SANDIA REPORT
SAND2001-2977
Unlimited Release
Printed September 2001

Compliance Assessment Document for the Transuranic Wastes in the Greater Confinement Disposal Boreholes at the Nevada Test Site

Volume 2: Performance Assessment
Version 2.0

John R. Cochran, Walt E. Beyeler, Doug A. Brosseau, Larry H. Brush, Theresa J. Brown, Bruce Crowe, Steve H. Conrad, Paul A. Davis, Tom Ehrhorn, Tom Feeney, Bill Fogleman, David P. Gallegos, Rick Haaker, Elena Kalinina, Laura L. Price, Dick P. Thomas, and Sharon Wirth

Prepared By
Sandia National Laboratories

Albuquerque, New Mexico 87185
and Livermore, California 94550

Sandia is a multiprogram laboratory operated by Sandia Corporation, a Lockheed Martin Company, for the United States Department of Energy under contract DE-AC04-94AL85000.

Sandia National Laboratories

Issued by Sandia National Laboratories, operated for the United States Department of Energy by Sandia Corporation.

Available to DOE and DOE contractors from
U.S. Department of Energy
Office of Scientific and Technical Information
P.O. Box 62
Oak Ridge, TN 37831

Telephone: (865)576-8401
Facsimile: (865)576-5728
E-Mail: reports@adonis.osti.gov
Online ordering: http://www.doe.gov/bridge

Available to the public from
U.S. Department of Commerce
National Technical Information Service
5285 Port Royal Rd
Springfield, VA 22161

Telephone: (800)553-6847
Facsimile: (703)605-6900
E-Mail: orders@ntis.fedworld.gov
Online order: http://www.ntis.gov/ordering.htm

SAND2001-2977
Unlimited Release
Printed September 2001

Compliance Assessment Document for the Transuranic Wastes in the Greater Confinement Disposal Boreholes at the Nevada Test Site, Volume 2: Performance Assessment

John R. Cochran, Walt E. Beyeler, and Doug A. Brosseau
Geohydrology Department
Sandia National Laboratories
P.O. Box 5800
Albuquerque, NM 87185-0735

Larry H. Brush
Repository Performance and Certification Department

Theresa J. Brown
Critical Infrastructure Surety Department

Bruce M. Crowe
Geologic Integration Group
Los Alamos National Laboratory

Steve H. Conrad, and Paul A. Davis
Geohydrology Department

Tom Ehrhorn
Duke Engineering and Services
Albuquerque, NM 87102

Tom Feeney
Geohydrology Department

Bill Fogleman
GRAM Inc.
Albuquerque, NM 87112

David P. Gallegos
Data Exploitation Department

Rick Haaker
AQ Safety Inc.
Albuquerque, NM 87111

Abstract follows

Elena Kalinina
GRAM Inc.
Albuquerque, NM 87112

Laura L. Price
BETA Corporation International
Albuquerque, NM 87109

Dick P. Thomas
Geohydrology Department

Sharon Wirth
I T Corp.
Albuquerque, NM 8710

ABSTRACT

Intermediate depth disposal operations were conducted by the U.S. Department of Energy (DOE) at the DOE's Nevada Test Site (NTS) from 1984 through 1989. These operations emplaced high-specific activity low-level wastes (LLW) and limited quantities of classified, "special case" transuranic (TRU) wastes in 37 m (120-ft) deep, 3 m (10 ft) diameter Greater Confinement Disposal (GCD) boreholes.

Four boreholes contain about 60,000 kg (132,000 lb.) of classified TRU waste packages, containing less than 330 curies of Plutonium-239. All of the TRU wastes emplaced in the GCD boreholes are classified for national security reasons and cannot be disposed of in the DOE's Waste Isolation Pilot Plant.

The U.S. Environmental Protection Agency's (EPA's) 40 CFR 191 defines the requirements for protection of human health from disposed TRU wastes. This EPA standard sets a number of requirements, including probabilistic limits on the cumulative releases of radionuclides to the accessible environment for 10,000 years. *This report presents the performance assessment (PA) that has been conducted to determine if disposal of TRU waste in the GCD boreholes complies with the EPA's 40 CFR 191 requirements.*

Sandia National Laboratories completed this PA using all available information and an Iterative PA Methodology, which focused work on uncertainty reduction in a cost-effective fashion that does not overestimate system performance and assured defensibility. Topics addressed in this PA include:

- Regulatory analysis
- Explanation of the Iterative PA Methodology
- Quality assurance and software quality
- Analysis and screening of features, events, and processes
- Analysis of human intrusion
- Nuclear criticality assessment
- Geochemical studies, including sorption and solubility
- Vadose zone characterization, including moisture content, water balance, and advective flux

- Development of plant and animal bioturbation models
- Climate change studies
- Landfill subsidence analysis
- 10,000 year surface water flooding analysis under current and glacial climates
- Conceptual model development
- Development of Flow and transport, and
- Dose Assessment modeling.

The desert southwest and the area surrounding the GCD boreholes have been studied intensively for over 20 years. These studies provide a very sound basis for the conceptual model of the disposal system:

- The GCD wastes are within a thick sequence of arid alluvium
- The arid alluvium is hydrologically homogeneous and isotropic on the scale of the disposal system
- The area is very stable geologically
- The tops of waste disposal zones are a minimum of 21 m (70 ft) below the land surface
- The bottoms of the waste disposal zones are almost 200 m (650 ft) above the water table
- Under current and undisturbed conditions, the pore water in the alluvium in the vicinity of the GCD boreholes moves very slowly upwards, toward the land surface
- There is no groundwater recharge under current climatic conditions
- Mammal and invertebrate burrowing can move soil from the subsurface to the land surface
- Desert plants can capture moisture and heavy metals, carrying them to the land surface
- No credit is taken for container degradation rates or other engineered barriers
- A return to the more dominant cooler and wetter climatic conditions, coupled with subsidence of the disposal cells, could result in deep infiltration, but no recharge to the water table.

The simplicity of the conceptual models of the GCD disposal system allowed them to be implemented in Microsoft® Visual Basic™ macros in an Access™ database. This PA model is built from a mathematical expression for mass conservation that includes the operation of a number of transport processes, including dissolution, precipitation, reversible chemical sorption onto soil, advection, diffusion, dispersion, radioactive decay and ingrowth, plant uptake, and bioturbation. The mathematical model and implementing code was used to calculate a complementary cumulative distribution function of integrated normalized release to the accessible environment for 10,000 years and probability distributions of dose based on two exposure conditions for the 1,000 year individual protection requirements.

The primary conclusions of this PA are that the disposal of TRU wastes in the GCD boreholes will, at most, result in minuscule doses to individuals, and that the GCD disposal system easily meets the EPA's 1985, 40 CFR 191 requirements for disposal of TRU waste. Further, there is a strong, reasonable expectation that actual system performance will be better than what is simulated in this PA.

ACKNOWLEDGMENTS

The GCD team would like to thank Angela Colarusso and Frank Di Sanza of the DOE, Nevada Operations Office (DOE/NV), for facilitating the completion of this 40 CFR 191 PA. The staff at Bechtel Nevada, Neptune and Company, Desert Research Institute, Harry Reid Center for Environmental Studies, and HSI GeoTrans have all supported this PA with review comments and suggestions on how to make this PA more readable and defensible. Faith Puffer and Jackie Ripple at Tech Reps worked long and hard hours to polish and publish this report.

Robert Guzowski, Gary Harms, Ahmed Hasan, Will Hareland, Terry Steinborn, and Harlan Stockman have all made important contributions to this PA.

Finally, the team would like to thank Beth Moore, Joe Ginanni, and Paul Dickman for their efforts to promote GCD as a safe and inexpensive method for disposing of difficult radioactive wastes.

PREFACE

Sandia National Laboratories has completed this Compliance Assessment Document (CAD) using all available information and an Iterative Performance Assessment Methodology. The Sandia National Laboratories team members provided the expertise in the broad suite of disciplines necessary to complete this CAD. The CAD, from its inception, has been peer reviewed by representatives of the DOE/NV, and DOE/NV contractors, including representatives from Bechtel Nevada, Neptune and Company, Desert Research Institute, Harry Reid Center for Environmental Studies, and HSI GeoTrans. *Sandia National Laboratories is comfortable defending the CAD as presented.* However, this CAD is undergoing a DOE Headquarters (DOE/HQ) peer review. As documented in Appendix R, many of the preliminary recommendations of the DOE/HQ Review Team have been incorporated in this Version 2.0.

Table of Contents

Figures

Tables

LIST OF ACRONYMS

ACH	air-changes-per-hour
AEA	Atomic Energy Act
AIC	active institutional control
AMC	antecedent moisture conditions
ANP	annual net primary
ASC	annual standing crop
ASME	American Society of Mechanical Engineers
CA	Composite Analysis
CAD	Compliance Assessment Document (GCD)
CCDF	Complementary Cumulative Distribution Function
CDF	cumulative distribution function
CERCLA	Comprehensive Environmental Response, Compensation, and Liability Act
CFR	Code of Federal Regulations
CR	containment requirements
CSRL	Criticality Safety Research Laboratory
DCF	dose conversion factor
DLLWMP	Defense Low-Level Waste Management Program
DOE	United States Department of Energy
DOE/NV	U.S. Department of Energy/Nevada Operations Office
DOE/HQ/EH	U.S. Department of Energy/Headquarters/Environmental Health
DNFSB	Defense Nuclear Facilities Safety Board
DQOs	date quality objectives
EDE	effective dose equivalent
EA	Environmental Assessment
EIS	Environmental Impact Statement
EPA	U.S. Environmental Protection Agency
ERDA	Energy Research and Development Administration
ES&H	Environment, Safety, and Health
FEPs	features, events, and processes
GCD	Greater Confinement Disposal
GCDT	GCD Test
GIS	Geographic Information System
GM	geometric means
GPR	Groundwater Protection Requirements
GWPR	ground water protection requirements
GSD	geometric standard deviation
HLW	high-level waste
ICRP	International Commission on Radiological Protection
IHI	inadvertent human intruder
IPR	individual protection requirement
LANL	Los Alamos National Laboratory
LHS	Latin Hypercube sampling
LLI	lower large intestine
LLNL	Lawrence Livermore National Laboratory

LLW	low-level waste
LLWMU	Low-Level Waste Management Unit
LWA	Land Withdrawal Act
MOP	member of the public
MPC	maximum permissible concentration
MSL	mean sea level
MTHM	metric tons of heavy metal
N&S	Necessary and Sufficient Process
NAS	National Academy of Sciences
NEPA	National Environmental Policy Act
NLLWMP	National Low-Level Waste Management Program
NRC	Nuclear Regulatory Commission
NTS	Nevada Test Site
NWAR	nuclear weapons accident residue
ORNL	Oak Ridge National Laboratory
PA	performance assessment
PDF	probability density function
PIC	passive institutional control
PMF	Probable Maximum Flood
PMP	Probable Maximum Precipitation
PPA	preliminary performance assessment
PVC	polyvinyl chloride
QA	quality assurance
QAMP	QA Management Plan
QAP	Quality Assurance Procedure
QARD	Quality Assurance Requirements and Description
RCRA	Resource Conservation Recovery Act
RFP	Rocky Flats Plant
RTG	radioisotopic thermoelectric generator
RWMS	Radioactive Waste Management Site
SCS	Soil Conservation Service
SLB	shallow land burial
SME	subject matter expert
SNF	spent nuclear fuel
SNL	Sandia National Laboratories
SPR	software problem report
TRU	transuranic
ULI	upper large intestine
U.S.	United States
USDA	United States Department of Agriculture
USGS	United States Geological Survey
WIPP	Waste Isolation Pilot Plant

This page intentionally left blank.

1.0 INTRODUCTION

1.1 Introduction and Scope

Intermediate depth disposal operations were conducted by the United States Department of Energy (DOE) from 1984 through 1989. These operations emplaced high-specific-activity low-level radioactive wastes (LLW) and limited quantities of classified transuranic (TRU) wastes in Greater Confinement Disposal (GCD) boreholes.

GCD boreholes are about 3 m (about 10 ft) in diameter and 36 m (120 ft) deep. The bottom 15 m (50 ft) of each borehole was used for waste emplacement and the upper 21 m (70 ft) was back-filled with native alluvium. The bottom of each GCD borehole is almost 200 m (650 ft) above the water table.

The GCD boreholes are located in the Area 5 Radioactive Waste Management Site (RWMS), which in turn is located on the Nevada Test Site (NTS), which occupies 3,500 km^2 (1,350 mi^2) of government-owned land (Figures 1-1 and 1-2). An aerial photograph of the Area 5 RWMS is presented in Figure 1-3.

The Area 5 RWMS is in one of the most arid portions of the United States (U.S.), with an average precipitation of 13 cm (5 in.) per year. The limited precipitation, coupled with plant uptake, generally warm temperatures and low humidities, results in a hydrologic system dominated by evapotranspiration; the limited surface water does not migrate to the water table. The Area 5 RWMS is situated on a thick sequence of arid alluvium, composed of weakly stratified, gravelly sand derived from the bordering mountains. An idealized cross-section through the Area 5 RWMS is presented in Figure 1-4. Importantly, there are no "preferential pathways" for water movement in the deeper alluvium; the alluvium is homogeneous on a large scale.

A total of 13 GCD boreholes were constructed. Radioactive wastes were emplaced in nine of the 13 boreholes. Of these 13 boreholes, Boreholes 1, 2, 3, and 4 contain the TRU wastes, which are classified for national security reasons.

This study presents the results of technical analyses undertaken to help DOE determine whether or not the TRU wastes in the GCD boreholes will endanger human health. The requirements for protection of human health from TRU wastes are defined by the U.S. Environmental Protection Agency's (EPA's) 40 Code of Federal Regulations (CFR) 191 Subpart B requirements promulgated in 1985.

40 CFR 191 includes four sets of requirements. The (1) Containment Requirements (CRs), (2) Groundwater Protection Requirements (GWPRs), and (3) Individual Protection Requirements (IPRs) are quantitative. Technical analyses that are conducted to determine compliance with requirements (1), (2), and (3) are referred to as "performance assessments" (PAs). The fourth set of requirements in 40 CFR 191 are the (4) Assurance Requirements, which are related to the physical closure of the disposal facility, and are qualitative.

Figure 1-1. Location Map of the NTS. Green Indicates Lowest Elevations, Reddish-Brown Indicates Highest Elevations.

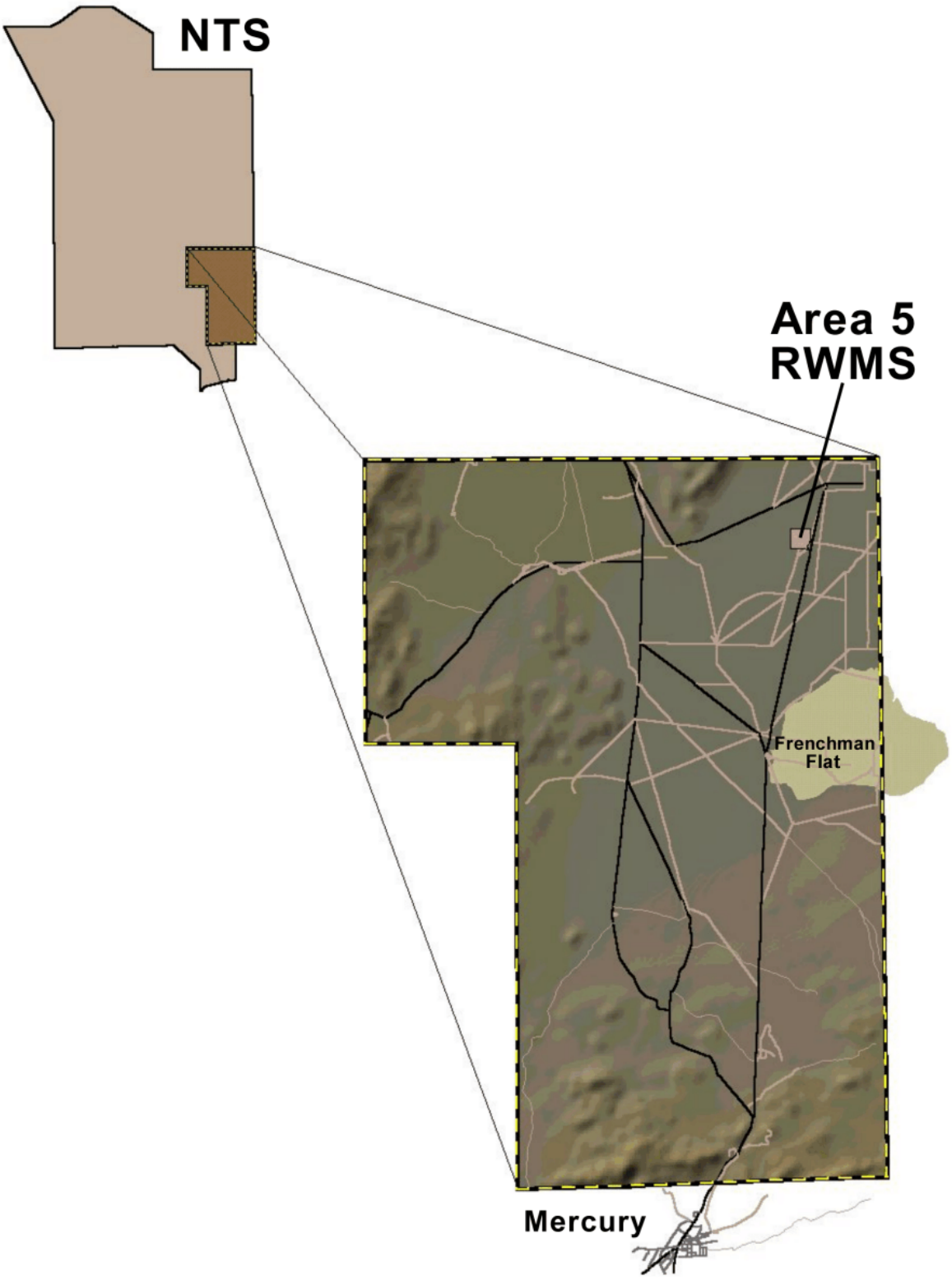

Figure 1-2. Location Map of Area 5 and the Area 5 RWMS within the NTS.

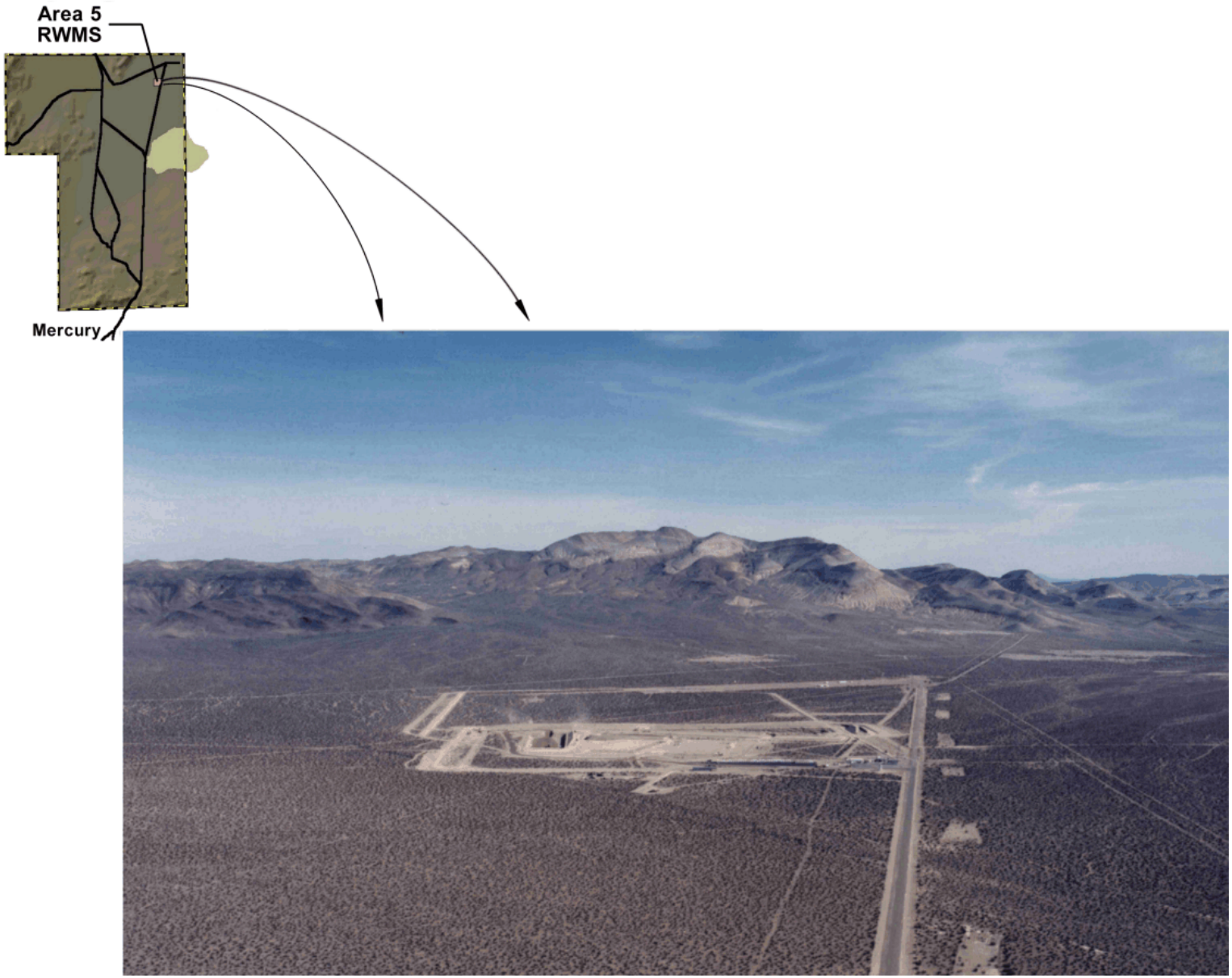

Figure 1-3. Aerial Oblique Photograph of the Area 5 RWMS (looking north).

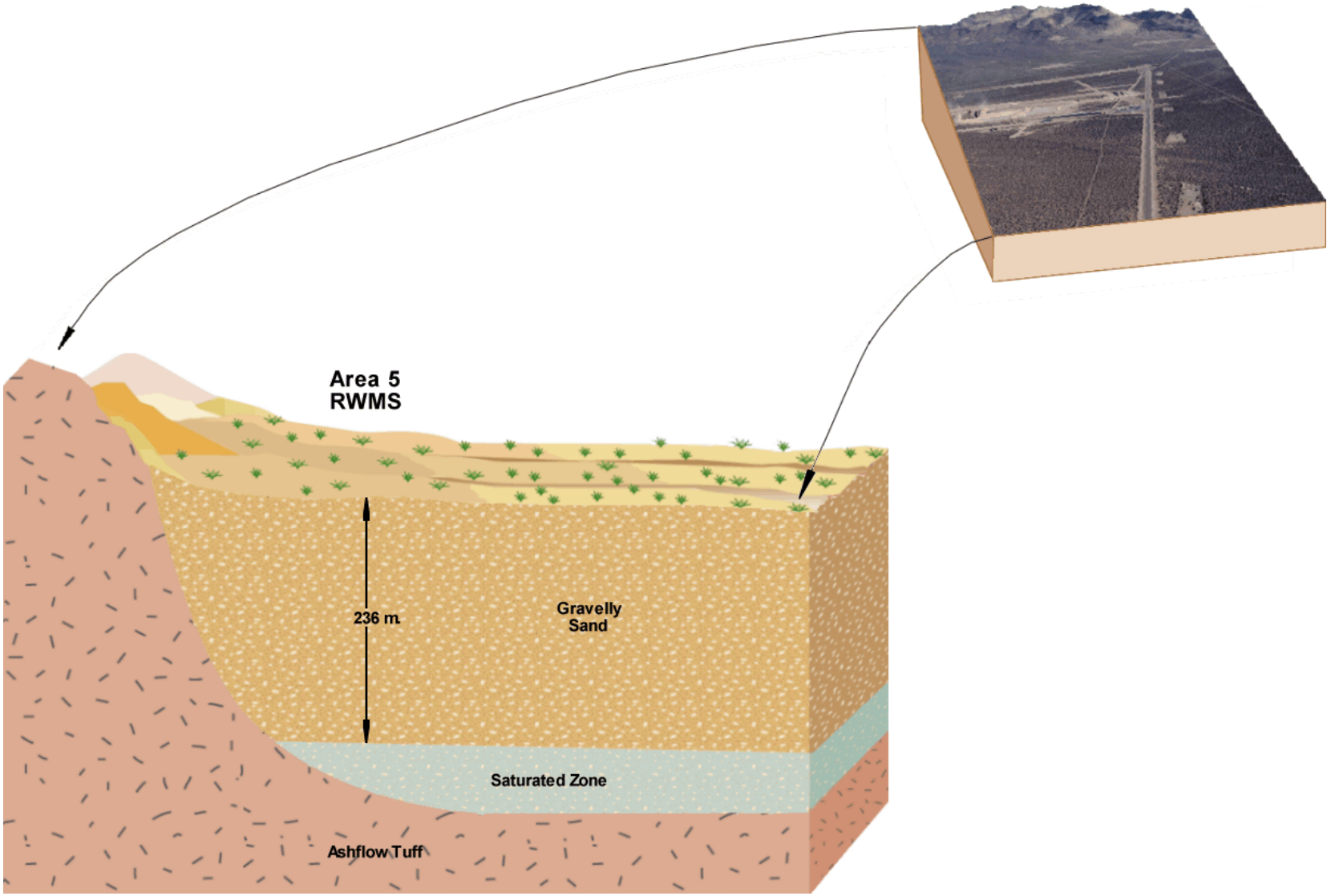

Figure 1-4. Idealized Cross-Section through the Area 5 RWMS.

This report (Volume 2) presents the PA for the TRU wastes in the GCD boreholes in a logical sequence:

C Introduction - provides an overview of Volume 2 and details the development of the GCD concept;

- Regulatory Requirements and Performance Measures - this section summarizes the regulatory requirements. This PA is conducted in the context of 40 CFR 191 and its 10,000-year probabilistic standards;

- Performance Assessment Methodology - this section describes the PA methodology used in this report. This methodology provides confidence beyond that required by 40 CFR 191.

- Quality Assurance Program - describes the planning and implementation procedures used to provide traceability, replication, and accountability of information in this PA;

- Current Disposal System Description - describes the current Area 5 RWMS setting and develops the conceptual and mathematical models and input parameters used to assess performance under current conditions;

- Future Evolution of the Disposal System - describes how the Area 5 RWMS setting may evolve (e.g., landfill subsidence is expected after closure) and develops the conceptual and mathematical models and input parameters used to assess performance under possible future conditions;

- Transport and Exposure Models - summarizes the human exposure scenarios and describes the implementation of the mathematical models used to assess performance;

- Consequence Analysis - as required by regulation, the results of this PA are presented as a complementary cumulative distribution function (CCDF) of the integrated normalized releases. Doses to the public, a resident farmer, are presented as a histogram;

- Summary and Conclusions - presents conclusions drawn from the PA; and

- References.

This report is part of a four-volume set. Volume 1 summarizes the entire study in nontechnical terms. Volume 2 presents the PA. Volume 3 documents the computer code used in the PA, and Volume 4 describes how DOE will demonstrate compliance with the qualitative Assurance Requirements. Taken together, these reports make up the Compliance Assessment Document (CAD) for the TRU wastes in the GCD boreholes.

1.2 Disposal History

In implementing its atomic energy defense mission, the DOE generates and is responsible for the safe disposal of LLW; by-product material; high-level waste (HLW); spent nuclear fuel (SNF);

and TRU waste. In general, each of these five different categories of waste is disposed using different techniques and/or facilities. LLW is generally disposed of using shallow land burial (SLB) techniques, HLW and SNF may be destined for the proposed repository at Yucca Mountain in Nevada, and the Waste Isolation Pilot Plant (WIPP) near Carlsbad, New Mexico, has been approved by the EPA for disposal of certain TRU wastes.

There are some wastes that do not meet the waste acceptance criteria for the default disposal techniques and/or facilities. Such "special-case wastes" have been given a number of titles over the years, including "orphan wastes," "special-case wastes," "performance assessment limited wastes," and most recently, "wastes with no identified path to disposal." These special-case wastes are not a new category of wastes; they are subsets of the existing five general categories of radioactive wastes. For example, the classified TRU waste generated by DOE is a "special-case" TRU waste that does not meet the waste acceptance criteria for disposal at WIPP.

Development of GCD boreholes grew out of the need to manage a special-case LLW. According to Dickman [1989]:

> In 1978, DOE established the ... Defense Low-Level Waste Management Program (DLLWMP) to address emerging technical and regulatory issues for generating and disposing of LLW. One of the early goals ... was to seek improved methods for disposing of mobile radionuclide species, in particular, tritium. ... The NTS was the disposal location for small volumes of concentrated tritium from Mound Laboratories. These wastes were disposed in a conventional SLB trench. Due to its high environmental mobility, minute quantities of tritium were soon detected at environmental monitoring stations ... While the amounts detected posed no hazards to workers or the environment, it was recognized that SLB did not provide sufficient confinement for these wastes. ...
>
> To address the issue of tritium waste disposal, DOE/NV proposed to develop an "intermediate depth" disposal project .... In October 1979, the DLLWMP requested that DOE/NV prepare a report on criteria necessary for development of an "intermediate" depth disposal facility.... In 1981, the DLLWMP approved funding for a project at the NTS with the specific goal to demonstrate GCD technology in an arid region.

The goals of GCD were to:

- Protect workers from high-specific-activity LLW;
- Develop equipment for handling and disposing of high-specific-activity wastes;
- Protect groundwater resources;
- Eliminate potential for wastes to be exposed at the land surface (e.g., by erosion);
- Minimize long-term maintenance;
- Minimize the potential for inadvertent human intrusion; and
- Protect members of the public from high-specific-activity LLW.

The development of the GCD technology in an arid region can be divided into three phases: Research, Testing, and Operations.

1.2.1 Initial Research of Greater Confinement Disposal Technology

The DOE authorized numerous studies of GCD technology prior to using the technique to dispose of waste. This research was conducted in three main areas:

- Risk Assessments/Cost-Benefit Analyses;
- Design and Operational Procedures; and
- Design of a GCD Test (GCDT) borehole.

In addition to the DOE-funded studies, the U.S. Geological Survey (USGS) [Winograd, 1981] suggested that the NTS, with an arid climate, dry alluvium, deep water table, and low population densities might provide an ideal location for disposal of radioactive waste.

Risk Assessments/Cost-Benefit Analyses

A number of DOE-funded studies were undertaken (1) to determine if implementation of intermediate depth GCD technology would be protective of human health, and (2) to determine if the GCD concept would be cost-effective. Because these studies were done prior to construction, most of these studies used a "reference GCD facility" as the basis for the evaluation. The reference GCD facility consisted of 100 equally-spaced GCD boreholes in a 200 m × 200 m (656 ft × 656 ft) facility where each borehole was assumed to be 46 m (150 ft) deep, with the top of the wastes 22 m (73 ft) below the land surface.

The first of these studies, *Limited Risk Assessment and Some Cost-Benefit Considerations for Greater Confinement Disposal as Compared to Shallow Land Burial*, was published by Science Applications Inc. [Belanger et al., 1981]. For the scenarios analyzed, the study concluded that there was no cost advantage of GCD over SLB at the NTS; that there was a cost advantage of GCD over deep geologic disposal; and that GCD "would generally be acceptable for TRU wastes." Science Applications Inc. then completed a second study in 1982 titled *Comparative Assessment of Disposal of TRU Waste in a Greater Confinement Disposal Facility* [Cohen et al., 1982].

The *Safety Assessment for Area 5 Radioactive Waste Management Site* was completed by Ford, Bacon & Davis [Hunter et al., 1982]. Then in 1984, the final risk assessment by Science Applications Inc., called *Limited Risk Assessment and Some Cost-Benefit Considerations for Greater Confinement Disposal as Compared to Shallow Land Burial*, was published [Hunter et al., 1984]. This study assessed the dose consequences to a Farmer/Intruder. Some of the conclusions of that study were that the "GCD concept seems to be an acceptable and cost-effective means of disposing of TRU wastes," and that GCD is more cost-effective than deep geologic disposal.

Hunter et al. [1984] also estimated the costs of operating the reference GCD facility. Assuming the GCD boreholes were co-located with an existing LLW disposal facility, the cost of drilling,

waste emplacement, and backfill at the reference GCD facility would be approximately $480 per cubic meter of waste emplaced.

These risk assessments were undertaken for "reference wastes," in the reference GCD facility, using limited site-specific data . The reference wastes included 22 curies per cubic meter (Ci/m^3) (0.63 Ci/ft^3) of plutonium-239 (^{239}Pu), plus other radionuclides. The RADTRAN code was typically used to calculate doses.

Although a number of these studies assessed potential doses from disposal of TRU wastes, none of these studies assessed compliance with the EPA's standard for disposal of TRU wastes, 40 CFR 191. EPA issued a draft of 40 CFR 191 in 1982, and the legally applicable version was issued by the EPA in 1985.

In addition, Los Alamos National Laboratory (LANL) conducted a study to determine the potential for a nuclear criticality, assuming that 15 containers of "Nuclear Weapons Accident Residue" stored at the DOE's Pantex Plant were buried in GCD boreholes [Caldwell and Bieri, 1983]. The study notes that most of the wastes are in a "stable aluminum-plutonium-uranium or aluminum-uranium slag form." The authors recommended burying these 15 containers in three GCD boreholes, and using approximately 160 tons of probertite (a borate ore and a neutron poison) as backfill around the waste packages in each of the three boreholes. As discussed in Section 5.9, these LANL recommendations were implemented by U.S. Department of Energy/Nevada Operations Office (DOE/NV).

Design and Operational Procedures

Design and operational considerations were addressed by several panel workshops, meetings, and reports:

- "Panel Workshop E (Greater Confinement Disposal) Report," *Proceedings of the Third Annual Information Meeting DOE Low-Level Waste Management Program* [Wiley and Hunter, 1981]
- *Criteria for Greater Confinement of Radioactive Wastes at Arid Western Sites* [Card et al., 1981]
- *Evaluation of the Need of Greater Confinement than Shallow Land Burial of Low-Level Waste*, Technical Position Paper [Mezga, 1981]
- *Technical Concept for a Greater Confinement Disposal Test Facility at the Nevada Test Site*. [Hunter and White, 1982]

The most comprehensive of these studies is *Operational Technology for Greater Confinement Disposal* [Dickman et al., 1984], which describes how to design, construct and operate a GCD facility.

Prior to construction and operation of a set of GCD boreholes, DOE wanted to test the GCD concept with a single borehole; therefore, a GCDT borehole needed to be designed and constructed.

Design of a Greater Confinement Disposal Test Borehole

The first GCD borehole was designed to provide "operations research and a technology demonstration" of the GCD concept. The GCDT borehole was to be heavily instrumented and contain a large enough inventory of radioactive wastes to test the ability of the arid alluvium to isolate mobile tritium wastes from the land surface and workers.

The design of the test borehole is documented in:

- *Test Plan for the Greater Confinement Disposal Facility at the Nevada Test Site* [Dickman and O'Neal, 1982];
- *Procurement Specifications - Downhole Instrumentation for Test of Greater Confinement Disposal of Radioactive Waste at the Nevada Test Site* [Hunter and Card,1982]; and
- *Soil Characterization for the GCDT Demonstration Project at the NTS* [Holmes and Narver, Inc., 1983].

1.2.2 Testing the Greater Confinement Disposal Concept

With the GCD Test Plan defined and a technical basis for the disposal concept, the GCDT borehole was constructed in 1983. The initial design was for a 46 m (150 ft) deep, 3 m (10 ft) diameter borehole; however, auger rigs available at the NTS were capable of achieving only a 36 m (120 ft) depth, so the test proceeded with the 36 m (120 ft) depth.

A photograph of the drilling of the GCDT borehole is provided in Figure 1-5. The equipment used to auger a GCD borehole is not much more complicated than the equipment used to construct a SLB trench.

To monitor the GCDT borehole performance, a total of nine 60 cm- (2 ft-) diameter shafts were drilled around the central GCDT borehole. Nine instrument lines, with a total of 144 monitoring stations were placed in the ground. Three of the instrument lines were placed in GCDT, as shown in Figure 1-6. Six more lines were placed in six of the nine monitoring shafts. A full set of photographs of the drilling and instrumenting of the GCDT borehole is available [DOE, 1983].

To test the remote-handling equipment, and to fully test the ability of the GCD concept to isolate tritium from the land surface, heat-producing radioactive sealed sources were buried with a large amount of tritium. In December of 1983, waste loading operations began with the remote transfer and disposal of a 345,000 Ci strontium 90 (^{90}Sr) source. The ^{90}Sr was contained in four stainless-steel capsules. The skin temperature of the capsules was approximately 600^{o} C (1100^{o} F). A specially constructed 1.2 m × 1.2 m (4 ft × 4 ft) "bucket" filled with metal turnings was placed at the bottom of the GCDT borehole to receive the remote-handled wastes. A 20,500 Ci Cesium 137 capsule, two 250 Ci Cobalt 60 capsules, and a 10,000 Ci ^{90}Sr source were also remotely placed in the bucket. Subsequent wastes were contact-handled and included over 690,000 Ci of tritium in 80 drums and over 40,000 Ci of ^{90}Sr from decommissioned radioisotopic thermoelectric generators (RTGs).

Figure 1-5. Drilling of the GCDT Borehole.

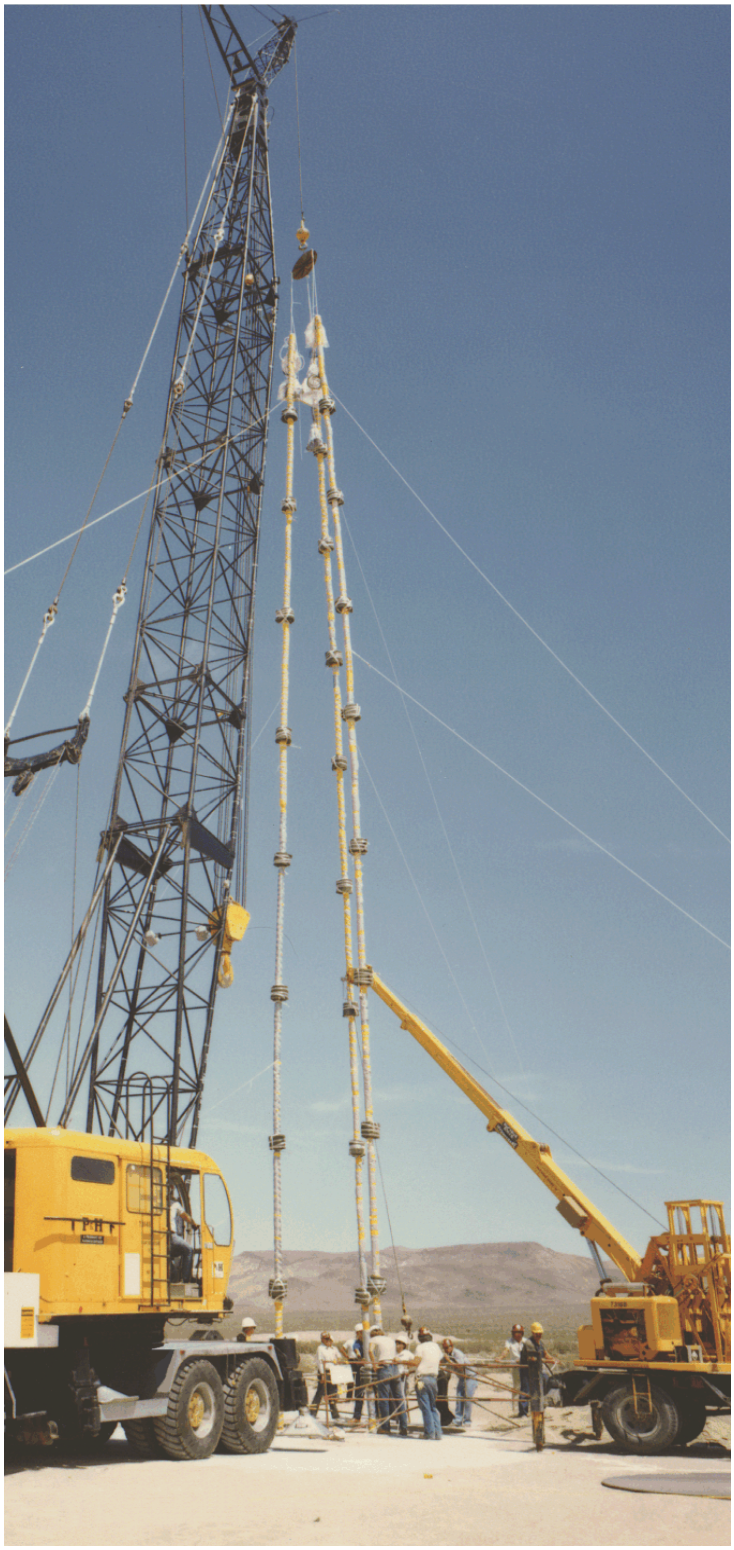

Figure 1-6. Placement of Monitoring Equipment in the GCDT Borehole.

In total, over 1,000,000 Ci of high-specific activity LLW was loaded into the GCDT borehole. These waste-loading operations are described in Boland and Dickman [1986].

Four years of monitoring soil temperature, soil moisture, and a fluorocarbon tracer gas are described by Dickman [1989] and results of the tritium monitoring are described by Swanson et al. [1988] and Pottororff et al. [1988]. One conclusion of the GCDT was that GCD borehole technology is an effective method to dispose of high-specific-activity tritium wastes.

The nine monitoring shafts have been grouted to the land surface and the GCDT borehole is covered by a 15 cm- (6 in.-) thick concrete pad with a concrete monument marking the location of the GCDT borehole under the pad.

1.2.3 Greater Confinement Disposal Operations

Based on technical analyses and an operational demonstration of the technology, 12 operational boreholes were augered in the Area 5 RWMS. The locations of all 13 GCD boreholes (GCDT plus 12 operational boreholes) are shown in the orthophotograph of the Area 5 RWMS (Figure 1-7).

From 1984 through 1989, eight of these 12 operational boreholes were used to dispose of special-case wastes. Shown in Figure 1-8 is an idealized cross-section of a GCD borehole loaded with wastes and backfilled with alluvium. In terms of curies, most of the wastes were LLW, with 2,300,000 Ci of tritium comprising the majority of the LLW.

Four of the boreholes were used to dispose of special-case TRU wastes. Boreholes 1, 2, and 3 were used to dispose of 15 containers of Nuclear Weapons Accident Residue (NWAR) waste, which is packaged in "CONEX" metal boxes, plywood boxes, and in metal barrels. Most of the NWAR wastes are in a "stable aluminum-plutonium-uranium or aluminum-uranium slag form." The TRU wastes in Borehole 4 are from DOE's Rocky Flats Plant (RFP). The Rocky Flats wastes are in fiberboard containers which have been bagged in heavy plastic and placed inside 200-L (55-gal) drums. Non-TRU wastes from Lawrence Livermore National Laboratory (LLNL) are also disposed in Borehole 4.

In total, about 60,000 kg (132,000 lb) of classified TRU waste packages, containing less than 330 Ci of ^{239}Pu, are buried in the four boreholes. All of the TRU wastes emplaced in the GCD boreholes are classified for national security reasons, and, therefore, do not meet the waste acceptance criteria for the WIPP. The inventory is described in greater detail in Section 5.9. All radionuclides exist in the solid phase except for isotopes of radon, which are gaseous. Presented in Figure 1-9 is a timeline of the operational use of the GCD boreholes and the timing of certain regulations governing radioactive waste disposal [Vocke et al., 1999].

1.3 Regulatory Requirements

This section provides a brief overview of the regulatory requirements governing the wastes in the GCD boreholes. Section 1.3.1 discusses the regulations governing the LLW in the GCD boreholes and the studies that have been conducted to determine if those wastes meet applicable

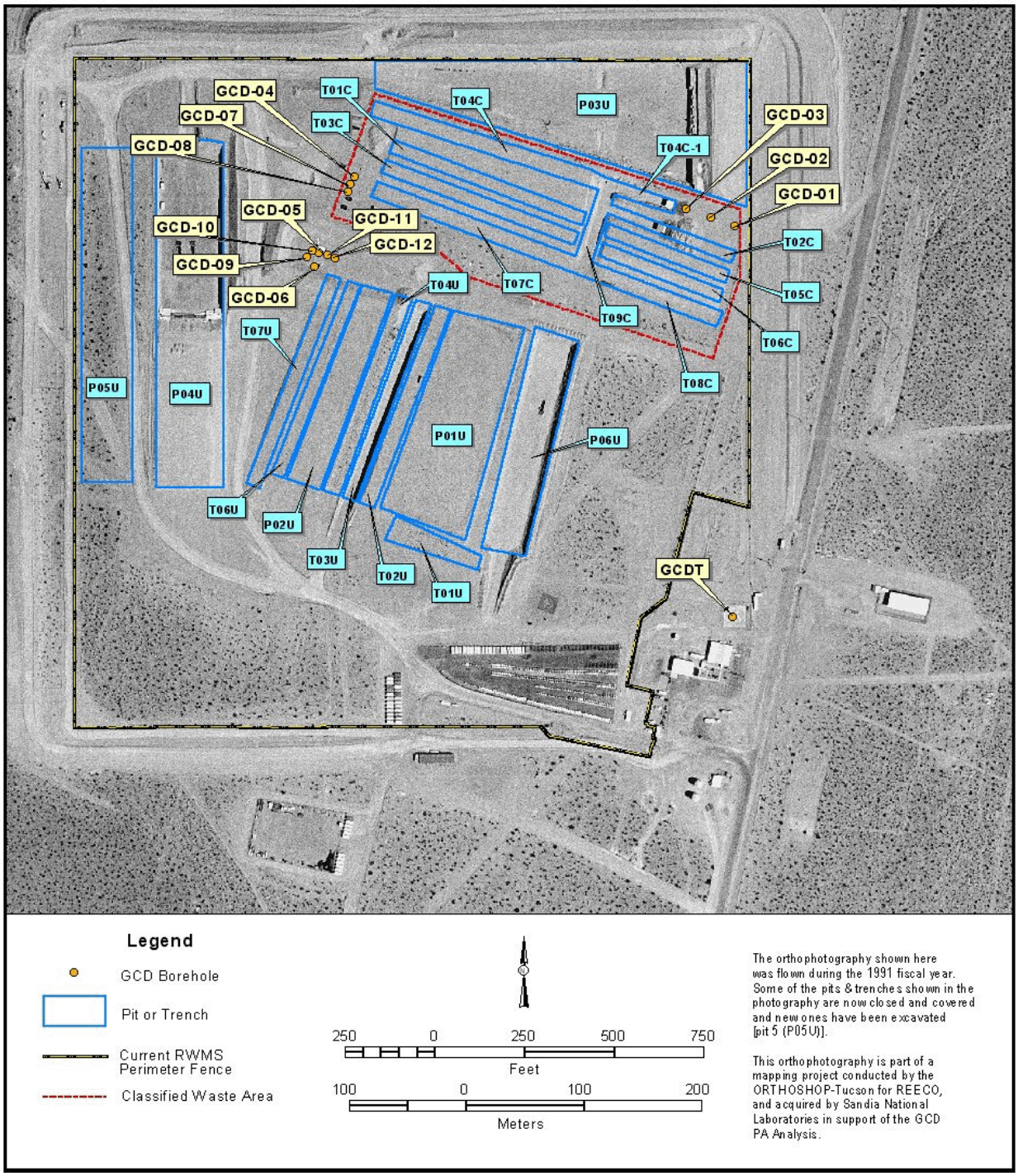

Figure 1-7. Orthophotography Showing Locations of GCD Boreholes in the Area 5 RWMS.

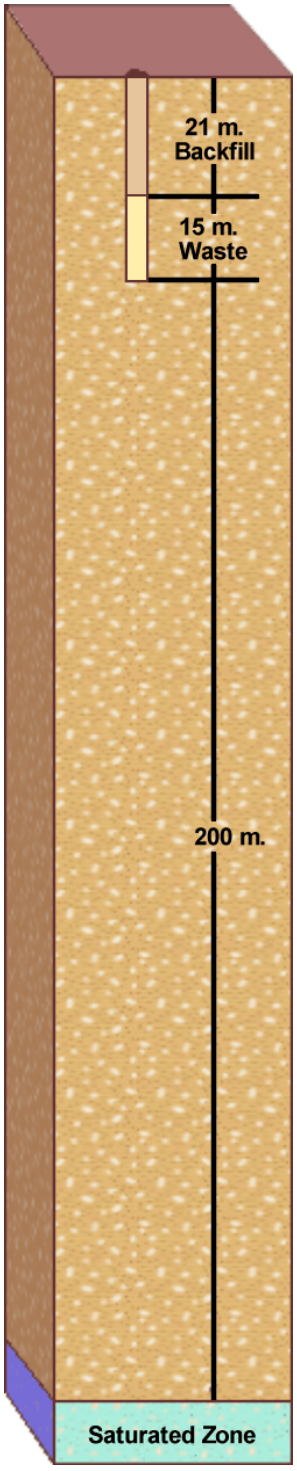

Figure 1-8. Idealized Cross-Section through a GCD Borehole.

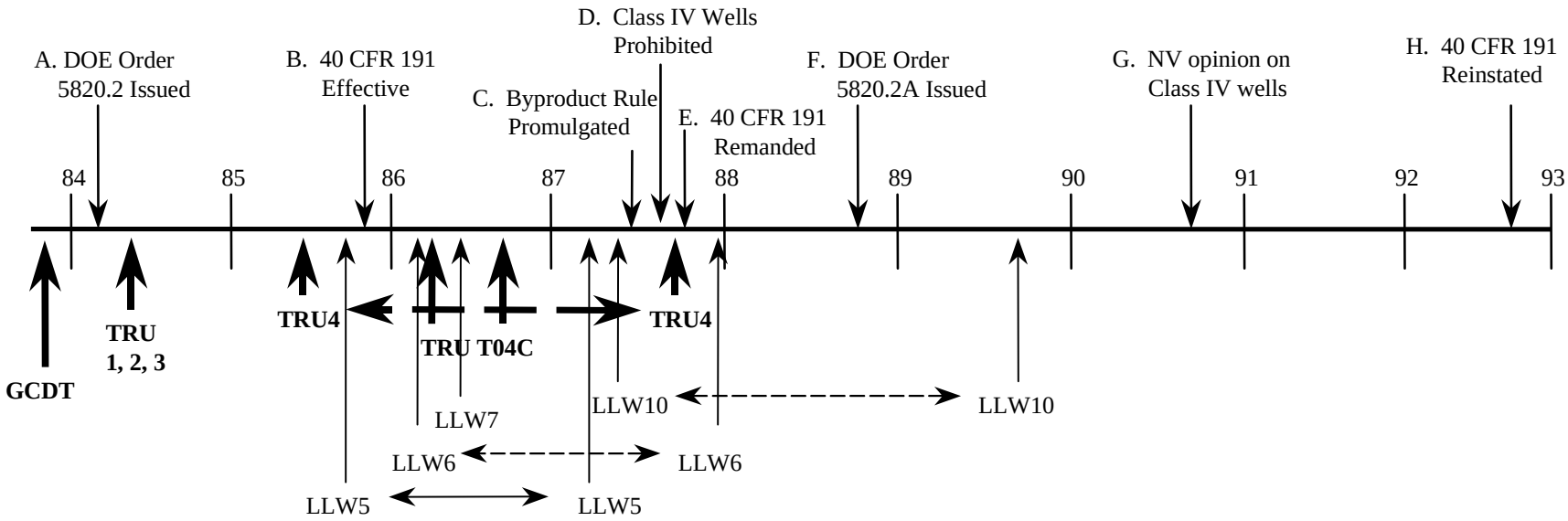

NOTES:

A. February 6, 1984: DOE Order 5820.2 issued to regulate management of DOE-titled radioactive waste.

B. November 18, 1985: Effective date for EPA 40 CFR Part 191, which established environmental radiation protection standards for TRU wastes.

C. June 1, 1987: DOE's Byproduct Rule becomes effective clarifying that the DOE exclusion from RCRA for byproduct material applies only to the radionuclides themselves, not the entire waste matrix.

D. July 22, 1987: Nevada prohibition on Class IV underground injection wells.

E. September 1987: 40 CFR Part 191 remanded by the First Circuit Court.

F. September 26, 1988: DOE Order 5820.2A issued to regulate management of DOE-titled radioactive waste.

G. October 1990: Nevada expresses written opinion that GCD boreholes are Class IV wells. This may not be their first statement of concern.

H. October 1992: WIPP Land Withdrawal Act reinstates most of 40 CFR Part 191.

Numbers indicate the borehole in which the waste was emplaced.

Figure 1-9. Disposal Timeline for GCD Boreholes. [from Vocke et al., 1999]

LLW standards. Section 1.3.2 provides an overview of the EPA's 40 CFR 191 Subpart B, which is the EPA's standard for the disposal of TRU wastes.

In the U.S., radioactive waste is divided into five categories: SNF, HLW, TRU waste, by-product material, and LLW. Three federal entities have the majority of the regulatory authority for the disposal of the five categories of radioactive waste: the EPA, the DOE, and the U.S. Nuclear Regulatory Commission (NRC). Each of these entities has instituted various laws, Orders, Directives, guidance documents, and Branch Technical Positions that govern the various categories of radioactive wastes.

In very general terms, the EPA has authority to write standards, the DOE has authority to write and enforce standards for radioactive wastes from "atomic energy defense activities," and the NRC has authority to write and enforce regulations for disposal of commercially-generated LLW and for disposal of SNF and HLW. There are many notable exceptions to these generalizations. Without going into details, the EPA has the authority to develop standards for the disposal of LLW and TRU wastes and the DOE has the responsibility to enforce those EPA standards for the disposal of LLW and TRU waste in the GCD boreholes.

1.3.1 Safety of Low-Level Waste in Greater Confinement Disposal Boreholes

Introduction

DOE implements its Atomic Energy Act (AEA) authority through a set of Directives, DOE Orders (which are not codified), and regulations. The most relevant of these is DOE Order 5820.2A [DOE, 1988a], which establishes "... policies, guidelines and minimum requirements by which the DOE manages its radioactive and mixed waste and contaminated facilities." Order 5820.2A has been in effect since September 1988. Recently, DOE Order 5820.2A was replaced by DOE Order 435.1, as discussed in Section 2.0. Through the "necessary and sufficient" process, DOE/NV continues to honor the requirements of DOE Order 5820.2A and has not adopted the requirements of DOE Order 435.1.

Definition of Low-Level Waste

LLW is radioactive waste that is not HLW, SNF, TRU waste, or by-product materials as defined in Section 11e(2) of the AEA. The NRC, consistent with existing law, can also classify a waste as LLW. LLW is defined by what it is not (it is not HLW, SNF, TRU, or by-product material).

U.S. Department of Energy Standards for Disposal of Low-Level Waste after September 1988

The EPA has the authority to set standards for disposal of LLW; however, EPA has yet to finalize 40 CFR 193 as the general disposal standard for LLW. The DOE sets and enforces its own standards for disposal of LLW from atomic energy defense activities. The DOE standards were contained in Chapter III of DOE Order 5820.2A. In summary, the DOE Order requires:

1. that doses to members of the public (MOP) be less than 25 mrem per year;
2. the effective dose equivalent to an inadvertent human intruder (IHI) be less than 100 mrem per year for continuous exposure or 500 mrem for a single acute exposure; and
3. protection of groundwater resources consistent with state and Federal standards.

This standard was applied to LLW disposed after September 1988, and the regulatory timeframe has been interpreted as being 1000 years.

As noted in Figure 1-9, LLW was disposed in GCD borehole 10 after September 1988. Shott et al. [1998] have prepared a PA for all LLW disposed of in the Area 5 RWMS after September 1988 and have found that these wastes meet the DOE requirements to protect the MOP, the IHI, and groundwater resources.

U.S. Department of Energy Standards for Low-Level Waste Disposed Before 1988

An external oversight board (the Defense Nuclear Facilities Safety Board [DNFSB]) found in DNFSB 94-2 that DOE should assess the possible impact to human health from both pre- and post-1988 LLW. In response to DNFSB 94-2, the DOE committed to prepare "composite analyses" (CAs).

The standards for the CAs are similar to the DOE 5820.2A standards for disposal of post-1988 LLW, with four major exceptions:

1. the source term for the CA includes all sources of radioactive contamination that could interact to affect the dose to the MOP (not just the post-1988 LLW);
2. the dose limit for the MOP is 100 mrem/yr (not 25 mrem/yr);
3. there is no requirement to protect the IHI; and
4. the point of compliance is a future DOE land use boundary, not the 100-m (330-ft) boundary typically assumed for post-1988 LLW.

Like the DOE standard for post-1988 LLW, the DOE requirements for CAs require protection of groundwater resources consistent with state and Federal standards. As noted in Figure 1-9, GCD Boreholes 4, 5, 6, 7, 10, and GCDT contain LLW, as do all the trenches in the Area 5 RWMS. A CA for all radioactive wastes in the Area 5 RWMS, including the GCD wastes, has been drafted and is under DOE review. A PA for the post-September 1988 LLW and a CA for all interacting radioactive wastes are separate analyses, because the performance objectives are different. Finally, this report details a third PA which addresses 40 CFR 191 and the TRU wastes in the GCD boreholes.

1.3.2 Standards for Transuranic Wastes

At the time of emplacement, TRU waste was governed by Chapter II of former DOE Order 5820.2. That DOE Order defined two options for disposal of TRU wastes that could not be certified for disposal in WIPP; (1) storage or (2) "…*disposed by greater confinement*…" (DOE 5820.2 II 3. C. (3), emphasis added).

In addition to requiring disposal by greater confinement, Chapter II of DOE Order 5820.2 also required TRU waste disposal systems to meet the EPA's requirements for disposal of TRU wastes, 40 CFR 191. Although developed primarily for mined geologic repositories, the EPA notes the applicability of 40 CFR 191 to the TRU waste in the GCD borehole in the Federal Register:

> "Although developed primarily through consideration of mined geologic repositories, 40 CFR 191, including today's amendments, applies to disposal of the subject wastes by any method, with three exceptions." [EPA, 1993; p. 66399]

None of the EPA's three exceptions apply to the GCD boreholes. In the same discussion, EPA was clear:

> "EPA informed the Department of Energy, prior to the First Circuit decision in 1987, that the 1985 version of part 191 was applicable to any disposal activities at the Greater Confinement Disposal (GCD) Facility. Therefore, any radioactive waste as defined in §191.02 that was disposed of at the GCD facility is subject to all of the requirements of 40 CFR 191 promulgated in 1985, and neither the First Circuit decision, the WIPP LWA, nor today's promulgation of revised regulations change that determination." [EPA, 1993; p. 66413]

Given the clear applicability of 40 CFR 191 to the TRU wastes in the GCD boreholes,[1] the remainder of this section provides an overview of the four sets of requirements of 40 CFR 191 Subpart B and Section 2.0 provides a full presentation and interpretation of 40 CFR 191 Subpart B requirements.

40 CFR 191 includes four sets of requirements; the (1) CRs, (2) IPRs, (3) GWPRs, and the (4) Assurance Requirements. Each of these is overviewed in the next four subsections.

1.3.2.1 Containment Requirements

Protection of the general population is provided by the CRs defined at 40 CFR 191.13 which state that the disposal system shall provide the **reasonable expectation**, based on a PA, that the cumulative releases of radionuclides **to the accessible environment** for **10,000 years** after disposal from **all significant processes and events** shall:

(a) have a likelihood of less than one chance in 10 of having an EPA Sum greater than one, and
(b) have a likelihood of less than one chance in 1,000 of exceeding an EPA Sum of 10.

40 CFR 191 defines the **accessible environment** as the atmosphere and the land surface, and all of the lithosphere that is beyond the controlled area. 40 CFR 191 defines the **controlled area** as (1) a surface location, to be identified by passive institutional controls, that encompasses no more

[1] As noted in Section 2.0, 40 CFR 191 only applies to some of the TRU waste, although DOE has chosen to apply 40 CFR 191 to all the TRU in the GCD boreholes.

than 100 km^2 (38.6 mi^2) and extends horizontally no more than 5 km (3.1 mi) in any direction from the outer boundary of the original location of the radioactive wastes in a disposal system; and (2) the subsurface underlying such a surface location.

How Rigorous Are The CRs?

If a disposal system contained 330 Ci of pure ^{239}Pu, and there was no decay and ingrowth, then a cumulative release of 0.033 Ci, to the accessible environment over 10,000 years, would result in an EPA Sum of one.

The EPA Sum is a sum of the ratios of the calculated total curies of each radionuclide that reaches the accessible environment in 10,000 years divided by the number of curies set by the release limit. The release limit is based on the inventory and calculated according to 40 CFR 191.

The CRs require a probabilistic assessment of all events and processes that might affect the performance of a TRU waste disposal system for the next 10,000 years. Because there is great uncertainty about how society and human activities might evolve over the next 10,000 years, the EPA provides guidance on the interpretation of the CRs in Appendix B of 40 CFR 191. This PA *relies on the EPA's Appendix B Guidance* for an interpretation of the nature, types, probabilities, and severity of potential inadvertent human intrusions that might disrupt the GCD disposal system.

1.3.2.2 Individual Protection Requirements

Protection of an individual is provided by the IPRs (40 CFR 191.15), which state that the disposal system shall provide a **reasonable expectation** that, for **1,000 years** after disposal, **undisturbed performance** of the disposal system shall not cause the annual dose equivalent from the disposal system to any MOP **in the accessible environment** to exceed 25 mrem to the whole body or 75 mrem to any critical organ.

40 CFR 191 defines **undisturbed performance** as: the predicted behavior of a disposal system, including **consideration of the uncertainties** in the predicted behavior, **if the disposal system is not disrupted by human intrusion** or the occurrence of unlikely natural events.

The IPRs are, *by regulation, to be assessed under the assumption that the disposal system has not been disturbed by human intrusion.* The IPRs are constrained to 1,000 years of "expected performance," undisturbed by human intrusion or the occurrence of unlikely natural events.

1.3.2.3 Ground Water Protection Requirements

Protection of groundwater resources is provided by the GWPRs (40 CFR 191.16) which state that disposal systems shall be designed to provide a **reasonable expectation** that, for **1,000 years** after disposal**, undisturbed performance** of the disposal system shall not cause the radionuclide concentrations averaged over any year in water withdrawn from any portion of **a special source of ground water** to exceed standards defined in the regulation.

40 CFR 191 defines a **special source of ground water** as those Class 1 ground waters identified in accordance with the EPA's Ground-Water Protection Strategy published in 1984 that: (1) are within the Controlled Area boundary; (2) are supplying drinking water for thousands of persons, as of the date that the site was chosen for waste disposal; and (3) are irreplaceable, in that no reasonable alternative source of drinking water is available.

Because there is no special source of ground water within 5 km (3.1 mi) of the GCD boreholes, the GWPRs of 40 CFR 191 do not apply to the GCD boreholes.

1.3.2.4 Assurance Requirements

The Assurance Requirements state that the DOE must maintain active institutional controls (AICs) for as long as practicable; monitor the disposal system until there are no significant concerns to be addressed by further monitoring; and undertake other actions related to closure. The purpose of the Assurance Requirements is to provide confidence and defense in depth that the CRs will be met. Volume 4 of this CAD describes how DOE will demonstrate compliance with the Assurance Requirements.

1.3.2.5 Unique Aspects of 40 CFR 191

40 CFR 191 is a unique environmental standard. Some of these unique aspects are presented here.

Containment Requirements are Probabilistic

The EPA recognized that there are inherent uncertainties in assessing performance for the next 10,000 years, and the EPA requires that those uncertainties be addressed. The EPA requires reasonable assurance that there will be at least a 90% probability that certain release limits will not be exceeded, and the EPA also requires reasonable assurance that there will be at least a 99.9% probability that a higher release limit will not be exceeded. These are the only probabilistic environmental standards in the U.S.

Consideration of All Significant Processes and Events

The CRs also require the assessment of "all significant processes and events that may affect the disposal system" for 10,000 years. No other environmental standard requires such an explicit consideration of future events and processes.

Containment Requirements Protect the General Population

The basis of the CRs in 40 CFR 191 is that implementing 40 CFR 191 will not result in any more excess fatalities, *in the general population,* than would have occurred if the uranium had not been mined in the first place [EPA, 1985; p. 38067]. In contrast, standards for the disposal of LLW are based on doses *to any individual* (known as the MOP) and the belief that no individual should be exposed to ionizing radiation above a predefined threshold. There are requirements in 40 CFR 191 to protect the MOP under a specific set of circumstances. The philosophical basis

behind the CRs and the dose standards for disposal of LLW are different, and these philosophical differences are reflected in the disposal requirements; most notably in treatment of the IHI.

The Inadvertent Human Intruder is Not Protected

Protection of the IHI is one of the key objectives of LLW disposal standards. As discussed below, 40 CFR 191 offers no dose standard for the protection of the IHI. The EPA had good reason to exclude doses to the IHI from accidental releases:

> ... if human intrusion occurs, the individuals intruding may be exposed to high radiation doses. No regulatory scheme could prevent this for situations in which large amounts of radioactive material are confined to a relatively small area. [EPA, 1993; p. 66402]

The inability to protect the IHI is a negative aspect of the U.S. policy to concentrate large amounts of SNF, HLW, and TRU waste in relatively small areas. The U.S. could dispose of SNF, HLW, and TRU waste by spreading the wastes over large areas, thereby increasing the risk to the public at large. On the other hand, spreading radioactive waste over large areas protects the intruder, because the intruder can never be exposed to large amounts of waste. Stated another way; once the decision is made to concentrate large amounts of radioactive waste in a small area, there is no means of protecting an individual, if inadvertent intrusion does occur.

The Controlled Area Concept

In drafting 40 CFR 191, the EPA reasoned that it would be very difficult to isolate TRU wastes for at least 100 centuries. The EPA also reasoned that the best approach would be to use multiple barriers, where the adjacent geologic formations serve as part of the containment system [EPA, 1985; p. 58199].

Therefore, the "controlled area" was defined to contain the geologic formations adjacent to the disposal facility which serve as part of the containment system.

Because the controlled area is part of the disposal system, 40 CFR 191 does not set CR and IPR standards for releases within the controlled area. The CR and IPR standards apply to releases to the accessible environment, which is defined as (1) the atmosphere, (2) the land surface, (3) surface waters, (4) oceans, and (5) all of the litho-sphere beyond the controlled area.

Release Pathways

Releases from the GCD boreholes may reach the accessible environment through one of two paths, (a) upward 21 m (70 ft) to the land surface, or (b) downward 200 m (650 ft) to the water table and *then* 5,000 m (16,500 ft) in the groundwater to the accessible environment.

40 CFR 191 is a Very Deliberated Standard

These unique aspects are deliberate; the EPA's 40 CFR 191 is probably the most reviewed, and the most deliberated, environmental standard in U.S. history. At the request of President Ford,

the EPA began work on 40 CFR 191 in 1976. After a series of public meetings, technical studies, and a Draft Environmental Impact Statement (EIS), the EPA proposed 40 CFR 191 in 1982. The EPA then solicited additional written comments and held more public hearings. Additionally, the Agency's Science Advisory Board held nine public meetings reviewing the draft rule. The final rule was published in 1985 [EPA, 1985]. Then, in 1987, the U.S. Court of Appeals remanded the disposal portion of the standard. After additional deliberation and Congressional intervention, the EPA published the current version of 40 CFR 191 in 1993 [EPA, 1993; p. 66398]. Every aspect of this short standard and its associated Appendix B Guidance has been throughly reviewed.

1.4 Performance Assessment Methodology

Compliance with most environmental laws is directly verifiable. For example, compliance with the Safe Drinking Water Act standards can be verified by sampling and laboratory analysis. 40 CFR 191, Subpart B sets requirements for the *future* performance of a disposal system. In 40 CFR 191, the EPA requires the use of PA to demonstrate that a disposal system will be protective of human health for the next 10,000 years. The results of a PA cannot be directly verified, yet the PA is the basis for determining if the requirements of 40 CFR 191 have been met. This section overviews the PA methodology, which provides confidence in the PA analysis and results.

1.4.1 Performance Assessment Methodology Overview

Fundamental to this methodology is the philosophy that this PA is not a prediction of how the GCD system will actually perform. Actual performance cannot be assessed or verified. Rather, this PA provides simulations of a range of plausible outcomes, *which are developed in a manner to provide confidence that the results of the analysis do not overestimate the ability of the GCD boreholes to protect human health.*

This methodology is described in Section 3.0 and includes the following principles: (1) if more than one possible interpretation or conceptual model of the system can be justified, each interpretation is considered and resources are focused on evaluating those interpretation(s) that may lead to non-compliant results; (2) parameter uncertainty and/or variability is addressed by including and sampling from the unbiased distribution of possible parameter values; (3) Monte Carlo simulations are used to propagate parameter uncertainty through the analysis, (4) all events and processes that can adversely affect the system performance are analyzed, and (5) these principles are implemented in an iterative PA framework.

Estimating future performance requires the use of models. Developing and implementing models of a disposal system is typically composed of four substeps:

1. Developing conceptual model(s) based on existing information;
2. Developing mathematical model(s) that describe the conceptual model(s);
3. Defining the possible values for the input parameters; and
4. Developing computer code(s) to implement the mathematical model(s).

How these steps are carried out has a great bearing on the defensibility of the PA.

Conceptual Model Uncertainty and Screening

In simple terms, information about the disposal system is used to develop a conceptual model or models. A conceptual model is effectively a set of assumptions that describes the system for a specific purpose.

For example, because the spatial and temporal characteristics of a disposal system are imperfectly known and cannot be predicted for the next 10,000 years, there may be multiple conceptual models that are consistent with existing site data. Ideally, all possible conceptual models would be carried through the entire PA and results from all conceptual models could be presented; however, for practical reasons, the number of conceptual models addressed in this PA has been reduced through the use of a conceptual model screening process, which includes the following:

- identify alternative conceptual models that are consistent with existing knowledge;
- analyze all the conceptual models to assess which ones might lead to non-compliant results; and
- retain for further consideration and PA analysis those models that could lead to non-compliant results.

The first step may result in multiple descriptions of the disposal system. Often, a combination of technically-defensible arguments and quantitative analysis is used in the second step to screen out conceptual models. If the screening analysis indicates that the use of a particular model would improve disposal system performance (i.e., shifting the CCDF toward lower values or reducing doses), that conceptual model may be (but does not have to be) excluded from further consideration. This screening process is practical, and it maintains the defensibility of PA results.

Parameter Uncertainty and Variability

Parameter uncertainty is defined as a lack of knowledge about a given parameter value. Parameter variability, on the other hand, is heterogeneity in a population.

For this PA, probability distributions of *effective values* of parameters have been developed and used to represent the parameter values over the spatial and temporal scales defined in the PA mathematical model. Probability distributions used in this analysis represent both parameter uncertainty and variability.

Unbiased probability distributions are used to capture uncertainty in the effective values of parameters. *Unbiased*, as used here, is meant to indicate that the distribution chosen for a given parameter is an accurate representation of the current state of knowledge for that parameter. If there is little uncertainty in a parameter's value, the parameter will be described using a narrow range (or even a single value). If, there is significant uncertainty in a parameter's value, then the input parameter is described with a broad distribution which captures that uncertainty.

For example, the rate of upward specific discharge at a given location and at a given time is uncertain *and* variable in terms of space and time. The uncertainty in upward specific discharge at any location, and the variability from location to location and time to time, are captured in an effective parameter distribution that describes the range and probability of rates of upward specific discharge across the depth of burial for all four GCD boreholes over 10,000 years.

Iterative Framework

An iterative framework is a very important aspect of this PA methodology. The process advocates beginning the PA with simple, defensible models, in which model uncertainty and parameter uncertainty are managed as described above (and in Section 3.0). If compliance is demonstrated, the PA is complete; if not, sensitivity and data worth analysis are used to guide future activities (e.g., additional site characterization).

The first step in assessing the ability of the GCD boreholes was a preliminary PA (PPA). The PPA qualitatively estimated the likelihood that the site would meet the 40 CFR 191 requirements. The PPA was not a full PA, in that the future evolution of the disposal system (e.g., landfill subsidence) was not quantitatively assessed. The PPA [Price et al., 1993a,b,c] was completed *using only existing site data, and concluded that compliance was likely*. Given that the site was likely to comply, the second phase of the project consisted of site-specific studies on processes and parameters found to be important in the PPA. The second phase of studies were completed in 1994, and since then, the project has focused on developing the final PA models and corresponding set of input parameters to be used to assess compliance with 40 CFR 191. This report documents this final PA.

1.4.2 Geologic Processes and Future Human Activities

As described in Sections 5.0 and 6.0, the Area 5 RWMS is located in a very stable geologic setting. The climate has also been relatively stable, fluctuating cyclically between a cooler and wetter glacial climate and a warmer and drier interglacial climate. For millions of years, the Sierra Nevada and other mountain ranges have been blocking most of the moist Pacific air from the west, and the mountains surrounding the Frenchman Flat basin have been slowly eroding and gradually filling the basin with alluvium. For the next 10,000 years, it is expected that these processes will continue; the mountains surrounding Frenchman Flat will continue to erode and the Sierra Nevada Mountains will continue to block most of the moist air from the west. *Consequently, for geologic processes, this PA is based on the continuation of current conditions*. Note that current conditions include processes operating over tens of years (e.g., changing plant species) and processes operating over thousands of years (e.g., climate change).

Human history is much, much shorter than the geologic record. Human societies, with written languages and technological advances, have only existed for a few thousand years. Previous technologically-oriented societies have advanced, and then declined in this time period. Given this short record, projecting human activities for the next 10,000 years is more difficult. *For future human activities, this PA relies on the EPA's Appendix B Guidance on how to assess future human interactions with the GCD system.*

This approach for addressing geologic processes and future human activities is similar to the approach advocated by the National Academy of Sciences (NAS) [NAS, 1995a, pages 9–11].

1.4.3 Simplified Example of the Use of the Performance Assessment Methodology

GCD Boreholes 1, 2, and 3 contain NWAR wastes. These wastes are composed of "stable aluminum-plutonium-uranium or aluminum-uranium slag form" enclosed in a variety of original and overpack containers that are buried at least 21 m (70 ft) below the land surface. Over the next few hundred to few thousand years, these containers will decay. The decay is expected to be very slow, due to the aridity of the alluvium.

After the containers decay and collapse, the alluvium and its associated pore water will come in contact with the NWAR wastes. This collapse will also lead to localized subsidence above the GCD boreholes. Where pore waters do come in contact with metal slag, radionuclides will dissolve into the pore water. The timing and the associated geochemistry of these processes will be very complicated. In very simple terms, this is one conceptual model of what is expected to occur.

However, a much simpler model has been used in this PA. For this PA, it is assumed that the entire inventory of NWAR radionuclides is contained in "alluvium-like" material, which occupies the cylindrical waste zone (~ 3 m [10 ft] in diameter and 15 m [50 ft] thick) and the radionuclides instantly dissolve at their solubility limits into the pore water. The moisture content of the alluvium and the solubilities of various radionuclides are characterized by unbiased ranges of possible values that are based on field studies and other analyses.

Several important points can be made:

- The more complex conceptual model, and one that is thought to be a closer representation of reality, is not the model used for the quantitative PA analyses;

- The simple model used in this PA is conservative relative to the more complex model. That is, the use of a more complex model would result in lower releases (i.e., a shift of the final CCDF to the left and lower doses to the receptor);

- The uncertainty in the input parameters is captured by unbiased ranges of values (e.g., the ranges of solubilities for the radionuclides);

- This PA takes no credit for delay of releases due to waste form;

- This PA takes no credit for delay of releases due to the waste containers.

This same methodology is also used in defining how the PA addresses climate change and landfill subsidence. As discussed later, it is expected that the climate will eventually return to cooler and wetter glacial conditions, and that landfill and GCD borehole subsidence will focus precipitation and runoff. Both conditions are expected to move moisture (and radionuclides) away from the land surface and deeper into the vadose zone (with a decrease in releases to the accessible

environment) but not to the water table. However, the PA models a continuation of current conditions (with upward advection), coupled with deeper-rooted glacial climate plant species, which overestimates the releases, relative to expected conditions.

1.4.4 Summary

This PA simulates the future movement of radionuclides from deep in the GCD boreholes to the accessible environment or to a receptor in the accessible environment. Results of the PA are not directly verifiable. This PA utilizes a methodology that provides assurance that actual system performance will be better than that which is simulated.

1.5 Quality Assurance Program

Quality Assurance (QA) consists of those planning and implementation procedures that provide traceability, replication, and accountability of information. DOE Order 5700.6C establishes the current QA requirements for DOE activities. This DOE Order, in turn, requires adherence to applicable portions of the American Society of Mechanical Engineers, NQA-1.

The QA Program for the GCD PA consists of six elements: a QA Project Plan; a QA Management Plan (QAMP); Task Plans; a set of QA Procedures; Technical Plans and Procedures; and the Geographic Information System Quality Plan.

The QA Project Plan encompasses both the quality and technical requirements for the entire project. It establishes the basis for all subordinate QA activities. The QAMP documents the requirements and approach for implementation of the appropriate QA provisions. The QAMP defines those necessary and sufficient controls to provide adequate confidence that the customer requirements are being met. QA activities for an individual activity, such as Climate Change Studies are documented in annual Task Plans for that activity.

Finally, the QA Procedures provide the detailed requirements and guidelines for *how* to implement the QA provisions of the upper-tier QA Plans. QA Procedures have been developed for:

- Data Qualification;
- Software QA and Configuration Management;
- Project Reviews;
- Document Control;
- Records Management; and
- Surveillance.

GCD Data Acceptance Review sheets are used to verify the origin and justification for input parameters used in the GCD PA code. A full set of these Data Acceptance Review sheets are kept in the GCD Records Center at Sandia National Laboratories (SNL). The GCD Records Center also contains copies of references, interim reports, and information related to project administration.

Finally, Volume 3 presents all information necessary to reproduce the results of the PA, which includes a hard copy of the code, and input files. Software verification and validation are also discussed in Volume 3 of the CAD.

1.6 Disposal System Description

This section and Section 5.0 describes the current, "undisturbed" conditions at the Area 5 RWMS. Sections 1.7 and 6.0 describe how the Area 5 RWMS may evolve over time.

The NTS is located in southeastern Nevada, approximately 105 km (65 mi) northwest of Las Vegas, and is in the southern part of the Basin and Range geologic province. The Basin and Range geologic province is characterized by north-south trending mountains separated by alluvial filled basins. These north-south trending mountains can be seen in Figure 1-1. The Area 5 RWMS is located in and on the thick, arid alluvium of the Frenchman Flat basin. An idealized cross-section through the northern edge of Frenchman Flat basin is presented in Figure 1-4.

As summarized in Section 5.5.4, Frenchman Flat basin has been filling with alluvium for a long time. Drillholes UE-5i and UE-5k encountered alluvial fill from the land surface to about 290 m (950 ft) depth at the Area 5 RWMS. At 290 m (950 ft), a layer of basalt was encountered. The basalt has been dated as being between 8,400,000 and 8,700,000 years old. Therefore, this geologic environment (i.e., a basin filling with alluvium) has been stable for more than 8,000,000 years. The exact rate of basin filling is not known, but the average rate of filling is about 3 cm (1.3 in.) per 1000 years. This very slow average rate of basin filling is collaborated by the ages of the alluvial surfaces near the Area 5 RWMS. Some of the arroyos (alluvial channels) are currently active. However, many of the areas between the alluvial channels (the interfluve areas) have been unchanged for 5,000 to 10,000 years. To put this in perspective, all human civilizations have developed since these older interfluvial surfaces were deposited.

Based on measurements from a number of characterization wells, groundwater is approximately 236 m (774 ft) below the land surface. The average precipitation is 13 cm/yr (5 in./yr). Based on 30 years of record keeping, 23 cm (9 in.) of precipitation was received in the wettest year and 2.9 cm (1.1 in.) was received in the driest year. The limited precipitation, coupled with generally warm temperatures, plant uptake, and low humidities, results in a hydrologic system dominated by evapotranspiration. The movement of water within this 236 m (774 ft) thick unsaturated zone can be subdivided into two zones; the near surface zone and the deeper zone. A photograph of the arid alluvium is presented in Figure 1-10. *All the processes modeled in this PA occur in this arid alluvium.*

The near surface zone is the hydrologically "active" region of the unsaturated arid alluvium. In the near surface, precipitation is pulled downward by gravity and is either aided or resisted by the capillary tension of the soil (depending on the moisture content and textural properties of the soil). The forces acting to remove the moisture include evaporation and plant root uptake. The *average* volumetric moisture content in the near surface zone is very low, ranging from 1% to 3%. Based on a number of field studies, the balance of these forces is such that (approximately)

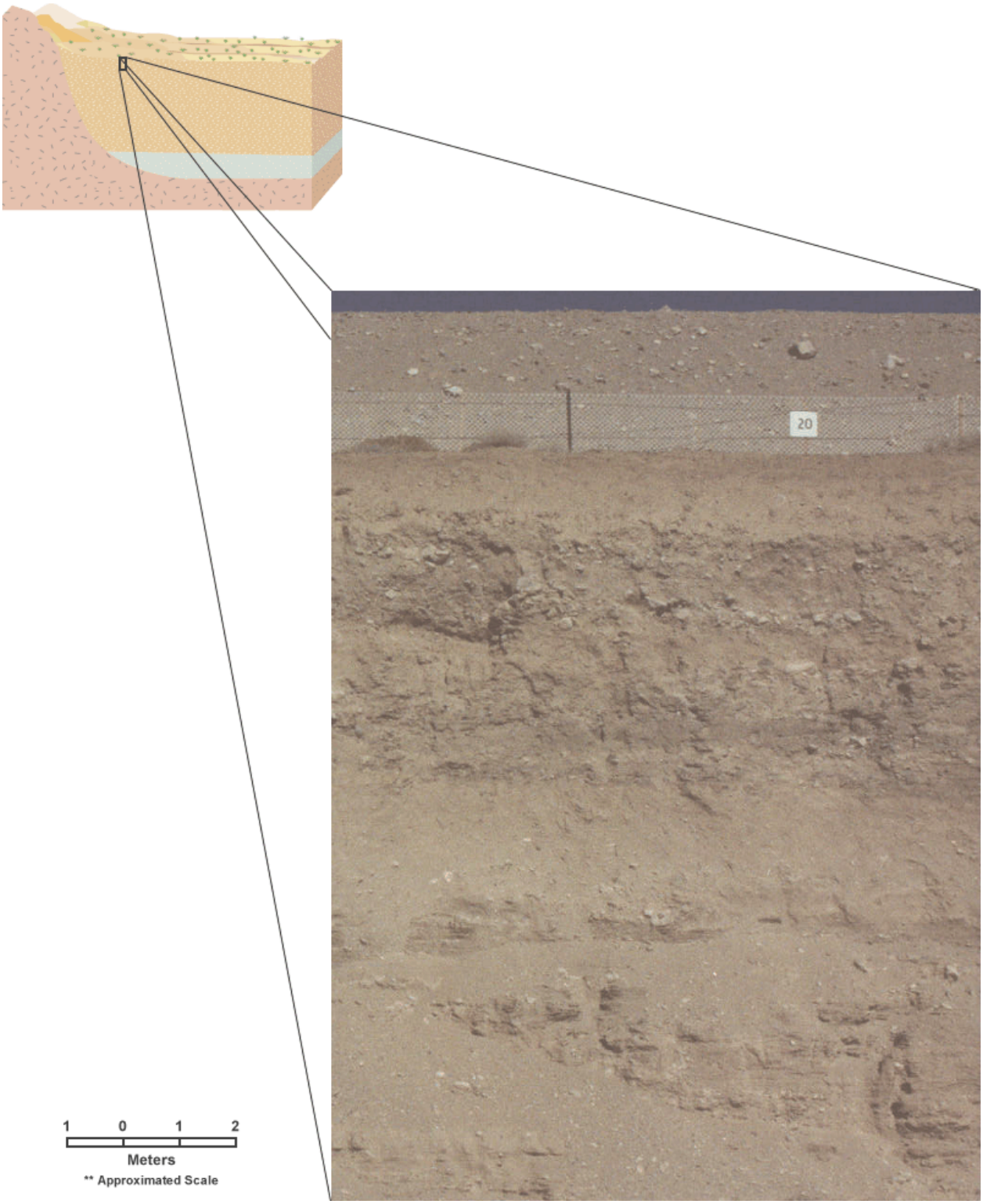

Figure 1-10. Photograph of Area 5 RWMS Alluvium. (Note: Fence is approximately 1 m (3 ft) high).

the upper 2 m (7 ft) is hydrologically active, and areally-distributed infiltration never infiltrates deeper than about 2 m (7 ft) in the interfluvial regions. The Area 5 RWMS is in an interfluvial region.

Under current climatic conditions, water-soluble constituents, such as chloride, are carried downward by infiltrating moisture, only to be deposited at about 2 m (7 ft) depth, as the infiltrating moisture is removed by evaporation and plant uptake. This process (a) moves water soluble constituents to the lower boundary of the near surface zone, and (b) provides a marker of the depth of infiltration. The bottom of this zone can be thought of as a "no-flux" liquid phase boundary based on the net effect of this transient cycling.

A number of plants have adapted to the arid climate of the desert southwest. These plants are able to rapidly capture infiltrating moisture and then hold that moisture through long dry periods. In addition to capturing soil moisture, plant roots also absorb minerals and heavy metals, carrying those minerals and metals to the plant's above-ground biomass. A plant uptake model which reflects rooting depths, biomass turnover, and the ability of plants to uptake radionuclides is described in Section 5.7.

In addition to plants, mammals and invertebrates burrow into the desert soils to seek refuge from temperature fluctuations; the dry, desiccating environment; and predators. Burrows can also function as routes taken in foraging activities and as storage areas for surplus food. All of these activities have the potential to transport contaminated soil from the subsurface to the surface. A model describing the effects of such bioturbation is presented in Section 5.8. Bioturbation and plant uptake occur primarily in the near surface vadose zone, although both processes can move limited amounts of radionuclides from the deeper vadose zone.

The plant uptake model and the bioturbation model are well developed, because these are the two processes that can move radionuclides across the no-flux liquid phase boundary to the accessible environment.

The deeper vadose zone is hydrologically inactive. The volumetric water content in the deeper zone is approximately 8%. This low-volumetric water content impedes the flow of liquid by significantly reducing the hydraulic conductivity. Between a depth of 2 and approximately 35 m (7 and approximately 115 ft), the alluvium shows decreasingly negative matric potential with depth (for example, (-) 10 bars at 35 m (115 ft) depth and (-) 75 bars at 5 m (15 ft) depth), indicating an *upward gradient in the pore water* (i.e., if the pore water moves, it moves upward and there is no groundwater recharge).

A static zone where the hydraulic gradient is negligible exists from approximately 35 to 90 m (115 to 300 ft), and from approximately 90 to 236 m (300 to 775 ft), very slow gravity drainage is still occurring. Detailed discussions of the deep vadose zone are presented in Shott et al. [1998].

The upward movement of pore water from 35 m (115 ft) deep has been studied extensively and is the result of a system in transition, where the transition times are on the order of thousands of years. As a simplification, the climate was significantly wetter and cooler 150,000 to 120,000

years ago (a super pluvial) and the water table received areally-distributed recharge. Subsequently, recharge decreased or ceased. Then, from 50,000 to 20,000 years ago, the climate was wetter and cooler (a pluvial). During this wetter and cooler time period, there was deep infiltration, but no areally-distributed recharge to the water table (see Figure 4 of Appendix A). Only under surface-water drainage features was there recharge to the water table 50,000 to 20,000 years ago. A more xeric environment now exists, and the drying of the land surface is pulling moisture from depth, resulting in the *very slow upward flux of pore water* evidenced by the soil matric potentials.

Deep Infiltration Without Recharge

The past occurrence of deep infiltration, without recharge, is identical to what may occur over the next 10,000 years as a result of landfill subsidence and the possible return to cooler and wetter conditions, which is discussed in Sections 1.7 and 6.6.

Because infiltrating moisture is recycled in the near surface, moisture movement in the deeper vadose zone is controlled by long-term climatic and geologic processes. The rates of moisture movement in the deep vadose zone are far too slow to be measured. Four studies, based on three techniques, were used to estimate the rate of upward specific discharge, as discussed in Section 5.6. Based on these studies, there is a 90% likelihood that the range will be from 0.01 to 0.4 mm/yr. At these low moisture contents (approximately 8%), the upward pore water velocities are about 10 times greater than the rate of upward specific discharge.

Over time, the waste containers in the GCD boreholes will decay and collapse and the radioactive wastes will come in contact with the pore water. Both time and water will be required to decay the waste containers; however, waste container disintegration is not modeled, and the wastes are assumed to dissolve into the pore water instantly. Because the GCD boreholes contain significant quantities of fissile materials (plutonium and highly enriched uranium), an analysis of the potential for a nuclear criticality to occur in the GCD boreholes is presented in Section 5.11.

Solubilities of the TRU-waste radionuclides in Area 5 RWMS pore water are developed in Section 5.10. Other factors influencing the movement of radionuclides include diffusion, dispersion, retardation, and radon gas transport. Each of these, and the general transport model, are discussed in Section 5.12.

1.7 Future Evolution of the Disposal System

The disposal system as it exists today was summarized above, and is detailed in Section 5.0. Over the next 10,000 years, the Area 5 RWMS will change. The changes will occur because:

- operation and closure of the Area 5 RWMS has “disturbed” the site conditions;
- future human activities could inadvertently alter site conditions; and
- natural processes that operate on long time scales may alter site conditions.

There is uncertainty in how much these driving forces will change the Area 5 RWMS over the next 10,000 years. Nonetheless, 40 CFR 191 requires the PA to identify, examine, and estimate

cumulative releases caused by "all significant processes and events" that could affect the disposal system for 10,000 years.

As a result of applying the scenario screening methodology (see Sections 6.3 and 6.6) to the GCD boreholes, four significant processes and events were identified: climate change, landfill subsidence, exploratory drilling accidently penetrates GCD TRU wastes, and irrigated agriculture accidently occurs on top of the Area 5 RWMS. Of these four, exploratory drilling and irrigated agriculture were assessed and screened out. Based on the EPA's 40 CFR 191 Appendix B Guidance, exploratory drilling was screened out because there is no (regulatory) consequence, and irrigated agriculture was screened out because it is not viable at the Area 5 RWMS. The two remaining events, climate change and landfill subsidence, are discussed below.

To assess the potential impact of climate change, this PA examined past global, regional, and site-specific empirical records of proxies of past climatic conditions. The records of the marine sediments and thick ice deposits provide global scale evidence of past climatic conditions. Studies of the isotopic composition of calcite deposits in Nevada's Devils Hole spring provide a 500,000 year record of past climate conditions in the southwestern U.S. Finally, studies of paleo vegetation from pack rat middens allow the reconstruction of the plant communities that existed during the last glacial climate at the NTS, which in turn allows a reconstruction of past climatic conditions at the NTS. The record is clear; open piñon-juniper woodlands existed at the elevations of the Area 5 RWMS.

All of the records showed a cyclic pattern of climate change in which the climate varies between relatively persistent glacial climates (cooler, wetter, pluvial periods) separated by interglacial climates (warmer, drier periods) of relatively short duration. At the Area 5 RWMS, cooler and wetter equates to 3^{o} to 5^{o} C cooler, with a doubling of average annual precipitation, from 13 to 26 cm/yr (5 to 10 in./yr). A conceptualization of the Area 5 RWMS under current and glacial conditions is presented in Figure 1-11.

The cyclic nature of past climatic conditions is solidly supported by a large number of studies of many different physical phenomena. However, the low resolution of some of the proxy records and the natural variability in the length of the climatic cycles does not allow an accurate estimation of the time when the climate will return to the more dominant, cooler, and wetter glacial conditions. It was concluded that (a) it is not possible to rule out a return to cooler and wetter conditions over the next 10,000 years, and (b) there is significant uncertainty in the timing of the return to those conditions. For this PA, it is assumed that the past climatic conditions can be used to estimate future conditions. Additional precipitation and cooler temperatures could cause the deep infiltration of surface moisture and the return of open piñon juniper woodlands, as discussed in Section 6.5 and 6.6.

The accumulation of anthropogenically-derived carbon dioxide (a greenhouse gas) may alter near term climatic conditions. The effects of anthropogenic climate change were assessed for the nearby Yucca Mountain facility using an expert elicitation based on available data and models and it was concluded that anthropogenic climate change will have a negligible impact at the NTS.

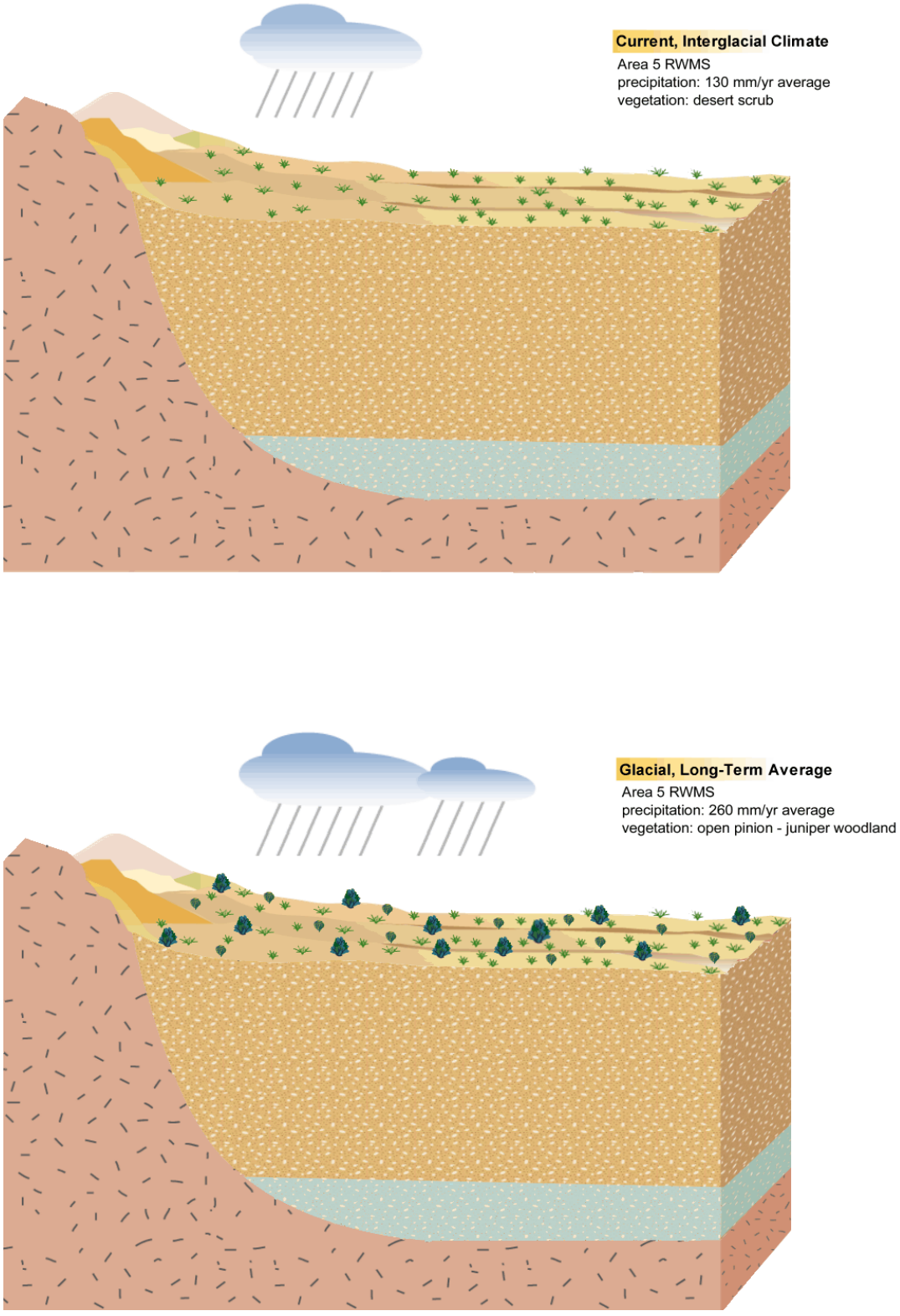

Figure 1-11. Visualization of the Area 5 RWMS Under Current Climatic Conditions and Under Glacial Climatic Conditions.

Wastes in the GCD boreholes and the RWMS pits and trenches contain a significant amount of void space, resulting from incomplete filling of waste containers, limited internal compaction of contents, and voids between containers. These voids will produce significant subsidence as the waste containers deteriorate and collapse.

To accommodate this subsidence, DOE/NV intends to construct an alternative cap consisting of a 2 m (7 ft) thick layer of compacted native alluvium. Based on forthcoming DOE guidance, DOE plans to operate the Area 5 RWMS until the year 2070. DOE would then assume AIC over the closed landfill. The EPA's standard does not allow the PA to take credit for more than 100 years of AIC (40 CFR 191.14). Therefore, this PA assumes loss of AIC in the year 2170.

A screening analysis was conducted to determine if the combined effects of landfill subsidence, precipitation, and a return to glacial climatic conditions might cause surface water to migrate to the aquifer during the next 10,000 years. Four coupled analyses were undertaken for the study: (1) modeling the geometry of future subsidence features; (2) using current climatic data to model precipitation, local runoff, and flooding; (3) using data for glacial climatic conditions to model precipitation, local runoff, and flooding; and (4) using the VS2DT code to model the two-dimensional movement of water in the subsurface.

Under current and undisturbed conditions in the vicinity of the GCD boreholes, the pore water in the upper 35 m (120 ft) of the arid alluvium is very slowly advecting upward. This very slow upward discharge, coupled with uptake by native plants, could move the GCD TRU waste radionuclides to the land surface, the shortest path to the accessible environment. The screening analysis was undertaken to determine if the operation and closure of the Area 5 RWMS could alter the natural conditions and induce movement of surface water through the GCD wastes and downward to the water table.

The screening analysis overestimated the potential for surface water to migrate to the aquifer by making a number of conservative assumptions, such as the assumption that all rare precipitation events were assumed to begin after the loss of institutional control. Under the current climate, 90 100-year storms, nine 1000-year storms, one 10,000-year storm, and one probable maximum precipitation storm were all assumed to occur at short intervals, beginning in year 2170. This screening analysis is summarized in Section 6.6.

The key result of the screening analysis was that there could be deep infiltration of surface moisture because of the capture and focusing of precipitation (current and glacial climates), but the moisture will not reach the water table in 10,000 years.

The movement of radionuclides was not modeled in the subsidence screening analysis; only the movement of water was modeled. Had the movement of radionuclides been modeled, the upward advection pathway (the shortest pathway to the accessible environment) would have been eliminated, and the radionuclides moving deeper into the vadose zone would not have reached the groundwater. Even if radionuclides had reached the groundwater, they would have to move 5 km (3 mi) laterally in the groundwater to reach the accessible environment. In essence, pushing radionuclides deeper into the vadose zone would reduce releases to the accessible environment.

Based on the PA methodology (Sections 1.4 and 3.0), the combined effects of subsidence, climate change, and flooding that result in downward movement of water are screened out of the PA, maintaining the more conservative upward pathway. To account for the concern that subsidence and/or subsidence plus climate change will cause the return of deeper-rooted piñon-juniper woodlands, all realizations of the PA model were made with the current upward movement of pore water, coupled with the downward, deeper-rooted piñon juniper woodland glacial plant community.

1.8 Exposure and Transport Models

Models of radionuclide release and transport were developed and used to assess compliance with the requirements of 40 CFR 191. These models are based on the geology, biology, climate, and undisturbed hydrology of the Area 5 RWMS, and include upward liquid-phase advection of radionuclides, along with diffusion and dispersion; diffusion of vapor-phase radionuclides; plant uptake; bioturbation; adsorption; precipitation; and radioactive decay and production. Modeling assumptions are discussed throughout Sections 5.0 and 6.0 and summarized in the summary tables in Sections 5.0 and 6.0.

The IPRs, presented in Sections 1.3.2.2 and 2.3.3, require estimation of doses to a MOP during the first 1000 years, assuming undisturbed performance of the disposal system. This involves (a) supplementing the transport model already implemented for the CRs, and (b) developing an exposure/dose model.

This PA uses a very simple (and very conservative) transport model and two exposure scenarios; a gardening scenario and a home construction and occupancy scenario. In the first scenario, all radionuclides released to the accessible environment for the first 1,000 years are "accumulated" and placed in a garden for the dose assessment model. The MOP receives a dose from ingesting contaminated food and soil, from inhaling contaminated soil particles, from external exposure to the contaminated garden, and from external exposure from immersion in a contaminated plume. In the second exposure scenario, all radionuclides released to the accessible environment for the first 1000 years are accumulated and placed over a GCD borehole. The MOP receives a dose from home construction and occupancy, including doses from radon. These models are discussed in detail in Section 7.6.

Models were developed to assess compliance with the CRs and IPRs of 40 CFR 191. The simplicity of these PA models allowed them to be implemented in Microsoft® Visual Basic™ macros in an Access™ database. The first set of macros calculates the movement and cumulative releases of 19 different radionuclides over a 10,000-year regulatory period, producing a CCDF that is used to assess compliance with the CRs of 40 CFR 191. The second set of macros calculates the movement and cumulative releases of 19 different radionuclides over a 1,000-year regulatory period and then approximates the dose to a MOP resulting from exposure to these 19 radionuclides and their progeny, producing an estimate of dose that is used to assess compliance with the IPRs. The same release and transport model is used in both sets of macros. *Figure 1-12 summarizes the conceptual and the mathematical models used to implement this PA.*

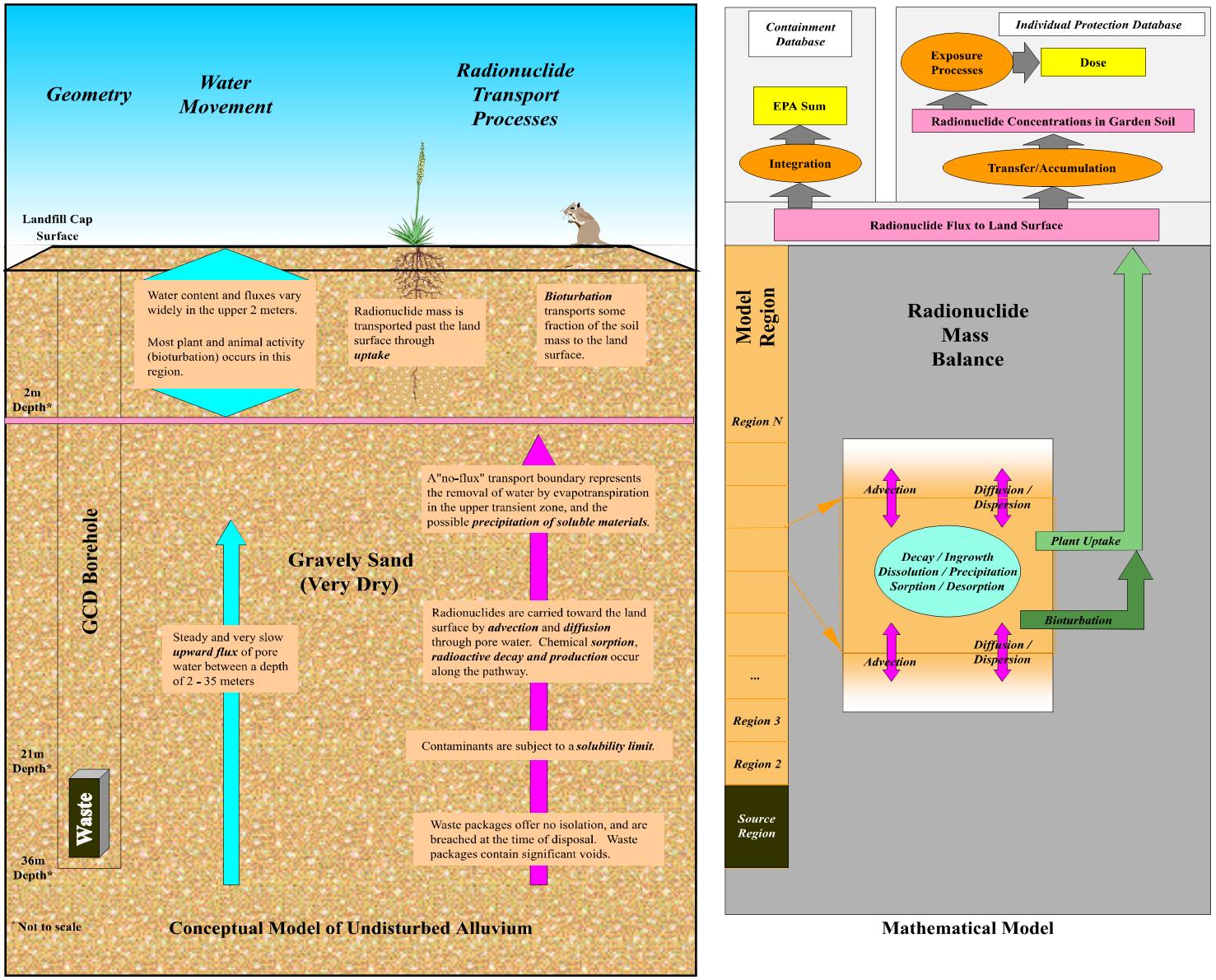

Figure 1-12. Conceptual Model and Mathematical Model of the Disposal System.

1.9 Consequence Analysis

Presented in Section 8.0 are the quantitative results of this PA. For the CRs, 5,000 realizations of the PA model were used to generate a CCDF of integrated normalized releases to the accessible environment. Based on the PA methodology and these analyses, there is a reasonable expectation that the cumulative releases of radionuclides to the accessible environment for 10,000 years will (a) have a likelihood of less than one chance in 10 of having an EPA Sum greater than one, and (b) have a likelihood of less than one in 1,000 of exceeding an EPA Sum of 10.

For the IPRs, the probability distribution for dose to a resident farmer was estimated using 1,000 samples of the uncertain parameters. All calculated dose values are far below the limits of 25 mrem for whole-body dose and 75 mrem for critical organ dose imposed by the IPRs.

1.10 Conclusions

The PA described in this document was performed to assess compliance with the quantitative requirements of 40 CFR 191. As such, the analyses have been tailored to these EPA standards, and provide a quantitative basis for deciding whether or not disposal of TRU waste in GCD boreholes is protective of human health and the environment.

The models used to analyze the release and transport of radionuclides are based on knowledge of the disposal system geology, biology, climate, geochemistry, and hydrology. Radionuclide releases and potential doses are estimated based on models of the system as it now exists and as it might exist in the future. The results of the PA indicate that disposal of TRU waste in GCD boreholes is protective of human health and the environment in that it meets the quantitative requirements of 40 CFR 191. Based on the PA methodology, there is a strong, reasonable assurance that actual performance will be better than that which is simulated in this PA.

This page intentionally left blank.

2.0 REGULATORY REQUIREMENTS AND PERFORMANCE MEASURES

2.1 Introduction

The AEA of 1954, as amended (Public Law 83-703), gives the DOE authority to develop and enforce standards for radioactive wastes from "atomic energy defense activities." In addition, the EPA has the authority to write standards that are applicable to radioactive waste from "atomic energy defense activities." However, the EPA only has authority to enforce those standards at DOE's WIPP and under the Comprehensive Environmental Response, Compensation, and Liability Act (CERCLA). Thus, the DOE is self-regulating; using regulations, directives, and orders that it has developed, as well as regulations that the EPA has promulgated. These regulations are presented and discussed in this section. The primary DOE regulations are presented first, followed by EPA regulations, concluding with a brief discussion of other regulatory requirements.

2.2 Department of Energy Orders

The first TRU wastes were disposed of in GCD Boreholes 1, 2, and 3 in March 1984 and the last TRU wastes were disposed of in GCD Borehole 4 in October 1987. Between those two dates, the most relevant DOE order to TRU waste disposal was DOE Order 5820.2, "Radioactive Waste Management." This order was in effect until September 26, 1988 when it was canceled and replaced by DOE Order 5820.2A, which had the same name. DOE Order 5820.2A was in effect until July 9, 1999 when it was canceled and replaced by DOE Order 435.1, which also has the same name. In addition, the DOE established Policy 450.3 on January 25, 1996, which authorized DOE Elements to select "necessary and sufficient" (N&S) Environment, Safety, and Health (ES&H) standards. The three relevant DOE Orders and the Policy are discussed in the following paragraphs.

DOE Order 5820.2. DOE Order 5820.2 required TRU waste that could not be certified for acceptance at the WIPP (i.e., waste that could not be confirmed to comply with WIPP waste acceptance criteria) to be evaluated for alternative means of disposal. For example, WIPP cannot accept classified TRU waste. The TRU waste disposed in the GCD boreholes is classified for national security reasons and therefore could not be certified for acceptance at the WIPP. Hence, an alternative disposal method (i.e, GCD boreholes) was required.

DOE Order 5820.2 also required operations involving TRU waste *to comply with applicable EPA standards*. The primary EPA regulation for disposal of TRU waste is 40 CFR 191, "Environmental Standards for the Management and Disposal of Spent Nuclear Fuel, High-Level and Transuranic Radioactive Wastes." Although available in 1982 as a draft for public comment [EPA, 1982, p. 58196], this regulation did not take effect until November 18, 1985 [EPA, 1985; p. 38066], after TRU waste was already disposed in Boreholes 1, 2, and 3 but before TRU waste was disposed of in Borehole 4. The applicability of 40 CFR 191 to the GCD boreholes containing TRU waste is discussed further in Section 2.3.

DOE Order 5820.2A. DOE Order 5820.2A took effect on September 26, 1988, after all the TRU waste had been disposed of in GCD boreholes. With respect to disposal of TRU waste in GCD boreholes, 5820.2A still required waste that could not go to WIPP to be disposed of using

alternative methods and still *required compliance with applicable EPA standards*. However, 5820.2A differed from 5820.2 in four ways: (1) the definition of TRU waste was slightly different, (2) 5820.2A did not specify the alternative disposal method for non-certifiable TRU wastes, *while 5820.2 specifically required GCD,* (3) 5820.2A explicitly required that alternative means of disposal be in compliance with the National Environmental Policy Act (NEPA) and State regulations, and (4) 5820.2A specified which offices at DOE Headquarters had the authority to approve of alternative means of disposal.

The first difference is not significant for the TRU wastes in the GCD boreholes. DOE Order 5820.2 defined TRU waste as "radioactive waste that at the end of institutional control periods is contaminated with alpha-emitting transuranium radionuclides with half-lives greater than 20 years and concentrations greater than 100 nCi/g." 5820.2A defined TRU waste as radioactive "waste that is contaminated with alpha-emitting transuranium radionuclides with half-lives greater than 20 years and concentrations greater than 100 nCi/g at the time of assay." Therefore, the difference between the two definitions is the time at which the physical characteristics (100 nCi/g of alpha-emitting transuranium radionuclides with half-lives greater than 20 years) are to be applied. For the wastes disposed of in the GCD boreholes, use of either definition yields identical designation of which waste packages are TRU waste and which packages are not TRU waste.

The second difference is not significant for the TRU wastes in the GCD boreholes because the disposal method is acceptable under either DOE order.

The third and fourth differences between 5820.2 and 5820.2A result in additional administrative requirements (e.g., an Environmental Assessment (EA) or an EIS under the NEPA and reports for DOE headquarters to obtain approval of alternative disposal methods). However, these are beyond the scope of this report and are not discussed further.

DOE Order and Manual 435.1. DOE Order 435.1, "Radioactive Waste Management," took effect on July 9, 1999. This order requires that radioactive waste be managed in accordance with the requirements of DOE Manual 435.1-1, "Radioactive Waste Management Manual," which also took effect on July 9, 1999, as well as other DOE Orders. Manual 435.1-1 differs slightly from DOE Orders 5820.2 and 5820.2A in that it does not specifically require waste that cannot be certified for disposal at WIPP to be disposed of by alternative methods, but it does state that "waste with no identified path to disposal shall be generated only in accordance with approved conditions which…shall address activities and plans for achieving final disposal of the waste" (DOE M 435.1-1, III.H.(2)). In contrast to DOE Orders 5820.2 and 5820.2A, the Manual explicitly states that disposal of TRU waste shall be in compliance with 40 CFR 191. Therefore, even though the wording is different, the result is the same.

> TRU wastes that cannot be disposed at WIPP shall be disposed by other methods, and these methods *shall comply with 40 CFR 191.*

DOE Policy 450.3. The subject of DOE Policy 450.3 is "Authorizing Use of the Necessary and Sufficient Process for Standards-Based Environment, Safety, and Health Management." It is implemented through Manual 450.3, "The Department of Energy Closure Process for Necessary

and Sufficient Sets of Standards." The N&S Process is one means of addressing the selection of ES&H standards. Use of the process is encouraged, but is not mandatory. This process provides a defensible, documented basis for defining the standards necessary to provide, among other things, adequate protection to the worker, the public, and the environment. If conducted properly, the N&S Process will produce a set of standards appropriately tailored to specific work and the hazards associated with that work. The set will include all applicable requirements in Federal, State, and local laws and regulations, as well as DOE directives, DOE Technical Standards, and nationally and internationally recognized industry consensus standards. The process provides a way to justify and pursue exemptions from laws and regulations that are judged not to add value to the achievement of adequate protection.

DOE/NV is currently implementing this process. DOE/NV has made the decision to continue to comply with DOE Order 5820.2A while DOE/NV evaluates 435.1. However, because both DOE Order 5820.2A and DOE Order 435.1 require compliance with applicable EPA standards, 40 CFR 191 still applies to the GCD boreholes containing TRU waste. 40 CFR 191 is discussed in the next section.

2.3 40 CFR 191

40 CFR Part 191 applies to the management and disposal of SNF, HLW, and TRU waste and is divided into Subparts A and B. Subpart A governs the management and storage of these three wastes, while Subpart B governs the disposal of such wastes by any method except directly into the oceans or ocean sediments. This PA addresses Subpart B requirements. Subpart B contains four requirements; three are quantitative and one is qualitative. These requirements are the CRs, GWPRs, IPRs, and Assurance Requirements. Following a discussion of which version of 40 CFR 191 is applicable to the GCD wastes, each requirement is discussed.

2.3.1 History of 40 CFR Part 191 and Applicability to Greater Confinement Disposal Wastes

As a result of legal challenges to the EPA and ensuing court rulings, two versions of 40 CFR Part 191 have been promulgated. The following paragraphs briefly discuss the history of 40 CFR Part 191 and answers the question of which version of the regulation is applicable to disposal of TRU waste in the GCD boreholes at the NTS.

Under authority derived from the AEA of 1954, as amended (42 U.S.C. 2011-2296), and Reorganization Plan No. 3 of 1970 (5 U.S.C. [app. at 1343]), EPA is responsible for developing standards for protection of the general environment from radioactive material. This includes standards for disposal of radioactive waste. After several years of research and regulatory development, on September 19, 1985, the EPA issued 40 CFR 191, final "Environmental Standards for the Management and Disposal of Spent Nuclear Fuel, High-Level, and Transuranic Radioactive Wastes" [EPA, 1985; p. 38066].

In March 1986, several States and environmental groups filed petitions for review of the law. On July 17, 1987 the First Circuit issued its ruling. The court found the IPR and GWPR to be "arbitrary and capricious" and therefore vacated and remanded the entire rule. At the request of

the government, upon rehearing, the court reinstated the management and storage standards (Subpart A of 40 CFR Part 191) but left the disposal standards (Subpart B) in remand.

On October 30, 1992, the WIPP Land Withdrawal Act (LWA) was enacted. This law reinstated all disposal standards originally issued in 1985 that had been remanded by the court in 1987 except for the GWPR and IPR. Finally, on December 20, 1993 [EPA, 1993; p. 66398], the EPA promulgated a new IPR and a new Subpart C that is intended to replace the original GWPR for disposal systems greater than one-quarter mile from an underground source of drinking water. These new requirements are different from the 1985 requirements. The three primary differences are that (1) the regulatory timescale for the new IPR and new Subpart C is 10,000 years, compared to 1,000 years for the 1985 IPR and GWPR; (2) the point of compliance for the new Subpart C is any underground source of drinking water outside the controlled area, as opposed to any special source of groundwater for the 1985 GWPR; and (3) the new Subpart C protects underground sources of drinking water in the accessible environment, while the 1985 GWPR protects special sources of groundwater.

It would seem, then, that the 1993 version of 40 CFR Part 191 applies to the GCD boreholes. However, in promulgating the new revised versions of the IPR and GWPR in 1993, the EPA made it clear that disposal of waste that occurred on or after November 18, 1985 (the effective date of the rule issued September 19, 1985) until January 19, 1994 is subject to the standards as they existed on November 18, 1985 [EPA, 1993; p. 66400, p. 66412].

The TRU waste in the GCD boreholes was disposed of between March 1984 and October 1987 [Chu and Bernard, 1991], making some of the waste not subject to 40 CFR 191 at all and some subject to the 1985 standards. However, DOE/NV has decided that all TRU waste in the GCD boreholes should be included in the 40 CFR 191 PA.

DOE/NV has decided that all of the TRU waste disposed in the GCD boreholes at the NTS is subject to the 1985 version of 40 CFR Part 191, and any definitions (and their references) given in this report are from this 1985 version.

Although the GCD boreholes are not subject to the 1993 version of 40 CFR 191, DOE/HQ, DOE/NV, and SNL have discussed demonstrating compliance with the 1993 version for informational purposes only. Additional analyses would have to be performed, and these analyses would be documented in a separate report.

2.3.2 Containment Requirements (40 CFR Part 191.13)

The CRs are the most complicated of the three quantitative requirements. The CRs (40 CFR Part 191.13) state that *(emphasis added)*:

> (a) Disposal systems for spent nuclear fuel or high-level or transuranic radioactive wastes shall be designed to provide a reasonable expectation, based upon *performance assessments*, that the cumulative releases of radionuclides to the *accessible environment* for 10,000 years after disposal from all significant processes and events that may affect the disposal system shall:

> (1) Have a likelihood of less than one chance in 10 of exceeding the quantities calculated according to Table 1 (Appendix A); and
> (2) Have a likelihood of less than one chance in 1,000 of exceeding ten times the quantities calculated according to Table 1 (Appendix A).

The italicized phrases in the requirements are defined by the EPA in 40 CFR Part 191 as follows.

> "Performance assessment"[2] means an analysis that (1) identifies the processes and events that might affect the disposal system; (2) examines the effects of these processes and events on the performance of the disposal system; and (3) estimates the cumulative releases of radionuclides, considering the associated uncertainties, caused by all significant processes and events. These estimates shall be incorporated into an overall probability distribution of cumulative release to the extent practicable. (40 CFR Part 191.12(q))

> "Accessible environment" means: (1) The atmosphere; (2) land surfaces; (3) surface waters; (4) oceans; and (5) all of the lithosphere that is beyond the controlled area. (40 CFR Part 191.12 (k)) "Controlled area" means (1) A surface location, to be identified by passive institutional controls, that encompasses no more than 100 square kilometers and extends horizontally no more than five kilometers in any direction from the outer boundary of the original location of the radioactive wastes in a disposal system; and (2) the subsurface underlying such a surface location. (40 CFR Part 191.12(g))

The controlled area may be established asymmetrically around a repository based upon the particular characteristics of a site. For the PA, the controlled area consists of a cylinder with a radius of 5 km (3.1 mi), but with a small piece of the eastern portion of that cylinder removed where it intersects with Nellis Air Force land. See Brosseau [Version 1.0, 2000] for a figure showing the location of the controlled area. The GCD boreholes are assumed to be at the center of this altered cylinder. Thus, the accessible environment consists of the ground surface and any point in the subsurface that is beyond the controlled area.

Note that the CRs call for a "reasonable expectation" that their various quantitative tests be met. As stated by the EPA:

> This phrase reflects the fact that unequivocal numerical proof of compliance is neither necessary nor likely to be obtained. [EPA, 1985; p. 38071]

Therefore, the EPA recognizes "the unique considerations likely to be encountered upon implementation of these disposal standards" [EPA, 1985; p. 38071]. Furthermore, the EPA did not use the phrase "reasonable assurance," a phrase used by the Nuclear Regulatory Commission (NRC), because that phrase has come to denote a level of confidence that the EPA believes is not

[2]The term "performance assessment" is often used to describe any set of analyses conducted for the purpose of assessing compliance with a set radioactive waste disposal requirement or performance goal.

"appropriate for the very long-term analytical projections that are called for by" the CRs. [EPA, 1985; p. 38071]

The estimated cumulative release of radionuclides is compared to the release limits calculated according to Table 1 in Appendix A of 40 CFR Part 191. This table is reproduced here as Table 2-1. The release limit is per 1,000 metric tons of heavy metal (MTHM) or other unit of waste. Because the GCD boreholes do not contain SNF, the release limits were calculated based on the "other unit of waste." The units of waste that apply to the GCD boreholes containing TRU waste are:

(a) Each 1,000,000 curies of other radionuclides (i.e., gamma or beta-emitters with half-lives greater than 100 years or any alpha emitters with half-lives greater than 20 years); or
(b) An amount of TRU wastes containing one million curies of alpha-emitting transuranic radionuclides with half-lives greater than 20 years.

Table 2-1. Release Limits for Containment Requirements

Radionuclide	Release limit per 1,000 MTHM or other unit of waste (curies)
Americium-241 or -243	100
Carbon-14	100
Cesium-135 or -137	1,000
Iodine-129	100
Neptunium-237	100
Plutonium-238, -239, -240, or -242	100
Radium-226	100
Strontium-90	1,000
Technetium-99	10,000
Thorium-230 or -232.	10
Tin-126	1,000
Uranium-233, -234, -235, -236, or -238.	100
Any other alpha-emitting radionuclide with a half-life greater than 20 years	100
Any other radionuclide with a half-life greater than 20 years that does not emit alpha particles	1,000

Therefore, the release limit for a given radionuclide depends on the amount of waste in the disposal system. For example, if a disposal system contained 5,000,000 curies of gamma-emitting radionuclides with half-lives greater than 100 years, the release limits for the disposal system would be the quantities in Table 2-1 (Table 1 of Appendix A of 40 CFR Part 191) multiplied by 5 (5,000,000 ÷ 1,000,000). If a disposal system contained 5,000,000 curies of gamma-emitting radionuclides with half-lives greater than 100 years *and* 10,000,000 curies of alpha-emitting TRU radionuclides with half-lives greater than 20 years, the release limits for the

disposal system would be the quantities in Table 2-1 multiplied by 15 ((5,000,000 ÷ 1,000,000) + (10,000,000 ÷ 1,000,000)). On the other hand, if a disposal system contained only 1,000 curies of alpha-emitting TRU radionuclides with half-lives greater than 20 years, the release limits for that system would be the quantities in Table 2-1 multiplied by $1 \times 10^{!3}$ (1,000 ÷ 1,000,000). *The release limits are dependent on the initial inventory of waste in the disposal system; systems that contain a large inventory of waste are allowed to release more than systems with smaller inventories.*

The rationale for inventory-dependent release limits is as follows. The risks allowed by the disposal standards are comparable to the risks that future populations would have been exposed to had the uranium ore used to produce the HLW never been mined [EPA, 1985]. "Specifically, the [EPA] estimates that compliance with the disposal standards would allow no more than 1,000 premature deaths from cancer in the first 10,000 years after disposal of the HLW from 100,000 metric tons of reactor fuel, an average of no more than one premature death every ten years" [EPA, 1985]. Thus, the health effects allowed by the disposal standards are proportional to the amount of waste disposed of, resulting in inventory-dependent release limits.

To determine compliance with the CRs, the projected release of each radionuclide is scaled by its corresponding release limit and these ratios are summed,

$$\sum_{i=1}^{n} \frac{Q_i}{L_i} = \text{ EPA Sum} = R \qquad (2\text{-}1)$$

where

Q_i = the estimated total release of radionuclide *i* over 10,000 years (Ci),
L_i = release limit for radionuclide *i*, adjusted for the inventory (Ci),
n = the number of radionuclides, and
R = EPA Sum.

It is the EPA Sum, as calculated by Equation (2-1), that must have a likelihood of less than one chance in ten of exceeding one and a likelihood of less than one chance in 1000 of exceeding ten. The likelihood, or probability, of the actual release exceeding a given value of R is given by equation (2-2),

$$P\left(Rel > R\right) = \sum_{i=1}^{m} P\left(Rel > R \middle| S_i\right) P\left(S_i\right) \qquad (2\text{-}2)$$

where

$P(Rel>R)$ = probability that the release is greater than R,
$P(Rel>R*S_i)$ = conditional probability that the release is greater than R for the i^{th} scenario,
$P(S_i)$ = probability that the i^{th} scenario occurs in 10,000 years, and
m = the number of scenarios.

This equation combines the results of multiple scenarios and assumes that the scenarios are mutually exclusive and exhaustive. Considering "all sources of uncertainty" as required by the regulation leads to each scenario having a distribution of releases because of parameter uncertainty. Each of these releases has a probability of exceeding R based on the calculated

release, the probability of the scenario, and the probability associated with a given set of model parameters.

The result of the calculation is presented as a CCDF, a curve that is plotted with $P(Rel>R)$ on the vertical axis and $R(EPA\ Sum)$ on the horizontal axis. Figure 2-1 gives two examples of CCDF curves. In this figure, the region labeled "EPA CR Violation" represents the "violation zone." The curve that does not pass through this region does not violate the CRs, while the curve that passes through the region violates the CRs.

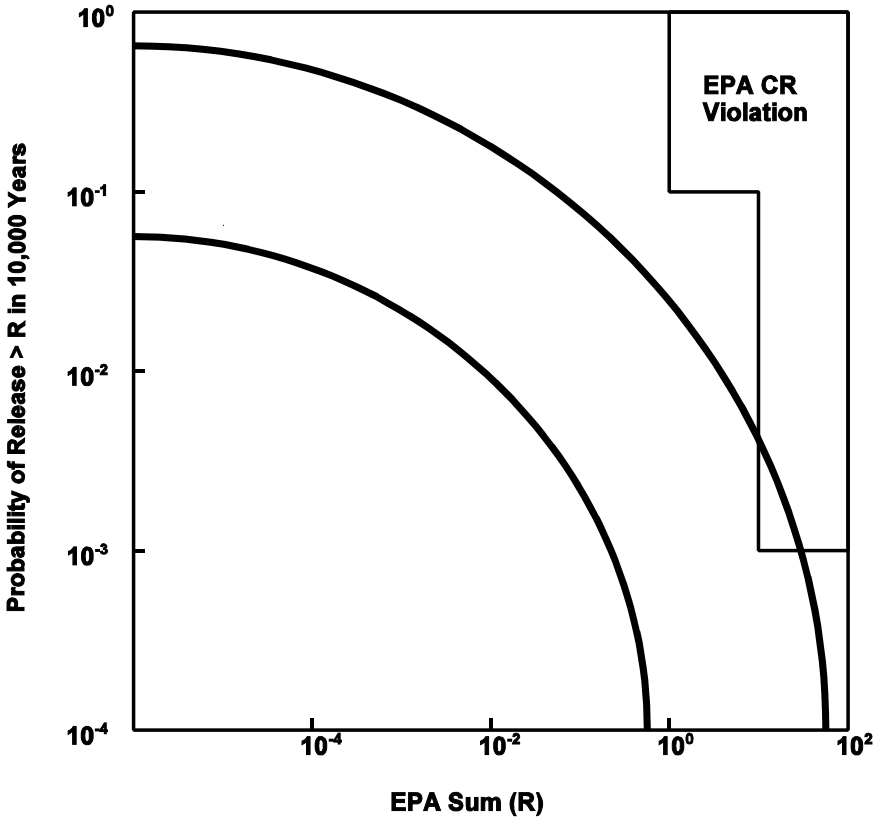

Figure 2-1. Examples of CCDF Curves in Relation to the EPA's CR.

2.3.3 Assurance Requirements (40 CFR Part 191.14)

The assurance requirements (40 CFR Part 191.14) state that *(emphasis added)*:

> To provide the confidence needed for long-term compliance with the requirements of 191.13, disposal of spent nuclear fuel or high-level or transuranic wastes shall be conducted in accordance with the following provisions, except that these provisions do not apply to facilities regulated by the Commission (see 10 CFR Part 60 for comparable provisions applicable to facilities regulated by the Commission):
>
> (a) *Active institutional controls* over disposal sites should be maintained for as long a period of time as is practicable after disposal; however, performance

assessments that assess isolation of the wastes from the accessible environment shall not consider any contributions from active institutional controls for more than 100 years after disposal.

(b) Disposal systems shall be monitored after disposal to detect substantial and detrimental deviations from expected performance. This monitoring shall be done with techniques that do not jeopardize the isolation of the wastes and shall be conducted until there are no significant concerns to be addressed by further monitoring.

(c) Disposal sites shall be designated by the most permanent markers, records, and other *passive institutional controls* practicable to indicate the dangers of the wastes and their location.

(d) Disposal systems shall use different types of barriers to isolate the wastes from the accessible environment. Both engineered and natural barriers shall be included.

(e) Places where there has been mining for resources, or where there is a reasonable expectation of exploration for scarce or easily accessible resources, or where there is a significant concentration of any material that is not widely available from other sources should be avoided in selecting disposal sites. Resources to be considered shall include minerals, petroleum or natural gas, valuable geologic formations, and ground waters that are irreplaceable because there is no reasonable alternative source of drinking water available for substantial populations or that are vital to the preservation of unique and sensitive eco-systems. Such places shall not be used for disposal of the wastes covered by this part unless the favorable characteristics of such places compensate for their greater likelihood of being disturbed in the future.

(f) Disposal systems shall be selected so that removal of most of the wastes is not precluded for a reasonable period of time after disposal.

The italicized phrases in the requirement are defined by the EPA in 40 CFR 191 as follows:

> "Active institutional control" means (1) controlling access to a disposal site by any means other than passive institutional controls, (2) performing maintenance operations or remedial actions at a site, (3) controlling or cleaning up releases from a site, or (4) monitoring parameters related to disposal system performance (40 CFR Part 191. 12(f)).

> "Passive institutional control" means (1) permanent markers placed at a disposal site, (2) public records and archives, (3) government ownership and regulations regarding land or resource use, and (4) other methods of preserving knowledge about the location, design, and contents of a disposal system (40 CFR Part 191.12(e)).

These requirements are qualitative, not quantitative, and compliance with them for the TRU waste in the GCD boreholes is discussed separately in Volume 4 [Brosseau, Version 1.0, 2000].

2.3.4 Individual Protection Requirements (40 CFR Part 191.15)

The IPRs (40 CFR Part 191.15) state that (*emphasis added*):

> Disposal systems for spent nuclear fuel or high-level or transuranic radioactive wastes shall be designed to provide a reasonable expectation that, for 1,000 years after disposal, *undisturbed performance* of the disposal system shall not cause the annual dose equivalent from the disposal system to any *member of the public* in the accessible environment to exceed 25 millirems to the whole body or 75 millirems to any *critical organ*. All potential pathways (associated with *undisturbed performance*) from the disposal system to people shall be considered, including the assumption that individuals consume 2 liters per day of drinking water from any *significant source of ground water outside of the controlled area*.

The italicized phrases in the requirement are defined by the EPA in 40 CFR Part 191 as follows. **(emphasis added)**:

> "Undisturbed performance" means the predicted behavior of a disposal system, including consideration of the uncertainties in predicted behavior, if the disposal system **is not disrupted by human intrusion or the occurrence of unlikely natural events**. (40 CFR Part 191.12(p))
>
> "Member of the public" means any individual except during the time when that individual is a worker engaged in any activity, operation, or process that is covered by the AEA of 1954, as amended. (40 CFR Part 191.02(p))
>
> "Critical organ" means the most exposed human organ or tissue exclusive of the integumentary system (skin) and the cornea. (40 CFR Part 191.02(q))
>
> "Significant source of ground water," as used in the Part, means: (1) an aquifer that: (a) Is saturated with water having less than 10,000 milligrams per liter of total dissolved solids; (b) is within 1,500 feet of the land surface; (c) has a transmissivity greater than 200 gallons per day per foot, provided that any formation or part of a formation included within the source of ground water has a hydraulic conductivity greater than 2 gallons per day per square foot; and (d) is capable of continuously yielding at least 10,000 gallons per day to a pumped or flowing well for a period of at least a year; or (2) an aquifer that provides the primary source of water for a community water system as of the effective date of this Subpart. (40 CFR Part 191.12(n))

Unlike the CRs, the IPRs apply only for "undisturbed performance" of the disposal system. For the PA, this means that the potential for complying with the IPRs needs to be assessed for the base case scenario only (discussed later), which includes only present-day conditions except for any changes that are almost certain to occur. In addition, the regulatory period for the IPRs is 1,000 years, not the 10,000-year period mandated by the CRs. This is discussed in more detail below.

Note that the requirements apply only to any "member of the public," which the EPA defines in 40 CFR Part 191.02(p) as any individual except during the time when that individual is a worker engaged in any activity, operation, or process that is covered by the AEA of 1954, as amended. Thus, anyone currently working at the NTS is not a "member of the public."

The performance measures for the IPRs are deterministic (e.g., 25 mrem, 75 mrem), not probabilistic. However, because many of the parameters that describe the performance of a disposal system are uncertain, the results of assessing the potential for complying with the IPRs may be probabilistic (i.e., have a probability associated with a given dose, similar to the EPA Sum of the CRs). The EPA recognizes this and, in Appendix B of 40 CFR Part 191, "assumes that compliance can be determined based upon 'best estimate' predictions (e.g., the mean or the median of the appropriate distribution, whichever is higher)."

The draft of 40 CFR Part 191 [EPA, 1982] differed from the final 1985 version in that it contained only two of the four disposal requirements that are in the 1985 version: CRs and Assurance Requirements. That is, it did not contain IPRs or GWPRs. The IPRs came about because of concerns expressed by some commenters during the rulemaking process that, even though overall population risks to future generations might be acceptably small, the risk to an individual was not regulated. The major concern was that an individual using contaminated groundwater in the future could receive a significant radiation exposure because groundwater generally provides relatively little dilution of contaminants. Hence, the EPA decided to supplement the CRs with the IPRs (which limit the dose to an individual) and GWPRs (which limit radionuclide concentrations in groundwater and resultant doses). Both of these "supplemental" requirements were written to evaluate the performance of the disposal system when functioning as designed.

The IPR analysis estimates the dose to an individual assuming "undisturbed performance," which the EPA has specifically defined to exclude "human intrusion" and "unlikely natural events."

The EPA does not define "human intrusion," but from the EPA's discussion of the issue in the preamble to the 1985 promulgation of 40 CFR Part 191 [EPA, 1985; p. 38066] and Appendix B of 40 CFR Part 191, it is clear that "human intrusion" does *not* include anthropogenic surface-disturbing activities. Instead, "human intrusion" refers to activities such as drilling or deep excavations that actually intrude into the waste or very close to the waste.

"Unlikely natural events" are low probability events that might alter the behavior of the disposal system. Processes and events such as faulting, volcanic intrusion, and meteorite impact are examples of unlikely natural events and these events are examined in more detail in Section 6.0.

2.3.5 Ground Water Protection Requirements (40 CFR Part 191.16)

The GWPRs (40 CFR Part 191.16) state that *(emphasis added)*:

> (a) Disposal systems for spent nuclear fuel or high-level or transuranic radioactive wastes shall be designed to provide a reasonable expectation that, for 1,000 years after disposal,

undisturbed performance of the disposal system shall not cause the radionuclide concentrations averaged over any year in water withdrawn from any portion of a *special source of ground water* to exceed:

(1) 5 picocuries per liter of radium-226 and radium-228;

(2) 15 picocuries per liter of alpha-emitting radionuclides (including radium-226 and radium-228 but excluding radon); or

(3) The combined concentrations of radionuclides that emit either beta or gamma radiation that would produce an annual dose equivalent to the total body or any internal organ greater than 4 millirems per year if an individual consumed 2 liters per day of drinking water from such a source of ground water.

(b) If any of the average annual radionuclide concentrations existing in a special source of ground water before construction of the disposal system already exceed the limits in 191.16(a), the disposal system shall be designed to provide a reasonable expectation that, for 1,000 years after disposal, undisturbed performance of the disposal system shall not increase the existing average annual radionuclide concentrations in water withdrawn from that special source of ground water by more than the limits established in 191.16(a).

The italicized phrase in the requirements is defined by the EPA in 40 CFR Part 191 as follows.

> "Special source of ground water" as used in this Part, means those Class I ground waters identified in accordance with the Agency's Groundwater Protection Strategy published in August 1984 that: (1) Are within the controlled area encompassing a disposal system or are less than five kilometers beyond the controlled area; (2) are supplying drinking water for thousands of persons as of the date that the Department chooses a location within that area for detailed characterization as a potential site for a disposal system (e.g., in accordance with Section 112(b)(1)(B) of the NWPA); and (3) are irreplaceable in that no reasonable alternative source of drinking water is available to that population. (40 CFR Part 191.12(o))

Section 5.6.3 provides the basis for concluding that the aquifer underlying the GCD boreholes is not a "special source of groundwater."

The requirements further state that if natural radionuclide concentrations exceed the limits given above, then the disposal system shall not increase concentrations in the groundwater by more than the given amounts. The limits in (1) and (2) apply to the combined concentration of radionuclides, not to individual radionuclides.

As with the IPRs, the GWPRs have a regulatory period of 1000 years, apply only to the "undisturbed performance" of the disposal system, and are deterministic.

The aquifer underlying the GCD boreholes does not meet the definition of a "special source of groundwater." Therefore, it is not necessary to perform analyses to demonstrate compliance with the GWPRs, and none are performed in this PA.

2.3.6 Environmental Protection Agency's Appendix B Guidance

Because there were no precedents for the implementation of long-term environmental standards such as those found in 40 CFR 191, the EPA provided "guidance for implementation" in Appendix B of 40 CFR 191. This guidance

> "describes certain analytical approaches and assumptions through which the Agency intends the various long-term numerical standards of Subpart B to be applied." [EPA, 1985; p. 38069]

The guidance covers several topics: limitations on the scope of PA, how results of the PA are expected to be presented, assumptions regarding institutional controls, and limiting assumptions regarding the frequency and severity of human intrusion. The EPA's guidance on these topics is examined below.

2.3.6.1 Scope of Performance Assessments

The EPA requires PAs in order to evaluate compliance with the CRs, but the EPA believes that events and processes estimated to have less than one chance in 10,000 of occurring over 10,000 years need not be included in the PA. Thus, releases from "events that are judged to have an incredibly small likelihood of occurrence" [EPA, 1985; p. 38068] need not be included in the estimate of total projected releases over 10,000 years. Furthermore, events and processes estimated to have a likelihood of occurrence greater than one chance in 10,000 over 10,000 years may be "omitted from the PA if there is a reasonable expectation that the remaining probability distribution of cumulative releases would not be significantly changed by such omissions" [EPA, 1985; p. 38088]. Thus, when estimating total projected releases over 10,000 years, the EPA suggests two criteria for eliminating (or screening out) processes and events from further consideration: probability and consequence. The application of this guidance to the PA process is discussed in greater detail in Sections 3.3 and 6.3.

2.3.6.2 Compliance with Individual Protection Requirements and Ground Water Protection Requirements

The IPRs and GWPRs (presented in Sections 2.3.4 and 2.3.5, respectively) are deterministic, but considering uncertainties in the performance of the disposal system may result in a range of estimated radiation exposures or radionuclide concentrations. In such cases, the EPA "assumes that compliance can be determined based upon 'best estimate' predictions (e.g., the mean or the median of the appropriate distribution, whichever is higher)" [EPA, 1985; p. 38088]. Thus, the results of a PA for the IPRs and GWPRs may be presented as a histogram, a cumulative distribution function (CDF), a CCDF, or in tabular form.

2.3.6.3 Compliance with Containment Requirements

The CRs are probabilistic, limiting the likelihood of cumulative releases exceeding certain values. The EPA assumes that "whenever practicable, the implementing agency will assemble all of the results of the PAs to determine compliance with § 191.13 into a CCDF that indicates

the probability of exceeding various levels of cumulative release. When uncertainties in parameters are considered in a PA, the effects of the uncertainties considered can be incorporated into a single such distribution function for each disposal system considered. The Agency assumes that a disposal system can be considered to be in compliance with § 191.13 if this single distribution function meets the requirements of § 191.13(a)" [EPA, 1985; p. 38088]. Thus, the EPA expects the results of a PA to be expressed as a CCDF.

2.3.6.4 Institutional Controls

The Assurance Requirements (presented in Section 2.3.3 and in Volume 4 of the CAD [Brosseau, Version 1.0, 2000]) require the use of AICs and passive institutional controls (PICs) in order to provide the confidence needed for long-term compliance with the CRs. Although these controls are required, the EPA limits the "credit" that can be taken in the PA as a result of the presence of these controls. For example, "none of the AICs prevent or reduce radionuclide releases for more than 100 years after disposal" even though the "Federal Government is committed to retaining ownership of all disposal sites for spent nuclear fuel and high-level and transuranic radioactive wastes" [EPA, 1985; p. 38088]. The Federal Government is also committed to establishing appropriate markers and records that, as long as they endure and are understood, can be assumed to (1) be "effective in deterring systematic or persistent exploitation of these disposal sites"; and (2) "reduce the likelihood of inadvertent, intermittent human intrusion" [EPA, 1985; p. 38088]. But these PICs "can never be assumed to eliminate the chance of inadvertent and intermittent human intrusion" [EPA, 1985; p. 38088]. The application of this guidance to the PA of the GCD boreholes is discussed in more detail in Section 6.7.

2.3.6.5 Inadvertent Human Intrusion

The CRs associate quantitative probabilities with two different levels of cumulative releases, noting that probabilities are to be assigned to the processes and events that cause these releases. The EPA recognized that inadvertent human intrusion required special attention because "it will not be possible to develop a 'correct' estimate of the probability of such intrusion" [EPA, 1985; p. 38077]. Thus, in Appendix B of 40 CFR 191, the EPA provides guidance regarding limits on the likelihood and consequences of human intrusion that must be considered in a PA.

In estimating the frequency of inadvertent intrusion into a repository, the EPA assumes that:

> the likelihood of such inadvertent and intermittent drilling need not be taken to be greater than 30 boreholes per square kilometer of repository area per 10,000 years for geologic repositories in proximity to sedimentary rock formations, or more than 3 boreholes per square kilometer per 10,000 years for repositories in other geologic formations [EPA, 1985; p. 38089].

Furthermore, EPA:

> assumes that the consequences of such inadvertent drilling need not be assumed to be more severe than: (1) Direct release to the land surface of all the ground water in the repository horizon that would promptly flow through the newly created

> borehole to the surface due to natural lithostatic pressure - or (if pumping would be required to raise water to the surface) release of 200 m^3 (65 ft^3) of ground water pumped to the surface if that much water is readily available to be pumped; and (2) creation of a ground water flow path with a permeability typical of a borehole filled by the soil or gravel that would normally settle into an open hole over time - not the permeability of a carefully sealed borehole [EPA, 1985; p. 38089].

The application of this guidance to the PA of the GCD boreholes is discussed in more detail in Section 6.7.

The EPA's Guidance requires the PA to determine if the favorable characteristics of the entire disposal system will be invalidated by an inadvertent "puncturing" by well drilling. Such an inadvertent puncturing of a GCD borehole does not alter the characteristics of the remainder of the GCD system.

Drilling an exploratory borehole or a water well through a GCD borehole is the only inadvertent human activity that could disturb the GCD wastes (see Section 6.7), and the probabilities and consequences of such a drilling event are independent of whether the wastes are 200 m (656 ft) deep (a mined geologic repository) or 36 m (118 ft) deep (intermediate depth burial).

The GCD wastes are so deep that inadvertent human intrusion, as envisioned in the EPA's Guidance, is directly applicable to the GCD wastes. Thus, there is no reason to deviate from any of the EPA's Guidance.

With regard to including drill cuttings in releases, the EPA states in their Preamble to 40 CFR 191:

> …the possibility of inadvertent human intrusion into or nearby a repository requires special attention. Such intrusion can significantly *disrupt the containment* afforded by a geologic repository … It will not be possible to develop a "correct" estimate of the probability of such intrusion. The Agency believes that performance assessments should consider the possibilities of such intrusion, but that limits should be placed on the severity of the assumptions used to make the assessments. Appendix B [the EPA Guidance] to the final rule describes a set of parameters about *the likelihood and consequences of inadvertent intrusion that the Agency assumed were <u>the most pessimistic that would be reasonable</u> in making performance assessments*. The implementing agencies may adopt these assumptions or develop similar ones of their own.… (emphasis added) [EPA, 1985; p. 38077]

It is assumed that the only reason an implementing agency would go to the effort to adopt and defend "similar" assumptions is if the implementing agency's PA failed compliance under the exact assumptions that the EPA provides, and that the implementing agency was looking for more lenient assumptions. The EPA Guidance is specific in presenting the most pessimistic limits on the likelihood and consequences of human intrusion events:

> Therefore, *inadvertent* and intermittent intrusion by *exploratory drilling for resources* (other than any provided by the disposal system itself) can be *the most severe intrusion scenario* assumed by the implementing agencies.
>
> … the Agency assumes that the likelihood of such inadvertent and intermittent drilling need not be taken to be greater than 30 boreholes per square kilometer of repository area per 10,000 years for geologic repositories in proximity to sedimentary rock formations, or more than 3 boreholes per square kilometer per 10,000 years for repositories *in other geologic formations*.
>
> Furthermore, the Agency assumes that the consequences of such inadvertent drilling need not be assumed to be more severe than:
> (1) Direct release to the land surface of all the ground water in the repository horizon that would promptly flow through the newly created borehole to the surface due to natural lithostatic pressure—or (if pumping would be required to raise water to the surface) release of 200 cubic meters of ground water pumped to the surface if that much water is readily available to be pumped; and (2) creation of a ground water flow path with a permeability typical of a borehole filled by the soil or gravel that would normally settle into an open hole over time—not the permeability of a carefully sealed borehole. (emphasis added) [EPA Appendix B Guidance]

This is very specific, very clear, bounding guidance that constrains what the implementing agency needs to consider and it is clear that the EPA did not include releases of wastes in drill cuttings.

Further proof of the EPA's intent was provided in the EPA's August 29, 1999 proposed, updated version of 40 CFR 191 for Yucca Mountain (i.e., 40 CFR 197). In that standard, the *EPA explicitly excludes cuttings from the release calculations* [see 40 CFR 197.26 in EPA, 1999; p. 47015]. Yucca Mountain is 28 miles from the GCD boreholes and both facilities are above the water table. Finally, note that including drill cuttings would unfairly evaluate a disposal system that does not have a groundwater pathway.

2.3.7 Relationship Between Requirements

As mentioned above, 40 CFR Part 191 has four requirements for disposal of TRU waste: CRs, GWPRs, IPRs, and Assurance Requirements. The Assurance Requirements are qualitative and thus require no analyses, and the GWPRs also require no analyses for demonstrating compliance because the aquifer underlying the GCD boreholes is not a special source of groundwater (see Section 2.3.5). The analyses that are carried out for the two remaining quantitative requirements need to be consistent with each other, even though the performance measures for the requirements are different (i.e., cumulative releases to the accessible environment vs. dose to an MOP). Hence, it is necessary to examine the IPRs and CRs to ensure consistency among the analyses for these requirements.

A comparison of the CRs and IPRs reveals several fundamental differences.

1. The regulatory timescale of the IPRs is 1,000 years (1985 version), while that of the CRs is 10,000 years.

2. The IPRs limit doses to an individual, which is equivalent to limiting radionuclide *concentrations* while the CRs limit the *cumulative release* of radionuclides into the accessible environment.

3. The IPRs assume "undisturbed performance" of the disposal system, while the CRs requires an analysis that includes "all significant processes and events that may affect the disposal system." Thus, the analysis for the CR must include processes and events that have only a small probability of occurring (anything with a probability greater than 1 in 10,000 over 10,000 years; see Appendix B of 40 CFR Part 191) if these processes and events have a significant effect on the cumulative release of radionuclides to the accessible environment, while the analyses for the IPRs include only those processes and events that are likely to occur.

4. The IPRs limit the dose received from *all* radionuclides released from the disposal system into the accessible environment, while the CRs limit the cumulative releases of only those radionuclides specified in Table 1 of Appendix A of 40 CFR Part 191. These specific radionuclides are long-lived (i.e., have a half-life greater than 20 years).

5. Finally, the quantitative requirements of the IPRs are deterministic while the CRs are probabilistic.

These differences between the CRs and the IPRs and their implications are discussed in more detail below.

To maintain consistency between the CR and IPR analyses, each analysis is based on the same conceptualization of the disposal system and of the transport of radionuclides to the accessible environment.

One similarity between the two analyses is that only those radionuclides that reach the accessible environment are included in calculating the performance measure of interest (cumulative release or dose). The difference between the two analyses is that one calculates the cumulative flux of long-lived radionuclides over 10,000 years (CR) while the other calculates the maximum dose to an MOP from all radionuclides (i.e., parents originally present in the waste and their daughter products) during the 1,000 years following disposal (IPR).

The primary difference between the CRs and the IPRs is that the analysis for the CRs must include the effects of *all* significant processes and events, even if the probability of occurrence is low; the analysis for the IPRs considers only the effects from "undisturbed performance" of the disposal system, which specifically excludes human intrusion and unlikely natural events. To account for the effects of all significant processes and events in conducting the analysis for the CRs, the significant processes and events that may occur in the future are categorized as being

either in the "base case" or a "disruptive scenario." The "base case" represents future conditions that may affect radionuclide movement and that have a high probability of occurrence. These are the events and processes that are almost certain to occur. "Disruptive scenarios" are unique combinations of processes and events that may significantly affect radionuclide movement and that have a probability of occurrence significantly less than one but greater than 1 in 10,000 in 10,000 years. Cumulative releases of radionuclides to the accessible environment are calculated for the "base case" and for all "disruptive scenarios;" then these releases and their associated probabilities are combined into a CCDF to determine compliance with the CRs.

2.4 Other Regulatory Requirements

Several other regulations apply to the wastes in the GCD boreholes in addition to the NEPA, DOE Order 5820.2A, and 40 CFR 191. Some apply because of the presence of radioactive waste, such as DOE Order 5400.5, "Radiation Protection of the Public and the Environment," and DOE Order 5480.11, "Radiation Protection for Occupational Workers." DOE Order 5400.5 requires DOE facilities to protect MOPs and the environment against undue risk from radiation, setting an annual limit of 100 mrem effective dose equivalent. Airborne emissions are not to result in an annual effective dose equivalent greater than 10 mrem, and radon fluxes are not to exceed 20 pCi/m^2sec (as established in 40 CFR 61). DOE Order 5480.11 requires the DOE to operate its facilities so that workers are protected from ionizing radiation. For example, an occupational worker should receive no more than 5,000 mrem annual effective dose equivalent and no more than 15,000 mrem annual dose equivalent to individual organs and tissues. The order also sets dose limits for specific groups of people: unborn children, minors, and students.

Other regulations apply because fissionable material is present in the boreholes. For example, DOE Order 5480.24, "Nuclear Criticality Safety" establishes "nuclear criticality safety program requirements to ensure that identifiable risks are reduced to acceptably low levels, management authorization of the operation is documented, and people and property are protected from the effects of a criticality incident" [Vocke et al., 1999]. It is not clear if the provisions of this order apply to the GCD waste, however.

Classified material has been disposed in GCD boreholes which triggers still other regulations. The DOE has standards for protecting classified information, and these are prescribed in DOE Order 5631.4A. Therefore, these guidelines must be followed when accessing and using classified information necessary for determining regulatory compliance.

In addition, the State of Nevada has taken the position that the GCD boreholes are Class IV underground injection wells, which are prohibited under EPA's Safe Drinking Water Act Underground Injection Control Program (40 CFR 144.13). The EPA does not share this view [EPA, 1993; p. 66408].

Wastes defined as hazardous under the Resource Conservation Recovery Act (RCRA) were disposed of in Boreholes 1, 2, 3, and 4. These wastes include lithium hydride, lithium deuteride, mercury, and lead. Therefore, closure of the boreholes must comply with RCRA requirements for a closure plan and closure permit.

Closure activities such as earthmoving; heavy equipment operations; removal or placement of fill material in floodplains; and obtaining sand, gravel, or other burrow materials for backfilling or closure cap construction could trigger additional regulatory requirements. For example, the Clean Air Act limits dust emissions from backfilling the GCD boreholes and dust emissions from constructing a closure cap. The Noise Control Act of 1972, as amended by the Quiet Communities Act of 1978, requires the DOE to comply with State and local requirements for noise control and abatement, so closure activities that generate a lot of noise would have to be in compliance with this act. Executive Order 11988, "Floodplain Management," requires the DOE to protect the 100-year floodplain that is within portions of the Area 5 RWMS that could be disturbed during construction of the closure caps.

Finally, requirements for the protection of natural, biological, archaeological, historical, and cultural resources will apply to closure of the GCD boreholes. For example, the Endangered Species Act of 1973 requires the DOE to protect the desert tortoise, a threatened species, in conducting its operations and in closing the boreholes. The Archaeological Resources Protection Act of 1979 obligates the DOE to protect any archaeological resources found during surface disturbing activities.

A complete list and discussion of the approximately 60 regulatory requirements that may apply to the GCD boreholes has been prepared by Vocke et al. [1999]. The actions required to comply with these regulations are many and varied; it is beyond the scope of this document to discuss compliance with these other requirements.

2.5 Conclusions

The primary DOE and EPA requirements that apply to the disposal of TRU waste in GCD boreholes are DOE Order 5820.2A and the 1985 version of 40 CFR 191, respectively. The DOE regulation establishes the need to comply with the NEPA and with EPA regulations (i.e., 40 CFR 191). The EPA's 40 CFR 191 has one qualitative requirement (the Assurance Requirements) and three quantitative requirements (CRs, IPRs, and GWPRs). Assessing compliance with the two of these three quantitative requirements that apply to GCD is the focus of this document.

In addition to DOE Order 5820.2A, NEPA, and 40 CFR 191, other regulations apply to the GCD waste because the waste is classified, radioactive, hazardous, or fissionable; because of certain closure activities; or because the closure activities require protection of natural, biological, archaeological, historical, or cultural resources. These other regulations are discussed in detail by Vocke et al. [1999] and are not discussed further in this document.

This page intentionally left blank.

3.0 PERFORMANCE ASSESSMENT METHODOLOGY

The PA methodology developed for GCD is iterative and is designed to facilitate site characterization and regulatory compliance decision making. The flow of this process is shown in Figure 3-1. The major components of this methodology are discussed below.

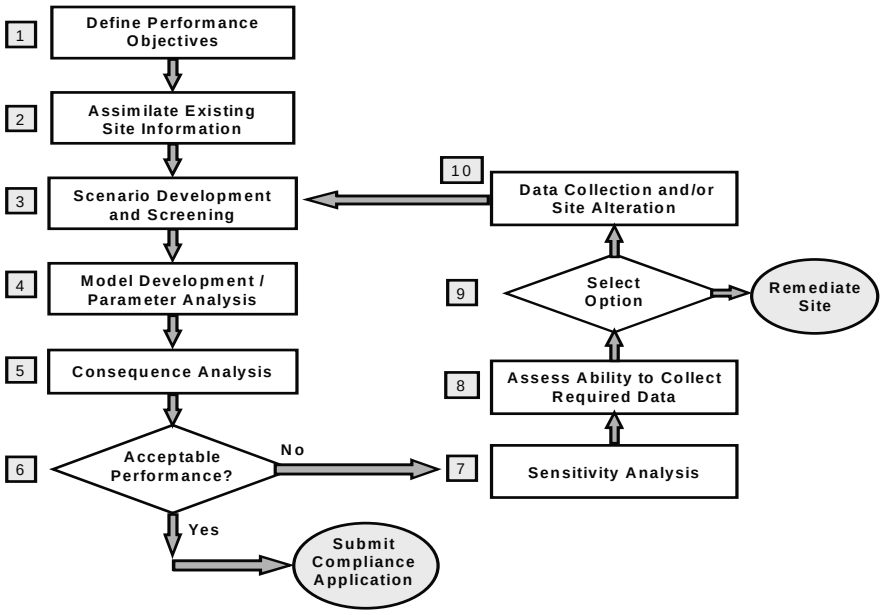

Figure 3-1. GCD PA Process.

For the TRU wastes in the GCD boreholes, the performance and reliability of the disposal system are assessed for up to 10,000 years and over spatial scales ranging from several square meters to several square kilometers. Consequently, uncertainty exists because we cannot know everything there is to know about the system today, nor can we predict with complete certainty what the system will look like in the future. We are uncertain about what events will occur in the future, how these events will manifest themselves, and what the magnitude of their impact will be. This uncertainty notwithstanding, compliance decisions based on the safety of the TRU wastes in the GCD boreholes are still required. This section provides a general overview of the PA methodology applied to the TRU waste, including the approaches taken in treating uncertainty. The specific implementation of the process is described in subsequent sections of this document.

The process used for assessing uncertainty, propagating uncertainty, and systematically reducing uncertainty applies the “risk” paradigm introduced by Kaplan and Garrick [1981] by assessing:

- what can happen?
- what is the likelihood/probability of occurrence,? and
- what are the resulting consequences?

A key point of the PA methodology is that uncertainty is quantified and propagated throughout the process rather than as a separate activity at the end of the process. Consequently, uncertainty analysis does not appear as a separate section in this CAD, but is described throughout. As a

matter of convenience, the types of uncertainty associated with assessing the system's performance have been separated into three general categories [Bonano and Cranwell, 1988; Davis et al., 1990]: (1) uncertainty about the occurrence of future events and conditions, (2) uncertainty in the models that describe the system both now and in the future, and (3) uncertainty in the parameter values that quantify the description and output of the models.

3.1 Define Performance Objectives

The first step in the PA methodology shown in Figure 3-1 is to define performance measures. For the TRU wastes in the GCD boreholes, the performance measure is the EPA regulation for disposal of SNF, TRU, and HLW, 40 CFR 191 [EPA, 1985], which is described in detail in Section 2.0 of this document. Recall that 40 CFR 191 has three quantitative requirements: the CRs, IPRs, and GWPRs. These requirements provide the performance objectives with which the results of the PA are compared.

In developing the regulation, EPA [1985] anticipated and acknowledged the existence of uncertainty by stating that "Because of the long time period involved and the nature of the events and processes of interest, there will inevitably be substantial uncertainties" [EPA, 1985; p. 38086]. In fact, 40 CFR 191 requires that all sources of uncertainty be included in a PA. To accommodate these uncertainties, 40 CFR 191 (in particular, the CRs of § 191.13) requires only a "reasonable expectation" that the performance objectives will be met, reflecting the "fact that unequivocal numerical proof of compliance is neither necessary nor likely to be obtained" [EPA, 1985; p. 38071]. Our interpretation of reasonable expectation for the GCD PA is that, given the uncertainty in the analyses, the likelihood of making an incorrect regulatory decision should be very low.

"Reasonable expectation" is provided by (1) quantifying, propagating, and reducing uncertainty systematically, and (2) representing the outcome of the analysis in a way that provides a measure of the probability that the correct option was chosen. An example of selecting the wrong option would be to approve an unsafe site. An example of selecting the correct option would be to approve a safe site. The EPA has defined the CRs in a way that directly facilitates assessing the probability of selecting the correct or incorrect option. If the probabilities of the EPA Sums of 1.0 and 10.0 do not exceed 0.1 and 0.001, respectively, then the site is considered "in compliance" (recognizing that actual compliance is determined through a regulatory process that considers many factors). By stating the CRs in this way, EPA has, in effect, stated how much decision risk they are willing to accept. By plotting the results as a CCDF (see Section 2.0), the conditional probability (conditioned on the models and scenarios used) that an EPA Sum of 1.0 or 10.0 would be exceeded can be assessed directly. In other words, if all uncertainties have been included, then the conditional probability of selecting the wrong option has been quantified and is represented directly by the CCDF.

The IPRs are not defined probabilistically, but rather as deterministic threshold values that must be met. However, the EPA recognized uncertainty in assessing these requirements. In guidance for 40 CFR 191 [EPA, 1985], the EPA states "that compliance can be determined based upon 'best estimate' predictions (e.g., the mean or median of the appropriate distribution, whichever is

higher)." The phrase "appropriate distribution" implies that a probabilistic methodology is necessary to assess compliance with the IPRs.

3.2 Assimilate Existing Site Information

As shown in Figure 3-1, the second step in the PA methodology is to assimilate existing site information in the context of Step 1 to understand the relevant properties of the waste and the physical systems and processes that might influence system performance. The implementation of this step for the GCD PA is discussed in some detail in Sections 5.0 and 6.0.

Describing the disposal system includes acquiring existing data and information about the characteristics of the waste, facility, and site. Waste characteristics that are of interest include, among other things, the form of the waste, the specific isotopes disposed of at the site, their quantities, decay chains, half-lives, solubilities in pore water, and decay modes. The characteristics of the facility include the size of the disposal system, emplacement configuration, and properties of any engineered barriers (e.g., backfill, waste packaging). Characteristics of the site include geology, hydrology, geochemistry, biology, climate, and geomechanical properties of the geologic formation containing the disposal system. The description of the GCD system is given in Sections 5.0 and 6.0.

Note that *new* site data collection does not take place until Step 10, at which point data that might make a difference in decision-making has been defined in the previous steps 7, 8, and 9. For the GCD PA, Price et al. [1993b] conducted an initial scoping analysis based only on existing information to assess the likelihood that the GCD site would comply with the performance objectives under 40 CFR 191. This provided the foundation for subsequent analyses. However, the PA conducted by Price et al. [1993b] was intended to have certain limitations (e.g., a full scenario analysis was not to be performed), so it did not fully implement the methodology given in Figure 3-1.

3.3 Scenario Development and Screening

The third step in the methodology is scenario development and screening. Scenario development and screening is a necessary part of the compliance assessment because the EPA's CRs stipulate that "all significant processes and events" be included in a PA. The EPA does not give specific guidance or instructions as to how these processes and events are to be included in the analysis. As a result, SNL developed a methodology that provides a systematic procedure for generating scenarios [Cranwell et al., 1990]. A scenario is a set of naturally-occurring or human-induced conditions that represent possible future states of the repository, geologic systems, and groundwater flow systems that might affect the release and transport of radionuclides from the repository to the accessible environment [Cranwell et al., 1990]. In simpler terms, a scenario represents a possible realization of the future state of the disposal system [Bonano and Cranwell, 1988].

The scenario methodology that has been applied for the CRs consists of six steps [Cranwell et al., 1990]:

1. Identify potentially disruptive events and processes,
2. Classify events and processes,
3. Screen events and processes,
4. Form scenarios from all combinations of events and processes,
5. Screen scenarios, and
6. Identify final set of scenarios.

The first step, identifying potentially disruptive events and processes, must be done carefully to increase the likelihood that potentially important scenarios are not overlooked; that is, the set must be as complete as possible. The second step, classifying events and processes, is often done iteratively with the first step because classifying events and processes helps increase the likelihood that the set of events and processes identified in Step 1 is complete. There are many ways of classifying events and processes: by the cause of the event or process (e.g., human-induced, naturally-occurring, waste- or repository-induced) or by how the event or process affects the disposal system (e.g., release or transport), for example.

For geologic and natural processes, the identification step was treated as comprehensively as possible. For human intrusion, EPA guidance was followed, in that EPA has specified the nature and maximum severity of a human intrusion event; that is, only the human-intrusion-through-exploratory-drilling event was given full consideration. The events and processes identified in Steps 1 and 2 are then screened to eliminate unlikely or inconsequential events and processes. As with classifying events and processes, screening events and processes can be accomplished in many ways. Cranwell et al. [1990] used the three criteria of physical reasonableness, likelihood of occurrence, and consequence. These three criteria were used to develop the scenarios included in the PA and are described in the following paragraphs.

The physical reasonableness criterion is used to eliminate events and processes whose occurrence is assumed to be impossible because of the characteristics of the geologic site or disposal facility. Examples of such events or processes are a tsunami occurring at the GCD site or a dissolution cavity forming where crystalline rock exists [Cranwell et al., 1990].

The likelihood of occurrence criterion eliminates events and processes whose probability of occurrence is less than 1 chance in 10,000 over 10,000 years (i.e., less than 1×10^{-8} per year). This is based on guidance given in Appendix B of 40 CFR Part 191 where the EPA assumes that "performance assessments need not consider categories of events or processes that are estimated to have less than one chance in 10,000 of occurring over 10,000 years."

For screening events and processes, the consequence criterion refers to the effect the event or process would have on the properties of the disposal system or the site. The consequence criterion is consistent with guidance from the EPA in Appendix B of 40 CFR Part 191. In this guidance, the EPA states that events and processes estimated to have a likelihood of occurrence that is greater than 1×10^{-8} "...may be omitted from the performance assessments if there is a reasonable expectation that the remaining probability distribution of cumulative releases (i.e., CCDF)

would not be significantly changed by such omissions." Within this PA, this criterion was applied to those events and processes whose inclusion would either (1) have no impact on the statistical properties of the CCDF, or (2) shift the weight of the CCDF toward lower values. In practical terms, the former condition cannot be determined without conducting a complete numerical PA analysis, after which there is little point in screening the event/process out; consequently, this was rarely applied. However, the latter condition can often be applied prior to conducting complex numerical analyses, and this is what was often done for the GCD TRU waste PA.

Step 4 in the scenario methodology, combining events and processes to form scenarios, consists of taking the events and processes remaining after the screening process and combining them in every possible way to form scenarios. Thus, 2^n scenarios are formed where *n* is the number of events and processes that survived the screening process in Step 3. For example, if only two events and processes, say, A and B, remained after Step 3, the four possible scenarios are: (1) only A occurs, (2) only B occurs, (3) both A and B occur, and (4) neither A nor B occurs. This last scenario in which neither A nor B occurs is known as the base case scenario. The base case scenario includes all events and processes that are likely to occur at the site during the regulatory time frame (i.e., have a probability of occurrence close to 1). The number of scenarios becomes extremely large quickly (e.g., 10 events and processes result in 1024 scenarios).

The scenario methodology does not address the time at which the events and processes that define a scenario occur. That is, A and B can occur at any time during the 10,000-year regulatory period. It is frequently assumed that the events and processes occur at the beginning of the 10,000-year period, when the disposal site closes.

The scenarios can then be screened (Step 5) using the same three criteria used to screen events and processes: physical reasonableness, probability, and consequence. At this stage of the screening process, the consequence criterion refers to the effect the scenario would have on the CCDF of the EPA Sum. The physical reasonableness criterion is often the easiest to apply in the process of screening scenarios. For example, the events "precipitation increases" and "precipitation decreases" cannot both occur in the same scenario. Thus, the scenarios in which those events occur together can be eliminated. If the consequence from a particular scenario is nonexistent or negligible (i.e., no releases to the accessible environment or exceedingly small releases), the scenario can be removed from further consideration. The probability of a given scenario is given by multiplying the probability of occurrence or nonoccurrence of all the constituent events and processes. If the scenario probability is less than some predetermined value (e.g., 1×10^{-8} per year), then the scenario can be removed from further consideration. The details of how scenarios were selected for the PA are given in Section 6.3 of this report.

3.3.1 Estimating Scenario Probabilities

The scenarios remaining after the screening process are assigned quantitative probabilities of occurrence and the results are combined into a single distribution of output upon which the final compliance decision is based. Approaches for estimating scenario probabilities and how they were applied in the GCD PA are provided in greater detail in Section 6.3.

3.3.2 Addressing the Individual Protection Requirements

To address the IPRs in this PA, two land-use/exposure scenarios were developed and applied to serve as the basis for decision-making. Consequently, the results from each IPR analyses were not weighted by scenario probabilities. The physical setting for this scenario was made to be consistent with the base-case scenario developed for the CR analyses. Dose was estimated by superimposing a defined MOP on to the radionuclide transport and release CR model. This is discussed in greater detail in Section 7.5.

3.4 Model Development and Parameter Analysis

Once scenarios have been developed and screened, models for each scenario were developed. This fourth step consists of developing models for the movement of pore water, source term release, transport of radionuclides in the geosphere, transport of radionuclides in the biosphere, and doses to man. These models are then used in Step 5 to produce numerical values that can be used to assess compliance with the performance criteria in 40 CFR Part 191.

Model development consists of identifying the significant processes that are occurring for a given scenario, developing conceptual models for these processes, developing mathematical models that correspond to the conceptual models, and solving the equations of the mathematical models. Significant processes that are thought to occur in a disposal system include; radionuclide dissolution, advection, diffusion, and radioactive decay; waste package corrosion; and radionuclide uptake by animals, to name a few. Identifying the processes of interest is coupled with the site description (see Sections 5.0 and 6.0). The conceptual models for these processes consist of sets of assumptions about these processes. These assumptions are based on information from the site and have some uncertainty associated with them. From these conceptual models, mathematical models (e.g., partial differential equations with associated boundary and initial conditions) are developed. The solutions to the equations in the mathematical models are usually embedded in a computer code or several computer codes. The parameters needed to run the computer codes are often uncertain, introducing further uncertainty into the calculations. Both conceptual model uncertainty and parameter uncertainty are discussed below.

3.4.1 Conceptual Model Uncertainty and Screening

A model is a simplification of the existing and future system. The underlying philosophy of this PA methodology is that no model is correct with regard to reality, but rather some models are useful for decision-making.

A conceptual model is effectively a set of assumptions that describes the system for a specified purpose. In developing the conceptual model, assumptions can be justified based on either of the following:

- the assumption is reasonable because it can be completely defended with site-specific information (e.g., transport occurs in three dimensions)

- the assumption is thought to be conservative in that a more realistic assumption based on *additional* site-specific knowledge would not yield higher output (e.g., one-dimensional transport of radionuclides without sorption).

For the purposes of this PA, the conceptual model describes how the contaminants move from the source to the accessible environment or to a defined receptor. When assessing dose to a receptor, identification of exposure pathways is key to the conceptual modeling process. Then, mathematical models are developed to implement the equations of the conceptual model.

When dealing with geologic systems where all the spatial characteristics cannot be known, and where the future cannot be perfectly known, a "realistic" conceptual model is not attainable. Consequently, uncertainty in the conceptual model is expected to exist. In other words, more than one possible interpretation of the system might be justified based on the existing information. This results in the possibility of alternative projected behaviors of the system into the future. Because development of an exhaustive suite of mutually exclusive models has not been shown to be practicable, assignment of probabilities to models is not really possible or meaningful. Given these presumptions, model uncertainty has been addressed in the TRU waste PA by:

- developing multiple alternative conceptual models of the system,

- performing screening analyses on all the conceptual models that are consistent with available data and current state of knowledge, and

- concentrating on those models that could result in releases that exceed the performance criteria.

Applying the conceptual model screening methodology may result in removing certain conceptual models from further consideration. That is, if screening analyses indicate that including releases calculated for a particular conceptual model shifts the CCDF to the left (i.e., that particular conceptual model represents an improvement in the disposal system's isolation capability), then that model can be, but does not have to be, removed from further consideration. By removing such a conceptual model from further consideration, resources can be focused on those conceptual models with releases that might exceed the performance measures.

For example, scenario analysis identified landfill subsidence as an event that could affect the performance of the disposal system. This event was deemed to be likely to occur and was thus included in the base case scenario. However, there was some uncertainty as to what the possible consequences of subsidence would be. One possibility was that subsidence would result in focusing enough precipitation to induce localized downward flow to the water table (i.e., induce recharge) within the regulatory period. Another possibility was that subsidence would not induce localized recharge but instead would change the types of plants growing above the boreholes (e.g., trees would take root) as well as the plant density, thereby changing the plant uptake model. Screening calculations were performed to determine whether or not localized recharge could occur (see Section 6.6 and Appendix B). The conclusion of the screening calculations was that subsidence would not cause localized recharge. In fact, assuming that subsidence induces downward flow in the vadose zone "improves" the performance of the site because contaminants

are no longer transported by pore water upward to the ground surface, 21 m (70 ft) away, but instead are transported downward, away from the closest point in the accessible environment. Therefore, the subsidence-causing-localized-recharge model was screened from further consideration, but the subsidence-changing-plant-community model was retained for the PA calculations (see Sections 6.6 and 6.8).

Models that result in noncompliance are of most interest because:

- the decision to accept the site should be made based on the models that result in failure to comply (under the premise that erroneously accepting a poor site is less desirable than erroneously ruling out a good site);

- the decision has been made to avoid assigning probabilities to conceptual models, thereby all conceptual models were assumed to be equally probable;

- if compliance can be demonstrated with all plausible models, then a high level of confidence in the decision to accept the site can be achieved; and,

- in the iterative PA process, it is much more likely that data collection activities can be defined that refute certain assumptions versus activities that will unequivocally support certain assumptions.

Section 5.0 provides a description of the conceptual model(s) for current conditions and Section 6.0 provides a description of the conceptual model(s) for future conditions.

3.4.2 Parameter Uncertainty and Variability

To assess performance quantitatively, the analyst must define the model parameter values and quantify the uncertainty and variability in each of the parameter values. Treatment of parameter uncertainty includes developing quantitative descriptions of possible parameter values, propagating uncertainty by exercising the models with a variety of possible parameter values, and reducing uncertainty through focused data collection.

In modeling the disposal site, effective values of parameters have been developed and used to represent the equivalent parameter value over some spatial or temporal scale. For example, the GCD disposal system is modeled using an effective value of the rate of upward specific discharge over the 21 m (70 ft) depth of burial, although it is known that a variety of values of the rate of upward specific discharge will likely exist at smaller scales. This is done because (1) for the purposes of the model, there may be no value in resolving the parameter at the smaller scales, or (2) it may not be possible or practical to measure the parameter at all scales and an approximation is required.

For the GCD PA, parameter uncertainty has been addressed by developing parameter distributions. The parameter distributions are quantitatively characterized in the form of probability density functions (pdfs). These pdfs reflect the current state of knowledge (based on physical limits, the results of laboratory and field studies, site characterization activities, analogous

situations, and models) and may incorporate information on both uncertainty and variability in the parameter value. To represent parameter uncertainty accurately, the distributions have been developed *to be representative and unbiased*, and not overconfident. By using this approach, the parameter distributions should progressively only narrow as additional information is collected. If there were a case of a variable parameter for which perfect information existed, then the distribution would reflect only variability. If there were a case of a deterministic parameter for which perfect information existed, then only a single value would be used.

3.5 Consequence Analysis

Step 5 of the PA process involves calculating cumulative releases of radionuclides to the accessible environment and dose to an MOP. These calculations generally require using computer codes to implement the conceptual models developed in Step 4 for all the scenarios developed in Step 3, all the while propagating the uncertainty in parameters developed in Step 4. Figure 3-2 shows how this is done for the CR analysis. The implementation of this step for the GCD PA is given in Section 7.0.

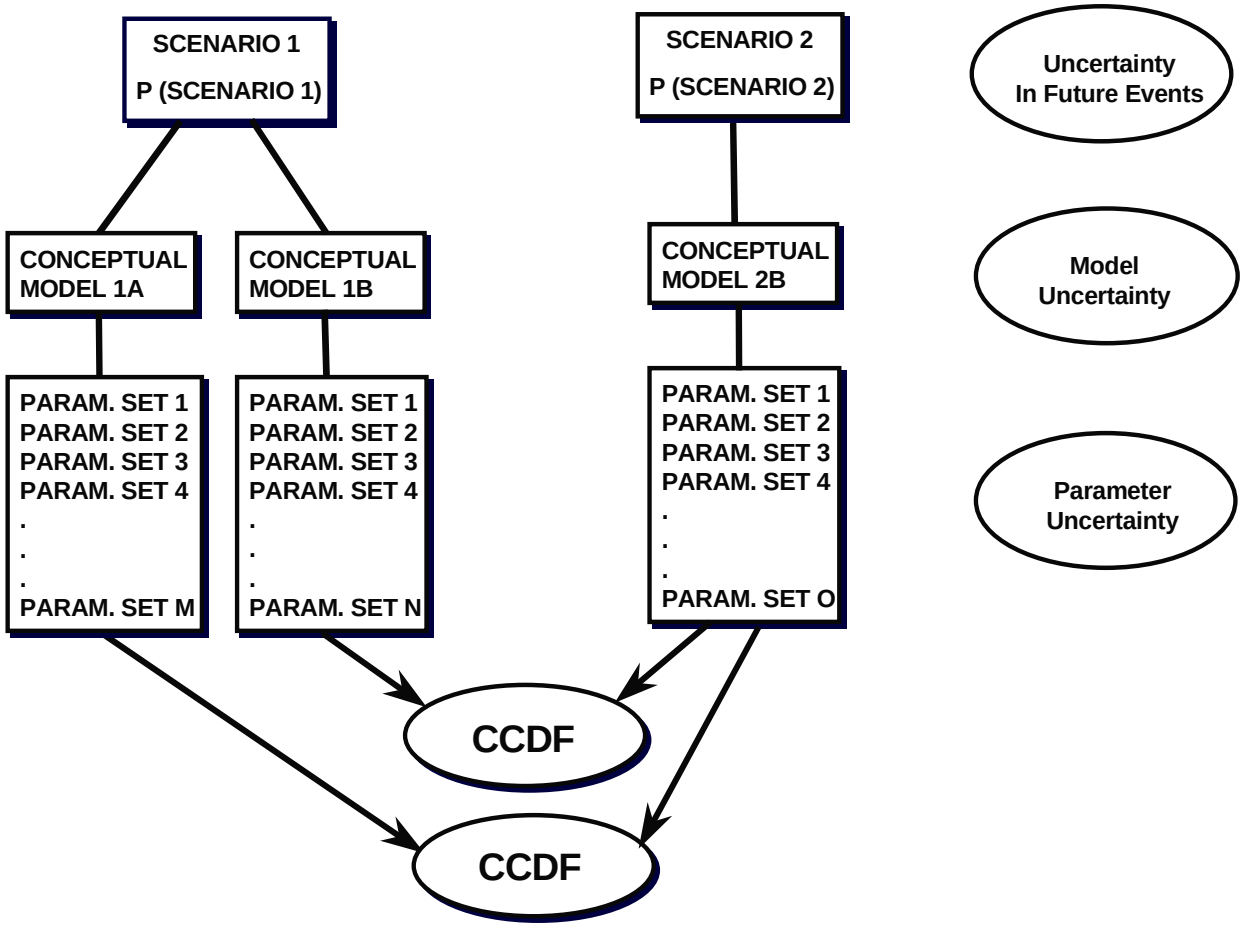

Figure 3-2. Process for Organizing and Propagating Uncertainty (adapted from Kozak et al. [1993]).

Uncertainty in the occurrence of future events is propagated through the assignment of probabilities to scenarios. *Note that consequences (model output in the form of EPA Sum or dose) are not downweighted (i.e., multiplied) by probability.* Rather, the consequence and the conditional probability of exceeding specified values are plotted against one another in the CCDF. Uncertainty in the evolution of the site is then propagated through the application of model(s) and parameters, as discussed below.

3.5.1 Conceptual Model Uncertainty

The most robust approach to propagating and displaying uncertainty in scenarios and models is to conduct an entire Monte Carlo analysis (described below) with all of the scenarios and all alternative models of concern, and then identify those assumptions that lead to noncompliance. However, this is not necessary if the scenarios and/or models can be ruled out early on in the process based on lack of consequence. That is, it may be possible to conduct deterministic or limited probabilistic screening analyses to rule out particular scenarios and models from further consideration. In the GCD PA, several alternative conceptual models were removed from further consideration based on screening analyses, as discussed in Section 6.0.

If multiple conceptual models were retained through the entire analysis, then multiple CCDFs (or other applicable distributions) would be produced, as shown in Figure 3-3. If several models result in outputs that exceed the performance objective, then all these "violating" models would have to be refuted for the GCD disposal to be deemed acceptable.

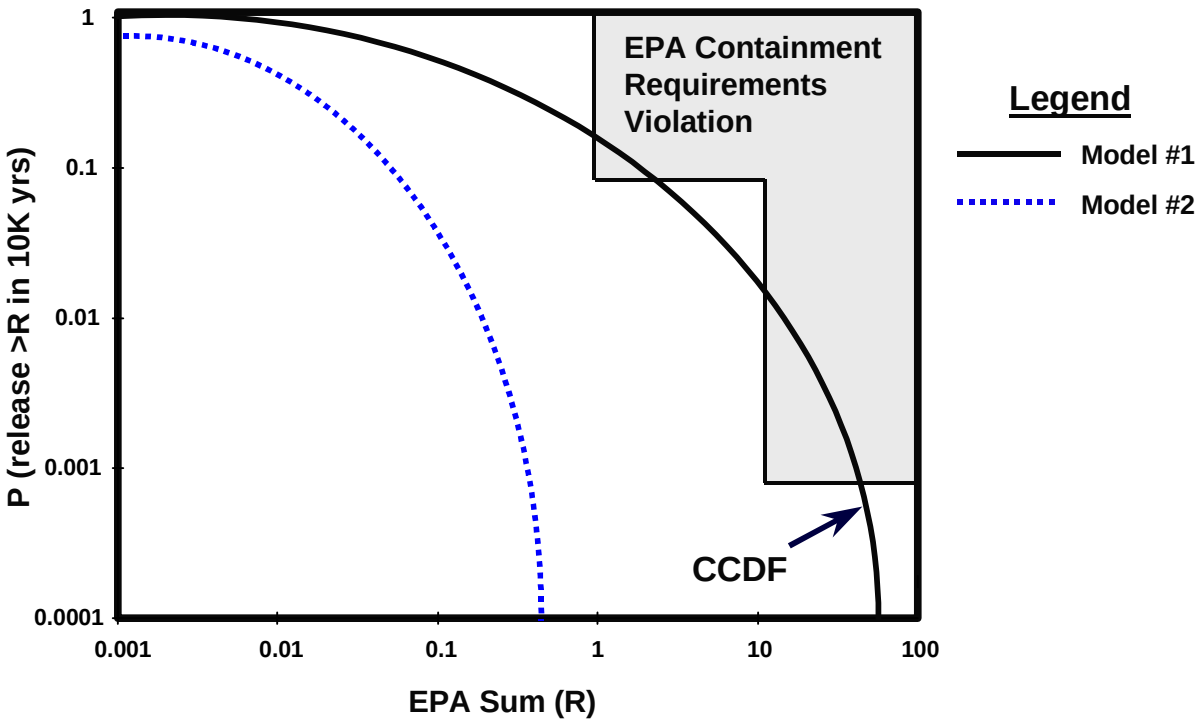

Figure 3-3. CCDFs for two Alternative Conceptual Models.

3.5.2 Parameter Uncertainty

Monte Carlo simulation has been used to propagate uncertainty in parameters to the results of the consequence analysis. This is a robust approach, particularly when the models are complex and parameter uncertainties are large [Helton et al., 1991]. In Monte Carlo simulations, the uncertainty in the numerical value of each uncertain input parameter is described with a pdf, as discussed above. Each pdf is randomly sampled to obtain one value of each uncertain parameter. The result of this sampling is an input parameter "vector." Each vector contains a single value for each parameter, and each vector serves as input to the computer codes for a single simulation of site performance. By sampling each of the pdfs multiple times, multiple vectors are produced and multiple simulations can be performed (i.e., one simulation for each input vector), producing a range of values for the performance measure of interest.

The Monte Carlo technique is used for several reasons. First, consequence analysis often involves a series of coupled computer codes, each having uncertain inputs. Analytical approaches (e.g., differential analysis techniques) are often intractable for this type of problem [Zimmerman et al., 1990]. Second, the CRs are concerned with the upper tail (i.e., 0.9 and 0.999 quantiles) of the output distribution. Deterministic methods (e.g., First Order Second Moment) typically yield only parametric descriptions of the output uncertainty (e.g., variance), whereas the entire output distribution can be described using the Monte Carlo technique. Third, many of the uncertain parameters typically have a very large range over which they can vary; Monte Carlo simulation allows the effects of these different values to be incorporated into the analysis in a straightforward manner. Fourth, correlations between parameters can be handled easily with this approach.

The Latin Hypercube Sampling (LHS) technique [McKay et al., 1979; Iman and Shortencarier, 1984] is used to obtain the samples for the Monte Carlo simulations because it ensures coverage of the extreme strata of each parameter's pdf with a relatively small number of samples. The LHS technique divides the pdf of each variable into n intervals of equal probability, where n is the desired number of samples. One value of the parameter is selected at random from each interval; these sample values are paired with samples generated in the same way from the pdfs of the other parameters. Sampled values are paired randomly except when a correlation between two parameters has been specified. Although this technique does not provide complete coverage of the joint probability space (i.e., all possible combinations of parameter values within the limits of the sampling density), it does reduce the number of samples needed to span the range of uncertainty in the input.

Once models have been defined, parameter values have been sampled, and simulations have been run, results are combined into a distribution of output. Each vector contains one value of each of the uncertain parameters and is used to perform one consequence analysis calculation. All simulations are equally probable; that is, the probability of each simulation is $1/n$ where n is the number of input vectors. For example, if 100 sample vectors have been created, then each output value has a probability of occurrence of 0.01. For the CRs, these probabilities are then multiplied by their respective scenario probability. Therefore, the probability of a given outcome becomes the probability of the random sample multiplied by the probability of the scenario. Bonano and Wahi [1990] provide details for how the results are combined into a CCDF. For the IPRs,

probability of scenarios does not come into play, as disruptive events beyond existing conditions are not considered (as specified by the regulation).

3.6 Compliance Decision

This evaluation corresponds to Step 6 in the framework (Figure 3-1). With the information available at this point, the results of the consequence analysis are evaluated to determine if the site meets the performance objectives. If the analyses demonstrate that the site complies with the regulatory performance objectives and the regulator (DOE in this case) agrees, then the process is complete. If the analyses do not demonstrate compliance, then the process proceeds to Step 7.

A defensible decision about compliance at this point is possible if the approach used to define scenarios, models, and parameters discussed above has been followed. That is, the analysis is based on existing information only and accounts for uncertainty. *The approach provides confidence that if additional information is collected, the range of results (EPA Sum or dose) will narrow (with reduction in parameter uncertainty) or completely shift toward lower values (with reduction in model uncertainty), and the maximum of the distribution will not increase.*

If the output from one or more of the models exceeds the performance objective, it is not necessary to conclude that the site is unacceptable, but rather, given the *current* state of knowledge, that acceptance of the site cannot be defended at this point. Because uncertainty has been accounted for coming into this step, the potential for reducing uncertainty through data collection, so that site compliance is defensible, can then be assessed.

3.7 Reduction of Uncertainty

The next four steps in the PA methodology, Steps 7–10, all serve to reduce uncertainty. Hence, they are discussed together in this section. In Step 7, a sensitivity analysis is conducted to identify the uncertain parameters that exhibit the greatest influence on the predicted quantity (e.g., EPA Sum or dose to an MOP). Thus, resources (i.e., time and money) are spent investigating those factors that "drive" the analysis, not those that are of little significance.

Note that although the PA described in this CAD represents the first comprehensive PA for the TRU waste in the GCD boreholes, Price et al. [1993c] were able to identify, using conditional PA calculations, parameters that were potentially important and others that were unimportant.

Many techniques are available for performing sensitivity analyses. One of the most commonly used techniques is regression analysis. In a regression analysis, a regression model is developed to relate the output to the input, with the simplifying assumption of linearity between input and output. Other techniques include graphical techniques, response-surface techniques, and differential analysis techniques; these are described in Zimmerman et al. [1990]. One drawback to these sensitivity analysis techniques is that they consider only the importance of the uncertainty in parameters, and not uncertainty in the conceptual model.

To assess the sensitivity of the results to model assumptions, Monte Carlo analyses for each conceptual model would be conducted, and the results are compared, relative to the performance

objectives. Based on these comparisons, it is often possible to identify the simplifying assumptions that lead to non-compliant results. The assumptions identified as important would then be possible candidates for further investigation. Because such analyses are often complex and intensive, many of the conceptual models are initially screened out based on defensible, qualitative arguments; that is, screening analyses eliminate more complex models or assumptions that would lead to lesser consequence than simpler, alternative models. Consequently, the logical progression of the modeling process is from simpler, higher-consequence models, to more complex, and perhaps lesser-consequence, models.

Once important model assumptions and/or parameters have been identified in Step 7, an evaluation is made in Step 8 as to whether or not the data can actually be collected. Several factors may lead to the decision that the data cannot be collected, including prohibitive cost and technical infeasibility.

To do this, criteria need to be defined to decide which parameters or model assumptions are important or critical to the compliance decision. *For an input parameter or model assumption (or sets of parameters and/or assumptions) to be considered important in this process, they must meet the following criteria:*

- the uncertainty in the input parameter or model assumption has a significant impact on the uncertainty in the output values (traditional definition of sensitive or important parameter/ assumption); and,

- a reduction in the uncertainty would change the decision from fail to pass.

For input parameters, the analysis should also be careful to recognize when the input parameter distribution includes uncertainty (and not simply variability) and data collection activities could actually reduce the range in the distribution.

In Step 9, a decision is reached to proceed either with data collection and/or site alteration, or with abandoning the site as unsafe. In the case of the GCD PA, because the TRU waste has already been disposed, the site would not be abandoned but the waste could be removed as part of a remediation effort or site characteristics could be altered to improve performance.

In Step 10, new information about the site is collected and/or the site is modified to enhance performance. This new information is then used to modify scenarios, models, and parameters as appropriate and the process begins again at Step 3 (Figure 3-1).

Data and information are collected to reduce uncertainty. Uncertainty has been treated going into this step so that new data collection should result only in a reduction of that uncertainty. In other words, as the analysis progresses and the state of knowledge improves, the number of plausible scenarios should decrease, the magnitude of disruptive scenario probabilities should decrease, the number of plausible conceptual models should decrease, and parameter distributions should narrow.

Note that *actual* reduction of uncertainty would not be realized until the completion of Step 10 in the framework. Steps 7 through 9 identify where to reduce uncertainty.

3.8 Termination of the Process

Termination and closure of this process under this framework is defined in one of two ways:

- the results from all models are less than the performance objective threshold values, and, therefore, a high level of confidence is provided that the site is acceptable, or

- the results from one or more of the models exceed the performance objective threshold values, and either reduction in uncertainty would not result in compliance or it is too costly to conduct the activities necessary to achieve compliance (i.e., it can be said with confidence that the site is not acceptable or there is not enough money to confidently demonstrate acceptability).

3.9 Data Quality Objectives and Performance Assessment

This CAD was evaluated by a DOE/HQ Review Team based on review criteria in the Transuranic Waste Disposal Facility Federal Review Group Manual. One of the review criteria in the TRU Federal Review Group Manual requires the PA to include:

> ...a discussion of how a *data quality objectives* or *similar process* was used as a planning tool and applied to the preparation of the analyses that support the conclusion of satisfying the (containment, individual protection, ground water protection) requirements (emphasis added).

This following section demonstrates that the Performance Assessment Methodology is a "similar process" as required by the above review criteria.

3.9.1 Data Quality Objectives Process

In 1994, the EPA developed a process designed to improve the effectiveness, efficiency, and defensibility of environmental data collection efforts [EPA, 1994]. This process is called the Data Quality Objectives Process (DQOs) and consists of seven iterative steps. The disposal requirements in 40 CFR 191 were developed before the DQO process was developed and, hence, do not require using DQOs to demonstrate compliance. Note that DQOs apply only to data collection, which is only one aspect of the PA Methodology summarized above.

The seven steps of the DQO process are summarized below [EPA, 1994].

> **Step 1: State the Problem -** Concisely describe the problem to be studied. Review prior studies and existing information to gain a sufficient understanding to define the problem.

Step 2: Identify the Decision - Identify what questions the study will attempt to resolve and what actions may result.

Step 3: Identify the Inputs to the Decision - Identify the information that needs to be obtained and the measurements that need to be taken to resolve the decision statement.

Step 4: Define the Study Boundaries - Specify the time periods and spatial area to which decisions will apply. Determine when and where data should be collected.

Step 5: Develop a Decision Rule - Define the statistical parameter of interest, specify the action level, and integrate the previous DQO outputs into a single statement that describes the logical basis for choosing among alternative actions.

Step 6: Specify Tolerable Limits on Decision Errors - Define the decision maker's tolerable decision error rates based on a consideration of the consequences of making an incorrect decision.

Step 7: Optimize the Design - Evaluate information from the previous steps and generate alternative data collection designs. Choose the most resource-effective design that meets all DQOs.

3.9.2 Comparison of DQO Process and PA Methodology

Although the DQO process was not used explicitly in preparing the PA analyses, the PA methodology that was used for the PA analyses qualifies as a "similar process." In the following sections, each of the seven steps of the DQO process is presented, along with a discussion of how the PA methodology is similar.

3.9.2.1 State the Problem

The purpose of this step is to develop a concise definition of the problem to be studied. This step is similar to the first step of the PA methodology, "Define Performance Objectives," as shown in Figure 3-1. The PA methodology begins with the understanding that there is radioactive waste and there is a disposal system, so these components of the "problem statement" do not have to be stated explicitly. Therefore, the first step of the PA methodology, defining performance objectives applicable to radioactive waste disposal, is similar to defining the problem in the DQOs process.

In the GCD PA, the problem to be studied was whether or not disposal of TRU waste in four GCD boreholes at the NTS Area 5 RWMS meets the disposal criteria of 40 CFR 191. This problem definition is unambiguously given in Section 1.1.

3.9.2.2 Identify the Decision

The purpose of this step is to identify exactly which questions will be answered by the study, and what actions may result. These purposes are achieved by a combination of the first step of the PA methodology, "Define Performance Objectives," and the sixth step of the PA methodology, the "Acceptable Performance?" decision. The first step of the PA methodology defines the questions that will be answered and the sixth step defines the actions that may result. If the answer in step six is "no," then steps seven through ten are executed. If the answer in step six is "yes," then a compliance application is submitted.

In the GCD PA, the decision to be made was whether or not disposal of TRU waste in four GCD boreholes at the NTS Area 5 RWMS meets the disposal requirements of the 1985 version of 40 CFR 191: containment requirements, assurance requirements, individual protection requirements, and ground water protection requirements. Specifically, is the probability of certain levels of cumulative release of radionuclides to the accessible environment over 10,000 years below regulatory limits given in the containment requirements? Is the disposal system sited so as to avoid resources? Is the disposal system designed so as not to preclude future removal of waste? Has the waste been adequately isolated from humans and the environment? Is the disposal system going to be monitored? Is access to the disposal system going to be prevented? Are future generations going to be warned of the presence of the disposal system? Are estimated doses to a member of the public in the accessible environment over 1,000 years less than 25 mrem to the whole body and 75 mrem to any critical organ? Are radionuclide concentrations in special sources of ground water and doses from ingesting water withdrawn from a special source of ground water below limits specified in 40 CFR 191? The final answers to these questions are "yes," although the PA methodology is iterative and at times during the course of the investigation some of the answers were "no." When this was the case, steps 7-10 of the methodology (Figure 3-1) were executed in order to increase the state of knowledge so that the consequence analyses could be run again.

3.9.2.3 Identify the Inputs to the Decision

The purpose of this step is to identify the information needed to arrive at the decisions identified in step 2 of the DQO process. This step is similar to steps two, three, four and five of the PA methodology: "Assimilate Existing Site Information," "Develop and Screen Scenarios," "Develop Models and Parameters," and "Perform Consequence Analysis." To decide whether disposal of radioactive waste meets the performance objectives established in step one of the PA methodology, it is necessary to collect and use available data (step 2 of the PA methodology) to develop and screen potential future states of the disposal system (step 3); develop conceptual models, mathematical models, and appropriate values of input parameters (step 4); and model the performance of the disposal system (step 5). The outputs from modeling the performance of the disposal system include cumulative radionuclide release to the accessible environment over 10,000 years, dose to a member of the public in the accessible environment over 1,000 years, and radionuclide concentrations in special sources of ground water. These outputs serve as input to the compliance decision.

The information needed to make the compliance decision for the TRU waste in the GCD boreholes is contained in Section 5 (site information and parameter development), Section 6 (scenario development and screening), Section 7 (model development), and Section 8 (consequence analysis).

3.9.2.4 Define the Study Boundaries

This step involves specifying temporal and spatial boundaries at which the decisions identified in step 2 of the DQO process will apply. Although the PA methodology does not explicitly include a similar step, the first step of the PA methodology "Define Performance Objectives" implicitly incorporates this information because the performance objectives specified in step one generally include spatial and temporal boundaries.

The spatial boundary for the containment requirements and individual protection requirements is defined in 40 CFR 191 to be the accessible environment, as discussed in Section 2.3.2. The spatial boundary for the ground water protection requirements is defined in 40 CFR 191 to be ground water within the controlled area or less than five kilometers beyond the controlled area, as discussed in Sections 2.3.2 and 2.3.5. The spatial boundary for the assurance requirements is either the boundary of the Area 5 RWMS or the boundary of the NTS, depending on which of the six assurance requirements is being addressed. The temporal boundary for the containment requirements is defined in 40 CFR 191 to be 10,000 years, as discussed in Section 2.3.2, and the temporal boundary for both the individual protection requirements and ground water protection requirements is defined in 40 CFR 191 to be 1,000 years, as discussed in Sections 2.3.4 and 2.3.5. The only temporal boundary for the assurance requirements specified in 40 CFR 191 is a 100-year limit for considering contributions to waste isolation from active institutional controls. For the assurance requirements, it is assumed that LLW disposal continues until 2070 and the DOE maintains control over the NTS for the foreseeable future, as discussed in Volume 4 of the CAD.

3.9.2.5 Develop a Decision Rule

This step encompasses three steps: specifying a statistical parameter (e.g., mean, median, 95th percentile) to characterize the population, specifying the action level (e.g., a concentration greater than 1 mg/kg), and defining the conditions that would cause the decision maker to choose among alternative actions. In the PA methodology, it is generally not necessary to specify statistical parameters to characterize the population or to specify the action level because these have already been specified in the form of the performance objectives defined in step 1 of the PA methodology. The decision maker may have to choose between alternative actions, however, as shown in step 6 of the PA methodology. As discussed above in DQO step 2, in step 6 of the PA methodology the decision-maker decides whether the performance objectives have been met. If the answer is "yes," then the PA can be submitted to the certifying authority. If the answer is "no," then steps seven through ten are followed to determine the best course of action.

For the containment requirements, the statistical parameters of interest are the 90th percentile and the 999th percentile, while the corresponding action levels are a summed normalized release of one and a summed normalized release of 10, as discussed in Section 2.3.2. For the individual

protection requirements, the statistical parameter of interest is the mean or median, whichever is higher, and the action levels are annual dose equivalent of 25 mrem to the whole body and 75 mrem to a critical organ, as discussed in Section 2.3.4. For the ground water protection requirements the statistical parameter of interest is the mean or median, which ever is higher and the action levels are ground water concentrations of 5 picocuries/L of ^{226}Ra and ^{228}Ra, 15 picocuries/L of alpha-emitting radionuclides (including ^{226}Ra and ^{228}Ra but excluding radon), and radionuclide concentrations that would produce an annual dose equivalent to the total body or any internal organ greater than 4 mrem/year.

3.9.2.6 Specify Tolerable Limits on Decision Errors

The purpose of this step is to minimize the likelihood of making a decision error, either a false positive decision error or a false negative decision error. That is, the decision-maker could decide that a disposal site is "safe" when it really isn't, or the decision maker could decide that a disposal site is not "safe" when it really is. Under the premise that it is more desirable to err on the side of safety, the likelihood of deciding that a site is "safe" when it really isn't is minimized in step 4 of the PA methodology in the way that conceptual models are developed and screened, and uncertainty is quantified. The PA methodology concentrates resources on those models with releases that exceed the performance criteria and uses conservative screening calculations as possible to save resources.

This concept is discussed in Section 3.4 and is applied throughout the analyses presented in this document. For example, the analysis for the individual protection requirements presented in Section 7.5 is a very conservative screening calculation, assuming that all radionuclides released to the accessible environment over 1,000 years accumulate in a the garden. Such an assumption clearly leads to overestimating the annual dose equivalent, yet estimated doses are still well below regulatory limits, building confidence in the decision that the site complies with the individual protection requirements.

3.9.2.7 Optimize the Design for Obtaining Data

The purpose of this step is to develop a cost-effective data collection design that still satisfies the DQOs specified in the preceding steps. The entire PA methodology is similar to this step in that the PA methodology is a cost-effective method for supporting site characterization and regulatory compliance decisions.

3.9.3 Summary and Conclusions

The PA methodology is similar to the DQO process. The PA methodology is the more appropriate process to use in the GCD PA analyses because the DQOs process was designed to optimize data collection; it was never intended to guide a PA.

3.10 Conclusions

In 40 CFR 191, the EPA requires the use of PAs to demonstrate that TRU waste disposal sites will be protective of human health and the environment for 10,000 years, even though the processes and events that could affect the movement of radionuclides over the next 10,000 years are uncertain. Therefore, a systematic methodology that incorporates uncertainty was used in the PA for the TRU wastes in the GCD boreholes. Fundamental to this methodology is the philosophy that PA models are not a prediction of how the system will respond. Rather, they provide simulations of a range of plausible outcomes given a state of knowledge. These simulations provide information for decision-making and are consistent with the EPA's requirement of a "reasonable expectation" of future performance.

The basic steps of this methodology are (1) define performance objectives, (2) assimilate existing site information, (3) develop and screen scenarios, (4) develop models and parameter values, (5) perform consequence analyses, (6) decide if the simulated performance of the site is acceptable, (7) conduct sensitivity analyses if the answer to Step 6 was "no," (8) assess the ability to collect desired data, (9) decide whether to proceed with another iteration of the PA or to declare the site unacceptable, and (10) collect data and/or modify the site and begin the PA process again, depending on the decision reached in Step 9. The PA methodology is similar to the DQO process.

This methodology was implemented in the GCD PA as follows:

1. The performance objectives are those given in 40 CFR 191. (Section 2.0)

2. Site information has been gathered. (Sections 5.0 and 6.0)

3. The scenario development and screening process identified several events and processes that could affect the performance of the disposal system (e.g., landfill subsidence, climate change, flooding, human intrusion). Some scenarios were screened from the quantitative PA and the remainder were screened to the base case. (Section 6.0)
4. Models were developed describing the site as it now exists and as it might exist in the future. Multiple conceptual models were developed, but only one was retained for the consequence analyses; the remainder were removed from further consideration through the use of screening analyses. (Sections 5.0 and 6.0)

5. Consequence analyses were conducted. (Sections 7.0 and 8.0)

6. This CAD provides a technical basis for DOE's decision in Step 6.

This page intentionally left blank.

4.0 QUALITY ASSURANCE PROGRAM

4.1 Introduction

A QA Program was specifically developed and implemented by SNL for the compliance assessment of the TRU wastes in the GCD boreholes. The QA Program is described in planning documents and implementing procedures that contain detailed instructions for each process or activity. The QA Program serves as a resource to the technical staff to ensure that the results of the compliance assessment are traceable and reproducible, that accountability is maintained, and that conclusions are based on sound practices.

4.2 Establishing Requirements

The original establishment of the QA requirements, as they applied to the GCD Project, are fully detailed in a letter report [Brosseau, 1990] issued July 12, 1990. The letter report submitted to DOE/NV provided an in-depth analysis of the QA requirements for the GCD Project and a recommended approach for implementation. In summary, the report determined that the regulations at that time referenced DOE Order 5700.6B [DOE, 1986] as the applicable DOE Order governing QA requirements. This order, in turn, required adherence to applicable portions of the American Society of Mechanical Engineers (ASME) NQA-1 [ASME, 1989] through the "judicious and selective application of appropriate requirements." SNL recommended that the development and implementation of the QA Program be tailored to the technical activities for the GCD Project. Although the applicable requirements of NQA-1 would be included, there would be no attempt to force-fit the program to the 18-criteria structure of NQA-1. A proposed outline for a GCD QAMP was submitted to DOE/NV in 1990 and they approved the outline which serves as the basis of the GCD QA program.

Following implementation of technical and QA activities during FY90, FY91, and early FY92, DOE Order 5700.6C [DOE, 1991] was issued and 5700.6B was canceled. This change in requirements was the driving force for the issuance of another QA report [Brosseau, 1993]. The purpose of this report was to analyze the 5700.6C requirements in order to address the impact on the QA Program and to identify any changes that may be required. The report analyzed the requirements of 5700.6C and the SNL laboratory-wide QA program. The products of this analysis were matrices that cross-referenced those portions of SNL QA documents that implemented each applicable requirement. The letter report concluded that the impact of requirement changes on the original GCD QA Program were minimal. Ten changes that resulted from the requirements review are listed in the report. These changes were made to the GCD Program based on programmatic and personnel-related considerations separate from the requirements definition. The QAMP and implementing procedures required few format or structural modifications. It was considered important to maintain the original structure based on project activities, rather than reorganizing the plan and procedures to directly correspond to the ten criteria of 5700.6C. In summary, it was determined that the QA provisions for the GCD Project at SNL must meet the basic requirements of DOE Order 5700.6C. Since the original GCD QA Program was developed under DOE 5700.6B and met the applicable requirements of NQA-1, the overall impact of conforming to the new requirements was minimal and easily accomplished.

Though most of the GCD PA activities at SNL were conducted in accordance with DOE Order 5700.6C, a cross-walk was performed to compare GCD QA Program provisions with the requirements of DOE Order 414.1A, as well as DOE Order 5700.6C. The cross-walk comparison concluded that the GCD QA Program implements all of the applicable QA requirements of DOE Orders 5700.6C and 414.1A.

4.3 Quality Assurance Program Overview

To attain quality on the GCD Project, the emphasis is placed on prevention through proper planning, reviews of work-in-progress, and assessment. The technical staff was involved in all phases of the development of the QA Program and can claim a sense of ownership in the program provisions. The policy for the overall QAMP emphasizes that quality is the responsibility of all project participants and that the QA Program applies to all activities and all personnel involved. It was considered imperative to keep the plans and procedures as simple, brief, and clear as possible. This QA approach emphasizes flexibility in planning and implementation. The structure is modular and task-oriented. Emphasis is placed on project activities and those elements of the program that will help achieve the desired objectives of the QA Program. Project technical activities that received primary emphasis include:

- Planning
- Analysis Documentation
- Data Qualification
- Control of Tests, Experiments, and Scientific Investigations
- Software QA and Configuration Management
- Reviews

Other areas of QA emphasis include:

- Procurement
- Document Control
- Records Management
- Nonconformance and Corrective Action Reporting
- Surveillance
- Personnel Certification and Training

The QAMP contains the requirements and in some cases the “how-to” needed to ensure that the customer’s needs are met. When the QAMP details only the requirement, a Quality Assurance Procedure (QAP) is issued. The primary purpose of QAPs is to provide the detailed requirements and guidelines for how to implement the QA provisions specified in upper-tier QA plans. In general, procedures are referred to for specific requirements, forms, and documentation methods.

4.4 Organization

The SNL GCD organization responsibilities, authorities, and interfaces are detailed in the QAMP [Alletzhauser, 1998]. As the Project Administrator, DOE is the focal point of interface between SNL and other DOE contractors.

4.5 Quality Assurance Program Documents

There are six document elements that define the overall SNL QA Program:

- GCD Project Plan
- QAMP
- Task Plans
- QAPs
- Technical Plans and Procedures
- Geographic Information System (GIS) Quality Plan

The GCD Project Plan encompasses both the quality and the technical requirements for the entire project. It establishes the basis for all subordinate planning, implementation, and assessment activities. The Project Plan addresses management methods used to accomplish the SNL GCD objectives, such as organizational structure, accountability and responsibility, work breakdown structures, communications, conflict resolution, quality policy and scope, schedule and cost control provisions, milestones and deliverables, and other pertinent information. It is periodically updated as work progresses, or conditions change.

The QAMP documents the requirements and approach for implementation of the appropriate QA provisions. The QAMP defines those necessary and sufficient controls to provide adequate confidence that customer requirements are being met throughout the life of the GCD Project. The QAMP is based upon management's policy that each person is individually responsible for the achievement and maintenance of quality in the work they perform. As such, the QAMP applies to all SNL project participants, including management, staff, support organizations, and SNL subcontractor's employees.

The Task Plan is meant as a vehicle for communication and to focus task activities, reviews, and task documentation. This plan specifies requirements (both technical and quality), outlines the approach and strategy for accomplishing the work, specifies the requirements for project reviews, and defines the requirement for, and scope of, any detailed technical plans and procedures. Applicable QA plans and procedures may be incorporated into Task Plans by reference. Task Plans are "living documents" and are revised periodically to reflect changes in project direction or scope. As task activities are completed, the associated task plan is closed. As new activities are undertaken, new Task Plans are written. Thus, the Task Plans reflect the overall project activities at any given time.

QAPs are implementation documents that provide detailed requirements regarding *how* the QA requirements specified in QA Plans or Task Plans will be met. These procedures are written in sufficient detail to allow personnel to easily comprehend and implement them. QAPs provide

specific documentation requirements for a given QA control provision. QAPs are generated when detailed implementation guidance is required by the QAMP, and may be incorporated by reference in Task Plans by Task Leaders.

Technical Plans generally describe *what* is required to meet the established requirements and what approach will be used to implement those requirements. They are the planning documents for a given task and also serve as valuable communication tools. Technical Procedures are implementation documents that provide detailed requirements and steps to follow, including prerequisites, to ensure that the conduct of specific technical activities are controlled, repeatable, and documented. Technical Procedures are closely tied to Task Plans or similar technical planning documents and prescribe *how* requirements will be met. Technical procedures may be supplemented with drawings, sketches, instructions, data sheets, etc. When required, these supplemental documents include the necessary steps to ensure that contractual requirements are accomplished, including compliance with established acceptance criteria.

The GIS is used as a tool for the capture, storage, management, retrieval, manipulation, analysis, and display of data collected for the GCD Project in support of the PA modeling of the TRU wastes in the GCD boreholes. The GIS Quality Plan is intended to define the requirements that must be met to ensure that data collected and managed for the GCD Project meets the quality standards defined in the GCD QAMP. The plan sets guidelines to ensure that data are handled in a manner consistent with recognized quality standards. The GIS Quality Plan identifies responsibilities within the GIS management team for oversight and documentation of compliance to QAPs.

4.6 Greater Confinement Disposal Quality Assurance Procedures

Table 4-1 provides a current listing of GCD Procedures together with the latest revision number and date.

Table 4-1. GCD Project QA Procedures

Doc. No.	Title	Rev.	Date
QP 4-2	Plan and Procedure Preparation, Format, and Content	4	11/97
QP 4-4	Data Qualification	4	04/98
QP 4-5	Tests, Experiments, and Scientific Investigations	3	12/94
QP 4-8	Reviews	5	07/98
QP 4-9	Software Quality Assurance (see section 4.8)	0	03/00
QP 4-10	Software Configuration Management (see section 4.8)	0	03/00
QP 5-2	Document Control	2	11/97
QP 5-3	Records Management	2	11/97
QP 5-5	Surveillance	4	11/97
QP 5-6	Personnel Certification and Training Program	4	04/98

4.7 Implementation Highlights

4.7.1 Task Plans

To address the flexibility and modular-structured approach desired, the use of Task Plans was established as a major aspect of the GCD QA Program. The plans specify requirements (both technical and quality-related) and outline the strategy and approach for accomplishing and reviewing the work. Task Plans provide Task Leaders with the flexibility to designate, on a task-specific basis, which QA provisions of the QA Program apply and which do not. Task plans are "living documents" and are revised and updated as necessary.

4.7.2 Personnel Certification and Training

The first step toward implementation of the QA Program was the development and conduct of informal QA awareness training sessions to provide all project staff with comprehensive, project-specific, QA information.

The responsibility for certification of personnel qualifications belongs to the Department Manager and the GCD Project Leader. A "Certification of Personnel Qualifications" form is provided to each new staff member for documenting their basis for qualification and certification. The Project Leader verifies that the qualification statements are factual and that they meet project requirements for the stated position. The Department Manager certifies the qualification by signing and dating the document.

As new project staff are assigned to the GCD Project, they are provided with QA indoctrination training. The purpose of this training is to provide newly assigned personnel with an overall familiarization with QA principles and an adequate knowledge of the purpose, scope, and implementation of the GCD procedures. Emphasis is placed on procedures for activities that the individual is most likely to be involved with.

Annual QA training was initiated in FY91. The purpose of this training is to serve as a refresher on the QA Program for all GCD Project personnel. It is intended to increase staff awareness of the QA provisions in place and to field comments and questions. The training consists of a general overview of the QA Program with an emphasis on any changes or problems that took place during the previous year.

The training program includes other elements, such as informal training during surveillance, ad hoc training sessions to address problems of significant consequence, and documentation of QA and technical training received outside the GCD Project.

4.7.3 Data Qualification

All data that are used as input for the software governed by the QAMP are qualified. An independent staff member, who has not participated in either code development or data selection, reviews each and every data item and ensures that the data items are traceable to a "qualified source." That source is usually a commonly-accepted reference (e.g., The Handbook of

Chemistry and Physics) or a previously prepared technical report that has been reviewed and accepted by the scientific or engineering community. Data are further reviewed for acceptability and the rationale for acceptance or rejection is documented. The final step is to issue a GCD Data Acceptance Review Sheet covering each data parameter addressed in the CAD.

4.7.4 Surveillance

Surveillance is planned and performed by SNL GCD QA personnel as an integral part of the SNL GCD QA Program. Surveillance makes use of qualified personnel to monitor work in process, assess compliance with requirements, identify actual or potential deficiencies, promote prompt corrective action, and provide management information on the status and effectiveness of quality program implementation. Surveillance is conducted in accordance with the provisions set forth in an approved procedure. Checklists are developed for selected provisions of the QA Program in order to review relatively small portions of the program at any given time. All surveillance activities are documented, and the observations, findings, and any recommendations are summarized. Copies of completed surveillance reports are, as a minimum, sent to the responsible technical staff and the Project Leader. All action items are tracked to completion. Surveillance documentation is sent to, and maintained by, the GCD Records Center.

DOE/NV completed a review of the GCD project in FY 2001, focusing on data qualification and software quality [HAZMED, 2001]. No significant findings were noted that invalidated the data or the software or the conclusions of this PA.

4.8 Software and Configuration Management

The GCD software QA/configuration management programs were patterned after those used at Yucca Mountain and described in the Quality Assurance Requirements and Description (QARD) [QARD, 2000] and other Yucca Mountain procedures. The Yucca Mountain process was modified to meet the needs of the GCD project.[1] The modified process is summarized below.

4.8. Software Quality Assurance

As with the entire QA Program, the implementation of software QA is designed to provide traceability, replication, and accountability based on a graded approach.

The approach is graded in that not every code requires the same level of scrutiny as every other code. Codes that do not contribute directly to the results of the PA (e.g., word processing software, project management software, plotting software) have no QA requirements. Codes which do contribute to the final PA are divided into three categories.

[1] The majority of software development and use did not occur until the later phases of the project. Prior to finalizing the Software QA Procedure in March 2000, the GCD Project followed draft procedures and processes similar to those specified by the Yucca Mountain Project. Though the draft software procedures for the GCD Project were not finalized until late in the PA process, the underlying processes met the procedural requirements.

The first category identifies codes obtained from a source that has a documented software QA Program at least as strict as GCD's (e.g., WIPP, Yucca Mountain). Codes obtained from such programs (e.g., VS2DT, EQ3/6, and LHS) that are used "as is," with no modifications, and within the ranges for which they were validated are considered to meet all software quality requirements. These codes are widely used by other laboratories and government agencies to support analyses for major projects such as WIPP and Yucca Mountain. By virtue of their widespread use, the codes are considered acceptable for use on the GCD Project without further testing or qualification. Staff members document that the QA Program from which the code was obtained was evaluated and that it is sufficient.

The second category is codes obtained from a source that does not have a documented software QA Program that is at least as strict as GCD's (e.g., the United States Department of Agriculture [USDA]). In this case, two steps are taken. First, staff members ensure that the package received is adequate for their needs: there is sufficient documentation to run the code as it was intended to be run; input ranges are defined; the revision is clearly identified; etc. The code is then validated to ensure that it is sufficiently accurate within the range of inputs for which it will be used. The validation is normally accomplished by comparing the results of the code with some other standard (e.g., published material, hand calculations, results of another code that has been qualified, etc.).

The final category includes computer codes developed by SNL in-house or those codes acquired from other sources which SNL modified. In this case, the graded approach requires that the GCD Project fully qualify the code. The process begins with a life cycle plan that documents why and how the code is being developed and tested. Next, the code is designed, developed, and fully documented. Perhaps most importantly, the code is validated to ensure that it produces accurate results for a specific range of input parameters.

This approach ensures that GCD codes are developed, documented, and tested in such a manner that the GCD Project has traceability and the ability to replicate results. Also, the software QA documentation is designed so that staff members can always determine how a particular code came to be designated as "qualified."

4.8.2 Software Documentation and Benchmarking

All software documentation was developed and controlled throughout the life of the project (and maintained in configuration management control as noted below). Independent review and verification of the documentation of the GCD PA code (i.e., the Unnamed Code (TUC)) was performed by PAI, as well as HAZMED personnel. Documentation for the TUC includes the Life Cycle Plan, and the Computer Software Documentation and Users Manual Version 3.0.

DOE/NV initiated two independent benchmarking exercises to provide additional confidence in the validity of the TUC. The results of these benchmarking exercises are documented in analysis packages prepared by Bechtel Nevada and Neptune and Company personnel and summarized by DOE/NV. One benchmark exercise was completed by Bechtel Nevada staff with the suite of codes used for the Area 5 PA/CA [Bechtel Nevada, August 16, 2001]. The second benchmark was completed by Neptune personnel using the GoldSim computer code platform developed by

Golder Associates and used and documented on the Yucca Mountain Project [Neptune and Company, August 15, 2001]. Both benchmarking exercises demonstrated that the TUC conservatively overestimates releases relative to the Area 5 PA/CA codes and the Neptune GoldSim models. Code comparisons and evaluations of differences in code parameters were made, noting similarities, differences, and discrepancies but no major concerns. As noted in the Bechtel Nevada documentation, "recognizing those differences, the TUC output results are generally compatible but are consistently more conservative than the Area 5 CA model results." Also, with respect to the GoldSim comparison, "the complexity of the modeled processes and numerical estimations used by the two codes results in reasonably close output results and general acceptability of the TUC computer code."

4.8.3 Configuration Management

Configuration management is essential to maintain traceability and the ability to replicate results. Any code, therefore, that contributes to the final PA results (any code that must be qualified) and its documentation are entered into the GCD configuration management system. The system is traditional, in that it provides for configuration identification, status accounting, and change control.

GCD configuration management uses Microsoft® Visual SourceSafe™ as a tool. After a code is identified as contributing to the PA results, a copy of the code and the documentation is entered into the SourceSafe™ database. (Note: If only hard copy documentation is obtained, it is submitted to the Records Center in lieu of being added to the database.) The database is controlled and the number of people authorized write or destroy access is limited.

Changes to codes or documentation that have been entered into configuration management are controlled by the configuration authority, a staff member designated by the Project Leader to perform that function. Requests for changes are entered into a software problem report (SPR) system where they are tracked. The SPR provides the reason for changes, when the change was made, what was changed, who made the change, how it was tested, etc., providing the necessary accountability. The SPRs are maintained as records in a Microsoft® Access™ database.

4.9 Conclusions

SNL has documented a QA Program that has been planned, implemented, and maintained. This is an ongoing effort to ensure that activities performed by SNL on behalf of DOE/NV produce results that are traceable and reproducible, that accountability is maintained, and that conclusions are based on sound practices. Establishment of the requirements for the QA Program were developed in conjunction with, and concurred by, DOE/NV. Implementation of the QA Program has been verified by periodic surveillance and audits.

A major goal of the SNL QA Program was to emphasize up-front planning. This was accomplished through the use of Task Plans. A strong commitment to quality together with quality training sessions ensured that quality plans and procedures were understood and followed.

All data collected and used in computer models has been reviewed and qualified. Software QA controls have been put in place and software has been placed under configuration controls. In conclusion, SNL has enforced a Quality Program that is both cost- and quality-effective.

This page intentionally left blank.

5.0 CURRENT DISPOSAL SYSTEM DESCRIPTION

5.1 Introduction

This section describes our conceptual model of the current GCD borehole disposal system for TRU waste, including:

- site location and topography
- GCD disposal
- climate
- geology
- hydrology
- plant uptake
- animal bioturbation
- source term
- pore water
- liquid and vapor phase transport

The description of the disposal system includes a discussion of why each topic is relevant to the PA, a presentation of what is known about the topic, how that knowledge is used to develop conceptual and mathematical models, and a listing of input parameters and their values.

5.2 Site Location and Topography

5.2.1 Regional Setting

Bechtel Nevada [1998a] has described the regional setting of the NTS as follows:

> The NTS is located in southern Nevada, approximately 105 km (65 mi) northwest of Las Vegas (see Figure 1-1). Approximately 3,500 km^2 (1,350 mi^2) of land is encompassed by the current site boundary. The combined area of the NTS and the surrounding Air Force-controlled land, referred to as the NTS-NAFR complex, is approximately 14,200 km^2 (5,480 mi^2). The NTS-NAFR complex is isolated further by U.S. Department of Interior-controlled land that surrounds much of the complex. Counties falling within an 80-km (50-mi) radius of the Area 5 RWMS include portions of Nye, Lincoln, and Clark Counties in Nevada; and Inyo County, California (Table 5-1).
>
> Las Vegas is the largest major metropolitan area near the NTS, with an estimated 1998 population of about 441,000 (U.S. Census Bureau [1999]). Other population centers surrounding the NTS-NAFR complex and their distances from the Area 5 RWMS are: Indian Springs (42 km [26 mi]), Lathrop Wells (52 km [32 mi]), Pahrump (80 km [50 mi]), Beatty (82 km [51 mi]), Alamo (96 km [60 mi]), Goldfield (165 km [103 mi]), Warm Springs (177 km [110 mi]), and Tonopah (195 km [121 mi]). The permanent settlement closest to the RWMS is Indian Springs.

Table 5-1. Estimated 1998 Populations in Vicinity of RWMS

County, State	Approximate Population [U.S. Census Bureau, 1999]
Clark, Nevada	1,200,000
Lincoln, Nevada	4,200
Nye, Nevada	29,000
Inyo, California	18,000

5.2.2 Topography

The local setting of the Area 5 RWMS is described by Bechtel Nevada [1998a] as follows:

> Mercury, a restricted access government facility that houses NTS administrative and support facilities, is located at the southeastern corner of the NTS. The Area 5 RWMS is located approximately 22 km (14 mi) north of Mercury, within the physiographic boundaries of Frenchman Flat. Frenchman Flat is an alluvium-filled closed basin in the southeast corner of the NTS (see Figure 1-2). Frenchman Flat playa, a dry lake bed at the physiographic low of the basin (939 m [3,080 ft]) above mean sea level), occupies approximately 14 km^2 (5 mi^2) and is perhaps the most prominent feature of the basin.
>
> The Area 5 RWMS is located in the northern region of Frenchman Flat at the juncture of three coalescing alluvial fan systems [Snyder et al., 1995]. The RWMS elevation ranges from 969 to 975 m (3,180 to 3,200 ft) above mean sea level. The RWMS is 3.8 km (2.4 mi) north of the playa and 30 to 36 m (98 to 120 ft) upslope of the playa.

5.3 Greater Confinement Disposal

GCD units are vertical boreholes drilled in the unsaturated desert alluvium. The boreholes are unlined and all but two are 3 m (10 ft) in diameter, with a total depth of 36 m (120 ft). Boreholes 1 and 2 are 3.6 m (12 ft) in diameter. Waste packages were placed in the bottom of the GCD boreholes to approximately 21 m (70 ft) below the land surface. The holes were then backfilled with native alluvium, although probertite was added to Boreholes 1, 2, and 3 after waste emplacement and before the backfilling. The backfill in all cases is not compacted. A 1.8-m (6-ft) tall concrete monument indicating the location and contents of the borehole is placed approximately 1.5 m (5 ft) below the surface in each hole. Figure 1-8 shows the design of a GCD borehole. Waste disposed of in GCD boreholes includes TRU waste, high-specific activity tritium waste, irradiated fuel rod cladding, and sealed sources. Wastes disposed since the inception of DOE Order 5820.2A contain only ^3H and depleted uranium.

GCD boreholes were used for the disposal of waste from 1983 through 1989 as described in Section 1.2. Thirteen GCD boreholes were developed (see Figure 1-7). Seven boreholes have been filled and operationally closed. Two GCD boreholes have received waste and remain open; four GCD boreholes are empty. Table 5-2 lists the GCD boreholes and their status.

Table 5-2. GCD Boreholes at the Area 5 RWMS [Chu and Bernard, 1991]

GCD Borehole	Disposal Area	Status
1	Classified	Closed, Full
2	Classified	Closed, Full
3	Classified	Closed, Full
4	Classified	Closed, Full
5	Unclassified	Closed, Full
6	Unclassified	Open, Full
7	Classified	Open, Full
8	Classified	Open, Empty
9	Unclassified	Open, Empty
10	Unclassified	Closed, Full
11	Unclassified	Open, Empty
12	Unclassified	Open, Empty
GCDT	Unclassified	Closed, Full

The PA analyses focused on the four GCD boreholes that contain TRU wastes: Boreholes 1, 2, 3, and 4 (see Figure 1-7). The TRU waste consists of various isotopes of Pu, U, and Am, along with their decay products. All radionuclides exist in the solid phase except for isotopes of radon (a progeny of U), which exist in the vapor phase. The inventory of TRU wastes is described in detail in Section 5.9.

5.4 Climate

The climate at the NTS has been described by Bechtel Nevada [1998a] as follows:

> The NTS lies within a region of the southwestern United States known for its arid intermontane deserts. Orographic lifting of humid Pacific air masses by coastal mountain ranges to the west causes a majority of the moisture destined for the continent to fall on the intercoastal mountain ranges before reaching the interior. The NTS lies in a region that is transitional between the Nevadan Desert and the Mojave Desert. The climate is characterized by a large number of cloudless days, low precipitation, and high daily temperatures, especially in the summer. Death Valley, California, the driest region of the country, lies approximately 80 km (50 mi) to the southwest of the NTS.

5.4.1 Precipitation

Annual precipitation over the NTS ranges from 8 to 25 cm (3 to 10 in.), depending on the elevation. Valley floors such as Frenchman Flat tend to be arid, while higher mountains such as Pahute Mesa are subhumid. The average annual precipitation in Frenchman Flat is approximately 10 cm (3.9 in.). Table 5-3 summarizes the monthly precipitation for a 30-year period from January 1963 through December 1993 at Well 5B in Area 5.

Table 5-3. Monthly Precipitation Frenchman Flat Well 5B (cm), 1964 –1999

Year	JAN	FEB	MAR	APR	MAY	JUN	JUL	AUG	SEP	OCT	NOV	DEC	YEAR
1964	-	-	0.76	1.24	0.23	0.69	0.30	1.68	-	0.18	0.36	-	5.44
1965	0.46	-	0.99	4.22	0.53	0.69	0.76	1.83	0.03	0.03	3.53	5.79	18.85
1966	0.41	0.79	0.15	0.18	0.41	0.08	1.45	0.03	0.53	-	0.03	1.68	5.72
1967	2.41	-	0.64	1.80	0.38	0.56	0.64	0.79	1.80	-	2.90	0.58	12.50
1968	0.23	1.24	0.08	0.56	-	0.43	2.18	0.10	-	0.71	0.36	0.20	6.10
1969	4.62	7.09	1.12	0.28	0.41	2.24	0.56	-	1.02	1.04	0.53	0.08	18.97
1970	0.05	2.03	0.71	0.76	-	0.05	-	1.35	-	-	1.55	0.71	7.21
1971	-	0.30	0.20	0.08	2.11	-	0.15	2.16	0.05	0.03	-	3.23	8.31
1972	-	-	-	0.18	0.08	2.29	0.03	0.99	1.52	1.93	2.62	-	9.63
1973	1.65	3.25	6.10	0.30	1.40	0.13	0.03	0.08	0.05	0.36	1.37	2.39	17.09
1974	3.35	0.05	0.23	-	-	-	4.14	-	-	1.93	0.20	3.30	13.21
1975	0.18	0.33	1.45	1.47	0.46	-	0.38	0.10	1.27	0.61	-	0.05	6.30
1976	-	3.33	0.10	0.66	1.04	-	1.75	-	2.57	2.87	-	0.03	12.34
1977	1.57	-	-	-	2.62	0.56	0.20	3.84	1.70	0.08	-	1.19	11.76
1978	4.90	5.64	4.90	1.27	0.13	-	-	-	0.05	0.53	3.23	1.50	22.15
1979	2.44	0.76	2.21	-	0.28	-	1.91	1.98	-	0.03	0.03	1.12	10.74
1980	3.43	2.79	3.66	0.38	0.58	0.15	2.16	-	0.48	0.05	-	-	13.69
1981	0.58	0.23	2.29	0.89	0.86	-	-	0.41	3.28	0.05	0.81	-	9.40
1982	0.79	1.02	4.29	0.97	2.06	0.30	1.68	2.13	2.57	0.53	1.57	0.79	18.69
1983	2.44	0.33	2.26	1.12	0.28	0.05	0.08	9.50	3.10	0.38	1.37	1.42	22.33
1984	-	0.41	-	0.13	0.13	-	6.65	6.43	0.25	0.69	3.18	5.69	23.55
1985	1.37	0.13	0.25	0.03	0.18	0.28	2.72	-	0.58	0.61	1.70	0.48	8.33
1986	3.05	0.86	2.21	0.25	0.81	-	1.40	2.57	0.08	1.22	1.65	1.07	15.16
1987	2.08	0.56	0.61	1.14	5.00	0.18	1.80	0.81	-	2.49	1.37	1.75	17.81
1988	3.40	0.66	-	3.86	0.51	0.25	0.08	1.47	0.18	0.05	0.28	0.33	11.07
1989	0.61	0.61	0.30	-	0.41	0.05	-	0.76	0.05	0.10	-	-	2.90
1990	1.50	0.36	0.25	0.56	0.97	0.23	1.24	0.86	0.84	0.03	1.14	0.05	8.03
1991	0.56	1.40	3.05	-	0.23	0.20	0.25	0.41	1.40	0.43	0.05	1.35	9.32
1992	0.81	3.33	3.84	0.05	0.76	-	0.58	0.10	-	1.88	-	2.74	14.10
1993	5.03	6.81	1.40	0.03	-	0.25	-	0.64	-	0.51	0.91	1.14	16.71
1994	0.61	1.78	1.04	1.09	0.25	-	0.64	0.43	0.38	-	0.69	3.86	10.77
1995	6.12	1.63	3.91	1.17	1.85	0.13	0.33	0.43	-	-	-	0.08	15.65
1996	0.30	0.94	0.41	0.25	0.18	0.30	0.18	0.25	-	1.52	1.47	1.19	7.01
1997	1.40	0.15	-	-	-	1.91	0.46	-	3.30	0.10	1.37	0.74	9.42
1998	0.74	9.63	2.57	1.45	0.51	4.01	1.78	1.45	1.35	0.41	0.69	-	24.56
1999	0.61	0.18	0.30	3.99	0.66	0.36	1.55	-	1.96	-	-	-	9.60
Mean	1.86	1.89	1.69	1.01	0.85	0.65	1.23	1.56	1.17	0.71	1.29	1.54	12.62
Max	6.12	9.63	6.10	4.22	5.00	4.01	6.65	9.50	3.30	2.87	3.53	5.79	24.56
Min	-	-	-	-	-	-	-	-	-	-	-	-	2.90
Stdev	1.66	2.30	1.63	1.10	0.98	0.84	1.36	1.93	1.06	0.77	1.05	1.52	5.61

"-" indicates zero precipitation

Rainfall varies markedly with the seasons as well as with elevation. The majority of rain falls during two seasons, with a larger peak in the winter and a smaller one occurring during the summer months. This bi-modal precipitation pattern results from two distinctive global weather patterns that develop during the summer and winter. During the summer, the lower Great Basin experiences frequent intrusions of warm moist tropical air, due to the formation of a high-pressure ridge located over the southern United States and northern Mexico. It has been widely accepted that the clockwise rotation of the air mass brings warm moist air up from the Gulf of Mexico to create a "summer monsoon season," characterized by local high-intensity thunderstorm activity of relatively short duration [Bryson and Lowry, 1955; Green and Sellers, 1964; Jurwitz, 1953; French, 1985]. Additional investigation by Hales [1974] reveals that much of this summer moisture may be credited to moisture driven up from the Pacific Ocean by way of the Gulf of California. Precipitation during the winter months is governed by the formation of a high-pressure ridge in the Pacific and an accompanying low-pressure cell in the Gulf of Alaska, known as the Aleutian low. This combination often forces cold, wet air masses from the Pacific Northwest over the Great Basin and Rocky Mountains. Although these storms are less intense than their summer counterparts, they are often longer in duration and they account for most of the annual moisture at the NTS. Snowfall is frequently observed at elevations greater than approximately 1,675 m (5,495 ft), but is rarely observed at the RWMS.

5.4.2 Temperature

NTS air temperatures vary widely with the seasons. Average daily temperatures range from 2EC (35EF) in January to 24EC (75EF) in August. Large daily fluctuations are common, especially on the playas and valley floors. Typical daily temperature ranges for the Area 5 RWMS run from !3E to 12EC (27E to 54EF) in January, and from 17E to 36EC (63E to 97EF) in July [Magnuson et al., 1992].

5.4.3 Evaporation

Due to the exposure of the ground surface to high levels of incident solar radiation and wind, the pan evaporation rate at the NTS is very high. The estimated *annual* pan evaporation rate ranges from a minimum of 93 cm (37 in.) in January to a maximum of 595 cm (243 in.) in July, with an average of approximately 310 cm (122 in.), as measured by REECo on Frenchman Flat (1956–1958) and Jackass Flats (1967–1969) [Magnuson et al., 1992].

5.4.4 Wind

Three major effects influence wind direction on the NTS: (1) large-scale movement of global pressure systems, (2) intermediate orographic effects due to regional mountain ranges, and (3) localized small-scale convection currents due to nearby topography and terrain [Quiring, 1968]. Northern winds tend to dominate in the winter and southern winds in the summer. Localized differential heating of the land surface during the day, coupled with a topographic trend toward greater

elevation in the northern section of the NTS, result in southern winds flowing upslope during the day and northern winds moving downslope at night.

Wind speeds tend to be greater in the spring than in the fall. Because surface vegetation is sparse in the area, surface wind speed is categorized as calm only 2% of the time. Over a 30-year period, winds have most often originated out of the southwest [Bechtel Nevada, 1998a].

5.5 Geology

The following sections discuss the geology of the NTS as presented by Bechtel Nevada [1998a].

5.5.1 Regional Setting

The geology of the NTS consists of a thick section (more than 10,600 m [34,780 ft]) of Paleozoic and older sedimentary rocks, locally intrusive Cretaceous granitic rocks, a variable assemblage of Miocene volcanic rocks, and locally thick deposits of postvolcanic sands and gravels that fill the present-day valleys [Frizzell and Shulters, 1990]. Figure 5-1 is a generalized geologic map of the NTS. More detailed stratigraphic information is available from recently updated maps of the NTS [Frizzell and Shulters, 1990]. A summary of the general stratigraphy beneath the NTS, including lithologies and mode of emplacement, appears in Appendix C.

The NTS and surrounding areas are in the southern part of the Great Basin, the northernmost subprovince of the Basin and Range Physiographic Province. The Basin and Range Province is generally characterized by more or less regularly spaced, generally north-south trending mountain ranges separated by alluvial basins that were formed by faulting. The Great Basin subprovince is an internally drained basin; i.e., precipitation that falls over the basin has no outlet to the Pacific Ocean.

The topography of the eastern and southern NTS is typical of the Great Basin, with numerous north-south trending mountain ranges and intervening alluvial basins. In the northwest portion of the NTS, the physiography is dominated by the volcanic highlands of the Pahute and Rainier Mesas. There are three primary valleys on the NTS: Yucca Flat, Frenchman Flat, and Jackass Flats. Both Yucca and Frenchman Flats are topographically closed, with playas in the lowest portion of each basin. Jackass Flats is topographically open, with drainage via Fortymile Wash off the NTS.

5.5.2 Local Setting

Frenchman Flat is an intermontane basin typical of basin-and-range structure. The alluvium- and tuff-filled valley is rimmed mainly by Proterozoic and Paleozoic sedimentary rocks and Cenozoic volcanic rocks. Frenchman Flat is bounded by

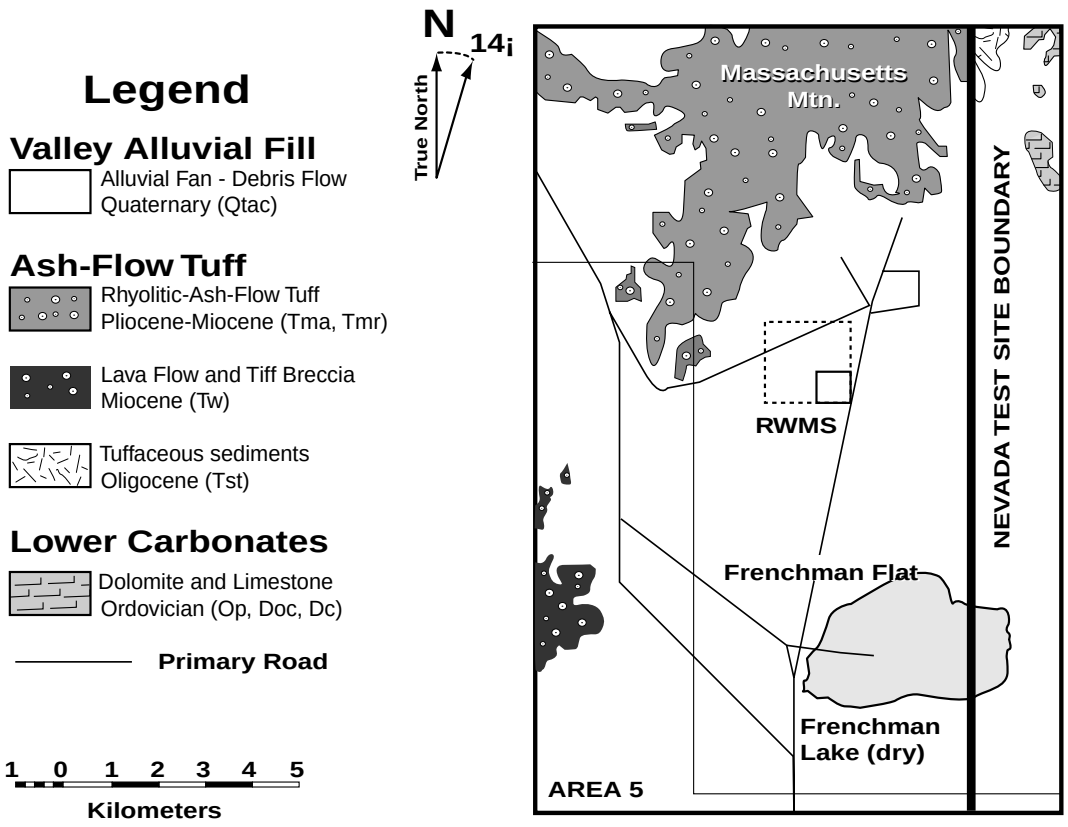

Figure 5-1. Surficial Geology of the Frenchman Flat Basin in the Vicinity of the Area 5 RWMS [Bechtel Nevada, 1998a].

the Halfpint Range to the north, the Ranger Mountains and the Buried Hills to the east-southeast, Mount Salyer to the west, and Mercury Ridge and Red Mountain to the south (Figure 5-2). It ranges in elevation from approximately 1,600 m (5,250 ft) above mean sea level in the surrounding mountain ranges to 939 m (3,080 ft) at Frenchman Flat Lake, a playa lake at the lowest point of the basin. The basin drains a 1,200 km^2 (460 mi^2) watershed.

Proterozoic and Paleozoic rocks are extensive and occur under Frenchman Flat as basement rocks. In the lowlands areas of the basin, the basement rock units are overlain with alluvium and volcanic and Tertiary sedimentary rocks. The infilling alluvium is 910 m (3,000 ft) deep at its maximum thickness. On the alluvial fans, the alluvium comprises interbedded gravel, sand, and silt with varying degrees of cementation. These coarse-grained deposits grade to the predominantly clayey silt deposits of the playa. Limited areas of wind-blown sand and silt are also present in portions of the lowland areas.

To the northwest and southeast, thrust faulting causes the exposure of repeated sections of the Paleozoic and Precambrian rocks, and low-angle gravity faulting has created isolated blocks of the Paleozoic rocks out of stratigraphic order.

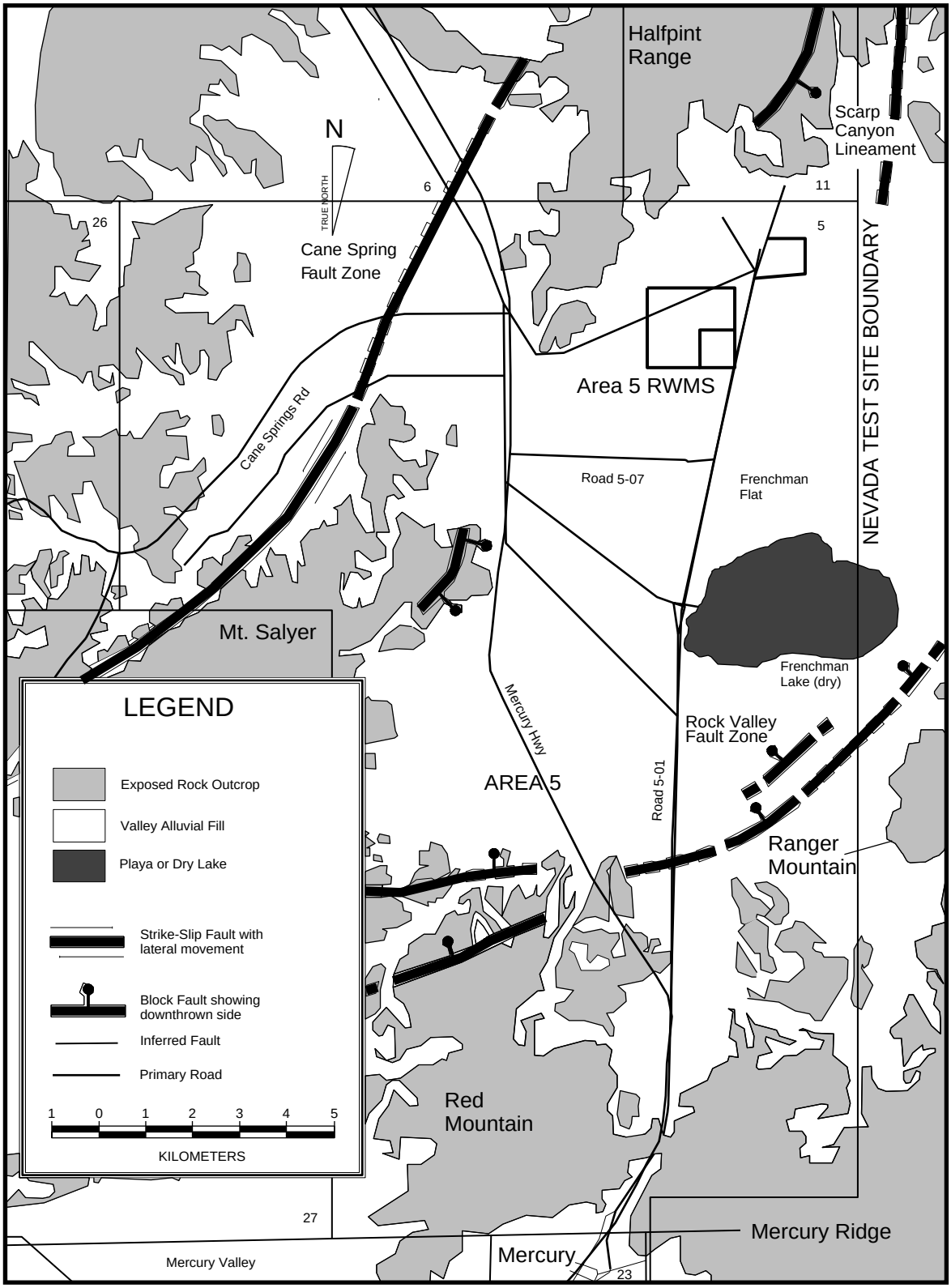

Figure 5-2. Map Showing the Major Structural Features of the Frenchman Flat Basin in the Vicinity of the Area 5 RWMS.

Today, most prominent structures are related to basin-and-range extensional faulting that is younger than the volcanic rocks. In southern Frenchman Flat, fault strike mostly east-northeast with a significant strike-slip component of displacement. In northern Frenchman Flat, fault strike north-northeast with dominantly dip-slip normal faults.

Outflow sheets of ash-flow tuffs from the volcanic centers west and northwest of the basin occurred during the Tertiary Period. The youngest sediments of the valley are sand and gravel, derived from the volcanic and sedimentary rocks in the surrounding highlands.

5.5.2.1 Potential for Seismic Activity [Bechtel Nevada, 1998a]

Rogers et al. [1977], Campbell [1980], Battis [1978], and Hannon and McKague [1975] have conducted seismic hazard studies of the NTS. They agree that the predicted maximum magnitude for an earthquake ranges from 5.8 to 7.0, with peak accelerations of 0.7 to 0.9 g. The estimated return period for the largest amplitude earthquakes expected (5.8 to 7.0) ranges from 12,700 to 15,000 years. These data suggest that there is the potential for a large earthquake somewhere within the NTS during the next 10,000 to 15,000 years.

The probability of the occurrence of at least one earthquake greater than 6.8 on the Richter scale is estimated in Appendix C. These calculations suggest there is about a 54% chance of one or more earthquakes greater than 6.8 in the next 10,000 years.

In August 1971, an earthquake of magnitude 4.3 occurred along the Cane Spring fault zone approximately 7.2 km (4.5 mi) northwest of the RWMS. An earthquake of 4.5 magnitude occurred in February 1973 along the Rock Valley fault system, approximately 7.2 km (4.5 mi) southwest of the RWMS. No surface displacement was associated with these two earthquakes. In 1999, earthquakes ranging from 2.7 to 4.8 occurred along the Frenchman Flat section of the Rock Valley Fault.

Despite the moderate risk of seismic activity, the limited use of engineered structures at Area 5 RWMS makes the site intrinsically less prone to significant earthquake damage than an aboveground facility or a facility using engineered belowground vaults. Because the GCD boreholes are or will be backfilled with alluvium, a major earthquake centered on the Area 5 RWMS is expected to result in only limited compaction, caused by the consolidation of alluvium. Given the large return times associated with the largest events, coupled with the small likelihood that an event would be centered upon the Area 5 RWMS, it is unlikely that the integrity of the RWMS would be significantly compromised by seismic activity. [Modified from Bechtel Nevada, 1998a]

5.5.2.2 Potential for Volcanism

Studies focused primarily on the southwest NTS region are ongoing to assess the hazards of future volcanism for the Yucca Mountain Project [Perry et al., 1998]. Silicic volcanic centers nearest the RWMS include the Miocene-age Wahmonie-Salyer Center of rhyodacite to rhyolite composition, located 20 km (12 mi) west-southwest of the Area 5 RWMS. The closest basaltic volcanic centers include the basalt of Paiute Ridge (8.5 Ma), located about 26 km (16 mi) north-northeast of the RWMS [Crowe et al., 1983], the basalt of Scarp Canyon (8.7 Ma) located about 6 km (4 mi) northeast of the RWMS [Perry et al., 1998], and the basalt of Nye Canyon (7.2 Ma) located about 5 km (3 mi) east-northeast of the RWMS [Perry et al., 1998]. Basaltic volcanic rocks intersected in a drillhole in alluvium beneath Frenchman Flat [Carr, 1984] a few kilometers northeast of the RWMS have been dated at 8.6 Ma and are probably correlative with the basalt of Scarp Canyon [Perry et al., 1998].

Data concerning the hazards of future volcanism in the NTS region have been acquired from ongoing assessments of the volcanic hazard at Yucca Mountain. These data have been used to assess the potential for renewed volcanic activity in Appendix C. This analysis indicates that volcanism is unlikely to have a negative impact on the integrity of the Area 5 RWMS over the next 10,000 years, and may have a positive impact. Lava or ash flows could enhance the performance of the site, particularly from the view of inhibiting inadvertent intrusion.

5.5.3 Near-Surface Observations of Alluvial Sediments

The near-surface stratigraphy of alluvial sediments has been studied in detail to a depth of approximately 11 m (36 ft) [Raytheon Services Nevada, 1991; Snyder et al., 1993]. The near-surface structure displays features expected for lower-middle to distal alluvial fan deposition, including sheet-flood, stream channel, and debris flows. A grain-size analysis reveals alternating sequences of fine- and coarse-grained sediments, with occasional lenses of very coarse stream channel deposits [Raytheon Services Nevada, 1991]. All of the deposits are unconsolidated and were caused by water-based deposition. The debris is composed predominantly of pyroclastic tuff clasts with lesser amounts (averaging 5 to 10%) of nonvolcanic clasts. The lithology of the deposits, combined with paleoflow estimates, suggests that deposition was from the north or northeast; e.g. the Scarp Canyon and Nye Canyon watersheds are the source for most of the sediments.

Some accumulation of calcium carbonate, in the B and BC horizons as coatings on clasts and with pendants of pebbles and sand beneath, indicates repeated periods of surface stability in the Quaternary.

5.5.3.1 Chemical Composition of the Alluvial Sediments

The composition of sediments may be useful in determining the history of lithification and the source of sediments. Additionally, it provides insight into the potential for contaminants to be retarded through interactions with mineral surfaces. A complete analysis of elemental and oxide composition was performed on samples collected from the Pilot Wells and Science Trench Boreholes [REECo, 1993a,b]. Overall, the elemental composition of minerals and total oxide concentrations of the sediments remain fairly constant with depth. The alluvium has a composition of approximately 65% SiO_2 and 13% Al_2O_3. Very little clay was apparent in the samples.

Inorganic and organic carbon analyses were performed to help identify soil layers that might affect movement of chemical contaminants. Organic carbon can enhance the transport of some inorganic carbon species. Inorganic carbon measurements may also assist in the identification of caliche or variably cemented carbonate layers which, with their extremely low porosities and hydraulic conductivities, can greatly hinder the movement of water within the soil. Inorganic carbon concentrations were less than 1% by weight and nearly constant throughout the entire thickness of sampled alluvium [REECo, 1993a,b]. Only a small increase was found in a 3-m (10-ft) interval from 167.6 to 170.7 m (550 to 560 ft) below the surface in Pilot Well UE5PW-2. This increase was accompanied by elevated levels of chloride, bromide, and sulfate as well. This isolated occurrence may indicate some degree of carbonate cementation at depth. However, any calcium carbonate accumulation at depth is expected to be discontinuous and does not have a significant impact on groundwater flow. Organic carbon concentrations were generally an order of magnitude smaller than those of inorganic carbon.

5.5.3.2 Particle Size Analysis

Particle size distribution can influence the hydraulic conductivity of porous media and reflects the uniformity of an aquifer material. Particle size analysis by both the wet and dry sieve methods were performed on drill cuttings and core samples from all three Pilot Wells [REECo, 1993a] (Figure 5-3). The particle size analysis was limited to material less than the size of the core diameter (e.g., cobbles or boulders larger than approximately 0.09 m [0.3 ft] are not recovered in core samples).

Interpretation of the vertical distribution of gravel, sand, and fines within the three Pilot Wells varies according to hydrologic or geologic perspective. Although the sediment contains variable assemblages of grain sizes, and is therefore considered geologically heterogeneous, the variability does not significantly affect groundwater flow; thus, it is considered hydrologically homogeneous. UE5PW-1 displays a general fining upward sequence until approximately 40 m (130 ft) below the surface, where a coarsening upward sequence begins and continues to the surface. UE5PW-2 appears to have two fining upward sequences, one from

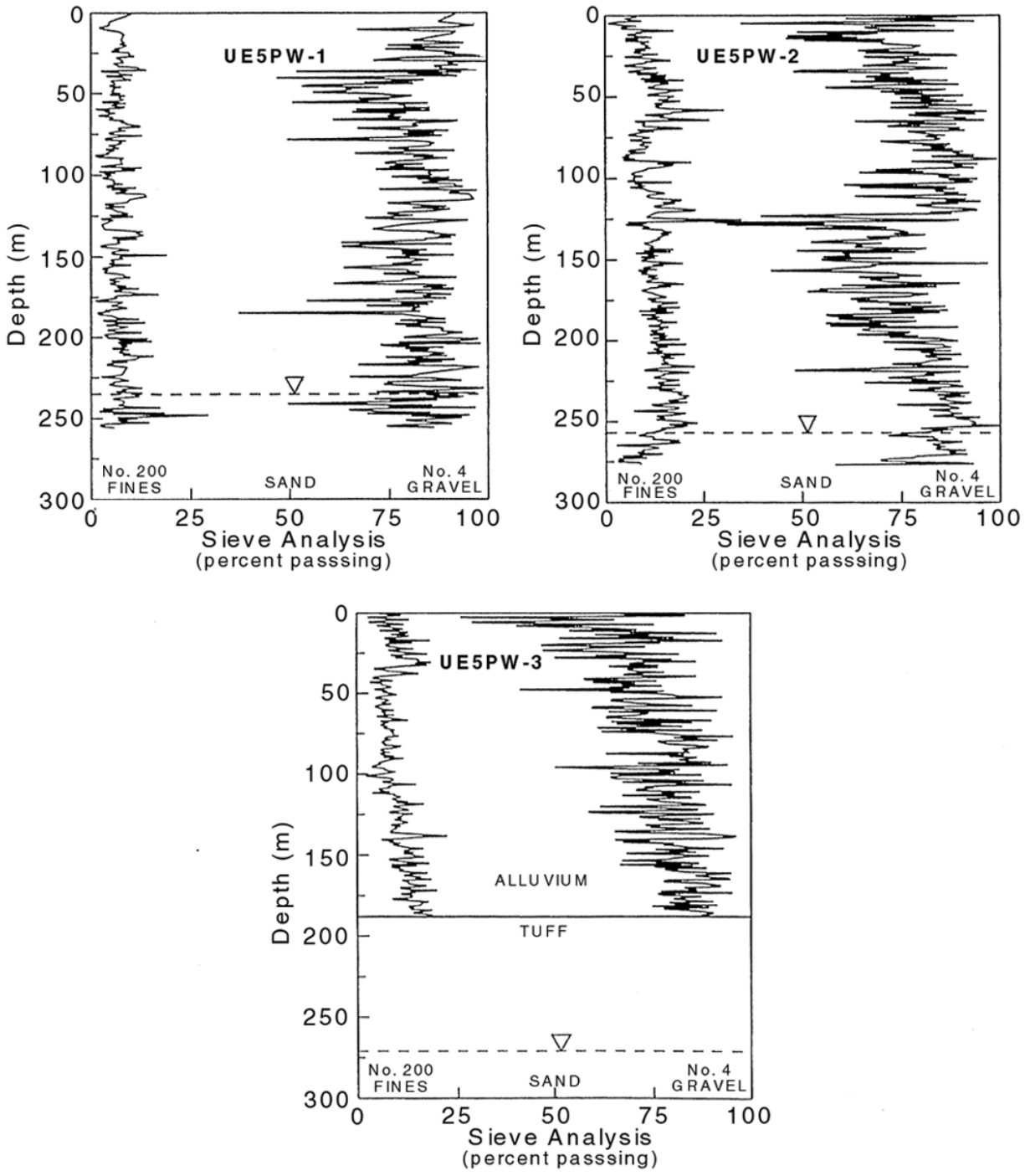

Figure 5-3. Depth Profile for the Grain-Size Distribution (Unified Soil Classification System) in the Three Pilot Wells [REECo, 1993a].

125 m (410 ft) to the surface, and another from 250 to 125 m (825 to 410 ft). UE5PW-3 has an overall fining upward sequence interrupted by a coarse section from approximately 75 to 85 m (246 to 279 ft) below the surface. In a gross sense, with the exception of the finer sections of UE5PW-2, the profiles are predominantly coarse sand and gravel with accessory silt and clay. Table 5-4 shows the relative percent of materials falling into the gravel, sand, and silt/clay size fractions, which were determined from analyses on 2,100 core samples at 0.76-m (2.5-ft) intervals from the Science Trench Boreholes [REECo, 1993b].

Table 5-4. Summary of the Mean Particle Size Fraction in the Alluvium as Sampled From the Science Trench Boreholes [Bechtel Nevada, 1998a]

Particle Size Fraction of Alluvium†										
Borehole Number	Mean Percent Passing Indicated Sieve Size									
	Gravel			Sands						Fines
	3/4	3/8	4	6	10	16	40	70	140	200
UE5ST-1	95.8	91.0	85.4	80.2	73.9	67.5	50.7	30.3	12.2	7.8
UE5ST-2A	98.6	94.3	86.8	81.9	75.5	68.4	51.7	32.8	13.4	8.5
UE5ST-2	96.0	91.1	84.4	79.2	72.8	66.5	51.1	32.4	13.3	8.5
UE5ST-4	94.1	89.6	84.5	80.2	74.9	69.2	54.3	35.2	15.1	9.6
UE5ST-5	98.5	96.0	88.7	84.8	80.5	74.3	53.7	32.1	14.2	10.2
UE5ST-6	94.6	88.2	82.4	78.0	73.2	67.3	50.1	29.9	12.5	8.1
UE5ST-7	94.5	89.1	83.3	78.0	72.4	66.1	47.8	29.6	9.9	5.0
Gross Mean	96.0	91.3	85.1	80.3	74.7	68.5	51.3	31.8	12.9	8.4

† Measured from 2,100 samples, Science Trench Borehole Project - REECo [1993b].

The alluvium composition was estimated to be 20% gravel, 70% sand, and less than 8.5% silt/clay using the Unified Soil Classification System [ASTM, 1990].

Using this classification, the grain-size distribution of the alluvium is classified as a well-graded sand with silt and gravel. The USDA [USDA, 1993] textural class is gravelly sand/loamy sand. The silt- and clay-sized fraction is composed primarily of silt rather than clay according to analysis by hydrometer. Individual particle density analyses on samples from the Science Trench Boreholes yielded a mean particle density (ρ_s) of 2.55 g cm^{-3} [REECo, 1993b].

5.5.3.3 Dry Bulk Density

The distribution of dry bulk density was estimated from 318 measurements of dry bulk density of Area 5 alluvium. The data were obtained from pilot wells Ue5PW-1, Ue5PW-2, and Ue5PW-3 [REECo, 1993a] and science trench boreholes Ue5ST-1, Ue5ST-2A, Ue5ST-2, Ue5ST-4, Ue5ST-5, Ue5ST-6, and Ue5ST-7 [REECo, 1993b].

The values of dry bulk density obtained from the pilot wells and science trench boreholes represent a relatively small volume of soil compared to the volume of soil modeled in the PA. Because of the difference between the scale at which the data were collected and the model scale, the average of a large number of observations at a single pilot well or borehole is assumed to be an appropriate value for the model. Each pilot well or borehole is assumed to be equally likely to represent the alluvium modeled in the PA, and the estimates from each borehole are assumed to be independent, and so are assigned an equal probability. For a given pilot well or borehole, individual dry bulk density measurements are assumed to be independent samples from a normal distribution. Table 5-5 provides summary statistics for the data obtained from the ten pilot wells and boreholes.

Figure 5-4 shows empirical distributions of dry bulk density created from individual measurements, along with the "effective" distribution created to represent dry bulk density in the model. The "effective" distribution is a normal distribution with a mean of 1600 kg/m^3, which is the average of the ten mean values given in Table 5-5, and a standard deviation of 109 kg/m^3, which is the average of the ten standard deviations given in Table 5-5. The individual measurements have a greater spread than the "effective" distribution because the individual measurements reflect small-scale spatial variability, while the model parameter reflects possible average (or effective) values over this small-scale variability.

5.5.4 Site Stability

The Basin and Range physiographic province, with its north-south trending mountain ranges and alluvial-filled basins, has been developing for over 30 million years [Winograd and Thordarson, 1975]. The actual age of the Frenchman Flat basin is unknown; however, the Frenchman Flat basin has been filling with alluvium for over 8 million years. Drillholes UE-5i and UE-5k encountered alluvial fill from the land surface to about 290 m (950 ft), depth at the Area 5 RWMS. At 290 m (950 ft), a layer of basalt was encountered. The basalt has been dated as

Table 5-5. Summary Statistics for Dry Bulk Density (kg/m^3)

Pilot Well/Borehole	Number of Observations	Mean	Standard Deviation
Ue5PW-1	76	1640	148
Ue5PW-2	34	1640	140
Ue5PW-3	23	1660	159
Ue5ST-1	41	1570	126
Ue5ST-2A	6	1600	91.2
Ue5ST-2	45	1540	88.0
Ue5ST-4	53	1520	56.5
Ue5ST-5	10	1620	96.0
Ue5ST-6	19	1580	73.8
Ue5ST-7	11	1600	116

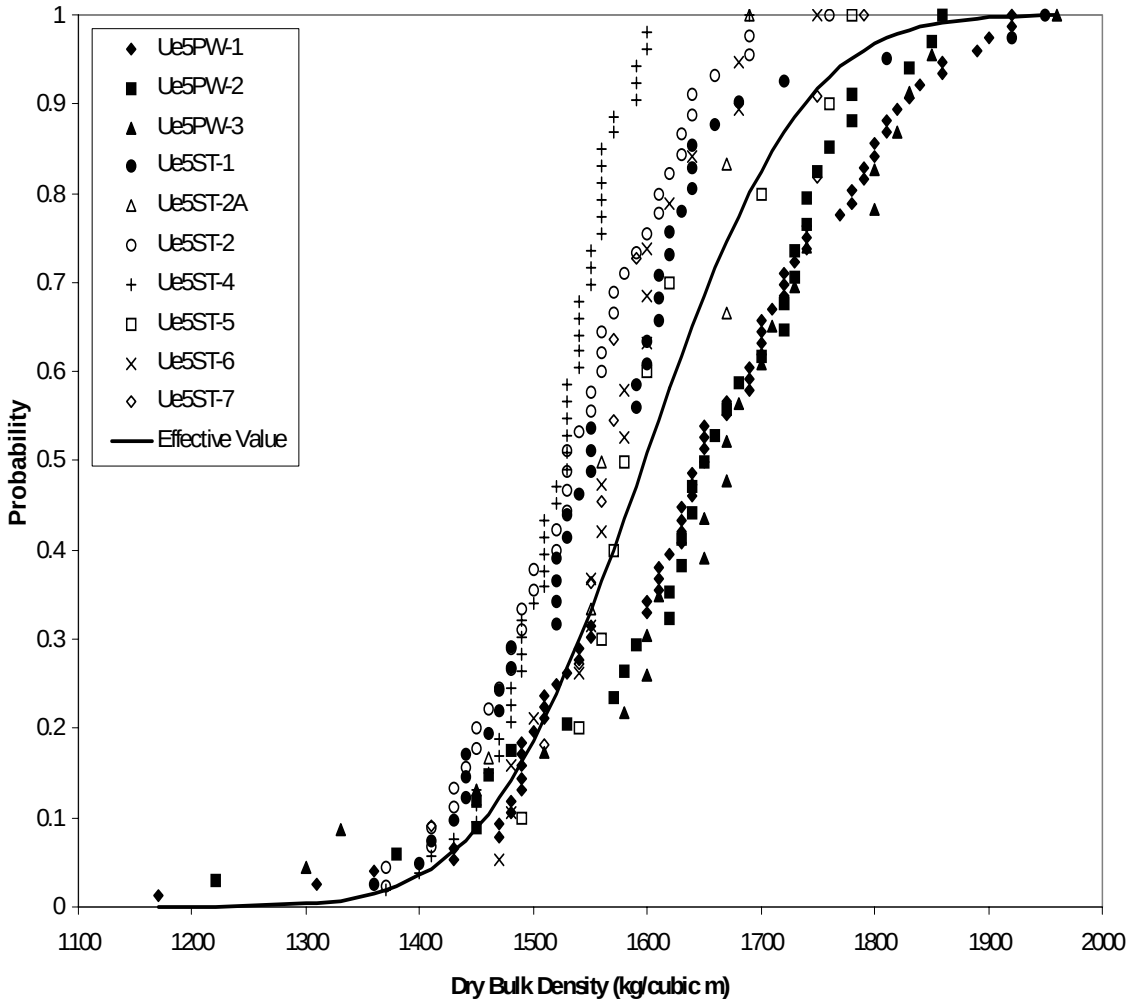

Figure 5-4. Distributions of Dry Bulk Density and Effective Dry Bulk Density.

being between 8.4 and 8.6 million years old. Therefore, this geologic environment (i.e., a basin filling with alluvium) has been in existence for more than 8 million years.

Computations based on the age and depth of this lava flow would indicate that the average aggradation rate has been 3.3 cm (1.3 in.) per 1000 years at Area 5 RWMS. Shott et al. [1998] reviews a number of other studies that conclude that the average rates of alluvial aggradation may range from 3.3 to 17 cm (1.3 to 6.7 in.) per 1,000 years. Given these very slow rates of aggradation, the land surface may be very stable, which has been confirmed by other studies. Some of the arroyos (alluvial channels) are currently active; however, many of the areas between the alluvial channels (the interfluve areas) have been unchanged for 5,000 to 10,000 years. To put this in perspective, all human civilizations have developed since these older interfluvial surfaces were deposited.

Trench and pit wall mapping in Area 5 found maximum depth of arroyo incision in the vicinity of the RWMS to be less than 1.5 m (5 ft). Based on these data, it is unlikely that natural geomor-

phic processes will result in erosion to a depth of more than approximately 2 m (7 ft) at the facility within the 10,000-year regulatory period [Snyder et al., 1995].

Faulting in the vicinity of the Area 5 RWMS is evidenced by seismic events measured along the Cane Spring fault at the western margin of the Frenchman Flat basin and the Rock Valley fault at its southern margin. Earthquakes in the vicinity of the Area 5 RWMS are not expected to have an adverse effect on the GCD wastes because the wastes are located in unconsolidated alluvium.

There is a very low likelihood of disruption by future basaltic volcanic activity at the Area 5 RWMS. Two lines of evidence support this inference. First, the location of eruptive vents for post-Miocene basaltic activity in the NTS shows a pattern of episodic, but progressive southwestward migration of sites of basaltic volcanic activity [Crowe and Perry, 1989; Crowe 1990; Crowe et al., 1998]. All sites of Quaternary basaltic volcanism (less than 1.6 million years ago) occur west of the western boundary of the NTS (see Appendix C, Figure C-2) at considerable distances from the RWMS. Second, Crowe et al. [1998] calculated disruption probabilities for the recurrence rate of small volume basaltic volcanic centers within relatively inactive areas (distant from sites of Quaternary volcanism) in the southern Great Basin. This calculation applies to the Area 5 RWMS in Frenchman Flat. They estimated, using regional counts of Quaternary volcanic events, the probability of disruption of a 6-km^2 (2.3-mi^2) site in an inactive area of the southern Great Basin to be about 10^{-9} per year. This estimate is an order of magnitude smaller than the 1 in 10,000 in 10,000 years probability-screening criteria used in 40 CFR 191 and allows elimination of volcanism as an issue for the RWMS.

The Area 5 RWMS, location of the GCD boreholes, has been a stable area with respect to geomorphic and volcanic processes for hundreds of thousands of years or more, well beyond the scale of the regulatory period of 10,000 years. While there is ongoing tectonic activity in the vicinity of the Area 5 RWMS, there is no expected consequence to the GCD site from seismic events due to its location in unconsolidated alluvium. From all studies, the location of the GCD boreholes appears to have been well-chosen for the purpose of waste disposal.

5.6 Hydrology

5.6.1 Surface Water Hydrology

Frenchman Flat and the NTS lie within the geographic area/climatic zone known as the "Great Basin," an arid to semi-arid region dominated by basin and range topography that covers most of Nevada and parts of adjacent states. Average annual precipitation within the valleys ranges between 7.5 and 15 cm (3.0 and 5.9 in.), while the ridges generally receive less than 25 cm (10 in.). At the Area 5 RWMS, mean annual precipitation is 12.6 cm (4.96 in.) Potential evaporation, which ranges from 152 to 208 cm (60 to 82 in.), greatly exceeds the annual rainfall. Surface water hydrology in this region is primarily ephemeral, meaning that watercourses flow only in response to rainfall and lose water along their course, rather than gaining it. The precipitation in this region is highly variable, both temporally and geographically, and is associated with two distinct weather patterns. Winter frontal storms associated with Pacific air masses that move from west to east provide about half the annual precipitation. Late summer thunderstorms provide the other half of the annual precipitation.

Frenchman Flat is a closed basin; that is, runoff generated in the basin flows to the center of the basin—there are no outlets. Rainfall on the surrounding mountain ranges may result in runoff if the intensity and duration of the storm is sufficient, but flood events are rare. Much of the runoff from these events will infiltrate into the coarse material that forms the alluvial fans at the foot of the mountain ranges. An analysis of the frequency and magnitude of floods that could potentially affecting Area 5 RWMS for the next 10,000 years is presented in Section 6.6.4.

5.6.2 The Vadose Zone

The disposal of radioactive wastes in thick alluvial unsaturated zones of arid regions has long been proposed (e.g., Winograd, 1981). The presumption of a very low rate of fluid movement provided confidence that radionuclides disposed of in arid alluvium would not migrate to the accessible environment. In the vicinity of the GCD boreholes, the vadose zone is approximately 235 m (770 ft) thick. It is comprised of alluvial deposits of unconsolidated gravelly sand with laterally discontinuous heterogeneities in the form of alternating fine- and coarse-grained layers that owe their existence to sheet flood and paleosol deposits (Figures 1-4 and 1-10). Annual precipitation is low, evapotranspiration is high, and infiltration under the current climatic conditions is limited to the upper 2 m (7 ft) of the profile.

The radionuclides disposed of in GCD boreholes and their decay products exist in the solid phase. (The one exception is radon; it exists in the gas phase and is discussed in Section 5.1.1.) While these wastes are somewhat soluble in water, dissolution is limited by low waste solubilities (discussed in Section 5.10) and the limited availability of water in the vadose zone. Barring intrusion, waste migration from the zone of disposal is limited to transport in the water phase. Moreover, as radionuclides move, their migration is impeded by sorption onto soil particles (discussed in Section 5.12).

Regulations governing waste migration in the vadose zone typically focus on limiting migration to an underlying aquifer. For radionuclides that reach the water table within 1000 years, concentrations in the aquifer are compared to the allowable limits in the GWPRs of 40 CFR 191.16. Also, radionuclides that reach the water table can potentially be extracted by a water well and ingested by an MOP, resulting in doses that are governed by the IPRs of 40 CFR 191.15. (This portion of the regulation is also operative for 1000 years.) In addition, radionuclides that reach the water table can be transported through the saturated zone to the accessible environment. The CRs of 40 CFR 191.13 consider integrated discharge to the accessible environment over a compliance period of 10,000 years. As described in detail below and in Section 6.4, inferences from extensive characterization of vadose zone conditions at the site demonstrate that:

- Water does not move downward under current climatic conditions in the portion of the vadose zone where the waste is disposed;

- It is extremely unlikely that a change to a more humid climate would be sufficient to result in recharging water carrying radionuclides to the water table within the 10,000-year compliance period; and,

- Even assuming an immediate climate change and landfill subsidence, calculations presented in Appendix B demonstrate that the site would still comply.

At the GCD site, upward radionuclide migration to the land surface is of far greater concern. The land surface is much closer to the waste disposal zone (21 m [70 ft]) than to the water table (almost 200 m [656 ft]) and the land surface also represents the accessible environment as defined by the CRs. At the land surface, radionuclides become accessible to human receptors and subsequent doses must be addressed via the IPRs. Transport mechanisms for this relatively short pathway from the waste to the land surface are advection, diffusion, bioturbation, and plant uptake.

5.6.2.1 Current Hydrologic Conditions

The GCD boreholes are located in one of the most arid portions of the U.S., with an average precipitation of 13 cm (5 in.) per year. The limited precipitation coupled with generally warm temperatures and low humidities results in a hydrologic system dominated by evapotranspiration.

Much effort has gone into measuring hydraulic properties of the vadose zone alluvium and in measuring concentrations of chemical species (mostly isotopes) that track the movement of water. The purpose of collecting this data was to elucidate attributes and significant processes of the hydrologic system regarding the suitability of the site for waste disposal. Data can be found in the following reports: Davis [1992], REECo [1993a,b,c], Blout et al. [1995], and Tyler et al. [1999].

The hydraulic properties for permeability and moisture retention have been shown to vary spatially as a function of textural variation from one lithologic unit to the next [Davis, 1992; McCord et al., 1997]. However, these properties can be considered homogeneous, because there appears to be no significant trends either laterally or with depth within a local region [Sully et al., 1993].

Volumetric water contents throughout the vadose zone are very small, ranging from about 5% to about 15% below about 2 m (7 ft) from the ground surface, showing an increasing trend with depth in the upper 35 m (115 ft). Very near the ground surface they can be as low as 1% to 3%. The overall average moisture content at depths beneath 35 m (115 ft) is less than 10%. With an average porosity of about 30%, water fills less than one third of the void space.

<u>The Hydrologically Dynamic Zone</u>

The near surface zone is the hydrologically dynamic region of the unsaturated arid alluvium. In this zone, hydraulic gradients are upward and very strong under the influence of high evaporative demand at the surface. However, the gradients are reversed under episodic infiltration events. The infiltrating water is cycled back to the atmosphere soon after the cessation of infiltration. This is a hydrologically active zone supporting plant life, whose transpiration plays a significant role in cycling water back to the atmosphere. Based on field studies [REECo, 1993a,b; Blout et al., 1995; Levitt et al., 1998], the balance of cycling between infiltration and evapotranspiration is such that approximately the upper 2 m (7 ft) is hydrologically active, and areally distributed

infiltration never infiltrates deeper than about 2 m (7 ft). The *average* volumetric moisture content in the near surface zone is very low, with values ranging from 1% to 3%.

Figure 5-5 provides a schematic diagram describing near-surface processes. The vast majority of roots are found near the land surface to capture transient water infiltration, as described in Section 5.6. Roots provide a major dietary component of burrowing animals and feeding tunnels exist at the same shallow depths as the roots (see Section 5.7). Between infiltration events, water contents are low, due to evaporation and efficient extraction by plants. The pulse of relatively high water content in Figure 5-5 depicts the shallow depth of intermittent infiltration following precipitation prior to extraction by evapotranspiration. Water-soluble constituents, such as chloride, are carried downward by infiltrating moisture, only to be deposited above the 2 m (7 ft) depth, as the infiltrating moisture is removed by evaporation and plant uptake. This process (1) moves water-soluble constituents toward the lower boundary of the near surface zone, and (2) provides a marker of the depth of infiltration. For example, analysis of chlorine-36 from near-surface soils in the vicinity has shown chlorine-36 from nuclear weapons testing to be restricted to the upper 2 m (7 ft) of the soil profile. The peak of the chlorine-36 bomb pulse was found to reside in the upper 1 m (3 ft) of soil. The bottom of this hydrologically active zone can be thought of as a "no-flux" liquid phase boundary for water based on the net effect of this transient cycling. Since it has been shown that precipitation never infiltrates beneath the upper 2 m (7 ft) of soil under current conditions, there is no groundwater recharge in the vicinity.

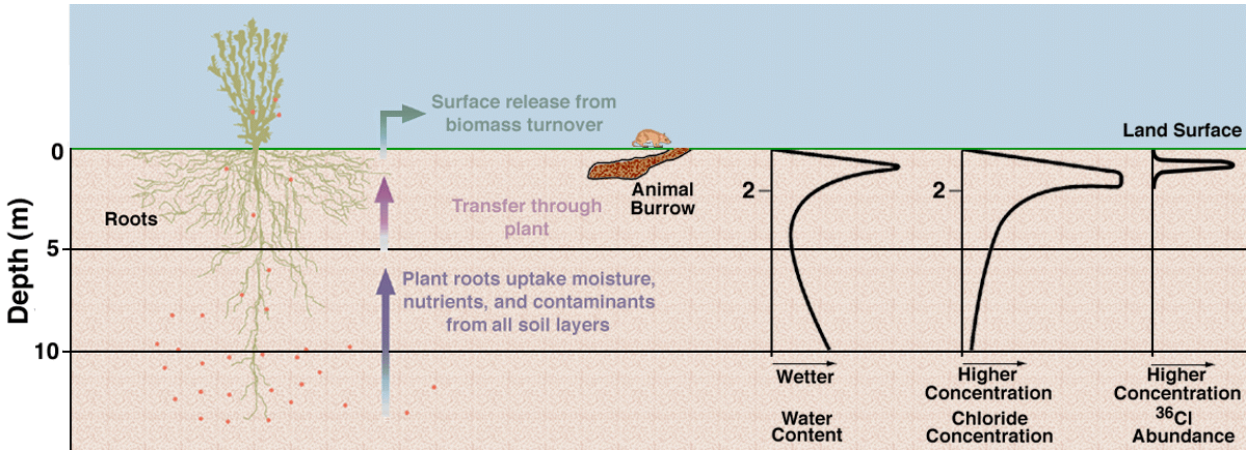

Figure 5-5. Schematic Describing Processes in the Near Surface Hydrologically Active Zone. Chloride and chlorine-36 serve as tracers of the depth of near surface water movement.

Beneath the Hydrologically Dynamic Zone

The zones beneath the upper 2 m (7 ft) of soil are hydrologically much less dynamic. Because infiltrating moisture is restricted to being recycled in the near surface, moisture movement in the deeper vadose zone is controlled by long-term climatic and geohydrologic processes. Uniformly low moisture contents throughout the profile at depth impede the flow of water by significantly reducing the hydraulic conductivity. A representative profile of hydraulic head versus depth is presented in Figure 5-6. In the vadose zone (in the absence of strong osmotic potentials),

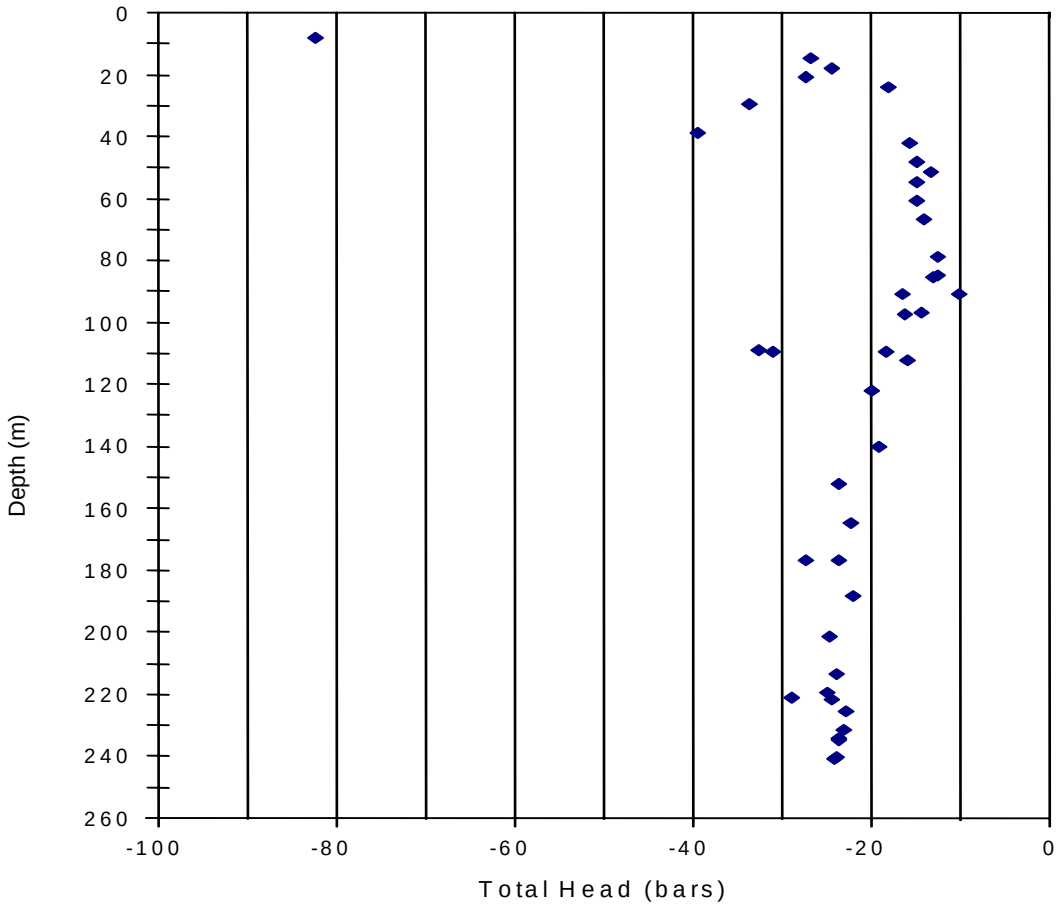

Figure 5-6. A Representative Profile of Total Water Potential Versus Depth. These data are for pilot well PW-1.

hydraulic head is the sum of capillary potentials and the potential imposed by gravity. Between a depth of 2 to 35 m (7 to 115 ft), the profile shows upward head gradients indicating a steady and very slow upward flux of pore water. This is the zone of interest for the GCD PA, for it is in this zone that the waste is emplaced. Waste dissolved in pore water can be transported upward where it would be more readily available for plant uptake or bioturbation. In the transport model (see Section 7.0), the top of this zone is treated as a zero-flux boundary for the dissolved waste; water is assumed to cross this boundary as water vapor with the dissolved contaminants left behind.

There is no groundwater recharge in this zone under the current climate, since the hydraulic gradients are upward.

The third zone, which extends to a depth of about 90 m (300 ft), is characterized by a near-zero hydraulic gradient, signifying negligible liquid water movement. Finally, the fourth zone, which extends to just above the water table (excluding the capillary fringe), is characterized by gravity drainage, remnant of a period when groundwater received recharge. Detailed discussions of the deep vadose zone are presented in Shott et al. [1998].

5.6.2.2 Evolution of the Hydrologic System in Response to Climatic Cycling

Disposal of radioactive waste in arid regions requires a thorough understanding of the occurrence of recharge. Recharge studies were conducted at the site to estimate the recharge rate under the current climate and the potential increase in recharge due to climate change [Strong and Conrad, 1992; Conrad, 1993; Conrad et al., 1993; Tyler et al., 1995; Appendix A]. Appendix A provides the most comprehensive analysis. The results of several complementary approaches to inferring recharge rates—chloride mass balance method, stable isotopes of water, cosmogenic chlorine-36, bomb-pulse chlorine-36, as well as the soil water potential measurements described above—all indicate that no recharge is occurring in the vicinity of the GCD boreholes under the current climate. In fact, in the upper 35 m (115 ft), stable isotope enrichment profiles indicative of evaporation corroborate the soil water potential data that indicate upward water movement. As stated previously, upward water advection has implications for PA, as water moving upward could carry radionuclides from the waste toward the accessible environment.

At depth, low chloride concentrations suggest that recharge has occurred at the site in the past. Chloride ages (derived from the mass of chloride contained in the profile above the low concentrations found at depth) indicate recharge during the last two glacial maxima. The stable isotopic composition of the soil water deep in the profiles is significantly more depleted in heavy isotopes than is modern precipitation, suggesting that recharge occurred under previous climatic conditions. These conditions would have to have been cooler, or more precipitation would have to have fallen in cooler months, or both.

Carbon-14 dating of groundwater beneath the site yields ages that span from 10,000 to 16,000 years before present. These groundwater ages imply recharge during the late Wisconsinan. Strong evidence indicating lack of recharge in the vicinity of the GCD facility during this time period suggests that recharge to the aquifer is likely to have occurred in the surrounding highlands and along ephemeral streams where conditions are most conducive to recharge. Indeed, there is further evidence that recharge in the basin is not always evenly distributed spatially. Chloride data collected from boreholes located proximal to a persistent stream channel show chloride accumulations on the order of about 25,000 years (coincident with retreat from the most recent glacial maximum), whereas boreholes located away from stream channels show chloride accumulations coincident with retreat from the preceding glacial maximum. Interestingly, boreholes located away from stream channels contain their chloride mass within two distinct bulges—one shallow, and one somewhat deeper (50 to 100 m [165 to 330 ft]). The presence of a deeper bulge suggests that the most recent glacial maximum was of sufficient magnitude to induce deep areally-distributed infiltration, but was of insufficient magnitude or duration to induce recharge.

To summarize the inferences from the environmental tracer data:

- there is no evidence of recharge occurring anywhere in the vicinity of the waste disposal site under current conditions;

- upward advection, driven by evapotranspiration at the surface, is occurring at the site;

- relatively mild pluvials are sufficient to cause recharge to the basin from surrounding highlands and along ephemeral streams having the largest catchments;

- the most recent glacial maximum was of sufficient duration and magnitude to induce recharge in the proximity of many stream channels;

- a climate change of greater magnitude and duration than the most recent glacial maximum is required to induce areally-distributed recharge; and

- areally-distributed recharge has not occurred in the vicinity of the waste disposal site in the last 120,000 years.

Although unlikely, if areally-distributed recharge were to occur, the GCD site would still be likely to comply. Screening calculations performed using estimates of past recharge rates (calculated using the chloride mass balance method and reported in Appendix A) indicate that the site is likely to meet the 40 CFR 191 containment requirements under those conditions [Price, 1993b]. As a result of the recharge studies conducted for the Area 5 RWMS, the focus of the PA analyses and climate change studies shifted to the upward pathway and modeling transport of contaminants to the ground surface.

An additional potential effect of climate change is that it may cause the water table to rise, thereby reducing the path length to the saturated zone. Jones [1982] suggests that the water table has remained relatively stable throughout the Pleistocene, based on the uniformity in clay hydration found in borehole U11g, 5 km (3 mi) north of the site.

All the analyses described above assume that no preferential water flow paths exist. Depending on conditions in the vadose zone, fractures can serve as either conduits or barriers to water flow. Regional tectonics together with subsurface detonations of nuclear explosives can cause fracturing of the alluvium and have been observed in Yucca Flat, a basin adjacent to Frenchman Flat to the north [Kao et al., 1994]. However, in Frenchman Flat, detailed mapping of waste disposal pits and trenches, video logging of one of the GCD boreholes, large-scale (1:60,000) air-photo analysis, and surficial mapping revealed no faults or open fractures in the alluvium [Gustafson and Rawlinson, 1994].

5.6.2.3 Establishing Parameter Distributions

As discussed in Section 5.11, the PA model requires parameter distributions for two hydrologic parameters – upward advective flux rates and effective moisture contents. The procedures used to develop these two distributions are discussed below.

Upward Advective Flux

Estimating upward advection is difficult under the very arid conditions that exist at the GCD site. Because the waste in the GCD boreholes is located relatively near to the land surface, and because the compliance period is lengthy (10,000 years for integrated discharge), even exceed-

ingly small rates of upward advection have the potential to result in radionuclide transport to the land surface.

Three approaches were taken to estimate upward advective flux: water balance, stable isotopic profiles, and soil physics. Each of these methods contains significant uncertainties. For the very low flux rates at the site, the errors associated with calculating the flux can be large relative to the magnitude of the calculated fluxes. Moreover, for any approach to estimating upward flux, assumptions must be made about how the system operates; clearly, the accuracy of the calculation depends of the veracity of these assumptions. Under the very arid conditions present at the site where water and water vapor move very slowly and conditions have taken thousands of years to evolve into their current state, it is often difficult to evaluate the appropriateness of assumptions underlying each approach. However, since three independent approaches were used to estimate upward advective flux, and to the extent that the results obtained from each of these three approaches are corroborative and not contradictory, the uncertainties associated with any one approach can be narrowed and a CDF of upward advection constructed for use in the PA. Each of the approaches, the results obtained, and the calculated uncertainties are presented below.

Water Balance

The beauty of the water balance approach lies in its simplicity. As the environment changed from a climate that was comparatively wet and cool to one characterized by lower precipitation and higher temperature, the evapotranspirative demand exceeded precipitation and soil moisture began to be extracted. As the near-surface soils dried out, capillary pressures increased and an upward pressure gradient was formed. This pressure gradient was sufficient to overcome the effect of gravity and cause the upward flow of water. Current soil water potential data indicate an upward flow gradient in the upper 35 m (115 ft) at the site.

The soil moisture contents of core samples extracted from several different boreholes were measured, and vertical profiles of soil moisture created for the current climate. One can postulate what a moisture content profile would look like under past wetter climatic conditions in which deep infiltration was occurring. It is likely that past profiles would look very similar to the current profiles at depth[3], but in the past profiles, the moisture contents found at depth would extend to very near the surface. The depletion of water from the upper portion of the current profiles represent water removed by evapotranspiration near the land surface as the climate changed from wetter to drier.

The estimate of upward advective water flux was obtained by calculating the total amount of water removed from the soil profile from the drying zones that have formed in the upper 20 m (65 ft) or so of the current profiles. Figure 5-7 provides one representative profile showing the decrease in near-surface moisture compared to higher average moisture contents seen at depth. In using a water balance approach, it is presumed that this water deficit is the result of upward liquid advective flow.

[3]Given the coarse texture of the soil, only a small increase in moisture content is necessary to accommodate infiltrating conditions.

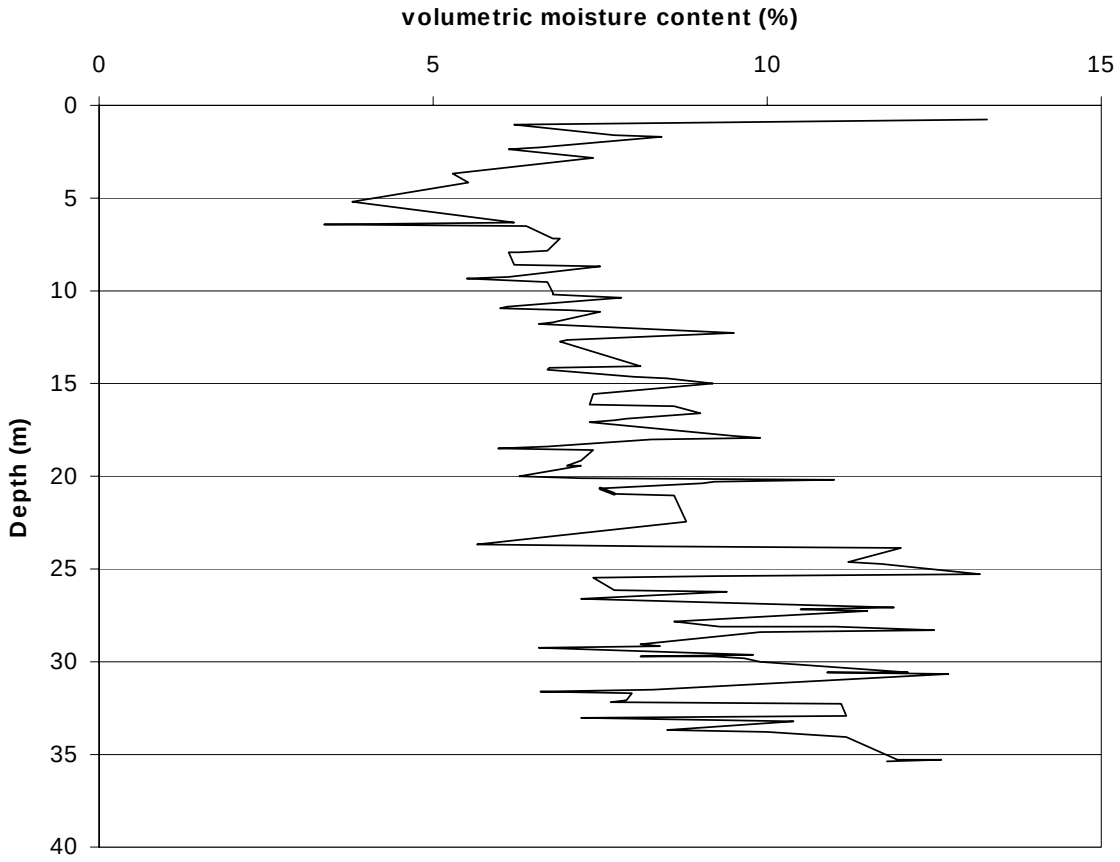

Figure 5-7. A Representative Profile of Moisture Content Versus Depth. These data are for borehole ST-1.

The upward flux estimate represents a long-term average based on the soil moisture deficit in the near subsurface and the years since drying began. The volume of water per unit area removed from the drying zone (a length of water, L) was calculated by subtracting moisture contents, θ_i, from the average moisture content found at depth, θ_{ave}, multiplied by the representative depth interval, d_i, for each moisture content measurement:

$$L = \sum \left(\theta_{ave} - \theta_i \right) d_i \tag{5-1}$$

The total length of water is then divided by the time interval, t, to obtain the upward advective flux, q:

$$q = L/t \tag{5-2}$$

A time interval of 10,000 years was selected because the climate literature indicates that the present arid climate has prevailed for at least that long, and probably longer [Brown et al., 1997a].

Conrad and Strong [1994] conducted water balance calculations of upward advective flux for the pilot wells. More recently, Beyeler [1999] calculated fluxes for the science trench boreholes using data from REECo [1993b]. These calculations yielded fluxes that ranged between $10^{!2}$ mm/y and $10^{!1}$ mm/y.

Stable Isotopes

A detailed discussion of the methods and results can be found in Tyler et al. [1999]. The brief description contained here is simply an abridged version of that work.

Under equilibrium conditions, strong isotopic fractionation occurs between liquid water and water vapor. Water vapor becomes isotopically light, that is, it contains proportionally more light isotopes, ^{1}H and ^{16}O, and is depleted in heavy isotopes, ^{2}H and ^{18}O. Conversely, the liquid becomes isotopically heavy, that is, it is enriched with the heavy isotopes. The result of this fractionation process is that water subjected to evaporation will become isotopically more heavy than it was initially. Therefore, the soil water very close to the land surface that is subject to evaporation will become markedly enriched in heavy isotopes relative to its original composition. This enriched water resides in proximity to water deeper in the profile that has not been subjected to evaporation. A profile containing such a contrast in isotopic concentrations is subject to the process of diffusion. The stable isotope approach to measuring upward advection is founded on the premise that this diffusive process is opposed by upward advection of water that has not been enriched. It is these opposing processes that lead to the development of isotopic profiles similar to the ones illustrated in Figure 5-8. Given enough time to equilibrate, these processes will balance one another, thereby forming a steady-state isotopic profile. The shape of the isotopic profile reflects the relative magnitude of the rate of upward advection. Relatively high rates of evaporation (sustained by upward advection of water) will be expressed with a high isotopic gradient and a relatively compressed enriched zone of stable isotopes near the land surface. Conversely, less upward advection will result in deeper diffusion of enriched isotopes. This is the basis for the theory developed by Barnes and Allison [1983]. Appropriate to the dry conditions that exist at the site, the upward advection calculations of Tyler et al. [1999] included isotopic diffusion in both the liquid and vapor phases following the approach of Cook et al. [1992].

Under the arid conditions present at the site, both of the competing processes—diffusion and upward advection—are very slow processes, and consequently, the time needed to reach a steady-state can be quite large. The consequence of the system not reaching steady-state, as assumed by the approach, is to overestimate the upward advection rate currently occurring. Tyler et al. [1999] calculated a characteristic time needed to approach steady-state and found it to be of similar magnitude to times postulated for when the climate turned more arid and the evaporative isotopic profile began to develop. Only when evaporative conditions have been known to exist for a period longer than characteristic time to reach steady-state can it be assured that the steady-state assumption has been met.

Tyler et al. [1999] calculated upward advection rates for both the isotopes of hydrogen and oxygen using the profiles recovered from ten boreholes yielding 20 measures of upward advection rates. These calculations yielded fluxes that ranged between 0.1 mm/y and 0.4 mm/y.

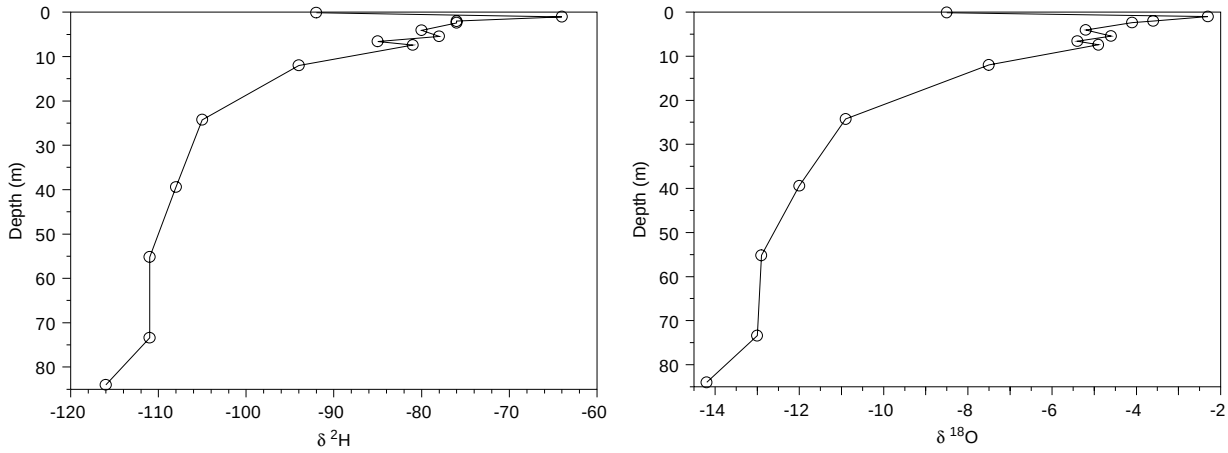

Figure 5-8. Representative Profiles of Stable Isotope Enrichment, ^{2}H (left) and ^{18}O (right). These data are for borehole AP-1.

Soil Physics

The soil physics approach was also used to calculate upward advection rates at the site. Bechtel Nevada [1998b] performed initial calculations. These initial calculations were updated by SNL and are included in Appendix D. The soil physics approach uses an unsaturated version of Darcy's Law:

$$q = -K(\theta)\,\partial H / \partial z \qquad (5\text{-}3)$$

where

$K(\theta)$ = unsaturated hydraulic conductivity (mm/y), and
$\partial H/\partial z$ = total head gradient.

$K(\theta)$is a function of the moisture content, θ, and total head is the sum of soil water capillary potentials and the potential due to gravity. Measurements of soil water potentials at the site are documented in Blout et al. [1995]. In-situ moisture contents were obtained for each of the core samples analyzed. Obtaining values for unsaturated hydraulic conductivity is more problematic. At low moisture contents, direct measurement of unsaturated hydraulic conductivity is not practical due to extremely low flow rates, although centrifuge methods are being developed (e.g., Conca and Wright, 1990). In the absence of direct measurement methods, standard practice is to use a theoretical model [Mualem, 1976] to calculate unsaturated conductivity as a function of moisture content. Saturated hydraulic conductivity and estimates of several fitting parameters that relate capillary pressure and moisture content are obtained from laboratory testing of the core sample. These parameters are used in the Mualem model to calculate unsaturated conductivity. The uncertainties associated with application of the Mualem theoretical model to very arid soil conditions have rarely been explicitly quantified, but are thought to be largely due to the non-linearity of the theoretical model.

Estimates of upward advection obtained from soil physics analyses on core samples are small-scale measurements and PA requires effective saturations that represent a spatial average for upward advection along the entire path length from the top of a GCD borehole to the bottom of

the zero-flux plane. To accomplish this, Monte Carlo analysis was used to convolve uncertainties in individual core-scale estimates of upward advection with the fact that estimates of effective values for upward advection must involve spatial averaging of small-scale estimates. Details are given in Appendix D. Estimates of effective upward advection ranged from $10^{!5}$ mm/y to $10^{!1}$ mm/y.

Creating an Overall CDF for Upward Advection

A graph showing the ranges obtained using each of the three techniques employed for estimating upward advection are given in Figure 5-9. Note the convergence of the three methods near an upward advective flux of $10^{!1}$ mm/yr, reflecting the upper end of the ranges for the water balance approach and the soil physics approach and the lower end of the range for the stable isotope approach. Also note the relatively tight ranges for the water balance and the stable isotope methods: one order of magnitude versus the broad, four-order of magnitude range for the soil physics method. This disparity reflects the large uncertainties associated with using the soil physics approach in dry sediments.

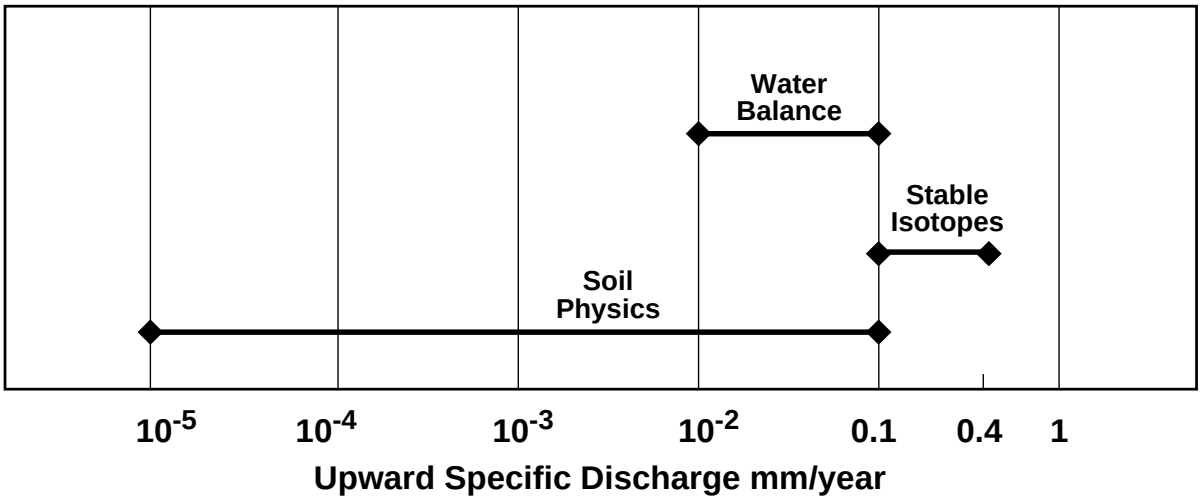

Figure 5-9. Range of Upward Specific Discharges Obtained From Three Methods.

It is important to impart a note of practicality. Even though the path length upward to the accessible environment is relatively short (on the order of about 21 m [70 ft]), very small upward advective flux rates result in negligible upward radionuclide transport for the purposes of PA by the water balance method.

An upward advective water flux of $10^{!2}$ mm/y results in upward advective migration of about 1 m over the 10,000-year regulatory period (assuming a volumetric moisture content of 10%). Operationally, the proportion of the CDF existing beneath 10^{-2} mm/y reflects the degree of belief in the possibility of negligible upward advection. For practical purposes, the density of the CDF at values less than 10^{-2} mm/y will prescribe the proportion of PA realizations in which liquid diffusion, plant root uptake, and bioturbation will constitute the radionuclide migration process. Of course, since rates lower than $10^{!2}$ mm/y are negligible, the details of the shape of the distribution beneath $10^{!2}$ mm/y have little practical significance.

Water balance uncertainties. True values for upward advection could be higher or lower than the range given. There are uncertainties as to whether the current moisture contents at depth actually represent the moisture conditions under the wetter previous climatic regime by the water balance method. If moisture contents at depth were actually higher under past climates, upward advection would have been underestimated. It is possible that moisture contents could have been as much as 2% to 3% higher than current moisture contents. Estimates of recharge under wetter climatic conditions were calculated using the chloride mass balance approach (Appendix A). Under this wetter previous climate, and assuming a unit gradient, the unsaturated hydraulic conductivity is equivalent to the recharge rate (approximately 10^{18} cm/s). Referring to K/θ relationships [REECo, 1993a], moisture contents could have been as much as 2% to 3% higher than current moisture contents. More likely, though, as the climate changed from wetter to drier, initial drainage of this moisture would have been downward.

The water balance estimate is based on integration over long timeframes. The rate represents a long-term average. To the extent that flux rates were higher at an early time, the method over-estimates the current rate. Conversely, one may postulate that little water need be taken out of the profile at early time to form the dry zero-flux boundary and therefore the long-term average may do a pretty good job of representing the current rates. Also at issue is the timeframe over which drying of the profile takes place. Conrad and Strong [1994] picked 10,000 years as a reasonable timeframe. However, it could have been somewhat shorter (considering the Younger Dryas occurred about 7,000 to 8,000 years ago) or could have been as much as two to three times longer (given uncertainties in the timing of departure from full glacial conditions), leading to an overestimate by a factor of 2 to 3. Even though the range of water balance estimates is relatively narrow, it does not preclude the possibility that true rates of upward advective flux could be either higher or lower than the range given.

Stable isotope uncertainties. The stable isotope results have the potential to be overestimates. As stated above, because the time since the beginning of isotopic profile formation and the time required to form a steady-state profile are similar, it is uncertain as to whether a steady-state profile has actually been achieved. In the absence of assurance that a steady-state profile has been achieved, the upward advective flux estimates from the stable isotope approach may be overestimates. Additionally, Tyler et al. [1999] considered the effects of non-isothermal conditions imparted by the geothermal temperature gradient at the site. They concluded that failure to account for temperatures that increase with depth in their isothermal analysis would lead to compaction of the isotopically-enriched zone closer to the surface due to upward thermally driven vapor flux and some, probably slight, overestimation of the upward advective flux.

Soil physics uncertainties. As discussed above, there is less confidence in the value of the soil physics calculations and, comparatively, they are given less weight. However, since the lower end of the range is 3 to 4 orders of magnitude lower than for either of the other methods, it forms a firm lower bound for the upward advective flux CDF. Also, as discussed above, since the practical lower limit for significant upward advection is 10^{12} mm/y, placement of the lower limit of the CDF is arbitrary.

The discussion above can be summarized as follows:

- There is moderate confidence in both the water balance results (ranging from $10^{!2}$ to $10^{!1}$ mm/y) and the stable isotope results ($10^{!1}$ to $4 \times 10^{!1}$ mm/y). There is less confidence in the soil physics results ($10^{!5}$ to $10^{!1}$ mm/y).

- Stable isotope results provide the highest flux rates. They provide either reasonable estimates or perhaps an overestimate. Therefore, the maximum of the stable isotope estimates is used, $4 \times 10^{!1}$ mm/y, as the upper bound of the CDF.
- Uncertainties in the water balance approach go either way — the flux estimates may be reasonable, they may be high, or they may be low. They provide no firm upper or lower bound for the CDF.

Using these arguments to build a subjective CDF, a 90% likelihood that the true, current, effective upward advective flux falls between $10^{!2}$ to $4 \times 10^{!1}$ mm/y is assigned. This forms the main body of the distribution. Since the ability to make further inferences due to limitations in the quality and quantity of the data is limited, a uniform distribution within this range was assigned. A 10% likelihood that the true upward advective flux falls below this range was assigned. The resultant CDF is shown in Figure 5-10.

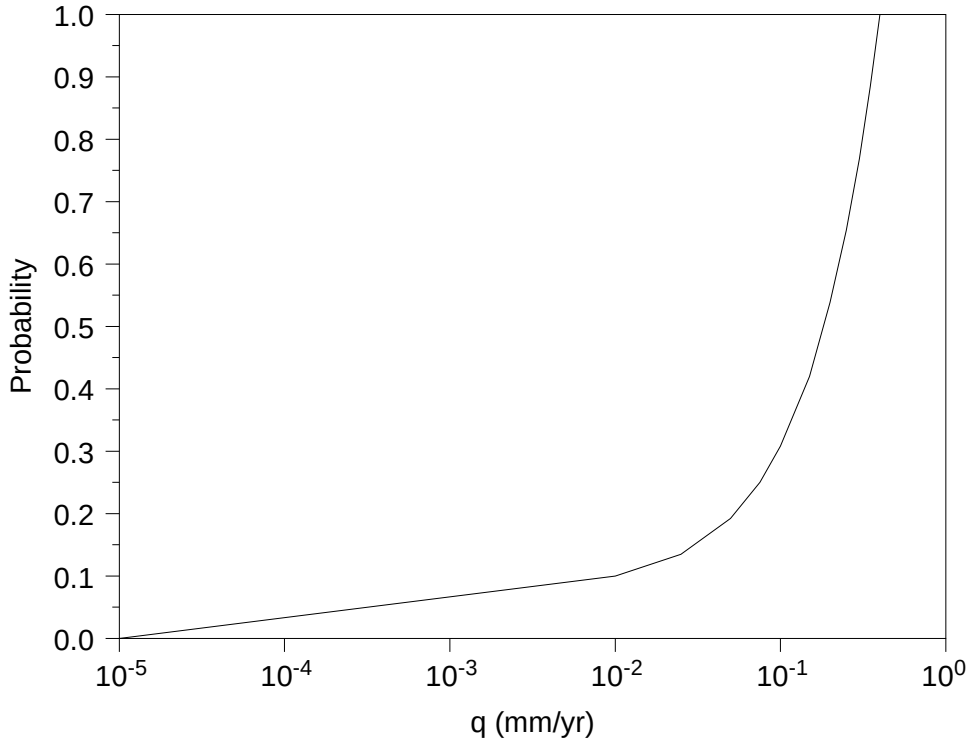

Figure 5-10. CDF of Upward Advection.

Effective Moisture Content

Moisture content, as used in the PA model, represents current climate conditions over a volume of soil that corresponds to the waste backfill. This parameter was estimated from the core sample data collected from boreholes AP-1, AP-2, RP-1, and RP-2 (data reported in Blout et al., 1995) and from the science trench boreholes Ue5ST-1, Ue5ST-2, Ue5ST-4, Ue5ST-5, Ue5ST-6, and Ue5ST-7 (data reported in REECo, 1993b). Data collected above the elevation of the waste and below a depth of 2 m (7 ft) were considered to be most representative of long-term conditions above the waste and to be isolated from the intense transient fluctuations nearer the land surface. Individual observations from the measurement boreholes represent a relatively small volume of soil compared to the volume described by the model parameter. Because of the difference between the measurement scale and the model scale, the average of a large number of observations at a single borehole was assumed to be an appropriate value for the model.

The process of developing a PDF from the borehole data is as follows. These two uncertainties are captured in the probability distribution for the moisture content parameter. First, each measurement borehole is assumed to provide an equally likely representation of the soil overlying the waste. Estimates from each borehole are assumed to be independent and are assigned an equal probability. Second, for a given borehole, the individual moisture content measurements are assumed to be independent samples taken from a normal distribution. Under this assumption, the estimate of the (true) average moisture content is also approximately normally distributed with a mean and standard deviation equal to the sample average and the standard error of the mean, respectively.

Table 5-6 lists the summary statistics from the AP and RP boreholes that define the uncertainty distributions for the (true) average values in each borehole. Table 5-7 lists the summary statistics for the science trench boreholes. The overall distribution for the model parameter is constructed by equally weighting each of the ten distributions of the average moisture content. Figure 5-11 shows empirical distributions created from the individual borehole measurements, along with the distribution for the model parameter. Note that the individual borehole measurements have a greater spread than the model parameter distribution. The individual measurements reflect small-scale spatial variability in moisture content, while the model parameter reflects possible average values over this small-scale variability.

Table 5-6. Moisture Content Summary Statistics from AP and RP Boreholes

	Measured Moisture Content (v/v)			
	AP-1	**AP-2**	**RP-1**	**RP-2**
Number of Observations	6	9	5	6
Average	0.0613	0.0631	0.0814	0.0663
Sample Standard Deviation	0.0120	0.0172	0.0316	0.0176
Standard Error	0.0049	0.0057	0.0141	0.0072

Table 5-7. Moisture Contents Summary Statistics from Science Trench Boreholes

	Measured Moisture Content (v/v)					
	Ue5ST-1	**Ue5ST-2**	**Ue5ST-4**	**Ue5ST-5**	**Ue5ST-6**	**Ue5ST-7**
Number of Observations	40	37	41	14	23	16
Average	0.0738	0.0826	0.0747	0.0539	0.0655	0.0523
Sample Standard Deviation	0.0136	0.0178	0.0147	0.0095	0.0128	0.0084
Standard Error	0.0022	0.0029	0.0023	0.0025	0.0027	0.0021

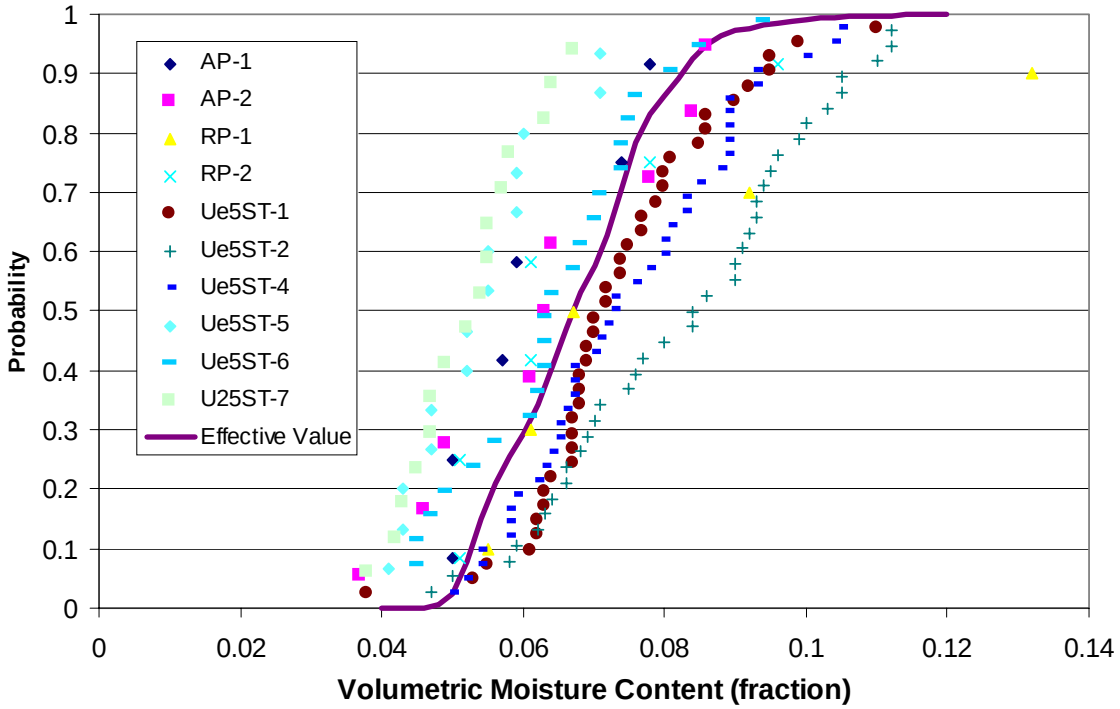

Figure 5-11. Distributions of Measured Moisture Content and Effective (Average) Moisture Content.

5.6.3 Special Source of Ground Water

This section provides an expanded evaluation of the Ground Water Protection Requirements (GWPRs) and provides the basis for concluding that none of the aquifers in Frenchman Flat meets the definition of a special source of ground water. The GWPRs (40 CFR Part 191.16) state that *(emphasis added)*:

> (a) Disposal systems for spent nuclear fuel or high-level or transuranic radioactive wastes shall be designed to provide a reasonable expectation that, for 1,000 years after disposal, undisturbed performance of the disposal system shall not cause the radionuclide concentrations averaged over any year in water withdrawn from any portion of a *special source of ground water* to exceed …:

In 40 CFR Part 191.12(o), the law defines a special source of ground water as:

> … those Class I ground waters identified in accordance with the Agency's Ground water Protection Strategy published in August 1984 that: (1) Are within the controlled area encompassing a disposal system or are less than five kilometers beyond the controlled area; (2) are supplying drinking water for thousands of persons as of the date that the Department chooses a location within that area for detailed characterization as a potential site for a disposal system (e.g., in accordance with Section 112(b)(1)(B) of the NWPA); and (3) are irreplaceable in that no reasonable alternative source of drinking water is available to that population.

The EPA describes specific requirements in defining special sources of ground water:

1. The ground water must be a Class I ground water, *and*
2. The ground water must be located within the controlled area, or < 5 km from the controlled area; *and*
3. The ground water must be supplying drinking water for thousands of persons as of the date that the Department selects the site for extensive exploration as a potential location of a disposal system; *and*
4. The ground water must be irreplaceable in that no reasonable alternative source of drinking water is available to *that* population.

All four of these requirements must be met to qualify as a special source of ground water, and these four requirements are examined in detail below. Before discussing each requirement, however, the aquifers below Frenchman Flat are briefly described.

5.6.3.1 Frenchman Flat Aquifers

The three aquifers in Frenchman Flat basin are described by Shott et al [undated draft of the Area 5 Compliance Assessment] as follows.

> Uppermost aquifers under the Frenchman Flat basin are the Alluvial Aquifer and the Timber Mountain Tuff Aquifer. The water table below the RWMS lies about 240 m (790) ft below the ground surface. The water table is nearly flat, indicating that there is no significant horizontal flow beneath the RWMS in the saturated zone. The Tuff Aquitard, which is estimated to be in excess of 1,370 m (4,496 ft) thick, lies below the alluvium. Because of its relatively large areal extent and thickness, it is a major barrier for ground water to move from the uppermost aquifers into the Lower Carbonate Aquifer below. The Lower Carbonate Aquifer is the regional aquifer underlying most of the eastern part of the NTS and is a part of the Ash Meadows Groundwater Basin which discharges at Ash Meadows in the Amargosa Desert, 30 km (18.6 mi) south of the NTS.

5.6.3.2 Class I Ground Water

The guidelines in the EPA's Ground-Water Protection Strategy are not enforceable requirements but are used generally to define different levels of protection for three classes of ground water: a)

Class I (special sources of ground water), b) Class II (ground water currently or potentially a source of drinking water), and c) Class III (ground water not a potential source of drinking water and of limited beneficial use). The guidance for determining if a ground water is Class I, II, or III is set forth in the EPA Guidelines for Ground-Water Classification [EPA, 1986].

An analysis of the classification of ground water at the NTS was completed in 1994 [Chapman, 1994] and the result of that analysis was incorporated in the Final Environmental Impact Statement for the Nevada Test Site and Off-Site Locations in the State of Nevada [DOE, 1996]. All ground water of all aquifers in the NTS were classified as Class II ground water [Chapman, 1994; see pages 49-51].

By EPA regulation, the GWPRs of the 1985 version of 40 CFR 191 do not apply *because the ground water is not a Class I ground water*. No further analysis of the GWPRs is required. However, the DOE/HQ Federal Review Group has requested additional information on other subjects related to the GWPRs, and so the other three requirements are analyzed below.

5.6.3.3 Within the Controlled Area or Less Than 5 km from the Controlled Area

As applied to ground water, the controlled area is defined in 40 CFR 191.12(g) as the subsurface underlying the disposal system. As discussed above, three major aquifers or hydrostratigraphic units are present beneath the GCD boreholes: 1) the alluvial aquifer composed of alluvial deposits of the Frenchman Flat basin, 2) the volcanic aquitard composed of Cenozoic volcanic rocks, and 3) the lower carbonate aquifer composed of limestone and dolomite of Middle Cambrian through Devonian age. Only these three aquifers meet the requirement of being within or less than 5 km from the controlled area.

5.6.3.4 Supply Drinking Water for Thousands of Persons

The town of Mercury is the primary entrance location and principal support site for activities on the NTS, and the only NTS location where “thousands of persons” were drinking water. The population of Mercury during the 1980’s included transient residents and onsite residents supporting weapons testing activities on the NTS. Much of the population commuted on a daily basis from the nearby cities (principally Las Vegas and Pahrump) and the onsite population increased dramatically during normal workdays and decreased in the evening and on weekends. Gillespie *et al.* [1996] report that a total of six water supply wells have been drilled in the Frenchman Flat Basin. Information on these six wells is given in Table Q-1 (Appendix Q).

Of the six wells, Chapman [1994] reports that two (#4 and #4A) were connected through a pipeline to the Yucca Flat water system and did not supply water to Mercury. One well (#5A) was abandoned in 1970 before the GCD project started. Another well provided water to Mercury but was taken out of service in 1994. The other two wells (Well-5B and Well-5C) provided water to Mercury and continue to do so.

An analysis of the Mercury drinking water supply is provided by Chapman [1994]. That reference notes that the population served with drinking water from the alluvial aquifer system of Frenchman Flat is slightly less than 1,500 people [Chapman, 1994; p. 43]. Chapman [1994]

describes several additional factors that must be considered in evaluating NTS populations that tend to decrease the assessed population. These factors are the transient patterns of the population (day-workers with limited permanent residents and seasonal work) and the use of bottled drinking water at the NTS (bottled water originates in the Las Vegas area). That reference concludes that the population relying on ground water at the NTS is *not* substantial but because of ambiguity in applying the population criterion, *assumes* the population *could be* substantial.

Two caveats must be expressed with respect to the Mercury population. First, the population is mostly working adults and is clearly different from a representative residential population of adults and children that meets the intent of the EPA protection guidelines. Second, the Mercury population works at the NTS, a government complex that works routinely under worker safety and radiation controls.

While the EPA ground water protection guidelines probably do not apply to the unique Mercury population, during periods of active underground testing at the NTS there *could* have been "thousands" of persons drinking water withdrawn from aquifers within the controlled area or less than 5 km from the controlled area.

5.6.3.5 Irreplaceable Water Supply

Discharge data from Gillespie *et al.*. [1996] for four wells that provided water for Mercury are summarized in Table Q-2 (Appendix Q). Three of these wells are in Frenchman Flat (5B, 5C, and UE-5C), while one (Army #1) is located southwest of Mercury (i.e., not in Frenchman Flat). The summed yearly discharge of water from the Frenchman Flat wells generally exceeds the discharge from Army #1. In some years (1989, 1990) the discharge from Army #1 exceeds the summed discharge from the Frenchman Flat wells. Chapman (1994) examined the water well production for a slightly longer period and she notes that for some years, about two-thirds of the Mercury water supply came from Frenchman Flat and that in latter years, after resumption of production in Water Well 5B, the Frenchman Flat wells account for less than 50% of the Mercury water supply.

The water wells of Frenchman Flat have clearly supplied significant percentages of the drinking water at Mercury. However, an important point is that the discharge data for the highest years of pumping from water well Army #1 are sufficiently high to have provided nearly all of the drinking water for Mercury, particularly in recent years when the NTS populations have declined dramatically. Further, other wells are now available and linked to the water-supply system of Mercury. The water-supply wells of Frenchman Flat could potentially be removed from the water-supply system of Mercury without adverse economic impacts. Therefore, *the drinking water provided by the alluvial and volcanic aquifers in Frenchman Flat is replaceable* in that there are alternative sources of drinking water.

Finally, Chapman (1994) used five screening tests recommended by the EPA to evaluate replaceability of drinking water. She argues that NTS waters are replaceable relative to the EPA screening tests and notes that no near-term changes are anticipated that would change the water supply status to irreplaceable.

5.6.3.6 Conclusions

There are two reasons why the alluvial and volcanic aquifers beneath the GCD boreholes are not special sources of ground water as defined in 40 CFR 191:

- All ground water in all aquifers of the NTS are classified as Class II ground water based on a 1994 review conducted independently of the GCD project and cited in the Environmental Impact Statement of the NTS (DOE, 1996).
- The water resource represented by the alluvial and volcanic aquifers in Frenchman Flat are replaceable.

5.7 Plant Uptake

Plant Transport and Release. The CRs of 40 CFR 191 regulate the release of radionuclides into the accessible environment. Thus, plant root uptake and within-plant transfer to aboveground biomass is the only release mechanism considered for plants.

Plant roots will contact radionuclides that are either dissolved in pore water and/or adsorbed on soil particles. These roots will absorb some fraction of the radionuclides and will transport them within the plant to both belowground and aboveground biomass. Once these radionuclides reach any portion of the aboveground biomass, they are considered to be released to the accessible environment for purposes of assessing compliance with the CRs. The plant uptake model estimates the quantity of radionuclides that could reach aboveground portions of native plants over 10,000 years.

5.7.1 Introduction

This section defines and defends the state of knowledge, conceptual and mathematical models, and associated input parameters for modeling the uptake of radionuclides by plants at the GCD facility.

Plants adapted to the arid climate of the NTS are able to rapidly capture infiltrating moisture. In addition to capturing soil moisture, plant roots absorb nutrients, minerals, and heavy metals, transporting them within the plant to both belowground and aboveground biomass. In this fashion, plant uptake affects the movement of radionuclides. The plant uptake model presented reflects rooting characteristics important to plant uptake, biomass turnover rates, and the ability of plants to take radionuclides from the soil. Movement of contaminants to the surface is the only transport mechanism evaluated with the model presented here. Parameters are provided in this section for modeling plant uptake of radionuclides and estimating surface contaminant flux due to plant uptake under current climate conditions.

The conceptual model of radionuclide release due to plant uptake begins by radionuclide absorption from the soil by plant roots, followed by radionuclide transport in the plant to the aboveground vegetative portions of the plant. A simple schematic of the uptake model is shown in Figure 5-12.

Contaminant transport from the soil is treated as a bulk flow process and is similar to that described by Murphy [1993]. This model is designed to estimate the concentration in above-ground vegetation as a function of the soil concentration in the soil layers from which plant roots access water and nutrients, weighted by the extraction of such resources by plant roots. The actual rate of contaminant withdrawal is a function of the number of roots present within a given depth, the rate of extraction by those roots, the amount of annual biomass produced by the vegetation at a site, and the degree to which those plants sequester contaminants in their aboveground tissues. The process of uptake is dynamic, depending not only on soil resources, but also on a plant's need for soil resources and its ability to extract those resources from the soil.

The conceptual model of plant uptake has three main components (Figure 5-12):

- Plant rooting characteristics. The near-surface soil layers contain the majority of roots to capture transient water infiltration;

- Plant concentration ratios of radionuclides, which are parameters used in an empirical model to describe the amount of radionuclides transferred from the soil to aboveground biomass as a function of the total contaminant mass in the soil (sorbed and liquid); and

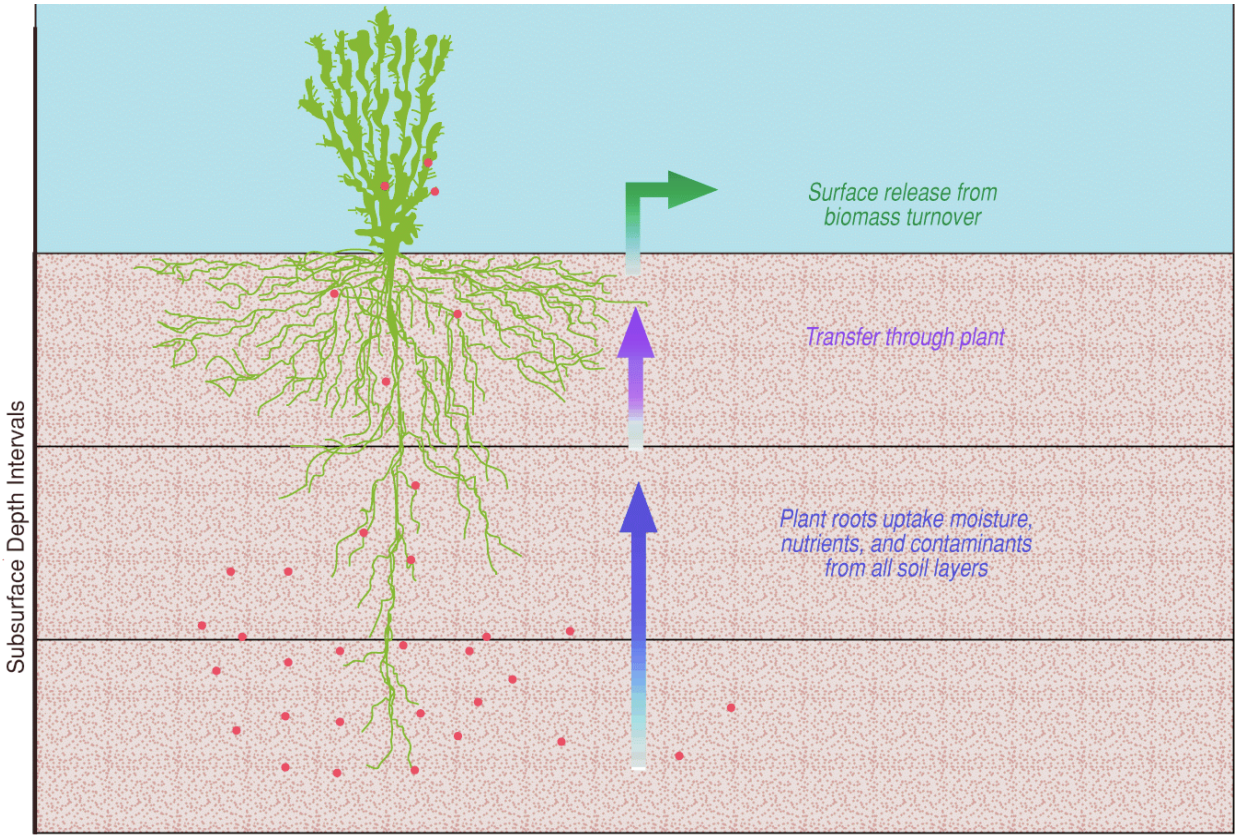

Figure 5-12. Conceptual Model of Uptake, Transfer, and Release by Plants.

- Plant biomass production and turnover.

This conceptual model is essentially the same as that used to model plant uptake in all NTS PAs [Shott et al., 1995 and 1998; Winkel et al., 1995; Brown et al., 1997b]. However, many model features are unique to this model, including treatment of parameter and model uncertainty, specific data used, and the model's applicability to both current and potential future conditions.

Plant uptake can be modeled mathematically as a function of soil depth, built from depth-dependent functions of the presence and activity of roots, radionuclide concentrations, and the amount of biomass produced by plants. It is also a "community scale" model in that it sums the contaminant uptake for all plant types within the community (e.g., annuals), defined simply as the assemblage of plants occupying the site at a specific point in time.

5.7.2 NTS Ecological Setting

5.7.2.1 Physiography and Ecology

The information on the NTS ecology presented in this section is summarized from Beatley [1976]. The NTS is located at the interface (ecotone) of the northern extent of the warm Mojave Desert and the southern limit of the cooler Great Basin Desert (Figure 5-13). The area where these two deserts overlap is called the Transition Desert. Mojave and Transition Desert communities occupy nearly all the land surface at the NTS below 1,500 m (4,920 ft) elevation, which includes about two-thirds of the area within the NTS boundaries. The remainder of the NTS area is above 1,506 m (4,920 ft) elevation and vegetation at these higher elevations belongs mostly to the Great Basin Desert, including the drainage basins and their surrounding mountains in the northern portion of the NTS. The Area 5 RWMS is approximately 972 m (3,190 ft) above mean sea level.

Overall controlling factors of the warm desert communities are the timing and amounts of individual precipitation events, with which most biological activity is synchronized. In the higher regions of the warm deserts and in most of the Great Basin Desert there are similar precipitation patterns as the warm deserts, but the rains occur in greater amounts and under conditions of lower temperatures, leading to a carryover of significant quantities of soil moisture from one period to the next. In these cooler areas, biological activity is more synchronized with seasons of higher temperatures than with the periods of rainfall.

5.7.2.2 Plant Ecology

The NTS can be characterized as a mosaic of communities in which the dominant and codominant species vary from site to site. It is the relative dominance of different shrubs, or shrubs and trees, that tends to define community boundaries, rather than the presence or absence of non-shrub species. Species composition is considered a site-specific characteristic that does not change from year to year; the number and sizes of individual plants within populations that are used to define NTS plant communities (shrubs and trees) tend to fluctuate within a narrow range. The communities are defined as climax communities in that they are self-perpetuating and in

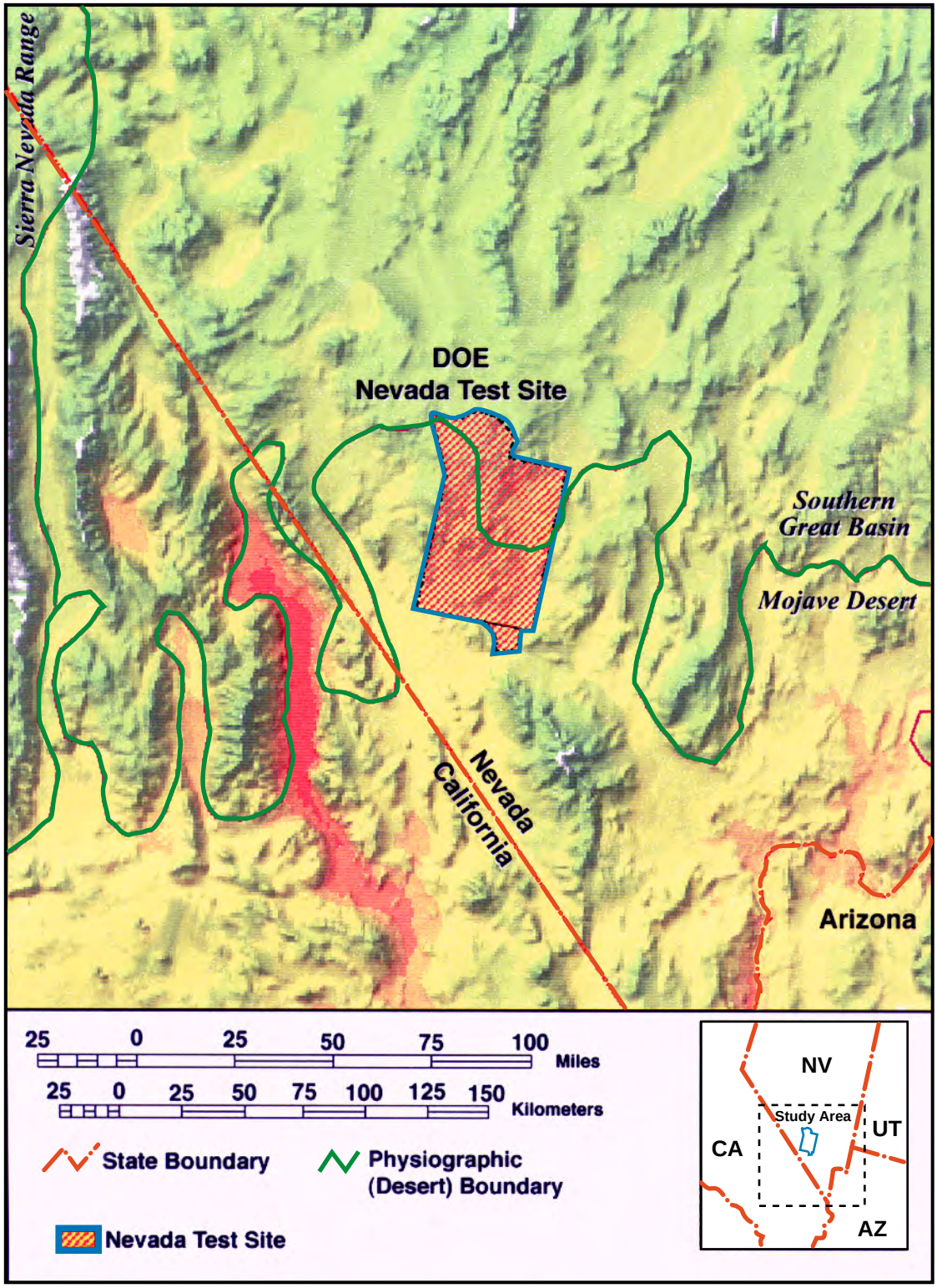

Figure 5-13. Physiographic Location of NTS.

equilibrium with the present climate and soils of the sites they occupy. Population sizes within the communities fluctuate within a range as expressions of climatic fluctuations.

The current plant community at low elevations within the NTS is desert shrubland. Higher elevations support either shrubland species adapted to relatively cooler and wetter conditions or woodland species. The vegetation has been extensively studied and is well characterized [Beatley, 1962; Beatley, 1965a; Beatley, 1965b; Rickard and Beatley, 1965; Beatley 1967; Beatley, 1969; Beatley, 1975; Beatley, 1976; Wallace and Romney, 1976; Hunter and Medica, 1989]. A photograph of a typical Mojave Desert shrubland is shown in Figure 5-14.

Species were grouped by the following four lifeforms to avoid excessively cumbersome analyses and computations, and to simplify the data collection and presentation: trees, shrubs/subshrubs, herbaceous perennials (hereafter referred to as "perennials"), and annuals. Trees and species that belong to the specialized habitats with elevated soil moisture are included only under potential future conditions (Section 6.0). The remaining three lifeforms are included under both current and future conditions.

Lifeform groups are "functional units" because species within the units tend to operate similarly [Walter, 1971; Wilcox and Breshears, 1995]. This categorization of plants is useful for describing plant communities at the NTS as it is consistent with numerous studies indicating that lifeform categories appropriately group similarly behaving species [Everett and Sharrow, 1985; DeLucia and Schlesinger, 1991; Johnson and Mayeux, 1992]. Details of the grouping of species within communities can be found in Brown et al. [1997a].

5.7.3 Conceptual Model

The process of root uptake of soil resources is a function of both the distribution of roots with depth and the distribution of resources in the soil. Because roots and soil resources are concentrated in the near-surface layers, most extraction occurs in these layers. Figure 5-15 illustrates how uptake is simulated, given what is known of plant roots and the relative uptake by roots at different depths. The model presented here uses a two-phased approach to simulate two known characteristics of roots relevant to plant uptake: (1) root depth and mass decrease with increasing soil depth, and (2) the majority of extraction of soil resources by roots occurs in near-surface soil layers (Figure 5-15). Also included are components to estimate the concentration of radionuclides expected in aboveground plant tissues as a function of soil concentrations and the annual amount of aboveground biomass produced (Figures 5-16 and 5-17). The actual data used and defense for parameter distribution choices of each model component are detailed in the remainder of Section 5.7.5 through 5.7.8.

If known, root densities can be used to directly estimate extraction with depth. However, data for root densities with depth are scarce and the data available describe maximum plant root lengths, not root density. Both root density and root depths are largely controlled by resource availability

Maximum Root Lengths. Measured maximum root lengths are used to create distributions of root depth through the soil profile for each lifeform, conservatively estimating the probability of roots expected in the deeper, subsurface layers.

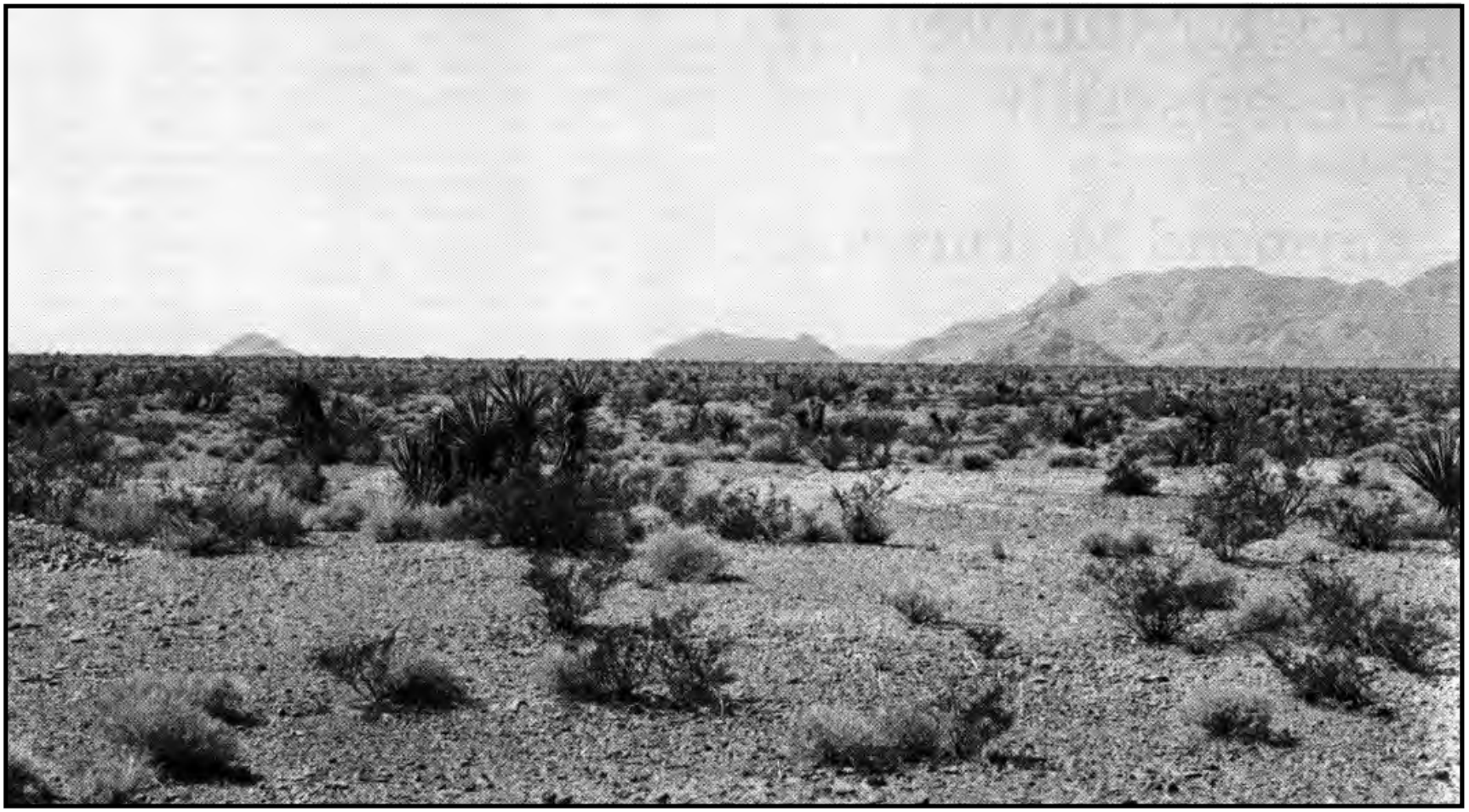

Figure 5-14. Mojave Desertscrub East of Spring Valley Mountains, Clark County, Nevada, ca. 1,220 m Elevation. A Creosotebush (Larrea tridentata)-Bursage (Ambrosia dumosa) series with yuccas present (Yucca schidigera, Y. baccata, Y. brevifolia) [Figure 90; Brown, 1982].

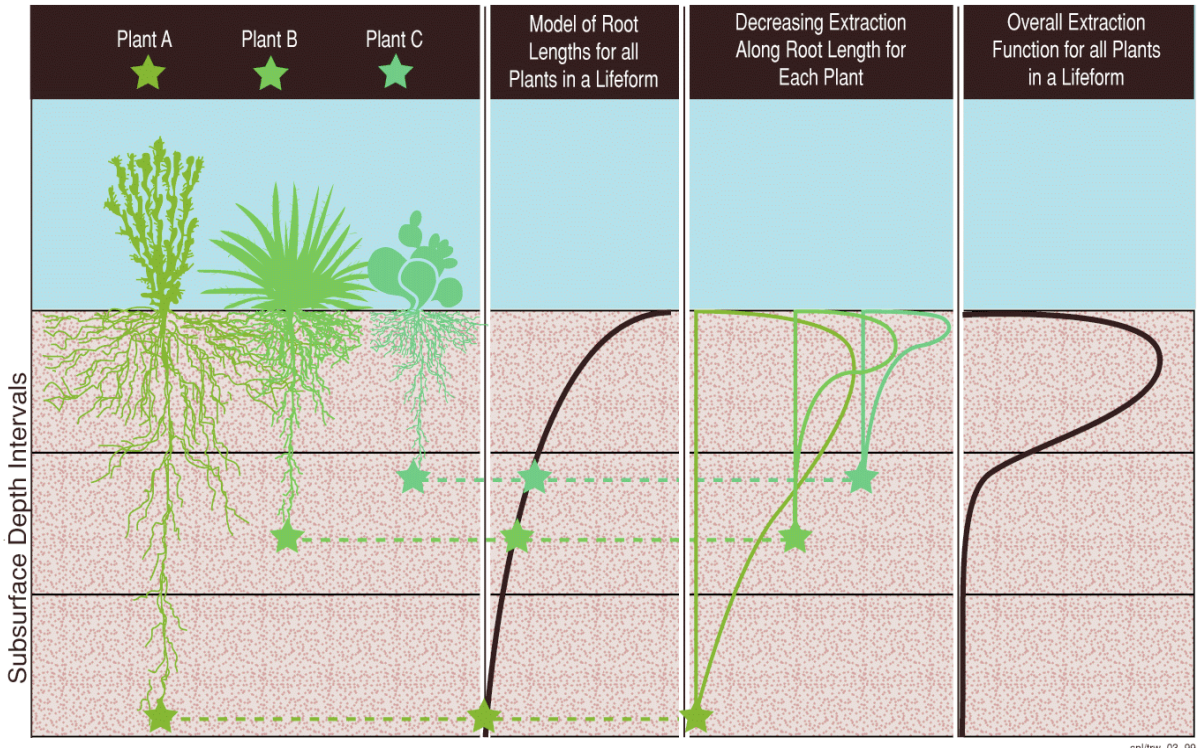

Figure 5-15. Simulating Uptake as a Function of Root Length and Extraction.

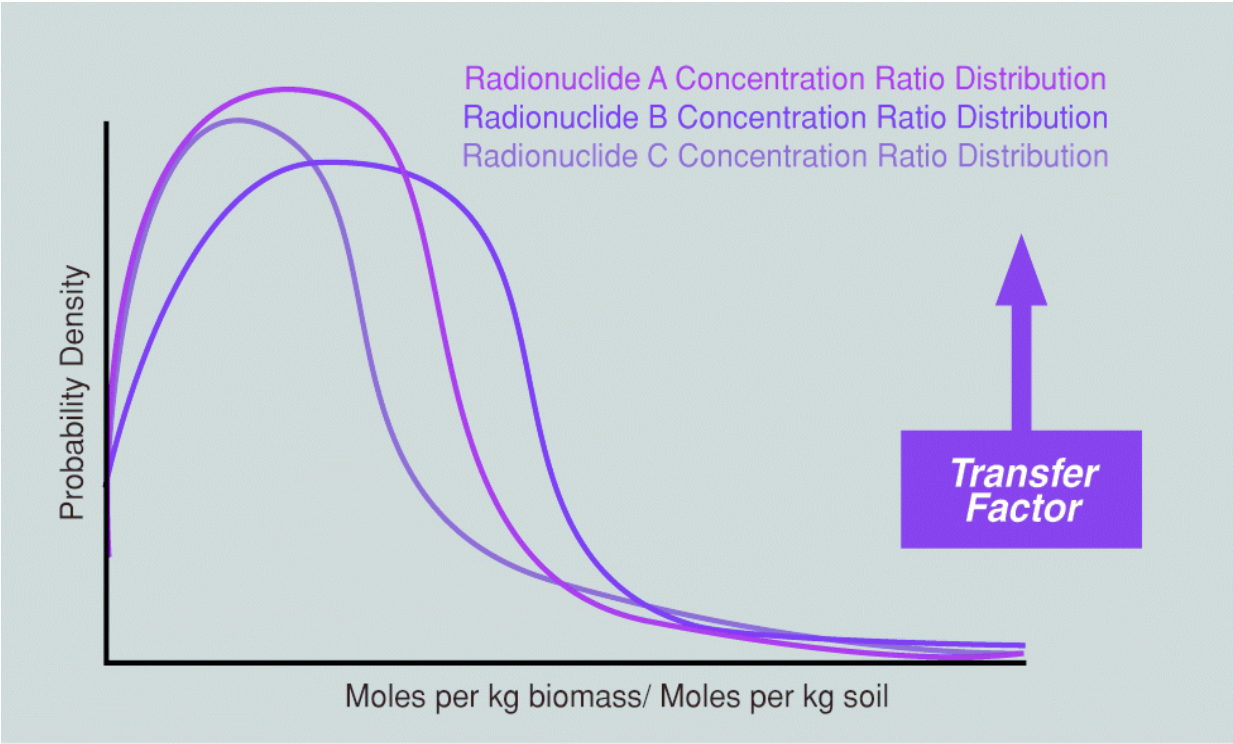

Figure 5-16. Simulating Uptake as a Function of Concentration Ratios.

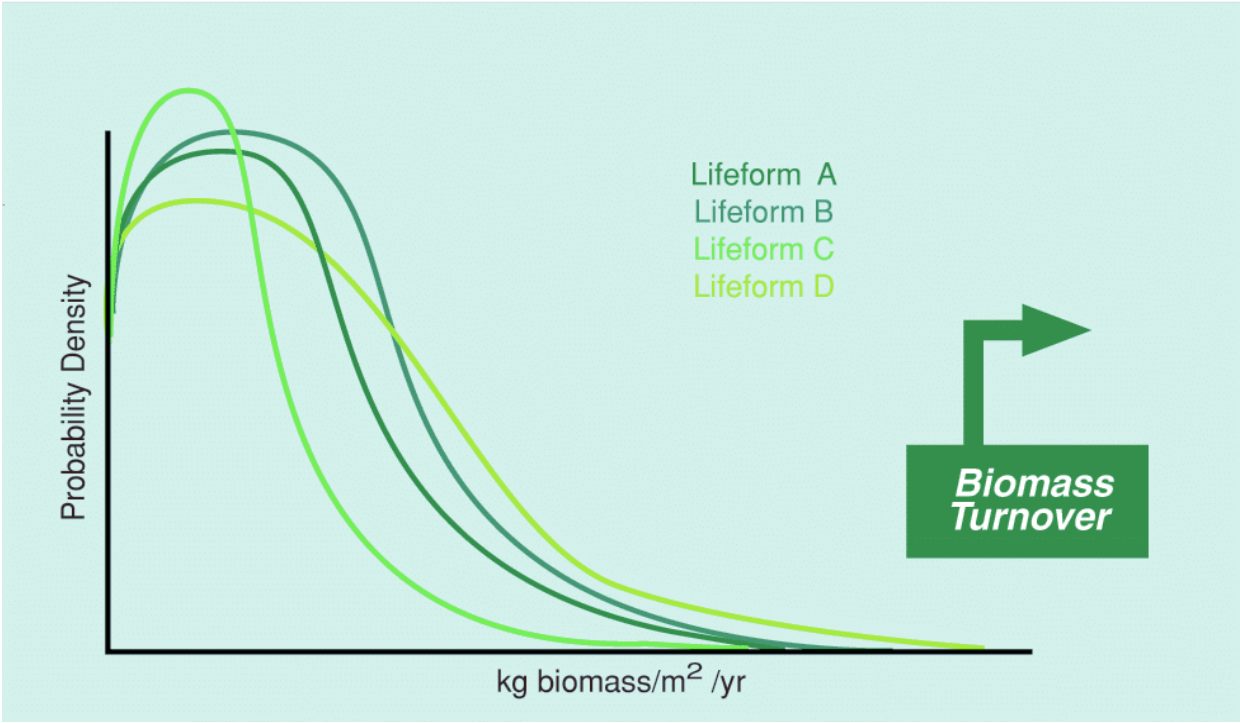

Figure 5-17. Simulating Uptake as a Function of Biomass Turnover.

and follow similar patterns with depth. That is, roots tend to terminate more readily in the near-surface layers where resources are available than they do at depth, where resources are more scarce. Figure 5-18 illustrates this, using shrub maximum root lengths as an example. Data on maximum root length and the knowledge that roots extract more resources near the surface than at depth are combined to develop a distribution that describes relative extraction rates by roots. Relative extraction rates are then used to estimate the relative amount of biomass supported by resources extracted from the soil by roots from any soil depth. In summary, the model is designed to account for the fact that roots and resources concentrate in the near-surface soil layers.

5.7.4 Numerical Model

Radionuclide release due to plant uptake is modeled as a concentration-dependent rate of mass transfer from the soil to the plant, transport within the plant from the point of uptake, and eventual death of the plant (or shedding of plant parts), releasing radionuclides to the land surface. Mathematically, plant uptake is modeled as:

$$Q_{pi} = \int_z U_{ci}(z)\, m_i\,(z)\, dz \qquad (5\text{-}4)$$

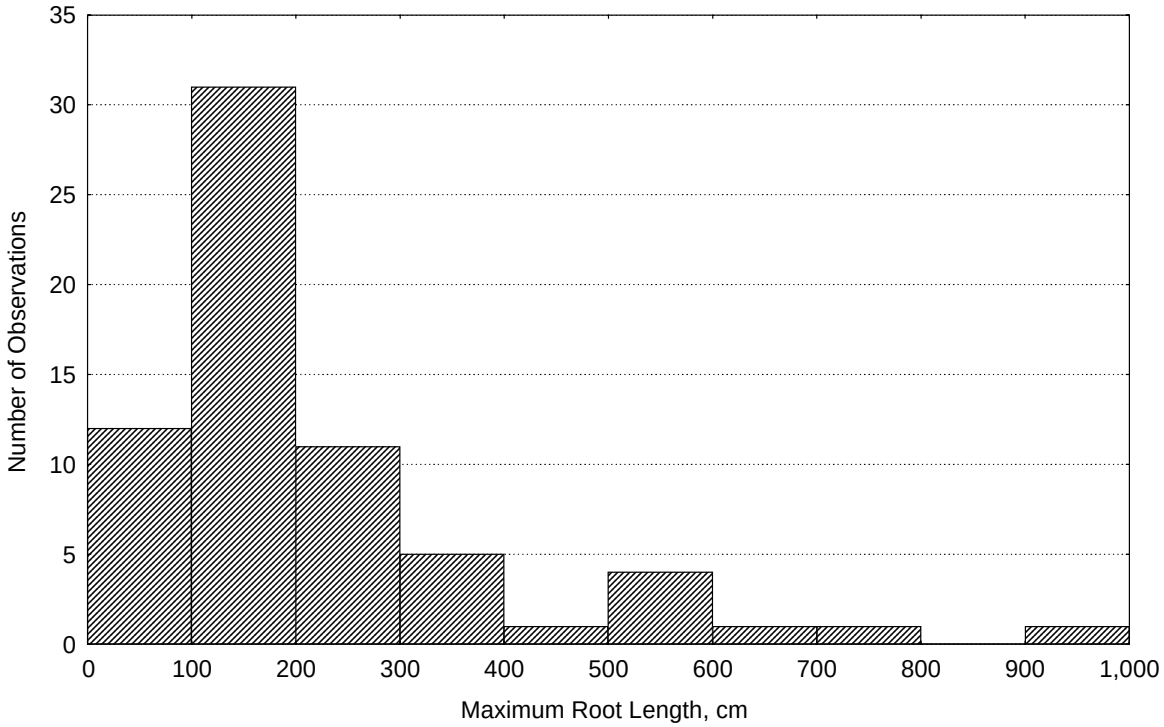

Figure 5-18. Frequency of Maximum Root Lengths for Shrubs.

where

Q_{pi} = total flux of radionuclide *i* due to plant uptake (moles removed from soil/m^2 yr);
$U_{ci}(z)$ = composite community transfer factor describing the rate of removal of radionuclide *i* by plants per unit soil concentration at depth *z* (moles in plant/yr/m^3 per moles in soil/m^3); and
$m_i(z)$ = total mass density of radionuclide *i* at depth *z* (moles in soil/m^3).

As described in the previous section, U_{ci} varies with depth *z*, reflecting variations in plant root mass and resource availability. The model does not vary with time and thus, U_{ci} represents the expected long-term average behavior of plants within a particular community. Community changes over time are modeled using different transfer factor functions, denoted by the subscript "*c*." U_{ci} is treated as a random variable with a probability distribution that describes uncertainty about its actual value. The probability distribution for U_{ci} is developed using the functional decomposition detailed below, which relates the value of U_{ci} to other properties of the plant community. Total mass density of radionuclide *i* at depth *z* ($m_i(z)$) is discussed in Section 7.0.

The plant community is divided into a number of lifeform groups (n_g). Each lifeform (*j*) is characterized by an overall biomass turnover rate (B_j), a concentration ratio for the particular radionuclide (CR_{ij}), and a relative extraction rate function, $R_j(z)$. All quantities are uncertain and are therefore described by random variables. The composite transfer factor, $U_{ci}(z)$, includes the annual contribution of all lifeforms in a community and is given by:

$$U_{ci}(z) = \sum_{j=1}^{n_g} B_j CR_{ij} R_j(z) / \rho \qquad (5\text{-}5)$$

where

$U_{ci}(z)$ = composite community transfer factor per year;
B_j = biomass turnover rate for lifeform j (kg plant biomass/m^2 yr);
CR_{ij} = concentration ratio for lifeform j (moles radionuclide i per kilogram plant biomass/moles radionuclide i per kilogram soil);
$R_j(z)$ = relative extraction by plant roots of lifeform j per m length of roots (1/m); and
ρ = mass density of soil (kg/m^3).

The function $R_j(z)$ describes the long-term average uptake by roots of the plants in each lifeform as a function of depth z, and is defined from the relative extraction functions for the individual plants in the community (n_I):

$$R_j(z) = \frac{\sum_{k=1}^{n_I} R_{Ijk}(z)}{n_I} \qquad (5\text{-}6)$$

However, Equation 5-6 cannot be used to estimate $R_j(z)$. Instead, measurements of the maximum observed root length for a number of individual plants that have been grouped into lifeforms by species are used to estimate $R_j(z)$. Each individual plant is characterized by its maximum root length l_{max}. $R_j(z)$ for each lifeform can be calculated as a weighted sum over the possible values of the maximum rooting length:

$$R_j(z) = \int_{l_{max}}^{\infty} X_j(l_{max}) R_{Lj}(z; l_{max})\, dl_{max} \qquad (5\text{-}7)$$

where

$X_j(l_{max})dl_{max}$ = number of individual plants in group j with a maximum root length of l_{max} (unitless); and
$R_{Lj}(z;l_{max})$ = relative extraction function for individual plants having a maximum root length of 1_{max} (1/m).

The function $X_j(l_{max})$ describes the relative frequency of maximum root length for individuals in each lifeform group. This function can be directly estimated from data on root lengths, as can confidence limits for the fitted parameters of this function which capture the uncertainty in the properties of the population given the available data on root lengths. Section 5.7.5 first describes the data compilation process for estimating l_{max}, followed by a specific discussion of the development of $X_j(l_{max})$.

The function $R_{Lj}(z;l_{max})$ describes the variability in contribution to biomass by a given portion of the root system. The relative extraction function for an individual plant is non-zero between the land surface and the maximum root depth, varying in some unknown way within this interval. This function, like $X_j(l_{max})$ is developed from data on root lengths. The development of $R_{Lj}(z)$ is discussed in Section 5.7.6. Sections 5.7.7 and 5.7.8 describe the modeling of CR_{ij} and B_j,

respectively. Figure 5-19 illustrates the steps involved in simulating plant uptake given this numerical model, and can be referenced as support to the information in the rest of Section 5.7.

5.7.5 Root Lengths

5.7.5.1 Introduction

Roots are a dynamic component of the soil environment, actively seeking soil water resources and drawing those resources to them [Everett et al., 1977]. In the arid southwest, the depth of infiltration tends to set the lower limit of rooting depths for all but exploratory roots, constraining most roots to near-surface layers receiving moisture from precipitation. Site-specific data support the assumption that most root depths are limited by the depth of infiltration but that roots can and will grow deeper in areas with increased effective moisture [Wallace and Romney, 1976; Wallace et al., 1980]. Note that both references indicate that infiltrating moisture and rooting depth is limited largely by the presence of a subsurface calcrete layer. Calcrete layer development is not found in all disposal areas at the NTS (e.g., Area 5).

While roots tend to concentrate in areas with high available water, exploratory roots can extend into relatively dry areas of the soil. The depth and extent of root exploration is primarily determined genetically [Foxx et al., 1984a]. For example, some plants have very shallow root systems, regardless of soil conditions at greater depths; other plants send roots to great depths, even though the soil at these depths may be considerably drier. Additionally, decreases in available soil water around roots may be compensated for by root growth [Weaver and Clements, 1938; Noy-Meir, 1973]. The presence of shrub and tree roots at great depths is often due to the ability of these long-lived plants to maintain extensive root systems both within soil and within and along subsurface heterogeneities, such as cracks and fissures, following (and creating) subsurface flowpaths for water. Thus, it is important to evaluate maximum root depth, as well as the depth of infiltration, when assessing the potential impact of plants on a waste site. This is particularly important at the NTS, as plants from arid environments or those from environments with a long dry season have the deepest rooting habits of all [Canadell et al., 1996].

All plants modify their root environment to some degree. One impressive example of this comes from big sagebrush (*Artemisia tridentata*), a shrub broadly distributed throughout the NTS but most common in the Transitional and Great Basin Deserts. Big sagebrush has been shown to act as a "hydraulic lift," actually increasing water content in dry soil layers by releasing water "mined" from wetter soil layers [Caldwell and Richards, 1989]. The water is released at night and during periods of low transpiration and is reabsorbed when transpiration resumes. The root system is considered "self-irrigating." Though the extent of the hydraulic lift phenomenon across plant species is unknown, the impact of this single species appears to improve transpiration on a landscape scale, dramatically influencing the partitioning of water between evapotranspiration and subsurface flow in arid areas [Caldwell and Richards, 1989]. Though this degree of root activity is not accounted for in this model, this information is provided as an example of the dynamic nature of root uptake. This example also emphasizes the possibility that exploratory roots will find and exploit soil layers with available soil moisture, often found in deeper vadose zones.

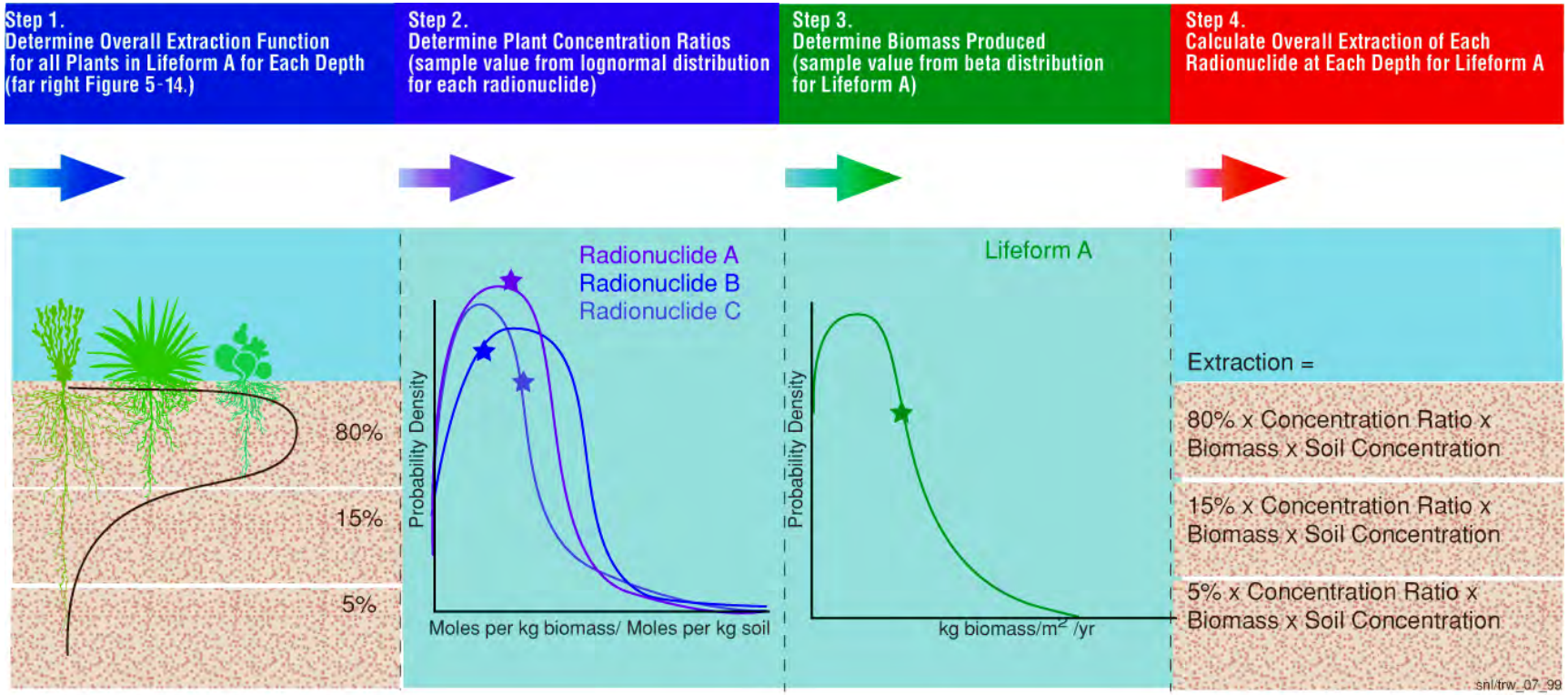

Figure 5-19. Simulation Example (repeat for many individual plants in a lifeform).

All reported root lengths are important to this plant uptake model for the development of $X_j(l_{max})$. For all plants, a maximum rooting depth exists, which may be a function of plant type, size, age, environmental conditions, and site hydrology. This maximum is estimated from existing data, as described in Sections 5.7.5.2 through 5.7.5.4. The modeling of relative uptake is illustrated as Step 1 in Figure 5-19.

5.7.5.2 Assumptions and Uncertainties

The following assumptions were made in compiling the root length data:

- Lateral root length serves as an appropriate analogue for vertical root length and vice versa. The distinction of lateral and vertical roots is often one of origin or form, not of function [T. Foxx, pers. comm, Weaver and Clements, 1938; Canadell et al., 1996]. While some roots may tend towards lateral orientation, in most plants these roots can and will grow vertically, following cracks, fissures, textural boundaries and discontinuities, and moisture zones in the soil. In other words, given similar conditions with depth, roots that grow laterally could extend vertically. Although average, long-term, near-surface conditions are not mirrored vertically, using data for lateral roots growing in more favorable conditions captures more of the uncertainty in how deep roots might grow in the future (either because of changes in moisture infiltration or because of root exploration into deeper soil layers);

Lateral Root Lengths. Assuming lateral roots—which can extend to significant lengths in near-surface soil layers—can also extend vertically, conservatively estimates the probability of roots expected in the deeper, subsurface layers.

- Maximum reported root lengths from appropriate analogue communities, including more mesic locations with potentially deeper-rooted individuals, provide an expected physical limit to rooting depths at the NTS. These analogue sites are from the southwest U.S.;

- Taxonomic similarities translate into physiologic similarities and data for one species can be applied to related species. Individual plants with root length data had to match NTS species, at the very least, at the taxonomic level of genus; and

- Root lengths are best described by continuous, rather than discrete, distributions.

5.7.5.3 Data Compilation

Data were retrieved from a database of plant rooting lengths of native southwestern and western arid and semi-arid plants compiled by T. Foxx [LANL from an extensive literature search of publications reporting root lengths, as well as original data derived from field excavations conducted by Foxx and others in northern New Mexico [Tierney and Foxx, 1987]. A number of reports document these database findings [Foxx et al., 1984a, b; Tierney and Foxx, 1987]. Appendix E includes the root length data used, by species.

Each root length reported in the literature is a separate record in the database; some citations contain numerous records. The values in the database for root lengths are the maximum values reported in the given citation, and as such, can only be considered maximum *observed* rooting lengths, not necessarily maximum *possible* rooting lengths. For example, if an excavation was performed only to a depth of 2 m (7 ft) and roots were found at that depth, then the value recorded in the database is 2 m (7 ft). For this reason, there might by a bias to shallow roots in the data sets compiled, as "maximum observed" samples may truncate the actual distribution of "maximum possible." Lateral root length data were also included in the data compilation in order to derive a distribution of maximum root depth.

5.7.5.4 Development of $X_j(l_{max})$

For each lifeform there are a number of observations of maximum root length for individual members of species in that lifeform, representing a lower bound on the length of the longest root for the individual. However, these data do not completely define the variability in the maximum root length for individuals of the lifeform because the number of observations is limited. For each lifeform, there are enough observations to estimate this distribution of maximum root length (with some uncertainty about the distribution remaining). This uncertainty can be described by assuming a functional form for the maximum root length distribution.

An exponential model for the variability of maximum root length has been assumed for several reasons. An exponential distribution is commonly used to model biological processes. Assuming that the longest root grows at a more or less constant rate over a plant's lifetime, and that rate is characteristic of the plant lifeform, then the distribution of root lengths should follow the distribution of plant lifetimes. Theoretically, the waiting time before the first occurrence of events governed by a Poisson process has an exponential distribution, such as the waiting time until death. Under this assumption of an exponential distribution of maximum root lengths, the relative frequency of maximum root length for individuals in lifeform group *j* is given by:

$$X_j\left(l_{\max}\right) = \frac{1}{L_j} e^{-l_{\max}/L_j} \tag{5-8}$$

where L_j = mean value of the maximum root length for individuals in lifeform group *j* (meters).

The value of L_j is uncertain, but a distribution describing this uncertainty can be developed from the root length observations in the database. Each lifeform consists of species that tend to behave similarly, exploit similar ecological niches, and is likely to be dominated by one or two species from the group of species in that lifeform. It is uncertain which species might dominate a given lifeform in a particular community, and there is no reasonable way of reducing this uncertainty. Assuming that environmental factors shape the distribution of maximum root lengths and that this process is similar for members within a lifeform group, the observed root lengths in the database for a given lifeform are *all* relevant for estimating root lengths for individual plants in an actual community, even though that community may be dominated by a single species from the lifeform. Thus, species-specific information in the database determines only lifeform group classification.

The maximum root length statistics provided in Appendix E (Table E-1) support the assumption of an exponential distribution for the maximum root length. The mean of an exponential distribution is equal to its standard deviation, and the median value is less than the mean by a factor of ln(2) (=0.693). The statistics in Table E-1 (see Appendix E) exhibit these properties with the exception of the median/mean ratio for annual plants. This lifeform has the fewest number of observations, however, and the distribution mean is correspondingly uncertain. Figure 5-20 shows the likelihood distributions for the mean value of maximum root length, L_j, based on the data in Table E-1 (see Appendix E). The 90% confidence interval for annuals is fairly broad, as noted above, ranging from approximately 30 to 60 cm (12 to 24 in.). In contrast, perennial plants have a much larger number of observations (196)—enough to establish the mean value for this lifeform with very little uncertainty.

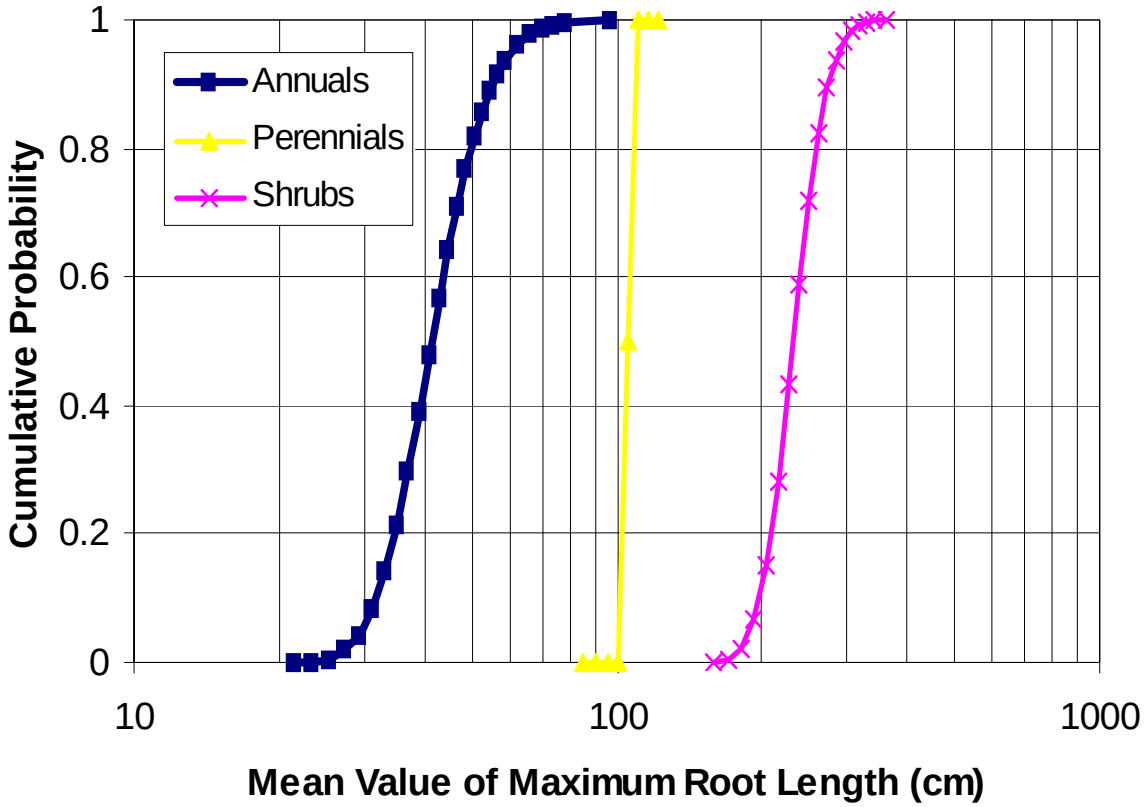

Figure 5-20. Likelihood Distributions for L_j.

The mean value of maximum root length, L_j, is sampled for each lifeform using LHS. The sampled value is used in Equation 5-8 to develop the distribution of maximum root lengths, which in turn is used in Equation 5-7 to calculate the relative extraction for a given lifeform. The pdfs for L_j are given as "continuous linear" functions in LHS, which provides piecewise uniform distributions. These distributions are given in Table 5-8. So, for example, for perennials, half of the sampled values of L_j will be between 1.007 and 1.06 m (3.3 and 3.5 ft), while the other 50% of the sampled values will be between 1.06 and 1.113 m (3.5 and 3.6 ft).

Table 5-8. LHS Input for Mean Value of Maximum Root Lengths

Annuals		Perennials		Shrubs	
Root Length (m)	**Cumulative Probability**	**Root Length (m)**	**Cumulative Probability**	**Root Length (m)**	**Cumulative Probability**
0.2145	0	1.007	0	1.4755	0
0.234	0.002	1.06	0.5	1.589	0.001
0.2535	0.006	1.113	1	1.7025	0.005
0.273	0.019			1.816	0.022
0.2925	0.043			1.9295	0.067
0.312	0.083			2.043	0.153
0.3315	0.141			2.1565	0.281
0.351	0.214			2.27	0.434
0.3705	0.299			2.3835	0.587
0.39	0.389			2.497	0.719
0.4095	0.48			2.6105	0.822
0.429	0.566			2.724	0.893
0.4485	0.644			2.8375	0.939
0.468	0.712			2.951	0.967
0.4875	0.771			3.0645	0.983
0.507	0.82			3.178	0.911
0.5265	0.859			3.2915	0.996
0.546	0.891			3.405	0.998
0.5655	0.917			3.632	1
0.585	0.936				
0.624	0.963				
0.663	0.979				
0.702	0.988				
0.741	0.993				
0.78	0.996				
0.975	1				

Examples of the relative frequencies of l_{max}, $X_j(l_{max})$, are shown in Figure 5-21. The functions produce no surprises: the shorter the average maximum root length, the higher the relative frequency at small values of l_{max}. In other words, the longer the average maximum root length, the lower the expectation of a root terminating in shallow soil depths.

The distributions of maximum rooting length have been designed conservatively for use in this PA for the GCD facility, a relatively deep disposal configuration. The distributions used available data on root lengths which can lead to modeled root depths at or near the waste. Note that these deep roots are rare, that very little extraction occurs at depth, and that there is limited sensitivity to this for the GCD PA. Note also that this insensitivity to root depth may not hold

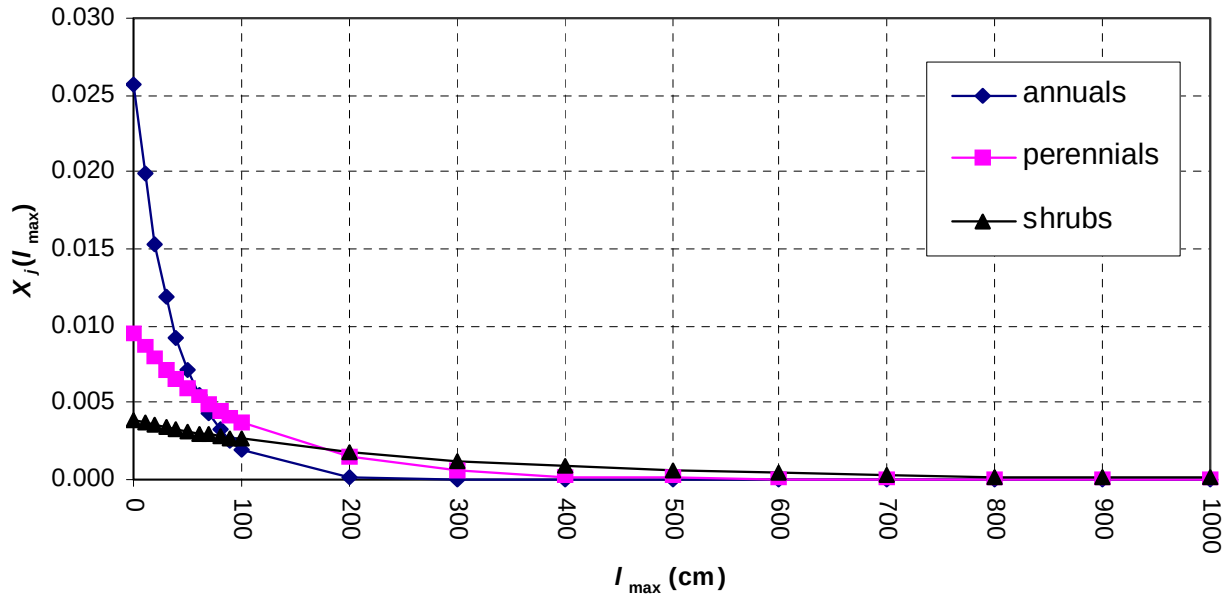

Figure 5-21. Examples of $X_j(l_{max})$.

true for PAs modeling the release of radionuclides from shallow buried waste; the maximum rooting depth may need additional consideration (i.e., the examination of site-specific data) for shallow, low-level radioactive waste disposal configurations at the NTS.

5.7.6 Development of $R_{Lj}(z; l_{max})$

Soil microsite conditions vary considerably across space and through time, producing variations in root activity. Local soil conditions influence root activity throughout a plant's root system. The actual contribution by a given portion of the root system to biomass depends largely on resource availability within a soil interval and the extraction that occurs by roots within that interval. The relative extraction function for an individual plant is non-zero between the land surface and the maximum root depth and varies in some unknown way within this interval. The model of extraction presented here assumes that the variations in extraction among individual plants of the same lifeform is due to the variation in the maximum rooting length over those individuals: the shape of the relative extraction function scales with maximum rooting length. Here, maximum root depth (l_{max}) is modeled and uptake is scaled as a function of l_{max} using a beta function bound by the land surface and l_{max}. The shape of the beta curve is treated as uncertain and is varied by altering the parameters of the beta function, as detailed below.

The beta "distribution" function is a good choice to represent the spatial variations in relative extraction rate because it is bounded, normalized (like the relative extraction), and can be warped into a wide variety of shapes reflecting the uncertainty about the behavior of individual plants. "Distribution" in this sense does not describe a probability density, but rather the variation of extraction rates with depth.

While not all possible relative extraction functions (e.g., multimodal functions) can be approximated by the beta function, it can represent preferential extraction from shallow roots. Thus, for

each individual plant we assume that $R_{Lj}(z; l_{max})$ is described by a beta function defined between the land surface and the maximum observed root length. Uncertainty in $R_{Lj}(z; l_{max})$ is represented by assigning probability distributions to the parameters of this beta function. Another assumption is that whatever the parameters of the beta function are, they are the same for all individuals of the lifeform.

Extraction throughout the soil profile is systematically described by a beta function between a depth of 0 and l_{max}:

$$R_{Lj}(z; l_{max}) = Cz^{\alpha}(l_{max} - z)^{\beta} \quad \text{with} \quad C = \frac{\Gamma(\alpha+\beta+1)}{\Gamma(\alpha)\Gamma(\beta) l_{max}^{\alpha+\beta+1}} \tag{5-9}$$

Values of parameters α and β are provided so that the relative extraction rate function allows for varying degrees of decreasing extraction with depth. The beta functions plotted in Figure 5-22 illustrate the way that extraction is modeled for different choices of α and β.

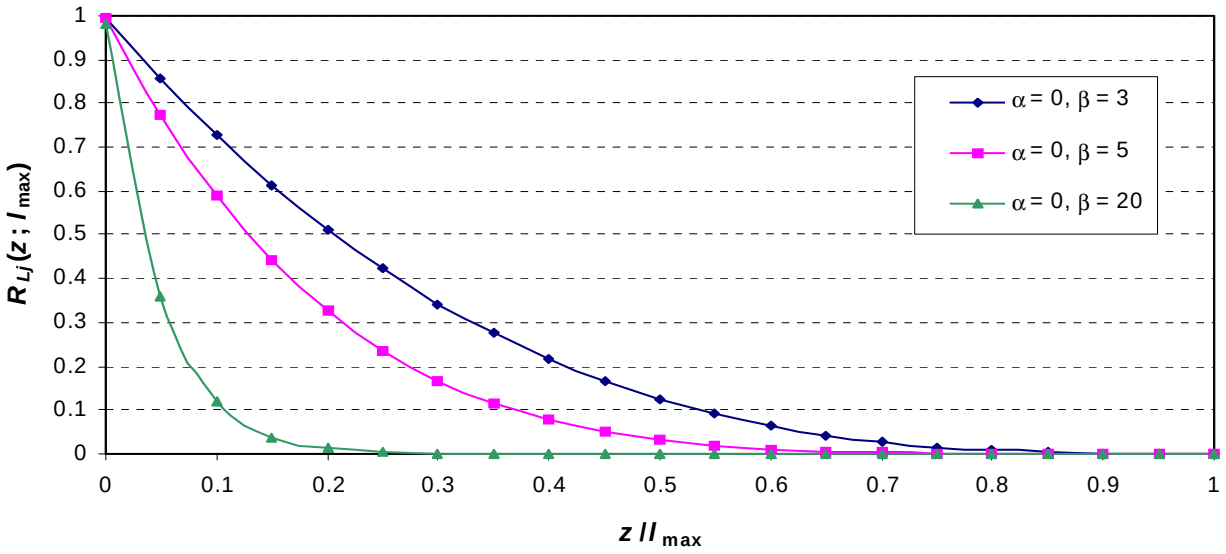

Figure 5-22. Beta Functions of Relative Extraction with Depth, Normalized to the Longest Observed Root Depth (z/l_{max}).

Holding α = 0 ensures that the maximum extraction rate will occur near the surface. Increasing β tends to shift the "mass" of the distribution toward the surface (x = 0); that is, extraction by near-surface roots exceeds that by deeper roots. At approximately β = 20, large increases in β are required to shift the position of the relative extraction curve, sometimes only slightly. As β falls below 3, the shape of the curve begins to "flatten," meaning that relative extraction is nearly uniform across depth. Given that there is little information on the specific mechanisms responsible for differential extraction with depth, the following sampling protocol is used:

- All beta functions describing relative extraction with depth are considered equally probable; thus, pdfs of α and β are uniform;

- Parameter α is held constant at zero to maximize relative extraction near the surface; and
- Parameter β ranges between 3 and 20 to model classes of extraction functions that provide for decreasing amounts of extraction with depth.

5.7.7 Concentration Ratios

5.7.7.1 Introduction

For plants growing in contaminated soil, the complex process of radionuclide uptake is simplified into a parameter called the concentration ratio, and as defined in Equation 5-10 is described as follows:

$$CR_{ij} = \frac{\text{pCi activity per kg dry above-ground biomass}}{\text{pCi activity per kg dry soil}} \qquad (5\text{-}10)$$

the units of radionuclide activity are not always in pCi. However, as long as the units of activity for the plant and the soil are the same, the ratio of plant to soil concentration is preserved and can be used to compare data from different sources. CR_{ij} is defined as zero when the soil concentration is zero.

One limitation of this concentration ratio model is that it is not necessarily applicable to an infinite range in plant and soil concentrations, as is predicted by the linear model. There will always be some concentration above which the uptake rate begins to decline with increasing soil concentrations, which would be observed as an asymptotic curve when plotting plant concentrations against soil concentrations. However, these limits are rarely observed experimentally, nor do they appear to apply to the concentration ratio data compiled here. Thus, a linear relationship between plant and soil concentrations is assumed across the ranges of concentration ratio values complied here. Additional defense for this assumption is provided below.

The process of uptake is an active process. Root surfaces are more than mere semi-permeable membranes that passively receive nutrients from the soil. Roots actively modify their environment, discharging chelating agents and other organic substances that can enhance nutrient extraction and uptake from the soil.

As Sheppard and Evenden [1988] point out, despite the simplicity of the concentration ratio model, the processes underlying plant uptake are very complex, resulting in substantial variability in concentration ratio data. Plant uptake is the result of many different chemical, biological, and physical processes and, as such, is affected by variability in factors such as climate, weather, growth conditions, plant metabolism, plant rooting traits, soil type, soil texture, soil moisture, and soil pH, to list a few. Concentration ratio distributions with several orders of magnitude difference between the minimum and maximum observed concentration ratio are not uncommon [Arkhipov et al., 1975; Dahlman et al., 1976; Whicker, 1978; Sheppard and Evenden, 1988]. This section presents concentration ratio data used to justify a concentration ratio model parameter value and the uncertainty in that model parameter value. A direct application of the

available concentration ratio data to the generation of pdfs for use within the GCD PA is provided. This component of the uptake model is illustrated in Step 2 of Figure 5-19.

5.7.7.2 Assumptions and Uncertainties

This section summarizes assumptions inherent to the concentration ratio model and identifies additional assumptions necessary for modeling plant uptake as a function of the concentration ratio.

One basic assumption of the concentration ratio model is that the plants and soil are in equilibrium. For a given species and a given radionuclide concentration in the soil, all that can be taken up by the plant has been taken up at the time the radionuclide concentrations in the soil and plant are measured. In the strictest interpretation of the concentration ratio model, two assumptions underlying that of plant and soil equilibrium are that plant and soil concentrations are linearly related and that the relationship has a zero intercept [Sheppard and Sheppard, 1985; Sheppard and Evenden, 1990]. As Sheppard and Evenden [1990] found, these assumptions were valid when plant and soil concentrations were averaged by element and that, despite the unique chemical behavior of each element, plant concentrations were linearly related to soil concentrations especially when the latter ranged over five orders of magnitude. Sheppard and Evenden [1990] note, however, that the true relationship of plant to soil concentrations is often difficult to demonstrate in the field, probably because the range of soil concentrations is narrow relative to the effect of other environmental sources of variability. The inclusion of environmental variables, such as soil texture and pH, reduced the variability in concentration ratio estimates only marginally [Sheppard and Evenden, 1990]. Without the means to quantify such variability, the assumption of a linear relationship between plant and soil concentrations must be made, and seems appropriate given the broad range of soil concentrations in many of the studies used here.

Also inherent in the concentration ratio model is the assumption that a given soil concentration results in the same equilibrium plant concentration, irrespective of the actual density of the roots in the soil. Thus, concentration ratio is a function only of root presence and soil concentration. For modeling, this eliminates the need to know root density to calculate plant concentration; the only rooting parameter of importance is the probability that a root is present at a given depth, rather than the actual number of roots present at that depth. Uncertainty in uptake as a function of depth and the change in density of roots with depth is treated separately from concentration ratios using $R_j(z)$.

Another assumption of the concentration ratio model is that the radionuclide isotopes of interest can be grouped by element. Often this was required due to a lack of sufficiently-sized data sets to determine if there were statistical differences (or similarities) among isotopes of a given element. Sheppard and Evenden [1988] provide support for this approach, as they found the variability among isotopes of a given element to be a minor source of the variation in uptake factors. Thus, isotopic specificity was not retained.

The concentration ratio model assumes that all roots extract radionuclides from the soil with equal efficiency and contribute in equal shares to the production of plant biomass. The uncer-

tainty in the contribution of different roots to plant uptake is addressed explicitly in the models of relative extraction as presented above.

This plant uptake model also assumes that all aboveground biomass tissue accumulates radionuclides similarly. The likelihood of different tissue types (e.g., woody versus herbaceous tissues) accumulating radionuclides differently is not addressed due to the scarcity of data available to make such a distinction between tissue types. Thus, the concentration ratio distributions developed for each radionuclide include all applicable data found for any aboveground tissue type.

One final assumption made in modeling radionuclide uptake through the incorporation of radionuclides into plant biomass is that release to the accessible environment via plants occurs only through aboveground plant biomass production and turnover.

5.7.7.3 Data Compilation

Concentration ratio data were compiled from a literature search for native, desert plants. Five criteria were used to screen the concentration ratio data:

1. The plant species had to be from arid or semi-arid locations in the western and southwestern U.S. For most of the studies used, the plants were either identical to species native to the NTS or from the same genera as plants native to the NTS.

2. Only concentration ratio data for aboveground plant parts were used. Roots are not part of the aboveground biomass that is shed from the plants and thus do not contribute to cumulative releases to the accessible environment. Additionally, root concentration ratio data are often suspect of surface contamination. Failure to take appropriate measures to wash contaminated soil from the root surfaces can result in gross overestimations of the concentration ratio. In most studies, it was impossible to verify that such precautions were taken, and as a result, it was deemed best to exclude all root concentration ratio data.

3. Only data from plant samples that were washed of potential surficial contamination were considered here, as unwashed samples can lead to erroneously high concentration ratio values and fail to adequately represent radionuclide uptake through plant roots. Washing is not always 100% effective at removing external foliar contamination and does not completely ensure that uptake through foliar deposition is eliminated as a pathway for radionuclides into plant biomass. This criterion eliminates potential surface contamination, which should not be confused with foliar contamination via root uptake from the soil. Foliar deposition from contaminated dust and airborne particles is an issue for other PA transport models, and data suspected of such “error” were excluded.

4. Only data reported as a function of the ratio of the plant sample’s dry weight to the soil sample’s dry weight were used. This was deemed important in reducing some of the variability in the concentration ratio data. Reducing this variability, which is difficult to control, has led most researchers to report concentration ratio data in units of plant and soil dry weight [Sheppard and Evenden, 1988].

5. Because radionuclides can be transported to all aboveground plant parts, no distinction among plant parts was made. In other words, there was no justification to exclude concentration ratio data for some plant parts, while including concentration ratio data from other plant parts. Accordingly, all concentration ratio data for aboveground vegetation were screened for inclusion in the data sets.

Building data sets for some of the radionuclides required a unique approach not fully addressed by the screening criteria. These "special cases" are detailed below.

- Lacking concentration ratio data for ^{227}Ac, ^{241}Am was used as an analogue for ^{227}Ac. This is in accordance to Grogan's [1985] assumption that the two radionuclides behave similarly because they share a dominant oxidation state (+3). Their chemical similarities and the fact that both are actinide elements are considered sufficient reasons to use Am as an analogue for Ac.

- Concentration ratio data for ^{237}Np were compiled as an analogue for ^{231}Pa data—again, due to a lack of data and in keeping with assumptions of chemical similarity between the radionuclides as detailed by Grogan [1985].

5.7.7.4 Statistical Analyses and Results

As with the other parameters used to estimate plant uptake, the model requires concentration ratio distributions that adequately describe the uncertainty associated with a single, lumped parameter which represents a value for a broad spatial area, a long time period, and a diverse mix of plant species. The concentration ratio data sets compiled are collections of measurements taken at relatively small spatial and temporal scales from studies where some factors affecting radionuclide uptake were experimentally controlled, other factors were experimentally varied, and still others were not controlled.

A lognormal distribution is suggested by Sheppard and Evenden [1988] to account for the uncertainty in concentration ratio data because concentration ratio values result from the product of several variables. This conclusion is consistent across many different uptake studies [Gilbert and Simpson, 1985; Sheppard and Evenden, 1988; Sheppard and Evenden, 1990; Murphy and Tuckfield, 1992]. Accordingly, parameters of the lognormal distribution of each data set were calculated from the measured data. Lacking concentration ratio values from the population of interest (lumped parameters for a specific disposal area), this is a reasonable next-best approach.

A perfect match of the collected data and the assumed distribution(s) is not a necessary requirement for data parameterization. Nonetheless, "goodness-of-fit" measures (Shapiro-Wilk and Lilliefors normality tests) were used to evaluate the lognormality assumption for each data set. The results of the distribution tests performed on the log-transformed concentration ratio data for the current shrubland and potential future communities are presented in Appendix F (Tables F-2 and F-3).

Statistical parameters for each data set are presented in Table 5-9. The mean and the standard deviation were determined from the underlying normal distribution of each data set, while the upper and lower quantiles were generated assuming lognormal distributions. Input to LHS is taken from the parameters given in Table 5-9. The pdf of native concentration ratio for each element is assumed to be lognormal and to have 0.001 and 0.999 quantiles as given in Table 5-9.

Table 5-9. Statistical Parameters for Concentration Ratio Data, Current Shrubland Conditions

Radionuclide Element	Parameter (pCi/dry plant mass per pCi/dry soil mass)						
	n	min.	max.	mean[a]	standard deviation[a]	0.001 quantile[b]	0.999 quantile[b]
Am (analogue for Ac)	12	6.0E!05	1.7E!02	2.2E!03	4.7E!03	1.7E!05	5.4E!02
Np (analogue for Pa)	12	7.0E!03	2.8E!01	1.1E!01	1.2E!01	5.2E!03	1.1E+00
Pb	20	1.4E!03	9.9E!01	3.2E!01	3.7E!01	1.3E!02	3.6E+00
Pu	13	1.4E!05	8.6E!04	1.6E!04	2.4E!04	1.5E!06	2.5E!03
Ra	30	4.7E!03	7.4E!01	1.7E!01	1.7E!01	9.4E!03	1.6E+00
Th	24	1.2E!02	1.1E+01	1.4E+00	3.1E+00	8.5E!03	3.5E+01
U	24	4.3E!03	1.9E+00	2.9E!01	4.8E!01	4.5E!03	5.1E+00

[a]This parameter is from the underlying normal distribution.
[b]This parameter is from the data's lognormal pdf.

5.7.8 Biomass Turnover

5.7.8.1 Introduction

This section addresses parameter selection for the amount of contaminated plant material produced annually (biomass productivity) or released to the environment through the shedding of vegetation (litterfall). This component of the plant uptake model is illustrated in Step 3 of Figure 5-19.

Productivity represents the sum total of a plant's ability to acquire resources of all kinds (e.g., water, light, nutrients) and survive when resources are scarce or unavailable. Productivity is a gross plant- or community-level response to the conditions at a site. It is also a highly variable response that differs from species to species, site to site, season to season, and year to year. The single, largest controlling factor to productivity in southwest deserts is precipitation. Other physiological (ability to tolerate drought or high temperatures, for example) or abiotic (such as climatic or edaphic constraints on growth) factors operate simultaneously in controlling productivity. The relative importance of these constraints can vary considerably, both temporally and spatially.

Over the lifetime of an individual plant, biomass not lost over short time scales through such processes as leaf shedding and herbivory is eventually lost upon the plant's death. Biomass gains and losses (which combined are termed "biomass turnover") within plant communities also balance over long time scales as individuals within the community die and are replaced. Of the

abiotic factors affecting productivity at the NTS, some years are favorable for some or all of the lifeforms present, while other years are less favorable for some or all of the lifeforms present. The possibility of a correlation in productivity among the lifeforms exists (with some species responding similarly to environmental cues and others responding quite differently), though the existing data are too limited to defensibly establish these correlations.

5.7.8.2 Assumptions and Uncertainties

The major assumption made in compiling and presenting data is that the total amount of biomass produced within a year can serve as an appropriate analogue for the amount of biomass shed in a year, or vice versa. This assumption holds true for long-term averages of productivity and litterfall in shrubland and woodland areas of the Great Basin north of the NTS [Passey et al., 1982]. Assuming equivalency of productivity and litterfall allows the prediction of biomass turnover when only productivity or litterfall data are available. This assumption also serves to increase the total usable information for predicting biomass turnover when both types of data are available.

Another assumption made is that productivity among the lifeforms is uncorrelated. Ignoring possible correlations would produce the greatest error in simulations where, in reality, two highly productive lifeforms are negatively correlated but the sampling procedure pulls out high values for each, resulting in simulated doses and fluxes exceeding expected values. Error could also occur in the opposite direction; if two low values are sampled when one should be high, the result would be simulated doses and fluxes that fall below expected values. The correlations could be evaluated probabilistically to determine if resolving the uncertainty would significantly alter the conclusions. If sensitivity analyses show this overestimation causes a false indication of failure to meet the performance objectives, then the benefit of collecting additional data to reduce uncertainty in the correlations should be further evaluated. However, it is unlikely that there is a cost-effective method for reducing uncertainty in the correlations, as field studies would require intensive sampling over long observation periods.

5.7.8.3 Data Compilation

Estimates of current shrubland productivity and litterfall were compiled from studies at various NTS locations, including areas within both the Mojave and Transitional Deserts [Strojan et al., 1979; Hunter and Medica, 1989; Turner and Randall, 1989]. The data represent a total of 12 years with both relatively large and small productivity measurements for all the lifeforms. The compilation of data from across the NTS is consistent with an NTS study by Hunter and Medica [1989] that found no significant differences among different basins for the total amount of biomass per hectare; these results indicate that the most important abiotic constraints to site-wide productivity operate at regional scales and produce similar community-level vegetation responses even among seemingly different areas within the NTS boundary. The results are also consistent with the assumption that precipitation (as expressed by effective moisture) is the single most important constraint on plant communities at the NTS. Ultimately, the proposed conceptual model of community changes through time conforms to the results by Hunter and Medica [1989] in assuming changes in both the total and relative percentages of lifeforms are driven by changes in the amount of effective moisture.

The data were treated as follows to compile litterfall and annual net primary (ANP) productivity data:

- Litterfall was reported for two years in Strojan et al. [1979]. The data were given by species, so it was possible to group the data into lifeform categories. There was one category in the report ("others") for which litterfall was estimated, not measured. The average relative percentages of measured shrub and perennial litterfall were applied to this value to estimate the approximate contribution of each lifeform to the unmeasured portion of litterfall.

- Turner and Randall [1989] report ANP for shrub and perennial species for six years and productivity of annuals for 11 years. There are three additional years with total productivity of non-annuals, though the data are not given by species; similar to the approach outlined above, the average relative percentages of measured shrub and perennial productivity were applied to these ANP totals to approximate the relative contribution of each lifeform. Turner and Randall [1989] also provide estimates of annual standing crop biomass (ASC) for two years. The average ratio of ANP to ASC was determined for perennial and shrub species. With these ratios, ANP could be estimated when only ASC was given.

- Standing biomass estimates of shrubs and perennials were given in Hunter and Medica [1989] for 18 plots across the NTS. These ASC values were converted to estimates of ANP with the ratios of ANP/ASC determined from Turner and Randall [1989]. Productivity of annuals was reported for seven plots located within five different alluvial basins or valleys at the NTS.

Appendix G includes the data for biomass productivity and litterfall.

5.7.8.4 Statistical Analyses and Results

Beta distributions were determined to be the best options for representing the biomass turnover data because of their flexibility in form and because they can be bound at a maximum value. The criteria that each distribution be bound at a maximum was deemed necessary since the productivity of individuals is limited at some upper value. The observed maximum was set as the upper bound, assuming this value reasonably represents the most growth that will occur for each lifeform under the particular sets of conditions at the analogue sites. Whether lognormal or normal, a distribution that is unimodal can be described with a beta function. Though not presented, histograms for each data set were examined for unimodality and all data sets passed this criteria. The cumulative probability distributions for each data set are shown in Figure 5-23. The statistical parameters for each data set are given in Table 5-10.

The statistical parameters given in Table 5-10 were used to develop input for LHS. For each lifeform, the beta distribution for biomass turnover was described by giving the minimum and maximum values of biomass turnover along with the α and β shape factors shown in this table.

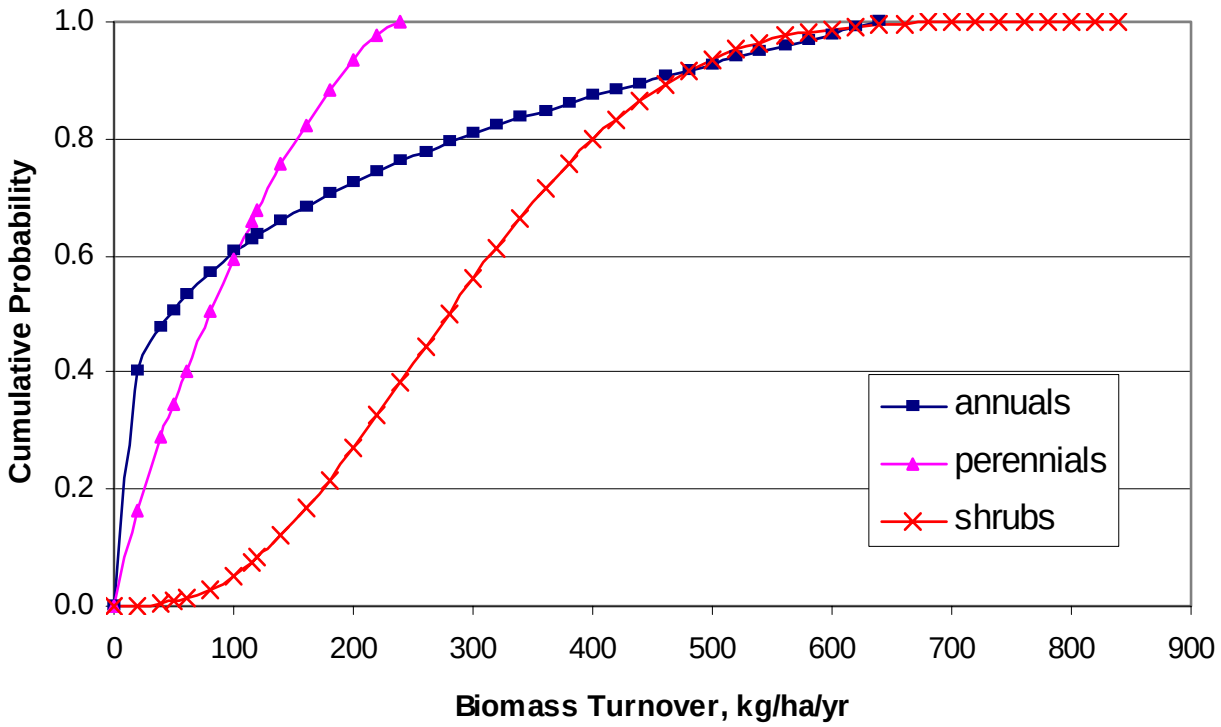

Figure 5-23. Biomass Turnover Cumulative Probability Distributions for Current Shrubland.

Table 5-10. Statistical Parameters of Biomass Turnover Data for Current Shrubland

Parameter, kg/ha/yr	Lifeform			Site-Wide Total
	Annual	Perennial	Shrub	
n	20	29	29	11
mean	140	91	306	485
median	52	80	276	350
minimum	0.24	2	120	194
maximum	644	242	842	1,326
standard dev.	180	65	175	337
α^a	0.255	0.848	2.01	na
β^a	0.918	1.43	5.79	na

[a]Scale parameter for beta distribution.

5.7.9 Conclusions of Plant Uptake Model

The plant uptake model for the GCD PA categorizes native plants into four lifeform groups: annuals, herbaceous perennials, shrubs, and trees. Trees are included only under future conditions (see Section 6.0), while the remaining three lifeforms are included under both current and future conditions.

The conceptual model of plant uptake has three main components: relative extraction by roots (Section 5.7.6), which is a function of root length (Section 5.7.5); plant/soil concentration ratios (Section 5.7.7); and plant biomass production and turnover (Section 5.7.8). Uncertainty and variability in plant uptake are addressed through the use of pdfs for input parameters: mean value of maximum root length for a lifeform, parameter β for the beta distribution describing relative extraction rate with depth for a lifeform, element-specific native plant concentration ratios, and plant biomass production for each lifeform. The model estimates the flux of radionuclides past the ground surface as a result of plant uptake, and is used in the PA analyses for the CR and IPR.

5.8 Animal Bioturbation

Rodents, invertebrates, and reptiles burrow into the desert soils to seek refuge from temperature fluctuations; the dry, desiccating environment; and predators. Burrows also function as routes taken in foraging activities and as storage areas for surplus food. All of these activities have the potential to transport contaminated soil from the subsurface to the surface. The bioturbation model presented below estimates the movement of radionuclides from the subsurface to the surface as a result of burrowing.

5.8.1 Introduction

The conceptual model of animal-induced release has two main components: (1) burrow depth and (2) burrow volume (or mass). These basic components provide a means for modeling the potential consequences of animal activity as part of the TRU wastes in the GCD boreholes. Data on burrow depth and mass of soil excavated and deposited by burrowing animals at the NTS are provided here. The burrow mass data include density information, so animal density estimates are not required. While the soil matrix (both surface and subsurface) can be altered by biological processes, such as burrowing, the effects of these processes are implicitly included in empirical studies of vadose zone water dynamics, and, as such, are not explicitly addressed in this report. In other words, the effects of historical burrowing activity cannot be removed from vadose zone field studies and measurements of soil characteristics such as moisture content and upward specific discharge include the effects of animal burrowing.

Similar to plant lifeforms, animal species were grouped by guilds. A guild is defined as a similarly-behaving group of species within an ecosystem, and is essentially a means to categorize either the various trophic levels within an ecosystem or the similar species within an ecosystem. Animal species are grouped by the following four main guilds of burrowing animals at the NTS: mammals, invertebrates, reptiles, and birds. A complete listing of animals at the NTS that excavate burrows can be found in Appendix H.

5.8.2 Current State of Knowledge

5.8.2.1 Introduction

In the southwest deserts, burrows function primarily as refuges from: (1) temperature fluctuations (diurnal and seasonal), (2) the dry, desiccating environment, and (3) predators. Burrows can also function as routes taken in foraging activities and as underground storage for surplus food.

Burrows that serve as refuges from the environment are typically built within a relatively narrow range of depths, with soil temperature fluctuations the most common constraint to burrowing activity [Cowels, 1941; Cloudsley-Thompson, 1975; Thompson, 1993]. Diurnal temperature fluctuations are not noticeable below 0.6 m (2 ft) and at depths greater than 1.2 m (4 ft) there is a long delay before the ground temperature warms up to the surface temperature in the spring [Cowels, 1941], suggesting that the optimum depth for burrowing animals seeking shelter from the harsh, arid environment is approximately 0.5 to 1.0 m (1.6 to 3.3 ft).

Burrows that function as pathways for foraging activities can extend to great depths, depending on the type of food being searched for. For example, pocket gopher burrow systems consist primarily of tunnels parallel to the ground surface at the plant rooting depth [Andersen, 1987]. For current conditions at the NTS, this sets a practical limit on burrow depth of approximately 3 m (10 ft), the depth at which nearly 90% of all plant roots can be expected to exist [Wirth et al., 1999].

Soil moisture conditions are sometimes cited as a constraint to burrowing for both mammals [Miller, 1948 and 1957] and invertebrates [Haverty and Nutting, 1976; Smith and Rust, 1994; Crist, 1998]. It is unclear if low soil moisture will inhibit burrowing at the NTS. Relative humidity in burrow systems is consistently higher than that at the surface, often near 100% [Hawkins and Nicoletto, 1992]. Additionally, at the NTS, soils have a small percentage of free water, suggesting soil relative humidities approaching 100% [Stockman, 1992]. Lastly, a study of burrowing mammals indicated burrowing was inhibited by lower plant productivity during dry seasons, not by low soil moisture conditions [Bandoli, 1981].

In some studies (typically those focused on burrow architecture), the term “excavated soil” describes only the soil mass moved during burrow construction. In other studies, like those that measure disturbance from burrowing by studying surface mounds, “excavated soil” describes only the mass of soil deposited onto the surface. A third usage of the term applies to the combination of soil moved for construction and the amount of soil deposited on the surface. Because both types of disturbance are important for the PA model (subsurface mixing and surface deposition), the following terms are defined for use in this report: *subsurface excavation* or just *excavation* applies only to the underground burrow system proper, as in the network of tunnels and underground chambers; *surface deposition* or just *deposition* describes only the soil that is deposited onto the soil surface as a direct result of burrowing activity. Studies that could not be described using these two terms were not useful and were not included.

The following sections (5.8.2.2 through 5.8.2.5) present the current state of knowledge concerning burrowing. This discussion is organized by the four guilds: mammals, invertebrates, reptiles, and birds.

5.8.2.2 Mammal Burrowing

General Ecology

Most studies of mammal burrowing have focused on two medium-sized rodents: the ground squirrel (*Sciuridae*) and the pocket gopher (*Geomyidae*),[4] both with similar counterparts at the NTS. The general ecology of burrowing mammals presented here is largely from reports focused on these two mammals, ubiquitous in western and central North America. They have highly specialized features for soil excavation: dense, massive skulls, large teeth, and heavily muscled forelimbs.

Rodent burrowing activity is seasonally variable, most notably correlated with soil moisture and temperature. Burrowing is minimal during the winter, increases in the spring, tapers off in the summer, and briefly increases again after autumn rains. As mentioned, some research suggests that this seasonal variability is due to favorable digging conditions [Miller, 1948; 1957], while other research suggests that the seasonality of burrowing activity is more closely related to seasonal patterns of primary productivity in the plant community [Bandoli, 1981]. Thus, the correlation of burrowing activity with soil moisture and temperature is likely due to the presence and/or absence of favorable conditions for plant growth. Cox and Hunt [1992] concluded that forage availability is the most important constraint to burrowing.

Vertical soil displacement is unidirectional. The only objects carried below the surface by rodents are plant materials, either for food or nest building. Otherwise, rodent movement of materials is a one-way process in which soil contents are transported from underground to the surface. Despite beliefs that burrowing causes erosion, most research demonstrates that rodent activity actually deepens the soil mantle [Hansen and Morris, 1968; Mielke, 1977; Chew, 1978; Johnson, 1989].

Burrowing activity most frequently affects small soil materials, which are displaced during tunneling, hauled to the surface, and deposited in backdirt mounds around burrow openings. Materials not hauled to the surface are deposited as backfill in older, unused tunnels and chambers. Ultimately, burrow diameter sets the limit on objects moved, with an average gopher burrow diameter of approximately 6 cm (2.4 in.) [Davis et al., 1938; Johnson, 1989]. Research shows that burrowing rodents habitually dig under, not alongside or over, large objects. Large materials eventually "sink" below the zone of burrowing activity, and smaller objects are carried toward the surface. There is evidence that in areas of extreme rodent activity, surface soils can be completely reworked within five to seven years [Thorp, 1949].

[4]Most of this information is taken from Bocek's [1986] review of the ecology and mechanisms of mammal burrowing. Information culled from other sources is called out separately in the text.

Feeding Habits

Burrowing mammals utilize a wide variety of plants. The regular feeding choices of pocket gophers at an Arizona site included an annual (*Lupinus kingii*), perennial herbs (*Cryptantha jamesii, Gutierrezia sarothrae, Hymenoxys richardsonii, Opuntia spp., Oxytropis lambertii,* and *Psilostrophe sparsiflora),* grasses *(Aristida fendleriana, Bouteloua gracilis*), and a shrub (*Chrysothamnus nauseosus*; Bandoli, 1981). Five of these species exist at the NTS and two have closely related counterparts in the same genus. The marginality of the habitat, including the harsh climatic regime and seasonally variable food sources, makes this Arizona study a likely analog for mammal burrowing activity at the NTS.

Roots are a major component of the diets of virtually all burrowing mammals, though above-ground plant parts can play a major dietary role [Huntly and Reichman, 1994]. Foraging is concentrated in patches of locally high productivity. Some burrowing mammals, such as pocket gophers, often preferentially consume certain annuals, forbs, or short-lived perennials. In the case of pocket gophers, preferred plants are often more abundant where pocket gophers are active [Huntly and Reichman, 1994].

Analogue Sites. Many sites with higher productivity than is expected for the NTS (particularly for grasses) were used in the data compilation of burrowing mammal depths. Thus, both high and low mammal population densities are considered in this PA.

Favorable conditions can promote high local abundance of burrowing mammals [Mohr, 1947 and Howard and Childs, 1959]. While population sizes are directly related to ground cover [Davis et al., 1938], local abundance is highest in their preferred habitat of grassland ecosystems. Cover type, as opposed to cover architecture, appears to most influence burrow abundance and pattern [Cameron et al., 1988]. Marginal habitats, with relatively sparse populations of grasses, such as those at the NTS, support lower densities of burrowing mammals than preferred habitats with higher grass coverage [Bandoli, 1981]. Many of the studies used for mammal burrowing data were from sites with higher plant productivity (and thus, more favorable conditions) than currently occurs at the Area 5 RWMS. However, given the uncertainty in possible future climate conditions, there will likely be periods of time with highly productive conditions conducive to rodent population booms. Thus, data for these sites are included in the analysis of animal burrowing impacts on the GCD facility.

Burrow Systems

Most burrow systems have surface openings, feeding tunnels, dens or nesting chambers, and food caches. Mammal burrow systems are basically linear, with a main tunnel, many short lateral foraging tunnels, and a deeper nest chamber that subtends the other tunnels [Cameron et al., 1988]. Feeding tunnels run parallel to the surface, with tunnel-to-surface depths determined by soil texture, horizon thickness, water table height, and depth of penetrating roots (their primary food source). Dens and storage chambers are usually constructed at greater depths than feeding tunnels. The excavated soil is deposited either in abandoned tunnels and chambers or as mounds on the surface. Huntly and Reichman [1994] report that the foraging tunnels comprise 80 to 95% of a burrow system.

The mature burrow system of burrowing mammals appears to reach a steady-state configuration in which size and shape are related to the animals' size and social system and to the physical and resource characteristics of the environment [Huntly and Reichman, 1994].

Burrow architecture is also correlated with dietary preferences, with shorter systems constructed by burrowing animals who also do significant foraging aboveground and more extensive systems maintained by those who are more exclusively underground feeders.

The total area affected by burrow systems ranges widely, depending, among other things, on the particular species present and the condition of the particular ecosystem. In an arid ecosystem study that is a likely analog to the arid conditions in Nevada, pocket gopher systems were found to underlay 7.5% of the study area [Bandoli, 1981].

Burrow Depths

Burrow depths of gophers, as measured in a Texas prairie ecosystem, varied seasonally; maximum depth occurred during summer and minimum depth occurred during late fall and early winter [Williams and Cameron, 1990]. The authors suggest that this was related to rooting depths of annuals, a more commonly consumed resource than perennials in that ecosystem. Thus, the deeper spring and summer burrows reflect foraging at the rooting depths of spring annuals that increase markedly in the diet during these seasons, while the more shallow fall burrows correspond to the root zone for fall annuals. Other research indicates that feeding tunnels created by pocket gophers can vary between 10 and 200 cm (4 and 80 in.) deep, though most are found between 15 and 30 cm (6 and 12 in.). In general, nests and cache chambers subtend the feeding tunnels and have been found as deep as 100 cm (40 in.), with an average depth of 50 cm (20 in.). This same pattern was observed by Erlandson [1984], who found a distinct bimodality of burrowing activity, with the majority of activity at 15 to 20 cm (6 to 8 in.) and 50 to 55 cm (20 to 22 in.). The shallow depth corresponded to feeding activities and the lower depth corresponded to the depth of breeding and nesting chambers. Johnson [1989] also found this bimodality at similar depths, but added that significant activity also occurred at depths below 100 cm (40 in).

Mole and ground squirrel burrow systems are slightly nearer the surface (less than 50 cm [20 in.] deep) than those measured for pocket gophers. Kangaroo rats create distinctive mounds and burrow systems which can extend 1 m (3.3 ft) or more into the soil [Hawkins and Nicolleto, 1992]. Unlike pocket gophers, kangaroo rats burrow to create subterranean caches, not to forage for soil invertebrates or below-ground plant materials.

Vertical tunnels are created as often as necessary to eject accumulated backdirt. This tends to minimize horizontal displacement, as objects are displaced only a short distance prior to being pushed up to the surface. Vertical tunnel spacing is directly related to the number of backdirt mounds created and the amount of soil ejected per mound.

Burrow Volume

Burrow volume data come in two basic forms: studies that focus on subsurface soil excavation and those that provide information on surface soil deposition. Ultimately, both types of data are

useful to the PA, as it is necessary to know the extent of subsurface soil mixing as well as the extent of surface deposition. Excavation data can be used to calculate the amount of soil mass moved from one subsurface soil compartment to another. Deposition data can be used to calculate the amount of soil actually released to the land surface. Data are presented here first for excavation and then for deposition.

Pocket gophers use up to 86% of excavated soil to backfill old tunnels [Andersen, 1988; 1990]. Huntly and Reichman [1994] present data from a number of studies that show gophers can excavate 40 L (10.6 gal) soil/d in a new habitat (equivalent to 64.8 kg/d (143 lb/d) at a bulk density of 1.62 g/cm^3; Brown et al., 1997b) and in longer-used sites can excavate 0.8–16 kg soil/m^2/yr. Other estimates of the annual volume of soil "dislodged" by rodent populations ranges from 0.4 to 4.4 kg/m^2 [Chew, 1978]. Bocek reports that a "reasonable range...is 3 to 15 m^3/ha." Other values for excavation are included in Section 5.8.3.

Deposition, as measured by surface mound production by individual gophers, ranges from 3 to 15 L/d (.8 to 4 gal/d) [Spencer et al., 1985; Andersen, 1987]. At an average bulk density of 1.62 g/cm^3 for NTS soils, deposition by mound production thus ranges from 1775 kg/yr (2 tons/yr) to more than 8875 kg/yr (10 tons/yr). Chew [1978] estimates a much lower daily value for deposition by mound production at 2.3 kg (5 lb) per gopher. Huntly and Inouye [1988] report a deposition rate of 1 to 8.5 kg/m^2/yr, considerably lower than the deposition rate reported by Anderson [1987] or Chew [1978].

Andersen [1987] estimated that mound deposition represented approximately 60% (with a range of 41 to 87%) of the total soil excavated in a burrow system. This should be contrasted with some later work by Andersen [1988; 1990] that estimates the rate of deposition at only 14% of total soil excavated within a burrow. Arthur and Markham [1983] concluded that only 0.05% of the estimated contamination in the surface soils (0 to 5 cm [0 to 2 in.]) was actually deposited on the surface by burrowing activity.

5.8.2.3 Invertebrate Burrowing

Invertebrates of all kinds burrow in the ground for shelter, nesting, and/or harvesting. This section focuses on invertebrates known to reside at the NTS—many of which also specifically reside at the Area 5 RWMS in Frenchman Flat—and are known to burrow, or in some other way disturb or alter soils. Much of the information given here is for ants and termites, two widely-studied insects groups that are also known to burrow somewhat deeper and/or more extensively than other burrowing insects found at the NTS, including desert cockroaches and scorpions [Thompson, 1993].

Both ants and termites excavate extensive subterranean systems, primarily for food storage, breeding, and nesting. Ant species at the NTS can excavate nest chambers as deep as 3 to 4 m (10 to 13 ft) [Blom and Johnson, 1991; Jensen and Hooten, 2000]. Excavated materials, including some particles gathered from the soil surface, are incorporated into surface mounds; "surficial contributions" to these mounds are slight [Jorgensen and Porter, 1982]. Vertebrates have been known to secondarily excavate ant mounds, presumably to exploit mound resources [Clark and Clark, 1989; Blom and Johnson, 1991]. Two experts on desert invertebrates indicated that desert

harvester ants of the families common to the NTS were not likely to construct nests to depths greater than 3 m (10 ft) because most of their foraging is aboveground [Thompson, 1993]. This observation was also made by Jensen and Hooten [2000]. Thus, as is the case for many of the burrowing animals in deserts, subterranean excavation by ants is primarily for protection and escape from the harsh, arid environment as well as for food storage and nesting and breeding activities, requirements that can be met by maintaining burrows within the top 3 to 4 m (10 to 13 ft) of soil.

Subterranean termites in the arid southwest are generally restricted to areas with suitable soil moisture conditions, though they obtain most of their water from the soil and litter they consume [Haverty and Nutting, 1976; Smith and Rust, 1994; Crist, 1998]. Nest chambers of subterranean termite colonies tend to be rather shallow, and are generally limited to the top meter of soil [Lee and Wood, 1971]. Subterranean termites are important detritivores on arid southwest watersheds, processing large fractions of surface plant litter and organic debris, and are reported to be responsible for 40 to 60% of litter decomposition during periods of peak activity from September through November [Lee and Wood, 1971; Elkins et al., 1986].

Subterranean termites transport soil to the surface in the building of gallery cartons—covered runways, shelters, and sheeting—by cementing together soil particles with saliva, fecal material, and occasionally undigested particles of wood and litter [Lee and Wood, 1971; Nutting et al., 1987]. Part of the carton is presumably brought from deep in the soil [MacKay and Whitford, 1988]. Though not directly applicable to the soils at the Area 5 RWMS, it is worth noting that subterranean galleries have been reported to extend into sandy soil to depths of 10 to 15 m (32.8 to 49.2 ft) [Lee and Wood, 1971]. This 10 m (32.8 ft) depth has been observed in areas of the desert southwest [Myles and Hooten, 2000]. In a semi-arid desert in Europe, termite galleries extended to "considerable depths" below the surface, sometimes penetrating masses of limestone [Lee and Wood, 1971]. Because of the difficulty of observing subterranean termites *in situ*, very little information, other than anecdotal accounts, exists for the depth and extent of soil disturbance by termites [Haverty et al., 1975].

The building of galleries is noticeably different from the soil excavation and deposition activities of ants and mammals, who rarely build with the soil they move. Ants and burrowing mammals simply remove soil from subterranean tunnels and chambers to the surface in mounds. Nutting et al. [1987] suggest that termites deposit as much soil on the surface as both ants and burrowing mammals combined, though data compiled here indicate disturbance by mammals is much more extensive than that by termites. Estimates of soil deposition by termite activity range from 95 to 272 kg/ha/yr (380.5 to 3,133 lb/acre/yr) in the Chihuahuan Desert [Whitford et al. 1982] to 70 to 575 kg/ha/yr (516.4 to 1,482 lb/acre/yr) in the Sonoran Desert [Nutting et al., 1987]. Nutting et al. [1987] suggest that most of the soil brought to the surface is usually eroded and returned to the A horizon with a period of 1 to 10 years.

Termite foraging groups are more numerous on deep sandy soil, but are virtually absent in other areas where a calcrete layer is within 30 cm (12 in.) of the surface [Johnson and Whitford, 1975]. Termites use plant roots as a primary food source, following roots to their termination at depth and consuming all food sources encountered to depletion, including plant roots. Myles and Hooten [2000] support this assumption that termites would "mine" roots to their termination.

However, Myles and Hooten [2000] also present evidence that at some point, the depth of this mining by termites is likely to be limited not to the presence of roots, but rather to surrounding microsite conditions, as in water or oxygen availability. Additionally, there exists an energetic metabolic limitation to deep burrowing. Interestingly, plant roots have been found to frequently follow deserted and soil-packed galleries [Lee and Wood, 1971]. Whether the galleries exist because of the roots or the roots because of the galleries, or both, is unknown. Under current conditions, 90% of the roots are in the top 5 m (16 ft) of soil, with a very small fraction of roots that might extend to much greater depths. Lacking information on the depths at which metabolic limitations may limit the mining for roots, this PA assumes that mining to the depth of root termination by termites can occur.

Termites have been observed as deep as 6 m (20 ft) in the arid southwest [Thompson, 1993] and 70 m (230 ft) in west Africa [Yakushev, 1968]. The African study concluded that the termites were mining water for construction and maintenance activities that require a relatively high soil humidity. Soils at the NTS have some small percentage of free water, suggesting soil relative humidities approaching 100% [Stockman, 1992]. Mining for water is not expected of termites at the NTS because favorable soil conditions and the depth to water preclude this type of burrowing.

5.8.2.4 Reptile Burrowing

Desert reptiles are adapted to a wide range of environments [Wallwork, 1982; Thompson, 1993]. Subterranean retreat is used as a mechanism by some reptiles to minimize exposure to the large diurnal temperature fluctuations and desiccating environment of the desert. Some reptiles bury themselves in either hard-packed soil or shifting desert sands. Both snakes and lizards have been observed utilizing abandoned mammal burrows, sometimes digging short, lateral tunnels into the sidewalls of the rodent burrow. Other reptile species find retreat under rock flakes or outcrops or native vegetation.

Dormant lizards have been found in burrows at depths ranging from 30 cm to 1.5 m (12 in. to 5 ft) [Bowers and Smith, 1947; Mayhew, 1968]. Other hibernating reptiles have been observed in burrows just below the soil surface down to 76 cm (30 in.) [Cowels, 1941].

A conspicuous inhabitant of the NTS due to its endangered species status, the desert tortoise, also burrows for hibernation. The desert tortoise is inactive approximately six months out of each year, spending this time within long, horizontal tunnels that do not appear to go very deep; burrowing information for other desert tortoise species is vague, using terms like “shallow” and “deep” without quantifying these terms [Wallwork, 1982; Thompson, 1993].

Reptiles are known to either use burrow systems created by mammals or to burrow below the surface for hibernation or escape from the environment, but they do not create actual burrow “systems.” Because of this, there is no requirement for additional data on the burrowing activities by this guild.

5.8.2.5 Burrowing Birds

The only bird known to burrow at the NTS is the burrowing owl, *Speotyte cunicularia*. The one study found that discussed the habit of burrowing owls [Desmond and Savidge, 1996] reports that these birds appear to favor habitat that already supports burrowing mammals. Because the owls inhabit abandoned burrows, there is no requirement for additional data on the burrowing activities by this guild.

5.8.3 Modeling Impact of Burrows

5.8.3.1 Introduction

Modeling burrow excavation and soil deposition is ultimately constrained by the type of information available, which comes in many forms. There are three basic categories of studies: complete and partial burrow excavations to determine burrow architecture, and direct measurements of the mass of soil moved through the subsurface or to the surface itself. This section describes the three data types and how they can be used to model contaminant flux due to burrow activity.

Burrow architecture is used by researchers to estimate burrow volume with depth. Direct measures of soil excavation and deposition are used to estimate the transfer of that soil among soil depth intervals (both within the subsurface and from the subsurface to the surface). A simple schematic of the burrow components detailed here is provided in Figure 5-24.

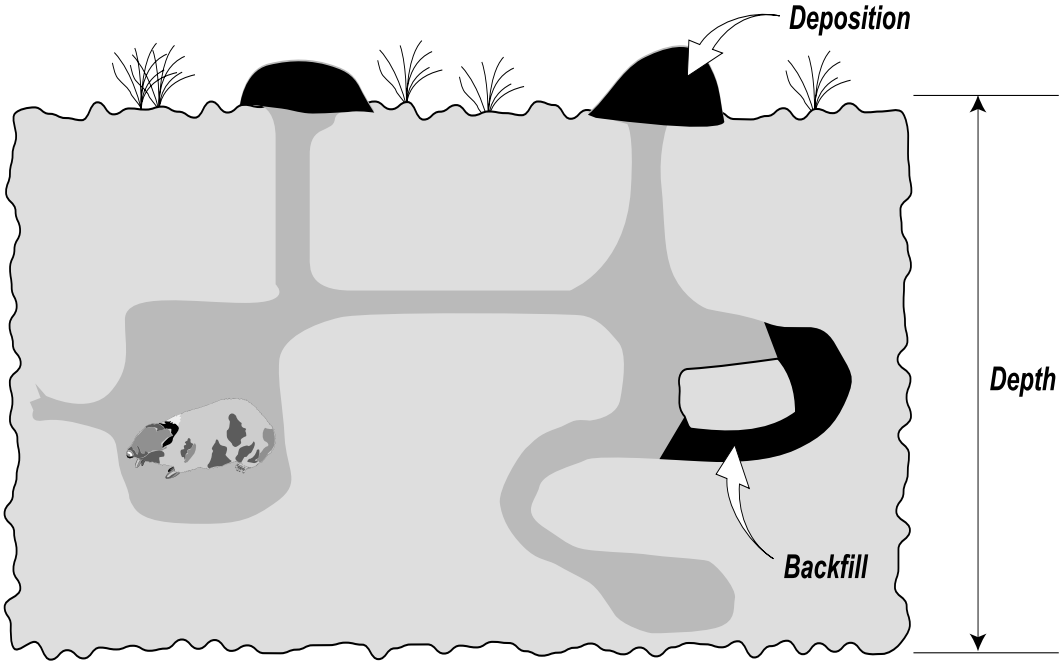

Figure 5-24. Basic Model Parameters Required to Estimate Impact of Burrows.

Complete excavations include studies of full burrow structure *in situ*. Most often, these are excavations performed after injecting polyurethane foam into burrows. The polyurethane foam preserves burrows while the surrounding soil is removed. Due to the intensive nature of such excavations, there are a limited number of these detailed studies reported in the literature. Information from partial excavations is more commonly available; however, more often than not, only one or two burrow characteristics are detailed in a single study—burrow length and diameter or burrow density and depth of nesting chambers, for example. This second type of data usually requires significant input from other sources in order to come up with complete estimates of burrow volume.

Most data available provide only a description of the mass of soil moved within a soil depth interval, not the rate of soil transfer among soil depth intervals. The approach proposed here is to use direct measures of soil moved during burrow excavation to estimate the fraction of burrow mass that is transferred from one soil compartment to the next.

Much of the information provided here was taken from three summaries of animal burrowing activities [Thompson, 1993; Winkel et al., 1995; Smallwood et al., 1998]. Two of these studies [Thompson, 1993; Winkel et al., 1995] specifically address the potential impact of animals on waste disposed at the NTS. Burrow data are limited to species that excavate their own burrows and are known to exist at the NTS (see Appendix H).

Unfortunately, there is a general lack of site-specific data to parameterize the bioturbation model components. This is less true for the mammals than the other guilds. There were enough data found for mammal burrowing parameters to screen for species known to occur at the NTS from studies analogous to the NTS site. For invertebrates, data were compiled for species closely related, but not identical, to those known to occur at the NTS, due to the small number of applicable studies available. Much of the definition of "applicability," however, depends on the appropriateness of extending information from a given study to the NTS; in this sense, site specificity was, in fact, addressed for building model parameters for invertebrates.

5.8.3.2 Numerical Model

The model presented here determines the amount of soil moved by burrowing animals. The model can be implemented to determine both the mixing of soil within subsurface intervals and the transfer of soil from subsurface intervals to the surface. Separate parameters are developed for mammals and invertebrates, as discussed in the following sections. The first step (Equation 5-8) is to calculate the total rate of soil mass excavated by the burrowing animals at the GCD facility as a function of depth. This equation is given as:

$$BR_z = B_m \, p_z \tag{5-11}$$

where

BR_z = soil mass excavated annually within each depth interval z as a function of the proportion of a burrow expected within each interval ($kg/m^2/yr$);
B_m = total mass of soil moved in burrowing activities annually ($kg/m^2/yr$); and
p_z = proportion of a burrow system expected within depth interval z (unitless).

A slight modification of Equation 5-11 describes the actual transfer of the amount of soil from one soil interval *z* to the next, as follows:

$$BR_{ztran} = B_m \, p_z \, p_{ztran} \qquad (5\text{-}12)$$

where

BR_{ztran} = total soil mass transferred annually from one soil interval *z* to another soil interval *z*, kg/m^2/yr; and

p_{ztran} = proportion of BR_z transferred from one soil interval to another, unitless.

The data available to estimate soil transfer among soil layers (Equation 5-12) are: B_m, the total annual rate of soil excavation, burrowing depths for estimating p_z, and excavation rates with depth to estimate p_{ztran}.

5.8.3.3 Burrow Data

The data provided here are from detailed reports that include information on burrowing animals at the NTS. A summary of the pertinent data culled from these reports is provided in Table 5-11.

The mammal excavation data are presented graphically in Figure 5-25. One interesting feature of this data set is the bimodal nature of the data. Examining the locations from which the data were derived indicates that there is not a simple explanation for the high values (e.g., the sites had more favorable climate or forage conditions, and thus, higher than expected rates of burrowing), nor any compelling reason why the high values should be excluded. Thus, all the data presented for mammal burrow excavation in Table 5-11 and Figure 5-25 were retained in the analysis.

Table 5-11. Burrow Data for NTS Guilds

Burrow Parameter	Mammals Depth (m)	Invertebrates Depth (m)
n	47	2
mean	0.81	3.5
minimum	0.10	1.0
maximum	2.0	6.0
	Excavation Mass (kg/m^2/yr)	Excavation Mass (kg/m^2/yr)
n	13	4
mean	24.9	0.0253
minimum	0.23	0.007
maximum	135	0.0575

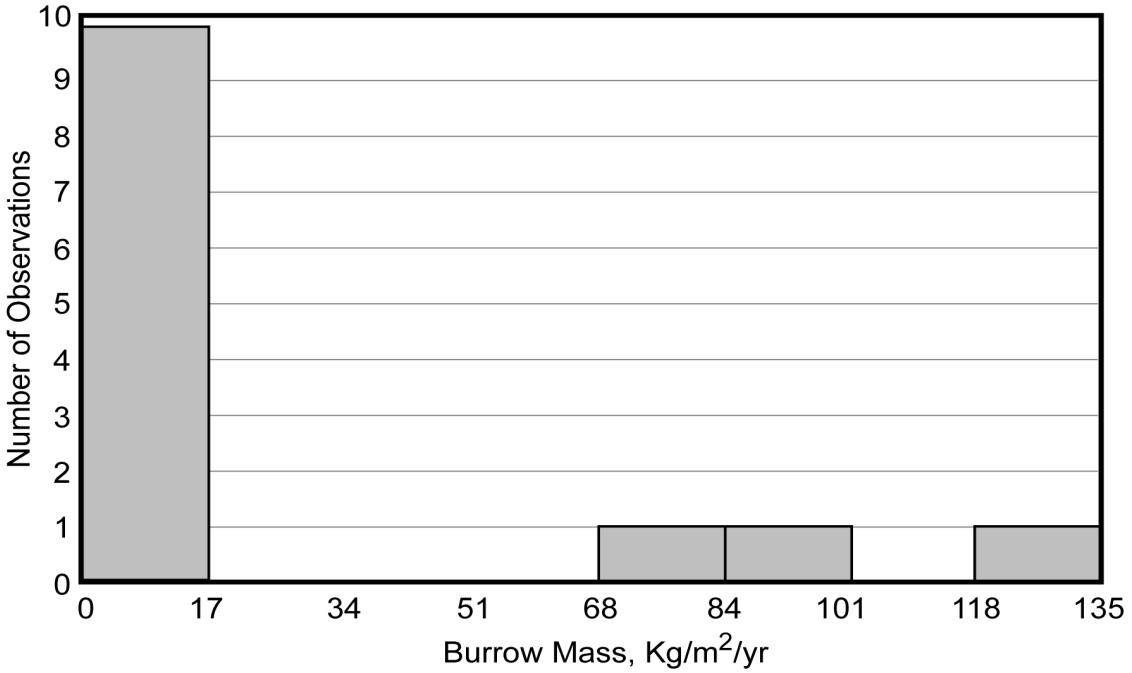

Figure 5-25. Annual Mass of Soil Excavated by Mammals.

The mammal burrow depth data are presented graphically in Figure 5-26. The maximum depth in Figure 5-26 (8.5 m [28 ft]) is from a study not applicable to the NTS; the remaining data are site-specific. Site-specific data indicate that burrowing at the NTS will be limited to the near-surface soil layers. However, some of the depths recorded in the site-specific studies (including the deepest observation at 2 m) are not maximum depths and the burrows could actually be deeper. Because of this uncertainty in the maximum burrow depth at the NTS, the 8.5 m (28 ft) observation is used as an upper limit to the distribution of burrow depths, even though the actual maximum at the NTS is likely to be closer to the surface. The 8.5 m (28 ft) limit is consistent with the expected depth of more than 95% of the roots (the below-ground food source) in the current community. The scarcity of roots below 8.5 m (28 ft) supports this depth as a plausible maximum, as the possibility of deep burrowing for roots is nearly eliminated based on the relative unavailability of food below 8.5 m (28 ft).

The data used to model the impact of burrowing mammals (Table 5-11), while derived from studies of pocket gophers, are inclusive of burrow depths and excavated burrow mass estimates expected for other NTS burrowing rodents [Winkel et al., 1995]. For example, Merriam's kangaroo rat (*Dipodomys merriami*), an ubiquitous inhabitant of the NTS, has shallower burrows and less extensive (shorter) burrow systems than those of pocket gophers. Because only one burrowing animal inhabits a location at a given time (except for species that prefer burrows already created by other animals), data for additional species are not required for the PA, provided that the parameters developed are inclusive of other animals, as is the case for the data compiled here.

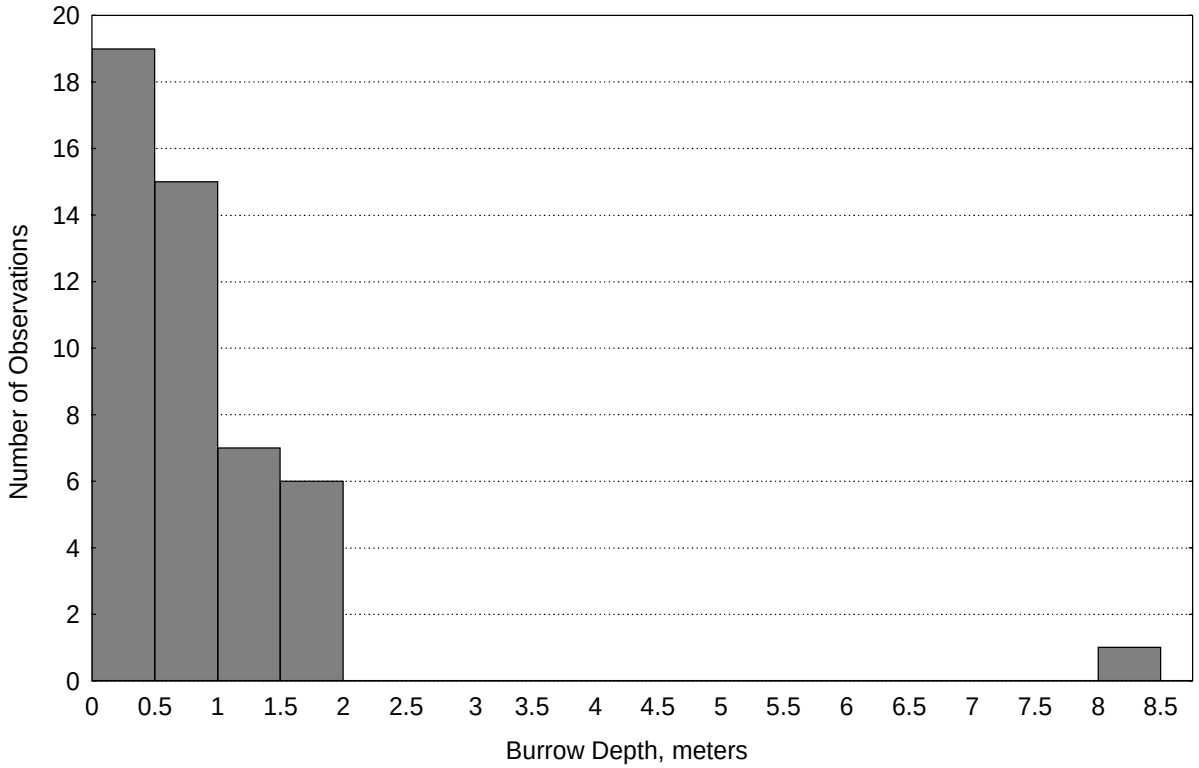

Figure 5-26. Mammal Burrow Depths.

5.8.3.4 Model Implementation

Mammals

The data summarized in Table 5-11 are 13 to 48 observations of individual burrow systems. For each system, either a measurement of the deepest excavation in that system or the average rate of excavation is given. A large number of individual burrow systems might occur over the GCD boreholes during the entire performance period. The PA must therefore consider a population of burrow systems with varying depths and rates, rather than a single burrow system.

The population of burrow systems that may occur over the GCD boreholes is assumed to have the same statistical characteristics as the population of current borehole systems. The statistical characteristics of the current population can be estimated from the available data; however, these estimates are uncertain. Uncertainty in the population of burrow systems is accounted for in the PA by defining probability distributions for the statistical parameters describing the population.

B_m

The burrow rate data are consistent with the assumption that the burrow rate is lognormally distributed across the population of burrow systems. The mean and standard deviation of the true population distribution were estimated by taking the logarithms of the burrow rate data and calculating their average and their standard deviation. The sample standard deviation was then

used to calculate the standard deviation of the uncertainty distribution for the true mean (i.e., the standard error (SE) of the mean):

$$SE = \frac{\text{sample standard deviation}}{\sqrt{13}} \quad (5\text{-}13)$$

Thus, the pdf of burrow rate was constructed from the average and standard error of the logarithms of the rate data. This pdf is given in Table 5-12. The pdf is empirical because the model requires mean burrow rate, not the mean of the logarithm of the burrow rate. The mean rate is given by

$$E(rate) = e^{\mu+\sigma^{2/2}} \quad (5\text{-}14)$$

where

$E(rate)$ = mean burrow rate
μ = mean of logarithms of burrow rate data
σ^2 = variance of logarithms of burrow rate data

Table 5-12. PDF of Average Mammal Excavation Rate (pdf is Continuous Linear)

Average Rate (kg/m^2 yr)	Cumulative Probability
4.6478	0.0000
5.8283	$1.3804 \times 10^{!3}$
7.2060	$4.3676 \times 10^{!3}$
8.8092	$1.1570 \times 10^{!2}$
10.670	$2.6430 \times 10^{!2}$
12.826	$5.322 \times 10^{!2}$
15.318	$9.6113 \times 10^{!2}$
18.193	$1.5786 \times 10^{!1}$
21.506	$2.3859 \times 10^{!1}$
25.317	$3.3518 \times 10^{!1}$
29.695	$4.4163 \times 10^{!1}$
34.718	$5.5026 \times 10^{!1}$
40.473	$6.5337 \times 10^{!1}$
47.060	$7.4475 \times 10^{!1}$
54.593	$8.2059 \times 10^{!1}$
63.1988	$8.7970 \times 10^{!1}$
73.019	$9.2306 \times 10^{!1}$
84.219	$9.5308 \times 10^{!1}$
96.981	$9.7270 \times 10^{!1}$
111.51	$9.8485 \times 10^{!1}$
128.05	$9.9198 \times 10^{!1}$
146.85	$9.9594 \times 10^{!1}$
168.22	$9.9804 \times 10^{!1}$
192.50	$9.9910 \times 10^{!1}$
200	1

The distribution for *E*(*rate*) was constructed using the above equation and the normal distribution for μ evaluated at several probability levels between 0 and 1.

p_z

Estimates of P_z, the proportion of a burrow in a given soil depth interval, can also be derived from the burrow data summarized in Table 5-11. The burrow depth data were found to be consistent with a log normally distributed population. As with the burrow rate data, logarithms of the 47 burrow depth observations were taken. The average and standard deviation of the logarithms of the sample data were calculated and used to estimate the mean and standard deviation of the true population. The uncertainty distribution for the log of the true mean value has a standard deviation equal to the standard error of the mean:

$$\text{SE} = \frac{\text{sample standard deviation}}{\sqrt{47}} \qquad (5\text{-}15)$$

This pdf is approximately normally distributed with a mean of !0.44 and a standard deviation of 0.13. The uncertainty distribution for the true variance is related to the chi-squared distribution with 47 degrees of freedom [Walpole and Myers, 1985]. LHS does not support chi-squared distributions so a continuous linear pdf was developed to describe the uncertainty in the true variance in burrow depth over the population of future burrow systems. This pdf is given in Table 5-13 and is continuous linear.

Table 5-13. PDF of Standard Deviation in Mammal Burrow Depth

Variance	Cumulative Probability
0.55	0
0.60	0.0026
0.65	0.0155
0.70	0.0619
0.75	0.1745
0.80	0.3637
0.85	0.5898
0.90	0.7856
0.95	0.9108
1.00	0.9707
1.05	0.9924
1.10	0.9985
1.15	0.9998
1.20	1

The log normal distribution for the depths of mammal burrows places no limit on the maximum depth of burrow systems. Physical and environmental constraints will establish a practical limit on the maximum burrow depth; however, the limiting depth is difficult to specify. The data collected for the NTS indicate that while mammal burrowing is limited to the near surface, the

maximum depth is undefined, given the available site-specific data. The distribution used for mammal burrow depths is assumed to be lognormal, but is truncated a 8.5 m (28 ft), as described in Section 5.8.3.3. Although the maximum observed depth in the 13 samples of the data set is 2 m (7 ft), it is unlikely that this represents an upper limit on possible burrow depths. Mammal burrowing depths were assumed to be limited by the availability of plant roots (as described in above in Section 5.8.2.2). Specifically, mammal burrowing was assumed to be confined to the soil interval containing 98% of the root mass of the lifeform with the deepest plant roots.

The resulting model for burrow depths places the majority of future burrow systems near the land surface. Deeper systems are also included, although the frequency of these systems decreases as the depth increases. In rare cases, the limit established by plant roots is below the elevation of the top of the waste, and a very small fraction of mammal burrows are therefore assumed to penetrate the waste. In the data sets used in this analysis, there is no observational evidence for mammal burrowing extending to the waste burial depth. This possibility is an extrapolation from the existing burrow depth measurements based on the probability distributions fitted to these measurements.

p_{ztran}

Data for deposition rates are used to estimate p_{ztran}. As mentioned in Section 5.8.2.2.5, 14 to 87% of the soil excavated in burrowing is deposited on the surface. Observations of surface deposition can be used to model soil movement between compartments with the following assumptions:

- Vertical soil movement is always unidirectional towards the surface;
- Surface deposition is from the soil compartment directly beneath the surface; and
- Surface deposition can be used to estimate subsurface deposition to a given interval, with the soil coming also from the soil compartment directly below.

A total of four data points are available on the proportion of a burrow system that is deposited on the surface. Lacking adequate data for even simple statistical analyses of the distribution type that might best describe deposition rates, sampling for this parameter is performed on a uniform distribution that ranges from the minimum value (0.14) to the maximum value (0.87).

Invertebrates

B_m

The data on soil excavation rates (Table 5-11) indicate a range from 0.7 to 5.77 kg/m^2/yr. The small sample size (n = 4) precludes anything but a uniform distribution of excavation rates that ranges between the minimum and maximum value. This distribution implies that these are possible long-term average rates of excavation appropriate for use in the PA model, with uncertainty about the actual distribution of these rates.

P_z

The data on burrow depths presented in Table 5-11 show that invertebrate burrowing has been observed to impact up to 6 m (20 ft). Termite burrowing depths are linked to their primary food source (plant roots). The expected distribution of l_{max} for the community (a combination of the expected root length for each lifeform) is used to estimate the proportion of termite burrowing within each soil interval *z*. Specifically, a community average maximum root length (weighted by the biomass production of the community lifeforms) is generated to estimate termite burrow depths. First, the average maximum root length for each lifeform is sampled for each simulation. Each lifeform's average maximum root length is then weighted by the biomass turnover rate sampled for that lifeform and an overall community average maximum root length is determined for the community. This community average maximum root length is then used to develop a single exponential "distribution" function that describes the variability of the length of the longest roots over all plants in the community. For the current community, the average maximum root length tends to fall between 1 and 2 m (3 and 7 ft). The range of expected frequencies of termite burrow depths based on the endpoints from this range of community average maximum root lengths are shown in Figure 5-27.

Although most of the distributions shown in Figure 5-27 are confined to depths near the land surface, the exponential distribution has no fixed upper limit, and some amount of invertebrate burrowing can occur at any depth. In particular, some very small fraction of invertebrate burrows can extend below the top of the waste. The current data set includes a maximum observed burrow depth of 6 m (20 ft); however, the number of observations is insufficient to support a

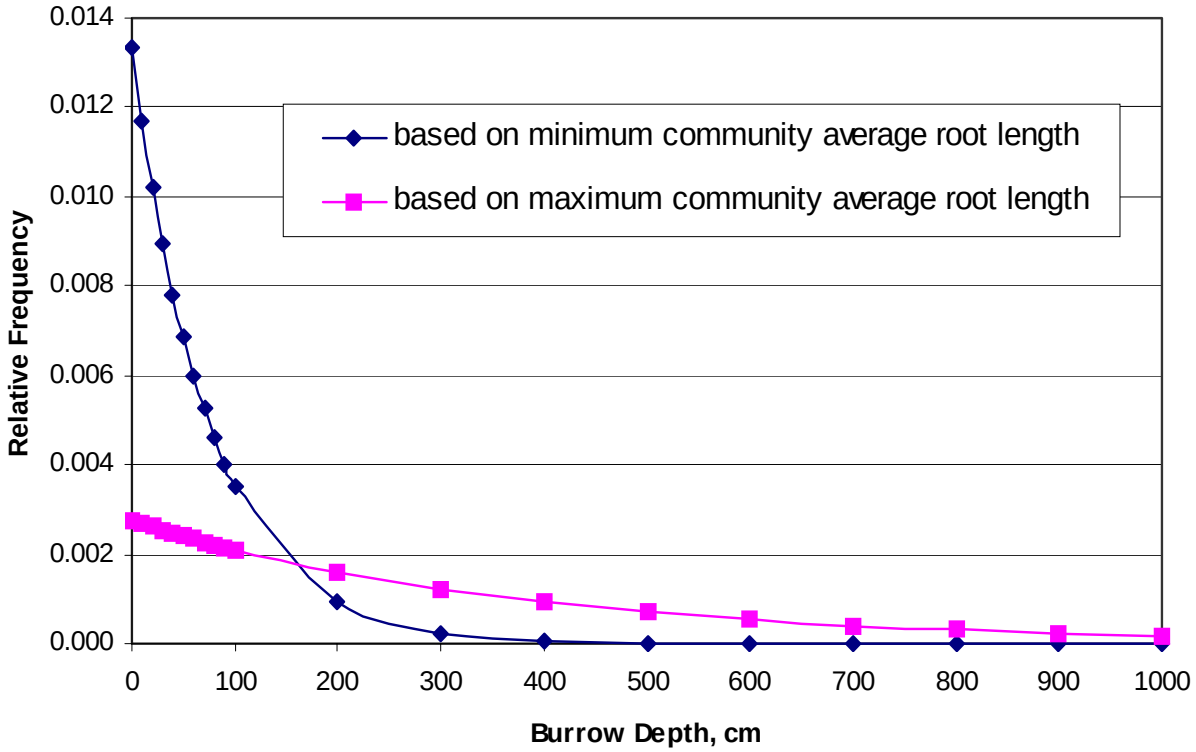

Figure 5-27. Range of Termite Burrow Frequencies, Current Conditions.

limit on the maximum depth of burrow systems. The probability of invertebrate burrows extending into the waste region is based on the assumed connection between burrow depth and root depth, and an extrapolation from existing root depth data, rather than on direct observations of burrows at these depths.

P_{ztran}

No data could be found to estimate the proportion of the burrow system that is either deposited on the surface or between soil depth intervals. It is proposed that the entire amount of burrowing within a given depth interval (the mass of excavated soil B_m times the proportion of the burrow within that interval p_z) is assumed to be deposited on the surface. This represents a conservative approach to estimating the flux of contaminants to the surface from subsurface burrowing activity, as it is likely that some proportion of the soil excavated is redistributed among subsurface intervals.

5.8.4 Conclusions of Animal Bioturbation

Bioturbation in NTS soils is most strongly affected by burrowing mammals and invertebrates in relatively shallow depths. Reptiles and birds either use abandoned burrows or burrow only for protection, rather than creating their own burrow systems. Mammals tend to excavate shallow (2.0 m [6 ft]), but extensive burrow systems. Invertebrates, on the other hand, tend to have deeper (6.0 m [20 ft]), but much less extensive burrow systems.

5.9 TRU Waste Source Term

5.9.1 Introduction

This section of the PA documentation identifies and defines the source term of TRU wastes disposed of in the GCD boreholes. This source term consists of the initial inventory of radionuclides in the TRU wastes in the GCD boreholes and the processes that will release those radionuclides into the subsurface at the GCD site. The original inventory information was presented by Chu and Bernard [1991].

The boreholes that make up the GCD are described in Section 5.3. From 1984 to 1987, DOE/NV disposed of TRU waste in GCD Boreholes 1, 2, 3, and 4. This TRU waste consisted of NWAR and TRU-contaminated material from nuclear weapon production or disassembly at the Rocky Flats Plant (RFP).

5.9.2 Definition of TRU Waste

TRU waste is defined by the EPA as (40 CFR 191.02(i)):

> Waste containing more than 100 nanocuries of alpha-emitting transuranic isotopes, with half-lives greater than twenty years, per gram of waste, except for: (1) high-level radioactive wastes, (2) wastes that the Department has determined, with the concurrence of the administrator, do not need the degree of isolation

required by this part; or (3) wastes that the commission has approved for disposal on a case-by-case basis in accordance with 10 CFR Part 61.

The DOE requires that the determination of whether a particular waste is TRU waste be made on a package-by-package basis (DOE Order 5820.2a, Chapter II.3.a(2)). Thus, if a particular waste package contains more than 100 nanocuries of alpha-emitting TRU isotopes, with half-lives greater than 20 years, per gram of waste, *then that particular waste package would be considered TRU waste*. A waste package that did not meet the definition of TRU waste but was disposed of in the same borehole as other waste packages that did meet the definition is not included in the initial inventory for the 40 CFR 191 PA of the GCD boreholes.[6] Only GCD Boreholes 1–4 contain TRU wastes. Although some of the wastes were emplaced before promulgation of the regulation, all nuclides regulated under 40 CFR 191 in packages that meet the definition of TRU waste are considered as part of source term for the 40 CFR 191 PA.

5.9.3 Source Term

5.9.3.1 Waste Form and Inventory for Boreholes 1, 2, and 3

Boreholes 1, 2, and 3 contain NWAR; that is, waste from accidents involving nuclear weapons. Much of this waste consists of damaged weapons parts recovered from accident sites that were subjected to fire or (non-nuclear) detonation. These residues are described as highly charred, irregular lumps of material. In the opinions of those who investigated the accidents, the fires were intense enough to melt metallic parts of the weapons and the molten parts mixed in undetermined fractions prior to solidifying. The shapes are relatively flat with jagged edges, and some have crusted edges. The final mixture of metals is not known, but evaluations indicate that, in addition to uranium and plutonium, the principal constituent is aluminum. The detonation fragments consist of uranium and plutonium fragments embedded in larger weapon components and component fragments [Caldwell and Bieri, 1983; Chu and Bernard, 1991].

The inventory of radionuclides in the15 packages is summarized in Chu and Bernard [1991]. Chu and Bernard developed the summary through an analysis of six sources of information:

1. REECo's Form (waste receipt form)
2. A classified NWAR document
3. Two classified Los Alamos reports
4. Classified DOE Form 741
5. Criticality study report by Los Alamos [Caldwell and Bieri, 1983].

As documented in the classified Los Alamos reports, the fissile and fertile isotope contents for each package were estimated using high-resolution gamma-ray spectrometry, passive neutron outputs, and both gamma-ray and neutron scans. In addition, extensive radiography was performed on these waste containers.

[6] The DOE/HQ Review Team that reviewed this PA disagreed with this conclusion. As a result, additional IPR analyses were performed to calculate the dose consequence of including the co-located, non-TRU wastes. These analyses are presented in Section 8.3.1.

These NWAR wastes were disposed in 15 packages which were constructed of steel and plywood. The plywood boxes were coated with fiberglass. Table 5-14 summarizes information on the 15 items of NWAR wastes.

Package #6 in Borehole 2 contains ^{137}Cs, but does not contain any TRU waste [Lewis, 1999, Appendix I], thus removing it from the 40 CFR 191 analyses. There are discrepancies reported between DOE Form 741s, REECo, and the other sources, especially for depleted uranium. In addition, ^{235}U, ^{238}U, and ^{239}Pu are often used interchangeably with the terms enriched uranium, depleted uranium, and weapon-grade plutonium, respectively. Because it is not possible to reconcile the differences among the reported values, it is assumed that the reported inventory values are all equally valid. Therefore, a range of values is used to represent the inventory. The smallest and largest numbers reported are used as the lower and upper bound of the possible inventory range.

Table 5-14. Information on NWAR Waste Packages

Item No.	Overpack Description			Container Within Overpack		
	Gross Weight (kg)	Volume (m^3)	Dimensions (Length × Width × Height)	Type	Dimensions (Length × Width × Height)	Type
1	4,309.2	11.3	2.7 × 2.0 × 2.1 m	Metal Pan w/ply cover	2.6 × 1.9 × 2.1 m	CONEX
2	3,175.2	11.3	2.7 × 2.0 × 2.1 m	Metal Pan w/ply cover	2.6 × 1.9 × 2.1 m	CONEX
3	3,175.2	11.3	2.7 × 2.0 × 2.1 m	Metal Pan w/ply cover	2.6 × 2.0 × 2.1 m	CONEX
4	6,350.4	11.3	2.7 × 2.0 × 2.1 m	Metal Pan w/ply cover	2.6 × 1.9 × 2.1 m	CONEX
5	1,905.1	11.3	2.7 × 2.0 × 2.1 m	Metal Pan w/ply cover	2.6 × 2.0 × 2.1 m	CONEX
6	1,587.6	3.4	2.1 × 1.2 × 1.3 m	744-7A Plywood	Transferred from dumpster container	
7	1,496.9	3.7	1.6 × 1.5 × 1.5 m	Metal	As received; heavy metal	
8	145.2	0.2	0.9 × 0.6 × 0.7* m	55 gal	0.7 × 0.5 D. m	AN CAN
9	172.4	0.4	0.7 × 0.7 × 0.7 m	Plywood	0.5 × 0.6 D. m	AN CAN
10	154.2	13.0	0.7 × 0.7 × 0.7 m	Plywood	0.5 × 0.6 D. m	AN CAN
11	544.3	1.8	1.2 × 1.5 × 1.0 m	Plywood	0.5 × 0.4 D. m	AN CAN
					0.6 × 0.6 D. m	AN CAN
					0.5 × 0.7 D. m	AN CAN
					0.6 × 0.6 D. m	AN CAN
12	172.4	0.4	1.0 × 0.7 × 0.7* m	314.2 L	0.9 × 0.6 D. m	208.2 L
13	181.4	0.4	1.0 × 0.7 × 0.7* m	314.16 L	0.9 × 0.6 D. m	208.2 L
14	680.4	2.1	1.4 × 1.3 × 1.1 m	Plywood	4.3 × 3.8 × 2.8 m	Wood
15	793.8	2.6	1.7 × 4.8 × 1.1 m	Plywood	1.5 × 1.4 × 0.9 m	Wood
Total	24843.7	84.5				

* The height of these packages were not reported; therefore, they were assumed to be similar to package No. 15.

These NWAR wastes are "classified wastes," because they contain shapes and isotopic compositions (isotopic signatures) that are classified for national security reasons. These 15 packages were disposed in GCD Boreholes 1, 2, and 3 in March 1984. As discussed in Section 5.11, these NWAR wastes contain approximately 25 kg of ^{235}U, or equivalent, fissile material. To prevent any possibility of a nuclear criticality event, the 15 waste items were buried in a specific configuration and backfilled with probertite (a borate ore and neutron poison). Figure 5-28 shows a schematic diagram of the arrangement of NWAR packages in GCD Boreholes 1, 2, and 3.

The waste in Boreholes 1, 2, and 3 was disposed of prior to the effective date of 40 CFR 191, November 18, 1985. However, as discussed in Section 2.3.1, DOE/NV decided to include this waste in the PA to demonstrate compliance with the strictest known regulation.

5.9.3.2 Waste Form and Inventory for Borehole 4

Borehole 4 contains classified wastes from the RFP and the LLNL. The RFP wastes were generated during the manufacture of new weapons or during disassembly of retired weapons. These wastes are typically contained in 200-L (55-gal) drums. Wastes were packed in cylindrical fiberboard containers, then two of these were bagged in heavy plastic and placed in the barrels. Figure 5-29 shows a typical container for RFP TRU wastes.

According to the records, 258 drums of RFP TRU waste were placed in GCD Borehole 4 between July 1985 and October 1987 in five shipments. Five specific waste forms have been identified for RFP wastes depending on the source of waste generation [Bauman, 1989]:

1. Graphite shapes – used for casting parts at RFP.
2. Tooling – bits used in machine castings.
3. Plastic shapes – used to secure parts during shipment to RFP.
4. Studs from uranium parts – lugs on plastic shapes to facilitate handling.
5. Metal shapes – parts removed from retired nuclear weapons.

Each part in the waste has a small amount of surface contamination resulting from contact with uranium or plutonium. The concentration of transuranic elements ranges from 2,000 to more than 14,000 nCi/g of waste, according to DOE Form 741s.

Eight boxes of wastes from LLNL were disposed in GCD Borehole 4 in January 1987. These wastes contain ^{3}H, ^{238}U, ^{232}Th, and ^{6}Li. Four boxes contain classified metal parts contaminated with ^{238}U, one box contains classified metal parts contaminated with ^{238}U and ^{232}Th, and one box contains LiH in classified assemblies. According to DOE Form 741s, these wastes also contain 252 g of ^{235}U. These eight boxes of waste were not included in the 40 CFR 191 PA because none of them meet the definition of TRU waste.

5.9.3.3 Initial Radionuclide Inventory

Table 5-15 presents the initial inventory of radionuclides included in the PA. This table is derived from Tables 2.7 and 2.8 of Chu and Bernard [1991], and is allocated among the various isotopes of U and Pu. The uranium nuclide inventories were converted from data for "enriched

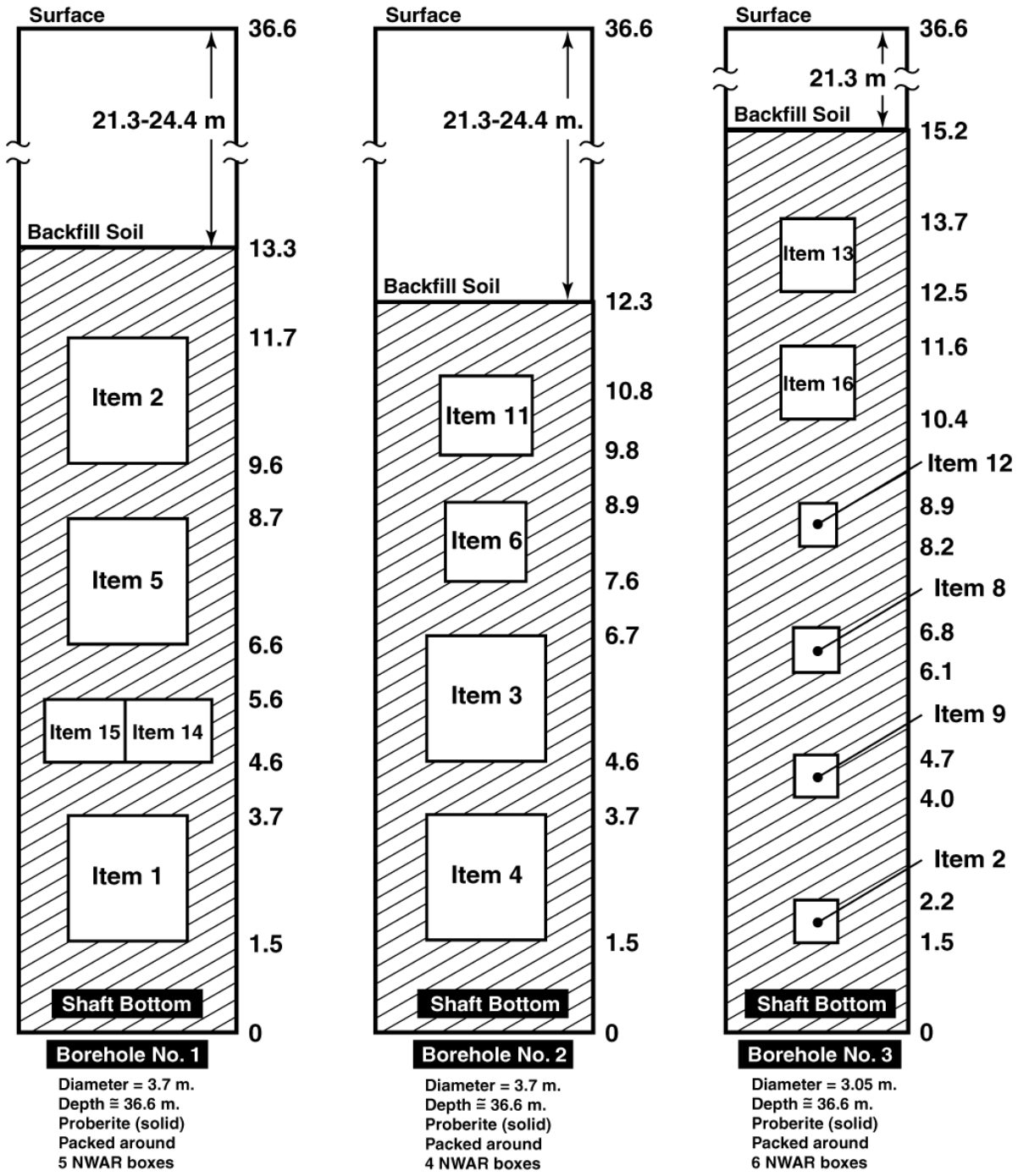

Figure 5-28. Schematic of NWAR Wastes in GCD Boreholes 1, 2, and 3.

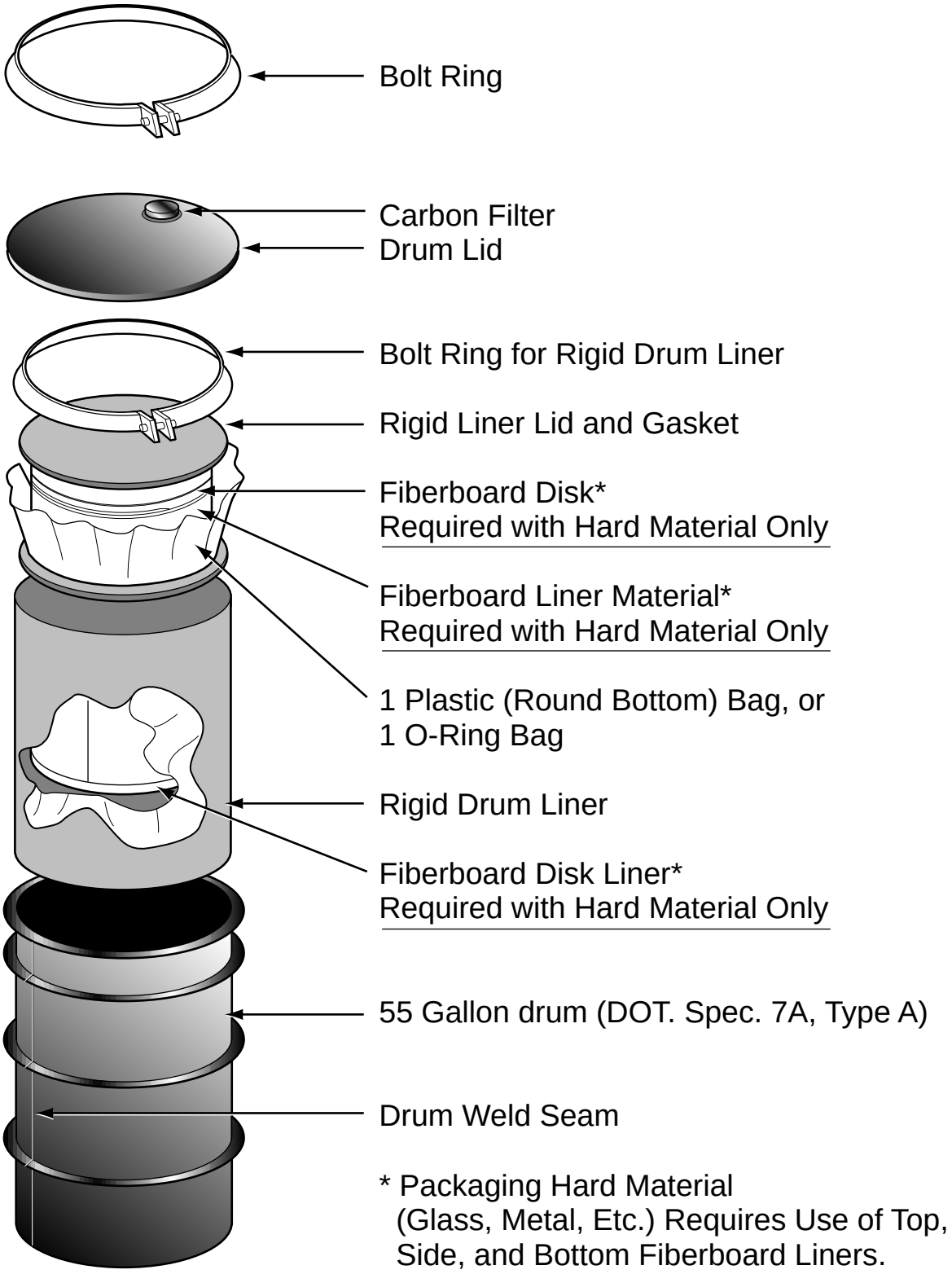

Figure 5-29. Typical Container for RFP TRU Wastes.

Table 5-15. Inventory of Radionuclides in TRU Waste Packages in GCD Boreholes Included in PA

Isotope	BH-1(kg)	BH-2 (kg)	BH-3 (kg)	BH-4 (kg)	Total (kg)	Total (Ci)
U-234	2.17E-2 - 3.78E!2	1.33E-3 - 2.81E-2	1.68E-3 - 1.34E-2	5.40E-05	2.48E-2 - 7.94E!2	1.53E!1 - 4.90E!1
U-235	17.87 - 31.05	1.05 - 22.17	1.33 - 10.67	4.23E-02	20.3 - 63.9	4.87E-2 - 1.53E-1
U-238	423.7 - 722.9	2.69 - 69.9	6.17 - 10.8	2.66E-03	432.6 - 803.6	1.44E-1 - 2.68E-1
Total U					**452.9 - 867.6**	
Pu-238	8.95E-5 - 2.03E-4	4.40E-06	1.27E-4 - 1.43E-4	2.23E-04	4.41E-4 - 5.73E-4	7.54 - 9.83
Pu-239	8.40E-1 - 1.90	4.13E-02	1.19 - 1.34	2.09	4.16 - 5.37	2.55E+2 - 3.29E+2
Pu-240	5.19E-2 - 1.18E-1	2.55E-03	7.37E-2 - 8.29E-2	1.29E-01	2.57E-1 - 3.22E-1	5.94E+1 - 7.44E+1
Pu-241	1.16E-3 - 2.63E-3	5.72E-05	1.65E-3 - 1.86E-3	2.90E-03	5.77E-3 - 7.45E-3	6.59E+2 - 8.51E+2
Pu-242	1.79E-4 - 4.06E-4	8.80E-06	2.54E-4 - 2.86E-4	4.46E-04	8.88E-4 - 1.15E-3	3.46E-3 - 4.47E-3
Total Pu					**4.42 - 5.70**	
Am-241	2.25E-3 - 1.45E-2	2.1E-04	5.79E-3 - 6.15E-3	5.91E-03	1.42E-2 - 2.68E-2	4.86E+1 - 9.04E+1

uranium" and "depleted uranium," assuming that enriched uranium contains 0.12% ^{234}U, 94% ^{235}U and 5.9% ^{238}U and depleted uranium contains 0.2% ^{235}U and 99.8% ^{238}U. Weapons-grade Pu is assumed to consist of 0.01% ^{238}Pu, 93.8% ^{239}Pu, 5.8% ^{240}Pu, 0.13% ^{241}Pu, and 0.02% ^{242}Pu, with 0.22% ^{241}Am [National Academy of Sciences (NAS), 1995a]. All quantities were calculated to a common time of January 1991. There is some uncertainty in the exact quantities of TRU waste disposed of in the GCD boreholes; hence the initial radionuclide inventory is given in terms of a distribution of values. For each radionuclide the initial inventory is assumed to be uniformly distributed between the minimum and maximum values given in Table 5-15. The constituent radionuclides of weapons grade plutonium were correlated with a correlation coefficient of 0.99 in LHS, and the sampled values of ^{235}U and ^{234}U were also correlated with a correlation coefficient of 0.99.

Figure 5-30 shows the four decay chains produced by radioactive decay of the radionuclides shown in Table 5-15. Only radionuclides with half-lives greater than 20 years are shown.[7] This is because the CR limit releases of only long-lived radionuclides; there are no release limits for radionuclides with half-lives less than 20 years. Therefore, the radionuclides in Figure 5-29 are the only radionuclides of concern to the CR. The IPRs are concerned with the dose that results from exposure to all radionuclides, whether short- or long-lived. Dose from short-lived radionuclides not shown in Figure 5-30 is accounted for as described in Section 7.6.

Complete radioactive decay chains and a table giving the half-life of each radionuclide are given in Appendix J.

[7]The exception is ^{241}Pu with a half-life of 14.4 years. ^{241}Pu is included in the decay chain because not including it would result in underestimating the quantities of daughters produced. However, ^{241}Pu is not included in the calculation of the release limit scale factor or the estimated cumulative releases.

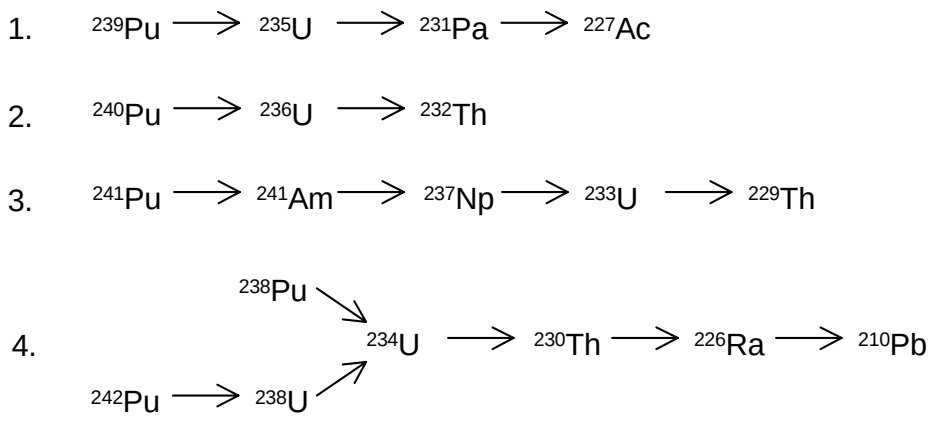

Figure 5-30. Decay Chains Resulting from Initial Inventory.

5.9.3.4 Disposal Configuration

The various waste packages have been placed in the boreholes as shown in Figure 1-8. The space between the containers is filled with probertite, a borate mineral, to reduce the potential for criticality, except in Borehole 4, where sifted native alluvium was used as backfill. Borate is toxic to plants and insects at the expected concentration levels in the boreholes. Each of the containers contains some void space, since no effort was made to compact the waste before packaging, or in placing the containers in the steel drum or other overpacks which were placed in the boreholes. Void space also exists among the waste containers in the borehole, as the backfill was not placed to minimize voids, nor was any effort made to compact it after placement. Arnold [1996] estimated that the waste packages contain 85 to 90% void volume, and that the extra-container void volume in the disposal zone varies from 0 to 30%.

The waste is located from 21 to 37 m (70 to 120 ft) below the surface in the alluvium. The bottom of the borehole is approximately 200 m (650 ft) above saturated alluvium (i.e., the water table), placing it well within the unsaturated zone.

5.9.3.5 Assumptions and Interpretations

A number of assumptions have been made in order to simplify the highly complex natural and engineered system. First, the four boreholes containing TRU waste are considered to be a single hole, with effective cross-sectional area equal to the sum of the four individual boreholes, or 35.6 m^2 (383 ft^2). This virtual borehole is assumed to be a 15-m (50-ft) tall cylinder containing the radionuclides described above. Combining these boreholes into one virtual borehole for ease of calculation should have no significant impact on the calculated system PA, since the movement of water will be upward, with only minor lateral movement through diffusion (see Section 5.12). Second, the radionuclides are assumed to be evenly dispersed throughout the waste zone, which is assumed to be filled with material that has properties identical to alluvium. The fact that one of the four boreholes does not contain probertite is not expected to increase the solubility or mobility of nuclides in that borehole relative to the other three. The probertite was included only to decrease the possibility of criticality of the fissionable nuclides. [This topic is discussed

by Harms et al., 1998.] Third, the top 21.3 m (70 ft) of the borehole (from the waste disposal zone to the surface), which was backfilled with sifted native alluvium, is assumed to have physical, hydrologic, and geochemical properties similar to the surrounding undisturbed soils. This assumption is supported by studies of collapse zones beneath nuclear test craters in alluvium in Area 3 of the NTS [Bechtel Nevada, 1997]. Data collected from these studies indicate that the physical properties of alluvium (e.g., bulk density, porosity) in the collapse zones are similar to those in the undisturbed alluvium. The same is true for hydrologic properties (e.g., saturated hydraulic conductivity and van Genuchten parameters) and for geochemical properties. Fourth, materials in the boreholes, pits, and trenches that are not regulated by 40 CFR 191 are expected to not interact chemically with the materials in the regulated boreholes.

5.9.4 Release Processes

5.9.4.1 Description

The availability of water in the waste disposal zone controls the release of radionuclides from this zone to the alluvium. Any water in contact with the wastes will dissolve radionuclides and other materials. Free water in the liquid phase must be available to dissolve radionuclides from the waste and transport them away from the disposal volume. Vapor phase water is available to corrode metallic materials such as waste packages, but liquid water must be present and mobile to permit migration of dissolved species. However, the available water will interact with all materials in the boreholes, including backfill materials, overpacks, waste packages, and wastes. Many of the chemical reactions resulting in package degradation and corrosion of wastes consume water. For example, iron in the steel waste containers and overpacks will corrode under oxidizing conditions to produce iron oxides, notably limonite, a mineral similar to common rust in composition. Also, many of the weapons parts consist of metallic aluminum, which generally develops a relatively inert coating of Al_2O_3 upon exposure to the atmosphere. However, the aluminum may corrode in water containing chloride, such as the pore waters at the site.

During excavation of the trenches, it was found that samples collected near the excavated surface had significantly dehydrated [Estrella et al., 1993]; it is assumed that the alluvium surrounding the boreholes also lost a significant amount of pore water, the degree of dehydration depending on the length of time the holes were open. Because of the low amount of pore water in the native alluvium, the low ambient humidity at the NTS, and the very low water migration rate, the back-fill and the alluvium around the borehole will return to ambient (undisturbed) water content slowly.

5.9.4.2 Assumptions and Interpretations

To model the release of TRU radionuclides from the waste for PA calculations, a number of assumptions must be made to simplify the highly complex natural system. The most important assumption concerns the amount of water available to dissolve and transport radionuclides. In the unsaturated zone, pore water is present, and radionuclides can move only by advection and diffusion in the liquid phase. Because water is consumed by the reactions that must take place to corrode and deteriorate the waste packages before nuclides can be dissolved, the actual amount of water available for radionuclide dissolution and transport will be highly time-dependent and

limited. In fact, consumption of water during corrosion will delay the migration of radionuclides away from the source region, perhaps significantly. An additional delay will result from the time taken to reestablish the ambient pore water in and near the boreholes. However, because of the difficulties in modeling these delays, the simplifying assumption is made that an adequate amount of water will be available to dissolve waste at all times. This is a highly conservative assumption. This water-availability assumption leads to the further assumption that the concentration of nuclides for transport in groundwater is limited only by their solubility under the pertinent chemical conditions.

The organic compounds derived from decay of cellulosic packaging in the boreholes may contribute to the mobility of TRU nuclides, as discussed in the previous section. The amount of organic materials in the native alluvium at the site is extremely small, less than 4 Fg/g (1.4 $e^{!7}$ oz/.03 oz) of soil, so they can safely be disregarded. Stockman [1997] points out that the subsurface conditions in the alluvium, especially in the presence of the borate (from the probertite backfill) are not conducive to decay of the cellulosics, and, in fact, he estimated several thousand years for the process to reach its maximum. Stockman [1997] found that isosaccharinate was the dominant organic chelating species under GCD conditions, and that the stability of isosaccharinate complexes was much lower than for other organic complexes, such as gluconates and saccharinates. The isosaccharinates will also form complexes with other metals, such as iron, which are in great abundance relative to the TRU nuclides in the boreholes. For these reasons, and the limitations on the methodology discussed in the previous section, the decision has been made to exclude the effects of organic complexing in the PA.

5.10 Solubilities

5.10.1 Geochemical Environment

The alluvium at the Area 5 RWMS has been characterized by Stockman [1992], based on studies of samples collected in Trench 8, in the vicinity of the GCD boreholes. The alluvium is dominated by quartz, feldspar, and cristobalite, with calcite, gypsum, and minor amounts of clays and zeolites. These samples were determined to be derived from devitrified tuff, which is a common rock type in the hills surrounding the Area 5 RWMS, with some contribution from the Paleozoic sedimentary rocks also present in the area. Local thin caliche layers are found at various depths in the alluvium.

For the solubility calculations, a pH range of 7 to 9 was used for the vadose-zone fluids in the alluvium. This range was selected based on a recommendation by R.L. Jacobson of the Desert Research Institute in Reno, Nevada. This range is narrow enough that the biggest source of uncertainty is in selecting the dominant nuclide-bearing solid phases. The range of solubilities generated by consideration of different controlling solid phases is sampled for the PA. This approach maintains internal geochemical consistency and accounts for uncertainties in estimating radionuclide solubilities.

Two geochemical environments will determine the mobility of radionuclides: the waste disposal region and the native alluvium. The water in the immediate vicinity of the wastes will be chemically conditioned by its interactions with materials in the disposal zone, notably the iron in the

steel overpacks. This interaction will consume oxygen and some water, so that the remaining water available for dissolving radionuclides will be relatively low in dissolved oxygen, and therefore low in oxidation potential. During migration, the nuclides must move through a transition zone to the region containing alluvium-dominated water (relatively high dissolved oxygen). Radionuclide solubilities will generally be different in the two sets of conditions. Nuclides that are soluble in low oxidation potential conditions may precipitate (or coprecipitate) under more oxidizing conditions, effectively reducing the mobility of those nuclides. Increased solubility under more oxidizing conditions will not result in increased mobility, since the nuclide availability in that zone is limited by the conditions in the waste-dominated environment. Highly complex geochemical modeling is necessary to predict the behavior and fate of radionuclides as they move through regions of different chemical characteristics; the modeling reported here uses the simplifying approach of modeling the entire system as if it were in the alluvium-dominated region. This is a conservative assumption, liable only to overestimate solubilities relative to the actual conditions.

The decay of organic materials in the GCD boreholes may result in the formation of organic chelating compounds, as suggested by Stockman [1997]. Stockman's paper modeled the interactions among the wastes (including the lithium), the cellulosic materials of their containers, the probertite backfill, and the surrounding alluvium and produced a sensitivity study of these effects. The rate at which cellulosic materials decay is expected to be inhibited in the presence of the high borate concentrations which exist in the boreholes containing probertite. The assumptions, specialized data, and calculational algorithms used in Stockman's study are not well documented, and therefore cannot be used directly in the PA. Stockman found that the decay of cellulosics, such as the plywood and fiberboard in the NWAR boreholes may produce organic compounds such as saccharates, isosaccharinate, and gluconate, reaching a maximum concentration in about 3,000 years. These compounds may chelate with plutonium (and other metals and TRU radionuclides), thus effectively increasing its solubility relative to those values calculated without consideration of organic compounds. Several factors are expected to reduce the effectiveness of organic chelation: (1) A limited amount of chelating species will be formed over several thousand years. (2) Chelating species will also form stable complexes with other metals. (3) Chelated radionuclides will still be retarded by sorption. (4) Radionuclides may precipitate in response to changes in chemical conditions. The extent to which these processes occur may be affected by the stability of any chelated species formed. These factors cannot be properly evaluated at this time in the GCD PA because of the limitations mentioned above.

5.10.2 Geochemical Modeling Methodology

The complex system cannot be modeled in detail with existing thermodynamic data. However, one of the simplifying assumptions is that the waste region and overlying alluvium begins and remains in equilibrium with the atmosphere, thus ensuring that oxidizing conditions dominate corrosion, waste dissolution, and radionuclide transport. Rapid equilibrium with the atmosphere is based on the relatively shallow (21 to 37 m [70 to 120 ft]) burial depth of the wastes, and the generally unconsolidated (uncemented) nature of the alluvium, especially in the backfilled boreholes. This assumption is conservative, since oxidizing conditions lead to higher TRU radionuclide solubilities than more reducing conditions; in any case, oxidizing conditions will certainly prevail as nuclides migrate upward from the disposal zone. It is possible that the very

low water availability will retard the system's attainment of equilibrium. This same lack of water will also severely limit the mobility of dissolved contaminants, so the assumption of equilibrium is clearly conservative.

The solubilities were estimated using the thermodynamic equilibrium model embodied in the EQ3/6 computer code, developed by Wolery and others at LLNL. The EQ3/6 geochemical software package is a set of computer codes and supporting thermodynamic and kinetic databases that calculates the solubilities of minerals and other solids and the speciation of solutes in aqueous solutions (EQ3NR), and predicts chemical reactions between these solutions and solids, gases, or other aqueous solutions (EQ6).

Wolery [1978] first developed EQ3/6 to model basalt-seawater reactions in hydrothermal systems at mid-ocean ridges; he patterned EQ3/6 after the PATHI code developed by Helgeson [1968] and Helgeson et al. [1970]. Subsequently, Wolery and his colleagues at LLNL have continued the development of EQ3/6, mainly for application to various radioactive-waste repositories. Daveler and Wolery [1992]; Wolery [1992a,b]; Wolery and Daveler [1992] describe the latest release (Version 7.2) of EQ3/6. The component codes, EQ3NR and EQ6 are described in the above references, and are summarized in Appendix K.

The thermodynamic database for EQ3/6 was originally a reformatted version of the database for PATHI [Helgeson, 1968; Helgeson et al., 1970]. This database included stability constants for many ion pairs and complexes. Subsequent versions of the PATHI database included revised equilibrium constants for mineral dissolution reactions and a few aqueous redox reactions from the work of Helgeson and Kirkham [1974; 1976], Helgeson et al. [1978], and Helgeson et al. [1981]. Helgeson and his colleagues did not, however, revise the stability constants for dissolved species. Since Wolery brought EQ3/6 to LLNL, personnel there have periodically expanded and updated the database. They have continued to incorporate the results from the ongoing efforts of Helgeson and his coworkers to correlate and predict the thermodynamic properties of the major rock-forming minerals and many aqueous species found in geochemical systems.

The EQLIB library supports both EQ3NR and EQ6. EQLIB contains mathematical routines, routines that perform various computer-system functions, and routines that evaluate chemical submodels used by both EQ3NR and EQ6, such as activity-coefficient models.

5.10.3 Use of EQ3/6 for Estimating Solubilities

EQ3/6 was used to predict the solubilities of several Am-, Np-, Pu-, Th-, Ra-, Pb, and U-bearing solid phases in vadose-zone water from a depth of 25.2 to 25.3 m (82.5 to 82.75 ft) in Science Trench borehole Ue5ST-1 (see Sample #24499 in Table 5-15). Estrella et al. [1993] reported chemical analyses for this and other vadose-zone fluids obtained from boreholes close to the GCD disposal boreholes. These fluids are more representative of those likely to interact with TRU waste in the GCD boreholes than those used in previous PA calculations [Chu and Bernard, 1991].

Conceptually, it was assumed that solubility equilibria between Am, Np, Pu, Th, Ra, Pb, or U and vadose-zone water with the composition of Sample #24499 would determine the concen-

trations of these radionuclides at or near their point of release from the waste. Chemical reactions between other constituents of the waste and the vadose-zone water might affect the composition of these fluids in the immediate vicinity of the waste. However, reactions among the alluvial materials in and around the boreholes, atmospheric CO_2 and O_2, and these fluids will restore them to their ambient compositions, or at least to compositions similar to ambient, prior to significant transport from the waste. Therefore, the results reported by Estrella et al. [1993] for Sample #24499 were used without any modifications for the EQ3NR calculations.

The concentrations of $Br^{!}$, Ca^{2+}, $Cl^{!}$, $CO_3^{2!}$, $HCO_3^{!}$, K^{+}, Mg^{2+}, Na^{+}, $NO_3^{!}$, and $SO_4^{2!}$ from Sample #24499 were used for the EQ3NR calculations. However, Estrella et al. [1993] did not report analyses for $B(OH)_{3,aq}$, Eh, $O_{2,\,aq}$, pH, nor $SiO_{2,aq}$. For $B(OH)_{3,aq}$ and $SiO_{2,aq}$, values reported by Harrar et al. [1990] were used. For $O_{2,\,aq}$, the concentration of $O_{2,\,aq}$ was used in equilibrium with atmospheric O_2 estimated by Harrar et al. [1990] for these conditions. For Eh, a value of 0.209 atm [Weast and Astle, 1982] was used for the fugacity (essentially the partial pressure) of O_2. This was equivalent to assuming that the vadose-zone fluids are in equilibrium with atmospheric O_2. Because actinide elements that speciate in more than one oxidation state (Np, Pu, and U in the case of these calculations) are more mobile (have higher solubilities and lower distribution coefficients, or K_ds) in their higher oxidation states, assuming equilibrium with atmospheric O_2 is conservative. This assumption is also consistent with the concentration of $O_{2,\,aq}$ estimated by Harrar et al. [1990]. For pH, a range of 7 to 9 was assumed. Table 5-16 provides all of the compositional data used in the EQ3NR calculations. A temperature of 25EC [77 EF] was assumed for these calculations.

The computer code runs are described in Steinborn and Brush [1999, Section 4.1.1], along with the rationale for the various runs. Appendix B of that report gives the EQ3NR files used to obtain the solubilities summarized below.

5.10.4 Results

Tables 5-17 through 5-24 show the solubilities of Am-, Np-, Pu-, Th-, U-, Ra- and Pb-bearing solids obtained from the EQ3NR calculations described above. The recommended solubility ranges for use in the PA calculations are summarized in Table 5-24. The numbers in the table are based on credible mineral phases in GCD site pore water, as discussed above. The variation over the designated pH range is small compared to the variation from selecting controlling mineral phases. The solubilities of Ac and Pa could not be calculated using EQ3NR because there are no thermodynamic data for Ac- or Pa-bearing solids or dissolved species in the EQ3/6 database. Therefore, Ac was estimated to have the same solubility range as Am and Pa was estimated to have the same solubility range as Np, based on the oxidation-state analogy. The oxidation-state analogy refers to commonly observed similarities in the chemical behavior of actinide elements in the same oxidation state. For example, Am(III) and Pu(III) behave very similarly. The reason for these similarities is that the solid phases, dissolution products for these solids, dissolved species, stability constants for dissolved species, solubilities, and Kds for actinides in the same oxidation state are usually very similar. Ac speciates exclusively in the +III oxidation state under geochemical conditions, the same state as Am. Pa speciates in the +IV and +V oxidation states

Table 5-16. GCD Vadose-Zone Water Compositions

Element or Chemical Property	Ue5ST-1, 82.5 – 82.75` Sample #24499 (mg/L)[a]	Ue5ST-1, 82.5 – 82.75` Sample #24499 (mM)b	Ue5ST-1, 115.0 – 115.25` Sample #24494 (mg/L)c	Ue5ST-1, 115.0 – 115.25` Sample #24494 (mM)d
B(OH)	0.766e	0.0124[f]	0.766[e]	0.0124[f]
Br^-	15	0.19	17	0.21
Ca^{2+}	44.1	1.10	203	5.06
Cl^-	2,130	60.1	2,310	65.2
CO^-	226	3.77	46	0.77
HCO	1,160	19.0	1,260	20.6
K^+	102	2.61	104	2.66
Mg^{2+}	28.1	1.16	92.0	3.78
Na^+	2,000	87.0	1,710	74.4
NO	24.0	0.387	2.8	0.045
$O_{2,\,aq}$	8.00[g]	0.500	8.00[g]	0.500
f_{O2} (atm)[g]	0.209	0.209	0.209	0.209
pH (std. units)	7.00 – 9.00[h]	7.00 – 9.00[h]	7.00 – 9.00[h]	7.00 – 9.00[h]
SiO	60.970[e]	1.01[f]	60.970[e]	1.01[f]
SO^-	373	3.88	276	2.87

a. From Estrella et al. [1993, Table C.3, p. 50].
b. Recalculated from Estrella et al. [1993, Table C.3, p. 50].
c. From Estrella et al. [1993, Table C.3, p. 51].
d. Recalculated from Estrella et al. [1993, Table C.3, p. 51].
e. From EQ3/6 input file J13WSF.3i [Daveler and Wolery, 1992; Wolery, 1992a,b; Wolery and Daveler, 1992].
f. Recalculated from EQ3/6 input file J13WSF.3i.
g. See text.
h. See Appendix D.

Table 5-17. Solubilities (M) of Am-Bearing Solids in Vadose-Zone Water from Ue5ST-1, 25.2 to 25.3 m (82.5 to 82.75 ft) Deep, Sample #24499, f_{O_2} = 0.209 atm

Solid	pH = 7.00	pH = 8.00	pH = 9.00
$Am(OH)_3$	4.50×10^{-13}, a	3.79×10^{-14}, a; 3.56×10^{-14}, b	3.03×10^{-15}, a; 3.01×10^{-15}, c
$AmOHCO_3$	1.02×10^{-17}, a	5.37×10^{-18}, a; 5.37×10^{-18}, d	4.43×10^{-18}, a; 4.43×10^{-18}, d

a. Solubility with no Np, Pu, Th, nor U.
b. Solubility with Np, Pu, Th, and U = 1.00×10^{-14} M each.
c. Solubility with Np, Pu, Th, and U = 1.00×10^{-15} M each.
d. Solubility with Np, Pu, Th, and U = 1.00×10^{-18} M each.

Table 5-18. Solubilities (M) of Np-Bearing Solids in Vadose-Zone Water from Ue5ST-1, 25.2 to 25.3 m (82.5 to 82.75 ft) Deep, Sample #24499, f_{O_2} = 0.209 atm

Solid	pH = 7.00	pH = 8.00	pH = 9.00
$NpO2(OH)_2$	2.86×10^{-11} [a]	4.09×10^{-12} [a]; 2.96×10^{-12} [b]	1.57×10^{-12} [a]; 6.15×10^{-13} [c]
Np_2O_5	1.00×10^{-12} [a]	5.32×10^{-13} [a]; 3.61×10^{-13} [c]	6.03×10^{-13} [a]; 3.94×10^{-13} [c]
$NpO_2(OH)_{am}$	3.21×10^{-13} [a]	2.98×10^{-13} [a]; 1.74×10^{-13} [c]	4.76×10^{-13} [a]; 2.87×10^{-13} [c]
NpO_2	1.51×10^{-15} [a]	3.08×10^{-15} [a]; 3.05×10^{-15} [e]	2.05×10^{-14} [a]; 1.89×10^{-14} [d]
$NaNpO_2CO_3 \cdot 3.5H_2O$	1.21×10^{-15} [a]	2.21×10^{-15} [a]; 2.20×10^{-15} [e]	1.66×10^{-14} [a]; 1.57×10^{-14} [d]

a. Solubility with no Am, Pu, Th, nor U.
b. Solubility with Am, Pu, Th, and U = 1.00×10^{-12} M each.
c. Solubility with Am, Pu, Th, and U = 1.00×10^{-13} M each.
d. Solubility with Am, Pu, Th, and U = 1.00×10^{-14} M each.
e. Solubility with Am, Pu, Th, and U = 1.00×10^{-15} M each.

Table 5-19. Solubilities (M) of Pu-Bearing Solids in Vadose-Zone Water from Ue5ST-1, 25.2 to 25.3 m (82.5 to 82.75 ft) Deep, Sample #24499, f_{O_2} = 0.209 atm

Solid	pH = 7.00	pH = 8.00	pH = 9.00
$PuO_2(OH)_2$	3.59×10^{-16} [a]	4.56×10^{-16} [a]; 4.56×10^{-16} [b]	3.85×10^{-16} [a]; 3.84×10^{-16} [b]
PuO_2	9.51×10^{-11} [a]	1.21×10^{-10} [a]; 1.21×10^{-10} [c]	1.02×10^{-10} [a]; 1.02×10^{-10} [c]

a. Solubility with no Am, Np, Th, nor U.
b. Solubility with Am, Np, Th, and U = 1.00×10^{-16} M each.
c. Solubility with Am, Np, Pu, Th, and U = 1.00×10^{-10} M each.

Table 5-20. Solubilities (M) of Th-Bearing Solids in Vadose-Zone Water from Ue5ST-1, 25.2 to 25.3 m (82.5 to 82.75 ft) Deep, Sample #24499, f_{O_2} = 0.209 atm

Solid	pH = 7.00	pH = 8.00	pH = 9.00
$Th(OH)_4$	5.69×10^{-17} [a]	5.69×10^{-17} [a]; 5.69×10^{-17} [b]	5.69×10^{-17} [a]; 5.69×10^{-17} [b]

a. Minimum solubility or solubility with no Am, Np, Pu, nor U.
b. Solubility with Am, Np, Pu, and U = 1.00×10^{-17} M each.

Table 5-21. Solubilities (M) of U-Bearing Solids in Vadose-Zone Water from Ue5ST-1, 25.2 to 25.3 m (82.5 to 82.75 ft) Deep, Sample #24499, f_{O_2} = 0.209 atm

Solid	pH = 7.00	pH = 8.00	pPH = 9.00
$UO_3 \cdot 2H_2O$[b]	6.49×10^{-3}[a]	6.54×10^{-3}[a];	6.98×10^{-3}[a];
(schoepite)		5.21×10^{-3}[d]	5.32×10^{-3}[d]
$CaUO_4$	ND[c]	ND[c]	ND[c]
$Na_2U_2O_7$	ND[c]	ND[c]	ND[c]
$Mg(H_3O)_2(UO_2)_2(SiO_4)_2 \cdot 4H_2O$	5.74×10^{-3}[a]	5.22×10^{-3}[a];	5.70×10^{-3}[a];
(sklodowskite)		3.77×10^{-3}[d]	3.76×10^{-3}[d]
$(UO_2)_2SiO_4 \cdot 2H_2O$	3.89×10^{-5}[a]	6.26×10^{-4}[a];	2.94×10^{-3}[a];
(soddyite)		5.83×10^{-4}[e]	1.53×10^{-3}[d]
$Ca(UO_2)_2(Si_2O_5)_3 5H_2O$	1.97×10^{-6}[a]	3.18×10^{-5}[a];	6.26×10^{-4}[a];
(haiweeite)		3.16×10^{-5}[f]	5.79×10^{-4}[e]

a. Minimum solubility or solubility with no Am, Np, Pu, nor Th.
b. This phase constitutes the end member of a series of phases in the EQ3 output files with the compositions (in order of increasing stability and decreasing solubility): $UO_3 \cdot 0.393H_2O$, $UO_3 \cdot 0.648H_2O$, $UO_3 \cdot 0.85H_2O$, $UO_3 \cdot 0.9H_2O$, and $UO_3 \cdot 1.0H_2O$. The solubility of the end member of this series was the only one calculated.
c. Not determined because it is unlikely to form under these conditions.
d. Solubility with Am, Np, Pu, and Th = 1.00×10^{-3} M each.
e. Solubility with Am, Np, Pu, and Th = 1.00×10^{-4} M each.
f. Solubility with Am, Np, Pu, and Th = 1.00×10^{-5} M each.

Table 5-22. Solubilities (M) of Ra-Bearing Solids in Vadose-Zone Water from Ue5ST-1, 25.2 to 25.3 m (82.5 to 82.75 ft) Deep, Sample #24499, f_{O_2} = 0.209 atm

Solid	pH = 7.00	pH = 8.00	pH = 9.00
RaSO4	8.53×10^{-8}[a]	8.61×10^{-8}[a]	8.61×10^{-8}[a]

a. Solubility with no Am, Np, Pb, Pu, Th, or U.

Table 5-23. Solubilities (M) of Pb-Bearing Solids in Vadose-Zone Water from Ue5ST-1, 25.2 to 25.3 m (82.5 to 82.75 ft) Deep, Sample #24499, f_{O_2} = 0.209 atm

Solid	pH = 7.00	pH = 8.00	pH = 9.00
PbO_2 (plattnerite)	4.68×10^{-6}[a]	4.70×10^{-8}[a]	4.71×10^{-10}[a]
$PbCO_3$ (cerussite)	1.96×10^{-8}[a]	1.74×10^{-9}[a]	1.91×10^{-10}[a]

a. Solubility with no Am, Np, Pu, Ra, Th, or U.

Table 5-24. Values of Solubility (M) Used in the PA Calculations

Element	Distribution	0.001 Quantile or Minimum	0.999 Quantile or Maximum
Am	loguniform	4×10^{-8}	4×10^{-3}
Np	loguniform	1×10^{-5}	3×10^{-1}
Pu	loguniform	1×10^{-10}	5×10^{-6}
Th	loguniform	6×10^{-8}	6×10^{-6}
U	loguniform	2×10^{-6}	7×10^{-3}
Ra	loguniform	9×10^{-9}	9×10^{-7}
Pa	loguniform	1×10^{-5}	3×10^{-1}
Pb	loguniform	2×10^{-10}	5×10^{-6}
Ac	loguniform	4×10^{-8}	4×10^{-3}

under geochemical conditions, the same oxidation states as Th and Np. It is conservative to assume that Pa will speciate as Pa(V), not Pa(IV), under these conditions. Therefore, Pa is assumed to have the same range of solubilities as Np(V) under these conditions.

5.10.5 Conclusions

The solubilities used in the PA calculations have been calculated based on recent site geochemical data. The range of pH conditions reflects the range of pH observed in native alluvial waters collected at the site. This narrow pH range reflects the high chemical buffering capacity of the alluvium. The variability in solubilities reflects the set of potentially controlling solid phases for the equilibrium calculations.

5.11 Criticality Potential

5.11.1 Introduction

The potential for nuclear criticality is of concern for the GCD boreholes, because they contain fissionable materials, i.e., plutonium and enriched uranium [Chu and Bernard, 1991]. With these constituents in the inventory, the possibility of nuclear criticality either as a result of the waste emplacement in the GCD boreholes itself or as a result of postclosure radionuclide migration is a concern when assessing disposal-system performance. This section presents a summary of criticality analyses performed for the GCD boreholes. A more detailed discussion can be found in Appendix L and in Harms et al. [1998].

Analyses were performed to evaluate the potential for nuclear criticality to determine whether this process can or cannot be eliminated as a concern when assessing disposal system performance. If nuclear criticality can occur, but the probability of occurrence is less than the value provided by the U.S. EPA as guidance (i.e., less than one chance in 10,000 in 10,000 years [EPA, 1985]), the process can be screened out of scenario development. If the occurrence of nuclear criticality either alone or in combination with other events and processes does not affect the

performance of the disposal system (i.e., no or low consequence), the process need not be considered further. If the conditions necessary for nuclear criticality to occur are not physically reasonable or possible, the process need not be considered further. A detailed discussion of the calculations and assumptions of these analyses are available in Harms et al. [1998]. This discussion is taken from that report, and presents no new analyses.

The approach used to screen nuclear criticality was to establish bounding conditions by modeling various highly idealized (i.e., noncredible) configurations of fissile radionuclides consistent with the radionuclide inventories present in the TRU boreholes and the physical properties of the materials within the disposal system. These bounding conditions optimized the conditions necessary for nuclear criticality to occur. This approach was selected as a more computationally-efficient alternative to attempting to simulate the relatively complex processes of radionuclide dissolution, migration, and reconcentration within and surrounding the TRU boreholes. If nuclear criticality cannot occur under these idealized conditions, then nuclear criticality certainly cannot occur under the actual conditions within the GCD disposal system, and the process need not be considered further. If nuclear criticality can occur under these idealized conditions, the next step is to examine less idealized configurations. If the analyses indicate that nuclear criticality can occur in modeled systems deemed to be sufficiently similar to the actual disposal system, the possible effects of nuclear criticality on system performance must be considered.

5.11.2 Basics of Nuclear Criticality

Nuclear criticality is commonly misunderstood to be the same as a nuclear explosion. Whereas the same radionuclides can participate in both phenomena, the specific conditions that will result in criticality are substantially different from the conditions resulting in an explosion. A nuclear explosion can occur only when the neutron chain reaction within a mass of radionuclides becomes supercritical with exponentially increasing energy levels occurring within a fraction of a second. Achieving the necessary geometry of this supercritical mass of radionuclides within the necessary time constraints is very difficult. No realistic mechanism for assembling a supercritical mass of radionuclides on the short time scales required for an explosion has been proposed in a repository or geologic setting, as discussed in Harms et al. [1998, Appendix A]. Nuclear explosions resulting from reconcentration of radionuclides within the GCD boreholes or along possible migration routes are excluded from further discussion because of the unrealistic conditions required for such events to occur. Because of these constraints, only nuclear criticality is considered further.

Nuclear criticality is a self-sustaining neutron chain reaction in which there is an exact balance between the production of neutrons [by the splitting of atomic nuclei] and the loss of neutrons in the absence of extraneous neutron sources. When the net production of neutrons exceeds the neutron leakage, the system will be supercritical, and a divergent chain reaction will occur. If, on the other hand, too many neutrons are lost through leakage, the effective reproduction factor for the system will be less than unity, and a self-sustaining chain reaction will not be possible [Wick, 1967, p. 877].

The state of a neutron multiplying system is most concisely described by its effective multiplication factor (k_{eff}). The k_{eff} is defined as the ratio of the production rate to the loss rate of neutrons

in a system. When k_{eff} is less than one, the system is subcritical and has a decreasing or zero power level depending on the initial conditions. When k_{eff} is greater than one, the system is supercritical and has an increasing power level. When k_{eff} is exactly equal to one, the system is critical and has a constant power level.

5.11.3 Assessment of Nuclear Criticality

The TRU waste inventory is given in Table 5-15 and is based on information examined in an earlier study [Chu and Bernard, 1991]. Only Boreholes 1, 2, 3, and 4 were found to contain either enriched uranium or plutonium, and thus only these boreholes are considered for criticality evaluation.

The material in Boreholes 1, 2, and 3 is the remains of weapons parts that were recovered from four nuclear weapon accident scenes. In all four accidents, the weapons were involved in either a fire or high-explosive detonation. In the accidents involving fire, the heat was intense enough to melt the weapon parts. The fissile material mixed with an undetermined amount of structural material before resolidifying. The fissionable material recovered from detonation accidents was embedded in surrounding structural material by the blast. The material buried in Boreholes 1, 2, and 3 was packaged in 15 containers of differing construction. Five containers were buried in Borehole 1, four in Borehole 2, and six in Borehole 3.

The plutonium buried in Borehole 4 is divided among 258 208.2-L drums (55-gal) and consists of surficial plutonium contamination on metal, plastic, and graphite items used in the manufacture and disassembly of weapons. A minor amount of ^{235}U (up to 45 g][1.6 oz]) is also contained in these drums. The large amount of depleted uranium buried in this hole is contained in eight boxes separate from the drums.

This study began with a bounding analysis based on highly conservative assumptions. Required assumptions were made in the direction that increased the criticality of the system. For example, because the locations of the materials in the boreholes were not well known, all of the material in a given borehole was assumed to be localized in a small volume with the optimum geometry to promote criticality. In reality, the fissionable materials are dispersed within the boreholes, a configuration much less likely to lead to criticality.

The multigroup Monte Carlo code KENO-IV [Petrie and Cross, 1975] was used to calculate k_{eff} for the various configurations investigated in this study. KENO-IV is a standard tool used in criticality safety analyses and was chosen over other Monte Carlo codes because this code is simple and thus computationally very fast without compromising accuracy.

Four situations were examined in the analyses: (1) the radionuclides in each borehole are concentrated within the backfill as a metallic sphere having no porosity, (2) the radionuclides are dissolved in groundwater and maintained in a spherical shape within the backfill, (3) the radionuclides are deposited within the pore volume available within the backfill, and (4) the radionuclides are deposited in the pore space within the undisturbed alluvium outside the boreholes.

For radionuclides concentrated in metallic spheres, the analyses considered an absence of reflectors and the presence of probertite and water as reflectors. Of the 12 analyses for the four boreholes and three reflector arrangements, only the radionuclides in Borehole 2 when concentrated in a sphere of radius 6.1 cm (2.4 in.) with probertite and water reflectors resulted in values of k_{eff} in excess of 0.95, which is the value assumed for criticality to occur. Even relatively minor dispersal of the radionuclides from the spherical geometry (e.g., separating the hemispheres) resulted in values of k_{eff} substantially below 0.95.

For fissionable radionuclides in a spherically-shaped solution within the backfill and surrounded by a water reflector, the radionuclide inventories can result in values of k_{eff} equal to or greater than 0.95 for certain sphere radii and mass ratios of the solutions. The mass ratios necessary for criticality to occur require radionuclide solubilities at least one order of magnitude greater than the solubilities determined for the groundwater composition in the vicinity of the GCD facility. Criticality under these conditions is not possible, because no mechanism exists that can create the geometry of this analysis in the field, other materials in solution with the fissionable radionuclides will absorb neutrons, and the radionuclide solubilities necessary for criticality to occur are not physically achievable for GCD-specific groundwater properties.

Concentration of the fissile radionuclides of each borehole in the pore volume in the probertite backfill was also analyzed. The radionuclides were assumed to occupy a spherical volume within the backfill with the pores filled with various proportions of radionuclides and either air or water. For all analyses of all borehole inventories, k_{eff} did not exceed 0.6. In addition to the lack of a mechanism to concentrate the radionuclides within the backfill, the porosities of the backfill required for criticality to be a concern are physically unrealistic (> 0.91).

Complete segregation of the fissile radionuclides in the alluvium was also analyzed. The radionuclides were assumed to be concentrated in a spherical shape, occupying the pores within the alluvium. Calculation of the minimum porosity in the alluvium for criticality to occur indicates that only the porosity associated with the Borehole 2 inventory is within the range of porosity values measured for samples associated with the GCD facility. No mechanism has been identified that can result in complete radionuclide concentration of a borehole's entire inventory. Fractional concentrations of radionuclides may be possible, but the porosities required for fractions of the radionuclide inventory to achieve criticality are higher than expected for alluvial deposits. A mechanism to achieve significant (i.e., with respect to criticality) fractional concentrations of radionuclides in the required geometry is also lacking.

Criticality analyses based on radionuclide inventories in the TRU boreholes do not consider the possible contributions to criticality by daughter products of the fissile radionuclides. Analyses of k_{eff} as a function of time (to 1 billion years) for radionuclides in Borehole 2 (nearly all uranium) and Borehole 4 (all plutonium) indicate that k_{eff} does not increase during this timeframe for either inventory. These results are also applicable to the radionuclide inventories in Boreholes 1 and 3.

5.11.4 Conclusions

Based on the results of bounding analyses of criticality safety for the fissile-radionuclide inventories in the TRU boreholes at the GCD location, criticality cannot occur under conditions that

either currently exist within the disposal system or will occur during the evolution of the disposal system. The conclusion derived from this study is that nuclear criticality is not just physically unreasonable, but physically impossible.

5.12 Radionuclide Transport

Radionuclides disposed of in the GCD boreholes will decay, producing the radionuclides shown in the decay chains in Figure 5-30. All of these radionuclides, with the exception of radon isotopes, are solids under the conditions existing in the boreholes and could only be transported in the liquid phase as dissolved solids. Radon is transported in the vapor phase. This section presents the PA models for liquid phase transport and vapor phase transport.

5.12.1 Liquid Phase Transport

Radionuclides dissolved in pore water can be transported by the upward flow of water (advection) and diffusion as a result of the existence of concentration gradients. Variations in pore size and structure can lead to uneven advection rates (dispersion), and the chemical bonding of radionuclides to the alluvium can slow radionuclide migration (adsorption). These four processes are included in the model of liquid phase transport and are discussed in the following sections. The mathematical models developed from the conceptual models of transport given below are discussed and presented in Section 7.0.

5.12.1.1 Advection

Assuming 1-D advection also provides the shortest radionuclide travel time to the ground surface for a given quantity of radionuclides released from the source.

As discussed in Section 5.6, data collected at the Area 5 RWMS indicate that pore water in the alluvium is slowly moving upward toward the ground surface. Any radionuclides dissolved in this water will move upward as well. Although in reality this upward movement may have some lateral component, advection is modeled one-dimensionally for the PA in order to simplify the calculations and overestimate releases. The flux of radionuclide *i* across a plane parallel to the ground surface is therefore given by

$$q_{a,i} = q_l \, C_i \qquad (5\text{-}16)$$

where

$q_{a,i}$ = advective flux of radionuclide *i* (moles/m^2 yr)
C_i = concentration of radionuclide *i* in the pore water (moles/m^3)
q_l = liquid advective flux density (m^3 water/m^2 alluvium yr).

As discussed in Section 5.6.2.1, the upward advection of water is assumed to end at the no-advective flux boundary, which is assumed to be at a depth of 2 m (7 ft) below the ground surface. Commensurately, the upward advection of radionuclides is also assumed to end at this boundary. Upward-moving pore water is assumed to evaporate as it reaches this hypothetical boundary, and any radionuclides dissolved in the water are assumed to precipitate if their

concentrations exceed their solubilities. Although radionuclides are no longer moving upward in the liquid phase, they can continue to be transported upwards only by plants and animals instead of by water movement.

The liquid phase concentration of each radionuclide is assumed to be limited by its solubility (see Section 5.10 for radionuclide solubilities). This assumption places a reasonable upper limit on the amount of radioactive material that can be dissolved in the pore water. Solubilities are uncertain and are element-specific. The volume of pore water available for dissolution is based on the volumetric moisture content of the alluvium and the volume of the portion of the boreholes in which waste was emplaced.

It is assumed that radionuclides will precipitate chemically if their solubilities are exceeded along the transport pathway. Precipitated radionuclides are not available for transport, but they are available for plant uptake.

Because the GCD inventory contains multiple isotopes of U and Pu (see Section 5.9), the elemental solubility is apportioned among all the isotopes of a particular element based on the initial molar inventory. For example, the solubility of ^{239}Pu is calculated by multiplying the Pu solubility by the ratio of the moles of ^{239}Pu in the initial inventory to the total moles of all isotopes of Pu in the initial inventory. This calculation is performed only at the beginning of the simulation; therefore, this assumption applies only to those radionuclides initially present in the waste and does not account for the change in relative molar abundance as a result of radionuclide transport away from the source or radioactive decay and production. This assumption does not apply to those radionuclides not present in the initial inventory (e.g., Pb); therefore, the solubility of each isotope of such elements equals the elemental solubility.

Assuming that the initial molar fractions can be used to apportion solubility among the various isotopes of U and Pu (i.e., not updating the molar fractions spatially and with each time step) does not result in a significant underestimation of radionuclide releases. Figure 5-31 shows the molar fractions of the U and Pu isotopes initially present in the GCD waste inventory and how these molar fractions change over 10,000 years as a result of decay and ingrowth. For this figure, average values of initial radionuclide inventory were used. As demonstrated by the figure, the molar fractions of all isotopes except ^{238}Pu change very little. The molar fraction of ^{238}Pu drops dramatically because of its short half-life.

For those isotopes of U and Pu that have *decreasing* molar fractions over 10,000 years, using initial molar fractions to estimate isotopic solubility for the entire 10,000 years results in overestimating the quantity of that isotope present and thus does not result in underestimating releases of those isotopes. For those isotopes of U and Pu that have *increasing* molar fractions over 10,000 years, using initial molar fractions to estimate isotopic solubility for the entire 10,000 years results in underestimating the quantity of that isotope present. However, for such isotopes of U and Pu, this underestimation is not a significant source of error. Three isotopes of U and Pu have molar fractions that *increase* over 10,000 years: ^{235}U, ^{239}Pu, and ^{242}Pu. The molar fraction of ^{235}U increases 3% (from 0.064 to 0.066), the molar fraction of ^{239}Pu also increases 3% (from 0.941 to 0.972), while the molar fraction of ^{242}Pu increases 35% (from 1.99×10^{-4} to $2.69 \times 10^{!4}$). Solubility values for isotopes of U and Pu vary over three to four orders of magnitude, so

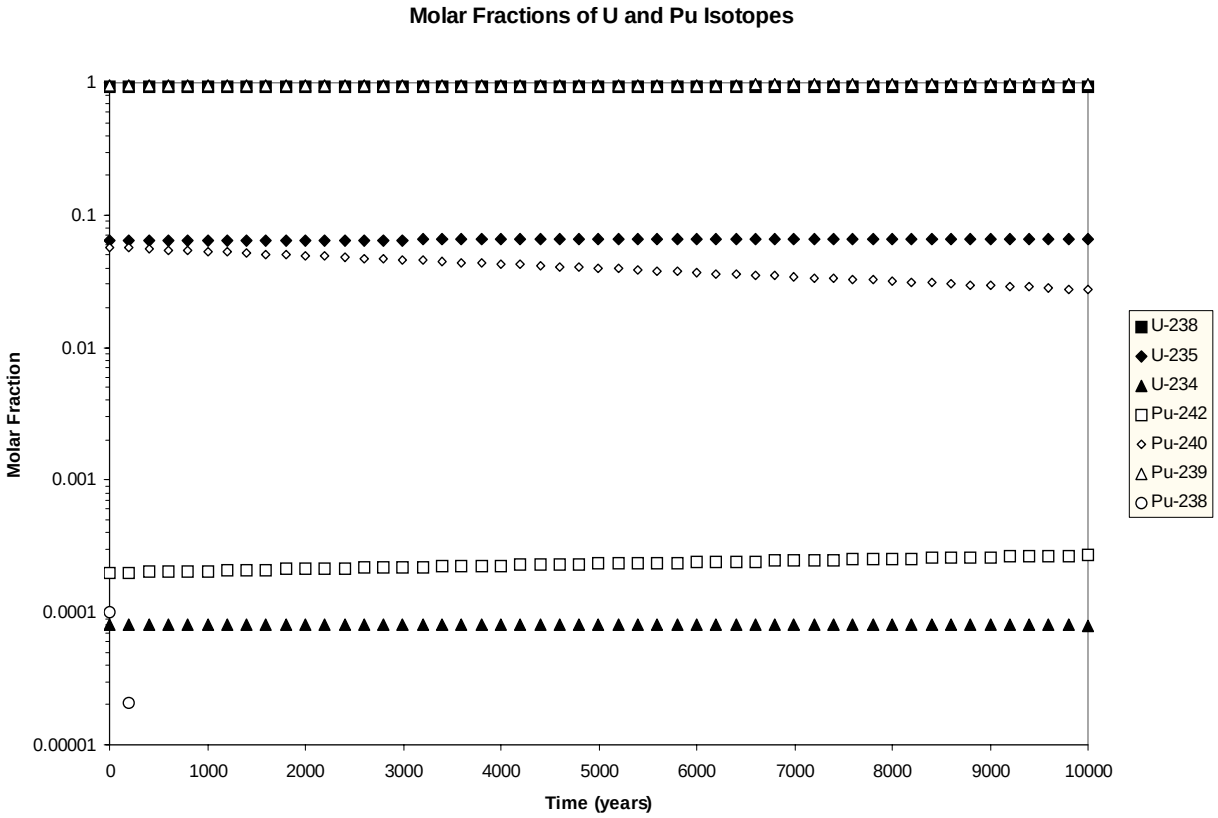

Figure 5-31. Molar Fractions of Isotopes of U and Pu.

underestimating the molar fractions of ^{235}U and ^{239}Pu by 3% is insignificant compared to the uncertainty in solubility. For ^{242}Pu, while the relative percentage increase in molar fraction is large (35%), the quantity of ^{242}Pu is so small, both in terms of mass and curies, that releasing all of it to the accessible environment results in an EPA Sum of about 0.1. Therefore, underestimating the molar fraction of ^{242}Pu is also insignificant.

The molar fractions shown in Figure 5-31 were calculated in the absence of transport away from the source. However, the analysis shown in this figure is still a reasonable approximation of what happens when transport occurs, as in the PA calculations. The isotopes of Pu are not produced by decay of any other radionuclides, and they all have identical transport parameters (sorption coefficients, diffusion coefficients, plant uptake parameters, etc.) and so will all be transported at the same rate. Therefore, the molar fractions of the Pu isotopes should be the same anywhere in the transport column. For example, if ^{239}Pu has a molar fraction of 0.94 in the source, it will have a molar fraction of 0.94 at any point in the transport column. The isotopes of U all have identical transport parameters but are produced by decay of Pu isotopes, which have transport parameters that are different from those of U isotopes, so the molar fractions of U isotopes will be somewhat different in the transport column than they are in the source. However, because the mass of U in the initial inventory is so much greater than the mass of Pu, over 10,000 years, less than the 3% of the mass of any U isotope is a result of Pu decay. For example, the quantity of ^{235}U present at 10,000 years, assuming no production by ^{239}Pu, is 97.2% of the quantity of ^{235}U present at 10,000 years, assuming production by ^{239}Pu. Therefore, the molar

fractions of the U isotopes in the transport column are only slightly different than they are in Figure 5-31 and the analysis shown in this figure is a reasonable approximation of what happens when transport occurs.

Therefore, molar fractions of the isotopes of U and Pu change very little spatially or temporally (over 10,000 years). Any underestimation of quantities of individual isotopes that results from using initial molar fractions to estimate solubilities of U and Pu isotopes throughout the simulation period is insignificant given the significant uncertainties in other related parameters (e.g., initial inventory, elemental solubility).

5.12.1.2 Diffusion/Dispersion

Diffusion

Radionuclides dissolved in pore water will diffuse away from the disposal region as a result of concentration gradients in the surrounding alluvium. Diffusion occurs whether or not the pore water is flowing and will transport radionuclides both laterally and upwardly. Upward diffusion is assumed to occur in conjunction with upward advection and dispersion and is assumed to end at the no-advective flux boundary 2 m (7 ft) below the ground surface. Lateral diffusion is modeled separately, as discussed below.

The diffusion coefficient used to calculate the diffusive flux is the "effective" diffusion coefficient. It is not radionuclide-specific and does not vary spatially or temporally. The effective diffusion coefficient is defined as

$$D_{eff} = \frac{D_m}{\tau} \tag{5-17}$$

where

D_{eff} = the effective diffusion coefficient (m^2/sec),
D_m = the molecular diffusion coefficient (m^2/sec), and
τ = the tortuosity (dimensionless).

The molecular diffusion coefficient is not radionuclide-specific because it is inversely related to the radius of the diffusing species [Bird et al., 1960, p. 514], and all the diffusing species are likely to be of similar size because the radionuclides themselves are of similar size. Furthermore, the larger source of uncertainty in calculating the *effective* diffusion coefficient is the tortuosity, not the molecular diffusion coefficient. For the PA, the molecular diffusion coefficient was assumed to equal $4.3 \times 10^{!6}$ cm^2/sec based on free-solution tracer diffusion coefficients reported by Brush [1996]. The values appropriate for the oxidizing conditions at the GCD site ranged from $1.53 \times 10^{!6}$ cm^2/sec to $4.26 \times 10^{!6}$ cm^2/sec, so the largest value was selected for use in the PA.

Tortuosity is a dimensionless number that reflects the fact that radionuclides are diffusing through alluvium that contains a variety of pore sizes and that may not have a continuous water phase. As defined and used in the PA, the tortuosity is always equal to or greater than one. Low

values of tortuosity signify that the path taken through the alluvium *is not* very tortuous, so that the effective diffusion coefficient is not much smaller than the molecular diffusion coefficient. Conversely, large values of tortuosity indicate that the path taken through the alluvium *is* tortuous and that the effective diffusion coefficient is much smaller than the molecular diffusion coefficient.

Developing appropriate values of tortuosity for the PA was accomplished by conducting a literature search to find tortuosity models [Shearer et al., 1973; Wright, 1990; Sadeghi et al., 1989] and data with which to test these models [Sadeghi et al., 1989; Sallam et al., 1984; Jurinak et al., 1987; Wright, 1990; Conca and Wright, 1990; Conca et al., 1992]. Several different models were considered and all were compared with published data (see Appendix M for a detailed discussion of the process). The result of this study was that, for the PA, tortuosity is modeled as a function of volumetric moisture content. The equation for this model is

$$\tau = \frac{1.01}{\theta^{1.75}} \tag{5-18}$$

where

θ = volumetric moisture content (dimensionless).

Because the moisture content is uncertain, tortuosity is also uncertain. If the sampled value of moisture content is 0.05, the tortuosity is 191. If the sampled value of moisture content is 0.12, the tortuosity is 41. Because of the way effective diffusion coefficient is defined and the way the tortuosity model was developed, the effective diffusion coefficient accounts for two phenomena: (1) a greater microscopic path length for the pore fluid compared to the macroscopic distance, and (2) only a small fraction (θ) of the porous medium being available for transport. Therefore, the diffusive flux of radionuclide *i* across an imaginary plane parallel to the ground surface is given as

$$q_i = \frac{-D_m}{\tau} \frac{\partial C_i}{\partial x} \tag{5-19}$$

where

q_i = flux of radionuclide *i* (moles/m^2 yr)

Dispersion

Dispersion results from the variety of pathways and path lengths in the alluvium through which advection occurs. The importance of dispersion in a porous medium (i.e., alluvium) under the conditions that are thought to exist (low moisture contents and low advection rates) is debatable, but including longitudinal dispersion in this one-dimensional model should not lead to an underestimation of radionuclide releases. Dispersion across an imaginary plane parallel to the ground surface is proportional to the upward water flux (q_i); therefore, dispersion is described by a dispersion coefficient that is equal to a constant dispersivity multiplied by the upward water flux rate (not the velocity),

$$D_\alpha = q_l \, \alpha \tag{5-20}$$

where

D_α = dispersion coefficient (m^2/yr),
q_l = liquid phase advective flux density (m^3 of water/m^2 of alluvium per yr), and
α = longitudinal dispersivity (m).

For the PA, data on chloride profiles in boreholes PW-1 and PW-3, along with conclusions regarding the history of infiltration at the GCD site presented in Appendix A, were used to estimate the dispersivity for unsaturated flow. These analyses are discussed in detail in Appendix N, and resulted in the dispersivity being described by a uniform distribution ranging from 0.01 m to 0.3 m (0.4 in. to 12 in.). The analyses documented in Appendix N were completed several years before this PA was conducted. Several changes occurred in those intervening years: (1) the tortuosity model was selected (see Equation 5-17) and it differed from the models used in the original dispersivity analysis, and (2) the definition of effective diffusion coefficient changed (see Equation 5-16). Repeating the analyses documented in Appendix N with the changes noted above results in values of dispersivity with a maximum of 15 cm (.50 ft). Therefore, the upper value of the distribution recommended in Appendix N was changed to 0.15 m (.50 ft) from 0.30 m (1 ft), resulting in a uniform distribution of dispersivity ranging from 0.01 m (.3 ft) to 0.15 m (.5 ft).

The total diffusion/dispersion coefficient is therefore given by combining Equations 5-19 and 5-20,

$$D_T = \alpha\, q_l + \frac{D_m}{\tau} \tag{5-21}$$

and the flux of radionuclide *i* across a plane parallel to the ground surface from mechanical dispersion and molecular diffusion is given by

$$q_{D,i} = -\left(\alpha\, q_l + \frac{D_m}{\tau}\right)\frac{\partial Ci}{\partial x} \tag{5-22}$$

Lateral Diffusion

Lateral diffusion can cause the actual movement of radionuclides to differ from the one-dimensional approximation in two ways. First, radionuclides that are transported through the top of the waste region will spread as they move toward the land surface, rather than remaining confined to the borehole region as assumed in the one-dimensional model. Lateral spreading of such radionuclides does not significantly affect the total mass transported to a particular elevation, but would tend to increase the area of contamination while decreasing contaminant concentrations. The models for the mass transfer processes that can bring contamination to the surface (plant uptake and bioturbation) are linear in both the total contaminated area and in the soil concentration. The increase in the contaminated area is proportional to the associated decrease in contaminant concentrations. Therefore, the estimate of mass discharged to the ground surface is unaffected by lateral spreading, and the one-dimensional model is adequate for describing the transport of waste that leaves through the top of the waste region.

Second, diffusion and dispersion can cause radionuclides to move laterally through the sides of the disposal boreholes, where they can be carried towards the land surface by advection of the pore water near the boreholes. The one-dimensional model does not include radionuclides that diffuse or disperse through the sides of the disposal boreholes, so the following model is used to estimate the mass of radionuclides released through the sides of the boreholes that is discharged to the ground surface in 10,000 years.

The amount of mass released from the waste region by lateral diffusion and dispersion is estimated using a simplifying assumption of radial transport laterally away from the disposal borehole. To simplify this calculation, radial diffusion and upward advection are assumed to operate independently of each other. This assumption leads to an expression for the rate of mass release laterally from the borehole, per unit length of borehole, as a function of time.

Conceptually, the pore water surrounding the borehole is divided into many thin annular regions which are carried upward past the borehole at the upward advection rate. As each annulus passes by the waste-containing region of the borehole, radionuclides diffuse into each thin section from the outer surface of the borehole. Diffusion and dispersion between regions as the regions are carried upward by the moving pore water are not considered in this calculation.

The mass released through the sides of the disposal boreholes by diffusion and dispersion and carried above the elevation of the top of the waste in the annular regions is compared to the mass released by advection through the top of the waste region. This comparison results in an "enlargement factor" for the area of the borehole. The enlargement factor is the relative amount that the disposal cell cross-sectional area would have to be increased, in the one-dimensional transport calculation, to compensate for the mass added by lateral diffusion and dispersion through the borehole sides. The geometry of a single borehole (1.5 m [5 ft] radius, 15 m [50 ft] height) is used to calculate the enlargement factor. The mathematical model of lateral diffusion is presented in Section 7.3.9.

5.12.1.3 Adsorption

Radionuclides dissolved in pore water will adsorb onto the alluvium as they are transported away from the waste, increasing the travel time to the accessible environment (i.e., retardation). Because of low fluid velocities and the assumption of steady-state flow conditions (see Section 5.6), it is reasonable to assume that adsorption of dissolved radionuclides onto the alluvium is an equilibrium process. Low radionuclide concentrations (see Section 5.10) make it reasonable to assume that the adsorption isotherm is linear (i.e., the amount of a given radionuclide adsorbed equals a constant multiplied by the radionuclide's liquid phase concentration). Assuming that adsorption is in equilibrium and that the adsorption isotherm is linear results in the following expression for retardation

$$R_i = 1 + \frac{\rho K_{d,i}}{\theta} \qquad (5\text{-}23)$$

where

R_i = retardation of radionuclide *i* (dimensionless),
ρ = bulk density of alluvium (kg/m^3),

$K_{d,i}$ = sorption coefficient for radionuclide *i* (m^3/kg)
θ = volumetric moisture content (dimensionless)

Values of bulk density and volumetric moisture content are given in Sections 5.5.3.3 and 5.6.2.3, respectively. Sorption coefficients are element-specific, not radionuclide-specific. The coefficients used in the PA were derived from experiments conducted on devitrified tuff, the rock that eroded to form the alluvium surrounding and backfilling the GCD boreholes [OCRWM, 1998; Stockman, 1992] and are given in Table 5-25. The sorption coefficients are uncertain variables, as shown in Table 5-25. The resulting values of retardation are used in the transport model as described in Section 7.3.4.

Table 5-25. Values of Sorption Coefficients

Element	Shape of pdf	Lower Endpoint (m^3/kg)	Upper Endpoint (m^3/kg)	Shape Factors for Beta Distribution	
				(α)	(β)
Pu	beta	2×10^{-2}	2×10^{-1}	8.45	10.6
U	beta	0	4×10^{-3}	5.06	5.06
Am	uniform	1×10^{-1}	2		
Np	beta	0	6×10^{-3}	9.09	45.5
Ra	uniform	1×10^{-1}	5×10^{-1}		
Th	uniform	1×10^{-1}	2		
Pa	uniform	0	1×10^{-1}		
Pb	uniform	1×10^{-1}	5×10^{-1}		
Ac	uniform	1×10^{-1}	2		

5.12.2 Vapor Phase Transport

The isotopes of radon are the only radionuclides released from the TRU waste disposed of in the GCD boreholes that are transported in the vapor phase. Radon exists as a gas under ambient conditions; it is one of the noble gases; and its daughter products can produce a significant dose to the lung if it is inhaled, which is relevant to the dose calculations for the IPRs. Radon is not of concern with respect to the CR. Three isotopes of radon are produced by the TRU waste: ^{219}Rn ($t_{1/2}$ = 3.96 sec), ^{220}Rn ($t_{1/2}$ = 55.6 sec), and ^{222}Rn ($t_{1/2}$ = 3.8 days). Because of their short half-lives, ^{219}Rn and ^{220}Rn will decay before they can be transported in the gas phase from below the ground surface to above the ground surface; thus, they are not of concern in modeling gas phase transport. ^{222}Rn is the only radon isotope whose vapor phase transport is modeled in the PA.

The source of ^{222}Rn is its parent radionuclide, ^{226}Ra, which is a daughter product of ^{242}Pu, ^{238}Pu, ^{238}U, and ^{234}U, all radionuclides that were originally emplaced in the bottom 15.2 m (50 ft) of the boreholes. As the simulation progresses, radium is produced by radioactive decay and is transported upward in the liquid phase (as discussed above). This upward movement of radium is accounted for in modeling the upward vapor-phase movement of radon.

It is assumed that radon is transported upwards by diffusion only. This assumption is reasonable, given the depth of burial, the nature of advective gas-phase flow in the unsaturated zone, and the time scale of interest. Advective transport is driven by thermal and pressure gradients. The *temperature difference* from disposal depth to the ground surface is approximately 2.5EC (36.5EF), not great enough to induce advection [Price et al., 1993a,b,c]. The *pressure* gradient is dominated by barometric effect effects in the shallow subsurface. Barometric pressure fluctuations result in cyclical flow into and out of the soil such that over the time scale of interest (i.e., 1,000 years), changes in the net flux as a result of barometric pumping will be negligible. This conclusion is consistent with those of Nazaroff [1992] and Peterson et al. [1987]. Because advective transport is not likely to contribute to radon migration, diffusion is assumed to be the primary transport mechanism.

It is further assumed that radon does not dissolve in the liquid phase. This assumption simplifies the radon transport calculations, and is conservative because dissolution into the pore water would serve only to decrease the flux of radon past the ground surface.

The mass balance equation for radon in the alluvium above the waste is thus given by

$$\frac{\partial m_{Rn}}{\partial t} = D_{Rn}\frac{\partial^2 C_{Rn}}{\partial x^2} - \lambda_{Rn} m_{Rn} + \lambda_{Ra} m_{Ra} \qquad (5\text{-}24)$$

where

m_{Rn} = mass of radon is a given volume of alluvium (moles/m^3),
D_{Rn} = effective diffusion coefficient for radon in alluvium (m^2/yr),
C_{Rn} = mass of radon in the air-filled porosity of the alluvium (moles/m^3),
λ_{Rn} = decay constant for radon = ln 2/radon half-life (1/yr),
λ_{Ra} = decay constant for radium = ln 2/radium half-life (1/yr), and
m_{Ra} = mass of radium in a given volume of alluvium (moles/m^3 alluvium).

The effective diffusion coefficient is assumed to equal 113.6 m^2/yr (1222 ft^2/yr) based on measurements taken at the NTS [Tanner, 1980]. The decay constants for radium and radon are calculated from their half-lives given in Appendix J, while the mass of radium in a given volume of alluvium is calculated by application of the liquid phase transport model.

There are two sources of radon in the air that is of concern for the IPRs: 1) radon resulting from the decay of radium that has been transported to the ground surface via advection, diffusion, and bioturbation, and 2) radon that has diffused upward from the waste to the ground surface. The concentration of radon in air resulting from radium that has already been deposited on the ground surface is given by

$$C_{radium,a} = g\,\rho\,C_{Ra,g}\frac{A_{Ra}}{A_{Rn}}\sqrt{\lambda_{Rn} D_{Rn}}\tanh\left(d_{grd}\sqrt{\frac{\lambda_{Rn}}{D_{Rn}}}\right)\frac{1-e^{\left(-\frac{r_{grd}\lambda_{Rn}}{U}\right)}}{\lambda_{Rn} H} \qquad (5\text{-}25)$$

where

$C_{radium,a}$ = concentration of radon in the air resulting from radium on the ground surface (moles/m^3)

g = radon emanation coefficient (.),
$C_{Ra,g}$ = concentration of radium in the soil (moles/kg),
A_{Ra} = specific activity of radium (Ci/mole),
A_{Rn} = specific activity of radon (Ci/mole),
d_{grd} = depth of surficial radium contamination (m),
r_{grd} = radius of surficial radium contamination (m),
U = wind speed (m/yr), and
H = height into which plume is uniformly mixed (m).

The radon emanation coefficient is the fraction of radon that is released from the soil matrix (which contains decaying radium) into the air-filled pore space. The radon emanation coefficient is assumed to equal 0.35 as given by the NRC [1989]. The concentration of radium in the soil is calculated by the liquid phase transport model, while the specific activities of radium and radon are given in Appendix O. The depth of surficial radium contamination is assumed to equal 0.15 m (0.5 ft), a typical garden depth. The area of the surficial radium contamination is equal to the area of the garden, which is 70 m^2 (750 ft^2). The wind speed is an uncertain parameter with a pdf estimated from wind data collected at weather station Well 5B. This pdf is given in Table 5-26. The height into which the radon plume is uniformly mixed is 2 m (7 ft), a standard assumption for dose calculations [Yu et al., 1993].

Table 5-26. Wind Speed PDF

Wind Speed (m/yr)	Cumulative Probability
0	0
4.7×10^7	0.37
1.3×10^8	0.62
2.1×10^8	0.82
2.8×10^8	0.92
4.1×10^8	1.0

The concentration of radon in the air directly above the virtual GCD borehole due to upward diffusion through the alluvium is given by:

$$C_{diff,a} = \frac{q_{Rn}^F}{\lambda_{Rn} H}\left(1 - e^{\frac{-X\lambda_{Rn}}{2U}}\right) \qquad (5\text{-}26)$$

where
$C_{diff,a}$ = concentration of radon in the air resulting from diffusion of radon upward through the alluvium (moles/m^3),
q_{Rn}^F = flux of radon diffusing up from the ground into the air (moles/m^2 yr), and
X = diameter of virtual borehole (m).

The flux of radon diffusing up from the ground into the air is calculated by the vapor phase diffusion model, while the diameter of the virtual borehole is 6.7 m (22 ft).

The radon concentrations in air as calculated by the two above equations are summed to obtain the total radon concentration in the air, as described in Section 7.5.3.2.

5.13 Conclusions

Describing the disposal system includes characterizing the site in terms of its location, topography, climate, geology, hydrology, plant biology, and animal burrowing behavior; and characterizing the waste in terms of quantities of specific radionuclides disposed of, identification of their progeny, and estimation of their solubilities. Models of radionuclide release from the waste, radionuclide transport through the alluvium, radionuclide uptake by plants, and radionuclide release to the ground surface were developed based on this description of the disposal system.

Developing a quantitative assessment of radionuclide release or doses resulting from releases involves collecting data about radionuclide transport, developing a conceptual model of radionuclide movement, developing a numerical model based on the conceptual model, and selecting numerical values of input parameters needed for the numerical model. Various assumptions must be made during this process, and these assumptions need to be defensible. The end result of this process are models of the disposal system that can be used to assess compliance with the quantitative requirements of 40 CFR 191. Table 5-27 summarizes what we know about the disposal system, how that knowledge was translated into models, and a brief justification for the modeling assumption.

Table 5-27. Summary of Conceptual Model for Current Conditions

Actual and Expected Conditions	Modeled Conditions	Justification
Alluvial fill is composed of alternative sequences of poorly sorted, weakly stratified, gravelly sand.	Alluvial fill is hydrologically homogeneous.	Realistic; on the scale of the disposal system (21 m [70 ft] to surface), alluvium is hydrologically homogeneous (Section 5.5.3.2).
Dry bulk density of alluvium varies spatially.	Dry bulk density of alluvium is an uncertain variable; the value for each simulation represents an effective value for the modeled region.	Reasonable; variability in bulk density accounted for by using a pdf to describe possible values of bulk density (Section 5.5.3.2).
Moisture content in alluvium varies spatially.	Moisture content in alluvium is an uncertain variable; the value for each simulation represents an effective value for the modeled region.	Reasonable; variability in moisture content accounted for by using a pdf to describe possible values of moisture content (Section 5.6.2).
Pore water in the upper 2 m (7 ft) is continuously removed by plant uptake and evaporation.	Upward advection, diffusion, and dispersion in the liquid phase cease at a depth of 2 m (7ft).	Realistic; pore water removed by evaporation and plant uptake is not available for liquid-phase transport (Section 5.6.2).

Table 5-27. Summary of Conceptual Model for Current Conditions (Continued)

Actual and Expected Conditions	Modeled Conditions	Justification
Pore water between 2 and 35 m (7 and 115 ft) is moving upward slowly as a result of an upward head gradient.	Pore water between 2 and 35 m (7 and 115 ft) is moving upward one-dimensionally.	Reasonable; head gradients indicate upward flow, 1-D assumption provides shortest pathway to ground surface (Section 5.6.2).
Rate of upward specific discharge of pore water in alluvium is uncertain.	Rate of upward specific discharge of pore water in alluvium is uncertain.	Realistic; uncertainty in rate of upward specific discharge accounted for by using a pdf to describe possible values of upward specific discharge (Section 5.6.2).
Several different plant species currently exist at the Area 5 RWMS.	All plants are categorized into one of the three functional units: annuals, perennials, or shrubs.	Reasonable; species within each unit tend to operate similarly (Section 5.7.2.2).
Maximum root lengths are uncertain.	Maximum root lengths are uncertain.	Realistic; variability and uncertainty accounted for with a pdf for average value of maximum root length (Section 5.7.5).
Majority of extraction of soil resources by roots occurs in near-surface soil layers, which have the highest densities of roots.	Majority of extraction of soil resources by roots occurs in near-surface soil layers, which have the highest densities of roots.	Realistic; uncertainty and variability accounted for by using pdfs to describe distribution of roots with depth (Section 5.7.5).
Extraction with depth can be estimated with *root density* data.	Extraction with depth is estimated with *maximum root length* data.	Reasonable; maximum root length is a reasonable analogue for root density (Section 5.7.5).
Plant uptake of radionuclides is affected by climate, weather, growth conditions, plant metabolism, plant rooting traits, soil type, soil texture, soil moisture, and soil pH.	Plant uptake of radionuclides is a linear function of soil radionuclide concentration (i.e., can be described with a concentration ratio).	Simplifying assumption; resulting uncertainties accounted for by using pdfs to describe element-specific concentration ratios (Section 5.7.7).
The total amount of contaminated plant material produced annually (biomass productivity) may or may not be correlated with the amount of vegetation shed annually (litterfall).	Biomass productivity is an appropriate analogue for litterfall, and vice versa.	Reasonable; assumption supported by long-term averages of productivity and litterfall (Section 5.7.8).

Table 5-27. Summary of Conceptual Model for Current Conditions (Continued)

Actual and Expected Conditions	Modeled Conditions	Justification
The amount of biomass produced annually is uncertain.	The amount of biomass produced annually is uncertain.	Realistic; uncertainty and variability accounted for by using pdfs to describe possible values of biomass production (Section 5.7.8).
Many different animals burrow into desert soils.	All animals are categorized into one of four guilds: mammals, invertebrates, reptiles, and birds.	Reasonable; animals within a particular guild have similar burrowing habits (Section 5.8.1).
The abundance of burrowing mammals is directly related to plant productivity.	The density of burrowing mammals at the NTS, a marginal habitat, can be modeled with data from more favorable habitats.	Conservative; also, there will likely be periods with conditions conducive to rodent population booms (Section 5.8.2).
Reptiles do not create burrow systems.	Reptile burrowing is not modeled separately.	Realistic; reptiles are observed inhabitating abandoned burrow systems (Section 5.8.2).
The only bird known to burrow at the NTS inhabits abandoned burrows.	Burrowing by birds is not modeled separately.	Realistic; birds do not create burrow systems (Section 5.8.2).
The inventory of radionuclides in the TRU waste is uncertain.	The inventory of radionuclides in the TRU waste is uncertain.	Realistic; uncertainty in inventory described by pdfs (Section 5.9.3).
TRU waste is disposed of in four separate boreholes.	TRU waste is contained in a single "virtual" borehole with effective cross-sectional area equal to the sum of the cross-sectional areas of the four individual boreholes. (Boreholes were modeled separately for criticality analyses)	Reasonable; given the one-dimensional nature of the flow and transport model (Section 5.9.3.4).
The bottom 15 m (50 ft) of three of the four boreholes is backfilled with probertite, a borate mineral, to preclude criticality.	The "virtual" borehole is backfilled with a material that has properties identical to alluvium.	Reasonable; should not affect solubility or mobility of radio-nuclides. This is a necessary assumption, as required data are not available for probertite (Section 5.9.3.4).
TRU waste is contained in discrete containers.	Radionuclides are evenly dispersed throughout the waste zone.	Simplifying and conservative assumption (Section 5.9.3.4).

Table 5-27. Summary of Conceptual Model for Current Conditions (Continued)

Actual and Expected Conditions	Modeled Conditions	Justification
The section of the borehole from the top of the waste to the ground surface (i.e., the top 21 m [70 ft]) is filled with native alluvium that was sifted to remove large pieces.	The alluvium in the top 21 m [70 ft] of the borehole has physical, hydrologic, and geochemical properties identical to the surrounding undisturbed soils.	Reasonable assumption; supported by data (Section 5.9.3.4).
Water, which controls radionuclide release from the waste disposal zone to the undisturbed alluvium, may not be immediately available for radionuclide transport because it will be consumed by the chemical reactions that corrode the waste packages and because of the delay in reestablishing ambient pore water in and near the boreholes.	An adequate amount of pore water is available to dissolve and transport waste at all times. This implies that pore-water radionuclide concentrations in the source equal radionuclide solubilities.	Conservative (Section 5.9.4.2).
Two geochemical environments exist: the waste disposal region and the native alluvium.	The geochemical effects of the waste disposal region are not modeled.	Simplifying and conservative assumption (Section 5.10.1).
Oxidizing conditions exist in the alluvium.	Oxidizing conditions exist in the alluvium and in the waste region.	Conservative assumption (Section 5.10.2).
Radionuclide solubility is a complicated function of many variables.	Radionuclide solubility is based on the observed pH range and the credible radionuclide-bearing mineral phases for that pH range.	Reasonable; uncertainty in which mineral phase will exist is accounted for by using pdfs to describe possible values of solubility (Section 5.10.3).
Radionuclides initially disposed of will decay, producing radioactive decay chains.	Radioactive decay and production are explicitly modeled.	Realistic (Section 5.12).
All radionuclides (except isotopes of radon) are solids and are transported in the liquid phase as dissolved solids.	The liquid-phase transport of all radionuclides with half-lives greater than 20 years is modeled.	Reasonable (Sections 5.12 and 5.9).
Radionuclides dissolved in pore water could potentially be transported in any direction.	Radionuclides dissolved in pore water will move upward as a result of advection, diffusion, and dispersion; and will move laterally as a result of diffusion.	Simplifying; uncertainty in the rates of these transport processes is accounted for by using pdfs (Section 5.6 and 5.12).

Table 5-27. Summary of Conceptual Model for Current Conditions (Continued)

Actual and Expected Conditions	Modeled Conditions	Justification
The chemical interaction between radionuclides dissolved in pore water and alluvium (i.e, adsorption) is a complicated function of many variables.	Adsorption is proportional to radionuclide pore water concentrations and is an equilibrium process at all times (i.e., adsorption can be described with a K_d).	Simplifying assumption; uncertainty in K_d values is accounted for by using pdfs (Section 5.12.1.3).
The three isotopes of radon produced by the TRU waste are gases under ambient conditions and can be transported in the vapor phase.	^{222}Rn is the only radon isotope whose vapor phase transport is modeled in the PA.	Reasonable; it is the only radon isotope with a long enough half-life for vapor phase transport (Section 5.12.2).

6.0 FUTURE EVOLUTION OF THE DISPOSAL SYSTEM

6.1 Introduction

The Area 5 RWMS, as it exists today, was described in Section 5.0. This section presents, and defends, a conceptual model of how the RWMS may change over the next 10,000 years. The forcing agents for the changes are:

- operation and closure of the Area 5 RWMS has "disturbed" the site conditions;
- future human activities could inadvertently alter site conditions; and
- natural processes, which operate on long time scales, may alter site conditions.

The nature of these forcing agents and their potential effects on the movement of radionuclides in the GCD boreholes are described in the following sections. It is recognized that there is no absolute boundary between "current conditions" (Section 5.0) and "future conditions" in this section. For example, the current climate is part of a climate change continuum, which is expressed over long timeframes. The boundary between what is presented in Section 5.0 and what is presented in this Section was made to facilitate the presentation of information.

Section 6.2 describes the near-term future of the RWMS. The near-term future includes continued operations, closure, and a period of AIC following closure.

How the Area 5 RWMS may evolve after the AICs cease is the subject of Sections 6.3 through 6.8. A methodology for addressing uncertainty in the overall PA is described in Sections 1.4 and 3.0. A scenario screening methodology for identifying all significant processes and events that could affect the disposal system was developed by Cranwell et al. [1990] and its implementation is described in Section 6.3. Beginning with an all-inclusive list of potential events and processes, the scenario screening methodology was used to narrow the list of concerns to four events and processes: IHI (drilling an exploratory well through a GCD borehole), irrigated agriculture over the Area 5 RWMS, climate change, and landfill subsidence. The screening process is summarized in Section 6.3 and future human activities are addressed in Section 6.7.

The potential for the climate to change over the next 10,000 years is addressed in Section 6.4. Section 6.4 overviews a prior study that examined numerous long-term records of past climate change and focused on the potential effects of future climate change on processes important to the movement of GCD TRU wastes. A return to "glacial" climatic conditions which existed at the Area 5 RWMS about 10,000 years ago could lead to deeper infiltration of surface water and significant changes in the plant community.

How the plant community at the Area 5 RWMS might evolve, in response to cooler and wetter "glacial conditions," is presented in Section 6.5. A piñon-juniper open woodland probably existed at the Area 5 RWMS as recently as 10,000 years ago, and if future climate change is similar to past climate changes, a piñon-juniper woodland plant community could return to the Area 5 RWMS. This change is significant in that the woodland species have greater rooting depths than the current shrubland species, and the annual biomass turnover rates are also greater for the woodland species.

Operation of the Area 5 RWMS has placed wastes in GCD boreholes and in pits and trenches, and these wastes contain a significant amount of void space. Over time, as the waste containers decay and lose their structural integrity, these voids will be expressed as landfill subsidence. The subsidence features, in turn, could capture and focus precipitation, sheet-flow, and possibly flood waters from arroyos. The focusing of surface water by subsidence features could cause the downward movement of surface water, and also lead to the localized return of a piñon-juniper woodland plant community.

As an extreme analogue, subsidence craters from the underground testing of nuclear weapons currently focus precipitation and cause deep infiltration of surface water and a change in the plant community (e.g., "ephemeral wetlands"). The results of a "Screening Analysis of the Potential to Contaminate Groundwater Beneath the GCD Boreholes Based on the Combined Effects of Subsidence, Precipitation, Flooding, and Climate Change" is presented as Appendix B and is summarized in Section 6.6.

Section 6.8 summarizes the information presented in Section 6 and also summarizes how the PA will be conducted to account for the future evolution of the Area 5 RWMS.

6.2 Area 5 Radioactive Waste Management Site Operations and Closure

At the Area 5 RWMS, pits and trenches have been used since 1961 for the disposal of LLW and, in 1987, for disposal of TRU waste. High-specific-activity LLW and TRU wastes were also disposed in the GCD boreholes from 1984 though 1989.

DOE/NV is responsible for the future closure and monitoring of the Area 5 RWMS. DOE plans to operate the Area 5 RWMS until the year 2070. Current pits, trenches, and GCD boreholes will be capped in the next few years, and disposal operations will continue within the RWMS directly north of the current disposal operations.

An important issue related to closure is the future subsidence of the disposal cells; DOE [1998] describes the situation.

> Review of waste disposal operations indicated that the waste already placed in the RWMS contains a *significant amount of void space* resulting from incomplete filling of waste containers, limited internal compaction of contents, and voids between containers. These voids *will produce significant subsidence* as the waste containers deteriorate and collapse over time. Additional sources of subsidence include the decomposition of containers, waste, and dunnage. ... over long time periods, the waste and containers would collapse, decompose, and ultimately reach a density similar to that of the surrounding soil materials. (emphasis added)

DOE [1998] recommends the construction of an alternative cap that would consist of a single thick layer of compacted native alluvium, constructed to 2 m (7 ft) above the land surface to accommodate this subsidence. The intent of this design is to simulate the natural system at the NTS, with particular emphasis on (1) limiting infiltration by enhancing evapotranspiration and

(2) using soil materials which have suitable durability and longevity. This PA assumes that this cap of native alluvium will be built to 2 m (7 ft) above the existing landscape.

After operations cease in 2070, DOE would then assume AIC over the closed RWMS. The EPA's standard for disposal of TRU wastes does not allow an analysis to take credit for more than 100 years of AIC (40 CFR 191.14). Through DOE may, in reality, maintain AIC for more than 100 years after closure, the PA only takes credit for 100 years of AIC.

Based on forthcoming DOE guidance, this PA assumes disposal operations will continue until the year 2070, and then, through AICs, the landfill cap will be maintained for 100 more years. Therefore, the RWMS will be under direct DOE control and maintenance for 170 years, and AIC will be lost in the year 2170. How the RWMS may evolve after loss of AICs is the subject of the next section.

6.3 Scenario Analysis for Naturally-Occurring Events

Section 3.0 of this CAD provides a comprehensive summary of the PA process; the treatment of uncertainty while conducting an iterative, probabilistic PA; and the regulatory environment within which the PA for the TRU wastes contained in the GCD boreholes is being completed. Figure 3-1 of Section 3.0 introduced the PA process. Step 1, Define Performance Objectives, was developed in Section 2.0 of the CAD. Step 2, Assimilate Existing Site Information, was documented in Section 5.0 (additional discussion of the existing state of knowledge regarding the site during the early phases of the PA is also provided in other portions of the CAD). This section addresses Step 3, Scenario Development and Screening and the treatment and reduction of uncertainty about the occurrence of future events.

This section of the CAD identifies those significant events, processes, and scenarios that could alter disposal system performance. The ultimate objective is to develop a manageable set of scenarios in order to assess compliance of the GCD disposal system for TRU wastes against the CRs of 40 CFR 191 [EPA, 1985]. For those scenarios that describe a plausible future state of the disposal system, an estimate of probability of occurrence is determined for the combination of events and processes represented by the scenario. The probabilities of all scenarios, including the probability applicable to the "base case," are used to develop the final output distribution (the CCDF). See Sections 2.0 and 3.0 for more detailed discussions of the process and mechanics involved in propagating the results of scenario analysis through the PA analysis.

This scenario analysis is limited to those disruptive events and processes that may have a negative impact on the capability of GCD boreholes to contain and isolate TRU wastes for the next 10,000 years. These events and processes may be naturally-occurring (such as climate change or earthquakes), disposal system-induced (subsidence), or human-induced (such as mining or drilling for natural resources). A comprehensive scenario development and screening process was used for everything except direct human intrusion. EPA guidance associated with 40 CFR 191 was then used for the inadvertent human intrusion. Scenario development included assessment of both the potential for actually intruding into the wastes by inadvertent human intrusion (exploratory drilling), as well as the likelihood of occurrence for surface activities and

events (irrigation) that might alter the disposal system without physically disturbing the wastes. Section 6.3.2 provides details for application of this process.

In addition, this section presents the results of a site-specific expert elicitation [Black et al., 1998] on the potential for inadvertent human intrusion into the NTS RWMSs. The original process and results of the expert elicitation were reapplied to the GCD TRU disposal concept to develop probabilities of occurrence for those events and to defend site-specific application of the EPA Guidance. This approach relies on the EPA Guidance supported by the results of the expert elicitation. Section 6.7.3 provides a general discussion of the expert elicitation process and its applicability to the GCD TRU boreholes. In Section 6.7.4, the general process and results from the expert elicitation are used to support the analysis of human intrusion based on the EPA Guidance discussed in Section 6.7.1.

6.3.1 Regulatory Basis

A comprehensive discussion of the regulatory basis for the scope of the GCD system PA is provided in Section 2.0. This subsection outlines and summarizes the aspects of that regulatory basis pertinent to assessing compliance with the CRs and for scenario development and analysis.

6.3.1.1 Requirements From the Environmental Protection Agency Standard

The CRs from 40 CFR 191.13 set limits on the probability that specified levels of cumulative releases of radionuclides from the controlled area can reach the accessible environment during the 10,000 years following closure of the disposal system. When complied with, the CRs establish protection for the general population. As stated in the EPA Standard:

> (a) Disposal systems for spent nuclear fuel or high-level or transuranic radioactive wastes shall be designed to provide a *reasonable expectation*, based on *performance assessments*, that the cumulative releases of radionuclides to the accessible environment for 10,000 years after disposal from *all significant processes and events that may affect the disposal system* shall [meet certain criteria, as noted in Section 2.0 of this CAD] (emphasis added)

From the Preamble discussion for 40 CFR 191 [EPA, 1985; p. 38071], the EPA stated that the phrase “reasonable expectation”:

> reflects the fact that unequivocal numerical proof of compliance is neither necessary nor likely to be obtained.

EPA defined “performance assessment” in § 191.12(q) as:

> an analysis that: (1) *Identifies the processes and events that might affect the disposal system*; (2) examines the effects of these processes and events on the performance of the disposal system; and (3) estimates the *cumulative releases* of radionuclides, considering the associated uncertainties, *caused by all significant processes and events.* These

estimates shall be incorporated into an overall probability distribution of cumulative release to the extent practicable. (emphasis added)

Concepts Used in Scenario Analysis

- base case: processes and events expected to occur
- disruptive scenarios: processes and events not part of the base case; these include IHI and unlikely natural events
- all significant processes and events: base case plus human intrusion and unlikely natural events; considered for the CRs
- undisturbed performance: base case alone, not including human intrusion and unlikely natural events; considered for IPRs and GWPRs

The EPA Standard is clear on the need to include "all significant processes and events" in the PA analysis. However, the EPA Standard provides no definition for this term nor guidance on how to identify significant processes and events for inclusion in PAs. To develop an overall probability distribution of cumulative radionuclide release, probability estimates are required for the occurrence of all significant processes and events, and, by implication, all combinations of these processes and events. In LLW PAs, human exposure scenarios are used to describe a set of circumstances leading to a dose to humans. In contrast, in TRU PAs, combinations of processes and events define possible future states of the disposal system and are generally referred to as "scenarios" (the term scenario is used once in the EPA Standard, in Appendix B of Subpart B, but it is not defined). These scenarios are used to develop the final CCDF of cumulative release to the accessible environment. The analysis in this section provides an assessment of combinations of all significant processes and events for assessment against the CR.

As already noted in this CAD and in the sidebar, the Individual Protection Requirements of § 191.15 and the Groundwater Protection Requirements of § 191.16 are concerned with "undisturbed performance of the disposal system." In § 191.12 (p), "undisturbed performance" means:

> the predicted behavior of a disposal system, including consideration of the uncertainties in predicted behavior, if the disposal system is *not disrupted by human intrusion or the occurrence of unlikely natural events*. (emphasis added)

The IPRs in 40 CFR 191 specifically exclude direct human intrusion from the analysis; therefore, there is no dose-based standard for the human intruder. The CRs require consideration of IHI as a cause of release of contaminants, but the CRs are not dose-based. Therefore, potential doses to an intruder are not calculated in a 40 CFR 191 PA.

6.3.1.2 Rationale Behind the Criteria Established by Environmental Protection Agency for the Containment Requirements

In the Preamble to the 1985 version of the final rule established in 40 CFR 191 [EPA, 1985; p. 38071], it is noted that:

> The containment requirements apply to accidental disruptions of a disposal system as well as to any expected releases. Accordingly, they are stated in terms of the probability of releases occurring. This is done in two steps.

The first step includes those releases that may be exceeded with a likelihood of greater than 0.1:

> the total releases from those processes that are expected to occur [i.e., the base case] as well as relatively likely disruptions (which the Agency assumes will primarily include predictions of inadvertent human intrusion).

The second step includes those releases that may be exceeded with a likelihood of greater than 0.001:

> releases that might occur from the more likely natural disruptive events, such as fault movement and breccia pipe formation (near soluble media such as salt formations). This range of probabilities was selected to include the anticipated uncertainties in predicting the likelihood of these natural phenomena. Greater releases are allowed for these circumstances because they are so unlikely to occur.

Finally, it is also noted that:

> the containment requirements place no limits on releases projected to occur with a cumulative probability of less than 0.001 over 10,000 years. Probabilities this small would tend to be limited to phenomena such as the appearance of new volcanoes outside of known areas of volcanic activity, and the Agency believes there is no benefit to public health or the environment from trying to regulate the consequences of such very unlikely events.

Though no specific guidance is provided on the identification of scenarios and quantification of the probabilities associated with disruptive events and human intrusion, the EPA does offer some basis for determining, through both qualitative and quantitative processes, those events that are reasonable for consideration in scenario development.

6.3.1.3 Environmental Protection Agency Guidance for Screening Processes and Events

Appendix B of the EPA Standard is “Guidance for Implementation of Subpart B,” herein referred to as the EPA Guidance. This Guidance “describes the Agency’s assumptions regarding the implementation of Subpart B” and how the Agency intends the various numerical standards to be applied. EPA felt the guidance was particularly important “...because there are no precedents for the implementation of such long-term environmental standards, which will require consideration of extensive analytical projections of disposal system performance.” [EPA, 1985; p. 38069]. Appendix B discusses (1) consideration of all barriers in PAs, (2) reasonable limitations on the scope of PAs, (3) the use of average or “mean” values in expressing results, (4) assumptions regarding institutional controls, and (5) “...limiting assumptions regarding the frequency and severity of inadvertent human intrusion into geologic repositories.”

The EPA felt it was important for implementing agencies to develop assumptions compatible with those used in developing the rule. Otherwise, it was felt that implementation under different assumptions "...may have effects quite different than those anticipated by EPA." [EPA; 1985, p. 38074] EPA felt that addition of the Guidance "...should discourage overly restrictive or inappropriate implementation of the containment requirements." [EPA, 1985; p. 38077] Therefore, EPA recommended that the Guidance "...be carefully considered in the planning for the application of 40 CFR Part 191."

EPA recognized the significant uncertainties involved with projections into the future. Therefore, this guidance was offered as a means to constrain the problem. While there is flexibility to deviate from the Guidance, that deviation requires adequate defense, backed with supporting information and data.

The EPA Guidance includes an indication of what constitutes a "significant" event by giving a lower limit for probability of occurrence in the future:

> The Agency assumes that such performance assessments need not consider categories of events or processes that are estimated to have less than one chance in 10,000 of occurring over 10,000 years.

This criterion for *likelihood of occurrence* provides a probability cutoff (i.e., less than a probability of 1×10^{-4} over the 10,000-year time frame) for removal of some processes and events from consideration.

The EPA Guidance also suggests a criterion for screening processes and events based on *consequence,* by limiting consideration of other more likely processes and events:

> Furthermore, the performance assessments need not evaluate in detail the releases from all events and processes estimated to have a greater likelihood of occurrence. Some of these events and processes may be omitted from the performance assessments if there is a reasonable expectation that the remaining probability distribution of cumulative releases would not be significantly changed by such omissions.

Some events and processes may occur, but their impact on the disposal system may be inconsequential and have no significant effect on the calculation of overall release of radionuclides from all processes. Other events and processes may have significant impacts that *improve* the performance of the disposal system. Subsidence was screened from consideration in the PA for this reason (see Section 6.6).

6.3.2 Scenario Development and Screening Using Environmental Protection Agency Guidance

A comprehensive set of scenarios is required to assure that no significant potential contributors to radionuclide releases are omitted from the PA. The scenarios should be mutually exclusive so that radionuclide releases and probabilities of occurrence can be unambiguously associated with specific scenarios. With radionuclide releases and probabilities of occurrence corresponding to

unique scenarios, a CCDF can be constructed for all of the scenarios for comparison to the performance measures in the CRs.

A PA methodology previously developed at SNL [Campbell et al., 1978; Cranwell et al., 1987; Davis et al., 1990] formed the general framework for this analysis of the GCD TRU boreholes. In addition, application of a comprehensive scenario development procedure [Cranwell et al., 1990] to identify possible future states of the disposal system identified a comprehensive set of mutually exclusive scenarios amenable to both consequence analysis and probability estimation. This section documents the implementation of that procedure to the GCD boreholes.

6.3.2.1 General Scenario Development and Screening Process

Cranwell et al. [1990] defined scenarios as sets of naturally occurring, human-induced, and waste- and repository-induced events and processes that represent realistic future changes to the disposal, geologic, and hydrologic systems. These changes, in turn, may affect the release and transport of radionuclides from the disposal facility to the accessible environment. *Because of the large number of possible scenarios, the goal of the scenario development procedure is to identify only those scenarios that may have adverse effects on overall disposal system performance.* Scenarios that would improve performance are not identified. The procedure to identify scenarios defined in this way consists of the following five steps. Guzowski and Newman [1993] and Guzowski [1996] provide a more complete summary of this general process used for scenario development and screening.

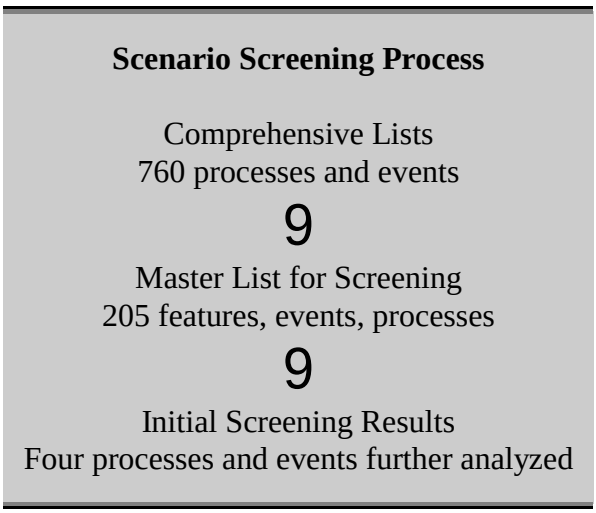

Step 1: Compilation of a comprehensive list of events and processes that could affect the performance of the disposal system. The first step in the procedure identifies those events and processes that may affect the performance of the disposal system so that these events and processes can be combined to form scenarios. Application of Step 1 began with comprehensive lists of over 760 processes and events and resulted in identifying a master list of 205 features, events, and processes (FEPs) to begin the screening analysis [Guzowski and Newman, 1993]. The complete list of references used to develop the master list are provided in Appendix B of Guzowski and Newman [1993]. The complete master list of 205 FEPs was published as Appendix C of Guzowski and Newman [1993].

Step 2: Classification of the events and processes as an organizational tool and in addressing completeness arguments. Classifying the events and processes in the initial list was helpful for organizational purposes, to assist in addressing the issue of completeness (i.e., have any potentially important events and/or processes not been considered?), and

to provide some insights into what needs to be included when developing conceptual models of the disposal system. The first level of classification divided the events and processes into naturally-occurring, human-induced, or waste/disposal system-induced groups. Each of these groups was then further subdivided following the schemes used in the original sources of the lists. Some consolidation of the subdivisions was necessary because of duplication on different lists. The full list of FEPs in Appendix C of Guzowski and Newman [1993] was developed based on the classification scheme established in this step.

Step 3: Screening of the events and processes to identify those that can be eliminated based on specific criteria. Events and processes are screened based on specific criteria noted in Table 6-1 (and discussed in more detail in Guzowski and Newman [1993]). The original and primary screening criteria are consistent with the EPA Guidance for screening based on low probability or negligible consequence (see Section 6.3.1.3). The product of this step is a list of events and processes the combinations of which are assumed to define all possible future states of the disposal system. When developing scenarios, all possible combinations of all possible events and processes that could occur produces an unmanageably large number of scenarios. The number of scenarios is 2^n, where *n* is the number of events and processes. Those events and processes that are not applicable to the GCD disposal system or do not have the potential to significantly affect the integrated radionuclide releases to the accessible environment are eliminated from scenario development, reducing the number of scenarios to a number that can be reasonably addressed in PA analyses.

Table 6-1. Criteria for Screening Events and Processes

Original Screening Criteria in Cranwell et al. [1990]:

- Probability of occurrence
- Physical reasonableness
- Consequence

Implied Screening Criteria in Cranwell et al. [1990]:

- Regulatory restrictions for performance assessments include:
  - < post-closure conditions only
  - < inadvertent human intrusion (not advertent human intrusion)
  - < only events after 100 years of institutional controls
  - < limits on the severity of human intrusion events
  - < limits on the consequences associated with exploratory drilling (no cuttings)
  - < removal of surface transport and biological pathways-to-man
- Base-case condition

Additional Screening Criteria for GCD Analysis (*see Guzowski and Newman [1993] for discussion*)

Step 4: Development of comprehensive and mutually exclusive scenarios by combining the events and processes that remain after screening. The goal of this step is to construct scenarios from the events and processes that survive screening through use of logic

diagrams (these are explained and depicted in more detail in Guzowski and Newman [1993]). For scenario construction, it is assumed that the combinations of events and processes that survived screening define all possible future states of the disposal system. This assumption assures that the scenarios used in this construction are comprehensive so that the sum of the scenario probabilities (including the base case scenario) will be 1. The scenarios in this construction must also be mutually exclusive so that probability values can be unambiguously assigned to each scenario.

Step 5: Screening scenarios to identify those that have no bearing on compliance with the performance measure. Screening based on probability of occurrence or consequence can identify scenarios for which full-scale PAs can be omitted. As noted in Section 6.3.1.3, some scenarios, though likely to occur, may be omitted from the PA if their impact on cumulative releases is negligible (or positive, as is the case with subsidence). Scenarios with sufficiently low probability of occurrence will have no effect on the performance measure no matter how large the releases to the accessible environment caused by these scenarios. Also noted in Section 6.3.1.3, the EPA Guidance provided a lower limit to scenario probabilities for screening purposes, a limit of 1 chance in 10,000 in 10,000 years. This limit is directly applicable to individual events and processes and was proposed for application to scenarios as well by Cranwell et al. [1990] and Guzowski [1990].

6.3.2.2 Results of Screening for the Greater Confinement Disposal Transuranic Boreholes

Appendix D of Guzowski and Newman [1993] provided full documentation of the rationale used for screening, or retaining for further analysis or scenario development, the compiled list of 205 FEPs. The initial screening process identified four events and processes that were retained for scenario development, as listed in Table 6-2. The screening process also assigned many events and processes to the base case because these events and processes are likely to occur. For example, climate change, chemical reactions, advection and dispersion, bioturbation, plant uptake, and decay product gas generation were all assigned to the base case and, therefore, are part of the base case model.

Table 6-2. Events Remaining After Initial Screening

Human-Induced FEPs:
Postclosure Surface Activities
• Irrigated Agriculture Occurs at the RWMS
Postclosure Subsurface Activities
• Exploratory Drilling for Resources Penetrates a TRU Borehole
• Drilling of Withdrawal/Injection Well Penetrates a TRU Borehole
Waste- and Disposal System-Induced FEPs:
Mechanical FEPs
• Landfill Subsidence/Caving Occurs Within the RWMS

Both irrigated farming and landfill subsidence were retained for scenario development because each of these FEPs may increase the amount and depth of infiltration (with corresponding effects on, for example, soil moisture, plant evolution and rooting density/depths, and potentially enhanced plant uptake and/or bioturbation). The drilling events were retained because of potential releases in the drilling fluid and/or from pumping contaminated groundwater to the surface.

Following the initial screening process, project team discussions resulted in further screening and refinement of the list of events and processes needed for scenario development. The drilling of withdrawal wells was originally retained as a mechanism to transport contaminated water from the water table to the surface. From the standpoint of potential consequences, drilling a withdrawal well is the same as drilling an exploratory borehole for some other resource. Therefore, the *event of drilling a withdrawal well was merged into the event of exploratory drilling for resources*.

The potential for landfill subsidence was initially retained for scenario development due to uncertainty regarding the extent and timing of subsidence relative to the institutional control period. However, project discussions later assigned this event to the base-case scenario since it is very likely to occur. Subsidence from compaction of the backfill and shifting and collapse of waste packages will occur due to overburden pressure and container decay, with most of the compaction occurring within a few hundred years after closure [DOE, 1998]. Organic decay of wooden boxes and corrosion of metals requires moisture, a slow process in this dry environment that could take hundreds to thousands of years. As such, there is a high likelihood that significant subsidence will occur well after the end of the institutional control period (as discussed in Section 6.6, this was recently defined to be the first 170 years following waste emplacement based on the assumption that closure of the Area 5 RWMS is planned for the year 2070).

In summary, the comprehensive screening process of all significant processes and events resulted in:

- Eliminating all "unlikely natural events,"
- Retaining as part of the base case all likely natural events (subsidence, climate change), and
- Retaining for analysis the human-induced events "Exploratory Drilling Penetrates a TRU Borehole," and "Irrigated Agriculture Occurs at the RWMS."

Climate Change is discussed in Section 6.4, and changes in the plant community resulting from a change in climate are discussed in Section 6.5. Subsidence is analyzed in Section 6.6, while Section 6.7 examines the two human-induced events.

6.4 Climate

To assess the potential impact of climate change on GCD performance, a study was undertaken to define plausible future climate states at the Area 5 RWMS for the next 10,000 years and to quantify the effects of the projected climate change on the performance of the TRU wastes in the GCD boreholes [Brown et al., 1997a]. That study was divided into four sections: (1) how the Frenchman Flat area responded to past climate changes, (2) time series analysis of proxy climate change records, (3) anthropogenic effects on climate, and (4) conclusions.

Since the wastes in the GCD boreholes are at least 21 m (70 ft) below the land surface, transient effects will have negligible effects on the ability of the system to isolate wastes, and the study focused on longer-term climatic effects.

Numerous studies of various phenomena indicate that the climate oscillates between the current, warmer and drier interfuture climate, and a cooler and wetter future climate. The future climate (also called a pluvial climate) has been dominant over the past 500,000 years. Of the future climate periods, a few are especially cold and wet, termed "superpluvials."

6.4.1 How the Frenchman Flat Area Responded to Past Climate Changes

Site-specific and regional data were used to bound potential changes in the hydrologic, geomorphic, and biologic systems over the next 10,000 years. To evaluate how past climate changes affected the hydrologic system, concentrations of stable chlorine, chlorine-36, deuterium and oxygen-18, as well as carbon-14 dating were used by a number of prominent researchers (a) to estimate the rates of movement of soil water and (b) to reconstruct the water infiltration history at the Area 5 RWMS (Appendix A).

As a simplification, the climate was much wetter and cooler 120,000 years ago and the water table received area-distributed recharge. This time period is recognized in many studies as being especially wet and cool (a superpluvial). Subsequently, recharge significantly decreased, or ceased. Then, from 50,000 to 20,000 years ago, the climate was wetter and cooler again (a glacial or pluvial period), resulting in recharge to the water table under surface water drainage features. The climate change of 50,000 to 20,000 years ago caused deep infiltration, but was not significant enough in magnitude and duration to cause area-distributed recharge to the water table. The isotopic signature of this aborted recharge event can be seen in Figure 4 of Appendix A. Area-distributed precipitation has not reached the water table in the past 120,000 years.

A warmer and drier interglacial climate now exists, and the drying of the land surface is pulling moisture from depth, resulting in the very slow upward flux of pore water evidenced by the soil matric potentials. The Appendix A study provides direct evidence of how the pore water in the thick vadose zone at the Area 5 RWMS has responded to past climate changes.

Site characterization studies (trenching and mapping) were conducted to estimate the amount of erosion under past climate conditions at the Area 5 RWMS [Snyder et al., 1995]. Overall, Frenchman Flat is an aggrading basin. However, local erosion has resulted in shallow drainage features. The study concluded that the maximum erosion depth was approximately 1.5 m (5 ft), with most channels on the order of 0.8 m (2 ft) or less. It was concluded that if future climate conditions are no more severe than those encountered during the last future climate, the maximum depth of erosion will be less than 2 m (7 ft).

Finally, studies of pack rat middens allowed the reconstruction of the plant communities that existed during the last future climate at the NTS (e.g., Spaulding, 1990). Pack rat middens are pack rat nests which contain deposits of fossil plant remains (e.g., leaves, pine needles, and seeds) cemented by crystallized urine. Analysis of the middens provides information on past

climate conditions, because the plants available to the rats are indicative of existing conditions and because the plants and other organic matter can be dated by radiocarbon techniques.

Figure 6-1 plots the presence and absence of juniper trees against elevation and time. The record is very clear that juniper trees were common at the Area 5 RWMS elevation (1,000 m or 3,300 ft above mean sea level [msl]) from approximately 35,000 to 10,000 years ago. If future climate changes are similar to past climate changes, open juniper woodlands will return to the Frenchman Flat. A return to woodland species is significant in that these plants have deeper roots than the existing shrubland species, and they also have a greater biomass turnover rate than current species.

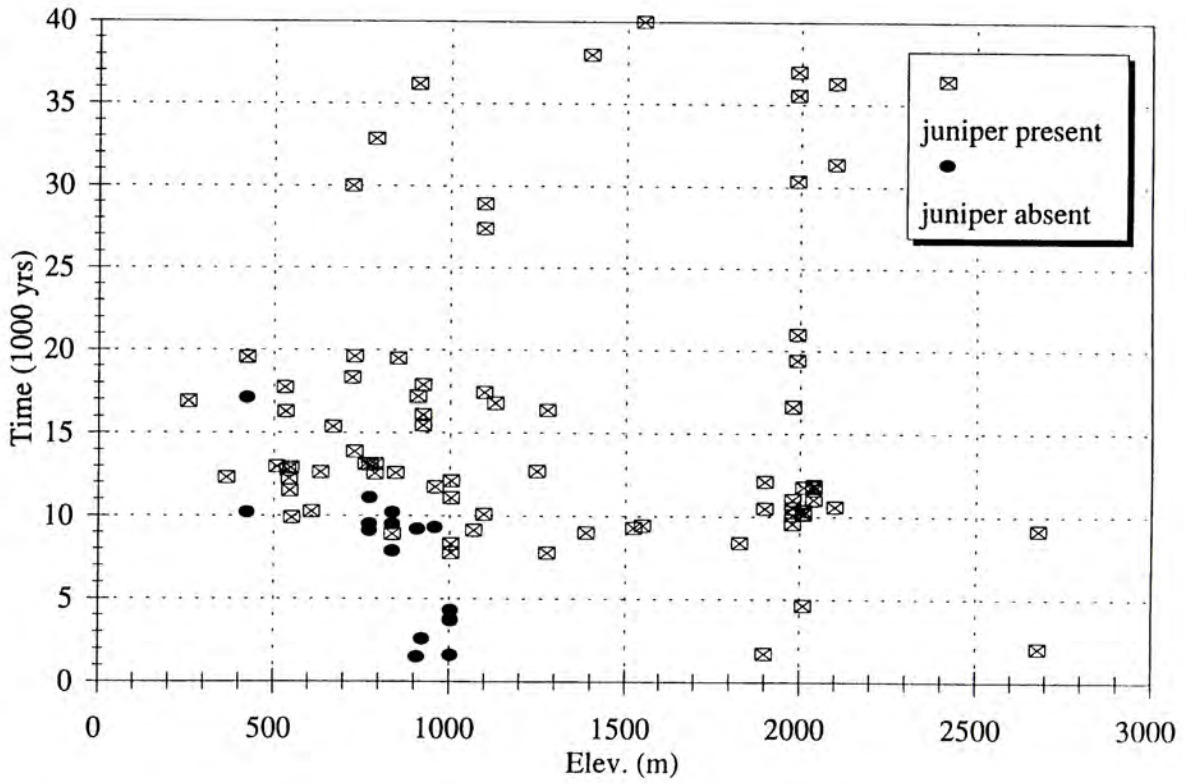

Figure 6-1. Midden Record of Juniper Presence and Absence as a Function of Time and Elevation [after Brown et al., 1997a].

6.4.2 Time Series Analysis of Proxy Climate Change Records

Brown et al. [1997a] also examined past global, regional, and site-specific empirical records of proxies of past climatic conditions. Because the ratios of stable isotopes of oxygen vary with climatic conditions, analysis of the isotopic ratios of oxygen, which are locked in media such as marine sediments and calcite spring deposits, provides a proxy, or substitute, for direct observation of past climates. Similarly, ice cores taken from the ice caps of Greenland and Antarctica provide high-resolution records of changes in the isotope values of precipitation caused by change in the earth's climate.

The records of the isotopic oxygen composition of marine sediments [Williams, 1988] and thick ice deposits provide *global* scale evidence of past climatic conditions. Studies of the isotopic composition of calcite deposits in Nevada's Devils Hole spring [Winograd et al., 1988; 1992] provide a 500,000-year *local* record of past climate conditions in the southwestern U.S.

All of the records showed a cyclic pattern of climate change in which the climate varies between relatively persistent future climates (cooler, wetter periods) separated by interglacial climates (warmer, drier periods) of relatively short duration. The ice core data, in addition to revealing the broader climate changes, also reveals rapid shifts between glacial and interglacial conditions (termed the "flickering switch") [Dansgaard et al., 1993]. It is not known whether these variations reflect global climate changes or whether they reflect changes in the regional climate of the Atlantic Ocean, an area thought to be particularly sensitive to changes in global circulation patterns.

There is very good agreement between the global ice core records, the local Devils Hole record, and the local pack rat midden records. Figure 6-2 plots several proxy records of past climate change.

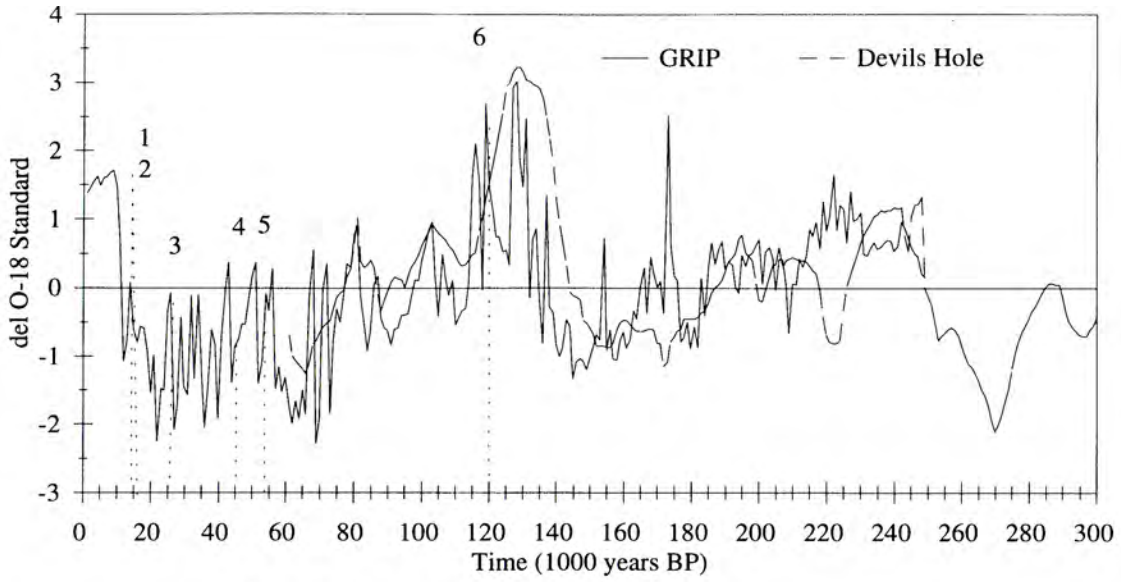

Figure 6-2. Time Series for Past Climatic Conditions in the Vicinity of the Area 5 RWMS: GRIP and Devils Hole Oxygen Isotope Data and Major Hydrologic and Biologic Events. [after Brown et al., 1997a]

At the Area 5 RWMS, cooler and wetter equates to 3EC to 5EC (5EF to 9EF) cooler, with a doubling of average annual precipitation, from 13 cm to 25 cm/yr (5 in. to 10 in./yr). A conceptualization of the Area 5 RWMS under current and glacial conditions is presented in Figure 1-11.

The cyclic nature of past climatic conditions is solidly supported by a large number of studies of many different physical phenomena. However, the low resolution of some of the proxy records and the natural variability in the length of the climatic cycles does not allow accurate estimation of the time when the climate will return to the more dominant, cooler, and wetter conditions. It was concluded that (a) it is not possible to rule out a return to cooler and wetter conditions over the next 10,000 years, and (b) there is significant uncertainty in the timing of the return to those conditions. For the PA, the key aspects of a return to a future climate are that additional precipitation and cooler temperatures could cause the deep infiltration of surface moisture, and that open piñon-juniper woodlands could return to Frenchman Flat.

6.4.3 Anthropogenic Effects on Climate

The accumulation of anthropogenically derived carbon dioxide (a greenhouse gas) in the Earth's atmosphere may alter near-term climatic conditions. The effects of anthropogenic climate change were assessed for the nearby Yucca Mountain facility using an expert elicitation and it was concluded that anthropogenic climate change will have a negligible impact at the NTS because the dominant rain shadow caused by the Sierra Nevada mountain range limits the number of storms capable of generating precipitation in the Great Basin [Dewispelare et al., 1993].

6.4.4 Conclusions

Analysis of proxy records for past climates showed a cyclic pattern of climate change in which the climate varies between relatively persistent future climates (cooler, wetter periods) separated by interglacial climates (warmer, drier periods) of relatively short duration. At the Area 5 RWMS, cooler and wetter equates to 3EC to 5EC (5EF to 9EF) cooler, with a doubling of average annual precipitation from 13 to 25 cm/yr (5 to 10 in./yr).

The cyclic nature of past climatic conditions is solidly supported by a large number of studies of many different physical phenomena. However, the low resolution of some of the proxy records and the natural variability in the length of the climatic cycles does not allow an accurate estimation of the time when the climate will return to the more dominant, glacial conditions. It was concluded that (a) it is not possible to rule out a return to cooler and wetter conditions over the next 10,000 years, and (b) there is significant uncertainty in the timing of the return to those conditions. For the PA, the key aspects of a return to a future climate would be the deep infiltration of surface moisture and the return of piñon-juniper woodlands.

6.5 Changes in Plant Community

6.5.1 Introduction

This section summarizes changes in the plant community that are assumed to occur as a result of returning to a future climate. The basis for including particular plant communities for

parameterizing uptake model components is given. A more detailed discussion and analysis can be found in Brown et al. [1997a]. Predicting the most likely vegetation community that will develop at NTS disposal areas following closure uses two lines of evidence. The first line utilizes relatively short-term revegetation studies for determining how quickly certain components of the communities will appear after site closure. These studies describe general revegetation patterns common throughout the region. However, they do not define the specific species that might inhabit a particular site. The actual plants that may inhabit a site in both the near and far future can be predicted using evidence of past species' movement and community change. This section describes the successional patterns that may be expected at the NTS given a change to cooler, wetter conditions.

There is uncertainty in predicting specifically which plant communities will develop at the NTS in the future. Instead of attempting to make specific predictions about resident species and community types, analogues to the NTS environment are used to predict which lifeforms within a community may become established at the site. Appropriate community analogues for current conditions include all the shrubland communities now found at the NTS. Areas with higher elevations at the NTS are analogues for predicting potential future communities that may establish under conditions of increased effective moisture. Pack rat midden data incontrovertibly demonstrate that past climate shifts to cooler, wetter conditions—creating an increase in effective moisture—provided for the establishment of piñon-juniper woodland associations at elevations below the lowest NTS elevation, at locations that are currently hotter and drier than the NTS. Species found within those past assemblages have since retreated to higher, cooler elevations which are appropriate analogues for potential future conditions of increased effective moisture.

Communities Under Climate Change Conditions. Both higher elevation shrublands and woodlands might be expected at the low elevation of the GCD facility given increases in effective moisture at the site. By considering only woodland communities, the climate change community is conservative in considering the addition of species (trees) that have the deepest roots of all the lifeforms at the NTS.

Many edaphic factors, such as texture and organic matter content, are highly correlated with elevational changes and may have a large impact on species presence and community development, as well. The term "effective moisture" is intended to be inclusive of all the variables that control soil water available to plants at a site (e.g., aspect, slope, precipitation, temperature, soil texture, and soil chemistry).

The general pattern of succession that can be expected at the NTS is shown in Figure 6-3. Regional studies suggest that under relatively arid conditions, shrublands develop from bare soil in less than 50 years [Erdman, 1970; Barney and Frischknecht, 1974; Tausch and Tueller, 1977].

These regional studies focused on "secondary" succession, the patterns of plant community development after disturbance to previously vegetated sites. "Primary" succession is a term used for describing plant community development of previously unvegetated or drastically disturbed soils. Primary succession is much slower than secondary succession due to the absence of propagules (seeds, spores, etc.) in the soil. Secondary succession is assumed for the GCD site

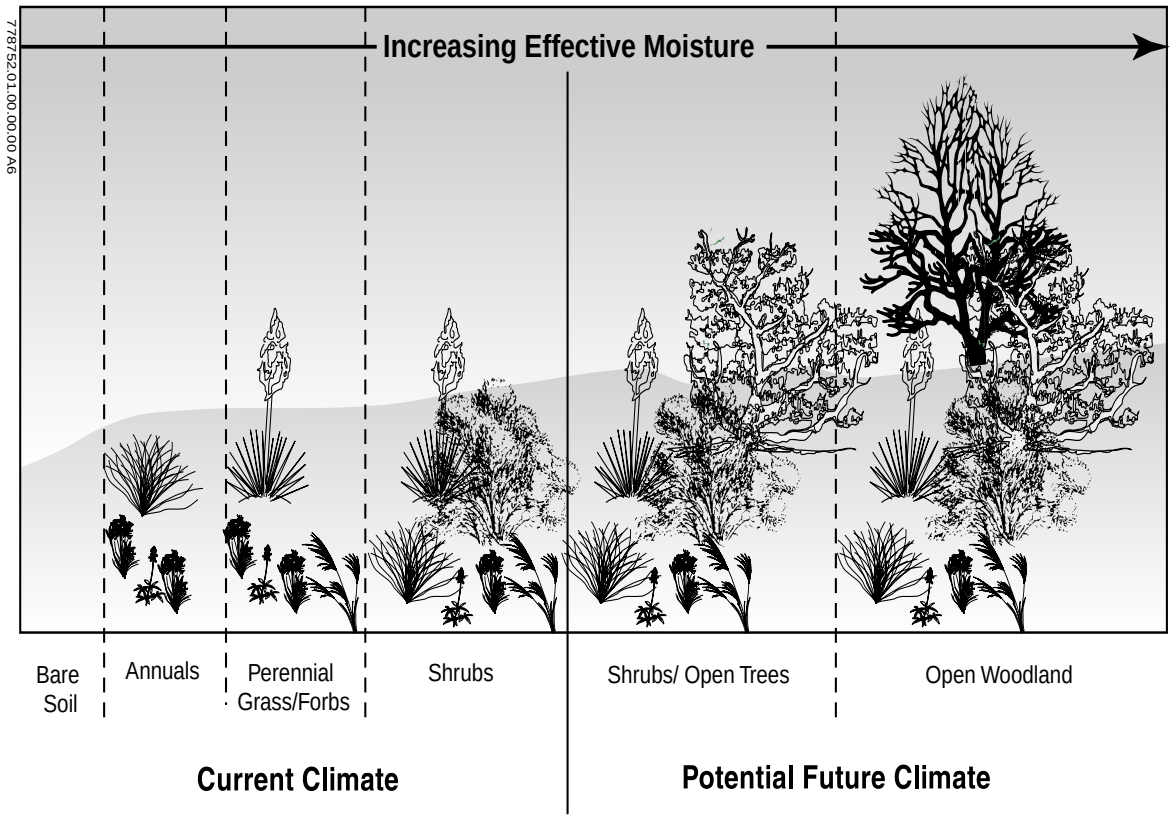

Figure 6-3. General Pattern of Succession at the NTS.

even though it is located in the active portion of the Area 5 RWMS and is currently unvegetated. The inactive portions of the Area 5 RWMS are vegetated and desert shrublands exist just beyond the RWMS boundary; therefore, seeds, spores, and remnant plants are readily available for revegetation at the site. More details on the successional patterns assumed for the GCD site can be found in Brown et al. [1997a].

With sufficient soil moisture conditions, deeper-rooted species can become established where currently there is not enough moisture to support anything but shrublands. The two most-likely successional endpoints under conditions of increased effective moisture are as follows:

- Under long-term conditions of climate change, the woodland ecotone can shift downward in elevation, just as it has in the past. At the lowest end of this ecotone, the interface between shrubland and woodland, juniper establishes among the shrubland first, followed by piñon. Establishment of this community can take 50 to 300 years.

Future Community Establishment. The 50- to 300-year establishment of woodlands under climate change is a conservative assumption, as the NTS woodlands are not proximal to the Area 5 RWMS. Thus, the establishment of seeds and propagules is likely to take longer than the PA assumes.

- Under conditions of subsidence, in the absence of climate change, it is more likely that the wetter microsites surrounded by "undisturbed" areas will be inhabited not by woodland

species, but by species currently found in analogous locations (e.g., washes and craters). These are termed "ephemeral wetland species" and can differ from species found in the surrounding higher elevation piñon-juniper ecosystem. For example, an "ephemeral wetland" exists in the U5a crater a few miles south of the Area 5 RWMS. These communities can be expected to establish within 50 years.

6.5.2 Current State of Knowledge

6.5.2.1 Woodland Communities

Because regulations governing radioactive waste disposal have protection requirements up to 10,000 years in the future, a conceptual model of potential community changes is also proposed with an estimated post-closure return to current shrubland communities in the near future and, given a shift to conditions of increased effective moisture, a potential future community comprised of more mesic shrubland or woodland species. Over shorter time periods, enhanced infiltration can support ephemeral wetland species that currently occupy sites receiving relatively large amounts of seasonal run-on.

At higher, cooler elevations in the NTS, shrub dominance gives way to tree dominance. At the lowest elevations, desert shrub intergrades with piñon-juniper (*Pinus monophylla-Juniperus osteosperma*) woodland at approximately 1800 m (5,900 ft). The piñon-juniper woodland gives way to other communities near 2,200 m (7,200 ft), the composition of which differs from site to site. Within the piñon-juniper woodlands themselves, relative species dominance varies as a function of elevation, which can be primarily attributed to differences in the availability of soil moisture from low to high elevations. Across one continuous local elevational gradient, juniper has greater amplitude in distribution than piñon, usually due to the extension of juniper into lower and more xeric elevations [Woodin and Lindsay, 1954; Barnes and Cunningham, 1987].

Within narrow elevation ranges, slope and aspect can also drive the relative dominance of junipers and piñons, with junipers more prevalent on warmer, drier, south-tending slopes. Physiological studies show that juniper is the more drought-resistant species and that piñon distribution is limited by its lack of water stress tolerance [Barnes and Cunningham, 1987; Wilkins and Klopatek, 1987; Breshears, 1993].

A piñon-juniper woodland is defined as an area where the dominant woody, non-shrub species is juniper, piñon, or both. As described in this section, the woodlands being proposed as analogues for potential future communities develop and persist under relatively dry conditions at sites currently receiving annual precipitation of only 25 to 33 cm (10 to 13 in.). It should be noted that these are not woodlands with massive trees and lush, multiple layers of undergrowth, a future scenario that is almost entirely implausible in the next 1000 to 10,000 years at the low elevations of the NTS. At the NTS, these woodlands are, in general, sparsely vegetated, with a tree canopy coverage of less (often much less) than 35%. Paleorecords of the NTS region show that it is not improbable to assume juniper and piñon-juniper woodlands can inhabit even the lowest elevations at the NTS, given appropriate soil moisture conditions [Brown et al., 1997a]. A piñon-juniper dominated community is shown in Figure 6-4.

Figure 6-4. Piñon (Pinus edulis) Dominated Great Basin Conifer Woodland on Fish Tail Mesa, Kaibab National Forest, Arizona ca. 1,585 m (5,200 ft) elevation. The major understory species on this ungrazed site is Big Sagebrush [Artemisia tridentata (Figure 25; Brown, 1982)]

6.5.2.2 Ephemeral Wetlands

There are a number of low elevation sites at the NTS where elevated, seasonal soil moisture conditions provide for analogues to subsidence conditions (such as washes and catchment areas).

Within these sites the vegetation differs markedly from the surrounding shrubland [Beatley, 1976; Hansen et al., 1997]. At some of these sites, wetland species (e.g., rushes and sedges) thrive, while at others, the wetter environment supports tree species, including some species that are usually associated with even wetter riparian systems (e.g., tamarix). The persistence of trees and wetland species at these sites with seasonally elevated soil moisture points to the impressive ability of desert-adapted plants to take advantage of enhanced water resources.

6.5.3 Parameters for Modeling Changes in the Plant Community

As discussed above, a change to cooler and wetter climatic conditions is assumed to alter the plant community at the NTS. It is assumed that the potential future communities in the low elevations of the NTS where the GCD site exists will be an admixture of species found currently in the low elevation shrublands and species growing in areas with higher effective moisture (i.e., ephemeral wetlands or woodlands). The plant uptake model accounts for this shift from shrubland species to woodland species by using different values for biomass turnover and for concentration ratios, and by adding trees to the possible lifeform types in the future community. The "distribution" function describing termite burrow depths also changes because termite burrowing depths are linked to plant roots. These three parameters and their values under climate change are discussed below, as well as the relative extraction function for trees.

6.5.3.1 Biomass Turnover Parameters — Climate Change

The data used for estimating productivity and litterfall for future communities came from a single study conducted within Great Basin shrubland and open juniper woodland ecosystems across northern Nevada, central and northern Utah, southern Idaho, and west-central Wyoming [Passey et al., 1982]. The shrubland sites are representative of those currently found in the northern half of the NTS. The juniper woodland sites are within the Great Basin piñon-juniper range [as defined by Miller and Wigand, 1994], also encompassing the NTS.

Only sites with woodlands or annual precipitation required for woodland development at the NTS were considered. At relatively cool locations in the northern Great Basin, junipers require approximately 20 cm (7.9 in.) of annual precipitation. At relatively warm locations in the southern Mojave Desert, juniper and piñon-juniper woodlands persist in regions that receive 25 to 33 cm (10 to 13 in.) of precipitation annually [Brown et al., 1997a]. Twelve sites were thus deemed appropriate as analogues for future conditions at the NTS, with average annual precipitation between 20 and 30 cm (8 and 12 in.). Two of the sites support open juniper woodland-shrubland ecosystems, and the remaining ten sites support Great Basin shrub-grass ecosystems. Increased infiltration will produce some variation of these communities.

Pertinent data collected for a ten-year period (1960 through 1969) include: species abundance, yearly productivity by species, and total yearly site litterfall. Not all 12 sites were studied each year, though all have data for 1961 through 1967. Two sites were studied for all ten years and three sites have data spanning eight years. With the data given at the species level it was possible to combine the data into lifeform groups.

Because litterfall was given only as a site total for each year, it was necessary to estimate the litterfall contributed by each lifeform. The amount of litterfall by a lifeform was calculated by multiplying the total litterfall by the relative percent productivity of that lifeform on a per year and per site basis. This assumes that for each unit of productivity, an equally proportionate amount of litterfall is produced. Thus, the distribution of litterfall among the lifeforms was weighted towards those that produce more biomass.

There were a few instances for which the productivity of annuals was reported as zero. While there is some slight chance that absolutely no annuals grew at these sites during these years, it is more likely that sampling techniques failed to detect measurable amounts of annuals. In these cases, the zero was changed to one half of the lowest value recorded for annuals for a given data set, an approach analogous to setting non-detections to one half the detection limit in chemical analyses. This assumes that the reported zero value represents some small, undetected number greater than zero and that the lowest recorded value represents the lowest detection limit for the sampling techniques used.

Appendix G includes the data for biomass productivity and litterfall.

Whether short-term productivity and litterfall data can be used interchangeably was tested using data found in Passey et al. [1982]. Specific details of the data screening and compilation are presented in the previous section. In the analysis presented here, total yearly site-wide productivity and litterfall data for 12 sites and from seven to ten years were used, for a total of 93 pairs of data. Because the data are paired by site, a t-test for the differences between population means of dependent variables was performed. Assumptions of the t-test (i.e., normality and equal variances) were investigated prior to performing the t-test and held true for each sample population. The test failed to prove a statistical difference between total site productivity and total site litterfall (see Appendix G for supporting documentation). Thus, the assumption of equivalency of short-term, site-wide productivity and litterfall data is appropriate for the modeling of biomass turnover for potential future communities, and is assumed to hold true for the current community, as well.

Equivalency of productivity and litterfall was also tested with the data for each lifeform, since the uptake model is lifeform-specific. As with the site-wide totals, the assumption of equivalency was determined appropriate for all lifeforms (see Appendix G).

The yearly litterfall data represent the long-term accumulation of dead plant materials in the soil; the data are actually the amount of all litter accumulated at a site up to, and including, that year. Because litterfall was not simply the amount of vegetation shed in a given year, the possibility that litterfall was dependent on previous years' productivity was investigated using a cross-correlation analysis technique (see Appendix G for analysis details).

For all the sites and all the years, the only significant correlation was for productivity and litterfall measured in the same year at one of the shrubland sites (p-value less than $\alpha = 0.05$). The remaining results, though not statistically significant, were used to evaluate possible trends that might lead to different litterfall data transformations. In general, the patterns in productivity were somewhat reflected in the patterns of litterfall. Eight of the 12 sites showed a positive correlation for data measured the same year. Only half of the sites showed litterfall to be positively correlated to the previous year's productivity and slightly more than half of the sites had positive correlations of litterfall to the previous two and three years' productivity. The most consistent trend across sites was the correlation of litterfall with the same year's productivity. Based on these results, the method of calculating litterfall for each lifeform as a function of the productivity of those lifeforms within the same year was deemed acceptable.

The cross-correlation results indicate that on a community level, yearly productivity and long-term litterfall trends can be quite different. A possible explanation is that the abiotic factors controlling productivity, such as precipitation, temperature, and soil nutrient levels, are either not the same factors controlling litterfall or they control leaf shedding to a different degree than they do productivity.

In the woodland community, for all the lifeforms, average litterfall was very close to average productivity. This indicates that the litterfall present on a site at any particular time is a good estimator of the long-term average productivity. The converse of this statement is true, as well—average productivity can be used to estimate the long-term biomass turnover in similar communities.

As with biomass turnover for current shrublands, biomass turnover for potential future communities is represented with beta distributions for each lifeform. Statistical parameters used to generate pdfs for the data set (Figure 6-5) are given in Table 6-3. In this model of community change from current conditions to potential future conditions, there is not a complete species replacement at the onset of climate change. Instead, there is merely a shift to a community with a broader possibility of species. This "broader possibility" includes all the current species with the possible addition of species now found in more mesic locations at the NTS. Because of this species persistence (i.e., community similarity), there is an assumption that what controls productivity in one community will tend to also control productivity in the other. Thus, a value of 0.9 is used to correlate the sampling of productivity for each lifeform in future woodlands with productivity of each lifeform in current shrublands.

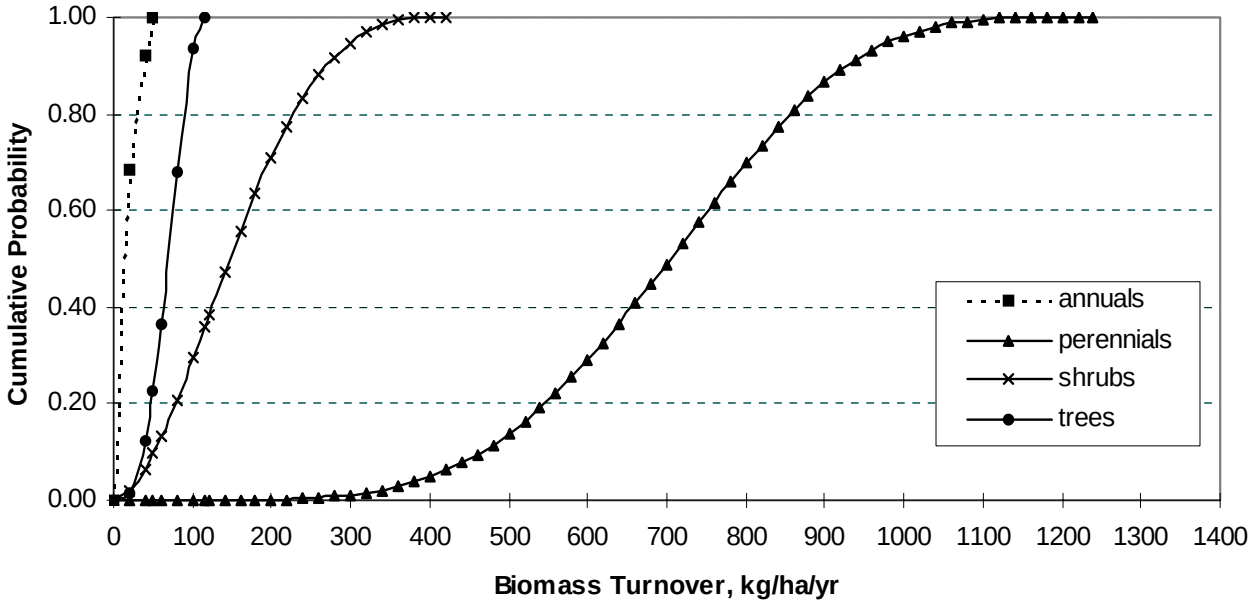

Figure 6-5. Biomass Turnover Cumulative Probability Distributions for Potential Future Woodlands.

Table 6-3. Statistical Parameters for Biomass Turnover, Potential Future Woodlands

Parameter, kg/ha/yr	Lifeform				Site-Wide Total
	Annual	Perennial	Shrub	Tree	
n	28	28	28	28	28
mean	14	700	155	68	936
median	10	663	134	69	915
minimum	1	437	48	28	666
maximum	47	1244	426	115	1523
standard dev.	14	176	82	22	187
α^a	0.469	0.622	1.05	4.70	na
β^a	1.23	1.29	2.67	5.61	na

[a]Scale parameter for beta distribution.

6.5.3.2 Concentration Ratios — Climate Change

Concentration ratios for plants expected in the community under potential future conditions are shown in Table 6-4. As with the concentration ratios for current shrublands, distributions are lognormal, with 0.001 and 0.999 quantiles given in the tables, and were developed as described in Section 5.7.7. Similar to the treatment of productivity sampling when the community shifts (Section 6.5.3.1), a value of 0.9 is used to correlate the sampling of concentration ratios for each element for future woodlands with the sampling of concentration ratios for each element for current shrublands. This correlation assumes that what controls the transfer of radionuclides from the soil to the plant in one community tends to control transfer in the other.

Table 6-4. Statistical Parameters for Concentration Ratio Data, Potential Future Woodlands

Radionuclide Element	Parameter						
	n	min.	max.	mean[a]	standard deviation[a]	0.001 quantile[b]	0.999 quantile[b]
Am (analogue for Ac)	14	5.0E!05	1.7E!02	1.9E!03	4.4E!03	1.2E!05	5.0E!01
Np (analogue for Pa)	12	7.0E!03	2.8E!01	1.1E!01	1.2E!01	5.2E!03	1.1E+00
Pb	26	1.4E!03	3.0E+00	4.3E!01	6.3E!01	8.9E!03	6.6E+00
Pu	15	8.0E!06	8.6E!04	1.7E!04	2.4E!04	3.9E!06	2.5E!03
Ra	41	2.2E!03	7.4E!01	1.3E!01	1.7E!01	3.9E!02	1.7E+00
Th	58	3.1E!05	1.1E+01	6.9E!01	2.1E+00	2.1E!03	2.4E+01
U	56	7.0E!04	3.5E+00	3.1E!01	6.3E!01	2.7E!03	7.1E+00
all data (generic)	239	8.0E!06	6.2E+01	6.6E!01	4.2E+00	2.8E!04	3.9E+01

[a]This parameter is from the underlying normal distribution.
[b]This parameter is from the data's lognormal pdf.

6.5.3.3 Relative Extraction for Trees

Because trees are assumed to be a part of the potential future community, it is necessary to estimate the relative extraction of tree roots (see Section 5.7.5). This requires an estimation of the relative frequency of maximum root length for individuals in each lifeform j, $X_j(l_{max})$, and the relative extraction function, $R_{Lj}(z; l_{max})$. The relative extraction of annuals, perennials, and shrubs for current conditions is assumed to remain unchanged under potential future climatic conditions.

Data for estimating the relative frequency of maximum root length were collected as described in Section 5.7.5. The root length data used are given in Appendix E (Table E-1), and the pdf used in the PA to describe relative frequency of maximum tree root length is given in Table 6-5. Figure 6-6 shows the likelihood distribution for the mean value of maximum root length, L_j, based on the data in Appendix E.

Table 6-5. LHS Input for Mean Value of Maximum Root Lengths for Trees

Length (m)	Cumulative Probability
2.834	0
3.052	0.002
3.27	0.01
3.488	0.034
3.706	0.086
3.924	0.172
4.142	0.29
4.36	0.425
4.578	0.56
4.796	0.681
5.014	0.78
5.232	0.855
5.45	0.908
5.668	0.943
5.886	0.966
6.104	0.98
6.322	0.989
6.54	0.994
6.976	0.998
7.412	0.999
7.848	1

The relative extraction function for trees under potential future woodland conditions is assumed to be identical to that of annuals, perennials, and shrubs under current conditions (see Section 5.7.6). That is, the relative extraction function for trees is a beta function with an α scale factor of 0, and a β scale factor varying uniformly between 3 and 20.

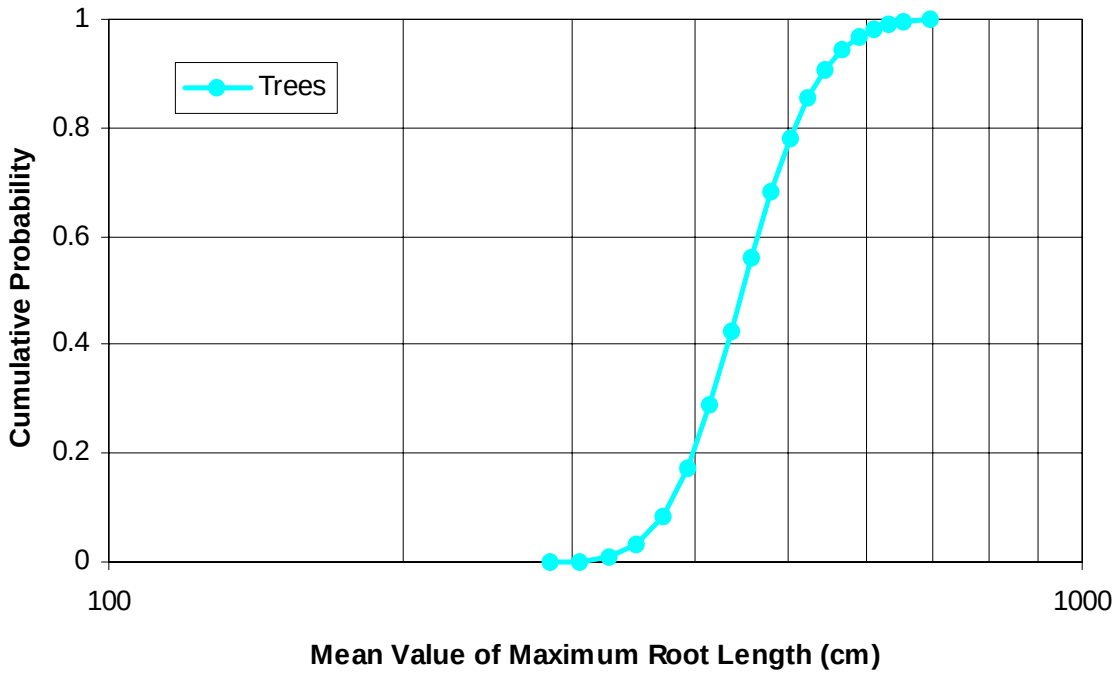

Figure 6-6. Likelihood Distribution for L_j.

6.5.3.4 Invertebrate Burrow Depth - P_z

Expected distributions of l_{max} for potential future woodland communities (a combination of all root length data for all lifeforms) can be used to estimate the proportion of termite burrowing within each soil interval *z* under potential future conditions. Root length data for all lifeforms were used to develop an exponential "distribution" function that describes the variability of the length of the longest root over all plants in the community. Root length observations greater than 6 m (20 ft) were not included in this distribution (see Section 5.8.3.4). This distribution was used to calculate the frequency of termite burrows with depth, and is shown in Figure 6-7.

6.6 Screening of Subsidence and Climate Change

6.6.1 Introduction

The GCD boreholes and Area 5 RWMS trenches contain a significant amount of void space resulting from the incomplete filling of waste containers, limited internal compaction of contents, and voids between containers. As the waste containers deteriorate and collapse, significant subsidence will occur.

Surface depressions resulting from subsidence have the potential to collect precipitation and runoff. This ponded water may infiltrate and move downward through the GCD wastes to the underlying aquifer. Additionally, numerous studies have shown that over long time spans, the climate could return to cooler and wetter glacial conditions, which could increase the amount of water collecting in the subsidence features.

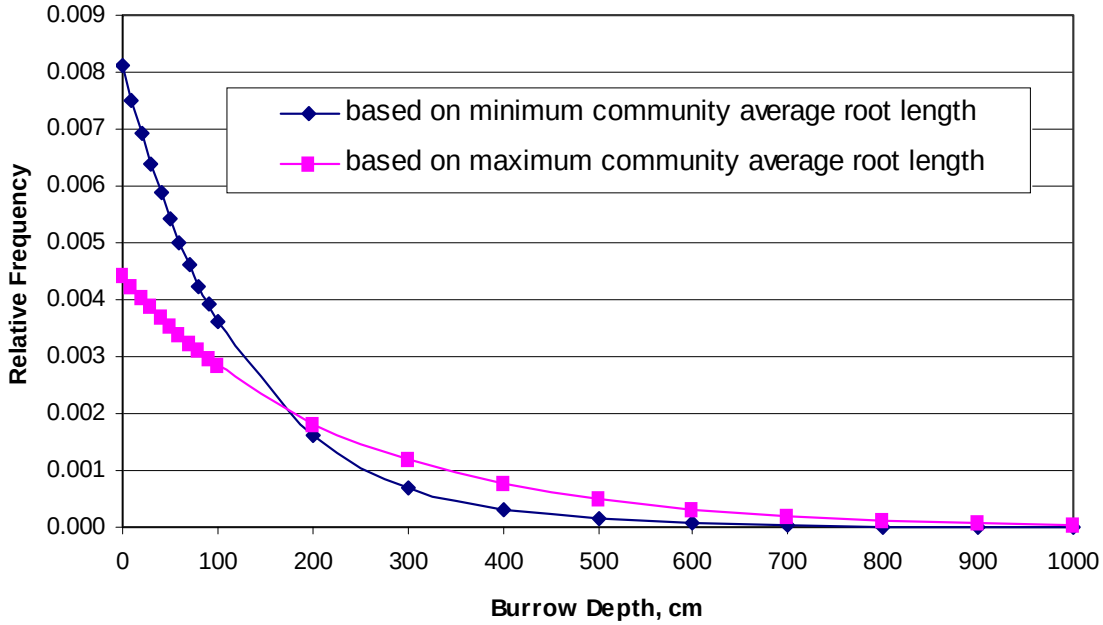

Figure 6-7. Range of Termite Burrow Frequencies, Potential Future Conditions.

6.6.1.1 Why This Screening Analysis was Undertaken

This section describes the results of a screening analysis conducted to determine if surface depressions resulting from subsidence could collect enough surface water to induce the movement of water through the vadose zone to the underlying aquifer during the next 10,000 years. The complete report on the detailed analysis of subsidence can be found in Appendix B.

If surface water has the potential to reach the aquifer and then the accessible environment in the next 10,000 years, this pathway would have to be included in the calculation of releases in the PA. On the other hand, if it can be shown that water moving through the GCD wastes will not reach the aquifer in 10,000 years, then it is clear that radionuclides will not be transported from the wastes to the accessible environment via the groundwater pathway in the same timeframe.

Four coupled analyses were undertaken for this study:

- the geometry of future subsidence features was estimated;
- precipitation, local runoff, and flooding were modeled using current climatic data;
- precipitation, local runoff, and flooding were modeled assuming an immediate return to glacial climatic conditions;
- 2-D and quasi-3-D flow of water in the unsaturated subsurface was modeled, assuming the landfill cap remains intact for 10,000 years, and also assuming the landfill cap is instantly removed at the end of the institutional control period.

6.6.1.2 Site Setting

A detailed discussion of the site setting was provided in Section 5.0. A brief discussion of the features and processes related to subsidence and climate change is included here.

The limited precipitation in the vicinity of the RWMS, coupled with generally warm temperatures and low humidities, results in a hydrologic system dominated by evapotranspiration. The movement of water within this 236 m (774 ft) thick unsaturated zone can be subdivided into two zones, the near surface zone and the deeper zone.

The near surface zone is the hydrologically "active" region of unsaturated alluvium. The forces acting to remove the moisture include evaporation and plant root uptake. Based on a number of field studies, the balance of these forces is such that only the upper 2 m (7 ft) is hydrologically active, and spatially distributed infiltration does not reach deeper than about 1 m (3 ft) [Appendix A; Shott et al., 1998].

The deeper vadose zone is hydrologically inactive. Between a depth of approximately 2 to 35 m (7 to 120 ft), the alluvium shows matric potentials with depth indicating a steady and *very slow upward flux of pore water,* i.e., there is no groundwater recharge.

A static zone where the hydraulic gradient is negligible exists between approximately 37 to 90 m (120 to 300 ft). From 90 to 236 m (300 to 774 ft) very slow gravity drainage is still occurring. Detailed discussions of the deep vadose zone are presented in Shott et al. [1998]. Based on measurements from a number of characterization wells, groundwater is approximately 236 m (774 ft) below the land surface.

6.6.1.3 Climate Change

To assess the potential impact of climate change, past global, regional, and site-specific empirical records of proxies of past climatic conditions were examined [Brown et al., 1997a]. The following paragraphs provide a summary of that work and the reader is referenced to Brown et al. [1997a] for details.

The records of the isotopic oxygen composition of marine sediments [Williams et al., 1988] and thick ice deposits [Dansgaard et al., 1993] provide global scale evidence of past climatic conditions. Studies of the isotopic oxygen composition of calcite deposits in Nevada's Devils Hole spring [Winograd et al., 1988; 1992] provide a 500,000-year record of past climate conditions in the southwestern U.S.

Studies of paleo-vegetation from pack rat middens (e.g., Spaulding, 1990) allow the reconstruction of past vegetation assemblages (and climatic conditions) at the NTS. It is clear that open piñon-juniper woodlands existed at the elevations of the Area 5 RWMS in the geologically recent past.

There is very good agreement between the global ice core records, the regional Devils Hole record, and the local pack rat midden records (e.g., Figure 16 of Brown et al., 1997a). *All of the records showed a cyclic pattern of climate change in which the climate varies between relatively persistent glacial climates (cooler, wetter periods) separated by interglacial climates (warmer, drier periods) of relatively short duration.*

At the Area 5 RWMS, cooler and wetter equates to 3E to 5E C cooler, with an average precipitation of about 30 cm (10 in.). A doubling of the amount of precipitation is dramatic; however, climatic conditions at the Area 5 RWMS were still relatively warm and semiarid, with open piñon-juniper woodlands.

The cyclic nature of past climatic conditions is solidly supported by a large number of studies of many different physical phenomena. However, the low resolution of some of the proxy records and the natural variability in the lengths of the climatic cycles does not allow an accurate estimation of the time when the climate will return to the more dominant, cooler, and wetter conditions.

For the PA, it is assumed that the past climatic conditions can be used to estimate future conditions and responses. Based on this assumption, it was concluded that (1) it is not possible to rule out a return to cooler and wetter conditions over the next 10,000 years, and (2) there is significant uncertainty in the timing of the return to those conditions. For this screening analysis, precipitation, local runoff, and flooding simulations were conducted assuming that the current climatic conditions persist for 10,000 years. Glacial climatic conditions were assumed to persist for 10,000 years in simulations of precipitation, local runoff, flooding, and the movement of pore water in the vadose zone.

6.6.1.4 Closure

As noted earlier, DOE/NV operates the Area 5 RWMS for the disposal of radioactive wastes, and DOE/NV is responsible for the future closure and monitoring of the Area 5 RWMS. An important issue related to closure is the future subsidence of the disposal cells; DOE [1998] describes the situation.

> Review of waste disposal operations indicated that the waste already placed in the RWMSs contains a significant amount of void space resulting from incomplete filling of waste containers, limited internal compaction of contents, and voids between containers. These voids will produce significant subsidence as the waste containers deteriorate and collapse over time. Additional sources of subsidence include the decomposition of containers, waste, and dunnage. ... over long time periods, the waste and containers would collapse, decompose, and ultimately reach a density similar to that of the surrounding soil materials.

DOE [1998] recommends the construction of an alternative cap that would consist of a single, thick layer of compacted native alluvium constructed to 2 m (7 ft) above the land surface. The intent of this design is to simulate the natural system at the NTS, with particular emphasis on (1) limiting infiltration by enhancing evapotranspiration and (2) using soil materials that have suitable durability and longevity. Figure 6-8 presents a visualization of the capped Area 5 RWMS in the year 2170, and Figure 6-9 presents a visualization of how the Area 5 RWMS might look in the year 2171, assuming that the remaining voids are instantly translated into subsidence features.

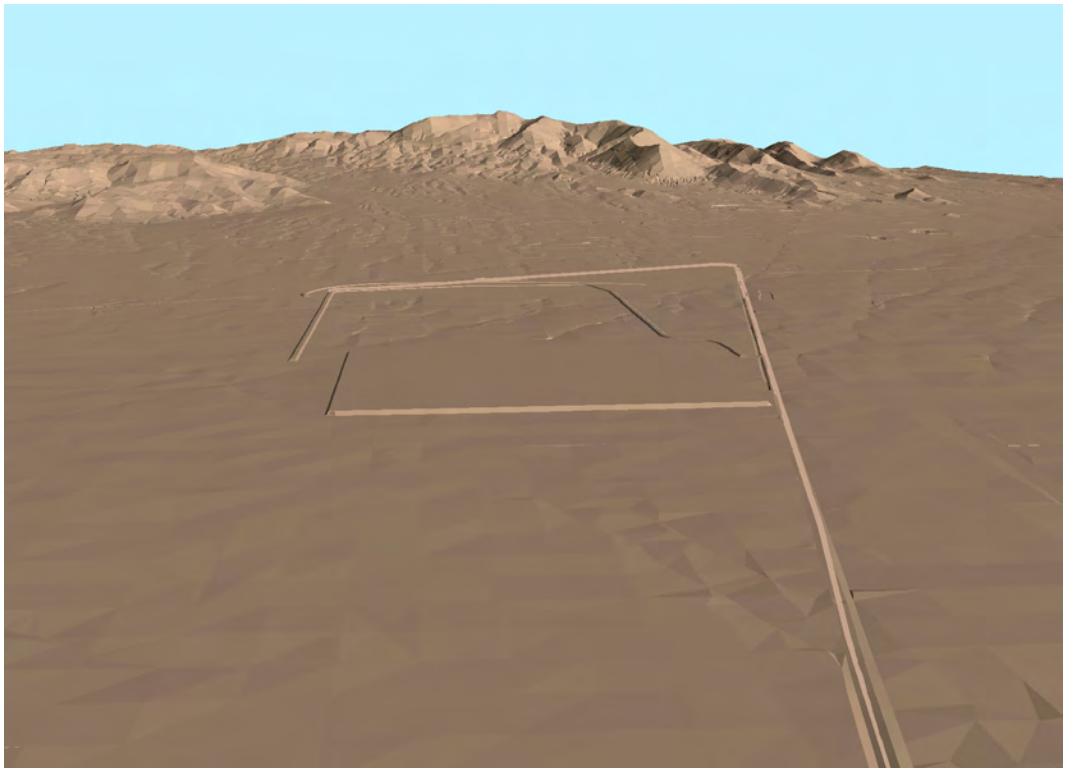

Figure 6-8. Visualization of the Capped Area 5 RWMS in the Year 2170.

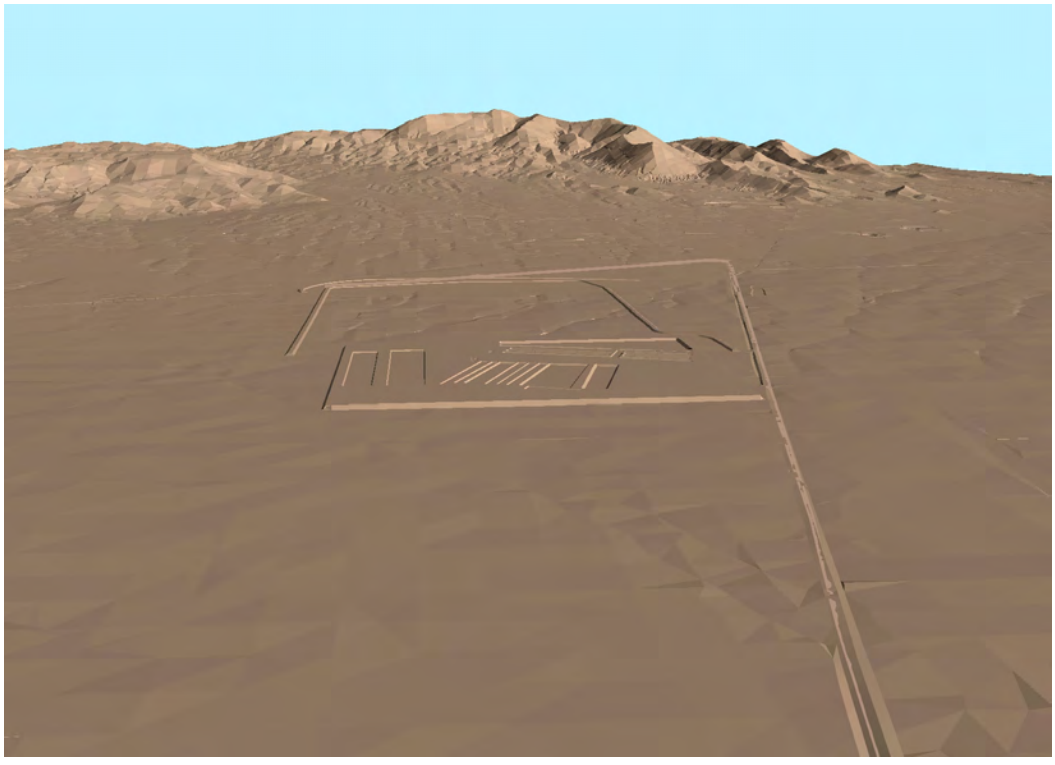

Figure 6-9. Visualization of the Capped Area 5 RWMS in the Year 2171.

Based on forthcoming DOE guidance, DOE plans to operate the Area 5 RWMS until the year 2070. During the next 70 years, a landfill cap that consists of a single, thick layer of compacted native alluvium will be constructed to 2 m (7 ft) above the land surface. DOE would then assume AIC over the closed landfill. The EPA's standard for disposal of TRU wastes does not allow the PA to take credit for more than 100 years of AIC (40 CFR 191.14, EPA [1985]). This screening analysis assumes loss of AIC 170 years from now, in the year 2170.

6.6.1.5 Overview of Subsidence Analysis

The subsidence analysis is based on a systematic evaluation of the potential for surface water to migrate to the water table during the next 10,000 years, due to the combined effects of landfill subsidence, precipitation, flooding, and a return to glacial climatic conditions.

Section 6.6.2 describes how the geometry of the subsidence features was calculated. This section provides a defensible methodology for estimating the volumes and surface expressions of subsidence features used in this analysis.

Section 6.6.3 provides an analysis of the quantity of precipitation and surface water runoff that could accumulate in the subsidence features. The magnitude of the PMP event is also calculated. Standard techniques are then used to translate this information into frequencies and volumes of surface water runoff that might accumulate in the subsidence features. These calculations are done for both existing and glacial climatic conditions.

Flooding analysis is provided in Section 6.6.4, including an estimation of the magnitude and frequency of rare flood events and the PMF for specific watersheds in the Area 5 RWMS. These calculations are done for both existing and glacial climatic conditions to estimate the potential for floods to overtop the landfill cap.

Section 6.6.5 describes the conceptual models of the unsaturated zone. The mathematical models, initial conditions, boundary conditions, parameters, and other relevant information are presented, as is the calibration of the vadose zone models.

Modeling of flow in the vadose zone as a result of infiltration from ponded water in subsidence features is the subject of Section 6.6.6. These calculations are performed for glacial climatic conditions, *assuming the landfill cap remains intact.* The redistribution of moisture from both subsided GCD boreholes and subsided LLW trenches is assessed. Additional calculations are performed *assuming the cap is instantly removed* and that the subsidence features will eventually fill with sediment entrained in the surface waters.

The sensitivity of these models to specific assumptions is briefly addressed in Section 6.6.7. Section 6.6.9 then summarizes the key findings of this study.

6.6.1.6 Bias in the Screening Analysis

These screening analyses are not a prediction of how the Area 5 RWMS system will actually respond to subsidence. These analyses were developed in a manner to bias (overestimate) the

downward movement of surface water. Some of the assumptions which clearly bias the outcome are:

- Pits and trenches were assumed to contain only steel containers, and the degradation rates of the steel containers were assumed to be one-half of the degradation rates used in previous studies; these assumptions maximize the amount of long-term void space in the Area 5 RWMS.

- All voids remaining in the Area 5 RWMS are assumed to be instantly expressed as subsidence features in the year 2170, the time at which AICs are assumed to be lost.

C The subsidence features are then assumed to instantly enlarge, based on the angle of repose.

C For the intact cap analysis, *the enlarged subsidence features are assumed to remain intact, capturing precipitation and precipitation runoff for 10,000 years.*

C To simulate glacial climatic conditions, it was assumed that the average number of precipitation events that occur under the current climate continues to occur under glacial climatic conditions, and that each event produces twice as much precipitation - *this results in approximately five times as much precipitation runoff* as is produced under the current climate (the less conservative approach is to assume that each event under glacial conditions produces the same amount of precipitation as under the current climate, and then double the number of events - this less conservative approach produces only a doubling of precipitation runoff)

C All rare precipitation events were assumed to begin occurring after the loss of AIC in the year 2170. For example, under glacial conditions, the PMP was assumed to occur at time zero (the year 2170), followed by the 10,000-year storm 1.125 years later. A 1000-year storm was assumed to occur 1.125 years after the 10,000-year storm. The 1000-year storm is followed by nine 100-year storms, each 1.125 years apart. Then this sequence of a 1,000-year storm and nine, 100-year storms was repeated at the year 1000, 2,000, etc., through the year 9000.

C High initial moisture conditions were assumed in the runoff analysis, so as to overestimate the volume of precipitation that flows into the subsidence features as precipitation runoff.

C No credit was taken for the future construction of RWMS disposal cells to the north (upstream) of the existing RWMS cells; such cells would block arroyo flood waters from the disposal cells analyzed in this study.

C The vadose zone was assumed to be homogeneous and isotropic.

- The subsidence models do not include the removal of soil moisture by plants.

These assumptions, and others discussed in this report, provide confidence that the potential for surface water to migrate to the water table is overestimated. If surface water will not reach the water table in 10,000 years, then it is clear that radionuclides will not reach the 5-km (3.1-mi) accessible environment boundary in 10,000 years.

6.6.2 Conceptual Model of Subsidence

The current configuration of the Area 5 RWMS includes 7 pits, 16 trenches, 12 GCD boreholes, and GCDT. The waste disposed in the pits, trenches, and GCD boreholes is not compacted and is expected to significantly subside with time.

This section discusses the analyses done to:

- estimate the range of subsidence depths and geometry of the subsided features in the LLW trenches and pits and over GCD boreholes due to degradation and compaction of waste and waste containers;
- reproduce the landscape of the Area 5 RWMS after the year 2170; and
- generate input for the surface water runoff analysis and for the unsaturated flow analysis.

6.6.2.1 Estimation of the Subsidence Depths in Pits and Trenches after Site Closure

The working group analysis [DOE, 1998] concluded that "the Area 5 RWMS could experience subsidence of the waste equal to about 30 percent of the trench/pit depth after about 100 years." This number (30%) was used then in Brown et al. [1998] to calculate the depth of subsidence expected in the trenches and pits after site closure. This estimate of subsidence depth represents the "expected depth value" calculated using what is believed to be the "best estimates" of the parameter values taken from DOE [1998].

Based on guidance from DOE, it is now assumed that the Area 5 RWMS will be an operational facility until the year 2070. Then, based on 40 CFR 191.14(a) [EPA, 1985], it is assumed that DOE will actively maintain the closed landfill until the year 2170 (i.e., 170 years from present).

DOE [1998] assumed that each column of waste consists of one type of container and/or a dunnage. The following types of containers were considered: cardboard boxes, wooden boxes, steel drums, and steel boxes. Maximum reduction values, C_i, were defined for each of four container types, wooden dunnage, and for the wooden pallets under containers (Table 6-6).

Table 6-6. Maximum Reduction Volume as a Percentage of the Total Initial Volume

Material	Maximum Reduction Volume
Cardboard	44%
Wooden Boxes	44%
Steel Drums	54%
Dunnage	100%
Wooden Dunnage (pallets)	100%
Steel Boxes	44%
Void Space	100%

Values for container volume, dunnage volume, and soil volume V_i of the total column volume (Table 6-7) were calculated assuming eight stacking patterns:

- cardboard boxes, dunnage, and soil
- wooden boxes, dunnage, and soil
- wooden dunnage and soil
- steel boxes and soil
- steel drums stacked horizontally and soil
- steel drums stacked vertically, dunnage, and soil
- steel drums stacked randomly and soil
- steel drums stacked horizontally in triangular array and soil

The compression of each container type and dunnage due to degradation and compaction was estimated for the following discrete times: 20, 50, 75, 100, 150, 300, 500, 1000, and 10,000 years (Table 6-8). The decay rates used in these calculations represent the expected values. It was noted in DOE [1998] that "*the decay rate for any of the containers could probably vary by at least a factor of 2*." Consequently, the decay rate of each container can change within a large range.

The greatest uncertainty is the amount of void space in the containers and the compressibility of the waste. Another uncertainty is the percentage of different types of containers within the trench and their location. No information is available to reduce this uncertainty except some photographs taken at the moment of waste emplacement. An example of such a photograph is presented in Figure 6-10.

As shown in Table 6-8, all container types will experience noticeable subsidence before the site closure (within the 170-year period). It is assumed that these subsidence features will be filled during the period of AIC (years 2070 through 2170).

All of the prior studies point out great uncertainty in the values of the parameters that define the magnitude and timing of subsidence. Moreover, the parameter variability was not characterized. To bound the effects of this uncertainty/variability, the minimum, maximum, and probable values of the expected potential subsidence depths in the pits and trenches were calculated.

Minimum Potential Subsidence Depth in Pits/Trenches

The minimum potential subsidence in pits and trenches after site closure was calculated assuming that the pits and trenches consist only of cardboard containers placed on wooden dunnages. The results of calculations are demonstrated in Figure 6-11. As it shows, 97% of subsidence occurs before the year 2170, leaving 3% of the subsidence after the year 2170. For the deepest pit at the site (PO6U), this would mean a depth equal to 0.40 m (1.3 ft). For most of the trenches, this would mean a depth equal to 0.10 m (.33 ft). Consequently, subsidence features will hardly be noticeable.

Table 6-7. Percentage of Different Materials in Waste Column for Different Waste Placement Patterns

Pattern Number	Pattern Composition	Percentage of Material
1	Cardboard boxes	77%
	Dunnage	14%
	Voids	9%
2	Wooden Boxes	77%
	Dunnage	14%
	Voids	9%
3	Wooden Dunnage	33%
	Voids	67%
4	Steel Boxes	90%
	Voids	10%
5	Steel Drums, Horizontal	78%
	Voids	22%
6	Steel Drums, Random	80%
	Voids	20%
7	Steel Drums, Vertical	68%
	Dunnage	13%
	Voids	19%
8	Steel Drums, Horizontal-Triangular	91%
	Voids	9%

Table 6-8. Time-Dependent Volume Reduction of Different Materials Due to Degradation

Material	Time (yr)									
	0	**20**	**50**	**75**	**100**	**150**	**300**	**500**	**1000**	**10000**
Cardboard	0%	90%	95%	100%	100%	100%	100%	100%	100%	100%
Wooden Boxes	0%	10%	50%	75%	90%	100%	100%	100%	100%	100%
Steel Drums	0%	5%	35%	60%	75%	85%	100%	100%	100%	100%
Dunnage	0%	0%	50%	75%	100%	100%	100%	100%	100%	100%
Wooden Dunnage	0%	5%	20%	50%	75%	90%	100%	100%	100%	100%
Steel Boxes	0%	0%	5%	10%	20%	50%	70%	80%	95%	100%
Dumped Soil	0%	15%	25%	50%	60%	70%	75%	80%	95%	100%

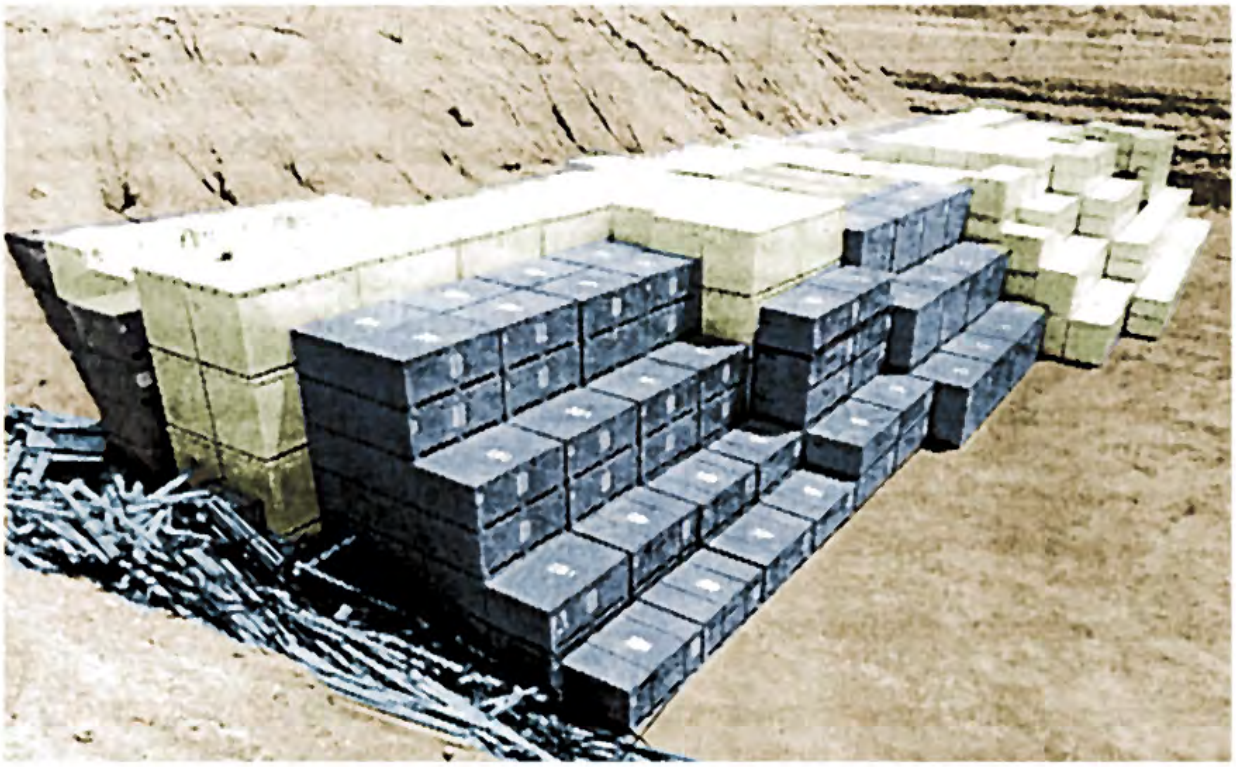

Figure 6-10. Waste Container Emplacement in a Typical Trench, Area 5 RWMS.

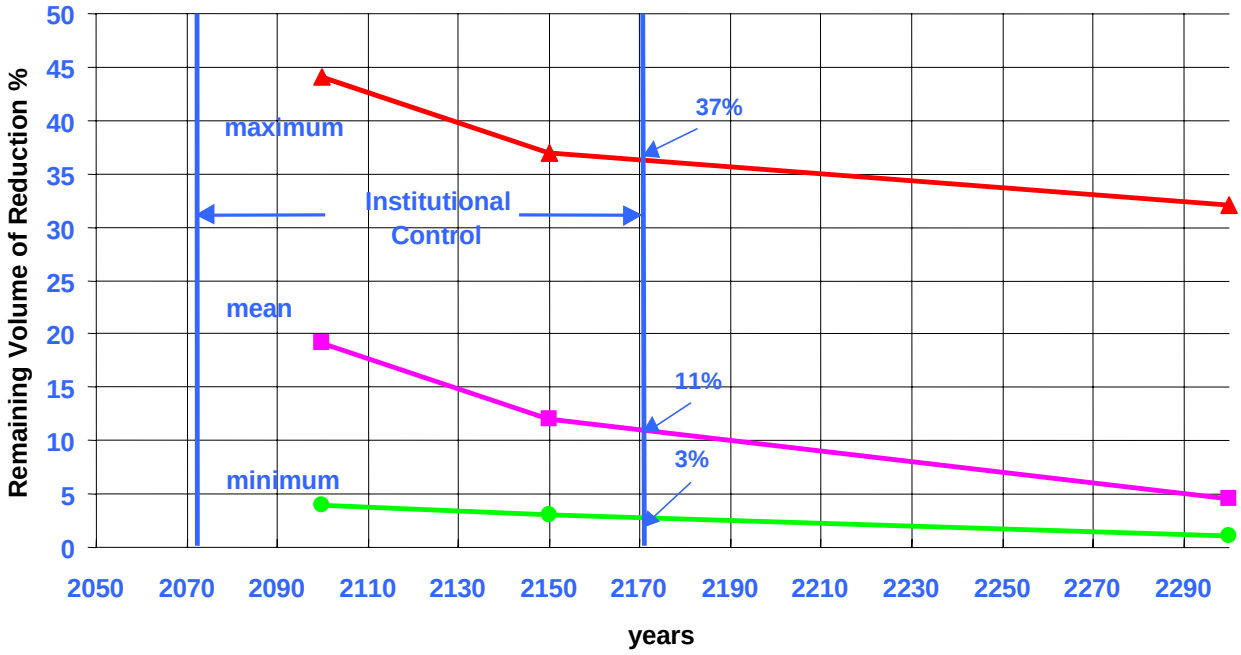

Figure 6-11. Remaining Volume of Reduction in Pits/Trenches, Area 5 RWMS.

Maximum Potential Subsidence Depth in Pits/Trenches

The maximum potential subsidence in pits and trenches was calculated using data from Tables 6-6 and 6-7 and assuming that the pits and trenches consist only of steel boxes. The decay rates for the steel boxes were assumed to be two times slower than the rates shown in Table 6-8. The results of calculations are demonstrated in Figure 6-11. As it shows, 63% of subsidence occurs before the year 2170, leaving 37% of the subsidence after the year 2170. Consequently, the maximum subsidence after the site closure would be from 1.2 m (3.9 ft) (most of the trenches) to 5.0 m (16 ft) (Pit PO6U).

Probable Potential Subsidence Depth in Pits/Trenches

The screening subsidence depths provided above are calculated assuming the very unlikely situation that only cardboard or steel boxes are placed in the pits and trenches. In reality, a combination of different containers was placed in the pits and trenches. However, there is not enough data to simulate a more realistic situation with different containers and patterns in the pits and trenches. Thus, the random situation was modeled to calculate the most likely subsidence depth. It was assumed that it is equally likely to find any of eight patterns listed previously in any pit or trench. The resulting probable subsidence depth was calculated using data from Tables 6-6 through 6-8. As shown in Figure 6-11, the most likely subsidence depth to occur after 170 years, according to these calculations, is 11% of the pit/trench depth or 0.4 m (1 ft) (most of the trenches).

In an attempt to simulate a more realistic trench, Figure A-1 from DOE [1998] was used to estimate the percentage of each stacking pattern within the trench. These percentages were used to calculate weighted average subsidence depth from data presented in Tables 6-6 through 6-8. The weighted average subsidence depth after the year 2170 was equal to 14% of the trench depth, which is comparable to an estimate based on the assumption that each stacking pattern has an equal likelihood of occurring.

Conclusions

Additional subsidence within the LLW trenches and pits is expected to occur after AIC ceases, 170 years from now. The estimated subsidence depth varies from 3% to 37% of the initial depth. The subsidence features with a depth of 3% of the trench/pit depth could be so small (0.15 m [.49 ft] for a typical trench) that it would be barely distinguishable from the original relief. The subsidence features with a depth of 37% could be deep enough (1.2 m [3.9 ft] for a typical trench) to look like a large pit. The difference in estimates is due to the uncertainties in the maximum volume reduction for different types of containers, container decay rates, and container stacking patterns. Assuming that all types of containers are equally likely to be found in the trench brings the subsidence depth down to 11% of the original depth or 0.4 m (1 ft) for a typical trench. This depth is the most likely to be observed in the trenches and pits after site closure when the compaction is complete. This time is related to the degradation period of the different types of the waste containers, which could be anywhere from 100 to 2000 years. Since the different types of waste containers could be distributed very differently within the trenches/pits,

different depths of subsidence and different rates of subsidence are likely to be observed within the trenches and pits, leading to differential subsidence. However, with time, the subsidence in trenches and pits will become more uniform.

6.6.2.2 Estimation of the Subsidence Depths and Radii above the Greater Confinement Disposal Boreholes after Site Closure

The GCD boreholes contain NWARs (Boreholes 1, 2, and 3) and classified waste (Borehole 4) [Chu and Bernard, 1991], located within the depth interval from 21 to 36 m (69 to 120 ft). All of the boreholes were backfilled using native alluvium.

The magnitude of potential subsidence over the GCD boreholes was estimated in Arnold [1996]. The conceptual model used in this estimate assumes a piston settlement of the waste and backfill soil within a GCD borehole, resulting in piston settlement at the surface with subsequent sidewall collapse in accordance with the angle of repose and formation of the cone-shaped depression. The completion of the GCD borehole is shown in Figure 6-11. The volume of this cone depression is assumed to be equal to the reduction volume of the waste and soil within the borehole. The depth d and the radius R of the cone at the time t are given by the following equations:

$$d(t) = [3V(t)\ tan^2\ \eta]^{1/3} \qquad (6\text{-}1)$$

and

$$R(t) = d(t) / tan\ \eta \quad , \qquad (6\text{-}2)$$

where $V(t)$ is reduction volume at the time t and η is the repose angle. This conceptual model is schematically presented in Figure 6-12.

The estimates of the degradation rates for different container types provided in DOE [1998] were not available in 1996 and only the maximum reduction volumes were calculated for each of the GCD boreholes in Arnold [1996] (see Appendix B). In Brown et al. [1998], the subsidence depths and radii were calculated using maximum reduction volume values from Arnold [1996] (see Appendix B), assuming that the reduction volume at 100 years will be 60% of the maximum reduction volume.

The same conceptual model used in Brown et al. [1998] was used to estimate the depths and radii of subsidence depressions above the GCD boreholes after the year 2170, the only difference being in the calculation of reduction volume at the year 2170. This calculation used a conceptual model and degradation rate data from DOE [1998]. The waste stored in GCD Boreholes 1, 2, and 3 is placed in metal boxes with the plywood covers [Chu and Bernard, 1991]. The waste in Borehole 4 is placed in 258 drums and 8 boxes. Since no data are available from DOE [1998] on the degradation rates of boxes that have both metal and plywood lids, the degradation rates for steel boxes were used. The degradation rate of drums was assumed to be the same as the degradation rate of boxes, even though according to data provided in Table 6-8, steel drums degrade faster than steel boxes. The minimum and maximum subsidence depth and radius values were estimated to define the range for these parameters.

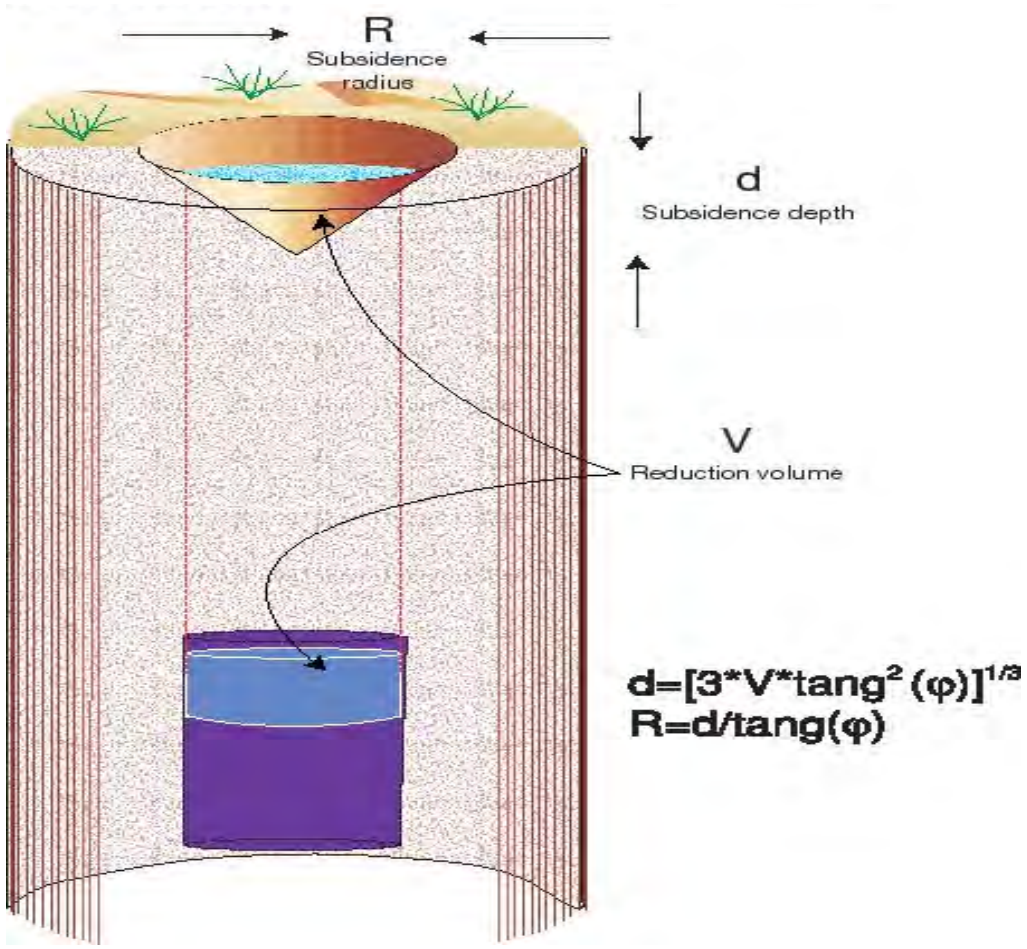

Figure 6-12. Conceptual Model of Subsidence Above the GCD Borehole.

Maximum Potential Subsidence Depths and Radii above the Greater Confinement Disposal Boreholes

The maximum reduction volume within the GCD borehole was calculated using the following assumptions:

- The waste container degradation rate is two times slower than the steel box degradation rates from Table 6-8.

- The maximum volume reduction of the metal boxes is 85% of the initial volume of the boxes based on calculations from Arnold [1996], which is significantly greater than the 44% volume reduction assumed for steel boxes in DOE [1998]. This is due to the loose packaging of waste in the GCD containers.

- The void volume of the backfill is 10% of the backfill column volume, which is the same as in DOE [1998]. In Arnold [1996], it was noted that this volume is extremely uncertain and is

probably within the 0% to 30% range. A value of 10% was selected to maintain consistency with the DOE [1998] estimates.

Using Equation (6-1) with these parameters yields a change in the subsidence depth with time (which is equivalent to the change in reduction volume) demonstrated in Figure 6-13. As this figure shows, the reduction volume at the year 2170 is 36%. The corresponding subsidence depth calculated using Equation (6-2) and expressed as a percentage of maximum subsidence depth is 86%. The calculated subsidence radius is also expressed as a percentage of maximum subsidence radius. The absolute values of the subsidence depths and radii for the GCD Boreholes 1, 2, 3, and 4 are summarized in Table 6-9.

Minimum Potential Subsidence Depths and Radii above the GCD Boreholes

The following assumptions were made to calculate minimum reduction volumes within the GCD boreholes:

- The waste container degradation rate is two times faster than the steel box degradation rates from Table 6-8.

- The maximum volume reduction of the metal boxes is 85% of the original volume.

- The void volume of the backfill due to poor compaction comprises 30% of the backfill column volume, equivalent to the value given in Arnold [1996].

The change in the reduction volume over time for the case considered is demonstrated in Figure 6-13. As this figure shows, the reduction volume at the year 2170 is 80%. The corresponding subsidence depth and radius after the year 2170 calculated using Equations (6-1) and (6-2) and expressed in percentages are both 59%. Due to the cube root relationship between the reduction volume and subsidence depth and radius, only a small decrease in the depth/radius values occurs with noticeable changes in the reduction volume. The minimum values of the subsidence depths and radii for the GCD Boreholes 1, 2, 3, and 4 are presented in Table 6-9.

Conclusions

After the assumed loss of AIC, 170 years from now, the waste containers within the GCD boreholes will not be fully compacted. This will result in subsidence of the land surface and the formation of a cone-shaped depression with the side walls sloping in accordance with the angle of repose. The formation of such a depression will depend on the degradation rates of the waste containers. Most of the compaction is expected to take place in the first 2000 years, but could be completed in the first 500 years.

After the compaction is fully completed, the expected depth of such a depression will be from 2.1 to 3.0 m (6.9 to 9.8 ft) (Boreholes 1 and 4); from 2 to 2.9 m (7 to 9.5 ft) (Borehole 2); and from 1.6 to 2.7 m (5.2 to 8.9 ft) (Borehole 3). The radius of the depression will be from 3.0 to 4.3 m

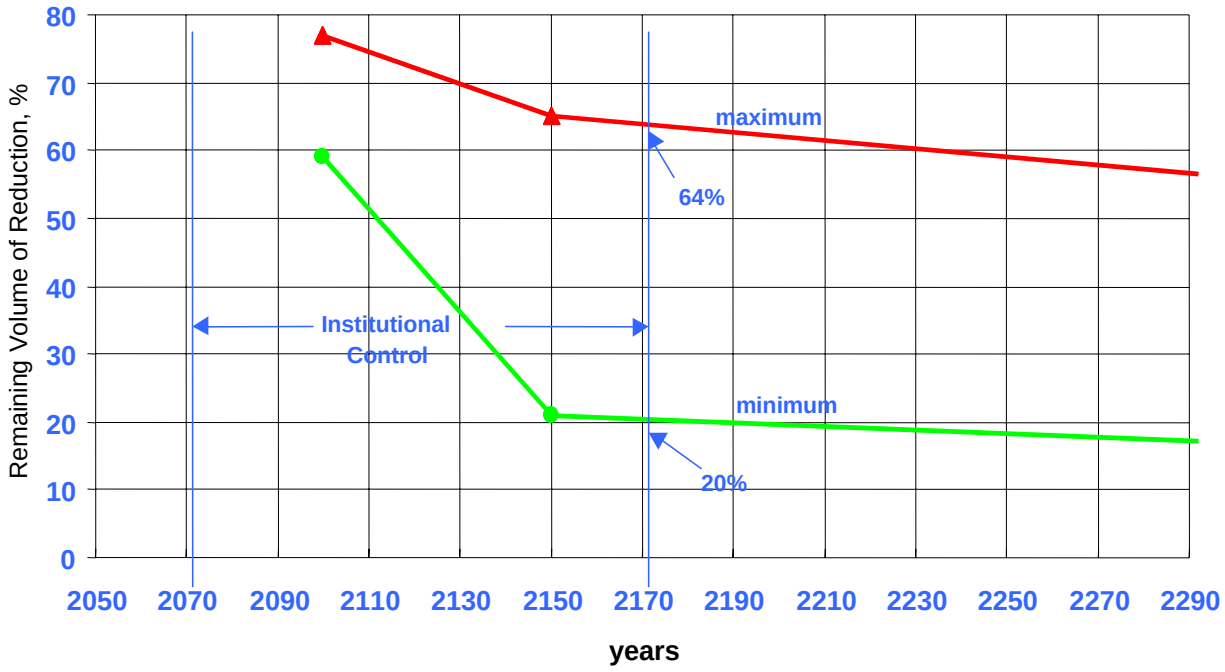

Figure 6-13. Remaining Volume of Reduction in GCD Boreholes, Area 5 RWMS.

Table 6-9. Depths and Radii of Subsidence above the GCD Boreholes after Site Closure

Borehole	Depth, m		Radius, m	
	Minimum	Maximum	Minimum	Maximum
1	2.1	3.0	3.0	4.3
2	2.0	2.9	2.8	4.1
3	1.6	2.3	2.2	3.3
4	2.1	3.0	3.0	4.3

(9.8 to 14 ft) (Boreholes 1 and 4); from 2.8 to 4.1 m (9.2 to 13 ft) (Borehole 2); and from 2.3 to 3.3 m (7.5 to 11 ft) (Borehole 3). The ranges of these values are obtained by estimating minimum and maximum possible reduction volumes remaining after site closure. Although the wide ranges of the parameter values were used in these calculations, the resulting ranges of the depth and radius values are relatively narrow.

6.6.3 Analysis of Precipitation and Surface Water Runoff

6.6.3.1 Purpose

The purpose of this precipitation analysis was to develop rainfall characteristics for Area 5 that can be used to estimate the total amount of local runoff that could flow into the RWMS subsidence features during the 10,000-year period for each of two conceptual models.

6.6.3.2 Data Used

The 36 years of daily precipitation at the National Weather Service gauge at Well 5B (1964–1999) were analyzed to create the statistics used for the computation of local runoff.

Tables and graphs in U.S. Department of Commerce publication, Hydrometeorological Report No. 49, Probable Maximum Precipitation (PMP) Estimates, Colorado River and Great Basin Drainages, were used to compute the PMP values.

6.6.3.3 Drainage Areas

Area 5 RWMS is situated on the lower portion of coalesced alluvial fans that emanate from the Massachusetts Mountains and the Halfpint Range (Figure 6-14). There are four defined drainages to the north, northwest, and northeast of the RWMS that could cause flooding onto the northwest corner of the cap where the GCD boreholes are located. The specific drainages that could contribute flow to the RWMS, as shown in Figure 6-15, are HP3, HP4, HP2, and the basin that is a combination of HP5, HP6, HPFa, and HPFb [Schmeltzer et al., 1993]. The drainage basins to the west and southwest of RWMS, namely HP1a, HP1b, and MM2, are not expected to flow onto the northern portion of the cap where the GCD boreholes are located. However, flooding from HP1a and HP1b were included for the case where the cap is instantly washed away.

6.6.3.4 Local Precipitation

Analysis of the rainfall record at Well 5B produces the general statistics shown in Table 6-10.

6.6.3.5 Conceptual Assumptions about the Future Glacial Climate

The current climate is characterized as being interglacial. Interglacial climatic conditions have occurred at fairly regular intervals over the last 400,000 years, generally lasting from 16,000 to 28,000 years [Brown, 1997a], whereas the glacial periods have generally lasted about 100,000 years [Brown, 1997a]. During the past 400,000 years the climate has been in the glacial state about 80% of the time [DOE, 1998].

Most precipitation in the glacial climate is expected to be winter-type frontal storms. Estimates of long-term mean precipitation for glacial conditions at Yucca Mountain are 200% of the current precipitation, although Brown et al. [1997a] estimated that the long-term mean increase in precipitation would be less than 50%. For the computations in this report, precipitation is assumed to be twice the current precipitation. These conceptual assumptions are summarized in Table 6-11.

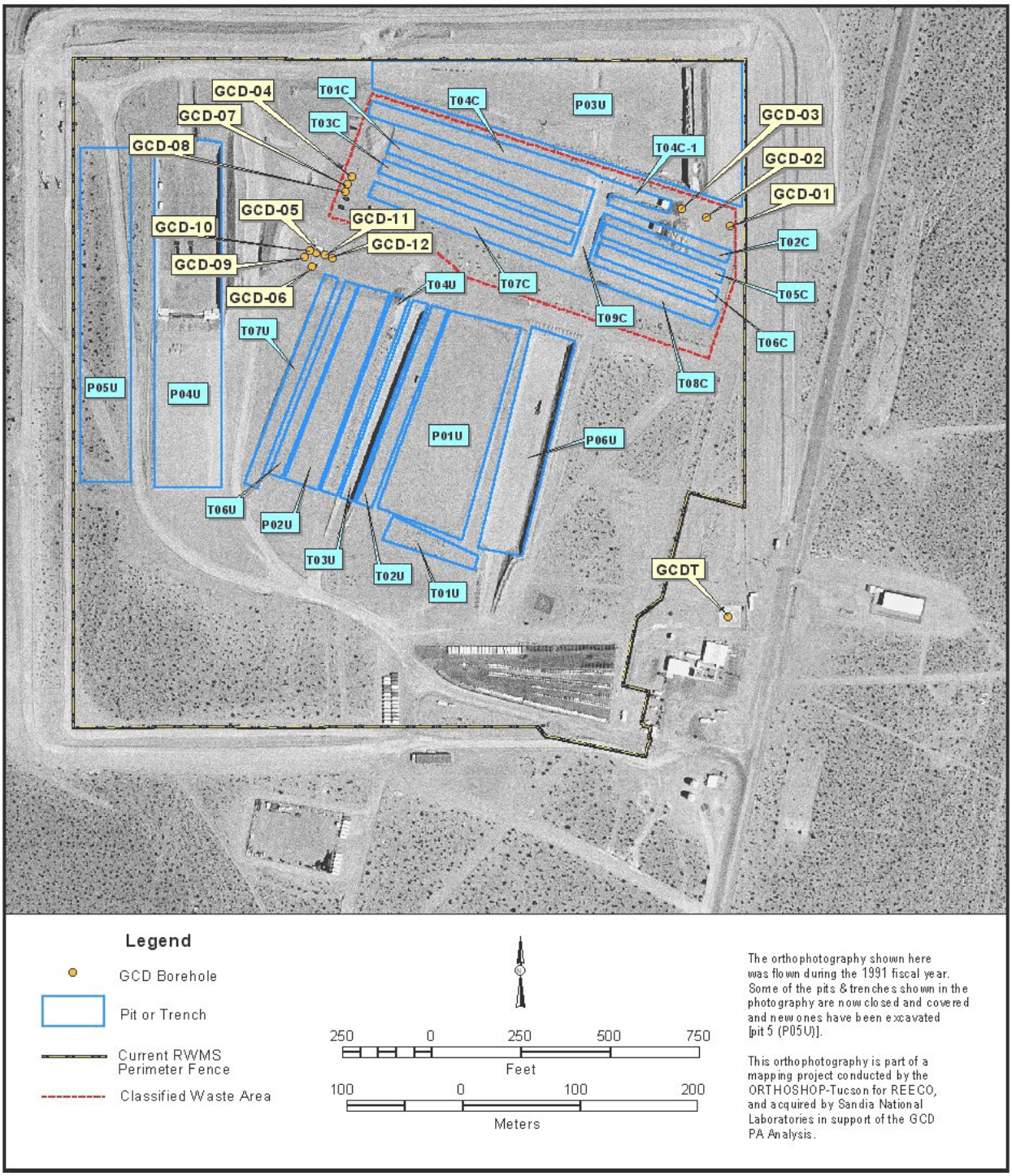

Figure 6-14. Orthophotograph of Area 5 RWMS.

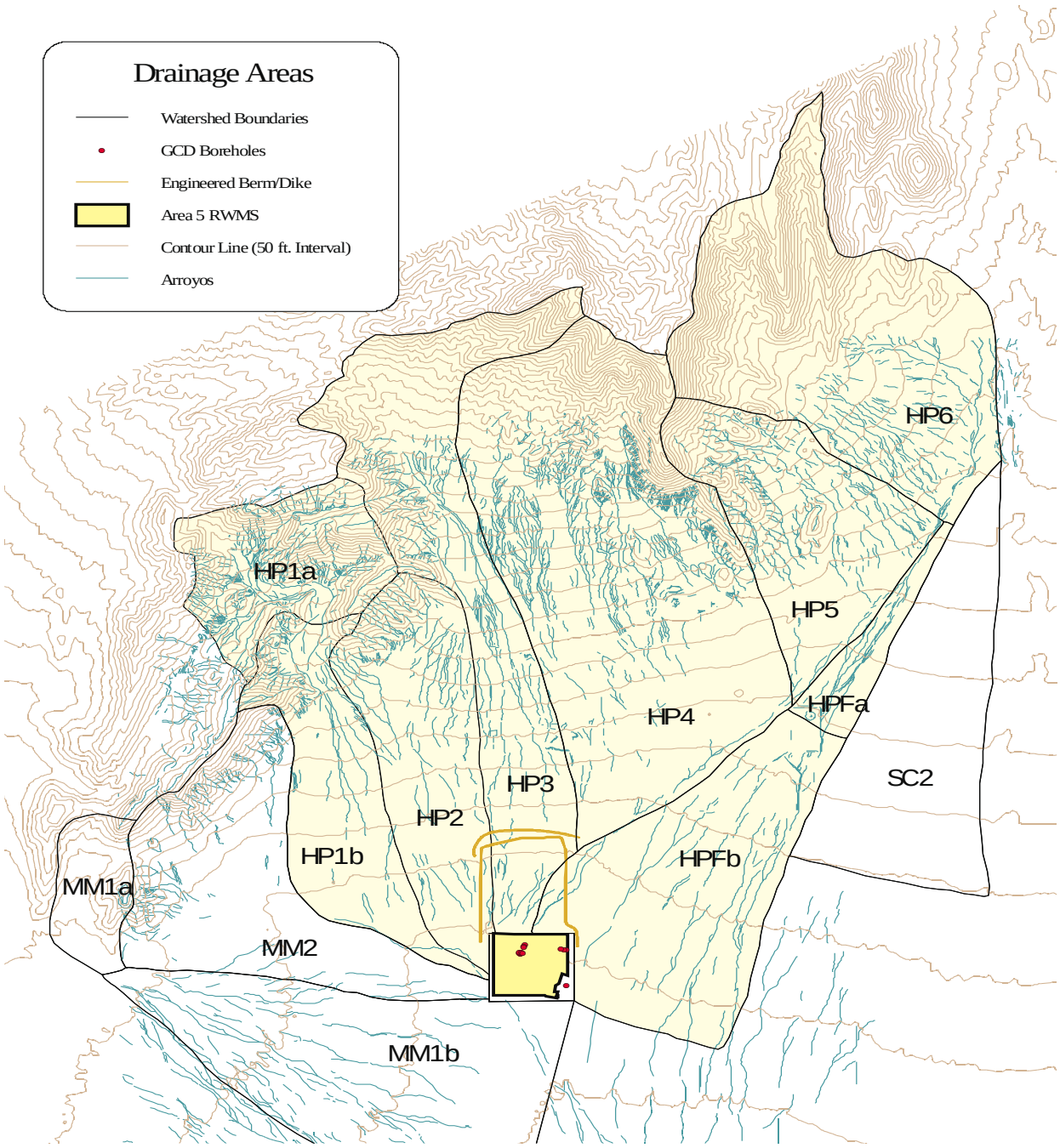

Figure 6-15. The Shaded Drainage Areas Have the Highest Potential to Flood the Northeast Portion of the RWMS. HP2 has some potential. HP1a, HP1b, and MM2 do not have potential to flood the northeast portion.

Table 6-10. Well 5B Precipitation Record

Length of Record:	36 years
Period of Record:	1964–1999
Mean annual precipitation	12.6 cm (4.97 in.)
Maximum Daily Rainfall	4.72 cm (1.86 in.)
Maximum Annual Rainfall	24.6 cm (9.67 in.)
Minimum Annual Rainfall	2.90 cm (1.14 in.)

Table 6-11. Climate Assumptions

Climatic Phenomenon	Current Interglacial Climate	Glacial Climate
Precipitation Pattern	Combination of convective thunderstorms in the summer and frontal storms in the winter.	Dominated by winter type frontal storms
Precipitation amount	~ 12.6 cm (4.97 in) per year	Two times the current precipitation, i.e. ~ 25.2 cm (9.94 in) per year.
Flooding	Floods are typically of short duration and high intensity as associated with summer thunderstorms.	Floods are expected to have a longer duration and a lower intensity as would be associated with a winter frontal storm.

The Yucca Mountain Site Description [DOE, 1998] describes the glacial climate as a situation where the polar front would commonly be over, or not far north, of Nevada; this polar front would dominate temperature and precipitation patterns in the area of Yucca Mountain and Frenchman Flat. Major floods in the glacial climate are expected to look a lot like those resulting from current winter storms and are expected to have characteristics associated with a winter frontal storm–longer duration and lower intensity than thunderstorm floods.

6.6.3.6 Computation of Runoff into Subsidence Features – Intact Cap

The computation of runoff into subsidence features is done for the two opposite bounding conceptual models, both of which have extremely low likelihoods. The future conditions are expected to lie somewhere between these two bounds. The first bounding case is a conceptual model where the cap and subsidence features stay intact for the entire 10,000 years. In this computation mean daily precipitation is used to compute mean daily local runoff and the magnitude and frequency of local precipitation is used to compute runoff from rare events.

The second bounding case assumes: (1) the cap is washed away before the subsidence features are fully subsided, (2) the subsidence features continue to subside after the cap is washed away, and (3) the features lie in the path of a watercourse. In this computation, the magnitude and frequency of precipitation on drainages up slope from Area 5 were used to compute runoff for a series of runoff events ranging from 2- to 200-year frequency.

In reality, the cap is not expected to wash away completely, nor is it expected to stay completely intact. It is expected that it will be eroded by floods emanating from the alluvial fan and by local runoff from the cap itself. The run-on areas for subsidence features will radiate outward and the features themselves will become partially or wholly filled in. As each of the features fill in, fine-grained alluvial sediments will be deposited in the bottom of depressions retarding infiltration of surface water. If an alluvial fan watercourse is "captured" by one of the subsidence features, the bed load and suspended sediment carried by that water course will quickly fill in the feature.

In the first bounding case, the cap stays intact throughout the 10,000-year period. Runoff from the run-on areas for each of the features is considered to be clear water (no sediment). Therefore, subsidence features do not erode or fill in. Runoff from these run-on areas continues at the same rate for the entire 10,000-year period.

The analytical procedure used to compute local runoff into the subsidence features is based on the 36-year period of rainfall at Well 5B. This procedure was to: (1) compute the excess daily precipitation from each day rainfall; (2) use the excess rainfall to compute the volume of runoff into the subsidences feature for each day; (3) compute the mean annual volume of runoff; (4) multiply the mean annual volume of runoff by 10,000 years; and (5) compute and add runoff from rare flood events, including the PMP. The local mean runoff for the glacial climate was computed in a similar fashion, with the exception that each value of daily rainfall was multiplied by two prior to the computation of excess rainfall.

Excess Daily Precipitation

Excess daily precipitation represents the portion of a rainfall event that will run off. This value was computed using the Soil Conservation Service (SCS) Curve Method [SCS, 1972]. In this method, a value for the abstraction of an initial retention of soil moisture is computed on the basis on the SCS curve number. Excess precipitation represents sheetflow runoff into the subsidence features from the run-on area.

$$Q = (P - 0.2S)^2/P + 0.8S \quad (Q = 0 \text{ if } P < 0.2S) \qquad (6\text{-}3)$$

where

- S = $(1000/CN) - 10$ = Potential maximum retention (in.)
- Q = Precipitation excess or runoff (in.)
- P = Cumulative precipitation (in.)
- CN = SCS Curve number

It is assumed that the cap will be constructed from compacted local alluvium and under current climate conditions will have a fair cover of desert brush and under glacial climate will have a piñon-juniper cover. Curve numbers with a medium potential for runoff, representing average antecedent moisture conditions (AMC-II),

Curve Numbers: In the dry conditions that exist at Area 5, computations for average and low frequency events should actually be done with curve numbers that represent the lowest runoff potential (AMC-I).

were used for rainfall events with a recurrence interval less than 100 years, while curve numbers with the highest potential for runoff, representing conditions where the soil is nearly saturated from antecedent rain (AMC-III), were used for rainfall events with a recurrence interval greater than or equal to 100 years. The curve numbers for AMC-II and AMC-III conditions under both current and glacial conditions are shown in Appendix B, Table 3.3.

Volume of Local Runoff

The total amount of runoff that flows into each subsidence feature is based on the rainfall that falls within the feature itself, and on excess rainfall generated by the run-on area immediately up-slope of the feature. If the runoff from the run-on area is significant, the analysis used is runoff plus the whole amount of rainfall that falls into the pit–under the assumption that a pond has been created in the subsidence feature and that the SCS abstraction process is not applicable. If the runoff from the run-on area is not significant, this analysis does not use any of the rainfall in the pit, under the assumption that there is no pond and that rainfall abstraction occurs.

The significance of the excess rainfall is based on a 2 mm (0.08 in) threshold. If the excess rainfall from the run-on area is greater than the threshold value, the runoff within the subsidence feature is the total rainfall multiplied by the area of the feature. If the excess rainfall from the run-on area is less than or equal to the threshold value, the runoff within the subsidence feature is zero.

The 2 mm (0.08 in) threshold that was used represents a four-year rainfall event (24 mm [0.94 in.]) under current climate conditions and a three-year event (33 mm [1.3 in.]) under glacial conditions. The VS2DT code was run to test the validity of this threshold using 40 mm (1.6 in) rainfall over a span of one day. The results of this model run show no downward pathway and that moisture conditions in the top meter (the only affected zone) essentially return to normal within a month (see Appendix B, Attachment B).

The subsidence features and their run-on areas are shown in Figure 6-16 and are summarized in Appendix B, Table 3.6.

Mean Annual Volume of Runoff

Runoff volumes were computed using the 36 years of rainfall at Well 5B as a representative record for the current climate and a simple doubling of the amount of rainfall in each rainfall event as representative of the glacial climate. Under a glacial climate, there would actually be an increase in the number of events. However, for modeling, the number of events was kept the same as the current climate–partly because it is difficult to quantify the actual number of events that would occur, but also because using fewer events with more rainfall per event has a greater potential for creating a downward flux of water in the subsurface than do more frequent events of lesser rainfall. Since the SCS method abstracts a threshold amount of rainfall from each event, a doubling of the rainfall with the same number of events increases the runoff fivefold. If the number of events are doubled, the runoff would be significantly less, since the threshold abstraction is subtracted from each rainfall event.

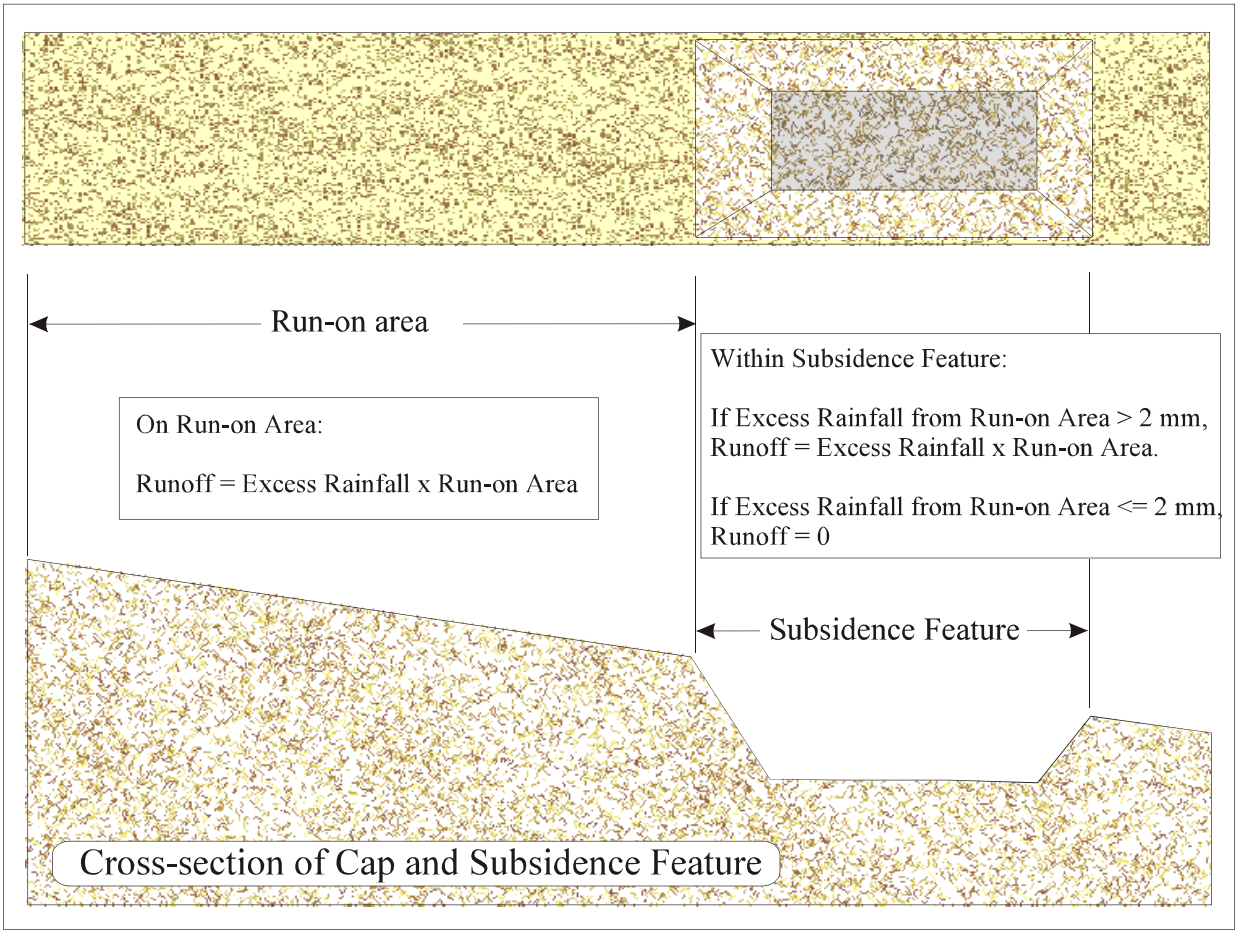

Figure 6-16. Runoff Diagram.

The mean annual volume of runoff is the arithmetic mean of the annual sums for each year of the 36-year period. Table 3.5 in Appendix B presents the mean annual volumes computed for both the current interglacial period and the glacial period.

Runoff from Flood Events

To estimate runoff from rare flood events, the maximum annual 24-hour rainfall events at Well 5B were analyzed and fitted to the Log-Pearson III (LP-III) frequency distribution through the use of the USGS PEAKFQ program [USGS, 1998]. Table 3.6 in Appendix B presents the entire range of LP-III estimated magnitudes and the values for the 95% confidence intervals through 500 years.

Rainfall magnitudes for the 1000-year and 10,000-year rainfall events were estimated graphically.

A synthetic frequency curve was developed to compute rainfall and runoff for rare events in the glacial climate. This curve was based on the Well 5B frequency curve above the 100-year storm and on the previously stated doubling of rainfall at the lower frequencies.

The values used in the computation of total runoff were those for the 100-, 500-, 1000-, and 10,000-year storms. The runoff for these events was computed using the SCS method, as described previously.

Probable Maximum Precipitation

PMP was computed using the methodology set forth in Hydrometeorological Report No. 49 [U.S. Department of Commerce, 1977]. Both local storm and general storm PMPs were computed for each watershed; the properties of these events are presented in Appendix B, Table 3.7. Computation sheets for the local and general storm PMPs are in Appendix B, Attachment C.

The runoff for the PMP was computed using the SCS method, as described previously.

Total Runoff Into Subsidence Features

Runoff into each subsidence feature for both the current climate and the glacial climate was computed by adding: (1) the total volume of mean runoff; (2) the volume of 90 100-year floods; (3) the volume of nine 1000-year floods; (4) the volume of one 10,000-year flood; and (5) the volume of one PMP. These values are presented in Appendix B, Tables 3.8 through 3.11.

These computations show that the mean runoff is significantly more important than rare events in estimating total volume. Hokett and French [1998] and French et al. [1996] also concluded that for estimating infiltration, extreme events are likely to be less important than the more frequent, average events.

6.6.3.6 Computation of Runoff into Subsidence Features – Case 2

In the conceptual model for the second bounding case, a series of events are presumed to happen: (1) the cap is washed away before the subsidence features are fully subsided; (2) the subsidence features continue to subside after the cap is washed away; and (3) the features lie in the path of a watercourse. In this computation, the magnitude and frequency of precipitation on drainages up slope from Area 5 were used to compute runoff for a series of runoff events ranging from 2- to 200-years in frequency.

Subsidence Feature Volumes: The fully subsided volume of each subsidence feature was used in these computations. The expected volume would be much smaller, because the portion of the volume of each feature that had occurred within the cap would have been washed away with the cap.

Runoff from Flood Events

Curve Numbers: In the dry conditions that exist at Area 5, computations for average and low frequency events would more accurately be done with curve numbers that represent the lowest runoff potential (AMC-I).

The same rainfall frequency statistics that were developed in the analysis described in Section 6.6.3.4 were used for these computations. The frequency curve developed for Well 5B was used to estimate rainfall and runoff for the current climate, and the synthetic curve developed for the glacial climate was used to develop rainfall and runoff for the glacial climate. For these computations, the rainfall magnitudes were used to compute runoff from the up-slope watersheds to the north, east, and west of Area 5.

The curve numbers for each watershed for AMC-II and AMC-III conditions under both current and glacial conditions are shown in Appendix B, Table 3.3.

Flooding: In reality, only a partial set of the up-slope drainages would contribute any amount of flow to the subsidence features, and for any given flood event, it is unlikely that each of these drainages would contribute a flood of the same magnitude and frequency at the same time.

In this bounding computation, runoff was assumed to come from the combined up-slope drainages to the north, east, and west of Area 5. Rainfall magnitudes for each frequency were applied to each basin and the computed runoff values were combined to arrive at the total input to the subsidence features.

A series of runoff events were then used to compute the amount of runoff and sediment that would flow into each of the four subsidence features in question: GCD Borehole 1, RWMS TO4C, RWMS PO3U, and RWMS TO7C (Figure 6-16). Each event was assumed to flow first into the feature furthest up-slope, PO3U, and when the flood volume exceeded the capacity of that pit the flood would overflow into the next two features, Borehole 1 and TO4C. When the capacity of those features was exceeded, the flood would overflow into the last feature, TO7C. Floods with recurrence intervals of 2, 5, 10, 25, 50, 100, and 200 years were simulated to occur at those exact intervals, i.e., a two-year flood every two years, a five-year flood every five years, etc. When more than one flood could occur in the same year, only the highest flood was used.

Suspended Sediment Concentration: In the hyperconcentrated sediment flows that can typically occur in the southwestern U.S., sediment concentrations can range from 20% to 45%.

For these computations, each flood event was presumed to carry a 15% volume of suspended sediment [Federal Emergency Management Agency, January 1995]. A volume sediment equal to 15% of the ponded flood volume in each feature was assumed to be deposited in those features during each event. Over time, the capacity of each feature was incrementally reduced in accordance to the amount of sediment deposited. All of the subsidence features were filled with sediment in less than 250 years (Appendix B, Table 3.9).

When the subsidence features are filled with sediment, the accumulation of flood volumes stops, and the infiltration process stops. The total volume of flooding is the same for both the current and the glacial climate, but the time to fill the features with sediment is shorter for the glacial climate, because the glacial flood volumes are larger and hence the sediment loads are larger.

Bed Load: In addition to suspended sediment, floods in the sandy, gravely environment found in alluvial plains carry a large volume of bed load. Bed load is a layer of sand, gravel, and rocks within the channel bottom that moves with the flood. Bed load was neglected for these computations.

6.6.4 Analysis of Flooding

6.6.4.1 Purpose

The purpose of these flooding analyses is to determine the range of flood events that would be expected to occur on the alluvial fan above the Area 5 RWMS, to evaluate the potential of these events to top the cap, and to evaluate the consequences to the GCD boreholes if they did.

6.6.4.2 Method of Analysis

The analytical procedure was to:

1. Compute the magnitude and frequency of flood events that might occur at the Area 5 RWMS using all reasonable estimation methods. The methods used were:

    a) the computation of Probable Maximum Floods (PMF) based on PMP computations;
    b) the estimation of the maximum expected floods based on a flood envelope curves; and
    c) the computations of specific flood magnitudes and frequencies based on regional flood equations.

2. Compute channel depth for the estimated floods.
3. Compute possible freeboard of the Area 5 RWMS cap.
4. Compare cap freeboard with flood depth.
5. Develop assumptions for the consequences of flooding.

The drainages considered in these analyses are shown in Figure 6-15.

6.6.4.3 Flood Analysis

Extreme flood events were estimated for the Area 5 RWMS drainages based on the PMP, flood envelope curves, and regional flood equations.

Computation of Probable Maximum Flood

The PMF for each of these watersheds was computed using HEC Hydrologic Modeling System (HMS) [U.S. Army Corps of Engineers, 1998]. HMS computes the flood hydrograph based on data that defines the watershed and the storm event. The watershed properties presented in Appendix B (Table 4.1) are from Schmeltzer et al. [1993] with updated curve numbers from a recent Bechtel Nevada study [Yucel, 2000]. The storm event used for the PMF is based on the PMP computed using the methodology set forth in Hydrometeorological Report No. 49 [U.S. Department of Commerce, 1977]. Both local storm and general storm PMFs were computed for each watershed; the properties of these events are presented in Appendix B, Table 4.2. Computation sheets for the local and general storm PMPs are in Appendix B, Attachment B.

The local storm PMF and the general storm PMF were both computed assuming that for the current climate, the local storm PMF is most likely to be applicable and for the glacial climate, the general storm PMF is most likely to be applicable. In the current climate, the local storm PMF are those flood events that are produced from convective-type thunderstorms that occur during the summer and early fall. These are the storms that produce the most intense rainfall and the largest peak discharges. In the case of the glacial climate, frontal-type storms are assumed to predominate, and therefore, the general storm PMF would be the correct flood model to use.

Estimation of Maximum Flood Using Flood Envelope Curves

For comparison to the computed PMF values, a second set of maximum flood magnitudes was estimated from maximum discharge envelope curves developed by Christensen and Spahr [1980] and Thomas et al. [1997]. An envelope curve is drawn along the top of all points on a plot of maximum measured floods versus the drainage areas for these floods. The Christensen and Spahr [1980] envelope curve is based on extreme events that occurred in Nevada, Utah, Arizona, and New Mexico. Thomas et al. [1997] developed an envelope curve for gauged watersheds in an area of the southwest that covers eastern Oregon to west Texas. The values from the Thomas et al. [1997] curve are significantly smaller than those from the Christensen and Spahr [1980] curve. This difference may be due to the fact that the data used to develop the Thomas et al. [1997] curve was limited to gauged watersheds. The largest maximum floods from the Christensen and Spahr [1980] envelope curve are 24 to 45% larger than the computed PMF local storm discharges (Appendix B, Table 4.3).

Computations of Flood Magnitudes and Frequencies Based on Regional Flood Equations

The magnitudes of 100- and 500-year floods were computed using three different sets of regional equations. These events were computed as a comparison and cross-check to the computed maximum flood events.

Flood magnitudes of 100-year frequency were developed using equations from by Christensen and Spahr [1980] for Topopah Wash in Jackass Flats, Nevada. This equation is based on the basin drainage area (A) in square miles, the mean basin elevation (E) in feet above mean sea level, and the latitude of the basin minus 35^{o} (L). Since this equation was derived on the basis of

English units, the flood magnitudes were computed in ft^3/s and converted to m^3/s, as shown in Appendix B, Table 6-25.

$$Q_{100} = 11900\ A^{0.55}\ E^{-1.28}\ L^{-1.16} \quad (6\text{-}4)$$

100- and 500-year flood magnitudes were developed using two sets of equations from Roeske [1978] for two regions in Arizona. The equations for Region 1 are based on flood events that occurred in northwestern Arizona, while the equations for Region 2 are based on flood events that occurred in southwestern Arizona. The Region 1 equation is not valid at drainage areas of less than 1.84 mi^2 (4.77 km^2). French and Lombardo [1984] suggested that, although Region 1 is conterminous to Southern Nevada, Region 2 may more closely resemble the NTS Area. The Roeske equations are based on basin drainage area (A) in square miles. Since this equation was derived on the basis of English units, the flood magnitudes were computed in ft^3/s and converted to m^3/s, as shown in Appendix B, Table 4.4.

Thomas et al. [1997] developed regional equations for each of 16 regions from eastern Oregon to west Texas, and from southwestern Wyoming to southeastern California. Frenchman Flat lies in Region 6 - the northern Great Basin region. The equations presented by Thomas et al. [1997] are based on basin area (A) in square miles and mean basin elevation (E) in feet above mean sea level (msl). The 100-year flood was computed for comparison with the other estimated and computed floods using the equation below. Since this equation was derived on the basis of English units, the flood magnitudes were computed in ft^3/s and converted to m^3/s, as shown in Appendix B, Table 4.4.

$$Q_{100} = 20{,}000\ A^{0.51}\ (E/1000)^{-2.3} \quad (6\text{-}6)$$

6.6.4.4 Compute Channel Depths

The widths and depths for each of the flood events were computed using equations developed by Dawdy [1979] and as applied to the Area 5 RWMS by French and Lombardo [1984]. These equations, based on the peak discharge (Q), estimate the top width (T) and the channel depth (y) of the flood peak on the alluvial fan. The computed channel depths and widths are presented in Tables 4.5 through 4.10 in Appendix B.

$$T = 9.5\ Q^{0.4}$$
$$Y = 0.07\ Q^{0.4} \quad (6\text{-}7)$$

6.6.4.5 Aggradation

The alluvial fan that RWMS Area 5 is located on is considered to be an active or aggrading fan; however, it is difficult to predict how much that fan will aggrade over the next 10,000 years. For the flooding bounding case, the highest estimated aggradation was assumed to have occurred in either the current climate or the glacial climate.

While the alluvial fans in the area of the Area 5 RWMS show signs of both active fans and inactive fans, it is assumed most of the aggradation on these fans occurred during the glacial conditions of the Pleistocene.

Surface geology mapping shows that the oldest alluvial fan surfaces at Area 5 RWMS are of Late Pleistocene to Middle Holocene age (~100,000 to 5,500 years ago) and that recent geomorphic activity during the Late Holocene (5,500 years ago to today) has been limited to erosion and deposition along small channels [Snyder et al., 1995]. The age estimates of the surface geologic mapping were corroborated by cosmogenic exposure age dating methods [Caffee et al., 1995]. This supports the assumption that active aggradation occurred during the last Glacial period and that this process has diminished during the current interglacial period.

Aggradation Rates

Although average rates of alluvial fan aggradation at Area 5 RWMS are fairly low, it is reasonable to expect that the rate of deposition has not been constant, but has varied with climatic changes and other factors [French and Lombardo, 1984; Rachocki, 1981]. Computations of average aggradation rates at Area 5 RWMS vary from 33 to 170 mm (1.3 to 6.7 in.) per millennia. French and Lombardo [1984] computed an aggradation rate of 71 mm (2.8 in.) per 1000 years based on an estimated alluvial fan age of 7 million years and a depositional thickness of 490 m (1600 ft). Shott et al. [1998] encountered basalt from about 270 to 300 m (880 to 900 ft) below the surface in wells UE5k and UE5i, and reported the age of the basalt at between 8.4 and 8.6 million years. Computations based on these numbers would indicate an average deposition rate of 32.5 mm (1.28 in.) per 1000 years.

There is an absence of consensus among alluvial fan investigators as to the optimum conditions for alluvial fan development; some researchers favor humid climates while others favor arid or semi-arid environments [Rachocki, 1981].

6.6.4.6 Cap Freeboard

The freeboard of the Area 5 RWMS Cap was estimated by subtracting alluvial fan aggradation (if any) from the original cap height.

Under the assumption that the glacial period will produce a higher aggradation rate, a maximum rate of 6.0 inches per 1000 years has been used for the computation of cap freeboard in the bounding case where floods overtop the cap. Table 4.11 in Appendix B presents the accumulated aggradation by millennia; Figure 6-17 show the relationship between the cap freeboard and the depths of the largest expected floods.

Assumptions Regarding Area 5 Radioactive Waste Management Site Cap and Subsidence Features

1. At year 2170, institutional control will end and the top of the cap will be at 2.0 m (6.7 ft) above the original surface of the alluvial fan.

2. At year 2170, all subsidence features will have been filled in, and the surface of the cap will be flat.

3. For computational purposes, it is assumed that maximum subsidence occurs (instantaneously) one year after control ends, and that the angle of repose for sidewalls is reached within each subsidence feature. Subsidence at the deepest GCD feature is 3 m (10 ft), which would be 1 m (3 ft) below the surface of the alluvial plain. For modeling purposes, it is assumed this occurs at the beginning of this period and that the geometry of the subsidence features remains the same.

4. At any point in time the cap freeboard is computed to be 2.0 m (6.7 ft) minus any accumulated aggradation. Table 4.11 in Appendix B presents the computed cap freeboard for the glacial climate.

5. Engineered barriers up-slope of Area 5 RWMS are ignored.

6. There is no additional landfill north of the present extent of Area 5 RWMS.

Compare Cap Freeboard to Flood Depths

The frequency of flood events that will top the cap is dependent on both the frequency and magnitude of expected flood events and on the freeboard of the cap at the time of the flood. The cap freeboard (the height of the cap above the alluvial fan) is dependent on how much the alluvial fan has aggraded. Although the alluvial fan that RWMS Area 5 is located on is considered to be an active or aggrading fan, it is difficult to predict how much that fan will aggrade over the next 10,000 years.

Figure 6-17 shows the relationship of the cap freeboard to the depths of the maximum floods when high alluvial fan aggradation is combined with the largest expected floods from the envelope curves, the PMF, and the 500-year flood computations. The maximum expected aggradation of 15 cm (6.0 in) per 1,000 years would result in 1.5 m (5.0 ft) of aggradation at the end of 10,000 years. If the minimum proposed cap height of 2.0 m (6.6 ft) is used, the freeboard at the end of 10,000 years would be 0.50 m (1.6 ft). The depth of the largest 500-year flood would not surpass the cap freeboard until about 9,000 years, when the freeboard is less than 0.64 m (2.1 ft).

Although the depth of the largest envelope curve maximum flood would surpass the cap freeboard at about 3,500 years, the recurrence interval of this flood and the PMF is estimated to be well over 10,000 years. Under this bounding case and given this relationship between the cap and the potential floods, there is a possibility that the cap could be topped by 500-year or larger floods during the last half of the 10,000-year period.

6.6.4.7 Consequences of Flooding on the Cap

Rare flood events may top the cap and fill the subsidence features with water, but they will also cause severe erosion and will leave large amounts of sediment, decreasing the capacity of the

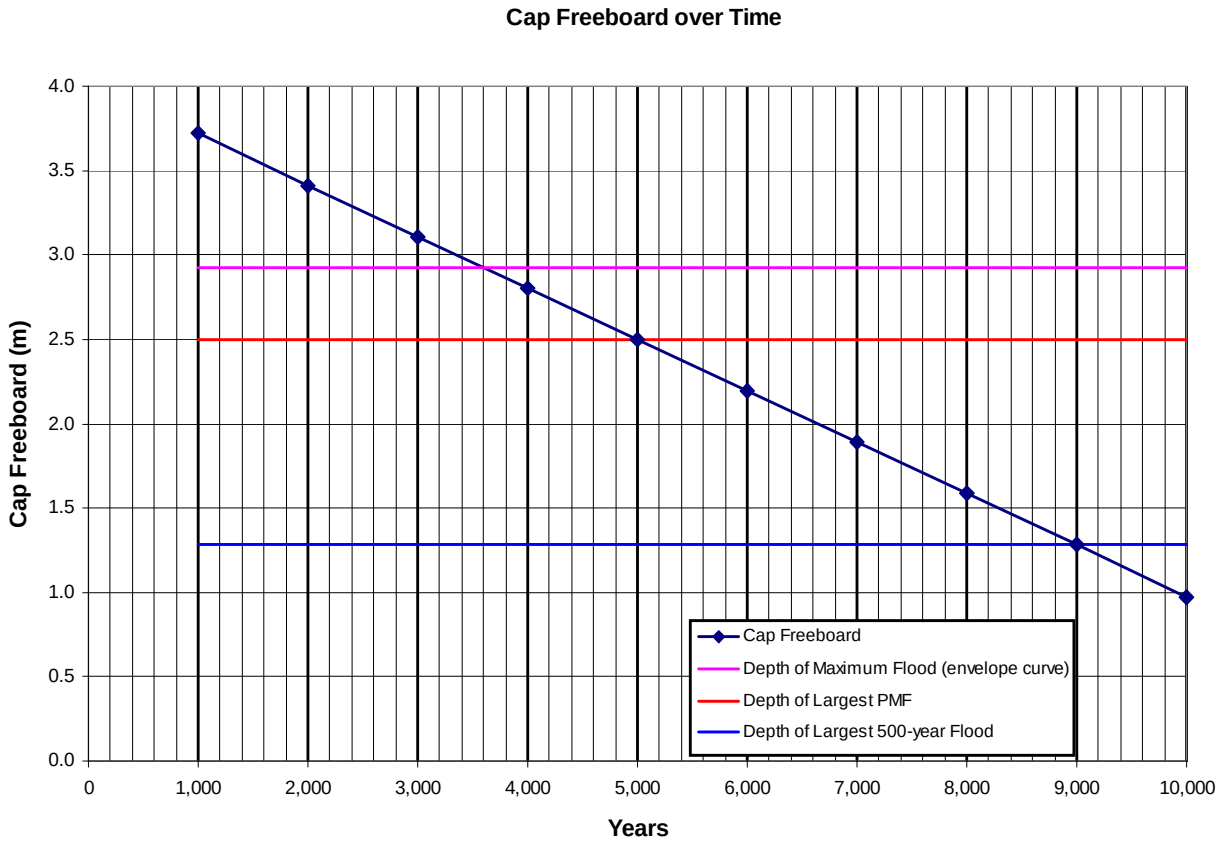

Figure 6-17. Under an Assumed Aggradation Rate of 15 cm (6 in.) per 1000 Years, the RWMS 5 Cap Freeboard Diminishes Relative to the Depths of the Largest Estimated Floods.

features to hold water for infiltration. Although a portion of the flood volume that flows onto the cap could flow into the subsidence features, the features are likely to be filled already with local runoff from the cap. These floods would primarily diminish the capacity of the subsidence features by depositing sediments.

The capability of alluvial fan floods to cause massive erosion and deposition were highlighted in a report by Anstey [1965]; he described an alluvial fan flash flood that deposited 1.2 m (4.0 ft) of debris in some areas and eroded 1.8 to 2.4 m (6.0 to 8.0 ft) deep channels in other areas, moving boulders up to 2.4 m (6.0 ft) in diameter. Hooke [1965] described a similar alluvial fan flash flood in Utah. Beaty [1963] reported one alluvial fan flood that moved 1.5 m (5.0 ft) boulders distances of up to 1.6 to 3.2 km (1.0 to 2.0 mi).

6.6.4.8 Conclusions

The conceptual model of floods eroding and occasionally topping the cap is believed to be far more likely than are either of the two highly unlikely bounding cases, intact cap for 10,000 years or cap completely washed away at 170 years. The results of this flooding model, in terms of water for infiltration, lie somewhere between those two bounding cases. The cap is not expected

to wash away completely, nor is it expected to stay completely intact. It is likely to be eroded by floods emanating from the alluvial fan and by local runoff from the cap itself. The run-on areas for subsidence features will radiate outward and the features themselves will become partially or wholly filled in. As each of the features fill in, fine-grained alluvium will be deposited in the bottom and hence, over time, infiltration will be retarded.

Since subsequent local runoff and overtopping flood events would be filling subsidence features that have diminished capacities, the total volume expected over 10,000 years will be less than the volume calculated for intact cap.

6.6.5 Conceptual Model of Unsaturated Flow

6.6.5.1 Purpose

As discussed in previous sections, the LLW trenches and pits and the GCD boreholes located in the Area 5 RWMS are expected to subside after the end of the institutional control and, as a result, will collect run-off and precipitation in the resulting depressions. The unsaturated flow analysis is therefore designed to address the following questions:

- Will the surface water collected in the subsidence depressions above the GCD boreholes infiltrate into the unsaturated zone and reach the water table within 10,000 years under current or glacial climate conditions?

- Will the surface water collected in the subsidence depressions within the LLW trenches and pits infiltrate into the unsaturated zone and spread laterally far enough to influence the moisture conditions around the GCD boreholes under current or glacial climate conditions?

- Will infiltrating surface water collected in the subsidence depressions above the GCD boreholes interact with infiltrating surface water from the LLW trenches in such a way that water from the GCD boreholes could reach the water table within 10,000 years under current or glacial climate conditions?

In this section, unsaturated flow conceptual models are developed to overestimate the potential of the water collected in the subsidence features to enter the vadose zone and to move downward.

The conceptual model of collecting precipitation and run-off in the subsided features is described in Section 6.6.5.2. The conceptual model for unsaturated flow analysis is discussed in Section 6.6.5.3. The mathematical formulation of the conceptual model and the general modeling approach used in the unsaturated flow analysis are then provided in Section 6.6.5.4. The evaluation of the mathematical model's bias is considered in Section 6.6.5.5. Finally, a summary of all the assumptions that cause the mathematical model to overestimate downward flow is provided in Section 6.6.5.6.

6.6.5.2 Conceptual Model of Collecting Precipitation in Subsided Features

The conceptual model of collecting precipitation in the subsided features represents the link between the subsidence model, the surface water model, and the unsaturated flow model through the specification of the upper boundary conditions of the unsaturated zone model. In this analysis, two conceptual models were considered. The first conceptual model assumes that the cap remains intact for 10,000 years and subsided features collect all of the local runoff from the cap and all precipitation falling in the subsidence feature starting from the end of the institutional control period and lasting for 10,000 years. The second conceptual model assumes that the cap is instantaneously removed at the end of the institutional control period and that the subsided features collect the regional runoff and sediment, as well as local precipitation, until they are totally filled with the sediment. Consequently, the main differences between the two models are in the volumes and frequencies of surface water runoff and the longevity of the subsided features.

Both conceptual models assume that at the end of the institutional control period, the voids no longer exist in the pits, trenches, and GCD boreholes, which, in effect, assumes instantaneous maximum subsidence. In reality, the remaining subsidence will occur gradually over several hundred years and some of the features may not collect the run-on water for a long time after the site closure. However, this assumption is used to maximize the overall volume of runoff into the subsidence features.

Conceptual Model 1 – Intact Cap

Major results of the precipitation and surface water runoff analyses (Section 6.6.3) include the following:

- estimation of the total volumes of surface water focused in the different subsidence features over the next 10,000 years under current and glacial climate conditions;

- estimation of the surface water volumes collected in the different subsidence features due to the low-probability events, such as the PMP, the 10,000-, 1000-, and 100-year storms under current and glacial climate conditions; and

- estimation of the number and volumes of the remaining high-frequency events that focus surface water in the different subsidence features under the current and glacial climate conditions.

A summary of these results is presented in Table 6-12. The following conclusions can be drawn from this table:

- Most of the surface water collected in the subsidence features is from the low-intensity high-frequency events (rather than from the low-probability events).

- The total amount of water focused into subsidence features under glacial climate conditions is significantly greater than the amount of focused surface water under current climate

Table 6-12. Volumes and Numbers of Ponding Events for the Different Subsidence Features from the Precipitation and Runoff Analysis – Intact Cap Conceptual Model

Subsided Features	GCD Borehole 1	Trench TO4C	Trench TO7C	Pit PO3U
Current Climate Conditions				
Total Volume, m^3	**14,869**	**488,220**	**305,145**	**2,764,205**
PMP, m^3	118	2,429	1,427	11,401
10,000-year storm, m^3	32	683	403	3,248
Nine 1000-year storms, m^3	198	4,325	2,567	20,956
90 100-year storms, m^3	1,222	28,406	17,016	141,730
Number of Low Probability Events	101	101	101	101
Total Volume of Low Probability Events, m^3	1,571	35,843	21,412	177,335
Number of Events Other than Low Probability Events	23,333	23,333	23,333	23,333
Total Volume of Events Other than Low Probability, m^3	13,298	452,377	283,733	2,586,870
Glacial Climate Conditions				
Total Run-On, m^3	**54,145**	**2,052,959**	**1,300,445**	**12,071,154**
PMP, m^3	108	2,231	1,313	10,512
10,000-year storm, m^3	28	642	383	3,162
Nine 1000-year storms, m^3	166	4,001	2,409	20,289
90 100-year storms, m^3	1,050	27,513	16,758	144,449
Number of Low Probability Events	101	101	101	101
Total Volume of Low Probability Events, m^3	1,352	34,387	20,863	178,412
Number of Events Other than Low Probability Events	35,833	35,833	35,833	35,833
Total Volume of Events Other than Low Probability, m^3	52,793	2,018,565	1,279,582	11,892,742

conditions; four times greater for GCD Borehole 1 and 4.5 times greater for trench TO4C. Consequently, assuming that the glacial climate will be established at the end of the institutional control period and will remain during throughout the 10,000 years will result in overestimating the infiltration flux.

The analysis of precipitation and runoff has also demonstrated that the number of high-frequency events over 10,000 years is very large (see Table 6-12). For example, under glacial climate conditions there would be 35,833 events that would result in accumulation of some volume of surface water within trench TO4C. A number of these events result in such shallow ponding

depths that it is not practical or necessary to simulate all of them. As an example, a volume of surface water equal to 10 m^3 evenly distributed over the 2169 m^2 (23350 ft^2) area of the Trench TO4C bottom would produce a pond with a depth of 0.5 cm (0.02 in).

The following approach was used to overestimate the infiltration flux on one hand while attempting to minimize computational and modeling effort on the other hand. Instead of simulating every single event, each with different volumes and spacing in time, a smaller number of events having some average volume and spaced evenly in time was simulated.

The number of events to be simulated, n_p, was calculated as the number of ponding events that have volumes equal to or greater than the median volume, $V_{50\%}$. This means that 50% of all the ponding events have a volume equal to or greater than $V_{50\%}$ and 50% have a volume less than $V_{50\%}$. The relationships between the frequencies and cumulative volumes of the ponding events are shown on Figures 6-18 and 6-19. Note that $V_{50\%}$ is equal to 109 m^3 (3850 ft^3)for trench TO4C and $V_{50\%}$ is equal to 1.7 m^3 (60 ft^3) for the GCD Borehole 1.

The volume of an average ponding event to be simulated, V*av*, and the average frequency of ponding, *fp*, were calculated as follows:

$$Vav = Vtot/np \tag{6-8}$$

$$fp = 10{,}000/n_p \tag{6-9}$$

where *Vtot* is the total volume of surface water captured by the subsidence feature over 10,000 years, excluding low-probability events. This approach accounts for all the surface water accumulated in the subsidence features over all 10,000 years and, thus, overestimates the infiltration flux. In reality, many small ponding events would dry off due to evaporation from the open water and the land surface before any infiltration occurs.

The information on average ponding volumes and frequencies for trench TO4C and for GCD Borehole 1 is summarized in Table 6-13 for the glacial climate conditions. The average ponding event in the subsided trench TO4C (*Vav* = 227 m^3 (8020 ft^3)) and in the subsidence feature above the GCD Borehole 1 (*Vav* = 5.9 m^3 (210 ft^3)) would occur every 1.125 years.

The low-probability events could be spread out over the entire simulation period with a frequency corresponding to their probability of occurrence. However, in order to overestimate the infiltration flux, the most significant events were placed at the beginning of the simulation. That is, the ponding event corresponding to the PMP was specified at time zero. The ponding corresponding to the 10,000-year storm was specified at time of 1.125 years. The ponding corresponding to the first of nine 1000-year storms was specified at time equal to 2.55 years. The other low-probability events were simulated as shown in Table 6-13.

With the volume and the frequency of the ponding events defined, the representation of this event will depend on the subsidence feature geometry and model dimensionality.

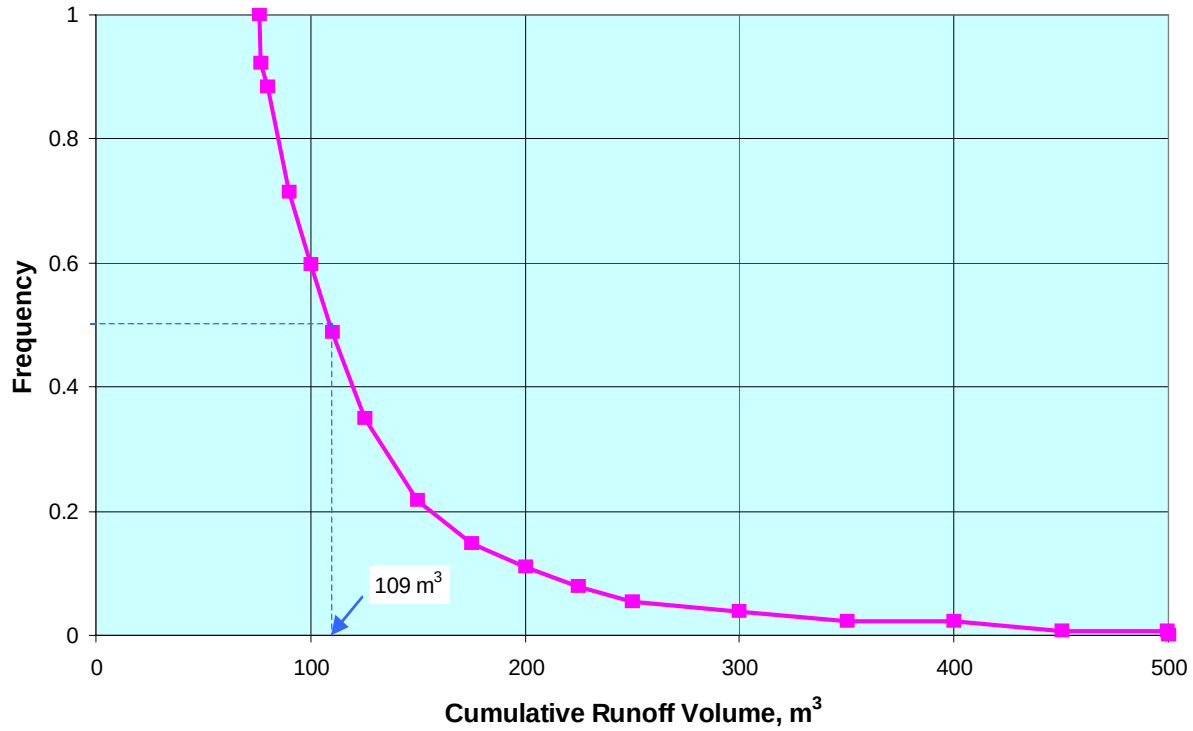

Figure 6-18. Frequencies and Volumes of Ponding Events in Subsided Trench TO4C Under the Glacial Climate. Conceptual Model 1 – Intact Cap.

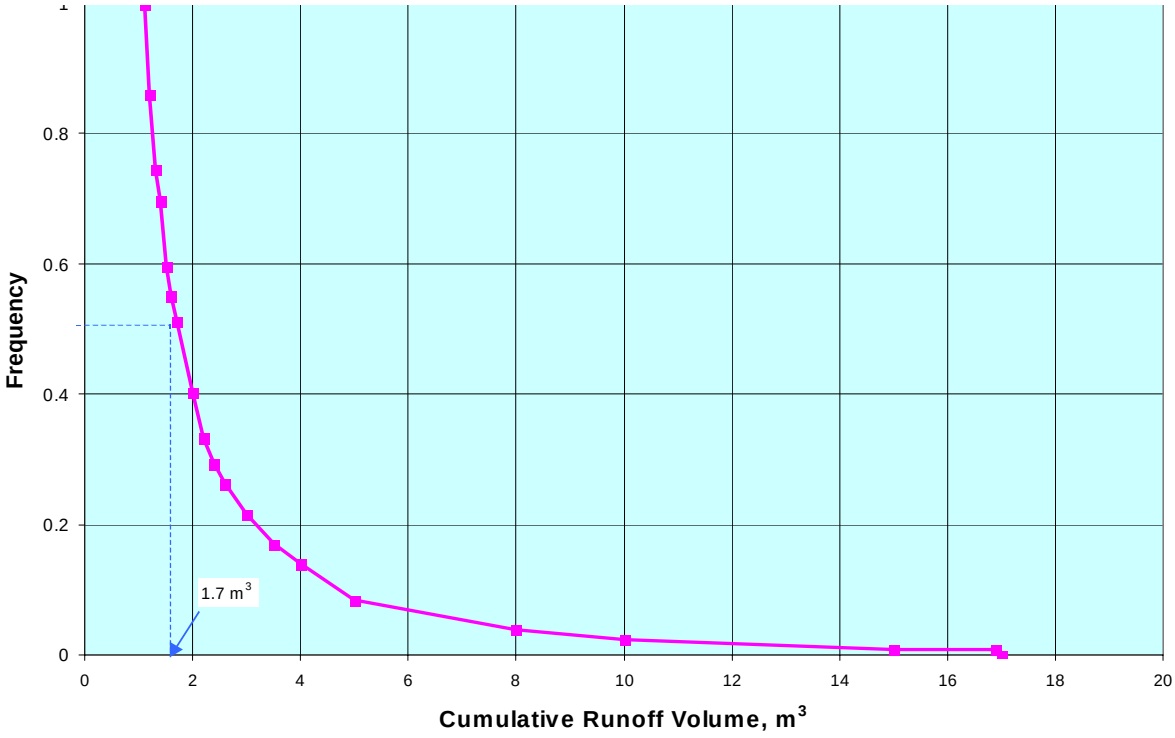

Figure 6-19. Frequencies and Volumes of Ponding Events in Subsidence Feature Above GCD Borehole 1 Under the Glacial Climate. Conceptual Model 1 – Intact Cap.

Table 6-13. Simulated Frequencies, Volumes, and Durations of the Different Ponding Events – Intact Cap Conceptual Model

Type of Event	Frequency, yrs^{-1}	Event Volume, m^3	Event Duration, d
Trench TO4C			
PMP	0.0001	2,231	1.25
10,000 year storm	0.0001	642	0.36
1,000 year storm	0.0009	445	0.25
100 year storm	0.009	306	0.17
Average event	0.889	227	0.13
GCD Borehole 1			
PMP	0.0001	59	5.42
10,000 year storm	0.0001	28	4.87
1,000 year storm	0.0009	18	3.13
100 year storm	0.009	12	2.09
Average event	0.889	5.9	1.03

The subsided features above the GCD boreholes are cone-shaped and are modeled with the quasi-three-dimensional model in radial coordinates (see Section 6.6.5.3 for details). All ponding events are assumed to instantaneously fill these features to a depth that corresponds to the event volume. The duration of the ponding event t_p is calculated as:

$$t_p = Vp/(Sp*Ksat) \quad (6\text{-}10)$$

where *Vp* is the volume of the average or low-probability ponding event, *Sp* is the surficial area associated with the portion of the cone-shaped depression that is filled with water, and *Ksat* is saturated hydraulic conductivity of the alluvial deposits. A prescribed flux boundary condition is then specified along the depression walls for a period of time equal to t_p to simulate the infiltration process.

The subsided trench is modeled as a two-dimensional vertical cross-section along the trench (see Section 6.6.5.3). Surface water is assumed to instantaneously fill the subsidence depression within the trench to the depth d_p which corresponds to the volume of the ponding event. The duration of the ponding event t_p is calculated as:

$$t_p = d_p/Ksat \quad (6\text{-}11)$$

A prescribed flux boundary condition is specified along the bottom of the trench for the period of time equal to t_p to simulate the infiltration process. The volume of water introduced to the system with each ponding event v_p is defined as:

$$v_p = V_p/w, \quad (6\text{-}12)$$

where *w* is the trench width in the direction orthogonal to the cross-section.

In this manner, each ponding event almost instantly introduces a volume of water equal to *Vp (GCD borehole)* or to v_p (trench) to the unsaturated system. Table 6-13 provides the duration of the average and low-probability events for these features.

Conceptual Model 2 – No Cap

The following results from the precipitation and runoff analysis (Section 6.6.3) were used to develop the conceptual model of collecting precipitation in the different subsided features assuming no cap:

- the time required to fill in the subsidence features with sediment; and
- the total volumes of water accumulated within the subsided features and the timing and volume of each ponding event under current and glacial climate conditions.

A summary of these results is presented in Table 6-14. Note that the total volume of the surface water accumulated in a specific subsidence feature under the current climate conditions is the same as under the glacial climate conditions. However, the time it takes to fill the features with sediment is different under current and glacial climate. Specifically, subsidence features fill with sediment faster under glacial climate conditions. For example, 37,413 m^3 (1,321,200 ft^3) of water would be captured within the subsided Trench TO4C during 220 years assuming the current climate or during 175 years assuming the glacial climate. In other words, 37,413 m^3 of water carries the amount of sediment required to fill the subsidence depression associated with TO4C.

Table 6-14. Volumes of Ponding Events and Lifetimes of the Different Subsidence Features from the Precipitation and Runoff Analysis – No Cap Conceptual Model

Subsided Features	GCD Borehole 1	Trench TO4C	Trench TO7C	Pit PO3U
Current Climate Conditions				
Total Volume, m^3	393	37,413	24,967	478,453
Life Time, yrs	168	220	236	224
Glacial climate Conditions				
Total Volume, m^3	393	37,413	24,967	478,453
Life Time, yrs	125	175	178	190

Introducing the same amount of water into the vadose zone in a shorter period of time will result in a higher downward flux, since there will be less time for the soil to dry between the ponding events. Consequently, assuming glacial climate conditions provides an upper bound or screening estimate of the downward flux.

The total volumes of water accumulated in Trench TO4C and GCD Borehole 1 under the glacial climate conditions assuming no cap (Conceptual Model 2) were compared to the corresponding total volumes of water accumulated assuming intact cap (Conceptual Model 1).
In the case of Trench TO4C, the total volume of water associated with Conceptual Model 2 is 18% of the total volume associated with Conceptual Model 1. However, the average intensity of precipitation/runoff events into the trench, and therefore into the vadose zone, is higher for Conceptual Model 2 (214 m^3 (7560 ft^3) versus 202 m^3 (7130 ft^3) for Conceptual Model 1). Therefore, it is difficult to assess *a priori* which model will result in the most downward flow. Given the higher intensity events of Model 2 and numerous other assumptions which cause both models to overestimate infiltration, Trench TO4C under the glacial climate conditions assuming no cap (Conceptual Model 2) was chosen as the screening model.

For the GCD boreholes, the total volume in Conceptual Model 2 is less than 1% of the total volume in Conceptual Model 1. In addition, the average intensity of introducing water into the vadose zone is much lower in Conceptual Model 2 (3.1 m^3/year (110 ft^3/yr)) than in Conceptual Model 1 (5.3 m^3/yr (190 ft^3/yr)). Therefore, GCD Borehole 1 was modeled using only Conceptual Model 1 (intact cap) under only glacial climate conditions.

The data used to estimate the volume of collected precipitation and runoff in the subsided Trench TO4C assuming no cap are presented in Appendix B, Table 5.4. The first ponding in the subsided trench occurs 25 years after the end of the institutional control period. Then, 59 ponding events occur over the trench lifetime (175 yrs). However, most of the water (over 99%) is introduced over the first 114 years by 33 ponding events. The remaining 26 ponding events span the next 44 years and add less than 1% of the total volume.

The following approach was used to overestimate the downward flux:

- The first of the 33 ponding events that occur prior to 114 years was assumed to occur at the beginning of the simulation (time zero) instead of at 25 years, as indicated in Appendix B, Table 5.4. The remaining 32 events occurred at the time given in Appendix B, Table 5.4 minus 25 years.

- The 26 ponding events that occur after 114 years were combined into two ponding events with the time between them equal to one year (the smallest frequency observed). The first of these events was assumed to occur one year after the first 33 events. Six of the 26 events were combined into a single event with a total volume of 180 m^3 (6400 ft^3). The remaining 22 events were combined into a single event with a total volume of 106 m^3 (3740 ft^3).

As a result, the volume of 37,410 m^3 (1,321,000 ft^3) is introduced into the vadose zone during the first 91 years of the simulation, instead of 175 years. The proposed distribution of the ponding volumes over the time is shown on Figure 6-20. The duration of each ponding event was calculated using Equation 6.6.5.3. The maximum duration of a ponding event was three days.

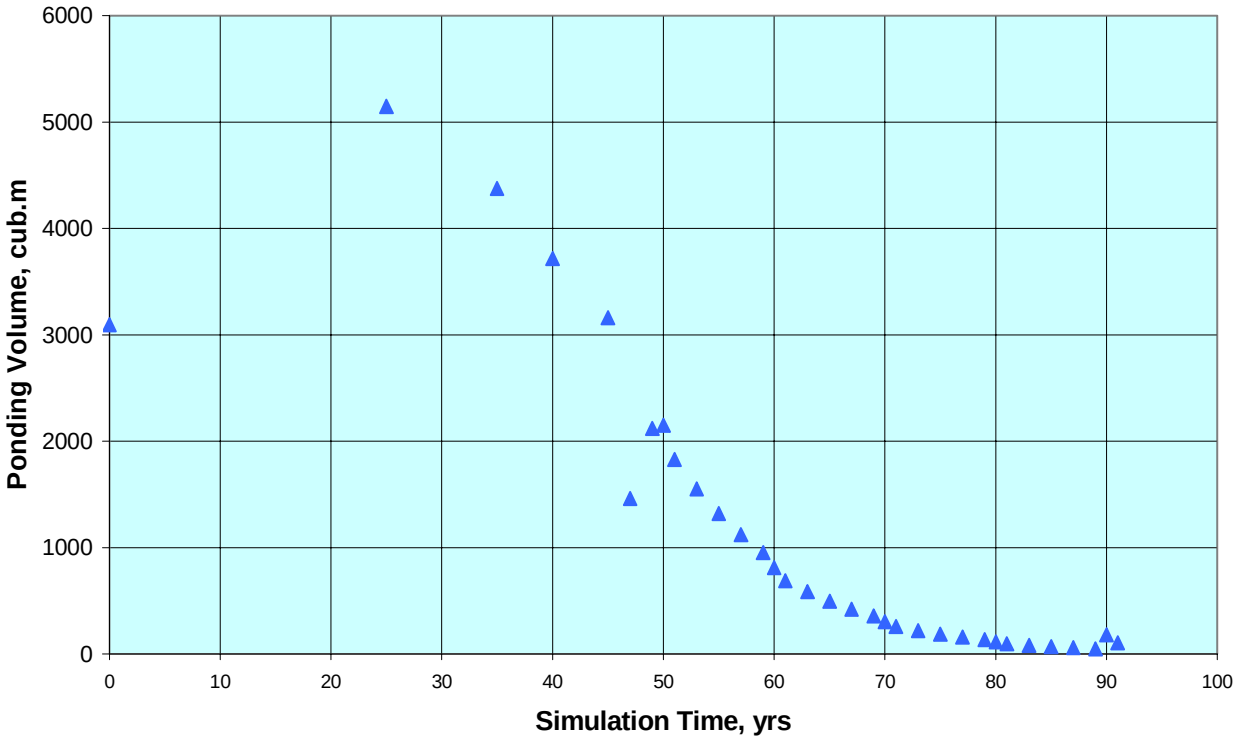

Figure 6-20. Volumes of Ponding Events in the Subsided Trench TO4C. Conceptual Model 2 – No Cap.

6.6.5.3 Unsaturated Zone Conceptual Model

The following concepts summarize the current state of knowledge about the vadose zone:

- The unsaturated zone at the site is very dry from the land surface all the way to the aquifer. Increases in moisture content occur only in close proximity to the water table. No groundwater recharge is occurring under the current climate conditions. All precipitation falling onto the undisturbed land surface at the site gets recycled by evaporation and evapotranspiration processes that occur within the top 2 m (7 ft) of soil. Thus, fluctuations in moisture contents are only observed within this shallow depth.

- The absence of spatially-distributed groundwater recharge during a significant period of time (in the order of the past 100,000 years) followed by a long drying out period has resulted in upward advection and evaporation of pore water from the upper part of the unsaturated zone to a depth of approximately 35 m (115 ft). Even though the upward pressure gradient is large, the upward movement is very slow due to the low moisture content and the correspondingly low unsaturated hydraulic conductivity. The velocity of the upward movement is currently estimated to be less than 0.4 mm/yr.

- Downward moisture movement currently occurs only at depths below 80 m (262 ft) from the land surface. The pore water encountered at this depth is believed to be surface water from

the previous climatic conditions that is moving downward very slowly. A transition zone with zero potential is located between the depth of 35 m (115 ft) and 80 m (262 ft). No moisture movement occurs in this transition zone.

- The unsaturated zone is made up of heterogeneous alluvial deposits. However, no extensive layers or anisotropy have been observed. Thus, the alluvium can be considered homogeneous and isotropic for modeling purposes.

- Among the physical parameters of the alluvium, the most important for the unsaturated flow simulation are: saturated porosity, residual moisture, saturated hydraulic conductivity, and parameters that describe functional relationships between moisture content and pressure head (water retention curve) and moisture content and unsaturated hydraulic conductivity. Detailed discussions of these parameters, including their probability distribution functions for the Area 5 RWMS, are provided in Shott [1998] and in Appendix D.

The above concepts form the basis for the development of the conceptual model and parameters used in simulating unsaturated flow resulting from infiltration of water collected in different subsided features.

Unsaturated Zone Parameters

Due to the screening character of the calculations and the significant computational effort needed to incorporate probabilistic representations of the unsaturated zone, only mean parameter values were used. Issues related to the sensitivity of the model to these parameter values are considered in Section 6.6.8.

The hydraulic conductivity characteristic curve was defined using Mualem model [Mualem, 1976]:

$$K(S_e) = K_{sat} S_e^1 \left[1 - \left(1 - S_e^{1/m} \right)^m \right]^2 \qquad (6\text{-}13)$$

where K_{sat} is saturated hydraulic conductivity, S_e is the effective saturation, and *l* and *m* are fitting parameters.

The moisture retention curve was described using van Genuchten relationship [van Genuchten, 1978]:

$$S_e = \frac{\theta - \theta_r}{\theta_S - \theta_r} = \frac{1}{\left[1 + (\alpha\psi)^n \right]^m}, \quad m = 1 - 1/n \qquad (6\text{-}14)$$

where Ψ is the pressure head, θ_r is residual moisture, θ_s is saturated porosity, and α and *n* are fitting parameters.

The unsaturated zone parameter values are summarized in Table 6-15. The mean parameter values are based on the data collected for the wells AP-1, AP-2, RP-1, and RP2. The actual measurements in these wells and the method used to fit these measurements into the van Genuchten function and into the Mualem function are discussed in Appendix D.

The mean parameter values of the distributions developed in Shott et al., [1998] are provided in Table 6-15 for the sake of comparison. The last two columns of Table 6-15 list the unsaturated zone parameters used in modeling unsaturated flow around the U5a Crater [Hokett and French, 1998] and around the Cambric Trench [Ross, 1994]. As shown in Table 6-15, the mean parameter values are comparable and fall within a relatively narrow range.

Table 6-15. Summary of the Unsaturated Zone Parameter Estimates

Unsaturated Zone Parameter	Notation Units	Mean Parameter Value	Parameter Value from Shott et al. [1998]	Parameter Value from Hokett [1998]	Parameter Value from Ross [1994]
Saturated Hydraulic Conductivity	K_{sat} m/d	0.82	0.72	3.5	0.54
Residual Moisture Content	θ_r unitless	0.06	0.065	0.057	0.084
Saturated Moisture Content	θ_s unitless	0.33	0.36	0.41	0.33
van Genuchten Fitting Parameter	α cm^{-1}	0.071	0.036	0.124	0.018
van Genuchten Fitting Parameter	n unitless	1.4	1.94	2.28	2.36

The Atmospheric Boundary

The atmospheric boundary, or the upper boundary of the unsaturated zone, is the subsided land surface. This section discusses potential evaporation (PE) and potential evapotranspiration (PET) from this boundary.

Evaporation estimates for use in the unsaturated flow modeling were based on average monthly bare soil PE estimates and an annual PET estimate for the Area 5 RWMS by Levitt et al., [1998]. Using the Penman equation, the estimated average annual PET was 156.8 cm/yr (61.73 in/yr). Monthly estimates of PE were calculated using the computer code CREAMS (Levitt et al., [1998]). The PE rates calculated by CREAMS were then adjusted by Levitt et al. to sum to the annual PET rate calculated from the Penman equation. These adjusted values are the basis for the values used in the subsidence analysis unsaturated flow modeling.

Under glacial conditions the climate will be cooler and wetter. As a result, PET may not significantly change. To assess this statement, analog sites in Boise, Idaho and Golodnaya Step, Ukraine were chosen to represent Area 5 under glacial climate conditions. PET was analyzed for these analog sites and results were found to be similar to the estimates of annual PET/PE for the GCD site. Consequently, the current PET rates were used for modeling glacial climate conditions. The sensitivity of the unsaturated flow model to these rates is considered in Section 6.6.7.

This modeling effort assumes only evaporation from the land surface and neglects plant transpiration. Ignoring plant transpiration underestimates the amount of water that is potentially removed from the subsurface and therefore overestimates infiltration into the vadose zone. Because plant transpiration is not included in the evaporation estimate, uncertainty related to the representation of different plant communities, especially under glacial climate conditions, need not be considered. In addition, overestimating infiltration is in line with the screening nature of the calculation.

Other Flow Boundaries and Dimensionality

The lower boundary of the unsaturated zone is the water table which is located at the depth of approximately 236 m (774 ft) below the land surface. It was assumed that the location of this boundary will remain constant over the next 10,000 years. This will be true in the absence of significant areal recharge to the region. According to the simulation results of the Death Valley regional flow model for the past, current, and glacial climate conditions [D'Agnese et al., 1999], there will not be areal recharge in the Frenchman Flat over this time period.

There are no natural boundaries that would limit the extent of the unsaturated zone in horizontal plane anywhere in the vicinity of the site. Assuming that there will be percolation of water from the subsided features, the horizontal boundaries should be placed outside of the zone of influence of the moving moisture front. However, in simulations horizontal boundaries were placed in vicinity of the subsided features to limit the horizontal spread of the moisture in order to overestimate downward flow.

Given that the subsided features above the GCD boreholes are assumed to be cone-shaped, flow was considered within a cylinder using a quasi-three-dimensional model in radial coordinates. Using a principle of symmetry of the flow within such a cylinder, the modeling domain can be defined as a half cylinder, as shown in Figure 6-21.

The most adequate representation of the subsided features within the trenches and pits would be with a three-dimensional model in Cartesian coordinates. However, the challenge of this modeling effort exceeds by far its purpose and possible outcome. Therefore, a two-dimensional vertical cross-sectional model was used instead (Figure 6-22). Such a two-dimensional model assumes that the trench/pit has infinite extent in the third direction or, in other words, an infinite width. This assumption provides an overestimation of the downward and lateral flow. The symmetry of the flow can be used in this case as well to model only one half of the domain. The no-flow symmetry boundary is placed in the middle of the trench, as shown in Figure 6-22.

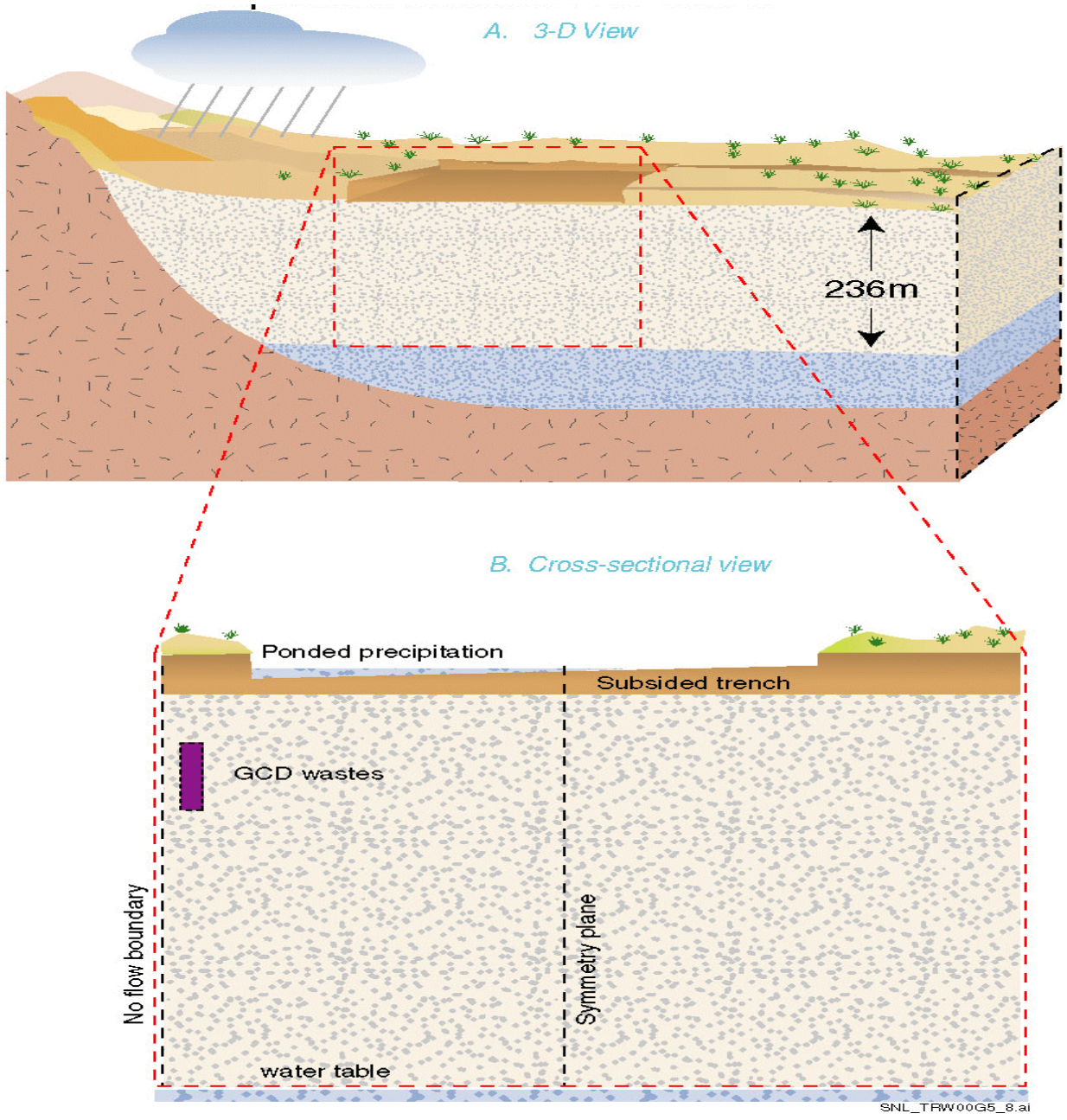

Figure 6-21. Conceptual Representation of Modeling Domain for Depression within the LLW Trench.

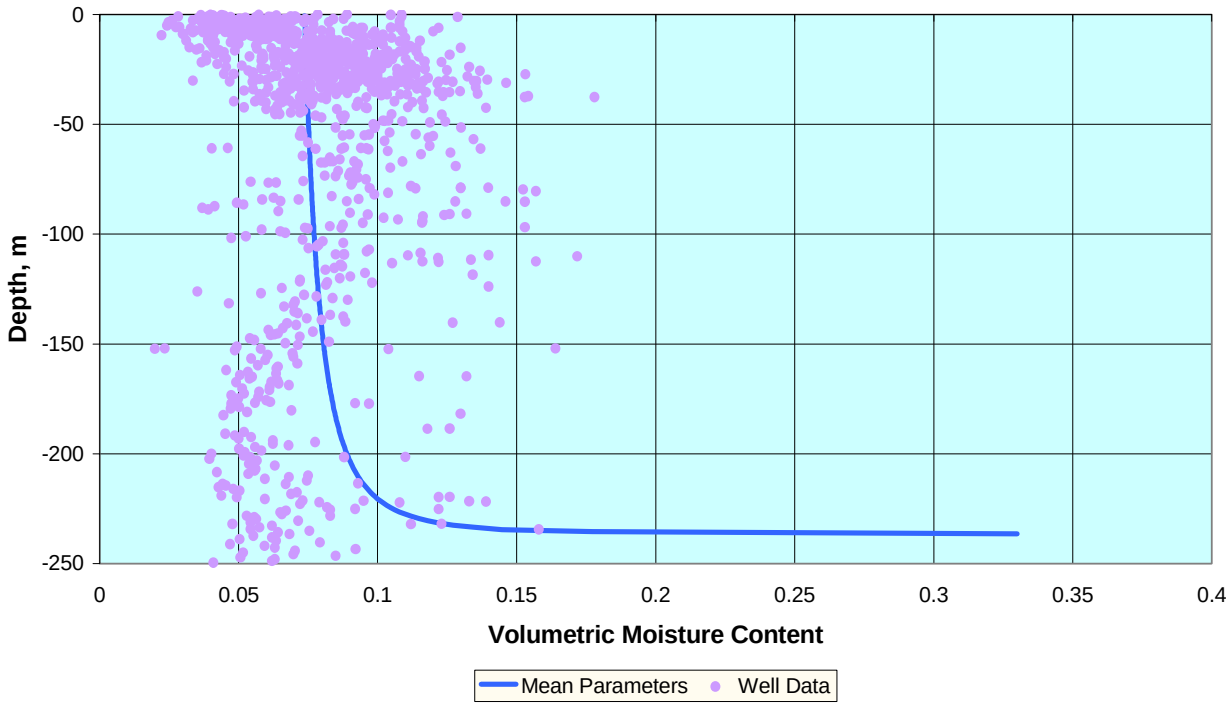

Figure 6-22. Moisture Profile for Calculated Equilibrium Conditions and Site Characterization Data.

Initial Conditions

The initial flow conditions are prescribed in terms of pressure heads or moisture contents within the modeling domain. The prescribed initial conditions are those that are assumed to exist at the end of the institutional control period. Since DOE intends to fill all subsidence features as they form, no collection of precipitation is anticipated in subsidence features before the end of the institutional control period. As a result, the initial distribution of moisture/pressure heads would be similar to that observed today. This distribution of moisture corresponding to the drying conditions was described above. However, for the subsidence modeling effort, an equilibrium profile was used instead. This equilibrium profile implies steady-state conditions within the system with zero velocities (i.e., no water flow) in any direction. In this case, introducing water into the system will immediately change the equilibrium and generate downward flow. On the other hand, Area 5 vadose zone data indicate an upward flow, or "drying" profile. Introducing water to a vadose zone demonstrating upward flow would not generate the downward flow until the upward gradient is reversed. Thus, by ignoring the upward flow profile and starting with the equilibrium profile, downward flow is overestimated. This approach supports the screening nature of the calculation.

6.6.5.4 Mathematical Representation of the Unsaturated Flow Conceptual Model

The mathematical representation of the unsaturated flow conceptual model and the method of modeling the unsaturated flow are described below.

Mathematical Formulation

Changes that are going to occur at the upper boundary of the unsaturated zone due to collection of precipitation in subsidence features will result in changes in pressure and moisture in the vadose zone. For the subsidence analysis, the Richards' equation [Richards, 1931] is used to simulate changes in moisture and pressure within the 2-D Cartesian coordinates unsaturated flow domain. This equation can be written as:

$$\left[K(\psi)\frac{\partial\psi}{\partial x}\right]+\frac{\partial\psi}{\partial x}\left[K(\psi)\left(\frac{\partial\psi}{\partial z}+1\right)\right]\frac{\partial\psi}{\partial z}=C(\psi)\cdot\frac{\partial\psi}{\partial t}$$
$$C(\psi)=\frac{\partial\theta(\psi)}{\partial\psi} \qquad (6\text{-}15)$$

where ψ is the pressure head, $K(\psi)$ is hydraulic conductivity characteristic curve, $C(\psi)$ is specific moisture capacity, and $\theta(\psi)$ is the moisture retention curve. A similar equation can be written for quasi-three-dimensional flow (i.e., radial coordinates).

The relationship between the total head h and the pressure head ψ is defined by the formula:

$$h = \psi + z \qquad (6\text{-}16)$$

Equation (6-12) assumes the isothermal conditions in the flow domain. As shown in Shott et al. [1998], the thermal gradient in most of the unsaturated zone is upward and very small and can be excluded from the screening calculations. The thermal gradient within the upper portion of the unsaturated zone can be upward or downward, but influences only the thin near-surface layer [Shott et al., 1998].

6.6.5.4 Computer Code used to Simulate Unsaturated Groundwater Flow

The computer code VS2DT [Lappala et al., 1987] was selected for modeling unsaturated flow. This code is well known and tested, widely used, can handle strong nonlinearity, and, most importantly, allows for numerical implementation of the conceptual models described above. The simplified way that VS2DT simulates evaporation and plant transpiration results in underestimating evapotranspiration flux and is appropriate for this screening approach.

The code solves the Richards' equation using a finite difference method. The form of the nonlinear equation solved for each finite difference grid block within the flow domain is as follows [Lappala et al., 1987]:

$$v\left\{\rho\left[C_m+sS_s\right]\right\}\frac{\partial H}{\partial t}-\rho\sum_{k=1}^{m}A_k K_{sat} Kr(\psi)\frac{\partial H}{\partial n_k}-\rho q v=0 \qquad (6\text{-}17)$$

where H is total head, v is the volume of the porous medium confined within the grid block, ρ is liquid density, s is liquid saturation, C_m is specific moisture capacity, S_s is specific storage, K_{sat} is saturated hydraulic conductivity, $Kr(\psi)$ is the hydraulic conductivity characteristic curve, q is the volumetric source-sink term accounting for liquid added to $(+q)$ or taken away from $(-q)$ the volume v, n_k is a direction normal to the face k, A_k is the area of the k-th face, and m is the number of the corresponding face of the grid block.

The following boundary conditions are implemented in the code.

- Liquid flux across the boundary $\hat{u}_k$ in the direction n:

$$\rho \hat{u} k = f_1, \left(x, t, \nabla H, \psi \right)_K \tag{6-18}$$

where f_1 is a general function depending on the boundary location x, time t, gradient in total head ∇H across the face k and the pressure head ψ at the face k.

- Total head H_k along the boundary:

$$H_k = f_2 \left(x, t, \psi \right)_k \tag{6-19}$$

where f_2 is a general time-dependent function.

Evaporation and infiltration are the boundary conditions that cannot be specified in the code. The method the code employs for modeling infiltration and evaporation are summarized below.

Infiltration is modeled as a vertical positive flux of liquid described by Equation (6-18) as long as the conductive and sorptive capacity of the boundary block is not exceeded. After that, ponding occurs and the boundary condition changes to the specified head as described by Equation (6-19). The point in time when this occurs is determined by the simulation.

Similarly, evaporation is modeled as a vertical negative flux (Equation 6-18) equal to the potential evaporative demand until the liquid cannot be conducted fast enough toward the land surface to meet this demand. After that, the boundary condition changes to a specified flux based on the gradient in pressure potential between the soil and atmosphere. The point in time at which this occurs is determined by the simulation as well.

The spatial derivatives of Equations (6-17) through (6-19) are approximated by central differences written about grid-block boundaries. Time derivatives are approximated by a fully implicit backward scheme. Nonlinear parameters of the equation are linearized either implicitly (conductance and boundary conditions) or by using Newton-Raphson method (storage term). The Strongly Implicit Procedure (SIP) is used to solve the resulting system of equations.

6.6.5.5 Evaluation of the Unsaturated Flow Model's Potential for Bias in Overestimating Downward Flow

Potential bias of the unsaturated flow model in overestimating downward flow was tested by simulating the current undisturbed conditions at the Area 5 RWMS with the same conceptual and mathematical model used in the flooding and subsidence analysis. As mentioned previously, recharge to the groundwater is not occurring anywhere within the RWMS under the current climate conditions. In other words, all of the current precipitation is recycled to the atmosphere by evaporation and transpiration in the upper portion of the unsaturated zone. Consequently, if simulation results based on current conditions and the conceptual and mathematical models described above indicate infiltration below the transition zone (about 2 m (7 ft)), then downward flow is being overestimated. Note that reproducing the observed moisture content distribution within the unsaturated zone and calibrating the conceptual and mathematical model were not the goals of this effort.

A one-dimensional model was set up to simulate the unsaturated flow under the current undisturbed conditions. Mean values of the unsaturated zone parameters modeled were used (see Table 6-15). PE rates were specified in accordance with the rates shown in Figure 6-23. A recurring annual cycle of the rate of PE was specified for a period of simulation equal to 1000 years. The lower boundary was placed at the water table and initial pressure heads were based on an equilibrium profile.

The upper boundary condition was specified at the land surface. Two major processes were simulated at this boundary: infiltration of precipitation, and evaporation from the top soil layer. Evaporation is a continuous process, the rate of which is limited by PE and availability of moisture in the upper portion of the unsaturated zone. However, it was assumed that evaporation during precipitation can be neglected.

Infiltration of precipitation, on the other hand, is a discrete process associated with a precipitation event. The rate of infiltration is equal to the precipitation rate unless ponding or run-off takes place, in which case the infiltration rate is equal to the saturated conductivity of the soil. For the flow model bias investigation, all precipitation was assumed to be available for infiltration.

The rates, durations, and frequencies of precipitation events were defined based on the data analysis provided in Hokett and French [1998]. The recurring annual cycle of precipitation for a typical year was based on the mean number of days with precipitation in every month of the year and a mean precipitation depth for each day of precipitation. The number of precipitation events was defined to represent the observed tendency in distribution of one-day, two-day, and three-day events within the specified month. The total annual precipitation was equal to the mean annual precipitation of 12.63 cm (4.972 in) (see Table 5.6 in Appendix B and Figure 6-24). The annual distribution of precipitation defined for the typical year was used for every year of the 1000-year period of simulation. The low-probability events, such as the 1000-year storm, 100-year storms, and others, were not simulated. These events have much higher intensity than the average events considered, and excluding the more intense events from the simulation results in an underestimate of the infiltration flux.

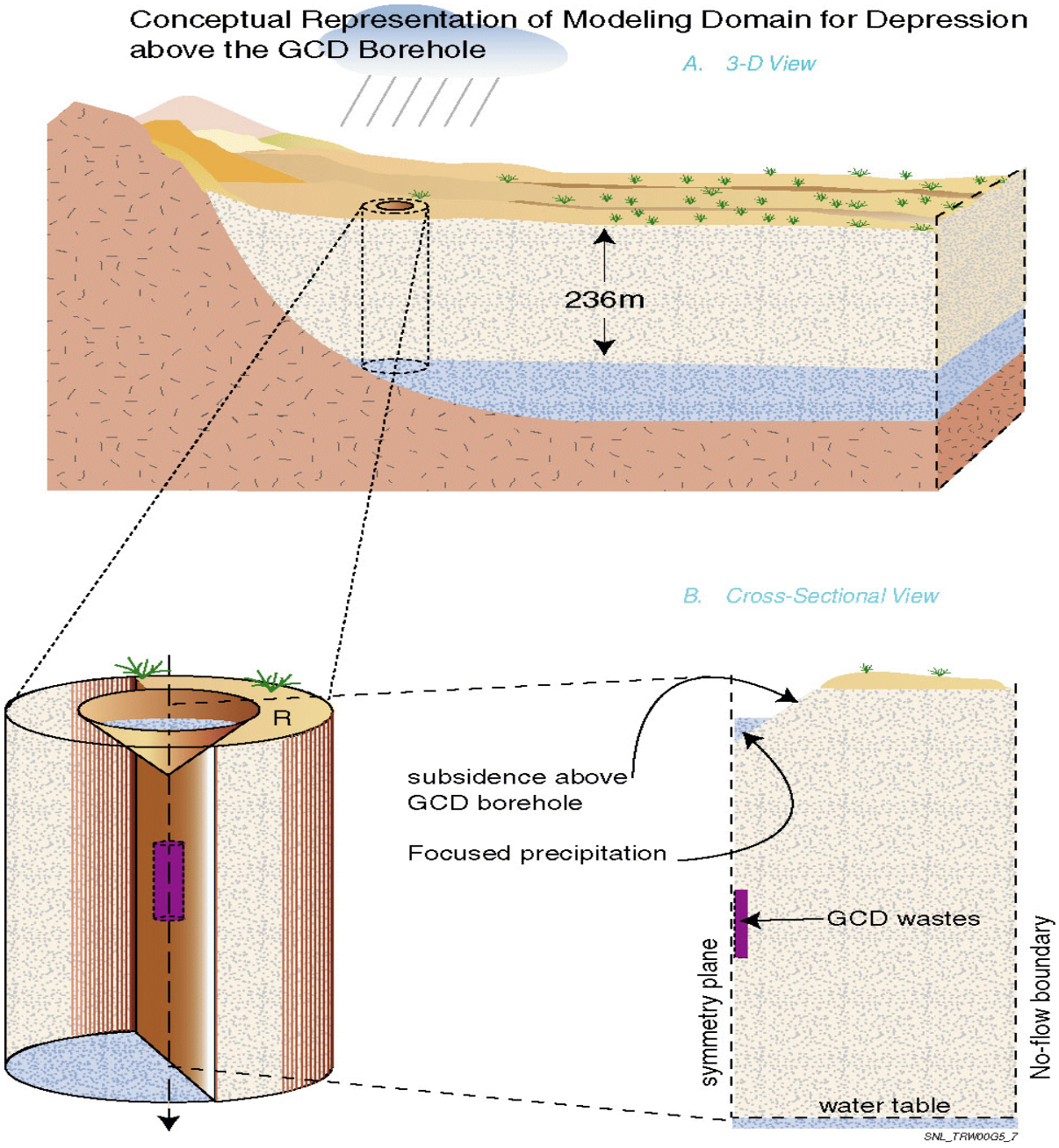

Figure 6-23. Conceptual Representation of Modeling Domain for a Depression above the GCD Borehole.

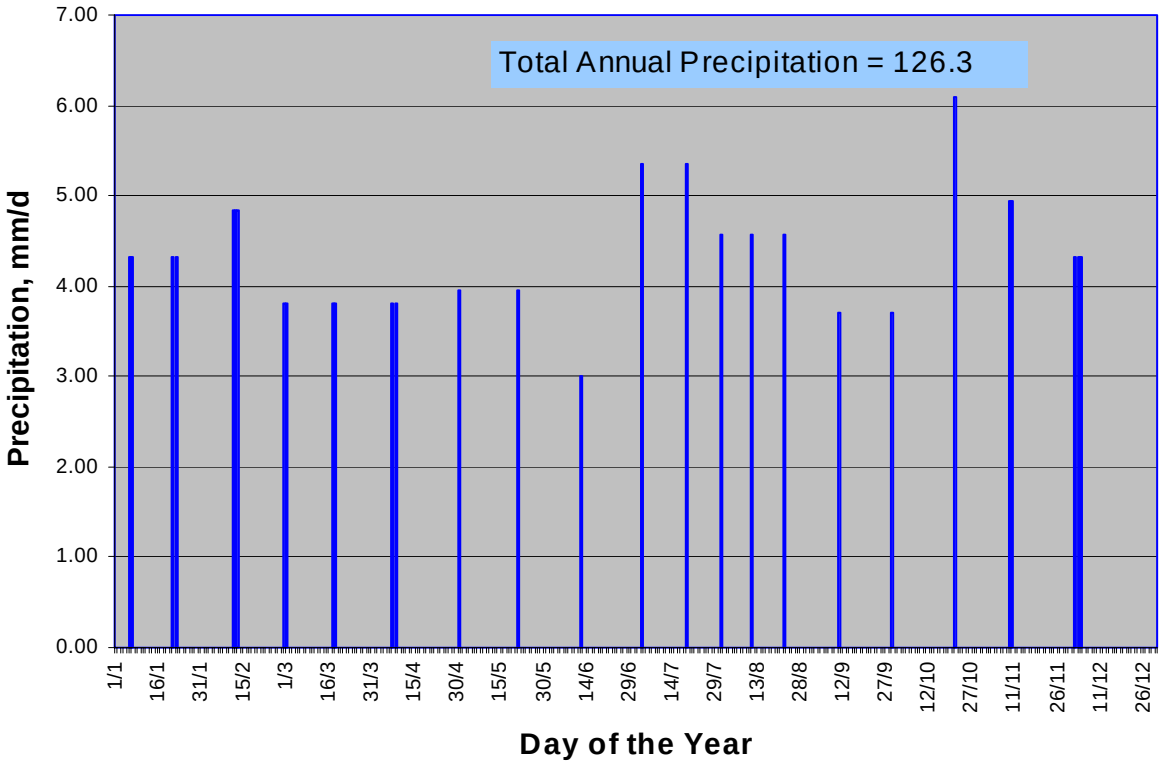

Figure 6-24. Annual Distribution of the Precipitation Used in 1-D Model of Unsaturated Flow Under Current Undisturbed Conditions.

Infiltration during precipitation was modeled by specifying a downward liquid flux at the upper flow boundary equal to the corresponding rate of precipitation. The duration of the flux corresponded to the event duration. Soil evaporation was assumed to occur between the precipitation events. The upward evaporation flux during these periods was calculated from the pressure-potential gradient between the soil and the atmosphere and compared to the PE flux at each time step during the simulation. The smaller of the two fluxes was then applied at the boundary.

Results and Conclusion of Investigation into Model Bias

The results of this simulation are presented on Figure 6-25 for four different times. As this figure indicates, the moisture introduced by the precipitation events is not all recycled to the atmosphere. By the end of the simulation period, 1000 years, the moisture front penetrates to a depth of 8.5 m (28 ft). Note that this is true even though the infiltration flux was intentionally underestimated and the current undisturbed conditions were simulated for a significantly smaller time period than the duration of the current climate (last 20,000 years).

This simulation demonstrates that the unsaturated flow conceptual and mathematical models cause an overestimate of the downward flow and, therefore an overestimation of the potential for the groundwater recharge. Based on this conclusion, these models were used for all further screening calculations.

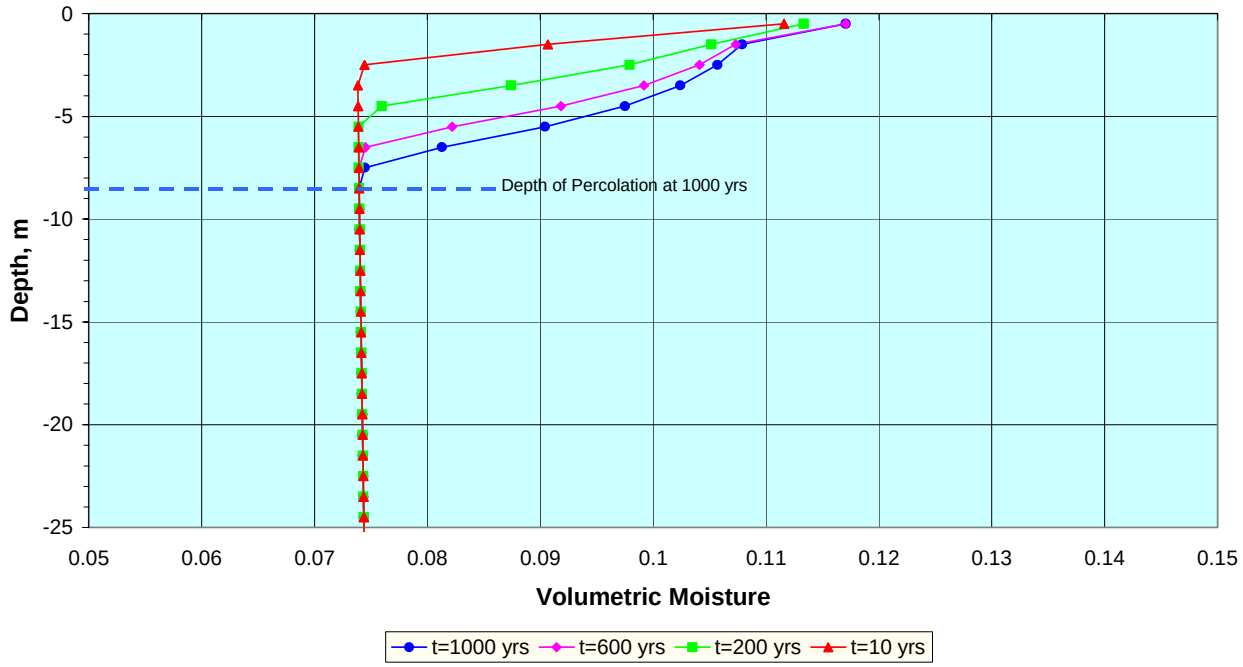

Figure 6-25. Moisture Profiles at Different Simulation Times from 1-D Model of Unsaturated Flow Under Current Undisturbed Conditions.

6.6.5.6 Additional Assumptions that Bias the Unsaturated Model Toward Overestimating Downward Flow

Following is a summary of additional model assumptions that bias the unsaturated flow model toward overestimating downward flow resulting from collection of precipitation and runoff in the subsidence features within the LLW trenches and pits and above the GCD boreholes at Area 5 RWMS.

- Instantaneous subsidence with removal of all remaining void spaces in the waste at the end of the institutional control period was assumed to occur. This results in the maximum possible depth of the subsided features being used in calculating subsidence volumes.

- The volumes of runoff into the subsided features under the glacial climate conditions were significantly overestimated by assuming that under the glacial climate the number of precipitation events will be the same as under the current climate, but the amount of precipitation per event will be two times higher. This results in five times more runoff compared to the runoff calculated by doubling the number of events.

- The likely formation of a low-permeability silt/clay crust at the depression bottoms due to runoff and associated sedimentation was excluded.

- All the surface water collected in the subsidence features was introduced into the vadose zone. No evaporation from the open water surface during the ponding was accounted for. This is true even for very small ponding events.

- The additional extraction of water from the upper unsaturated zone by plant transpiration was not incorporated. Only evaporation from the top soil was assumed to take water out of the unsaturated flow system.

- Initial conditions were specified as an equilibrium profile (zero gradient within the profile); the existence of the known upward flux in the upper zone was neglected.

- Extreme events, such as the PMP, the 10,000-year storm, one 1000-year storm, and nine 100-year storms, were all placed at the beginning of the simulations (first 14 years) when the intact cap (Conceptual Model 1) was considered.

< Unsaturated flow associated with runoff into the trench was approximated by a two-dimensional model, thereby assuming an infinite width for the trench.

6.6.6 Modeling Unsaturated Flow Under Climate Change and Subsidence

6.6.6.1 Introduction

This section focuses on the modeling set-up and analysis of the modeling. Two conceptual models were considered. In the first conceptual model, the infiltration of surface water from subsided Trench TO4C and from the cone-shaped depression above GCD Borehole 1 assimilated for 10,000 years assuming that the glacial conditions will be established instantly at the end of institutional control period and that the cap will remain intact during the entire simulation period. In the second conceptual model, the infiltration of surface water from subsided Trench TO4C was simulated for 10,000 years assuming that the glacial conditions will be established instantly and that the cap will be washed away completely at the end of institutional control period.

6.6.6.2 Modeling Set-Up

Subsided Trench TO4C – Intact Cap (Conceptual Model 1)

As discussed in Section 5.0, the major purpose of modeling unsaturated flow due to the collection of precipitation and runoff in the subsided trench was to estimate the extent of the lateral spreading of the moisture front and its possible effects on moisture conditions around the GCD boreholes. Trench TO4C was simulated since it has a greatest potential to impact the GCD boreholes. Trench 4 is located closer to GCD Borehole 3 than any other trench or pit and collects more water per unit width than the other trenches

The modeling set up for Trench TO4C is shown in Figure 6-26. The trench is modeled along the cross-section that extends from the land surface to the groundwater table. In the vertical direction, 230 blocks with a size of 1 m (3 ft) were defined everywhere except the middle part of

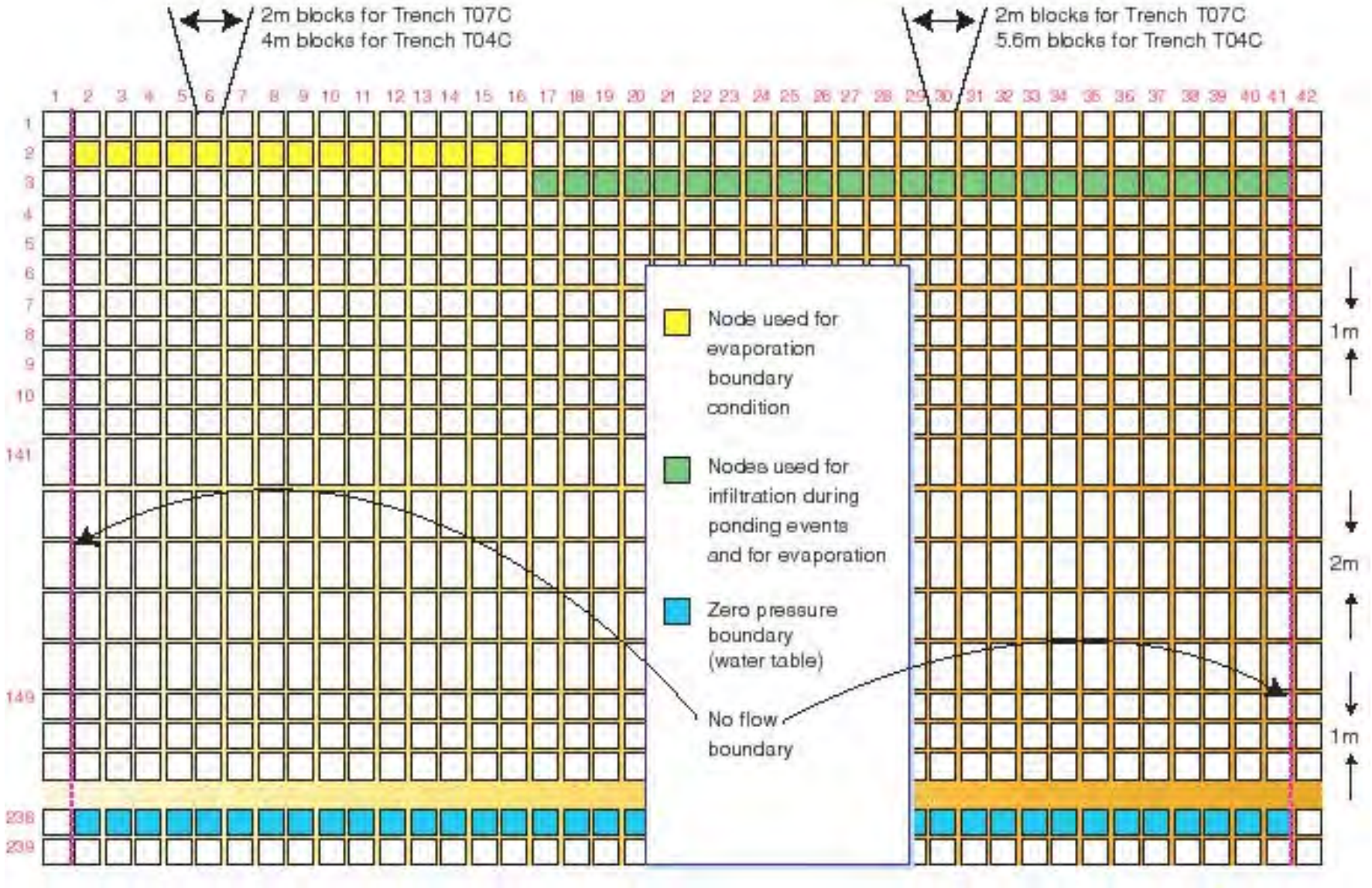

Figure 6-26. Cross-Section Showing 2-D Model Set-Up.

the vadose zone, where the vertical dimension of nine blocks was 2 m (7 ft). This was done to minimize the total number of the nodes while maintaining fine discretization in the areas close to the upper and lower flow boundaries.

No-flow boundary conditions were specified along the vertical boundaries of the modeling domain. A zero-pressure boundary condition was specified at the lower boundary. The subsided depression within the trench was modeled as a pit having a flat bottom and vertical walls with a depth of 1 m (3 ft). The prescribed flux boundary condition was specified in each boundary block representing the bottom of the trench during the ponding event. An evaporation boundary condition was maintained in all the other blocks representing the undisturbed land surface. After the ponding event was completed, the prescribed flux boundary condition at the bottom of the trench boundary blocks was switched to the evaporation boundary condition until the next ponding event. The recurring annual cycles of potential evaporation rates and the vadose zone parameters used in these simulations were discussed in Section 5.0. The potential evaporation rates were specified as shown in Figure 5.6 of Appendix B. The parameters used were the mean values (see Table 5.5, Appendix B).

The volumes, frequencies, and durations of the ponding events were discussed in detail in Section 6.6.5 and Appendix B (see Appendix B, Table 5.2). The following distribution of these events within the first 1000-year time period was used. The ponding event corresponding to the PMP was placed at time zero, the 10,000-year storm began at 1.125 years, the 1000-year storm was placed at 2.25 years, and the nine 100-year storms were placed starting from the time 3.375 years with the time interval between them equal to 1.125 years. The average ponding events were placed starting from the time equal to 13.5 years with a time interval equal to 1.125 years between them for the remaining 986.5 years of simulation. The second 1000-year time period included the 1000-year storm at time equal to 2,000 years, and the nine 100-year storms starting from time equal to 2,001.125 years with the time interval between them equal to 1.125 years. The average ponding events were placed starting from time equal to 2,011.25 years with the time interval equal to 1.125 years between them for the remaining 988.75 years of simulation. The third through the tenth 1000-year time periods were identical to the second 1000-year time period. The total simulation time was 10,000 years.

Volumes introduced into the vadose zone by every ponding event were normalized by the trench width. The ponding event was modeled by maintaining the specified flux boundary condition until the pond volume infiltrated into the vadose zone.

Subsided Trench TO4C – No Cap (Conceptual Model 2)

The total volume of water accumulated in Trench TO4C is greater than in Trench TO7C and its lifetime is shorter. Thus, more water is introduced from Trench TO4C to the vadose zone than Trench TO7C. The volume of water accumulated in Pit PO3U is larger, but normalized volume is smaller than in Trench TO4C.

The only difference in modeling set-up from the intact cap conceptual model described above was in the timing and volumes of water introduced to the trench. As described in Section 6.6.5.2,

the simulated lifetime of Trench TO4C assuming no cap and glacial climate conditions was 91 years. Thirty-three ponding events were simulated over this time period. No ponding events were simulated from the year 92 until the year 10,000.

The bottom of the trench was maintained at the same place, even though it rises with every ponding event until it is at the undisturbed land surface. This provides some overestimation of the depth of the moisture front at the end of the simulation period and is consistent with the screening approach used.

Subsidence Depression Above GCD Borehole 1 – Intact Cap

The modeling set-up is shown in Figure 6-27 for one of the vertical cross-sections through the vertical cylinder that extends from the land surface to the water table. Figure 6-28 shows a horizontal view of the modeling domain. The depth of the vadose zone equal to 236 m (774 ft) is represented by 255 grid blocks.

The no-flow boundary condition is specified along the vertical plane of symmetry and along the vertical cylinder walls. The zero-pressure boundary condition is specified at the bottom of the cylinder. The cone-shaped depression is specified at the top blocks so that the depression depth and radius would correspond to the maximum dimensions of the deepest subsidence features, which are 3.04 m (10 ft) (depth) and 4.34 m (14 ft) (radius). Eight blocks represent the wall of the depression. The prescribed flux boundary condition is specified in the nodes of the blocks located below the water level corresponding to the depth of the ponding event modeled. The constant flux rate in these blocks is maintained until the total volume of the ponded water infiltrates into the vadose zone. When the depression is totally filled with water, the prescribed flux boundary condition is specified in the nodes of all eight boundary blocks. The boundary blocks located above the water level on the depression wall during the corresponding ponding event are specified with the evaporation flux. The evaporation flux boundary condition is maintained in the other blocks representing the land surface. When the ponding event is completed, the prescribed flux boundary condition is switched to the evaporation flux boundary condition until the next ponding event. As discussed in Section 6.6.5, the actual evaporation flux out of the system is not prescribed, but calculated during every time step.

The volumes, frequencies, and durations of the ponding events were discussed in detail in Section 6.6.5 (See Table 5.2 of Appendix B) and in Section 5.0 of Appendix B. The same timing of the low probability and the average ponding events for subsided Trench TO4C was used in simulating the subsidence depression above GCD Borehole 1.

All the ponding events, except the ponding event corresponding to the PMP, have volumes smaller than half of the total subsidence volume, which is 59 m^3 (2100 ft^3). The maximum ponding depth at the subsidence depression focal point corresponding to the average ponding event is 1.4 m (4.6 ft). Four blocks shown in Figure 6-28 are located below this water level. These blocks were specified as the prescribed flux blocks. The low-probability ponding events, except the PMP, were modeled by specifying a prescribed flux in four bottom blocks, since the difference in the ponding depths was not significant. The ponding event corresponding to the

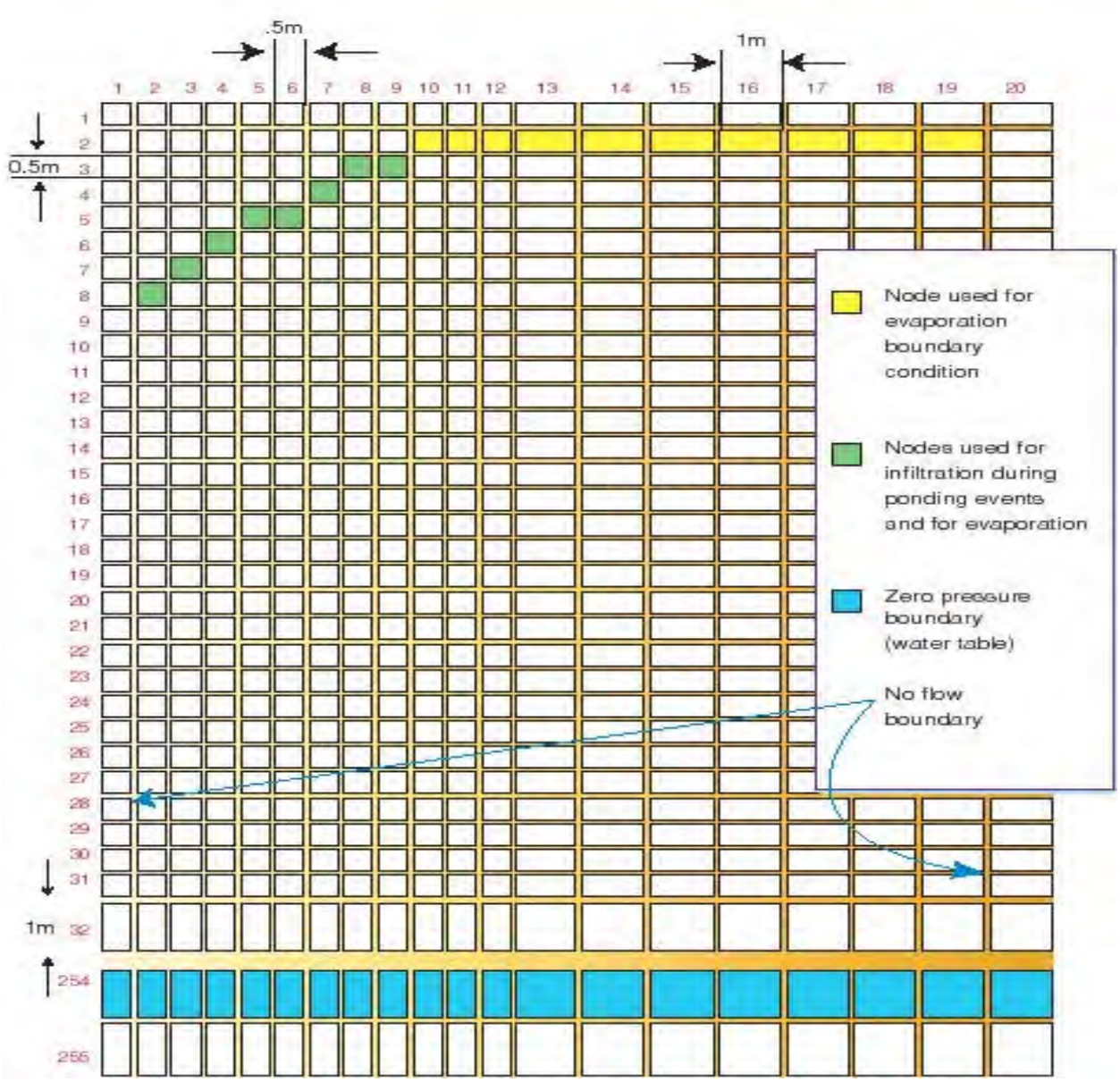

Figure 6-27. Cross-Section Showing Radial Coordinates of Model Setup.

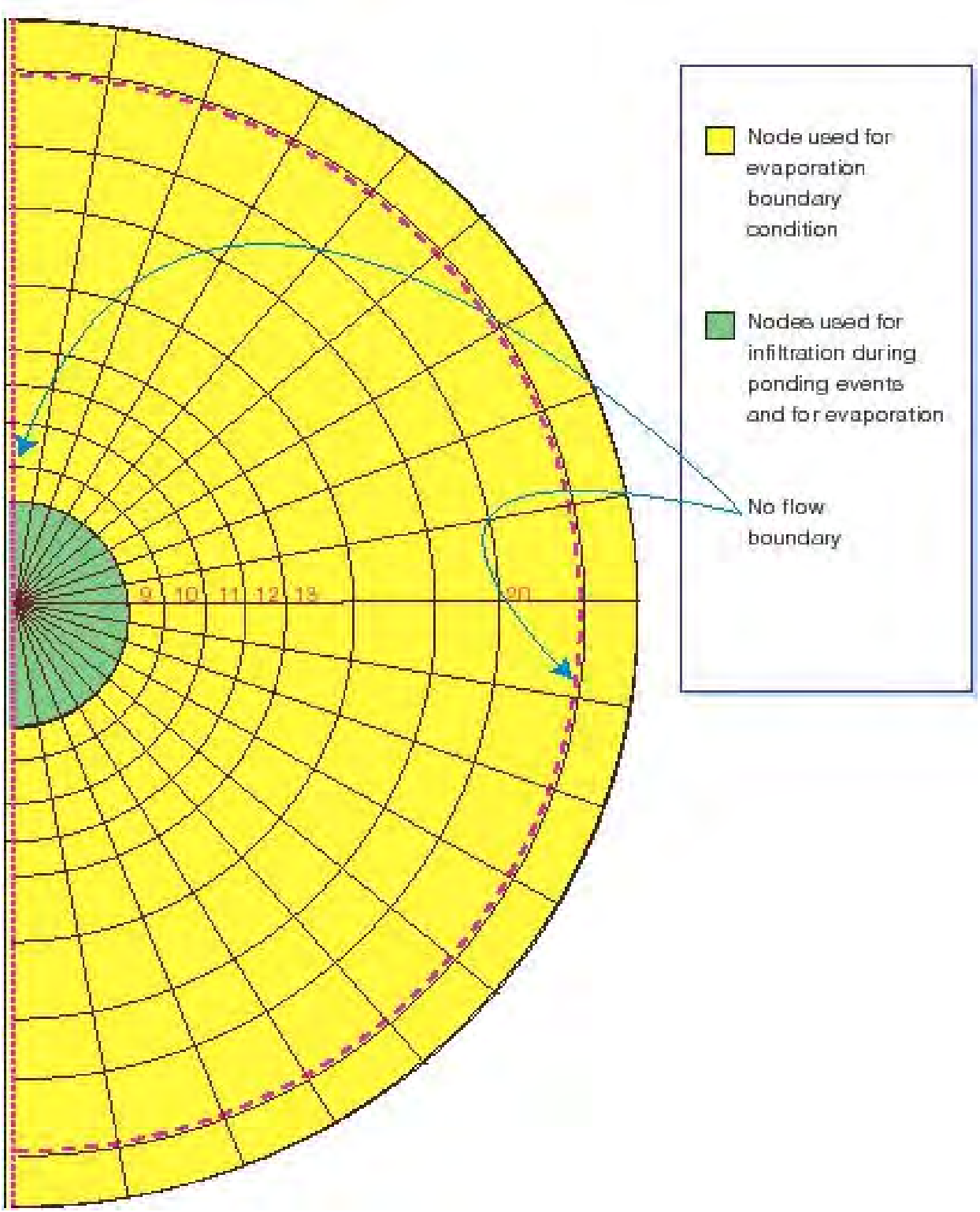

Figure 6-28. 2-D Plane View Showing Radial Coordinates Model Set Up.

PMP was simulated by specifying prescribed flux boundary condition in eight boundary blocks representing the depression wall up to the undisturbed land surface.

6.6.6.3 Unsaturated Flow Due to Collection of Precipitation in the Subsidence Features

Subsided Trench TO4C – Intact Cap (Conceptual Model 1)

The distribution of moisture obtained around Trench TO4C at 10,000 years assuming an intact cap and glacial climate conditions during 10,000 years of simulation is shown in Figure 6-29. At this time, the moisture front beneath the trench is at the water table. The moisture front spreads laterally to a distance of approximately 35 m (120 ft) and reaches close to GCD Borehole 1. GCD Boreholes 2 and 3 are outside of the zone affected by the movement of moisture from the trench. If Trench TO7C was simulated, GCD Borehole 4 would probably be on the edge of the zone of influence, since it is located 24 m (79 ft) away from the trench. Consequently, the moisture conditions around two GCD boreholes can potentially be affected by water infiltrating from the trenches.

However, as shown in Figure 6-29, the changes in moisture beneath GCD Borehole 3 at 10,000 years impact the vadose zone down to a depth of 185 m (607 ft) with most changes being above 150 m (490 ft). The changes in moisture beneath GCD Borehole 4 would occur down to 170 m (560 ft).

The development of the moisture front in time in a vertical cross-section through GCD Borehole 3 is shown in Figure 6-30. As seen in this figure, only minimal changes above the GCD borehole can be observed at 1000 years. Two components of the velocity vector are plotted in Figure 6-30: horizontal and vertical velocities. The depth of the moisture front at the specified moment in time is equal to the point where the vertical velocity is equal to zero. The vertical velocity is upward in the upper 5 m (16 ft) of the vadose zone and downward at greater depth. The maximum downward velocity at 10,000 years was at the depth of 70 m (200 ft). The horizontal velocity is negative or in the direction opposite to the trench at all times and at all depths, indicating that there is no movement from the borehole toward the trench.

The downward flow over the period of simulation expressed as a percentage of the total amount of water introduced to the vadose zone due to the infiltration from the trench is shown in Figure 6-31. The total amount of water accumulated in Trench TO4C was approximately 2.053×10^6 m^3 (7.250×10^7 ft^3). By the end of the 10,000 year period, 6.8% of the total amount accumulated, or approximately 139,600 m^3 (4.930×10^6 ft^3), contributed to downward flow.

The moisture profiles in the vertical cross-section through GCD Borehole 3 are shown in Figure 6-32. Moisture content data from the different wells located in Area 5 RWMS are plotted on this figure for the sake of comparison. The maximum increase in the moisture content in the upper part of the vadose zone is 4%; from 8% corresponding to the equilibrium profile to 12% at 10,000 years. This increase in moisture is smaller than the variability of moisture content in the different wells, as demonstrated in Figure 6-32.

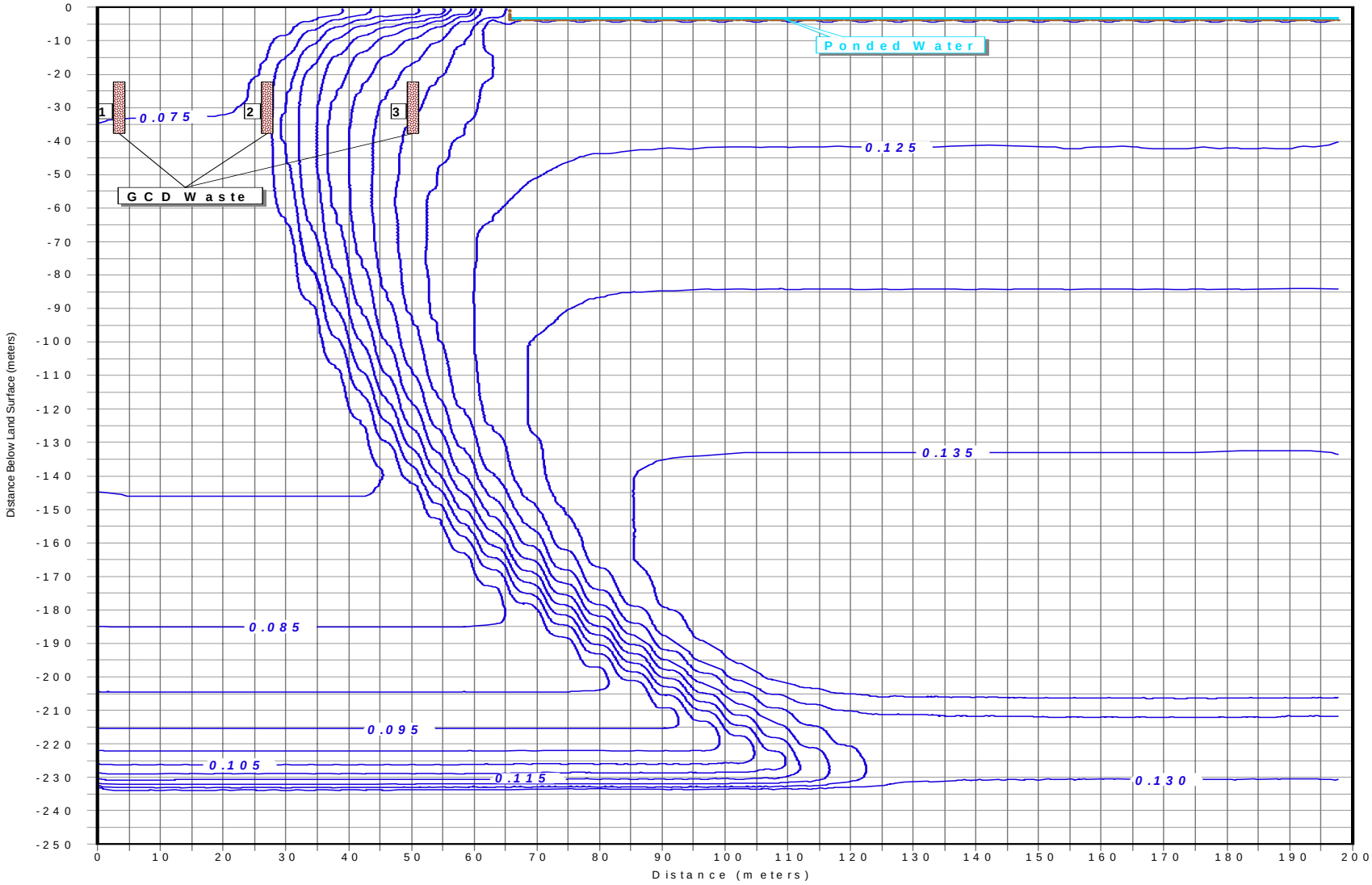

Figure 6-29. Intact Cap Conceptual Model. Distribution of Moisture Beneath Trench TO4C at 10,000 Years.

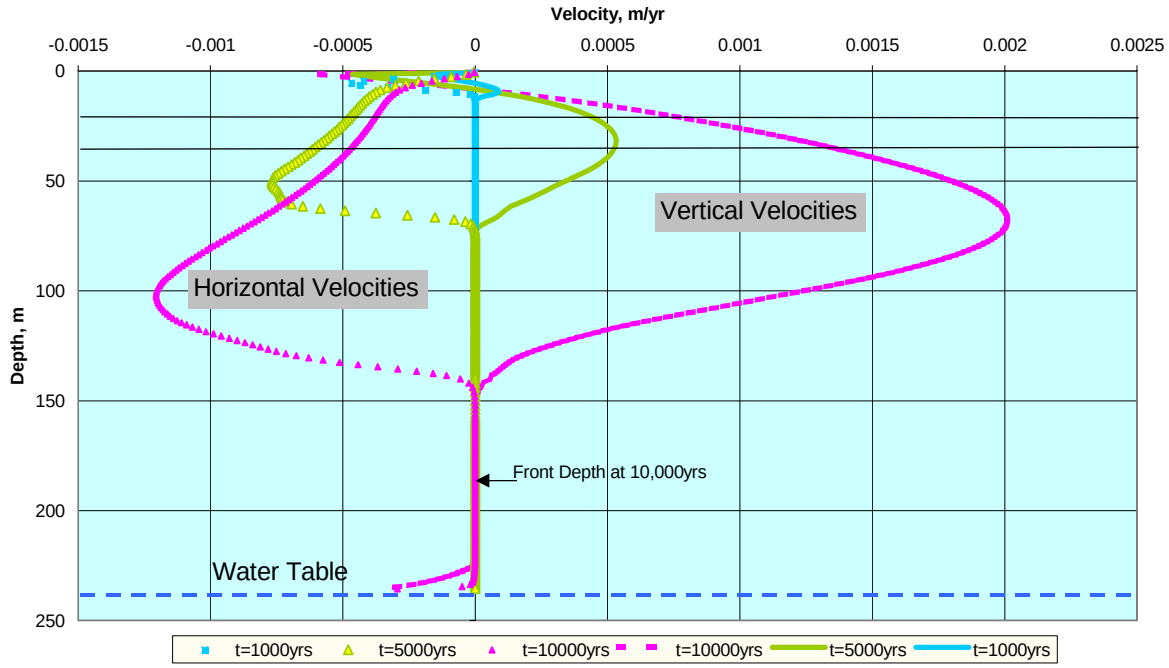

Figure 6-30. Conceptual Model 1 – Intact Cap. Results of the Trench TO4C Modeling Velocity Profiles for the Cross-Section through GCD Borehole 3.

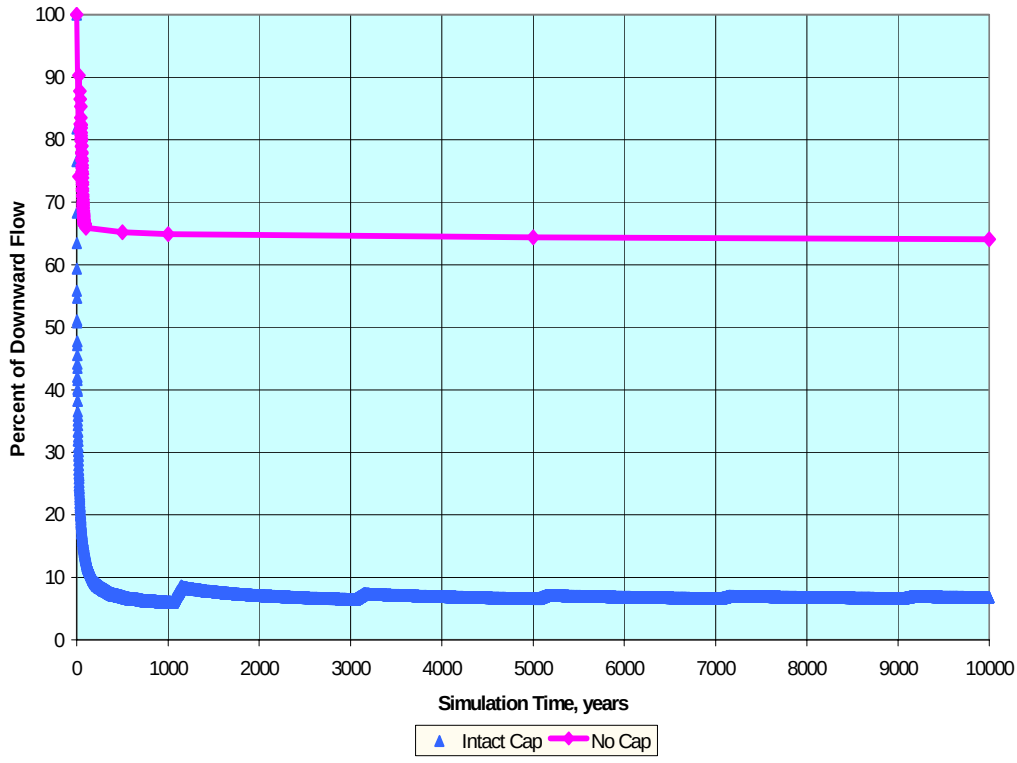

Figure 6-31. Results from the Trench TO4C Modeling Downward Flow as a Percentage of the Total Volume of Surface Water.

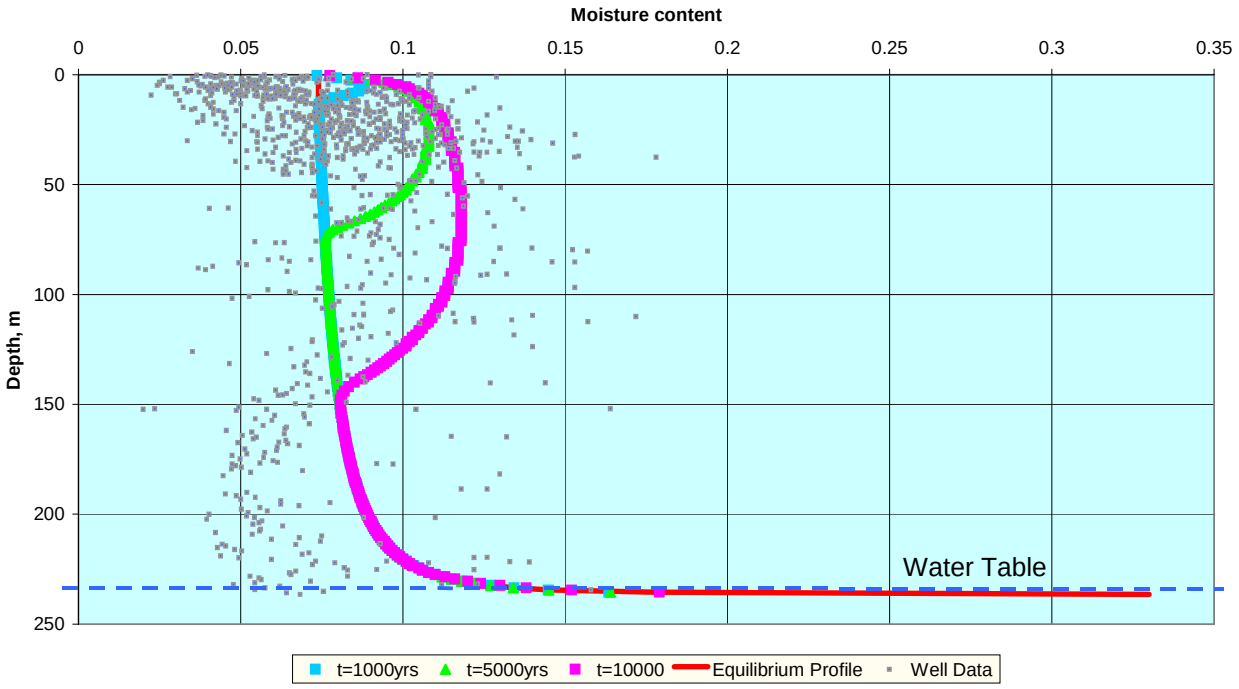

Figure 6-32. Conceptual Model 1 – Intact Cap. Results of Trench TO4C Modeling Moisture Profiles for the Cross-Section through GCD Borehole 3.

The conclusion from this analysis is that the infiltration of water from the trenches and pits in the Area 5 RWMS will not have any impact on GCD Boreholes 1 and 2 and may have an impact on GCD Boreholes 3 and 4. The impact on these boreholes is later estimated by specifying higher initial moisture conditions in simulating unsaturated flow around the GCD boreholes.

Subsided Trench TO4C – No Cap (Conceptual Model 2)

The distribution of moisture obtained around Trench TO4C at 10,000 years assuming no cap and glacial climate conditions during 10,000 years of simulation is shown in Figure 6-33. A total of approximately 37,410 m^3 (1.321×10^6 ft^3) of water accumulated in the subsided trench during the simulation, mostly within the first 91 years due to the assumption of aggradation built into the runoff estimates for Model 2. By the end of the 10,000-year period, 64% of the total amount accumulated, or approximately 23,940 m^3 (8.455×10^5 ft^3), contributed to downward flow. The maximum depth of the moisture front beneath the trench at 10,000 years is 115 m (377 ft). The lateral spread of the moisture front is 30 m (100 ft). GCD Boreholes 3 and 4 are affected by the moisture front movement. The depth of the moisture front at 10,000 years beneath GCD Borehole 3 is 88.5 m (290 ft) and beneath GCD Borehole 4 is 83.5 m (274 ft). Since no water movement is expected in this conceptual model from subsidence depressions above GCD boreholes, this is the only impact of subsidence and climate change on the moisture conditions around GCD Boreholes 3 and 4. No changes in moisture will occur around GCD Boreholes 1 and 2. Consequently, Model 1 provides a wider lateral spread of increased moisture and deeper infiltration than Model 2. In other words, the intact cap model is more bounding than the model that assumes no cap.

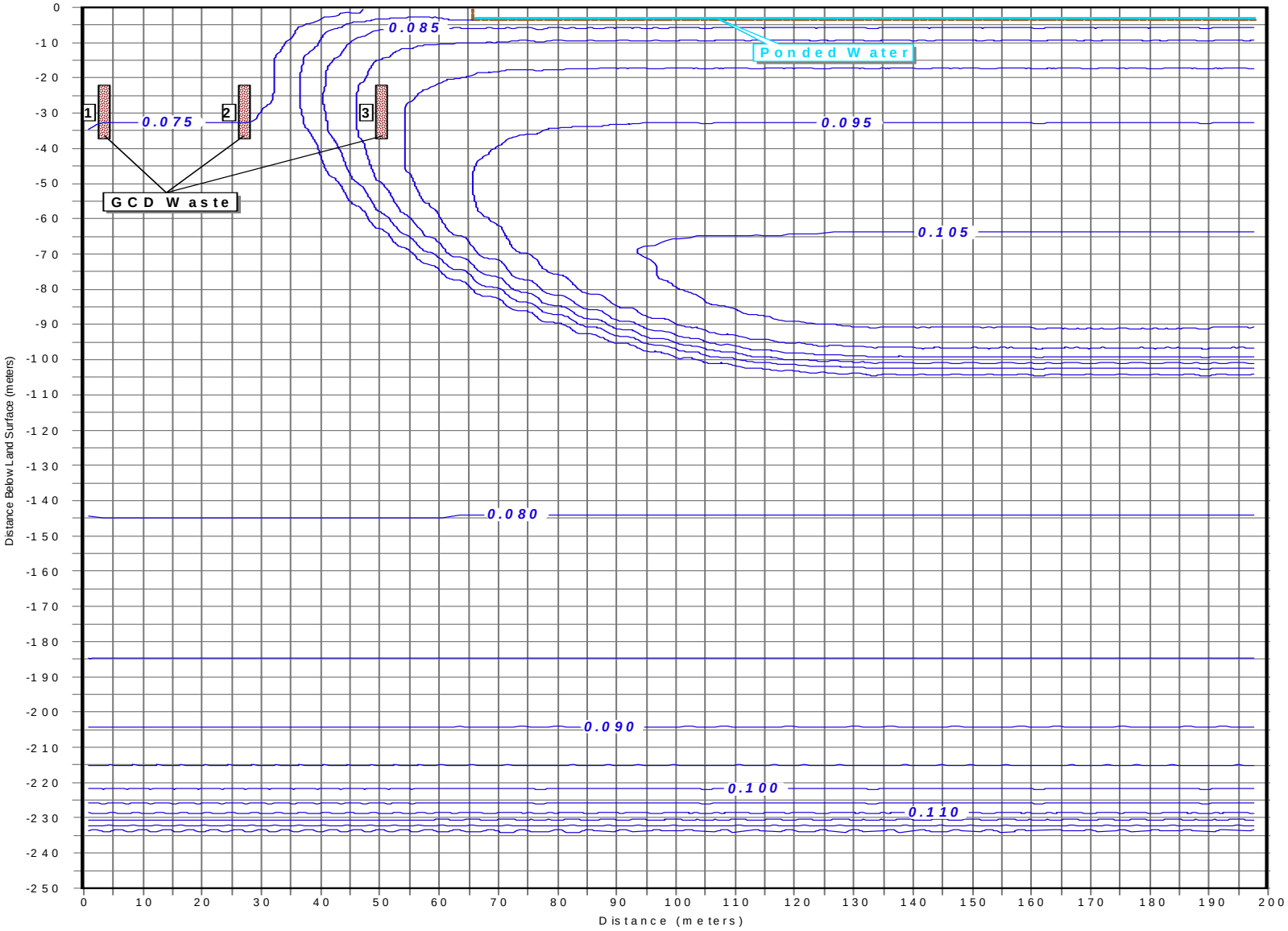

Figure 6-33. No Cap Conceptual Model. Distribution of Moisture Beneath Trench TO4C at 10,000 Years.

The only significant difference between Model 1 (intact cap) and Model 2 (no cap) is in the ratio between the total volume of water introduced into vadose zone and the total volume of water that became downward flow. The downward flow obtained in Model 1 is 6.8% of the total volume of the surface water available for infiltration. The downward flow obtained in Model 2 is 64% of the total volume of the surface water. This is the result of introducing a large amount of water over short period of time in Model 2 – there is not enough time for evaporation to extract the water from the vadose zone. However, the total volume of water introduced into the unsaturated zone in Conceptual Model 1 is far greater than the volume introduced in Conceptual Model 2.

Subsidence Depression Above GCD Borehole 1

The distribution of moisture obtained around GCD Borehole 1 at 10,000 years assuming an intact cap and glacial climate conditions during 10,000 years of simulation is shown in Figure 6-34. The depth of the moisture front at 10,000 years is 100 m (300 ft). The lateral spread of the moisture front is about 10 m (30 ft) from the center of the borehole. Taking into account the distance of 22 m (72 ft) between GCD Boreholes 1, 2, and 3, no interference between the moisture infiltrating from the subsidence depression above GCD boreholes is expected. In addition, the total volume of water accumulated by the depressions above Boreholes 2 and 3 is smaller due to the smaller capture areas.

The borehole subsidence simulation was also performed with higher initial moisture conditions to investigate the possible influence of the trench. The higher initial moisture conditions were defined to obtain the moisture content of about 10% in the upper part of the vadose zone. Model parameters were modified to provide the physically correct distribution of moisture with depth corresponding to the higher moisture conditions.

The moisture and vertical velocities profiles at the subsidence depression center-line for a few different times are shown in Figure 6-35 and 6-36 for two different initial conditions; with undisturbed initial moisture conditions and with high initial moisture conditions due to the influence from the trench. The depth of the moisture front in the case of the higher initial moisture is 25 m deeper (125 m (410 ft)) at 10,000 years than the undisturbed case. In both cases, the moisture front does not reach the water table in 10,000 years. The most significant changes in moisture occur near the surface where the moisture content reaches its highest values. The moisture gradually decreases down to a depth of about 25 m (82 ft) from the land surface and then remains constant all the way to the moisture front depth.

The difference between the two calculations is in the volume of water that becomes downward flow. A larger volume of water (12%) percolates into the vadose zone assuming undisturbed (drier) moisture conditions. This water significantly increases the moisture content within the relatively narrow depth interval. The smaller volume of water (3%) percolates into the vadose zone under the higher initial moisture conditions. However, increases in moisture content occur over a larger depth interval.

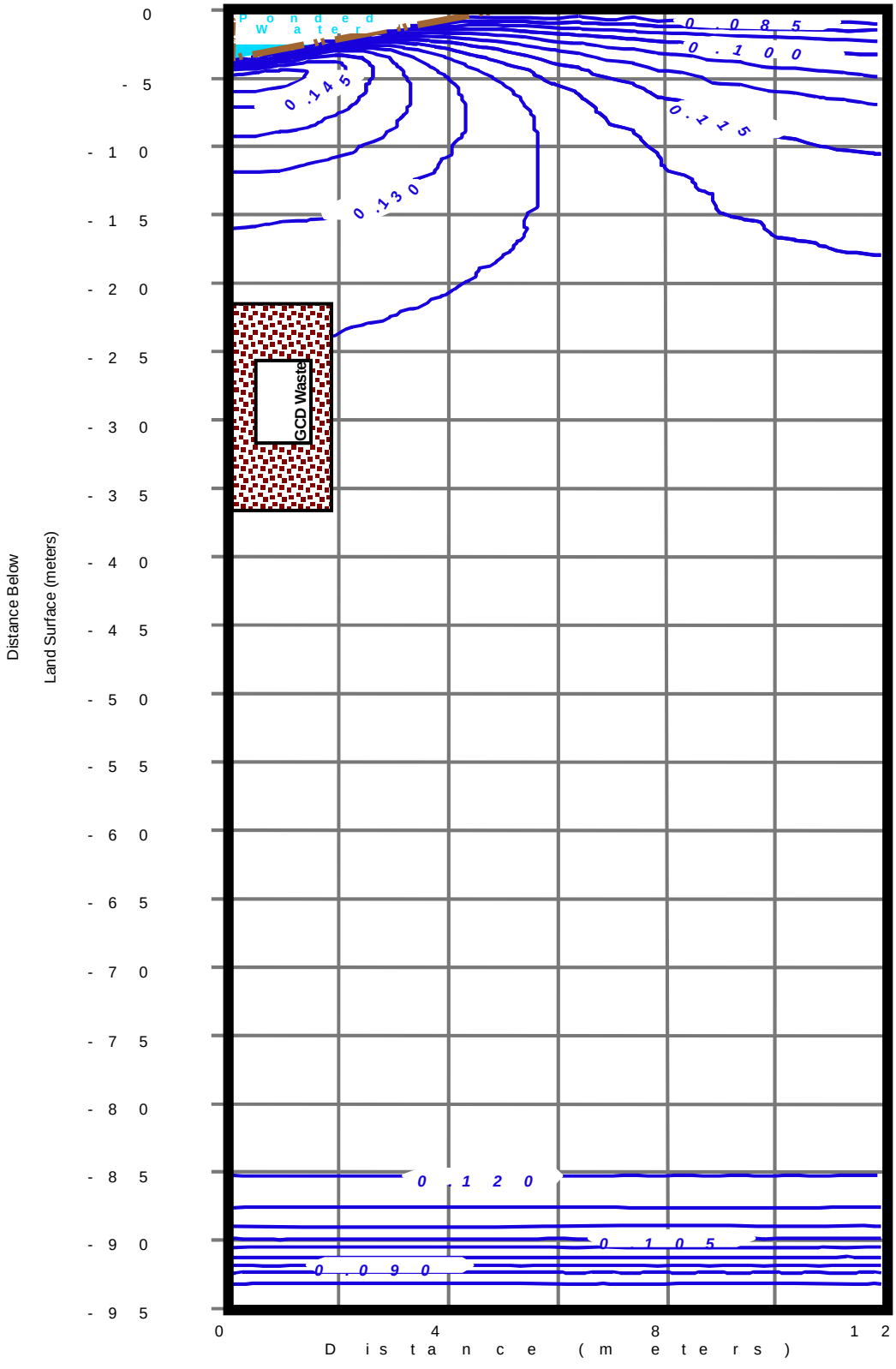

Figure 6-34. Intact Cap Conceptual Model. Distribution of Moisture Beneath GCD Borehole 1 at 10,000 Years.

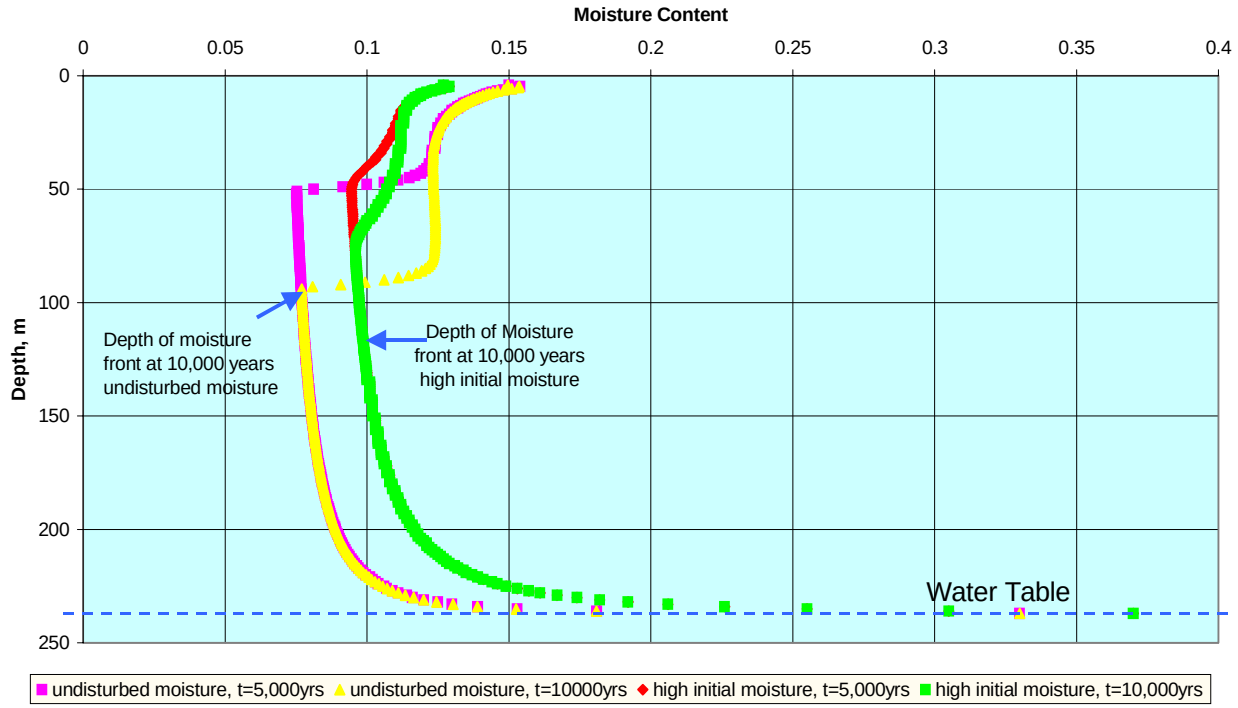

Figure 6-35. Conceptual Model 1 – Intact Cap. Results of the GCD Borehole Modeling Moisture Profiles at the Vertical Cross-Section through the GCD Borehole.

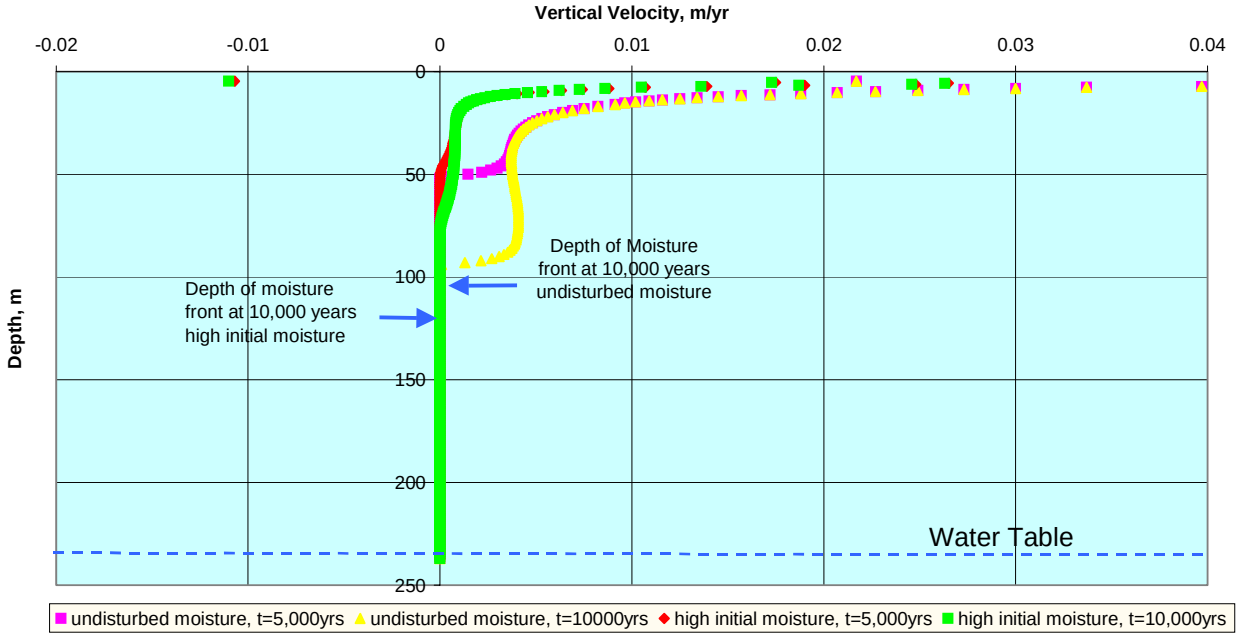

Figure 6-36. Conceptual Model 1 – Intact Cap. Results of the GCD Borehole Modeling Vertical Velocity Profiles at the Vertical Cross-Section through the GCD Borehole.

6.6.6.4 Conclusions

Four simulations were performed to estimate the effects of subsidence and climate change on the moisture conditions around GCD boreholes.

In the first simulation, Trench TO4C was modeled assuming glacial climate conditions and an intact cap for 10,000 years. The conclusions from this simulation are that the moisture conditions around GCD Boreholes 1 and 2 will not be affected by the infiltration of water from the trench and that the moisture content around GCD Boreholes 3 and 4 may increase slightly.

In the second simulation, Trench TO4C was modeled assuming glacial climate conditions and no cap for 10,000 years. Based on the results of this simulation, it is concluded that the moisture conditions around GCD Boreholes 3 and 4 will be affected by the infiltration of water from the trench, but no groundwater recharge will occur anywhere in the area in 10,000 years. It can also be concluded that the intact cap conceptual model (Model 1) provides a bounding estimate of downward flow in comparison to the no cap conceptual model (Model 2).

In the third simulation, GCD Borehole 1 was modeled assuming glacial climate conditions and an intact cap for 10,000 years with undisturbed initial moisture conditions. The results of this simulation showed that the depth of the moisture front beneath GCD Boreholes 1 and 2 will be 100 m (300 ft) at 10,000 years. Consequently, no groundwater recharge will occur in 10,000 years.

In the fourth simulation, the GCD borehole was modeled assuming glacial climate conditions and an intact cap for 10,000 years with high initial moisture conditions to account for the influence of infiltration from Trench TO4C. The results of this simulation showed that the depth of the moisture front beneath GCD Boreholes 3 and 4 will be 125 m (410 ft) at 10,000 years and no groundwater recharge will occur in 10,000 years.

The major conclusions from the simulations performed were the following:

- The infiltration of water collected in the LLW trenches will result in the spreading of moisture downward and laterally. The lateral spread of the moisture has a potential to affect the moisture conditions around GCD Boreholes 3 and 4 that are in the closer vicinity to the trenches.

- Collection of precipitation within the subsidence depressions above the GCD boreholes and its infiltration into the vadose zone may result in downward unsaturated flow. However, the moisture front will not reach the water table within 10,000 years under the current or future climate conditions either when the moisture movement around the GCD boreholes is affected by the trench (GCD Boreholes 3 and 4) or when it is not (GCD Boreholes 1 and 2).

6.6.7 Sensitivity of Unsaturated Flow Model

The unsaturated flow model was investigated to determine the sensitivity of model results to these components:

- unsaturated flow parameters
- dimensionality of the model domain
- potential evaporation rates
- low-probability ponding events
- slope of the trench bottom

Model dimensionality was found to have the most significant effect on model results. The comparison of a 1-D model, with a quasi-three-dimensional (3-D) model in radial coordinates showed that in the case of the 1-D model, the moisture front moves down to a depth of a few meters above the water table (234 m (768 ft) below the land surface), while the moisture front in the quasi-3-D model reached a depth of only 10 m (30 ft) by 1000 years. In a homogeneous, isotropic system, a quasi-3-D model is a closer approximation of actual infiltration behavior than in a 1-D model because the infiltrating front is allowed to move in all directions according to 3-D gradients instead of being forced down a 1-D column.

The model is also very sensitive to the unsaturated flow parameters. Assuming higher moisture conditions in the unsaturated zone results in a noticeable increase in the moisture front depth. For example, the moisture front beneath Trench TO4C was 30 m (100 ft) when the mean parameters were used and 80 m (300 ft) when the parameters corresponding to the higher than measured moisture conditions were used.

The potential evaporation rates have a relatively small effect on the modeling results. Assuming total annual evaporation 1.4 times lower increases the depth of the moisture front by only 7 m (20 ft).

Finally, assuming a sloped trench bottom instead of a flat bottom has a negligible influence on the modeling results.

6.6.8 Summary and Conclusions

RWMS trenches contain a significant amount of void space resulting from the incomplete filling of waste containers, limited internal compaction of contents, and spaces between containers. As the waste containers deteriorate and collapse, subsidence will result as these voids are filled. The depressions caused by subsidence have the potential to collect precipitation and runoff, which may cause the downward movement of pore water and the formation of ephemeral wetlands. Additionally, numerous studies have shown that over long time spans, the climate could return to cooler and wetter, glacial conditions.

This report presents the results of a detailed screening analysis conducted to determine if surface water might migrate to the water table during the next 10,000 years because of the combined

effects of landfill subsidence and a possible return to a glacial climate. If surface water and radionuclides have the potential to reach the accessible environment in the next 10,000 years, this pathway would have to be included in the PA for the TRU wastes in the GCD boreholes.

Four coupled analyses were undertaken for this study:

- the geometry of future subsidence features was estimated;
- using current climatic data, precipitation, local runoff, and flooding were modeled;
- assuming an immediate return to glacial climatic conditions, precipitation, local runoff, and flooding were modeled; and
- the 2-D and quasi-3-D movement of water in the subsurface was modeled in two ways–first, assuming the landfill cap is intact for 10,000 years and second, assuming the landfill cap is instantly "removed" at the end of the institutional control period.

This screening analysis does not model the movement of radionuclides, nor does it model the movement of water to the accessible environment. The movement of radionuclides would be much slower than the movement of pore water due to chemical sorption of radionuclides onto the alluvium. Therefore, if it can be shown that pore water moving through the GCD wastes will not reach the water table in 10,000 years, then it is clear that radionuclides will not reach the 5-km (3.1-mi) accessible environment boundary in 10,000 years.

The actual evolution of the site with respect to subsidence and climate change is unknown. Therefore, this analysis was systematically constructed to overestimate the potential for downward migration of water. With respect to subsidence, this meant maximizing the amount of subsidence that occurs after institutional control. That is, for the next 170 years, the site will be under institutional control and DOE will fill in any subsidence that occurs. Therefore, this analysis chose rates of subsidence that maximize the post-170 years subsidence. The entire remaining void volume is then assumed to instantly collapse and form a subsidence depression. The effects of natural erosion of the cap were investigated first by an analysis of flooding potential and second by postulating two bounding conditions. The flooding analysis indicated that it is not very likely that floods will overtop the cap during the next 10,000 years. However, due to uncertainty in this calculation, two bounding conditions were analyzed. First, the cap with associated subsidence features was assumed to stay intact for 10,000 years. Second, the cap was assumed to be instantly removed at the end of the institutional control period. In the case of no cap, sedimentation associated with flooding filled in the subsidence features in a few hundred years, which halted the accumulation of floodwaters. Since the subsidence features associated with the intact cap were assumed to last 10,000 years, this case became the bounding analysis. That is, much more water entered the deep unsaturated zone in the intact cap case.

Climate studies indicate that a doubling of precipitation is very likely to occur in the next 10,000 years. However, the timing of climate change is uncertain. Therefore, this analysis assumed that climate change begins immediately and lasts the entire 10,000-year period. Climate change was

represented by a doubling of each precipitation event instead of doubling the number of precipitation events. This approach maximizes total runoff because in each precipitation event a certain volume of rainfall must be absorbed by the soil before runoff begins.

Based on the results of the subsidence and climate change analysis, models of unsaturated groundwater flow were developed. These models simulated the migration of water collected by the subsidence features as it infiltrated into the unsaturated zone and migrated toward the water tables. These models were also biased toward high migration rates. In both the analyses of current and glacial climatic conditions, all rare precipitation events were assumed to begin soon after the loss of institutional control. For example, under glacial conditions, the PMP was assumed to occur at time zero (the year 2170), followed by the 10,000-year storm 1.125 years later. A 1000-year storm was assumed to occur 1.125 years after the 10,000-year storm. The 1000-year storm is followed by nine 100-year storms, each 1.125 years apart. Then, beginning at 2,000 years, this sequence of a 1000-year storm and nine 100-year storms was repeated every 1000 years through the year 9,000. In addition, only evaporation from the land surface was modeled. That is, *the model does not include the removal of soil moisture by plants*.

The results of these studies indicate that:

- The infiltration of the water collected in the LLW trenches will result in downward and lateral spreading of moisture. The lateral spread of the moisture has a potential to affect the moisture conditions around GCD Boreholes 3 and 4 (the boreholes closest to the trenches).

- Focusing precipitation within the subsidence depressions above the GCD boreholes and its infiltration into the vadose zone may result in downward unsaturated flow. However, the moisture front will not reach the water table within 10,000 years under the current or glacial climate change. This conclusion is true when moisture is also migrating laterally from the trench (GCD Boreholes 3 and 4) and when it is not (GCD Boreholes 1 and 2).

Therefore, subsidence with or without climate change can be ruled out as a scenario that needs to be included in the PA.

6.7 Scenario Analysis for Human-Induced Events

Section 6.3 summarized the process applied in this PA to identify and screen all significant processes and events. This screening process leads to a manageable list of processes and events that are either analyzed as part of the base case or developed as mutually-exclusive scenarios.

The initial screening analysis in Section 6.3 resulted in four events requiring further analysis (the two drilling events were combined into a single event). Climate change is expected to occur and was discussed in Section 6.4. Subsidence is also likely to occur, was added to the base case, and was further analyzed in Section 6.6. Note that this subsequent analysis screened subsidence from further consideration in the PA. This section examines the two remaining events: "Exploratory Drilling Penetrates a TRU Borehole," and "Irrigated Agriculture Occurs at the RWMS." The

discussion begins with a review of the regulatory basis in 40 CFR 191 relative to human intrusion.

6.7.1 EPA Guidance For Inadvertent Human Intrusion

EPA determined that inadvertent human intrusion required "special attention." From EPA, 1985; p. 38077, in discussing the possibility of inadvertent human intrusion:

> "...the possibility of inadvertent human intrusion into or nearby a repository requires special attention. Such intrusion can significantly disrupt the containment afforded by a geologic repository (as well as being dangerous for the intruders), and repositories should be selected and designed to reduce the risks from such potential disruptions. However, assessing the ways and the reasons that people might explore underground in the future—and evaluating the effectiveness of passive controls to deter such exploration near a repository—will entail informed judgment and speculation. It will not be possible to develop a "correct" estimate of the probability of such intrusion. The Agency believes that performance assessments should consider the possibilities of such intrusion, but that *limits should be placed on the severity of the assumptions* used to make the assessments. Appendix B to the final rule describes a set of parameters about the likelihood and consequences of inadvertent intrusion that the Agency assumed were the most pessimistic that would be reasonable in making performance assessments. The implementing agencies may adopt these assumptions or develop similar ones of their own...." "...if they develop information considered adequate to support those judgments." [latter quote from EPA, 1985; p. 38080] (emphasis added)

6.7.1.1 Scenario Definition for Inadvertent Human Intrusion

The EPA provided guidance on the question of what can go wrong (the first question posed by Kaplan and Garrick [1981]), and placed practical and reasonable limits on what types of events, processes, and scenarios need to be considered:

> "...it is possible to conceive of intrusions (involving widespread societal loss of knowledge regarding radioactive wastes) that could result in major disruptions that no reasonable repository selection or design precautions could alleviate. The Agency believes that the most productive consideration of inadvertent intrusion concerns those *realistic probabilities* that may be usefully mitigated by repository design, site selection, or use of passive institutional controls (although passive institutional controls should not be assumed to completely rule out the possibility of intrusion). Therefore, *inadvertent and intermittent intrusion by exploratory drilling for resources* (other than any provided by the disposal system itself) *can be the most severe intrusion scenario assumed* by the implementing agencies." (emphasis added)

In describing and implementing this scenario, the EPA Guidance provides the following limitations on the scenario definition:

> Furthermore, the implementing agencies can assume that passive institutional controls or the intruders' own *exploratory procedures are adequate for the intruders to soon detect*, or be warned of, the incompatibility of the area with their activities. (emphasis added)

Appendix B provides additional guidance on the likelihood and significance of this type of human intrusion activity (in answer to the second and third questions posed by Kaplan and Garrick [1981]):

> *Frequency and Severity of Inadvertent Human Intrusion into Geologic Repositories*. The implementing agencies should consider the effects of each particular disposal systems' site, design, and passive institutional controls in judging the likelihood and consequences of such inadvertent exploratory drilling. However, the Agency assumes that the likelihood of such inadvertent and intermittent drilling *need not be taken to be greater* than 30 boreholes per square kilometer of repository area per 10,000 years for geologic repositories in proximity to sedimentary rock formations, or more *than 3 boreholes per square kilometer per 10,000 years* for repositories in other geologic formations. (emphasis added)

Section 6.7.2 summarizes application of probability estimation techniques to the exploratory drilling event *based on a drilling density of 3 boreholes per km^2 per 10,000 years deemed applicable to the GCD disposal facility location*.

6.7.1.2 National Academy of Sciences Views on Inadvertent Human Intrusion Scenarios

To provide guidance to the EPA for writing a 40 CFR 191-equivalent standard for the proposed Yucca Mountain repository, Congress asked three specific questions of the NAS in Section 801(a)(2) of the Energy Policy Act of 1992. The responses to these questions were included in the Technical Bases for the YMP Standards [NAS, 1995b]. Of those three questions, Question 3 provides insight to this discussion:

> Question 3. Whether it is reasonable to make scientifically supportable predictions of the probability that a repository's engineered or geologic barriers will be breached as a result of human intrusion over a period of 10,000 years.

One of the primary concerns in addressing the consequences of human intrusion was that "the consideration of human intrusion cannot be integrated into a fully risk-based standard because the results of any analysis of increased risk as a consequence of intrusion events would be driven mainly by *unknowable factors*" (emphasis added). In a consequence-based analysis, the following recommendation was made for the Standard that will govern YMP:

> Although it would be desirable if the risks associated with the disturbances to a repository by human intrusion could be integrated into a risk assessment of the undisturbed repository performance, technically, it is not appropriate to do so. Rather than a complete risk analysis, one alternative is to examine the site- and design-related aspects of repository performance under an assumed intrusion scenario to inform a qualitative

judgment. In this approach, the objective would be to perform a consequences-only analysis without attempting to determine an associated probability for the analyzed scenario. We recommend that the Yucca Mountain standard require such an analysis.

On the question of the usefulness of such an analysis for evaluating the proposed repository site and design, it was noted in the Technical Bases that:

> "…the key performance issue is whether the repository would continue to be able to isolate wastes from the biosphere, or if its performance would be substantially degraded as a consequence of an intrusion of the type postulated."

Along with developing assumptions regarding conceptual models and critical groups, guidance is needed for scenario development to help assess the resilience of the repository to intrusion. Selecting an intrusion scenario for analysis requires judgment. The following recommendation was made:

> To provide for the broadest consideration of what scenario or scenarios might be most appropriate, we recommend that EPA make this determination in its rulemaking to adopt a standard.

6.7.1.3 Consequences Associated with the Defined Inadvertent Human Intrusion Scenario

The EPA Guidance provides limits on the severity (or consequence) of inadvertent human intrusion:

> Furthermore, the Agency assumes that the consequence of such inadvertent drilling need not be assumed to more severe than: (1) Direct release to the land surface of all the ground water in the repository horizon that would promptly flow through the newly created borehole to the surface due to natural lithostatic pressure—or (if pumping would be required to raise water to the surface) release of 200 cubic meters of ground water pumped to the surface if that much water is readily available to be pumped; and (2) creation of a ground water flow path with a permeability typical of a borehole filled by the soil or gravel that would normally settle into an open hole over time—not the permeability of a carefully sealed borehole.

EPA placed an emphasis on analysis of a "punctured" disposal system and the immediate and long-term releases of water via the pathway opened by the exploratory drilling activity. *Therefore, the consequences from drill cuttings are not included in this scenario analysis.* As such, the EPA Standard will not be interpreted more rigorously than what the EPA intended. The following discussion provides defense for omitting drill cuttings from the PA.

6.7.1.4 Justification for Omission of Drill Cuttings[6]

If an individual inadvertently drills through the buried TRU wastes, should the radionuclides that may be brought to the surface in the drill cuttings be counted as a release to the accessible environment?

Evaluation of this question requires review of some interesting aspects of the 40 CFR 191 regulation. For example, the portion of 40 CFR 191 that is concerned with doses to an individual (the IPRs) specifically states that the doses are to be calculated under the assumption that the "disposal system is not disrupted by human intrusion." This requirement to exclude doses that might result from inadvertent human intrusion may seem counterintuitive. However, the EPA had good reason to exclude doses from accidental releases (e.g., drill cuttings) from the IPRs:

> The individual protection requirements apply only to the undisturbed performance of the disposal system. … This aspect of the standard was included because, if human intrusion occurs, the individuals intruding may be exposed to high radiation doses. No regulatory scheme could prevent this for situations in which large amounts of radioactive material are confined to a relatively small area. [EPA, 1985; p. 66402]

The inability to protect the intruder is a negative aspect of concentrating large amounts of radioactive waste in relatively small areas. An alternative disposal method would be to spread the waste over large areas, such as by ocean disposal. Spreading radioactive waste over large areas protects the intruder because the intruder can never be exposed to large amounts of waste. Once the decision is made to concentrate large amounts of radioactive waste in a small area, there is no means of protecting an intruder.

The question addressed here is: if an individual inadvertently drills through the buried TRU wastes, should the radionuclides brought to the surface as drill cuttings be counted as a release to the accessible environment under the 40 CFR 191 CRs? Recall that the CRs require consideration of all events and processes, which would seem to include releases caused by inadvertent human intrusion. As noted above, however, the EPA Guidance provided a specific interpretation for assessing the limits on severity of releases caused by IHI(s). This interpretation of the Guidance suggests that the EPA is not concerned about releases of TRU wastes in drill cuttings, although under very specific circumstances the EPA is concerned about the performance of a disposal system which has been "punctured."

Possibly the EPA did not want to count releases in drill cuttings because *no regulatory scheme could prevent high releases in the drill cuttings for situations in which large amounts of radioactive material are confined to a relatively small area*.

---

[6] The DOE/HQ Review Team reviewing this PA disagreed with this conclusion. As a result, additional analyses were performed to address Review Team concerns. These additional analyses are documented in Section 8.3.1.

Unless a repository is sufficiently shallow and wide, the releases due to drill cuttings may be a relatively large fraction of the total waste volume, since the waste has been confined to a relatively small area. To count releases from drill cuttings might invalidate otherwise reasonable repository designs, such as that used for the GCD boreholes. On the other hand, different repository designs may perform very differently once punctured. Based on the EPA Guidance, the EPA is concerned about repository performance after a puncture and the EPA is very specific in limiting the potential releases from such a punctured repository. As an example, puncturing WIPP changes the future performance of WIPP by creating a groundwater flow path, since WIPP lies within the saturated zone; puncturing a GCD borehole does not generally change the future performance of a dry GCD borehole.

To complicate the situation, the WIPP Project did include releases that might occur in drill cuttings. Analysis and interpretation from the WIPP Project [Bertram and Guzowski, 1995] determined that the EPA specifically intended to exclude drill cuttings from the consequences associated with the most severe exploratory drilling scenarios. Unfortunately, it was late in the WIPP Project that the regulatory analysts determined that drill cuttings should not be included, and to exclude cuttings would be inconsistent with Project precedence. Notwithstanding, the WIPP analysis and the GCD analysis both conclude that the EPA did not intend that cuttings be included as a release mechanism to be assessed under the 40 CFR 191 CRs.

In summary, an individual receiving a dose from drill cuttings has been excluded by regulation. In addition, releases of TRU wastes via drill cuttings is excluded from consideration by consistent interpretation of the EPA Guidance.

6.7.2 Application of Probability Estimation Techniques to Events

This section presents probabilities of occurrence of the human-induced events as calculated by Guzowski [1996]. Those events were (1) exploratory drilling for resources penetrates a TRU borehole, and (2) irrigation occurs at the RWMS. The goal of that effort was to determine event probabilities for use in the scenario construction procedure (Step 4) in Section 6.3.2.1.

6.7.2.1 Exploratory Drilling Into a Transuranic-Waste Borehole

Based on the EPA Guidance, exploratory drilling for resources is the most severe type of direct human intrusion that must be considered for this PA.

Event Definition Based on Interpretation of EPA Guidance

An interpretation (and therefore, definition) of the exploratory drilling scenario as specified in the EPA Guidance is as follows: From the outset (and following the 100-year AIC period), potential human intruders could be warned by effective PICs and not drill in the area at all. Failing that, if one assumes that the PICs are only partially effective or not effective at all in imparting the required knowledge, humans might then locate and drill an exploratory borehole until they intersect the waste. That event brings up waste in the drill cuttings that, by whatever means, are "soon detected." The drillers then recognize the hazards this drilling site represents and cease

their operations. What is then left is an uncased borehole exposing a pathway from the location of the waste packages to the accessible environment—a "punctured repository."

An extension of this event definition could involve drilling through the GCD wastes to the water table, where the only viable resource located in the region—water—is the objective of the exploratory drilling. In this event, drilling would intersect the wastes, which go undetected, and result in a borehole (cased or uncased) and potential pathway from the water table to the waste region and potentially to the accessible surface environment.

What is the likelihood that this inadvertent and intermittent drilling might occur at the GCD TRU boreholes? The EPA provides very specific, very clear, bounding guidance. The upper limit of 30 boreholes per km^2 of repository area per 10,000 years applies to areas relatively rich in resources (such as significant oil or gas deposits) in sedimentary rock formations; this is not the case for the GCD boreholes located in the deep alluvium of Frenchman Flat on the NTS (see discussion in Section 5.0). Therefore, as noted in Section 6.7.1, the GCD boreholes are located in "other geologic formations" and *the analysis can assume that there are no more than 3 boreholes per km^2 of repository area per 10,000 years*.

Probability Estimation Results for Exploratory Drilling

Guzowski [1996] provides a detailed discussion of the application of a number of probability estimation techniques to the various components of the exploratory drilling for resources event. Evaluation of the details behind these summaries must be left to the reader. In particular, Guzowski utilized both the Poisson and geometric modeling techniques to estimate the probability that at least one exploratory borehole penetrates a GCD borehole. The analysis was broken down to an assessment of drilling rate within a given area, along with exploratory borehole size and area ratios. For comparison, this analysis also included drilling rates of 15 and 30 boreholes/ km^2/10,000 years.

Use of the Poisson model to estimate the probability of drilling into a GCD borehole is based on the assumption that site selection for each exploratory borehole is a random process for as long as drilling occurs. The results utilizing the Poisson model yielded the conditional probabilities noted in Table 6-16. These probabilities are conditional in that they do not include any credit for the effectiveness of some of the components of the event, most notably the effectiveness of AICs or PICs. As will be shown, use of these conditional probabilities is both conservative and consistent with results obtained from the DOE expert elicitation (see Section 6.7.4). For the drilling density applicable to the GCD boreholes from EPA Guidance, *the probability associated with exploratory drilling for resources is quite low, approaching the EPA screening cutoff value of 1.0 E-4 in 10,000 years*.

Guzowski [1996] used the geometric model with two components of the exploratory drilling event: (1) the likelihood of drilling within the secured area, and (2) the intrusion component. The binomial model was used to calculate the probability of any given number of boreholes being drilled within a target area. The geometric model is based on the assumption that the probability of a randomly drilled exploratory borehole hitting a TRU borehole is equal to the ratio of the

areas of the TRU boreholes (the target area) and the area within which the random drilling occurs (the disposal facility area, in this case 0.37 km^2). The results of applying the geometric model are given in Table 6-17.

Table 6-16. Results of Probability Estimation for Exploratory Drilling - Poisson Model

Drilling Density (Boreholes/km^2/10,000 years)	**Estimated Probability in 10,000 Years**
3	1.2 E ! 4
15	6.0 E ! 4
30	1.2 E ! 3

Table 6-17. Results of Probability Estimation for Exploratory Drilling - Geometric Model

Drilling Density (Boreholes/km^2/10,000 years)	**Estimated Probability in 10,000 Years**
3	3.3 E ! 4
15	1.6 E ! 3
30	3.3 E ! 3

Screening Based on Consequence

An abandoned exploratory borehole (cased or uncased) provides a pathway for immediate potential release of water to the surface as well as an exposure pathway for long-term migration of wastes to the surface (the definition of these potential pathways for migration are based on the EPA Guidance, not what is specifically postulated to occur at the GCD location). In the short term, this means either natural or pumped removal of 200 m^3 (7,063 ft^3) of water. In the long-term, such a borehole *could* provide a preferential pathway for flow of water and transport of radionuclides. The first consequence listed by the EPA (in Section 6.7.1), "direct release to the land surface of all the ground water in the repository horizon…" applies only to repositories located within the saturated zone. Because the GCD boreholes are not in the saturated zone, this consequence cannot occur and does not apply. The second consequence listed, "creation of a ground water flow path…" applies to the GCD boreholes but is not expected to result in radio-nuclide releases. First, if such a drillhole reached the water table but was cased, downward flowing water would not contact the waste and so radionuclides would not be transported to the saturated zone. Second, if such a drillhole were not cased, it would likely be filled rapidly by the dry, unconsolidated alluvium in which it was drilled, and thus would not provide a preferential path to groundwater for the radionuclides. Finally, in the unlikely event that such a drillhole were not cased and did not fill in with alluvium, it still would not provide a preferential path to groundwater for the radionuclides because water flowing downward through the drillhole would be flowing quickly and thus would have very little contact time with radionuclide-contaminated

groundwater. Therefore, exploratory drilling through a GCD borehole does not result in radionuclide releases in water, either upward to the ground surface or downward to the saturated zone.

Conclusions for the Exploratory Drilling Event

Given the nature of the GCD borehole site and the provisions of EPA Guidance, there is a very low likelihood that exploratory drilling will intersect the GCD TRU wastes. Because the GCD boreholes are located in the vadose zone, no free-flowing water is available to transport radionuclides upward to the ground surface or downward to the saturated zone. Therefore, exploratory drilling for resources can be removed from further consideration because of lack of consequences.

6.7.2.2 Irrigation Occurs at the Radioactive Waste Management Site

Irrigated agriculture is not considered disruptive human intrusion or a disruptive event. This event could affect disposal system performance, so it was included in the preliminary scenario analysis. Guzowski [1996] provides a brief summary of the application of each of the probability estimation techniques to the irrigation event to derive conditional and final estimates of the probability of irrigation at the RWMS. Evaluation of the details behind these summaries must be left to the reader.

Regardless of the estimation technique used, under current conditions, irrigation from groundwater located at least 244 m (800 ft) below the ground surface is not economically viable. It is assumed and understood that irrigation means commercial agricultural irrigation as opposed to yard or garden irrigation. *Given these assumptions, the probability of irrigation at the GCD site is considered very unlikely*. Also, demand for other residential and commercial uses may preclude allocation of groundwater for what is perceived to be a lower priority use of water. In addition, the land at the RWMS (and Frenchman Flat) may not be suitable for long-term sustainable irrigated agriculture. Therefore, the irrigated agriculture event was eliminated from further consideration in scenario analysis. This conclusion was supported by information obtained during an independent expert elicitation that is presented in Section 6.7.3.

DOE commissioned an expert elicitation to assess probability of inadvertent human intrusion into the Area 3 and Area 5 RWMSs for the NTS LLW PA [Black et al., 1998]. Section 6.7.3 provides a summary of the implementation of that expert elicitation to assess the probability of inadvertent human intrusion into the Area 5 RWMS facilities. Section 6.7.4 then applies the process and results from the expert elicitation to the TRU wastes in the GCD boreholes. This expert elicitation provides supporting arguments for estimates of probability for direct human intrusion into the GCD TRU boreholes.

6.7.3 Expert Elicitation Process

An assessment of inadvertent human intrusion was the focus of a subject matter expert (SME) panel, which examined the site-specific probability of inadvertent human intrusion events through a formal process of expert elicitation [Black et al., 1997]. While this elicitation was

targeted at assessing inadvertent human intrusion into intermediate-depth buried LLW at the NTS RWMSs [Shott et al., 1998], much of the process is directly applicable to the GCD TRU wastes. Although the original expert elicitation of inadvertent human intrusion focused on the LLW-based intruder drilling scenario (estimating the dose to the homesteader via the ingestion of produce grown in a garden contaminated with cuttings from the drilling of a production water well), rather than the inadvertent human intrusion-type event from 40 CFR 191 Guidance (which considers only the potential releases to the environment resulting from exploratory drilling as a breach of containment), the expert elicitation can be effectively used to support the analysis based on 40 CFR 191 guidance. The essential part of the elicitation shared by both scenarios is the estimation of the probability of drilling into the waste, ignoring, for now, the consequences of doing so. The following sections discuss the elicitation process and summarize the results that are relevant to the GCD TRU PA.

6.7.3.1 The Use of Expert Elicitation in Scenario Development

In 1996, an expert elicitation involving participation of stakeholders, the public, and environmental professionals was conducted to develop likely scenarios[7] for inadvertent human intrusion at the NTS Area 3 and Area 5 RWMSs and to better represent the probabilistic nature of inadvertent human intrusion in support of the NTS LLW PAs. A stakeholder workshop was convened early in the project to involve the public in the probabilistic process development. The stakeholders confirmed that the inclusion of site-specific community scenarios should be considered in addition to the default homesteader scenario. They also verified that appropriate variables had been identified for consideration in the intrusion scenarios to be used. In addition, they strongly endorsed the probabilistic process and underlying assumptions [Black et al., 1997]. Details regarding the general elicitation process are provided in Black et al. [1998].

Traditionally, LLW PAs are deterministically based, assuming that inadvertent human intrusion will occur with a probability of one at some time during the evaluation period (in this case, 10,000 years). This expert elicitation was conducted as a first step towards bringing a probabilistic perspective to this aspect of LLW PA, and the approach is more consistent with the probabilistic PA methodology outlined for TRU wastes in 40 CFR 191. The NTS LLW inadvertent human intrusion elicitation was not dependent on the specific waste inventory or configuration, and so it was deemed by DOE/NV to be applicable to the GCD TRU wastes, which are sited adjacent to the LLW disposal pits and trenches. In addition, many of the major issues surrounding both the LLW and TRU waste disposal cells are the same, especially with respect to disruptive activities.

Expert judgment has proven to be a particularly useful tool for evaluating probabilistic estimates for rare or poorly understood phenomena and for forecasting future events [Geomatrix, 1997, 1998; Kotra et al., 1996; Morgan and Henrion, 1995; Meyer and Booker, 1991; Keeney and

[7] As noted elsewhere in this report,"events and processes" are analyzed for probability and then combined in logic diagrams to form "scenarios," or collections of events and processes. The SMEs in the expert elicitation developed community and homesteader "scenarios" to help define possible occurrences of human habitation of Frenchmen Flat and the probability of human intrusion via the water well drilling event they postulated. This usage by the SMEs of the term "scenario" is distinguished with usage of the term for the balance of this report.

Raiffa, 1993; Raiffa, 1968]. These topics have significant uncertainty that commonly cannot be reduced by conventional means of data gathering. The issue of inadvertent human intrusion for the GCD boreholes in the Area 5 RWMS in Frenchman Flat is a prime example, involving multiple factors with largely non-reducible uncertainty. There is uncertainty in the future missions and institutional control of the NTS, uncertainty in the viability, values, and practices of future societies, and uncertainty in future hydrogeologic processes that make arid desert lands either more or less desirable to society. The purpose of the elicitation is to quantify that uncertainty probabilistically.

The elicitation was conducted in the following stages:

- Develop the logic of the pertinent factors affecting inadvertent human intrusion through influence diagrams,

- Hold open workshops involving participation of stakeholders, environmental and waste management professionals, and the public to examine the logic and acceptability of the approach taken for the probabilistic study, and

- Assess the probabilities of intrusion into waste units by convening and formally eliciting expert judgments from a panel of SMEs.

An external review was conducted through a workshop to ensure that stakeholders shared a basic understanding of the probabilistic approach [Black et al., 1998]. Results of the stakeholder and public interactions were used to tailor the probabilistic assessments to the NTS and to validate the logic used in the influence diagrams for the management controls and settlement scenarios. In particular, the workshop participants concluded that, based on current population trends, a scenario of community settlement in Frenchman Flat (as well as the neighboring Yucca and Jackass Flats) is plausible and should be considered for evaluation.

The SMEs found it necessary to establish assumptions for the modeling process. The first assumption concerns the effectiveness of site management controls. Management control factors that may affect inadvertent human intrusion were developed in the stakeholder workshop and were defined during the SME elicitation sessions. These factors include AICs, such as maintained fences and the presence of waste management and security personnel, and PICs, including site knowledge, placards and markers, surface barriers, and subsurface barriers. If any of these management controls is effective, it was assumed by the SMEs that inadvertent human intrusion could not then occur.

The current boundaries of the NTS are subject to AIC, so open public access to waste disposal sites is prohibited. As long as institutional control of the NTS is actively maintained, the SMEs found it reasonable to assume that all public development on the site will be precluded and that inadvertent human intrusion will be avoided. While institutional control and site knowledge may be important factors for the first few centuries, they would not be significant over the evaluation period of 10,000 years. This conclusion supports the regulatory limit for contributions to system performance from AICs to no more than 100 years after disposal (which, for the GCDs, has been

interpreted by DOE/NV to mean 100 years after closure of the site, anticipated in the year 2070, so that credit for the AICs would be extended to the year 2170). The SMEs decided that the potential for institutional control or site knowledge to last for 10,000 years was very low. Their opinions concurred with those of the workshop participants. Elicited input for the institutional control and site knowledge factors indicated less than 500 years of combined effectiveness. For this assessment of inadvertent human intrusion for the GCD boreholes, no credit is taken for effectiveness of institutional controls or maintenance of site knowledge.

The SMEs argued that placards and markers designed to current societal interpretations are unlikely to maintain their intended meaning in the future, unless their design is relatively simple. Since no system of placards or markers has been devised, no credit is taken for this management control in developing the probability of inadvertent human intrusion for the GCD boreholes. The SMEs also concluded that surface barriers can be designed that would, for example, deter the siting of a drill rig over the waste site with an effectiveness of 95%, but that subsurface barriers and placards and markers will not prevent inadvertent human intrusion as effectively. Since this design theme has not been planned for implementation over the GCD boreholes, no credit is taken for surface barrier effectiveness against inadvertent human intrusion. It was concluded that cost-effective subsurface barriers cannot be designed or constructed, because human curiosity or technology would eventually penetrate all barriers. No subsurface design has been established for the GCD boreholes; thus no credit is taken for this management control provision. Unless and until these PICs are adopted by DOE for implementation, credit may not be taken for them in the PA. However, the EPA Standard acknowledges AICs and PICs as part of the Assurance Requirements, discussed in greater detail in Volume 4 of this CAD.

A second assumption addresses prediction of future changes in society and technology. Past studies have shown that many aspects of science and technology, particularly social sciences that are more susceptible to the vagaries of human behavior, are inherently unpredictable [Casti, 1990]. At best, stochastic or probabilistic models of future events can be developed. Accurate prediction of most events is impossible, so a working assumption for this probabilistic study of inadvertent human intrusion is that forecasting of future patterns must be based on current technology and current societal practices.

A third assumption by the SMEs was also noted by Black et al. [1997]. The SMEs proposed a periodic review of intrusion at an interval of 25 years, in order to reassess probabilistic estimates given that changes in society or technology will affect the results of the evaluation. They recommended that sufficient funds be allocated to ensure a periodic review of intrusion.

The final assumption for the basic approach concerns the mechanisms by which an inadvertent intruder who gains access to NTS chooses to settle in a remote alluvial valley. Several settlement scenarios are possible, and a range of factors may affect the outcome of the probabilistic assessment of inadvertent human intrusion for these scenarios. Examples of such factors include the suitability of the land surface for expected settlement activities and future groundwater availability. The factors and the models developed by the SMEs for each scenario provided the necessary focus for the expert elicitation.

In summary, the principal assumptions concerning the assessment of inadvertent human intrusion are that management controls, if implemented by DOE, will preclude inadvertent human intrusion as long as they are effective (but will be insignificant over the 10,000-year compliance period), that forecasts of future activities must be grounded in the present, that review of intrusion occur at least each generation, and that any inadvertent human intrusion that would occur would be the result of settlement of Frenchman Flat.

6.7.3.2 Scenarios For Direct Human Intrusion

At this point, it is instructive to reflect on what sort of human activities could possibly cause a release of contaminants from the GCD boreholes to the accessible environment. Recall the simple intermediate-depth borehole geometry: The wastes are packed in boxes in a vertically oriented cylindrical cavity 3 and 3.7 m (10 and 12 ft) in diameter and 15 m (50 ft) in height. Most importantly, the top of this cylinder is 21 m (70 ft) below the ground surface. In order to actually disturb the waste, an inadvertent intruder would have to dig below 21 m (70 ft). This excludes some of the standard inadvertent human intrusion scenarios prescribed by, for example, DOE Order 5820.2A for LLW [Wood et al., 1994], which assume that the intruder is excavating a basement for a dwelling. Excavation of the waste is possible, however, in a drilling scenario in which a homesteader drills a well for water. This event was corroborated by the work of Guzowski [1996], which was discussed in Section 6.3.2. Other credible direct intrusion scenarios are lacking, since the only other known natural resource in Frenchman Flat is gravel, which would not be mined to a depth of 21 m (70 ft). Of course, the GCD wastes are not regulated under Chapter III of 5820.2A (as is the adjacent LLW), but rather under 40 CFR 191, which also recognizes the possibility of drilling as the most serious type of inadvertent human intrusion event which need be considered.

The SMEs also concluded that drilling was the only plausible way to disturb the waste. They were asked to consider all possible scenarios that might result in intrusion into the waste, and were encouraged to consider scenarios that go beyond the default scenarios considered in LLW PAs. Although the SMEs were not provided with the exhaustive list of FEPs used by Guzowski, they came to the same basic conclusion that drilling was the only plausible mechanism to unwittingly exhume this intermediate-depth waste. From that point they proceeded to examine scenarios of human activities which would result in drilling in Frenchman Flat.

Exploratory drilling through the thick alluvium of Frenchman Flat might occur in the exploration for natural resources. There is no exploitable amount of oil and gas in the area, and the only conceivable mineral resource is gravel of poor grade. The principal exploitable resource is water, which, although deep, is of potable quality. While the SMEs ruled out the possibility of supporting commercial-scale agricultural enterprises, they did concede that the water could be used to support a limited number of homesteads or communities.

The probability of drilling into waste was judged to be driven primarily by two settlement scenarios: (1) the homestead scenario, consisting of scattered individual homesteaders, each homestead with its own well, and (2) a community scenario incorporating a cluster of settlers that share drilling and distribution systems for groundwater. The SMEs were given complete

freedom to discuss and revise the scenarios and management control factors as necessary. This process resulted in acceptance of the homestead scenario and refinement of the community scenario. Three separate community scenarios were identified:

- a small community located in the alluvial basins of Frenchman Flat (Base Community Scenario),

- urban expansion of Las Vegas north up the valley corridor and into the alluvial basins of NTS, including "commuting homesteaders" (Las Vegas Expansion Scenario), and

- a small community located in Jackass Flats, or in another area nearby Frenchman Flat, including "commuting homesteaders" (Jackass Flats Scenario).

The SMEs defined "commuting homesteaders" as settlers who commute regularly from their homes located outside of the community or urban resource base, but who do not share water wells or distribution systems. This was distinguished from the homestead scenario for which homesteaders were assumed to be isolated from any central community. The homestead scenario, in addition to the three community scenarios, yields the four scenarios that the SMEs considered in this study.

The four settlement scenarios follow a common basic model represented by the influence diagram in Figure 6-37. The rectangular elements in the diagram indicate inputs which are single-valued, such as the duration of the compliance period specified in the EPA Standard (the compliance period is identical for both DOE Order 5820.2A and 40 CFR 191). Oval elements represent inputs that are probabilistic in nature, such as the lifetime of an individual well. Probability distributions for the primary factors were elicited from the SMEs (unshaded ovals), whereas others are derived from these factors (shaded ovals). The number of wells likely to be drilled was evaluated separately for each scenario. Inputs obtained from the SMEs for each scenario provided information relevant to the top-level factors: the number of wells at a point in time (well density) and the well lifetime. Elicitation of these inputs depended on other factors specific to each scenario. The inputs were used to assess the total number of wells that are anticipated to be drilled in the region during the 10,000-year compliance period.

Several factors were included in the scenario-specific influence diagrams, all of which affect assessment of the number of wells to be drilled during the evaluation period. For example, suitability of the land surface and hydrogeologic factors may influence the likelihood of establishing a settlement in the vicinity of the RWMS. The suitability of the land surface may be influenced by the remoteness of the alluvial basins, playas (dry lakes) that are contained within these basins, and surface-collapse craters that were formed by underground testing.

Several scenarios were considered by the SMEs, including isolated and independent homesteads in Frenchman Flat, a single small independent community with shared resources, a community of commuting homesteaders resulting from the expansion of Las Vegas, and a community of commuting homesteaders associated with a central community in Jackass Flats. Analysis by the SMEs indicated that independent homesteading without an associated support community is

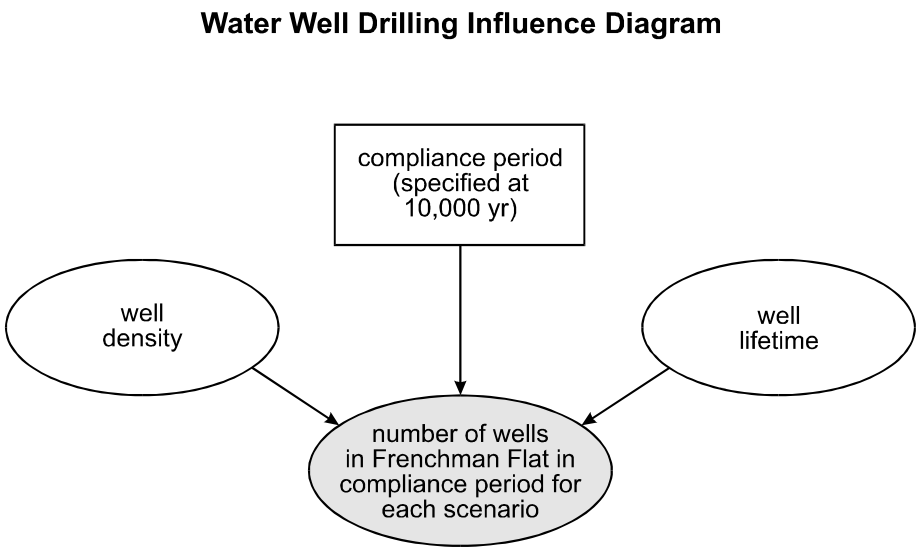

Figure 6-37. Influence Diagram of Factors to Determine the Number of Wells Drilled for Each Settlement Scenario.

extremely unlikely to occur in Frenchman Flat. Of the community scenarios, the Jackass Flats scenario was judged by the SMEs to clearly dominate the assessment of well densities in Frenchman Flat, so the other scenarios have been discarded. The Jackass Flats Scenario consists of locating a community in an area near Frenchman Flat. Jackass Flats is centrally located in the vicinity of the Flats of interest. The assumption is that there are many areas around NTS that would be more desirable than Frenchman Flat for community settlement, but that such communities would place population pressure on these two areas. For example, a community that develops in Jackass Flats, or around the current infrastructure of Mercury, is considered large enough to spill population over into neighboring valleys. The opinion of the SMEs was that this type of scenario is likely to occur, and that communities of this type can be expected to be present intermittently for approximately 5,000 years during the evaluation period. The number of wells drilled in Frenchman Flat was estimated by Black et al. [1998] to be approximately 5,000.

Given the four settlement scenarios and the presence of management controls, the high-level influence diagram for determining the probability of inadvertent human intrusion in Frenchman Flat is shown in Figure 6-38. The dimensions and locations of the GCD boreholes are well known, but the locations of the future water wells are not, and are considered a random variable in the assessment of the probability of accidentally drilling through a GCD borehole. The complete method of estimating the probabilities of inadvertent human intrusion by drilling through a GCD borehole is developed in Section 6.7.4.

6.7.4 Analysis of Direct Human Intrusion

The basic rationale for conducting a probabilistic PA is outlined in Section 3.0. The essence of

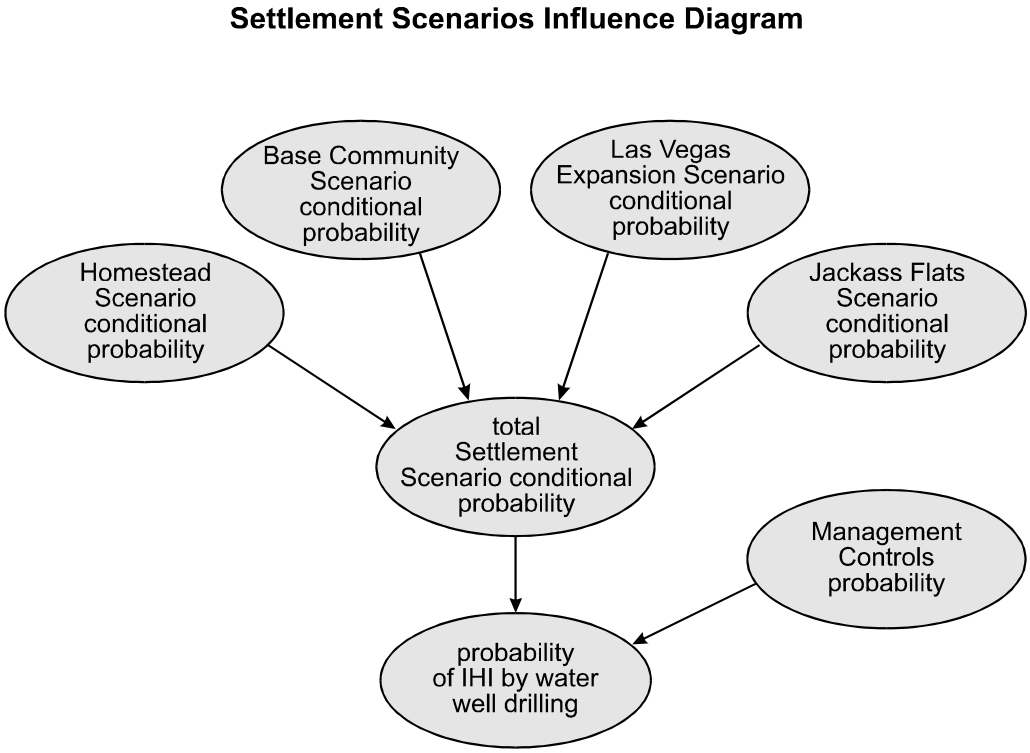

Figure 6-38. Influence Diagram for the Probability of Inadvertent Human Intrusion.

the probabilistic approach in application to human intrusion scenarios is that a conceptual model of inadvertent human intrusion for each scenario is developed, uncertain factors are identified and assigned probability distributions, and the uncertainties are propagated through a simulation that combines samples from the specified probability distributions based on the conceptual model. The expert elicitation study [Black et al. 1998] provided a rigorous and defensible subjective technique for developing scenario conceptual models and estimating probability distributions for uncertain factors. This section discusses the application of the elicitation in a probabilistic assessment of GCD inadvertent human intrusion as outlined in Section 6.7.3.

6.7.4.1 Application of Expert Elicitation to Intrusion Scenarios

Scenario influence diagrams (e.g., Figure 6-39) provide a qualitative description of the interrelationships between important factors prescribed by the SMEs. Each unshaded oval node in the influence diagram represents an uncertain factor for which probability distributions were elicited from the SMEs. Thus, the SMEs have provided the foundation for the underlying structure of the influence diagrams as well as the probability distributions assigned to each uncertain factor. The uncertainty in each factor, as defined by the elicited probability distributions, was propagated through the relationships defined in the influence diagrams resulting in a final scenario-specific probability distribution.

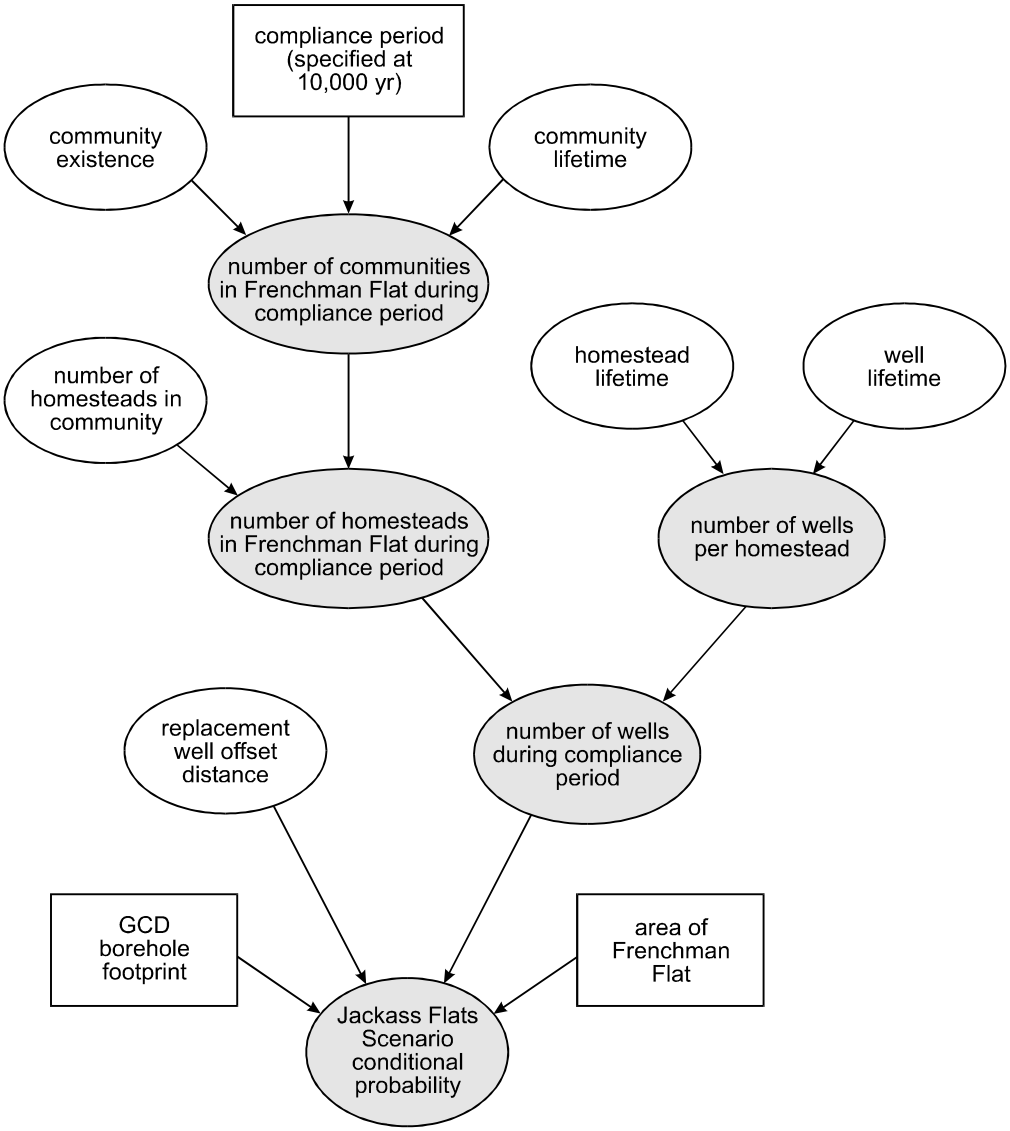

Figure 6-39. Influence Diagram for the Jackass Flats Community Scenario.

Probability distributions for uncertain factors were elicited from the SMEs in the form of quantiles, as demonstrated in the following sections. Fitting the elicited quantile data using polynomial regression generated CDFs. These CDFs were then used as the basis for a Monte Carlo simulation to propagate the uncertainty in each factor. In this approach, samples were drawn randomly from the fitted CDFs, ultimately generating samples of uncertain output factors and the scenario-specific probability distribution of inadvertent human intrusion.

The sample of probabilities resulting from the simulation is used to estimate the scenario probability distribution. Thus, the final results of the uncertainty propagation are presented in the form of probability distributions providing an indication of the uncertainty associated with these probabilities. These distributions reflect the assumptions and conditions imposed by the elicitation process and, therefore, do not represent all possible sources of uncertainty.

As previously detailed in Section 6.7.3, the probabilistic assessment of intruder well drilling scenarios clearly indicated that the Jackass Flats scenario with commuter homesteads in Frenchman Flat was the most likely scenario by which inadvertent human intrusion might occur [Black et al. 1998]. Thus, the focus of scenario analysis for the GCD TRU PA is the Jackass Flats community scenario, which dominates so strongly that the others may be ignored. The objective in applying the elicitation results in an inadvertent human intrusion assessment of the GCD is to estimate the probability of drilling a well into a GCD TRU borehole.

The Jackass Flats Community Scenario

The Jackass Flats community scenario is essentially a hybrid of the base community and homestead settlement scenarios, in that homesteaders settle in Frenchman Flat only because of the existence of a support community in Jackass Flats. The influence diagram model for the Jackass Flats scenario includes the following constant input factors (represented as rectangles in Figure 6-39):

- the compliance period of 10,000 years as defined in 40 CFR 191;
- the area of Frenchman Flat (35,000 ha or 86,000 acres); and
- the area of the GCD TRU boreholes (two 10-ft and two 12-ft diameter boreholes).

The influence diagram also includes uncertain input factors (represented as unshaded ovals in Figure 6-33) relating to:

- the cumulative length of time during which communities would exist during the compliance period;
- the lifetime of a single community;
- the number of homesteads associated with the community;
- homestead lifetime (the number of years that a homestead might be expected to remain viable in this area);
- well lifetime; and
- the distance a replacement well (if needed) would be placed from the original well.

Information needed to generate probability distributions for these uncertain input factors was elicited from the SMEs. From this elicited information, CDFs were estimated using polynomial regression for use in the probabilistic simulation.

Several uncertain factors (represented as shaded ovals in Figure 6-39) are generated through the simulation of the scenario influence diagram, including:

- the total number of communities during the compliance period;
- the total number of homesteads settled during the compliance period;
- the number of wells drilled for each homestead; and
- the total number of wells drilled during the compliance period.

The total number of wells is then used in conjunction with the total area of the GCD TRU boreholes and the area of Frenchman Flat to calculate the conditional probability of a well accidentally being drilled into a GCD TRU borehole, excluding the influence of management controls.

A summary of the elicited information, in the form of quantiles, and the estimated CDFs are provided in the following discussion.

Community Existence

The first issue to be addressed by the SMEs for this scenario concerned the potential for a community to be located in the vicinity of Jackass Flats, putting population pressure on Frenchman Flat in the form of commuter homesteading. The SMEs were asked to provide the number of years (out of the next 10,000 years) a Jackass Flats community might exist, providing a limit on the time frame for which inadvertent human intrusion could occur for this scenario. The SMEs provided the following input for community existence:

- There will be communities for no less than 25% of the time.
- There will most likely be communities for about half of the time.
- There will not be communities for more than 75% of the time.

This corresponds to a period of time of between 2,500 and 7,500 years uniformly distributed over the next 10,000 years (i.e., not necessarily consecutive years). To randomly simulate values for this factor, a uniform distribution between 2,500 and 7,500 is used.

Community and Homestead Lifetime

The SMEs agreed, based on knowledge of historical trends of small, single-purpose communities and their personal experiences, that the expected lifetime of a community would be quite short. The SMEs' input on the lifetime of a community was as follows:

- Ten percent of the communities are expected to collapse within 10 years.
- Twenty-five percent of the communities are expected to collapse within 35 years.
- Fifty percent of the communities are expected to collapse within 50 years.
- Seventy-five percent of the communities are expected to collapse within 65 years.
- Approximately 5% of the communities are expected to last longer than 100 years.

The SMEs also indicated that homesteads that occur as a result of nearby communities are expected to have the same lifetime as the corresponding community. While this is a somewhat conservative assumption, the SMEs regarded it as reasonable given the relatively short expected lifetimes for the envisioned communities.

Number of Homesteads per Community

Assuming a community were to come into existence in Jackass Flats, the number of related homesteads that might be located in Frenchman Flat was elicited from the SMEs. When there is a community nearby, the SMEs would expect:

- There will be one or more homesteads in Frenchman Flat 90% of the time.
- There will be more than 50 homesteads in Frenchman Flat 50% of the time.
- There will be more than 100 homesteads in Frenchman Flat 5% of the time.
- There will be more than 200 homesteads in Frenchman Flat 1% of the time.

Well Lifetimes

The SMEs agreed on an assumption of one primary water well per homestead. Knowledge of local well traits dominated the discussion of well lifetimes for future homesteaders in Frenchman Flat. The SMEs projected that polyvinyl chloride (PVC) pipe will be in common use for these private wells. The SMEs cited many potential difficulties that could bring an end to a well's useful lifetime, including the pipe breaking as the pump is dropped down, breakdown of the casing, encrustation, sand, cave-ins, and earthquakes. The input for this variable was elicited directly as the following:

- The median well lifetime is expected to be 35 years.
- Twenty-five percent of the wells are expected to fail within 20 years.
- Only 5% of the wells are expected to fail within 10 years.
- Similarly, only 5% of the wells are expected to last longer than 60 years.

Replacement Well Offset Distance

The SMEs indicated that when a well fails, a replacement well would be necessary for the homestead to remain viable. Under this assumption, the SMEs were asked how far from the original well a replacement well would be drilled. The offset distance between an original well and its replacement was important because wells that are close to one another by design may not have the same opportunity to intersect the waste footprint as wells that are randomly sited throughout Frenchman Flat. The following inputs from the SMEs were obtained:

- The median distance between the original well and the replacement well was assessed as 9 m (30 ft).
- Ten percent of the replacement wells are expected to be less than 3 m (10 ft) from their corresponding original well.
- Ten percent of the replacement wells are expected to be more than 15 m (50 ft) from their corresponding original well.

Probabilistic Assessment Through Simulation

The estimated CDFs are the basis for the random draws used in the simulation of the scenario influence diagram (Figure 6-39). The simulation is conducted by:

- Randomly drawing a community existence period.

- Randomly drawing community lifetimes until the sum of the individual community lifetimes exceeds the previously drawn community existence (from step 1). This provides the number of communities that may exist during the compliance period.

- Randomly drawing from the number of homesteads per community distribution for each community that may exist during the compliance period (from step 2).

- Summing the simulated number of homesteads per community to calculate the total number of homesteads during the compliance period.

- Randomly drawing well lifetime for each homestead (from step 3) until the cumulative well lifetime for a homestead exceeds the simulated community lifetimes (from step 2). This provides the total number of wells drilled during the compliance period, under the assumption that each homestead will only have one active well at a time.

This process is simulated many times generating a large sample for each of the uncertain factors represented in the scenario influence diagram (Figure 6-39).

Assumptions:

- Homesteads are randomly placed across the whole area of Frenchman Flat;
- The waste is homogeneously distributed in a borehole so that drilling into any portion of a borehole results in waste being brought to the surface;
- Well diameter is insignificant in relation to borehole diameter;
- Homestead lifetimes equal the lifetime of the associated community; and
- Replacement wells do not significantly increase the likelihood of drilling into the waste.

The first three assumptions allow the further assumption that the probability of a well being drilled into a GCD borehole is a binomial random variable. Following this assumption the scenario probability is calculated as

$$P(\text{IHI}) = 1 - (1 - p)^n \qquad (6\text{-}20)$$

where p is the ratio of the total GCD borehole footprint to the area of Frenchman Flat and n is the number of wells drilled in Frenchman Flat during the compliance period. Thus the total number of wells and the ratio of the waste footprint to the area of Frenchman Flat are the critical factors that determine the scenario probabilities.

6.7.4.2 Results of Jackass Flats Scenario

The SMEs clearly indicated that the Jackass Flats scenario was the most likely scenario by which inadvertent human intrusion could occur. The SME panel concluded that the probability that a community of commuter homesteaders would be established in Frenchman Flat, at any given point in time, would be between 0.25 and 0.75. This corresponds to a period of occupation (not necessarily consecutive years) of between 2,500 and 7,500 of the next 10,000 years. Because of the long timeframe involved, the number of wells (approximately 5,000) drilled in Frenchman Flat under this scenario is comparatively large.

Replacement wells are of concern, but the impact of simulating replacement wells on the conditional scenario probability is minimal. Based on simulations, approximately 72% of the homesteads were expected to require a replacement well [Black et al., 1998]. Since the distance the replacement well is drilled from the primary well is small relative to the area of Frenchman Flat, if a primary well does not intersect a GCD borehole, then a replacement well is extremely unlikely to intersect a borehole. The computational burden of the simulations is greatly reduced by only considering primary wells.

Simulation results for the Jackass Flats scenario are presented in Figures 6-40 and 6-41. These conditional probabilities represent the likelihood of a well being drilled into a GCD borehole in the next 10,000 years. The median scenario probability is 0.0006 and ranges from a low value of 0.0002 to a high of 0.0011.

These estimates for the density of exploratory wells in Frenchman Flat compare favorably to the EPA Standard. As outlined in Sections 6.3.1.2 and 6.7.1, the EPA Guidance limits the likelihood of inadvertent and intermittent drilling in "sedimentary rock formations" to 30 boreholes per square kilometer of repository area over 10,000 years and in "other geologic formations" to 3 boreholes per km^2. The higher value presumably reflects the more likely occurrence of exploration in sedimentary rock for mineral resources extractable by drilling, such as oil and gas, which occur in sedimentary formations. Water, however, occurs in all rock formations, and so would be expected to fall somewhere between the 3 and 30 boreholes per km^2 values. *The median number of homesteads simulated for the Jackass Flats scenario is approximately 5,000, which, when divided by the area of Frenchman Flat, gives a median value of about 16 boreholes drilled per km^2, a value derived by methods completely independent of the EPA Standard.* The simulated number of boreholes drilled per km^2 ranges from 1 to 30 (Figure 6-42).

6.7.5 Conclusions and Recommendations for the Performance Assessment

As stated in Section 6.3, the purpose of the GCD screening analyses was to identify those events, processes, and scenarios that may affect the ability of the GCD boreholes to isolate TRU wastes from the accessible environment over the next 10,000 years, as defined in 40 CFR 191.

The CRs of 40 CFR 191 are concerned with base case processes and events as well as disruptive scenarios. The scenario analysis identified the disruptive scenarios necessary for assessing compliance with the CRs.

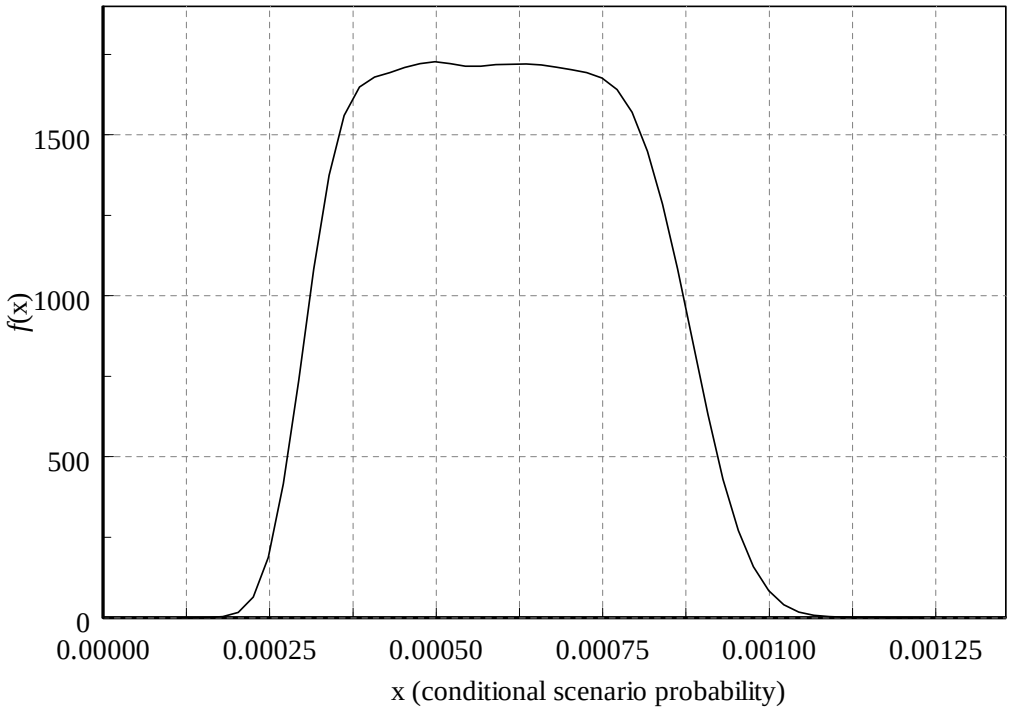

Figure 6-40. Estimated Distribution for the Conditional Scenario Probability of Inadvertent Human Intrusion for the Jackass Flats Community Scenario.

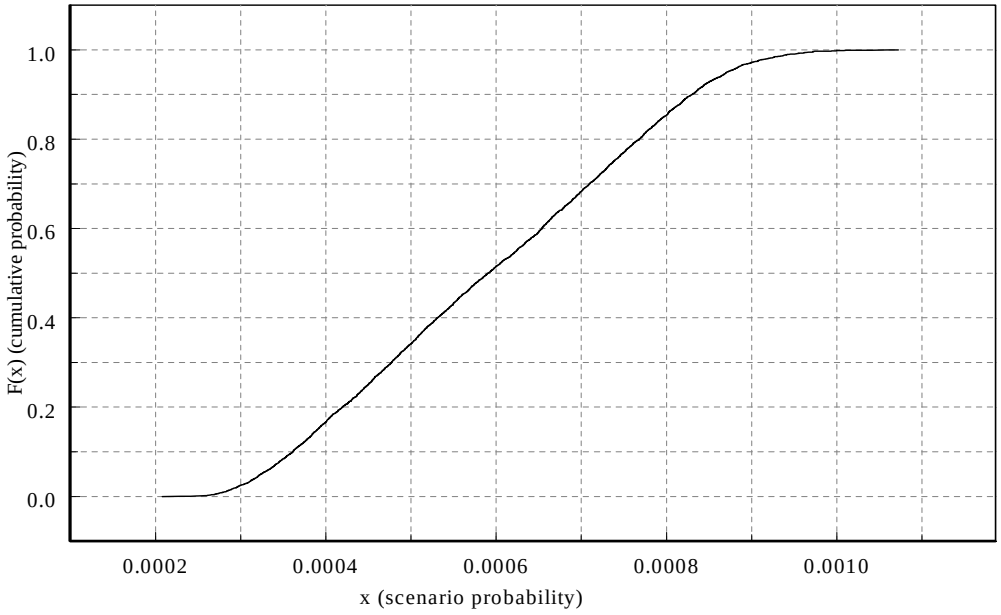

Figure 6-41. Estimated CDF for the Scenario Probability of Inadvertent Human Intrusion for the Jackass Flats Community Scenario.

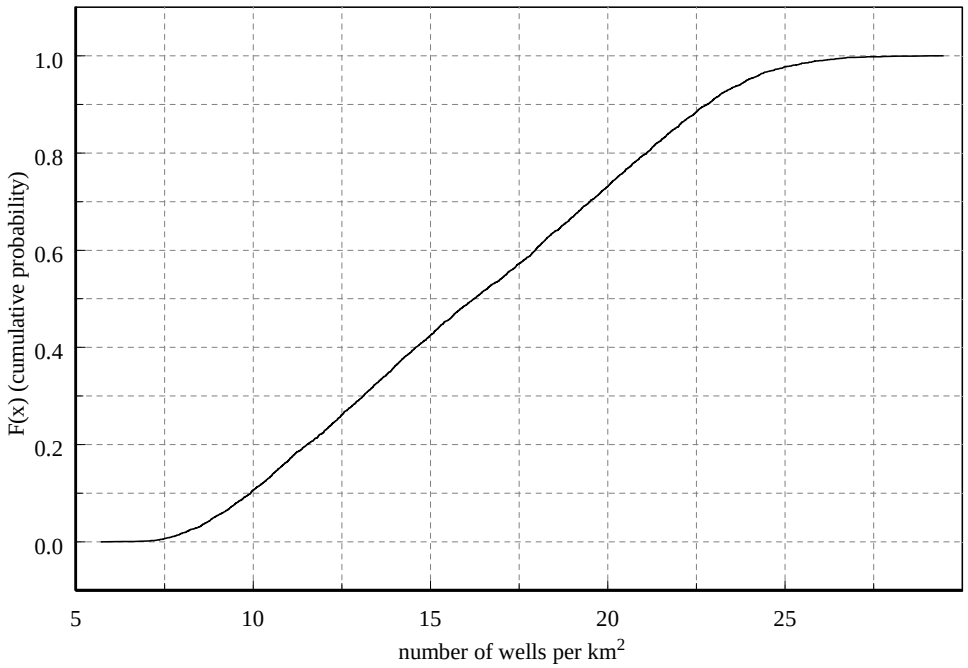

Figure 6-42. Estimated CDF for the Number of Wells Drilled per Square Kilometer in Frenchman Flat for the Jackass Flats Community Scenario.

A systematic, comprehensive, and consistent process was used to identify all significant processes and events that could adversely affect disposal system performance. Those events and processes that could have a positive impact on performance were not considered (as such, events like subsidence were screened from the PA). As noted in Section 6.3.2, use of the systematic process either eliminated all naturally-induced and disposal system-induced events and processes or considered those events/processes in the base case analysis. Climate change and landfill subsidence are notable examples of events and processes considered in the base case.

The EPA Guidance was relied upon for the analysis of direct human intrusion. As prescribed in the EPA Guidance, limits were placed on the severity of the assumptions made in the assessment of inadvertent human intrusion. The screening process and analysis were limited to inadvertent intrusion events. Specifically, for the analysis of inadvertent human intrusion, inadvertent and intermittent exploratory drilling for resources was considered the most severe intrusion scenario that need be considered. In addition, the EPA Guidance specified limits on the frequency of such events. As such, this analysis adopted EPA Guidance on the frequency or density of exploratory drilling that may occur: that the likelihood of exploratory drilling need not be taken to be greater than 3 boreholes per square kilometer per 10,000 years.

As noted in Sections 6.7.3 and 6.7.4, the expert elicitation provided arguments supporting the assumptions made about inadvertent human intrusion. It is important to note that the expert elicitation was conducted as an independent analysis not related to the GCD TRU PA or the requirements of 40 CFR 191. The SMEs considered drilling for water resources the most plausible mechanism to inadvertently intersect and intrude upon the intermediate depth waste.

The analysis of the Jackass Flats scenario concluded that homestead density will result in a median value of about 16 water wells drilled per km^2 in Frenchman Flat over the 10,000-year timeframe. Given that water, as a resource, may occur in any rock formation, this drilling density is consistent with that based on the EPA Guidance.

As noted in Section 6.7.2, different probability estimation techniques yielded the results for the EPA Guidance-based exploratory drilling event noted in Table 6-18. The high and median results from the expert elicitation for water well drilling are included for comparison.

Table 6-18. Final Results of Probability Estimation for Exploratory Drilling

Drilling Density (wells/ km^2)	Poisson	Geometric	Elicitation
3	1.2 E ! 4	3.3 E ! 4	n/a
15	6.0 E ! 4	1.6 E ! 3	6.0 E ! 4 (median)

These results are consistent given the variety of estimation techniques used and the uncertainties involved in developing these kinds of estimates. Clearly, the likelihood of occurrence that exploratory drilling might intersect GCD TRU waste is quite low. As noted in Section 6.7.2, the consequences of exploratory (or water well) drilling on disposal system performance are zero. Therefore, this event was screened from the final PA analysis.

In Section 6.7.2, commercial irrigated agriculture was analyzed and not considered a viable activity in Frenchman Flat; this conclusion was corroborated by the expert elicitation. Therefore, the event was screened from further consideration in scenario development.

The goal of Step 4 in the scenario development procedure (see Section 6.3.2.1) is to construct scenarios by combining the events and processes that survive the screening process, using logic diagrams. This scenario development process identifies the unique and mutually exclusive set of scenarios, including the base-case scenario (defined by the pathway through the logic diagram resulting from "no" decisions at each of the branch points). The base case consists of the geo-hydrologic conditions within the disposal system at the time of closure, and those changes expected to occur to this system during the 10,000 years after closure. From a conceptual-model point of view, the base case scenario consists of the parameter values that define the physical characteristics of the disposal system and those processes that will occur during the "normal" undisturbed evolution of the disposal system. Any other scenario developed within the logic diagram consists of a modification to this expected evolution.

Since all of the identified significant processes and events were either eliminated or were considered part of the base case, there was no need to perform Steps 4 and 5 of the scenario development and screening process. *All that remains from the scenario analysis for the GCD TRU PA are those processes and events that are considered part of the base case and analyzed in other portions of this CAD.*

6.8 Conclusions

Over the next 10,000 years, the Area 5 RWMS will change. The forcing agents for the changes are:

- activities associated with operation and closure of the Area 5 RWMS that could "disturb" site conditions;
- future human activities that could inadvertently alter site conditions; and
- natural processes, which operate on long time scales, that may alter site conditions.

The nature of these forcing agents and their potential effects on the movement of radionuclides in the GCD boreholes were analyzed in this section and summarized in Table 6-19.

Table 6-19. Summary of Conceptual Model for the Future Evolution of the Disposal System

Actual and Expected Conditions	Modeled Conditions	Justification
Area 5 disposal operations will continue through year 2070; disposal cells, boreholes, pits, and trenches will be uniformly covered with a 2-m [7-ft] native alluvium cap.	None, the PA is performed only for the post-closure period. The GCD boreholes will be uniformly covered with a 2-m (7-ft) native alluvium cap	Realistic; cap is part of the closure plan (Section 6.2). Credit for the cap is allowed by 40 CFR 191.14(d)
During the 100-year AIC period from 2070 to 2170, natural processes that may impact disposal system performance will be mitigated (e.g., erosion; formation of subsidence depressions; and human intrusion).	No impacts from flooding or erosion, plant or animal intrusions, subsidence or human intrusion or human-induced surface disturbances are modeled during AIC.	Realistic; the DOE is committed to maintaining AICs and credit for mitigation during AIC is allowed by 40 CFR 191.14(a) (Section 6.2)
After 2170, AICs and PICs will eventually become ineffective.	The PA does not take credit for AICs or PICs after the year 2170.	Conservative; actual AICs and PICs implementation and durability are unknown; 100 years credit taken for AICs, per 40 CFR 191.14(c).
Under current *interglacial* climate conditions (after year 2170):		
a. Unmitigated subsidence occurs, creating collapse features which capture and focus precipitation - causing increased moisture content in alluvium and potential downward movement of moisture	Increased moisture content and potential downward movement of moisture is not modeled in quantitative PA (was modeled in subsidence screening analysis).	Conservative; modeling fastest, shortest pathway (22 m [72 ft]) to accessible environment, using upward advection would result in higher releases than modeling downward advection. Screening analysis of subsidence shows upward advection reduced/ eliminated by focused precipitation, and without groundwater impact (Section 6.6)

Table 6-19. Summary of Conceptual Model for the Future Evolution of the Disposal System (Continued)

Actual and Expected Conditions	Modeled Conditions	Justification
b. Flooding occurs in arroyos from intense storm events; if flood waters go into subsidence features, will fill them with sediment.	Not modeled in PA.	Subsidence analysis showed that arroyo flooding of subsidence features will have less impact on vadose zone moisture than 10,000 years of sheetflow runoff. (Section 6.6)
c. Changes in plant species to deeper-rooted woodland and "ephemeral wetland species" could occur locally in subsidence features	Ephemeral and woodland species, coupled with upward advection of pore water.	Conservative; modeling fastest, shortest pathway (22 m [72 ft]) to accessible environment using upward advection, coupled with the woodland species plant model.
Under future cooler and wetter (*glacial*) climate conditions (after year 2170):		
a. Unmitigated subsidence occurs, creating collapse features which capture and focus precipitation - causing increased moisture content in alluvium and potential downward movement of moisture	Increased moisture content and potential downward movement of moisture is not modeled in quantitative PA (was modeled in subsidence screening analysis).	Conservative; modeling fastest, shortest pathway (22 m [72 ft]) to accessible environment using upward advection, coupled with the woodland species plant model.
b. Flooding occurs in arroyos from intense storm events	Not modeled in PA.	Subsidence analysis showed that arroyo flooding of subsidence features will have less impact on vadose zone moisture than 10,000 years of sheetflow runoff. (Section 6.6)
c. Plant species change to ephemeral wetland and woodland species.	Ephemeral wetland, and piñon-juniper woodland plant species in all realizations.	Reasonable; woodland plant species expected to eventually return (Sections 6.4 and 6.5)
Additional subsidence occurs after year 2170 and top of wastes drops deeper into ground increasing distance from top of waste to surface, minimum distance is 22.3 m (73 ft)	Distance from waste to land surface is 22 m [72 ft]	Reasonable; 2 m [7 ft] cap, plus top of waste drops deeper into profile (Section 6.6)
After year 2170, potential human intrusion or other surface disturbing activities are no longer prevented from occurring:	N/A	N/A

Table 6-19. Summary of Conceptual Model for the Future Evolution of the Disposal System (Continued)

Actual and Expected Conditions	Modeled Conditions	Justification
a. Surface disturbances may occur	These processes are not modeled.	Scenario screening eliminated these events (e.g., irrigated agriculture not commercially viable) from further consideration in the PA (Section 6.7)
b. Human intrusion directly into waste may occur	These events are not modeled.	Screened out based on EPA Appendix B Guidance.
Following loss of AIC, many other potential natural-occurring, disposal system-induced, or human-induced events and processes could occur at the site.	Other than those events and processes already discussed in this tabular summary, all other significant processes and events were either modeled as part of the undisturbed condition (the base case) or were not modeled.	All events that were not considered part of the base case were eliminated from consideration in the final PA via qualitative, well-documented screening assessments or via more detailed quantitative screening analyses (such as those for flooding and subsidence) (Sections 6.3 and 6.6)

7.0 TRANSPORT AND EXPOSURE MODELS

7.1 Introduction

The PA for the GCD boreholes for 40 CFR 191 required a relatively simple computational model. This simplicity results from inherent features of the system, but it is also a consequence of the PA approach described in Section 3.0, where the model is designed to be a sufficient basis for regulatory decision-making given the existing state of knowledge. This approach naturally requires simplifying conservative assumptions about uncertain aspects of system behavior. The simplicity of the PA models allowed them to be implemented in Microsoft® Visual Basic™ macros in an Access™ database.

7.2 Types of Models and Conditions

Figure 7-1 illustrates the modeled processes that affect waste migration and potentially contribute to integrated release or dose. The model of transport processes is common to both CR and IPR calculations; however, the IPR regulatory period is only 1000 years. The CR model integrates radionuclide releases across the accessible environment boundary (land surface) over 10,000 years. The IPR model accumulates releases over a 1000 year period, and calculates the dose that would result from including the entire amount of released radionuclides in the garden soil cultivated by a resident farmer. In addition to the transport model, the IPR model includes an exposure model for the various pathways from the contaminated garden soil to the resident farmer. The transport model used for both the CR and IPR is described in Section 7.3. The IPR exposure model is described in Section 7.5.

Based on the scenario analysis, transport through the system was simulated for base case conditions and increased vegetation resulting from subsidence and climate change. Although parameter values differ for the different conditions, the transport model itself is the same for all conditions.

7.3 Overview–Transport

Both CR and IPR calculations use the same mathematical model for radionuclide transport. This model is built from a mathematical expression for mass conservation that includes the operation of a number of transport processes, including dissolution and precipitation of radionuclides, advection and diffusion of radionuclides dissolved in pore water, reversible chemical sorption onto soil, and radionuclide uptake and transport by plants and burrowing animals. The mathematical expressions for each of these processes reflect the underlying conceptual models of the process, and are described above in Section 5.0. The overall mass balance formulation, which includes the combined effects of these diverse processes, is described in this section. The mathematical models for the individual transport processes, developed in Section 5.0, are repeated here for convenience.

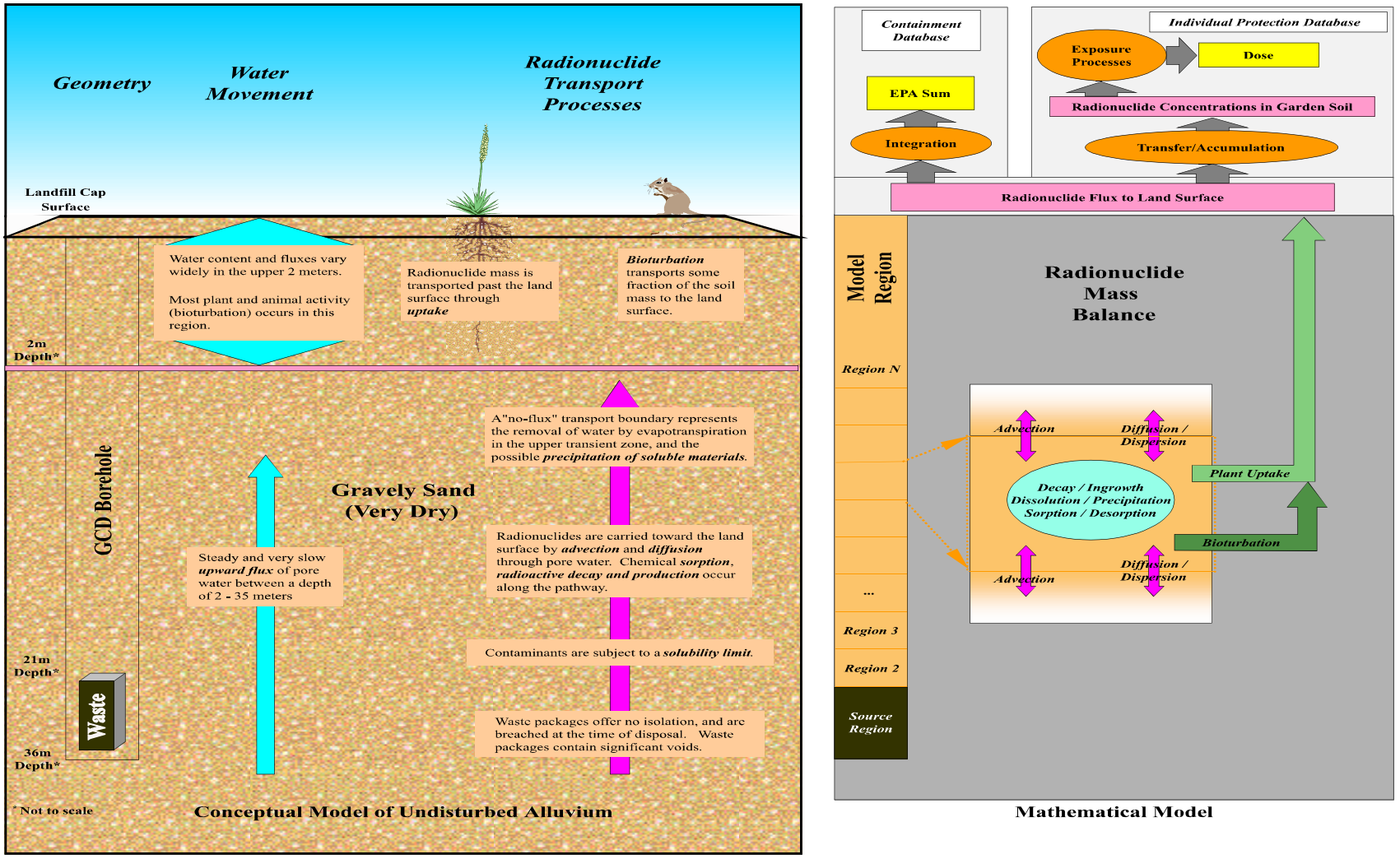

Figure 7-1. Mass Transfer Processes Considered in the Transport Model

7.3.1 Geometry

The waste disposal region and overburden is divided into a number of discrete horizontal regions (Figure 7-1). The regions are numbered beginning with the waste disposal region, with region numbers and coordinate values increasing upwards towards the land surface. The top of the last region corresponds to the land surface. Liquid water flows upward through the waste region, and is uniform and constant in time. This flowing pore water is removed through evapo-transpiration near the land surface, and this loss is assumed to occur at a single depth, creating a zero-flux boundary for radionuclides at this depth. This zero-flux boundary is imposed at the top of a designated region.

7.3.2 Mass Balance for Water-Borne Radionuclides

The equation describing the change in mass density of radionuclide *i* in transport region *x* is given by:

$$\frac{dm_i^x}{dt} = \frac{q_i^{x-1}}{L^x} - \frac{q_i^x}{L^x} - q_{dist,i}^x + \lambda_{i-1} m_{i-1}^x - \lambda_i m_i^x \qquad (7\text{-}1)$$

where:

- m_i^x = mass density of radionuclide *i* in transport region *x* (moles/m^3 of alluvium),
- t = time (yr),
- q_i^{x-1} = flux of radionuclide *i* out of transport region *x - 1* into the overlying transport region *x* as a result of advection, diffusion, and dispersion in pore water (moles/m^2 of alluvium yr),
- q_i^x = flux of radionuclide *i* out of transport region *x* into the overlying transport region *x+1* as a result of advection, diffusion, and dispersion in pore water (moles/m^2 of alluvium yr),
- L^x = height of transport region *x* (m),
- $q_{dist,i}^x$ = flux of radionuclide *i* out of transport region *x* due to distributed sinks such as plant uptake and bioturbation (moles/m^3 yr),
- λ_i = decay constant for radionuclide $i = \ln(2)/t_{1/2}$, (1/yr).

In this equation and the equations that follow, the superscript *x* refers to a spatial region, while the subscript *i* refers to radionuclide *i*.

The flux of radionuclide *i* out of transport region *x* due to distributed sinks is assumed to be a linear function of mass density:

$$q_{dist,i}^x = a_i^x + b_i^x \, m_i^x \qquad (7\text{-}2)$$

where:

- a_i^x = total of constant sinks of radionuclide *i* in transport region *x* (moles/m^3 yr),
- b_i^x = total of mass-dependent sinks for radionuclide *i* in transport region *x* (moles/m^3 yr per mole/m^3 of alluvium),

7.3.3 Advection, Dispersion, and Diffusion

The flux of radionuclide *i* out of transport region *x* and into transport region *x + 1* is a result of advection, dispersion, and diffusion (see Section 5.12.1). This flux can be approximated by:

$$q_i^x = q_l\left(\gamma C_i^x + (1-\gamma) C_i^{x+1}\right) - \left(\frac{\alpha q_l + D_m/\tau}{\left(L^x + L^{x+1}\right)/2}\right)\left(C_i^{x+1} - C_i^x\right) \qquad (7\text{-}3)$$

where:

q_l = liquid phase advective flux density (m^3 of water/m^2 of alluvium yr),
γ = upstream weighting factor for evaluating advective concentration (dimensionless)
C_i^x = concentration of radionuclide *i* in pore fluid (moles/m^3 of water).
α = longitudinal dispersivity (m),
D_m = molecular diffusion coefficient (m^2/yr),
τ = tortuosity (dimensionless).

The second term on the right-hand side models the effects of both diffusion and dispersion. The tortuosity, τ, in this model is defined as D_m/D_{eff} where D_{eff} is the effective molecular diffusion coefficient in alluvium. The tortuosity parameter includes both the effects of limiting transport to the saturated portion of the pore space, and of greater microscopic transport distances compared to macroscopic distances (see Section 5.12.1.2). The tortuosity is related to the volumetric moisture content, θ:

$$\tau = \frac{1.01}{\theta^{1.75}} \qquad (7\text{-}4)$$

where:

θ = volumetric moisture content (m^3 of water/m^3 of alluvium),

7.3.4 Sorption, Dissolution, and Precipitation

A linear sorption process partitions radionuclide mass between the liquid phase and the soil (see Section 5.12.1.3). The liquid-phase concentration of radionuclide *i* cannot exceed a specified solubility, $C_{i,sol}$. The liquid-phase concentration of radionuclide *i* in transport region *x*, C_i^x, is related to the mass density of radionuclide *i* in transport region *x*, m_i^x (moles/m^3):

$$C_i^x = \min\left(\frac{m_i^x}{R_i\,\theta}, C_{i,sol}\right) \qquad (7\text{-}5)$$

where:

$C_{i,sol}$ = isotopically apportioned solubility of radionuclide *i* (moles/m^3 of water).
R_i = retardation coefficient of radionuclide *i* (dimensionless).

If $C_i^x = C_{i,sol}$, region x is *saturated* with respect to radionuclide *i*; if $C_i^x < C_{i,sol}$, region x is *undersaturated* with respect to radionuclide *i*.

The isotopically apportioned solubility of each isotope of a given element is determined by multiplying its elemental solubility by the ratio of the amount of that particular isotope in the initial inventory to the total amount of all isotopes of that element in the initial inventory (e.g., moles of ^{239}Pu/moles of all isotopes of Pu). The elemental solubility was estimated using the thermodynamic equilibrium models described in Section 5.10.

The retardation coefficient of radionuclide *i*, R_i, is given by:

$$R_i = 1 + \frac{\rho K_{d,i}}{\theta} \tag{7-6}$$

where:

$K_{d,i}$ = sorption coefficient for radionuclide *i* (m^3 of water/kg of alluvium),
ρ = dry bulk density of alluvium (kg dry of alluvium/m^3 of alluvium),

The apparent dispersion coefficient between regions *x* and *x* + 1 is defined as:

$$q_D^x = \frac{\alpha q_l + D_m/\tau}{\left(L^x + L^{x+1}\right)/2} \tag{7-7}$$

7.3.5 Plant Uptake and Bioturbation

Two processes, plant uptake and bioturbation, can create a distributed sink for radionuclide *i* in region *x*:

$$q_{dist,i}^x = q_{plant,i}^x + q_{bio,i}^x \tag{7-8}$$

where $q_{plant,i}^x$ and $q_{bio,i}^x$ are the fluxes of radionuclide *i* from region *x* due to plant uptake and bioturbation, respectively.

For regions other than the source region, plant roots may access all dissolved, sorbed, and precipitated mass. In the source region, roots may access dissolved and sorbed mass, but radionuclides are assumed to be unavailable to roots in their original physical and chemical form until mobilized by dissolution (see Section 5.7). For non-source regions, and for undersaturated conditions in the source region, the flux of radionuclide *i* due to plant uptake from transport region *x* in terms of the mass density, m_i^x, is given by:

$$q^{x}_{plant,i} = \sum_{j=1}^{n_g} B_j \overline{R_j^x} \frac{CR_i}{\rho L^x} m_i^x \qquad (7\text{-}9a)$$

and for the source region under chemically saturated conditions, the flux is:

$$q^{x}_{plant,i} = \sum_{j=1}^{n_g} B_j \overline{R_j^x} \frac{CR_i}{\rho L^x} C_{i,Sol} R_i \theta \qquad (7\text{-}9b)$$

where:

B_j = annual biomass turnover of plant functional group j (kg dry above-ground plant/m^2 yr),

$\overline{R}_r^x = \int_{z=z_1}^{z_2} R_r^x(z)dz =$ average relative extraction by plant functional group j within transport region x (dimensionless),

CR_i = concentration ratio for radionuclide i (moles/kg dry above-ground plant per moles/kg dry of alluvium),

j = plant functional unit (annual, perennial, shrub, or tree),

N_g = number of plant functional units.

The flux of radionuclide i from transport region x by bioturbation in terms of the mass density, m_i^x, is given by:

$$q^{x}_{bio,i} = \sum_{l=1}^{n_a} p^x_{z,l} \frac{B_{m,l}}{\rho L^x} m_i^x \qquad (7\text{-}10)$$

where:

$B_{m,l}$ = annual soil excavation rate of burrower guild l (kg soil /m^2 yr),

$p_{z,l}^{x}$ = fraction of soil excavation by burrowers in guild l from region x (dimensionless)

l = burrower guild (mammals, invertebrates),

n_a = number of burrower guilds.

The mass-density-dependent distributed sink coefficients for region x combine the effects of plant uptake and burrowing. For non-source regions, and for the source region when undersaturated:

$$b_i^x = \sum_{j=1}^{n_g} B_j \overline{R_j^x} \frac{CR_i}{\rho L^x} + \sum_{l=1}^{n_a} p^x_{z,l} \frac{B_{m,l}}{\rho L^x} \qquad (7\text{-}11a)$$

while for the saturated source region:

$$b_i^x = \sum_{l=1}^{n_a} p_{z,l}^x \frac{B_{m,l}}{\rho L^x} \qquad \text{(7-11b)}$$

7.3.6 Lowering of the Zero-Flux Boundary

Mass can be instantaneously transferred from overlying regions to represent the lowering of the zero-flux boundary from the top of region N to the top of region M:

$$m_{n+1}^M = m_{i,n}^M + \frac{\sum_{k=M+1}^{N} L^k m_{i,n}^k}{L^M} \qquad \text{(7-12)}$$

where

$m_{i,n}$ = mass density of radionuclide *i* in transport region *x* at time step *n* (moles/m^3 of alluvium)

7.3.7 Radionuclide Discharge to the Land Surface

The total of constant sinks in Equation (7-2) can be used to model the deposition in region *l* of radionuclide mass by plant uptake and bioturbation. This mass may come from any of N_x regions:

$$a_i^l = \sum_{x=1}^{N_x} \left\{ h_{lp}^x \left(\sum_{j=1}^{n_g} B_j \overline{R_j^x} \frac{CR_i}{\rho L^x} \right) + p_{ztran,l}^x \left(\sum_{l=1}^{n_a} p_{z,l}^x \frac{B_{m,l}}{\rho L^x} \right) \right\} \left(\omega m_{i,n+1}^x + (1-\omega) m_{i,n}^x \right) \frac{L^x}{L^l} \qquad \text{(7-13a)}$$

where ω is a weighting factor for terms evaluated at the end of a simulation timestep (see Section 7.6.2.1).

If the source region *S* is saturated, the summand for that region is:

$$\left\{ h_{lp}^S \left(\sum_{j=1}^{n_g} B_j \overline{R_j^S} \frac{CR_i}{\rho L^S} \right) + R_i \theta C_{i,sol} + p_{ztran,l}^S \left(\sum_{l=1}^{n_a} p_{z,l}^S \frac{B_{m,l}}{\rho L^S} \right) \right\} \left(\omega m_{i,n+1}^S + (1-\omega) m_{i,n}^S \right) \frac{L^S}{L^l} \qquad \text{(7-13b)}$$

where:

h_{lp}^x = fraction of the mass removed by plants from region *x* that is deposited in region *l*

$p^x_{ztran,l}$ = fraction of the mass removed by bioturbation from region *x* that is deposited in region *l*

The total discharge rate to region *l*, $L^l a_i^l$, is the radionuclide discharge rate per unit area required for the CR calculations and the IPR calculations.

7.3.8 Mass Balance for Gas-Phase Contaminant (Radon)

Recall from Section 5.12.2, that there are two sources of radon in the air: (1) decay of radium that has already been transported to the ground surface and (2) upward vapor phase diffusion of radon from the waste source to the ground surface. The following paragraphs describe the model for upward vapor phase diffusion of radon. The model for radon concentration in air resulting from decay of radium already at the ground surface is discussed in Sections 5.12.2 and 7.5.3.2.

The equation describing the mass density of radon in region *x* includes the effects of diffusive flux, production by radium decay, and loss by radon decay:

$$\frac{dm_{Rn}^{x}}{dt} = \frac{q_{Rn}^{x-1}}{L^{x}} - \frac{q_{Rn}^{x}}{L^{x}} + \lambda_{Ra} m_{Ra}^{x} - \lambda_{Rn} m_{Rn}^{x} \qquad (7\text{-}14)$$

where:

m_{Rn}^{x} = mass of radon in transport region *x* (moles/m^3),
q_{Rn}^{x} = flux of radon out of transport region *x* (moles/m^2 yr),
λ_{Ra} = decay constant for radium (1/yr),
m_{Ra}^{x} = mass of radium in transport region *x* (moles/m^3),
λ_{Rn} = decay constant for radon (1/yr).

The mass of radium in transport region *x* is calculated by the dissolved contaminant transport model described in Section 7.3.2.

The flux of radon out of transport region *x*, q_{Rn}^{x}, is the result of diffusion alone and is given by:

$$q_{Rn}^{x} = \frac{2 D_{Rn}}{L^{x} + L^{x+1}} (C_{Rn}^{x} - C_{Rn}^{x+1}) \qquad (7\text{-}15)$$

where:

D_{Rn} = effective diffusion coefficient for radon in alluvium = D_{MRn} ε (m^2/yr),
D_{MRn} = molecular diffusion coefficient for radon in air (m^2/yr),
ε = air-filled porosity of the alluvium(dimensionless), and
C_{Rn} = concentration of radon in control volume *x* (moles/m^3 of air).

The concentration of radon in transport region *x*, C_{Rn}^{x}, is related to the mass density of radon in transport region *x*, m_{Rn}^{x}:

$$C_{Rn}^{x} = \frac{m_{Rn}^{x}}{\in} \tag{7-16}$$

The air-filled porosity of the alluvium is assumed to equal the porosity minus the volumetric moisture content. Radon concentration is not subject to a solubility limit.

Using Equation (7-16) in Equation (7-15), the flux of radon out of transport region *x* in terms of the radon mass density in regions *x* and *x + 1* is given by:

$$q_{Rn}^{x} = \frac{2\ D_{MRn}}{\left(L^{x} + L^{x+1}\right)}\left(m_{Rn}^{x} - m_{Rn}^{x+1}\right) \tag{7-17}$$

The flux of radon out of the topmost region is calculated assuming that the radon mass density at the land surface is zero:

$$q_{Rn}^{F} = \frac{2D_{MRn}}{L^{F}} m_{Rn}^{F} \tag{7-18}$$

The concentration of radon in the air directly above the GCD boreholes that is there as a result of diffusion upward through the alluvium is calculated by the following Equation (7-19):

$$C_{a} = \frac{q_{Rn}^{F}}{\lambda_{Rn} H}\left[1 - e^{\left(\frac{-x\lambda_{Rn}}{2U}\right)}\right] \tag{7-19}$$

where:

C_a = outdoor concentration of radon (moles/m^3),
H = height into which plume is uniformly mixed (m),
X = diameter of contaminated area (m), and
U = annual average wind speed (m/y).

7.3.9 Approximate Effect of Lateral Diffusion and Dispersion

Diffusion and dispersion can cause radionuclides to move laterally through the sides of the disposal boreholes, where they can be carried towards the land surface by advection through the pore water near the boreholes. The 1-D model does not include radionuclides that diffuse or disperse through the sides of the disposal boreholes. For solubility-limited conditions, the radionuclide discharge calculated using the 1-D model is therefore incomplete.

The amount of mass released from the waste region by lateral diffusion and dispersion was estimated using a simplifying assumption of radial transport laterally away from the disposal borehole. Radial diffusion and upward advection are assumed to be independent in order to

simplify this calculation.[7] Radionuclide concentrations along the sides of the disposal boreholes were assumed to be fixed at the solubility limit. These assumptions lead to an expression for the rate of mass released laterally from the borehole, per unit length of borehole, as a function of time. Considering a small thickness of soil near the top of the waste, the pore water in this region will have been carried upward past the waste by advection. The mass of mobile radionuclides in this region was calculated by integrating the mass that is added to this region at each elevation as it is carried upward. The mass released from the waste by diffusion and dispersion, which is then carried above the elevation of the top of the waste, is compared to the mass released by advection through the top of the waste region.

This comparison results in an "enlargement factor" for the area of the borehole. Conceptually, the enlargement factor is the relative amount that the cross-sectional area of the top of the virtual GCD borehole would have to be increased, in the 1-D transport calculation, in order to compensate for the mass added by lateral diffusion and dispersion through the borehole sides.

The effect of lateral diffusion can be pictured as an increase in the cross-sectional area of the virtual GCD borehole; however, the 1-D calculations cannot be modified to include the effect of lateral diffusion by a simple increase in the cross-sectional area used in the model. The enlargement factor depends on the radionuclide transport parameters, and is therefore different for different radionuclides. Because the factor is different for each radionuclide in the decay chain, a single enlargement factor cannot be used for an entire decay chain. Instead, the enlargement factor can be directly applied to the discharges calculated for the individual radionuclides (see Section 7.3.7). This use of the enlargement factor is valid because the transport processes that move waste from the top of the virtual GCD borehole to the land surface are linear in the mass of radionuclides that cross the elevation of the top of the waste.

The mass balance equation for radionuclide *i* in the soil surrounding the waste borehole is:

$$\frac{\partial m_i^r}{\partial t} = -\vec{\nabla} \bullet \vec{q}_i^{\,r} \tag{7-20}$$

where m_i^r is the bulk mass density of radionuclides, given by:

$$m_i^r = C_i^r R_i \theta \tag{7-21}$$

and the radionuclide flux $\vec{q}_i^{\,r}$ is given by:

$$\vec{q}_i^{\,r} = -\left(\alpha_t q_l + D_{eff}\right) \nabla C_i^r \tag{7-22}$$

where

[7] Radial *dispersion*, however, does depend on the upward advection rate.

C_i^r is the concentration of radionuclide *i* in pore water in the region *r* surrounding a GCD borehole (mole/m^3)

α_t is the transverse dispersivity (m)

$D_{eff} = D_m / \tau$ is the effective diffusivity of the radionuclide in pore water (m^2/y)

and the other terms are as previously defined.

Assuming that transport occurs radially, Equations (7-20) through (7-22) give:

$$\theta R_i \frac{\partial C_i^r}{\partial t} = D_c \nabla^2 C_i^r = D_c \left[\frac{1}{r} \frac{\partial C_i^r}{\partial r} + \frac{\partial^2 C_i^r}{\partial r^2} \right] \tag{7-23}$$

where $D_c = \alpha_t q_l + D_m / \tau$.

The concentration is fixed at the solubility limit at the radius of the GCD borehole, and goes to zero at large distances from the borehole:

$$C_i^r (r_w, t) = C_{i,sol} \tag{7-24a}$$

$$\lim_{r \to \infty} C_i^r (r, t) = 0 \tag{7-24b}$$

and the initial concentration around the borehole is zero:

$$C_i^r (r, 0) = 0 \quad r_w < r \tag{7-25}$$

Lohman [1979] presents a solution for an analogous set of equations and evaluates the flux Q around the inner boundary at $r = r_w$. Using the coefficients of Equation (7-23), this flux is given by:

$$Q = -2\pi D_c r_w \frac{\partial C_i^r}{\partial r} = 2\pi D_c C_{i,sol} G(\gamma) \tag{7-26}$$

where

$$\gamma = \frac{D_c t}{\theta R_i r_w^2} \tag{7-27}$$

and

$$G(\gamma) = \frac{4\gamma}{\pi} \int_0^\infty x e^{-\gamma x^2} \left[\frac{\pi}{2} + \tan^{-1}\left(\frac{Y_0(x)}{J_0(x)} \right) \right] dx \tag{7-28}$$

where J_0 and Y_0 are zero-order Bessel functions of the first and second kind, respectively.

Equation (7-26) describes the lateral flux, per unit length along the waste borehole, into a region of pore water that has been exposed to the saturated boundary condition (Equation 7-24a) for a time *t*. Consider a small thickness of the unsaturated zone at the top of the waste disposal region at time *t*. The total mass per unit length in the pore water in this region is the integral of the mass flux (Equation (7-26)) over the time that the pore water has been exposed to saturated conditions at the borehole boundary.

Upward advection will have moved this pore water from some lower elevation at time 0 to its current location at the top of the waste at time *t*. If the location of the pore water at time 0 was above the bottom of the waste region, then the pore water has been exposed to saturated conditions during the entire time from 0 to *t*. If the location of the pore water at time 0 was below the waste region, however, then the pore water would only have been exposed to the concentration boundary during the time required for upward advection to move the pore water from the bottom of the waste to the top of the waste. The total mass per unit length along the borehole in the pore water at the top of the waste is obtained by integrating Equation (7-26) over the time during which the fixed concentration boundary acts on this pore water:

$$M(t) = \int_{t'=0}^{t'=\min(t,t_{adv})} Q(t')dt' \tag{7-29}$$

where t_{adv} is the time required for upward advection to move pore water from the bottom to the top of the waste region:

$$t_{adv} = \frac{h_w}{q_l / \theta} \tag{7-30}$$

and h_w is the height of the waste disposal region. Equation (7-29) can be expanded using Equation (7-26) to give:

$$\begin{aligned} M(t) &= 2\pi D_c C_{i,sol} \int_{t'=0}^{t'=\min(t,t_{adv})} G(t)dt' = 2\pi D_c C_{i,sol} \frac{dt}{d\gamma} \int_{t'=0}^{\gamma'=\min(\gamma,\gamma_{adv})} G(\gamma)\, d\gamma' \\ &= 2\pi C_{i,sol} \theta R_i r_w^2 H \left(\min(\gamma, \gamma_{adv}) \right) \end{aligned} \tag{7-31}$$

where:

$$H(\gamma) = \int_0^{\gamma} G(\gamma')d\gamma' \tag{7-32}$$

During a small time increment Δt, upward advection will displace the mobile radionuclide mass in a small thickness Δz from just below the top of the waste to just above the top of the waste. Because the retardation R_i represents the ratio of the total mass density to the mobile mass density, the mass that crosses the elevation of the top of the waste during this time is:

$$M_A(t) = \frac{M(t)\Delta z}{R_i} = \frac{M(t)\frac{q_l \Delta t}{\theta}}{R_i} \tag{7-33}$$

In the 1-D transport model, the mass introduced into the transport region above the waste is based on advection and diffusion through the top of the waste during the time Δt. Equation (7-33) represents the additional mass introduced into the transport region above the waste due to lateral diffusion from the sides of the borehole. This mass is not included in the 1-D transport calculation. The relative amount of extra mass is the ratio of M_A to the mass introduced through the top of the waste during the time interval:

$$E_l = \frac{M_A(t)}{\pi r_w^2 q_l C_{i,sol} \Delta t} \tag{7-34}$$

From Equations (7-33) and (7-31):

$$E_l = \frac{\frac{2\pi C_{i,sol} \theta R_i r_w^2 \; H\left(\min\left(\gamma, \gamma_{adv}\right)\right)\frac{q_l \Delta t}{\theta}}{R_i}}{\pi r_w^r \; q_l C_{i,sol} \Delta t} = 2H\left(\min\left(\gamma, \gamma_{adv}\right)\right) \tag{7-35}$$

Equation (7-35) was evaluated for several combinations of parameter values appropriate for the GCD site. The borehole size and molecular diffusivity were assigned single values. High and low values were defined for the remaining parameters, as shown in Table 7-1. Lohman [1979] provides tabulated values for $G(\gamma)$. $H(\gamma)$ was estimated from these values by trapeziodal integration. Table 7-2 lists the values of $G(\gamma)$ and $H(\gamma)$ used in evaluating Equation (7-35).

Table 7-1. Parameter Values and Ranges

Parameter (units)	Value	
D_m (m^2/y)	1.35×10^{-12}	
r_w (m)	1.5	
h_w (m)	15	
	Low	**High**
R_i (dimensionless)	1	100
θ (dimensionless)	0.05	0.10
α_t (m)	0.0	0.03
q_l (m/y)	1×10^{-6}	4×10^{-4}

Table 7-2. Values of G(γ) and H(γ) used to Evaluate Equation (7-35)

γ	G(γ)	H(γ)[a]	γ	G(γ)	H(γ)[a]
1.00E-04	56.9		2.00E-01	1.716	5.94E-01
2.00E-04	40.4	4.87E-03	3.00E-01	1.477	7.54E-01
3.00E-04	33.1	8.54E-03	4.00E-01	1.333	8.95E-01
4.00E-04	28.7	1.16E-02	5.00E-01	1.234	1.02E+00
5.00E-04	25.7	1.44E-02	6.00E-01	1.16	1.14E+00
6.00E-04	23.5	1.68E-02	7.00E-01	1.103	1.26E+00
7.00E-04	21.8	1.91E-02	8.00E-01	1.057	1.36E+00
8.00E-04	20.4	2.12E-02	9.00E-01	1.018	1.47E+00
9.00E-04	19.3	2.32E-02	1.00E+00	0.985	1.57E+00
1.00E-03	18.3	2.51E-02	2.00E+00	0.803	2.46E+00
2.00E-03	13.11	4.08E-02	3.00E+00	0.719	3.22E+00
3.00E-03	10.79	5.27E-02	4.00E+00	0.667	3.92E+00
4.00E-03	9.41	6.28E-02	5.00E+00	0.63	4.56E+00
5.00E-03	8.47	7.17E-02	6.00E+00	0.602	5.18E+00
6.00E-03	7.77	7.99E-02	7.00E+00	0.58	5.77E+00
7.00E-03	7.23	8.74E-02	8.00E+00	0.562	6.34E+00
8.00E-03	6.79	9.44E-02	9.00E+00	0.547	6.90E+00
9.00E-03	6.43	1.01E-01	1.00E+01	0.534	7.44E+00
1.00E-02	6.13	1.07E-01	2.00E+01	0.461	1.24E+01
2.00E-02	4.47	1.60E-01	3.00E+01	0.427	1.69E+01
3.00E-02	3.74	2.01E-01	4.00E+01	0.405	2.10E+01
4.00E-02	3.3	2.37E-01	5.00E+01	0.389	2.50E+01
5.00E-02	3	2.68E-01	6.00E+01	0.377	2.88E+01
6.00E-02	2.78	2.97E-01	7.00E+01	0.367	3.25E+01
7.00E-02	2.6	3.24E-01	8.00E+01	0.359	3.62E+01
8.00E-02	2.46	3.49E-01	9.00E+01	0.352	3.97E+01
9.00E-02	2.35	3.73E-01	1.00E+02	0.346	4.32E+01
1.00E-01	2.25	3.96E-01			

[a]Estimated by numerically integrating G(γ)

Figure 7-2 shows a plot of Equation (7-35) over the CR performance period for 8 of the 16 parameter combinations implied by Table 7-1. The result is insensitive to transverse dispersivity over the parameter ranges considered. For clarity, only the results for the lower bound of 0 are shown on the figure. The highest relative flux rates occur for low values of q_l and low values of retardation. For these cases, the amount of mass introduced into the transport region due to lateral diffusion from the sides of the borehole can exceed the amount introduced through the top of the borehole by more than an order of magnitude over much of the performance period. At low flux rates, however, contaminants are not likely to reach the active zone near the surface and the integrated release from the system is quite small. Although the *relative* error due to neglecting lateral diffusion may be large in these cases, the error does not affect compliance because the integrated release is very small. High rates of flux and low retardations, however, can result in relative flux rates approaching an order of magnitude. At high flux rates, an upper limit on the relative mass flux from lateral diffusion occurs before 2000 years. At these rates, the amount of mass introduced into the pore water passing the borehole is limited by the amount of time the water spends adjacent to the borehole. Note that this limiting time, from Equation (7-30), is based on the rate of water movement, and is therefore not sensitive to the retardation coefficient.

The total integrated release from the system, including the mass introduced by lateral diffusion, can be estimated by scaling the integrated release that is calculated when this mass is neglected (see Section 7.3.7) using a representative constant value for the mass ratio E_l. The representative value of E_l will be different for each radionuclide. Scaling integrated release is appropriate because the transport processes that operate between the top of the waste region and the land surface are generally linear in the amount of mass that crosses the elevation of the top of the waste.

There are, however, some assumptions underlying this scaling. First, radioactive decay and production are not included. The estimated releases are therefore only appropriate for radionuclides with long half lives compared to the performance period, and which are not produced by radioactive decay in significant quantities during the performance period. Second, mass transport above the top of the waste is not strictly linear if radionuclide precipitation occurs near the upper transport boundary. Third, E_l is a function of time, and this time-dependence cannot be reflected in a constant scaling factor. Based on the parametric combinations shown in Figure 7-2, however, the assumption of a constant value over the performance period appears to be a good approximation for those parameter combinations likely to lead to relatively large discharges. If the value at 10,000 years is used as the constant value, the approximation is conservative when inaccurate. Fourth, the integrated release calculated in the 1-D model (see Section 7.3.7) includes plant roots and animal borrows that can extend below the elevation of the top of the waste, and move radionuclides directly from the waste region to the land surface. Direct removal does not contribute to releases from the region outside the disposal boreholes. For this reason, the integrated release scaled by E_l should include only those releases from the regions above the waste. Fifth, Equation (7-29) does not include the effects of vertical dispersion. Because concentrations in the soil around the waste region will tend to increase with elevation, including dispersion would tend to reduce the mass per unit length from the estimate provided by Equation (7-29). Lastly, the 1-D model only underestimates the mass that leaves the source region when transport is solubility limited. When concentrations are not solubility-

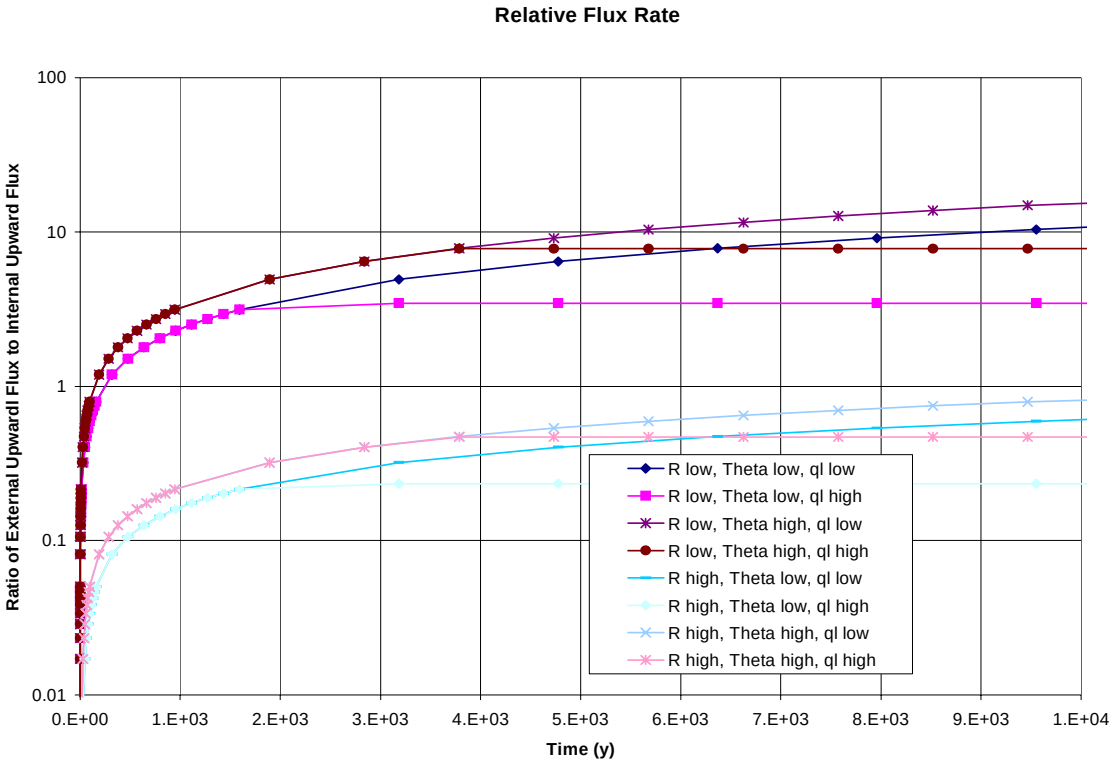

Figure 7-2. Relative Rate of Mass Flux into the Transport Region of Radionuclides Diffused through the Borehole Sides.

limited, the 1-D model correctly accounts for the transport of all available mass, and no convection for lateral diffusion is needed.

7.3.10 Parameter Values

Each of the transport processes included in the transport model is described by one or more parameters. Some of these parameters are assigned constant values because the values can be defined with little uncertainty or because appropriate bounding values have been adopted. Other parameters were assigned probability distributions that describe uncertainty in the appropriate value. The values and distributions for the process model parameters are described in Section 5.0, and are summarized here for convenience.

Values for each of the model parameters were assigned based on available information from diverse sources. Some parameters, such as radionuclide half-lives, are universal physical constants. Common literature values were used for such parameters. Other parameters, such as upward flux rates, describe specific characteristics of the site, and assigned values were based on analyses of site characterization data. The values for some parameters, such as sorption coefficients, would not change with the onset of subsidence. Some parameters, such as porosity and bulk density, would change during subsidence, however, the relative change would be small.

These parameters were assigned constant values representing conditions following subsidence. Parameters such as those that describe radionuclide uptake by native plants depend on assumptions about effective pore moisture. Parameter values are discussed for both current conditions and for the conditions that might exist after the landfill subsides. The woodland community discussed in Section 6.4 is assumed to represent the plant community that might exist after subsidence occurs.

Parameter values were assigned considering the way they are used in the model. Most of the parameters are effective values which describe a large region of space (e.g., the backfill overlying the waste) for the entire performance period. In many cases, experimental data related to these parameters describes a much smaller region under current conditions. The differences between the experimental scale and the model parameter scale are important considerations in defining parameter values.

For some parameters (radionuclide half-lives, for example), existing information can adequately establish the parameter value with very little uncertainty. Other parameters (dose conversion factors, for example) may be established as part of the regulation or by common practice in regulatory assessments. Such parameters were assigned constant values. For many other parameters, especially those characterizing specific conditions at the site, there is considerable uncertainty about the appropriate value. Probability distributions, describing this uncertainty, were assigned to these parameters.

This section presents a summary of the constant values and distributions assigned to the model parameters. For each parameter, the value or distribution is given, along with a reference to the other section(s) of this report that discuss the justification for the assigned value or distribution. Some parameters, for example the rather lengthy tables of dose conversion factors, are tabulated in Appendix O and, for brevity, are not repeated here.

7.3.10.1 Constant Parameter Values

In Equation (7-19), the height H into which the radon plume is uniformly mixed is assumed to be 2 m (7 ft), and the annual average wind speed U is assumed to be 2 m/s (7 ft/s) (see Figure 5-1). The diameter of the contaminated area X is assumed to be equal to the diameter of the "virtual" borehole, 35.6 m^2 (1,257 ft^2) (see Section 5.9).

Table 7-3 lists the constant values for the transport model parameters, along with reference information for the source of the value. The model geometry is defined by the sum of the areas of the four disposal boreholes and by the thicknesses of the waste region and overlying backfill regions. Thicknesses are listed in Table 7-4. The values include the effects of subsidence and mitigating backfill over an assumed 170 year operational and monitoring period. This table also describes which regions are assumed to have flowing liquid under current and future conditions. The height H of the atmospheric mixing zone, the annual average wind speed U, and the diameter D of the contaminated area are also used in the IPR dose model, and are described below in Section 7.8. Table 7-5 lists the half-lives of the modeled radionuclides. The radionuclide decay chains used in the model are discussed in Section 5.9.3.

Table 7-3. Transport Model Parameters with Constant Values

Symbol	Parameter Description	Value	Reference
A_b	Total area of disposal boreholes (m^2)	35.6	Section 5.9.3.4
$t_{1/2}$	Radionuclide half-lives	See Table 7-5	Section 5.9.3.2 and Appendix J
D_m	Molecular diffusion coefficient for radionuclides in water (m^2/yr)	0.0136	Section 5.12.1.2
D_{Rn}	Radon diffusion coefficient (m^2/yr)	113.607	Section 5.12.2
H	Height into which the radon plume is uniformly mixed (m)	2	Section 7.8
D	Diameter of the contaminated area (m)	6.7	$= 2\sqrt{A_b / \pi}$

Table 7-4. Thicknesses and Liquid Flow Conditions of the Model Transport Regions

Region Name	Thickness (m)	Upward Advection Occurs	
		Current Conditions	Subsidence
Dynamic	2	No	No
Transport	20.3	Yes	Yes
Source	15	Yes	Yes

Table 7-5. Radionuclide Half-Lives

Radionuclide	Half-Life (years)	Radionuclide	Half-Life (years)
Ac-227	2.18E+01	Ra-226	1.60E+03
Am-241	4.32E+02	Th-229	7.90E+03
Np-237	2.14E+06	Th-230	7.54E+04
Pa-231	3.25E+04	Th-232	1.40E+10
Pb-210	2.26E+01	U-233	1.59E+05
Pu-238	8.77E+01	U-234	2.45E+05
Pu-239	2.41E+04	U-235	7.04E+08
Pu-240	6.54E+03	U-236	2.34E+07
Pu-241	14.4		
Pu-242	3.76E+05	U-238	4.46E+09

7.3.10.2 Distributions of Uncertain Parameters

Probability distributions were assigned to describe uncertainty about the value of some parameters. These parameters typically describe conditions over the entire site for the full performance period. Much of the uncertainty about the parameter values come from the inability to make measurements at the appropriate scales, and from the potential variability in conditions over the performance period. This is discussed further in Section 3.0.

Table 7-6 summarizes the uncertain parameters of the transport model. For each parameter, a reference is given for the section of this report that discusses the state of knowledge about the parameter and develops the distribution used in the model. Some parameters are described by distributions with common functional forms, such as normal and uniform distributions: these distributions are defined directly in Table 7-6. Empirical distributions have been developed for other parameters. These distributions are defined by a list of paired values specifying points on the CDF. Empirical distributions are defined in the subsequent tables referenced in Table 7-6. Solubilities, sorption coefficients, and concentration ratios have different values for each chemical element. Element-specific distributions for these parameters are provided in the tables referenced in Table 7-6.

Most of the parameters listed in Table 7-6 are defined above in Sections 7.3.1 through 7.3.8. Three of the uncertain parameters in Table 7-6 are used to calculate values for the model parameters. The average length of plant roots (L_j) and the relative extraction shape parameter (β) are used to evaluate the relative extraction function $\overline{R}_r^x$ as described in Sections 5.6.6 and 7.3.5. The average depth of mammal burrows, D_b, is used to calculate the soil excavation fraction $p_{z,l}^x$ for mammals. (For invertebrates, the soil excavation fraction is based on the distribution of roots, as described in Section 5.8.3.4.)

7.4 Subsidence and Climate Change

As discussed above, scenario analysis identified subsidence and a change in climate as events/processes that might affect the performance of the disposal system. Because such changes are considered likely to occur over the 10,000-year regulatory period, subsidence and climate change were included in the base case (i.e., the effects of subsidence and climate change are included in every simulation).

The potential effects of subsidence and climate change in the disposal system were discussed at length in Sections 6.4 and 6.5. This analysis ruled out the potential for a downward water pathway. This left a shift in the plant community to species more representative of a woodland community as the only effect of subsidence and climate change that had to be included in the PA.

The shift in the plant community is modeled by: (1) adding trees to the plant community, (2) developing different biomass turnover pdfs, (3) developing different CR pdfs, and (4) developing a different "distribution" of termite burrows with depth. The relative extraction

Table 7-6. Transport Model Parameters with Uncertain Values

Symbol	Description	Distribution	Reference
$M_i^1(0)$	Initial radionuclide inventory	See Table 7-7	Section 5.9.3.2
q_l	Liquid phase advective flux (m/y)		Section 5.6
α	Longitudinal dispersivity, m	Uniform, 0.01 to 0.15	Section 5.12.1.2
θ	Volumetric moisture content	See Table 7-8	Section 5.6.2.3
-	Total porosity	Normal, 0.16 to 0.42	Section 5.12.2
C_{sol}	Elemental solubility	See Table 7-9	Section 5.10.4
$K_{d,i}$	Sorption coefficient	See Table 7-9	Section 5.12.1.3
ρ	Dry bulk density of alluvium (kg/m^3)	Normal, mean=1,600, F = 109	Section 5.5.3.2
B_r	Annual biomass turnover	See Table 7-10	Section 5.7.8
L_j	Average length of a plant's longest root	See Table 7-11	Section 5.7.5
B	Shape parameter β for the relative extraction function		Section 5.7.6
	Annuals:	Uniform, 3 to 20	
	Perennials:	Uniform, 3 to 20	
	Trees:	Uniform, 3 to 20	
CR_i	Concentration ratios for native plants	See Table 7-12	Section 5.7.7
$B_{m,l}$	Annual soil excavation rate (kg/m^2/yr)		Section 5.8.3.4
	Invertebrates:	Uniform, $7 \times 10^{!3}$ to $5.77 \times 10^{!2}$	
	Mammals:	See Table 7-13	
D_b	Average depth of mammal burrows	log(mean): normal, μ = !0.44, σ = 0.13	Section 5.8.3.4
S_g	Standard deviation of natural log of mammal burrow depth	See Table 7-12	Section 5.8
$p^x_{z,l}$	Fraction of soil excavation		
	Invertebrates:	Based on root length distribution	Section 5.8.3.4
	Mammals:	Based on the average burrow depth, *Db*	

Table 7-7. Inventory of Radionuclides in TRU Waste Packages in GCD Boreholes Included in PA

Isotope	BH-1(kg)	BH-2 (kg)	BH-3 (kg)	BH-4 (kg)	Total (kg)	Total (Ci)
U-234	2.17E!2– 3.78E!2	1.33E!3 – 2.81E!2	1.68E!3 – 1.34E!2	5.40E!05	2.48E!2 – 7.94E!2	1.53E!1 – 4.90E!1
U-235	17.87– 31.05	1.05 – 22.17	1.33 – 10.67	4.23E!02	20.3 – 63.9	4.87E!2 – 1.53E!1

Table 7-7. Inventory of Radionuclides in TRU Waste Packages in GCD Boreholes Included in PA (Continued)

Isotope	BH-1(kg)	BH-2 (kg)	BH-3 (kg)	BH-4 (kg)	Total (kg)	Total (Ci)
U-238	423.7 – 722.9	2.69 – 69.9	6.17 – 10.8	2.66E!03	432.6 – 803.6	1.44E!1 – 2.68E!1
Total U					**452.9 – 867.6**	
Pu-238	8.95E!5 – 2.03E!4	4.40E!06	1.27E!4 – 1.43E!4	2.23E!04	4.41E!4 – 5.73E!4	7.54 – 9.83
Pu-239	8.40E!1 – 1.90	4.13E!02	1.19 – 1.34	2.09	4.16 – 5.37	2.55E+2 – 3.29E+2
Pu-240	5.19E!2 – 1.18E!1	2.55E!03	7.37E!2 – 8.29E!2	1.29E!01	2.57E!1 – 3.22E!1	5.94E+1 – 7.44E+1
Pu-241	1.16E!3 – 2.63E!3	5.72E!05	1.65E!3 – 1.86E!3	2.90E!03	5.77E!3 – 7.45E!3	6.59E+2 – 8.51E+2
Pu-242	1.79E!4 – 4.06E!4	8.80E!06	2.54E!4 – 2.86E!4	4.46E!04	8.88E!4 – 1.15E!3	3.46E!3 – 4.47E!3
Total Pu					**4.42 – 5.70**	
Am-241	2.25E!3 – 1.45E!2	2.1E!04	5.79E!3 – 6.15E!3	5.91E!03	1.42E!2 – 2.68E!2	4.86E+1 – 9.04E+1

Table 7-8. Cumulative Distribution Function for the Moisture Content Parameter

Moisture Content (V/V)	Cumulative Probability
0.042	0.0
0.044	0.0006
0.046	0.0013
0.048	0.0053
0.05	0.0249
0.052	0.0773
0.054	0.1501
0.056	0.2111
0.058	0.2550
0.06	0.2951
0.062	0.3430
0.064	0.4040
0.066	0.4720
0.068	0.5314

Table 7-8. Cumulative Distribution Function for the Moisture Content Parameter (Continued)

Moisture Content (V/V)	Cumulative Probability
0.088	0.9646
0.07	0.5769
0.072	0.6285
0.074	0.7054
0.076	0.7830
0.078	0.8310
0.08	0.8609
0.082	0.8924
0.084	0.9253
0.086	0.9504
0.09	0.9722
0.092	0.9773
0.094	0.9814
0.096	0.9849
0.098	0.9880
0.1	0.9906
0.102	0.9928
0.104	0.9945
0.106	0.9959
0.108	0.9970
0.11	0.9979
0.112	0.9985
0.114	0.9989
0.116	0.9993
0.118	0.9995
0.12	1.0

functions do not change, except for the addition of relative extraction functions for trees (see Table 7-9). The biomass turnover pdfs for climate change are given in Table 7-8 while the CR pdfs for climate change are given in Table 7-10. The "distribution" of termite burrows with depth was presented in Section 6.4.3.4.

The time at which the plant community begins to shift is unknown, as is the length of time it will take for these transitions to become complete. Any additional subsidence that occurs after the institutional control period ends is assumed to occur quickly. Therefore, subsidence is assumed to occur within a few hundred years. It was assumed that changes in the plant community occur instantaneously.

Table 7-9. Distributions for Solubility and Sorption Coefficient

Element	Distribution for Solubility (M)	Distribution for Sorption Coefficient (m^3 of water/kg of alluvium)
Pu	Loguniform, 1×10^{-10} to 5×10^{-6}	Beta, 2×10^{-2} to 2×10^{-1}; $\beta = 10.6$, $\alpha = 8.45$
U	Loguniform, 2×10^{-6} to 7×10^{-3}	Beta, 0 to 4×10^{-3}; $\alpha = 5.06$, $\beta = 5.06$
Am	Loguniform, 4×10^{-8} to 4×10^{-3}	Uniform, 1×10^{-1} to 2
Np	Loguniform, 1×10^{-5} to 3×10^{-1}	Beta, 0 to 6×10^{-3}, $\alpha = 9.09$, $\beta = 45.5$
Ra	Loguniform 9×10^{-9} to 9×10^{-7}	Uniform, 1×10^{-1} to 5×10^{-1}
Th	Loguniform, 6×10^{-8} to 6×10^{-6}	Uniform, 1×10^{-1} to 2
Pa	Loguniform, 1×10^{-5} to 3×10^{-1}	Uniform, 0 to 1×10^{-1}
Pb	Loguniform, 2×10^{-10} to 5×10^{-6}	Uniform, 1×10^{-1} to 5×10^{-1}
Ac	Loguniform, 4×10^{-8} to 4×10^{-3}	Uniform, 1×10^{-1} to 2

Table 7-10. Parameters of the Beta Distributions for Biomass Turnover

Plant Functional Group	Current Climate				Subsidence			
	Minimum ($kg/m^2/yr$)	Maximum ($kg/m^2/yr$)	α	β	Minimum ($kg/m^2/yr$)	Maximum ($kg/m^2/yr$)	α	β
Annuals	2.4×10^{-5}	6.44×10^{-2}	0.255	0.918	1×10^{-4}	4.7×10^{-3}	0.469	1.23
Perennials	2×10^{-4}	2.42×10^{-2}	0.848	1.43	4.37×10^{-2}	1.244×10^{-1}	0.622	1.29
Shrubs	1.2×10^{-2}	8.42×10^{-2}	2.01	5.79	4.8×10^{-3}	4.26×10^{-2}	1.05	2.67
Trees	Not Present				2.8×10^{-3}	1.15×10^{-2}	4.70	5.61

Table 7-11. Cumulative Distribution Functions for Root Lengths of Native Plants

Annuals		Perennials		Shrubs		Trees	
Root Length (m)	Cumulative Probability	Root Length (m)	Cumulative Probability	Root Length (m)	Cumulative Probability	Root Length (m)	Cumulative Probability
0.2145	0	1.007	0	1.475	0	2.834	0
0.234	0.002	1.06	0.5	1.589	0.001	3.052	0.002
0.2535	0.006	1.113	1	1.702	0.005	3.270	0.010
0.273	0.019			1.816	0.022	3.488	0.034
0.2925	0.043			1.930	0.067	3.706	0.086
0.312	0.083			2.043	0.153	3.924	0.172
0.3315	0.141			2.156	0.281	4.142	0.290
0.351	0.214			2.270	0.434	4.360	0.425
0.3705	0.299			2.384	0.587	4.578	0.560
0.39	0.389			2.497	0.719	4.796	0.681

Table 7-11. Cumulative Distribution Functions for Root Lengths of Native Plants (Continued)

Annuals		Perennials		Shrubs		Trees	
Root Length (m)	Cumulative Probability	Root Length (m)	Cumulative Probability	Root Length (m)	Cumulative Probability	Root Length (m)	Cumulative Probability
0.4095	0.48			2.610	0.822	5.014	0.780
0.429	0.566			2.724	0.893	5.232	0.855
0.4485	0.644			2.838	0.939	5.450	0.908
0.468	0.712			2.951	0.967	5.668	0.943
0.4875	0.771			3.064	0.983	5.886	0.966
0.507	0.82			3.178	0.991	6.104	0.980
0.5265	0.859			3.292	0.996	6.322	0.989
0.546	0.891			3.405	0.998	6.540	0.994
0.5655	0.917			3.632	1	6.976	0.998
0.585	0.936					7.412	0.999
0.624	0.963					7.848	1
0.663	0.979						
0.702	0.988						
0.741	0.993						
0.78	0.996						
0.975	1						

Table 7-12. Concentration Ratios for Native Plants (pCi/dry plant mass per pCi/dry soil mass) (all distributions are lognormal)

Element	Current Climate Conditions			Cooler, Wetter Climate		
	Geometic Mean	0.001 Quantile	0.999 Quantile	Geometic Mean	0.001 Quantile	0.999 Quantile
Pu	1.6×10^{-4}	1.5×10^{-6}	2.5×10^{-3}	1.7×10^{-4}	3.9×10^{-6}	2.5×10^{-3}
U	2.9×10^{-1}	4.5×10^{-3}	5.1	3.1×10^{-1}	2.7×10^{-3}	7.1
Am	2.2×10^{-3}	1.7×10^{-5}	5.4×10^{-2}	1.9×10^{-3}	1.2×10^{-5}	5.0×10^{-1}
Np	1.1×10^{-1}	5.2×10^{-3}	1.1	1.1×10^{-1}	5.2×10^{-3}	1.1
Ra	1.7×10^{-1}	9.4×10^{-3}	1.6	1.3×10^{-1}	3.9×10^{-2}	1.7
Th	1.4	8.5×10^{-3}	$3.5 \times 10^{+1}$	6.9×10^{-1}	2.1×10^{-3}	2.4×10^{1}
Pa	1.1×10^{-1}	5.2×10^{-3}	1.1	1.1×10^{-1}	5.2×10^{-3}	1.1
Pb	3.2×10^{-1}	1.3×10^{-2}	3.6	4.3×10^{-1}	8.9×10^{-3}	6.6
Ac	2.2×10^{-3}	1.7×10^{-5}	5.4×10^{-2}	1.9×10^{-3}	1.2×10^{-5}	5×10^{-1}

Table 7-13. PDF of Average Mammal Excavation Rate ($Kg/m^2/g$) (pdf is Continuous Linear)

Average Rate	Cumulative Probability
4.6478	0.0000
5.8283	1.3804×10^{-3}
7.2060	4.3676×10^{-3}
8.8092	1.1570×10^{-2}
10.670	2.6430×10^{-2}
12.826	5.322×10^{-2}
15.318	9.6113×10^{-2}
18.193	1.5786×10^{-1}
21.506	2.3859×10^{-1}
25.317	3.3518×10^{-1}
29.695	4.4163×10^{-1}
34.718	5.5026×10^{-1}
40.783	6.5337×10^{-1}
47.060	7.4475×10^{-1}
54.593	8.2059×10^{-1}
63.198	7.7970×10^{-1}
73.019	9.2306×10^{-1}
84.219	9.5308×10^{-1}
96.981	9.7270×10^{-1}
111.51	9.8484×10^{-1}
128.05	9.9198×10^{-1}
146.85	9.9594×10^{-1}
168.22	9.9804×10^{-1}
192.50	9.9910×10^{-1}
200	1

Because of the manner in which subsidence and climate change are assumed to affect the disposal system, the equations presented above do not need to be modified in order to model climate change. Only parameter values are modified to model these changes.

7.5 Individual Protection

7.5.1 Introduction

Because the performance measure of the IPR is dose to a MOP, the IPR analysis must include an individual and the conditions under which that individual is exposed to radioactive waste.

Table 7-14. PDF of Standard Deviation in Mammal Burrow Depth

Standard Deviation	Cumulative Probability
0.55	0
0.60	0.0026
0.65	0.0155
0.70	0.0619
0.75	0.1745
0.80	0.3637
0.85	0.5898
0.90	0.7856
0.95	0.9108
1.00	0.9707
1.05	0.9924
1.10	0.9985
1.15	0.9998
1.20	1

Unfortunately, it is not possible to know the nature of exposure conditions[8] in the distant future, creating a large source of uncertainty that cannot be eliminated. The EPA does not provide guidance in 40 CFR 191 as to the exposure conditions that should be considered, but some guidance can be obtained from other sources, namely PAs for LLW disposal.

7.5.2 Creation of a Set of Exposure Conditions

Requirements for disposal of LLW, which is typically disposed of in shallow pits and trenches, are similar to the IPR in that they limit the dose received by a MOP. Both the NRC and the DOE are responsible for approving of LLW PAs. As a result, both DOE [Wood et al., 1994] and NRC [NRC, 1981; 1982] have developed reasonable but conservative exposure conditions that serve as surrogates for unknowable future exposures. The EPA has recommended the use of these LLW exposure conditions for IPR calculations for the GCD PA (memo of July 10, 1996 from D. Gallegos to Distribution; see Beyeler et al. [1999]). Hence, we use these LLW exposure conditions to build a set of exposure conditions for the IPR, recognizing that there may be some differences between IPR and LLW exposure conditions because of differences in disposal practices and disposal standards. The two most significant differences between IPR and LLW exposure conditions are that: (1) the IPR is for undisturbed conditions only, meaning that well cuttings do not contribute to dose; and (2) the IPR dose is based on only those radionuclides that have reached the accessible environment.

[8]The circumstances under which an individual receives a dose from radioactive waste to which he has been exposed are commonly called "exposure scenarios." To avoid confusing "exposure scenarios" with "disruptive scenarios" that are used in the CR analysis (discussed above), these circumstances are called "exposure conditions" in this report.

The DOE's recommendations on the types of exposure conditions that should be considered for calculating doses to off-site individuals from buried LLW are as follows [Wood et al., 1994].

1. If groundwater is expected to be contaminated by off-site transport of radionuclides, then an exposure scenario involving use of the contaminated groundwater as a domestic drinking water supply and for agricultural purposes (i.e., watering livestock, irrigating a vegetable garden, and irrigating pasture grass consumed by livestock) should be considered. However, such a scenario should be evaluated only if contaminated groundwater reasonably could be used by off-site individuals under present conditions. For example, only contaminated groundwater at depths that do not exceed the depth of a well that reasonably could be constructed using the types of drilling techniques normally used near the disposal site should be considered; the quantity of water that could be drawn from the contaminated aquifer should be sufficient for domestic use; the ambient water quality in the aquifer should be acceptable for domestic use without the need for treatment; and doses from irrigation need not be considered if irrigation is not commonly practiced near the disposal site.

2. If releases of radionuclides to surface waters are potentially important at off-site locations, then the same scenario described above involving use of contaminated groundwater should be considered. In addition, use of surface waters for recreational purposes (e.g., swimming, boating) and consumption of contaminated fish should be considered, provided such scenarios are reasonable under present conditions for surface waters near the disposal site.

3. If releases of radionuclides to the atmosphere are potentially important, e.g., for such volatile radionuclides as ^{3}H, ^{14}C, and radon, then a scenario for off-site individuals involving exposure to airborne radioactivity should be considered.

Because groundwater contamination is not expected in the next 1000 years (see discussion in Section 5.5.2 on the Vadose Zone) and because there are no surface waters nearby, the first two exposure conditions can be eliminated from further consideration. The third exposure condition should be retained for further consideration because radon is a daughter product of TRU waste.

The DOE's recommendations on the types of exposure conditions that should be considered for individuals who come onto the disposal site after loss of AIC and who have no prior knowledge of waste disposal activities at the site are as follows [Wood et al., 1994].

1. An acute construction scenario and a chronic agriculture (homesteader) scenario involving excavation into disposal units, mixing exhumed waste in an intruder's vegetable garden, and permanent residence in a home on top of disposal units.

2. An acute discovery scenario and a chronic resident scenario involving an attempted excavation into disposal units, which is assumed to be precluded by the presence of intact engineered barriers.

3. An acute drilling scenario and a chronic post-drilling scenario involving drilling through disposal units and mixing the drilling waste in an intruder's vegetable garden.

The first exposure condition must be revised to account for the depth of the waste in GCD boreholes. A typical basement depth is 3 m (10 ft), placing the basement floor approximately 18 m (60 ft) above the waste in the borehole and making it is physically unreasonable for construction of a basement over a GCD borehole to result in exhuming the waste itself. Furthermore, human intrusion is not to be included in the analysis for the IPR. Eliminating this direct intrusion from the first exposure condition leaves the construction of a house (with garden) on or near the boreholes. Eliminating human intrusion from the second and third conditions leaves an individual living in a house on or near the boreholes. That individual may have a garden, but no exhumed waste has been placed or mixed in the garden.

The exposure conditions developed by the NRC for its draft environmental impact statement on 10 CFR 61 [NRC, 1981] are as follows.

1. An intruder-construction scenario involving the construction of a house with a basement directly into the disposed waste. Exposure occurs during construction of the house and would principally occur through inhalation of contaminated dust, exposure to direct gamma radiation from standing on contaminated ground, and immersion in a dust cloud.

2. An intruder-agriculture scenario involving a situation in which an individual or individuals live in the house constructed in #1 above and the soil from basement excavation is mixed in the garden. In addition to the exposure pathways for the construction case, the individuals could be exposed through consumption of food grown in contaminated soil.

3. A population exposure scenario consisting of waste that has been uncovered and brought to the surface through inadvertent intrusion being transported off-site by surface water and wind. Exposures to the surrounding population are then calculated.

As before, eliminating direct human intrusion from the first and second exposure conditions leaves an individual living in a house with a basement and a garden on or near the boreholes. The third condition can be eliminated from further consideration because it involves a population exposure and the IPR does not limit exposure to a population, only to an individual.

After tailoring the LLW disposal exposure conditions proposed by the DOE and NRC to the IPR, the following exposure condition remains: an individual living next to the boreholes, having a garden that does not contain exhumed waste. The particulars are as follows.

1. The MOP is a subsistence farmer that lives in a house near all four boreholes. The house is not on top of the boreholes because a house in such a location is not part of the "base case" for the CR. Construction of a house on top of the boreholes is very unlikely because of the unmitigated subsidence that is likely to occur. A future occupant of the site will likely avoid the entire RWMS because the terrain will be highly irregular and unusual. After the pits, trenches, and boreholes have been covered with the 2-m (7-ft) thick alluvial cap, and after

unmitigated subsidence has occurred, the RWMS will have hills several meters high and valleys several meters deep. Over time the hills will erode and the valleys will fill with sediment, but that process is not likely to be complete in 1000 years. Such a location will not be attractive to a future resident. Therefore, a future resident is more likely to choose to live off-site than on-site. Hence, the MOP lives near all four boreholes, but not on top of them.

2. The house may have a basement, but the basement does not contribute to the dose. No dose is received by the individual either in constructing the basement or in living in the basement after construction because the alluvium on which the house is constructed is not contaminated with radionuclides from the GCD boreholes. All radionuclides released from the GCD boreholes to the ground surface are assumed to be in the garden (discussed below). Furthermore, the tailings from basement construction are not contaminated, so the individual does not receive a dose from being exposed to contaminated tailings from basement construction.

3. The individual spends his time indoors, outdoors, and outdoors working in the garden. Water for drinking and irrigation is taken from the aquifer that is 236 m (774 ft) below the ground surface and is not contaminated by radionuclides from the boreholes. The water source is outside the controlled area, as required by the IPR.

4. The MOP has a contaminated garden which is also near the boreholes. Leafy vegetables, root vegetables, and fruits are grown in the garden. The MOP eats these contaminated leafy vegetables, root vegetables, and fruits. The MOP inadvertently ingests soil as well.

5. Under undisturbed conditions, upward liquid-phase advection, diffusion, and dispersion; and plant uptake and bioturbation move radionuclides from depth to the land surface. Contamination of the garden soil occurs as radionuclides are transported in the wind from the ground surface above the boreholes to the nearby garden. *It is assumed that all radionuclides released to the ground surface over 1000 years accumulate and are transported to the garden*. Radionuclides are uniformly distributed in the garden, which is 70 m^2 (750 ft^2). This garden area is large enough to grow a year's supply of fruits and vegetables and is twice the surface area of the virtual borehole (see Section 5.9.3.4). The area has been increased by a factor of two to account for the effects of lateral diffusion over 10^3 years (see Section 7.3.9 and Figure 7-2).

6. The MOP is assumed to be exposed to radionuclides both internally (by inhaling contaminated air, eating contaminated food, and eating contaminated soil) and externally (by being exposed to the contaminated garden and being immersed in a contaminated plume). The contaminated food the MOP ingests consists of produce grown in the contaminated garden (leafy vegetables, root vegetables, and fruit). The exposure period is one year. As discussed earlier, the water source is not contaminated by radionuclides from the GCD boreholes. Figure 7-3 illustrates the exposure pathways that are included in the dose calculations.

Each radionuclide released to the accessible environment over 1,000 years is assumed to be transported to the MOP's garden via the wind without diffusion, dispersion, or mixing with uncontaminated air and is uniformly mixed into the dirt in the garden. The transport model used

in estimating the release of radionuclides over 1,000 years for the IPR analysis is identical to the transport model used for modeling the first 1,000 years of the "base case" for the CR. Radionuclide concentrations in the garden dirt are then calculated and are used to estimate the dose to the MOP, as discussed below.

Assuming that *all* the mass released to the accessible environment is transported to the garden is very conservative. This assumption is made for the purpose of doing a screening calculation. *The results of the analyses indicated that the MOP's dose is likely to be below the dose limits given in the IPR; therefore, this very conservative assumption will not be changed. If the results of the analyses had indicated that the MOP's dose is likely to exceed dose limits given in the IPR, additional work would have been needed to determine what fraction of the waste released to the accessible environment is transported to the garden.*

For this off-site MOP exposure condition, concentrations of radionuclides in the air (used to calculate crop contamination from foliar deposition and to calculate doses from inhalation and immersion) are related to their concentrations in the garden by factors representing the fraction of dirt suspended in the air. Radionuclide concentrations in soil and garden products (used to calculate doses from ingestion and external exposure to contaminated soil (i.e., groundshine)) are also based on radionuclide concentrations in the garden. Radon in the air inhaled by the MOP is assumed to have two sources: (1) radium in the garden and (2) radon diffusing up through the alluvium. The concentration of radon in the air from the radium that is in the garden is calculated and used to calculate dose from inhalation. The concentration of radon in the air from upward diffusion of radon is calculated as well (assuming no dispersion) and is also used to calculate dose from inhalation. The garden is assumed to be 15 cm (6 in.) deep and to be 70 m^2 (750 ft^2), large enough to provide the subsistence farmer MOP with a year's supply of fruits and vegetables.

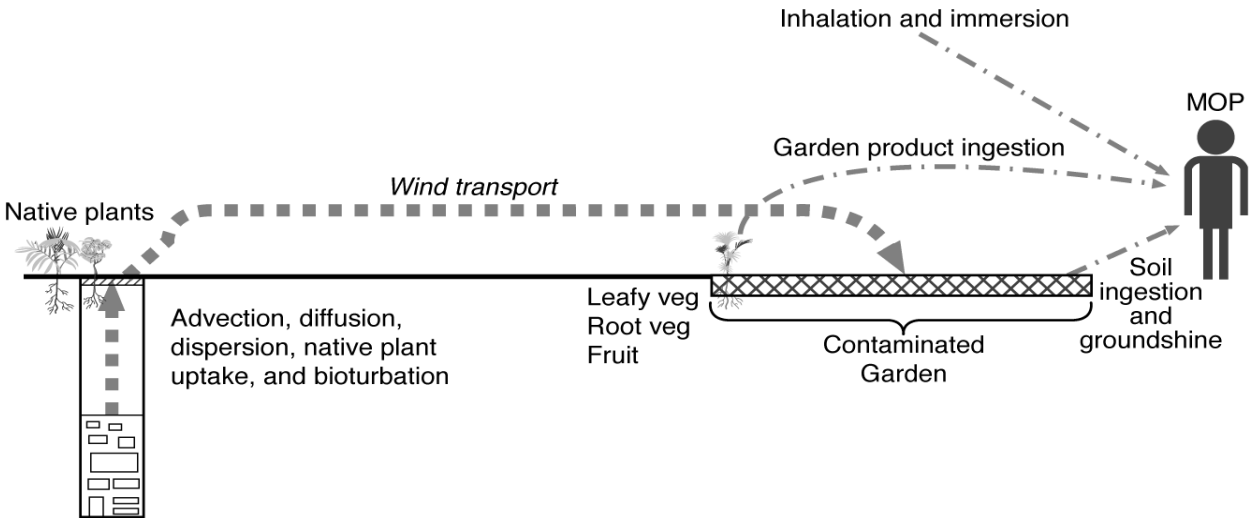

Figure 7-3. Exposure Pathways.

Because of the way the exposure condition is constructed (e.g., no loss of radionuclides as they are transported to the MOP's garden; garden area approximately equal to the surface area of the boreholes, correcting for possible effects of lateral diffusion), the doses calculated are similar to those that would be calculated if the MOP were to construct a garden directly on top of the boreholes. Therefore, the off-site MOP exposure condition is equivalent to an on-site MOP exposure condition with one exception: exposure to radon from residing in a house constructed on top of the boreholes.

To address this one exception, the PA analyses include an estimate of the dose to an MOP resulting from constructing and living in a residence with a basement on top of the virtual borehole 1000 years after closure. This MOP constructs a house on the contaminated alluvium; thus, there is no contaminated garden. Radiation dose results from inhalation of airborne particulate (excluding ^{222}Rn and progeny) during construction, incidental ingestion of particulate (excluding ^{222}Rn and progeny) during construction, external exposure from gamma emitters from excavated material during construction, inhalation of ^{222}Rn during occupancy, inhalation of airborne particulate (excluding ^{222}Rn and progeny) during occupancy, ingestion of particulate (excluding ^{222}Rn and progeny) during occupancy, and external exposure from gamma emitters beneath the basement during occupancy. These pathways and activities are summarized in Table 7-15.

Table 7-15. Summary of Exposure Pathways for an MOP Constructing and Occupying a House on Top of the Virtual Borehole

	Inhalation of ^{222}Rn	Inhalation of Airborne Particulate	Ingestion of Particulate	External Gamma Radiation
Construction of House		V	V	V
Occupation of House	V	V	V	V

^{220}Rn and ^{219}Rn were excluded from the assessment for two reasons. First, the total activities of these two isotopes of radon are expected to be much smaller than that of ^{222}Rn. Second, the diffusion barrier presented by a concrete foundation and walls will prevent these short-lived radon isotopes from entering the structure.

In contrast to ^{220}Rn and ^{219}Rn, ^{222}Rn has a much higher potential to penetrate a foundation and accumulate in structures. The degree of protection against ^{222}Rn afforded by a concrete slab will vary with the number of cracks and expansion joints in the slab as well as the method of sealing penetrations in the slab for utilities. An old slab that is extensively fractured may not be a very effective ^{222}Rn barrier. Given the uncertainties about future construction practices and the integrity of the slab, the foundation is not considered to be a ^{222}Rn diffusion barrier in the dose calculations.

The GCD boreholes are in close proximity to LLW disposal pits and trenches, raising the question of whether any dose from the LLW is included in the IPR analysis. The answer is no; dose from LLW is *not* included in the IPR dose analysis. There are two reasons for this. First, 40 CFR 191 does not apply to LLW. Requirements for the disposal of LLW are found in DOE Order 5820.2A, Chapter III and in the DOE requirements for a "composite analysis." Second, the argument can be made that an individual who might receive a dose sometime in the future cannot distinguish a dose from TRU waste from a dose from LLW. This is true, and a composite PA that will be conducted to determine compliance with DOE Order 5400.5 will look at the dose received by a MOP from all sources.

Furthermore, hazardous wastes that were disposed of in Boreholes 1–4 are not included in the IPR analysis because exposure to hazardous wastes does not result in radiological damage to the human body. That is, any damage to human tissue resulting from exposure to hazardous materials cannot be measured in terms of millirems, which is the performance measure of the IPR. Likewise, health effects resulting from exposure to radionuclides that are heavy metals (e.g., U, Pu) are not included in the IPR analyses because such health effects cannot be measured in terms of millirem. Thus, only radiological effects resulting from exposure to radionuclides is included in the PA.

7.5.3 Dose Calculations

The IPR sets limits on the annual dose equivalent to the whole body or to any critical organ. This type of dose, the "annual dose equivalent" was, in 1985, the standard method for measuring internal doses received by an individual. Since then, a new method, the "effective dose equivalent (EDE)," has been adopted as the standard method for measuring internal dose received by an individual. The two methods are not interchangeable. Therefore, the method for calculating internal dose for the IPR may be different from methods for calculating internal dose for other PAs, such as LLW disposal PAs, having requirements that use the newer internal dose calculation method.

7.5.3.1 Dose Conversion Factors

Internal Dose Conversion Factors

The method for calculating internal dose for the IPR was recommended by Committee II of the International Commission on Radiological Protection (ICRP 2) [ICRP, 1959]. The methodology presented by ICRP 2 contains (a) recommendations for maximum permissible doses to the whole body and to critical organs and (b) maximum permissible concentrations (MPCs) of radionuclides in air and water corresponding to these maximum permissible doses. These maximum permissible doses and concentrations were given for workers who are occupationally exposed, but they can be used for the present application by calculating dose conversion factors (DCFs) based on the maximum permissible doses and MPCs given in ICRP2. The manner in which this was done is described below.

Rearranging Equation (11) of ICRP 2 and inserting necessary unit conversion factors yields an effective inhalation DCF for organ *j* for inhalation of radionuclide *i*:

$$DCF_{i,j}^{inh} = \frac{MPDose_j \; A_i \; 10^6}{MPC_{i,j}^{air} \; RInh} \tag{7-36}$$

where

$DCF_{i,j}^{inh}$	=	inhalation dose conversion factor for organ *j* and radionuclide *i* (mrem/mole),
$MPDose_j$	=	maximum permissible dose to organ *j* from ICRP 2 (mrem/yr),
A_i	=	activity of radionuclide *i* (Ci/mole),
$MPC_{i,j}^{air}$	=	maximum permissible air concentration of radionuclide *i* associated with maximum permissible dose to organ *j* from ICRP 2 (μCi/cm^3),
RInh	=	inhalation rate of air from ICRP 2 (cm^3/yr).

Recommended maximum permissible doses to the whole body and to each organ are given in Table 7-16. Hereinafter in this report, it should be understood that a reference to organ *j* also includes the whole body.

The air MPC associated with the maximum permissible doses are given in Table O-1 (Appendix O), along with the activity of each radionuclide. The inhalation rate of air given in ICRP 2, which was used to calculate inhalation dose conversion factors, is 2.5×10^9 cm^3/yr. This rate reflects the amount of air inhaled by an occupationally exposed worker in a year and is used *only* to calculate inhalation dose conversion factors. The resulting inhalation DCFs are given in Table O-2.

As is evident from Table O-1, ICRP 2 does not provide air MPCs for all radionuclides included in the PA. The radionuclides for which MPCs were not provided were examined to determine whether or not it was necessary to calculate MPC values. The conclusions from this examination are as follows.

Table 7-16. Maximum Permissible Doses to Organs from ICRP 2 [1959]

Organ	mrem/yr
Whole Body	5000
Bone	30000
Liver	15000
Kidney	15000
Lower Large Intestine	15000
Lung	15000
Spleen	15000
Upper Large Intestine	15000
Stomach	15000

Rn-222 daughters: Po-218, Pb-214, Bi-214, Po-214–These radionuclides are already taken into account by the MPC for Rn-222. It is not necessary to calculate MPC values for these radionuclides.

Rn-220 daughters: Po-216, Tl-208–These radionuclides are already taken into account by the MPC for Rn-220. It is not necessary to calculate MPC values for these radionuclides.

Rn-219 and daughters: Po-215, Pb-211, Bi-211, Tl-207–A composite MPC (air) should be calculated for Rn-219 in equilibrium with its daughters.

Thorium-229 and daughters: Ra-225, Ac-225, Fr-221, At-217, Bi-213, Po-213, Pb-209–Based on analogy to Th-228, Th-230, and Th-232, calculate a composite MPC (air) for Th-229 in equilibrium with its daughters.

Therefore, air MPCs were calculated for these radionuclides: ^{229}Th, ^{225}Ra, ^{225}Ac + daughters, and ^{219}Rn + daughters. The organs for which ^{229}Th and ^{225}Ac MPCs were calculated are whole body, bone, kidney, liver, lung, lower large intestine (LLI), upper large intestine (ULI), and stomach. For ^{225}Ra, MPCs were calculated for whole body, bone, liver, kidney, and lung. For ^{219}Rn, a MPC was calculated for lung only. These values are shown in Table O-1, and the memos documenting the calculation of these MPCs along with printouts of the spreadsheets with which the calculations were performed are in Beyeler et al. [1999].

The ingestion DCF for organ *j* for ingestion of radionuclide *i* was also obtained by rearranging Equation (11) of ICRP 2 and was calculated as

$$DCF_{i,j}^{ing} = \frac{MPDose_j \; A_i \; 10^6}{MPC_{i,j}^{water} \quad RIng} \tag{7-37}$$

where

$DCF_{i,j}^{ing}$ = ingestion dose conversion factor for organ *j* and radionuclide *i* (mrem/mole),
$MPDose_j$ = maximum permissible dose to organ *j* from ICRP 2 (mrem/yr),
A_i = specific activity of radionuclide *i* (Ci/mole),
$MPC_{i,j}^{water}$ = maximum permissible water concentration of radionuclide *i* associated with maximum permissible dose to organ *j* from ICRP 2 (μCi/cm^3),
$RIng$ = ingestion rate of water from ICRP 2 (cm^3/yr).

Maximum permissible doses are given in Table 7-14. Water MPCs associated with maximum permissible doses are given in Table O-3 of Appendix O. ICRP 2 assumed that water was the only source for ingesting radionuclides. The ingestion rate of water given in ICRP 2, which was used to calculate ingestion DCFs, is 2.75×10^5 cm^3/year. As with the inhalation rate, this water ingestion rate is used *only* to calculate ingestion DCFs. The resulting ingestion DCFs are given in Table O-4 in Appendix O.

ICRP 2 does not provide water MPCs for all radionuclides included in the PA. As with air MPCs, most of the radionuclides for which water MPCs are not given in ICRP 2 are taken into

account by the water MPC for a parent. However, this is not true for several radionuclides that can produce a significant dose upon ingestion (^{229}Th, ^{225}Ra, and ^{225}Ac + daughters) and thus MPCs were calculated for these radionuclides. These values are shown in Table O-3 of Appendix O, and printouts of the spreadsheets with which the MPC calculations were performed are in Beyeler et al. [1999].

External Dose Conversion Factors.

ICRP 2 does not address the dose that results from exposure to a contaminated volume of soil, nor does it address the external dose that results from immersion in a contaminated plume, except for the noble gases (i.e., argon, krypton, and xenon). Therefore, an alternative method for estimating external dose must be utilized. Both the DOE [DOE, 1988b] and the EPA in Federal Guidance Report #12 [Eckerman and Ryman, 1993] have published DCFs for calculation of dose resulting from external exposure. Either set of DCFs would be acceptable to use to calculate the dose from external exposure, as the values in each set are similar to each other. However, the DCFs published by the EPA tend to be slightly higher (i.e., would estimate a higher dose than the DOE values, given the same levels of exposure), and the EPA has DCFs for exposure to ground that is contaminated to a depth of 15 cm (5.85 in.), which the DOE does not have. Therefore, for these two reasons, we used the DCFs published by the EPA [Eckerman and Ryman, 1993] to calculate the dose resulting from external exposure.

The DCFs published by the EPA [Eckerman and Ryman, 1993] are in SI units (Sv/s per Bq/m^3). To convert from these units to (mrem/yr per mole/m^3) the following equation was used:

$$DCF_i\left(\frac{mrem/yr}{mole/m^3}\right) = 1\times10^5\left(\frac{mrem}{Sv}\right)\ 3.156\times10^7\left(\frac{s}{yr}\right)$$
$$3.7\times10^{10}\left(\frac{Bq}{Ci}\right)\ A_i\left(\frac{Ci}{mole}\right)\ DCF_i\left(\frac{Sv/s}{Bq/m^3}\right) \qquad (7\text{-}38)$$

The external DCFs used in the PA are given in Tables O-5 and O-6 of Appendix O. It is evident from Tables O-2, O-4, O-5, and O-6 of Appendix O that internal DCFs are *not* available for all radionuclides and for only nine organs, whereas external DCFs *are* available for all radionuclides and for 24 organs. For this PA, doses are calculated for all radionuclides and for 24 organs; as a result, doses to organs for which only external DCFs are available (e.g., adrenals) represent only external doses. Doses to organs for which both external and internal DCFs are available (e.g, bone) represent the sum of external and internal doses.

The EPA gives DCFs for specific organs and for the EDE, but not for the whole body. Dose to the whole body can be estimated by calculating a mass-weighted dose equivalent (sum of DCFs for each organ weighted by the mass fraction of that organ in the total body). However, calculations indicate that the EDE can serve as an approximation to the whole-body dose (memo from R. Haaker to L. Price, September 12, 1997, given in Beyeler et al. [1999]). Therefore, the DCFs

for EDE given in Eckerman and Ryman [1993] will be used to estimate the dose to the whole body from external exposure.

Finally, Eckerman and Ryman [1993] give DCFs for skin. These are not used in the PA because the definition of "critical organ" in 40 CFR 191 specifically excludes the skin and the cornea.

7.5.3.2 Calculation of Radionuclide Concentrations

Off-Site MOP. The concentration of radionuclide *i* in the garden is calculated by summing the release of that radionuclide to the accessible environment over 1,000 years and dividing this quantity by the volume of dirt in the garden. The garden is assumed to be 15 cm (6 in.) deep and to have an area of 70 m^2 (750 ft^2). Thus:

$$C_{i,g} = \frac{Tot_i}{\rho \, 10.5 \text{ m}^3} \tag{7-39}$$

where

Tot_i = total mass of radionuclide *i* released to the accessible environment over 1000 years (moles),
$C_{i,g}$ = concentration of radionuclide *i* in garden soil (moles/kg soil), and
ρ = bulk density of alluvium (kg/m^3).

The concentrations of radionuclide *i* in the air and in food are based on the concentration of that radionuclide in the garden. Concentrations of radionuclides in air are related to their concentrations in the garden soil by a dust suspension factor. More radionuclides are likely to be suspended above the garden while gardening than in other outdoor areas, and more radionuclides are likely to be suspended in the air outside than inside. Hence, radionuclide concentrations in air are calculated for three separate regions: air above the garden while gardening, air outside (not gardening), and air inside. The concentration of radionuclide *i* in the air above the garden while gardening (i.e., while the soil is being actively disturbed by the MOP) is given by:

$$C_{i,ag} = S_g \, C_{i,g} \tag{7-40}$$

where

$C_{i,ag}$ = concentration of radionuclide *i* in the air above the garden while gardening (moles/m^3 air), and
S_g = dust suspension factor for gardening activities (kg soil/m^3 air).

The concentration of radionuclide *i* in outside air (not gardening) is given by:

$$C_{i,ax} = S_x \, C_{i,g} \tag{7-41}$$

where

$C_{i,ax}$ = concentration of radionuclide *i* in the outside air (not gardening) (moles/m^3 air), and
S_x = dust suspension factor for outside air (kg soil/m^3 air).

The concentration of radionuclide *i* in air inside the MOP's residence is given by:

$$C_{i,ai} = S_i \, C_{i,g} \tag{7-42}$$

where

$C_{i,ai}$ = concentration of radionuclide *i* in inside air (moles/m^3 of air), and
S_i = dust suspension factor for inside air (kg soil/m^3 of air).

The concentration of radon in the air resulting from upward radon diffusion in the alluvium and from decay of radium in the garden soil (see Section 5.12.2) is given by [NRC, 1989]:

$$C_{Rn,a} = \frac{q_{Rn}^F}{\lambda_{Rn} H}\left[1 - e^{\left(\frac{-X\lambda_{Rn}}{2U}\right)}\right] + g\,\rho\,C_{Ra,g}\frac{A_{Ra}}{A_{Rn}}\sqrt{\lambda_{Rn} D_{Rn}} \tanh\left(d_{grd}\sqrt{\frac{\lambda_{Rn}}{D_{Rn}}}\right)\frac{1}{\lambda_{Rn} H}\left[1 - e^{\left(\frac{-r_{grd}\lambda_{Rn}}{U}\right)}\right] \tag{7-43}$$

where

$C_{Rn,a}$ = concentration of radon in the air (moles/m^3),
q_{Rn}^F = flux of radon diffusing up from the ground into the air (moles/m^2 yr),
λ_{Rn} = decay constant for radon (1/yr),
H = height into which plume is uniformly mixed (m),
X = diameter of "virtual" borehole (6.7 m),
g = radon emanation coefficient (dimensionless),
$C_{Ra,g}$ = concentration of radium in the garden (moles/kg),
A_{Ra} = specific activity of radium (Ci/mole),
A_{Rn} = specific activity of radon (Ci/mole),
D_{Rn} = effective radon diffusion coefficient (m^2 /yr),
d_{grd} = garden depth (m), and
r_{grd} = radius of garden (m)
U = wind speed (m/yr)

The concentration of radionuclide *i* in food *f* grown in the garden (leafy vegetables, root vegetables, and fruit) is given by:

$$C_{i,f} = C_{i,g}\,(CR_{i,f}\,DWC_f + FAR_f\,S_g) \tag{7-44}$$

where

$C_{i,f}$ = concentration of radionuclide *i* in food *f* (moles/kg wet food),
$CR_{i,f}$ = concentration ratio of radionuclide *i* in plant that produces food *f* (moles/kg dry food per moles/kg dry soil),
DWC_f = dry-to-wet conversion factor for food *f* (kg dry food/kg wet food), and
FAR_f = plant-food/air concentration ratio for food *f* (m^3 air/kg wet food).

FAR_f = plant-food/air concentration ratio for food f (m^3 air/kg wet food).

Construction of and Residence in a House. For the exposure condition involving construction of and residence in a house on top of the virtual borehole, the concentration of radon in the house is calculated as follows. The time rate of change of radon concentration in the house is given by:

$$\frac{dC_{Rn,h}}{dt} = q_{Rn}^{f}\frac{A}{V} - \lambda_{Rn}C_{Rn,h} - \frac{k}{V}C_{Rn,h} \tag{7-45}$$

where

$C_{Rn,h}$ = concentration of radon in the house (moles/m^3),
A = area of contamination (i.e., cross-sectional area of virtual borehole) (m^2),
V = volume of residence (m^3), and
k = fresh air infiltration rate for the residence (m^3/yr).

Only the steady-state solution is of interest, resulting in the following expression for radon concentration in the house:

$$C_{Rn,h} = \frac{q_{Rn}^{f}\frac{A}{V}}{\lambda + \frac{k}{V}} \tag{7-46}$$

For the exposure condition involving construction of a residence in a house on top of the virtual borehole, the concentration of radionuclides used to calculate inhalation, ingestion, and external doses is calculated as described in Section 7.3.2. Concentrations at a depth of 3 to 4 m (10 to 13 ft) and 1000 years are used.

7.5.3.3 Obtaining Doses from Concentrations

Off-Site MOP. To calculate doses from inhalation, ingestion, and external exposure concentrations of radionuclide i in the garden and in air and food calculated from Equations (7-41), (7 42), (7-43), and (7-44) are needed. The annual dose to organ j from inhalation of radionuclide i (including radon) is given by:

$$D_{i,j}^{inh} = \left(T_x\ BR_x\ C_{i,ax} + T_g\ BR_g\ C_{i,ag} + T_i\ BR_i\ C_{i,ai}\right) DCF_{i,j}^{inh} \tag{7-47}$$

where

$D_{i,j}^{inh}$ = annual dose to organ j from inhalation of radionuclide i (mrem),
T_x = time per year spent outdoors (yr),
T_i = time per year spent indoors (yr),
T_g = time per year spent gardening (yr),
BR_x = outdoor breathing rate (m^3 air/yr).

BR_i = indoor breathing rate (m^3 air/yr), and
BR_g = breathing rate while gardening (m^3 air/yr).

The annual dose to organ *j* from ingestion of garden foods *f* and soil contaminated with radionuclide *i* is given by:

$$D_{i,j}^{ing} = DCF_{i,j}^{ing}\left(\sum_f C_{i,f} HC_f + C_{i,g} HC_s\right) \quad (7\text{-}48)$$

where
$D_{i,j}^{ing}$ = annual dose to organ *j* from ingestion of radionuclide *i* (mrem),
HC_f = consumption rate of food *f* (kg/yr), and
HC_s = consumption rate of soil (kg/yr).

The annual dose to organ *j* from immersion in a contaminated plume of radionuclide *i* is given by:

$$D_{i,j}^{imm} = DCF_{i,j}^{imm}\left(T_x C_{i,ax} + T_i C_{i,ai} + T_g C_{i,ag}\right) \quad (7\text{-}49)$$

where
$D_{i,j}^{imm}$ = annual dose to organ *j* from immersion in a plume of radionuclide *i* (mrem), and
$DCF_{i,j}^{imm}$ = immersion dose conversion factor for organ *j* and radionuclides *i* (mrem/yr per mole/m^3),

The annual dose to organ *j* from exposure to ground contaminated with radionuclide *i* to a depth of 15 cm (6 in.) is given by:

$$D_{i,j}^{grd} \text{ ' } DCF_{i,j}^{grd} \rho \left(T_x \% T_i \; SF^{ext} \% T_g\right) C_{i,g} \quad (7\text{-}50)$$

where
$D_{i,j}^{grd}$ = annual dose to organ *j* from exposure to ground contaminated with radionuclide *i* (mrem),
SF^{ext} = shielding factor for indoor external exposure, and
$DCF_{i,j}^{grd}$ = dose conversion factor for organ *j* for exposure to soil contaminated with radionuclide *i* to a depth of 15 cm (6 in.) (mrem/yr per mole/m^3).

The total annual dose to organ *j* is obtained by summing the doses from inhalation, ingestion, immersion, and ground shine over all radionuclides:

$$D_j^{total} = \sum_i D_{i,j}^{inh} + D_{i,j}^{ing} + D_{i,j}^{imm} + D_{i,j}^{grd} \quad (7\text{-}51)$$

This total annual dose is compared to the dose limits given in the IPRs (25 mrem to the whole body and 75 mrem to any critical organ).

Construction of and Residence in a House. For the exposure condition involving construction and occupancy of a residence on top of the virtual borehole, the MOP is assumed to inhale airborne particulate (excluding ^{222}Rn and progeny) during construction of the residence. The dose from this exposure is calculated as:

$$D_{i,j}^{inh} = T_{ch}\, BR_{ch}\, S_{ch}\, C_{i,3-4\,\mathrm{m}}\, DCF_{i,j}^{inh} \tag{7-52}$$

where

T_{ch} = time spent constructing the house (yr),
BR_{ch} = breathing rate while constructing the house (m^3 air/yr),
S_{ch} = dust suspension factor during construction of the residence (kg/m^3), and
$C_{i,\,3\text{-}4\,\mathrm{m}}$ = concentration of radionuclide *i* in the alluvium layer having a depth of 3 –4 m (10 to 13 ft) (moles/kg).

The MOP is also assumed to ingest particulate (excluding ^{222}Rn and its progeny) accidentally during construction of the residence. The ingestion dose from this pathway is calculated as:

$$D_{i,j}^{ing} = HC_s T_{ch} DCF_{i,j}^{ing} C_{i,3-4\,\mathrm{m}} \tag{7-53}$$

Detailed modeling of the external exposure that the MOP receives during construction of the residence is a complex problem. External radiation exposure would occur in a variety of exposure geometries both with and without the shielding that would be provided by the basement foundation and walls. In addition, the soil concentrations have a depth dependency. Thus, the average concentration at a depth of 3 to 4 m (10 to 13 ft) is most appropriate for assessing dose from gamma emitters present beneath the slab. On the other hand, the 0 to 3 m (0 to 10 ft) average concentrations are most appropriate for modeling the dose from the sides of the excavation or from the walls of the foundation. In addition, the area presented by the footing of the structure is greater than the total area of the virtual GCD borehole. Thus, not all the alluvium under the basement slab is contaminated with radionuclides. Contaminated alluvium from the excavation could be used as backfill behind the basement walls, and the remainder might be spread out as a uniform layer on the ground surface. Also, most of the time required for house construction occurs after the alluvium is excavated and after the foundation and walls are in place.

Therefore, a bounding external dose is calculated for exposure to gamma emitters during construction of the residence. This bounding dose is easily calculated and does not underestimate dose. A more complicated and sophisticated external dose assessment would only be performed if this bounding external dose estimate is high enough to prevent demonstration of compliance with the IPRs.

The dose rate within the basement excavation is assumed to result only from alluvium at the bottom of the excavation and not from the sides, because the footprint of the house is larger than the area of the virtual borehole. Excavation spoils are assumed to be placed back from the edge of the excavation during construction to prevent cave-ins; thus, the MOP receives no dose from the excavation spoils while in the excavation. Thus, the (bounding) external dose to the MOP during construction of a house is calculated as:

$$D_{i,j}^{grd} = T_{ch}\ \rho\ 1.271\, DCF_{i,j}^{grd} C_{i,3-4\mathrm{m}} \tag{7-54}$$

The factor of 1.271 in Equation (7-54) is the largest difference between DCFs for exposure to soil contaminated to a depth of 15 cm (6 in.) (Table III-6 of Eckerman and Ryman [1993]), which is the DCF in Equation (7-54), and DCFs for exposure to soil contaminated to an infinite depth (Table III-7 of Eckerman and Ryman [1993]). Using this factor allows the use of the DCFs already tabulated in Appendix P and provides a reasonable approximation of dose, given that this is a bounding calculation. Note that attenuation from the concrete walls and slab of the basement (nominally 15 and 9 cm (6 and 3.5 in.) thick, respectively) is ignored. These walls and floor would attenuate exposure to about half of what would be expected for an infinite plane (100 m^2 house assumed).

After the house has been constructed, the MOP is assumed to occupy the house and receive a dose from inhaling ^{222}Rn (and its progeny) that is diffusing up from the alluvium, through the basement slab, and into the house. Recall that the basement slab is not assumed to be a ^{222}Rn diffusion barrier. The dose to the lung from inhalation of ^{222}Rn during occupancy of the house is calculated as:

$$D_{Rn,lung}^{inh} = BR_i\, T_i\, C_{Rn,h}\, DCF_{Rn,lung}^{inh} \tag{7-55}$$

The MOP is also assumed to inhale airborne particulate (excluding ^{222}Rn and progeny) during occupancy of the residence. The source of the airborne particulate is the spoils from excavating the basement. The dose from this exposure pathway is calculated as:

$$D_{i,j}^{inh} = \left(T_i\, BR_i\, S_i + T_x\, BR_x\, S_x\right) C_{i,3-4\mathrm{m}}\, DCF_{i,j}^{inh} \tag{7-56}$$

The MOP is also assumed to ingest particulate (excluding ^{222}Rn and its progeny) accidentally during occupancy of the residence. The source of the particulate is the spoils from excavating the basement. The dose from this exposure pathway is given by:

$$D_{i,j}^{ing} = HC_s \left(T_i + T_x\right) DCF_{i,j}^{ing} C_{i,3-4\mathrm{m}} \tag{7-57}$$

As with estimating external dose from exposure to gamma-emitting radionuclides beneath the slab during construction of the house, a bounding approach is taken to estimate the dose from this pathway during occupancy of the house. Making the same assumptions as were used to develop Equation (7-55), the external dose during occupancy of the house is calculated as:

$$D_{i,j}^{grd} = (T_i + T_x)\rho\ 1.271\ DCF_{i,j}^{grd} C_{i,3-4\mathrm{m}} \quad (7\text{-}58)$$

The total annual dose to an MOP who constructs and occupies a residence built on top of the virtual borehole is thus calculated by summing the inhalation, ingestion, and external exposure doses for each organ and for the whole body as given in Equations (7-52) through (7-58).

7.5.3.4 Parameter Values

As is evident from the equations above, calculation of dose involves many parameters: dust suspension factors, radon emanation coefficient, mixing height, wind speed, CRs, dry-to-wet conversion ratios, time spent doing various activities, breathing rates, human consumption rates, and bulk density. These parameters and their values are discussed below.

Values of the dust suspension factors (or dust loading) used in the PA are given in Table 7-17. They are taken from NUREG/CR-5512, Volume 3 [Beyeler et al., 1999], which was a study and analysis of parameter values used in assessing potential dose from exposures to residual radioactive contamination after decommissioning NRC-licensed facilities. Values of the outdoor dust suspension factor, S_x, given by Beyeler et al. [1999] include values representative of both humid and arid sites. Because values of S_x for humid sites are not applicable to the NTS, only data from desert sites was considered in constructing the pdf for S_x. The data were taken from three arid sites given in Table 6.47 of Beyeler et al. [1999]. The values of S_x obtained from this table vary from $1.6 \times 10^{!9}$ kg/m^3 to $1 \times 10^{!7}$ kg/m^3. For reasons given by Beyeler et al. [1999], the distribution of S_x is best represented by a log-uniform distribution. Suspension of dust as a result of gardening is not as dependent on whether the site is arid or humid, and so the distribution presented by Beyeler et al. [1999] was adopted for use the PA. The distribution of S_g is uniform between $1 \times 10^{!7}$ kg/m^3 to $4 \times 10^{!7}$ kg/m^3. Suspension of dust indoors is related to the suspension outdoors. Ratios of indoor to outdoor dust loading varied from 0.2 to 0.7, as reported by Beyeler et al. [1999]. Therefore, consistent with Beyeler et al. [1999], S_i is not sampled separately but is assumed to be related to S_x:

Table 7-17. Values of Dust Suspension Factors

Parameter	Distribution	Reference
Outdoor dust suspension factor, S_x	$1.6 \times 10^{!9} – 1 \times 10^{!7}$ kg/m^3 loguniform	Beyeler et al. [1999, p. 6-71]
Gardening dust suspension factor, S_x	$1 \times 10^{!7} – 4 \times 10^{!7}$ kg/m^3 uniform	Beyeler et al. [1999, p. 6-72]
Ratio of indoor to outdoor dust suspension, *PF*	0.2 – 0.7 uniform	Beyeler et al. [1999, p. 6-72]

$$S_i = PF \otimes S_x \quad (7\text{-}59)$$

where

PF = ratio of indoor to outdoor dust loading (dimensionless),

and *PF* is uniformly distributed between 0.2 and 0.7.

The hours per year that the MOP spends gardening, outdoors but not gardening, and indoors are approximated by distributions reported by Beyeler et al. [1999]. These three parameters are related in that the time the MOP spends in a given context is constrained by the time spent in each of the other two contexts. Following the recommendation of Beyeler et al. [1999], each pair of time categories is assigned a rank correlation of !0.35. The distributions are given in Table 7-18 and the correlations are given in Table 7-19.

When the exposure time parameters are correlated as given in Table 7-19, the total time ranges from 0.66 yr to 0.93 yr with a median value of 0.78 yr. The remainder of the time is assumed to be spent away from home.

The shielding factor for indoor external radiation exposure, SF^{ext}, is a measure of attenuation of gamma radiation by the structural materials of the MOP's residence. It is defined as the ratio of shielded dose to unshielded dose, and is a function of the building material as well as the gamma energy. Most of the radionuclides considered in the dose calculation have gamma energies greater than about 0.06 MeV. Further, assuming that the residence is constructed of wood, which is not as effective at attenuating gamma radiation as concrete, SF^{ext} varies from 0.608 to 0.857, according to Beyeler et al. [1999, Table 6.16]. Therefore SF^{ext} is assigned a uniform distribution between 0.608 and 0.857. This is shown in Table 7-20.

Just as exposure times and dust suspension are different for the three regions (garden, outside not gardening, and inside), the MOP's breathing rate is different for the three regions. The highest breathing rate is assumed to occur while gardening, the second highest breathing rate is assumed to occur while outside not gardening, and the lowest to occur while inside. The values of breathing rate recommended by Beyeler et al. [1999] are used in the PA for the dose calculations and are given in Table 7-20.

The distribution of dry bulk density was discussed in Section 5.5.3.3, but is repeated here in Table 7-20 for convenience.

Table 7-21 gives element-specific crop CR values. Only those radionuclides with internal DCFs were included in the crop uptake calculations. For all radionuclides except Np, the geometric means (GM) of measured CR values were taken from Baes et al. [1984], while GMs of measured CR values for Np were taken from Ng et al. [1982]. Geometric standard deviation (GSD) values were obtained from Sheppard and Evenden [1997] and represent the average GSD for 19 different elements, with the actual range of GSDs varying from 2.4 to 16. Lognormal pdfs were developed from the GM and the GSD by assuming that the 0.001 and 0.999 quantiles of the lognormal distribution could be estimated as GM/GSD^3 and $GM*GSD^3$, respectively.

Table 7-18. Quantile Values for Exposure Period Distributions

Probability	T_g (yr)	T_x (yr)	T_i (yr)
0	$5.5 \times 10^{!5}$	$4.60 \times 10^{!2}$	$4.76 \times 10^{!1}$
0.001	$9.6 \times 10^{!5}$	$4.61 \times 10^{!2}$	$4.77 \times 10^{!1}$
0.011	$2.60 \times 10^{!4}$	$5.78 \times 10^{!2}$	$5.20 \times 10^{!1}$
0.051	$8.90 \times 10^{!4}$	$6.79 \times 10^{!2}$	$5.53 \times 10^{!1}$
0.101	$1.23 \times 10^{!3}$	$7.64 \times 10^{!2}$	$5.69 \times 10^{!1}$
0.201	$1.97 \times 10^{!3}$	$8.90 \times 10^{!2}$	$5.97 \times 10^{!1}$
0.301	$2.82 \times 10^{!3}$	$9.69 \times 10^{!2}$	$6.19 \times 10^{!1}$
0.401	$3.70 \times 10^{!3}$	$1.05 \times 10^{!1}$	$6.35 \times 10^{!1}$
0.501	$4.76 \times 10^{!3}$	$1.20 \times 10^{!1}$	$6.52 \times 10^{!1}$
0.601	$7.01 \times 10^{!3}$	$1.21 \times 10^{!1}$	$6.68 \times 10^{!1}$
0.701	$9.80 \times 10^{!3}$	$1.31 \times 10^{!1}$	$6.82 \times 10^{!1}$
0.801	$1.43 \times 10^{!2}$	$1.43 \times 10^{!1}$	$6.98 \times 10^{!1}$
0.901	$1.94 \times 10^{!2}$	$1.59 \times 10^{!1}$	$7.28 \times 10^{!1}$
0.951	$2.31 \times 10^{!2}$	$1.74 \times 10^{!1}$	$7.47 \times 10^{!1}$
0.981	$3.01 \times 10^{!2}$	$1.91 \times 10^{!1}$	$7.67 \times 10^{!1}$
0.999	$4.57 \times 10^{!2}$	$2.3 \times 10^{!1}$	$8.16 \times 10^{!1}$
1	$4.65 \times 10^{!2}$	$2.46 \times 10^{!1}$	$8.21 \times 10^{!1}$

Table 7-19. Correlations Among Exposure Times

Parameters	Rank Correlation Coefficient
T_i, T_x	!0.35
T_i, T_g	!0.35
T_g, T_x	!0.35

Table 7-20. Values of Shielding Factor, Breathing Rates, and Bulk Density

Parameter	Distribution	Reference
Shielding factor for indoor external radiation, SF^{ext}	0.608 – 0.857 uniform	Beyeler et al. [1999, Table 6.16]
Breathing rate while gardening, BR_g	1.49×10^4 m^3/yr	Beyeler et al. [1999, Table 6.29]
Breathing rate while outside, BR_x	1.23×10^4 m^3/yr	Beyeler et al. [1999, Table 6.29]
Breathing rate while indoors, BR_i	7.89×10^3 m^3/yr	Beyeler et al. [1999, Table 6.29]
Dry bulk density of alluvium, ρ	mean = 1600 kg/m^3, std dev = 109; normal	See Section 5.5.3.3

Table 7-21. Values of Element-Specific Crop Concentration Ratios

Element	Leafy (non-reproductive) vegetation (pCi/dry plant mass per pCi/dry soil mass)			Reproductive vegetation (pCi/dry plant mass per pCi/dry soil mass)		
	GM	GSD	0.001 and 0.999 Quantiles	GM	GSD	0.001 and 0.999 Quantiles
Pu	4.5E!4	5.7	2.4E!6, 8.3E!2	4.5E!5	5.7	2.4E!7, 8.3E!3
U	8.5E!3	5.7	4.6E!5, 1.6E0	4.0E!3	5.7	2.2E!5, 7.4E!1
Am	5.5E!3	5.7	3.0E!5, 1.0E0	2.5E!4	5.7	1.3E!6, 4.6E!2
Np	1.1	4.9	9.3E!3, 1.3E2	6.0E!2	3	2.2E!3, 1.6E!3
Ra	1.5E!2	5.7	8.1E!5, 2.8E0	1.5E!3	5.7	8.1E!6, 2.8E!1
Th	8.5E!4	5.7	4.6E!6, 1.6E!1	8.5E!5	5.7	4.6E!7, 1.6E!2
Pa	2.5E!3	5.7	1.3E!5, 4.6E!1	2.5E!4	5.7	1.3E!6, 4.6E!2
Pb	4.5E!2	5.7	2.4E!4, 8.3E0	9.0E!3	5.7	4.9E!5, 1.7E0
Ac	3.5E!3	5.7	1.9E!5, 6.5E!1	3.5E!4	5.7	1.9E!6, 6.5E!2
Po	2.5E!3	5.7	1.3E!5, 4.6E!1	4.0E!4	5.7	2.2E!6, 7.4E!2
Bi	3.5E!2	5.7	1.9E!4, 6.5E0	5.0E!3	5.7	2.7E!5, 9.3E!1

Dry-to-wet conversion factors are given in Table 7-22. These were obtained from Beyeler et al. [1999, Table 6.79] and are used to correct for the moisture content in edible parts of plants, since both dry-weight and wet-weight factors are used in dose modeling. The pdf describing the dry-to-wet conversion factor for vegetables and fruit is a gamma distribution with a mean of 0.11 and lower and upper limits of 0.04 and 0.23, respectively.

Table 7-22. Dry-to-Wet Conversion Factors

Plant Type	Factor (kg dry-weight/kg wet-weight)
Leafy vegetables	gamma distribution, α= 2.68, β= 35.1
Root vegetables	gamma distribution, α= 2.68, β= 35.1
Fruit	gamma distribution, α= 2.68, β= 35.1

Plant food/air concentration ratios are taken from RESRAD and are calculated as follows [Yu et al., 1993; Appendix D]:

$$FAR_K = \frac{395\left(\frac{m}{y}\right)\left(1-e^{-20t_{ek}}\right)T_k}{CY_k} \qquad (7\text{-}60)$$

where

t_{ek} = time of exposure of plant k to contamination during the growing season (0.25 yr for leafy vegetables; 0.17 year for all other plants) (yr),

T_K = foliage-to-food transfer factor for plant *k* (1 for leafy vegetables; 0.1 for all other plants), (dimensionless)
CY_k = crop yield for plant *k* (kg wet plant/m^2y)

Fixed parameters used in calculating the concentration of radon in the air are given in Table 7-23. The mixing height is a standard assumption [Yu et al., 1993] in such calculations. The radon emanation coefficient is given by the NRC [1989], and the effective diffusion coefficient for radon is taken from measurements at the NTS [Tanner, 1980].

Table 7-23. Parameters for Calculating Radon Concentrations in Air

Parameter	Value
Mixing height, H	2 m
Radon emanation coefficient, g	0.35
Effective diffusion coefficient, D_{Rn}	113.6 m^2/yr

The average wind speed, *U*, was estimated from the wind rose. The resulting pdf is given in Table 7-24.

Table 7-24. Wind Speed Quantile Values

Wind Speed (m/yr)	Cumulative Probability
0	0
4.7×10^7	0.37
1.3×10^8	0.62
2.1×10^8	0.82
2.8×10^8	0.92
4.1×10^8	1.0

To model the exposure condition involving construction of and residence in a house on top of a borehole, five additional parameters are needed: the volume of the residence (*V*), the fresh air infiltration rate (*k*), the breathing rate during construction of the house (BR_{ch}), the time the MOP spends constructing the house (T_{ch}), and the dust loading during house construction (S_{ch}). Values of these parameters are discussed below and are summarized in Table 7-25.

The volume of the residence is used to calculate the concentration of radon in the house. However, the indoor concentration of radon is only slightly dependent on the volume of the house, because the volume, *V*, appears in both the numerator and denominator of the equation that calculates radon concentration in the house (see Equation (7-46)). For the purposes of this calculation, it is assumed that the house has an area of 100 m^2 (1,080 ft^2) and that the basement is 3.0 m (10 ft) deep. This results in a basement volume of 300 m^3 (1.06×10^4 ft^3). This volume is used in Equation (7-46) to calculate radon concentration.

Table 7-25. Values of Parameters for Construction of and Residence in a House on Top of the Virtual Borehole

Parameter	Distribution	Reference
Volume of residence, V	300 m^3	assumption
Fresh air infiltration rate, k	1.31×10^5 to 5.26×10^6 m^3/yr, lognormal	Fisk et al. [1987]
Breathing rate during construction, BR_{ch}	1.49×10^4 m^3/yr	Beyeler et al. [1999, Table 6.29]
Time spent constructing the house, T_{ch}	0.14 yr (52 days)	Beyeler et al. [1999, Table 6.12 and Section 6.2.3.6.3]
Dust loading during house construction, S_{ch}	$1 \times 10^{!7}$ to $4 \times 10^{!7}$ kg/m^3, uniform	Beyeler et al. [1999, page 6.72]

The fresh air infiltration rate is also used to calculate the concentration of radon in the house and is estimated from air-changes-per-hour (ACH) information obtained from Fisk et al. [1987]. This reference indicates that fresh air infiltration rates vary from "less than 0.1 to several ACH" and "an average air exchange rate ... has been estimated to be in the range of 0.5 to 0.9 ACH." It is assumed that the fresh air infiltration rate ranges from 0.05 $hr^{!1}$ to 2 $hr^{!1}$, with a mean value of 0.53 $hr^{!1}$. The fresh air infiltration rate, k, is obtained by multiplying the ACH by the volume of the house (300 m^3) and the number of hours in a years (8766 hr/yr). Performing this multiplication results in a minimum value of 1.31×10^5 m^3/yr and a maximum value of 5.26×10^6 m^3/yr. Assigning a lognormal distribution to these values results in a mean value of 1.39×10^6 m^3/yr for k, which corresponds to an ACH of 0.53 $hr^{!1}$. Therefore, the fresh air infiltration rate, k, is assumed to be lognormally distributed between 1.31×10^5 m^3/yr and 5.26×10^6 m^3/yr.

To estimate the breathing rate during construction, it is assumed that construction activities are similar to gardening activities in their physical exertion characteristics. Therefore, the breathing rate during construction is assumed to equal the breathing rate during gardening, 1.49×10^4 m^3/yr.

The time spent constructing the house is based on information obtained from Section 6.2.3.6.3 of Beyeler et al. [1999] and was estimated in a manner that ensures that time constructing the house plus time outdoors plus time indoors does not exceed one year (365 days). When the distributions of time spent indoors, outdoors not gardening, and gardening as given in Table 7-18 are correlated as given in Table 7-19, the 99th percentile value for total time on-site is 325 days. The MOP constructing a house on top of the virtual borehole does not garden, so subtracting 12 days, which is the 99th percentile of gardening time (Table 6.12 of Beyeler et al. [1999]) from 325 days yields 313 days spent outdoors and indoors. This leaves 52 days (0.14 yr) to construct the house. This is a reasonable amount of time to erect the walls and roof of the house, after which the occupancy portion of the exposure condition is assumed to commence.

The dust suspension factor during construction of the residence is assumed to be similar to the dust suspension factor during gardening. Therefore, S_{ch} is assumed to equal S_g, $1 \times 10^{!7}$ kg/m^3 to $4 \times 10^{!7}$ kg/m^3, uniform distribution.

Table 7-26 gives the various parameter values associated with the different activities of the MOP who has constructed a house and occupies it.

7.5.3.5 Calculation of Food Consumption Rates

The quantity of food grown and consumed by the MOP is assumed to be a function of garden size, crop yield, and quantity of each type of food consumed (i.e., leafy vegetables, root vegetables, fruit). The garden size is assumed to be fixed at 70 m^2 (750 ft^2). Crop yields used in the PA are given in Table 7-27 and are taken from Beyeler et al [1999].

Table 7-26. Comparison of Parameter Values for Construction and Occupation

Activity	Time (*T*)	Breathing Rate (*BR*)	Dust Suspension Factor (*S*)
Construction	0.14 yr	1.49×10^4 m^3/yr	1×10^{-7} to 4×10^{-7} kg/m^3
Occupation	See Table 7-1 for time spent outside and time spent inside	1.23×10^4 m^3/yr (outside) 7.89×10^3 m^3/yr (inside)	$1.6 \times 10^{!9}$ to $1 \times 10^{!7}$ kg/m^3 loguniform (outside) 0.2 to 0.7 times the outside values of *S* (inside)

Table 7-27. Crop Yields (kg/m^2)

Crop	Distribution
Leafy vegetables	2.7 – 3.2, normal
Root vegetables	2.3 – 2.5, normal
Fruit	2.2 – 2.6, normal

Ingestion rates of homegrown foods are uncertain and highly variable; however, because the garden is fixed at 70 m^2 (750 ft^2), the sampling procedure for ingestion rates would have to be constrained to be consistent with the garden size. Rather than sample ingestion rates, it is assumed that the *ratio* of annual fruit consumption to leafy vegetable consumption to root vegetable consumption is fixed, but the actual quantities consumed are determined by the (fixed) garden size and (variable) crop yields. Table 6.21 of Beyeler et al. [1999] gives statistical characteristics of ingestion rates of homegrown food. From the data in this table, it is assumed that the MOP grows and consumes equal amounts of fruit and root (non-leafy) vegetables, and consumes half as much leafy vegetables as non-leafy vegetables. Therefore, the following equation relates garden size, crop yield, and crop ingestion:

$$\text{Garden Area} = \frac{HC_{fruit}}{CY_{fruit}} + \frac{HC_{fruit}}{CY_{root}} + \frac{0.5\, HC_{fruit}}{CY_{leafy}} \tag{7-61}$$

where

Garden Area	=	70 m^2 (750 ft^2),
HC_{fruit}	=	Annual consumption rate of fruit = HC_{root} = 2 HC_{leafy} (kg/yr),
CY_{fruit}	=	crop yield for fruit (kg/m^2),
CY_{root}	=	crop yield for root vegetables (non-leafy) (kg/m^2), and
CY_{leafy}	=	crop yield for leafy vegetables (kg/m^2).

Therefore, for each simulation, the annual growth and consumption of fruit, root vegetables, and leafy vegetables is given by:

$$HC_{fruit} = HC_{root} = 2\, HC_{leafy} = \frac{\text{Garden Area}}{\frac{1}{CY_{fruit}} + \frac{1}{CY_{root}} + \frac{1}{2CY_{leafy}}} \tag{7-62}$$

Based on these assumptions, the minimum amount of fruit, root vegetables, and leafy vegetables grown and consumed by the MOP in a year is 65 kg, 65 kg, and 33 kg, respectively. The maximum amounts are 74 kg, 74 kg, and 37 kg, respectively. This places the MOP between the 75th and 90th percentiles in terms of fruit and vegetable consumption, according to Table 6.21 of Beyeler et al. [1999].

The ingestion rate of contaminated soil is assumed to equal 0.0365 kg/yr, as recommended by Wood et al. [1994].

7.6 Computer Codes and Procedures

The simple mathematical model defined above was implemented as Microsoft® Visual Basic™ modules in an Access™ database. The Monte Carlo analysis used for both the CR and the IPR entails a large number of calculations, but the simple model structure allows acceptable performance when these calculations are implemented as Basic macros. The database produces a CCDF for assessing compliance with the CR, and calculates doses to the whole body and specific organs for assessing compliance with the IPR.

Figure 7-4 illustrates the transport and exposure processes simulated in the database models along with the important system properties. Both databases have the same radionuclide transport model that simulates mobilization of the waste, advection, diffusion, and dispersion of dissolved radionuclides up towards the ground surface, and transport of radionuclides to the ground surface by plant uptake and animal burrowing. The common transport model also includes radioactive decay and production, adsorption, and chemical precipitation of radionuclides. This transport model is a numerical approximation of the mass balance equations described above in Section 7.3.

The requirements differ in their use of the calculated radionuclide discharge. The CR requires integrated radionuclide flux over a 10,000-year performance period. A weighted sum over all radionuclides is then calculated for comparison against the regulatory requirement. The IPR calculation accumulates all discharged radionuclide mass over a 1,000-year performance period. All of this mass is assumed to be transferred to the MOP's garden. The exposure model then calculates the dose resulting from the garden soil contamination due to the diverse ingestion, inhalation, and external exposure pathways described above in Section 7.7.

Figure 7-5 illustrates the flow of information through the PA process, including parameter definition, parameter sampling, system simulation, and performance measure calculation. This figure applies to both requirements. Both perform multiple simulations using multiple sets of parameter values generated using LHS. The sample parameter values generated by LHS are imported into a database table. The transport model is then executed for each of the parameter sample sets in the table. Probability distributions for integrated release and dose are constructed from the results of these repeated simulations.

As Figure 7-5 illustrates, much of the PA information flow takes place within the database, and can be easily exported for graphing and analysis. The database contains most of the information used in the PA, including the code that implements the transport and exposure calculations. This implementation helps make the calculations transparent and verifiable, but has some cost in computational efficiency. Because of the simplicity of the model, however, the execution time for a set of parameter samples is quite acceptable: for the CR calculations, 1000 simulations can be run in approximately one-half hour; for the IPR workbook, 1000 simulations can be run in less than two hours.

The database models are being verified and validated as part of the QA process for the GCD PA . This process includes review of the underlying mathematical model, review of the implementing code, and comparison of the model results to analytical solutions where appropriate.

7.6.1 Sampling Uncertain Parameters

The CR model uses more than 100 input parameters to characterize the disposal system. Of these, 70 are considered to be uncertain, and are assigned probability distributions based on the existing state of knowledge. The IPR model use more than 200 input parameters, 104 of which are considered to be uncertain. For both models, parameters that were not considered uncertain were assigned fixed values based on generally accepted sources (such as radionuclide half-lives), regulatory stipulation, or convention.

For both models, LHS was used to produce a set of samples of the input parameter values and the PA model was executed in turn for each of these parameter sets. For each set of sampled values of uncertain input parameters, the model calculates the integrated release (for the CR) or the dose to the MOP (for the IPR). For the CR, the distribution of possible integrated releases is explicitly required by the regulation. A dose distribution is not explicitly required by the IPR, however the input parameter values are still uncertain. Characterizing the effect of this uncertainty on the

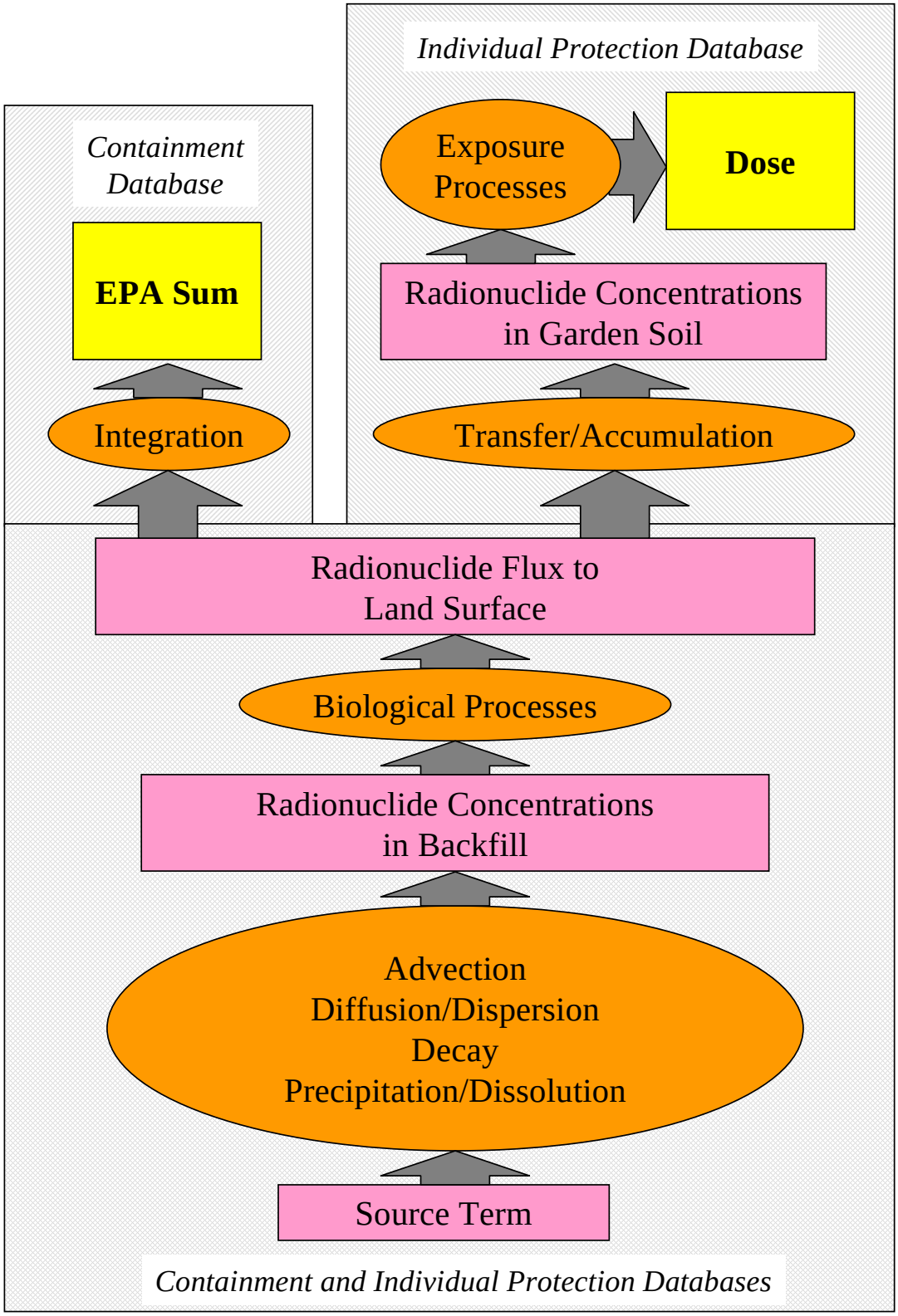

Figure 7-4. Transport and Exposure Processes in the Containment and Individual Protection Database Models.

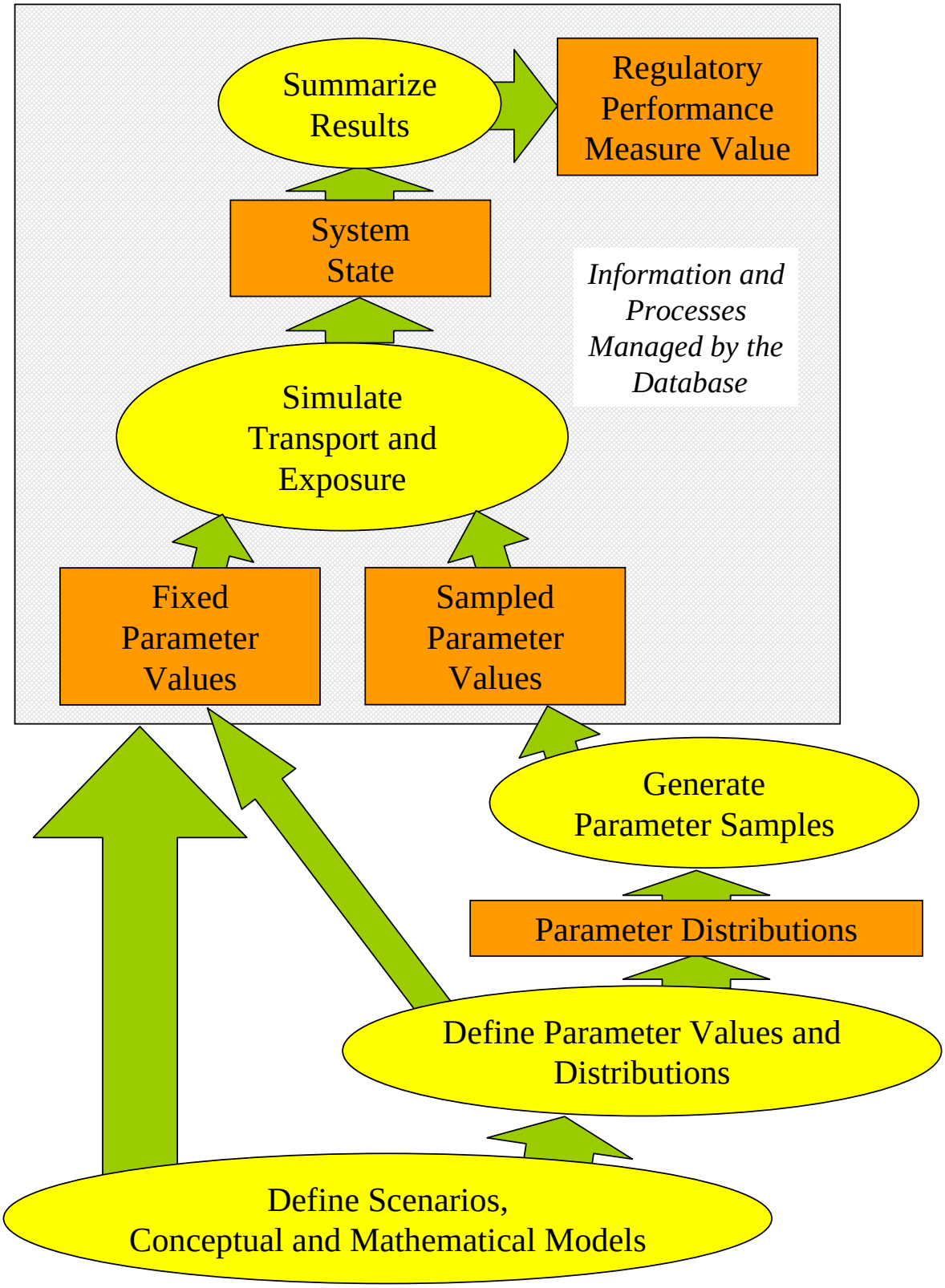

Figure 7-5. Flow of Information in the PA Process.

regulatory performance measure is good practice, and is anticipated by the EPA in 40 CFR 191 (see Section 2.3).

7.6.2 Calculating Performance Measures

7.6.2.1 Numerical Model for Transport

General Formulation

The mass density of each radionuclide *i* in each region *x* was estimated at a series of discrete timesteps by approximating Equation (7-1). The right-hand side of Equation (7-1) was evaluated to estimate the average rate of change in mass density in region *x* between time intervals *n* and *n+1*:

$$\frac{m_{i,n+1}^{x} - m_{i,n}^{x}}{\Delta t} = \overline{Rate} = (1-\omega)\, Rate(t_n) + \omega\, Rate(t_{n+1}) \tag{7-63}$$

where:

ω = weighting factor for rate terms evaluated at the end of the timestep (implicit rate terms)

As Equation (7-63) shows, the effective rate between timesteps n and n+1 was approximated by a weighted combination of the rates at timesteps n and n + 1. An expression for mass density at timestep n + 1 was obtained by substituting the equations for these rates, in terms of the radionuclide mass density, into Equation (7-63), and solving for mass density at timestep n + 1. The weighting factor ω determines the accuracy, stability, and ease of implementation of the approximation.

The general numerical approximation was obtained by substituting the expressions for the rate terms in Equation (7-63):

$$\begin{aligned}
\frac{m_{i,n\%1}^{x} \& m_{i,n}^{x}}{\Delta t} \cdot \frac{\omega}{L^{x}} & \left[q_l\left(\gamma C_i^{x\&1} \% (1\&\gamma) C_i^{x}\right) \& q_D^{x\&1}\left(C_i^{x} \& C_i^{x\&1}\right) \right. \\
& \left. \& q_l\left(\gamma C_i^{x} \% (1\&\gamma) C_i^{x\%1}\right) \% q_D^{x}\left(C_i^{x\%1} \& C_i^{x}\right) \right]_{n\%1} \\
& \% \omega \left[\& a_i^{x} \& b_i^{x} m_i^{x} \% \lambda_{i\&1} m_{i\&1}^{x} \& \lambda_i m_i^{x} \right]_{n\%1} \\
\% \frac{(1\&\omega)}{L^{x}} & \left[q_l\left(\gamma C_i^{x\&1} \% (1\&\gamma) C_i^{x}\right) \& q_D^{x\&1}\left(C_i^{x} \& C_i^{x\&1}\right) \right. \\
& \left. \& q_l\left(\gamma C_i^{x} \% (1\&\gamma) C_i^{x\%1}\right) \% q_D^{x}\left(C_i^{x\%1} \& C_i^{x}\right) \right]_{n} \\
\% (1\&\omega) & \left[\& a_i^{x} \& b_i^{x} m_i^{x} \% \lambda_{i\&1} m_{i\&1}^{x} \& \lambda_i m_i^{x} \right]_{n}
\end{aligned} \tag{7-64}$$

Collecting terms for the various mass densities and concentrations, with the values at the new timestep n + 1 on the left-hand side:

$$
\begin{aligned}
&-\Delta t\omega A_D^x C_{i,n+1}^{x-1} + (1+\Delta t\omega B_M^x) m_{i,n+1}^x + \Delta t\omega B_C^x C_{i,n+1}^x - \Delta t\omega A_U^x C_{i,n+1}^{x+1} \\
&= \Delta t(1-\omega) A_D^x C_{i,n}^{x-1} + (1-\Delta t(1-\omega) B_M^x) m_{i,n}^x - \Delta t(1-\omega) B_C^x C_{i,n}^x + \Delta t(1-\omega) A_U^x C_{i,n}^{x+1} \\
&\quad + \Delta t\left(\lambda_{i-1}\left((1-\omega) m_{i-1,n}^x + \omega m_{i-1,n+1}^x\right) - a_i^x\right)
\end{aligned}
\tag{7-65}
$$

where:

$$
\begin{aligned}
A_D^x &= \frac{\gamma q_l + q_D^{x-1}}{L^x} \\
A_U^x &= \frac{q_D^x - (1-\gamma) q_l}{L^x} \\
B_{Mi}^x &= b_i^x + \lambda_i \\
B_C^x &= B_D^x + B_U^x \\
B_D^x &= \frac{(\gamma-1) q_l + q_D^{x-1}}{L^x} \\
B_U^x &= \frac{\gamma q_l + q_D^x}{L^x}
\end{aligned}
\tag{7-66}
$$

If fluid-based transport from region $x-1$ does not occur:

$$
\begin{aligned}
A_D^x &= 0 \\
B_D^x &= 0
\end{aligned}
\tag{7-67}
$$

If fluid-based transport to region $x+1$ does not occur:

$$
\begin{aligned}
A_U^x &= 0 \\
B_U^x &= 0
\end{aligned}
\tag{7-68}
$$

Effect of Solubility Limits

The relationships between fluid concentration and mass density in regions $x-1$, x, and $x+1$ are determined by Equation (7-5). If a particular region is undersaturated, concentration is a linear function of mass density, and the terms multiplying concentration in Equation (7-65) are combined with the terms multiplying mass density as follows:

If region $x-1$ is undersaturated:

$$A_D^x C_i^{x\&1} \;'\; A_D^x \frac{m_i^{x\&1}}{R_i \theta} \tag{7-69}$$

If region x + 1 is undersaturated:

$$A_U^x C_i^{x\%1} \;'\; A_U^x \frac{m_i^{x\%1}}{R_i \theta} \tag{7-70}$$

If region x is undersaturated:

$$B_M^x m_i^x \;\%\; B_C^x C_i^x \;'\; \left(B_M^x \% \;\frac{B_C^x}{R_i \theta} \right) m_i^x \tag{7-71}$$

If a particular region is saturated, the corresponding concentration in Equation (7-65) is equal to the solubility limit, and the terms involving concentration in that region are evaluated as part of the right-hand side of the mass density equation for region *x*. If region $x \,!\, 1$ is saturated, for example, then:

$$C_{i,n\%1}^{x\&1} \;'\; C_{i,n}^{x\&1} \;'\; C_{i,sol} \tag{7-72}$$

and the terms involving the concentration in region *x*-1 are included in the evaluation of the right-hand side:

$$\Delta t(1\&\omega) A_D^x C_{i,n}^{x\&1} \;\%\; \Delta t \omega A_D^x C_{i,n\%1}^{x\&1} \;'\; \Delta t A_D^x C_{i,sol} \tag{7-73}$$

Stability and Accuracy Considerations

The numerical approximation in Equation (7-65) is stable provided errors in mass density tend to zero with successive iterations [Al-Khafaji and Tooley, 1986]. Assuming a mass density error of magnitude ξ_n at timestep *n*, the mass density error at timestep *n* + 1 can be bounded using Equation (7-65). Assuming undersaturated conditions in regions $x \,!\, 1$, *x*, and *x*:

$$\left(1 + \Delta t\,\omega\,B_M^x\right)\xi_{n+1} + \Delta t\,\omega\,B_C^x\,\frac{\xi_{n+1}}{R_i\theta} = \left(1 - \Delta t(1-\omega)\,B_M^x\right)\xi_n - \Delta t(1-\omega)\,A_D^x\,\frac{\xi_n}{R_i\theta} - \Delta t(1-\omega)\,B_C^x\,\frac{\xi_n}{R_i\theta} + \Delta t(1-\omega)\,A_U^x\,\frac{\xi_n}{R_i\theta} \tag{7-74}$$

The requirement that the error amplification, $\left|\frac{\xi_{n+1}}{\xi_n}\right|$, be less than 1 leads to limits on ω:

$$1 - \frac{2 + \Delta t\left(B_M^x + \frac{B_C^x}{R_i\theta}\right)}{\Delta t\left\{2B_M^x + \frac{1}{R_i\theta}\left(2B_C^x + A_D^x + A_U^x\right)\right\}} < \omega \le 1 \tag{7-75}$$

This expression implies that a fully implicit approximation (ω = 1) may be needed as the timestep becomes large. For sufficiently small timesteps, an explicit (ω = 0) approximation will be stable; however, the more accurate semi-implicit (ω = ½) approximation is preferred when it does not lead to instability. The following function provides the desired limiting behavior, and defines a stable and accurate numerical scheme:

$$\omega = \frac{1/2 + \Delta t P}{1 + \Delta t P} \tag{7-76}$$

where:

$$P = \frac{\Delta t\left\{2B_M^x + \frac{1}{R_i\theta}\left(2B_C^x + A_D^x + A_U^x\right)\right\}}{2 + \Delta t\left(B_M^x + \frac{B_C^x}{R_i\theta}\right)} \tag{7-77}$$

When region $x - 1$, x, or $x + 1$ is saturated, then the corresponding advection coefficient (A_D^x, B_C^x, or A_U^x) does not appear in Equation (7-74) and therefore does not appear in Equation (7-77). When all three regions are saturated, for example, all advection terms are removed, which gives:

$$P \;=\; \frac{2\Delta t B_M^x}{2 \;+\; \Delta t B_M^x} \qquad (7\text{-}78)$$

Solution Algorithm

Equations for mass density for each region *x* are based on Equation (7-65). The resulting equations are coupled through the coefficients A_D and A_U, and are solved simultaneously. The mass density equation for a region depends on the saturation conditions in that region and in adjacent regions. The saturation condition in any region may change during a timestep. In addition, each region has a separate stability requirement based on Equation (7-77), and the weighting factor ω must satisfy the stability requirements of all regions.

The following algorithm was used to calculate the mass densities in all regions at timestep $n + 1$ from the mass densities at timestep n in consideration of potential changes in saturation conditions and global stability requirements. The algorithm was implemented in Visual Basic™ modules within the PA database.

1) The distributed sink coefficients a_i^x and b_i^x are calculated for all regions for this timestep.

2) Using the saturation conditions at the beginning of the timestep, the weighting factor ω is calculated for each region, and the largest value, ω_{max}, is identified.

3) Using ω_{max}, mass densities at time $n + 1$ are calculated for all regions by solving the simultaneous set of difference equations based on Equation (7-65).

4) In each region, the saturation condition at time $n + 1$ is compared to the saturation condition at time n. If they differ, the mass densities are used to calculate the time at which the saturation condition changes. The minimum time at which saturation conditions change is tracked over all regions.

5) If the saturation conditions have not changed in any region, the timestep is complete.

6) If the saturation conditions have changed, a smaller timestep, based on the minimum time at which conditions change in any region, is used. Mass densities in all regions are calculated at this intermediate time, and the saturation condition is updated in the region whose transition defined the limit on timestep size.

7) The rate of discharge to the surface during the timestep, due to the activities of plants and animals, is calculated using Equation (7-13a) or (7-13b). The mass of radionuclides in the soil region is updated by solving Equation (7-65) for the soil region, which is only coupled to the underlying regions through Equation (7-13).

8) A new timestep size is calculated based on the current (intermediate) simulation time and the desired ending time for step n + 1. The algorithm is then repeated from step (2).

Gas-Phase (Radon) Transport

The radon mass balance Equation (7-14) is a special case of Equation (7-1) in which advection and distributed sink terms are excluded and a different diffusion coefficient is used. The numerical approximation for the mass density of radon *i* in each region *x* is therefore a special case of Equation (7-64) with the corresponding terms excluded:

$$\begin{aligned}\frac{m_{Rn,n+1}^{x} - m_{Rn,n}^{x}}{\Delta t} = & \frac{\omega}{L^{x}}\left[-q_{D_{Rn}}^{x-1}\left(m_{Rn}^{x}-m_{Rn}^{x-1}\right)+ q_{D_{Rn}}^{x}\left(m_{Rn}^{x+1}-m_{Rn}^{x}\right)\right]_{n+1} \\ & +\omega\left[\lambda_{Ra} m_{Ra}^{x}-\lambda_{Rn} m_{Rn}^{x}\right]_{n+1} \\ & +\frac{(1-\omega)}{L^{x}}\left[-q_{D_{Rn}}^{x-1}\left(m_{Rn}^{x}-m_{Rn}^{x-1}\right)+ q_{D_{Rn}}^{x}\left(m_{Rn}^{x+1}-m_{Rn}^{x}\right)\right]_{n} \\ & +(1-\omega)\left[\lambda_{Ra} m_{Ra}^{x}-\lambda_{Rn} m_{Rn}^{x}\right]_{n}\end{aligned} \tag{7-79}$$

where:

$$q_{D_{Rn}}^{x} = \frac{2\,D_{Rn}}{\left(L^{x}+L^{x+1}\right)} \tag{7-80}$$

Collecting terms for the various mass densities and concentrations, with the values at the new timestep n+1 on the left-hand side:

$$\begin{aligned}-\Delta t\omega\frac{A_D^{x}}{\varepsilon} m_{Rn,n+1}^{x-1} + \left(1+\Delta t\omega\left(B_M^{x}+\frac{B_C^{x}}{\varepsilon}\right)\right) m_{Rn,n+1}^{x} - \Delta t\omega\frac{A_U^{x}}{\varepsilon} m_{Rn,n+1}^{x+1} \\ = \Delta t(1-\omega)\frac{A_D^{x}}{\varepsilon} m_{Rn,n}^{x-1} + \left(1-\Delta t(1-\omega)\left(B_M^{x}+\frac{B_C^{x}}{\varepsilon}\right)\right) m_{Rn,n}^{x} + \Delta t(1-\omega)\frac{A_U^{x}}{\varepsilon} m_{Rn,n}^{x+1} \\ +\Delta t\lambda_{Ra}\left((1-\omega) m_{Ra,n}^{x}+\omega m_{Ra,n+1}^{x}\right)\end{aligned} \tag{7-81}$$

where:

$$
\begin{aligned}
A_D^x &= \frac{q_{D_{Rn}}^{x\&1}}{L^x} \\
A_U^x &= \frac{q_{D_{Rn}}^{x}}{L^x} \\
B_M^x &= \lambda_{Rn} \\
B_C^x &= A_D^x \% A_U^x
\end{aligned}
\tag{7-82}
$$

No diffusion is assumed to occur through the lower boundary of the source. This condition is enforced by specifying:

$$A_D^1 = 0 \tag{7-83}$$

Mixing in the atmosphere is assumed to reduce radon concentration at the land surface to low values compared to concentrations in the soil. This condition, which is conservative with respect to radon flux from the soil, is enforced by specifying the following terms in the mass balance expression for the uppermost region N_x :

$$
\begin{aligned}
m_{Rn}^{N_x+1} &= 0 \\
L^{N_x+1} &= 0
\end{aligned}
\tag{7-84}
$$

The weighting factor for radon transport, ω, is given by Equation (7-76) with:

$$P = \frac{\Delta t \left\{ 2 B_M^x \% \frac{1}{\mathrm{g}} \left(2 B_C^x \% A_D^x \% A_U^x \right) \right\}}{2 \% \Delta t \left(B_M^x \% \frac{B_C^x}{\mathrm{g}} \right)} \tag{7-85}$$

7.6.2.2 Containment Requirements

For each set of parameter values and for each transported radionuclide, the rate of discharge to the surface, which is due to the activities of plants and animals, was calculated using Equation (7-13). The total integrated discharge over 10,000 years for each nuclide was then calculated by integrating this discharge rate.

Integrated discharge due to lateral diffusion of nuclides through the borehole sides was then estimated (as described in Section 7.3.9) by the product of the integrated discharge for the nuclide (excluding direct release from the waste) and a nuclide-specific scale factor. The original integrated discharge and the discharge due to lateral diffusion were then added to produce the total integrated discharge for each nuclide.

The total integrated discharge for the system was obtained by summing the total integrated discharges for each nuclide, normalized by their respective release limits. The probability distribution for integrated discharge was then constructed from the set of integrated discharge values for all parameter vectors.

7.6.2.3 Individual Protection Requirements

For each parameter sample vector and for each transported radionuclide, the rate of discharge to the surface due to the activities of plants and animals was calculated using Equation (7-13). The mass of each radionuclide in the soil region was updated by solving Equation (7-65) for the soil region, which is only coupled to the underlying regions through Equation (7-13). The calculated mass in the soil region at the end of a 1000-year simulation period was then assumed to be available to the MOP in the garden soil. The exposure model was then used to calculate the dose resulting from this concentration. The exposure pathway models are algebraic expressions that do not require numerical approximation. They were implemented directly as defined in Section 7.5. The probability distribution for dose to the MOP was then constructed from the set of calculated doses for all parameter vectors.

7.7 Conclusions

This section has presented the equations used to model the various processes that are assumed to affect radionuclide releases to the accessible environment for the current climate and for a wetter, cooler climate: advection, dispersion, diffusion, adsorption, dissolution, precipitation, radionuclide decay and production, plant uptake, and bioturbation. In addition, the assumptions and equations used to model a dose to an MOP were also presented. Finally, the procedure for sampling uncertain parameters and calculating performance measures was also discussed.

Because the conceptual models implemented are relatively simple, it was possible to implement them in Microsoft® Visual Basic™ macros in an Access ™ database. Such an implementation makes the calculations transparent and traceable; the input and output for each equation in each macro can be verified.

8.0 CONSEQUENCE ANALYSIS

8.1 Introduction

This section presents the results of the PA and compares the results to the regulatory limits defined in the CRs and IPRs of 40 CFR 191. These results are built on the work presented in the previous sections of this PA. Sections 5.0 and 6.0 detail the conceptual model of processes that may affect the movement of TRU radionuclides. This conceptual model is then described mathematically in Section 7.0, which also details how the mathematical model was implemented in the PA computer code. The PA computer code and input parameters were then used to calculate a CCDF of integrated normalized release of radionuclides for the CRs and histograms of dose for the IPRs. This section presents the CCDF and the histograms of dose, which are then compared to the regulatory limits defined in the CRs and IPRs.

8.2 Results

8.2.1 Containment Requirements

The probability distribution for integrated normalized release was estimated using 5,000 samples of the uncertain parameters for the CR model. For each parameter sample set, integrated release was calculated over the 10,000-year performance period of the CR. Figure 8-1 shows the resulting CCDF of integrated normalized release. The critical points of regulatory compliance for comparison against the CR are also shown on the figure. The CR requires that the integrated release at a probability level of 0.1 be less than 1, and that the integrated release at a probability level of 0.001 be less than 10. The region representing violation of the CR is shaded. The corresponding integrated release values based on the 5,000-sample CCDF in Figure 8-1 are 4.6×10^{-4} and 6.0×10^{-3}. The estimated CCDF satisfies both quantitative limits defined in the CR.

The calculated probability distribution quantifies uncertainty about integrated release given the scenarios and conceptual models that underlie the calculations. The uncertainty in scenarios and conceptual models is not quantified, and is not directly reflected in the calculated distribution. Instead, the PA methodology treats this uncertainty by focusing only on those scenarios and conceptual models that have the greatest potential performance consequence. Therefore, reduction in uncertainty about the scenarios and conceptual models should cause the resulting CCDF to fall to the left of the calculated CCDF.

The CCDF is an approximate reflection of the mathematical models and parameter distributions that follow from the selected scenarios and conceptual models. Numerical approximations are used in three areas: the soil column is divided into discrete layers; discrete timesteps are used to approximate dynamic behavior; and a finite number of parameter samples are used to approximate the assigned distributions, and to estimate the distribution of integrated release. These approximations each introduce some inaccuracy in the estimated CCDF. As discussed in Appendix P, this inaccuracy is quite small compared to the distance between the CCDF and the CR limits.

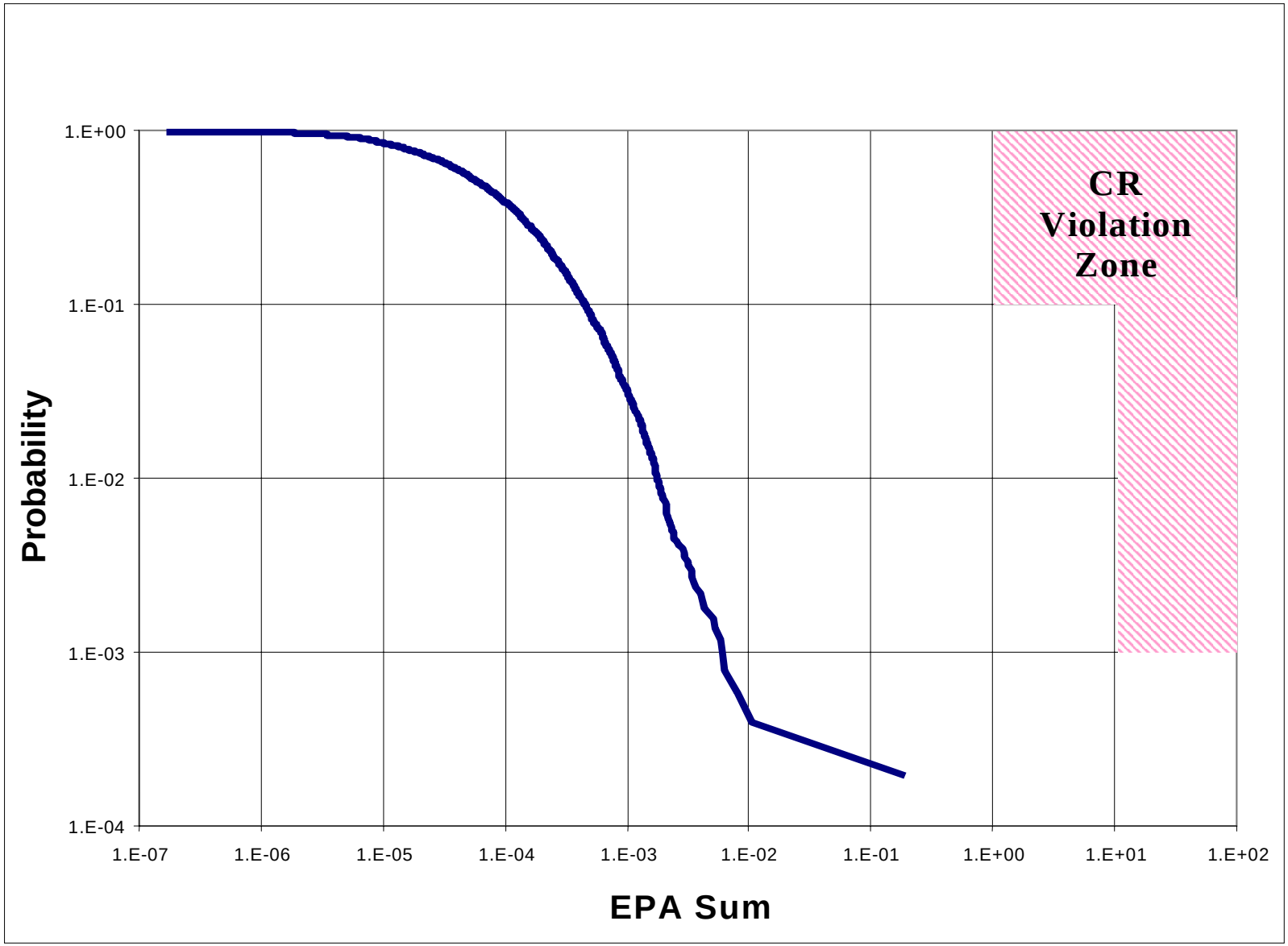

Figure 8-1. CCDF for the PA Analysis of the TRU Wastes in the GCD Boreholes. Analyses of Alternative Scenarios and Conceptual Models are Expected to Result in Reduced Releases, Shifting the CCDF to the Left

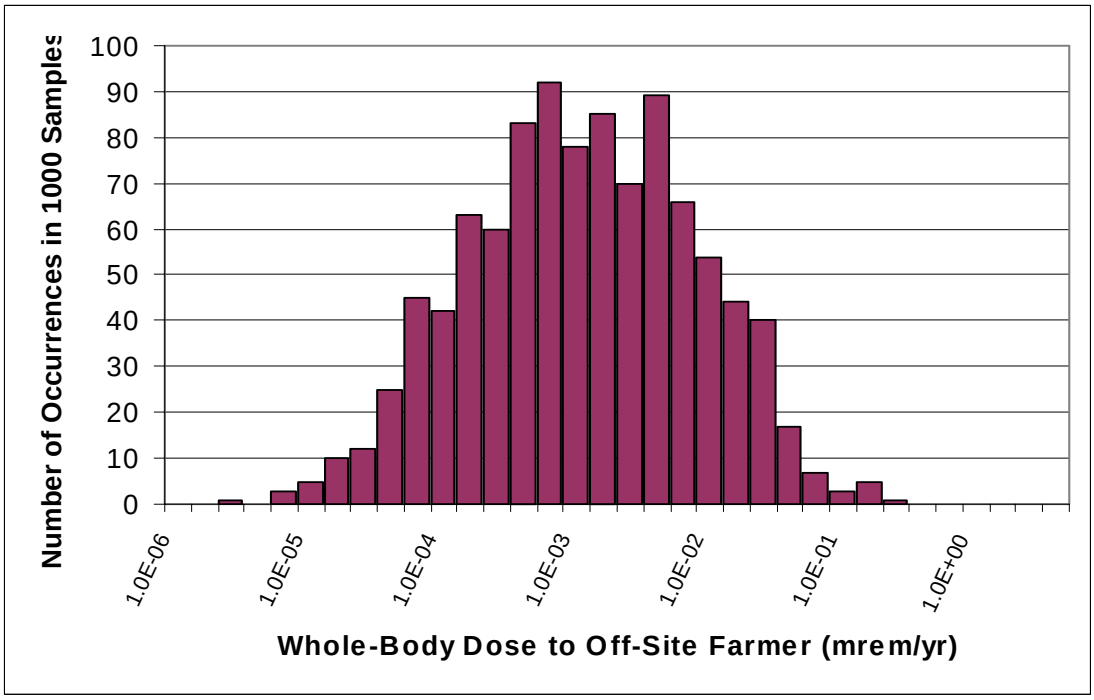

Figure 8-2. Histogram of Calculated Whole-Body Dose Values for the GCD TRU Waste IPR Analysis.

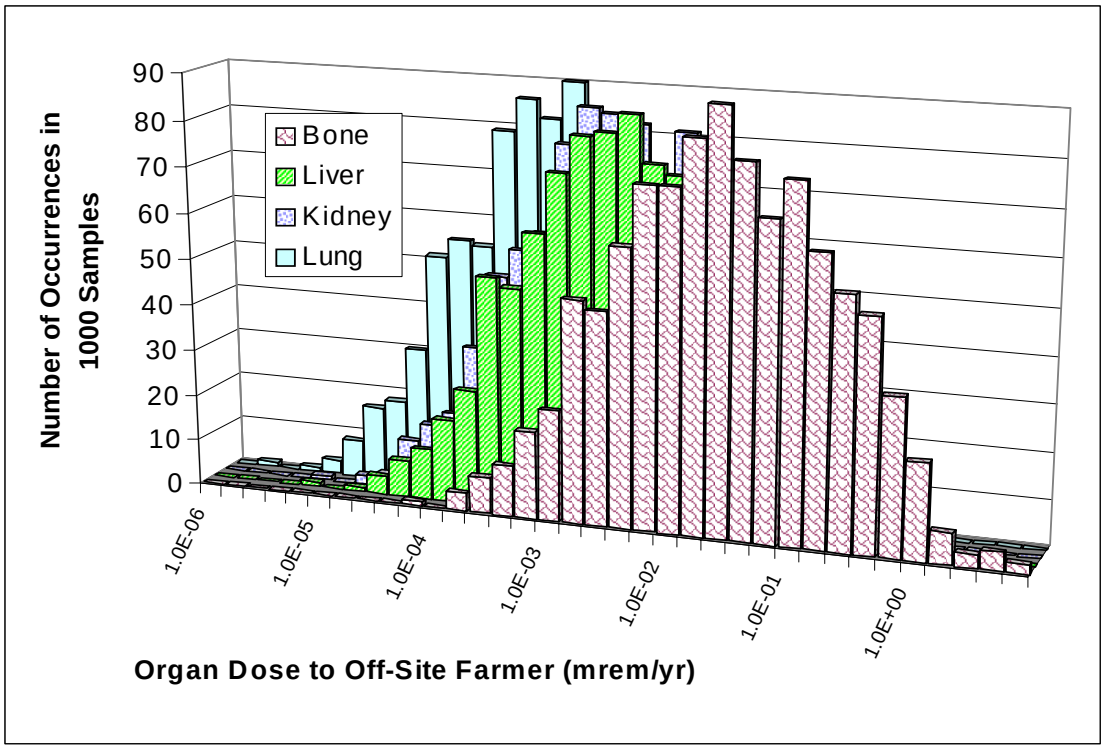

Figure 8-3. Histogram of Calculated Values of Dose to Critical Organs for the GCD TRU Waste IPR Analysis.

8.2.2 Individual Protection Requirements

Probability distributions for dose were calculated using two exposure conditions: an off-site resident farmer, and an on-site homebuilder. In both conditions, dose was estimated using 1000 samples of the uncertain transport and exposure parameters. For each parameter sample set, dose was calculated at the end of the 1000-year performance period. In the off-site farmer condition, all radionuclides crossing the land surface boundary during the 1000-year period were assumed to have collected in the garden soil. Figure 8-2 shows the resulting histogram of whole-body dose values, and Figure 8-3 shows the histogram of doses to those organs receiving relatively large doses. The average whole-body dose was 4.7×10^{-3} mrem and the average dose to bones, which typically received the largest dose of any organ, was 0.12 mrem. The median values were 8.8×10^{-4} mrem for the whole-body dose and 2.0×10^{-2} mrem for dose to bones. The radionuclides ^{234}Pa, ^{241}Am, ^{240}Pu, and ^{239}Pu were the only radionuclides to contribute more than 10% to total dose in one or more parameter sample sets.

The maximum calculated whole-body dose value was 0.16 mrem, and the largest calculated dose to any organ was 4.5 mrem.[9] All calculated dose values are far below the limits of 25 mrem for whole-body dose and 75 mrem for critical organ dose imposed by the IPR.

In the on-site homebuilder condition, all radionuclides crossing the land surface boundary during the 1000-year period were assumed to be retained in the soil over the virtual borehole. The homebuilder is exposed to this soil while constructing and occupying the residence, and is also exposed to radon from the waste and backfill that accumulates in the basement. In the on-site homebuilder condition, radionuclides accumulate in the soil profile due to upward advection during the 1000-year performance period. The homebuilder is exposed to soil 3 to 4 m (10 to 13 ft) below the ground surface while constructing and occupying the residence, and is also exposed to radon from the waste and backfill that accumulates in the basement. The probability distribution of dose was calculated using 1000 samples of the uncertain transport and exposure parameters. Whole-body dose under this condition was practically zero: the maximum calculated value was 7×10^{-10} mrem. Figure 8-4 shows the histogram of doses to the lung, which was the only organ receiving significant doses under this condition. The lung doses were entirely due to Rn-222 exposure. No other radionuclide contributed as much as 0.001% in any parameter sample set.

The calculated average and median values of whole-body dose under this condition are 9.0×10^{-13} and 8.7×10^{-19} mrem, respectively, and the corresponding statistics for the calculated lung doses are 2.0×10^{-3} and 1.6×10^{-3} mrem. The maximum calculated lung dose was 1.2×10^{-2} mrem. These quantities are substantially below their respective regulatory limits of 25 mrem and 75 mrem.

[9]Concentrations in garden soil for the vector producing the largest whole-body dose are given in Appendix P.

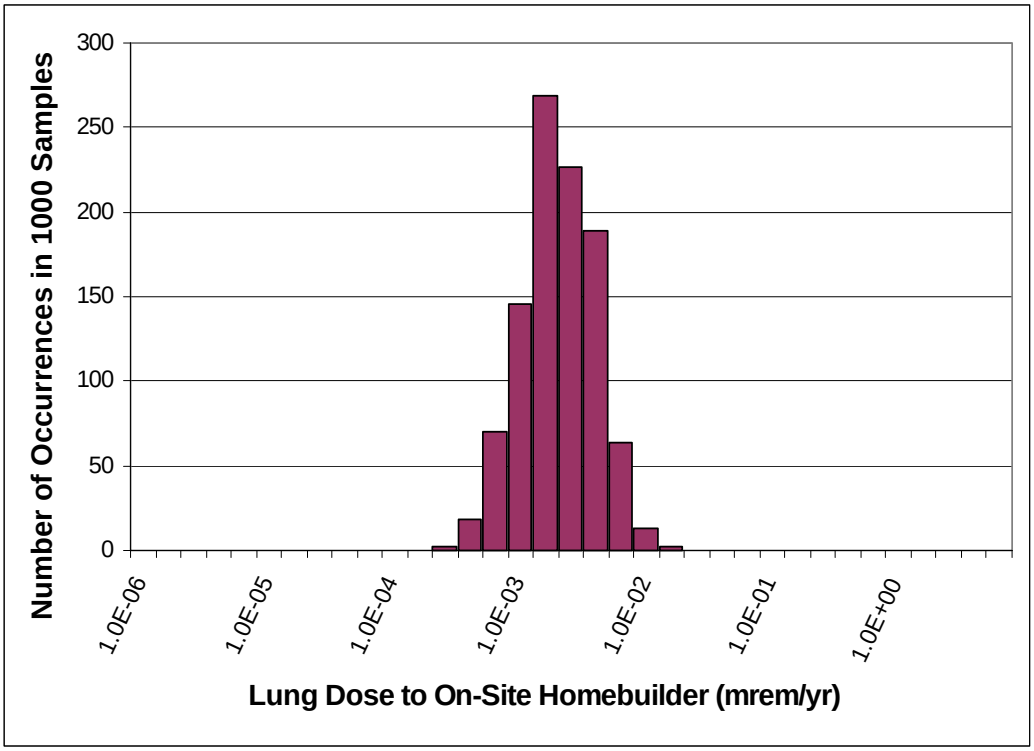

Figure 8-4. Histogram of Calculated Values of Dose to Lungs for the GCD TRU Waste IPR Analysis.

8.2.3 Groundwater Protection Requirements

Because the groundwater beneath the GCD boreholes is not a "special source of ground water," as defined in 40 CFR 191, there is no regulatory requirement to demonstrate protection of groundwater resources in this PA.

8.2.4 Sensitivity Analysis

In the PA methodology described in Section 3.0, sensitivity and data worth analyses are performed only if one or more calculated performance measures are above their regulatory limits. The goal of these analyses is to discover whether and how the calculated performance measure values can be defensibly brought within regulatory limits by, for example, collecting information to reduce parameter uncertainty or disqualifying certain conceptual models, or by modifying certain features of the disposal system. Sensitivity and data worth analyses are used to discover whether it is both possible and practical to demonstrate compliance at a site, given that existing information is inadequate to support such a demonstration.

In the current case, a defensible interpretation of existing information indicates compliance with all quantitative requirements.

In this case, sensitivity and data worth analyses are unnecessary because additional information has no regulatory value. A sensitivity analysis was performed nonetheless (see Appendix P) only

to shed light on the model results. The results of this analysis should not, however, be given the conventional interpretation of providing insight into the behavior of the disposal system. Instead, sensitivity analysis identifies those aspects of the mathematical model that control its output given the parameter values and distributions used in the assessment. Modeled releases from the system were typically dominated by invertebrate burrowing that can occasionally extend below the top of the waste, resulting in direct transport from the waste region to the land surface. Uncertainty about the system performance is accordingly controlled by uncertainty in the model of this process. As emphasized in Section 3.0, the mathematical model is designed to defensibly evaluate compliance and not to mimic the behavior of the disposal system. It is therefore inappropriate to draw extra-regulatory inferences about disposal system behavior from incidental properties of the model.

8.3 Additional Analyses Conducted to Address Review Team Concerns

Four additional analyses were conducted to address concerns expressed by the Federal Review Team following their review of the PA. These analyses examined 1) the effects on the CCDF of including drill cuttings, 2) the effects on the CCDF of extending the simulation time from 10,000 years to 20,000 years, 3) the effects on the CCDF of including extreme values of upward advection, and 4) the effects on estimated doses of including radionuclides in non-TRU waste packages disposed of in boreholes 2 and 4. In all four cases, the transport model and the values and distributions for all input parameters were the same as those used in the previous calculations (Section 8.2.1), except as noted. Additionally, the revised calculations were completed under the GCD quality assurance requirements. These four analyses are discussed below.

8.3.1 Analysis of Inclusion of Drill Cuttings in CCDF

A PA simulation was conducted that included release to the ground surface of TRU waste in drill cuttings resulting from inadvertent drilling of a water well through buried GCD waste. The simulation was conducted at the request of the Federal Review Team who argued that the CCDF could not be judged to satisfy the limits specified in the CRs without inclusion of a drilling scenario.

For the simulation, it is assumed that all active and passive markers have failed, that site knowledge is lost, the top of the GCD boreholes looks exactly like the surrounding landscape, and a water well is randomly drilled through the GCD waste. It is also assumed that the intruder drills through the virtual borehole (see Section 5.9.3.5). Three pieces of information are needed for the simulation: the probability of the water well striking the GCD wastes, the diameter of the drill hole, and the timing of the inadvertent intrusion.

DOE/NV commissioned an expert elicitation study to assess the probability of inadvertent intrusion into the Area 5 RWMS for the Area 5 PA. Section 6.7.3 provides a summary of the elicitation and the elicitation results. Based on the elicitation, the median number of random water wells drilled in Frenchman Flat is about 16 random water wells per km^2 in 10,000 years. This well density results in a median probability of 6×10^{-4} of randomly intersecting TRU waste in the GCD boreholes in 10,000 years (see discussion in Section 6.7.4.2).

The drill hole diameter of the water well is assumed to be 30 cm (1 ft) consistent with the Area 5 PA (Shott et al., 1998; the same diameter used in the acute drilling scenario; page 3-88) and consistent with an expected drill-hole diameter for 235-m depth homesteader water well. The surface area of a 30 cm-diameter drill hole is about 0.07 m^2, which is about two one-thousandths of the surface area of all four boreholes. Accordingly, it is assumed that drilling the water well results in approximately two one-thousandths of the waste being removed in the drill cuttings.

The inadvertent human intrusion is assumed to occur in the year 2170, which is the first year after cessation of active institutional control. The timing of the intrusion is conservative for two reasons. First, the inventory is largest at the onset of the simulation. Second, the GCD boreholes must look like the surrounding alluvial surface for the intrusion to be inadvertent. This is not expected to occur for thousands of years.

The EPA sum from just the release in the drill cuttings is 20. Note that this calculation is deterministic; hence, the EPA Sum is a single value. However, the release of wastes in the drill cuttings does not alter the releases assumed to occur as a result of natural processes. Therefore, the base case releases from the natural processes must be added to the release from the drill cuttings. To do this, each of the 5,000 EPA sums associated with releases from natural processes is added to the EPA sum for releases in the drill cuttings. For simplicity, the same 5,000 EPA sums for the undisturbed "natural processes" system (section 8.2.1) were used.

Figure 8-5 shows the resulting CCDF of the normalized integrated releases. This CCDF plots 10,000 EPA Sums: the 5,000 EPA Sums shown in Figure 8-1 and the 5,000 EPA Sums generated as described above.

The release of TRU radionuclides from the drilling event is a low probability, high consequence event (removing two one-thousands of the inventory is a high-consequence event under the CRs in 40 CFR 191). The high consequences are a result of the thickness of the waste zone relative to the lateral extent of the waste zone (high aspect ratio). A 30-cm drill hole moves a cylinder of waste with dimensions of 30-cm diameter and 16-m height into the accessible environment. Because of the small width of the virtual borehole, a large relative fraction of the waste is removed by a single drilling event. However, while the consequences are high, the intrusion probability is low because of the small cross-sectional area of the virtual borehole. In contrast, if the GCD boreholes were placed on their sides, the probability of intrusion would increase and the EPA sum would decrease.

From the perspective of the release sensitivity, the drill cuttings releases *do not* result in a violation of the CRs as long as the probability of an intrusion event is less than 1 in 1,000 (assuming the existing configuration of the GCD boreholes).

8.3.2 Analysis of Extending Simulation Time from 10,000 to 20,000 Years

The law (40 CFR 191) sets the time frame of compliance at 10,000 years for the CRs. The Federal Review Team requested additional information to examine the robustness of the modeled disposal system. To provide this additional information, the simulation time was increased from

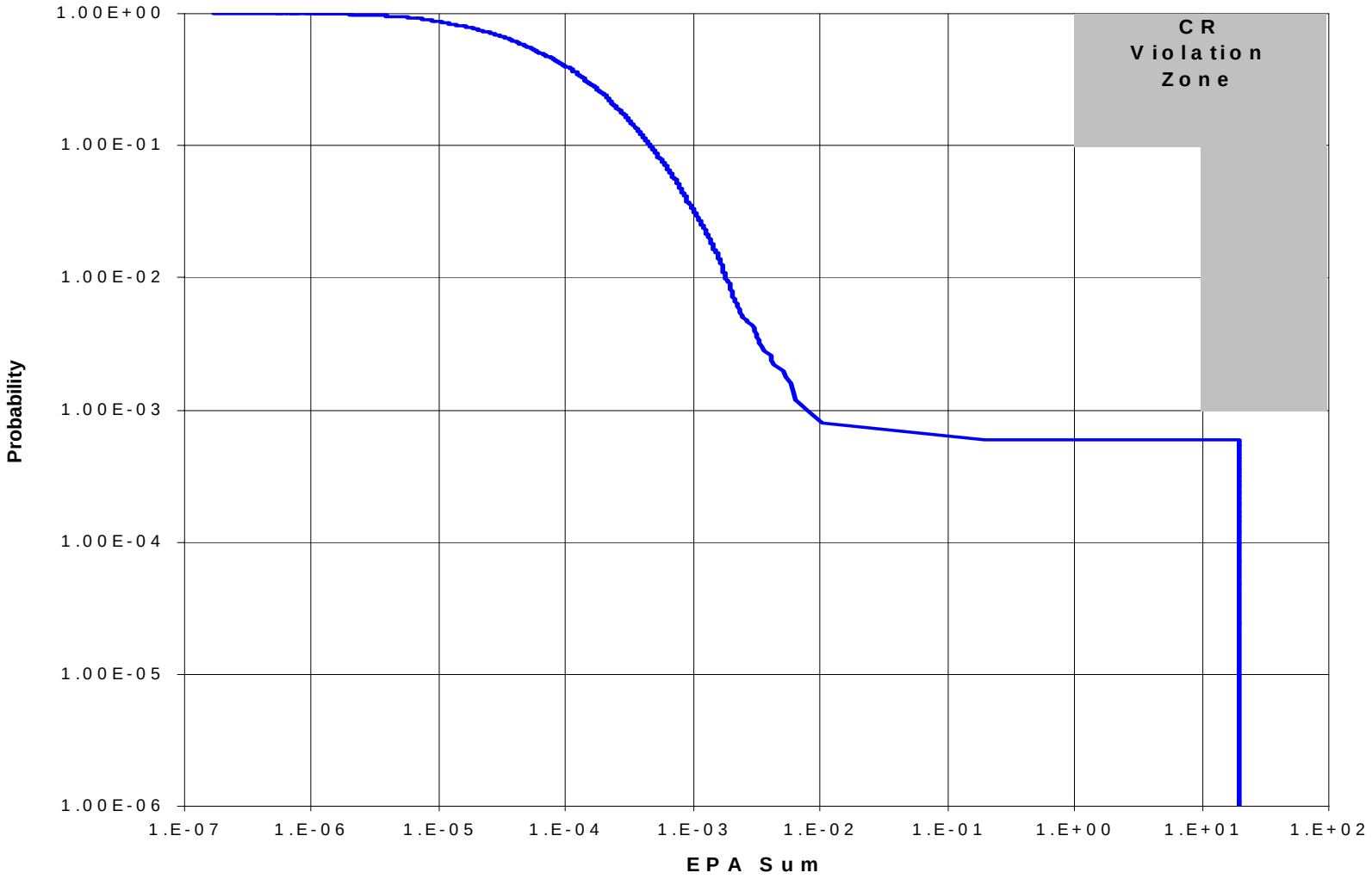

Figure 8-5. Revised CCDF for the PA analysis of the TRU wastes in the GCD boreholes. Compare with Figure 8-1, which does not include releases from a drilling event.

10,000 years to 20,000 years. This analysis is discussed below. The transport model and the distributions of input parameter values were the same as those used in the compliance calculations except 1) two hundred timesteps were used in the new calculations so that the timestep size of 100 years is the same in both simulations, and 2) the onset of cooler and wetter conditions occurs at 150 years, and not at 200, as in the compliance calculation. Figure 8-6 shows the resulting CCDF of normalized integrated releases.

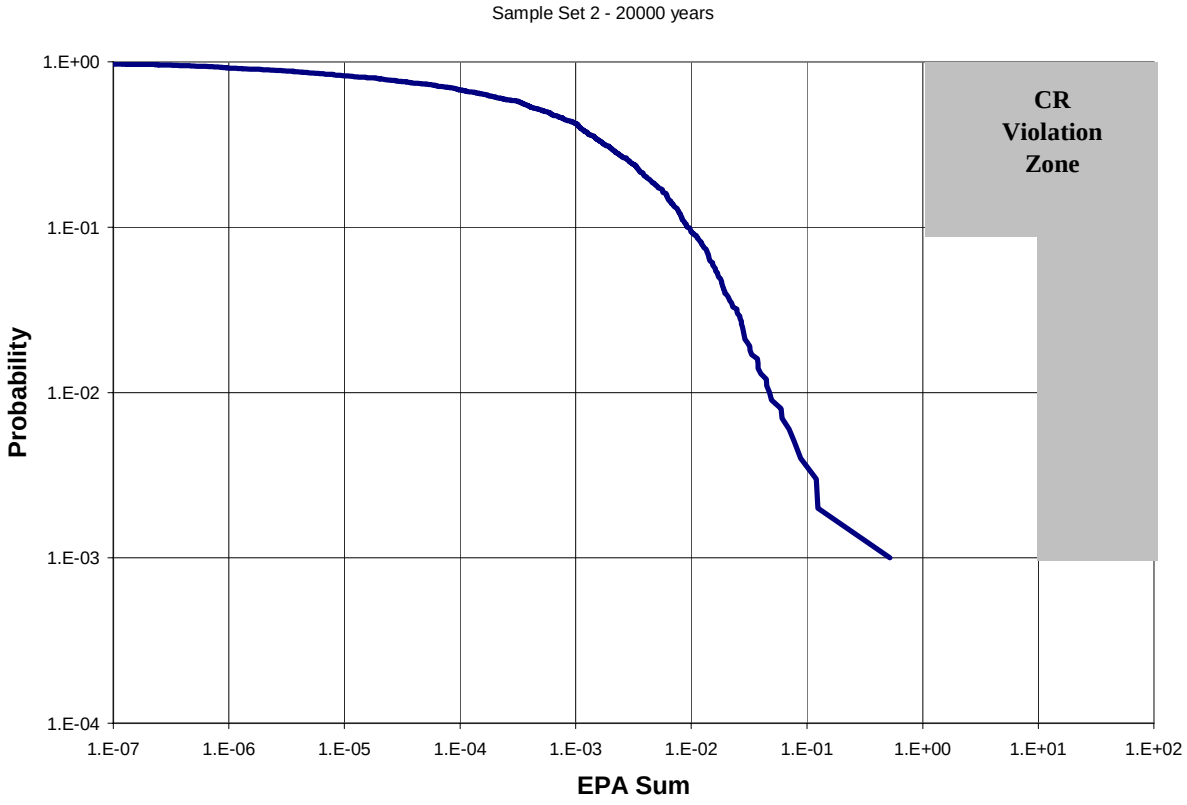

Figure 8-6 CCDF for Comparison and Information - Time Frame of Simulation Increased to 20,000 Years.

Doubling the simulation time allows more time for upward advection to move radionuclides towards the land surface, where the waste is more likely to be removed into the accessible environment by plant uptake and bioturbation. This simulation demonstrates that the *rate* that radionuclides reach the accessible environment does not increase dramatically after 10,000 years.

8.3.3 Analysis of Extreme Values of Upward Advection

At the request of the Federal Review Team, for comparison and information, a simulation was conducted using extreme rates of upward advection. The transport model and the distributions of input parameter values were the same as those used in the compliance calculations except 1) the distribution of the upward advection rates (q_l) was increased by two orders of magnitude and 2) the

onset of cooler and wetter conditions was assumed to occur at 150 years, not at 200, as in the compliance calculation.

Such high advection rates are physically impossible for a number of reasons, including 1) the fact that this rate would rapidly remove all the pore water, and 2) at even lower soil moisture contents, the unsaturated hydraulic conductivities decrease dramatically, preventing the further liquid phase movement of water. The thickness of the vadose zone is 236 m and the average volumetric moisture content is about 7%, therefore, the total amount of water in the vadose zone beneath a one square meter area is 16 cubic meters (236 m x 0.07). Increasing the rate of upward specific discharge by a factor of 100 means that there is a good probability of upward specific discharge rates around 10 mm / year; at such a rate, all of the pore water would exit to the land surface in 1,600 years, which is not physically possible.

Figure 8-7 shows the resulting CCDF of normalized integrated releases. Using an upward advection rate increased by two orders of magnitude significantly reduces the advective travel time from the waste region to the land surface for uranium isotopes, so that the travel time is much less than the simulation period for many of the sampled parameter values. For several simulations, the combination of small travel time and high solubility results in near-complete depletion of the original inventory of uranium isotopes (i.e., kilograms of uranium would be moved to the land surface). This simulation demonstrates that an absurd increase in the rate of upward advection would results in wholesale violation of the CRs.

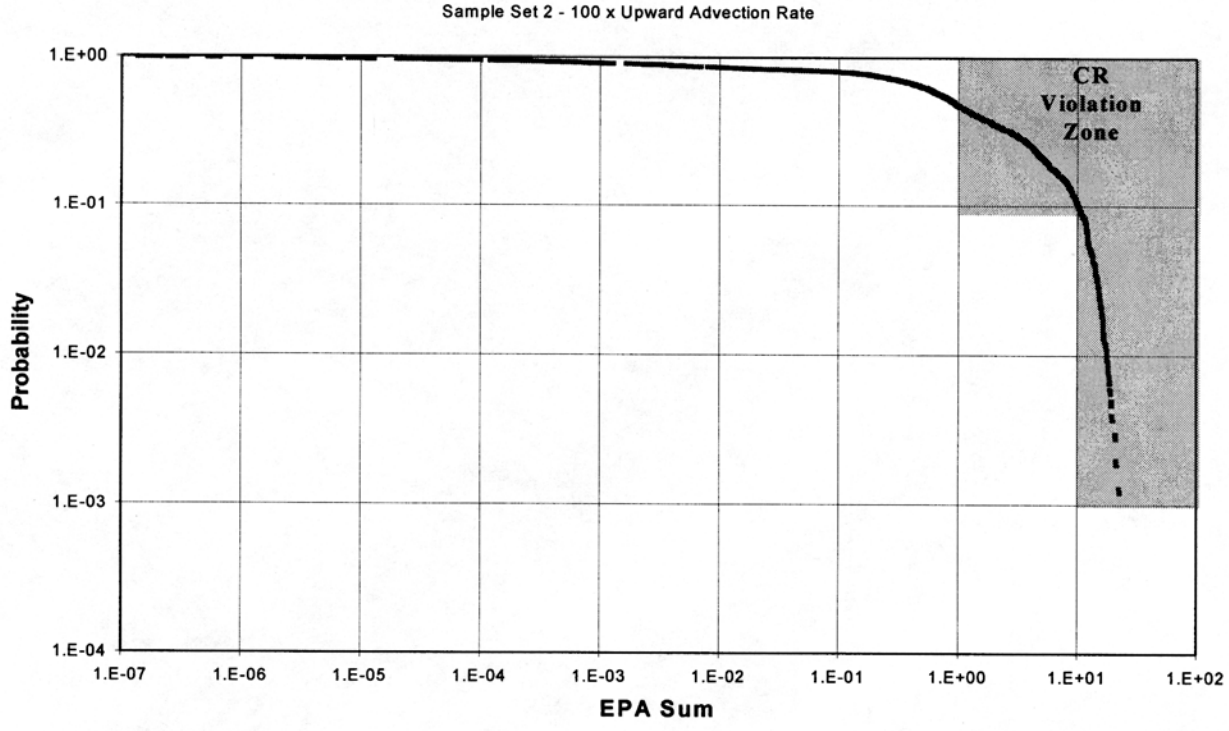

Figure 8-7 CCDF for Comparison and Information - Two Order of Magnitude Increase in Rates of Upward Advection.

8.3.4 Estimation of Dose Including Radionuclides from Non-TRU Waste Packages

While GCD boreholes 1, 2, 3, and 4 contain primarily TRU waste, they also contain some non-TRU waste. This non-TRU waste is LLW and its inventory is given in Table 8-1. This non-TRU waste was not included in the PA because the 1985 version of 40 CFR 191 does not require the inclusion of such waste. However, the Federal Review Team requested that this non-TRU waste be included in the dose calculations that were performed for the IPRs of 40 CFR 191. Therefore, for comparison and information, this section presents the dose calculated when non-TRU waste that is co-located in GCD boreholes 1-4 with TRU waste is included in the initial inventory for the IPR compliance assessment.

Table 8-1. Non-TRU waste in GCD Boreholes 1-4 not in the PA

Borehole	^{235}U(grams)	^{137}Cs(grams)	^{238}U(grams)	^{232}Th(grams)	^{3}H (grams)
2	-	11.51	-	-	-
4	252	-	1.28×10^{6}	1.85×10^{5}	0.0013

It was determined that it was not necessary to model the dose resulting from the ^{137}Cs and ^{3}H present in boreholes 2 and 4, respectively, because of their small quantities and relatively short half-lives. As discussed in Volume 4 of the CAD, it is assumed that institutional controls remain effective until 2170; accordingly, it is assumed that a "member of the public," the recipient of the dose calculated for the IPRs, will not be present at the site until 2170. In 2170, approximately 0.2 grams (about 1.5 Ci) of ^{137}Cs will remain and approximately 5×10^{-8} grams (about 5×10^{-4} Ci) of ^{3}H will remain. These quantities are insignificant compared to the quantities of other longer-lived wastes present in the boreholes. Hence, doses resulting from exposure to ^{137}Cs and ^{3}H were not modeled.

To model the ^{235}U, ^{238}U, and ^{232}Th present in the non-TRU waste, the initial inventories of ^{235}U and ^{238}U (shown in Table 5-15) were increased by 252 grams (1.07 moles) and 1.28×10^{6} grams (5380 moles), respectively. The initial inventory of ^{232}Th was set to 1.85×10^{5} grams (797 moles) in TUC and the code was modified so that ^{232}Th would be included in the initial inventory.

The results of the dose calculations with the non-TRU waste in the initial inventory are summarized in Table 8-2 for the Off-Site Farmer exposure condition and in Table 8-3 for the On-Site Homebuilder exposure condition. The numbers in Table 8-2 indicate a slight increase in whole body dose to the farmer when the co-located non-TRU waste is included in the initial inventory. The increase in bone dose (the organ typically receiving the greatest dose) is almost imperceptible. The results in Table 8-3 show that the maximum whole-body dose increases significantly, with a commensurate increase in average whole-body dose, while the median whole-body dose increases only slightly. The dose to the lung is almost unchanged. Note that all doses are still well below the limits of 25 mrem whole-body dose and 75 mrem organ dose established by the IPRs.

Table 8-2. Comparison of Doses Calculated for IPRs With Only TRU Waste and With Addition of non-TRU Waste, Off-Site Farmer Exposure Condition

Organ	Doses with only TRU waste (mrem)	Doses with non-TRU waste (mrem)
Whole Body	Maximum: 0.16 Mean: 4.7×10^{-3} Median: 8.8×10^{-4}	Maximum:0.31 Mean: 6.2×10^{-3} Median: 1.3×10^{-3}
Bone	Maximum: 4.5 Mean: 0.12 Median: 2.0×10^{-2}	Maximum: 7.3 Mean: 0.12 Median: 2.2×10^{-2}

Table 8-3. Comparison of Doses Calculated for IPRs With Only TRU Waste and With Addition of non-TRU Waste, On-Site Homebuilder Exposure Condition

Organ	Doses with only TRU waste (mrem)	Doses with non-TRU waste (mrem)
Whole Body	Maximum: 7×10^{-10} Mean: 9×10^{-13} Median: 8.7×10^{-19}	Maximum: 6.7×10^{-7} Mean: 6.7×10^{-10} Median: 1.2×10^{-18}
Lung	Maximum: 1.2×10^{-2} Mean: 2.0×10^{-3} Median: 1.6×10^{-3}	Maximum: 1.3×10^{-2} Mean: 2.0×10^{-3} Median: 1.6×10^{-3}

8.4 Conclusions

Given the assumptions used to develop the transport and exposure models, and the probability distributions describing our current uncertainty about the parameter values for these models, the calculated performance measure values for the CR and the IPR are less than their regulatory limits. These calculations were based on specific conditions and conceptual models. The PA methodology followed here provides confidence that analyses of alternative conditions and conceptual models would lead to reduced estimates of release. In fact, the PA has been constructed so that inclusion of these additional scenarios and models would lead to lower doses and releases.

9.0 SUMMARY AND CONCLUSIONS

Intermediate depth disposal operations were conducted by the DOE from 1984 through 1989. As a part of those operations, 60,000 kg (132,000 lb) of classified TRU waste packages were disposed in four GCD boreholes. This study presents the results of a PA undertaken by SNL to help DOE determine whether these TRU wastes meet the EPA's 1985, 40 CFR 191 requirements for disposal of TRU wastes.

40 CFR 191 includes four sets of requirements. The CRs set probabilistic limits for the cumulative releases to the accessible environment for the next 10,000 years. Dose limits to protect individuals are set by the IPRs. This PA was tailored to these two EPA requirements. Because there is no "special source of groundwater" beneath the GCD boreholes, the EPA's GWPRs do not apply. Demonstrating compliance with the Assurance Requirements of 40 CFR 191 is addressed in Volume 4 of the CAD.

The results of a PA cannot be verified in the usual sense of the word; therefore, this PA utilized a methodology which provides confidence in the PA analysis and results. Fundamental to this methodology is the philosophy that this PA is not a prediction of how the GCD system will actually perform. Rather, this PA provides simulations of a range of plausible outcomes, which are developed in a manner to provide confidence that the results of the analysis do not overestimate the ability of the GCD boreholes to protect human health.

The GCD wastes are emplaced a minimum of 21 m (70 ft) below the land surface at the Area 5 RWMS. The desert southwest, and the Area 5 RWMS, have been studied intensively for over 15 years. These studies have revealed that:

- this is one of the most arid portions of the U.S.,
- the average annual precipitation is 13 cm (5 in.),
- the water table is at least 200 m (665 ft) below the GCD wastes,
- the GCD wastes are within a thick sequence of arid alluvium,
- the arid alluvium is hydrologically homogeneous and isotropic,
- under current and undisturbed conditions, the pore water in the alluvium in the vicinity of the GCD boreholes moves very slowly upwards, toward the surface,
- there is no groundwater recharge,
- mammal and invertebrate burrowing can move soil from the subsurface to the surface, and
- desert plants can capture moisture and heavy metals, carrying them to the surface

Although the area is very stable geologically, certain changes are expected to occur over the next 10,000 years. The forcing agents for the changes are:

- future human activities that could inadvertently alter site conditions;
- activities associated with operation and closure of the Area 5 RWMS that have "disturbed" the site conditions; and
- natural processes, which operate on long time scales, that may alter site conditions.

Over the next few thousand years, control and knowledge of the buried wastes could be lost and future human activities could inadvertently disturb the wastes. Fortunately, the GCD wastes are buried beyond the depths of most human activities (e.g., construction of a home with a basement and buried utilities). Drilling an exploratory borehole or a water well through a GCD borehole is the only inadvertent human activity that could disturb the GCD wastes. This PA utilizes the EPA's Appendix B Guidance for addressing the nature of inadvertent human activities. The EPA's Guidance requires the PA to determine if the favorable characteristics of the entire disposal system will be invalidated by inadvertent "puncturing" by well drilling. Such inadvertent puncturing of a GCD borehole does not alter the characteristics of the remainder of the GCD disposal system.

Operation and closure of the Area 5 RWMS will result in future landfill subsidence. This subsidence has the potential to focus precipitation and runoff, which may result in the downward movement of pore water and the formation of ephemeral wetlands. Additionally, numerous studies have shown that, over long time scales, the climate cycles between the current, warmer and drier conditions, and cooler and wetter glacial conditions. At the Area 5 RWMS, past glacial conditions included a doubling of precipitation (to 26 cm/yr [10 in./yr]) and temperatures three to five degrees Celsius cooler. Glacial conditions may result in downward movement of pore water and the return of open piñon-juniper woodlands.

A detailed screening analysis was conducted as part of this PA to determine the effects of subsidence and the eventual return to a glacial climate. The result of the screening analysis was that subsidence and climate change will result in the downward movement of pore water and development of ephemeral wetlands and/or piñon-juniper woodlands. Both subsidence and climate change are expected to move moisture (and radionuclides) away from the land surface and deeper into the vadose zone (with a decrease in releases to the accessible environment). Importantly, surface water will not infiltrate to the water table in 10,000 years, even assuming that subsidence and a glacial climate begin 170 years from now.

Based on the PA methodology, this PA models a continuation of current conditions (with upward advection of the pore water), coupled with deeper-rooted, glacial-climate plant species, which overestimates the releases, relative to expected conditions.

The simplicity of the conceptual models allowed them to be implemented in Microsoft® Visual Basic™ macros in an Access™ database. This PA model is built from a mathematical expression for mass conservation that includes the operation of a number of transport processes, including dissolution, precipitation, reversible chemical sorption onto soil, advection, diffusion, dispersion, radioactive decay and ingrowth, plant uptake, and bioturbation. The first set of macros calculates the movement and cumulative releases of 19 different radionuclides over a 10,000-year regulatory period, producing a CCDF that was used to assess compliance with the CRs of 40 CFR 191. The second set of macros calculates the movement and cumulative releases of 19 different radionuclides over a 1000-year regulatory period and then approximates the dose to an individual resulting from exposure to these 19 radionuclides and their progeny, producing an estimate of doses that is used to assess compliance with the IPRs. The same release and transport model is used in both sets of macros. Figure 1-12 summarizes the conceptual and mathematical models used to implement this PA.

The primary conclusions of this PA are that the disposal of TRU waste in the GCD boreholes will at most result in minuscule doses to individuals, and that the GCD disposal system easily meets the EPA's 1985 requirements for disposal of TRU waste. Further, there is a strong, reasonable expectation that actual system performance will be better than what is simulated in this PA.

The arid climate, intermediate depth burial, deep water table, and hydrologically homogeneous and isotropic alluvium make GCD an ideal system for isolating radioactive wastes from the biosphere.

This page intentionally left blank.

10.0 REFERENCES

Al-Khafaji, A. W. and J. R. Tooley. 1986. *Numerical Methods in Engineering Practice*, Holt, Rinehart and Winston, New York, New York.

Alletzhauser, G.J. 1998. "Quality Assurance Management Plan for the Greater Confinement Disposal Compliance Assessment Program," Revision 5, Sandia National Laboratories, New Mexico, April 1998.

Andersen, D. C. 1987. *Geomys bursarius* burrowing patterns: influence of season and food patch structure. Ecology 68(5):1306-1318.

Andersen, D. C. 1988. "Tunnel-construction methods and foraging path of a fossorial herbivore, *Geomys bursaruis*." *Journal of Mammalogy* 69:565-582.

Andersen, D. C. 1990. "Search path of a fossorial herbivore, *Geomys bursarius*, foraging in structurally complex plant communities." *Journal of Mammalogy* 71:177-187.

Anstey, R.L., *Physical Characteristics of Alluvial Fans*, U.S. Army Natick Laboratories, Technical Report ES-20, Natick, Mass., 1965.

Arkhipov, N. P., Ye. A. Fedorov, R. M. Aleksakhin, P. F. Bondar´, T. L. Kozhevnikova, and V.V. Suslova. 1975. "Soil chemistry and root accumulation of artificial radionuclides in the crop harvest." *Soil Science* 11:690-711.

Arnold, W.W. 1996. "Estimating Subsidence for GCD PA (memo/96/S34)." Sandia National Laboratories, Memo from W.W. Arnold to T. Brown, May 29. 1996.

Arthur, W. J., III, and O. D. Markham. 1983. "Small mammal soil burrowing as a radionuclide transport vector at a radioactive waste disposal area in southeastern Idaho." *Journal of Environmental Quality* 12(1):122-117.

ASME NQA-1, ASME. 1989. "Quality Assurance Requirements for Nuclear Facilities," The American Society of Mechanical Engineers. 1989 Edition.

ASTM-D-2488-90. 1990. Standard Recommended Practice for the Description of Soils–Visual Manual Procedure, American Society for Testing Materials, Philadelphia, PA.

Baes, C. F. III, R. D. Sharp, A.L. Sjoreen, and R. W. Short. 1984. *A Review and Analysis of Parameters for Assessing Transport of Environmentally Released Radionuclides Through Agriculture*, ORNL-5786, Oak Ridge National Laboratory, Oak Ridge, TN

Bandoli, J. H. 1981. "Factors influencing seasonal burrowing activity in the pocket gopher, *Thomomys bottae*." *Journal of Mammalogy* 62(2):293-303.

Barnes and Allison. 1983. "The distribution of Deuterium and ^{18}O in Dry Soils 1. Theory." *J. Hydrology,* v. 60, pp. 141-156.

Barnes, F. J. and G. L. Cunningham. 1987. "Water relation and productivity in pinyon-juniper habitat types," in *Proceedings: Pinyon-Juniper Conference*, Reno, NV, January 13-16. 1986. USDA Forest Service Intermountain Research Station General Technical Report INT-215, p. 406-411.

Barney, M. A. and N. C. Frischknecht. 1974. "Vegetation changes following fire in the pinyon-juniper type of west central Utah." *Journal of Range Management* 17:91-96.

Battis, J. D. 1978. Geophysical Studies for Missile Basin: Seismic Risk Studies in the Western United States. TI-ALEX(02)-FSR-78-01. Texas Instruments Inc., Houston, Texas.

Bauman, R.S. 1989. Rockwell International, Rocky Flats Plant, Personal Communication.

Beatley, J. C. 1962. Vascular plants of the U.S. Atomic Energy Commission's Nevada Test Site, Nye County, Nevada. USAEC Report UCLA-12-508, 33 p.

Beatley, J. C. 1965a. Ecology of the Nevada Test Site. I. Geographic and ecologic distributions of the vascular flora (annotated check list). USAEC Report UCLA-12-553, 69 p.

Beatley, J. C. 1965b. Ecology of the Nevada Test Site. II. Status of introduced species. USAEC Report UCLA-12-554, 39 p.

Beatley, J. C. 1967. "Survival of winter annuals in the northern Mojave Desert." *Ecology* 48(5):745-750.

Beatley, J. C. 1969. Vascular plants of the Nevada Test Site, Nellis Air Force Range, and Ash Meadows (northern Mojave and southern Great Basin Deserts, south-central Nevada). USAEC Report UCLA-12-705, 122p.

Beatley, J. C. 1975. "Climates and vegetation pattern across the Mojave/Great Basin Desert transition of southern Nevada." *American Midland Naturalist* 93:53-70.

Beatley, J. C. 1976. Vascular plants of the Nevada Test Site and central-southern Nevada: ecologic and geographic distributions. TID-26881, NTIS, U.S. Department of Commerce, Springfield, VA 22161. 308 pp.

Beaty, C.B. 1963. *Origin of Alluvial Fans, White Mountains, California and Nevada,* Annals of the Association of American Geographers, Vol. 53, pp. 516-535. Blakemor.

Bechtel Nevada. 1997. Performance Assessment/Composite Analysis for the Area 3 Radioactive Waste Management Site at the Nevada Test Site, Nye County, Nevada (Rev. 2.0). Prepared for U.S. Department of Energy, Nevada Operations Office under Contract Number DE-AC08-96NV11718.

Bechtel Nevada. 1998a. Performance Assessment for the Area 5 Radioactive Waste management Site at the Nevada Test Site, Nye County, Nevada (Rev. 2.1). Prepared for U.S. Department of Energy, Nevada Operations Office under Contract Number DE-AC08-96NV11718. DOE/NV/11718-176 UC-721.

Bechtel Nevada. 1998b. Estimation of Upward Advective Water Flux at the Greater Confinement Disposal Facility. Work performed by Bechtel-Nevada under contract no. DE-AC08-96NV11718, submitted to the Nevada Operations Office, U.S. Department of Energy, Las Vegas, Nevada.

Bechtel Nevada. August 16, 2001. Memorandum from R. G. Lahoud, Bechtel, Nevada to Angela Colarusso, NNSA/NVO with attached reports:(1) "Test Case 11, Benchmarking of the Unnamed Code (TUC) with the Area 5 Radioactive Waste Management Site Composite Analysis Model," and (2)"Validation and Verification Plan for TUC Version 2.0."

Belanger, R., D.H. Lester, L.D. Robertson, M.E. Spaeth, J.A. Stoddard, R.T. Stula, J.J. Cohen, C.F. Smith. 1981. *Limited Risk Assessment and Some Cost-Benefit Considerations for Greater Confinement Disposal as Compared to Shallow Land Burial*. SAI01381-369-LJ, Science Applications Inc., La Jolla, CA.

Bertram, S.G and R.V. Guzowski. 1995. Results of management discussion of a draft issue paper entitled *Issue Paper on the Treatment of Cuttings in PA Analyses*. Memo to L.E. Shepherd, WIPP Project, Sandia National Laboratories.

Beyeler, W. E., T. J. Brown, W. A. Hareland, S. Conrad, N. Olague, D. Brosseau, E. Kalinina, D. P. Gallegos, and P. A. Davis. 1998. "Review of Parameter Data for the NUREG/CR-5512 Residential Farmer Scenario and Probability Distributions for the DandD Parameter Analysis," Letter report to M. C. Daily, Office of Nuclear Regulatory Research, Radiation Protection and Health Effects Branch, NRC.

Beyeler, W. E., T. F. Ehrhorn, G. Alletzhauser, and L. L. Price. "Compliance Assessment Document for the TRU Wastes in the Greater Confinement Disposal Boreholes at the NTS, Volume 3: Modeling Details," Sandia National Laboratories, Albuquerque, NM, to be published.

Beyeler, W.E. 1999. E-mail transmittal of excel spreadsheet from Walt Beyeler to Steve Conrad on 7/14/99.

Beyeler, W. E., W. A. Hareland, F. A. Duran, T.J. Brown, E.Kalinina, D. P. Gallegos, and P.A. Davis. *Residual Radioactive Contamination from Decommissioning; Parameter Analysis; Draft for Comment*. NUREG/CR-5512, Volume 3, Sandia National Laboratories, Albuquerque, NM.

Bird, R.B., W.E. Stewart, and E.N. Lightfoot. 1960. *Transport Phenomena*, John Wiley and Sons, New York, NY.

Black, P.K., B. Moore, B. Crowe, M.M. Hooten, K.J. Black, S.E. Rawlinson, and L.E. Barker. 1997. *A Common-Sense Probabilistic Approach to Assessing Inadvertent Intrusion into Low-Level Radioactive Waste at the Nevada Test Site*, Proceedings of the Waste Management '97 Conference, Tuscon, AZ.

Black, P.K., K.J., Black, M.M. Hooten, L.P. Mathai, and M.D. Neptune. 1998. *Assessing the Probability of Inadvertent Human Intrusion at Nevada Test Site Radioactive Waste Management Sites*, U.S. Department of Energy, Nevada Operations Office, Draft Report (Yet to be published).

Blom, P. E. and J. B. Johnson. 1991. "Concentrations of ^{137}Cs and ^{60}Co in nests of the harvester ant, *Pogonomyrmex salinus*, and associated soils near nuclear reactor waste water disposal ponds." *American Midland Naturalist* 126:140-151.

Blout, D. O., W. S. Birchfiel, D. P. Hammermeister, and K. A. Zukosky. 1995. Site Characterization Data from the Area 5 Science Boreholes, Nevada Test Site, Nye County, Nevada. Report No. DOE/NV11432-170, U.S. Department of Energy, Nevada Operations Office, Las Vegas, Nevada.

Bocek, B. 1986. "Rodent ecology and burrowing behavior: predicted effects on archaeological site formation." *American Antiquity* 51(3):589-603.

Boland, E.J., and P.T. Dickman. 1986. "High-Specific-Activity Waste Handling for Greater Confinement Disposal," *Abstract for Waste Management '86*. Proceedings of the Symposium on Waste Management at Tucson, AZ.

Bonano, E. J., and R. M. Cranwell. 1988. "Treatment of Uncertainties in the Performance Assessment of Geologic High-Level Radioactive Waste Repositories," *Mathematical Geology*, vol. 20, pp. 543-565.

Bonano, E.J., and Wahi, K.K. 1990. Use of Performance Assessment in Assessing Compliance With the Containment Requirements in 40 CFR 191, NUREG/CR-5521, SAND90-0127, U.S. Nuclear Regulatory Commission, Washington, DC.

Bowers, C. C. And H. M. Smith. 1947. "Hibernation of lizards in western Texas." *Herpetologica* 4:80.

Breshears, D. D. 1993. Spatial partitioning of water use by herbaceous and woody life forms in semiarid woodlands. Dissertation. Colorado State University, Fort Collins, Colorado.

Brosseau, D.A. 1990. "Quality Assurance Requirements for the Greater Confinement Disposal Project," Letter Report prepared for Sandia National Laboratories, New Mexico, July 12, 1990.

Brosseau, D.A. 1993. "Revised Quality Assurance Requirements for the Greater Confinement Disposal Project," Letter Report prepared for Sandia National Laboratories, New Mexico, November 30, 1993.

Brosseau, D. A. Draft 2000. "Compliance Assessment Document for the TRU Wastes in the Greater Confinement Disposal Boreholes at the NTS, Volume 4: Application of Assurance Requirements," Sandia National Laboratories, Albuquerque, NM.

Brown, D.E. (ed.). 1982. "Biotic communities of the American Southwest-United States and Mexico." *Desert Plants* 4 (1-4).

Brown, T., S.H. Conrad, S. Wirth, J.R. Cochran, and J. Emery. 1997a. "Plausible Future Climate States at the Area 5 Radioactive Waste Management Site, Nevada Test Site," Letter Report transmitted J. Ginanni (DOE/NV/WMD), January 31, 1997, under Contract DE-AC04-76DP00789, Sandia National Laboratories, Albuquerque, NM.

Brown, T. J., W. Beyeler, J. Cochran, H. Stockman, L. Price, and S. Wirth. 1997b. Performance Assessment Analyses of Fernald IIe(2) Byproduct Material for Disposal in Deep Trenches at the Area 5 RWMS on the Nevada Test Site. Prepared for the U.S. Department of Energy/Las Vegas under Contract No. DE-AC04-94AL-8500.

Brown, T., R. Thomas, W. Fogleman. 1998. "Modeling Potential Effects of Subsidence at the Area 5 RWMS for the GCD Compliance Assessment Analyses," SNL.

Brush, L.H., "Revised Free-Solution Tracer Diffusion Coefficients (D sol S) for Dissolved Pu, Am, U, Th, Np, Cm, and Ra in Boreholes and the Culebra for Use in PA Calculations to Support the WIPP PA," unpublished memorandum to M.S. Tierney, May 11, 1996, Sandia National Laboratories, Albuquerque, NM.

Bryson, R.A., and W.P. Lowry. 1955. "The Synoptic Climatology of the Arizona Summer Precipitation Singularity." *Bull. Amer. Meteor. Soc.* 36:329-339.

Burmaster, D.E., and Anderson, P.D. 1994. "Principles of Good Practice for the Use of Monte Carlo Techniques in Human Health and Ecological Risk Assessments," *Risk Analysis*, vol. 14, no. 4, pp. 477-481.

Caffee, M., K.E. Snyder, and D.L. Gustafson. 1995. *Letter Report of Cosmogenic Exposure Dating of Geomophic Surfaces at Frenchman Flat, Southern Nevada*.

Caldwell, J.T. and J.M. Bieri. 1983. *Technical Study of the Proposed Greater Confinement Disposal for NWAR, Phases I and II*. LA-Q2TN-83-311, Los Alamos National Laboratory, NM.

Caldwell, M.M. and J.H. Richards. 1989. "Hydraulic lift: water efflux from upper roots improves effectiveness of water uptake by deep roots." *Oecologia* 79:1-5.

Cameron, G. N., S. R. Spencer, B. D. Eshelman, L. R. Williams, and M. J. Gregory. 1988. "Activity and burrow structure of Attwater's pocket gopher (*Geomys attwateri*)." *Journal of Mammalogy* 69(4):667-677.

Campbell, J.E., R.T. Dillon, M.S. Tierney, H.T. Davis, P.E. McGrath, F.J. Pearson, Jr., H.R. Shaw. J.C. Helton, and F.A. Donath. 1978. *Risk Methodology for Geologic Disposal of Radioactive Waste: Interim Report*, SAND78-0029 (NUREG/CR-0458), Sandia National Laboratories, Albuquerque, NM.

Campbell, K. W. 1980. Seismic Hazard Analysis for the NTS Spent Reactor Fuel Test Site. UCRL-15620. Lawrence Livermore National Laboratory, Livermore, California.

Canadell, J., R.B. Jackson, J.R. Ehleringer, H.A. Mooney, O.E. Sala, and E.-D. Schulze. 1996. "Maximum rooting depth of vegetation types at the global scale." *Oecologia* 108:583–595.

Card, D.H., P.H. Hunter, J.A. Adam, and R.B. White. 1981. *Criteria for Greater Confinement of Radioactive Wastes at Arid Western Sites*. NVO-234, U.S. Department of Energy, Las Vegas, NV.

Carr, W.J., Regional Structural Setting of Yucca Mountain, Southwestern Nevada, and Late Cenozoic Rates of Tectonic Activity in Part of the Southwestern Great Basin, Nevada and California, U.S. Geological Survey Open-File Report 84-854, 109 p. (1984)

Casti, J.L. 1990. *Searching for Certainty: What Scientists Can Know About the Future*, William Morrow and Company, Inc.

Chapman, Jenny B. 1994. *Classification of Groundwater at the Nevada Test Site*, Desert Research Institute Pub. #45069, DOE/NV/10384-28.

Chew, R. M. 1978. The impact of small mammals on ecosystem structure and function. In *Populations of Small Mammals Under Natural Conditions*, D. P. Snyder (ed.), Pymatuning Laboratory of Ecology Special Publication Series, vol. 5. University of Pittsburgh, Linesville, Pennsylvania, pp. 167-180.

Christensen, R.C. and N.E. Spahr. 1980. *Flood Potential of Topopah Wash and Tributaries, Eastern Part of Jackass Flats, Nevada Test Site, Southern Nevada*, Open File Report 80-963, U.S. Geological Survey, Lakewood, Colorado.

Chu, Margaret S. Y. and Emile Bernard. 1991. *Waste Inventory and Source Term Model for the Greater Confinement Disposal Site at the Nevada Test Site*, SAND91-0170, Sandia National Laboratories, Albuquerque, NM.

Clark, W. H., and C. J. Clark. 1989. "White-Tailed Prairie Dog (*Cynomys leucurus* Merriam) Diggings in Western Harvester Ant, *Pogonomyrmex occidentalis* (Cresson), Mounds." *Great Basin Naturalist* 49:36-37.

Cloudsley-Thompson, J. L. 1975. "Adaptations of Arthropods to Desert Environments." *Annual Review of Entomology* 20:261-283.

Cohen, J.J, C.F. Smith, F.J. Ciminesi, P.T. Dickman, and D.A. O'Neal. 1982. *Comparative Assessment of Disposal of TRU Waste in a Greater Confinement Disposal Facility*. DOE/NV/00410-68.

Conca, J. L., M. Apted, and R. Arthur. 1992. "Aqueous Diffusion in Repository and Backfill Environments, " *Scientific Basis for Nuclear Waste Management,* 16th Symposium, ed. C. G. Interrante and R. T. Pabalan, pp. 395–402.

Conca, J. L. and J. Wright. 1990. "Diffusion Coefficients in Gravel Under Unsaturated Conditions," *Water Resources Research,* Vol. 26, No. 5, pp. 1055–1066.

Conrad, S.H., and W. Strong. 1994. "An Estimate of Upward Advective Moisture Flux at the Greater Confinement Disposal Site." Letter report submitted to the Nevada Operations Office, U.S. Department of Energy, Las Vegas, Nevada.

Conrad, S.H., S.W. Tyler, and J.B. Chapman. 1993. "Inferring Paleo-Recharge Using Several Naturally-Occurring Tracers Taken from a Thick Alluvial Vadose Zone in the Nevada Test Site." *Eos*, Transactions of the American Geophysical Union, 74(43), pp. 296-297.

Conrad, S.H. 1993. Using Environmental Tracers to Estimate Recharge through an Arid Basin. Proceedings, Fourth Annual High-Level Radioactive Waste Management Conference, April 26-30, Las Vegas, Nevada, pp. 132-137.

Cook, P.G., W.M. Edmunds, and C.B. Gaye. 1992. "Estimating Paleorecharge and Paleoclimate from Unsaturated Zone Profiles." *Water Resources Research*, 28(10):2721-2731.

Cowels, R.B. 1941. "Observations on the Winter Activities of Desert Reptiles." *Ecology* 22:125-140.

Cox, G. W. and J. Hunt. 1992. "Relation of Seasonal Activity Patterns of Valley Pocket Gophers to Temperature, Rainfall, and Food Availability." *Journal of Mammalogy* 73:123-134.

Cranwell, R.M., J.E. Campbell, J.C. Helton, R.L. Iman, D.E. Longsine, N.R. Ortiz, G.E. Runkle, and M.J. Shortencarier. 1987. *Risk Methodology for Geologic Disposal of Radioactive Waste: Final Report,* SAND81-2573 (NUREG/CR-2452), Sandia National Laboratories, Albuquerque, NM (original version of this report published in 1982 under the same title and report numbers).

Cranwell, R.M., R.V. Guzowski, J.E. Campbell, and N.R. Ortiz. 1990. *Risk Methodology for Geologic Disposal of Radioactive Waste: Scenario Selection Procedure,* NUREG/CR-1667 (SAND80-1429), U.S. Nuclear Regulatory Commission, Washington DC (original version of this report published in 1982 under same title and report numbers).

Crist, T. O. 1998. "The Spatial Distribution of Termites in Shortgrass Steppe: a Geostatistical Approach." *Oecologia* 114:410-416.

Crowe, B. M. 1990. "Basaltic Volcanism Episodes of the Yucca Mountain Region. p. 65-73. In: High-Level Radioactive Waste Management." Proceedings of the international topic meeting sponsored by the American Society of Civil Engineers for the American Nuclear Society. Co-sponsored by the American Chemical Society . . . [et al.]. Hosted by the University of Nevada, Las Vegas, Nevada; American Nuclear Society, Inc., La Grange Par., Illinois; and American Society of Civil Engineers. New York. April 8-12. 1990.

Crowe, B. M., S. Self, D. Vaniman, R. Amos, and F. Perry, Aspects of Potential Magmatic Disruption of a High-Level Radioactive Waste Repository in Southern Nevada, Journal of Geology, v. 91, p. 259-276 (1983)

Crowe, B.M. Basaltic Volcanic Episodes of the Yucca Mountain Region, *Proceedings High-Level Radioactive Waste Management Conference, Las Vegas, Nevada* (American Nuclear Society, La Grange Park Illinois) p. 65-73 (1990).

Crowe, B.M., and F.V. Perry. 1989. "Volcanic Probability Calculations for the Yucca Mountain Site; Estimation of Volcanic Rates," in *Proceedings Nuclear Waste Isolation in the Unsaturated Zone, Focus '89* (American Nuclear Society, La Grange Park, IL.) p. 326-334.

Crowe, B.M., P. Wallmann, and L.M. Bowker. 1998. Probabilistic Modeling of Volcanism Data: Final Volcanism Hazard Studies for the Yucca Mountain Site, in Perry, F.V., B.M. Crowe, G.A. Valentine, and L.M. Bowker (eds). *Volcanism Studies: Final Report for the Yucca Mountain Project.* Los Alamos National Laboratory Report LA-13478 554 p.

D'Agnese, F.A., G.M. O'Brien, C.C. Faunt, and C.A. San Juan. 1999. "Simulated Effects of Climate Change on the Death Valley Regional Ground-Water Flow System, Nevada and California." U.S. Geological Survey, Water-Resources Investigations Report 98-4041.

Dahlman, R. C., E. A. Bondetti, and L. D. Eyman. 1976. Biological pathways and chemical behavior of plutonium and other actinides in the environment, in A. M. Friedman (ed.), *Actinides in the Environment*, ACS Symposium Series, American Chemical Society, Washington, DC., pp. 47-80.

Dansgaard, W.S., J. Johnsen, H.B. Clausen, D. Dahl-Jensen, N.S. Gundestrup, C.U. Hammer, C.S. Hvldberg, J.P. Steffensen, A.E. Sveinbjornsdottir, J. Jouzel, and G. Bond. 1993. "Evidence for general instability of past climate from a 250-kyr ice-core record," Nature, v. 364 p. 218-220.

Daveler, S.A., and T.J. Wolery. 1992. *EQPT, A Data File Preprocessor for the EQ3/6 Software Package: User's Guide and Related Documentation (Version 7.0).* UCRL-MA-110662 PT II. Livermore, CA: Lawrence Livermore National Laboratory.

Davis, J.M. 1992. Greater Confinement Disposal Heterogeneity Study, Nevada Test Site, Area 5, Radioactive Waste Management Site. DOE/NV/10630-26, UC-721, 57p.

Davis, P. A., E. J. Bonano, K. K. Wahi, and L. L. Price. 1990. Uncertainties Associated with Performance Assessment of High-Level Radioactive Waste Repositories: A Summary Report, SAND88-2703, NUREG/CR-5211, Sandia National Laboratories, Albuquerque, NM.

Davis, P.A., L.L. Price, K.K. Wahi, M.T. Goodrich, D.P. Gallegos, E.J. Bonano, and R.V. Guzowski. 1990. *Components of an Overall Performance Assessment Methodology*, NUREG/CR-5256 (SAND88-3020), U.S. Nuclear Regulatory Commission, Washington, DC.

Davis, W. B., R. R. Ramsey, and J. M. Arendale, Jr. 1938. "Distribution of pocket gophers (*Geomys breviceps*) in relation to soils." *Journal of Mammalogy* 19:412-418.

Dawdy, D.R. 1979. "Flood Frequency Estimates on Alluvial Fans." *Journal of the Hydraulics Division,* Proceedings of the American Society of Civil Engineers, Vol. 105, No. HY11.

DeLucia, E. H. and W. H. Schlesinger. 1991. "Resource-use efficiency and drought tolerance in adjacent Great Basin and Sierran plants." *Ecology* 72 (1):51-58.

Desmond, M. J. and J. A. Savidge. 1996. "Factors influencing burrowing owl (*Speotyto cunicularia*) nest densities and numbers in western Nebraska." *American Midland Naturalist* 136:143-148.

Dewispelare, A.R., L. T. Herren, M. P. Mikalas, and R.T. Clemen. 1993. "Expert Elicitation of Future Climate in the Yucca Mountain Vicinity: Iterative Performance Assessment Phase 2.5," Center for Nuclear Waste Regulatory Analyses, San Antonio TX, Report CNWRA 93-016.

Dickman, P.T. and D.A. O'Neal. 1982. *Test Plan for the Greater Confinement Disposal Facility at the Nevada Test Site*.

Dickman et al. 1986. Reference currently unavailable.

Dickman, P.T. 1989. *Greater Confinement Disposal Test at the Nevada Test Site - Final Technology Report*, prepared by Science Applications International Corp., for Reynolds Electrical and Engineering Company.

Dickman, P.T., A.T. Vollmer, and P.H. Hunter. 1984. "Operational Technology for Greater Confinement Disposal," DOE/NV/10327-14.

DOE. 1983. "Greater Confinement Disposal Test, at the Nevada Test Site," Reynolds Electrical & Engineering Co., Inc., Las Vegas, NV, DOE/NV/00410-79.

DOE. 1986. DOE Order 5700.6B, DOE 1986, "Quality Assurance," U.S. Department of Energy, September 23, 1986.

DOE. 1988a. "Radioactive Waste Management," DOE Order 5820.2A, September 26, 1988.

DOE. 1988b. *External Dose-Rate Conversion Factors for Calculation of Dose to the Public*, DOE/EH-0070, U.S. Department of Energy, Washington, DC.

DOE. 1991. DOE Order 5700.6C, DOE 1991, "Quality Assurance." U.S. Department of Energy, August 21, 1991.

DOE. 1996. *The Environmental Impact Statement for the Nevada Test Site and Off-Site Locations in the State of Nevada*, DOE/EIS/0243, Nevada Operations Office, Las Vegas, Nevada.

DOE. 1998. "Modeling the Potential Effects of Subsidence at the Area 5 RWMS for the GCD Compliance Assessment Analysis."

DOE. 1998. "Consequences of Subsidence for the Area 3 and Area 5 Radioactive Waste Management Sites, Nevada Test Site (Working Group Report)." DOE/NV-502 U.S. Department of Energy, Nevada Operations Office, Waste Management Division.

DOE. 1999. DOE Order, Manual, and Guide, 435.1-1, "Radioactive Waste Management," U.S. Department of Energy, July 9, 1999.

DOE. 2000 (draft). *Transuranic Waste Disposal Facility Federal Review Group Manual*, U.S. Department of Energy, Washington, DC.

Eckerman, K. F., and J. C. Ryman. 1993. *Federal Guidance Report No. 12: External Exposure to Radionuclides in Air, Water and Soil*, EPA-402-R-93-081, U.S. Environmental Protection Agency, Washington, DC.

Elkins, N. Z., G. V. Sabol, T. J. Ward, and W. G. Whitford. 1986. "The influence of subterranean termites on the hydrological characteristics of a Chihuahuan desert ecosystem." *Oecologia* 68:521-528.

EPA. 1982. "40 CFR 191: Environmental Standards for the Management and Disposal of Spent Nuclear Fuel, High-Level and Transuranic Radioactive Wastes, Draft Rule," *Federal Register*, Vol. 47, pp. 58196–58206.

EPA. 1984. *A Ground-Water Protection Strategy for the Environmental Protection Agency*, Office of Ground-Water Protection, Office of Water.

EPA. 1985. "40 CFR 191: Environmental Standards for the Management and Disposal of Spent Nuclear Fuel, High-Level and Transuranic Radioactive Wastes; Final Rule," *Federal Register*. Vol. 50, no. 182, 38066–38089.

EPA. 1986. *Guidelines for Ground-Water Classification under the EPA Ground-Water Protection Strategy*, Office of Ground-Water Protection, Office of Water.

EPA. 1993. "40 CFR 191: Environmental Radiation Protection Standards for the Management and Disposal of Spent Nuclear Fuel, High-Level and Transuranic Radioactive Wastes; Final Rule," *Federal Register*, Monday, December 20, 1993.

EPA. 1994. *Guidance for the Data Quality Objectives Process*, EPA QA/G-4, EPA/600/R-96/055, U.S. Environmental Protection Agency, Washington, DC.

EPA. 1999. "40 CFR 197: Environmental Radiation Protection Standards for Yucca Mountain, Nevada; Proposed Rule," *Federal Register*. Vol. 64, no. 166, 46976–47016.

Erdman, J. A. 1970. "Pinyon-juniper succession after natural fires on residual soils of Mesa Verde, Colorado." *Brigham Young University Science Bulletin*, Biological Series 11(2), 26 p.

Erlandson, J. M. 1984. "A case study in faunalturbation: delineating the effects of the burrowing pocket gopher on the distribution of archaeological materials." *American Antiquity* 49(4):785–790.

Estrella, R., S. Tyler, J. Chapman, and M. Miller. 1993. "Area 5 Site Characterization Project - Report of Hydraulic Property Analysis Through August 1993." Water Resources Center Publication #45121, Desert Research Institute, DOE/NV/10845-41.

Everett, R. L., R. O. Meeuwig, P. T. Tueller, and R. A. Evans. 1977. "Water potential in sagebrush and shadscale communities." *Northwest Science* 51(4):271-281.

Everett, R. L. and S. H. Sharrow. 1985. "Understory response to tree harvesting of singleleaf pinyon and Utah juniper." *Great Basin Naturalist* 45(1):105-113.

Federal Emergency Management Agency, Mitigation Directorate. 1995. "Engineering Principles and Practices for Retrofitting Flood Prone Residential Buildings, Chapter IV: Determination of Hazards."

Fisk, W.J., R.J. Spencer, D.T. Grimsrud, F.J. Offermann, B. Pedersen, and R. Sextro. 1987. *Indoor Air Quality Control Techniques: Radon, Formaldehyde, Combustion Products*. Noyes Data Corporation, Park Ridge, New Jersey.

Foxx, T. S., G. D. Tierney, and J. M. Williams. 1984a. Rooting depths of vascular plants as related to biological and environmental factors. Los Alamos National Laboratory Report LA-10254-MS.

Foxx, T. S., G. D. Tierney, and J. M. Williams. 1984b. Rooting depths of vascular plants found on low-level waste sites. Los Alamos National Laboratory Report LA-10253-MS.

French, R. H. 1985. A Preliminary Analysis of Precipitation in Southern Nevada. Pub. No. 45042. Desert Research Institute, University of Nevada, Reno, Nevada.

French, R.H. and W. S. Lombardo. 1984. *Assessment of Flood Hazard at the Radioactive Waste Management Site in Area 5 of the Nevada Test Site*, Publication 45036, Water Resources Center.

French, R.H., R.L. Jacobson and B.F. Lyles. 1996. Threshold precipitation events and potential groundwater recharge, ASCE, *Journal of Hydraulics Engineering*, 11(10):573-578.

Frizzell, V. L., Jr., and J. Shulters. 1990. Geologic Map of the Nevada Test Site, Southern Nevada. USGS Map 1-2046. Miscellaneous Investigation Series. U.S. Geological Survey, U.S. Government Printing Office, Washington, DC.

Geomatrix Consultants, Inc. 1997. *Unsaturated Zone Flow Model Expert Elicitation Project*, prepared for the DOE/NV Yucca Mountain Site Characterization Office, North Las Vegas, NV, by Geomatrix Consultants, Inc., San Francisco, CA, and TRW, Las Vegas, NV.

Geomatrix Consultants, Inc. 1998. *Saturated Zone Flow and Transport Expert Elicitation Project*, prepared for the DOE/NV Yucca Mountain Site Characterization Office, North Las Vegas, NV, by Geomatrix Consultants, Inc., San Francisco, CA, and TRW, Las Vegas, NV.

Gilbert, R. O. and J. C. Simpson. 1985. "Comparing computing formulas for estimating concentration ratios." *Environ. Antl.* 11:25-47.

Gillespie, D., D. Donithan, and P. Seaber. 1996. *Nevada Test Site Water-Supply Wells*, Desert Research Institute," Water Resources Center, Publication #45138, DOE/NV/10845-56.

Green, C. R., and W. D. Sellers (eds.). 1964. Arizona Climate. The University of Arizona Press, Tucson, Arizona.

Grogan, H. A. 1985. Concentration ratios for BIOPATH: selection of the soil-to-plant concentration ratio database. Swiss Federal Institute for Reactor Research, EIR-Bericht Nr. 575.

Gustafson, D.K. and S.E. Rawlinson. 1994. Summary of Fault Investigations at the Area 5 Radioactive Waste Management Site, DOE/Nevada Test site, Nye County, Nevada. Raytheon Services Nevada.

Guzowski, R.V. 1990. *Preliminary Identification of Scenarios that May Affect the Escape and Transport of Radionuclides from the Waste Isolation Pilot Plant, Southeastern New Mexico*. SAND89-7149, Sandia National Laboratories, Albuquerque, NM.

Guzowski, R.V. (revised by T.L. Steinborn). 1996. *Preliminary Estimation of Probabilities of Occurrence For Potentially Disruptive Scenarios at the Greater Confinement Disposal Facility, Area 5 of the Nevada Test Site.* Memo to J. Ginanni, US DOE/NV, Sandia National Laboratories.

Guzowski, R.V. and G. Newman. 1993. *Preliminary Identification of Potentially Disruptive Scenarios at the Greater Confinement Disposal Facility, Area 5 of the Nevada Test Site*, SAND93-7100, Sandia National Laboratories, Albuquerque, NM.

Hales, J. H. Jr. 1974. "Southwestern United States Summer Monsoon Source–Gulf of Mexico or Pacific Ocean?" *Jour. Appl. Meteor.* 13:331-342.

Hannon, W. J., and H. L. McKague. 1975. An Examination of the Geology and Seismology Associated With Area 410 at the Nevada Test Site. UCRL-51830. Lawrence Livermore National Laboratory, Livermore, California.

Hansen, R. M. and M. J. Morris. 1968. "Movement of rocks by northern pocket gophers." *Journal of Mammalogy* 49:391-399.

Hansen, D. J., P. D. Greger, C. A. Wills, and W. K. Ostler. 1997. Nevada Test Site wetlands assessment. NTIS, Springfield, VA, DOE/NV/11718-124.

Harms, G.A., T.L. Steinborn, and R.V. Guzowski. 1998. *An Assessment of Nuclear Criticality for the Greater Confinement Disposal Facility, Area 5 of the Nevada Test Site*, SAND94-1854, Sandia National Laboratories, Albuquerque, NM.

Harrar, J.E., J.E. Carley, W.F. Isherwood, and E. Raber. 1990. "Report of the Committee to Review the Use of J-13 Well Water in Nevada Nuclear Waste Storage Investigations." Lawrence Livermore National Laboratory Report UCID-21867.

Hattis, D., and Burmaster, D. E. 1994. "Assessment of Variability and Uncertainty Distributions for Paractical Risk Analyses," *Risk Analysis*, vol. 14, no. 5, pp. 713-730.

Haverty, M. I. and W. L. Nutting. 1976. "Environmental factors affecting the geographical distribution of two ecologically equivalent termite species in Arizona." *American Midland Naturalist* 95(1):20-27.

Haverty, M. I. and W. L. Nutting, and J. P. LaFage. 1975. "Density of colonies and spatial distribution of foraging territories of the desert subterranean termite, *Heterotermes aureus* (Snyder)." *Environmental Entomology* 4(1):105-109.

Hawkins, L. K. and P. F. Nicoletto. 1992. "Kangaroo rat burrows structure the spatial organization of ground-dwelling animals in a semiarid grassland." *Journal of Arid Environments* 23:199-208.

HAZMED, 2001. Letter from Susan Krenzien, HAZMED, to Angela Colarusso, DOE Nevada Operations, Las Vegas Nevada, March 26, 2001.

Helgeson, H.C. 1968. "Evaluation of Irreversible Reactions in Geochemical Processes Involving Minerals and Aqueous Solutions. I. Thermodynamic Relations." *Geochimica et Cosmochimica Acta*, Vol. 32, 853–877.

Helgeson, H.C., and D.H. Kirkham. 1974. "Theoretical Prediction of the Thermodynamic Behavior of Aqueous Electrolytes at High Pressures and Temperatures: I. Summary of the Thermodynamic/Electrostatic Properties of the Solvent." *American Journal of Science*, Vol. 274, 1089–1188.

Helgeson, H.C., and D.H. Kirkham. 1976. "Theoretical Prediction of the Thermodynamic Behavior of Aqueous Electrolytes at High Pressures and Temperatures: III. Equation of State for Aqueous Species at Infinite Dilution." *American Journal of Science, Vol. 276*, 97–240.

Helgeson, H.C., D.H. Kirkham, and G.C. Flowers. 1981. "Theoretical Prediction of the Thermodynamic Behavior of Aqueous Electrolytes at High Pressures and Temperatures: IV. Calculation of Activity Coefficients, Osmotic Coefficients, and Apparent Molal Properties to 600EC and 5 kb." *American Journal of Science, Vol. 281*, 249–1516.

Helgeson, H.C., T.H. Brown, A. Nigrini, and T.A. Jones. 1970. "Calculation of Mass Transfer in Geochemical Processes Involving Aqueous Solutions." *Geochimica et Cosmochimica Acta*, Vol. 34, 569–592.

Helgeson, H.C., J.M. Delany, H.W. Nesbitt, and D.K. Bird. 1978. "Summary and Critique of the Thermodynamic Properties of Rock-Forming Minerals." *American Journal of Science*, Vol. 278A, 1–229.

Helton, J.C., J.W. Garner, R.D. McCurley, D.K. Rudeen. 1991. Sensitivity Analysis Techniques and Results for Performance Assessment at the Waste Isolation Pilot Plant, SAND90-7103, Sandia National Laboratories, Albuquerque, NM.

Hokett, S.L. and R.H. French. 1998. Evaluation of Recharge Potential at Crater U5a (Wishbone), Publication No. 45160, Water Resources Center, Desert Research Center, Las Vegas, Nevada.

Holmes and Narver, Inc. 1983. *Soil Characterization for the GCDT Demonstration Project at the NTS*. Material Testing Laboratory, Mercury, NV.

Hooke, R.L. 1965. *Alluvial Fans*, Ph.D. Thesis, California Institute of Technology, Pasedena, CA.

Howard, W. E. and H. E. Childs, Jr. 1959. Ecology of pocket gophers with emphasis on *Thomomys bottae mewa*. Hilgardia 29:277-358. California Agricultural Experiment Station, Sacramento.

Hunt, C. B., T. W. Robinson, W. A. Bowles, and A. L. Washburn. 1966. Hydrologic Basin, Death Valley California. U.S. Geological Survey Prof. Paper 494-B. U.S. Geological Survey, U.S. Government Printing Office, Washington, DC.

Hunter, R. B. and P. A. Medica. 1989. Status of the flora and fauna on the Nevada Test Site: results of continuing basic environmental research January through December 1987. DOE/NV/10630-2.

Hunter, P. and D. Card. 1982. *Procurement Specifications - Downhole Instrumentation for Test of Greater Confinement Disposal of Radioactive Waste at the Nevada Test Site*. DOE/NV-10253-3 (FBDU 427-001).

Hunter, P.H., et al. 1982. *Safety Assessment for Area 5 Radioactive Waste Management Site*. DOE/NV-10253-1, Ford, Bacon & Davis Utah and Reynolds Electrical and Engineering Co.

Hunter, P. and R. White. 1982. *Technical Concept for a Greater Confinement Disposal Test Facility at the Nevada Test Site*. NVO-238

Hunter, P.H., D.H. Lester, L.D. Robertson, M.E. Spaeth, J.A. Stoddard, R.T. P.T. Dickman. 1984. *Limited Risk Assessment and Some Cost-Benefit Considerations for Greater Confinement Disposal as Compared to Shallow Land Burial*. DOE/NV/10327-6.

Huntly, N. and R. Inouye. 1988. "Pocket gophers in ecosystems: patterns and mechanisms." *BioScience* 38(11):786-793.

Huntly, N. and O. J. Reichman. 1994. "Effects of subterranean mammalian herbivores on vegetation." *Journal of Mammalogy* 75(4):852-859.

Iman, R. L. and M. J. Shortencarier. 1984. A FORTRAN 77 Program and User's Guide for the Generation of Latin Hypercube and Random Samples for Use With Computer Models, NUREG/CR-3624, SAND83-2365, U.S. Nuclear Regulatory Commission, Washington, DC.

International Commission on Radiological Protection. 1959. *Report of Committee II on Permissible Dose for Internal Radiation*, International Commission on Radiological Protection Publication 2, Pergamon Press, New York.

Jensen, P. and M.M. Hooten. 2000. "Burrowing Depths of Ant Species of the Transition Desert and Piñon-Juniper Plant Communities of the Nevada Test Site." http://www.neptuneandco.com/pubs.html (Access date: July 10, 2000).

Johnson, K.A. and W.G. Whitford. 1975. "Foraging ecology and relative importance of subterranean termites in Chihuahuan Desert ecosystems." *Environmental Entomology* 4(1): 66–70.

Johnson, D. L. 1989. "Subsurface stone lines, stone zone, artifact-manuport layers, and biomantles produced by bioturbation via pocket gophers (*Thomomys bottae*)." *American Antiquity* 54(2):370-389.

Johnson, H. B. and H. S. Mayeux. 1992. "Veiwpoint: a view on species additions and deletions and the balance of nature." *Journal of Range Management* 45:322-333.

Jones, B.F. 1982. Mineralogy of fine grained alluvium from Borehole U11g, Northern Frenchman Flat Area, Nevada Test Site. U.S. Geological Survey Open File Report, 82-765.

Jorgensen, C. D. and S. D. Porter. 1982. "Foraging behavior of *Pogonomyrmex owheei* in southeastern Idaho." *Environmental Entomology* 11:381–384.

Jurinak, J. J., S. S. Sandhu, and L. M. Dudley. 1987. "Ionic Diffusion Coefficients as Predicted by Conductometric Techniques," *Soil Science Society of America Journal*, Vol. 51, pp. 625–630.

Jurwitz, L. R. 1953. "Arizona's Two-Season Rainfall Pattern." *Weatherwise* 6(4):96-99.

Kao, C.S., D.K. Smith, and W.B. McKinnis. 1994. New Observations of Infiltration through Fractured alluvium in Yucca Flat, Nevada Test site: A Preliminary Field Investigation. Lawrence Livermore National Laboratory.

Kaplan, S. and B.J. Garrick. 1981. "On the Quantitative Definition of Risk," in *Risk Analysis*, Vol. 1, No.1, p. 11–26.

Keeney, R.L. and H. Raiffa. 1993. *Decisions with Multiple Objectives*, Cambridge University Press.

Kennedy, W. E. and D. L. Strenge. 1992. *Residual Radioactive Contamination from Decommissioning. Technical Basis for Translating Contamination Levels to Annual Total Effective Dose Equivalent. Final Technical Report*, NUREG/CR-5512, Vol. 1; PNL-7994, Vol. 1, Office of Nuclear Regulatory Research, Nuclear Regulatory Commission, Washington DC.

Kinnear, J.G., A. Wallace, and E.M. Romney. 1981. Frequency Distribution of ^{241}Am in a Population of Bush Bean Plants Grown in Soil in a Glass House." *Soil Science* 132(1):122–126.

Kotra, J.P., M.P. Lee, N.A. Eisenberg, and A.R. DeWispelare. 1996. *Branch Technical Position on the Use of Expert Elicitation in the High-Level Radioactive Waste Program*, U.S. Nuclear Regulatory Commission, NUREG-1563.

Kozak, M.W., Olague, N.E., Rao, R.R., and McCord, J.T. 1993. Evaluation of a Performance Assessment Methodology for Low-Level Radioactive Waste Disposal Facilities, Evaluation of Modeling Approaches, NUREG/CR-5927, SAND91-2802, vol. 1, U.S. Nuclear Regulatory Commission, Washington, DC.

Lappala, E.G., R. W. Healy, and E.P. Weeks. 1987. Documentation of Computer Program VS2D to Solve the Equations of Fluid Flow in Variably Saturated Porous Media. Water-Resources Investigations Report 83-4099. Denver, CO.

Lee, K. E. and T. G. Wood. 1971. *Termites and Soils*. Academic Press, New York.

Levitt, D. G., M. J. Sully, B. L. Dozier and C. F. Lohrstorfer. 1998. Determining the Performance of an Arid Zone Radioactive Waste Site Through Site Characterization, Modeling and Monitoring. Proceedings of the American Geophysical Union 1998 Fall Meetings, December 6-10, 1998, San Francisco, CA.

Lohman, S.W. 1979. *Ground-Water Hydraulics Geological Survey.* Professional Paper 708, USGS.

MacKay, W. P. and W. G. Whitford. 1988. "Spatial variability of termite gallery production in Chihuahuan Desert plant communities." *Sociobiology* 14(1):281-289.

Magnuson, S. O., S. J. Maheras, H. D. Nguyen, A. S. Rood, J. I. Sipos, M. J. Case, M. A. McKenzie-Carter, and M. E. Donahue. 1992. Radiological Performance Assessment for the Area 5 Radioactive Waste Management Site at the Nevada Test Site, Revision 1. Idaho National Engineering Laboratory, Idaho Falls, Idaho.

Mayhew, W. W. 1968. Biology of desert amphibians and reptiles. In *Desert Biology*, G. W. Brown (ed.). Academic Press, New York, pp. 21-50.

McCord, J.T., C.A. Gotway, and S.H. Conrad. 1997. "Impact of geologic heterogeneity on recharge estimation using environmental tracers: numerical modeling investigation." *Water Resources Research*, vol. 33, no. 6, pp. 1229-40.

McKay, M. D., W. J. Conover, and R. J. Beckman. 1979. "A Comparison of Three Methods for Selecting Values of Input Variables in the Analysis of Output from A Computer Code," *Technometrics*, vol. 21, no.2, pp. 239-245.

McKone, T.E. 1994. "Uncertainty and Variability in Human Exposures to Soil Contaminants Through Home-Grown Food: A Monte Carlo Assessment," *Risk Analysis*, vol. 14, no. 4, pp. 449-463.

Meyer, M. and J. Booker. 1991. *Eliciting and Analyzing Expert Judgment: A Practical Guide*, Academic Press.

Mezga, L.J. 1981. *Evaluation of the Need of Greater Confinement than Shallow Land Burial of Low-Level Waste*, Technical Position Paper, ORNL/NFW -81/29.

Mielke, H. W. 1977. "Mound building by pocket gophers (*Geomyidae*): their impact on soils and vegetation in North America." *Journal of Biogeography* 4:171-180.

Miller, M. A. 1948. "Seasonal trends in the burrowing of pocket gophers." *Journal of Mammalogy* 29:38-44.

Miller, M. A. 1957. "Burrows of the Sacramento Valley pocket gopher in flood-irrigated alfalfa fields." *Hilgardia* 26:431-452.

Miller, R. F. and P. E. Wigand. 1994. "Holocene changes in semiarid pinyon-juniper woodlands: response to climate, fire, and human activities in the U. S. Great Basin." *BioScience* 44(7):465–474.

Mohr, C. O. 1947. "Table of equivalent populations of North American small mammals." *American Midland Naturalist* 37:223-249.

Morgan, M.G. and M. Henrion. 1995. *Uncertainty: A Guide to Dealing with Uncertainty in Quantitative Risk and Policy Analysis*, Cambridge University Press.

Mualem, Y. 1976. "A New Model for Predicting the Hydraulic Conductivity of Unsaturated Porous Media." *Water Resources Research*, 12:513-522.

Murphy, C.E., Jr., and J. C. Tuckfield. 1992. Transuranic element uptake and cycling in a forest established over an old burial ground (U). Westinghouse Savannah River Company. WSRC-MS-92-110.

Myles, T.G. and M.M. Hooten. 2000. "Evaluation of the Occurrence of Termite Species and Potential Termite Burrowing Depths in the Area of the Nevada Test Site: Present Day and for the Next 10,000 Years." http://www.neptuneandco.com/pubs.html (Access date: July 10, 2000).

Murphy, C. E., Jr. 1993. "Tritium transport and cycling in the environment." *Health Physics* 65(6):683-712.

NAS. 1995a. *Technical Bases for Yucca Mountain Standards*, National Academy Press, Washington, D.C.

NAS. 1995b. "Management and Disposition of Excess Weapons Plutonium." National Academy of Sciences, Washington, DC.

Nazaroff, W. W. 1992. "Radon Transport from Soil to Air," *Reviews of Geophysics*, 30/2, pp. 137–160.

Neptune and Company. August 15, 2001. Memorandum from Paul Black, Neptune and Company, Inc to Angela Colarusso, NNSA/NVO with attached report, "Benchmarking Aspects of TUC for the NTS GCD PA Models Using GoldSim."

Ng, Y. C., C. S. Colsher, and S. E. Thompson. 1982. *Soil-to-Plant Concentration Factors for Radiological Assessments*, NUREG/CR - 2975.

Noy-Meir, I. 1973. "Desert ecosystems: environment and producers." *Annual Review of Ecology and Systematics* 4:25-41.

NRC. 1977. Regulatory Guide 1. 109 Calculation of Annual Doses to Man from Routine Releases of Reactor Effluents for the Purpose of Evaluating Compliance with 10 CFR Part 50, Appendix I, U.S. Nuclear Regulatory Commission, Washington, DC.

NRC. 1981. *Draft Environmental Impact Statement on 10 CFR Part 61 "Licensing Requirements for Land Disposal of Radioactive Waste*," NUREG-0782, U. S. Nuclear Regulatory Commission, Office of Nuclear Material Safety and Safeguards, Washington, DC.

NRC. 1982. *Final Environmental Impact Statement on 10 CFR Part 61 "Licensing Requirements for Land Disposal of Radioactive Waste*," NUREG-0945, U. S. Nuclear Regulatory Commission, Office of Nuclear Material Safety and Safeguards, Washington, DC.

NRC. 1988. "Disposal of High-Level Radioactive Wastes in Geologic Repositories," *Code of Federal Regulations*, Title 10, Part 60, U.S. Government Printing Office, Washington, DC.

NRC. 1989. *Calculation of Radon Flux Attenuation by Earthen Uranium Mill Tailings Covers*, Regulatory Guide 3.64, U.S. Nuclear Regulatory Commission, Office of Nuclear Regulatory Research, Washington, DC.

Nutting, W. L., M. I. Haverty, and J. P. LaFage. 1987. Physical and chemical alteration of soil by two subterranean termite species in Sonoran Desert grassland. Journal of Arid Environments 12:233-239.

OCRWM. 1998. Total System Performance Assessment—Viability Assessment Technical Basis Report, Office of Civilian Radioactive Waste Management, Washington, DC.

Passey, H. B., V. K. Hugie, E. W. Williams, and D. E. Ball. 1982. Relationships between soil, plant community, and climate on rangelands of the intermountain west. USDA Soil Conservation Service, Technical Bulletin No. 1669.

Perry, F.V., B.M. Crowe, S.G. Wells, L.D. McFadden, J.W. Geissman, J. Poths, M.T. Murrell, M.T. Heizler, L.M. Bowker, K.P. Finnegan, and G.A. Valentine, Geology and Geochronology of Basaltic Volcanism in the Yucca Mountain Region, *in* Perry, F.V., B.M. Crowe, G.A. Valentine and L.M. Bowker (eds), *Volcanism Studies: Final Report for the Yucca Mountain Project*, Los Alamos National Laboratory Report LA-13478 554 p. (1998).

Peterson, E. W., K. Lie, and R. H. Nilson. 1987. "Dispersion of Contaminant During Oscillatory Gas-Motions Driven by Atmospheric Pressure Variations," *Fourth Symposium on Containment of Underground Nuclear Explosions, Volume 2*, United States Air Force Academy, Colorado Springs, CO, September 21–24, 1987, p. 30.

Petrie, L.M., and N.F. Cross. 1975. *KENO-IV—An Improved Monte Carlo Criticality Program*, ORNL-4938, Oak Ridge National Laboratory, Oak Ridge, TN.

Pottororff, E.T., H.A. Phillips, and D.A. Kreamer. 1988. *Analysis of Gaseous Tracer Migration for the Greater Confinement Disposal Test Five-A.* Report Submitted to Reynolds Electrical and Engineering Co. Department of Civil Engineering, Arizona State

Price C.E., and W. Thordarson. 1961. Groundwater Test Well A, Nevada Test Site, Nye County Nevada: A Summary of Lithologic Data, Aquifer Tests, and Construction. USGS Open File Report TEI-800. U.S. Geological Survey, U.S. Government Printing Office, Washington, DC.

Price, L. L., S.H. Conrad, D.A. Zimmerman, N. E. Olague, K.C. Gaither, W.B. Cox, J.T. McCord, and C. P. Harlan. 1993a. *Preliminary Performance Assessment of the Greater Confinement Disposal Facility at the Nevada Test Site - Volume 1: Executive Summary*, SAND91-0047, Sandia National Laboratories, Albuquerque, NM.

Price, L. L., S.H. Conrad, D.A. Zimmerman, N. E. Olague, K.C. Gaither, W.B. Cox, J.T. McCord, and C. P. Harlan. 1993b. *Preliminary Performance Assessment of the Greater Confinement Disposal Facility at the Nevada Test Site - Volume 2: Technical Discussion*, SAND91-0047, Sandia National Laboratories, Albuquerque, NM.

Price, L. L., D. A. Zimmerman, N. E. Olague, S. H. Conrad, and C. P. Harlan. 1993c. *Preliminary Performance Assessment of the Greater Confinement Disposal Facility at the Nevada Test Site - Volume 3: Supporting Details*, SAND91-0047, Sandia National Laboratories, Albuquerque, NM.

Price, L. 1993. Analysis of climate change for PAIII -Round 2 (memo/94/534). Sandia National Laboratories Internal Memo, December 23, 1993, p.6.

QARD. 2000. Quality Assurance Requirements and Description, DOE/RW-0333P, Revision 9.

Quiring, R.F. 1968. Climatological Data, Nevada Test Site and Nuclear Rocket Development Station. ERLTM-ARL 7. Environmental Sciences Administration Report. U.S. Department of Commerce, U.S. Government Printing Office, Washington, DC.

Rachocki, A. 1981. *Alluvial Fans, an Attempt at an Empirical Approach*, John Wiley & Sons, Inc., New York, NY.

Raiffa, H. 1968. *Decision Analysis: Introductory Lectures on Choices Under Uncertainty*, Addison-Wesley.

Raytheon Services Nevada. 1994. Summary of Volcanic Activity at the Area 5 Radioactive Waste Management Site DOE/Nevada Test Site, Nye County, Nevada. Letter Report. Raytheon Services Nevada, Las Vegas, Nevada.

REECo. 1993a. Site Characterization and Monitoring Data From Area 5 Pilot Wells, Nevada Test Site, Nye County, Nevada. Reynolds Electrical & Engineering Co. Inc., Las Vegas, Nevada.

REECo. 1993b. Hydrogeologic Data for Science Trench Boreholes at the Area 5 Radioactive Waste Management Site, Nevada Test Site, Nye County Nevada. Special Projects Section, Environmental Restoration & Technology Development Department, Environmental Management Division, Reynolds Electrical & Engineering Co., Inc., Las Vegas, Nevada.

REECo. 1993c. Hydrogeologic Data for Existing Excavations at the Area 5 Radioactive Waste Management Site, Nevada Test Site, Nye County Nevada. Special Projects Section, Environmental Restoration & Technology Development Department, Environmental Management Division, Reynolds Electrical & Engineering Co., Inc., Las Vegas, Nevada.

REECo. 1994. Site Characterization and Monitoring Data From Area 5 Pilot Wells, Nevada Test Site, Nye County, Nevada. Reynolds Electrical & Engineering Co. Inc., Las Vegas, Nevada.

Richards, L.A. 1931. Capillary conduction of liquids through porous mediums. Physics, 1, pp. 318-333.

Rickard, W. H. and J. C. Beatley. 1965. "Canopy-coverage of the desert shrub vegetation mosaic of the Nevada Test Site." *Ecology* 46(4):524-529.

Roeske, R.H. 1978. *Methods for Estimating the Magnitude and Frequency of Floods in Arizona*, U.S. Geological Survey, Tucson, AZ.

Rogers, A. M., D. M. Perkins, and F. A. McKeon. 1977. "A Preliminary Assessment of the Seismic Hazard of the Nevada Test Site Region." *Bull. Seismol. Soc. Amer.* 67:1587-1606.

Ross, W.C. and S.W. Wheatcraft. 1994. A Two-Dimensional Simulation of Tritium Transport in the Vadose Zone at the Nevada Test Site. Publication #45098, DOE/NV/10162-21.

Sadeghi, A. M., D. E. Kissel, and M. L. Cabrera. 1989. "Estimating Molecular Diffusion Coefficients of Urea in Unsaturated Soil," *Soil Science Society of America Journal*, Vol. 53, pp. 15–18.

Sallam, A., W. A. Jury, and J. Letey. 1984. "Measurement of Gas Diffusion Coefficient under Relatively Low Air-filled Porosity," *Soil Science Society of America Journal*, Vol. 48, pp. 3–6.

Schmeltzer, J.S., J.J. Miller, and D.L. Gustafson. 1993. *Flood Assessment at the Area 5 Radioactive Waste Management Site and the Proposed Hazardous Waste Storage Unit DOE/Nevada Test Site, Nye County, Nevada*, Ratheon Services Nevada, Las Vegas, NV.

Shearer, R. C., J. Letey, W. J. Farmer, and A. Klute. 1973. "Lindane Diffusion in Soil," *Soil Science Society of America Proceedings*, Vol. 37, pp. 189–193.

Sheppard, M. I. and S. C. Sheppard. 1985. "The plant concentration ratio concept as applied to natural U." *Health Physics* 48:494-500.

Sheppard, S. C. and W. G. Evenden. 1990. "Characteristics of plant concentration ratios assessed in a 64-site field survey of 23 elements." *Journal of Environmental Radioactivity* 11:15-36.

Sheppard, S. C. and W. G. Evenden. 1997. "Variation in Transfer Factors for Stochastic Models: Soil-to-Plant Transfer," *Health Physics*, 72(5):727–733.

Sheppard, S.C. and W.G. Evenden. 1988. "Critical compilation and review of plant/soil concentration ratios for uranium, thorium, and lead." *Journal of Environmental Radioactivity* 8:255–285.

Shott, G. J., L. E. Barker, S. E. Rawlinson, M. J. Sulley, and B. A. Moore. 1998. Performance Assessment for the Area 5 RWMS at the Nevada Test Site, Nye County Nevada (Rev 2.1). DOE/NV/11718-176. Report to the U.S. Department of Energy, Nevada Operations Office, Las Vegas, Nevada.

Shott, G.J., V. Yucel, B.A. Moore. In Draft. "Draft Composite Analysis for the Area 5 RWMS at the Nevada Test Site, Nye County Nevada (Rev. 1.0)," prepared for the U.S. DOE, Nevada Operations Office, DOE/NV-XXX (Yet to be published).

Shott, G., C. Muller, L. Barker, D. Cawlfield, F. Lindstrom, D. Linkenhel, M. Sully, D. Thorne, and L. McDowell-Boyer. 1995. Performance Assessment for the Area 5 Radioactive Waste Management Site at the Nevada Test Site, Nye County, Nevada. DOE/NV/11432-196.

Smallwood, K. S., M. L. Morrison, and J. Beyea. 1998. "Animal burrowing attributes affecting hazardous waste management." *Environmental Management* 22: 831-847.

Smith, J. L. and M. K. Rust. 1994. "Temperature preferences of the western subterranean termite, *Reticulitermes hesperus* Banks." *Journal of Arid Environments* 28:313-323.

Snyder, K. E., S. M. Parsons, and D. L. Gustafson. 1993. Field Results of Subsurface Geologic Mapping at the Area 5 Radioactive Waste Management Site, DOE/Nevada Test Site, Nye County, Nevada. Raytheon Services Nevada, Las Vegas, Nevada.

Snyder, K. E., D. L. Gustafson, H. E. Huckins-Gang, J. J. Miller, and S. E. Rawlinson. 1995. Surficial Geology and Performance Assessment for A Radioactive Waste Management Facility at the Nevada Test Site. U.S. Department of Energy Report DOE/NV/10833-25, UC721, 5 pp.

SCS. 1972. SCS National Engineering Handbook, Section 4, U. S. Department of Agriculture.

Spaulding, W.G. 1990. "Vegetational and Climatic Development of the Mojave Desert: The Last Glacial Maximum to the Present," in: Packrat Middens: The Last 40,000 Years of Biotic Change, J. L. Betancourt, T. R. Van Devender and P.S. Martin, eds., University of Arizona Press, Tucson AZ, p.166-199.

Spencer, S. R., G. N. Cameron, B. D. Eshelman, L. C. Cooper, and L. R. Williams. 1985. "Influence of pocket gopher mounds on a Texas coastal prairie." *Oecologia* 66:111-115.

Steinborn, Terry L. and Laurence H. Brush. 1999. "Source Term and Solubilities for the Greater Confinement Disposal 40 CFR 191 Performance Assessment." Sandia National Laboratories, Report to DOE/NV.

Stockman, H.W. 1992. "Preliminary Geochemical Characterization of Alluvium from Trench 8 at the Area 5 RWMS, Area V, Nevada Test Site." Interim Report to USDOE Nevada Operations Office.

Stockman, H.W. 1997. "Long-Term Modeling of Plutonium Solubility at a Desert Disposal Site, Including CO2 Diffusion, Cellulose Decay and Chelation." Draft Report to USDOE, Nevada Operations Office.

Strojan, C. L., F. B. Turner, and R. Castetter. 1979. "Litter fall from shrubs in the northern Mojave Desert." *Ecology* 60(5):891-900.

Strong, W. and S. H. Conrad. 1992. "Using a Suite of Environmental Tracers to Estimate Recharge Through an Arid Basin." *Eos*, v.73(14), p. 128.

Sully, M.J., D.E. Cawlfield, D.O. Blout, L.E. Barker, B.L. Dozier, D.P. Hammermeister. 1993. Characterization of the Spatial Variability of Hydraulic Properties of an Arid Region Vadose Zone, EOS, Transaction of AGU, 74 (43), Fall Meeting Supplement, 286.

Swanson, D.E., et al. 1988. *Preliminary Report: Initial Studies of Tritium Migration at the Greater Confinement Disposal Test (GCDT) Facility; February 1987 – July 1988*. DOE/NV/10327-40.

Tanner, A. B. 1980. "Radon Migration in the Ground: A Supplementary Review," in *Natural Radiation Environment III*, Volume I, Proceedings of a symposium held at Houston, Texas, April 23 – 28. 1978, edited by Thomas F. Gesell and Wayne M. Lowder.

Tausch, R.J. and P.T. Tueller. 1977. "Plant succession following chaining of pinyon-juniper woodlands in eastern Nevada." *Journal of Range Management* 30(1):44-49.

Thomas, B.E., H.W. Hjalmarson, and S.D. Waltemeyer. 1997. Methods for Estimating Magnitude and Frequency of Floods in the Southwestern United States, U.S. Geological Survey Water Supply Paper 2433, Denver, CO.

Thompson, M. 1993. Burrowing animals at the Nevada Test Site: a literature study. Unpublished supporting documentation for the Area 5 GCD Performance Assessment, prepared by Sandia National Laboratories for the U.S. Department of Energy under Contract DE-AC04-94AL85000.

Thordarson, W., M.S. Garber, and G.E. Walker. 1962. Groundwater Test Well D, Nevada Test Site, Nye County, Nevada. U.S. Geological Survey Open File Report TEI-803. U.S. Geological Survey, U.S. Government Printing Office, Washington, DC.

Thorp, J. 1949. "Effects of certain animals that live in the soil." *Science Monthly* 68:180-191.

Tierney, G. D. and T. S. Foxx. 1987. Root Lengths of Plants on Los Alamos National Laboratory Lands. Los Alamos National Laboratory Report LA-10865-MS.

Turner, F. B. and Randall. 1989. "Net production by shrubs and winter annuals in southern Nevada." *Journal of Arid Environments* 17:23-36.

Tyler, S.W., J.B. Chapman, and C. Cooper. 1999. Estimates of Upward Advection at the Area 5 Radioactive Waste Management Site, Nevada Test Site: Evaluation of Estimates Based on Stable-Isotopes and Comparison to Other Methods. Submitted the Nevada Operations Office, U.S. Department of Energy, Las Vegas, Nevada.

Tyler, S. W., J. B. Chapman, S. H. Conrad, D. P. Hammermeister, D. O. Blout, J. J. Miller, M. J. Sully, and J. M. Ginanni. 1996. "Soil-Water Flux in the Southern Great Basin, USA: Temporal and Spatial Variations Over the Last 120,000 years." *Water Resources Research*, Vol. 32, No. 6, pp. 1481-1499.

Tyler, S. W., J. B. Chapman, S. H. Conrad, and D. P. Hammermeister. 1995. "Paleoclimatic Response of a Deep Vadose Zone in Southern Nevada, USA, as Inferred from Soil Water Tracers." *Application of Tracers in Arid Zone Hydrology, Proceedings of an International Symposium Held at Vienna, 22-26 August 1994*. E.M. Adar and C. Levbundgut, eds., IAHS publication no. 232, International Association of Hydrological Sciences, p. 351-361.

U.S. Army Corps of Engineers. 1998. *HEC-HMS Hydrologic Modeling System - User's Manual Version 1.0*, Hydrologic Engineering Center, Davis California.

U.S. Census Bureau. 1999. County Population Estimates for July 1, 1998 and Population change for July 1, 1997 to July 1, 1998. CO-98-1. Population Estimates Program, Population Division. 301-457-2422. Internet Release Date: March 12, 1999. www.census.gov/publication/estimates/county/co-98-1/98C1_32.txt

USDA. 1993. Reference currently unavailable.

USDA. 1995. *Chickens and Eggs: Final Estimates for 1998–1993*, Agricultural Statistics Board, National Agricultural Statistics Service, USDA, Washington, DC.

USDA. 1997. *Poultry Slaughter, 11/04/97*, National Agricultural Statistics Service, USDA, Washington, DC.

U.S. Department of Commerce. 1977. National Oceanic and Atmospheric Administration, *Hydrometeorological Report NO. 49, Probable Maximum* Prec*ipitation Estimates, Colorado River and Great Basin Drainages*, Silver Spring, MD.

USGS. 1998. *PEAKFQ - flood frequency analysis based on Bulletin 17B Version 2.4*, http://water.usgs.gov/software/peakfq.html (Access date: July 10, 2000).

van Genuchten, R. 1978. Calculating the Unsaturated Hydraulic Conductivity with a New Closed-Form Analytical Model. Water Resources Program. Department of Civil Engineering. Princeton University, Princeton, NJ, 67-WR-08.

Vocke, William T., John R. Cochran, and Laura L. Price. 1999. *Identification of Applicable Regulations and Compliance Strategy for Closure of the Greater Confinement Disposal Boreholes at Area 5 of the Nevada Test Site*, unpublished, Sandia National Laboratories, Albuquerque, NM.

Wallace, A. and E. M. Romney. 1976. Radioecology and ecophysiology of desert plants at the Nevada Test Site. Technical Information Center, Office of Technical Information, Energy Research and Development Administration. TID-25954.

Wallace, A., E. M. Romney, and J. W. Cha. 1980. "Depth distribution of roots of some perennial plants in the Nevada Test Site area of the northern Mojave Desert." *Great Basin Naturalist Memoirs* 4:201-207.

Wallwork, J. A. 1982. *Desert Soil Fauna*. Praeger, New York.

Walpole and Myers. 1985. Probability and Statistics for Engineers and Scientists, Macmillan Publishing Co., New York, NY.

Walter, H. 1971. *Ecology of Tropical and Subtropical Vegetation*. Edinburgh: Oliver and Boyd.

Weast, R.C., and M.J. Astle. 1982. "CRC Handbook of Chemistry and Physics." Boca Raton, FL: CRC Press.

Weaver, J. E. and F.E. Clements. 1938. *Plant Ecology*. McGraw-Hill Book Co., Inc.

Whicker, F. W. 1978. Biological interactions and reclamation of uranium mill tailings. Symposium on Uranium Mill Tailings Management, Fort Collins, Colorado, November 20-21.

Whitford, W.G., Y. Steinberger, and G. Ettershank. 1982. "Contributions of subterranean termites to the "economy" of Chihuahuan Desert ecosystems." *Oecologia* 55:298–302.

Wick, O.J., ed. 1967. *Plutonium Handbook. A Guide to the Technology. Volume II*, Gordon and Breach, Science Publishers, Inc., New York, NY.

Wilcox, B. F. and D. D. Breshears. 1995. Hydrology and ecology of piñon-juniper woodlands: conceptual framework and field studies. In *Proceedings: Desired Future Conditions for Piñon-Juniper Ecosystems*. USDA Forest Service General Technical Report RM-258, pp. 109-119.

Wiley J. and P. Hunter. 1981. "Panel Workshop E (Greater Confinement Disposal) Report," *Proceedings of the Third Annual Information Meeting DOE Low-Level Waste Management Program*, ORNL/NFW-81/34, Convened by the DOE Low-Level Waste Management Program, New Orleans, LA.

Wilkins, S. D. and J. M. Klopatek. 1987. Plant water relations in ecotonal areas of pinyon-juniper and semi-arid shrub ecosystems. In *Proceedings: Pinyon-Juniper Conference*, Reno, NV, January 13-16. 1986. USDA Forest Service Intermountain Research Station General Technical Report. INT-215, p. 412-417.

Williams, D.F., R.C. Thunell, E. Tappa, D. Rio, and I. Raffi. 1988. "Chronology of the Pleistocene Oxygen Isotope Record: 0 -1.88 my BP," Paleog., Palaeoc., and Palaeoe. 64:221-240.

Williams, L. R. and G. N. Cameron. 1990. "Dynamics of burrows of Attwater's pocket gopher (*Geomys attwateri*)." *Journal of Mammalogy* 71(3):433-438.

Winkel, V. K., J. P. Angerer, D. B. Hall, M. W. Fariss, and K. R. Johnejack. 1995. Plant and Burrowing Animal Characteristics. Integrated Closure Program for the Area 3 and Area 5 Radioactive Waste Management Sites, Nevada Test Site. Prepared for U.S. Department of Energy, Nevada Operations Office under Contract No. DE-AC08-94-NV11432.

Winograd, I.J., and W. Thordarson. 1975. *Hydrogeologic and Hydrochemical Framework, South-Central Great Basin, Nevada-California, with Special Reference to the Nevada Test Site,* U.S. Geological Survey Professional Paper 712-C.

Winograd, I.J., B.J. Szabo, T.B. Coplen, and A.C. Riggs. 1988. "A 250,000-year climatic record from Great Basin vein calcite: Implications for Milankovitch Theory," Science, v. 242, p. 1275-1280.

Winograd, I.J. 1981. "Radioactive Waste Disposal in Thick Unsaturated Zones." *Science*, Vol. 212, p. 1457-1464.

Winograd, I.J., T.B. Coplen, J.M. Landwehr, A.C. Riggs, K.R. Ludwig, B.J. Szabo, P.T. Kolesar, and K.M. Revesz. 1992. "Continuous 500,000-year record from vein calcite in Devils Hole, Nevada," Science, v. 258, p. 255- 260.

Wirth, S., T.J. Brown, and W. Beyeler. 1999. *Native Plant Uptake Model for Radioactive Waste Disposal Areas at the Nevada Test Site*. SAND98-1789.

Wolery, T.J. 1978. *Some Chemical Aspects of Hydrothermal Processes at Mid-Ocean Ridges - A Theoretical Study*. Unpublished Ph.D. Thesis. Evanston, IL: Northwestern University.

Wolery, T.J., and S.A. Daveler. 1992. EQ6, A Computer Program for Reaction-Path Modeling of Aqueous Geochemical Systems: Theoretical Manual, User's Guide, and Related Documentation (Version 7.0). UCRL-MA-110662 PT IV. Livermore, CA: Lawrence Livermore National Laboratory.

Wolery, T.J. 1992a. *EQ3/6, A Software Package for Geochemical Modeling of Aqueous Systems: Package Overview and Installation Guide (Version 7.0).* UCRL-MA-110662 PT I. Livermore, CA: Lawrence Livermore National Laboratory.

Wolery, T.J. 1992b. *EQ3NR, A Computer Program for Geochemical Aqueous Speciation-Solubility Calculations: Theoretical Manual, User's Guide, and Related Documentation (Version 7.0).* UCRL-MA-110662 PT III. Livermore, CA: Lawrence Livermore National Laboratory.

Wood, D. E., T. E. Buhl, J. R. Cook, R. U. Curl, M. R. Dolenc, D. C. Kocher, B. A. Napier, K. W. Owens, E. P. Regnier, G. W. Roles, R. R. Seitz, D.J. Thorne, and M. I. Wood. 1992. *Performance Assessment Task Team Progress Report*, DOE/LLW -157, Revision 0, Idaho National Engineering Laboratory, Idaho Falls, ID.

Wood, D.E., R.U. Curl, D.R. Armstrong, J.R. Cook, M.R. Dolenc, D.C. Kocher, K.W. Owens, E.P. Regnier, G.W. Roles, R.R. Seitz, and M.I. Wood. 1994. *Performance Assessment Task Team Progress Report*, Revision 1, DOE/LLW-157, Idaho National Engineering Laboratory, EG&G Idaho, Inc., Idaho Falls, ID.

Woodin, H. E. and A. A. Lindsay. 1954. Juniper-pinyon east of the Continental Divide, as analysed by the line-strip method. Ecology 35:473-489.

Wright, J. 1990. "Diffusion Coefficients and Hydraulic Conductivity in Unsaturated Hanford Soils and Sediments," *Proceedings of the First International High-Level Radioactive Waste Management Conference*, Vol. 1, pp. 835–842.

Yakushev, V. M. 1968. "Influence of termite activity on the development of laterite soil." *Soviet Soil Science* 1:109-111.

Yu, C, A. J. Zielen, J.-J. Cheng, Y. C. Yuan, L. G. Jones, D.J. LePoire, Y. Y. Wang, C. O. Loureiro, E. Gnanapragasam, E. Faillace, A. Wallo II., W. A. Williams, and H. Peterson, *Manual for Implementing Residual Radioactive Material Guidelines Using RESRAD, Version 5.0*, ANL/EAD/LD-2, Argonne National Laboratory, Argonne, Illinois. 1993.

Yucel, V. 2000. personal communication.

Zimmerman, D. A., Wahi, K.K., Gutjahr, A.L., Davis, P.A. 1990. A Review of Techniques for Propagating Data and Parameter Uncertainties in High-Level Radioactive Waste Repository Performance Assessment Models, NUREG/CR-5393, SAND89-1432, U.S. Nuclear Regulatory Commission, Washington, DC.

Appendix A

Soil-Water Flux in the Southern Great Basin, United States: Temporal and Spatial Variations Over the Last 120,000 Years

This page intentionally left blank.

WATER RESOURCES RESEARCH, VOL. 32, NO. 6, PAGES 1481–1499, JUNE 1996

Soil-water flux in the southern Great Basin, United States: Temporal and spatial variations over the last 120,000 years

S. W. Tyler,[1,2] J. B. Chapman,[3] S. H. Conrad,[4] D. P. Hammermeister,[5,6]
D. O. Blout,[5,7] J. J. Miller,[8,9] M. J. Sully,[5,9] and J. M. Ginanni[10]

Abstract. The disposal of hazardous and radioactive waste in arid regions requires a thorough understanding of the occurrence of soil-water flux and recharge. Soil-water chemistry and isotopic data are presented from three deep vadose zone boreholes (>230 m) at the Nevada Test Site, located in the Great Basin geographic province of the southwestern United States, to quantify soil-water flux and its relation to climate. The low water contents found in the soils significantly reduce the mixing of tracers in the subsurface and provide a unique opportunity to examine the role of climate variation on recharge in arid climates. Tracing techniques and core data are examined in this work to reconstruct the paleohydrologic conditions existing in the vadose zone well beyond the timescales typically investigated. Stable chloride and chlorine 36 profiles indicate that the soil waters deep in the vadose zone range in age from approximately 20,000 to 120,000 years. Secondary chloride bulges that are present in two of the three profiles support the concept of recharge occurring at or near the last two glacial maxima, when the climate of the area was considerably wetter and cooler. The stable isotopic composition of the soil water in the profiles is significantly more depleted in heavy isotopes than is modern precipitation, suggesting that recharge under the current climate is not occurring at this arid site. Past and present recharge appears to have been strongly controlled by surface topography, with increased incidence of recharge where runoff from the surrounding mountains may have been concentrated. The data obtained from this detailed drilling and sampling program shed new light on the behavior of water in thick vadose zones and, in particular, show the sensitivity of arid regions to the extreme variations in climate experienced by the region over the last two glacial maxima.

Introduction

In recent years, investigations into the hydrogeology of arid regions have focused on the flow and transport processes of the vadose zone. Much of this work has been driven by the need to find safe disposal sites for hazardous and radioactive wastes and by the search for water resources to feed the growth of urban areas. In this work, data collected during characterization of the Area 5 Radioactive Waste Management Site (RWMS), located on the Nevada Test Site (NTS), in the southern portion of the Great Basin geographic province, are examined (Figure 1). The Area 5 RWMS is approximately 95 km northwest of Las Vegas, Nevada [*Sully et al.*, 1993]. The current climate at the study site is arid, with a mean precipitation of 124 mm/yr for 30 years of record (1963–1992) at a National Weather Service station 6 km south of the RWMS. There is great variability in the amount of precipitation from year to year, with a recorded minimum of 29 mm/yr, maximum of 230 mm/yr, and standard deviation of 55 mm/yr. The southern Great Basin experiences two distinct precipitation periods: a winter season characterized by cyclonic frontal systems originating in the Pacific Ocean off the western coast of the United States, and a summer monsoon of high-intensity convective thunderstorms carrying moisture originating in the Gulf of California. About 25% of the annual precipitation falls during this summer monsoon season.

Seven shallow (ST series) and three deep (PW series) boreholes were drilled and cored to characterize the thick vadose zone in the vicinity of the radioactive waste disposal site. The PW series boreholes were drilled to the water table approximately 230 to 270 m below land surface. In this work we focus on the paleoclimate response of the vadose zone as inferred from the distribution of environmental tracers in the soil water. These data clearly show the response of the vadose zone to major climatic variations over the last 120,000 years and represent a unique opportunity to study the paleohydrology of the southern Great Basin.

The Role of Tracers in Vadose Zone Studies

In this work we define net infiltration as the soil-water flux below the active rooting zone and define recharge as that flux

[1]Water Resources Center, Desert Research Institute, Reno, Nevada.
[2]Also at Department of Environmental and Resource Sciences, University of Nevada, Reno.
[3]Water Resources Center, Desert Research Institute, Las Vegas, Nevada.
[4]Sandia National Laboratories, Albuquerque, New Mexico.
[5]Reynolds Electrical and Engineering Company, Las Vegas, Nevada.
[6]Now at Silver City, New Mexico.
[7]Now at Daniel B. Stephens and Associates, Incorporated, Silver City, New Mexico.
[8]Raytheon Services Nevada, Las Vegas.
[9]Now at Bechtel Nevada Corporation, Las Vegas.
[10]Nevada Operations Office, U.S. Department of Energy, Las Vegas.

Paper number 96WR00564.
0043-1397/96/96WR-00564$09.00

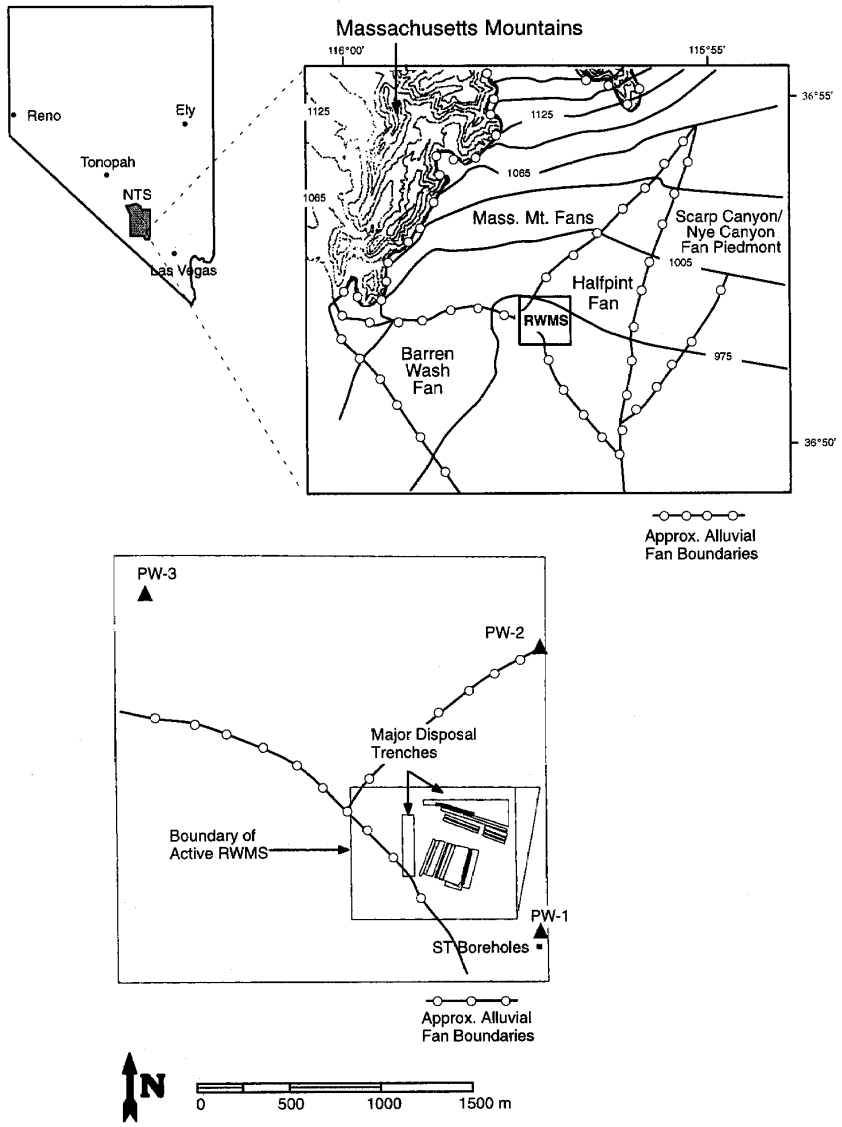

Figure 1. Locations of wells and boreholes discussed in the text relative to the Area 5 Radioactive Waste Management Site (RWMS). Contour interval is 30 m.

reaching the saturated zone. In vadose/groundwater systems at steady state, these terms are interchangeable; however, the response time of these systems may be much longer than the shifts in climate and it is necessary to differentiate these fluxes.

Study of environmental tracers in net infiltration and groundwater recharge investigations began in the early 1960s, when tracking of tritium (^{3}H) from atmospheric nuclear weapons testing was used to examine movement of soil water [*Zimmermann et al.*, 1967]. Use of radiotracers was subsequently expanded to include chlorine 36 (^{36}Cl) by *Phillips et al.* [1988]. As the fallout of these tracers is well documented, the rate of movement and dispersion of soil water can easily be estimated by noting the location of these tracers in the vadose zone. *Scanlon* [1992] and *Phillips et al.* [1988] present comparisons of both tritium and ^{36}Cl in arid portions of the western United States. Since tritium may travel as both liquid and vapor, whereas ^{36}Cl is limited to the liquid phase, both *Scanlon* [1992] and *Phillips et al.* [1988] were able to estimate the relative proportion of vapor and liquid fluxes, which suggest that vapor flux at these arid sites accounted for 37 to 80% of the total water flow.

Radiogenic decay of ^{36}Cl has also been used to date groundwater, yet its long half-life (301,000 years) makes it of limited use in most vadose zone studies. Of considerable hydrologic interest, however, are the variations in isotope production resulting from shifts in strength and orientation of the Earth's magnetic field [*Mazaud et al.*, 1991]. Shifts in the field have resulted in a time-varying cosmic ray bombardment of the upper atmosphere. *Tric et al.* [1992] used cores of marine sediments to construct a continuous estimate of the geomag-

netic field strength over the last 80 kyr and found three periods of significantly reduced field strength, between 15 and 25 ka, between 35 and 45 ka, and between 60 and 67 ka ("ka" denotes a date before present; "kyr" denotes a time period). Because both carbon 14 (^{14}C) and ^{36}Cl are produced by cosmic ray bombardment, their concentration in their respective reservoirs has not remained fixed. This variation in production was first noted by discrepancies between ^{14}C and uranium-thorium age dates in corals [*Bard et al.*, 1990] and was subsequently extended to ^{36}Cl [*Phillips et al.*, 1991]. Because of the long half-life of ^{36}Cl, these variations may provide a chronological dating technique if preserved in the soil water.

Decay of ^{14}C is the most commonly applied radioactive dating method for groundwaters with residence times beyond the point when tritium is useful (>40 years). With a half-life of 5,730 years, ^{14}C can be used to date carbon which has been isolated from the atmosphere for up to 30,000 to 50,000 years. With the development of accelerator mass spectrometry, ^{14}C measurements can be performed with great accuracy on small volume samples. Despite complications presented by geochemical reactions and diffusion of carbon dioxide (CO_2) in the gas phase [*Thorstenson et al.*, 1983], thick unsaturated sections in arid regions may offer the possibility of dating successive infiltration events from hundreds to thousands of years in age.

Nonradiogenic isotopes, principally deuterium (^2H) and oxygen 18 (^{18}O), have also been extensively used in studying processes in the vadose zone. *Barnes and Allison* [1983] developed models of both liquid and vapor flow based on the fractionation that occurs under evaporation to estimate vertical water fluxes in the vadose zone. Under evaporating conditions the profiles of ^2H and ^{18}O can be divided into three general regimes. In the uppermost portion of the soil profile, where vapor flow is dominant, the isotopic composition of the soil water is influenced by the atmospheric concentration which is always more depleted in heavy isotopes than the liquid phase. Moving deeper into the profile, the composition of the soil water becomes enriched in heavy isotopes selectively left behind by the evaporation process. At the point in the profile, where liquid flow begins to dominate (often within 10 to 20 cm of the land surface), the isotopic composition reaches its maximum enrichment [*Barnes and Allison*, 1983]. Below this point the isotopic composition tends toward that of the underlying source water as a result of downward diffusion against the upward advective flux. *Barnes and Allison* [1983] developed simple expressions to estimate the rate of evaporation based on the depth of the vapor transmission zone as well as the shape of the lower, liquid-dominated profile.

One of the simplest techniques proposed for net infiltration and recharge estimation is the chloride mass-balance method [*U.S. Department of Agriculture*, 1954; *Allison and Hughes*, 1978]. By noting that in most environments, the major source of chloride in the soil solution is from atmospheric deposition, either in precipitation or as dry deposition, a simple mass-balance expression of chloride may be developed to predict net water flux at any point in the profile.

The chloride mass-balance method has gained wide acceptance and has been applied to a wide variety of sites to estimate recharge. It suffers from several assumptions (e.g., all fluxes are steady and there are no additional sources of chloride present in the soil) and data limitations (e.g., the chloride flux to the soil surface is both variable and difficult to accurately measure); however, it has proven to be a robust estimator, particularly for low rates of net infiltration [*Allison et al.*, 1994]. Under steady flow the ratio of the net infiltration or recharge to the precipitation flux is given as

$$PC_P/C_R \tag{1}$$

where P is the precipitation rate and C_P and C_R are the chloride concentrations in the precipitation and soil water, respectively.

It is convenient to consider C_P to be an "effective chloride concentration," which accounts for both wet and dry deposition. The concentration of chloride in precipitation is strongly controlled by the distance to its oceanic source [*Junge and Werby*, 1957] and is therefore unlikely to vary significantly over the timescales of most hydrologic interest. In arid settings a significant component of chloride input is also derived from dry deposition and dust [*Dettenger*, 1989]. In a study of chloride and groundwater recharge in the Great Basin of Nevada and Utah, *Dettenger* [1989] suggested that dry deposition may contribute as much as 33% of the total influx of chloride. For low rates of flux, errors introduced by the uncertainty of the effective chloride concentration and/or precipitation may have to be tolerated, as other tracers also suffer uncertainties at low flux rates.

In many arid systems where the net infiltration may be less than 0.1 mm/yr, the assumption of a steady state flux of water throughout the vadose zone required in the chloride mass-balance method may not be appropriate. For example, under a flux of 0.1 mm/yr, a vadose zone 20 m deep at an average water content of 10% by volume will contain soil water as old as 20,000 years at the bottom of the profile. Particularly in North America, where the last 20,000 years have been a time of significant climate change, we cannot expect the net infiltration rate to have remained steady over such a period. In such cases the chloride concentration deep in the vadose zone will not reflect the current conditions. To overcome this difficulty, the chloride mass-balance method can be modified to develop a chloride age of the soil water. If we assume that the chloride input has remained constant over time and that no additional sources of chloride are present in the soil, the chloride age, $A(z)$, at any depth in the soil profile, z, is simply taken as the ratio of the cumulative chloride concentration (mass Cl/unit volume of soil) from the soil surface to the depth of interest divided by the annual chloride deposition:

$$A(z) = \frac{\int_{\text{surface}}^{z} \theta_\ell C_R \, dz}{PC_P} \tag{2}$$

where θ_ℓ is the volumetric water content.

Rather than yielding a direct measure of net infiltration, (2) provides an estimate of age of the soil-water chloride (and by assumption, the age of the water) at any depth in the profile. The only major assumption in this technique is that the rate of chloride deposition (PC_P) to the surface is constant. While this will certainly vary, it is unlikely to vary greatly for the following reasons. Because the concentration of chloride in precipitation is most strongly controlled by the proximity to its ocean source, the wet deposition flux should be linearly proportional to the precipitation assuming the source of the precipitation has remained constant. Paleoclimatic reconstructions for southern Nevada suggest that the two major sources of precipitation through the late Pleistocene have been the Pacific Ocean and the Gulf of California, both at approxi-

mately equal distances. At the same time, the dry deposition component may have varied significantly due to both local and regional sources.

Recent data from Greenland [*Mayewski et al.*, 1994] have shown that chloride concentrations preserved in Greenland ice cores were almost an order of magnitude higher during the last glacial maximum. Extrapolation of this record to the southern Great Basin may not be appropriate, however, given the major differences in factors controlling the region's climate and wind patterns and Greenland's proximity to oceanic sources of chloride. Consistency in the local chloride deposition rate is, however, supported by correlation between climatic variation and chloride ages calculated from modern accumulation rates in the vicinity of the study area, as shown by *Fouty* [1989] and *Phillips* [1994]. Correlations between major climatic shifts and chloride age found by these workers support the assumption of consistency in chloride deposition and therefore support the dating of soil waters based on chloride. Based on the above discussion, it is clear that care must be used in assigning chloride age dates in the absence of other evidence for the timing of recharge and climate change.

The Role of Paleoclimate in Recharge

Acceptance of tracers and the increasing awareness and interest in the nature and extent of climate change have led several workers to investigate thick vadose zones as sources of climate change information. Because many of the arid zones of the world have seen dramatic climate changes over the last 10,000 to 15,000 years, the relationship of climate to recharge may be inferred from the distribution of tracers in the vadose zone. Low flow velocities and water contents found in arid vadose zones significantly reduce the effects of diffusion and should help to preserve information in the soil water concerning the geochemical signature of precipitation and root zone processes.

The first research to recognize the potential for paleoclimate reconstruction from vadose zone chemistry was that by *Edmunds and Walton* [1980]. *Stone* [1992] used chloride profiles from Australia and suggested that shifts in the slope of the chloride-age-versus-depth relationship reflected changes in net infiltration in the region. These ages were shown to be correlated to paleoclimate changes inferred from other independent sources including paleolake levels, pollen analysis, and packrat midden data. *Scanlon* [1991] showed similar results for profiles from west Texas. *Cook et al.* [1992] analyzed vadose zone chloride data from north Africa and found very good agreement between recent (<400 year) climatic events and the rate of residual flux based on chloride mass balance. *Cook et al.* [1992] also presented analyses that century-scale fluctuations in climate might be preserved for >1000 years under recharging conditions.

Phillips [1994] presented an encompassing study of chloride profiles from the southwestern United States, where chloride ages suggest that soil water is as old as 16,000 years. Many of the chloride profiles showed a characteristic maximum in chloride concentration just below the root zone, with decreasing concentrations below the maximum. This chloride "bulge" was suggested to be the result of a cessation of recharge to the water table between 13,000 and 15,000 years ago, when the climate of the western United States began to shift from a cooler and wetter climate to the current arid conditions. As will be shown in this work, even this most recent pluvial period may not have been sufficient to induce recharge in one of the most arid portions of the southwestern United States.

Paleoclimate of the Southern Great Basin

In contrast to the present arid climate, evidence from a variety of sources clearly indicates that the paleoclimate in the southern Great Basin over the last 100,000 to 150,000 years (100–150 kyr) has been dramatically different and at times significantly less arid. *Smith* [1984] identified paleohydrologic regimes in the southwestern Great Basin on the basis of lacustrine deposits at Searles Lake (located 160 km southwest of the study site) and found reasonable correlation with global ice sheet histories. *Jannick et al.* [1991] found evidence for a shallow lake at Searles between 290 and 150 ka, with evidence for the last major highstand and overflow event at 150 ka, lasting through 120 ka. They interpret a sequence of fluctuating shallow lakes from 100 to 24 ka with an additional overflow event between 24 and 10 ka. For the last 10 kyr, with the exception of one unspecified brief Holocene pluvial period, Searles has been a small- to moderate-sized saline lake.

Winograd et al. [1988, 1992] present a detailed examination of the oxygen isotope record of spring deposits at Devils Hole, located approximately 60 km southwest of the study site in the major discharge zone for the groundwater flow basin encompassing the RWMS. These paleohydrologic reconstructions identified the periods of 250 to 160 ka and 120 to 60 ka before present as relatively wet periods. There are differences in the timing of the end of Isotope Stage 6 between the Devils Hole and Searles records, with *Winograd et al.* [1992] favoring 160 ka, whereas *Jannick et al.* [1991] record Searles overflowing until 120 ka. A major stadial at 65 ka is the last pluvial event recorded by Devils Hole because the last 50 ka are missing from the record. *Szabo et al.* [1994] combined calcite morphology with uranium series dating to create a record of water table fluctuations in Browns Room at Devils Hole. They identified at least two major episodes of wetter conditions during the period 10 to 160 ka: between 116 and 53 ka and between 44 and 20 ka. For after 17 ka they found the water level continued to decline to its present level.

Persistent pluvial-period lakes did not exist in the vicinity of the RWMS; the closest were in Groom and Kawich playas, approximately 60 km to the north [*Mifflin and Wheat*, 1979]. Marsh deposits have been identified 50 to 70 km south of the RWMS in an area characterized today by isolated springs [*Quade*, 1986]. The more moist, marsh-forming periods occurred between 40 to 60 ka and between 30 and 15 ka (the most widespread period of standing water). Between 14 and 7.2 ka, surface water gradually decreased, whereas after 7.2 ka there was a lowering of the water table accompanied by widespread erosion [*Quade*, 1986], though conditions remained more moist than today until as late as 8.6 ka. Similar chronologies have been found at other locations south of the RWMS [*Quade and Pratt*, 1989; *Haynes*, 1967].

Plant macrofossils from ancient packrat middens have been used to reconstruct vegetation and climatic conditions over the last 50 kyr, with several intensive studies conducted at and near the Nevada Test Site [*Wells and Jorgensen*, 1964; *Wells and Berger*, 1967; *Spaulding*, 1985; *Spaulding and Graumlich*, 1986]. Juniper woodlands and steppe shrubs were widespread in the area from at least 45 to 10 ka, but the development of desert vegetation in the lowlands had begun by around 15 ka. The period from 45 to 35 ka was marked by plants adapted to

rainfall amounts similar to present, but more of that rain occurred during the winter season and temperatures may have been slightly cooler (1° to 3°C). This was followed by a progressive increase in available moisture up to about 25 ka. The latest period of major continental ice sheet expansion is recorded as beginning around 22 ka in the Mojave Desert, based on major biotic turnover marking the initiation of a stadial climatic regime. Maximum (full glacial) conditions may have occurred locally between 19 and 16 ka and were marked by plants adapted to relatively cold, dry environments, suggesting a large decrease in winter temperatures (up to 7°C), a pronounced absence of summer rain (making up less than 10% of the total), and a relative increase in winter precipitation by as much as 70% above current values. The change to postglacial vegetation took place earlier at some NTS sites than as recorded elsewhere. At elevations comparable to the RWMS, woodlands gave way to desert scrub prior to 14 ka. The transformation took time to spread across the elevational range, but was nearly complete by 9 ka. Between 12 and 10 ka, the number of plants dependent on summer rainfall increased so that by 10 ka, it is estimated that summer and fall precipitation around the NTS may have been 50% more than that at present. Current plant communities were not established until after 5 ka, presumably owing to migration times for warm-weather species. There is also evidence of a mid-Holocene increase in effective moisture and summer precipitation probably exceeded present amounts until 3 or 4 ka [*Spaulding and Graumlich*, 1986].

In summary, the paleoclimate of the region was significantly different than the modern climate. Various paleoclimatic indicators, each with a different spatial and temporal resolution, suggest periods of extensive groundwater and surface water discharge were associated with glacial maxima at approximately 120–150 ka and 15–35 ka. In the following sections we examine the response of the vadose zone to these two periods of documented pluvials.

Results From the Nevada Test Site

Ten core holes were drilled adjacent to the RWMS facility to characterize the vadose zone. Three of these boreholes (PW-1, PW-2, and PW-3) were drilled to the water table, with the remaining boreholes (ST-1 through 7) limited to the upper 40 m. The ST series boreholes were drilled using either casing advance, under ream, or hollow stem auger techniques to provide preliminary data for the deep drilling efforts. The PW series boreholes were drilled and cored using a casing advance, under ream drilling method, and air percussion coring [*Detty et al.*, 1993; *Sully et al.*, 1993]. Air was used as the drilling fluid to minimize disturbance of the in situ water contents, water potentials, and tracer signatures.

The ST boreholes were drilled and sampled in January and February 1992, with shallow sampling completed prior to the onset of unusually heavy rainfall in February (monthly total precipitation of 3.3 cm). Drilling and sampling from PW-1 were conducted from March through June 1992, coinciding with additional heavy precipitation in March (monthly total of 3.8 cm). PW-2 was sampled from June through September 1992, and PW-3 was drilled and sampled from September through November 1992, with no marked excursions from normal precipitation patterns.

As part of the drilling program, intact core and cutting samples were analyzed for both geochemical and radiotracers as well as for a suite of hydraulic properties [*Sully et al.*, 1993; *Reynolds Electrical and Engineering Company* (*REECo*), 1994]. Cores were collected in 76-cm lengths. At each core depth, subcores (7.6 cm in length) were collected in plastic liners, sealed, and sent to the laboratory for hydraulic and geochemical analysis. Tracer analysis included chloride, bromide, sulfate, ^{36}Cl, ^{18}O, ^{2}H, and ^{14}C. In addition to these tracers, core splits were analyzed for water potential, water content, saturated hydraulic conductivity, water retention, porosity, and grain size distribution. Cuttings samples from the drilling were also collected at 0.76-m intervals for textural and chloride analysis. Groundwater samples from each of the PW boreholes were also analyzed for the tracers listed above. Core data from the shallow boreholes (ST series) were similar to those found in the upper portions of the deep boreholes, and we therefore focus our attention on these deep boreholes.

Boreholes PW-1, PW-2, and PW-3 are located within 3 km of each other at surface elevations of 968.7, 989.4, and 1004.9 m above mean sea level (AMSL), respectively [*REECo*, 1994] (Figure 1). The vegetation is similar at each borehole, consisting predominantly of *Larria tridentata*, *Atriplex canescens*, and *Ephedra nevadensis* [*Wallace et al.*, 1974]. Sediments encountered in each of the boreholes consisted of sandy-textured alluvial deposits, with generally less than 10% acid soluble inorganic carbon. At PW-3, volcanic tuff was encountered at a depth of 188 m. Groundwater was intersected in PW-1, PW-2, and PW-3 at 235.2, 256, and 271.6 m below land surface at elevations of 733.5, 733.4, and 734.3 m AMSL, respectively, indicating that the water table beneath the RWMS has little or no gradient.

Alluvial sediments exposed in the existing waste pits and trenches show considerable bedding and limited soil development; however, the hydraulic properties from each of the three deep boreholes show less variation in water retention, saturated hydraulic conductivity, and in situ water content with depth [*Sully et al.*, 1993] than would be expected from visual inspection of these outcrops. In the tuffaceous units encountered below 188 m in PW-3, the saturated hydraulic conductivity measured on the few available cores from this unit is several orders of magnitude lower than that of the alluvium.

Soil-Water Chloride

Soil-water chloride was measured on core samples from selected intervals and from cutting samples on 0.76-m intervals. Analysis by ion chromatography was performed on 1:2 soil-water extracts (50 g of dried soil diluted with 100 g of distilled water). Owing to the alluvial nature of most sediments, it was assumed that the extracts represented soil water only and that no additional chloride was leached from the soil matrix. Concentrations were then reported as milligrams of chloride per kilogram of dried soil. Figure 2 shows the chloride concentration from both cores and cuttings from PW-1, PW-2, and PW-3. Because of limited recovery in the upper portions of PW1, core chloride concentration from borehole ST-1, 61 m to the south, has been used to represent the chloride concentrations in the upper 8 m of PW-1. Good correlation between the core concentrations and adjacent cuttings was found at most depths, suggesting that measured concentrations in the cuttings can be used where core data are sparse or missing. This is particularly important when analyzing the data from PW-2 and PW-3, where core sample density was less. The apparent lack of agreement in the upper portion of PW-1 is primarily

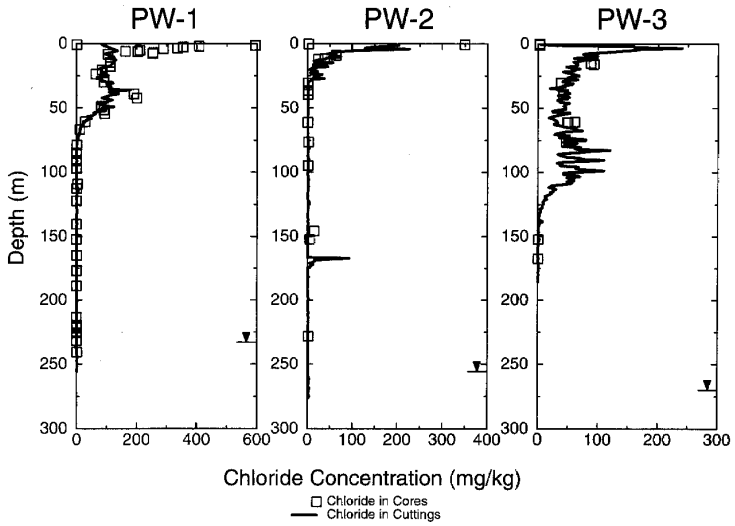

Figure 2. Chloride concentration in cores and cuttings from boreholes PW-1, PW-2, and PW-3. Chloride concentrations from the upper 8 m of ST-1, 61 m to the south, are used to augment the core record from PW-1. All concentrations are reported as milligrams of chloride per kilogram of dry soil.

attributable to the limited core available in this high-chloride zone and to difficulties in obtaining representative cutting samples in the shallow parts of the borehole. As both water content and bulk density varied over only a narrow range, soil-water concentration (as milligrams per liter) versus depth profiles were essentially identical in shape to those shown in Figure 2.

Each of the boreholes shows similar characteristics. In the upper 1 to 2 m of the vadose zone the chloride concentration is very low, reflecting repeated flushing by precipitation. This is also the zone of active rooting, based on observations from the waste pits and trench walls. Below 2 m, each of the profiles quickly reaches a maximum concentration of between 250 and 600 mg/kg. Such a peak concentration is typical in many chloride profiles in arid regions [*Phillips*, 1994] and indicates either a net infiltration rate that has changed over time, significant nonpiston flow, or a combination of these two processes.

Below this characteristic bulge the profiles differ somewhat. In both PW-1 and PW-3 the chloride profile shows a second bulge at 40 and 85 m, respectively. These bulges are not as pronounced as the first peak, and both show considerable spreading. The secondary bulges show evidence of diffusion or dispersion and may represent a previously developed chloride bulge in the near surface that has been advected downward under a subsequent, more pluvial condition. Below these secondary bulges the chloride concentration quickly drops, ranging from 0.5 to 2.0 mg/kg. Using the measured gravimetric water contents of core samples, the calculated soil-water concentration ranges from 10 to 30 mg/L in the deeper portions of each borehole. Groundwater samples collected from the boreholes showed slightly lower concentrations of chloride.

In contrast, PW-2 shows a very rapid decrease in chloride concentration to a depth of 25 m, with low chloride concentrations throughout the rest of the profile. A small spike does appear in several cutting samples at a depth of approximately 175 m. This may be the result of contamination of the cuttings during drilling, although no core data are available from the interval to confirm this. Using the cuttings data, the total mass of chloride stored in the PW-2 profile is roughly 70% lower than the mass stored in either PW-1 or PW-3, suggesting either a shorter time of chloride accumulation or a significantly smaller input flux of chloride at the soil surface. Given the geographic proximity of the boreholes, it is unlikely that differences in the input flux could be responsible for this large difference.

The chloride profiles show that the profiles are not at steady state and are accumulating chloride in the upper 125 m. Two possible explanations are plausible for the profile shapes: a water table much higher than that which currently exists or a period of significantly wetter surface conditions that resulted in significant net infiltration and a flushing of the vadose zone. Given the coarse texture of the soil, the water table would have to be very near the land surface to maintain the significant evaporation rate needed to accumulate the chloride found in the boreholes. It has been suggested [*Winograd and Doty*, 1980] that the water table in Frenchman Flat may have risen by as much as 30 m in the late Pleistocene; however, simple evaporation from this depth could not produce the secondary bulges found in both PW-1 and PW-3. In addition, *Jones* [1982] suggests that the water table has remained relatively stable throughout the Pleistocene, based on the uniformity in clay hydration found in a borehole (U11g) 5 km north of the study site. It is more probable that at some time in the past, the regional climate was sufficiently wet to induce a significant recharge with resulting low chloride concentrations in the lower portion of the vadose zone.

While it is not appropriate to estimate a recharge rate from the upper portions of the boreholes where chloride is currently accumulating, it is possible to use the deeper data (>100 to 150 m) to estimate the paleorecharge rate. The very low and uniform chloride concentrations at depth indicate that at some time in the past, the vadose zone was in equilibrium and significant recharge must have occurred. An estimate of the recharge represented by the low chloride concentrations at depth in each of the boreholes requires knowledge of the chloride

flux at the surface at the time recharge was occurring. Although the magnitude of the precipitation when the recharge occurred is unknown, it must have been greater than present conditions (124 mm/yr; from French [1986]), under which recharge and net infiltration are negligible [*Detty et al.*, 1993; *Tyler et al.*, 1994]. At this time, data are not available for chloride fluxes at the site. *Junge and Werby* [1957] and *Dettenger* [1989] report chloride concentrations in precipitation in the general area averaging 0.4 mg/L and also reported dry deposition measurements from several stations. On the basis of these measurements, *Dettenger* [1989] suggested using an "effective" concentration of 0.6 mg/L to account for the additional flux due to dry deposition. Chloride concentrations in bulk precipitation samples (both wet fall and dry deposition combined) collected in 1985 from several sites across the NTS ranged from a minimum of 0.2 mg/L to a maximum of 1.3 mg/L (unpublished data, 1985). These samples showed no apparent trend attributable to elevation. In addition to these data, several authors [*Phillips*, 1994; *Fouty*, 1989; *Fabrika-Martin et al.*, 1993] have estimated chloride flux in the region to range from 80 and 150 mg/m^2/yr, with most estimates close to 100 mg/m^2/yr.

The calculated chloride flux based on average annual precipitation (124 mm/yr) and *Dettenger*'s [1989] estimate of effective chloride concentration is 74.4 mg/m^2/yr, somewhat lower than those used in other studies. The paleoclimate record clearly shows that more mesic conditions prevailed through much of the Pleistocene, and it is therefore logical to assign a higher value of precipitation (and therefore chloride flux) when estimating paleorecharge. Packrat midden data suggest that precipitation over the last 35 ka was often 20 to 50% higher than present precipitation. Prior to these dates, other paleoclimatic indicators in the region also suggest a more pluvial period than at present. Using an assumed 50% increase in precipitation, the estimated paleochloride flux is 105 mg/m^2/yr, similar to the estimated chloride paleoflux used by *Fouty* [1989] and *Fabryka-Martin et al.* [1993]. While the paleochloride flux remains an open question, it is important to point out that calculated recharge rates are linearly related to this estimate and are therefore less sensitive to uncertainties than traditional soil physics methods used to estimate recharge.

An estimate of the paleorecharge preserved in the deeper portions of each of the three boreholes can be made based on their average deep chloride concentrations (C_R = 13.9 mg/L in PW-1, 23.7 mg/L in PW-2, and 17.9 mg/L in PW-3). Using the above estimated chloride flux, the calculated paleorecharge rates from deep in the profiles range from 7.6 mm/yr at PW-1 to 4.4 mm/yr at PW-2 to 5.9 mm at PW-3. These rates of recharge are currently found at much higher elevations in the southern Great Basin. Modern recharge of this magnitude is associated with areas with cooler average temperatures and higher annual precipitation. Increased precipitation and cooler temperatures characterized glacial climates of the region and suggest that conditions at the site during recharging periods were similar to those found only at higher elevations today.

The combination of low chloride concentrations at depth, of large differences in stored chloride between the boreholes, and of the presence of secondary bulges suggests that a series of recharging events have occurred and that the profiles have responded in different ways. At PW-1 and PW-3 significant recharge was interrupted by a long period of chloride accumulation in the near surface. This accumulation was presumably the result of a climatic shift from a more pluvial period. During this same period PW-2 may have also experienced chloride accumulation (and hence little or no recharge); however, this signal is no longer present. At some more recent time a return to pluvial conditions initiated deep infiltration at all three boreholes. This infiltration was of sufficient magnitude or temporal length to induce infiltration to the water table at PW-2, carrying with it most of the accumulated chloride. At PW-1 and PW-3 the infiltration was not sufficient to reach the water table but, rather, advected the near-surface chloride bulges deeper into the profile. The results of this "aborted" recharge are witnessed by the presence of the secondary bulges in both PW-1 and PW-3. Following this paleorecharge period, the profiles show the beginning of another period of chloride accumulation that is still occurring today.

Timing the age of these postulated periods may be estimated from (2), provided the input chloride flux is known. As shown in the discussion of paleorecharge rates, above, the input flux requires knowledge of both the chloride concentration of the precipitation and the precipitation rate, both of which have clearly varied over recent geologic time. Figures 3a–3c show the estimated chloride ages from the three boreholes under an assumed chloride flux of 105 mg/m^2/yr. The use of constant flux in the chloride age calculations is at best a simplification of the climatic conditions over the last 100 kyr; as discussed above, the choice of a flux slightly higher than that presently occurring appears appropriate given the known changes in climate over the period of interest. The chloride ages shown in Figures 3a–3c show the significant differences between the PW-1, PW-3, and PW-2 profiles. Age estimates at both PW-1 and PW-3 suggest that these profiles have accumulated chloride for at least 100 to 120 kyr. In contrast, the chloride age calculated at PW-2 (Figure 3b) is 25 to 35 kyr, with almost all of the chloride contained in the upper 25 m. As will be discussed later, these ages may represent the last two major pluvial periods in the paleoclimatic history of the region.

If the secondary bulges in PW-1 and PW-3 represent a more pluvial period in which recharge was occurring in PW-2, the chloride age of the bulges should be commensurate with the age at the bottom of the chloride bulge in PW-2. From Figures 3a and 3c the break in slopes of the chloride ages represents the secondary bulges and clearly shows an apparent age of approximately 60 to 70 kyr, much older than that estimated for the timing of recharge at PW-2. This apparent discrepancy may be the result of dispersive mixing, rather than of the simple piston displacement assumed by the chloride age model. The secondary bulges clearly show spreading, reflecting additional mixing during the advective phase of transport from the near surface. The accumulated chloride above the secondary peaks at 40 and 85 m in PW-1 and PW-3, respectively, therefore represents not only chloride added since the aborted recharge, but also a significant amount of chloride that was initially present but that has spread, owing to the transport. By assuming a simple piston model of displacement the calculated age of the peak will overestimate the actual age.

To address the effect of the dispersed chloride, a two-step modeling process was conducted. In the first step a simple Gaussian model was fit to both secondary bulges in PW-1 and PW-3. The initial conditions assumed a Dirac distribution of chloride centered on the current peak of the respective secondary bulges. The only parameter which was allowed to vary to obtain a best fit was the variance of concentration. In the second step the actual age of the chloride peak was calculated from the chloride accumulated above the peak, after subtracting that portion of the chloride which resulted from dispersion

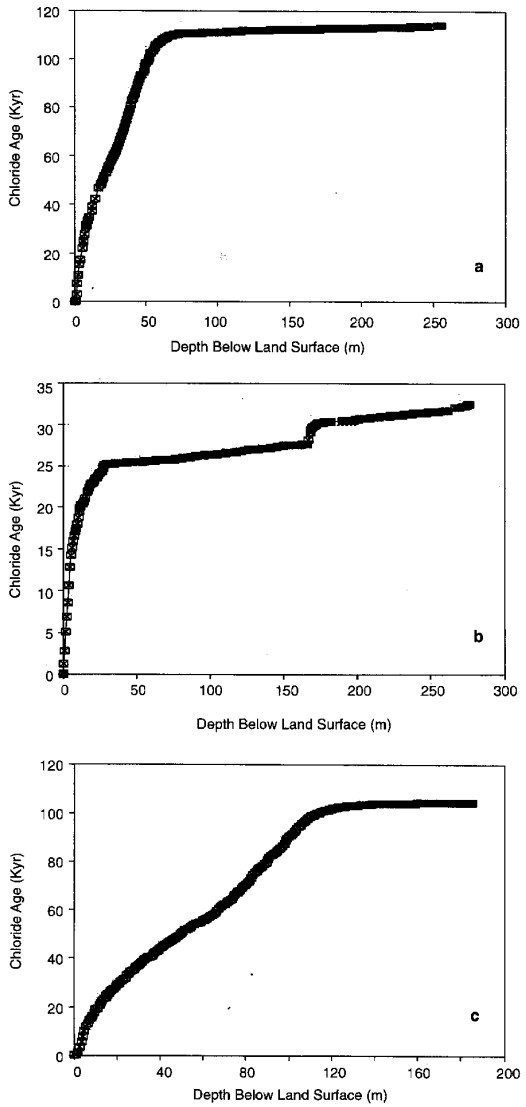

Figure 3. Estimated soil water age based on chloride accumulation for (a) borehole PW-1, (b) borehole PW-2, and (c) borehole PW-3. In each case a chloride accumulation rate of 0.105 gr/m^2/yr was assumed.

of the original peak. This age also corresponds to the trough between the primary and secondary bulges. The average velocity of the secondary bulge was then calculated by dividing the peak depth by the adjusted age. The best fit simulated results are compared with the measured concentrations in Figures 4a and 4b. The solid line represents the distribution of chloride that would be present if no further chloride had been input to the soil following the advective phase of the transport. The Gaussian model fits the leading (deeper) edges of the secondary bulges very well, but it is not possible to assess the accuracy along the trailing edge since it is obscured by more modern chloride.

At PW-1 the Gaussian model reduces the age of the secondary bulge from 82 kyr to 53 kyr, while at PW-3 the age was reduced from 75 kyr to approximately 46 kyr. These ages are closer to the total age at PW-2 but are still much older and indicate different timing for recharge. There are several other possible explanations for this apparent lack of consistency. The secondary bulge ages represent the time when the aborted recharge events began, while the accumulated chloride age at PW-2 represents the amount of time since recharge ceased. It is quite plausible that recharging conditions continued to prevail at PW-2 for an additional 20 to 30 kyr, well after the aborted recharge had been initiated at PW-1 and PW-3. The paleoclimatic indicators clearly demonstrate that throughout much of the late Wisconsin, conditions were conducive to recharge. Another explanation for the difference may be due to nonpiston or nonuniform flushing of the accumulated chloride by the aborted recharge at PW-1 and PW-3. Incomplete removal of chloride has been reported by *Jolly et al.* [1989] in studies of land clearing and chloride flushing in Australia. Complete flushing would only occur after several pore volumes of recharge had moved through the profile, such as what may have occurred at PW-2. This phenomenon leaves accumulated chloride behind, resulting in a skewed upward distribution (long tail) of chloride. While the leading edge of secondary bulges is well defined by the advection dispersion model (Figures 4a and 4b), the tails cannot be modeled with any certainty, as they intersect the primary bulges in both cases. If the leaching of the chloride was not complete, this older chloride left behind would increase the apparent age of the recharging period. If tailing is the major source of the disparities in estimated timing, the calculated leaching efficiency needed to reconcile the timing of the aborted recharge was approximately 75% for both boreholes, with 25% of the initial mass of chloride remaining outside of the calculated Gaussian distribution. From the chloride data alone it does not appear possible to resolve which, if either, of these explanations is most appropriate.

The modeling of the secondary bulges can also be used to investigate the magnitude of the average dispersion coefficient. Average in this sense represents both spatial and temporal variations. In the spatial sense the dispersive characteristics are assumed to be homogenous from the land surface to the bulge position. The chloride profiles shown in Figures 2a and 2c display significant scatter attributable to both sample collection methods (primarily drill cuttings) and small-scale heterogeneity in the flow velocities. The dispersion coefficient therefore represents a profile-scale measure of dispersion. From a temporal framework the dispersive process has varied from an advective case under past recharging conditions to one dominated by diffusion today. The dispersion coefficients which best fit the secondary bulges in PW-1 and PW-3 are 4×10^{-11} and 1×10^{-10} m^2/s, respectively. The ratio of the dispersion coefficients is very close to the ratio of the depths of the maximum concentration of the secondary bulges, suggesting that the difference may be attributable to differences in advective velocity rather than to differences in the intrinsic dispersivity. The magnitude of the dispersion coefficient is only somewhat higher than that expected for molecular diffusion, indicating that the advective velocity was small and supporting the small estimated recharge rates of 7.6 and 5.9 mm/yr deeper in the profiles of PW-1 and PW-3, respectively.

It is important to note that the secondary bulge velocity in PW-3 is almost twice that of PW-1, while the deep chloride concentrations imply a higher rate of recharge in PW-1. The soil textures in PW-1 are coarser, which would result in slower wetting front velocities during displacement of the secondary

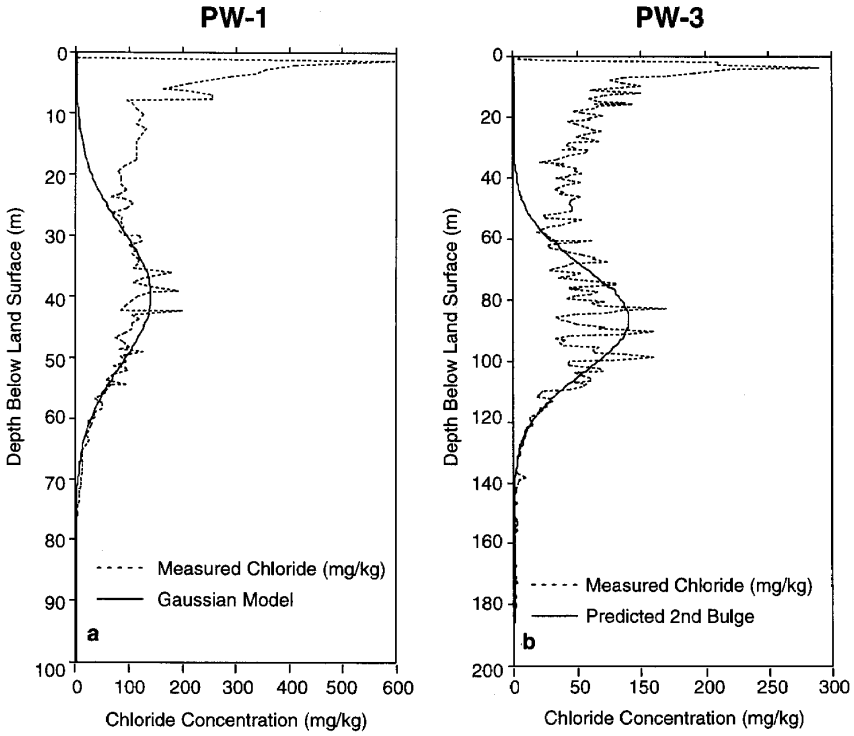

Figure 4. Gaussian model fit to the secondary chloride bulge in (a) borehole PW-1 and (b) borehole PW-3.

bulges yet higher overall recharge rates. It is also possible that surface conditions, particularly vegetation communities, may have differed between recharging periods at these two boreholes. PW-3 is located at a slightly higher elevation and further up the fan surface. These factors may have resulted in different conditions during these two recharging periods separated by almost 100 kyr.

Chlorine 36 in Soil Water

Analysis of ^{36}Cl from the near-surface soils in the vicinity of the RWMS has shown the ^{36}Cl from nuclear weapons testing to be restricted to the upper 2 m of the soil profile [*REECo*, 1994]. This is consistent with the chloride mass-balance results (presented above) and hydraulic data [*Detty et al.*, 1993], which indicate that infiltration is recycled in the root zone.

Isotopic ratios for ^{36}Cl were measured on 27 core samples from the PW series boreholes. The chloride content of the soil was precipitated in the form of AgCl using standard procedures [*Mattick et al.*, 1987]. The ratio of ^{36}Cl to chlorine 35 (^{35}Cl) was measured using tandem accelerator mass spectroscopy [*Elmore et al.*, 1979]. Between the land surface and the water table, 14 samples were analyzed from borehole PW-1, four samples were analyzed from borehole PW-2, and nine samples were analyzed from borehole PW-3.

Chlorine-36 ratios versus depth are shown in Figure 5. The solid symbols represent raw data, that is, the ^{36}Cl ratio as measured by the accelerator mass spectrometer. The open symbols show ^{36}Cl ratios corrected for decay and represent the estimated ^{36}Cl ratios at the time of deposition. Decay corrections were calculated using chloride mass-balance ages corresponding to the depth from which the sample was taken. The corrected ^{36}Cl ratios from all three boreholes are significantly higher than the modern ratio of approximately 500×10^{-15} ($^{36}Cl/^{35}Cl$) for the region measured at Yucca Mountain by *Fabrika-Martin et al.* [1993] from samples taken just beneath the ^{36}Cl peak. According to *Tric et al.* [1992], the beginning of the first period of reduced field strength occurred approximately 15 ka, suggesting that even the most shallow soil-water samples must be at least 15 kyr old. An age estimate of at least 15 ka is consistent with the chloride mass-balance results.

The PW-1 profile shows one anomalously low ratio of 184×10^{-15} at a depth of 91 m. This ratio is much lower than what would be expected from the geomagnetic fluctuations. If this low ratio was attained by decay of ^{36}Cl, the decay age is 433 kyr, significantly older than the water above it or beneath it in the profile and inconsistent with their chloride ages. Two samples deeper in the profile (152 m and 213 m) show much higher ratios as well as excellent agreement in ^{36}Cl ratio. All three samples were taken from beneath the chloride bulge in the region of low chloride concentrations where chloride was added as a carrier during analysis, and therefore the likelihood of analytical error was significantly increased. It is most likely that this anomalously low ratio does not represent very old water but, rather, analytical error.

Figure 6 shows the decay-corrected ^{36}Cl data as a function of their calculated chloride ages from all three boreholes plotted along with the estimated atmospheric fallout at the site over time following the method of *Mazaud et al.* [1991]. Here, the data presented previously in Figure 5 have been normalized relative to the modern ratio of 500×10^{-15} so that they may be compared against the curve of ^{36}Cl production. Figure 6 shows three peaks of ^{36}Cl production corresponding to the three

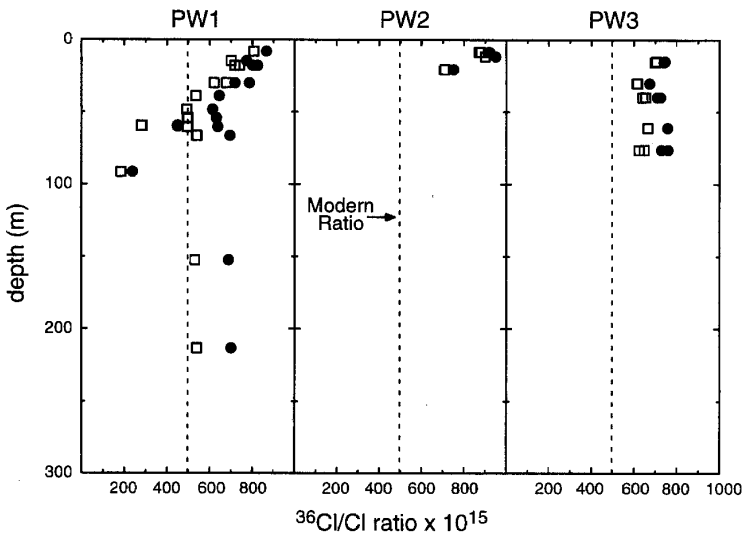

Figure 5. Chlorine 36 concentrations in soil water from PW-1, PW-2, and PW-3. Open symbols represent decay-corrected concentrations based on chloride ages estimated for the sample depth. Dashed line represents approximate modern ratio of $^{36}Cl/Cl$ deposition at the site.

periods of significantly reduced strength in the magnetic field. Over these time periods of increased ^{36}Cl production, the soil-water samples are also elevated in ^{36}Cl relative to the modern ratio. However, during periods of reduced ^{36}Cl production, the ^{36}Cl ratios of soil water remain elevated rather than decreasing toward the modern ratio, as predicted. This lack of lower concentration of observed ^{36}Cl may be the result of dispersion during transport or nonpiston displacement through the vadose zone. However, the elevated levels of ^{36}Cl are consistent with waters infiltrated during the late Pleistocene.

Stable Isotopes in Soil Water

The stable isotopes of hydrogen and oxygen provide an excellent indicator for evaluating paleofluxes, as their ratios in precipitation are sensitive to changes in both temperature and origin of moisture. Thus changes in the net infiltration and recharge are likely to be directly recorded in the isotopic ratios of the soil waters [*Fontes*, 1981]. Stable isotopic analysis was performed on core samples from both the ST series and the PW series boreholes. Subsamples (7.6 cm in length) from each core run were collected in plastic liners, sealed in the field, and

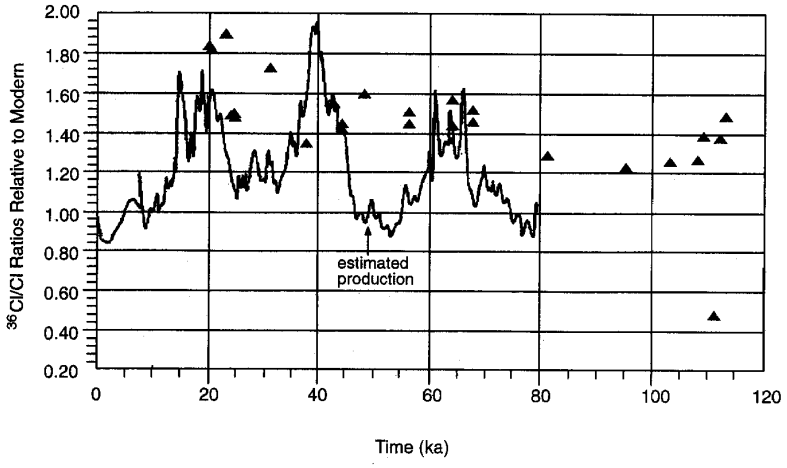

Figure 6. Decay corrected ^{36}Cl ratios relative to the modern ratio at the site (500×10^{-15} atoms of ^{36}Cl/atoms of ^{35}Cl) from all three deep boreholes. The solid line represents the estimated fallout from cosmic production as influenced by variations in the geomagnetic field intensity.

sent to the laboratory for soil-water extraction. After completion of the PW series boreholes beneath the water table, groundwater samples were collected for isotopic analysis.

Drilling techniques may have a significant impact on the quality of subsurface samples. This is particularly true of the stable isotopic samples if drying of the core occurs. Although all core samples were collected by percussion coring, compressed air was used to drill all of the PW series boreholes and some of the ST series boreholes. Significant amounts of drilling air were often injected into the formation during several stages of drilling the deeper boreholes, which could cause drying of the formation and possibly the core samples. The potential magnitude of this problem was tested by comparing the isotopic composition between two ST boreholes drilled 1.5 m apart; one drilled by a hollow-stem auger and the other using the air casing advance, under the ream-drilling method. Three sample pairs, where core depth was within 2 m of each other vertically, were available for comparison. For these three pairs the greatest difference in $\delta^{18}O$ is 0.3‰ and the greatest difference in δD is 2‰, in both cases just slightly greater than the analytical reproducibility (discussed below). Minor drying at depth is evidenced by small (<2.5 MPa) excursions in the water potential at depth [*Detty et al.*, 1993]. The coarse texture of the material suggest that had significant drying occurred during drilling, the water potential excursion would have to be much larger to also be reflected in the isotopic composition of the soil water.

The isotopic content of precipitation was not collected as part of this study. In a study of precipitation and springs in southern Nevada, *Ingraham et al.* [1991] operated 14 precipitation sampling stations, including a station located 450 m from the RWMS. The station elevation was 960 m AMSL, only 10 m lower than the land surface at PW-1. The station was designed only to collect monthly averaged precipitation chemistry and isotopic ratios. *Ingraham et al.* [1991] reported the results of 40 samples collected from 1982 to 1986, although 13 of the samples report ^{18}O only. An additional 19 samples (from January 1987 through October 1988) were archived and analyzed as part of this study. These samples had been stored in glass, and several samples analyzed shortly after collection were compared to their archived duplicates. These checks on sample integrity showed the archived samples to be within the standard analytical error of the previously analyzed precipitation.

Laboratory analysis of cores began with a toluene extraction [*Ingraham and Shadel*, 1992] on approximately 100 g of moist soil from the cores. The extractions were run to completion, with generally 3 to 4 mL of water being derived from each extraction. For the oxygen analysis, approximately 10 μL of water was completely converted to carbon dioxide using guanidine hydrochloride, and the CO_2 was directly introduced into a Delta E Finnigan-Matt triple collector mass spectrometer. Hydrogen analyses were conducted after quantitative conversion of 5 μL of water to hydrogen gas using uranium as the reducing agent and direct injection into a Nuclide 3-60 HDD double collector mass spectrometer. All data are reported in standard delta notation, with respect to standard mean ocean water (SMOW). The reproducibility of the ^{2}H is ±1‰, while the oxygen results are ±0.2‰.

Isotope Composition of Precipitation and Soil Water

A total of 46 analyses of precipitation isotope pairs are available covering the period from January 1984 through October 1988. The $\delta^{18}O$ value of precipitation ranged from +2.9‰ to −19.7‰, while the δD values ranged from −15‰ to −152‰. The annual mean composition, weighted by the volume of precipitation, is −10.5‰ for $\delta^{18}O$ and −80‰ for δD. An important factor is the relative proportion and isotopic composition of the seasonal component. Considering the summer season to include precipitation from May through October, the weighted mean summer precipitation is −7.1‰ and −57‰ for $\delta^{18}O$ and δD, respectively. The weighted mean for winter precipitation is −12.5‰ and −93‰, respectively, reflecting the cooler temperatures. The winter δD mean agrees well with that reported by *Smith et al.* [1992] of −95‰ for recharge in the Amargosa Desert area, just southwest of the study site.

A local meteoric water line (LMWL) can be defined by a linear regression through the precipitation data and is shown in Figure 7 along with the weighted average values. This line is described by $\delta D = 6.26 \cdot \delta^{18}O - 15.3$. The difference between this locally derived line and the global water line is small over the range of isotopic values encountered at the study site.

The measured ^{2}H and ^{18}O content of soil waters and ground water from PW-1, PW-2, and PW-3 are plotted against depth in Figures 8a–8c and 9a–9c, respectively. In the upper portions of each borehole, both oxygen and hydrogen are enriched in heavy isotopes. This enrichment is maximum near the soil surface and decreases rapidly with depth. Below 50 m the isotopic composition is fairly consistent with depth in PW-1 and PW-3; however, PW-2 shows some differences, including its minimum isotopic value at approximately 50 m and several excursions of enriched water at depths of 150 and 225 m. As the water table is approached, the soil water isotopic signature resembles the groundwater signature in all three wells.

The relation of the soil-water, precipitation, and groundwater isotopic signatures is shown in Figure 7. Two populations can be clearly identified in the soil-water isotopic compositions: samples collected from the land surface to about 16 m (and to almost 40 m in PW-1) that exhibit evaporative enrichment of ^{18}O relative to ^{2}H (defined here as "shallow soil water") and deeper samples that trend on a line parallel to the LMWL (defined here as "deep soil water"). As a group, the shallow soil waters define a line described by $\delta D = 3.6 \cdot \delta^{18}O - 65$ ($n = 45$, $R^2 = 0.99$). The isotopic enrichment of this sample group is inversely related to depth (Figures 8 and 9). The deep soil waters define a line described by $\delta D = 6.64 \cdot \delta^{18}O - 22$ ($n = 41$, $R^2 = 0.90$). The maximum and minimum along this deeper trend are defined by samples from PW-2, which has more variation in the composition of the deeper samples than either PW-1 or PW-3.

Shallow Soil-Water Isotopic Composition

The isotopic composition of recharge water is generally believed to be reasonably represented by the isotopic composition of the mean precipitation in an area [*Gat*, 1981]. For example, *Yonge et al.* [1985] found that the isotopic ratios measured in cave seepage water approximately reflected the mean annual precipitation for the region, weighted by the volume of individual storms. Groundwaters in some arid regions, however, have been shown to deviate from the isotopic composition of mean precipitation, with either enrichment or depletion in heavy isotopes. Enriched compositions generally plot along evaporation lines from the local precipitation, indicating that evaporative enrichment occurs during the recharge process, either from precipitation or surface water prior to infiltration or by evaporative loss from the soil zone. Depleted

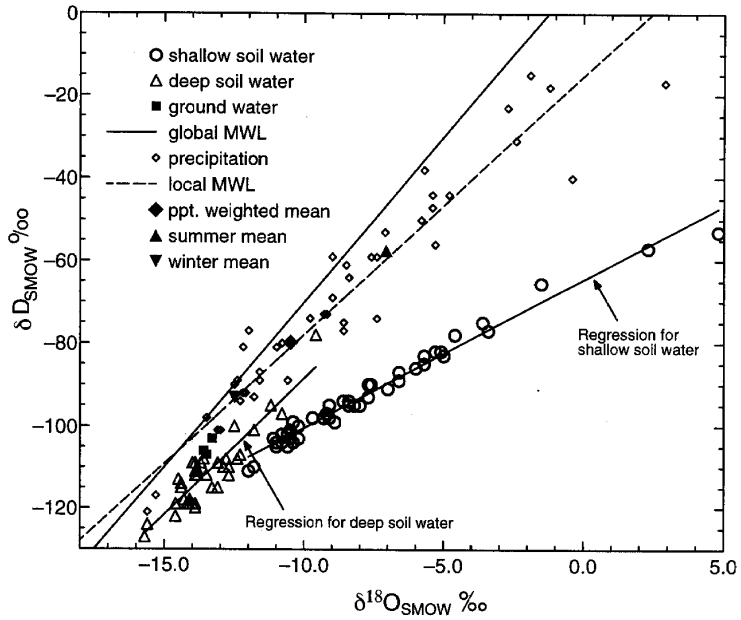

Figure 7. Stable isotopic concentrations of soil water, groundwater, and precipitation. Precipitation chemistry data consist of reported data from *Ingraham et al.* [1991] as well as additional samples analyzed during the present study.

groundwater relative to mean precipitation was found by *Vogel et al.* [1963] and *Vogel and Van Urk* [1975] and attributed to selective infiltration of rainfall from intense, large-volume, isotopically light rainfall events. Depleted values can also indicate infiltration of primarily cooler season precipitation. By comparing precipitation values and spring discharge in a desert range in California (Providence Mountains), *Smith et al.* [1992] concluded that most summer precipitation evaporates before reaching the groundwater and that recharge occurs mainly in winter. A study of southern Nevada precipitation and springs

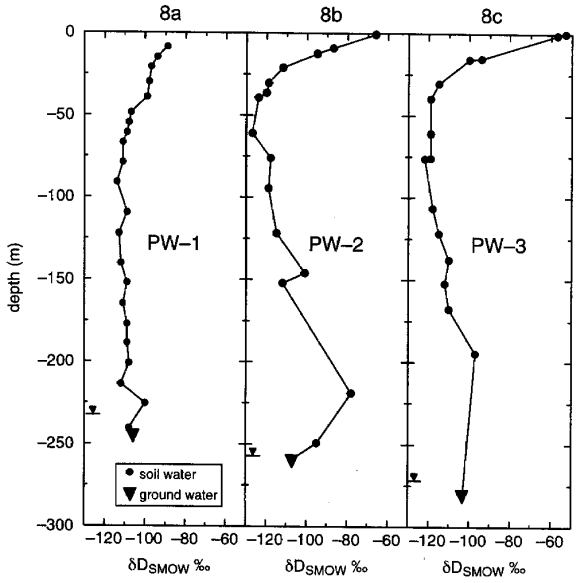

Figure 8. Soil water ^{2}H concentrations from boreholes PW-1, PW-2, and PW-3. Note the isotopic enrichment in the upper 25–35 m of each borehole, suggesting long-term evaporation. Solid triangle represents isotopic composition of groundwater.

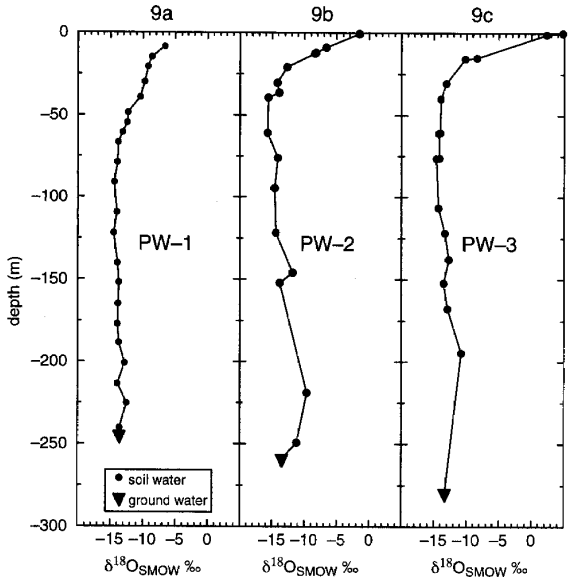

Figure 9. Soil water ^{18}O concentrations from boreholes PW-1, PW-2, and PW-3. Note the isotopic enrichment in the upper 25–35 m of each borehole, suggesting long-term evaporation. Solid triangle represents isotopic composition of groundwater.

[*Ingraham et al.*, 1991] concluded that both winter and summer precipitation events contributed to spring discharge in the NTS area, but that summer recharge occurred only as a result of exceptionally large precipitation events. One of the springs in the study is located approximately 13 km from our study area.

Several workers have established that direct rain infiltration and recharge is widespread in arid regions [*Mazor et al.*, 1974; *Gat and Issar*, 1974; *Dincer et al.*, 1974], but localized infiltration from runoff events, which may possess a different isotopic signature, can also be expected. Runoff from higher elevations, such as the adjacent Massachusetts Mountains (elevation 1,600 m), may introduce water of different isotopic signatures to lower elevation areas. Isotopic variation due to orographic effects on the NTS are generally small, however. An isotopic sampling station located 25 km north of the site at an elevation of 1,590 m had a mean weighted $\delta^{18}O$ composition of $-11‰$, very similar to that measured at the site. Runoff events have been documented during all seasons, which, combined with the similar isotopic composition of precipitation at higher elevations, implies that modern infiltration can be represented by the weighted mean of the local precipitation ($\delta^{18}O = -10.5‰$, $\delta D = -80‰$).

The progressive enrichment in heavy isotopes near the land surface (Figures 8 and 9), coupled with the low slope of the shallow soil data (Figure 7), indicates that the enrichment is due to evaporation occurring in the shallow soil zone. Low slopes were determined by *Allison* [1982] to be typical for the isotopic relationship developed by evaporation from relatively dry soils. The evaporation line defined by the shallow soil data joins the deeper samples as well as the meteoric water line at an isotopic composition much more depleted than both the modern precipitation mean and the mean of modern winter precipitation. This implies that the soil water, as well as groundwater, was infiltrated under previous climatic conditions, in concurrence with the soil chloride and ^{36}Cl results. The only evidence of current infiltration may be found in the three samples collected within 1 m of the surface at PW-2 and PW-3. A line formed by the samples from 7.5 cm and 91 cm in PW-3 and 60 cm in PW-2 intersects the LMWL between the weighted mean precipitation value and the weighted mean for winter precipitation. It is logical that these three very shallow samples represent current infiltration affected by evaporation under the present climate. This is also supported by the high water potentials, abundant root distribution, low chloride concentration found in the upper 1 to 2 m of the soil profile, and the shallow penetration of ^{36}Cl bomb pulse [*REECo*, 1994]. The timing of sampling of the PW series boreholes also coincided or directly followed the unusual wet spring of 1992, further supporting the conclusion that the shallowest soil water isotope samples are derived from modern precipitation. This infiltration does not penetrate to 3 m, the next most shallow sample available.

The effects of evaporation on the soil water isotopic composition can be seen to a depth of 39 m in PW-1, 8.5 m in PW-2, and 16 m in PW-3. However, it is not possible to distinguish between enrichment caused directly by evaporation and enrichment attributable to mixing between shallow, evaporated water and deeper soil water. Downward movement of the evaporative signature will occur under diffusive gradients but could also be accelerated by advective movement during brief periods of infiltration. In a diffusion-dominated system the isotope profile reaches a steady state, balanced by downward diffusion and upward evaporation. The characteristic depth of the diffusion profile is defined by the ratio of the combined liquid and vapor diffusivity to the evaporation rate. The great depth of the evaporative signature suggests a low evaporation rate, ranging from 0.2 to 1.0 mm/yr, using the approach of *Barnes and Allison* [1983], considering both liquid and vapor phase diffusion [*Walker et al.*, 1988; *Cook et al.*, 1992]. The diffusion calculations assumed a liquid-phase tortuosity of 0.2 and a gas-phase tortuosity of 0.45, resulting in an effective diffusion coefficient ($D_\ell + D_v$) ranging from 0.0025 to 0.003 m^2/yr, depending on water content. The total porosity used was 0.37, and a soil humidity of 0.99 was assumed for the vapor diffusivity. The upward evaporation rate is higher than that calculated for the geothermally driven vapor flux (0.019 mm/yr, from *Detty et al.*, [1993]) and may reflect enhanced drying owing to seasonal temperature gradients and an upward liquid flow component in addition to the geothermal gradient.

The depth of the observed isotopic enrichment implies a very long time of development. A simple estimate of the time required for these profiles to develop can be obtained by assuming a purely diffusional transport of isotopes from the evaporating front at the land surface through the underlying vadose zone and neglecting any advection due to evaporation. The upper boundary is taken to be constant and equal to that of the observed enriched concentration found at the soil surface while the rest of the profile initially has the concentration currently found at the water table. Solution of the diffusion equation for these boundary and initial conditions was calculated using the diffusion parameters described above. For borehole PW-2 these calculations result in an estimate of 20 to 30 kyr needed for the development of the observed isotope profile in PW-2. This time period agrees well with the chloride age dates of the soil water, suggesting that the soil profile has not experienced any significant infiltration events since the last time of groundwater recharge at the end of the Pleistocene. Calculations for PW-3 yield larger estimates of up to 60 kyr for diffusional profile development due to the deeper penetration of the enriched isotopic signature. The isotope profile at PW-1 does not exhibit the exponential shape expected for diffusion-dominated profiles, nor were sufficient shallow samples available to accurately fit the diffusion solution.

Although the above calculations provide a general range of time needed to develop such deep enriched profiles, application of a diffusion model is a simplification. Deep infiltration events may occur in response to short-term periods of increased rainfall and runoff that are not necessarily associated with major climate changes. Such infiltration would tend to carry the enriched water to depth, resulting in a diffuse profile. Occasional deep infiltration would increase the depth of enriched isotopes in the profile, and the estimated diffusion times would represent a maximum time of development.

Deep Soil-Water Isotope Profile

Soil-water data below the zone of evaporative enrichment record infiltration that must have occurred under past climate conditions. Similarity of the slopes of the current LMWL and the trend of the deep soil data suggests that recharge in the past was from moisture sources the same as those at present, although at a cooler temperature. The displacement of the soil trend to the right of the LMWL may reflect slight evaporation during infiltration, as suggested by *Allison et al.* [1984]. The spread in composition of the deep soil water data as shown in Figure 7 may be due to the preservation of "packets" of water infiltrated under slightly different, but still pluvial, climates.

Three packets are definable in the PW-2 profile: one containing the most depleted water in the soil profile, located just below the enriched zone and extending to at least 61 m below land surface; a section containing soil water with an intermediate composition (δD of -112 to -119‰) from 61 to 152 m; and then a more enriched bulge deeper in the profile containing water with an isotopic composition comparable to the current precipitation weighted mean. All of the profiles share the presence of enriched water to varying degrees at depth. These enriched values do not deviate from the deep soil water trend and are therefore not suggestive of evaporation from drying by the low-humidity air used during drilling, although this cannot be ruled out conclusively. Because they do not appear evaporated, their enrichment may be indicative of recharge under warmer climatic conditions or precipitation patterns dominated by summer precipitation.

The presence and persistence of these deep isotopic variations are somewhat surprising, given the estimated ages of the soil water deep in the vadose zone. However, these variations, or lack thereof, can be used to support the relative ages of soil water in the three boreholes. Both PW-1 and PW-3 show only modest variation in the distribution of ^{2}H and ^{18}O below approximately 100 m (see Figures 8 and 9). The chloride age dates for these deep waters are up to 110 ka. In contrast, PW-2, with its chloride age of only 20 to 35 kyr, shows significant departures at depths of approximately 150 m and 225 to 250 m, as well as a much more pronounced minimum at 50 to 60 m. The persistence of these departures is consistent with the chloride data, as the soil water in PW-2 may be much younger with less time to diffuse these pulses than both PW-1 and PW-3.

Direct age dating can be done only if the diffusive and advective constants (vapor diffusivity, thermal vapor diffusivity, liquid diffusivity, etc.) are known. However, by using reasonable estimates of diffusion constants, recharge rates, and input time periods, estimates of persistence times for pulses of isotopically different water can be made. Using the approach of *Cook et al.* [1992], the persistence time, t_p, can be calculated as

$$t_p \approx \frac{t_i^2 R^2}{D\pi^2\theta_\ell^2} \ln\left[\frac{4f}{\pi}\right] \quad (3)$$

where t_i is the timescale of the isotopically different recharge; R, the recharge rate during that time; D, the effective diffusion coefficient (including both vapor and liquid components); θ_ℓ, the water content; and f, a factor chosen to express the reduction in concentration over the persistence period. For the calculation of persistence time the reduction factor used was 5.0 [*Cook et al.*, 1992]. A single value for volumetric water content (0.10), representative of the deep soils at the site and the other parameters were as described previously, was used, resulting in an effective diffusion coefficient of 0.003 m^2/yr for combined liquid and vapor diffusion. Using a recharge rate of 10 mm/yr (roughly the rate suggested by the chloride concentrations at depth) and an input signal lasting 200 years (reflecting a short-term climate shift), the persistence time for the resulting 20-m-wide isotope pulse is 25,000 years. Such a signal could reasonably be preserved in the PW-2 profile, but would be lost from PW-1 and PW-3 if the waters are as old as predicted by the chloride profiles. The small isotopic variations seen deep in the PW-1 and PW-3 profiles may be the remnants of larger pulses, either recharged during periods of higher recharge rates or for longer periods of time (>500 years).

The groundwater collected from the PW series boreholes is significantly depleted in the heavy isotopes as compared to both the weighted mean of current precipitation and the weighted mean of winter-only precipitation. The depletion is large enough (>10‰ in δD even as compared to the winter values) to strongly indicate that the groundwater was recharged under previous climatic conditions. Either these conditions would have been cooler, or more precipitation would have fallen in the cooler months, or both. This coincides with estimates of conditions in the southern Great Basin during the last glacial interval and that prior to Termination II. The source of much of the aquifer recharge may not have been derived from the overlying vadose zone, however, as the chloride concentrations in the soil water are elevated slightly over the groundwater.

Carbon 14 Age Dating of Groundwater and Soil Water

Carbon 14 was used to date both groundwater and soil water from the site. Groundwater sampling was conducted with a low-volume piston pump to collect a large-volume sample (100 L), with the carbon precipitated within 24 hours as strontium carbonate. Two samples each were collected from PW-1 and PW-2, separated by several months, and one sample from PW-3. The samples from PW-1 differed markedly from one another at 21.2 ± 1% and 14.4 ± 0.4% modern carbon (PMC) (12,800 and 16,000 radiocarbon years, respectively). The two samples from PW-2 agreed closely with each other at 27.1 ± 0.4 and 28.4 ± 1.6 PMC. This gives an uncorrected ^{14}C age of approximately 10,500 radiocarbon years. The hydrogeologic setting and repeatability of the PW-2 samples argue against a temporal change in ^{14}C in PW-1 between samplings. Given that sample contamination by atmospheric CO_2 is more likely than contamination by dead carbon, the older age is considered more accurate. PW-3 contained 17.1 ± 0.4 PMC, yielding a radiocarbon age of approximately 14,500 years. These ages are consistent with ages reported from other wells in Frenchman Flat [*Byer*, 1991]. Carbon 13 (^{13}C) varied from δ values (as referenced to PDB) of -7.9 to -7.3‰.

All of the groundwater ages imply recharge during the late Wisconsinan, contrary to the chloride ages of soil water in PW-1 and PW-3. The discrepancy may be evidence that groundwater recharge in the Frenchman Flat basin is not always evenly distributed spatially. Recharge to the aquifer is likely to have occurred in the surrounding highlands and along ephemeral streams where conditions are most conducive to recharge.

Age dating of arid-zone soil water via ^{14}C is only recently possible due to the small sample sizes that can be analyzed with a tandem accelerator. Samples were collected and stored in the identical fashion as the stable isotope samples. Soil water was extracted by washing the soil with a CO_2-free water, created by boiling ultrapure distilled water. The washing and subsequent filtering and addition of strontium carbonate and sodium hydroxide were performed under a nitrogen atmosphere. The resultant precipitate was split, with part retained for ^{13}C determination, and part sent with an aliquot of wash water to Lawrence Livermore National Laboratory for ^{14}C analysis. The wash water was found to retain 0.5 to 1 mg/L HCO_3^-. This bicarbonate was assigned a ^{14}C concentration of 111 PMC and corrected from the soil wash analysis. Of greater concern is the possibility for contamination from the drilling air. For the deeper PW boreholes, generally more drilling air and difficulties were encountered which could have led to significant con-

tamination of the samples. As with the stable oxygen and hydrogen isotopes, there is no systematic difference between the samples collected during auger drilling at ST-1 and those collected during drilling with air in the PW holes (in both cases, the samples were collected by driving a core barrel ahead of the drill bit). However, ^{14}C is expected to be more sensitive to contamination problems than the stable isotopes because it is present in trace quantities. If contamination were to have occurred, the ^{14}C composition of the soil water would be shifted toward the modern value.

A total of five soil-water samples were analyzed; however, the results are not consistent with piston flow from the surface to the water table. For example, the sample collected at 30 m from PW-2 had 13 PMC, while a sample from 146 m in the same well had 19 PMC. The highest ^{14}C concentration, 25 PMC, was found in a sample from 54 m in PW-1. Two samples collected from near the same depth in ST-1 (at 30.8 and 33.5 m) agreed fairly well with 17 and 19 PMC, respectively.

The ^{14}C concentrations in PW-1 and ST-1 lead to soil-water ages (11,000 to 15,000 radiocarbon years) much younger than those indicated by the chloride accumulation, but the ages at PW-2 are in general agreement (14,000 to 17,000 radiocarbon years), well within the uncertainty of the chloride method. Though the discrepancy at PW-1 could be a result of inappropriate assumptions for the chloride calculations such as the presence of nonpiston flow, it is also likely that the ^{14}C content is not an accurate indicator of soil-water residence time. Diffusion of gaseous CO_2 through the unsaturated zone was shown to be an important transport mechanism by *Thorstenson et al.* [1983] and results in apparent ^{14}C ages much younger than the actual soil-water residence time. Calculations for ^{14}C diffusion in these soils using representative diffusion and exchange coefficients indicate that significant addition of atmospheric ^{14}C is likely. The interpretation of the soil-water ^{14}C data with respect to the other chemical and isotopic indicators must await continued research into the processes controlling gaseous carbon diffusion in the unsaturated zone.

Relation Between Paleoclimate and Borehole Tracers

The tracer data from the three boreholes show distinct similarities as well as major differences in their response to climatic changes. Each of the boreholes displays the characteristic chloride "bulge" and enriched isotopes found in many arid vadose zones having little or no current recharge [*Phillips*, 1994]. Prior to the beginning of the accumulation phase, the vadose zone appears to have experienced a period of areally widespread recharge to the water table to produce the low concentrations currently found at depth. Boreholes PW-1 and PW-3 both show a long duration of chloride accumulation (approximately 100 to 120 kyr) broken by a period of downward advective transport represented by a secondary chloride peak centered at 40 and 85 m, respectively. Based on chloride age dating and a simple model of dispersive transport, the timing of onset of the advective phase was approximately 40 to 50 ka. Stable isotopic profiles from these boreholes indicate net upward movement in the shallow soil zone (ranging from 8.5 to 39 m), owing to evapotranspiration and thermal gradients. The depletion of the isotopic composition of the deep soil water as compared to the current precipitation indicates that the soil waters infiltrated during a colder period when the precipitation was depleted in heavy isotopes. The only soil water resembling current precipitation is found in the upper 0.9 m of the vadose zone. The ^{36}Cl in all soil waters below the root zone shows enrichment compared to modern values, indicative of water infiltrated during times of a weaker geomagnetic field.

In contrast to these boreholes, PW-2 shows a much shorter duration of chloride accumulation, representing only the last 20 to 30 kyr. Chloride concentrations deep in the profile indicate a previous period of recharge. The isotopic profile is similar to the other boreholes, although once below the upper enriched section, the profile exhibits greater variation in isotopic concentration than either PW-1 or PW-3. These major differences in hydrologic responses and timing of events cannot be logically assigned to any climatic differences, as the boreholes are within 3 km of one another and differ in elevation by less than 40 m. Other evidence must be investigated to explain the tracer distributions. We first develop a simple chronology of events based on the inferred climatic history of the region over the last 150 kyr.

Figure 10 summarizes the general climatic trends in moisture as inferred from the paleoclimatic indicators in the region. Between 150 and 120 ka, the global climate record indicates a major transition (Termination II) from a full glacial maximum. Locally, the period was marked by a general warming, an increase in pluvial lake areas [*Smith*, 1987; *Jannick et al.*, 1991], and a period of significant groundwater recharge. From this time to the next glacial maximum at 18 ka the region experienced a general cooling. Several records (Browns Room and marsh deposits) also indicate moist conditions predominating up to 40 ka. Precipitation along with maximum cooling culminated at around 18 ka. As in the previous glacial maximum, pluvial lakes reached their maximum at or slightly after this termination.

The implications to vadose zone flux from these broad climatic regimes are significant and correlate well with the tracer data presented. At the time of Termination II (approximately 120 ka), precipitation was high and vegetation may have been in a transition phase. Opportunity for recharge at all three boreholes would have been high. This is the approximate age calculated for the accumulations of chloride found in both PW-1 and PW-3. After this period, recharge significantly decreased or ceased through the vadose zone at PW-1 and PW-3 with chloride beginning to accumulate. The flux conditions at PW-2 cannot be determined, owing to complete flushing of the profile at a much later time.

The period of advective transport responsible for the secondary bulges at PW-1 and PW-3 has been calculated to begin at 40 and 50 ka, respectively, based on the chloride ages of the soil water, but the data were not sufficient to estimate when this phase ended. Several of the paleoclimatic indicators suggest that this period was moist, although not to the same magnitude as the period from 15 to 35 ka. This aborted recharge event through the vadose zone was then followed by a chloride accumulation phase (that continues to this time), indicating an ending to recharge. The timing of the cessation of recharge at PW-2 is later, in the range of 20 to 30 ka. This period is recognized by all of the paleoclimate indicators as a major pluvial period. The disparity in timing of these events in the vadose zone may indicate that the recharging event lasted from 50 to 20 ka, and/or the age difference may be due to residual chloride in the upper portions of the vadose zone in both PW-1 and PW-3.

If the above hypothesis is correct, then the timing of re-

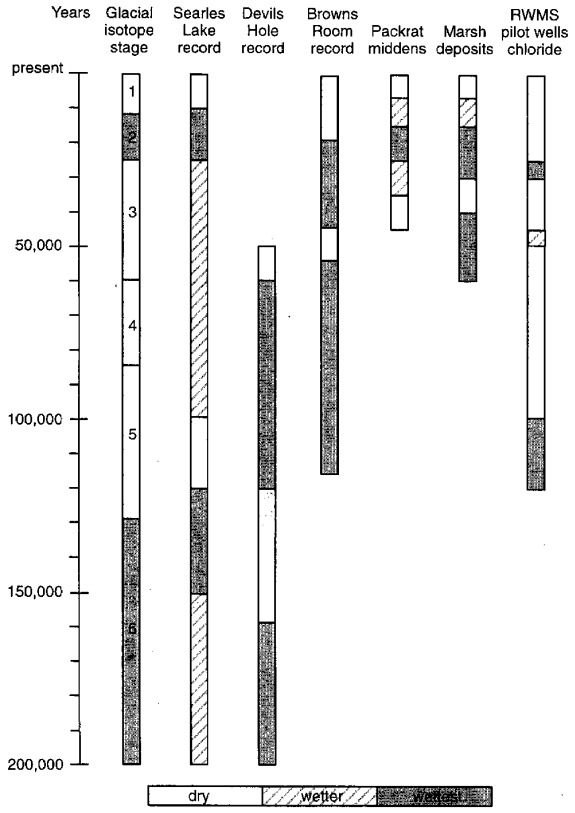

Figure 10. Summary of interpretations from paleoclimatic indicators. Glacial isotope stages are those from the marine $\delta^{18}O$ record. Our assignment of "wettest" corresponds to glacial maximum stages, when regional climates are often interpreted as cooler and wetter. The Searles Lake record is as reported by *Jannick et al.* [1991]. Periods of overflow are designated here as "wettest," with fluctuating lake levels designated as "wetter" than present. The Devils Hole record is from *Winograd et al.* [1988], with "wettest" periods corresponding to their periods of short groundwater residence time. The Browns Room record shows the water table fluctuations in a room of Devils Hole reported by *Szabo et al.* [1994]. The packrat midden record includes the plant fossil interpretations of *Spaulding* [1985], with "wettest" corresponding to his interpretation of late Wisconsin full glacial conditions and "wetter" coinciding with periods of increasing and decreasing effective moisture before and after. The marsh deposit record is from *Quade* [1986], with "wettest" periods coinciding with widespread standing water at groundwater discharge locations south of the RWMS. The RWMS pilot well record summarizes the chloride results presented in this paper. "Wettest" periods correspond to the flushing of chloride from PW-1 and PW-3 profiles (100 to 120 ka) and from PW-2 (24 to 30 ka). "Wetter" corresponds to the aborted flushing of the secondary chloride bulge in PW-1 and PW-3, assumed to have occurred at approximately 50 ka.

charge and aborted recharge corresponds to the period of pluvial conditions in the mid-Wisconsinan to late Wisconsinan glaciation between 15 and 30 ka. Following this period, the vadose zone at each borehole responded to the more xeric environment, and the evapotranspiration requirements utilized most of the precipitation. Recharge continued in favorable environments, perhaps along washes and at upland margins, as indicated by the younger ^{14}C ages of the regional groundwater; however, the vadose zone sampled at this lower elevation became effectively isolated from the underlying groundwater. *Szabo et al.* [1994] also found reasonable correlation between Great Basin paleoclimate records and water level fluctuations at Browns Room. Similar to the record from Browns Room, our vadose zone record contains no indication of increased infiltration subsequent to the last glacial maximum, despite records of intermittent high lake levels in other parts of the Great Basin near the Pleistocene-Holocene boundary.

While the timing of events can be reasonably correlated between the boreholes, the issue of the apparent spatial variability in recharge remains. During the last glacial maximum, significant recharge to the water table appears to have occurred only at PW-2. At the other two boreholes, infiltration was only able to move 40 to 80 m. Although the boreholes are close in proximity, there are several differences that may have led to different responses to the same climatic forcing.

Textural and hydraulic properties measured on cores from the three boreholes show slight but consistent differences. Of the three boreholes, cores and cuttings from PW-1 have the lowest average percentage of <200 mesh (74 μm) size particles, while PW-2 contains the highest percentage [*REECo*, 1994]. The difference is not readily explained, as PW-1 is located on the more distal portion of the Halfpint alluvial fan than is PW-2. However, the vadose zones of all three boreholes are derived from several alluvial fan systems with some significant differences in catchment size and in source rock, ranging from Tertiary volcanics to Paleozoic carbonates [*Snyder et al.*, 1994]. During the deposition of the vadose zone material, the relative dominance of any one of these sources has undoubtedly shifted with time. As a result, the underlying sediment sorting and distribution may not follow the current surface topography.

These slight differences in texture are also manifested in the differences in saturated conductivity measured on cores from the various boreholes. The saturated hydraulic conductivities from the upper 60 m of PW-2 are generally less than those found at similar depths in PW-1 [*Sully et al.*, 1993]. While the saturated conductivities may be greater at PW-1, this may indicate that the unsaturated conductivity in PW-1 may be less than that in PW-2 at the same water potential. Under these conditions, infiltrating water would move more slowly at PW-1 and could remain near the surface, where evapotranspiration may remove much of the water. As a result, net infiltration could be significantly reduced. In contrast, the higher unsaturated conductivity at PW-2, under the conditions of a wetter climate, may have allowed a deeper penetration of surface moisture beyond the reach of vegetation and evaporation.

Perhaps a more significant influence on recharge mechanisms in arid regions is surface topography [*Allison et al.*, 1994]. In arid regions, local ponding or concentration of runoff can be a major factor in controlling the magnitude of recharge. In particular, channelization of flow across the alluvial surfaces may lead to increased recharge. Surficial mapping and aerial photography of the fan surfaces have revealed the presence of a major lineament that crosses the PW-2 drill site from northeast to southwest [*Carr et al.*, 1967; *Miller et al.*, 1993]. Detailed trenching across this lineament in several locales has revealed no evidence of fault control, however. The likely explanation for the formation of this lineament is that it is associated with the alluvial fan morphology. At present, the western edge of

the Halfpint alluvial fan is coincident with this lineament. Coalescing alluvial fans emanating from the Massachusetts Mountains to the west intersect the western edge of the Halfpint alluvial fan, concentrating overland flow within a well-defined channelized zone along the lineament. At the PW-2 drill site a small confined active channel is presently located within 20 m of the PW-2 borehole. Field evidence also suggests that the edge of a series of older fans from the north also delineated this feature in the past [*Snyder et al.*, 1994], implying a consistency in enhanced runoff. During times of increased runoff it is probable that this feature would result in more frequent flooding of the area adjacent to borehole PW-2 and therefore increase the likelihood of recharge.

In contrast, no such flow-concentrating mechanism currently exists at either PW-1 or PW-3. The drill site of PW-1 lies on the more distal portions of the Halfpint alluvial fan and shows no evidence of channelized flow. The drill site of PW-3 lies on coalescing alluvial fans emanating from the Massachusetts Mountains. The drainage areas for these fans are smaller than that for the Halfpint fan and therefore does not supply the same volume of water for runoff and recharge. As at PW-1, there is no evidence of recurrent channel flow at the PW-3 drill site.

The importance of topography and channel control on recharge is further supported by recent shallow drilling around the perimeter of the RWMS. Boreholes drilled to depths of 80 m in clearly defined channels showed significantly less accumulated chloride and enriched isotopic concentration than those boreholes drilled in the interfluve areas. Such topographic features may be contributing recharge under the modern climate and are important hydrologic features to be considered in the design of waste disposal facilities.

Conclusions

The data presented represent the first use of very deep (>230 m) vadose zone borehole data to reconstruct paleohydrologic behavior. The results presented suggest that a variety of soil-water tracers are needed to reconstruct the paleohydrology of the vadose zone. Both soil-water chloride and ^{36}Cl clearly show that the soil waters were infiltrated during the late Pleistocene. The stable isotopic composition of the soil water demonstrates that recharge is not occurring under present climatic conditions at the deep boreholes and that the timescales needed for isotopic profile development are consistent with late Pleistocene recharge. Carbon 14 analysis of groundwater supports this conclusion, while soil-water ^{14}C shows the effect of gaseous diffusion. Local-scale heterogeneity in topography and soil texture also play a role in the magnitude of the vadose zone response to climate change. The vadose zone at the study site has responded to the major climatic shifts of the last 120 ka. Recharge is evident under more pluvial climates, most likely prior to full glacial maximum conditions at approximately 20 and 120 ka, when other indicators suggest general pluvials. The nature and extent of the pluvial at 120 ka were sufficient to induce recharge even in the lowest portions of the basin. The most recent pluvial, however, may not have been sufficient to induce deep infiltration everywhere, and recharge to the water table was not widespread. During this last period, recharge was controlled not only by climate, but also by surface geomorphology in which a drainage channel may have brought more surface water to the area above borehole PW-2. Soil textural differences which define the unsaturated hydraulic conductivity may also have played a role in determining the spatial distribution of recharge.

The strong correlation between climate and recharge in arid settings is clearly shown in the data from this site. Borehole profiles document up to 120,000 years of climate history and vadose zone response. The secondary chloride bulges represent the first known observations of aborted recharge during this period. Preservation of these responses is due to the low rates of diffusion and dispersion of the tracers in the extremely dry soil, the deep water table and the continuity of the sedimentary sequence. Such attributes are similar to those found in the deep ice core records. These data represent the first use of deep vadose zones to infer climatic histories over timescales commensurate with the detailed ice core records from Greenland and the Antarctic. The site drilled represents one of the more shallow vadose zones in the southern Great Basin [*Winograd*, 1981] and clearly opens the possibility for other records to be developed using the drilling and tracer technologies developed in this current effort.

Acknowledgments. The research upon which this paper is based was supported by grants and contracts from the United States Department of Energy. Accordingly, the U.S. Government retains a nonexclusive, royalty-free license to publish or reproduce the published form of this contribution, or allows others to do so, for U.S. Government purposes. Special thanks go to the analytic laboratory support from Donald Brandvold (Cl), Scott Wightman and Marc Caffee (^{36}Cl), Craig Shadel (^{2}H, ^{18}O, ^{13}C, and ^{14}C), and Lee Davisson (^{14}C). The authors also wish to express their appreciation to the anonymous reviewers, whose detailed comments were very helpful in improving the clarity and focus of the manuscript.

References

Allison, G. B., The relationship between ^{18}O and deuterium in water in sand columns undergoing evaporation, *J. Hydrol.*, *55*, 163–169, 1982.

Allison, G. B., and M. W. Hughes, The use of environmental tritium and chloride to estimate total local recharge to an unconfined aquifer, *Aust. J. Soil Res.*, *16*, 181–195, 1978.

Allison, G. B., C. J. Barnes, M. W. Hughes, and F. W. Leaney, Effect of climate and vegetation on oxygen-18 and deuterium profiles in soils, *IAEA-SM-270/20*, pp. 105–123, Int. At. Energy Agency, Vienna, 1984.

Allison, G. B., G. W. Gee, and S. W. Tyler, Vadose-zone techniques for estimating ground-water recharge in arid and semiarid regions, *Soil Sci. Soc. Am. J.*, *58*, 6–14, 1994.

Bard, E., B. Hamelin, R. G. Fairbanks, and A. Zinder, Calibration of the ^{14}C timescale over the past 30,000 years using mass spectrometric U-Th ages from Barbados corals, *Nature*, *345*, 405–410, 1990.

Barnes, C. J., and G. B. Allison, The distribution of deuterium and ^{18}O in dry soils, 1, Theory, *J. Hydrol.*, *60*, 141–156, 1983.

Byer, R. M., A carbon-14 calibrated discrete-state compartment model of the ground-water flow system, Yucca Mt. and vicinity, Nevada-California, M.S. thesis, 249 pp., Univ. of Nev., Reno, 1991.

Carr, W. J., G. D. Bath, D. L. Healey, and R. M. Hazlewood, Geology of northern Frenchman Flat, Nevada Test Site, *U.S. Geol. Surv. Techn. Lett. NTS-188*, 25 pp., 1967.

Cook, P. G., W. M. Edmunds, and C. B. Gaye, Estimating paleorecharge and paleoclimate from unsaturated zone profiles, *Water Resour. Res.*, *28*, 2721–2731, 1992.

Dettenger, M. D., Reconnaissance estimates of natural recharge to desert basins in Nevada, USA, by using chloride-mass balance calculations, *J. Hydrol.*, *106*, 55–87, 1989.

Detty, T. E., D. P. Hammermeister, D. O. Blout, M. J. Sully, R. L. Dodge, J. Chapman, and S. W. Tyler, Water fluxes in a deep arid-region vadose zone, *Eos Trans. AGU*, *74*(43), Fall Meet. Suppl., 297, 1993.

Dincer, T., A. Al-Mugrin, and U. Zimmermann, Study of the infiltration and recharge through the sand dunes in arid zones with special

reference to the stable isotopes and thermonuclear tritium, *J. Hydrol., 23*, 79–109, 1974.

Elmore, D., B. R. Fulton, M. R. Clover, J. R. Marsden, H. E. Gove, H. Naylor, K. H. Purser, L. R. Kilius, R. P. Beukens, and A. E. Litherland, Analysis of chlorine-36 in environmental water samples using an electrostatic accelerator, *Nature, 227*, 22–25, 1979.

Edmunds, W. M., and N. R. G. Walton, A geochemical and isotopic approach to recharge evaluation in semi-arid zones—past and present, in *Arid Zone Hydrology: Investigations with Isotopic Techniques*, pp. 47–68, Int. At. Energy Agency, Vienna, 1980.

Fabryka-Martin, J., S. J. Wightman, W. J. Murphy, M. P. Wickham, M. W. Caffee, G. J. Nimz, J. R. Southon, and P. Sharma, Distribution of chlorine-36 in the unsaturated zone at Yucca Mt.: An indicator of fast transport paths, paper presented at FOCUS '93: Site Characterization and Model Validation, Las Vegas, Nev., Sept. 26–29, 1993.

Fontes, J. C., Palaeowaters, in *Stable Isotope Hydrology, Deuterium and Oxygen-18 in the Water Cycle*, edited by J. R. Gat and R. Gonfiantini, pp. 273–302, Int. At. Energy Agency, Vienna, 1981.

Fouty, S. C., Chloride mass balance as a method for determining long-term ground-water recharge rates and geomorphic surface stability in arid and semiarid regions: Whiskey Flat and Beatty, Nevada, M.S. thesis, Univ. of Ariz., Tucson, 1989.

French, R. H., Daily, seasonal and annual precipitation at the Nevada Test Site, *Water Resour. Cent. Publ. 45042*, 58 pp., Desert Res. Inst., Reno, Nev., 1986.

Gat, J. R., Groundwater, in *Stable Isotope Hydrology, Deuterium and Oxygen-18 in the Water Cycle*, edited by J. R. Gat and R. Gonfiantini, pp. 223–240, Int. At. Energy Agency, Vienna, 1981.

Gat, J. R., and A. Issar, Desert isotope hydrology: Water sources of the Sinai Desert, *Geochim. Cosmochim. Acta, 38*, 1117–1131, 1974.

Haynes, C. V., Quaternary geology of the Tule Springs area, Clark County, Nevada, in *Pleistocene Studies in Southern Nevada, Pap. 13*, edited by H. M. Wormington and D. Ellis, pp. 1–104, Nev. State Mus. of Anthropology, Carson City, Nev., 1967.

Ingraham, N. L., and C. Shadel, A comparison of the toluene distillation and vacuum/heat method for extracting soil water for stable isotopic analysis, *J. Hydrol., 140*, 371–387, 1992.

Ingraham, N. L., B. F. Lyles, R. L. Jacobson, and J. W. Hess, Stable isotope study of precipitation and spring discharge in southern Nevada, *J. Hydrol., 125*, 243–258, 1991.

Jannick, N. O., F. M. Phillips, G. I. Smith, and D. Elmore, A ^{36}Cl chronology of lacustrine sedimentation in the Pleistocene Owens River system, *Geol. Soc. Am. Bull., 103*, 1146–1159, 1991.

Jones, B. F., Mineralogy of fine grained alluvium from Borehole U11g, Northern Frenchman Flat Area, Nevada Test Site, *U.S. Geol. Surv. Open File Rep., 82-765*, 1982.

Jolly, I. D., P. G. Cook, G. B. Allison, and M. W. Hughes, Simultaneous water and solute movement through the unsaturated zone, *J. Hydrol., 111*, 391–396, 1989.

Junge, C. E., and R. T. Werby, The concentration of chloride, sodium, potassium calcium and sulfate in rain water over the United States, *J. Meteorol., 15*(5), 417–425, 1957.

Mattick, J. L., T. A. Duval, and F. M. Phillips, Quantification of ground-water recharge rates in New Mexico using bomb ^{36}Cl, bomb ^{3}H and chloride as soil water tracers, *Rep. 220*, 184 pp., N. M. Water Resour. Res. Inst., Las Cruces, N. M., 1987.

Mayewski, P. A., et al., Changes in atmospheric circulation and ocean ice cover over the North Atlantic during the last 41,000 years, *Science, 263*, 1747–1751, 1994.

Mazaud, A., C. Laj, E. Bard, M. Arnold, and E. Tric, Geomagnetic field control of ^{14}C production over the last 80 KY: implications for the radiocarbon timescale, *Geophys. Res. Lett., 18*, 1885–1888, 1991.

Mazor, E., B. T. Verhagen, J. P. F. Sellschop, N. S. Robins, and L. G. Hutton, Kalahari groundwaters: Their hydrogen, carbon and oxygen isotopes, in *Isotope Techniques in Groundwater Hydrology*, pp. 203–225, Int. At. Energy Agency, Vienna, 1974.

Mifflin, M. D., and D. D. Wheat, Pluvial lakes and estimated pluvial climate of Nevada, *Nev. Bur. of Mines and Geol. Bull., 94*, 57 pp., Mackay School of Mines, Univ. of Nev., Reno, 1979.

Miller, J. J., D. L. Gustafson, and K. E. Snyder, Lineaments identified in northern Frenchman Flat, Nye, Lincoln and Clark counties, Nevada, scale 1:12,000, Raytheon Serv. Nev., Las Vegas, 1993.

Phillips, F. M., Environmental tracers for water movement in desert soils of the American southwest, *Soil Sci. Soc. Am. J., 58*, 15–24, 1994.

Phillips, F. M., J. L. Mattick, T. A. Duval, D. Elmore, and P. W. Kubick, Chlorine-36 and tritium from nuclear-weapons fallout as tracer for long-term liquid and vapor movement in desert soils, *Water Resour. Res., 24*, 1877–1891, 1988.

Phillips, F. M., P. Sharma, and P. Wigand, Deciphering variations in cosmic radiation using cosmogenic chlorine-36 in ancient rat urine, *Eos Trans. AGU, 72*(44), Fall Meet. Suppl. 72, 1991.

Quade, J., Late Quaternary environmental changes in the upper Las Vegas Valley, Nevada, *Quat. Res., 26*, 340–357, 1986.

Quade, J., and W. L. Pratt, Late Wisconsin groundwater discharge environments of the southwestern Indian Springs Valley, southern Nevada, *Quat. Res., 31*, 351–370, 1989.

Reynolds Electrical and Engineering Company (REECo), Site characterization and monitoring data from area 5 pilot wells, Nevada Test Site, Nye County, Nevada, *Contract. Rep. DOE/NV/11432-74*, Nev. Oper. Off., U.S. Dep. of Energy, Las Vegas, 1994.

Scanlon, B. R., Evaluation of moisture flux from chloride data in desert soils, *J. Hydrol., 128*, 137–156, 1991.

Scanlon, B. R., Evaluation of liquid and vapor movement in desert soils based on chlorine 36 and tritium tracers and nonisothermal flow simulations, *Water Resour. Res., 28*, 285–297, 1992.

Smith, G. I., Paleohydrologic regimes in the southwestern Great Basin, 0–3.2 my ago, compared with other long records of "global" climates, *Quat. Res., 22*, 1–17, 1984.

Smith, G. I., Searles Valley, California: Outcrop evidence of a Pleistocene lake and its fluctuations, limnology, and climatic significance, in *Centennial Field Guide*, vol. 1, edited by M. L. Hill, pp. 137–142, Geol. Soc. of Am. Cordillian Sect., Boulder, Colo., 1987.

Smith, G. I., I. Friedman, J. D. Gleason, and A. Warden, Stable isotope composition of waters in southeastern California, 2, Groundwaters and their relation to modern precipitation, *J. Geophys. Res., 97*, 5813–5823, 1992.

Snyder, K. E., D. L. Gustafson, J. J. Miller, and S. E. Rawlinson, Geological components of site characterization and performance assessment for a radioactive waste management facility at the Nevada Test Site, *DOE/NV/10833-20*, 13 pp., Raytheon Services Nevada, Las Vegas, Nev., 1994.

Spaulding, W. G., Vegetation and climates of the last 45,000 years in the vicinity of the Nevada Test Site, South-Central Nevada, *U.S. Geol. Surv. Prof. Pap. 1329*, 55 pp., 1985.

Spaulding, W. G., and L. J. Graumlich, The last pluvial climatic episodes in the deserts of southwestern North America, *Nature, 320*, 441–444, 1986.

Stone, W. J., Paleohydrological implications of some deep soil water chloride profiles, Murray Basin, South Australia, *J. Hydrol., 132*, 201–223, 1992.

Sully, M. J., D. E. Cawfield, D. O. Blout, L. E. Barker, B. L. Dozier, and D. P. Hammermeister, Characterization of the spatial variability of hydraulic properties of an arid region vadose zone, *Eos Trans. AGU, 74*(43), Fall Meet. Suppl., 286, 1993.

Szabo, B. J., P. T. Kolesar, A. C. Riggs, I. J. Winograd, and K. R. Ludwig, Paleoclimatic inferences from a 120,000-year calcite record of water-table fluctuation in Browns Room of Devils Hole, Nevada, *Quat. Res., 41*, 59–69, 1994.

Thorstenson, D. C., E. P. Weeks, H. Haas, and D. W. Fisher, Distribution of gaseous $^{12}CO_2$, $^{13}CO_2$ and $^{14}CO_2$ in the subsoil unsaturated zone of the western United States, *Radiocarbon, 25*(2), 315–346, 1983.

Tric, E., J. P. Valet, P. Pucholka, M. Paterne, L. Labeyrie, F. Guichard, L. Tauxe, and M. Fontugune, Paleointensity of the geomagnetic field during the last 80,000 years, *J. Geophys. Res., 97*(B6), 9337–9351, 1992.

Tyler, S. W., J. B. Chapman, S. H. Conrad, and D. Hammermeister, Paleoclimatic response of a deep vadose zone in southern Nevada as inferred from soil water tracers, in *Proceedings of the First International Symposium on Tracers in Arid Settings, Vienna, Austria, 1994.*

U.S. Department of Agriculture, Diagnosis and improvement of saline and alkali soils, *Agric. Handb., 69*, 160 pp., 1954.

Vogel, J. C., and H. Van Urk, Isotopic composition of groundwater in semi-arid regions of southern Africa, *J. Hydrol., 25*, 23–36, 1975.

Vogel, J. C., D. Ehhalt, and W. Roether, A survey of the natural isotopes of water in South Africa, in *Radioisotopes in Hydrology*, pp. 407–415, Int. At. Energy Agency, Vienna, 1963.

Walker, G. R., M. W. Hughes, G. B. Allison, and C. J. Barnes, The movement of isotopes of water during evaporation from a bare soil surface, *J. Hydrol., 97*, 181–197, 1988.

Wallace, A., S. A. Bamberg, and J. W. Cha, Quantitative studies of roots of perennial plants in the Mojave Desert, *Ecology, 55*, 1160–1162, 1974.

Wells, P. V., and C. D. Jorgensen, Pleistocene wood rat middens and climatic change in Mohave Desert—a record of juniper woodlands, *Science, 143*, 1171–1174, 1964.

Wells, P. V., and R. Berger, Late Pleistocene history of coniferous woodland in the Mojave Desert, *Science, 155*, 1640–1647, 1967.

Winograd, I. J., Radioactive waste storage in thick unsaturated zones, *Science, 212*, 1457–1464, 1981.

Winograd, I. J., and G. C. Doty, Paleohydrology of the southern Great Basin, with special reference to water table fluctuations beneath the Nevada Test Site during the late (?) Pleistocene, *U.S. Geol. Surv. Open File Rep. 80-569*, 91 pp., 1980.

Winograd, I. J., B. J. Szabo, T. B. Coplen, and A. C. Riggs, A 250,000-year climatic record from Great Basin vein calcite: Implications for Milankovitch Theory, *Science, 242*, 1275–1280, 1988.

Winograd, I. J., T. B. Coplen, J. M. Landwehr, A. C. Riggs, K. R. Ludwig, B. J. Szabo, P. T. Kolesar, and K. M. Revesz, Continuous 500,000-year climate record from vein calcite in Devils Hole, Nevada, *Science, 258*, 255–287, 1992.

Yonge, C. J., D. C. Ford, J. Gray, and H. P. Schwarcz, Stable isotope studies of cave seepage water, *Chem. Geol., 58*, 97–105, 1985.

Zimmermann, U., D. Ehhalt, and K. O. Munnich, Soil water movement and evapotranspiration: Changes in the isotopic composition of the water, in *Proceedings of the IAEA Symposium on Isotope Hydrology*, Int. At. Energy Agency, Vienna, 1967.

D. O. Blout, Daniel B. Stephens and Associates, Inc., 509 N. Texas St., Silver City, NM 88061.

J. B. Chapman, Water Resources Center, Desert Research Institute, P.O. Box 19040, Las Vegas, NV 89132.

S. H. Conrad, Sandia National Laboratories, P.O. Box 5800, Albuquerque, NM 87185.

J. M. Ginanni, U.S. Department of Energy, Nevada Operations Office, P.O. Box 98512, Las Vegas, NV 89193.

D. P. Hammermeister, 1500 W. Montana, Silver City, NM 88061.

J. J. Miller and M. J. Sully, Bechtel-Nevada Corporation, P.O. Box 98521, Las Vegas, NV 89193.

S. W. Tyler, Water Resources Center, Desert Research Institute, P.O. Box 60220, Reno, NV 89506.

(Received February 17, 1995; revised February 16, 1996; accepted February 19, 1996.)

This page intentionally left blank.

Appendix B

Scenario Analysis: The Affects of Climate Change and Subsidence on Unsaturated Flow Beneath the GCD Boreholes

This page intentionally left blank.

Scenario Analysis: The Effects of Climate Change and Subsidence on Unsaturated Flow Beneath the GCD Boreholes

Prepared by:

Elena Kalinina
GRAM, Inc.

Dick Thomas and John Cochran
Environmental Risk and Decision Analysis Department
Sandia National Laboratories

Bill Fogleman
GRAM, Inc.

March 31, 2000

ACKNOWLEDGEMENT

Special thanks to Faith Puffer of Tech Reps for her technical editing and publishing support.

LIST OF ACRONYMS

1-D	one-dimensional
2-D	two-dimensional
3-D	three-dimensional
AIC	active institutional control
AMC	antecedent moisture conditions
CAD	Compliance Assessment Document (GCD)
DOE	United States Department of Energy
DOE/NV	U.S. Department of Energy/Nevada Operations Office
EPA	U.S. Environmental Protection Agency
GCD	Greater Confinement Disposal
GCDT	GCD Test
HMS	Hydrologic Modeling System
LLW	low-level waste
LP-III	Log-Pearson III
msl	mean sea level
NTS	Nevada Test Site
PA	performance assessment
PE	potential evaporation
PET	potential evapotranspiration
PMF	Probable Maximum Flood
PMP	Probable Maximum Precipitation
RWMS	Radioactive Waste Management Site
SCS	Soil Conservation Service
SIP	strongly implicit procedure
SNL	Sandia National Laboratories
TRU	transuranic
USGS	United States Geological Survey

CONTENTS

FIGURES

TABLES

This page intentionally left blank.

1.0 INTRODUCTION

Intermediate depth disposal operations were conducted by the U.S. Department of Energy (DOE) from 1984 through 1989. As a part of those operations, classified transuranic (TRU) wastes were disposed in four Greater Confinement Disposal (GCD) boreholes. Sandia National Laboratories (SNL) has been tasked to conduct a performance assessment (PA) to help the DOE/Nevada Operations Office (DOE/NV) determine whether these TRU wastes meet the U.S. Environmental Protection Agency's (EPA's) 1985, 40 CFR 191 requirements for disposal of TRU wastes. This screening analysis was undertaken as a component of the GCD PA.

The GCD wastes are emplaced a minimum of 21 m (70 ft) below the land surface in the thick, arid alluvium at the Area 5 Radioactive Waste Management Site (RWMS). Under current conditions, surface water does not reach the water table at the Area 5 RWMS, and the long-term drying of the land surface is pulling moisture from depth, resulting in the very slow upward flux of pore water to the land surface.

This analysis does not address current conditions. Rather, this analysis addresses the potential for future conditions to be different from current conditions because of the operation of the Area 5 RWMS. Operation of the Area 5 RWMS has placed wastes in the GCD boreholes and the RWMS trenches, which contain a significant amount of void space resulting from the incomplete filling of waste containers, limited internal compaction of contents, and voids between containers. These voids will produce significant subsidence as the waste containers deteriorate and collapse.

This subsidence has the potential to focus precipitation and runoff, which may cause the downward movement of pore water and the formation of ephemeral wetlands. Additionally, numerous studies have shown that over long time spans, the climate could return to cooler and wetter, glacial conditions.

1.1 Why This Screening Analysis was Undertaken

This report presents the results of a detailed screening analysis, which was conducted to determine if surface water might migrate to the water table during the next 10,000 years because of the combined effects of landfill subsidence and the possible return to a glacial climate. If surface water and radionuclides have the potential to reach the accessible environment in the next 10,000 years, this pathway will have to be included in the PA for the TRU wastes in the GCD boreholes.

Four coupled analyses were undertaken for this study:

- the geometry of future subsidence features was modeled;
- using current climatic data, precipitation, local runoff, and flooding were modeled;
- assuming an immediate return to glacial climatic conditions, precipitation, local runoff, and flooding were modeled; and
- the two-dimensional (2-D), and quasi-three-dimensional (3-D) movement of water in the subsurface was modeled, assuming the landfill cap is intact for 10,000 years, and also assuming the landfill cap is instantly "removed."

This screening analysis does not model the movement of radionuclides, nor does it model the movement of water to the accessible environment. Conceptually, water moving through GCD wastes would become contaminated with long-lived radionuclides. The movement of regulated radionuclides would be much slower than the movement of pore water due to chemical sorption of radionuclides onto the alluvium. If it can be shown that pore water moving through the GCD wastes will not reach the water table in 10,000 years, then it is clear that regulated radionuclides will not reach the 5 km (3.1 mi) accessible environment boundary in 10,000 years.

1.2 Background and Site Setting

The DOE/NV operates the Area 5 RWMS, which has been used for disposal of low-level radioactive wastes (LLWs) and TRU wastes. LLWs have been disposed in pits and trenches since 1961. High-specific activity LLW and TRU wastes were disposed in intermediate depth GCD boreholes from 1984 though 1989. See Figure 1.1 for an orthophotograph of the Area 5 RWMS.

The average precipitation at the Area 5 RWMS is 13 cm (5 in.) per year. A number of plants have adapted to this arid climate. These plants are able to rapidly capture infiltrating moisture and then hold and use the moisture through long dry periods.

The Area 5 RWMS is founded in the thick, arid alluvium of Frenchman Flat. This thick alluvium is from coalesced alluvial fans that emanate from the Massachusetts Mountains and Halfpint Range. See Figure 1.2 for an aerial oblique photograph of the Area 5 RWMS and Figure 1.3 for a visualization of the digital terrain model of the Area 5 RWMS.

Based on measurements from a number of characterization wells, the water table is approximately 236 m (775 ft) below the land surface [REECo, 1994]. Figure 1.4 presents an idealized cross-section through the Massachusetts Mountains and Frenchman Flat. The movement of water within this 236-m (775-ft) thick unsaturated zone can be subdivided into two zones; the near surface zone and the deeper zone.

The near surface zone is the hydrologically “active” region of the unsaturated alluvium. In the near surface, precipitation is pulled downward by gravity and is either aided or resisted by the capillary tension of the soil (depending on the moisture content and textural properties of the soil). The forces acting to remove the moisture include evaporation and plant root uptake. The *average* volumetric moisture content in the near surface zone is very low, ranging from 1% to 3%. Based on a number of field studies conducted at the Area 5 RWMS, the balance of these forces is such that (approximately) the upper 2 m (7 ft) is hydrologically active, and areally-distributed infiltration never infiltrates deeper than about 2 m (7 ft).

The deeper vadose zone is hydrologically inactive. The volumetric water content in the deeper zone is approximately 8%. This low-volumetric water content impedes the flow of liquid by significantly reducing the hydraulic conductivity. Between a depth of 2 and approximately 35 m (7 and approximately 115 ft), the alluvium shows decreasingly negative matric potential with depth (for example, (-) 10 bars at 35 m (115 ft) depth and (-) 75 bars at 5 m (15 ft) depth), indicating an *upward gradient in the pore water* (i.e., if the pore water moves, it moves upward and there is no groundwater recharge).

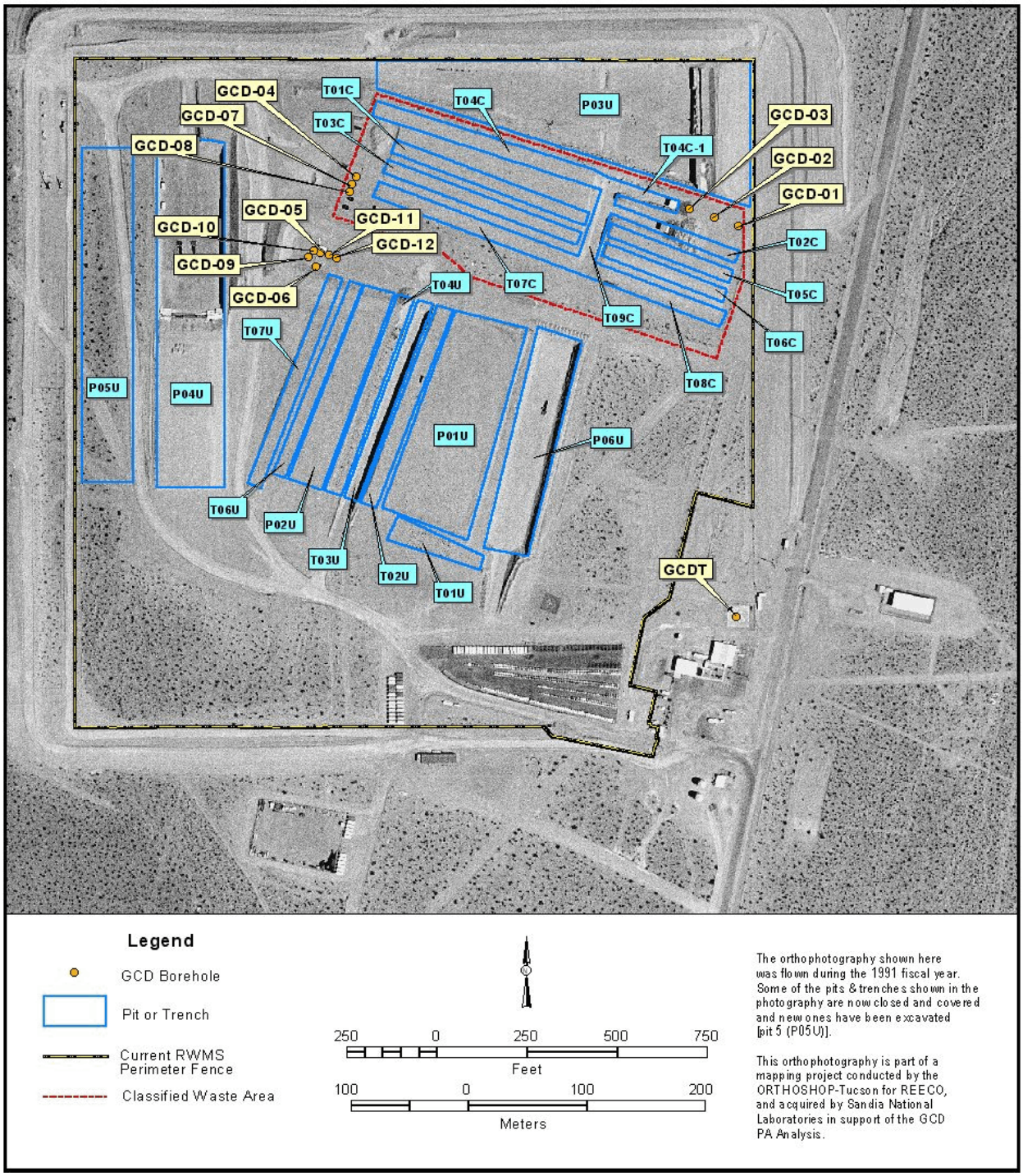

Figure 1.1. Orthophotograph of Area 5 RWMS.

Figure 1.2. Aerial Oblique Photograph of the Area 5 RWMS.

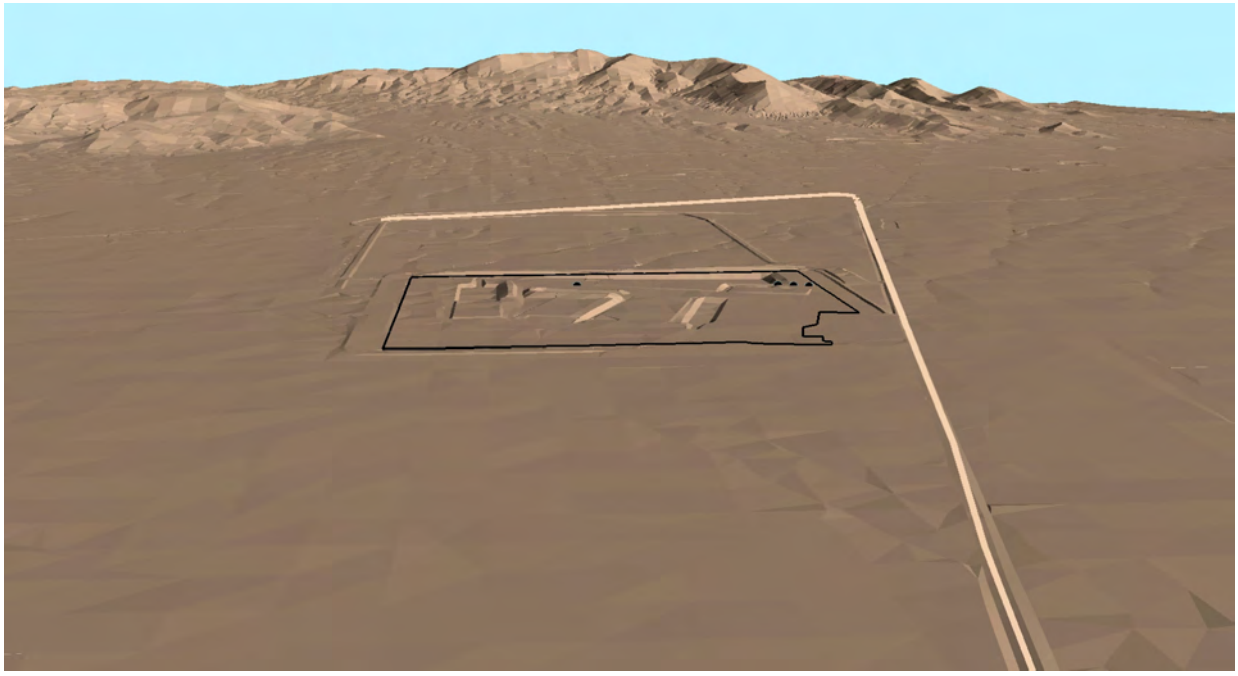

Figure 1.3. Visualization of the Digital Terrain Model of the Area 5 RWMS.

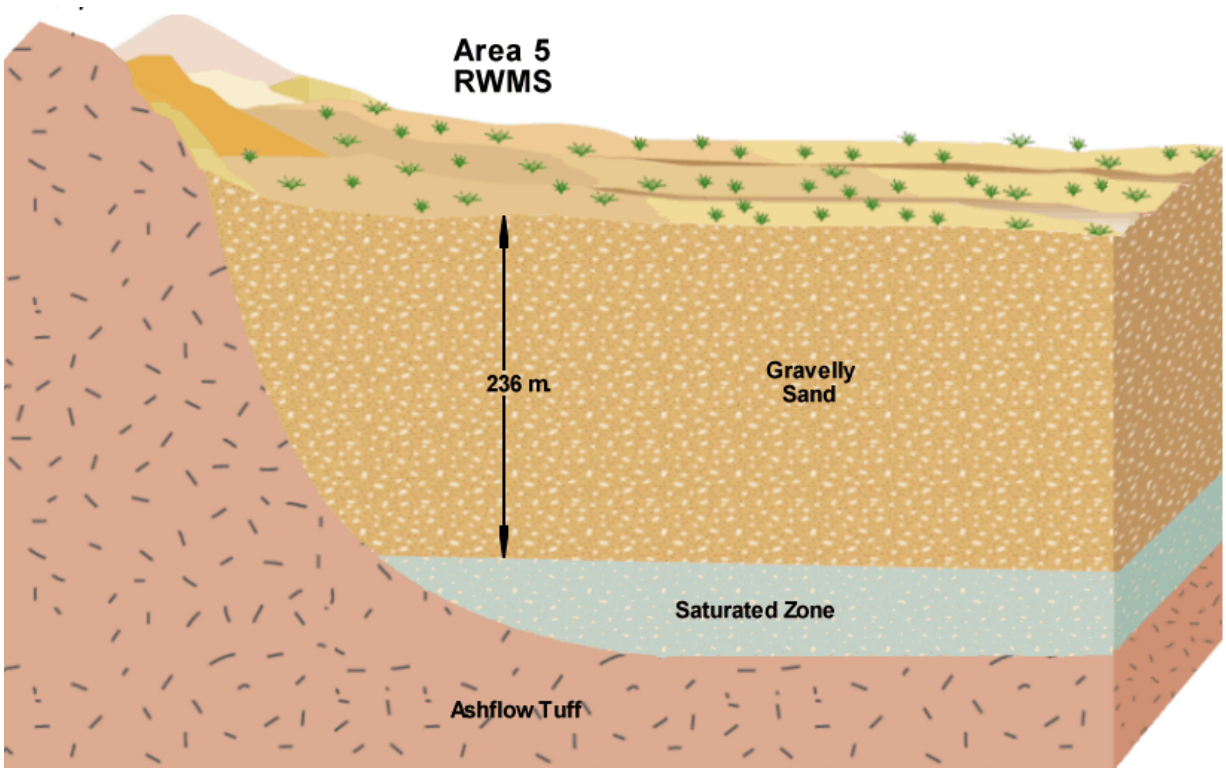

Figure 1.4. Idealized Cross-Section through the Massachusetts Mountains and Frenchman Flat.

A static zone where the hydraulic gradient is negligible exists from approximately 35 to 90 m (115 to 300 ft), and from approximately 90 to 236 m (300 to 775 ft), where very slow gravity drainage is still occurring. Detailed discussions of the deep vadose zone are presented in Shott et al. [1998].

The upward movement of pore water from 35 m (115 ft) deep has been studied extensively and is the result of a system in transition, where the transition times are on the order of thousands of years. As a simplification, the climate was significantly wetter and cooler 150,000 to 120,000 years ago (a superglacial climate) and the water table received areally-distributed recharge. Subsequently, recharge decreased or ceased. Then, from 50,000 to 20,000 years ago, the climate was wetter and cooler (a glacial climate). During this wetter and cooler time period, there was deep infiltration, but no areally-distributed recharge to the water table (see Figure 4 of Tyler et al., 1996). Only under surface-water drainage features was there recharge to the water table 50,000 to 20,000 years ago.

A more xeric environment now exists, and the long-term drying of the land surface is pulling moisture from depth, resulting in the very slow upward flux of pore water evidenced by the soil matric potentials. The limited precipitation, generally warm temperatures, low humidities, and plant uptake of moisture, coupled with the hydrologically homogeneous and isotropic alluvium, results in a hydrologic system dominated by evapotranspiration.

1.3 Climate Change

To assess the potential impact of climate change, SNL examined past global, regional, and site-specific empirical records of proxies of past climatic conditions [Brown et al., 1997]. The following paragraphs provide a summary of that work and the reader is referenced to Brown et al. [1997] for details.

The records of the isotopic oxygen composition of marine sediments [Williams et al., 1988], and thick ice deposits [Dansgaard et al, 1993] provide global scale evidence of past climatic conditions. Studies of the isotopic oxygen composition of calcite deposits in Nevada's Devils Hole spring [Winograd et al., 1988; 1992] provide a 500,000 year record of past climate conditions in the southwestern U.S.

Studies of paleo-vegetation from pack rat middens (e.g., Spaulding, 1990) allow the reconstruction of past vegetation assemblages (and climatic conditions) at the Nevada Test Site (NTS). It is clear that open piñon-juniper woodlands existed at the elevations of the Area 5 RWMS in the geologically recent past.

There is very good agreement between the global ice core records, the regional Devils Hole record, and the local pack rat midden records (e.g., Figure 16 of Brown et al., 1997). *All of the records showed a cyclic pattern of climate change in which the climate varies between relatively persistent glacial climates (cooler, wetter periods) separated by interglacial climates (warmer, drier periods) of relatively short duration.*

At the Area 5 RWMS, cooler and wetter equates to 3E to 5EC cooler, with an average precipitation of about 26 cm (10 in.). A doubling of the amount of precipitation is dramatic; however, climatic conditions at the Area 5 RWMS were still relatively warm and semiarid, with open piñon-juniper woodlands. See Figure 1.5 for a visualization of the Area 5 RWMS under the current interglacial climatic and under glacial, long-term climatic conditions.

The cyclic nature of past climatic conditions is solidly supported by a large number of studies of many different physical phenomena. However, the low resolution of some of the proxy records and the natural variability in the length of the climatic cycles does not allow an accurate estimation of the time when the climate will return to the more dominant, cooler, and wetter conditions.

The accumulation of anthropogenically-derived carbon dioxide (a greenhouse gas) may alter near-term climatic conditions. The effects of anthropogenic climate change were assessed for the nearby, proposed Yucca Mountain facility using an expert elicitation, and it was concluded that anthropogenic climate change will have a negligible impact at the NTS [Dewispelare, 1993].

For the PA, it is assumed that the past climatic conditions can be used to estimate future conditions and responses. Based on this assumption, it was concluded that (1) it is not possible to rule out a return to cooler and wetter conditions over the next 10,000 years, and (2) there is significant uncertainty in the timing of the return to those conditions. For this screening analysis, simulations of precipitation, local runoff, and flooding were conducted assuming that the current

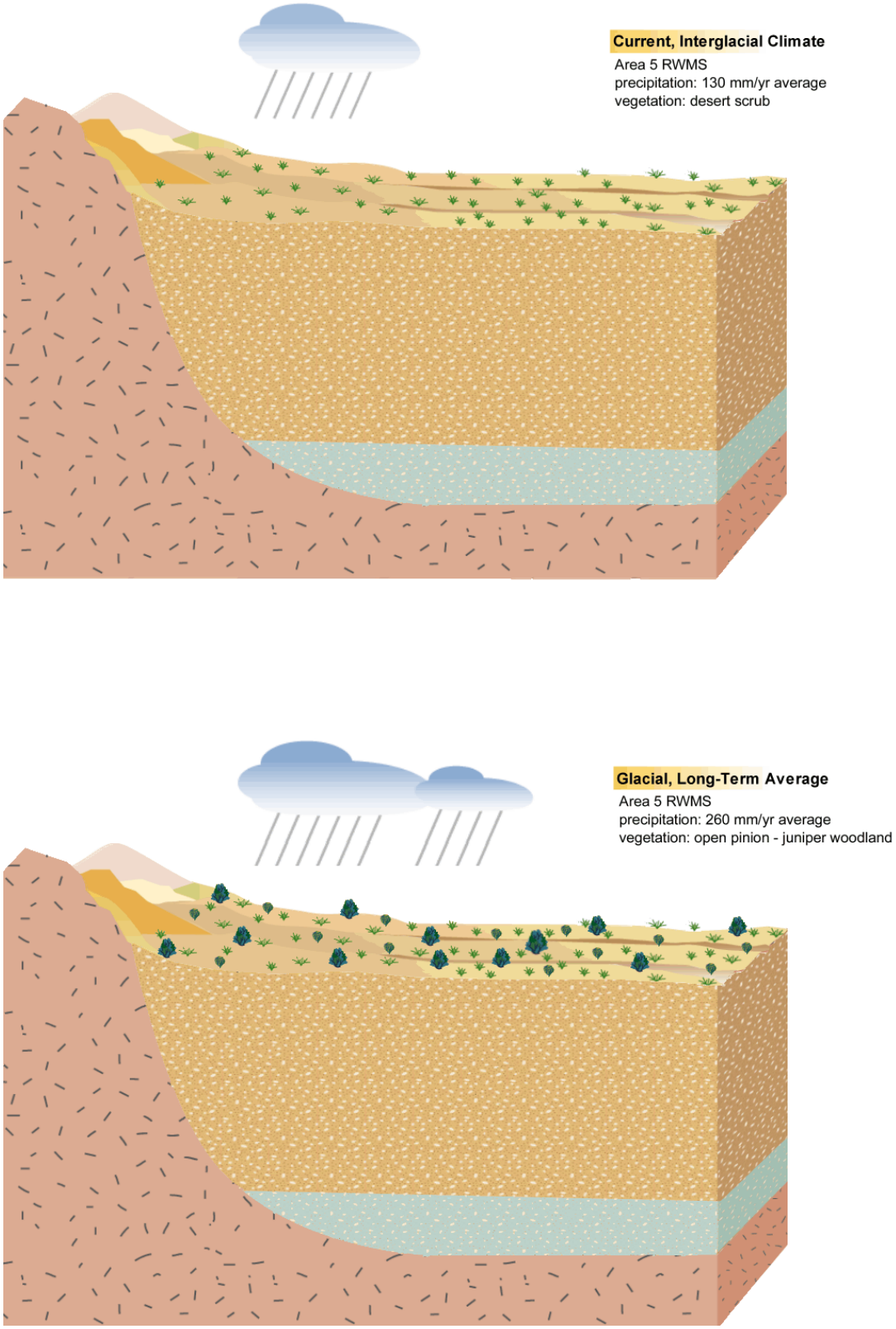

Figure 1.5. Visualization of the Area 5 RWMS Under Current Climatic Conditions and Under Future Glacial Climatic Conditions.

climatic conditions continue for 10,000 years, and simulations of precipitation, local runoff, flooding, and the movement of pore water in the vadose zone were also run assuming a full 10,000 years of glacial climatic conditions.

1.4 Closure

As noted earlier, DOE/NV operates the Area 5 RWMS for the disposal of radioactive wastes, and DOE/NV is responsible for the future closure and monitoring of the Area 5 RWMS. An important issue related to closure is the future subsidence of the disposal cells; DOE [1998] describes the situation.

> Review of waste disposal operations indicated that the waste already placed in the RWMSs contains a significant amount of void space resulting from incomplete filling of waste containers, limited internal compaction of contents, and voids between containers. These voids will produce significant subsidence as the waste containers deteriorate and collapse over time. Additional sources of subsidence include the decomposition of containers, waste, and dunnage. ... over long time periods, the waste and containers would collapse, decompose, and ultimately reach a density similar to that of the surrounding soil materials.

DOE [1998] recommends the construction of an alternative cap that would consist of a single, thick layer of compacted native alluvium constructed to 2 m (7 ft) above the land surface. The intent of this design is to simulate the natural system at the NTS, with particular emphasis on (1) limiting infiltration by enhancing evapotranspiration and (2) using soil materials that have suitable durability and longevity. Figure 1.6 presents a visualization of the capped Area 5 RWMS in the year 2170, and Figure 1.7 presents a visualization of how the Area 5 RWMS might look in the year 2171, assuming that the remaining voids are instantly translated into subsidence features.

Based on forthcoming DOE guidance, DOE plans to operate the Area 5 RWMS until the year 2070. During the next 70 years, a landfill cap that consists of a single, thick layer of compacted native alluvium will be constructed to 2 m (7 ft) above the land surface. DOE would then assume active institutional control (AIC) over the closed landfill. The EPA's standard for disposal of TRU wastes does not allow an analyses to take credit for more than 100 years of AIC (40 CFR 191.14, EPA [1985]). This screening analysis assumes loss of AIC 170 years from now, in the year 2170.

1.5 Overview of the Report

This analysis is based on a systematic evaluation of the potential for surface water to migrate to the water table during the next 10,000 years, due to the combined effects of landfill subsidence, precipitation, flooding, and a return to glacial climatic conditions.

Section 2.0 describes how the geometry of the subsidence features was calculated. This section provides background information and defends the volumes and surface expressions of subsidence features used in this analysis. There is significant uncertainty in the parameters that govern the

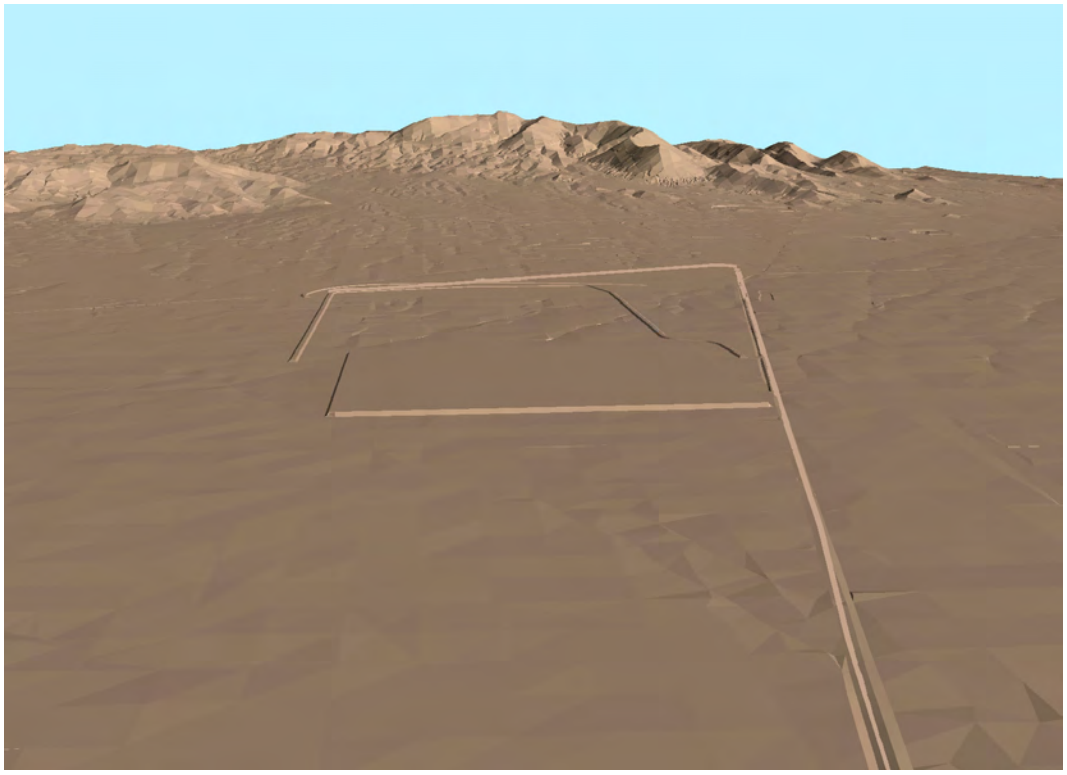

Figure 1.6. Visualization of the Capped Area 5 RWMS in the Year 2170.

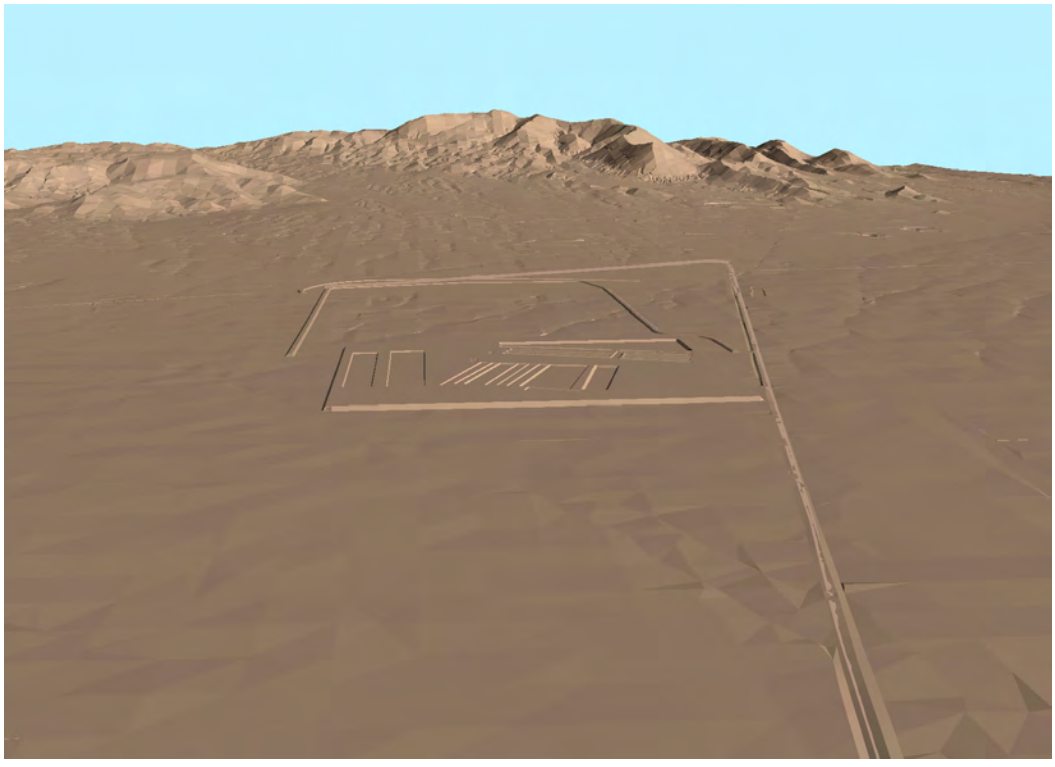

Figure 1.7. Visualization of C Area 5 RWMS in the Year 2171.

timing, volume, and surface expressions of subsidence features that may evolve after the assumed loss of AIC, 170 years from today. Therefore, a number of assumptions are made that maximize the potential volumes of the subsidence features.

Section 3.0 provides an analysis of how much precipitation and surface water runoff might accumulate in the subsidence features. Precipitation records from the local Station B-5 are used to calculate the frequency and magnitude of potential future precipitation events. The magnitude of the Probable Maximum Precipitation (PMP) event is also calculated. Standardized techniques are then used to translate that information into frequencies and volumes of surface water runoff that might accumulate in the subsidence features. These calculations are done for both existing and glacial climatic conditions.

Flooding analysis is provided in Section 4.0, including an estimation of the magnitude and frequency of rare flood events and the Probable Maximum Flood (PMF) for specific watersheds in the Area 5 RWMS. These calculations are done for both existing and glacial climatic conditions to estimate the potential for floods to overtop the landfill cap.

Section 5.0 describes the conceptual models of the unsaturated zone. The mathematical models, initial conditions, boundary conditions, parameters, and other relevant information are presented, as is the calibration of the vadose zone models.

Modeling of the movement of pore water in the vadose zone due to the focusing of surface water by subsidence is the subject of Section 6.0. These calculations are performed for glacial climatic conditions, assuming *the landfill cap remains intact.* It is also assumed that the subsidence features remain intact, focusing surface water for 10,000 years. The redistribution of moisture from both subsided GCD boreholes and subsided LLW trenches is assessed.

Section 6.0 also presents the results of modeling the movement of pore water in the vadose zone due to the focusing of surface water by subsidence. These calculations are performed for glacial climatic conditions, *assuming the cap is instantly removed* and that the subsidence features will eventually fill with sediment entrained in the surface waters. The redistribution of moisture from the most significant LLW trench is assessed.

The sensitivity of these models to specific assumptions is addressed in Section 7.0. A comparison between an "identical" one-dimensional (1-D) and 2-D flow model is also presented in Section 7.0. Section 8.0 then summarizes the key findings of this study.

1.6 Biased Screening Analysis

These screening analyses are not a prediction of how the Area 5 RWMS system will actually respond to subsidence. These analyses are developed in a manner to bias (overestimate) the downward movement of surface water. These biased analyses are not a worst-case, or "incredible" analyses, where all conceptual models and input parameters are maximized. Rather, this screening combines expected conditions, and some very biased conditions, which create an overall bias to the results. Some of the assumptions which clearly bias the outcome are:

- pits and trenches were assumed to contain only steel containers, and the degradation rates of the steel containers were assumed to be one-half of the degradation rates used in previous studies; these assumptions maximize the amount of long-term void space in the Area 5 RWMS

- all voids remaining in the Area 5 RWMS are assumed to be instantly expressed as subsidence features in the year 2170, the time at which AICs are assumed to be lost

C the subsidence features are then assumed to instantly enlarge, based on the angle of repose

C for the intact cap analysis, *the enlarged subsidence features are assumed to remain intact, capturing precipitation and precipitation runoff for 10,000 years*

C to simulate glacial climatic conditions, it was assumed that the average number of precipitation events that occur under the current climate continues to occur under glacial climatic conditions, and that each event produces twice as much precipitation - *this results in approximately five times as much precipitation runoff* as is produced under the current climate (the less conservative approach is to assume that each event under glacial conditions produces the same amount of precipitation as under the current climate, and then double the number of events - this less conservative approach produces only a doubling of precipitation runoff)

C all rare precipitation events were assumed to begin after the loss of AIC in the year 2170. For example, under glacial conditions, the PMP was assumed to occur at time zero (the year 2170), followed by the 10,000-year storm 1.125 years later. A 1,000-year storm was assumed to occur 1.125 years after the 10,000-year storm. The 1000-year storm is followed by nine 100-year storms, each 1.125 years apart. Then this sequence of a 1,000-year storm and nine, 100-year storms was repeated at the year 1000, 2000, etc., through the year 9000.

- high initial moisture conditions were assumed to overestimate the volume of precipitation that flows into the subsidence features as precipitation runoff

C no credit was taken for the future construction of RWMS disposal cells to the north (upstream) of the existing RWMS cells; such cells would block arroyo flood waters from the disposal cells analyzed in this study

C the vadose zone was assumed to be homogeneous and isotropic

C as modeled, soil moisture is only removed from the land surface. *The model does not include the removal of soil moisture by plants*

These assumptions, and others discussed in this report, provide confidence that the potential for surface water to migrate to the water table is overestimated. If surface water will not reach the water table in 10,000 years, then it is clear that regulated radionuclides will not reach the 5-km (3.1-mi) accessible environment boundary in 10,000 years.

This page intentionally left blank.

2.0 ESTIMATION OF SUBSIDENCE AFTER SITE CLOSURE

2.1 Introduction

The current configuration of the Area 5 RWMS includes seven pits, 16 trenches, 12 GCD boreholes, and GCD Test (GCDT). The waste disposed of in the pits, trenches, and GCD boreholes is not compacted and is expected to significantly subside with time. The estimation of the possible subsidence in Area 5 was considered in the following studies:

- Consequences of Subsidence for the Area 3 and Area 5 RWMSs, NTS, Working Group Report [DOE, 1998].

- Modeling Potential Effects of Subsidence at the Area 5 RWMS for the GCD Compliance Assessment Analyses [Brown et al., 1998].

The purposes of this study were:

- to estimate the range of subsidence depths and geometry of the subsided features in the LLW trenches and pits and over GCD boreholes due to degradation and compaction of waste and waste containers,

- to reproduce the landscape of the Area 5 RWMS after the year 2170,

- to generate an input for the surface water runoff analysis and for the unsaturated flow analysis.

The conceptual model and data from the previous studies were used to estimate the range of subsidence depths and geometry. The difference from the previous work was in estimating the range, rather then expected values, of the subsidence depths and in using a different time for the end of the institutional control period.

Estimating the range of subsidence depths in the pits and trenches is considered in Section 2.2. The conceptual model of subsidence above the GCD boreholes and the estimates of subsidence depression depths and radii are considered in Section 2.3.

2.2 Estimation of the Subsidence Depths in Pits and Trenches after Site Closure

The working group analysis [DOE, 1998] concluded that “the Area 5 RWMS could experience subsidence of the waste equal to about 30 percent of the trench/pit depth after about 100 years.” This number (30%) was used then in Brown et al. [1998] to calculate the depth of subsidence expected in the trenches and pits after site closure. This estimate of subsidence depth represents the “expected depth value” calculated using what is believed to be the “best estimates” of the parameter values taken from DOE [1998].

Based on guidance from DOE, it is now assumed that the Area 5 RWMS will be an operational facility until the year 2070. Then, based on 40 CFR 191.14(a) [EPA, 1985], it is assumed that

DOE will actively maintain the closed landfill until the year 2170 (i.e., 170 years from present). The data and conceptual assumptions provided in DOE [1998] were reviewed to calculate the minimum subsidence, probable subsidence, and maximum possible subsidence that may occur after 170 years.

The conceptual model proposed in DOE [1998] to estimate the depths of subsidence assumes a piston (uniform) settlement in a column that consists of waste containers, dunnage (may not be present), and backfill soil. The settlement of each container type is proportional to the container degradation rate and void volume. The total settlement at a specified time is the sum of settling by all the materials present in the columns. Using these assumptions, the total subsidence depth *d*, expressed as a percentage of the total trench/pit depth at a future time *t*, can be calculated as:

$$d(t) = \sum ; i_{=1,k}\ V_i * C_i * G_i(t) \qquad (2.1)$$

where *k* is the number of different container types in the waste column, V_i is the proportion of the *i*-th material volume expressed as a percentage of the total volume of the column, C_i is the maximum reduction volume of the container *i* expressed as a percentage of the total material volume, and $G_i(t)$ is the reduction of the material *i* volume that occurred by the time *t* due to the material degradation expressed as a percentage of the maximum reduction volume of this material.

Equation (2.1) was used to calculate the subsidence depths reported in DOE [1998]. In these calculations, it was assumed that each column of waste consists of one type of container and/or a dunnage. The following types of containers were considered: cardboard boxes, wooden boxes, steel drums, and steel boxes. Maximum reduction values, C_i were defined for each of four container types, wooden dunnage, and for the wooden pallets under containers (Table 2.2). Values for container volume, dunnage volume, and soil volume V_i of the total column volume (Table 2.3) were calculated assuming eight stacking patterns.

- cardboard boxes, dunnage, and soil
- wooden boxes, dunnage, and soil
- wooden dunnage and soil
- steel boxes and soil
- steel drums stacked horizontally and soil
- steel drums stacked vertically, dunnage, and soil
- steel drums stacked randomly and soil
- steel drums stacked horizontally in triangular array and soil

The compression of each container type and dunnage due to degradation and compaction was estimated for the following discrete times: 20, 50, 75, 100, 150, 300, 500, 1000, and 10,000 years (Table 2.1). The decay rates used in these calculations represent the expected values. It was noted in DOE [1998] that "*the decay rate for any of the containers could probably vary by at least factor of 2*." Consequently, the decay rate of each container can change within a large range.

Table 2.1. Time-Dependent Volume Reduction of Different Materials Due to Degradation

Material	Time (yr)									
	0	**20**	**50**	**75**	**100**	**150**	**300**	**500**	**1000**	**10000**
Cardboard	0%	90%	95%	100%	100%	100%	100%	100%	100%	100%
Wooden Boxes	0%	10%	50%	75%	90%	100%	100%	100%	100%	100%
Steel Drums	0%	5%	35%	60%	75%	85%	100%	100%	100%	100%
Dunnage	0%	0%	50%	75%	100%	100%	100%	100%	100%	100%
Wooden Dunnage	0%	5%	20%	50%	75%	90%	100%	100%	100%	100%
Steel Boxes	0%	0%	5%	10%	20%	50%	70%	80%	95%	100%
Dumped Soil	0%	15%	25%	50%	60%	70%	75%	80%	95%	100%

Table 2.2. Maximum Reduction Volume as a Percentage of the Total Initial Volume

Material	Maximum Reduction Volume
Cardboard	44%
Wooden Boxes	44%
Steel Drums	54%
Dunnage	100%
Wooden Dunnage (pallets)	100%
Steel Boxes	44%
Void Space	100%

Table 2.3. Percentage of Different Materials in Waste Column for Different Waste Placement Patterns

Pattern Number	Pattern Composition	Percentage of Material
1	Cardboard boxes	77%
	Dunnage	14%
	Voids	9%
2	Wooden Boxes	77%
	Dunnage	14%
	Voids	9%
3	Wooden Dunnage	33%
	Voids	67%
4	Steel Boxes	90%
	Voids	10%
5	Steel Drums, Horizontal	78%
	Voids	22%
6	Steel Drums, Random	80%

Table 2.3. Percentage of Different Materials in Waste Column for Different Waste Placement Patterns (Continued)

Pattern Number	Pattern Composition	Percentage of Material
	Voids	20%
7	Steel Drums, Vertical	68%
	Dunnage	13%
	Voids	19%
8	Steel Drums, Horizontal-Triangular	91%
	Voids	9%

The greatest uncertainty is in the amount of void space in the containers and the compressibility of the waste. Another uncertainty is related to the percentage of different types of containers within the trench and their location. No information is available to reduce this uncertainty except some photographs taken at the moment of waste emplacement. An example of such a photograph is presented in Figure 2.1.

Figure 2.1. Waste Container Emplacement in a Typical Trench, Area 5 RWMS.

As shown in Table 2.1, all container types will experience noticeable subsidence before the site closure (within the 170-year period). It is assumed that these subsidence features will be filled during the period of AIC (years 2070 through 2170). The total depth of subsidence that will occur after AIC ceases (i.e., after year 2170) is of most interest. This depth will be proportional to the difference between the maximum reduction volume and the reduction volume at the end of the 170-year period.

All of the prior studies point out great uncertainty in the values of the parameters that define the magnitude and timing of subsidence. Moreover, the parameter variability was not characterized. To bound the effects of this uncertainty/variability, the minimum, maximum, and probable values of the expected potential subsidence depths in the pits and trenches were calculated.

2.2.1 Minimum Potential Subsidence Depth in Pits/Trenches

The minimum potential subsidence in pits and trenches after site closure was calculated using data from Tables 2.2 and 2.3 and assuming that the pits and trenches consist only of cardboard containers placed on wooden dunnages. The decay rates for cardboard boxes and dunnages were assumed to be twice as fast as the rates shown in Table 2.1. The results of calculations are demonstrated in Figure 2.2. As it shows, 97% of subsidence occurs before the year 2170, leaving 3% of the subsidence after the year 2170. For the deepest pit at the site (P06U), this would mean a depth equal to 0.40 m (1.3 ft). For most of the trenches, this would mean a depth equal to 0.10 m (0.33 ft). Consequently, subsidence features will hardly be noticeable.

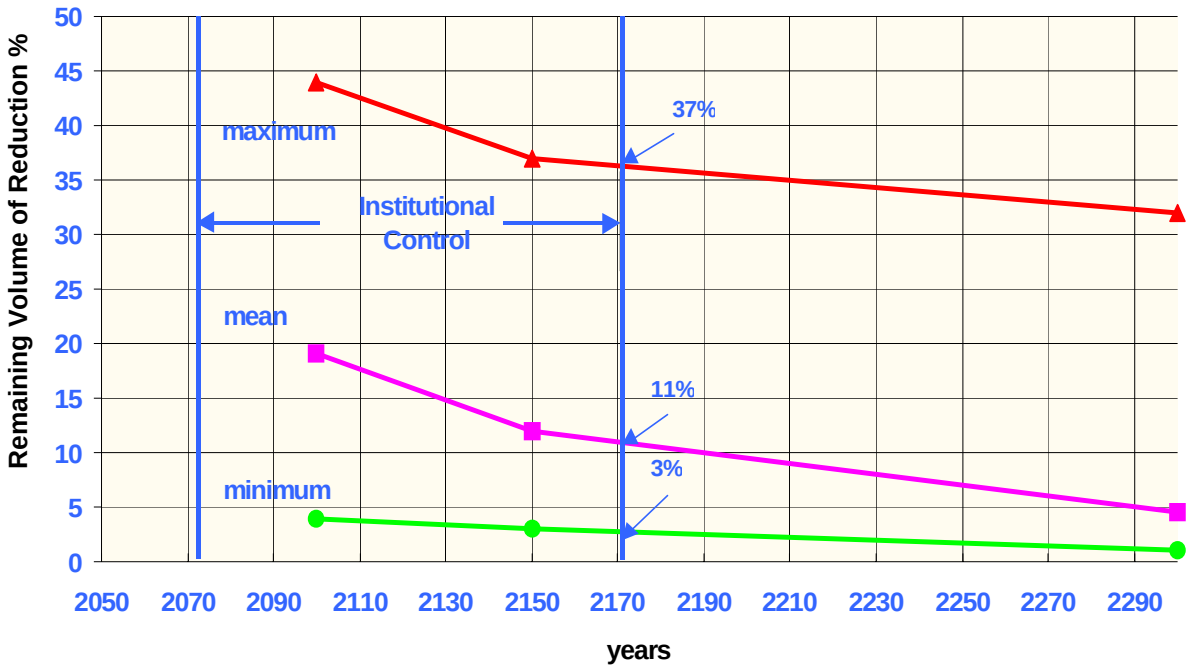

Figure 2.2. Remaining Volume of Reduction in Pits/Trenches, Area 5 RWMS.

2.2.2 Maximum Potential Subsidence Depth in Pits/Trenches

The maximum potential subsidence in pits and trenches was calculated using data from Tables 2.2 and 2.3 and assuming that the pits and trenches consist only of steel boxes. The decay rates for the steel boxes were assumed to be two times slower than the rates shown in Table 2.1. The results of calculations are demonstrated in Figure 2.2. As it shows, 63% of subsidence occurs before the year 2170, leaving 37% of the subsidence after the year 2170. Consequently, the maximum subsidence after the site closure would be from 1.2 m (3.9 ft) (most of the trenches) to 5.0 m (15 ft) (Pit PO6U).

2.2.3 Probable Potential Subsidence Depth in Pits/Trenches

The screening subsidence depth values provided above are calculated assuming very unlikely situations when only cardboard boxes or only steel boxes are placed in the pits and trenches. In reality, a combination of different containers were placed in the pits and trenches. However, there is not enough data to simulate a more realistic situation with different containers and patterns in the pits and trenches. Thus, the random situation was modeled to calculate the most likely subsidence depth. It was assumed that it is equally likely to find any of eight patterns listed above in any pit or trench. The resulting probable subsidence depth was calculated using data from Tables 2.1, 2.2, and 2.3. As shown in Figure 2.2, the most likely subsidence depth to occur after 170 years, according to these calculations, is 11% of the pit/trench depth or 0.4 m (1.3 ft) (most of the trenches).

In an attempt to simulate a more realistic trench, Figure A-1 from DOE [1998] gives a schematic diagram of a waste container disposal in Area 5 RWMS trenches (used to estimate compressibility and total void space for different container types and stacking geometries) to calculate the percentage of each pattern within the trench. These percentages were used to calculate weighted average subsidence depth from data presented in Tables 2.1, 2.2, and 2.3. The weighted average subsidence depth after the year 2170 was equal to 14% of the trench depth, which is comparable to an estimate based on an equal likelihood assumption.

2.2.4 Conclusions

Additional subsidence within the LLW trenches and pits is expected to occur after AICs cease 170 years from now. A wide range for the possible subsidence depths was obtained by estimating minimum and maximum possible reduction volumes remaining after site closure. The estimated subsidence depth varies from 3% to 37% of the waste initial depth. The subsidence features with a depth of 3% of the trench/pit depth could be so small (0.10 m (0.33 ft) for a typical trench) that it would be barely distinguishable from the original relief. The subsidence features with the depth of 37% could be deep enough (1.2 m (3.9 ft) for a typical trench) to look like a large pit. The difference in estimates is due to the uncertainties in the maximum volume reduction for different types of containers, container decay rates and container stacking patterns. No information was available to reduce this uncertainty. Assuming that all the different types of containers are equally likely to be found in the trench brings the subsidence depth down to 11% of the original depth or 0.4 m (1.3 ft) for a typical trench. This depth is the most likely to be observed in the trenches and pits after site closure when the compaction is complete. This time is related to the degradation period of the different types of the waste containers, which could be anywhere from 100 to 2000 years. Since the different types of waste containers could be distributed very differently within the trenches/pits, different depths of subsidence and different rates of subsidence are likely to be observed within the trenches and pits, leading to differential subsidence. However, with time, the subsidence in trenches in pits will become more uniform. This is schematically presented in Figure 2.3.

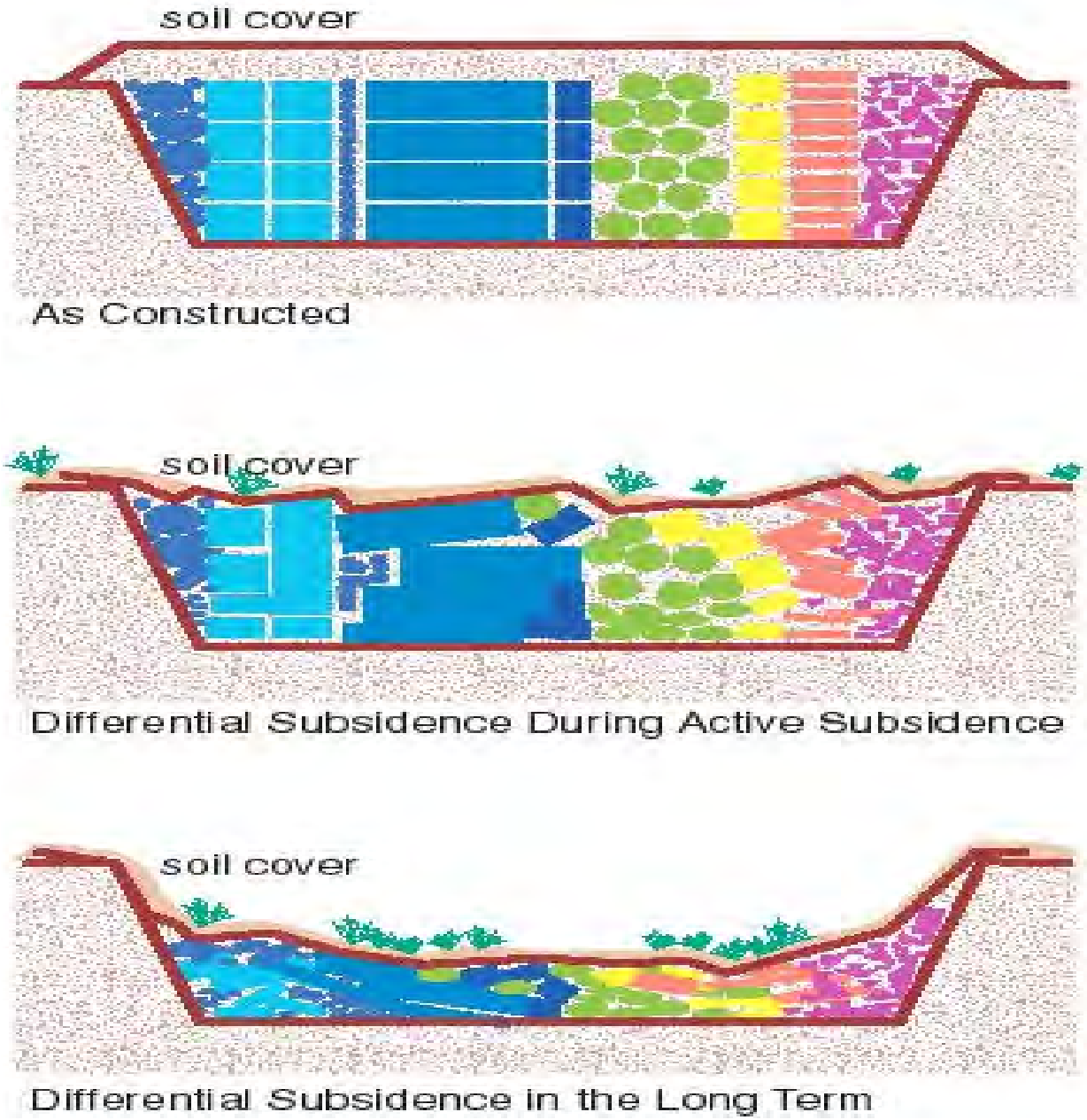

Figure 2.3. Conceptual Model of Waste Container Degradation and Subsidence Processes at the Area 5 RWMS (from Consequences of Subsidence Working Group).

2.3 Estimation of the Subsidence Depths and Radii above the Greater Confinement Disposal Boreholes after Site Closure

The GCD boreholes contain [Chu and Bernard, 1991] Nuclear Weapon Accident Residues (Boreholes 1, 2, and 3) and classified waste (Borehole 4), located at the depth interval from 21 to 36 m (69 to 118 ft). All the boreholes were backfilled using native alluvium. A backfilling of the GCD boreholes is shown in Figure 2.4.

Figure 2.4. The Backfilling of the GCD Borehole.

The magnitude of potential subsidence over the GCD boreholes was estimated in Arnold [1996]. The conceptual model used in this estimate assumes a piston settlement of the waste and backfill soil within a GCD borehole, resulting in piston settlement at the surface with subsequent sidewall collapse in accordance with the angle of repose and formation of the cone-shaped depression. The volume of this cone-shaped depression is assumed to be equal to the reduction volume of the waste and soil within the borehole. The depth *d* and the radius *R* of the cone at the time *t* are given by the following equations:

$$d(t) = \left[3 * V(t) * \mathrm{tang}^2(\varphi)\right]^{1/3} \tag{2.2}$$

and

$$R(t) = d(t) / \tan(\varphi), \tag{2.3}$$

where $V(t)$ is reduction volume at the time t and n is the repose angle. This conceptual model is schematically presented in Figure 2.5.

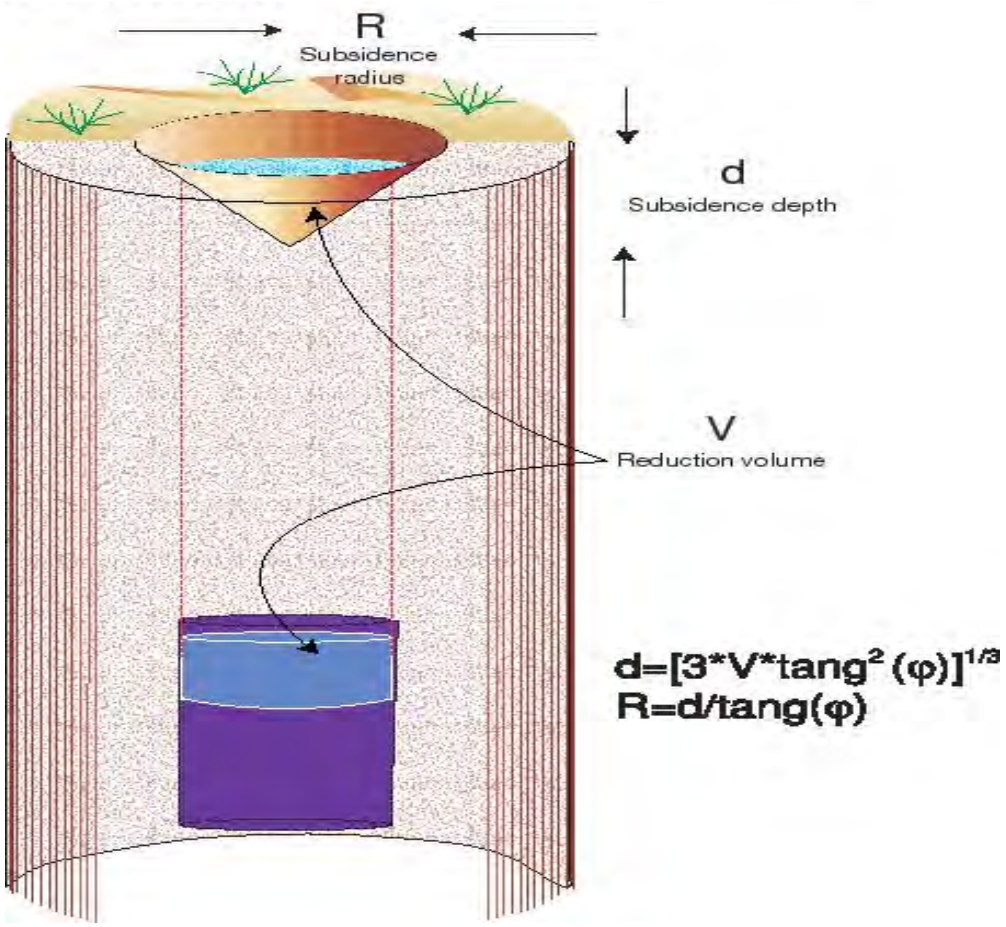

Figure 2.5. Conceptual Model of Subsidence above the GCD Borehole.

The estimates of the degradation rates for different container types provided in DOE [1998] were not available in 1996 and only the maximum reduction volumes were calculated for each of the GCD boreholes in Arnold [1996] (see Attachment A). This is summarized in Table 2.4. In Brown et al. [1998], the subsidence depths and radii were calculated using maximum reduction volume values from Arnold [1996] (see Attachment A), assuming that the reduction volume at 100 years will be 60% of the maximum reduction volume.

The same conceptual model was used to estimate the depths and radii of the subsidence depressions above the GCD boreholes after the year 2170. The only difference from Brown et al. [1998] was in the calculation of reduction volume at the year 2170. This calculation used

Table 2.4. Total Maximum Void Volume Estimated for the GCD Boreholes [Arnold, 1996; see Attachment A]

Borehole Number	Maximum Void Volume, m^3
1	93.87
2	81.11
3	42.29
4	93.87

conceptual model and degradation rate data from DOE [1998]. The waste stored in GCD Boreholes 1, 2, and 3 is placed in metal boxes with the plywood covers [Chu and Bernard, 1991]. The waste in Borehole 4 is placed in 258 drums and eight boxes. Since no data are available from DOE [1998] on the degradation rates of boxes that have both metal and plywood lids, the degradation rates for steel boxes were used. The degradation rate of drums was assumed to be the same as the degradation rate of boxes, even though according to data provided in Table 2.1, steel drums degrade faster than steel boxes. The minimum and maximum subsidence depth and radius values were estimated to define the range for these parameters.

2.3.1 Maximum Potential Subsidence Depths and Radii above the Greater Confinement Disposal Boreholes

The maximum reduction volume within the GCD borehole was calculated using the following assumptions:

- The waste container degradation rate is two times slower than the steel box degradation rates from Table 2.1.

- The maximum volume reduction of the metal boxes is 85% of the initial volume of the boxes based on calculations from Arnold [1996], which is significantly greater than the 44% volume reduction assumed for steel boxes in DOE [1998]. This is due to the loose packaging of waste in the GCD containers.

- The void volume of the backfill soil due to poor compaction of the backfill comprises 10% of the backfill column volume, which is the same as in DOE [1998]. In Arnold [1996] it was noted that this volume is extremely uncertain and is probably within the 0% to 30% range. A value of 10% was selected to maintain consistency with the DOE [1998] estimates.

Using Equation (2.1) with these parameter values yields a change in the subsidence depth with time (which is equivalent to the change in reduction volume) demonstrated in Figure 2.6. As this figure shows, the reduction volume at the year 2170 is 36%. The corresponding subsidence depth calculated using Equation (2.2) and expressed as a percentage of maximum subsidence depth is 86%, and so is the subsidence radius expressed as a percentage of maximum subsidence radius. The absolute values of the subsidence depths and radii for GCD Boreholes 1, 2, 3, and 4 are summarized in Table 2.5.

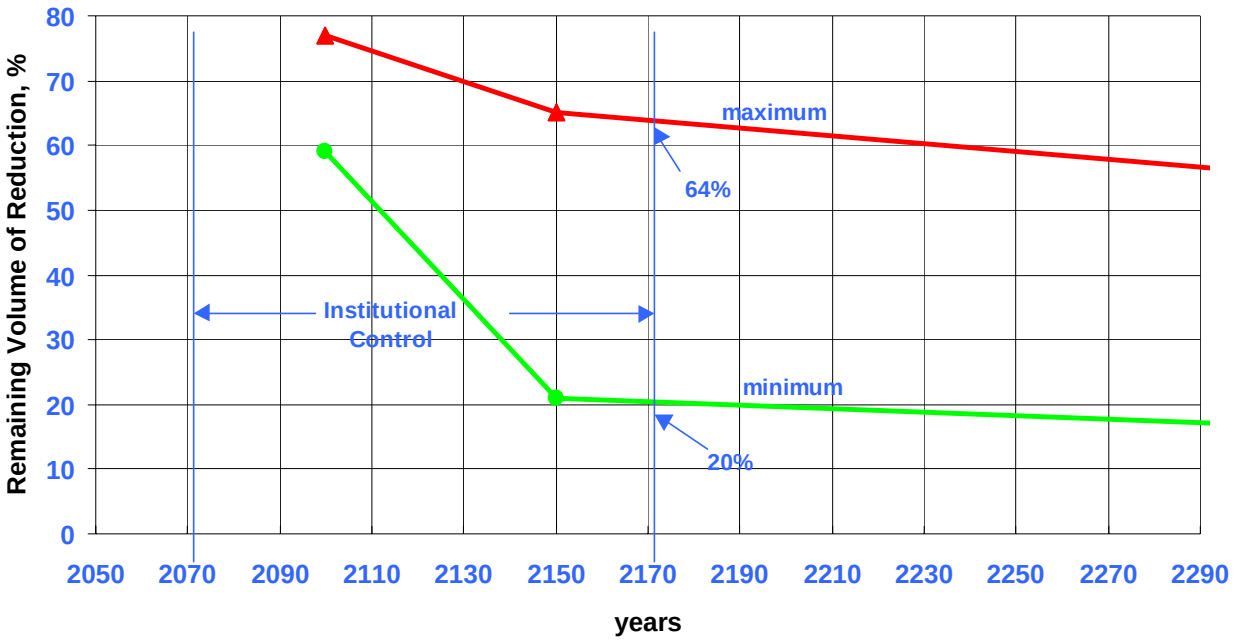

Figure 2.6. Remaining Volume of Reduction in GCD Boreholes, Area 5 RWMS.

Table 2.5. Depths and Radii of Subsidence above the GCD Boreholes after Site Closure

Borehole	Depth, m		Radius, m	
	Minimum	Maximum	Minimum	Maximum
1	2.1	3.0	3.0	4.3
2	2.0	2.9	2.8	4.1
3	1.6	2.3	2.2	3.3
4	2.1	3.0	3.0	4.3

2.3.2 Minimum Potential Subsidence Depths and Radii above the Greater Confinement Disposal Boreholes

The following was assumed to calculate minimum reduction volumes within the GCD boreholes:

- The waste container degradation rate is two times faster than the steel box degradation rates from Table 2.1.
- The maximum volume reduction of the metal boxes is 85% of the original volume.
- The void volume of the backfill soil due to poor compaction of the backfill comprises 30% of the backfill column volume, as it was assumed in calculations by Arnold [1996].

The change in the reduction volume over time for the case considered is demonstrated in Figure 2.6. As this figure shows, the reduction volume at the year 2170 is 80%. The corresponding subsidence depth and radius after the year 2170 calculated using Equations (2.2) and (2.3) and expressed in percentages are both 59%. Due to the cubical relationship between the reduction

volume and subsidence depth and radius, only a small decrease in the depth/radius values occur with noticeable changes in the reduction volume. The minimum values of the subsidence depths and radii for GCD Boreholes 1, 2, 3, and 4 are presented in Table 2.5.

2.3.3 Conclusions

After the assumed loss of AIC, 170 years from now, the waste containers within the GCD boreholes will not be fully compacted. This will result in subsidence of the land surface and the formation of a cone-shaped depression with the side walls sloping in accordance with the angle of repose. The formation of such depression will depend on the degradation rates of the waste containers. Most of the compaction is expected to take place in the first 2000 years, but could be completed in the first 500 years.

After the compaction is fully completed, the expected depth of such a depression will be from 2.1 to 3.0 m (6.9 to 9.8 ft) (Boreholes 1 and 4); from 2.0 to 2.9 m (2.6 to 9.5 ft) (Borehole 2); and from 1.6 to 2.71 m (5.2 to 8.9 ft) (Borehole 3). The radius of the depression will be from 3.0 to 4.3 m (9.8 to 14 ft) (Boreholes 1 and 4); from 2.8 to 4.1 m (9.2 to 13 ft) (Borehole 2); and from 2.3 to 3.3 m (7.5 to 11 ft) (Borehole 3). The ranges of these values were obtained by estimating minimum and maximum possible reduction volumes remaining after site closure. Although the wide ranges of the parameter values were used in these calculations, the resulting ranges of the depth and radius values are relatively narrow.

3.0 ANALYSIS OF PRECIPITATION AND SURFACE WATER RUNOFF

3.1 Purposes and Expected Results

The purpose of this precipitation analysis was to develop rainfall characteristics for Area 5 that can be used to estimate the total amount of local runoff that could flow into the RWMS subsidence features during the 10,000-year period for each of two conceptual models. In the first conceptual model, the cap and subsidence features stay intact for the entire 10,000-year period. In this case, mean daily precipitation was used to compute mean daily local runoff and the magnitude and frequency of local precipitation was used to compute local runoff from rare events. The PMP was computed using standard methods and was included in the computation of local runoff.

In the second computation conceptual model, the cap is washed away immediately and the trenches, pits, and GCD boreholes subside after this event. In this case, the magnitude and frequency of precipitation on drainages up-slope from Area 5 were used to compute runoff for a series of rainfall events ranging from two-year to 200-year frequency.

3.2 Data Used

Thirty-six years of daily precipitation at the National Weather Service gage at Well 5B (1964-1999) were analyzed to create the statistics used for the computation of local runoff. Well 5B is located about 5 km (3 mi) south of the Area 5 RWMS at 36 degrees, 48.1 minutes longitude, 115 degrees, 57.9 minutes latitude at an elevation of 939 m (3,080 ft) mean sea level (msl).

Tables and graphs in U.S. Department of Commerce publication, Hydrometeorological Report No. 49, Probable Maximum Precipitation Estimates, Colorado River and Great Basin Drainages, were used to compute the PMP values.

3.3 Hydrologic Setting

Area 5 RWMS is situated in Frenchman Flat on the lower portion of coalesced alluvial fans that emanate from the Massachusetts Mountains and the Halfpint Range (Figure 1.1). There are four defined drainages to the north, northwest, and northeast of the RWMS that could cause flooding onto the northeast corner of the cap where the GCD boreholes are located. The drainage names used in this document and the delineation of the drainage basins are from Schmeltzer et al. [1983]. The specific drainages that could contribute flow to the RWMS are HP3, HP4, HP2, and the basin that is a combination of HP5, HP6, HPFa, and HPFb (Figure 3.1). Although the drainage basins to the west and southwest of RWMS (HP1a, HP1b, and MM2) are not expected to flow onto the northern portion of the cap where the GCD boreholes are located, flood events from HP1a and HP1b were included in the series of events contributing to the subsidence features for the case where the cap is washed away. Curve numbers for these drainages are based on new computations by Bechtel Nevada [Yucel, 2000].

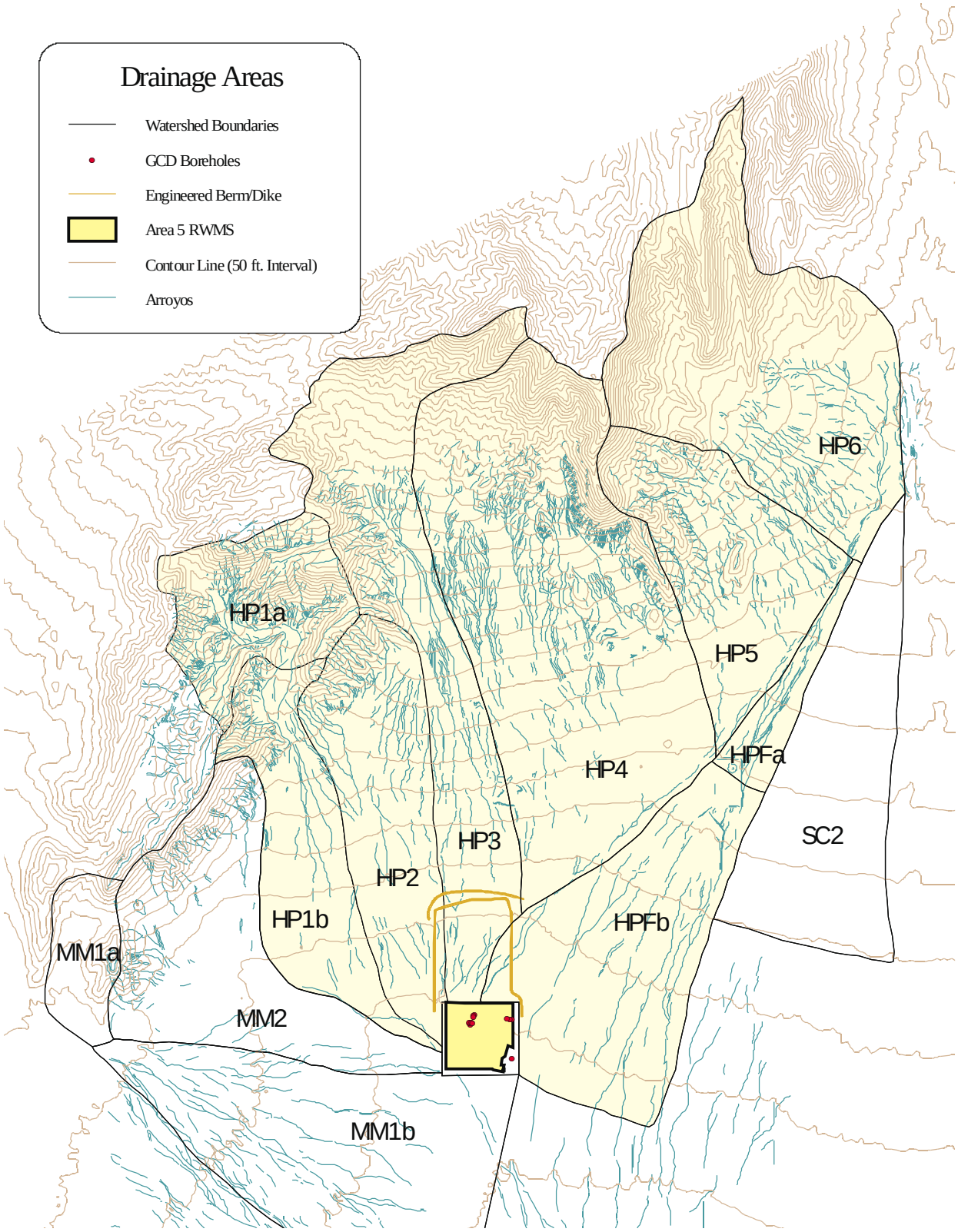

Figure 3.1. The Shaded Drainage Areas Have the Highest Potential to Flood the Northeast Portion of the RWMS. HP2 has some potential. HP1a, HP1b, and MM2 do not have potential to flood the northeast portion.

3.4 Method(s) of Analysis

3.4.1 Analysis of Local Precipitation

Analysis of the rainfall record at Well 5B produces the general statistics shown in Table 3.1.

Table 3.1. Well 5B Precipitation Record

Length of Record:	36 years
Period of Record:	1964–1999
Mean Annual precipitation	12.62 cm (4.97 in.)
Maximum Daily Rainfall	4.72 cm (1.86 in.)
Maximum Annual Rainfall	24.56 cm (9.67 in.)
Minimum Annual Rainfall	2.90 cm (1.14 in.)

3.4.2 Conceptual Assumptions about the Future Glacial Climate

The current climate is characterized as being interglacial. Interglacial climatic conditions, similar to current conditions, have occurred at fairly regular intervals over the last 400,000 years, generally lasting from 16,000 to 28,000 years [Brown et al., 1997], whereas the glacial periods have generally lasted about 100,000 years [Brown et al., 1997]. During the past 400,000 years, the climate has been in the glacial state about 80% of the time [DOE, 1998]. The break between the Pleistocene Epoch and the Holocene Epoch (interglacial) is generally considered to be at 10,000 years before present. The late Pleistocene includes the Sangamonian Stage, which is considered to be an interglacial, and the Wisconsinan Stage, which is generally considered to be glacial including periods of full glacial conditions (stades) and periods of climatic amelioration (interstades). The last stade during the Wisconsinan is generally recognized to have peaked between 18,000 and 22,000 years ago, with climatic deterioration going into the peak and amelioration coming out of the peak [Rawlinson, 1999]. Analysis of information on climate change and the potential for the return to more dominate glacial conditions is presented in detail in Brown et al. [1997] and is not repeated here.

Precipitation in the glacial climate is expected to be dominated by winter-type frontal storms. Estimates of long term mean precipitation for glacial conditions at Yucca Mountain are 200% of the current precipitation, although Brown et al. [1997] estimated that the long-term mean increase in precipitation would be less than 50%. For the computations in this report, precipitation is assumed to be twice the current precipitation. These conceptual assumptions are summarized in Table 3.2.

The Yucca Mountain Site Description [DOE, 1998b] describes the glacial climate as a situation where the polar front would commonly be over or not far north of Nevada; this polar front would dominate temperature and precipitation patterns in the area of Yucca Mountain and Frenchman Flat. Major floods in the glacial climate are expected to look a lot like those resulting from current winter storms and are expected to have characteristics associated with a winter frontal storm – longer duration and lower intensity than thunderstorm floods.

Table 3.2. Climate Assumptions

Climatic Phenomenon	Current Interglacial Climate	Glacial Climate
Precipitation Pattern	Combination of convective thunderstorms in the summer and frontal storms in the winter.	Dominated by winter type frontal storms
Precipitation amount	~ 12.7 cm (5 in.) per year	Two times the current precipitation, i.e. ~ 25.4 cm (10 in.) per year.
Flooding	Floods are typically of short duration and high intensity as associated with summer thunderstorms.	Floods are expected to have a longer duration and a lower intensity as would be associated with a winter frontal storm.

3.4.3 Computation of Runoff into Subsidence Features

The computation of runoff into subsidence features is done for the two opposite bounding conceptual models, both of which are not expected happen. The expected future lies somewhere between these two bounds. The first bounding case is a conceptual model where the cap and subsidence features stay intact for the entire 10,000 years. In this computation, mean daily precipitation is used to compute mean daily local runoff and the magnitude and frequency of local precipitation is used to compute runoff from rare events.

The second bounding case is a conceptual model where (1) the cap is washed away before the subsidence features are fully subsided; (2) the subsidence features continue to subside after the cap is washed away; and (3) the features lie in the path of a watercourse. In this computation, the magnitude and frequency of precipitation on drainages up-slope from Area 5 were used to compute runoff for a series of runoff events ranging from two-year to 200-year frequency.

In reality, the cap is not expected to wash away completely nor is it expected to stay completely intact. It is expected that it will be slowly eroded by floods emanating from the alluvial fan and by local runoff from the cap itself. The run-on areas for subsidence features will radiate outward and the features themselves will become partially or wholly filled in. As each of the features fill in, fine-grained alluvium will be deposited in the bottom, retarding infiltration. If an alluvial fan watercourse is "captured" by one of the subsidence features, the bed load and suspended sediment carried by that water course will quickly fill in the feature.

3.4.3.2 First Bounding Case – Cap Stays

In the first bounding case, the cap stays intact throughout the 10,000-year period. Runoff from the run-on areas for each of the features is considered to be clear water (no sediment). Therefore, subsidence features do not erode or fill in. Runoff from these run-on areas continues at the same rate for the entire 10,000-year period.

The analytical procedure used to compute total local runoff into the subsidence features is based on the 36-year period of rainfall at Well 5B. This procedure was to (1) compute the excess daily

precipitation from each days rainfall, (2) use the excess rainfall to compute the volume of runoff into the subsidence feature for each day, (3) compute the mean annual volume of runoff, (4) multiply the mean annual volume of runoff by 10,000 years, and (5) compute and add runoff from rare flood events, including the PMP. The total local runoff for the glacial climate was computed in a similar fashion, with the exception that each value of daily rainfall was multiplied by two prior to the computation of excess rainfall.

3.4.3.2.1 Computation of Excess Daily Precipitation

Excess daily precipitation represents the portion of a rainfall event that will run off. This value was computed using the Soil Conservation Service (SCS) Curve Method [SCS, 1972]. In this method, the potential maximum retention of soil moisture is computed on the basis of the SCS curve number and is used in the following equation to compute the maximum runoff for these conditions. Excess precipitation represents sheetflow runoff into the subsidence features from the run-on area.

$$Q = (P - 0.2S)^2/P + 0.8S \quad (Q = 0 \text{ if } P < 0.2S) \tag{3.1}$$

Where S = (1000/CN) -10 = potential maximum retention (inches)
Q = precipitation excess or runoff (inches)
P = cumulative precipitation (inches)
CN = SCS curve number

It is assumed that the cap will be constructed from compacted local alluvium, and under current climate conditions will have a fair cover of desert brush, and under glacial climate, will have a piñon-juniper cover. Curve numbers for the cap are based on new computations by Bechtel Nevada [Yucel, 2000]. Curve numbers with a medium potential for runoff, representing average antecedent moisture conditions (AMC-II), were used for rainfall events with a recurrence interval less than 100 years, while curve numbers with the highest potential for runoff, representing conditions where the soil is nearly saturated from antecedent rain (AMC-III), were used for rainfall events with a recurrence interval greater than or equal to 100 years. The curve numbers for AMC-II and AMC-III conditions under both current and glacial conditions are shown in Table 3.3.

Curve Numbers: In the dry conditions that exist at Area 5, computations for average and low frequency events would normally be done with curve numbers that represent the lowest runoff potential (AMC-I).

3.4.3.2.2 Compute Volume of Local Runoff

The total amount of runoff that flows into each subsidence feature is the sum of the rainfall that falls within the feature itself and the excess rainfall generated by the run-on area up-slope of the feature. If the runoff from the run-on area is significant, that runoff plus the total amount of rainfall that falls into the pit is used, under the assumption that a pond has been created in the subsidence feature and that the SCS abstraction process is not applicable. If the runoff from the

Table 3.3. Curve Numbers for RWMS Cap and Up-Slope Drainages [Yucel, 2000]

Drainage	Curve Numbers			
	Current Climate		Glacial Climate	
	AMC-II	AMC-III	AMC-II	AMC-III
RWMS Cap	81	92	73	87
HP1a	80	91	73	87
HP1b	66	82	61	78
HP2	66	82	60	78
HP3	75	88	68	84
HP4	68	84	63	80
HP5	69	84	63	80
HP6	69	84	64	81
HPFa	63	80	58	76
HPFb	63	80	58	76

run-on area is not significant, none of the rainfall in the pit is used, under the assumption that there is no pond and rainfall is abstracted as it is under current conditions.

The above approach results in a number of events with very small runoff volumes. These volumes are similar to many current rainfall events which do not result in infiltration. In order to avoid simulating very small events, a threshold was set. Only events with runoff values greater than the threshold were included in the analysis.

A 2 mm (0.08 in) threshold was used in this study. It represents a four-year rainfall event (24 mm (0.94 in.)) under current climate conditions and a three-year event (33 mm (1.3 in.)) under glacial conditions. The VS2DT code was run to test the validity of this threshold using a 40 mm (1.6 in) rainfall over a span of one day. Increased soil moisture from this rainfall essentially returned to normal within a 20-day period (see Attachment B).

The subsidence features and their run-on areas are shown in Figure 3.2. These areas are summarized in Table 3.4.

3.4.3.2.3 Compute Mean Annual Volume of Runoff

Runoff volumes were computed using the 36 years of rainfall at Well 5B as a representative record for the current climate and a doubling of the amount of rainfall in each rainfall event as representative of the glacial climate. Although it is likely that under a glacial climate there would actually be an increase in the number of events, the number of events were kept the same as the current climate – partly because it is difficult to quantify the actual number of events that would occur, but also because using fewer events with more rainfall per event is a more conservative approach. Since the SCS method abstracts a threshold amount of rainfall from each event, doubling the rainfall with the same number of events increases the runoff fivefold. If the

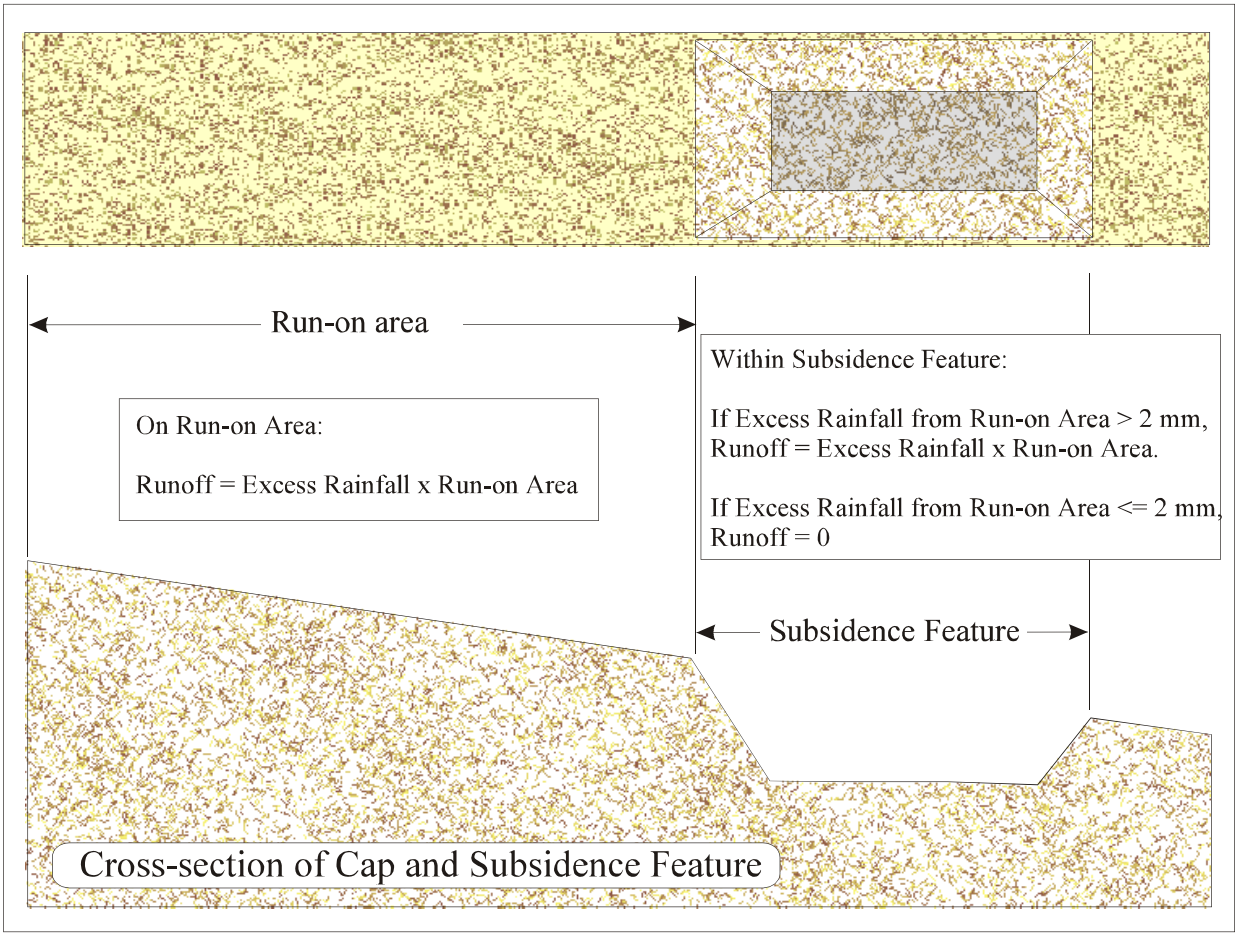

Figure 3.2. Runoff Diagram.

Table 3.4. Areas of Subsidence Features and Run-On for GCD and Selected RWMS Subsidence

Subsidence feature	Run-on Area for Subsidence Feature(m^2)*	Area of Subsidence Feature (m^2)*
GCD Borehole 1	334	59
RWMS TO4C	3,412	4,067
RWMS PO3U	7,021	26,493
RWMS TO7C	1,657	2,676

* 1 m^2 = 10.76 ft^2

number of events are doubled, the runoff would be significantly less, since the threshold abstraction is subtracted from each rainfall event.

The mean annual volume of runoff is the arithmetic mean of the annual sums for each year of the 36-year period. Table 3.5 presents the mean annual volumes computed for both the current interglacial period and the glacial period.

Table 3.5. Mean Annual Volume for GCD and RWMS Subsidence Features

Subsidence Feature	Mean Annual Volume (m^3)*	
	Current Interglacial Climate	Glacial Climate
GCD Borehole 1	1.3	5.3
RWMS TO4C	45.2	202
RWMS PO3U	259	1,189
RWMS TO7C	28.4	128

* 1 m^3 = 35.3 ft^3

3.4.3.2.4 Compute Runoff from Rare Flood Events

The maximum annual 24-hour rainfall events at Well 5B were analyzed and fitted to the Log-Pearson III (LP-III) frequency distribution through the use of the United States Geological Survey (USGS) PEAKFQ program [USGS, 1998]. The LP-III distribution has been shown by O'Connor and Clark [1971] to fit both peak discharge and peak rainfall events. Table 3.6 presents the entire range of LP-III estimated magnitudes and the values for the 95% confidence intervals through 500 years. Rainfall magnitudes for the 1,000-year and 10,000-year rainfall events were estimated graphically. Figure 3.3 shows the Well 5B data, the frequency curves, and the six-hour local PMP.

Table 3.6. Log-Pearson Statistics for Well 5B 36-Hour Storm Event

Recurrence Interval	Annual Exceedence Probability	LP-III Estimate (mm)*	95% Confidence Limits	
			Lower Conf. Limit (mm)*	Upper Conf. Limit (mm)*
1.05		10.4	8.6	11.9
1.11	0.9	11.7	9.9	13.2
1.25	0.8	13.7	11.9	15.2
2	0.5	18.5	16.8	20.8
5	0.2	26.2	23.4	30.0
10	0.1	31.5	27.7	37.3
25	0.04	38.9	33.3	48.0
50	0.02	44.7	37.6	56.9
100	0.01	51.1	42.2	66.8
200	0.005	57.7	46.7	77.5
500	0.002	66.8	53.3	93.0
1,000	0.001	73.9	-	-
10,000	0.0001	101.6	-	-

* 1 in = 25.4 mm

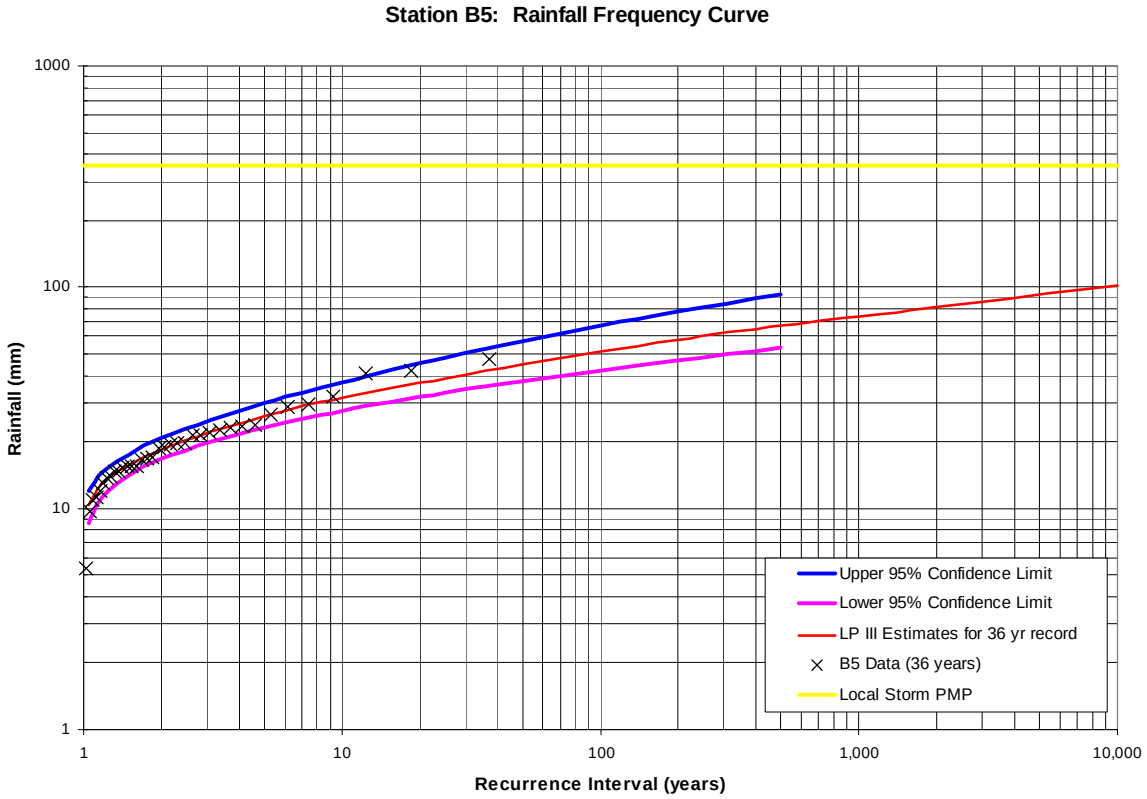

Figure 3.3. Log-Pearson Frequency Curve for Well B5–Daily Maximum Rainfall.

A synthetic frequency curve developed for the glacial climate was based on the Well 5B frequency curve above the 100-year storm and on the previously-stated doubling of rainfall at the lower frequencies. The synthetic curve for the glacial climate is shown in Figure 3.4. This curve was used to compute rainfall and runoff for rare events in the glacial climate.

3.4.3.2.5 Computation of Probable Maximum Precipitation

PMP was computed using the methodology set forth in Hydrometeorological Report No. 49 [U.S. Department of Commerce, 1977]. Both local storm and general storm PMPs were computed for each watershed; the properties of these events are presented in Table 3.7. Computation sheets for the local and general storm PMPs are in Attachment C.

The runoff for the PMP was computed using the SCS method, as described in Sections 3.4.3.2.2 and 3.4.2.2.1.

3.4.3.2.6 Total Runoff into Subsidence Features

Runoff into each subsidence feature for both the current integlacial climate and the glacial climate was computed by adding (1) the total volume of mean runoff, (2) the volume of 90 100-year floods, (3) the volume of nine 1000-year floods, (4) the volume of one 10,000-year flood, and (5) the volume of one PMP. These values are presented in Tables 3.8 through 3.11.

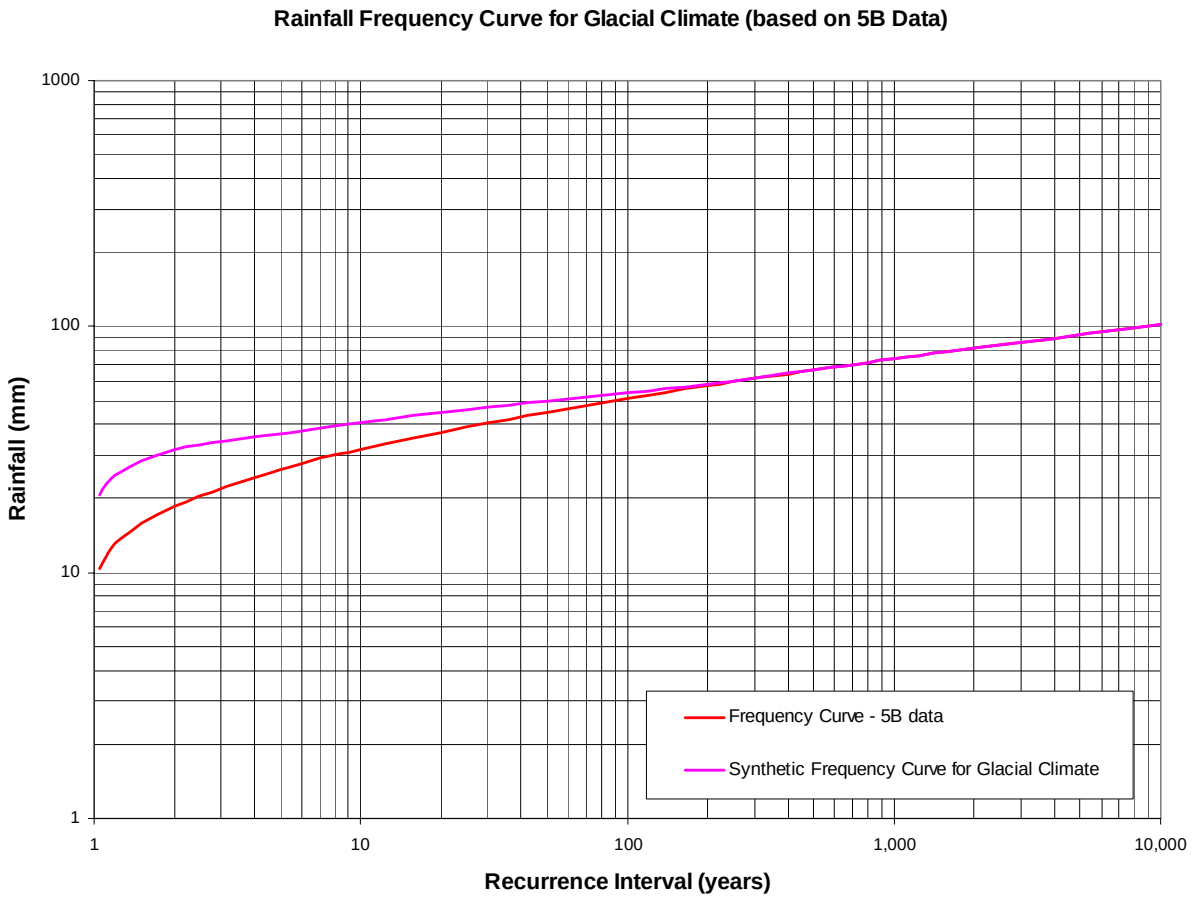

Figure 3.4. Synthetic Frequency Curve for Glacial Climate.

Table 3.7. Local and General Storm PMPs for RWMS Drainage Basins

Drainage	Local Storm 6-hr. PMP (mm)*	General Storm 72-hr. PMP (mm)*
HP3	353	327
HP4	338	
HP5, HP6, HPFA, HPFB	330	
HP2	353	
HP1a, HP1b	353	
MM2	353	

* 1 in = 25.4 mm

These computations show that the mean runoff is significantly more important than the rare events in estimating total volume. Hokett and French [1998] and French et al. [1996] also concluded that for estimating infiltration, extreme events are likely to be less important than the more frequent, average events.

Table 3.8. Total Volume of Runoff into GCD Borehole 1 Over 10,000 Years

Number of Events	Event Description	Current Climate		Glacial Climate	
		Flood Volumes (m^3)*	Total Volumes (m^3)*	Flood Volumes (m^3)*	Total Volumes (m^3)*
	Total Volume of Mean Runoff		13,298		52,739
90	100-year floods @	13.6	1,222	11.7	1,050
9	1000-year floods @	22.0	198	18.5	166
1	10,000-year floods @	32.4	32	28.4	28
1	PMP	118	118	108	108
	Total		**14,869**		**54,091**

* 1 m^3 = 35.3 ft^3

Table 3.9. Total Volume of Runoff into RWMS Trench T04C Over 10,000 Years

Number of Events	Event Description	Current Climate		Glacial Climate	
		Flood Volumes (m^3)*	Total Volumes (m^3)*	Flood Volumes (m^3)*	Total Volumes (m^3)*
	Total Volume of Mean Runoff		452,377		2,018,565
90	100-year floods @	316	28,406	306	27,513
9	1000-year floods @	481	4,325	445	4,001
1	10,000-year floods @	683	683	642	642
1	PMP	2,429	2,429	2,231	2,231
	Total		**488,220**		**2,052,952**

* 1 m^3 = 35.3 ft^3

Table 3.10. Total Volume of Runoff into RWMW Pit PO3U Over 10,000 Years

Number of Events	Event Description	Current Climate		Glacial Climate	
		Flood Volumes (m^3)*	Total Volumes (m^3)*	Flood Volumes (m^3)*	Total Volumes (m^3)*
	Total Volume of Mean Runoff		2,586,870		11,892,742
90	100-year floods @	1,575	141,730	1,605	144,449
9	1000-year floods @	2,328	20,956	2,254	20,289
1	10,000-year floods @	3,248	3,248	3,162	3,162
1	PMP	11,401	11,401	10,512	10,512
	Total		**2,764,205**		**12,071,154**

* 1 m^3 = 35.3 ft^3

Table 3.11. Total Volume of Runoff into Trench TO7C Over 10,000 Years

Number of Events	Event Description	Current Climate		Glacial Climate	
		Flood Volumes (m^3)*	Total Volumes (m^3)*	Flood Volumes (m^3)*	Total Volumes (m^3)*
	Total Volume of Mean Runoff		283,733		1,279,582
90	100-year floods @	189	17,016	186	16,758
9	1000-year floods @	285	2,567	268	2,409
1	10,000-year floods @	403	403	383	383
1	PMP	1,427	1,427	1,313	1,313
	Total		**305,145**		**1,300,445**

* 1 m^3 = 35.3 ft^3

3.4.3.3 Second Bounding Case – Cap is Washed Away

Subsidence Feature Volumes: The fully subsided volume of each subsidence feature was used in these computations. The expected volume would be much smaller because the portion of the volume of each feature that had occurred within the cap would have been washed away with the cap.

In the conceptual model for the second bounding case, a series of events are presumed to happen: (1) the cap is washed away before the subsidence features are fully subsided; (2) the subsidence features continue to subside after the cap is washed away; and (3) the features lie in the path of a watercourse. In this computation, the magnitude and frequency of precipitation on drainages up-slope from Area 5 were used to compute runoff for a series of runoff events ranging from two-year to 200-year frequency, until the features were filled with sediment.

3.4.3.3.1 Compute Runoff from Flood Events

The same rainfall frequency statistics that were developed in the analysis described in Section 3.4.3.2.4 were used for these computations. The frequency curve developed for Well 5B was used to estimate rainfall and runoff for the current climate and the synthetic curve developed for the glacial climate was used to develop rainfall and runoff for the glacial climate. For these computations, the rainfall magnitudes were used to compute runoff from the up-slope watersheds to the north, east, and west of Area 5. The specific drainages that could contribute flow to the RWMS are HP3, HP4, HP2, and the basin that is a combination of HP5, HP6, HPFa, and HPFb (Figure 3.1). Although the drainage basins to the west and southwest of RWMS HP1a, HP1b, and MM2, are not expected to flow onto the northern portion of the cap where the GCD boreholes are located, flood events from HP1a and HP1b are included in the series of events for this computation.

Curve numbers for these drainages were used in essentially the same way as in Section 3.4.3.2.1. Curve numbers for these drainages are based on new computations by Bechtel Nevada [Yucel, 2000] with the AMC-II curves used for those rainfall events with a recurrence interval less than 100 years, and the AMC-III curves used for rainfall events with a recurrence interval greater than or equal to 100 years. The curve numbers for each watershed for AMC-II and AMC-III conditions under both current and glacial conditions are shown in Table 3.3.

Curve Numbers: In the dry conditions that exist at Area 5, computations for average and low frequency events would more accurately be done with curve numbers that represent the lowest runoff potential (AMC-I).

In this bounding computation, runoff was assumed to come from the combined up-slope drainages to the north, east, and west of Area 5. Rainfall magnitudes for each frequency were applied to each basin and the computed runoff values were combined to arrive at the total input to the subsidence features.

Flooding: In reality, only a partial set of the up-slope drainages would contribute any amount of flow to the subsidence features, and for any given flood event, it is unlikely that each of these drainages would contribute a flood of the same magnitude and frequency at the same time.

A series of runoff events were then used to compute the amount of runoff and sediment that would flow into each of the four subsidence features in question: GCD Borehole 1, RWMS TO4C, RWMS PO3U, and RWMS TO7C (Figure 3.2). Each event was assumed to flow first into the feature furthest up-slope, PO3U, and when the flood volume exceeded the capacity of that pit, the flood would overflow into the next two features, Borehole 1 and TO4C. When the capacity of those features was exceeded, the flood would overflow into the last feature, TO7C. Floods with recurrence intervals of 2, 5, 10, 25, 50, 100, and 200 years were simulated to occur at those exact intervals, i.e., a two-year flood every two years, a five-year flood every five years, etc. When more than one flood could occur in the same year, only the highest flood would be used. For example, at year 10, a 2-, 5-, and 10-year flood could occur, but only the 10-year flood was used.

For these computations each flood event was presumed to carry a 15% volume of suspended sediment [Federal Emergency Management Agency, 1995]. A volume sediment equal to 15% of the ponded flood volume in each feature was assumed to be deposited in those features during each event. Over time, the capacity of each features was incrementally reduced in accordance to the amount of sediment deposited. All of the subsidence features were filled with sediment in less than 250 years (Table 3.12).

Suspended Sediment Concentration: In the hyperconcentrated sediment flows that can typically occur in the southwestern U.S., sediment concentrations can range from 20% to 45%.

Table 3.12. Total Runoff and Sediment into Subsidence Features for Bounding Case #2

Subsidence Feature	Initial Capacity (m^3)*	Years to fill with sediment		Total Volume of Floods for Current or Glacial Climate (m^3)*
		Current Climate	Glacial Climate	
GCD Borehole 1	59	155	112	391
RWMS TO4C	5,612	206	160	37,411
RWMS PO3U	71,768	210	164	478,451
RWMS TO7C	3,745	206	160	24,964

* 1 m^3 = 35.3 ft^3

When the subsidence features are filled with sediment, the accumulation of flood volumes stops, and the infiltration process stops. The total volume of flooding is the same for both the current and the glacial climate, but the time to fill the features with sediment is shorter for the glacial climate, because the glacial flood volumes are larger, and hence, the sediment loads are larger.

Bed Load: In addition to suspended sediment, floods in the sandy, gravelly environment found in alluvial plains carry a large volume of bed load. Bed load is a layer of sand, gravel, and rocks within the channel bottom that moves with the flood. Bed load was neglected for these computations.

4.0 ANALYSIS OF FLOODING

4.1 Purpose and Expected Results

The purpose of these flooding analyses is to determine the range of flood events that would be expected to occur on the alluvial fan above Area 5 RWMS, to evaluate the potential of these events to top the cap, and to evaluate the consequences to the GCD boreholes if they did.

4.2 Method of Analysis

The analytical procedure was to:

1. Compute the magnitude and frequency of flood events that might occur at the Area 5 RWMS using all reasonable estimation methods. The methods used are:
   a. the computation of PMF based on PMP computations,
   b. the estimation of the maximum expected floods based on flood envelope curves, and
   c. the computations of specific flood magnitudes and frequencies based on regional flood equations.
2. Compute channel depth for the estimated floods.
3. Compute possible freeboard of the Area 5 RWMS cap.
4. Compare cap freeboard with flood depth.
5. Develop assumptions for the consequences of flooding.

The drainages considered in these analyses are shown in Figure 3.1.

4.3 Flood Analysis

Extreme flood events were estimated for the Area 5 RWMS drainages based on the PMP, flood envelope curves, and regional flood equations.

4.3.1 Computation of Probable Maximum Flood

The PMF for each of these watersheds was computed using HEC Hydrologic Modeling System (HMS) [U.S. Army Corps of Engineers, 1998]. HMS computes the flood hydrograph based on data that defines the watershed and the storm event. The watershed properties presented in Table 4.1 are from Schmeltzer et al. [1993] with updated curve numbers from a recent Bechtel Nevada study [Yucel, 2000]. The storm event used for the PMF is based on the PMP computed using the methodology set forth in Hydrometeorological Report No. 49 [U.S. Department of Commerce, 1977]. Both local storm and general storm PMFs were computed for each watershed; the properties of these events are presented in Table 4.2. Computation sheets for the local and general storm PMPs are in Attachment B.

The local storm PMF and the general storm PMF were both computed because it is assumed that for the current climate, the local storm PMF is most likely to be applicable and for the glacial climate, the general storm PMF is most likely to be applicable. In the current climate, the local

Table 4.1. Drainage Areas and Properties for Drainages to the North of Area 5 RWMS (See Figure 3.1.)

Drainage Name	Drainage	Drainage Area (km^2)*	SCS Curve Number*		Lag Time (hrs)
			Current Climate	Glacial Climate	
HP3	drains the area to the north and north-northwest of the Area 5 RWMS	4.4	88	84	0.59
HP4	drains the area to the north and north-northwest of the Area 5 RWMS	8.5	84	80	0.52
HP5	drains areas to the northwest of the Area 5 RWMS	3.1	84	80	0.30
HP6	drains areas to the northwest of the Area 5 RWMS	5.7	84	81	0.55
HPFA	drains areas to the northwest of the Area 5 RWMS	0.8	80	76	0.33
HPFB	drains areas to the northwest of the Area 5 RWMS	4.1	80	76	0.44
HP2	drains areas to the northeast of the Area 5 RWMS	3.1	82	78	0.51
HP1a,	drains areas to the northeast of the Area 5 RWMS	2.1	91	87	0.30
HP1b		2.6	82	78	0.51
MM2	drains areas to the east of the Area 5 RWMS	4.7	83	79	0.47

* 1 km^2 = 0.386 mi^2

Table 4.2. Computed Properties of Local Storm and General Storm PMP and PMF for each Drainage Basin

Drainage	PMP				PMF			
	General Storm		Local Storm		General Storm		Local Storm	
	Rainfall (mm)*	Duration (hrs)	Rainfall (mm)*	Duration (hrs)	Peak (m^3/s)*	Volume ($m^3 \times 10^6$)*	Peak (m^3/s)*	Volume ($m^3 \times 10^6$)*
HP3	324	72	353	6	25.6	1.21	327	1.38
HP4			338		48.6	2.24	618	2.41
HP5, HP6, HPFA, HPFB			330		77.4	3.54	796	3.68
HP2			353		17.5	0.79	241	0.91
HP1a, HP1b			353		26.8	1.25	405	1.42
MM2			353		20.5	0.94	301	1.07

* 1 mm = 0.394 in; 1 m^3/s = 35.3 ft^3/s; 1×10^6 m^3 = 811 AF (Acre-Foot)

storm PMFs are those flood events that are produced from convective-type thunderstorms that occur during the summer and early fall. These storms produce the most intense rainfall and the largest peak discharges. In the case of the glacial climate, frontal-type storms are assumed to predominate, and therefore, the general storm PMF would be the correct flood model to use.

4.3.2 Estimation of Maximum Flood Using Flood Envelope Curves

For comparison to the computed PMF values, a second set of maximum flood magnitudes was estimated from maximum discharge envelope curves developed by Christensen and Spahr [1980] and Thomas et al. [1997]. An envelope curve is the curve that is drawn along the top of all points on a plot of maximum measured floods versus the drainage areas for these floods. The Christensen and Spahr [1980] envelope curve is based on extreme events that have occurred in Nevada, Utah, Arizona, and New Mexico. Thomas et al. [1997] developed an envelope curve for gauged watersheds in an area of the southwest that covers eastern Oregon to west Texas. The values from the Thomas et al. [1997] curve are significantly smaller than those from the Christensen and Spahr [1980] curve. This difference may be due to the limitation of the Thomas et al. [1997] curve to gauged watersheds. The largest maximum floods from the Christensen and Spahr [1980] envelope curve are 24 to 45% larger than the computed PMF local storm discharges (Table 4.3).

Table 4.3. Comparison of Peak Discharges for Maximum Floods Computed by the Local Storm PMF Method and as Estimated Using the Envelope Curve Developed by Christensen and Spahr [1980]

Drainage	Drainage Area	Local Storm PMF (m^3/s)*	Christensen and Spahr [1980] Envelope Curve (m^3/s)*	Thomas et al. [1997] Envelope Curve (m^3/s)*
HP3	4.4	309	411	173
HP4	8.5	586	722	306
HP5, HP6, HPFA, HPFB	13.7	761	1104	425
HP2	3.1	231	283	142
HP1a, HP1b	4.7	388	453	198
MM2	3.6	289	354	153

* 1 m^3/s = 35.3 ft^3/s

4.3.3 Computations of Flood Magnitudes and Frequencies Based on Regional Flood Equations

100- and 500-year Floods: The magnitude of 100- and 500-year floods were computed using three different sets of regional equations. These events were computed as a comparison and cross-checked to the computed maximum flood events.

4.3.3.1 Christensen and Spahr Regional Equation

100-year flood magnitudes were developed using equations developed by Christensen and Spahr [1980] for Topopah Wash in Jackass Flats, Nevada. This equation computes peak discharge in

ft^3/s and is based on the basin drainage area (A) in square miles, the mean basin elevation (E) in feet above msl, and the latitude of the basin minus 35° (L).

$$Q_{100} = 11900\ A^{0.55}\ E^{-1.28}\ L^{-1.16}$$

The computed magnitudes (in m^3/s) are shown in Table 4.4.

4.3.3.2 Roeske Regional Equations

100- and 500-year flood magnitudes were developed using two sets of equations developed by Roeske [1978] for two regions in Arizona. The equations for Region 1 are based on flood events that occurred on northwestern Arizona, while the equations for Region 2 are based on flood events that occurred on southwestern Arizona. The Region 1 equation is not valid at drainage areas of less than 1.84 mi^2 (4.77 km^2). French and Lombardo [1984] suggested that, although Region 1 is conterminous to Southern Nevada, Region 2 may more closely resemble the NTS. The Roeske equations compute peak discharge in ft^3/s and are based on basin drainage area (A) in square miles. The computed magnitudes (in m^3/s) are shown in Table 4.4.

Region 1	Region 2
$Q_{100} = 584\ A^{0.490}$	$Q_{100} = 1100\ A^{0.499}$
$Q_{500} = 1300\ A^{0.451}$	$Q_{500} = 2000\ A^{0.509}$

4.3.3.3 Thomas et al. [1997] Regional Equation

Thomas et al. [1997] developed regional equations for each of 16 regions spanning a southwest region that runs from eastern Oregon to west Texas, and from southwestern Wyoming to southeastern California. Frenchman Flat lies in Region 6, the northern Great Basin region. The equations presented by Thomas et al. [1997] compute peak discharge in ft^3/s and are based on basin area (A) in square miles and mean basin elevation (E) in feet above msl. The 100-year flood was computed for comparison with the other estimated and computed floods using the equation below. The computed magnitudes (in m^3/s) are shown in Table 4.4.

$$Q_{100} = 20{,}000\ A^{0.51}\ (E/1000)^{-2.3}$$

4.4 Compute Channel Depths

The widths and depths for each of the flood events were computed using equations developed by Dawdy [1979] and as applied to the Area 5 RWMS by French and Lombardo [1984]. These equations are based on the peak discharge (Q) in ft^3/s, estimate the top width (T) in feet, and the channel depth (y) in feet of the flood peak on the alluvial fan. The computed channel depths and widths are presented in Tables 4.5 through 4.10.

$$T = 9.5\ Q^{0.4}$$
$$Y = 0.07\ Q^{0.4}$$

Table 4.4. Comparison of Peak Discharges for 100- and 500-Year Floods Computed Using Regional Equations Developed by Christensen and Spahr [1980] and by Roeske [1978]

Drainage	Christensen and Spahr [1980]	Roeske [1978] Region 1		Roeske [1978] Region 2		Thomas et al. [1997] Region 6
	100-Year (m^3/s)*	100-Year (m^3/s)*	500-Year (m^3/s)*	100-Year (m^3/s)*	500-Year (m^3/s)*	100-Year (m^3/s)*
HP3	38.8	not applicable		40.6	74.2	34.4
HP4	57.8	29.7	63.1	56.5	104	51.4
HP5, HP6, HPFA, & HPFB	77.7	37.4	78.1	71.6	132	69.7
HP2	37.0	not applicable		34.1	62.1	37.2
HP1a, HP1b	42.9	not applicable		41.8	76.4	40.2
MM2	41.8	not applicable		36.8	67.2	43.2

*1 m^3/s = 35.3 ft^3/s

Table 4.5. HP3 - Summary of Flood Events and Computed Channel Parameters

Flood Event	Source	Discharge (m^3/s)*	Depth (m)*	Channel Top Width (m)*
Maximum Flood	Christensen and Spahr [1980] Envelope Curve	411	1.0	134
	Thomas et al. [1997] Envelope Curve	173	0.70	94.6
	PMF from Local Storm PMP	309	0.88	120
	PMF from General Storm PMP	25.7	0.34	44.2
500-year	Roeske [1978] Arizona Region 2	74.2	0.49	67.4
100-year	Christensen and Spahr [1980] Regional Equation	38.8	0.40	52.2
	Roeske [1978] Arizona Region 2	40.6	0.40	53.1
	Thomas et al. [1997] Great Basin Region 6	34.4	0.37	49.7

*1 m^3/s = 35.3 ft^3; 1 m = 3.28 ft

Table 4.6. HP4 - Summary of Flood Events and Computed Channel Parameters

Flood Event	Source	Discharge (m^3/s)*	Depth (m)*	Channel Top Width (m)*
Maximum Flood	Christensen and Spahr [1980] Envelope Curve	722	1.2	168
	Thomas et al. [1997] Envelope Curve	306	0.88	119
	PMF from Local Storm PMP	586	1.1	154
	PMF from General Storm PMP	49.0	0.43	57.3

Table 4.6. HP4 - Summary of Flood Events and Computed Channel Parameters (Continued)

Flood Event	Source	Discharge (m^3/s)*	Depth (m)*	Channel Top Width (m)*
500-year	Roeske [1978] Arizona Region 1	63.1	0.46	63.1
	Roeske [1978] Arizona Region 2	104	0.58	77.2
100-year	Christensen and Spahr [1980] Regional Equation	57.8	0.46	61.0
	Roeske [1978] Arizona Region 1	29.7	0.34	46.7
	Roeske [1978] Arizona Region 2	56.5	0.46	60.7
	Thomas et al. [1997] Great Basin Region 6	51.4	0.43	58.3

*1 m^3/s = 35.3 ft^3; 1 m = 3.28 ft

Table 4.7. HP5, HP6, HPFA, & HPFB - Summary of Flood Events and Computed Channel Parameters

Flood Event	Source	Discharge (m^3/s)*	Depth (m)*	Channel Top Width (m)*
Maximum Flood	Christensen and Spahr [1980] Envelope Curve	1104	1.5	199
	Thomas et al. [1997] Envelope Curve	425	1.0	136
	PMF from Local Storm PMP	761	1.2	171
	PMF from General Storm PMP	78.5	0.52	68.9
500-year	Roeske [1978] Arizona Region 1	78.1	0.52	68.9
	Roeske [1978] Arizona Region 2	132	0.64	85.1
100-year	Christensen and Spahr [1980] Regional Equation	77.7	0.52	68.6
	Roeske [1978] Arizona Region 1	37.4	0.37	51.2
	Roeske [1978] Arizona Region 2	71.6	0.49	66.5
	Thomas et al. [1997] Great Basin Region 6	69.7	0.49	65.9

*1 m^3/s = 35.3 ft^3; 1 m = 3.28 ft

Table 4.8. HP2 - Summary of Flood Events and Computed Channel Parameters

Flood Event	Source	Discharge (m^3/s)*	Depth (m)*	Channel Top Width (m)*
Maximum Flood	Christensen and Spahr [1980] Envelope Curve	283	0.85	115
	Thomas et al. [1997] Envelope Curve	142	0.64	87.5
	PMF from Local Storm PMP	231	0.79	106
	PMF from General Storm PMP	17.5	0.27	37.8
500-year	Roeske [1978] Arizona Region 2	62.1	0.46	62.8
100-year	Christensen and Spahr [1980] Regional Equation	37.1	0.37	50.9
	Roeske [1978] Arizona Region 2	34.1	0.37	49.4
	Thomas et al. [1997] Great Basin Region 6	37.2	0.37	51.2

*1 m^3/s = 35.3 ft^3; 1 m = 3.28 ft

Table 4.9. HP1a, & HP1b - Summary of Flood Events and Channel Computed Parameters

Flood Event	Source	Discharge (m^3/s)*	Depth (m)*	Channel Top Width (m)*
Maximum Flood	Christensen and Spahr [1980] Envelope Curve	453	1.0	139
	Thomas et al. [1997] Envelope Curve	198	0.73	100
	PMF from Local Storm PMP	389	0.98	131
	PMF from General Storm PMP	26.7	0.34	44.8
500-year	Roeske [1978] Arizona Region 2	76.4	0.52	68.3
100-year	Christensen and Spahr [1980] Regional Equation	42.9	0.40	54.2
	Roeske [1978] Arizona Region 2	41.8	0.40	53.6
	Thomas et al. [1997] Great Basin Region 6	40.2	0.40	52.7

*1 m^3/s = 35.3 ft^3; 1 m = 3.28 ft

Table 4.10 MM2 - Summary of Flood Events

Flood Event	Source	Discharge (m^3/s)*
Maximum Flood	Christensen and Spahr [1980] Envelope Curve	354
	Thomas et al. [1997] Envelope Curve	153
	PMF from Local Storm PMP	289
	PMF from General Storm PMP	20.5
500-year	Roeske [1978] Arizona Region 2	67.2
100-year	Christensen and Spahr [1980] Regional Equation	41.8
	Roeske [1978] Arizona Region 2	36.8
	Thomas et al. [1997] Great Basin Region 6	43.2

*1 m^3/s = 35.3 ft^3

4.5 Aggradation

Although the RWMS Area 5 is located on an active or aggrading alluvial fan, it is difficult to predict how much that fan will aggrade over the next 10,000 years. For the flooding bounding case, the highest estimated aggradation was assumed have occurred in either the current climate or the glacial climate.

While the alluvial fans in the Area 5 RWMS show signs of being active, it is assumed most of the aggradation on these fans occurred during the glacial conditions of the Pleistocene. Rachocki [1981] said that "it is recognized that the growth of alluvial fans was initiated during the Pleistocene epoch when the climate was more humid (pluvial)" and cites evidence of the decline in active sedimentation since the last glacial period. Bull [1964] estimated that the alluvial fans

in San Joaquin Valley had been formed in the mid-Pleistocene and were approximately 600,000 years old.

The alluvial fans in the vicinity of Area 5 RWMS show some of the signs of active fans and some of the signs of inactive fans. French and Lombardo [1984] noted terraces covered with desert varnish in the alluvial fan in HP2 and HP1B. He also noted evidence of recent flow including recent deposition in the fans within HP4. French and Lombardo [1984] noted conditions of entrenchment in upper portion of Scarp Canyon alluvial fan. Continuous channels, desert varnish, and channel entrenchment are all indicators of inactive alluvial fans [French et al., 1993].

Surface geology mapping shows that the oldest alluvial fan surfaces at Area 5 RWMS are of Late Pleistocene to Middle Holocene age (~100,000 to 5,500 years ago) and that recent geomorphic activity during the Late Holocene (5,500 years ago to today) has been limited to erosion and deposition along small channels [Snyder et al., 1995]. The age estimates of the surface geologic mapping were corroborated by cosmogenic exposure age dating methods [Caffee et al., 1995]. This confirms the assumption that active aggradation occurred during the last Glacial period and that this process has diminished during this current interglacial period.

4.5.1 Aggradation Rates

Although average rates of alluvial fan aggradation at Area 5 RWMS are fairly low, it is reasonable to expect that the rate of deposition has not been constant, but has varied with climatic changes and other factors [French and Lombardo, 1984; Rachocki, 1981]. Computations of average aggradation rates at Area 5 RWMS vary from 33 to 170 mm (1.3 to 6.7 in.) per millennia. French and Lombardo [1984] computed an aggradation rate of 71 mm (2.8 in.) per 1000 years based on an estimated alluvial fan age of 7 million years and a depositional thickness of 488 m (1600 ft). Shott et al. [1998] measured a lava flow at a depth of 274 m (900 ft) below the surface in well UE5k, and reported the age of the basalt flow to have been established at 8.4 million years. Computations based on these numbers would indicate an average deposition rate of 32.5 mm (1.28 in.) per 1000 years.

It might be reasonable to assume that when the climate is in the glacial state, the aggradation rate would be higher, since there would be more rainfall [Brown et al., 1997; DOE, 1998] and since much of the deposition on the local alluvial fans actually occurred during the last ice age in the late Pleistocene. However, in this current interglacial climate, the events that have produced large alluvial fan depositions have been associated with convective thunderstorms that occur during the summer [Beaty, 1963]. Rachocki [1981] presents observations of alluvial fan deposition associated with high intensity rainstorms.

Rachocki [1981] discussed the absence of consensus amongst alluvial fan investigators as to the optimum conditions for alluvial fan development; some researchers favor humid climates, while others favor arid or semi-arid environments. He pointed out that Langbein and Schumm [1958] consider the optimum annual rainfall to be 254 to 356 mm (10 to 14 in.). They felt that this amount of rainfall would provide adequate runoff for transport of materials, but inadequate water for extensive plant cover. Allen [1971] argued that intermittent rainfall was especially

conductive to the development of fans. Tuan [1962] presented conflicting hypotheses for alluvial fan formation:

> The classic theory that the coarse fans form in response to intensified mechanical weathering due to frost action during times of climate cooling, and equally classic theory that the fans form in response to the hypothetically intense mechanical weathering process and deficient runoff of hot arid climates, and that dissections are a product of the times of cool, wet climates.

4.6 Cap Freeboard

The freeboard of Area 5 RWMS cap was estimated by subtracting alluvial fan aggradation (if any) from the original cap height.

Under the assumption that the glacial period will produce a higher aggradation rate, a maximum rate of 15 cm (6 in.) per 1000 years has been used for the computation of cap freeboard in the bounding case where floods overtop the cap. Table 4.11 presents the accumulated aggradation by millennia; Figure 4.1 show the relationship between the cap freeboard and the depths of the largest expected floods.

Table 4.11. Projected Aggradation During Glacial Climate and Computed Area 5 RWMS Cap Freeboard

Parameters	Millennia									
	1	**2**	**3**	**4**	**5**	**6**	**7**	**8**	**9**	**10**
Aggradation (m)*	0.15	0.31	0.46	0.61	0.76	0.92	1.1	1.2	1.4	1.5
Cap Freeboard (m)*	1.9	1.7	1.6	1.4	1.2	1.1	1.0	0.79	0.64	0.49

* 1 m = 3.28 ft

4.7 Assumptions Regarding Area 5 Radioactive Waste Management Site Cap and Subsidence Features

1. At year 2170, institutional control will end and the top of the cap will be 2.0 m (6.6 ft) above the original surface of the alluvial fan.

2. At this point in time, all subsidence features will have been filled in, and the surface of the cap will be flat.

3. For computational purposes, it is assumed that maximum subsidence occurs (instantaneous) one year after control ends, and that the angle of repose for sidewalls is reached within each subsidence feature. Subsidence at the deepest GCD feature is 3 m (10 ft), which would be 1 m (3 ft) below the surface of the alluvial plain. For modeling purposes, it is assumed this occurs at the beginning of this period and that the geometry of the subsidence features remains the same.

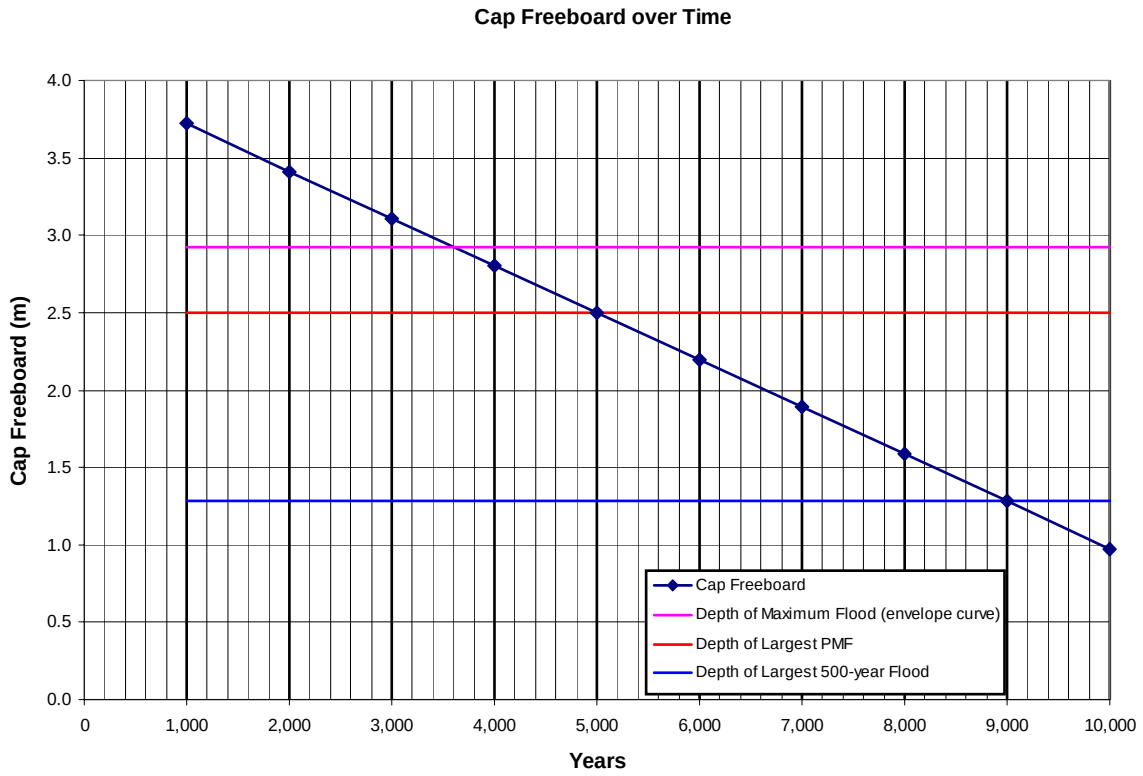

Figure 4.1. Under an Assumed Aggradation Rate of 15 cm (6 in.) per 1000 Years, the RWMS 5 Cap Freeboard Diminishes Relative to the Depths of the Largest Estimated Floods.

4. At any point in time, the cap freeboard is computed to be 2 m (7 ft) minus any accumulated aggradation. Table 4.11 presents the computed cap freeboard for the glacial climate.

5. Engineered barriers up-slope of Area 5 RWMS are ignored.

6. There is no additional landfill north of the present extent of Area 5 RWMS.

4.7.1 Compare Cap Freeboard to Flood Depths

The frequency of flood events that will top the cap is dependent on both the frequency and magnitude of expected flood events and on the freeboard of the cap at the time of the flood. The cap freeboard, the height of the cap above the alluvial fan, is dependent on how much the alluvial fan has aggraded. Although the alluvial fan at the RWMS Area 5 is located on an active or aggrading fan, it is difficult to predict how much that fan will aggrade over the next 10,000 years.

Figure 4.1 shows the relationship of the cap freeboard to the depths of the maximum floods when high alluvial fan aggradation is combined with the largest expected floods. From the envelope curves, the PMF, and the 500-year flood computations, the maximum expected aggradation of 15 cm (6 in.) per 1000 years would result in 1.5 m (5 ft) of aggradation at the end of 10,000 years. If the minimum proposed cap height of 2 m (7 ft) is used, the freeboard at the end of

10,000 years would be 0.5 m (1.6 ft). The depth of the largest 500-year flood would not surpass the cap freeboard until about 9,000 years, when the freeboard is less than 6.89 m (2.1 ft).

Although the depth of the largest envelope curve maximum flood would surpass the cap freeboard at about 3,500 years, the recurrence interval of this flood and the PMF is estimated to be well over 10,000 years. Figures 4.2 through 4.5 show the relationship of flood frequency curves to the maximum floods for each of the major drainages. Under this bounding case, given this relationship between the cap and the potential floods, there is a possibility that the cap could be topped by 500-year or larger floods during the last half of the 10,000-year period.

4.8 Consequences of Flooding on the Cap

The conceptual model of floods eroding and occasionally topping the cap is closer to the expected reality than are either of the two bounding cases, neither of which are expected to happen, and the results of this flooding model, in terms of expected water for infiltration, would lie somewhere between those two bounding cases. The cap is not expected to wash away completely, nor is it expected to stay completely intact. It is probable that it will be eroded by floods emanating from the alluvial fan and by local runoff from the cap itself. The run-on areas for subsidence features will radiate outward and the features themselves will become partially or wholly filled in. As each of the features fill in, fine alluvium will be deposited in the bottom, retarding infiltration over time.

Rare flood events may top the cap and fill the subsidence features with water, but they will also cause severe erosion and leave large amounts of sediment, decreasing the capacity of the features to hold water for infiltration. Although a portion of the flood volume that flows onto the cap could flow into the subsidence features, the features are likely to be filled already with local runoff from the cap. The primary impact of these floods would not increase the water for infiltration, but would diminish the capacity of the subsidence features by depositing sediments.

Since subsequent local runoff and overtopping flood events would fill subsidence features that have diminished capacities, the total volume expected over 10,000 years will have to be less than the volume calculated for bounding case #1. The potential water for infiltration would be distributed similarly to the first bounding case, but the total volume would be less.

The capability of alluvial fan floods to cause massive erosion and deposition was highlighted in a report by Anstey [1965]; he described an alluvial fan flash flood that deposited 1.2 m (4 ft) of debris in some areas and eroded 1.8- to 2.4-m (6- to 8-ft) deep channels in other areas, moving boulders up to 2.4 m (6 ft) in diameter. Hooke [1965] described a similar alluvial fan flash flood in Utah. Beaty [1963] reported several alluvial fan floods that occurred in the White Mountains of California in 1952. The event in Lone Tree Creek consisted of a massive debris flow that lasted 45 minutes to an hour, which was followed by 48 hours of high stream flow. Beaty [1963] described 1.5-m (5-ft) quartzite boulders that were moved for 1.6 to 3.2 km (1 to 2 mi) during these events, and documented boulders up to 4.6 to 6.1 m (15 or 20 ft) long that had been moved in other parts of the western U.S.

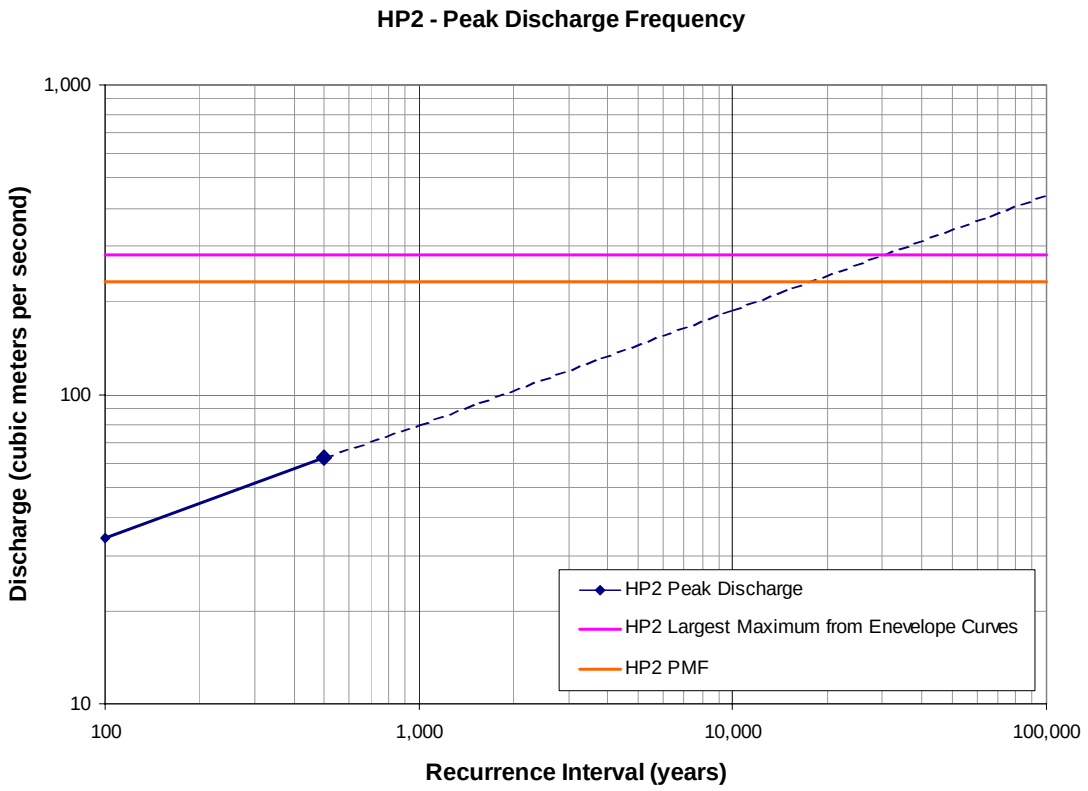

Figure 4.2. Peak Discharge Frequency for HP2 Compared to Maximum Floods.

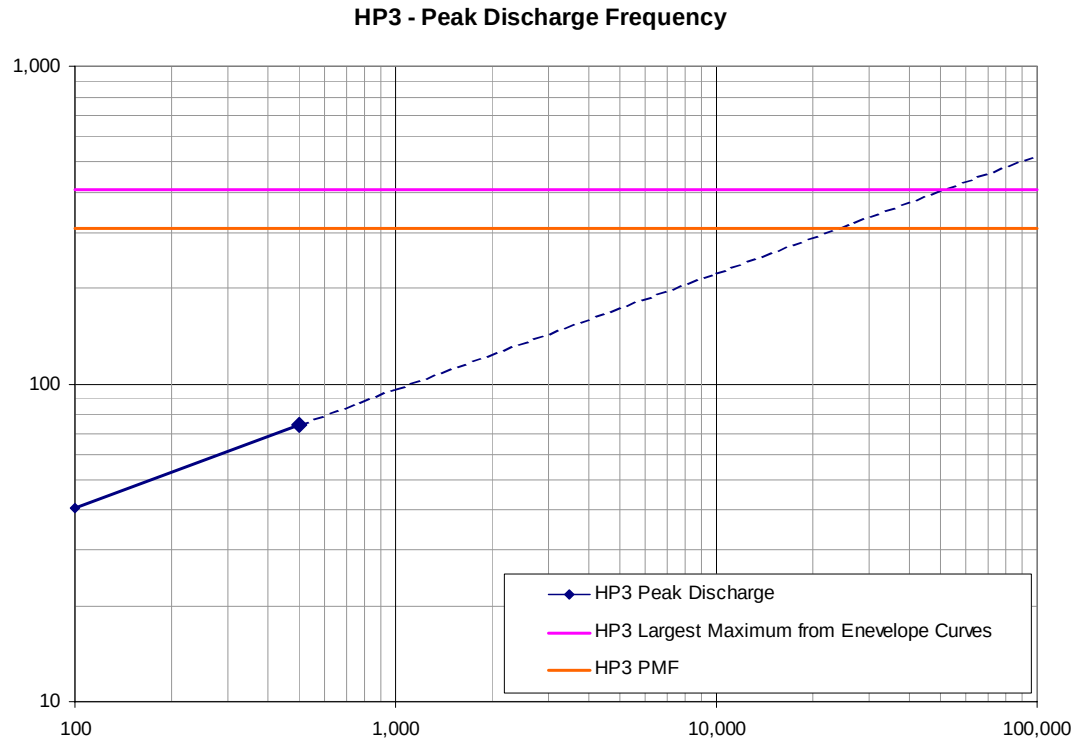

Figure 4.3. Peak Discharge Frequency for HP3 Compared to Maximum Floods.

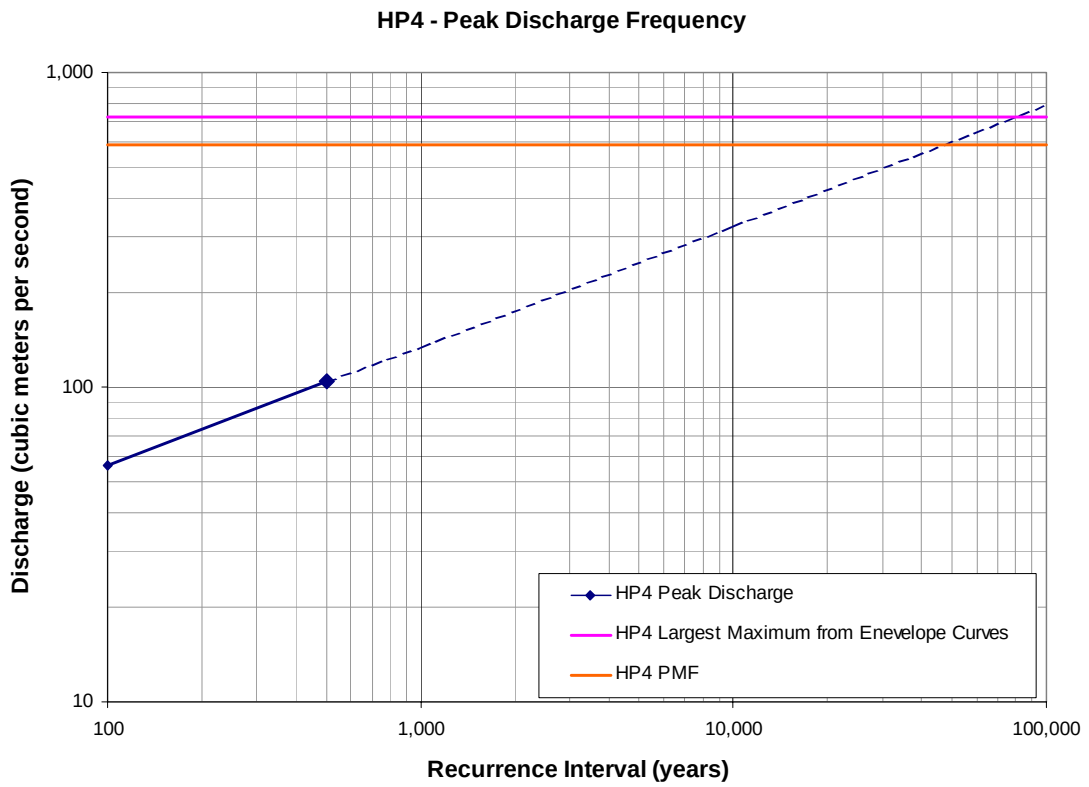

Figure 4.4. Peak Discharge Frequency for HP4 Compared to Maximum Floods.

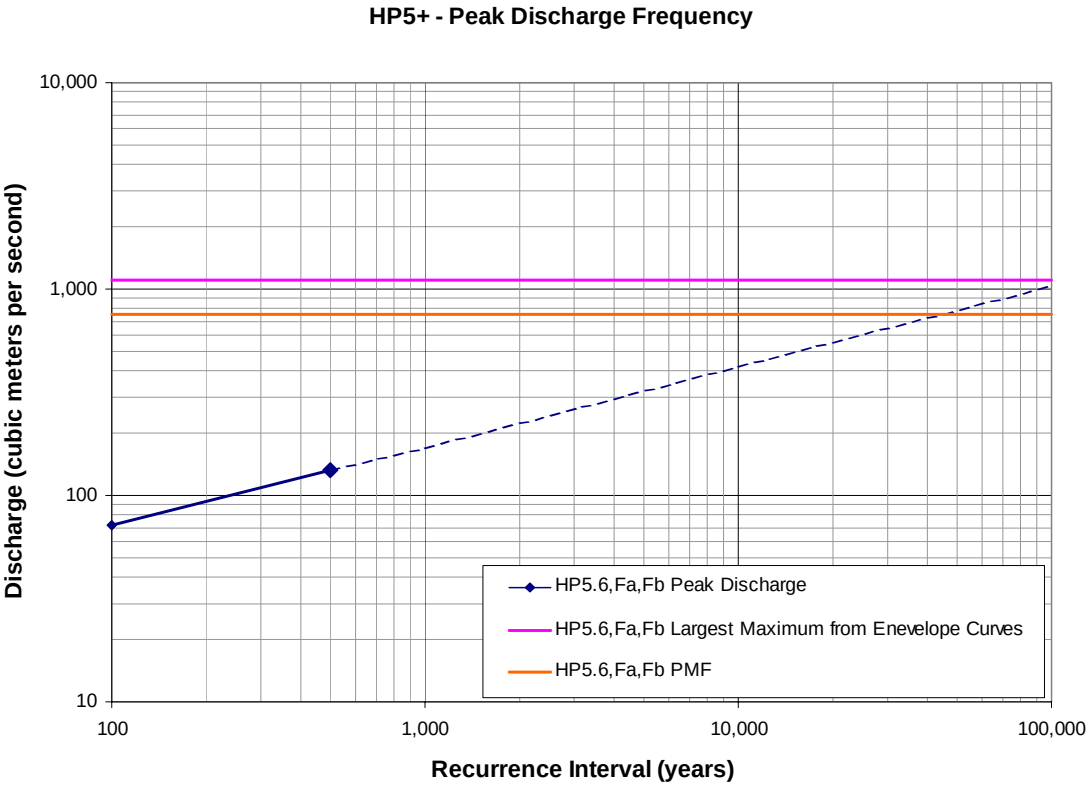

Figure 4.5. Peak Discharge Frequency for HP5+ Compared to Maximum Floods.

This page intentionally left blank.

5.0 UNSATURATED FLOW ANALYSIS

5.1 Purposes and Expected Results

As discussed in previous sections, the LLW trenches and pits and the GCD boreholes located in the Area 5 RWMS are expected to subside after the end of the institutional control and, as a result, will focus runoff and precipitation into the resulting depressions. The unsaturated flow analysis is therefore designed to address the following questions:

- Will the surface water focused in the subsidence depressions above the GCD boreholes infiltrate into the unsaturated zone and reach the groundwater table in <10,000 years under current or future climate conditions?

- Will the surface water focused in the subsidence depressions within the LLW trenches and pits infiltrate into the unsaturated zone and spread far enough laterally to influence the moisture conditions around the GCD boreholes under current or future climate conditions?

- Will infiltrating surface water focused in the subsidence depressions above the GCD boreholes interact with infiltrating surface water from the LLW trenches in such a way that water from the GCD boreholes could reach the groundwater table in <10,000 years under current or future climate conditions?

Depending on the answers to these questions, the scenarios of subsidence and climate change will either be screened out of the PA, or further work (i.e, radionuclide transport analyses) will be required to screen out this scenario.

The approach taken in this screening analysis is to develop unsaturated flow conceptual models that overestimate the potential of the focused water to enter the unsaturated zone and move downward. These models are largely based on the information provided in the previous sections on the geometry of the subsided features and subsidence depths (Section 2.0) and the volumes and frequencies of the events that focus surface water into the different subsidence features (Sections 3.0 and 4.0).

The conceptual model of focusing precipitation and run-off in the subsided features is described in Section 5.2. The conceptual model for unsaturated flow analysis is discussed in Section 5.3. The mathematical formulation of the conceptual model and the general modeling approach used in the unsaturated flow analysis are then provided in Section 5.4. The evaluation of the mathematical model's bias is considered in Section 5.5. Finally, a summary of all the assumptions that cause the mathematical model to overestimate downward flow is provided in Section 5.6.

5.2 Conceptual Model of Focusing Precipitation in Subsided Features

The conceptual model of focusing precipitation in the subsided features represents the link between the subsidence model, the surface water model, and the unsaturated flow model by specifying the upper boundary conditions of the unsaturated zone model. In this analysis, two conceptual models were considered. The first conceptual model assumes that the cap remains

intact for 10,000 years and subsided features collect all of the local runoff from the cap and all precipitation falling in the subsidence feature starting from the end of the institutional control period and lasting for 10,000 years. The second conceptual model assumes that the cap is instantaneously removed at the end of the institutional control period and that the subsided features collect the regional runoff and sediment as well as local precipitation until they are totally filled with the sediment. Consequently, the main differences between the two models are in the volumes and frequencies of surface water runoff and in longevity of the subsided features.

Both conceptual models assume that at the end of the institutional control period, all the remaining voids in the pits, trenches, and GCD boreholes will be instantly expressed. In reality, the remaining subsidence will occur gradually over several hundred years and some of the features may not collect the run-on water for a long time after the site closure. However, this assumption is used to maximize the overall volume of runoff into the subsidence features.

5.2.1 Conceptual Model 1 – Intact Cap

The conceptual model used to calculate runoff into subsided features assuming an intact cap is shown in Figure 5.1. Major results of the precipitation and surface water runoff analyses (Section 3.0) include the following:

- estimation of the total volumes of surface water focused in the different subsidence features over the next 10,000 years under current and future climate conditions;

- estimation of the surface water volumes focused in the different subsidence features due to low-probability events such as the PMP, the 10,000-, 1000-, and 100-year storms under current and future climate conditions; and

- estimation of the number and volumes of the remaining high-frequency events that focus surface water in the different subsidence features under the current and future climate conditions.

A summary of these results is presented in Table 5.1. The following conclusion can be drawn from this table:

- most of the surface water focused in the subsidence features is from the low-intensity, high-frequency events (rather than from the low-probability events). The total amount of water focused into subsidence features under glacial climate conditions is significantly greater than the amount of focused surface water under current climate conditions; 3.7 times greater for GCD Borehole 1 and 4.2 times greater for trench TO4C. Consequently, assuming that the glacial climate will be established at the end of the institutional control period and will remain throughout the 10,000 years will result in overestimating the infiltration flux.

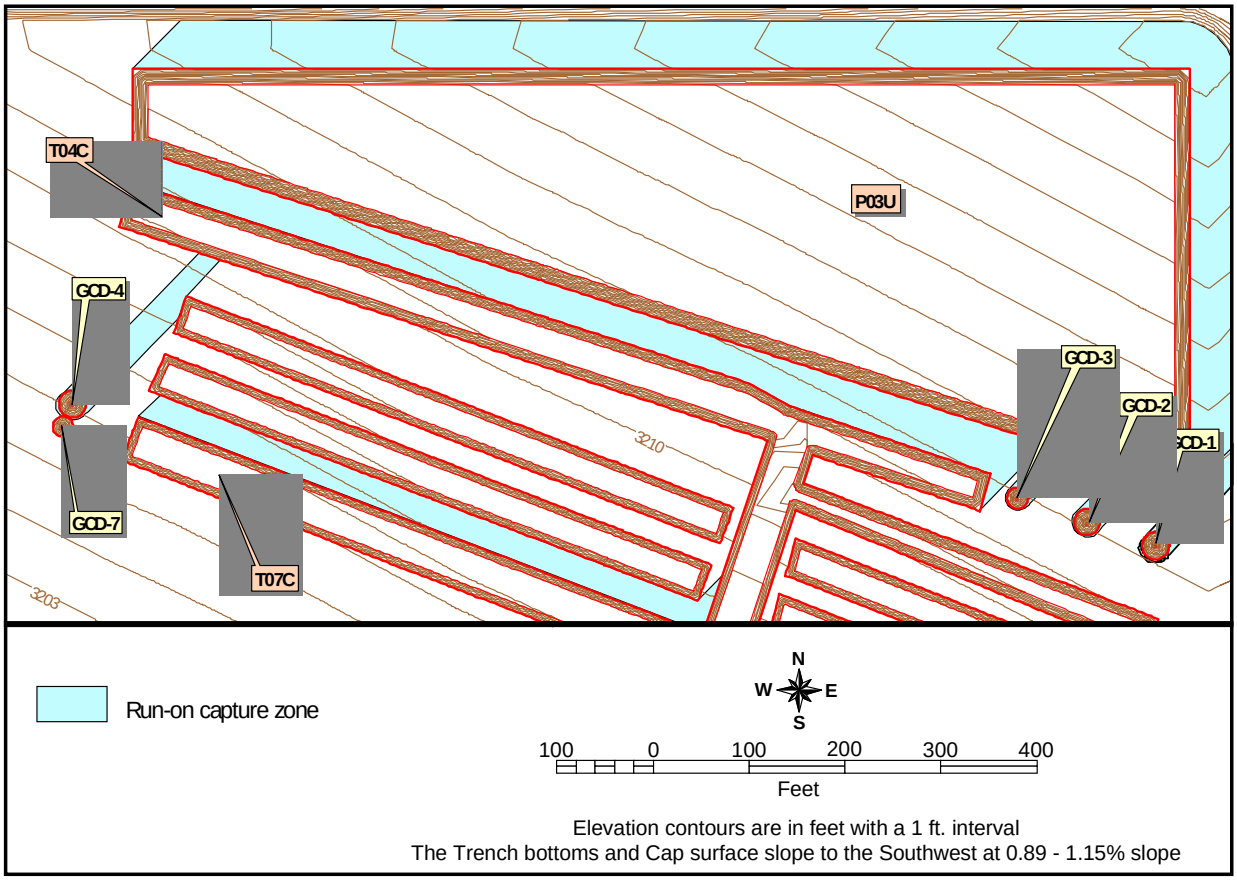

Figure 5.1. Northeast Corner of the Area 5 RWMS Capture Zones of the LLW Trenches/Pits and GCD Boreholes.

Table 5.1. Volumes and Numbers of Ponding Events for the Different Subsidence Features from the Precipitation and Runoff Analysis – Intact Cap Conceptual Model

Subsided Features	GCD Borehole 1	Trench TO4C	Trench TO7C	Pit PO3U
		Current Climate Conditions		
Total Volume, m^3	**14,869**	**488,220**	**305,145**	**2,764,205**
PMP, m^3	118	2,429	1,427	11,401
10,000-year storm, m^3	32	683	403	3,248
Nine 1000-year storms, m^3	198	4,325	2,567	20,956
90 100-year storms, m^3	1,222	28,406	17,016	141,730
Number of Low Probability Events	101	101	101	101
Total Volume of Low Probability Events, m^3	1,571	35,843	21,412	177,335
Number of Events Other than Low Probability Events	23,333	23,333	23,333	23,333

Table 5.1. Volumes and Numbers of Ponding Events for the Different Subsidence Features from the Precipitation and Runoff Analysis – Intact Cap Conceptual Model (Continued)

Subsided Features	GCD Borehole 1	Trench TO4C	Trench TO7C	Pit PO3U
Total Volume of Events Other than Low Probability, m^3	13,298	452,377	283,733	2,586,870
Future Climate Conditions				
Total Run-On, m^3	**54,145**	**2,052,959**	**1,300,445**	**12,071,154**
PMP, m^3	108	2,231	1,313	10,512
10,000-year storm, m^3	28	642	383	3,162
Nine 1000-year storms, m^3	166	4,001	2,409	20,289
90 100-year storms, m^3	1,050	27,513	16,758	144,449
Number of Low Probability Events	101	101	101	101
Total Volume of Low Probability Events, m^3	1,352	34,387	20,863	178,412
Number of Events Other than Low Probability Events	35,833	35,833	35,833	35,833
Total Volume of Events Other than Low Probability, m^3	52,793	2,018,565	1,279,582	11,892,742

The analysis of precipitation and runoff has also demonstrated that the number of high-frequency events over 10,000 years is very large (see Table 5.1). For example, under glacial climate conditions there would be 35,833 events that would accumulate some volume of surface water within trench TO4C. A number of these events result in such shallow ponding depths that it is not practical to simulate all of them. For example, a volume of surface water equal to 10 m^3 evenly distributed over the 2169 m^2 area of the trench TO4C bottom would produce a pond with a depth of 5 mm.

The following approach was used to overestimate the infiltration flux while attempting to minimize computational and modeling efforts. Instead of simulating every single event, each with different volumes and spacing in time, a smaller number of events having an average volume, spaced evenly in time, was simulated.

The number of events to be simulated, n_p, was calculated as the number of ponding events that have volumes equal to or greater than the median volume, $V_{50\%}$. This means that 50% of all the ponding events have a volume equal to or greater than $V_{50\%}$ and 50% have a volume less than $V_{50\%}$. The relationships between the frequencies and cumulative volumes of the ponding events are shown in Figures 5.2 and 5.3. Note that $V_{50\%}$ is equal to 109 m^3 for trench TO4C and $V_{50\%}$ is equal to 1.7 m^3 for GCD Borehole 1.

The volume of an average ponding event to be simulated, V*av*, and the average frequency of ponding, *fp*, were calculated as follows:

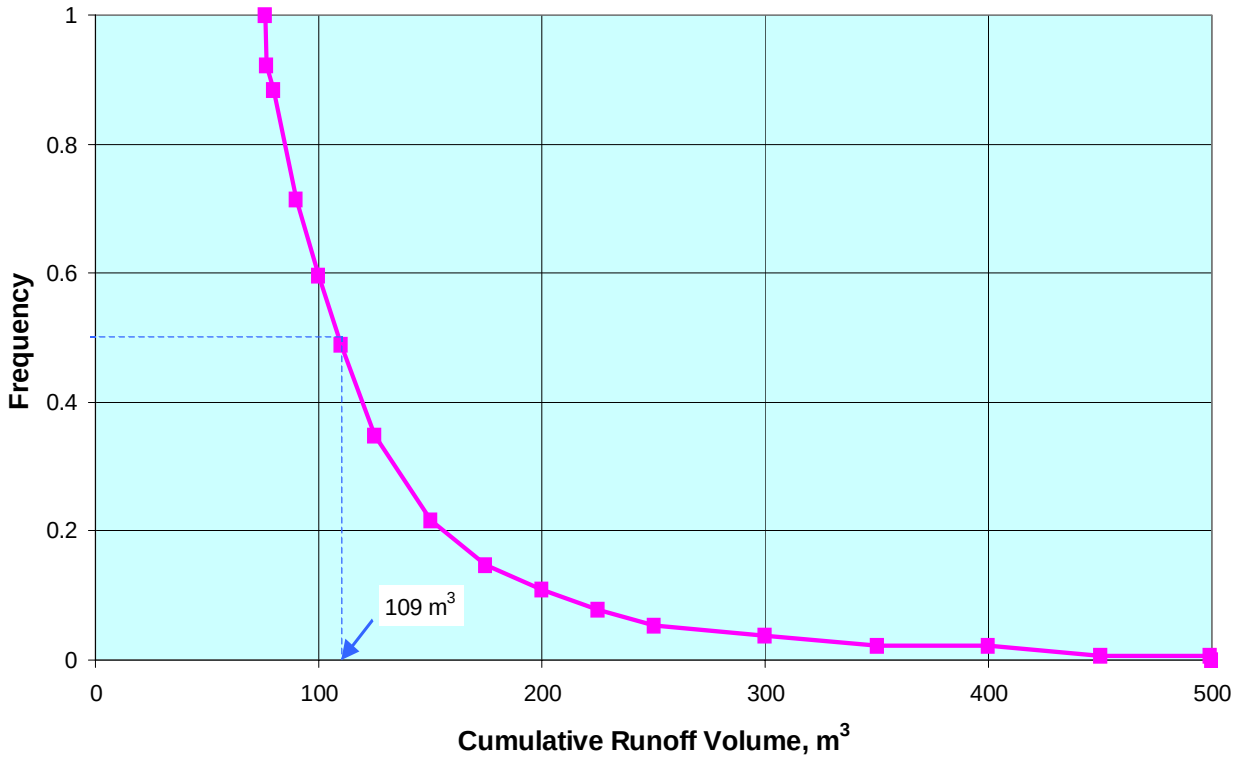

Figure 5.2. Frequencies and Volumes of Ponding Events in Subsided Trench TO4C Under the Glacial Climate. Conceptual Model 1 – Intact Cap.

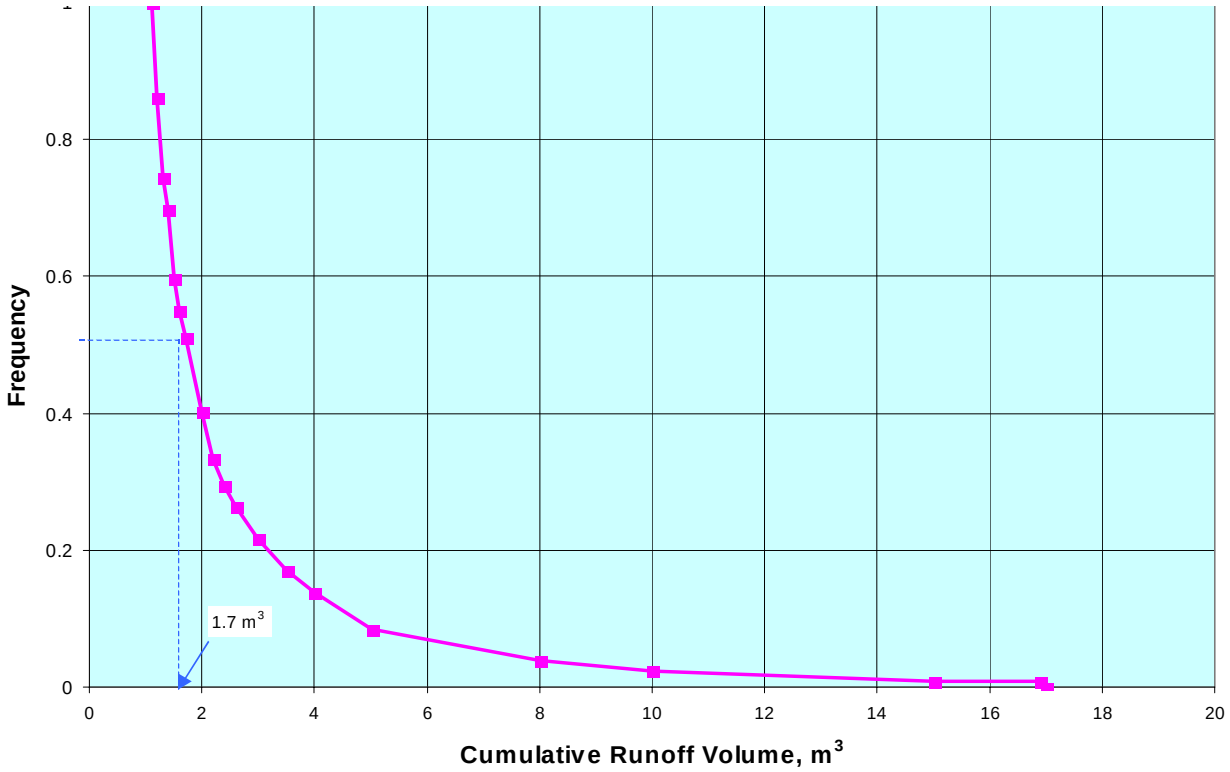

Figure 5.3. Frequencies and Volumes of Ponding Events in Subsidence Feature Above GCD Borehole 1 Under the Glacial Climate. Conceptual Model 1 - Intact Cap.

$$Vav = Vtot/n\text{p} \quad (5.1)$$

$$fp = 10{,}000/n_p \quad (5.2)$$

where *Vtot* is the total volume of surface water captured by the subsidence feature over 10,000 years, excluding low probability events. This approach accounts for all the surface water accumulated in the subsidence features over the period of simulation and, thus, overestimates the infiltration flux. In reality, many small ponding events would dry off due to evaporation from the open water and land surface before any infiltration occurs.

The information on average ponding volumes and frequencies for trench TO4C and for GCD Borehole 1 is summarized in Table 5.2 for the glacial climate conditions. The average ponding event in subsided trench TO4C (V*av* = 227 m^3) and in the subsidence feature above the GCD Borehole 1 (V*av* = 5.9 m^3) would occur every 1.125 years.

The low-probability events could be spread out over the entire simulation period with a frequency corresponding to their probability of occurrence. However, in order to overestimate the infiltration flux, the most significant events were placed at the beginning of simulation. That is, the ponding event corresponding to the PMP was specified at time zero. The ponding corresponding to the 10,000-year storm was specified at time equal to 1.125 years. The ponding corresponding to the first of nine 1000-year storms was specified at time equal to 2.55 years. The other low-probability events were simulated as shown in Table 5.2.

Table 5.2. Simulated Frequencies, Volumes, and Durations of the Different Ponding Events – Intact Cap Conceptual Model

Type of Event	Frequency, yrs^{-1}	Event Volume, m^3	Event Duration, d
Trench TO4C			
PMP	0.0001	2,231	1.25
10,000 year storm	0.0001	642	0.36
1000 year storm	0.0009	445	0.25
100 year storm	0.009	306	0.17
Average event	0.889	227	0.13
GCD Borehole 1			
PMP	0.0001	59	5.42
10,000 year storm	0.0001	28	4.87
1000 year storm	0.0009	18	3.13
100 year storm	0.009	12	2.09
Average event	0.889	5.9	1.03

When the volume and the frequency of the ponding events are defined, the representation of these events depends on the subsidence feature geometry and model dimensionality.

The subsided features above the GCD boreholes are cone-shaped and are modeled with the quasi-3-D model in radial coordinates (see Section 5.3 for details). All ponding events are

assumed to instantaneously fill these features to a depth that corresponds to the event volume. The duration of the ponding event t_p is calculated as:

$$t_p = Vp /(Sp*Ksat) \quad (5.3)$$

where *Vp* is the volume of the average or low-probability ponding event, *Sp* is the surficial area associated with the portion of the cone-shaped depression that is filled with water, and *Ksat* is saturated hydraulic conductivity of the alluvial deposits. A prescribed flux boundary condition is then specified along the depression walls for a period of time equal to t_p to simulate the infiltration process.

The subsided trench is modeled as a 2-D vertical cross-section along the trench (see Section 5.3). Surface water is assumed to instantaneously fill the subsidence depression within the trench to the depth d_p, which corresponds to the volume of the ponding event. The duration of the ponding event t_p is calculated as:

$$t_p = d_p /Ksat \quad (5.4)$$

A prescribed flux boundary condition is specified along the bottom of the trench for the period of time equal to t_p to simulate the infiltration process. The volume of water introduced to the system with each ponding event v_p is defined as:

$$v_p = V_p / w \quad (5.5)$$

where *w* is the trench width in the direction orthogonal to the cross-section.

In this manner, each ponding event almost instantly introduces a volume of water equal to *Vp* (GCD borehole) or to v_p (trench) to the unsaturated system. Table 5.2 provides the duration of the average and low-probability events for these features.

5.2.2 Conceptual Model 2 – No Cap

The following results from the precipitation and runoff analysis (Section 3.0) were used to develop the conceptual model of focusing precipitation in the different subsided features assuming no cap:

- the time required to fill in the subsidence features with sediment, the total volumes of water accumulated within the subsided features, and the timing and volume of each ponding event under current and future climate conditions.

A summary of these results is presented in Table 5.3. Note that the total volume of the surface water accumulated in a specific subsidence feature under the current climate conditions is the same as under the future climate conditions. However, the time it takes to fill the features with sediment is different under current and future climates. Specifically, subsidence features fill up with sediment faster under future climate conditions. For example, 37,413 m^3 of water would be

Table 5.3. Volumes of Ponding Events and Lifetimes of the Different Subsidence Features from the Precipitation and Runoff Analysis – No Cap Conceptual Model

Subsided Features	GCD Borehole 1	Trench TO4C	Trench TO7C	Pit PO3U
Current Climate Conditions				
Total Volume, m^3	393	37,413	24,967	478,453
Life Time, yrs	168	220	236	224
Future Climate Conditions				
Total Volume, m^3	393	37,413	24,967	478,453
Life Time, yrs	125	175	178	190

captured within the subsided trench TO4C during 220 years assuming the current climate or during 175 years assuming the glacial climate. In other words, 37,413 m^3 of water carries the amount of sediment required to fill up the subsidence depression associated with TO4C.

Introducing the same amount of water into the unsaturated zone in a shorter period of time will result in a higher downward flux, since there will be less time for the soil to dry between the ponding events. Consequently, assuming glacial climate conditions provides an upper bound or screening estimate of the downward flux.

The total volumes of water accumulated in trench TO4C and GCD Borehole 1 under glacial climate conditions assuming no cap (Conceptual Model 2) were compared to the corresponding total volumes of water accumulated assuming intact cap (Conceptual Model 1).

In the case of trench TO4C, the total volume water associated with Conceptual Model 2 is 18% of the total volume associated with Conceptual Model 1. However, the average intensity of precipitation/runoff events into the trench, and therefore into the unsaturated zone, is higher for Conceptual Model 2 (214 m^3 versus 202 m^3 for Conceptual Model 1). Therefore, it is difficult to assess *a priori* which model will result in the most downward flow. Given the higher intensity events of Model 2 and numerous other assumptions which cause both models to overestimate infiltration, trench TO4C under the glacial climate conditions assuming no cap (Conceptual Model 2) was chosen as the screening model.

In the case of the GCD boreholes, the total volume in Conceptual Model 2 is less than 1% of the total volume in Conceptual Model 1. In addition, the average intensity of introducing water into the unsaturated zone is much lower in Conceptual Model 2 (3.1 m^3/year) than in Conceptual Model 1 (5.3 m^3/yr). Therefore, GCD Borehole 1 was modeled using only Conceptual Model 1 (intact cap) under only glacial climate conditions.

The data used to estimate focused precipitation and runoff into subsided trench TO4C, assuming no cap, are presented in Table 5.4. The first ponding in the subsided trench occurs 25 years after the end of the institutional control period. Then, 59 ponding events occur over the trench lifetime (175 yrs). However, most of the water (over 99%) is introduced over the first 114 years by 31 ponding events. The remaining 28 ponding events span the next 44 years and add less than 1% of the total volume.

Table 5.4. Timing and Volumes of Ponding Events in Subsided Trench TO4C – No Cap Conceptual Model

Event Timing, yrs	Event Volume, m^3	Event Timing, yrs	Event Volume, m^3
25	3,095	114	51
50	5,148	115	43
60	4,376	116	37
65	3,719	118	31
70	3,161	120	27
72	1,462	122	23
74	2,120	124	19
75	2,150	125	16
76	1,827	126	14
78	1,553	128	12
80	1,320	130	10
82	1,122	132	9
84	954	134	7
85	811	135	6
86	689	136	5
88	586	138	4
90	498	140	4
92	423	141	3
94	360	143	3
95	306	144	2
96	260	145	2
98	221	146	2
100	188	148	1
102	160	150	1
104	136	152	1
105	115	154	1
106	98	155	1
108	83	156	1
110	71	158	1
112	60		

The following approach was use to overestimate the downward flux:

- the first of the 31 ponding events that occur prior to 114 years was assumed to occur at the beginning of simulation (time equal to zero), instead of the 25 years indicated in Table 5.4. The remaining 28 events occurred at the time given in Table 5.4 minus 25 years; and

- the 28 ponding events that occur after 114 years were combined into two ponding events with the time between them equal to one year (the smallest frequency observed). The first of these events was assumed to occur one year after the first 31 events. Six of the 28 events were combined into a single event with a total volume of 180 m^3. The remaining 22 events were combined into a single event with a total volume of 106 m^3.

As a result, the volume of 37,413 m^3 is introduced into the unsaturated zone during the first 91 years of the simulation, instead of 175 years, and by 33 ponding events instead of 59. The proposed distribution of the ponding volumes over the time is shown in Figure 5.4. The duration of each ponding event was calculated using Equation (5.4). The maximum duration of a ponding event was three days.

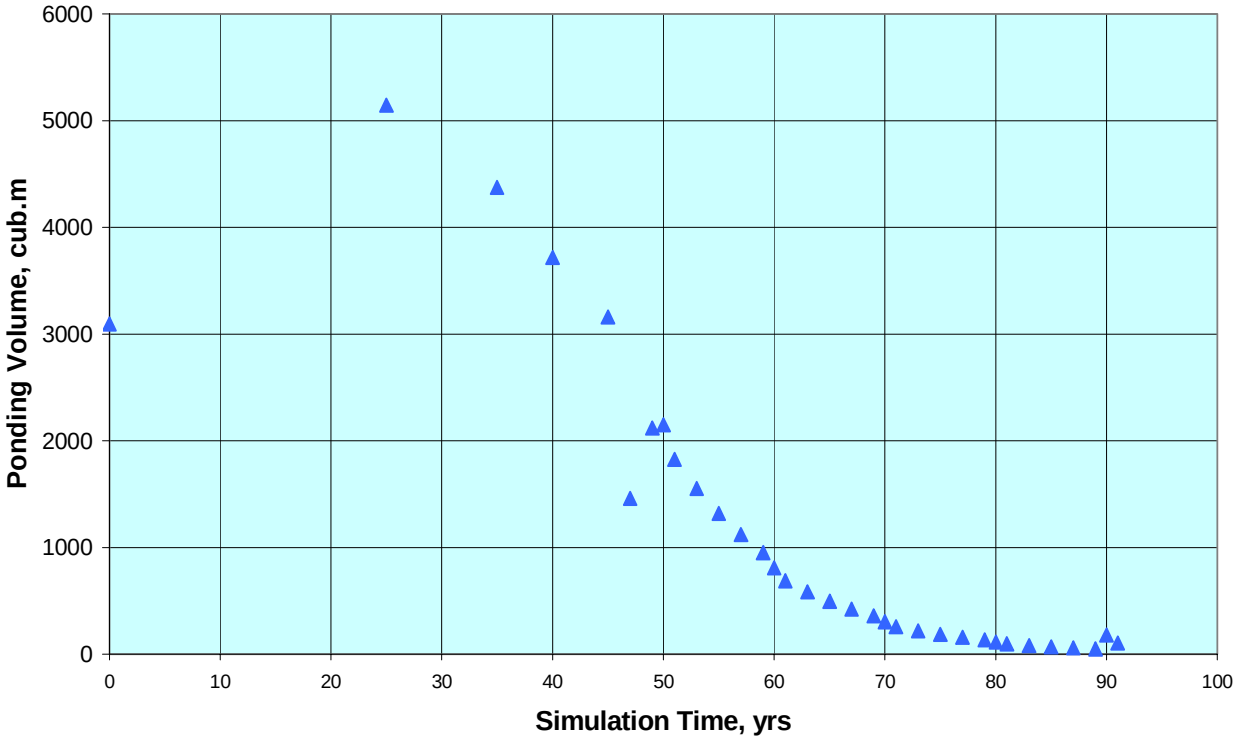

Figure 5.4. Volumes of Ponding Events in the Subsided Trench TO4C. Conceptual Model 2 – No Cap.

5.3 Unsaturated Zone Conceptual Model

5.3.1 Summary of Previous Research

This unsaturated zone conceptual model was developed based on the current state of knowledge about the unsaturated zone within the Area 5 RWMS, as summarized in Shott et al. [1998] and discussed in many previous reports. A number of studies have been conducted on the unsaturated zone within and around the Area 5 RWMS. Site characterization data are provided in McGrath [1987], Blout [1995], REECo [1993a], REECo [1993b], and REECo [1994]. The results of isotopic studies at the site are published in Chapman [1993] and Tyler [1996]. The modeling of unsaturated flow is discussed in Levitt et al. [1998a]. The modeling of the unsaturated zone in the vicinity of the site is discussed in Hokett and French [1998], Ross and Wheatcraft [1994], and Bryant [1992]. The current stage of knowledge about the unsaturated zone within the Area 5 RWMS and its conceptualization for different purposes (LLW PA, transport and flow simulation, etc.) are summarized in Shott et al. [1998] and are based on site characterization data, isotopic studies, and flow and transport simulations.

The following concepts summarize the current state of knowledge about the unsaturated zone:

- The unsaturated zone at the site is very dry from the land surface all the way to the aquifer. Increases in moisture content occur only in close proximity to the groundwater table.

- No groundwater recharge is occurring under current climate conditions. All precipitation falling onto the undisturbed land surface at the site gets recycled by evaporation and evapotranspiration processes that occur within the top 2 m (7 ft) of soil. Thus, fluctuations in moisture contents are only observed within this shallow depth.

- The absence of spatially-distributed groundwater recharge during a significant period of time (on the order of the past 100,000 years) followed by a long drying-out period has resulted in upward advection and evaporation of pore water from the upper part of the unsaturated zone to a depth of approximately 35 m (115 ft). Even though the upward pressure gradient is large, the upward movement is very slow due to the low moisture content and the correspondingly low unsaturated hydraulic conductivity. The velocity of the upward movement is currently estimated to be less than 0.4 mm/yr.

- Downward moisture movement currently occurs only at depths below 80 m (262 ft) from the land surface. The pore water encountered at this depth is believed to be surface water from previous climatic conditions that is very slowly moving downward. A transition zone with zero potential is located between the depth of 35 and 80 m (115 and 262 ft). No moisture movement occurs in this transition zone.

- The unsaturated zone is made up of heterogeneous alluvial deposits. However, no extensive layers or anisotropy have been observed. Thus, the alluvium can be considered homogeneous and isotropic for modeling purposes.

- Among the physical parameters of the alluvium, the most important for the unsaturated flow simulation are: saturated porosity, residual moisture, saturated hydraulic conductivity, and parameters that describe functional relationships between moisture content and pressure head (water retention curve) and moisture content and unsaturated hydraulic conductivity. Detailed discussions of these parameters, including their probability distribution functions for the Area 5 RWMS, are provided in Shott et al. [1998] and in Appendix D.

The above concepts form the basis for the development of the conceptual model and parameters used in simulating unsaturated flow resulting from infiltration of water collected in different subsided features.

5.3.2 Unsaturated Zone Parameters

Due to the screening character of the calculations and the significant computational effort needed to incorporate probabilistic representations of the unsaturated zone, only mean parameter values were used. Issues related to the sensitivity of the model to these parameter values are considered in Section 8.0.

The hydraulic conductivity characteristic curve was defined using Mualem model [Mualem, 1976]:

$$K(S_e) = K_{sat} S_e^1 \left[1 - \left(1 - S_e^{1/m} \right)^m \right]^2 \tag{5.6}$$

where K_{sat} is saturated hydraulic conductivity, S_e is the effective saturation, and *l* and *m* are fitting parameters.

The moisture retention curve was described using van Genuchten relationship [van Genuchten, 1978]:

$$S_e = \frac{\theta - \theta_r}{\theta_s - \theta_r} = \frac{1}{\left[1 + (\alpha \Psi)^n \right]^m}, \; m = 1 - 1/n \tag{5.7}$$

where Ψ is the pressure head, θ_r is residual moisture, θ_s is saturated porosity, and α and *n* are fitting parameters.

The unsaturated zone parameter values are summarized in Table 5.5. The moisture retention curves corresponding to the mean parameters are shown in Figure 5.5. The mean parameter values are based on data collected for the wells AP-1, AP-2, RP-1, and RP2. The actual measurements in these wells and the method used to fit these measurements into the van Genuchten function and into the Mualem function are discussed in Appendix D.

Table 5.5. Summary of the Unsaturated Zone Parameter Estimates

Unsaturated Zone Parameter	Notation Units	Mean Parameter Value	Parameter Value from Shott et al. [1998]	Parameter Value from Hokett and French [1998]	Parameter Value from Ross and Wheatcraft [1994]
Saturated Hydraulic Conductivity	K_{sat} m/d	0.82	0.72	3.5	0.54
Residual Moisture Content	θ_r unitless	0.06	0.065	0.057	0.084
Saturated Moisture Content	θ_s unitless	0.33	0.36	0.41	0.33
van Genuchten Fitting Parameter	α cm^{-1}	0.071	0.036	0.124	0.018
van Genuchten Fitting Parameter	n unitless	1.4	1.94	2.28	2.36

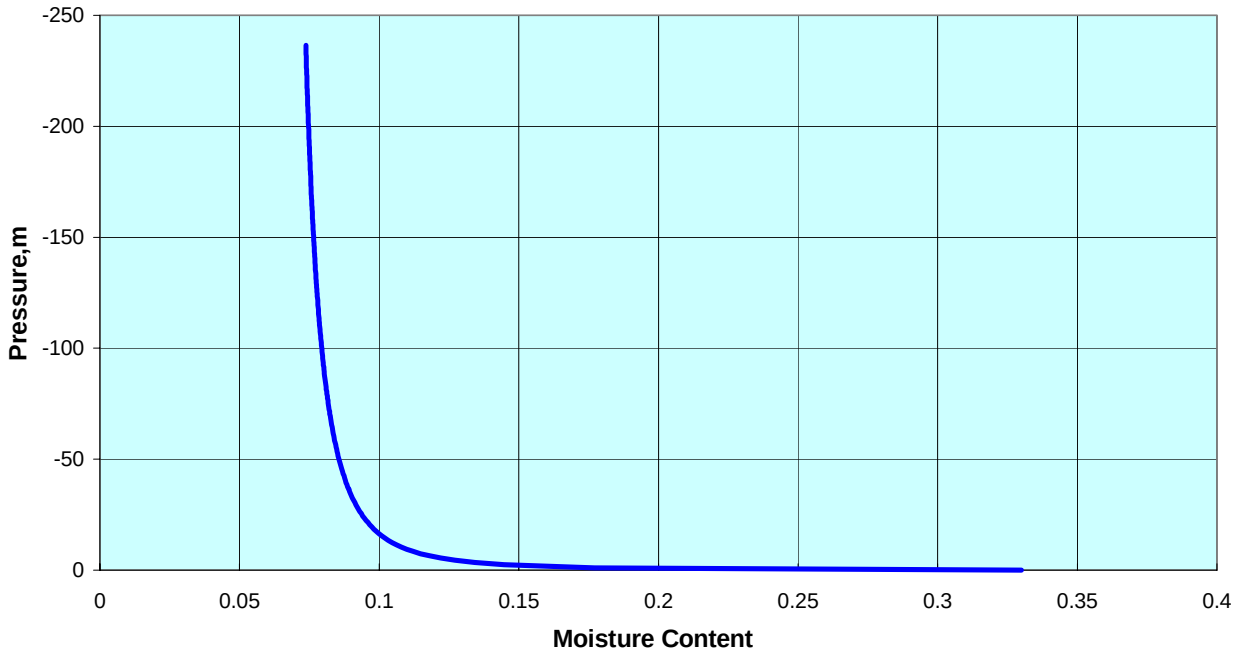

Figure 5.5. Pressure-Moisture Content Relationship.

The mean parameter values of the distributions developed in Shott et al. [1998] are provided in Table 5.5 for the sake of comparison. The last two columns of Table 5.5 list the unsaturated zone parameters used in modeling unsaturated flow around the U5a crater [Hokett and French, 1998] and around the Cambric trench [Ross and Wheatcraft, 1994], and are included for comparison. As shown in Table 5.5, the mean parameter values are comparable and fall within a relatively narrow range.

5.3.3 The Atmospheric Boundary

The atmospheric boundary, or the upper boundary of the unsaturated zone, is the subsided land surface. This section discusses potential evaporation (PE) and potential evapotranspiration (PET) from this boundary, and the source of the values used in the unsaturated flow modeling.

The maximum amount of water that can be extracted by evaporation and transpiration from the surface layer of the vadose zone by evaporation or from the upper portion of the vadose zone (or root zone) by plant transpiration is limited by several factors, including meteorological conditions and vegetation. The absolute upper limits of PE and PET at Area 5 are bounded by the average annual potential *pan evaporation* measured on Frenchman Flat, a value of 310.0 cm (122.0 in.) [Magnuson et al., 1992]. The average annual PET for Area 5 is likely to be similar to the estimated value for Area 6 of the NTS, which ranges from 169.8 to 178.5 cm/yr (66.85 to 70.26 in./yr) [French, 1993]. However, since Area 6 is located at a higher elevation than Area 5, the PET range for Area 5 is expected to be higher than the PET range in Area 6 [Shott et al., 1998].

The bare soil PE and PET at the Area 5 RWMS were estimated by Levitt et al. [1998]. Average annual PET was estimated with the Penman equation to be 156.8 mm/yr (61.73 in./yr). This

value is lower than would be expected based on the Area 6 estimate. Monthly PE estimates were computed with the CREAMS code [Levitt et al., 1998]. For modeling purposes, Levitt et al. [1998] adjusted the monthly PE values so that their sum over one year was equal to the Penman annual PET estimate. The adjusted PE values were used to model 1-D unsaturated flow within the 3 m (10 ft) cover proposed for Pit 3 of the Area 5 RWMS. The modeling results were then compared with four year's worth of weighing lysimeter data collected at the site, and matched to the experimental data [Levitt et al., 1998]. As noted by Levitt et al. [1998], the measured *evapotranspiration* rates from lysimeters located in vegetated areas were higher than measured *evaporation* rates from lysimeters located in non-vegetated areas.

The simplified relationship between *PE* and *PET* commonly used in agricultural practice is described as:

$$PE = C*PET, \tag{5.8}$$

where *C* is known as crop coefficient. While *PE* mainly depends on meteorological factors and the surface type, *PET* also depends on the surface characteristics of plants, depth of the rooting zone, distribution of roots within the rooting zone, and composition and physical properties of soil. The coefficient *C* in Equation (5.8) expresses the difference between PE and PET in a simple fashion. In many cases, such as Area 5, *PET* will be higher than *PE* and the crop coefficient would be less than 1.

Evaporation from bare soil occurs only within a thin surficial layer. Without precipitation, liquid flux from below the surface layer provides the water for evaporation. The liquid flux supplied to the surface from below is controlled by the suction pressure near the surface. Evapotranspiration by plants occurs from the depth that is occupied by the plant roots. In turn, the liquid flux into the plant roots is controlled by the difference in suction pressure in the root zone and in the plant, which can be very high in plants possessing high water-extraction capabilities.

This modeling effort chose to model only evaporation from the land surface, and PE values used in modeling unsaturated flow were based on the Area 5 work of Levitt et al., [1998], as discussed above. Assuming only PE will underestimate the amount of water removed from the subsurface and therefore overestimates the amount of infiltration into the vadose zone, which is in line with the purpose of these screening calculations. In addition, by using only PE, uncertainty related to the representation of different plant communities, especially under the future climate conditions, is eliminated.

The distribution of the PET rates within the year is shown in Figure 5.3.

Under glacial conditions, the climate will be cooler and wetter. As discussed in Section 3.0, the average annual temperature under future climate conditions will be about 4°C lower and the mean annual precipitation will be about two times higher. The lower temperature may result in the lower PE from the bare soil. The higher precipitation may result in higher potential transpiration. As a result, the total PET may not significantly change. To assess this statement, an analog site was identified and analyzed. The data used in searching for an analog site was the expected annual average temperature and the expected mean annual precipitation. The site identified was Boise, ID with average annual temperature of 10.4°C and mean annual precipitation of 30.76 cm/yr (12.11 in./yr).

The available reference crop evapotranspiration data for this location (http://snow.ag.uidaho.edu/Publications/pond_evap/Appendix_B.html [Access date: July 10, 2000]) are shown in Figure 5.3. As this figure shows, the annual PET for the analog site is close to the Levitt et al. [1998] estimate of PET for Area 5.

Another site found in the literature is Golodnaya Step, Ukraine with an average annual temperature of 13°C and mean annual precipitation of 25.8 cm/yr (10.2 in./yr). According to research described in Kats [1992], the annual average evapotranspiration at this site is 152.1 cm/yr (59.88 in./yr), which is comparable to the PET of 156.8 cm/yr estimated by Levitt et al. [1998] for the Area 5 RWMS.

Consequently, the PET and PE rates estimated by Levitt et al. [1998] for current conditions were used in simulating future climate conditions. The sensitivity of the unsaturated flow model to these rates is considered in Section 8.0.

5.3.4 Other Flow Boundaries and Dimensionality

The lower boundary of the unsaturated zone is the water table, which is located at a depth of approximately 236 m (774 ft) below the land surface. It was assumed that the location of this boundary will remain constant over the next 10,000 years. This will be true in the absence of significant areal recharge to the region. According to the simulation results of the Death Valley regional flow model for the past, current, and future climate conditions [D'Agnese et al., 1999], there will be no areal recharge in the Frenchman Flat over this time period.

There are no natural boundaries that would limit the extent of the unsaturated zone in the horizontal plane anywhere in the vicinity of the site. Assuming that there will be a percolation of water from the subsided features, the horizontal boundaries should be placed outside of the zone of influence of the moving moisture front. However, horizontal boundaries were placed in vicinity of the subsided features to limit the horizontal spread of the moisture in order to overestimate downward flow.

An adequate representation of the flow dimensionality depends on the geometry of the subsided feature. Even though the preferential movement of water that passes the upper zone is vertically downward, the horizontal velocity component may still be noticeable within and around the moving moisture front if the infiltration occurs through a relatively small surface area. The subsided features above the GCD boreholes are cone-shaped. In this case, it is adequate to consider flow within a cylinder using a quasi-3-D model in radial coordinates. Using a principle of symmetry of the flow within such a cylinder, the modeling domain can be defined as a half cylinder, as shown in Figure 5.6.

The most adequate representation of the subsided features within the trenches and pits would be with a 3-D model in Cartesian coordinates. However, the challenge of this modeling effort exceeds by far its purpose and possible outcome. A 2-D vertical cross-section model was used instead (Figure 5.7). Such a 2-D model assumes that the trench/pit has infinite extent in the third direction, or in other words, an infinite width. This assumption provides an overestimation of the

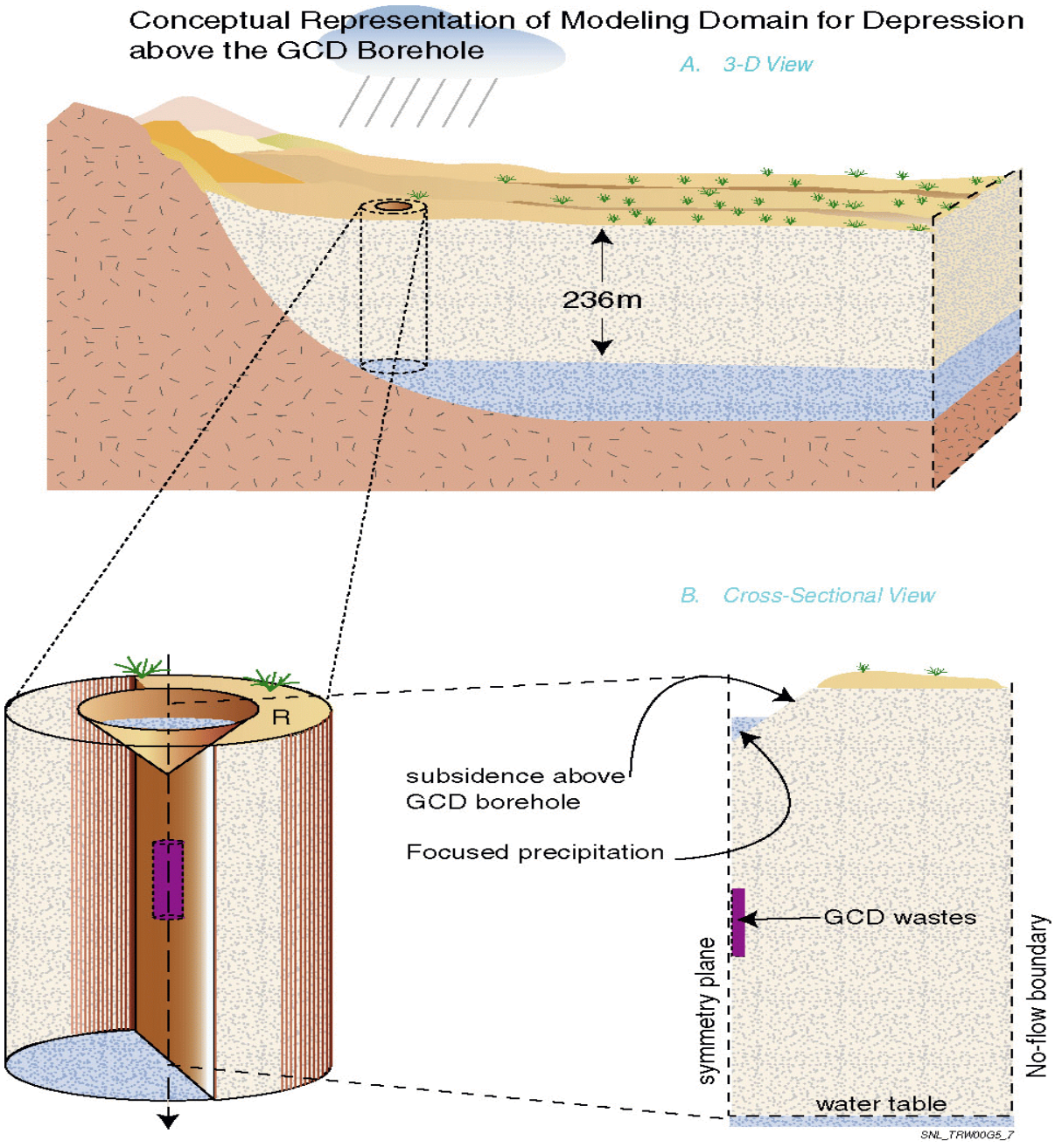

Figure 5.6. Conceptual Representation of Modeling Domain for Depression above the GCD Borehole.

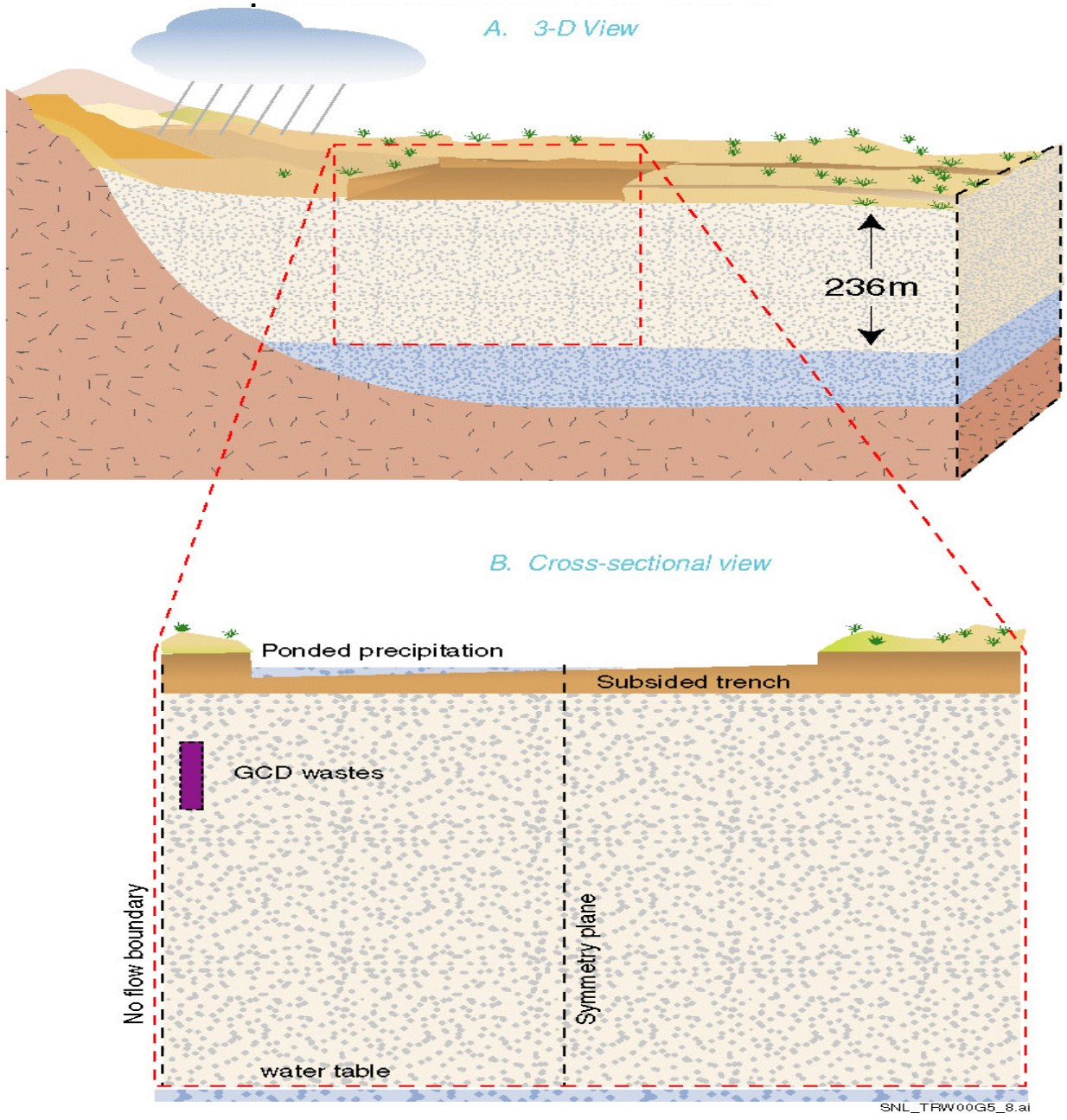

Figure 5.7. Conceptual Representation of Modeling Domain for Depression within the LLW Trench.

downward and lateral flow. The symmetry of the flow can be used in this case as well to model only one-half of the domain. The no-flow symmetry boundary is placed in the middle of the trench, as shown in Figure 5.7.

5.3.5 Initial Conditions

The initial flow conditions are prescribed in terms of pressure heads or moisture contents within the modeling domain. The prescribed initial conditions are those that are assumed to exist at the end of the institutional control period. Since DOE intends to fill all subsidence features as they form, no focusing of precipitation is anticipated before the end of the institutional control period. As a result, the initial distribution of moisture/pressure heads would be similar to that observed today. This distribution of moisture, corresponding to drying conditions, was described above. However, for this effort, an equilibrium profile was used instead. This equilibrium profile implies steady-state conditions within the system with zero velocities in any direction. In this case, introducing water into the system will immediately change the equilibrium and generate a downward flow. On the other hand, introducing water to the system with an upward flow (drying profile) would not generate the downward flow until the upward gradient is reversed. Thus, starting with the equilibrium profile supports the screening approach.

The equilibrium moisture profile is shown in Figure 5.8 for mean unsaturated zone parameters. The moisture data from the science trench boreholes, pilot wells, and boreholes AP-1, AP-2, RP-1, and RP-2 are plotted on this figure for the sake of comparison. As shown, the moisture profile corresponding to the mean parameter values approximates the average moisture conditions within the unsaturated zone.

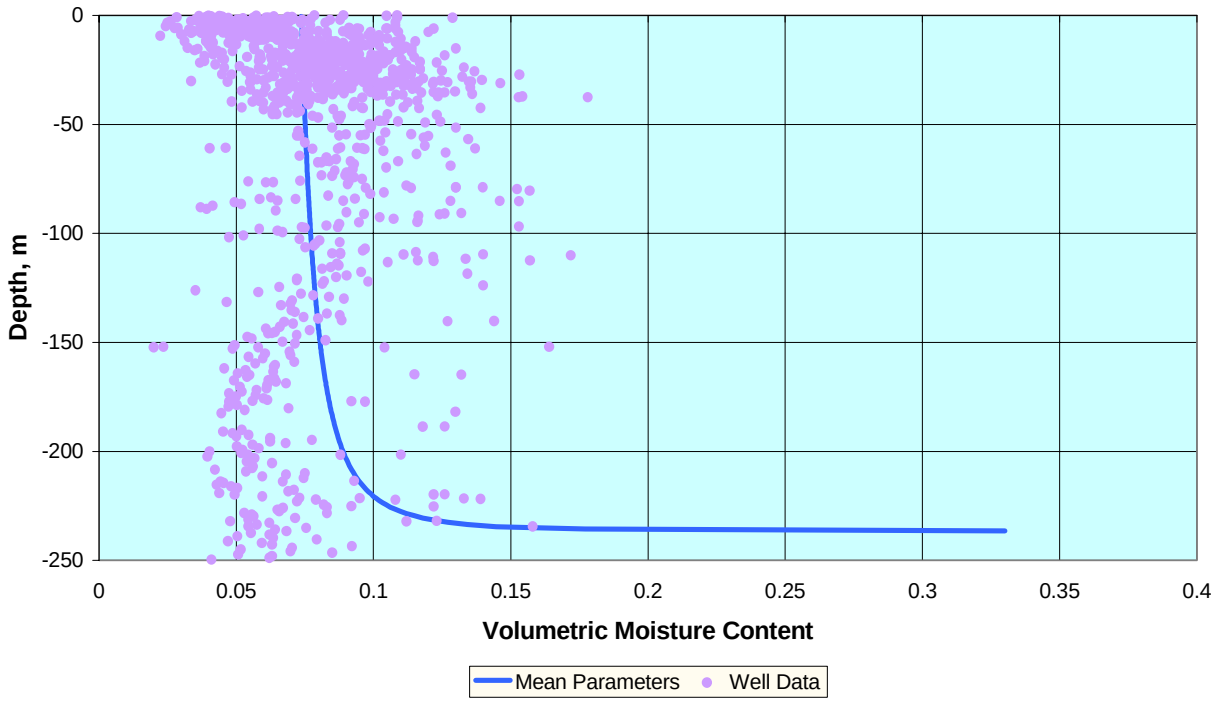

Figure 5.8. Moisture Profile for Calculated Equilibrium Conditions and Site Characterization Data.

5.4 Mathematical Representation of the Unsaturated Flow Conceptual Model

The mathematical representation of the unsaturated flow conceptual model and the method of modeling the unsaturated flow are described below.

5.4.1 Mathematical Formulation

Changes that are going to occur at the upper boundary of the unsaturated zone due to focusing precipitation in subsidence features will result in changes in pressure and moisture in the unsaturated zone. For this exercise, Richards equation [Richards, 1931] is used to simulate changes in moisture and pressure within the 2-D Cartesian coordinates unsaturated flow domain. This equation can be written as:

$$\left[K(\psi)\frac{\partial\psi}{\partial x}\right]+\frac{\partial\psi}{\partial x}\left[K(\psi)\left(\frac{\partial\psi}{\partial z}+1\right)\right]\frac{\partial\psi}{\partial z}=C(\psi)\cdot\frac{\partial\psi}{\partial t}$$
$$C(\psi)=\frac{\partial\theta(\psi)}{\partial\psi} \qquad (5.9)$$

where ψ is the pressure head, $K(\psi)$ is hydraulic conductivity characteristic curve, $C\psi$ is specific moisture capacity, and $\theta(\psi)$ is the moisture retention curve. A similar equation can be written for quasi-3-D flow (i.e., radial coordinates).

The relationship between the total head h and the pressure head ψ is defined by the formula:

$$h = \psi + z \qquad (5.10)$$

Equation (5.10) assumes the isothermal conditions in the flow domain. As shown in Shott et al. [1998], the thermal gradient in most of the unsaturated zone is upward and very small and can be excluded from the screening calculations. The thermal gradient within the upper portion of the unsaturated zone can be upward or downward, but influences only the thin near-surface layer [Shott et al., 1998].

5.5 Computer Code used to Simulate Unsaturated Groundwater Flow

The computer code VS2DT [Lappala et al., 1987] was selected for modeling unsaturated flow. This code is well known and tested, widely used, can handle strong nonlinearity, and, most importantly, allows for numerical implementation of the conceptual models described above. Besides, the simplified way that VS2DT simulates evaporation and plant transpiration results in underestimating evapotranspiration flux, which is appropriate for this screening approach.

The code solves the Richards equation using a finite difference method. The form of the nonlinear equation solved for each finite difference grid block within the flow domain is as follows [Lappala et al., 1987]:

$$v\{\rho[C_m + sS_s]\}\frac{\partial H}{\partial t} - \rho\sum_{k=1}^{m} A_k K_{sat} Kr(\psi)\frac{\partial H}{\partial n_k} - \rho q v = 0 \qquad (5.11)$$

where H is total head, v is the volume of the porous medium confined within the grid block, ρ is liquid density, s is liquid saturation, C_m is specific moisture capacity, S_s is specific storage, K_{sat} is saturated hydraulic conductivity, $Kr(\psi)$ is the hydraulic conductivity characteristic curve, q is the volumetric source-sink term accounting for liquid added to $(+q)$ or taken away from $(-q)$ the volume v, n_k is a direction normal to the face k, A_k is the area of the k-th face, and m is the number of the corresponding face of the grid block.

The following boundary conditions are implemented in the code.

- Liquid flux across the boundary $\check{u}_k$ in the direction n:

$$\rho \overset{>}{u} k = f_1, (x, t, \nabla H, \psi)_K \qquad (5.12)$$

where f_1 is a general function depending on the boundary location x, time t, gradient in total head ΔH across the face k and the pressure head ψ at the face k.

- Total head H_k along the boundary:

$$H_k = f_2 (x, t, \psi)_k \qquad (5.13)$$

where f_2 is a general time-dependent function.

Evaporation, infiltration, evapotranspiration, and seepage are the boundary conditions that cannot be specified in the code. The method the code employs for modeling infiltration and evaporation are summarized below. The other two processes were not modeled and are not described here.

Infiltration is modeled as a vertical positive flux of liquid described by Equation (5.12) as long as the conductive and sorptive capacity of the boundary block is not exceeded. After that, ponding occurs and the boundary condition changes to the specified head as described by Equation (5.13). The point in time when this occurs is determined by the simulation.

Similarly, evaporation is modeled as a vertical negative flux (Equation 5.13) equal to the potential evaporative demand until the liquid cannot be conducted fast enough toward the land surface to meet this demand. After that, the boundary condition changes to a specified flux based on the gradient in pressure potential between the soil and atmosphere. The point in time at which this occurs is determined by the simulation as well.

The spatial derivatives of Equations (5.11) through (5.13) are approximated by central differences written about grid-block boundaries. Time derivatives are approximated by a fully implicit backward scheme. Nonlinear parameters of the equation are linearized either implicitly (con-

ductance and boundary conditions) or by using Newton-Raphson method (storage term). The Strongly Implicit Procedure (SIP) is used to solve the resulting system of equations.

Some modifications were incorporated into the code to extend the maximum sizes of the grid, to output the specific information needed for the analysis, and to simplify working with the long simulation time periods. In addition, the flow balance was printed out for each time step during which a change at the upper flow boundary occurred. This balance included the total infiltration flux into the unsaturated zone by the time of change, the total evaporative flux out of the unsaturated zone, and the total change in storage.

5.6 Evaluation of the Unsaturated Flow Model's Potential for Bias in Overestimating Downward Flow

Potential bias of the unsaturated flow model in overestimating downward flow was tested by simulating the current undisturbed conditions at the Area 5 RWMS. As mentioned previously, recharge to the groundwater is not occurring anywhere within the RWMS under the current climate conditions. In other words, all of the current precipitation is recycled to the atmosphere by evaporation and transpiration in the upper portion of the unsaturated zone. Consequently, if simulation results based on current conditions and the conceptual and mathematical models described above indicate infiltration below the transition zone (about 2 m [7 ft]), then downward flow is being overestimated. Note that reproducing the observed moisture within the unsaturated zone and calibrating the conceptual and mathematical model were not the goals of this effort.

A 1-D model was set up to simulate the unsaturated flow under the current undisturbed conditions. Mean values of the unsaturated zone parameters modeled were used (see Table 5.5). PE rates were specified in accordance with the rates shown in Figure 5.9. A recurring annual cycle of the rate of PE was specified for a period of simulation equal to 1000 years. The lower boundary was placed at the water table and initial pressure heads were based on an equilibrium profile.

The upper boundary condition was specified at the land surface. Two major processes were simulated at this boundary: (1) infiltration of precipitation; and (2) evaporation from the top soil layer. Evaporation is a continuous process, the rate of which is limited by PE and availability of moisture in the upper portion of the unsaturated zone. However, it was assumed that evaporation during precipitation can be neglected.

Infiltration of precipitation, on the other hand, is a discrete process associated with the precipitation event. The rate of infiltration is equal to the precipitation rate unless ponding or run-off takes place in which case the rate is equal to the saturated conductivity of the soil. For this simulation, all precipitation was assumed to be available for infiltration.

The rates, durations, and frequencies of precipitation events were defined based on the data analysis provided in Hokett and French [1998]. The recurring annual cycle of precipitation for a typical year was based on the mean number of days with precipitation in every month of the year and a mean precipitation depth for each day of precipitation. The number of precipitation events

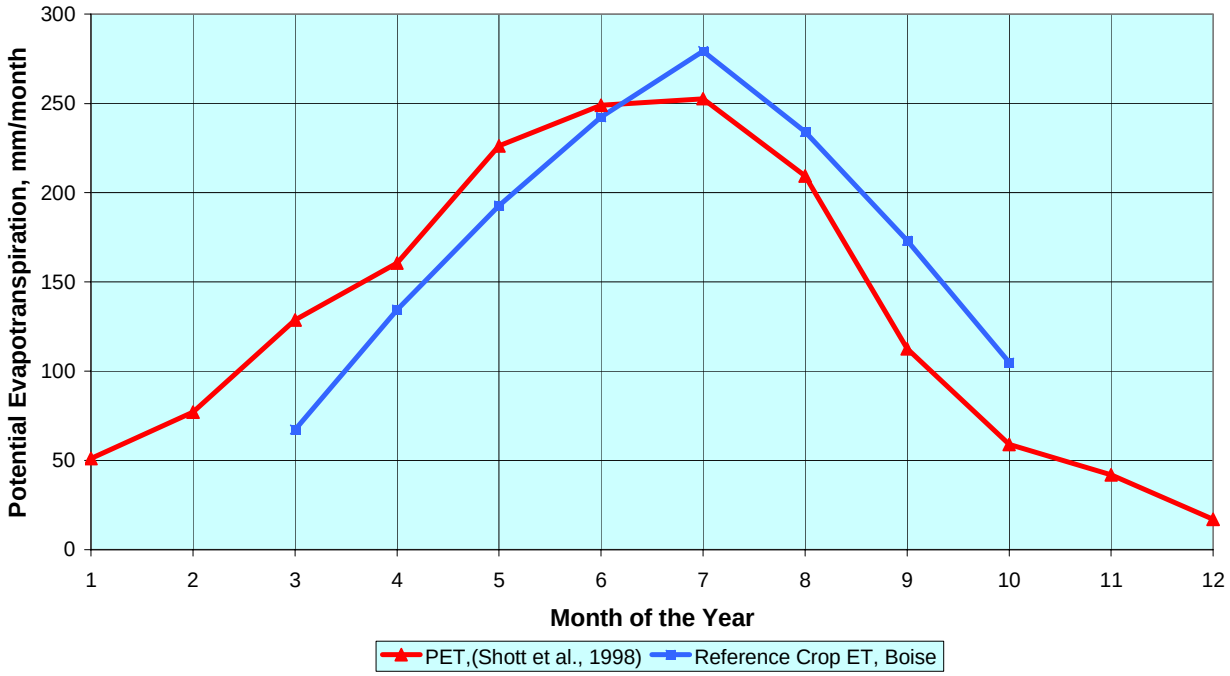

Figure 5.9. Potential Evaporation/Evapotranspiration Rates.

was defined to represent the observed tendency in distribution of one-, two, and three-day events within the specified month. The total annual precipitation was equal to the mean annual precipitation of 126.5 mm (see Table 5.6 and Figure 5.10). The annual distribution of precipitation defined for the typical year was used for every year of the 1000-year period of simulation. The low-probability events, such as 1000-year storm, 100-year storms, and others were not simulated. These events have much higher intensity than the average events considered. Excluding them from the simulation results in an underestimate of the infiltration flux.

Infiltration during precipitation was modeled by specifying a downward liquid flux at the upper flow boundary equal to the corresponding rate of precipitation. The duration of the flux corresponded to the event duration. Soil evaporation was assumed to occur between the precipitation events. The upward evaporation flux during these periods was calculated from the pressure-potential gradient between the soil and the atmosphere and compared to the PE flux at each time step during the simulation. The smaller of the two fluxes was then applied at the boundary.

The results of this simulation are presented in Figure 5.11 for four different times. As this figure indicates, the moisture introduced by the precipitation events is not all recycled to the atmosphere. By the end of the simulation period, 1000 years, the moisture front penetrates to a depth of 8.5 m (28 ft). This is true even though the infiltration flux was intentionally underestimated and the current undisturbed conditions were simulated for a period of time that was significantly smaller than the duration of the current climate (last 20,000 years).

Table 5.6. Distribution of Precipitation within the Typical Year Used in 1-D Simulation of Undisturbed Current Conditions.

Month of the Year	Number of Precipitation Events	Event Duration (days)	Precipitation Rate per Precipitation Day (mm)	Monthly Precipitation (mm)
January	2	2	4.33	17.3
February	1	3	4.83	14.5
March	2	2	3.8	15.2
April	1	2	3.8	7.6
May	2	1	3.95	7.9
June	1	1	3	3
July	2	1	5.35	10.7
August	3	1	4.57	13.7
September	2	1	3.7	7.4
October	1	1	6.1	6.1
November	1	2	4.95	9.9
December	1	3	4.33	13
Total	**19**	**29**	**-**	**126.3**

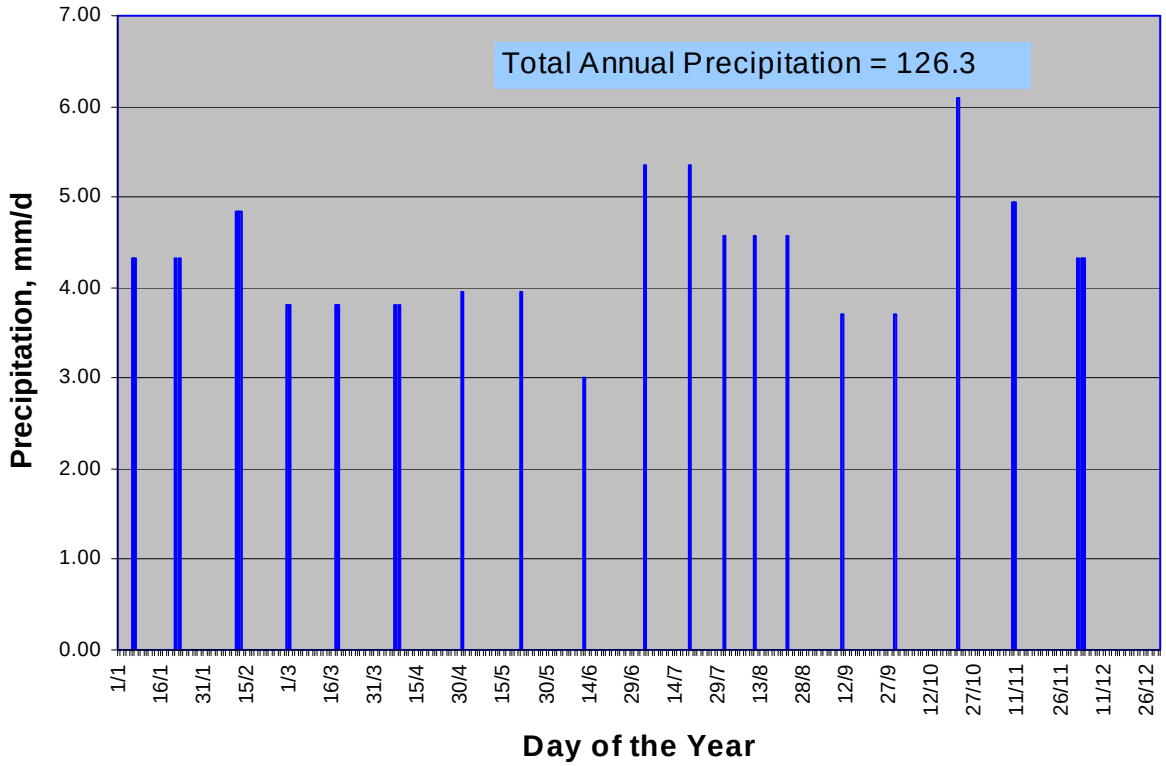

Figure 5.10. Annual Distribution of the Precipitation Used in 1-D Model of Unsaturated Flow Under Current Undisturbed Conditions.

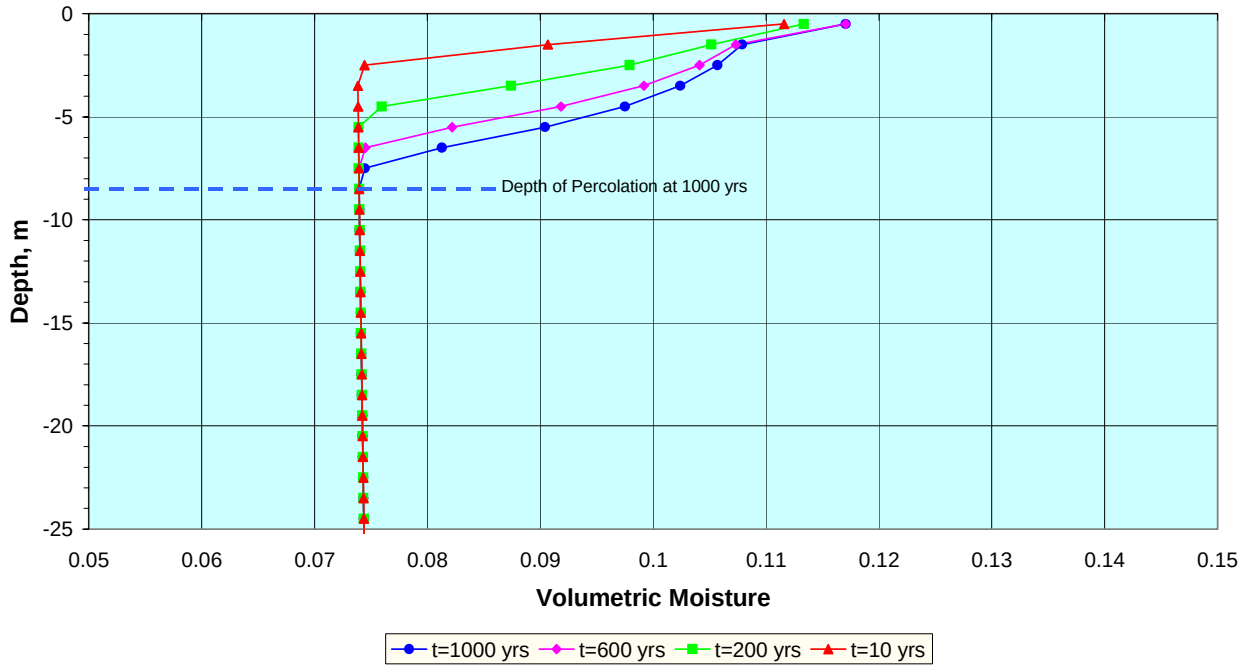

Figure 5.11. Moisture Profiles at Different Simulation Times from 1-D Model of Unsaturated Flow Under Current Undisturbed Conditions.

This simulation demonstrates that the unsaturated flow conceptual and mathematical models cause an overestimate of the downward flow and, therefore, an overestimation of the potential for groundwater recharge. Based on this conclusion, these models were used for all further screening calculations.

5.7 Additional Assumptions that Bias the Unsaturated Model toward Overestimating Downward Flow

Following is a summary of additional model assumptions that bias the unsaturated flow model toward overestimating downward flow due to the focusing of precipitation and runoff in the subsidence features within the LLW trenches and pits and above the GCD boreholes in the Area 5 RWMS.

- Instantaneous subsidence of all the void spaces remaining at the end of the institutional control period was assumed to occur. This results in the maximum possible depth of the subsided features being used in calculating subsidence volumes.

- The volumes of runoff into the subsided features under future climate conditions were significantly overestimated by assuming that under the glacial climate, the number of precipitation events will be the same as under the current climate, but the amount of precipitation per event will be two times higher. This results in five times more runoff compared to the runoff calculated by doubling the number of events..

- The likely formation of a low-permeability silt/clay crust at the depression bottoms due to runoff and associated sedimentation was excluded.

- All the surface water focused in the subsidence features was introduced into the unsaturated zone. No evaporation from the open water surface during the ponding was accounted for. This is true even for very small ponding events.

- Additional extraction of water from the upper unsaturated zone by plant transpiration was not incorporated. Only evaporation from the top soil was assumed to take water out of the unsaturated flow system.

- Initial conditions were specified as an equilibrium profile (zero gradient within the profile); the existence of upward flux in the upper zone was neglected.

- Extreme events, such as the PMP, the 10,000-year storm, one 1000-year storm, and nine 100-year storms, were all placed at the beginning of the simulations (first 14 years) when the intact cap (Conceptual Model 1) was considered.

- Unsaturated flow associated with runoff into the trench was approximated by a 2-D model, thereby assuming an infinite width for the trench.

This page intentionally left blank.

6.0 MODELING UNSATURATED FLOW UNDER CLIMATE CHANGE COUPLED WITH SUBSIDENCE

6.1 Introduction

The conceptual model and approach for simulating unsaturated flow associated with infiltration of precipitation and runoff in subsidence features were discussed in Section 5.0. This section focuses on the model-set up (Section 6.2) and analysis of model results (Sections 6.3). Two conceptual models were considered. In both models, a simulation period of 10,000 years was used and the climate was assumed to change to glacial conditions at the end of the institutional control period. In the first conceptual model, infiltration of surface water from the subsided TO4C trench and from a cone-shaped depression above GCD Borehole 1 were simulated assuming the cap remains intact for the entire 10,000 years. In the second conceptual model, infiltration of surface water from the subsided TO4C trench was simulated for 10,000 years assuming that the cap will be washed away completely at the end of institutional control period.

6.2 Model Set-Up

6.2.1 Subsided Trench TO4C – Intact Cap Conceptual Model

As discussed in Section 5.0, the purpose of modeling unsaturated flow beneath a subsided trench was to estimate the extent of the lateral spreading of the moisture front and its possible effects on moisture conditions around the GCD boreholes. Trench TO4C was chosen since it has a greatest potential impact on the GCD boreholes. First, Trench TO4C is nearest to a GCD borehole. It is 14 m (46 ft) from the eastern edge of the trench to Borehole 3. Second, less surface water is focused into Trench TO7C (which is 21 m (69 ft) from Borehole 4). Note that the volumes of water focused into pit PO3U could be very large. However, the volumes that could affect the GCD boreholes are only those assigned to the top of the 2-D model. Note that this does not neglect any volume of runoff. Quite the opposite; the model is assumed to be infinite in the dimension perpendicular to the trench (i.e., there is an infinite amount of water in that dimension). The volume of water seen by the model is then the volume of runoff and precipitation into the trench (or pit) normalized by the width of the trench (or pit). The result is that a larger volume of water is available from TO4C then for PO3U. For example, in the case of the pit PO3U, the average volume of a ponding event is 1350 m^3 (47,700 ft^3) which corresponds to 3.3 m^2 (36 ft^2) per unit pit width. On the other hand, the average volume of a ponding event for Trench TO4C is 227 m^3 (8,020 ft^3) which corresponds to 14.8 m^2 (159 ft^2) per unit trench width.

The model set up for the Trench TO4C is shown on Figure 6.1. The trench is modeled as a cross-section that extends from the land surface to the groundwater table. In the vertical direction, 230 1-m (3-ft) blocks are used everywhere except in the middle part of the unsaturated zone. In this zone, nine 2-m (7-ft) blocks were used. This was done to minimize the total number of the nodes while maintaining fine discretization close to the upper and lower boundaries. In the horizontal dimension, 42 blocks were defined. Sixteen 4-m (10-ft) blocks represented the undisturbed land surface and 26 5.6-m (18-ft) blocks represented the subsided bottom of the trench. The modeled length of the trench was 140 m (460 ft) , which is half the total length of Trench TO4C.

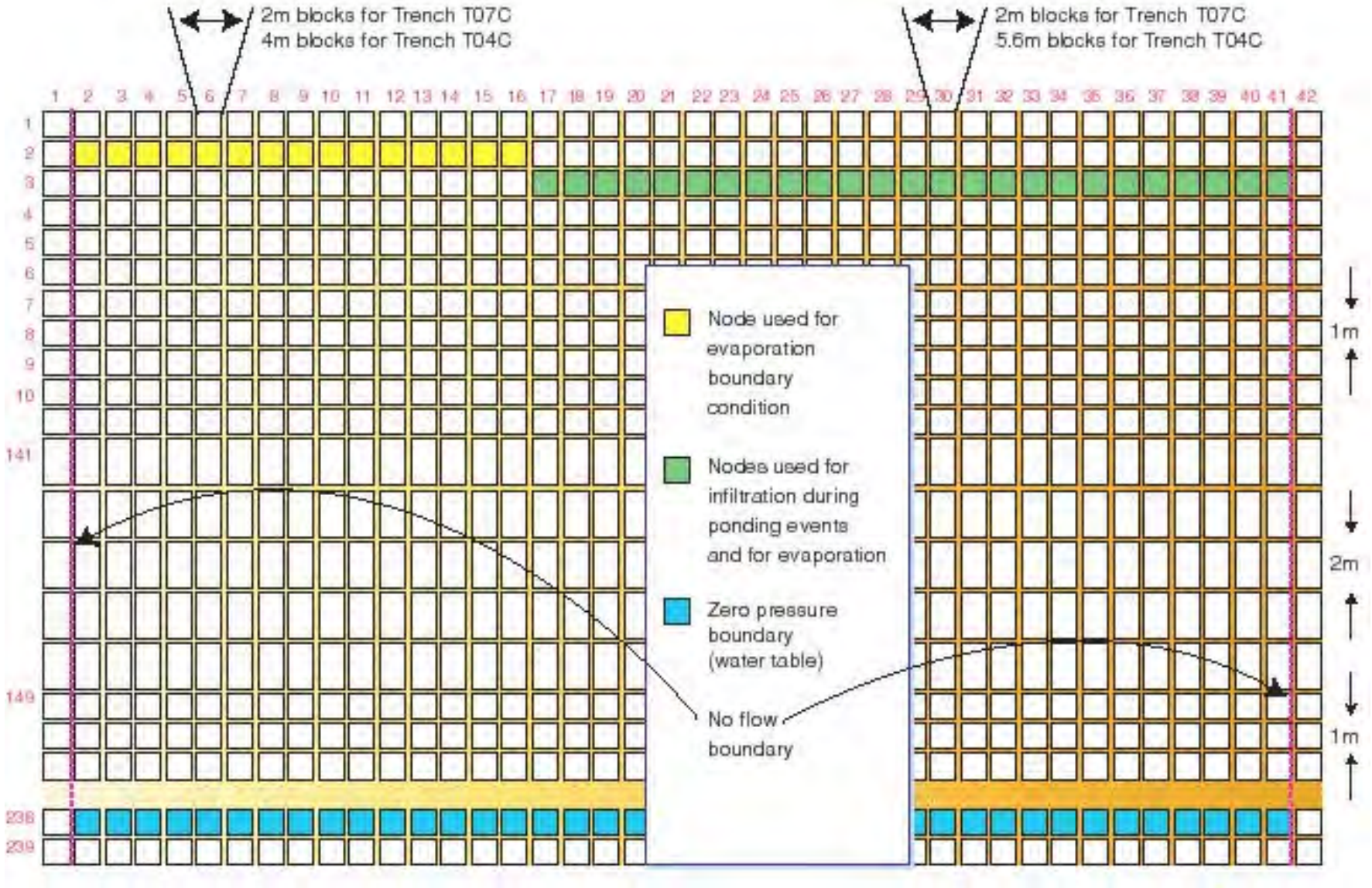

Figure 6.1. 2-D Model Grid for Trench TO4C.

No-flow conditions were specified along the vertical boundaries of the model domain. A zero-pressure condition was specified at the lower boundary. The subsided depression within the trench was modeled as a flat bottom with 1-m (3-ft) vertical walls. During a ponding event, a flux was specified in each boundary block representing the bottom of the trench. Evaporation was prescribed in all other land-surface blocks. Following a ponding event, the prescribed flux at the bottom of the trench was switched to an evaporation boundary condition until the next ponding event. Potential soil evaporation rates and unsaturated zone parameters used in these simulations were discussed in Section 5.0. The potential evaporation rates were prescribed in the manner shown on Figure 5.6 (Section 5.0). Mean values were used for the unsaturated zone parameters (see Table 5.5).

The volumes, frequencies, and duration of ponding events were discussed in detail in Section 5.0 (See Table 5.2). The sequencing of the events is described next. For the first 1000 years, a ponding event corresponding to the PMP was placed at time zero. Then a 10,000-year storm was input at a time of 1.125 years, a 1000-year storm at time of 2.25 years, and the nine 100-year storms were placed starting at 3.375 years recurring every 1.125 years. The average ponding events started at 13.5 years and recurred every 1.125 years for the remaining 986.5 years. The second 1000-year time period started with a 1000-year storm at 1000 years, followed by nine 100-year storms beginning at 1,001.125 years and recurring every 1.125 years. The average ponding events were placed starting from time equal to 1,011.25 years with the time interval equal to 1.125 years between them for the remaining 988.75 years of simulation. The third through the tenth 1000-year time periods were identical to the second 1000-year time period. The total simulation time was 10,000 years.

Only half of the trench was modeled; therefore, the volumes introduced into the unsaturated zone by each ponding event were half of the volumes listed in Table 5.2. These volumes in turn were normalized by the trench width for input in the 2-D model. The ponding event was modeled by maintaining the specified flux boundary condition in all the top 25 nodes of the model until all the pond volume infiltrated into the unsaturated zone.

6.2.2 Subsided Trench TO4C – No Cap Conceptual Model

The only difference in the no cap conceptual model from the intact cap conceptual model described above was in the timing and volumes of water introduced to the trench. A key difference between the two conceptual models is that runoff contains sediment in the no cap case. This sediment eventually fills the subsidence feature until the land surface elevation in the trench is equal to the surrounding region. Note that the increased thickness of the unsaturated zone associated with sedimentation is not accounted for in the unsaturated zone model. As described in Section 5.2.2, the simulated lifetime of the Trench TO4C assuming no cap and glacial climate conditions was 91 years. Thirty-three ponding events were simulated over this time period. No ponding events were simulated from the year 92 until the year 10,000.

6.2.3 Subsidence Depression Above the Greater Confinement Disposal Borehole 1 – Intact Cap Conceptual Model

The model set up for the GCD borehole is shown in Figure 6.2. Shown in this figure is a cross-section through a vertical cylinder that extends from the land surface to the groundwater table. Figure 6.3 shows a horizontal view of the modeling domain. The thickness of the unsaturated zone is 236 m (774 ft) which is represented by 255 grid blocks. These blocks have a vertical dimension of 0.5 m (2 ft) in the upper 15 m (49 ft) of the unsaturated zone and 1 m (3 ft) in the rest of the model. The radius of the cylinder is 12 m (40 ft) with 20 grid blocks specified in horizontal direction. The radial dimension of these blocks is 0.5 m (2 ft) from zero to 5.5 m (18 ft) from the cylinder axis. The remaining blocks have a horizontal dimension of 1 m (3 ft).

A no-flow boundary condition is specified along the vertical plane of symmetry (the axis of the cylinder) and along the outer vertical cylinder walls. A zero-pressure boundary condition is specified at the bottom of the cylinder. The depression depth and radius at the top of the model correspond to the maximum dimensions of the deepest subsidence features, which are 3.04 m (9.97 ft) (depth) and 4.34 m (14.2 ft) (radius). Eight blocks represent the wall of the depression. A prescribed flux is specified for blocks that are submerged by ponding. This flux rate is maintained until the total volume of the ponded water infiltrates into the unsaturated zone. Also, when the depression is totally filled with water, a prescribed flux is specified in all eight-boundary blocks. An evaporation flux is specified for the boundary blocks located above the water level on the depression wall. The evaporation flux boundary condition is also maintained in all other land-surface grid blocks. When all water from the ponding event has entered the unsaturated zone, the prescribed flux boundary condition is switched to the evaporation flux boundary condition until the next ponding event. As discussed in Section 5.0, the actual evaporation flux out of the system is not prescribed, but is calculated during every time step.

The volumes, frequencies, and duration of the ponding events were discussed in detail in Section 5.0 (See Table 5.2). The same timing and sequencing of the low-probability and the average ponding events described in Section 6.2.1 was used in the GCD Borehole 1 simulations. Because only half of the depression is modeled, the volumes introduced into the unsaturated zone by every ponding event were half of the volumes listed in Table 5.2.

All ponding events, except the event corresponding to the PMP, have volumes smaller than half of the total subsidence volume (59 m^3 (2,100 ft^3)). The maximum ponding depth corresponding to the average ponding event is 1.4 m (4.6 ft). Four blocks shown on Figure 6.2 are located below this water level. These blocks were specified as the prescribed flux blocks. The low probability ponding events, except the PMP, were modeled in the same way. That is, a prescribed flux was specified in four bottom blocks, since the difference in the ponding depths was not significant. The ponding event associated with the PMP was simulated by specifying prescribed flux boundary conditions in the eight boundary blocks representing the total height of the depression wall.

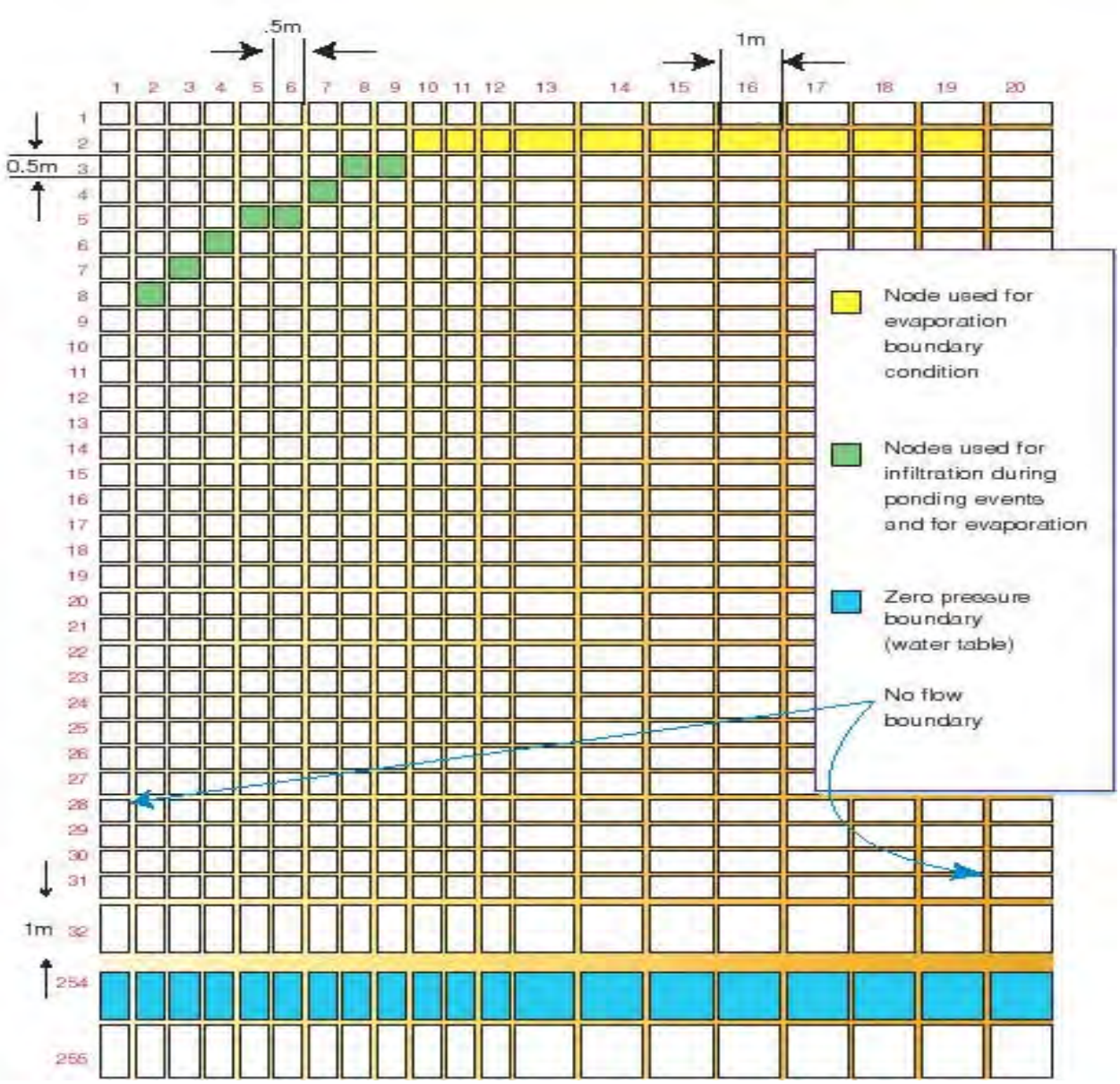

Figure 6.2. 2-D Cross-Section Showing Radial Coordinates of Modeling Set-Up.

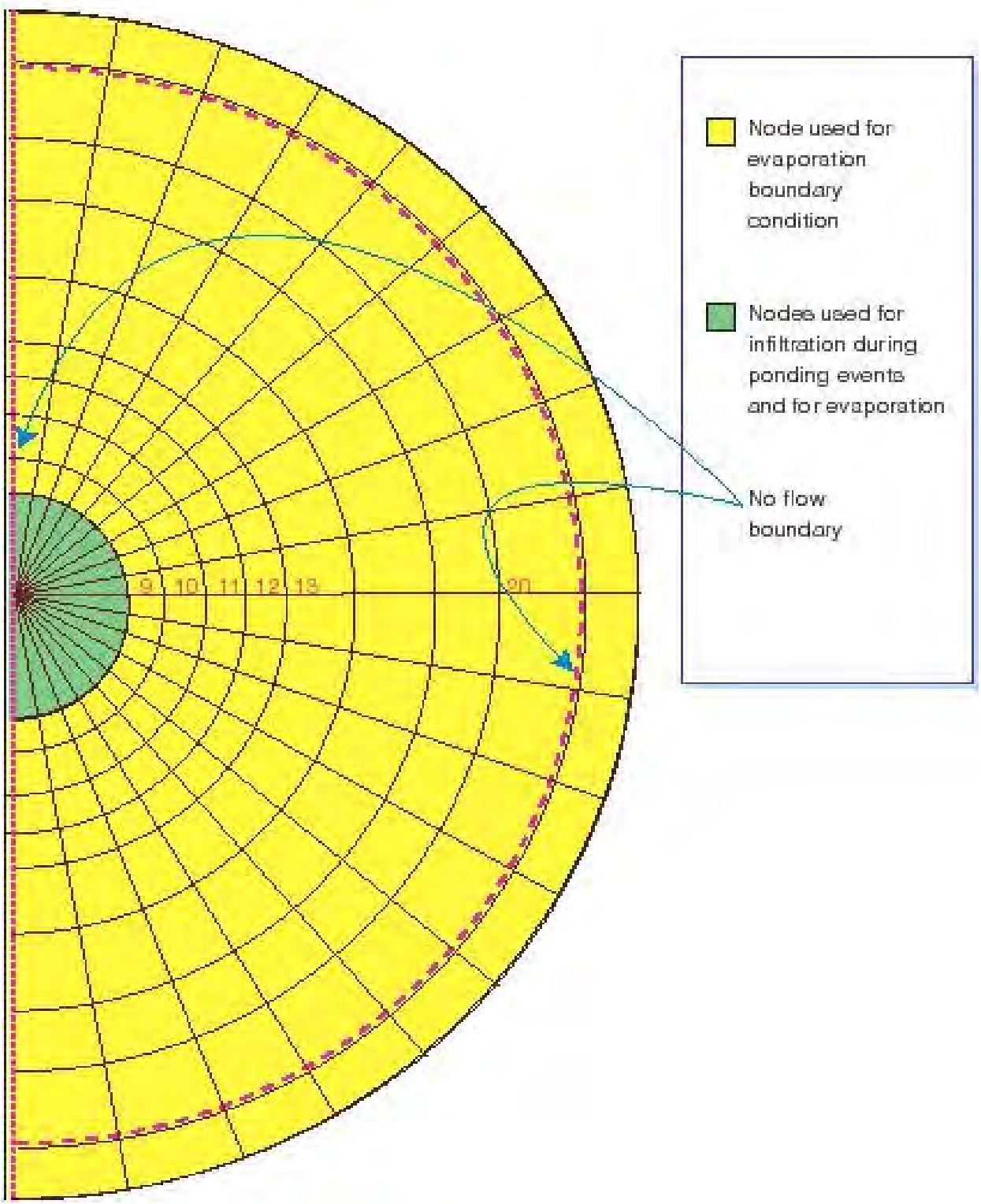

Figure 6.3. 2-D Plane View Showing Radial Coordinates Model Set-Up.

6.3 Unsaturated Flow Due to Focusing Precipitation in the Subsidence Features

6.3.1 Subsided Trench TO4C – Intact Cap Conceptual Model

The distribution of moisture resulting from infiltration of precipitation and runoff into Trench TO4C at 10,000 years assuming intact cap and glacial climate conditions during10,000 years is shown on Figure 6.4. At this time, the moisture front beneath the trench is at the groundwater table. The moisture front spreads laterally to a distance of approximately 35 m (128 ft) and reaches GCD Borehole 1. GCD Boreholes 2 and 3 are outside of the zone affected by the movement of moisture from the trench. If Trench TO7C had been simulated, GCD Borehole 4 would probably be on the edge of its zone of influence, since it is located 21 m (69 ft) away from the trench. Consequently, the moisture conditions around two GCD boreholes have potential to be affected by water infiltrating from the trenches.

However, changes in moisture beneath GCD Borehole 3 at 10,000 years only impact the unsaturated zone to the depth of 197 m (646 ft) with the most changes being in the upper 150 m (490 ft) (Figure 6.3). Changes in moisture beneath GCD Borehole 4 could be up to 180 m (590 ft).

The development of the moisture front with time at GCD Borehole 3 is shown in Figure 6.5. As seen from this figure, only minimal changes above the GCD borehole are observed at 1000 years. The horizontal and vertical components of the velocity vector are plotted in Figure 6.4. The depth of the moisture front at any given time is the point where the vertical velocity is equal to zero. The vertical velocity is upward in the upper 5 m (16 ft) of the unsaturated zone and downward at greater depths. The maximum downward velocity at 10,000 years occurs at a depth of 70 m (200 ft). The horizontal velocity is negative or in the direction opposite to the trench during all times and at all depths, indicating that there is no movement from the borehole toward the trench.

Following are general remarks about the results of the analysis. The downward flow over the period of simulation expressed as a percentage of the total amount of water introduced to the unsaturated zone due to the infiltration from the trench is shown in Figure 6.6. The total amount of water accumulated in Trench TO4C was 2,052,959 m^3 (72,496,140 ft^3). By the end of the 10,000-year period 6.8% of this amount, or 139,601 m^3 (4,929,730 ft^3), became the downward flow. The moisture profiles at the vertical cross-section through GCD Borehole 3 are shown in Figure 6.7. The moisture content data from the different wells located in Area 5 RWMS are plotted on this figure for the sake of comparison. The maximum increase in the moisture content in the upper part of the unsaturated zone is 4% - from 8% corresponding to the equilibrium profile to 12% at 10,000 years. This increase in moisture is smaller than the variability of moisture content in the different wells, as shown in Figure 6.7.

The conclusion of this analysis was that the infiltration of water from the trenches and pits in the Area 5 RWMS will not affect the moisture content at GCD Boreholes 1 and 2 and may slightly increase the moisture content near GCD Boreholes 3 and 4.

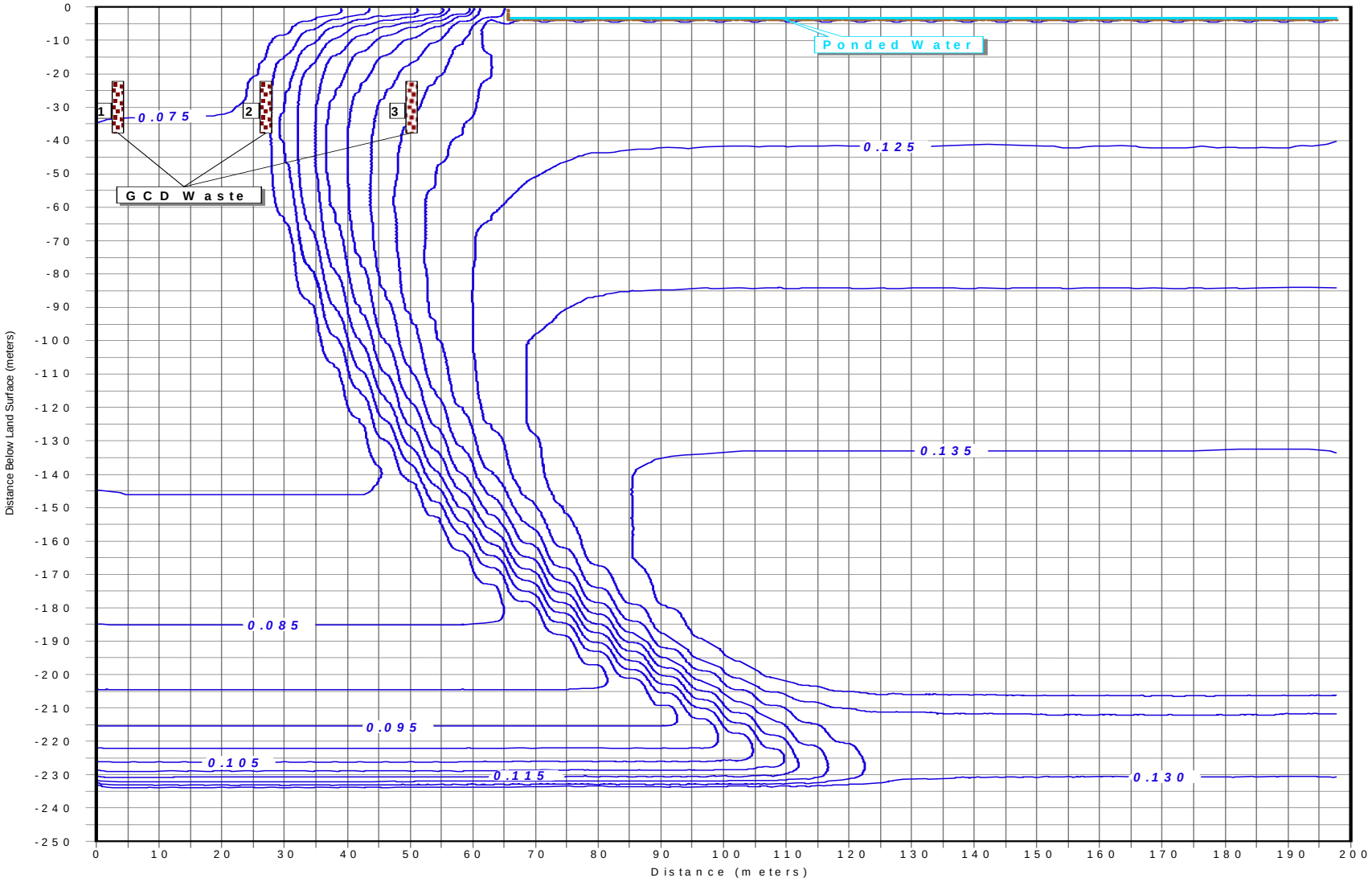

Figure 6.4. Intact Cap Conceptual Model. Distribution of Moisture Beneath Trench TO4C at 10,000 Years.

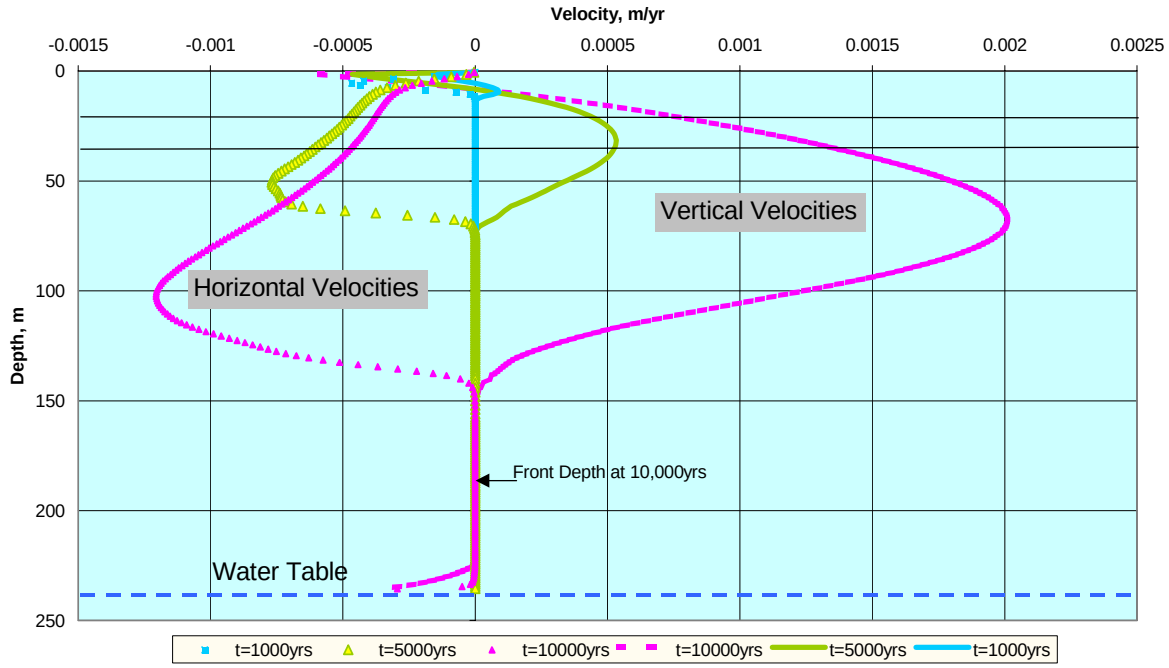

Figure 6.5. Conceptual Model 1 – Intact Cap. Results of the Trench TO4C Modeling Velocity Profiles for the Cross-Section through GCD Borehole 3.

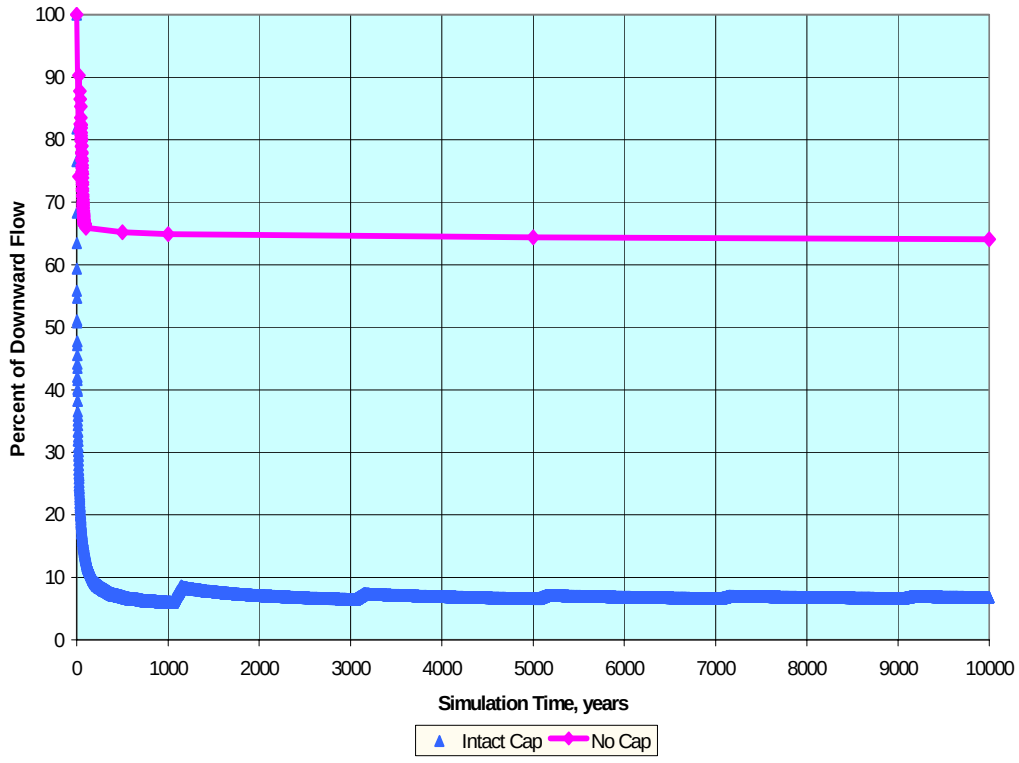

Figure 6.6. Results from the Trench TO4C Modeling Downward Flow as a Percentage of the Total Volume of Surface Water.

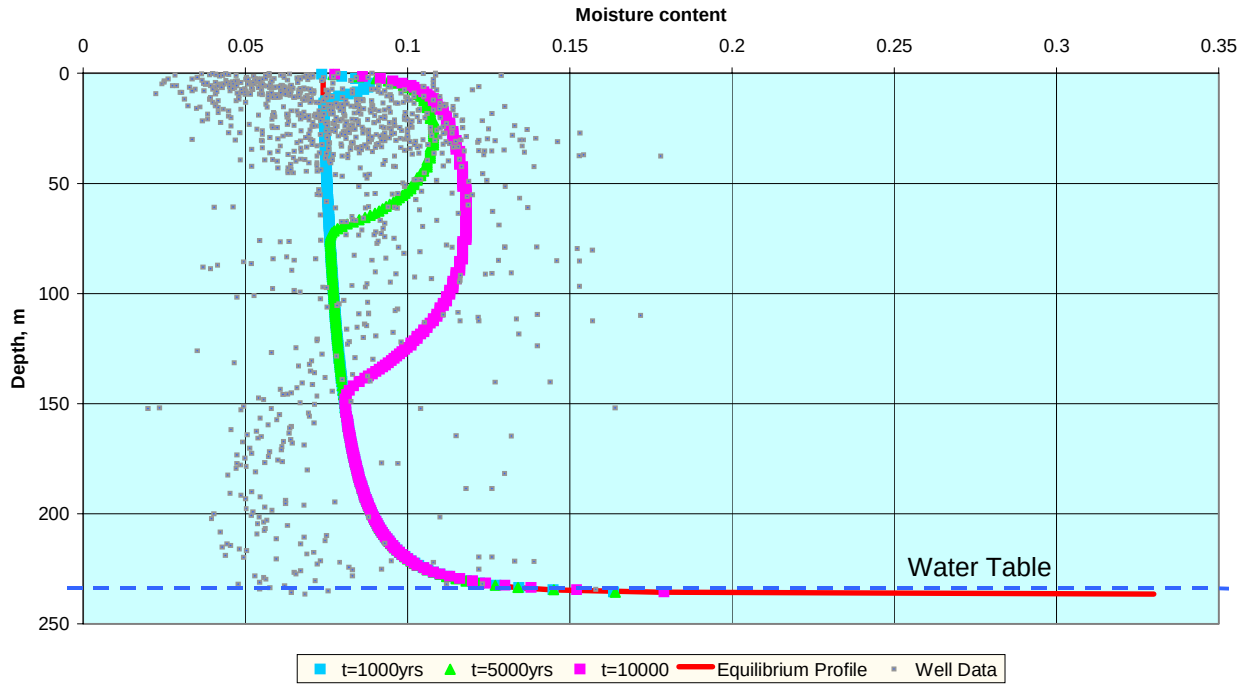

Figure 6.7. Conceptual Model 1 – Intact Cap. Results of Trench TO4C Modeling Moisture Profiles for the Cross-Section through GCD Borehole 3.

6.3.2 Subsided Trench TO4C – No Cap Conceptual Model

The distribution of moisture obtained around the Trench TO4C at 10,000 years assuming no cap and glacial climate conditions during all 10,000 years of simulation is shown in Figure 6.8. The maximum depth of moisture front beneath the trench at 10,000 years is 115 m (377 ft). The lateral spread of the moisture front is 30 m (100 ft). Two boreholes (GCD Boreholes 3 and 4) are affected by the moisture front movement. The depth of the moisture front at 10,000 years beneath GCD Borehole 3 is 88.5 m (290 ft) and beneath GCD Borehole 4 is 83.5 m (274 ft). Since no water movement is expected in this conceptual model (Section 5.2.2) from the subsidence depressions above GCD, this is the only impact of the subsidence and climate change on the moisture conditions around GCD Boreholes 3 and 4. No changes in moisture will occur around GCD Boreholes 1 and 2. Consequently, Conceptual Model 1 that assumes intact cap is more bounding than Conceptual Model 2 that assumes no cap.

One difference between the results from the two conceptual models is how much water leaves the near surface and continues to migrate deep into the unsaturated zone. In the first conceptual model (intact cap), the ratio of the total volume of water that became a downward flow to the total volume of water introduced into unsaturated zone is 6.8%. For the second conceptual model (no cap), the downward flow is 64% of the total injected. This difference is the result of introducing a large amount of water over a short period of time in the second conceptual model. In essence, there is not enough time for evaporation to extract the water from the unsaturated zone. However, the total volume of water injected into the first conceptual model (intact cap) is

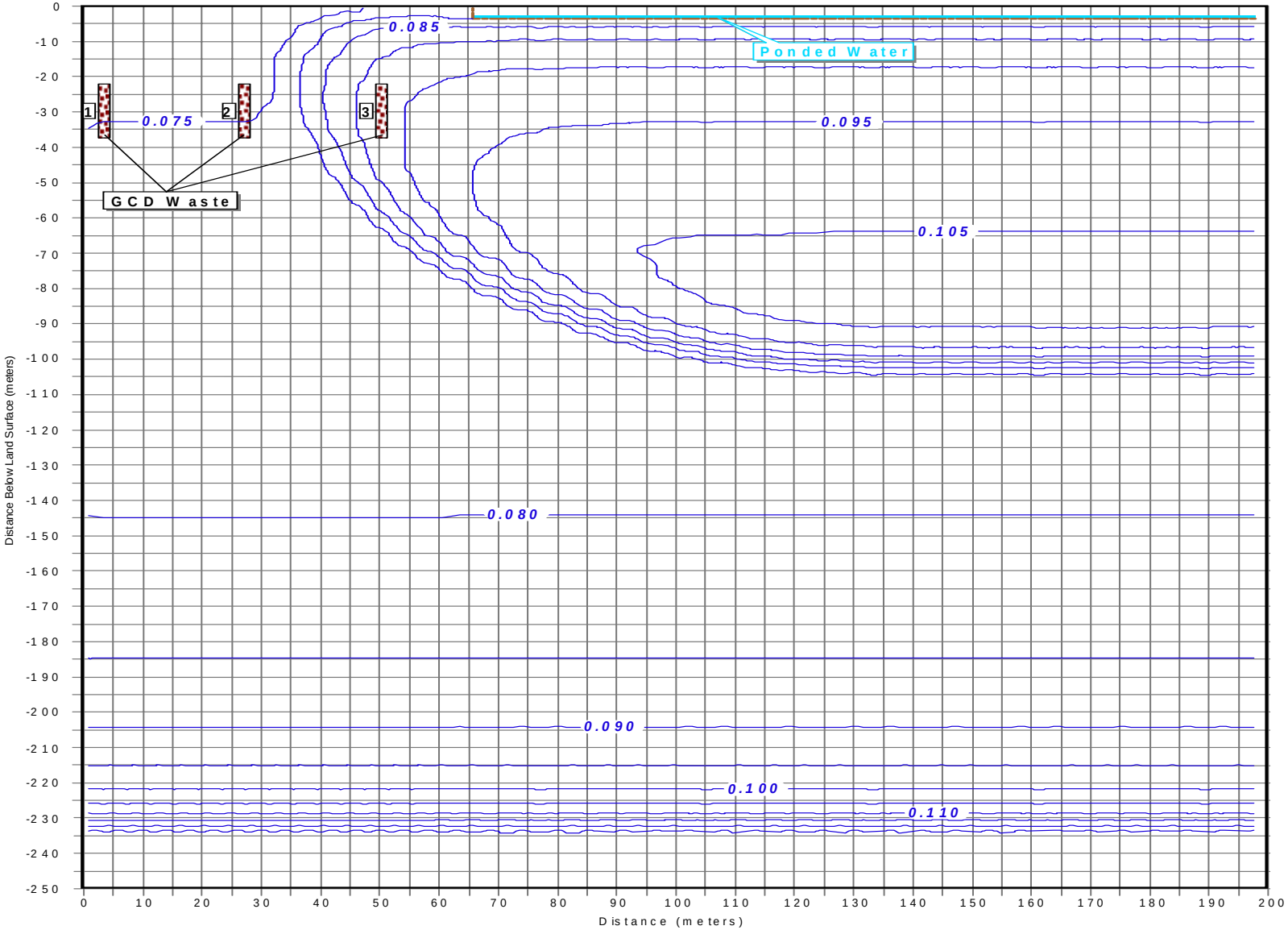

Figure 6.8. No Cap Conceptual Model. Distribution of Moisture Beneath Trench TO4C at 10,000 Years.

much larger than the total volume of water injected into the second conceptual model (intact cap). Therefore, the first conceptual model still shows more total water migrating downward toward the water table.

6.3.3 Subsidence Depression above Greater Confinement Disposal Borehole 1

The distribution of moisture obtained around GCD Borehole 1 at 10,000 years assuming intact cap and glacial climate conditions during all 10,000 years of simulation is shown in Figure 6.9. The depth of the moisture front at 10,000 years is 100 m (300 ft). The lateral spread of the moisture front is about 10 m (30 ft) from the center of the borehole. Taking in account the distance between GCD Boreholes 1, 2, and 3, which is 22 m (72 ft), no interference between the moisture infiltrating from the different GCD boreholes is expected. In addition, the total volume of water accumulated by the depressions above Boreholes 2 and 3 is smaller due to their smaller capture areas.

This analysis was repeated with higher initial moisture conditions to simulate the possible influence of moisture migrating laterally from the trench at the same time moisture is migrating downward from the GCD subsidence depression. For this simulation, a moisture content of about 10% in the upper part of the unsaturated zone was used. The saturated porosity, residual porosity, and the fitting parameters from Equation (5.7) were modified for consistency with the higher moisture conditions.

The moisture content and vertical velocities profiles along the centerline of the borehole are shown in Figure 6.10 and 6.11. Simulations for the undisturbed initial moisture conditions and for the 10% initial moisture content are shown for various times. The depth of the moisture front in the case of the higher initial moisture is 19 m (62 ft) deeper (119 m (390 ft)) at 10,000 years. In neither case does the moisture front reach the water table in 10,000 years.

6.4 Conclusions

Four simulations were performed to estimate the effects of subsidence and climate change on the moisture conditions around the GCD boreholes.

In the first simulation, Trench TO4C was modeled assuming glacial climate conditions and an intact cap for 10,000 years. Moisture conditions around GCD Boreholes 1 and 2 were not affected in this simulation. On the other hand, small changes in the moisture content around GCD Boreholes 3 and 4 were observed.

In the second simulation, Trench TO4C was modeled assuming glacial climate conditions and no cap for 10,000 years. Based on the results of this simulation, it was concluded that the moisture conditions around GCD Boreholes 3 and 4 will be affected by the infiltration of water from the trench, but no groundwater recharge will occur anywhere in the area in 10,000 years. It was also concluded that the intact cap conceptual model (first simulation) provides bounding estimation of the downward flow in relation to the no-cap conceptual model.

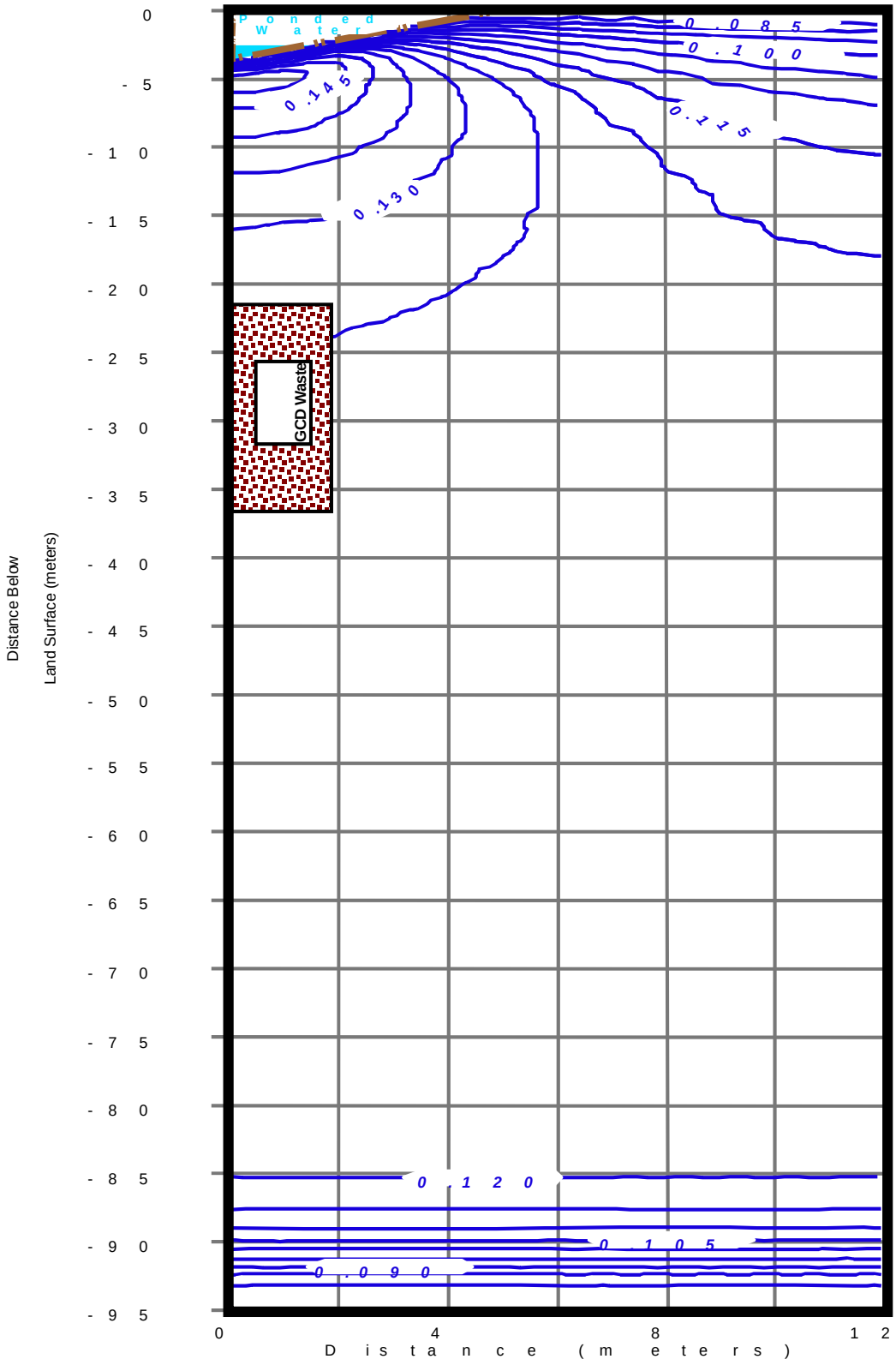

Figure 6.9. Intact Cap Conceptual Model. Distribution of Moisture Beneath GCD Borehole 1 at 10,000 Years.

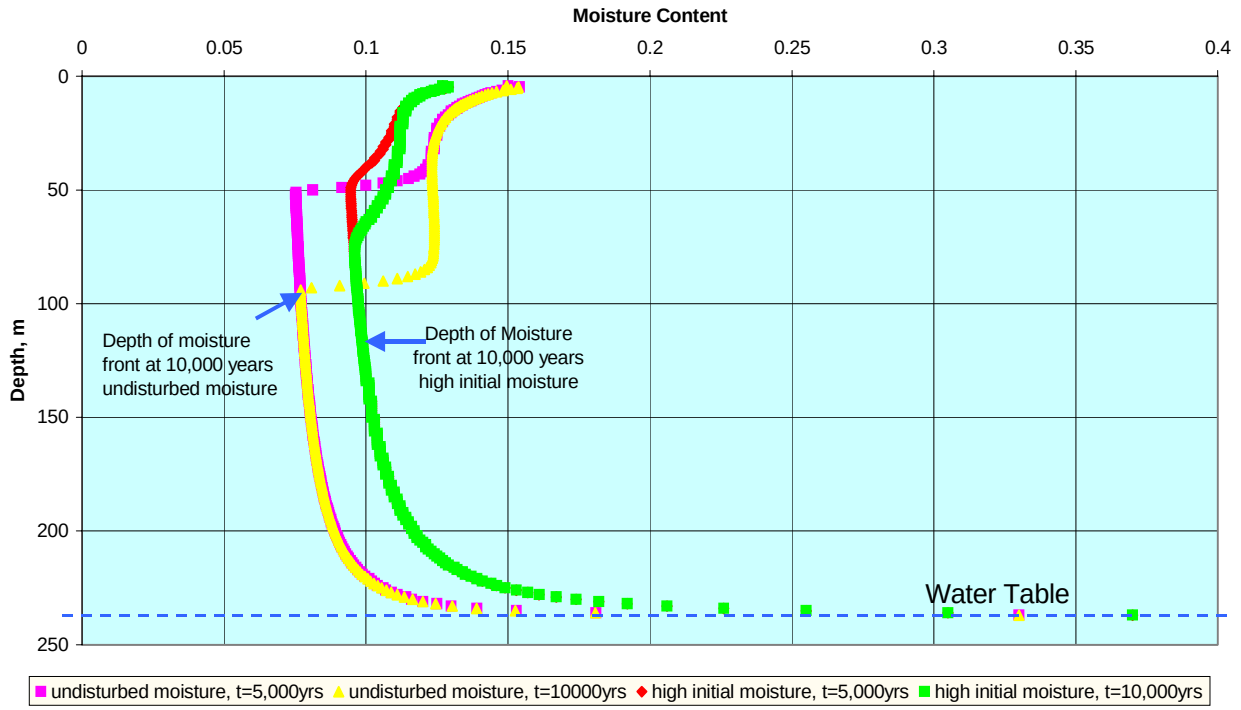

Figure 6.10. Conceptual Model 1 – Intact Cap. Results of the GCD Borehole Modeling Moisture Profiles at the Vertical Cross-Section through the GCD Borehole.

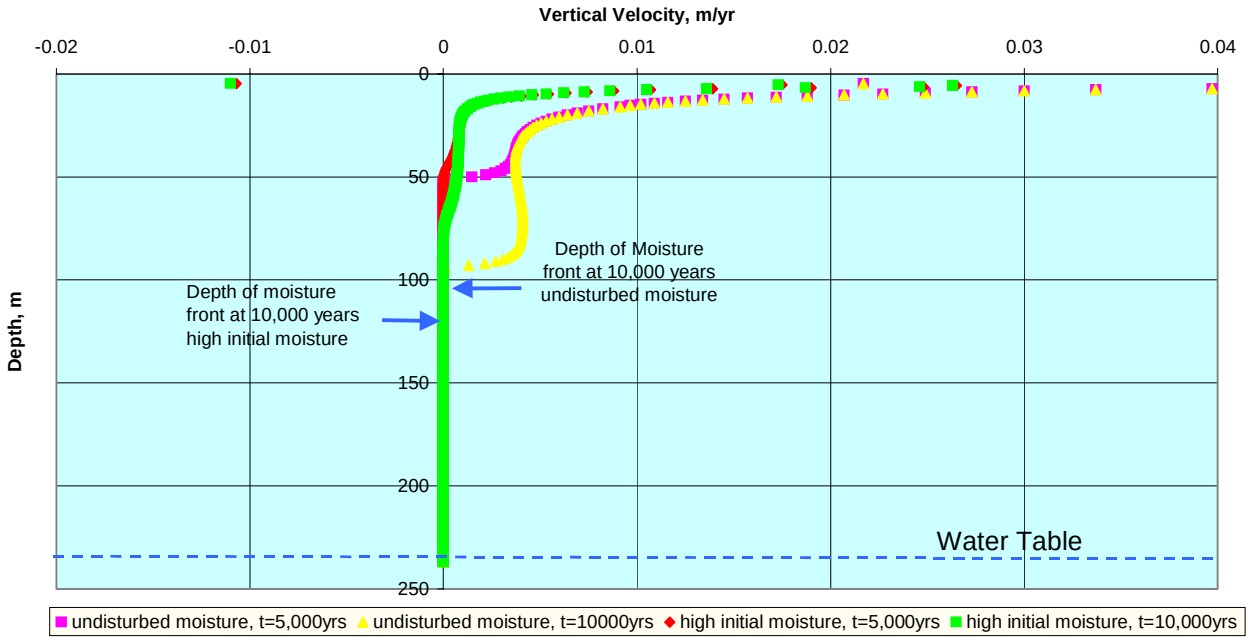

Figure 6.11. Conceptual Model 1 – Intact Cap. Results of the GCD Borehole Modeling Vertical Velocity Profiles at the Vertical Cross-Section through the GCD Borehole.

In the third simulation, GCD Borehole 1 was modeled assuming glacial climate conditions and an intact cap for 10,000 years and using undisturbed initial moisture conditions. The results of this simulation indicated that the depth of the moisture front beneath GCD Boreholes 1 and 2 could be at a depth of 100 m (300 ft) at 10,000 years. Consequently, no groundwater recharge will occur in 10,000 years.

Finally, the potential effect of the trench on GCD Boreholes 3 and 4 was estimated by specifying higher initial moisture in simulations of the infiltration of water from the subsidence depression above a GCD borehole. In this case, a GCD borehole was modeled assuming glacial climate conditions, an intact cap for 10,000 years, and a high (10%) initial moisture condition to account for the influence of moisture migrating from Trench TO4C. The results of this simulation indicated that the depth of the moisture front beneath GCD Boreholes 3 and 4 could be at a depth of 119 m (390 ft) at 10,000 years and no groundwater recharge will occur in 10,000 years.

The major conclusions from the simulations performed were the following:

- The infiltration of the water focused in the LLW trenches will result in downward and lateral spreading of moisture. The lateral spread of the moisture has a potential to affect the moisture conditions around GCD Boreholes 3 and 4 (the closest boreholes to the trenches).

- Focusing precipitation within the subsidence depressions above the GCD boreholes and its infiltration into the unsaturated zone may result in downward unsaturated flow. However, the moisture front will not reach the water table within 10,000 years under the current or future climate conditions. This conclusion is true when moisture is also migrating laterally from the trench (GCD Boreholes 3 and 4) and when it is not (GCD Boreholes 1 and 2).

This page intentionally left blank.

7.0 MODELING THE REDISTRIBUTION OF MOISTURE IN THE UNSATURATED ZONE DUE TO FOCUSING PRECIPITATION IN THE LLW TRENCHES

7.1 Introduction

The sensitivity analysis provided below is not a classic sensitivity analysis. The complexity of the unsaturated flow considered in 2-D and quasi-3-D formulation and long simulation time required (10,000 years) did not allow for applying the standard scheme based on performing a large number of simulations. The purpose of this analysis was to test the sensitivity of those assumptions used in the screening analysis and discussed in Section 5.0 that are not bounding for estimation of downward flow.

7.2 Model Sensitivity to the Unsaturated Flow Parameters

The mean unsaturated zone parameter values (see Section 5.3.2) were used in the unsaturated flow modeling. The moisture profile obtained with these parameters describes the mean moisture conditions within the unsaturated zone. However, the moisture content is highly variable and a range of values was observed for every depth within the unsaturated zone (see Figure 5.9). To estimate the effect that the different parameters may have on the modeling results, the moisture conditions near the surface were specified at the 95th percentile level from the moisture content distribution, which is equal to 0.09. The other unsaturated zone parameters, except the saturated hydraulic conductivity, were adjusted as described below to correspond to the higher moisture conditions within the unsaturated zone. The saturated conductivity, K_{sat}, is relatively well-established, and the uncertainty in this parameter contributes very little to overall uncertainty in the potential for deep recharge.

The constraint $m = 1 - 1/n$ [van Genuchten et al., 1991] was used to fit the retention curves, since the numbers of retention curve data points are too small to estimate both n and m. The values for the remaining parameters of Equation (5.7) were constrained by the measurements taken from core samples and boreholes.

Core sample data from the AP and RP boreholes have been analyzed to estimate values for the parameters θ_s, θ_r, θ_i, α, and n (Appendix D). θ_i is the moisture content within the upper 20 m (70 ft) of the unsaturated zone. These parameter estimates vary from sample to sample and the values for a given sample have some degree of uncertainty. The value used in the model represents a volume of soil much larger than the core sample volume. For the parameters θ_s and θ_i, the effective value is the average value over the modeled volume of soil. The scaling relationships between the core-scale values and the model-scale values for the other parameters are unknown. The model parameter values were established considering the range of core-scale values for these parameters under the assumption that the model-scale values would be bounded by the available core-scale estimates.

The prevailing high suction pressures in the upper 20 m (70 ft) interval of the unsaturated zone set a further restriction on the parameter values. The combination of retention curve parameters and the initial moisture content (θ_i) in this zone was required to produce a suction head of -300 m (-1000 ft), which is consistent with the range of suctions measured in this zone. With

this constraint, the remaining parameters were selected to produce a large value for the unsaturated hydraulic conductivity at the initial moisture content.

Equation (5.6) was used to define the relationship between K and S_e. Core samples from the AP and RP boreholes were analyzed assuming $l = 0.5$. $K(S_e)$ increases as S_e and m increase. Large values for these parameters, consistent with available data, were therefore selected. Using the constraint $m = 1 - 1/n$, large values of n correspond to large values of m. In interpreting the core data, the relative saturation S_e as a function of the suction pressure ψ was modeled using Equation (5.7).

For a given suction pressure, small values of α lead to large saturations, and therefore to large unsaturated hydraulic conductivities. Overall, a large value for n and a small value for α will lead to a relatively large unsaturated hydraulic conductivity for any given suction pressure. In addition, the moisture content in the upper zone, θ_i, along with the parameters θ_s and θ_r, should be consistent with a suction pressure of −300 m (−1000 ft) typically observed in this region.

The core samples from the AP and RP boreholes were analyzed to estimate the current advective flux in the undisturbed region in the upper zone (Appendix D). Over these core samples, the fitted values for α (including the uncertainty in the fitted values) range from 0 to 0.8 cm^{-1} (0 to 0.3 $in.^{-1}$). Fitted values for n range from 1 to 2.3. The reported confidence intervals for these parameters are typically quite large for a given sample, and the reported lower bound of the 95% confidence interval (which assumes a symmetric distribution around the estimated value) is often below the physically meaningful limits for both parameters. The parameter estimation errors for n and α also have a strongly negative correlation, so that the combination of a large value for n and a small value for α is consistent with the fit of Equation (5.7) to the retention data. Estimation errors for α and θ_r are also negatively correlated, suggesting that a large value of θ_r, in conjunction with a small value for α will be required for consistency with the available retention data.

Considering this correlation, the largest estimate of residual moisture content (0.08) from the analysis of the AP and RP core samples was adopted as a limiting estimate for θ_r. Because reported values for the saturated water content are much larger than values for the initial and residual water contents, the result is not expected to be sensitive to the value of the saturated water content given the relatively small uncertainty in this parameter. θ_s was assigned a value of 0.37, typical of the analyzed core samples.

The lower limit for α is 0, based on the confidence limits for the fits to retention data, is not physically plausible: it implies that saturation does not change as suction pressure increases. A value of 10^{-2} cm^{-1} (4×10^{-3} $in.^{-1}$) was chosen as a lower limit for this parameter based on the fitted values reported for various soil types in van Genuchten et al. [1991, Tables 3 and 4]. This value is an order of magnitude smaller than the values typically reported for sandy soil, and is therefore an appropriate lower limit for this analysis. With this value for α, n was constrained to produce a suction head of −300 m (−1000 ft) at the selected initial moisture content of 0.09 using Equation (5.7). The resulting value of 1.573 is less than the limit of 2.3 established by the largest value for the upper confidence limit of any individual core sample, and is smaller than some best

estimates for individual core samples. It is also well within the range of values reported for various soil types in van Genuchten et al. [1991].

As an overall check on the validity of the unsaturated flow parameters, Figure 7.1 shows the volumetric moisture content as a function of suction head using these parameter values. Measured retention data from the AP and RP core samples are included for comparison. The selected function appears consistent with these measurements, given the objective of screening the unsaturated hydraulic conductivity at high suction.

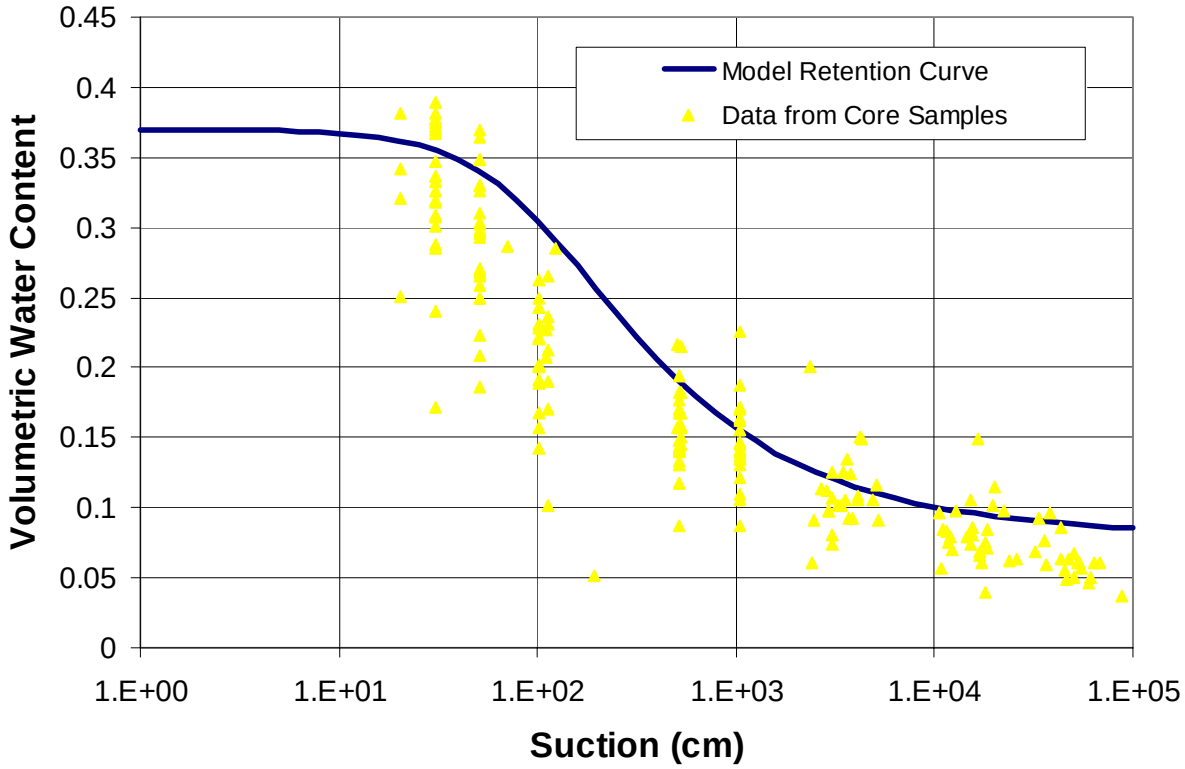

Figure 7.1. Retention Curve Using Model Parameters with Data from AP and RP Core Sample Analyses.

Two simulations for Trench TO4C were performed to estimate the sensitivity of the model to the unsaturated flow parameters. The same modeling setup, as discussed in Section 6.2.1, was used in these simulations. The volumes and durations of the ponding events were defined arbitrarily, but identical for two simulations. The mean parameter values were used in the first simulation and the parameter corresponding to the high moisture conditions were used in the second simulation. The distributions of moisture beneath Trench TO4C at 10,000 years obtained from these simulations are shown in the Figures 7.2 and 7.3. The depth of moisture front calculated using the mean parameters is 30 m (100 ft) and the lateral spread of the moisture front is 15 m (49 ft). The depth of moisture front calculated using parameters corresponding to the higher moisture conditions is more than two times deeper (80 m (300 ft)) and so is the lateral spread of the moisture front (35 m (120 ft)).

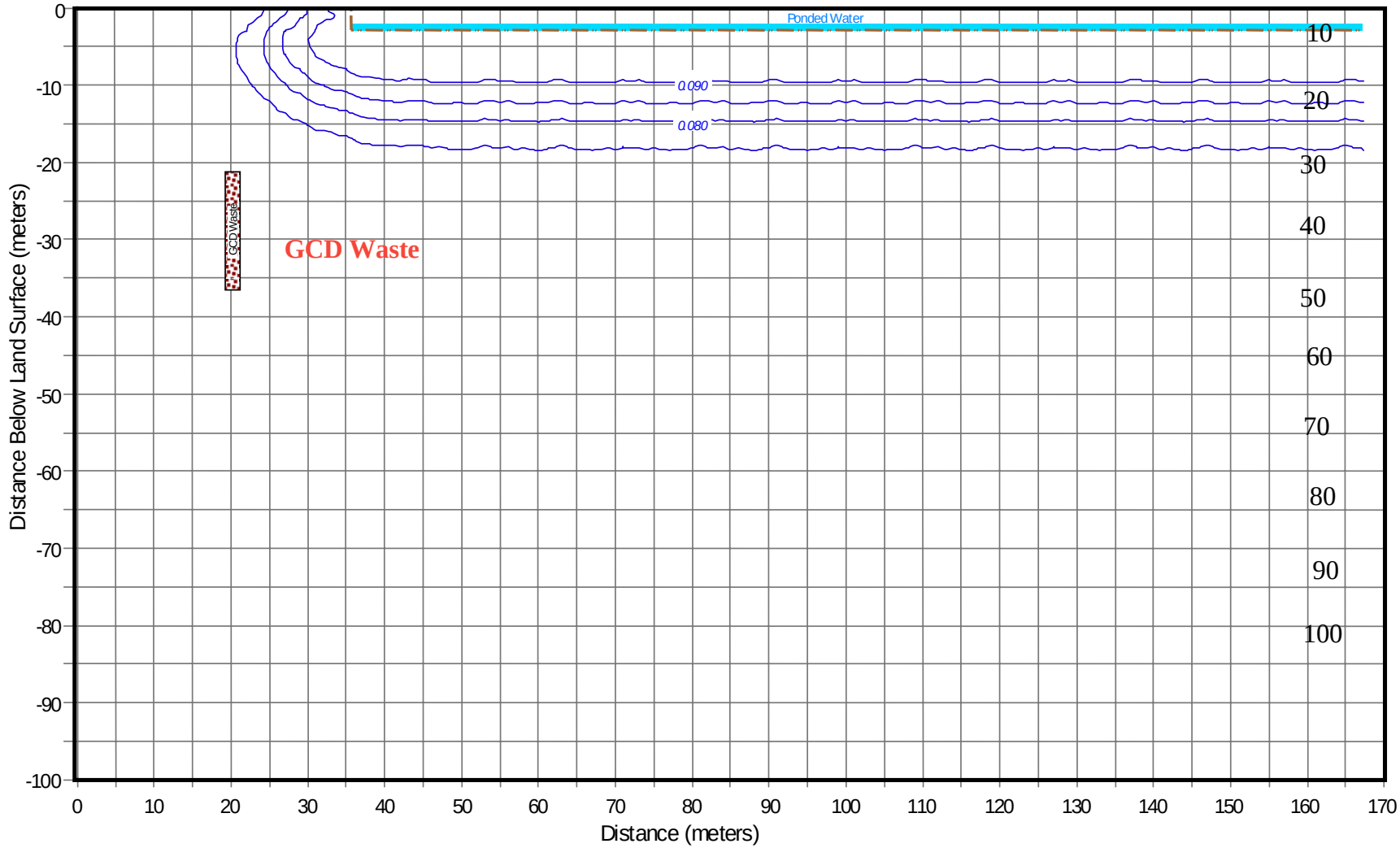

Figure 7.2. Distribution of Moisture Beneath Trench TO4C at 10,000 Years. Mean Unsaturated Flow Parameters.

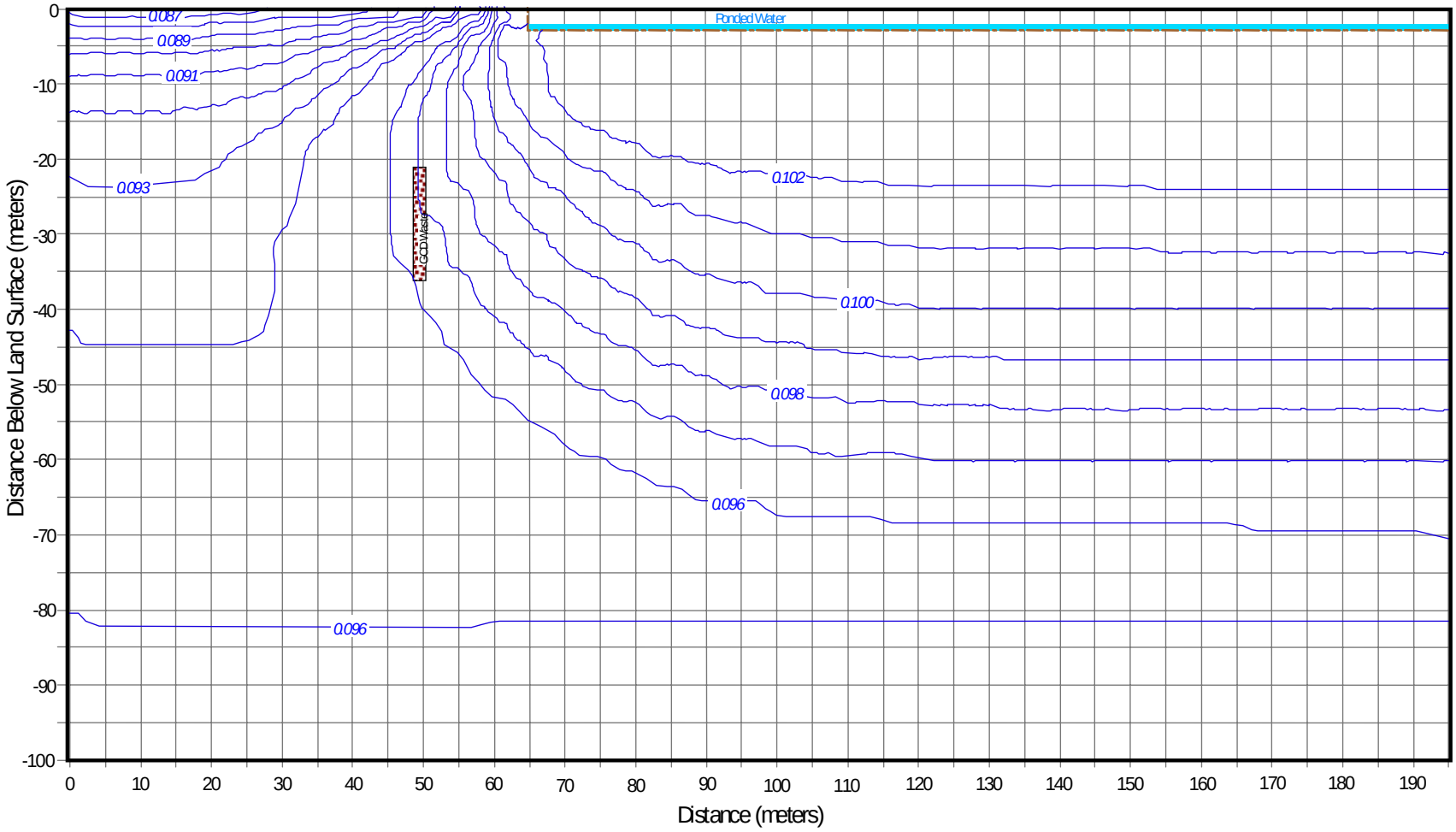

Figure 7.3. Distribution of Moisture Beneath Trench TO4C at 10,000 Years. Unsaturated Flow Parameters Corresponding to High Moisture Conditions.

7.3 Model Sensitivity to Dimensionality

The model sensitivity to the dimensionality was studied by comparing the results of models identical in everything except dimensionality. Two models were compared – a quasi-3-D model and an equivalent 1-D model.

The quasi-3-D model setup is the same as described in Section 6.2.3. The simulation time was 1000 years. The average ponding event with a volume of 1.9 m^3 (67 ft^3) and reoccurrence of 2.4 years was specified arbitrarily. The low-probability ponding events were not modeled.

The 1-D model was set up to provide the best match with the quasi-3-D model. This setup is shown in Figure 7.4. The 1-D model represents the vertical line that begins at the bottom of the cone-shaped depression and extends 234 m (768 ft) down to the water table. The spatial discretization used is the same as the spatial discretization of the quasi-3-D model in the vertical direction (see Section 6.2.3). The boundary conditions were defined in the nodes of two boundary blocks. Zero pressure was specified at the boundary block located at the lower end of the model. The upper boundary condition was specified in the upper boundary block as follows. The average ponding event was modeled by specifying prescribed flux q_p in the node of the boundary block for the period of time t_p. The q_p was calculated as:

$$q_p = V_{av}/S_p \tag{7.1}$$

where V_{av} is the volume of the average ponding event from the quasi-3-D model (1.9 m^3 (67 ft^3)) and S_p is the surficial area of the cone-shaped depression through which infiltration of the ponded water occurs. The value of S_p was calculated using the following formula:

$$S_p = \pi * R * (R^2 + d^2)^{½} \tag{7.2}$$

where d is the maximum depth of the ponding event and R is the radius of the depression corresponding to this depth. The parameters D and R from the quasi-3-D model were d = 1 m and R = 1.43 m. The corresponding value of the q_p specified for the 1-D model was 260 mm. This rate was maintained for the period of time t_p equal to 0.32 days and calculated from the following formula:

$$t_p = q_p/K_{sat} \tag{7.3}$$

The evaporation boundary condition was specified in the upper boundary node between the ponding events same way it was done in the quasi-3-D model, using potential soil evaporation rates shown on Figure 5.6.

The results of these two simulations at 1000 years are shown in Figures 7.5 through 7.7. According to the 1-D model, the moisture front is a few meters away from the water table (232 m (761 ft) deep) at 1000 years (Figure 7.5). The vertical velocity beneath the depth of 50 m (164 ft) is constant and equal to 200 mm/yr (Figure 7.6). The evaporation effect is noticeable in the upper 10 m (33 ft) of the unsaturated zone. The downward flow is 19.7% of the total

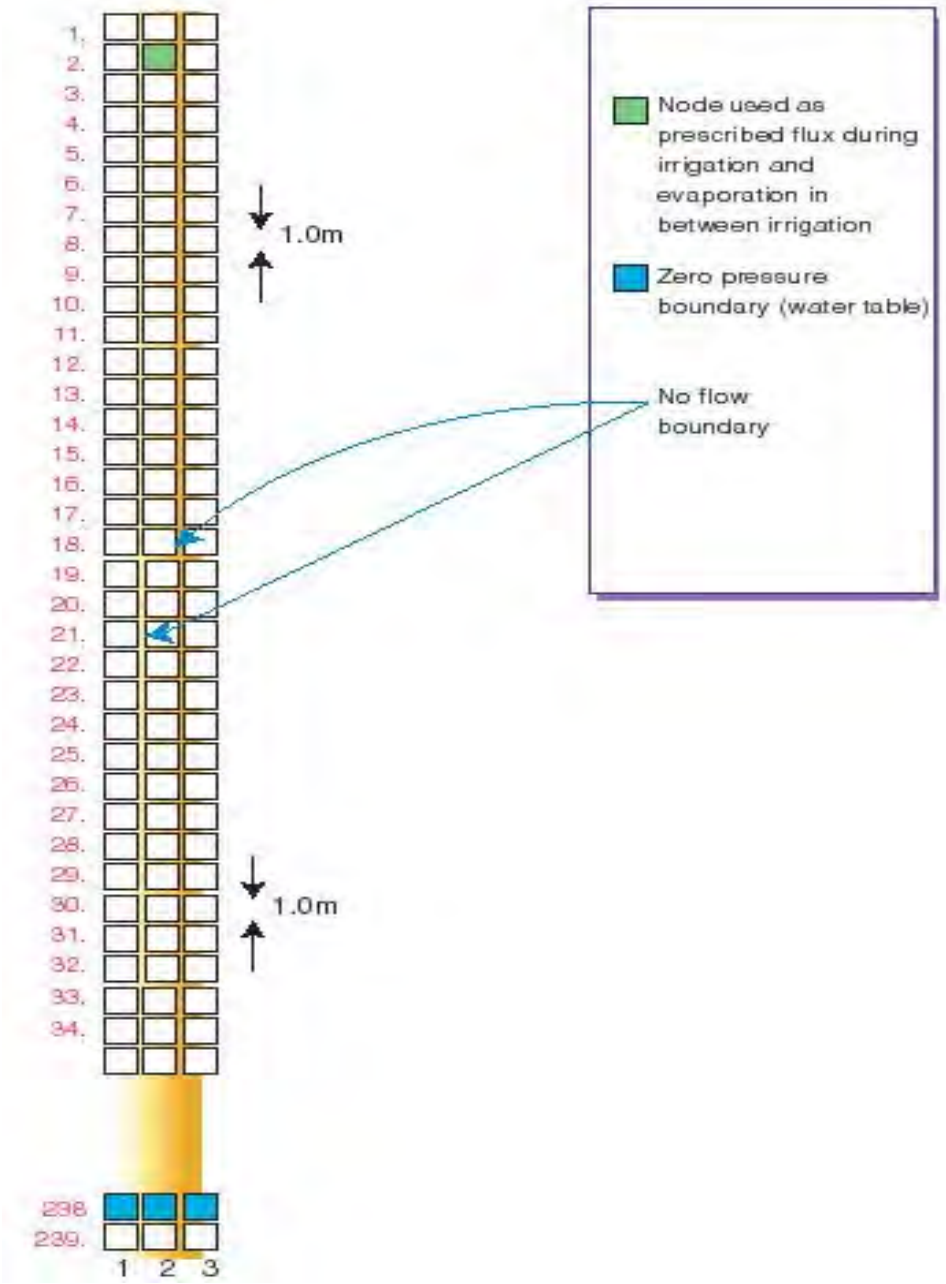

Figure 7.4. 1-D Model Set-Up.

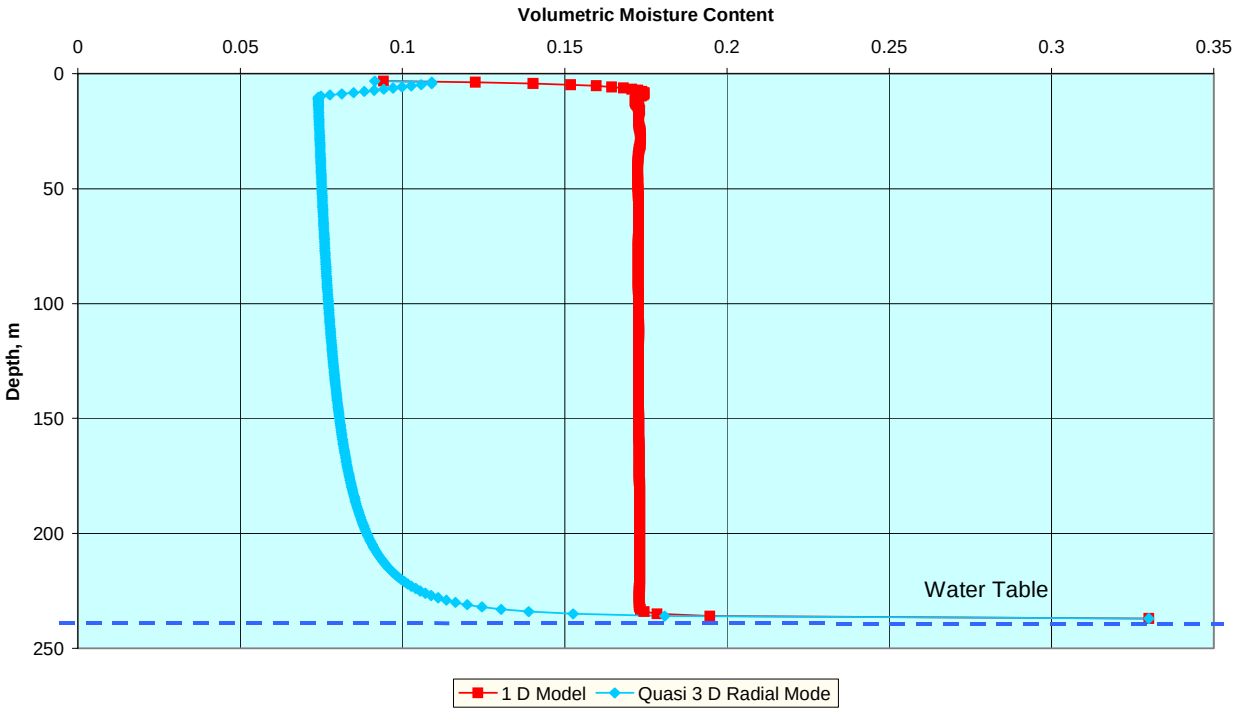

Figure 7.5. Model Sensitivity to Dimensionality Moisture Profiles at 1000 Years.

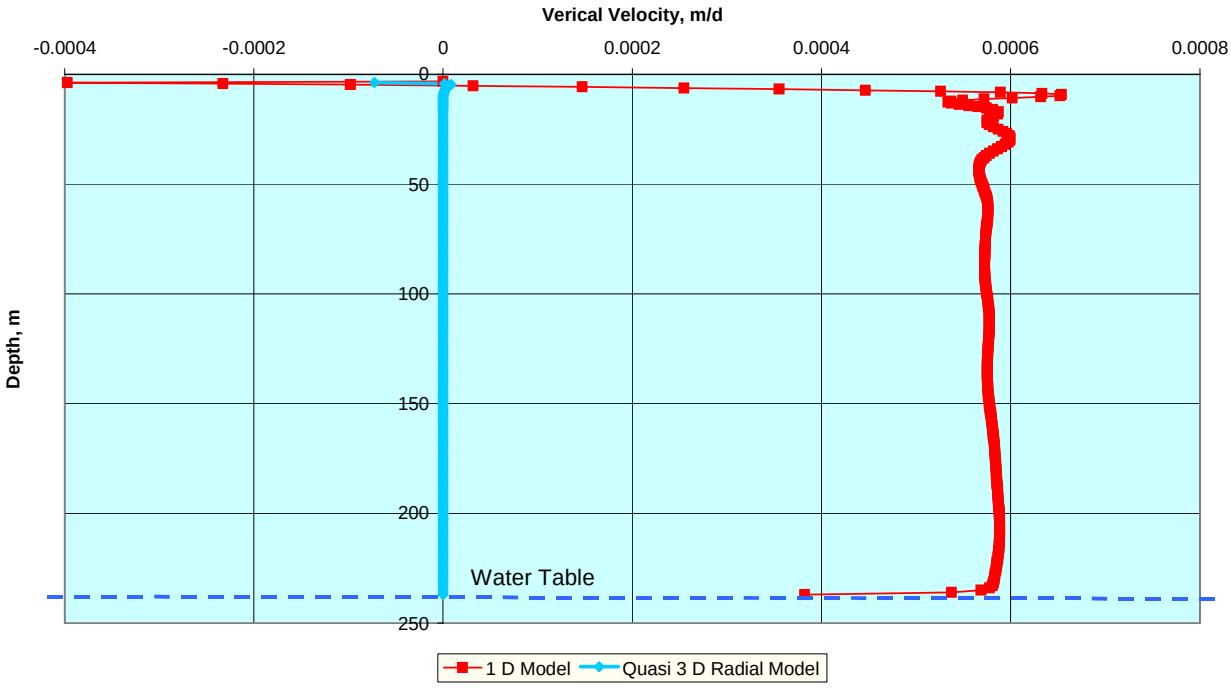

Figure 7.6. Model Sensitivity to Dimensionality Vertical Velocity Profile at 1000 Years.

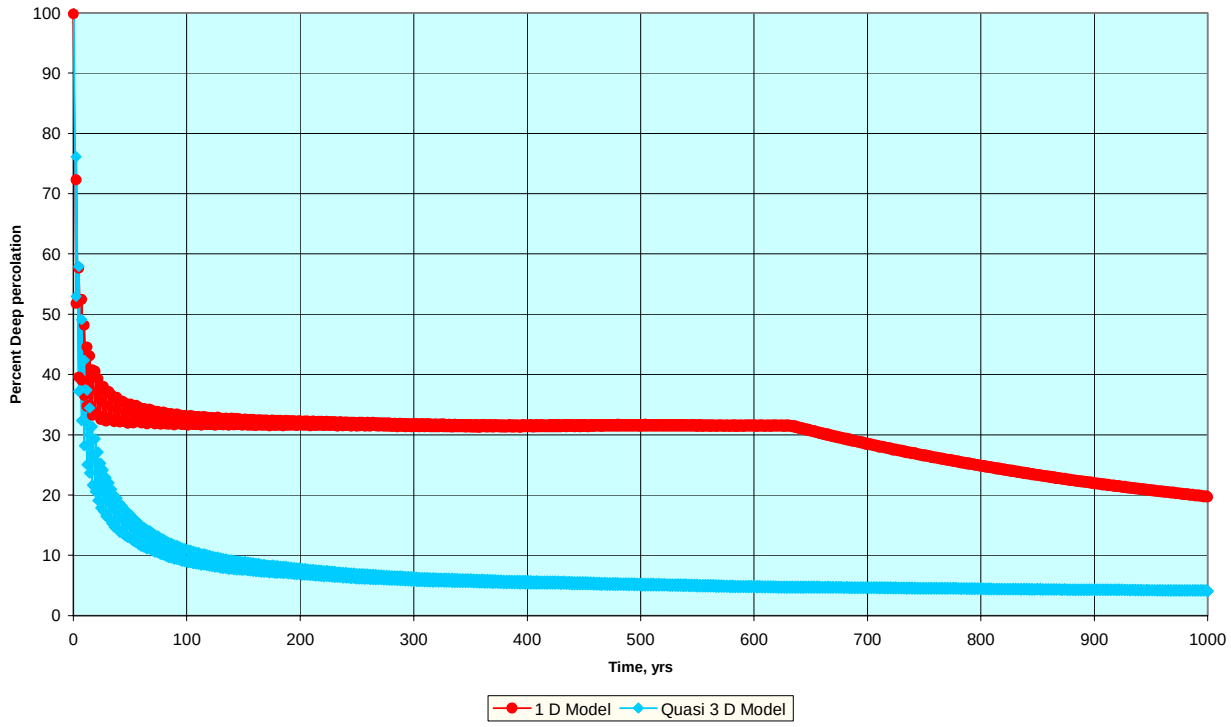

Figure 7.7. Model Sensitivity to Dimensionality Downward Flow as a Percentage of the Total Volume of Surface Water.

amount of water introduced into the unsaturated zone. According to the quasi-3-D model, the moisture front depth at 1000 years is only 10 m (33 ft). The downward vertical velocity ranges from 0 mm/yr (beneath the depth of 10 m [33 ft]) to maximum 35 mm/yr. The downward flow is 6.0% of the total amount of water introduced into the unsaturated zone.

The significant differences in these results are due to the fact that the quasi-3-D model takes into account the lateral flow around the cone-shaped depression. The lateral flow with the subsequent evaporation results in extracting 15.6% of the water introduced into the unsaturated zone out of the system.

7.4 Model Sensitivity to the Potential Evaporation Rates

To estimate the model sensitivity to the PE rates, the lower limit of the PE was defined assuming glacial climate conditions.

A simple empirical formula was used to calculate the average monthly PE rates. This formula relates average monthly PE PE_m to mean monthly temperature T_m, ratio of sum of daylight hours within the month and sum of daylight hours within the year D, and crop factor C [Blaney, 1950] as follows:

$$PE_m = T_m * C * D \qquad (7.4)$$

The crop factor *C* is time- and location-dependent. The ratio *D* is provided in Table 7.1. They were calculated based on the daily values of the duration of daylight hours at the GCD site latitude.

Table 7.1. Ratios of the Sum of Daylight Hours within the Month and Sum of Daylight Hours within the Year for the Area 5 RWMS

Month	Jan	Feb	Mar	Apr	May	Jun	Jul	Aug	Sep	Oct	Nov	Dec
D*10^{-2}	7.14	6.52	8.63	8.93	1.01	9.79	1.01	9.4	8.11	7.77	6.69	6.81

Equation (7.4) was used first assuming current climate conditions. Average monthly PE rates were calculated based on the current average monthly temperatures. The crop factor *C* was assumed to be constant and was adjusted to provide the match in the total annual PE calculated using Equation (7.4) and total annual, PE estimated using site-specific data, as described in Section 5.3.3. The obtained monthly evaporation rates were close to the monthly evaporation rates shown in Figure 5.6.

To simulate glacial climate conditions, the average monthly temperature was lowered by 5°C. The crop factor *C* and daylight ratio *D* remained the same. As a result, the total PE dropped from 1585 mm/yr to 1114 mm/yr, or 1.4 times.

Two simulations for GCD Borehole 1 were performed to estimate the sensitivity of the model to the PE rates. The same modeling setup, as discussed in Section 6.2.3, was used in these simulations. The average ponding event with a volume of 1.9 m^3 and reoccurrence of 2.4 years was specified arbitrarily. The low-probability ponding events were not modeled. The PE rates used in the first simulation were same as shown in Figure 5.6. The PE rates used in the second simulation were 1.4 times lower. The depth of moisture front calculated using the 1.4-times-lower PE rates was 7 m (23 ft) deeper at 10,000 years.

7.5 Model Sensitivity to the Low-Probability Ponding Events

The purpose of this analysis was to identify the contribution of the low-probability ponding events to the downward flow in comparison with the average ponding events. Three simulations for GCD Borehole 1 were performed in this analysis. The same modeling setup, as discussed in Section 6.2.3, was used in these simulations. The average volume of ponding event was arbitrarily defined as 1.9 m^3 with reoccurrence of 2.4 years. The difference was in the way of specifying low-probability events.

The first simulation modeled the average ponding events only. The second simulation modeled four low-probability events placed 2.4 years apart that totally filled the subsidence depression (total subsidence volume is 59 m^3) and average ponding events, with the first average ponding event occurring 2.4 years later than the last low-probability event, and other average ponding events occurring every 2.4 years during the period of simulation. The third simulation modeled a ponding event corresponding to PMP placed at the time equal to zero, one 10,000-year ponding event placed 2.4 years apart from the PMP, nine 1000-year ponding events placed 2.4 years apart

from the 10,000-year ponding event and from each other, 90 100-year ponding events placed 2.4 years from the last 1000-year ponding event and 2.4 years apart from each other, and average ponding events, with the first average ponding event occurring 2.4 years later than the last 100-year ponding event and other average ponding events occurring every 2.4 years during the period of simulation.

The results of these simulations are shown in Figure 7.8. The depth of moisture front at 1000 years obtained in the third simulation (all low-probability events and average ponding events) was only 4 m (13 ft) deeper than the depth of moisture front in the first simulation (the average ponding events only). The depth of the moisture front obtained in the second simulation was in between the first one and the third one. Consequently, the timing and volumes of the low-probability events have a low impact on the movement of the moisture front that is mainly defined by the average ponding events.

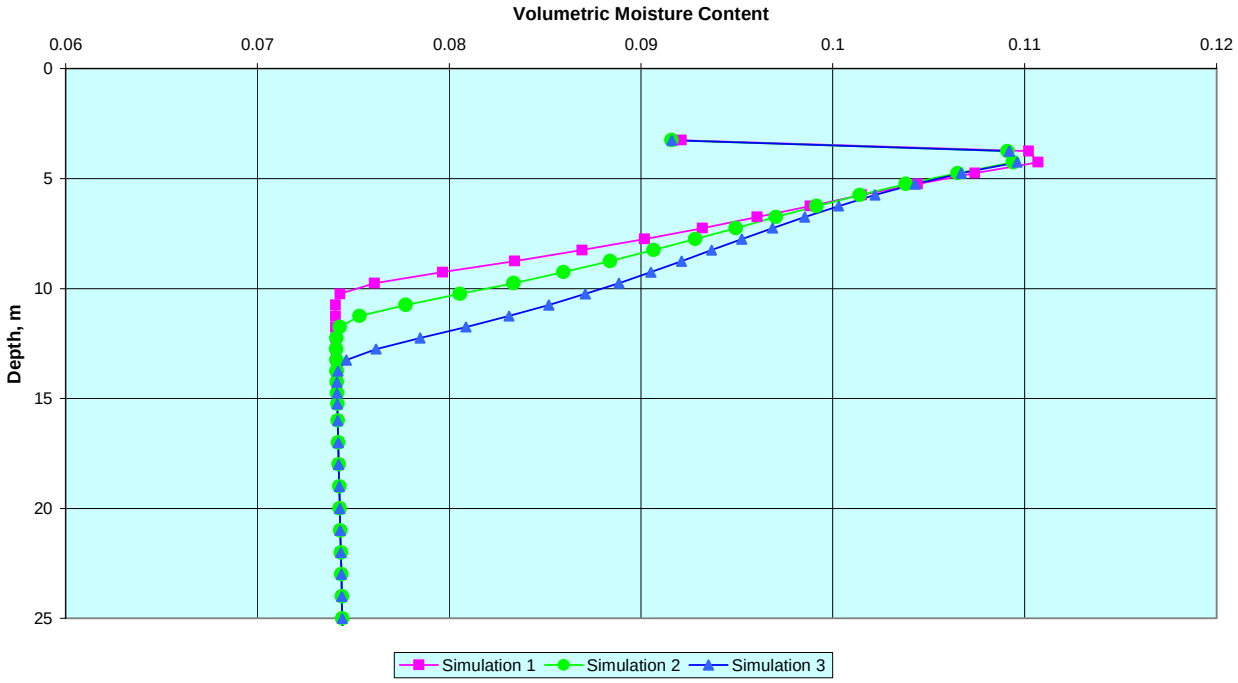

Figure 7.8. Model Sensitivity to the Low-Probability Ponding Events/Moisture Profile at the Depression Center Line at 1000 Years for GCD Borehole 1.

7.6 Model Sensitivity to the Assumption About the Trench Bottom

Under undisturbed conditions, the land surface in the Area 5 RWMS gradually slopes to the southwest and the bottom of the trenches and pits mimic the undisturbed land surface. Two situations can occur when the trenches and pits subside. In the first situation, the subsidence is uniform and the bottoms of the subsided features mimic the land surface. This situation results in collecting most of the surface water (low-intensity average ponding events) within the southwest corners of the subsided features. The only borehole of concern is GCD Borehole 4,

which would be in the vicinity of the ponded water in Trench TO7C. GCD Boreholes 1, 2, and 3 would be located too far from the water ponded in Trench TO4C and Pit PO3U to be impacted.

In the second situation, the subsidence is differential and consists of a number of features with different shapes and depths. This situation result in a somewhat even distribution of water within all the bottoms which can be conceptualized assuming a flat bottom of the trench. As discussed in Section 6.2.1, Trench TO4C has the greatest potential to affect GCD Boreholes 1, 2, and 3 in this situation.

Two simulations were performed to determine which assumption is more bounding for estimation of the downward flow. In the first simulation, Trench TO4C was modeled using the model set up described in Section 6.2.1. The arbitrarily-defined average ponding events in Trench TO4C were modeled during 10,000 years assuming a flat bottom of the trench (this is the first simulation described in Section 7.2).

In the second simulation, Trench TO7C was modeled. The same model setup as for Trench TO4C was used, except that all the blocks in horizontal dimension had the same size, equal to 2 m (7 ft), with 16 blocks representing the land surface and 26 blocks representing the subsided bottom of the trench. The modeled length of the trench was 50 m (164 ft), half the trench length that is filled with water during the average ponding event.

The distributions of moisture around Trenches T04C and TO7C at 10,000 years are shown in Figures 7.2 and 7.9, respectively. The unsaturated zone influenced by the infiltration of ponded water has a similar lateral and vertical extent in both cases. The moisture front beneath trench TO4C is located at a depth of 29 m (95 ft) from the bottom of the trench. The moisture front beneath Trench TO7C is at a depth of 32 m (105 ft). The lateral extent is about 10 m (33 ft) from the edge of the trench.

7.7 Conclusions

The sensitivity of the unsaturated flow model was considered using the following parameters/ assumptions:

- unsaturated flow parameters
- dimensionality
- PE rates
- low-probability ponding events
- assumption about the trench bottom

The most significant effect on the result was the model dimensionality. The comparison of the 1-D model and similar quasi-3-D model in radial coordinates showed that, in the case of the 1-D model, the moisture front at 1000 years is a few meters above the water table (232 m [761 ft] below the land surface). In the case of the quasi-3-D model, the depth of the moisture front at 1000 years is 10 m (33 ft).

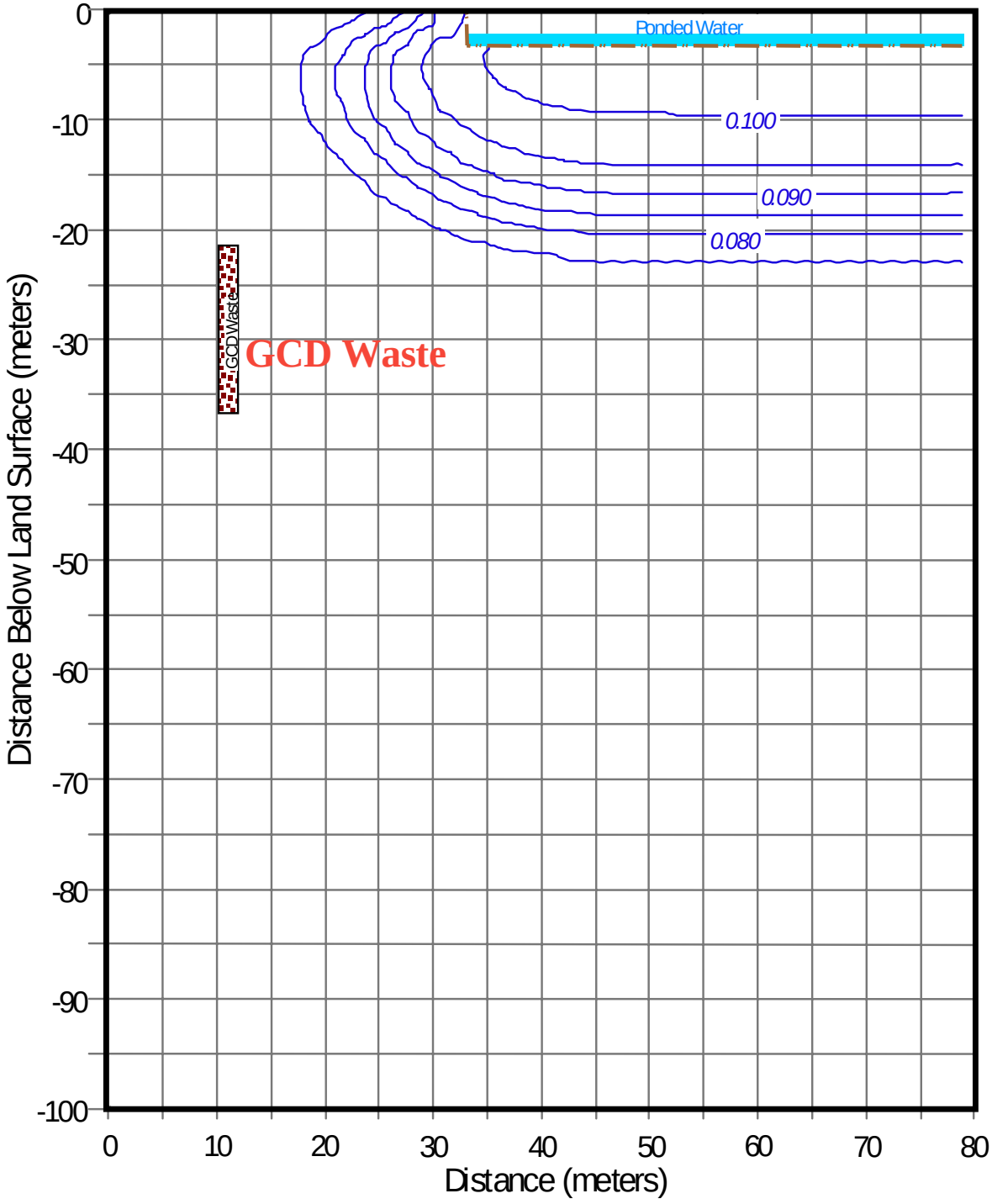

Figure 7.9. Distribution of Moisture Beneath Trench TO7 at 10,000 Years, Sloped Trench Bottom.

The model is also very sensitive to unsaturated flow parameters. Assuming higher moisture conditions in the unsaturated zone results in the noticeable increase in the moisture front depth. For example, the moisture front beneath Trench TO4C was 30 m (98 ft) when the mean parameters were used and 80 m (262 ft) when the parameters corresponding to the higher moisture conditions were used.

The PE rates have a relatively small effect on the modeling results. Assuming total annual evaporation 1.4 times lower results in increasing depth of the moisture front by only 7 m (23 ft).

Modeling the low-probability events along with the average ponding events results in some increase of the depth of moisture front (4 m [13 ft] deeper) in comparison with the simulation that models only average ponding events. This is a relatively small effect as well.

The model is not sensitive to the way the trench bottom is modeled. The same results were obtained by modeling Trench TO7C assuming a sloped bottom and Trench TO4C assuming a flat bottom.

8.0 SUMMARY

The Area 5 RWMS LLW trenches and pits contain a significant amount of void space resulting from the incomplete filling of waste containers, limited internal compaction of contents, and voids between containers. These voids will produce significant subsidence as the waste containers deteriorate and collapse. This subsidence has the potential to focus precipitation and runoff, which may cause the downward movement of pore water and the formation of ephemeral wetlands. Additionally, numerous studies have shown that over long time spans, the climate could return to cooler and wetter, glacial conditions.

This report presents the results of a detailed screening analysis conducted to determine if surface water might migrate to the water table during the next 10,000 years, because of the combined effects of landfill subsidence and a possible return to a glacial climate. If surface water and radionuclides have the potential to reach the accessible environment in the next 10,000 years, this pathway would have to be included in the PA for the TRU wastes in the GCD boreholes.

Four coupled analyses were undertaken for this study:

- the geometry of future subsidence features was estimated;
- using current climatic data, precipitation, local runoff, and flooding were modeled;
- assuming an immediate return to glacial climatic conditions, precipitation, local runoff, and flooding were modeled; and
- the 2-D), and quasi-3-D movement of water in the subsurface was modeled in two ways. First, assuming the landfill cap is intact for 10,000 years and second, assuming the landfill cap is instantly "removed" at the end of the institutional control period.

This screening analysis does not model the movement of radionuclides, nor does it model the movement of water to the accessible environment. The movement of radionuclides would be much slower than the movement of pore water due to chemical sorption of radionuclides onto the alluvium. Therefore, if it can be shown that pore water moving through the GCD wastes will not reach the water table in 10,000 years, then it is very clear that radionuclides will not reach the 5-km (3.1-mi) accessible environment boundary in 10,000 years.

The actual evolution of the site with respect to subsidence and climate change is unknown. Therefore, this analysis was systematically constructed to overestimate the potential for downward migration of water. With respect to subsidence, this meant maximizing the amount of subsidence that occurs after institutional control. That is, for the next 170 years the site will be under institutional control and DOE will fill in any subsidence that occurs. Therefore, this analysis chose rates of subsidence that maximize the post-170 years subsidence. Then the entire remaining void volume is assumed to instantly collapse and form a subsidence depression. The effects of natural erosion of the cap were investigated first by an analysis of flooding potential and second by postulating two bounding conditions. The flooding analysis indicated that it is not very likely that floods will overtop the cap during the next 10,000 years. However, due to uncertainty in this calculation two bounding conditions were analyzed. First, the cap with associated subsidence features was assumed to stay intact for 10,000 years. Second, the cap was assumed to be instantly removed at the end of the institutional control period. In the case of no

cap, sedimentation associated with flooding filled in the subsidence features in a few hundred years, which halted the accumulation of floodwaters. Since the subsidence features associated with the intact cap were assumed to last 10,000 years, this case became the bounding analysis. That is much more water entered the deep unsaturated zone in the intact cap case.

Climate studies indicate that a doubling of precipitation is very likely to occur in the next 10,000 years. However, the timing of climate change is uncertain. Therefore, this analysis assumed that climate change begins immediately and lasts the entire 10,000-year period. Climate change was represented by a doubling of each precipitation event instead of a doubling of the number of precipitation events. This approach maximizes total runoff because in each precipitation event a certain volume of rainfall must be absorbed by the soil before runoff begins.

- Based on the results of the subsidence and climate change analysis models of unsaturated groundwater flow were developed. These models simulated the migration of water collected by the subsidence features as it infiltrated into the unsaturated zone and migrated toward the water table. These models were also biased toward high migration rates. All low probability precipitation events were assumed to begin soon after the loss of institutional control. For example, under glacial conditions, the PMP was assumed to occur at time zero (the year 2170), followed by the 10,000-year storm 1.125 years later. A 1000-year storm was assumed to occur 1.125 years after the 10,000-year storm. The 1000-year storm is followed by nine 100-year storms, each 1.125 years apart. Then beginning at 1000 years, this sequence of a 1000-year storm and nine, 100-year storms was repeated every 1000 years through the year 9000. In addition, only evaporation from the land surface was modeled. That is, t*he model does not include the removal of soil moisture by plants*.

The results of these studies indicate that:

- The infiltration of the water focused in the LLW trenches will result in downward and lateral spreading of moisture. The lateral spread of the moisture has a potential to affect the moisture conditions around GCD Boreholes 3 and 4 (the closest boreholes to the trenches).

- Focusing precipitation within the subsidence depressions above the GCD boreholes and its infiltration into the unsaturated zone may result in downward unsaturated flow. However, the moisture front will not reach the water table within 10,000 years under the current or future climate conditions. This conclusion is true when moisture is also migrating laterally from the trench (GCD Boreholes 3 and 4) and when it is not (GCD Boreholes 1 and 2).

Therefore, the subsidence with or without climate change can be ruled out as a scenario that needs to be included in performance assessment.

REFERENCES

Allen, J.R.L., *Physical Processes of Sedimentation*, Allen and Unwin, London, 1971.

Anstey, R.L., *Physical Characteristics of Alluvial Fans*, U.S. Army Natick Laboratories, Technical Report ES-20, Natick, Mass., 1965.

Arnold, Bill W. 1996. Memorandum: Estimating Subsidence for GCD PA (memo/96/S34). Sandia National Laboratories, Albuquerque, NM.

Beaty, C.B., *Origin of Alluvial Fans, White Mountains, California and Nevada*, Annals of the Association of American Geographers, Vol. 53, 1963, pp. 516-535.Blakemor

Bechtel Nevada. 1998. Estimation of Upward Advective Water Flux at the Greater Confinement Disposal Facility. Project No. 04010. North Las Vegas, NV.

Blaney, H.F. and W.D. Criddle, Determining water requirements in irrigated areas from climatological and irrigation data. USDA Soil Conser. Surv. Tp-96, 48 pp., 1950.

Blout, D. O., W. S. Birchfiel, D. P. Hammermeister, and K. A. Zukosky. 1995. Site Characterization Data from the Area 5 Science Boreholes, Nevada Test Site, Nye County, Nevada. Report No. DOE/NV11432-170, U.S. Department of Energy, Nevada Operations Office, Las Vegas, Nevada.

Brown, T., S.H. Conrad, S. Wirth, J.R. Cochran, and J. Emery, "Plausible Future Climate States at the Area 5 Radioactive Waste Management Site, Nevada Test Site," Letter Report transmitted J. Ginanni (DOE/NV/WMD), January 31, 1997, Sandia National Laboratories, Albuquerque, NM (1997)

Brown, T., R. Thomas, W. Fogleman, "Modeling Potential Effects of Subsidence at the Area 5 RWMS for the GCD Compliance Assessment Analyses," SNL, 1998.

Bryant, Ernest A. 1992. The Cambric Migration Experiment, A Summary Report. LA-12335-MS. Los Alamos National Laboratory, Los Alamos, NM.

Bull, W.B., *Alluvial Fans and Near-Surface Subsidence in Western Fresno County*, California, Professional Paper 437-A, U.S. Geological Survey, Washington, D.C., 1964.

Caffee, Marc, K.E. Snyder and D.L. Gustafson, *Letter Report of Cosmogenic Exposure Dating of Geomophic Surfaces at Frenchman Flat, Southern Nevada*, December, 1995.

Chapman, J.B. 1993. Groundwater Investigations Near the RWMS. Letter Report, Desert Research Institute, Las Vegas, NV.

Christensen, Rulon C., and N.E. Spahr, *Flood Potential of Topopah Wash and Tributaries, Eastern Part of Jackass Flats, Nevada Test Site, Southern Nevada*, Open File Report 80-963, U.S. Geological Survey, Lakewood, Colorado, 1980.

Chu, Margaret S.Y. and Emile A. Bernard. 1991. Waste Inventory and Preliminary Source Term Model for the Greater Confinement Disposal Site at the Nevada Test Site. SAND91-0170. Sandia National Laboratories, Albuquerque, NM.

Crippen, J.R. and C. D. Bue, *Maximum Floodflows in the Conterminous United States*, U.S. Geological Survey Water-Supply Paper 1887, Washington, D.C., 1977.

D'Agnese, F.A., G.M. O'Brien, C.C. Faunt, and C.A. San Juan. 1999. "Simulated Effects of Climate Change on the Death Valley Regional Ground-Water Flow System, Nevada and California." U.S. Geological Survey, Water-Resources Investigations Report 98-4041.

Dawdy, D.R. 1979. "Flood Frequency Estimates on Alluvial Fans." *Journal of the Hydraulics Division*, Proceedings of the American Society of Civil Engineers, Vol.

Dansgaard, W.S., J. Johnsen, H.B. Clausen, D. Dahl-Jensen, N.S. Gundestrup, C.U. Hammer, C.S. Hvldberg, J.P. Steffensen, A.E. Sveinbjornsdottir, J. Jouzel, and G. Bond, "Evidence for general instability of past climate from a 250-kyr ice-core record," Nature, v. 364 pp. 218–220 (1993)

Dewispelare, A.R., L.T. Herren, M.P. Mikalas, and R.T. Clemen, "Expert Elicitation of Future Climate in the Yucca Mountain Vicinity: Iterative Performance Assessment Phase 2.5," Center for Nuclear Waste Regulatory Analyses, San Antonio TX, Report CNWRA 93-016 (1993)

DOE. 1998. Consequences of Subsidence for the Area 3 and Area 5 Radioactive Waste Management Sites, Nevada Test Site. DOE/NV-502.

EPA, "40 CFR Part 191: Environmental Radiation Protection Standards for the Management and Disposal of Spent Nuclear Fuel, High-Level and Transuranic Radioactive Wastes, Final Rule" 50 FR 38066-38089 (1985).

Estrella, Rocio, Scott Tyler, Jenny Chapman, and Mary Miller. 1993. Area 5 Site Characterization Project-Report of Hydraulic Property Analysis Through August 1993. Publication #45121. Desert Research Institute, University and Community College System of Nevada, DOE/NV/10845-41.

Federal Emergency Management Agency. 1995. Mitigation Directorate, "Engineering Principles and Practices for Retrofitting Flood Prone Residential Buildings, Chapter IV: Determination of Hazards."

Feeney, Thomas A., Stephen H. Conrad, and Walter Beyeler. In Progess. Estimation of Upwards Specific Discharge in Vadose Zone at Area 5 RWMS.

French, Richard H. and W. S. Lombardo, *Assessment of Flood Hazard at the Radioactive Waste Management Site in Area 5 of the Nevada Test Site*, Publication 45036, Water Resources Center, July 1984

French, Richard H., J.E. Fuller and S. Waters, *Alluvial Fan: Proposed New Process-Oriented Definitions for Arid Southwest*, Journal of Water Resources Planning and Management, Vol. 119, No. 5., September/October 1993.

French, Richard H., R.L. Jacobson and B.F. Lyles, *Threshold precipitation events and potential ground-water recharge*, ASCE, Journal of Hydraulics Engineering, 1996, 11(10):573-578.

French, R.H. 1993. Letter report of FY-93 evaporation studies at ER 6-1 ponds to Stephen J. Lawrence. USDOE Environmental Restoration & Waste Management. Desert Research Institute/Water Resources Center. Sept. 29, 1993. 20.

Hokett, Samuel L. and R.H. French, Evaluation of Recharge Potential at Crater U5a (Wishbone), Publication No. 45160, Water Resources Center, Desert Research Center, Las Vegas, Nevada, November 1998.

Hooke, R.L., *Alluvial Fans*, Ph.D. Thesis, California Institute of Technology, Pasedena, CA, 1965.

Kats, D.M., Shestakov, V.M. 1992. Irrigation Hydrogeology, Moscow State University Publication.

Langbein, W.B. and S.A. Schumm, *Yield of sediment in relation to mean annual precipitation*, American Geophysical Union Transactions, 39, 1076-1084.

Lappala, E.G., R. W. Healy, and E.P. Weeks. 1987. Documentation of Computer Program VS2D to Solve the Equations of Fluid Flow in Variably Saturated Porous Media. Water-Resources Investigations Report 83-4099. Denver, CO.

Levitt, Daniel G. and Michael J. Sully. 1998a. Performance of Proposed Cover for Pit 3, Area 5 Radioactive Waste Management Site, Nevada Test Site. Bechtel Nevada, Las Vegas, NV.

Levitt, Daniel G. and Michael J. Sully. 1998b. Simulation of Soil Water Flow at Pit 5 at the Area 5 Radioactive Waste Management Site Using VS2DT. Bechtel Nevada, Las Vegas, NV.

Magnuson, S.O., S.J. Maheras, H.D. Nguyen, A.S. Rood, J.I. Sipos, M.J. Case, M.A. McKenzie-Carter, and M.E. Donahue. 1992. Radiological Performance Assessment for the Area 5 Radioactive Waste Management Site at the Nevada Test Site, Revision 1. Idaho National Engineering Laboratory, Idaho Falls, Idaho.

McGrath, Daniel A. 1987. Monitoring of Heat and Moisture at the Greater Confinement Disposal Test from January 1983 through October 1986 A Preliminary Analysis. Radioactive Waste Management Project, Environmental Sciences Department, Reynolds Electrical & Engineering Co., Inc. Las Vegas, NV.

Mualem, Y. 1976. A new model for predicting the hydraulic conductivity of unsaturated porous media. Water Resour. Res. 12:513-522.

O'Connor, G.E. and R.A. Clark. 1971. *Applications of Climatology and Meteorology to Hydrologic Simulation*, Technical Report No. 38, Texas Water Resources Institute.

Rachocki, A., *Alluvial Fans, an Attempt at an Empirical Approach*, John Wiley & Sons, Inc., New York, New York, 1981.

Rawlinson, S.E. 1999. Personal communication.

Reynolds Electrical & Engineering Co. Inc. (REECo). 1993a. Site Characterization and Monitoring Data From Area 5 Pilot Wells, Nevada Test Site, Nye County, Nevada. Las Vegas, NV.

Reynolds Electrical & Engineering Co. Inc. (REECo). 1993b. Hydrogeologic Data for Science Trench Boreholes at the Area 5 Radioactive Waste Management Site, Nevada Test Site, Nye County Nevada. Special Projects Section, Environmental Restoration & Technology Development Department, Environmental Management Division, Las Vegas, NV.

Reynolds Electrical & Engineering Co. (REECo). 1994. "Site Characterization and Monitoring Data from Area 5 Pilot Wells, Nevada Test Site, Nye County, Nevada," Prepared for the U.S. Department of Energy, Nevada Operations Office by REECo, Las Vegas, NV, DOE/NV/11432-74.

Reynolds Electrical & Engineering Co. (REECo), "Site Characterization and Monitoring Data from Area 5 Pilot Wells, Nevada Test Site, Nye County, Nevada," Prepared for the U.S. Department of Energy, Nevada Operations Office by REECo, Las Vegas, NV, DOE/NV/11432-74 (1994)

Richards, L.A. 1931. Capillary conduction of liquids through porous mediums. Physics, 1, pp. 318-333.

Roeske, R.H., *Methods for Estimating the Magnitude and Frequency of Floods in Arizona*, U.S. Geological Survey, Tucson, Arizona, September, 1978.

Ross, Wyn. C. and Stephen W. Wheatcraft. 1994. A Two-Dimensional Simulation of Tritium Transport in the Vadose Zone at the Nevada Test Site. Publication #45098, DOE/NV/10162-21.

Schmeltzer, J.S., J.J. Miller, and D.L. Gustafson, *Flood Assessment at the Area 5 Radioactive Waste Management Site and the Proposed Hazardous Waste Storage Unit DOE/Nevada Test Site, Nye County, Nevada*, Ratheon Services Nevada, Las Vegas, Nevada, January 1993.

Shott, G. J., L. E. Barker, S. E. Rawlinson, M. J. Sully, and B. A. Moore. 1998. "Performance Assessment for the Area 5 RWMS at the Nevada Test Site, Nye County Nevada (Rev 2.1)," prepared for the U.S. DOE,. Nevada Operations Office, DOE/NV/11718--176.

Smart, Peter, *Understanding Hydrology, A Comparison of Hydrologic Methods*, 1989, Applied Microcomputer Systems, Chocorua, NH

Snyder, K.E., D.L. Gusafson, H.E. Huckins-Gang, J.J. Miller, S.E. Rawlinson, Surficial *Geology and Performance Assessment for a Radioactive Waste Management Facility at the Nevada Test Site, Ratheon Services Nevada*, DOE, Nevada Operations Office, February, 1995.

Soil Conservation Service. 1972. SCS National Engineering Handbook, Section 4, U. S. Department of Agriculture.

Spaulding, W.G. "Vegetational and Climatic Development of the Mojave Desert: The Last Glacial Maximum to the Present," in: Packrat Middens: The Last 40,000 Years of Biotic Change, J.L. Betancourt, T.R. Van Devender and P.S. Martin, eds., University of Arizona Press, Tucson AZ, pp. 166–199 (1990)

Thomas, B.E., H.W. Hjalmarson, and S.D. Waltemeyer, Methods for Estimating Magnitude and Frequency of Floods in the Southwestern United States, U.S. Geological Survey Water Supply Paper 2433, Denver, CO, 1997.

Tuan, Yi-Fu, *Structure, climate and basin landforms in Arizona and New Mexico*, Annals of the Association of American Geographers, Vol. 52, 1962, pp. 51-68.

Tyler, S.W., J.B. Chapman, S. H. Conrad, D. P. Hammermeister, D.O. Blout, M.J. Miller, M.J. Sully, and J.M. Ginanni, "Soil-water flux in the southern Great Basin, United States: Temporal and spatial variations over the last 120,000 years," Water Resources Research, Vol. 32, No. 6, pp. 1481–1499 (1996)

Tyler, Scott W. 1987. Review of Soil Moisture Flux Studies at the Nevada Test Site, Nye County, Nevada. Publication #45058. Desert Research Institute, University of Nevada System, DOE/NV/10384-17.

U.S. Army Corps of Engineers, *HEC-HMS Hydrologic Modeling System - User's Manual Version 1.0*, Hydrologic Engineering Center, Davis California, March 1998.

U.S. Department of Commerce, National Oceanic and Atmospheric Administration, *Hydrometeorological Report NO. 49, Probable Maximum* Prec*ipitation Estimates, Colorado River and Great Basin Drainages*, Silver Spring, Maryland, 1977

U.S. Geological Survey, *PEAKFQ - flood frequency analysis based on Bulletin 17B Version 2.4*, April 4, 1998, http://water.usgs.gov/software/peakfq.html.

van Genuchten, M. Thn., F.J. Leij and S.R. Yates. 1991. The RETC Code for Quantifying the Hydraulic Functions of Unsaturated Soils. U.S. Salinity Laboratory, U.S. Department of Agriculture, Agricultural Research Service, Riverside, CA. EPA/600/2-91/065.

van Genuchten, Rein. 1978. Calculating the Unsaturated Hydraulic Conductivity with a New Closed-Form Analytical Model. Water Resources Program. Department of Civil Engineering. Princeton University, Princeton, NJ, 67-WR-08.

University of Idaho, State Climate Services for Idaho, Daily Reference-Crop Evapotransportation, http://snow.ag.uidaho.edu/Publications/pond_evap/Appendix_B.html, July, 1999.

Williams, D.F., R.C. Thunell, E. Tappa, D. Rio and I. Raffi, "Chronology of the Pleistocene Oxygen Isotope Record: 0 -1.88 my BP," Paleog., Palaeoc., and Palaeoe. 64:221–240 (1988)

Winograd, I.J., T.B. Coplen, J.M. Landwehr, A.C. Riggs, K.R. Ludwig, B.J. Szabi, P.T. Kolesar, and K.M. Revesz, "Continuous 500,000-year record from vein calcite in Devils Hole, Nevada," Science, v. 258, pp. 255– 260 (1992)

Winograd, I.J., B.J. Szabo, T.B. Coplen, and A.C. Riggs, "A 250,000-year climatic record from Great Basin vein calcite: Implications for Milankovitch Theory," Science, v. 242, pp. 1275–1280 (1988)

Yaron, B., Danfors, E., and Y. Vaadia. 1973. Arid zone irrigation, pringer-Verlag New York, Heidelberg, Berlin.

Yucel, V. 2000. Personal Communication.

Attachment A: Estimating Subsidence for GCD PA

This page intentionally left blank.

Sandia National Laboratories

Albuquerque, New Mexico 87185-1326

INFORMATION ONLY

date: July 16, 1996

to: T. Brown, 6414, MS 1345

from: Bill W. Arnold, 6851, MS1326

subject: Estimating Subsidence for GCD PA (memo/96/S34)

The purpose of this memo is to present a preliminary analysis of subsidence above the GCD boreholes for incorporation in performance assessment calculations. Subsidence has the potential to impact performance of GCD waste isolation in three primary ways. Subsidence of the land surface over the boreholes would shorten the pathway from the waste to the environment (either at the ground surface or at rooting depth). The depression above the borehole formed by subsidence could effect the pattern of surface runoff in such a way that infiltration is enhanced in the center of the depression. This enhancement to infiltration could alter the pattern of groundwater flow in the unsaturated zone above the waste and/or could provide increased soil moisture resulting in increased plant growth and possibly the growth of deeper rooting plant species in the surface depression.

Conceptual Model

The conceptual model of the subsidence process used in this analysis includes three mechanisms for the reduction of volume resulting in subsidence. The first mechanism is the degradation and collapse of waste containers. Many of the waste containers buried in the GCD boreholes have significant void space, which would collapse after the waste containers lose their structural integrity. The second mechanism is movement of the backfill material into voids created around and between the waste containers during filling of the boreholes. The third mechanism is compaction of the backfill material itself. This general conceptual model of borehole subsidence and the decision to model subsidence in the performance assessment base case rather than as an event in scenario development are documented in a memo of record (Cochran, 1995).

The surface expression of subsidence in the boreholes is conceptualized to be a cone shaped depression. An alternative conceptualization of the depression is a cyllindrical pit formed by piston-like subsidence in the borehole. If, however, we assume that the subsidence is a relatively slow process, it is unlikely that the borehole walls would retain their structural integrity. Also, operational plans call for eventually covering the borehole sites with additional material. Native alluvium in this cover material would tend to form a cone shaped depression. The possible effects of a cement cap over the entire surface are unclear, although it is unlikely that such a cap would remain intact during the subsidence process.

For these reasons, a cone shaped depression, defined by the angle of repose of the surface material, is used in the conceptual model.

Intra-Container Void Space

Estimates of the total volume of voids within waste containers are made for each of the filled GCD boreholes based on historical records summarized in Chu and Bernard (1991). These records vary in completeness. Also, a number of simplifying assumptions have been made to perform these analyses. The possibility of additional void space being created by the decay of contents within containers is not considered in this analysis. Plastic waste has the highest potential for degradation, but the quantities of plastic and rates of decay are too uncertain for incorporation into the analysis. The estimates of void space presented here should be viewed as approximations. These analyses are summarized in Table 1.

Table 1: Estimates of Intra-Container Void Volume

Borehole Number	Contents	Total Volume (m^3)	Total Weight (kg)	Complete Inventory of Waste	Intra-Container Void Volume (m^3)
1	boxes	38.60	10,864	yes	34.57
2	boxes	27.86	11,657	yes	23.55
3	boxes	5.44	2,322	yes	4.58
4	drums, boxes	53.71	?	no	48.34
5	drums, boxes	25.19	?	no	2.52
6	cyllinders	8.63	?	yes	7.76
7	drums	9.99	?	yes	8.31
10	drums, boxes	17.70	?	no	1.77
GCDT	drums	15.82	?	no	1.58

Boreholes 1, 2, and 3 contain a number of relatively large metal and plywood boxes that hold Nuclear Weapon Accident Residues (NWAR). The volumes and gross weights of each container are given in Chu and Bernard (1991). The waste material consists primarily of aluminum parts. By assuming that the containers and contents have an average density equal to that of aluminum, the total void volume is calculated. Note in Table 1 that the void space in the containers in these boreholes ranges from about 85% to 90% of the total container volume.

Borehole 4 contains 258 drums and 8 boxes containing classified waste consisting of metal, plastic, and graphite shapes. Based on the relatively loose packing of waste material calculated for containers in boreholes 1, 2, and 3, it is assumed that these containers also contain approximately 90% void space. Information is not available on the volumes of the

boxes and they are not included in the analysis. The relatively high total intra-container void volume calculated for borehole 4 is probably an overestimate due to the likely denser packing of waste shapes in drums than in the large boxes in boreholes 1, 2, and 3. An overestimate of this void volume is conservative from the perspective of performance assessment.

Most of the waste emplaced in boreholes 5, 10, and GCDT was solidified in cement and further packed in bituminous asphalt within the waste containers. Because of this, it is assumed that the fraction of void space within the containers is relatively small and is calculated as 10% of the total volume. Note that the total volume of waste does not include several boxes that were not described in the waste inventory.

Borehole 6 contains 164 long, cylindrical cannisters of reactor fuel element cladding materials. No information is available on the internal packing of material or gross weights of these cannisters, but it is assumed that material is relatively loosely packed in these cannisters. The void volume is assumed to be 90% of the total volume of the cannisters.

Borehole 7 contains 38 drums of classified metal and plastic shapes. It is assumed that these containers are relatively loosely packed with 90% void space. It should be noted that GCD boreholes 6 and 7 remain open and the analyses presented in this memo assume that no additional waste will be added to these boreholes and that they will be backfilled in a manner similar to the other, completed boreholes.

Extra-Container Void Space

The quantity of void space created around the waste containers during the backfill process is difficult to assess. Waste containers were not optimally placed, especially in the case of the NWAR boxes in boreholes 1, 2, and 3. Attempts were made to minimize the void space left in the boreholes during backfilling. The backfill was sifted through a 1 inch mesh sieve and emplaced near the bottom of the borehole using a stemming tube. However, the effectiveness of these methods in completely filling the space between and around containers was not evaluated.

The highest potential for incomplete backfilling probably exists in boreholes 1, 2, 3, and 6. The relatively large NWAR waste containers were apparently not emplaced in any regular geometry. This created the potential for shielding of cavities beneath the upper boxes during the backfilling process. The long, thin (4.3 m by .12 m) cyllindrical cannisters in borehole 6 were also potentially emplaced in an irregular configuration, which may have created void spaces during backfilling.

A range of total extra-container void space is calculated for each borehole based on a percentage of the total container volume. The range considered is from 0% to 30%. The 30% upper limit is somewhat arbitrary, but simple geometric considerations (e.g. for regularly placed drums or irregularly stacked boxes) seem to preclude void volumes greater than this. See Table 2 for the estimates of maximum extra-container void volume for each of the boreholes.

Backfill Compaction

Reduction of volume within the boreholes due to compaction of the backfill material is a process that may continue over a relatively long period of time. Analysis of the potential reduction in volume due to compaction is based on average measured density of the native alluvium and the assumption that the backfill material will eventually compact to the density of native alluvium. It is not clear how the fact that the backfill material was sieved during emplacement affects the validity of this assumption.

These calculations are based on density data taken from the GCDT borehole. The average bulk density of the native alluvium is 1.74 g/cm^3 (REECo, 1983). Bulk density in the backfill material, following compaction by a vibrator used during backfilling, is 1.5 to 1.6 g/cm^3 (Hunter et al., 1982). It should be noted that the bulk density of 1.5 to 1.6 g/cm^3 for the backfill material is quoted as a recommendation for construction of the boreholes and has not been confirmed by measurements in the other GCD boreholes. The range of potential compaction from these values of bulk density is 8.0% to 13.8%. This range is used to estimate the minimum and maximum soil compaction volume shown in Table 2, based on the volume of backfill in each borehole. It should be noted that the effect of the probertite placed in boreholes 1, 2, and 3 is not considered in this analysis

Total Compaction and Subsidence

The minimum and maximum total compaction volume for each of the boreholes is calculated by summing the components of intra-container void space, extra-container void space, and soil compaction. These results are shown in Table 2. The largest maximum total compaction is estimated for boreholes 1 and 4. Calculations indicating the smallest minimum total compaction volume are for boreholes 5 and 10. The greatest contributions to total compaction from intra-container void space occur for boreholes 1, 2, and 4.

The rate and timing of the compaction processes considered in this analysis are very uncertain. The rate of reduction of extra-container and intra-container void space will depend primarily upon chemical degradation of the containers followed by structural collapse of the containers. Corrosion of steel containers will be enhanced by soil gas compositions of near 100% relative humidity. For some of the larger containers, such as the boxes in boreholes 1, 2, and 3, collapse of the containers could occur catastrophically, but it is not clear how quickly this event would propogate to the ground surface. Compaction of the backfill will probably occur at a steady, gradual rate, but could be enhanced by seismic activity. The simplest, most conservative approach for performance assessment calculations would be to assume that total compaction and subsidence occurs immediately after closure of the facility.

The total compaction volume is converted to subsidence depth by assuming that the surface depression is an inverted cone. The relationship between the volume of the depression and the maximum depth is given by:

$$V = \frac{1}{3} d \pi \left(\frac{d}{\tan\theta} \right)^2$$

where V is the volume of the cone, d is the maximum depth, and θ is the dip angle of the slope of the conical depression. Note the cubic relationship between depth and volume; this implies relatively smaller increases in depth with increasing compaction volume. For these calculations the slope angle is assumed to be 35^{o}. The angle of repose for talus is 30^{o} to 35^{o} (Compton, 1977).

Minimum and Maximum range of values of subsidence depth are given in Table 2. The smallest minimum value is 2.04 m for borehole 10 and the largest maximum value is 3.53 m for boreholes 1 and 4. The range of corresponding subsidence depression diameters is 5.83 m to 10.08 m.

It is possible that overlapping of conical depressions from closely spaced boreholes will occur. This overlap of subsidence depressions would tend to deepen the individual depressions somewhat and could lead to coalescence of deeper-rooting plant species clusters. Analysis of the proximity of boreholes shows that only three borehole pairs are within 10 m of each other (boreholes 9-10, 7-8, and 4-7). Boreholes 8 and 9 remain empty and their interactions with boreholes 7 and 10 cannot be evaluated. The centers of boreholes 4 and 7 are 7.77 m apart, leading to an overlap of 1.27 m if the maximum subsidence is assumed for both boreholes. This overlap of subsidence depressions would lead to the deepening of the depressions by only a few percent.

Performance Assessment

Based on this range of estimates for surface subsidence in the GCD boreholes and the relative uncertainties in the analysis I recommend that subsidence be modeled in performance assessment calculations using a uniform distribution from 2.0 to 4.0 m for all boreholes. This distribution of subsidence values can be included as a reduction of the travel distance to the accessible environment in a straightforward manner. The effects of subsidence on focusing of infiltration and on plant species and plant growth density will be addressed in further work.

Alternatively, each borehole can be assigned a possible range of subsidence based on the calculations shown in Table 2. Another possibility is to consider the TRU waste in boreholes 1-4 separately from the other boreholes (TRU + nonTRU), assigning a range of subsidence of 2.0 to 4.0 m for boreholes 1-4 and a range of 2.0 to 3.0 m to the other boreholes.

References

Chu, Margaret S.Y. and Emile A. Bernard, 1991. *Waste Inventory and Preliminary Source Term Model for the Greater Confinement Disposal Site at the Nevada Test Site.* SAND91-0170. Albuquerque, NM. Sandia National Laboratories.

Cochran, John, 1995. *Documentation of Significant Decision Concerning Borehole Subsidence Based on Meeting of 2/2/95.* Memo of Record memo/95/S33 & S34.

Compton, Robert R., 1977. *Interpreting the Earth.* New York. Harcourt Brace Jovanovich, Inc. 554 p.

Hunter, Preston H., Darrel Card, and Richard B. White, 1982. *Assembly and Installation Procedures, Downhole Instrumentation for a Test of Greater Confinement Disposal of Radioactive Waste at the Nevada Test Site.* DOE/NV/10253-4. Salt Lake City, Utah. Ford, Bacon & Davis Utah, Inc.

REECo, 1983. *Greater Confinement Disposal Test at the Nevada Test Site.* DOE/NV/00410-79. Las Vegas, NV. Reynolds Electric & Engineering Co., Inc.

cc:

MS 1345	6414	J. Cochran
MS 1345	6414	S. H. Conrad
MS 1345	6414	D. P. Gallegos
MS 1326	6851	H. A. Dockery
MS 1345		GCD Records

File: subsidence.memo.doc

Attachment B: PMP Computation Sheets

This page intentionally left blank.

The PMP computation sheets (one for each watershed) are based on the Computation sheets provided in Hydrometeorological Report NO. 49, Probable Maximum Precipitation Estimates, Colorado River and Great Basin Drainages (1977). Table 6.2 is for general storm PMP computation. Table 6.2A is for local storm PMP computation. All references to figures and tables in these computation sheets are to figures and tables in Hydrometeorological Report NO. 49.

Table 6.2A*. -- Local PMP computation, Colorado River, Great Basin and California Drainages. For drainage average depth PMP. Go to table 6.3B if areal variation is required.

Drainage: **HP1a,b** Area: 1.8 mi^2
Latitude: 36° 54' Longitude: 115° 57' mi^2

Steps correspond to those in sec. 6.3A.

1. Average 1-hour 1-mi^2 PMP for drainage (fig. 4.5). 10.3 in.

2. a. Reduction for elevation. (No adjustment for elevations up to 5,000 feet; 5% decrease per 1,000 feet above 5,000 feet.) 100 %

2. b. multiply 1 x 2a. 10.3

3. Average 6/1-hr ratio for drainage (fig 4.7). 1.35

	Duration (hours)									
	1/4	1/2	3/4	1	2	3	4	5	6	
4. Durational variation for 6/1-hr ratio of step 3 (table 4.4).	68	86	94	100	116	123	129	133	135	%
5. 1-mi2 PMP for indicated durations (2b x 4)	7.00	8.86	9.68	10.30	11.95	12.67	13.29	13.70	13.91	in.
6. Areal Reduction (Fig. 4.9)	95.5	96.4	97.4	98	98.9	99.8	100	100	100	%
Areal Reduced PMP (5 x 6)	6.69	8.54	9.43	10.09	11.82	12.64	13.29	13.70	13.91	in.

Table 6.2A*. -- Local PMP computation, Colorado River, Great Basin and California Drainages. For drainage average depth PMP. Go to table 6.3B if areal variation is required.

Drainage: **HP2** Area: 1.2 mi^2
Latitude: 36° 54' Longitude: 115° 57' mi^2

Steps correspond to those in sec. 6.3A.

1. Average 1-hour 1-mi^2 PMP for drainage (fig. 4.5). 10.3 in.

2. a. Reduction for elevation. (No adjustment for elevations up to 5,000 feet; 5% decrease per 1,000 feet above 5,000 feet.) 100 %

2. b. multiply 1 x 2a. 10.3

3. Average 6/1-hr ratio for drainage (fig 4.7). 1.35

	Duration (hours)									
	1/4	1/2	3/4	1	2	3	4	5	6	
4. Durational variation for 6/1-hr ratio of step 3 (table 4.4).	68	86	94	100	116	123	129	133	135	%
5. 1-mi2 PMP for indicated durations (2b x 4)	7.00	8.86	9.68	10.30	11.95	12.67	13.29	13.70	13.91	in.
6. Areal Reduction (Fig. 4.9)	98	99	100	100	100	100	100	100	100	%
Areal Reduced PMP (5 x 6)	6.86	8.77	9.68	10.30	11.95	12.67	13.29	13.70	13.91	in.

Table 6.2A*. -- Local PMP computation, Colorado River, Great Basin and California Drainages. For drainage average depth PMP. Go to table 6.3B if areal variation is required.

Drainage: **HP3** Area: 1.7 mi^2
Latitude: 36° 54' Longitude: 115° 57' mi^2

Steps correspond to those in sec. 6.3A.

1. Average 1-hour 1-mi^2 PMP for drainage (fig. 4.5). 10.3 in.

2. a. Reduction for elevation. (No adjustment for elevations up to 5,000 feet; 5% decrease per 1,000 feet above 5,000 feet.) 100 %

2. b. multiply 1 x 2a. 10.3

3. Average 6/1-hr ratio for drainage (fig 4.7). 1.35

	Duration (hours)									
	1/4	1/2	3/4	1	2	3	4	5	6	
4. Durational variation for 6/1-hr ratio of step 3 (table 4.4).	68	86	94	100	116	123	129	133	135	%
5. 1-mi2 PMP for indicated durations (2b x 4)	7.00	8.86	9.68	10.30	11.95	12.67	13.29	13.70	13.91	in.
6. Areal Reduction (Fig. 4.9)	96.2	97.2	97.9	98.6	99.3	100	100	100	100	%
Areal Reduced PMP (5 x 6)	6.74	8.61	9.48	10.16	11.86	12.67	13.29	13.70	13.91	in.

Table 6.2A*. -- Local PMP computation, Colorado River, Great Basin and California Drainages. For drainage average depth PMP. Go to table 6.3B if areal variation is required.

Drainage: **HP4** Area: 3.3 mi^2
Latitude: 36° 54' Longitude: 115° 57' mi^2

Steps correspond to those in sec. 6.3A.

1. Average 1-hour 1-mi^2 PMP for drainage (fig. 4.5). 10.3 in.

2. a. Reduction for elevation. (No adjustment for elevations up to 5,000 feet; 5% decrease per 1,000 feet above 5,000 feet.) 100 %

2. b. multiply 1 x 2a. 10.3

3. Average 6/1-hr ratio for drainage (fig 4.7). 1.35

	Duration (hours)									
	1/4	1/2	3/4	1	2	3	4	5	6	
4. Durational variation for 6/1-hr ratio of step 3 (table 4.4).	68	86	94	100	116	123	129	133	135	%
5. 1-mi2 PMP for indicated durations (2b x 4)	7.00	8.86	9.68	10.30	11.95	12.67	13.29	13.70	13.91	in.
6. Areal Reduction (Fig. 4.9)	89	91	92.4	93.1	94.5	94.8	95.2	95.5	95.7	%
Areal Reduced PMP (5 x 6)	6.23	8.06	8.95	9.59	11.29	12.01	12.65	13.08	13.31	in.

Table 6.2A*. -- Local PMP computation, Colorado River, Great Basin and California Drainages. For drainage average depth PMP. Go to table 6.3B if areal variation is required.

Drainage: **HP5,6,FA,FB** Area: 5.3 mi^2
Latitude: 36° 54' Longitude: 115° 57' mi^2

Steps correspond to those in sec. 6.3A.

1. Average 1-hour 1-mi^2 PMP for drainage (fig. 4.5). 10.3 in.

2. a. Reduction for elevation. (No adjustment for elevations up to 5,000 feet; 5% decrease per 1,000 feet above 5,000 feet.) 100 %

2. b. multiply 1 x 2a. 10.3

3. Average 6/1-hr ratio for drainage (fig 4.7). 1.35

	Duration (hours)									
	1/4	1/2	3/4	1	2	3	4	5	6	
4. Durational variation for 6/1-hr ratio of step 3 (table 4.4).	68	86	94	100	116	123	129	133	135	%
5. 1-mi2 PMP for indicated durations (2b x 4)	7.00	8.86	9.68	10.30	11.95	12.67	13.29	13.70	13.91	in.
6. Areal Reduction (Fig. 4.9)	83	86.5	88	89	90.8	91.4	92.2	92.8	93.5	%
Areal Reduced PMP (5 x 6)	5.81	7.66	8.52	9.17	10.85	11.58	12.25	12.71	13.00	in.

Table 6.2A*. -- Local PMP computation, Colorado River, Great Basin and California Drainages. For drainage average depth PMP. Go to table 6.3B if areal variation is required.

Drainage: **MM2** Area: 1.4 mi^2
Latitude: 36° 54' Longitude: 115° 57' mi^2

Steps correspond to those in sec. 6.3A.

1. Average 1-hour 1-mi^2 PMP for drainage (fig. 4.5). 10.3 in.

2. a. Reduction for elevation. (No adjustment for elevations up to 5,000 feet; 5% decrease per 1,000 feet above 5,000 feet.) 100 %

2. b. multiply 1 x 2a. 10.3

3. Average 6/1-hr ratio for drainage (fig 4.7). 1.35

	Duration (hours)									
	1/4	1/2	3/4	1	2	3	4	5	6	
4. Durational variation for 6/1-hr ratio of step 3 (table 4.4).	68	86	94	100	116	123	129	133	135	%
5. 1-mi2 PMP for indicated durations (2b x 4)	7.00	8.86	9.68	10.30	11.95	12.67	13.29	13.70	13.91	in.
6. Areal Reduction (Fig. 4.9)	97	98.2	98.8	99.2	100	100	100	100	100	%
Areal Reduced PMP (5 x 6)	6.79	8.70	9.57	10.22	11.95	12.67	13.29	13.70	13.91	in.

Table 6.1*. -- General Storm PMP computation, Colorado River and Great Basin.

Drainage: **RWMS** Area: 8.6 mi^2
Latitude: 36° 54' Longitude: 115° 57' mi^2

Month: September

Step		Duration (hours)						
		6	12	18	24	48	72	
A. Convergence PMP								
1. Drainage average value from one of figures 2.5 to 2.16	10.8 in.							
2. Reduction for barrier elevation. (Fig 2.18)	60 %							
3. Barrier-elevation reduced PMP (1 x 2)	6.48 in.							
4. Durational variation (figs. 2.25 to 2.27 and table 2.7)		68	85	94	100	115	122	%
5. Convergence PMP for indicated durations (3 x 4)		4.41	5.51	6.09	6.48	7.45	7.91	in.
6. Incremental 10 mi^2 PMP (successive subtraction in step 5)		4.41	1.10	0.58	0.39	0.97	0.45	in.
7. Areal reduction (select from figs 2.28 and 2.29)		100	100	100	100	100	100	%
8. Areally reduced PMP (6 x 7)		4.41	1.10	0.58	0.39	0.97	0.45	in.
9. Drainage average PMP (accumulated values of step 8)		4.41	5.51	6.09	6.48	7.45	7.91	in.
B. Orographic PMP								
1. Drainage average orographic index from figure 3.11a to d.			2.8	in.				
2. Areal reduction (figure 3.2)			100	%				
3. Adustment for month (one of figures 3.12 to 3.17)			100	%				
4. Areally and seasonally adjusted PMP (steps 1 x 2 x 3)			2.8	in.				
5. Durational variation (table 3.17)		32	59	81	100	152	177	%
6. Orographic PMP for given durations (4 x 5)		0.90	1.65	2.27	2.80	4.26	4.96	in.
C. Total PMP (Add steps A9 and B6)		5.30	7.16	8.36	9.28	11.71	12.86	in.

This page intentionally left blank.

Attachment C: Infiltration Model to Verify Storm Cutoff

This page intentionally left blank.

Purpose

An infiltration flow model was constructed to investigate the depth of infiltration and the residence time of the infiltrating water in the vadose zone at the Area 5 RWMS after a storm of 4 cm occurring within one day. The result of this modeling exercise is used in conjunction with observed infiltration data at the Area 5 RWMS to identify a rain intensity level below which it will be assumed that runoff from the watershed areas into the subsided trench does not need to be included in the subsidence and flooding analysis.

Conceptual Model

A rain storm of 4 cm infiltrates during one day into a vertical one-dimensional column that represents the alluvium. Prior to the infiltration event, an equilibrium condition exists in the vertical column in which the distribution of moisture is such that no upward or downward flow is occurring. The lower boundary of the column is the water table below the Area 5 RWMS at a depth of approximately 236 m. The top of the column is a flux boundary that first receives recharge with bare-soil evaporation during the rain event. After the event, evapotranspiration is initiated. The water infiltration is simulated under transient conditions over a several month period.

Numerical Model

The VS2DT computer code was used to construct a vertically oriented one-dimensional finite-difference grid to represent the column of alluvium. The van Genuchten unsaturated conductivity model was chosen as the function representing the relationship between water content, suction pressure, and unsaturated hydraulic conductivity in the vadose zone. Evaporation and transpiration functions in VS2DT were used to simulate these processes over time within the uppermost cells of the grid. The code simulated infiltration of water into the unsaturated soil column by finite difference approximation of the transient Richards equation of unsaturated single-phase water flow.

Equilibrium conditions were established initially in the column through an option in the VS2DT code. Simulation of evaporation and transpiration used averaged parameter values based on the plant uptake studies and site-specific hydrology data collected for the compliance assessment.

Results

The change in moisture content over time near the land surface was the most significant aspect of the model results with respect to the purpose of this modeling exercise (see Figure 1). The change in moisture content was dramatic in the near surface, but did not extend beyond a depth of approximately 0.4 m during the entire simulation. At the end of the first day, at which time the storm was terminated, the average water content ranged from 29% near the land surface to 7.4% (about equivalent to equilibrium conditions) at 0.6 m. By 20 days, water content above 3 m had dropped to 7.9%, within about 7% of the initial (equilibrium) conditions. At two months, water contents below 0.4 meters have returned to equilibrium conditions, while the zone from 0.4 meters to the land surface was within 1.6% of original conditions. By four months water contents essentially returned to equilibrium conditions.

Conclusions

Based on the results of the numerical model, a 4 cm rainfall occurring within a one day period will not result in deep infiltration in the vadose zone at the Area 5 RWMS, and only contributes water to the near-surface vadose zone for a period of between one day and two months before transpiration and evaporation removes the added water from the vadose zone.

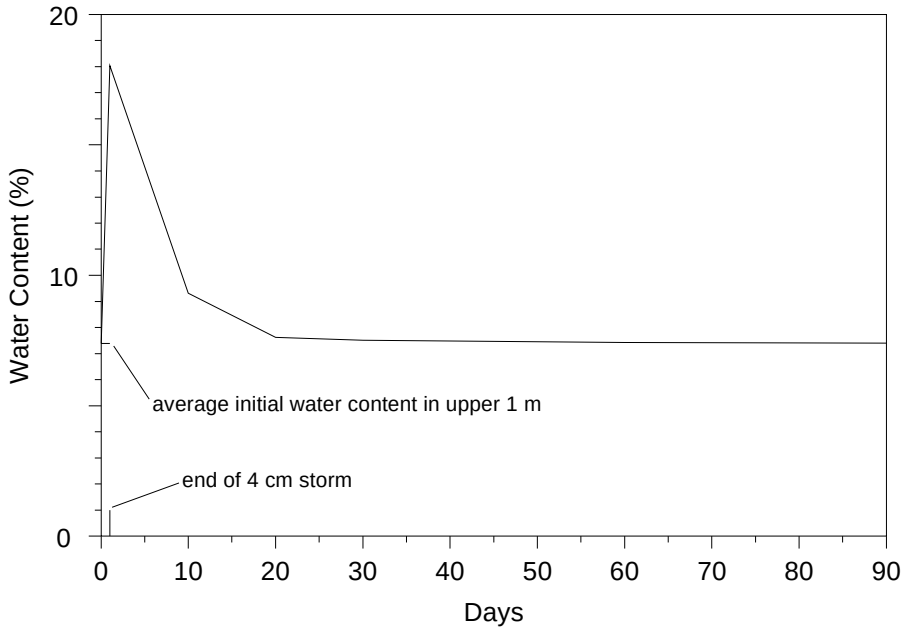

Figure 1. Average Water Content in Upper 1 Meter.

Appendix C

Supplemental Geological Information
[Modified from Bechtel Nevada, 1998]

This page intentionally left blank

General Stratigraphy Beneath the NTS

The stratigraphy beneath the NTS can be broadly classified, based on a hydrologic framework, into eight primary units with associated lithologic character as diagramed in Figure C-1 [Winograd and Thordarson, 1975]. Figure C-1 is a highly idealized conceptual perspective of a very complex region. Because of erosion and structural deformation, the complete stratigraphic section does not exist everywhere within the NTS, as seen on a surficial geological map of the area.

The stratigraphic units were deposited over long periods of geologic time under varying depositional environments. The lithologies range from older sedimentary rocks overlain by younger volcanic deposits of ash-fall and ash-flow tuff, and minor basalts. The topmost unit on which the Area 5 RWMS is located consists of unconsolidated valley fill alluvium. These units are described below from bottom to top, oldest to youngest.

Lower Clastic Rocks [modified from Bechtel Nevada, 1998]

The lowermost strata, which rests on Precambrian crystalline basement rock, are Precambrian sedimentary deposits. These deposits represent some of the first sediment deposited in the Cordilleran miogeosyncline, a gently subsiding, marine, depositional basin that was located off the western edge of North America. The Cordilleran miogeosyncline was a depositional basin from the Precambrian through Devonian period. The earliest deposits in the Cordilleran miogeosyncline were predominantly sandstones, siltstones, and shales derived from sediment eroded from the craton. These deposits have been classified into four formations [Burchfiel, 1964]: the Zabriskie Quartzite, Wood Canyon Formation, Stirling Quartzite, and the Johnnie Formation. The lower half of the Carrara Formation is also commonly included in the lower clastic rocks. These units are predominantly composed of quartzite and shale-siltstone layers, with a total thickness estimated at over 3,000 m (9,840 ft).

The clastic rock units are highly fractured, although fractures are commonly completely sealed by quartz and calcite. The only major outcrop in the NTS region is on the northeast side of the Halfpint Range [Frizzell and Shulters, 1990]. Elsewhere within the NTS, the unit is believed to be buried deep beneath overlying units of Paleozoic limestone and Tertiary volcanic rocks.

Lower Carbonate Rocks

The lower clastic rocks are directly overlain by a succession of carbonate rocks. These carbonate rocks consist of limestone and dolomite deposited when clastic deposition originating from the craton decreased, providing a clear, calm-water environment suitable for carbonate-producing organisms. Occasional influxes of sediment from the craton are recorded as minor sandstone, siltstone, and shale deposits interbedded with the carbonate rocks. This lower carbonate succession contains the Carrara Formation, Bonanza King Formation, Nopah Formation, Pogonip Formation, Eureka Quartzite, Ely Springs Dolomite, Laketown Dolomite, Sevy Dolomite, Simonson Dolomite, and the Guilmetted Formation. The Carrara Formation at the base of this succession contains sandstone and siltstone which are considered transitional with the underlying

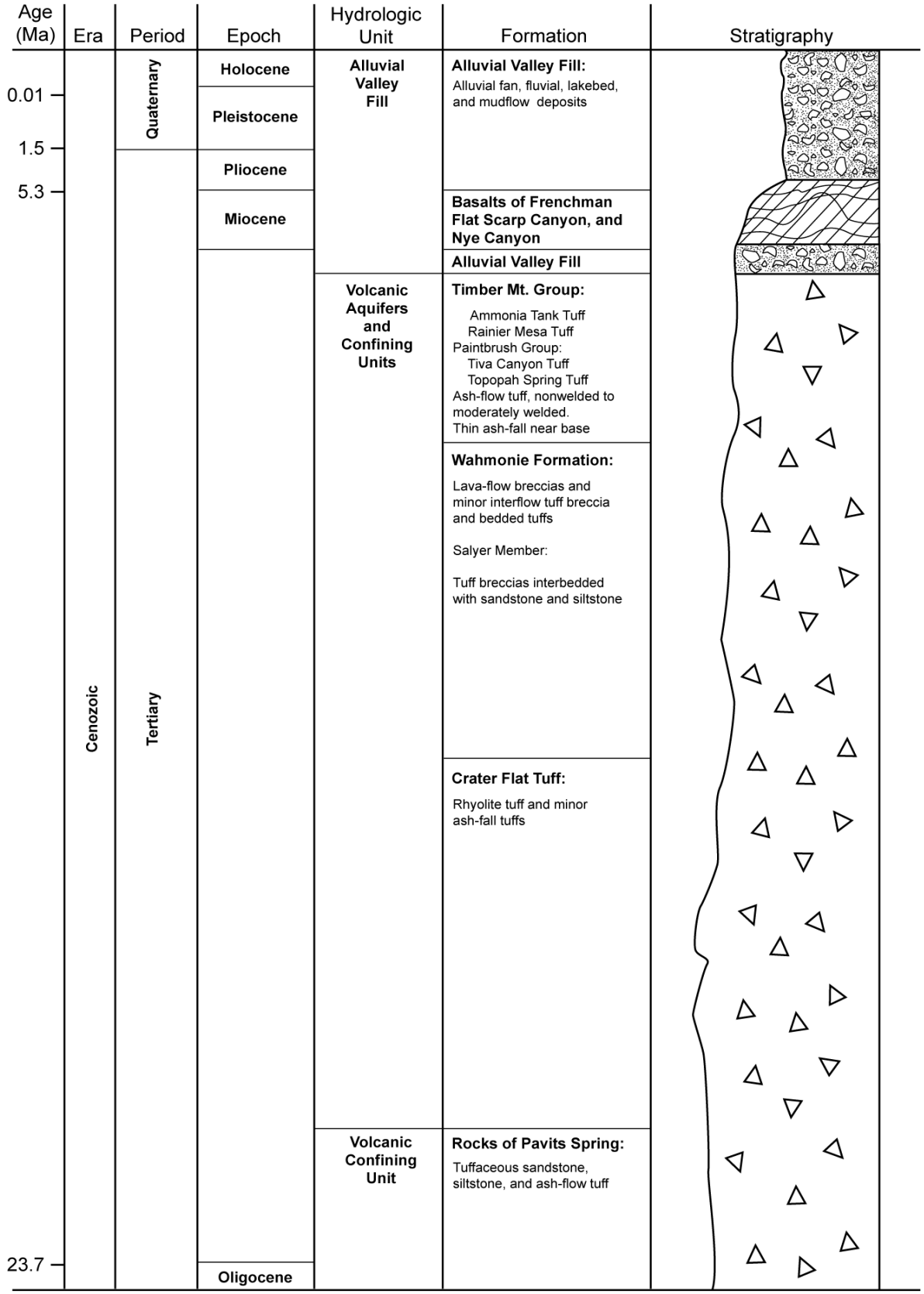

Figure C-1. General Stratigraphy and Time Sequence at the NTS [Bechtel Nevada, 1998].

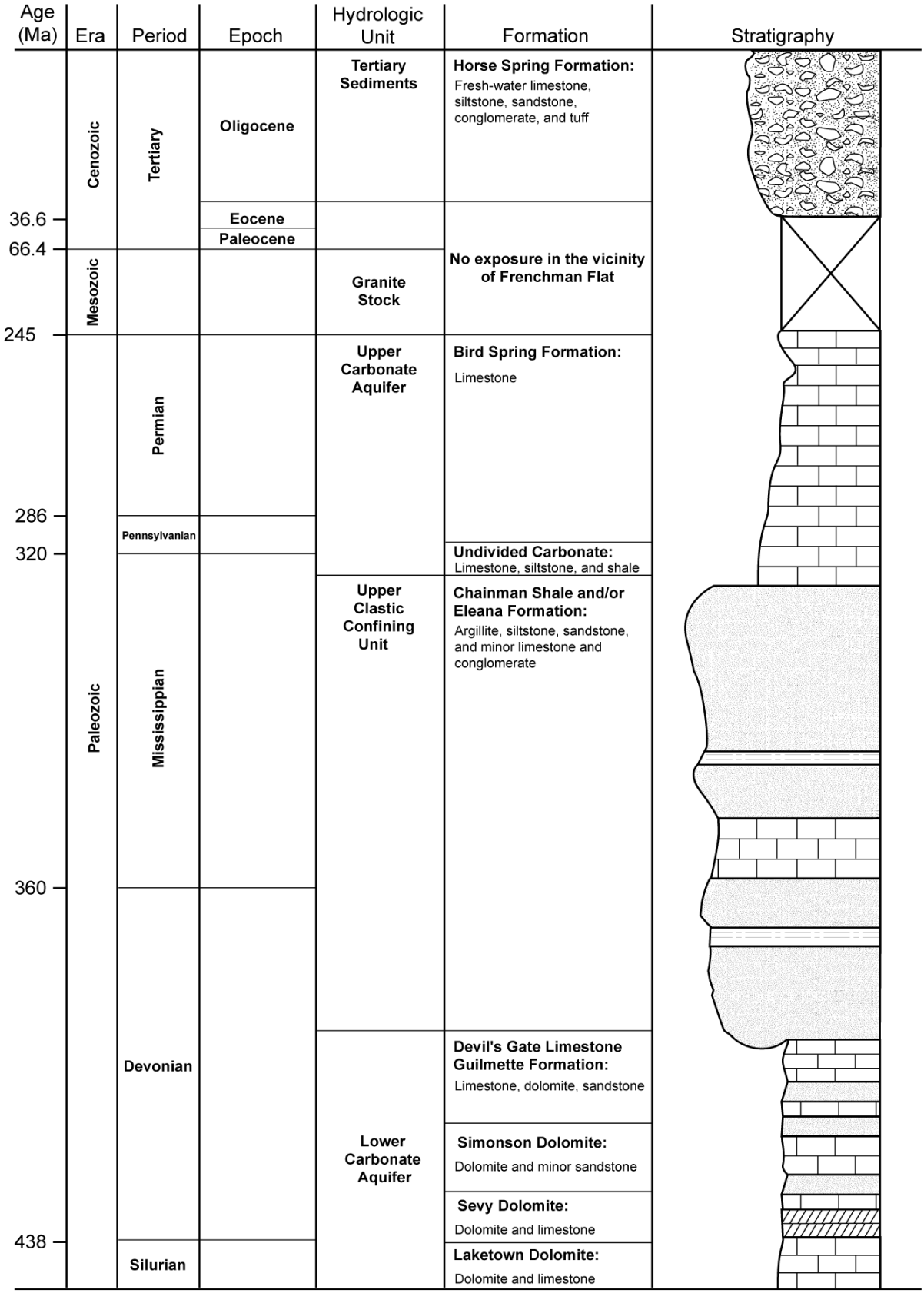

Figure C-1. General Stratigraphy and Time Sequence at the NTS (continued).

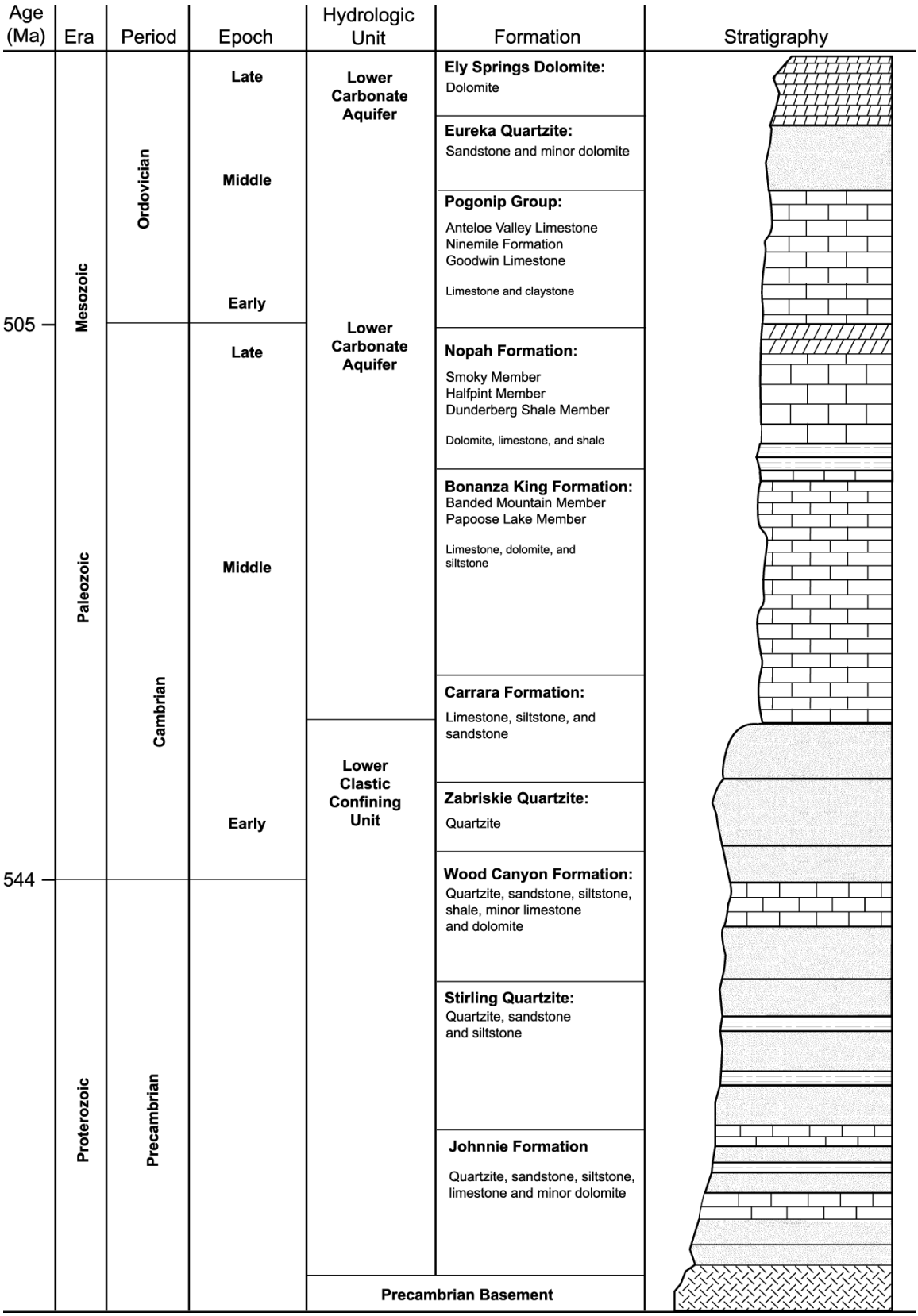

Figure C-1. General Stratigraphy and Time Sequence at the NTS (continued).

lower clastic rocks. These thick carbonate units are collectively more than 4,570 m (14,990 ft) thick.

The carbonates are highly fractured and locally brecciated near fault traces. Most outcrops exhibit three or more sets of joints and high-angle fractures [Winograd and Thordarson, 1975]. According to core logs, the fracture fill consists of breccia and clay gouge, calcite, and dolomite. Although clay gouge fill provides strong evidence for the existence of fault planes, the most common fill materials are calcite and dolomite, followed by quartz and iron-manganese oxides.

Upper Clastic Rocks

During the late Devonian Period (360 Ma), an island arc collided into the North American craton. The resulting Antler Orogeny resulted in uplift and deformation of the deposits of the Cordilleran miogeosyncline. Evidence of the collision is seen in the Roberts Mountains in central Nevada, where deep marine facies were thrust as far as 160 km (100 mi) over thinner platform deposits. The Antler Orogeny initiated a long period of alternating depositional environments. Influx of immature clastic sediments, due to turbidity and debris flows shed off the craton during periods of uplift during the Mississippian Period (330 Ma), probably formed the Eleana and Chainman Shale Formations. The Eleana Formation consists of a thick section of fine-grained sandstone to quartz-pebble conglomerate and comprises the upper clastic rocks unit, whereas the Chainman Shale is primarily finer grained shale. Near Yucca Flat, the unit is upwards of 1,210 m (4,000 ft) thick; however, outcrops are limited in the vicinity of Frenchman Flat to CP Basin.

Upper Carbonate Rocks

During the late Mississippian to Permian Period (330 to 240 Ma), when the basin experienced more stable, shallow-marine conditions, the 1,300-m (4,265-ft)-thick upper carbonate unit was deposited. This unit is composed of the limestones of an undivided carbonate rock succession and the Bird Spring Formation. These units are typically thin bedded and fossiliferous. During the Mesozoic Era, this unit, along with the underlying upper clastic rocks, was eroded from most of the NTS. Although study of the unit has been limited, visual inspection reveals that it has a similar fracture pattern and joint fill to the lower carbonate units [Winograd and Thordarson, 1975].

Granitic Stocks

The Mesozoic and early Cenozoic periods were dominated by granitic intrusions and thrust faulting. In the vicinity of Frenchman Flat, no intrusive bodies are present. The only significant occurrence of intrusive bodies on the NTS is in the extreme northern and northwestern portions of Yucca Flat. Here, coarse porphyritic monzonite-granite and quartz-monzonite magmas were extruded into limestone of the Pogonip group [Frizzell and Shulters, 1990].

During the Nevadan Orogeny, granitic intrusions were emplaced throughout the western United States. During the slightly younger Sevier Orogeny, the great compressional strain in the crust, caused by the subduction of the Pacific plate, thrust older Paleozoic strata over younger strata. Better-known thrust faults from this event are the Lee Canyon, Wheeler, and Keystone thrusts.

These strike roughly north and northeast along the Spring Mountains, 55 to 95 km (34 to 60 mi) to the southeast of the NTS [Fleck, 1970; Burchfiel, 1974]. Sedimentation was sparse throughout the area during this time, as shown by the unconformity on the stratigraphic column (Figure C-1) where rocks of Mesozoic and Early Cenozoic age should exist. This suggests that either very little strata were initially deposited during the Mesozoic or Early Cenozoic, or that these units eroded after deposition.

Ash-Flow and Ash-Fall Tuffs

Significant deposition of ash-fall and ash-flow tuff began during the Oligocene Epoch. This phase included silicic volcanism and associated deep crustal extension, producing both rotated and tilted block features and strike slip faulting. Volcanic activity climaxed approximately 11 Ma ago with the eruption of pyroclastic sheets in localized areas of the NTS [Christiansen et al., 1977; Byers et al., 1976]. Between nine and fourteen Ma, extensive caldera complexes formed, producing (in order of decreasing abundance) ash-flow tuff, ash-fall tuff, and rhyolite lavas. During eruptive hiatuses, minor erosion and sedimentation produced minor beds of conglomerate, tuffaceous sandstone, and freshwater limestone. The total thicknesses of the volcanic units vary, with thicker deposits generally located closer to the volcanic center. At the NTS, well over half of the exposed rock in the major mountain ridges contain some form of tuff or tuffaceous sediment, and the tuff often lies buried deep beneath valley fill alluvium [Frizzell and Shulters, 1990]. In Frenchman Flat, the total thickness of tuff may be more than 1,060 m (3,500 ft).

Typically, the ash-fall tuff units (bedded tuff) underlie the ash-flow units (welded tuff). Ash-fall tuff results from relatively prolonged periods of volcanic activity when variable thicknesses of tuff are emplaced near eruptive centers via precipitation from heavily laden ash clouds. The resulting units are generally fine-grained, well-sorted, and highly stratified.

Their mode of emplacement precludes welding often experienced upon cooling, creating highly porous and friable rocks. Accordingly, they do not exhibit a high degree of jointing and are often highly altered to zeolites and clay minerals.

Ash-flow tuffs, however, are consolidated rock formed by catastrophic explosions of hot pyroclastic material (volcanic ash and gases). The resulting deposits exhibit neither bedding nor sorting and could have taken years to cool after emplacement. During cooling, they experience much compaction and internal welding of particles. The degree of welding is generally greater in the center of the unit, resulting in a dense zone of little porosity sandwiched between zones of partial welding. Subsequent cooling of these units produces marked jointing and foliation patterns [Ross and Smith, 1961; Smith, 1960]. Such distinctions are important because the structure and mode of emplacement between ash-flow and ash-fall tuffs plays a considerable role in determining the difference between the two in water-bearing and transmission capabilities.

Basalts

Although the Miocene was dominated by silicic volcanism (i.e., ash-fall and ash-flow tuffs), minor basalt flows occurred in Frenchman Flat. The only basalts exposed at the land surface

near the RWMS are Miocene in age. These basalts include the Basalt of Nye Canyon [Crowe, 1990], dated at about 7.31 Ma; and the Basalt of Scarp Canyon, dated at about 8.7 Ma [Raytheon Services Nevada, 1994]. The Basalt of Frenchman Flat, dated at about 8.6 Ma, was encountered at about 290 m (950 ft) below the surface in drillholes UE-5i and UE-5k.

The transition from predominantly silicic volcanism to basaltic volcanism occurred approximately 10 Ma [Christiansen and Lipman, 1972]. Since 7.3 Ma, only scattered, short- duration volcanic activity occurred in Nevada. The volcanic rocks are primarily basaltic cinder cones and lava flows [Sawyer et al., 1990; Stewart, 1980]. All the lavas were most prevalent near their respective eruptive centers such as the Timber Mountain Caldera to the northwest of the RWMS and the Wahmonie-Salyer Center to the immediate west, near Skull Mountain. The lava flows are localized in extent; however, they can be of significant thickness close to their origin. Their primary hydrologic importance is restricted to the vicinity of east-central Jackass Flats. Because these flows are not in the immediate vicinity of Frenchman Flat, they are not included in the stratigraphic column.

Alluvial Valley Fill Sediments

The most recent deposits in the region are those that fill the valleys and basins due to faulting and erosion of the surrounding mountain ranges. They consist of typical alluvial fan and playa deposits, and are generally poorly sorted and stratified. The alluvial fan deposits are primarily composed of subangular pebbles and cobbles of tuff, carbonate, and sandstone in a sand and silt matrix [Raytheon Services Nevada, 1991]. Alluvial fan deposits contain evidence of several depositional subenvironments. The most common subenvironments are streamflow, sheetflow, and debris flow deposits. The alluvial fan itself is divided into the upper fan, the midfan, and the distal fan. The upper fan is dominated by coarse-grained streamflow and debris flow deposits. The midfan acts as a transition zone, with finer-grained debris flow and streamflow deposits and an increase in sheetflow deposits. The distal fan is dominated by sheetflow deposits and only minor streamflow deposits. The distal fan may be transitional to the playa deposits in the lowest point of the basin. Some accumulation of calcium carbonate has been observed in the B and BC soil horizons as coatings on clasts and pebbles from soil trenches in Frenchman Flat. Minor, discontinuous calcrete layers have also been identified in the near surface alluvium, suggesting past periods of stability on the fan surface. Because of their discontinuity, however, they are not believed to have a significant effect on groundwater flow within the basin. The alluvium, very thick in most valleys within the NTS, is estimated to be at least 500 to 600 m (1,640 to 1,968 ft) beneath central Yucca Flat and Frenchman Flat, and about 320 m (1,050 ft) beneath central Jackass Flats.

SEISMOLOGICAL RISK ANALYSIS

Intensities of Historical Earthquakes

Although the western margin of the NTS lies within an area believed to have a high risk for potential seismicity, activity has historically been low to moderate. The most recent earthquake of significance was of magnitude 5.6, occurring on June 29, 1992. Its epicenter was approximately 15 km (9 mi) to the southwest of the Area 5 RWMS near Skull Mountain, at a depth of

10 km (6 mi). The Area 5 RWMS was unaffected. In August 1971, an earthquake of magnitude 4.3 occurred along the Cane Spring Fault zone, approximately 7.2 km (4.5 mi) northwest of the RWMS. An earthquake of 4.5 magnitude occurred in February 1973 along the Rock Valley Fault system, approximately 7.2 km (4.5 mi) southwest of the RWMS. No surface displacement was associated with these two earthquakes.

There is a marked trend for increased seismic events in southern Nevada having a magnitude greater than 5.0 on the Richter scale to the northwest of the NTS. This parallels preexisting planes of weakness thought due to a 250-km- (155-mi)-long rift that formed 14 to 17 Ma ago in north-central Nevada [Stewart et al., 1975; Zoback and Thompson, 1978; and Zoback and Zoback, 1980].

Rogers et al. [1977], Campbell [1980], Battis [1978], and Hannon and McKague [1975] conducted seismic hazard studies of the NTS. They agree that the predicted maximum magnitude for an earthquake ranges from 5.8 to 7.0, with peak accelerations of 0.7 to 0.9 g.

Seismicity as a result of underground nuclear testing has been observed since 1963. Before the current moratorium on testing, tests with yields from 20 to 200 kilotons resulted in earthquakes of magnitude from 4.8 to 5.7 on the Richter scale [Hunter et al., 1982]. There is a current moratorium on underground nuclear testing at the NTS.

An early analysis by the Energy Research and Development Administration (ERDA) [ERDA, 1977] indicated that 95% of the disturbances and aftershocks associated with nuclear testing were within 14 km (8.6 mi) of the detonation site.

Forecast for Recurrence of Seismicity

The estimated return period for the largest amplitude earthquakes expected (5.8 to 7.0) ranges from 12,700 to 15,000 years (Table C-1). These data suggest that there is a possibility for the occurrence of a large earthquake somewhere within the NTS during the next 10,000 to 15,000 years.

Table C-1. Compilation of Estimated Seismic Hazard Analyses for the NTS

Potential Maximum Earthquake Magnitude[†]	Peak Ground Acceleration	Return Period	Source
7	0.7 g	15.0 Ka	Rogers et al. [1977]
6.8	0.7 g	12.7 Ka	Campbell [1980]
5.8-6.1	0.9 g	—	Hannon and McKague [1975]

[†] Richter Scale

An approximation of the seismic risk to the NTS region can be calculated using the binomial distribution [Parzen, 1960]. It is common to examine a sequence of independent events for which the outcome is either a success (an earthquake of magnitude 6.8 or greater occurs in a given year) or failure (no earthquake of magnitude 6.8 or greater occurs). This assumes that the

probability (p) of a success remains constant over time and that each year represents an independent Bernoulli trial. Given these assumptions, the risk (probability that at least one earthquake will occur over a given period) can be calculated from the well-known binomial distribution.

If there are n independent trials and, on each trial the probability of a success is p, then for x = 0, 1, 2,...,n,

$$P(\text{number of successes is } x) = \binom{n}{x} p^x (1-p)^{n-x} \tag{B.1}$$

where:

$$\binom{n}{x} = \frac{n!}{x!\,(n-x)!} \quad \text{for } x = 0, 1, 2, \ldots, n. \tag{B.2}$$

Because the probability of a success (earthquake of magnitude 6.8 or greater) is assumed to be a constant $7.87 \times 10^{-5}\ \text{yr}^{-1}$ (1/12,700 yr), and because the probability that there are 0, 1, 2, . . ., 10,000 earthquakes sums to one, the probability there are one or more earthquakes of magnitude 6.8 or greater is:

$$\begin{aligned} Risk &= \\ 1 - P(\text{no successes}) &= \\ 1 - \binom{10000}{0} (7.87\times10^{-5})^0 (1 - 7.87\times10^{-5})^{10000} &= 0.545. \end{aligned} \tag{B.3}$$

These calculations suggest there is a 54.5% chance of one or more earthquakes greater than 6.8 in the next 10,000 years. Note that if the calculations are repeated with the less conservative return time of 15,000 years, the probability of an earthquake falls to 0.486.

Despite the moderate risk of seismic damage, the limited use of engineered structures at Area 5 RWMS makes the site intrinsically less prone to significant earthquake damage than an above-ground facility or a facility using engineered belowground vaults. Because the GCD boreholes are or will be backfilled with alluvium, a major earthquake centered on the Area 5 RWMS is expected to result in only limited compaction, caused by the consolidation of alluvium. Given the large return times associated with the largest events, coupled with the small likelihood that an event would be centered upon the Area 5 RWMS, it is unlikely that the integrity of the RWMS would be compromised.

Volcanic Risk Analysis

Data concerning the hazards of future volcanism in the NTS region have been acquired from ongoing assessments of the volcanic hazard at Yucca Mountain, located approximately 45 km (28 mi) west of the RWMS. The close proximity of Yucca Mountain to the RWMS suggests that the volcanic hazard associated at the RWMS can be garnered from the data gathered at Yucca Mountain.

Crowe et al. [1983] concluded that further silicic volcanism was not realistic, given the age evidence by Christiansen et al. [1977] and Byers et al. [1976] for the ash-flow and ash-fall tuffs in nearby caldera systems. The most recent volcanism, associated with the Death Valley-Pancake Range Volcanic Belt [Wells et al., 1990], has been basaltic. The Death Valley-Pancake Range Volcanic Belt, a 50-km- (31-mi)-wide swath of activity that transects the NTS trending north-south throughout southern Nevada, is characterized by cinder cones and lava flows of limited extent (Figure C-2). Crowe and Carr [1980] identified four tectonic settings within the NTS where the risk of recurrent basaltic volcanism was assessed. Their data suggest the immediate vicinity of nearby caldera ring fracture zones or rift grabens possess the greatest likelihood for renewed volcanism. Ongoing studies at the proposed high-level waste repository at Yucca Mountain indicate significant activity in the past from the Timber Mountain-Oasis Valley Caldera and Lathrop Wells Volcanic Fields [Byers et al., 1976; Crowe, 1990]. Closer to the Area 5 RWMS, approximately 19 km (12 mi) west-southwest, lies the Wahmonie-Salyer Volcanic Center. The youngest basalt exposed at the land surface nearest the RWMS is that of Nye Canyon [Crow, 1990], dated at about 7.31 Ma [Raytheon Services Nevada, 1994].

Basalt flow and rubble, intercalated with near subsurface alluvium, occur in two nearby drill-holes. Basalt flows were encountered 290 m (950 ft) below the surface, approximately 2.4 km (1.5 mi) north of the Area 5 RWMS in borehole UE-5i and roughly 2.7 km (1.6 mi) to the north-northeast in borehole UE-5k. The ages of the flows in UE-5i and UE-5k have been determined at 8.6 and 8.4 Ma, respectively [Raytheon Services Nevada, 1994]. Approximately 2.3 km (1.4 mi) northwest of the Area 5 RWMS in Pilot Well UE5PW-3, two major lithologic tuff units were penetrated and identified from Pilot Well cuttings [REECo, 1993]. One silicic ash-flow tuff unit, encountered from 188 to 280 m (617 to 920 ft) below the surface, was identified as the Ammonia Tanks Tuff of the Timber Mountain Group (late Miocene). Below this unit lies a bedded tuff unit of the Ammonia Tanks Tuff that extends at least to the total borehole depth (291 m [955 ft]).

Crowe and Carr [1980] and Metcalf [1983] assessed volcanic risk assessment for the NTS region. These studies agree that the probability of an event is exceedingly small. Christiansen et al. [1977] and Byers et al. [1976] determined that silicic volcanic activity at the NTS climaxed 10 to 11 Ma ago, when an extensive network of calderas ejected a large volume of pyroclastic flow over much of the NTS. Because older calderas seldom show renewed activity during a hiatus after extended periods (10 Ma) of activity [Crowe and Carr, 1980], Crowe et al. [1983] concluded that the occurrence of additional silicic volcanism in the area was highly unlikely. More recently, Crowe [1990] suggested that the location with the highest probability for a small volume event was Lathrop Wells or Sleeping Butte volcanic centers, 50 to 75 km (31 to 47 mi) west of the RWMS.

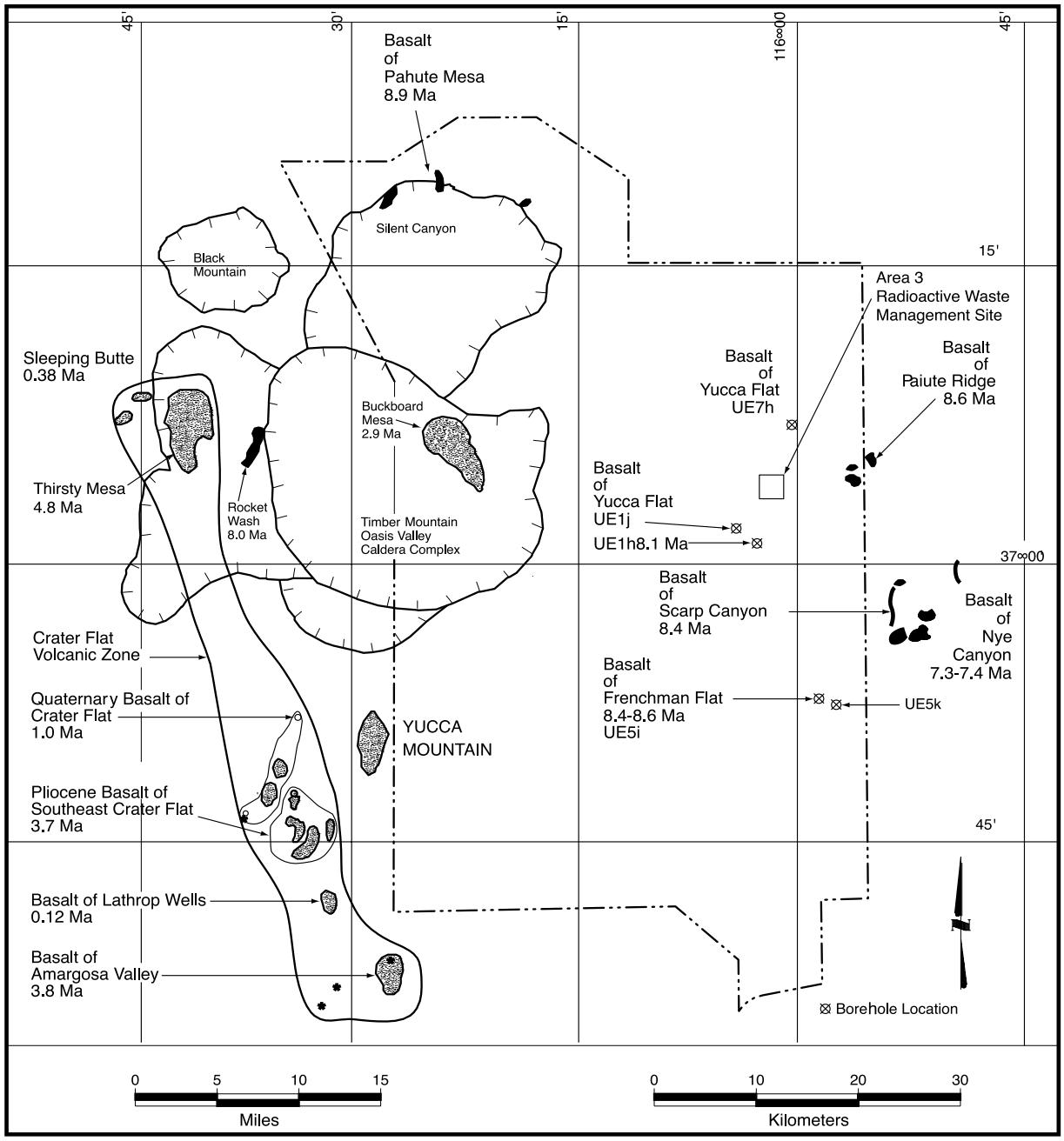

Figure C-2. Tertiary Volcanic Centers in the NTS Region (modified from Case et al., 1984).

Projected Volcanic Hazard

It is believed that the influence of renewed basaltic volcanism would be much more localized than that of earlier silicic eruptions. The extent of deposition would be restricted to the immediate vicinity of the eruption centers, probably within 2 to 10 km (1.2 to 6.2 mi) of the cinder cone and associated lava sheet [Case et al., 1984].

Two lines of evidence support the inference that there is a very low likelihood of disruption of the Area 5 RWMS by future basaltic volcanic activity. First, the location of eruptive vents for post-Miocene basaltic activity in the NTS shows a pattern of episodic but progressive, southwestward migration of sites of basaltic volcanic activity [Crowe and Perry, 1989; Crowe 1990; Crowe et al., 1998]. All sites of Quaternary basaltic volcanism (less than 1.6 Ma) occur west of the western boundary of the NTS (Figure C-2), at considerable distances from the RWMS. Second, Crowe et al. [1998] calculated disruption probabilities for the recurrence rate of small volume basaltic volcanic centers within relatively inactive areas (distant from sites of Quaternary volcanism) in the southern Great Basin. This calculation applies to the Area 5 RWMS in Frenchman Flat. They estimated, using regional counts of Quaternary volcanic events, the probability of disruption of a 6-km^2 site in an inactive area of the southern Great Basin to be about 10^{-9} per year. This estimate is an order of magnitude *smaller* than the 1 in 10,000 in 10,000 years probability-screening criteria used in 40 CRF 191 and allows elimination of volcanism as an issue for the RWMS.

References

Battis, J. D. 1978. Geophysical Studies for Missile Basin: Seismic Risk Studies in the Western United States. TI-ALEX(02)-FSR-78-01. Texas Instruments Inc., Houston, Texas.

Bechtel Nevada. January 1998. Performance Assessment for the Area 5 Radioactive Waste Management Site at the Nevada Test Site, Nye County, Nevada (Rev. 2.1). Prepared for U.S. Department of Energy, Nevada Operations Office under Contract Number DE-AC08-96NV11718. DOE/NV/11718-176 UC-721.

Burchfiel, B.C., R.J. Fleck, D.T. Secor, C.R. Vincelette, and G.A. Davis. 1974. Geology of the Spring Mountains, Nevada. Geol. Soc. Amer. 85:1013–1022.

Burchfiel, B.C. 1964. Precambrian and Paleozoic Stratigraphy of the Specter Range Quadrangle, Nye County, Nevada. Am. Assoc. Petroleum Geol. Bull. 48:40–56.

Byers, F.M. W.J. Carr, P.P. Orkild, and W.D. Quinlivan. 1976. Volcanic Suites and Related Caldrons of Timber Mountain–Oasis Valley Caldera Complex, Southern Nevada. U.S. Geological Survey Professional Paper 919. U.S. Geological Survey, U.S. Government Printing Office, Washington, DC.

Campbell, K. W. 1980. Seismic Hazard Analysis for the NTS Spent Reactor Fuel Test Site. UCRL-15620. Lawrence Livermore National Laboratory, Livermore, California.

Case, C., J. Davis, R. French, and S. Raker. 1984. Site Characterization in Connection With the Low-Level Defense Waste Management Site in Area 5 of the Nevada Test Site, Nye

County, Nevada, Final Report. Publication No. 45034. Water Resources Center, Desert Research Institute, University of Nevada, Las Vegas, Nevada.

Christiansen, R.L., and P.W. Lipman. 1972. Cenozoic Volcanism and Plate Tectonic Evolution of the Western United States, II, Late Cenozoic. Trans. of the Royal Soc. London. Ser. A. Vol. 271: 249–284.

Christiansen, R.L., P.W. Lipman, W.J. Carr, F.M. Byers, P.P. Orkild, and K.A. Sargent. 1977. Timber Mountain–Oasis Valley Caldera Complex of Southern Nevada. Geol. Soc. Am. Bull. 88:943–956.

Crowe, B. M. 1990. Basaltic Volcanism Episodes of the Yucca Mountain Region. p. 65-73. In: High-Level Radioactive Waste Management. Proceedings of the international topic meeting sponsored by the American Society of Civil Engineers for the American Nuclear Society. Co-sponsored by the American Chemical Society . . . [et al.]. Hosted by the University of Nevada, Las Vegas, Nevada; American Nuclear Society, Inc., La Grange Par., Illinois; and American Society of Civil Engineers. New York. April 8-12. 1990.

Crowe, B.M., S. Self, D. Vaniman, R. Amos, and F. Perry. 1983. Aspects of Potential Magmatic Disruption of a High-Level Radioactive Waste Repository in Southern Nevada. J. of Geology 91:259–276.

Crowe, B.M. and W.J. Carr. 1980. Preliminary Assessment of the Risk of Volcanism at a Proposed Nuclear Waste Repository in the Southern Great Basin. USGS Open File Report 80–357. U.S. Geological Survey, U.S. Government Printing Office, Washington, DC.

Crowe, B.M. 1990. Basaltic Volcanic Episodes of the Yucca Mountain Region, *Proceedings High-Level Radioactive Waste Management Conference, Las Vegas, Nevada* (American Nuclear Society, La Grange Park Illinois) p. 65–73.

Crowe, B.M., and F.V. Perry. 1989. Volcanic Probability Calculations for the Yucca Mountain Site; estimation of Volcanic Rates, in *Proceedings Nuclear Waste Isolation in the Unsaturated Zone, Focus '89* (American Nuclear society, La Grange Park, Illinois) p. 326–334.

Crowe, B.M., P. Wallmann, and L.M. Bowker. 1998. Probabilistic Modeling of Volcanism Data: Final Volcanism Hazard Studies for the Yucca Mountain Site, in Perry, F.V., B.M. Crowe, G.A. Valentine, and L.M. Bowker, (eds) *Volcanism Studies: Final Report for the Yucca Mountain Project* Los Alamos National Laboratory Report LA-13478 554.

Energy Research and Development Administration. 1977. Nevada Test Site Final Environmental Impact Statement. ERDA-155. U.S. Government Printing Office, Washington, DC.

Fleck, R.J. 1970. Tectonic Style, Magnitude, and Age of Deformation in the Sevier Orogenic Belt in Southern Nevada and Eastern California. Geol. Soc. Amer. Bull. 81:1705–1720.

Frizzell, V.L., Jr., and J . Shulters. 1990. Geologic Map of the Nevada Test Site, Southern Nevada. USGS Map 1-2046. Miscellaneous Investigation Series. U.S. Geological Survey, U.S. Government Printing Office, Washington, DC.

Hannon, W. J., and H. L. McKague. 1975. An Examination of the Geology and Seismology Associated With Area 410 at the Nevada Test Site. UCRL-51830. Lawrence Livermore National Laboratory, Livermore, California.

Hunter, P.H., D.H. Card, and K. Horton. 1982. Safety Assessment for Area 5 Radioactive Waste Management Site. DOE/NV/00410-54. Ford, Bacon and Davis Utah Inc., and Reynolds Electrical & Engineering Co., Inc., Las Vegas, Nevada.

Metcalf, L.A. 1983. A Preliminary Review and Summary of the Potential for Tectonic, Seismic, and Volcanic Activity at the Nevada Test Site Defense Waste Disposal Site. Publication 45029. Water Resources Center, Desert Research Institute, University of Nevada, Las Vegas, Nevada.

Parzen, E. 1960. Modern Probability Theory and Its Applications. John Wiley & Sons, Inc., New York, New York.

Raytheon Services Nevada. 1994. Summary of Volcanic Activity at the Area 5 Radioactive Waste Management Site DOE/Nevada Test Site, Nye County, Nevada. Letter Report. Raytheon Services Nevada, Las Vegas, Nevada.

REECo. 1993. Site Characterization and Monitoring Data from Area 5 Pilot Wells, Nevada Test Site, Nye County, Nevada. Reynolds Electrical and Engineering Co., Inc., Las Vegas, NV.

Rogers, A. M., D. M. Perkins, and F. A. McKeon. 1977. A Preliminary Assessment of the Seismic Hazard of the Nevada Test Site Region. Bull. Seismol. Soc. Amer. 67:1587-1606.

Ross, C.S., and R.L. Smith, 1961. Ash-Flow Tuffs – Their Origin, Geologic Relations, and Identification. USGS Professional Paper 366. U.S. Geological Survey, U.S. Government Printing Office, Washington, DC.

Sawyer et al. 1990. Reference not currently available.

Smith, R.L. 1960. Zones and Zonal Variations in Welded Ash Flows. USGS Professional Paper 354-F. U.S. Geological Survey, U.S. Government Printing Office, Washington, DC.

Stewart, J.H., G.W. Walker, and F.J. Kleinhampl. 1975. Oregon-Nevada Lineament. Geology 3:265–268.

Stewart. 1980. Reference not currently available.

Wells, S.G., L.D. McFadden, C.E. Renault, and B.M. Crowe. 1990. Geomorphic Assessment of Late Quaternary Volcanism in the Yucca Mountain Area, Southern Nevada: Implications for the Proposed High-Level Radioactive Waste Repository. Geology 18:549–553.

Winograd, I.J. and W. Thordarson. 1975. Hydrologic and Hydrochemical Framework, South-Central Great Basin, Nevada-California, With Special Reference to the Nevada Test Site, U.S. Geological Professional Paper 712-C. U.S. Government Printing Office, Washington, DC.

Zoback, M.L., and G.A. Thompson. 1978. Basin and Range Rifting in Northern Nevada: Clues From a Mid-Miocene Rift and its Sequent Offsets. Geology 6:111–116.

Zoback, M.L., and M.D. Zoback. 1980. Faulting Patterns in North-Central Nevada and Strength of the Crust. J. Geophys. Res. 85(B1):275–284.

This page intentionally left blank.

Appendix D

Estimation of Upward Specific Discharge in Vadose Zone at Area 5 RWMS

This page intentionally left blank.

Introduction

In this study, upward specific discharge is estimated at the depths of core samples in boreholes AP-1, AP-2, RP-1, and RP-2 at the Area 5 RWMS (Figure D-1). The region of investigation is the vadose zone extending from the near surface (below 1.8 m, or 6 ft depth) to the approximate depth of waste burial (about 21 m, or 70 ft). The choice of mathematical model for unsaturated conductivity followed that of Bechtel [1998], as did the general curve fitting procedures used to obtain unknown empirical constants. This study differs from Bechtel [1998] by 1) the way in which core and retention data are used, 2) calculation of effective saturation, and 3) in the depths at which specific discharge is estimated. The specific discharge estimates were used to assist in the construction of a defensible distribution for use in the GCD performance assessment model.

Figure D-1. Location of the AP- and RP- Science Boreholes, Area 5 RWMS.

Conceptual Model Assumptions

The specific discharge calculation was based on the unsaturated form of Darcy's Law oriented in the vertical direction. If it is assumed:

- the datum is ground surface,

- the vertical (z) axis is positive upward,
- vadose zone water pressures are treated as negative matric potentials,
- vadose zone water flow is vertical,
- vadose zone flow is one dimensional, and
- steady state exists in the vadose zone between depths of 3 to 21 m,

then the following equation for specific discharge, q, can be used:

$$q = -K(\theta)[d\psi/dz + 1] \qquad \text{(D-1)}$$

where:

q	=	specific discharge or flux (length/time),
$K(\theta)$	=	unsaturated hydraulic conductivity (length/time),
$d\psi/dz$	=	pressure head gradient (unitless).

The investigated region did not begin at the land surface or at the shallow-most core sample in any of the boreholes because each borehole showed a distinct, wetter (lower suction) zone between the land surface and a depth of up to approximately 2.7 m (9 ft). There is no specific evidence to explain why these values are observed in all four boreholes, although it is likely that surface wetting from dust control activities at the RWMS and precipitation events around the time of the sampling could have resulted in these values. Therefore, it was assumed for the purposes of this analysis that these near-surface suction pressures are anomalous and they do not represent a long-term trend toward steady state in the vadose zone. Instead, they are assumed to be near-surface artifacts of very recent infiltration events of unknown origin that have not disrupted the long-term stabilization of conditions in the vadose zone between about 3 m (10 ft) and 21 m (70 ft) depth. Based on this reasoning, core samples more shallow than 1.8 to 2.7 m depth were not considered in this analysis. In addition, samples deeper than the upper extent of waste burial, 21 m (70 ft) depth were not considered because the region of concern is above the shallowest depth of burial. The phrase "reference depth" was given to the depth at which specific discharge was calculated. For practical purposes it was the approximate depth of the sample core on which the water retention analyses were performed [Blout et al., 1995, Appendix D.1.27 through D.1.30]. Actual sampling at depth consisted of collecting several sample cores within selected depth intervals.

From inspection of (D-1), it can be seen that calculating specific discharge for each reference depth involves estimating unsaturated hydraulic conductivity as a function of water content, $k(\theta)$, or more precisely, as a function of reduced water content or "effective saturation," $K(S_e = (\theta - \theta_r)/(\theta_s - \theta_r))$, and estimating the pressure head gradient, $d\psi/dz$, at the location (depth) of each sample.

Estimate of Pressure head gradient at Sample Depths

The pressure head gradient was estimated by plotting sample depth (m) versus suction pressure (m of H_2O) for each borehole, and then fitting these data to a continuous, monotonic curve (Figures D-2 through D-5). A data-plotting package was used for the curve fitting and was judged to be adequate but approximate.

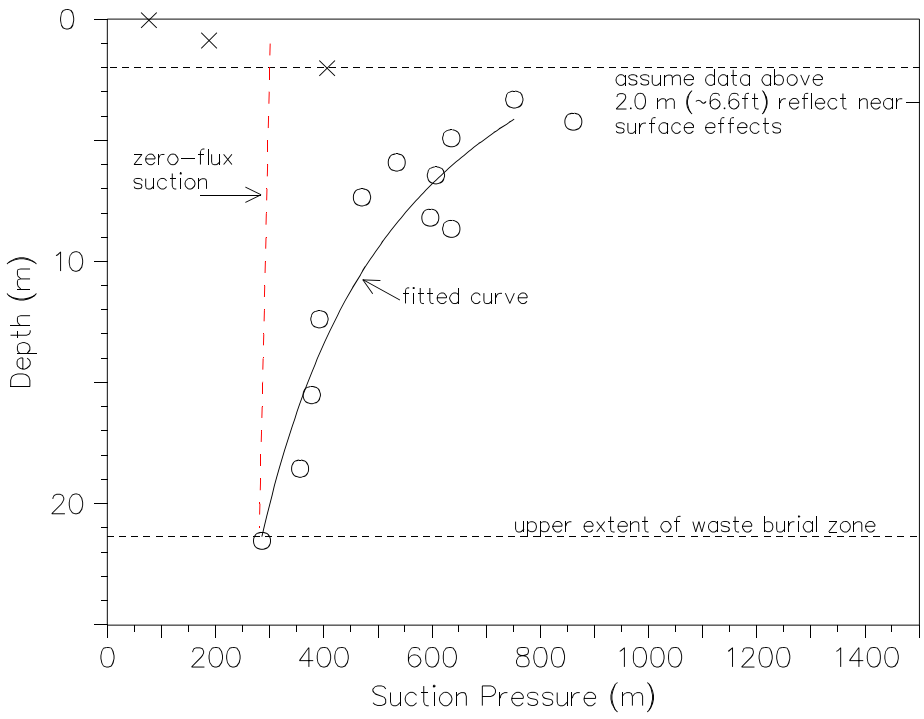

Figure D-2. AP-1 Suction Pressure with Depth.

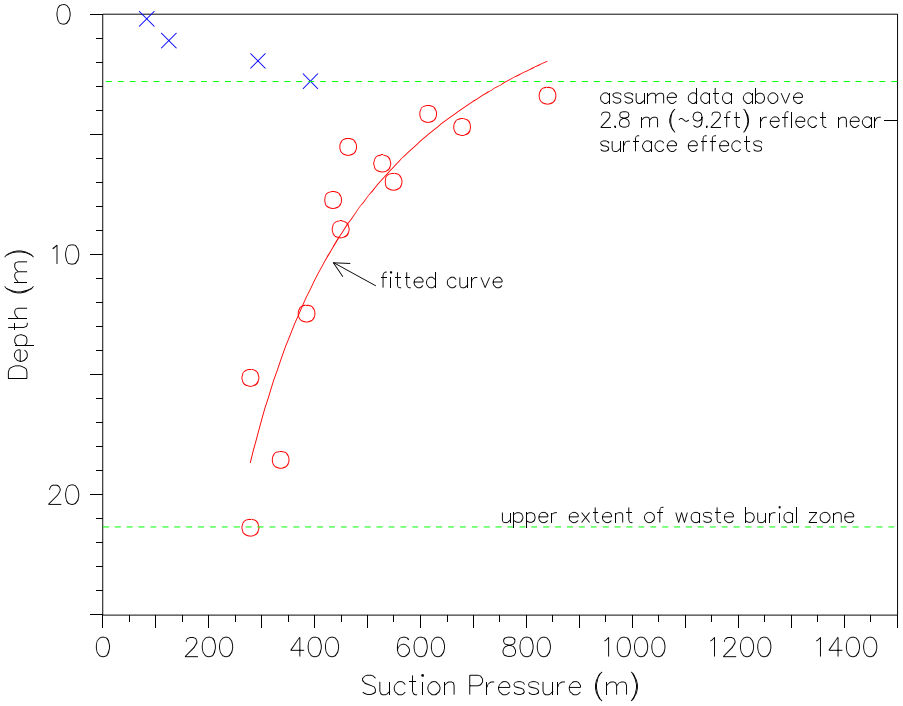

Figure D-3. AP-2 Suction Pressure with Depth.

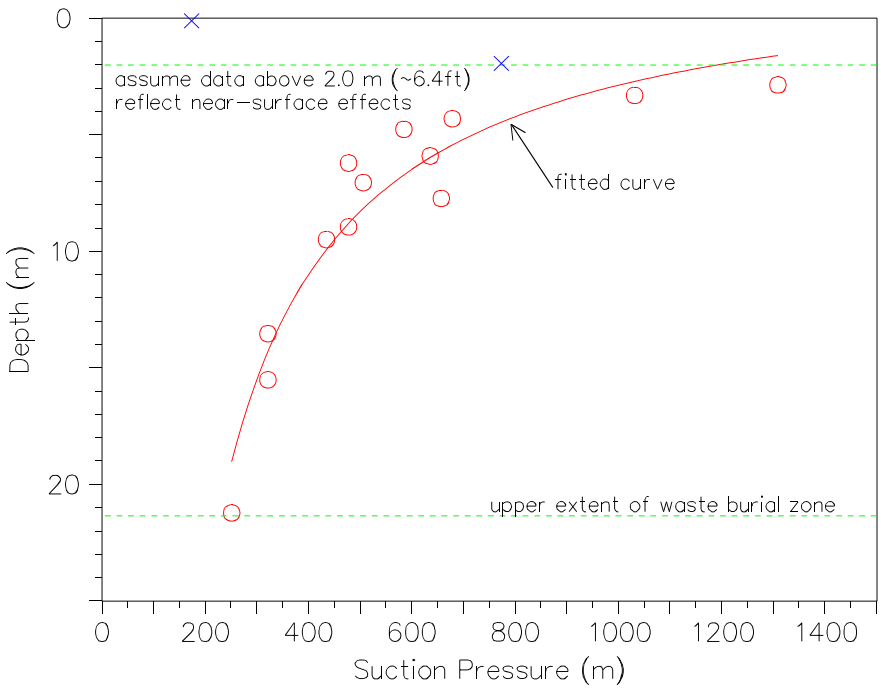

Figure D-4. RP-1 Suction Pressure with Depth.

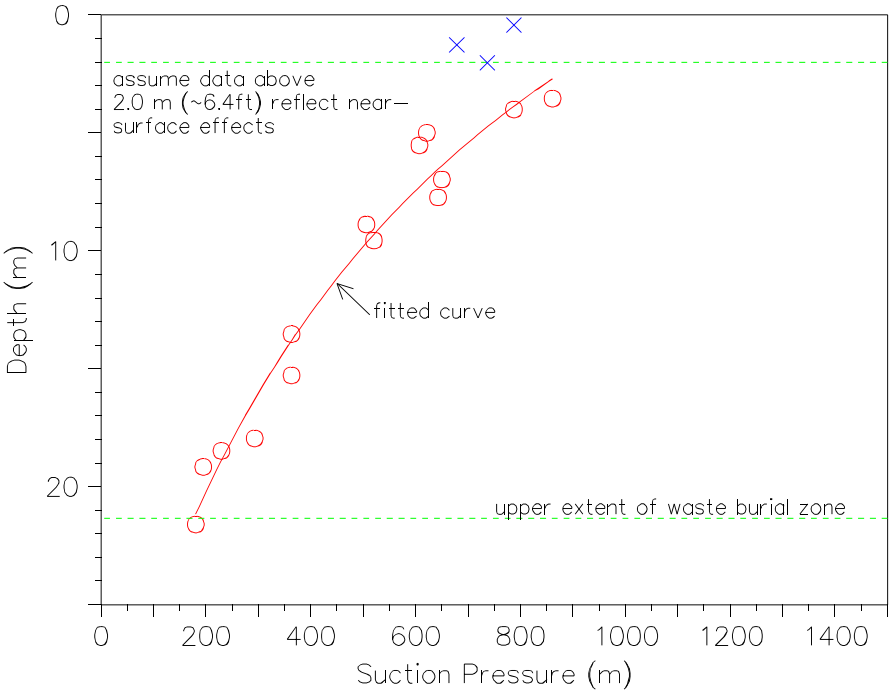

Figure D-5. RP-2 Suction Pressure with Depth.

Based on the results of the curve fitting, the pressure head gradient at the depth and pressure of each core sample is assumed to be equal to the reciprocal of the slope of the curve at the sample depth. The fitted equations for each borehole and their derivatives are included in Attachment 1.

Estimate of Unsaturated Hydraulic Conductivity at Sample's Effective Saturation

To estimate a value for unsaturated hydraulic conductivity at the depth of a core sample, a simplified form of the Mualem model was used. The Mualem expression for unsaturated hydraulic conductivity [Mualem, 1976] as a function of effective saturation (a.k.a. reduced water content) is

$$K(S_e) = K_{sat}\left(S_e^{l}\left[1-\left(1-S_e^{1/m}\right)^{m}\right]^{2}\right) \qquad \text{(D-2)}$$

where:

$K(S_e)$ = unsaturated hydraulic conductivity (length/time),
S_e = effective saturation,
K_{sat} = saturated hydraulic conductivity (length/time),
l, m = empirical constants, and $m = 1 - (1/n)$.

By inspection of the righthand side of (D-2) it can be seen that values for S_e, K_{sat}, l, and m must first be measured or estimated to calculate $K(S_e)$. Core samples from the AP and RP boreholes have been analyzed in the laboratory for K_{sat}, but S_e, l, and m must be estimated. To estimate the effective saturation, S_e, the standard equation was used:

$$S_e = (\theta-\theta_r)/(\theta_s-\theta_r) \qquad \text{(D-3)}$$

where:

θ = in-situ, i.e., "measured" volumetric water content,
θ_s = saturated volumetric water content,
θ_r = residual volumetric water content.

Actual measured values of θ and θ_s were obtained from laboratory analyses of each core sample [Blout, et al., 1995]. However, θ_r in (3) was unknown and was therefore estimated.

Estimate of Residual Water Content, θ_r

Observed water retention data [Blout et al., 1995] were used in conjunction with the RETC computer code [van Genuchten et al., 1991] to obtain an estimate of θ_r for each core. RETC was used to individually fit the van Genuchten model for effective degree of saturation, S_e, to water retention data from each core by setting the van Genuchten model equal to (D-3). The van Genuchten model for effective saturation (or, "reduced water content"), S_e, is:

$$S_e = 1/\left[1 + (\alpha\psi)^{n}\right]^{m} \qquad \text{(D-4)}$$

where

α (1/length), n, m = empirical parameters

ψ = suction pressure.

In the RETC fitting exercise, Equation D-3 was set equal to D-4. The θ versus ψ water retention analysis for each sample core [Appendix D.1.27 through D.1.30 of Blout et al., 1995] was the basis of the curve fit. The parameters n, α, and θ_r were fitted, and θ_s, θ, Ψ were a known quantity from laboratory analysis. Parameter m was set equal to 1 ! 1/n based on the recommendation of van Genuchten and Yates [1991] for coarse soils and less well-defined retention data sets. An additional effort was made to define the dry region of the curve by adding an actual in-situ data point to the water retention curve before the fitting exercise; measurements of in-situ water content and matric potential were available at all but one reference depth. These measurements originated from laboratory tests for hydrologic properties [see Blout et al., 1995, Appendix D.1.1, D.1.5, D.1.9, D.1.13]. If the additional measurement did not appear to fit in the retention curve or was not available, nothing was added to the analytical water retention data. Data from cuttings were not used in this analysis.

Calculation of Effective Saturation, S_e and $K(S_e)$

Effective saturation S_e was directly calculated in this analysis with equation (D-3), parameters θ_s, in-situ θ, and the fitted value of θ_r. The value for S_e was then inserted into the Mualem hydraulic conductivity model, along with parameter m, l, and the measured K_{sat}, to estimate unsaturated hydraulic conductivity as a function of saturation at the sample depth, matric potential, and water content in question. Parameter l was fixed at 0.5, as recommended for coarse textured soils [van Genuchten and Yates, 1991].

Now, given an estimate of unsaturated conductivity from (D-2) and the pressure head gradient at the in-situ suction pressure, the specific discharge can be calculated from (D-1). A summary of the specific discharge calculation results is presented in Table D-1. The actual spreadsheet table used for the calculation is included in Attachment 2.

Table D-1. Summary of Results: Upward Specific Discharge Estimates in Vadose Zone in Four Science Boreholes at the Area 5 RWMS - *Fitted Pressure Head gradient*

Borehole	Upward Specific Discharge, q (mm/yr)						
	Mean	Standard Deviation	Minimum	Maximum			
AP-1 (5 estimates)	9.2E!5	1.5E!4	7.1E!7	3.6E!4			
AP-2 (8 estimates)	3.1E!3	5.9E!3	4.8E!8	1.7E!2			
RP-1 (3 estimates)	6.8E!4	6.2E!4	9.8E!5	1.3E!3			
RP-2 (6 estimates)	2.9E!4	6.7E!4	3.3E!6	1.7E!3	median	skewness	kurtosis
All boreholes	1.3E!3	3.7E!3	4.8E!8	1.7E!2	3.4E!5	4.0	17
All boreholes, log of **q**	!4.3	1.4	!7.3	!1.8	!4.5	!0.19	0.39

Discussion

The 22 specific discharge flux estimates range from approximately $4.8 \times 10^{!8}$ to $1.7 \times 10^{!2}$ mm/yr across boreholes AP-1, AP-2, RP-1, and RP-2, while the individual borehole averages fall within a more narrow range, from $9.2 \times 10^{!5}$ to about $6.6 \times 10^{!3}$ mm/yr (Table D-1). Specific discharge estimates plotted versus sample depth, Figures D-6 through D-9, do not appear to show any significant trends within boreholes. However, when grouped into a single plot representing all four boreholes, as shown in Figure D-10a, there is an apparent trend of higher flux estimates, i.e., values greater than the median value of $3.4 \times 10^{!5}$, below 10 m (about 33 ft), while lower estimates are more numerous above 10 m. This trend with depth appears to be associated with the in-situ moisture contents, which show the same trend (Figure D-10b). The drier zone above 10 m is apparently affected to a much greater degree by evaporation and root uptake than the zone from about 10 m down to 21 m. A distinct zonation in matric potential above and below a depth of about 7 to 10 m is also observed in the science trench (ST) boreholes, and supports this observation.

Curve Fitting of Suction Pressure versus Depth

By imposing a continuous, monotonic function to the depth versus suction pressure data, the curve fitting procedure guaranteed, or forced, an upward direction to specific discharge for the observed data. Fitting polynomials of higher order to the data could impose localized changes in the direction of the gradient vector, but it was not assumed to be consistent with the vadose zone's steady state conceptual model of suction pressure distribution with depth. Curve-fitting, in general, smooths over observed variations in the measured suction pressure at local, adjacent core sample points. Some localized pressure head gradient reversals apparently do not fit the model of steady upward flux. However, these reversals may be a relic of the uncertainty involved in the direct measurement of in-situ matric potential in each core. Therefore, based on the bulk of the observed suction pressure data with depth in boreholes AP-1, AP-2, RP-1, and RP-2 it is assumed that the general trend of suction pressure is monotonic from a depth of about 2 or 3 m to a depth of about 21 m. The observed reversals are not consistently maintained vertically or horizontally with depth on the scale of the investigation and were therefore not assumed to be part of the conceptual model of steady state upward flux. In addition, the uncertainty in the curve-fitting procedure was not incorporated into the calculation because it was observed to have a much smaller effect on the outcome than other aspects in the method.

Curve Fitting of Water Retention Data

The RETC curve fitting procedure is approximate, particularly at the dry end of the retention curve. This was evident in four particular water retention data sets because RETC estimated residual water content, θ_r, that was higher (wetter) than the dry end of the retention data set, which was marked by an in-situ (observed) θ. If residual water content is greater than in-situ, it may indicate that liquid-phase water flux is zero at that point, or it may suggest that the theoretical model is invalid under those conditions because a negative saturation is calculated. Although in-situ θ values greater than θ_r were available in three of these cases, these higher in-situ θ values were not measured in the same core that was analyzed for suction pressure, and using them would not be consistent with the rest of the analyses. In an effort to improve the

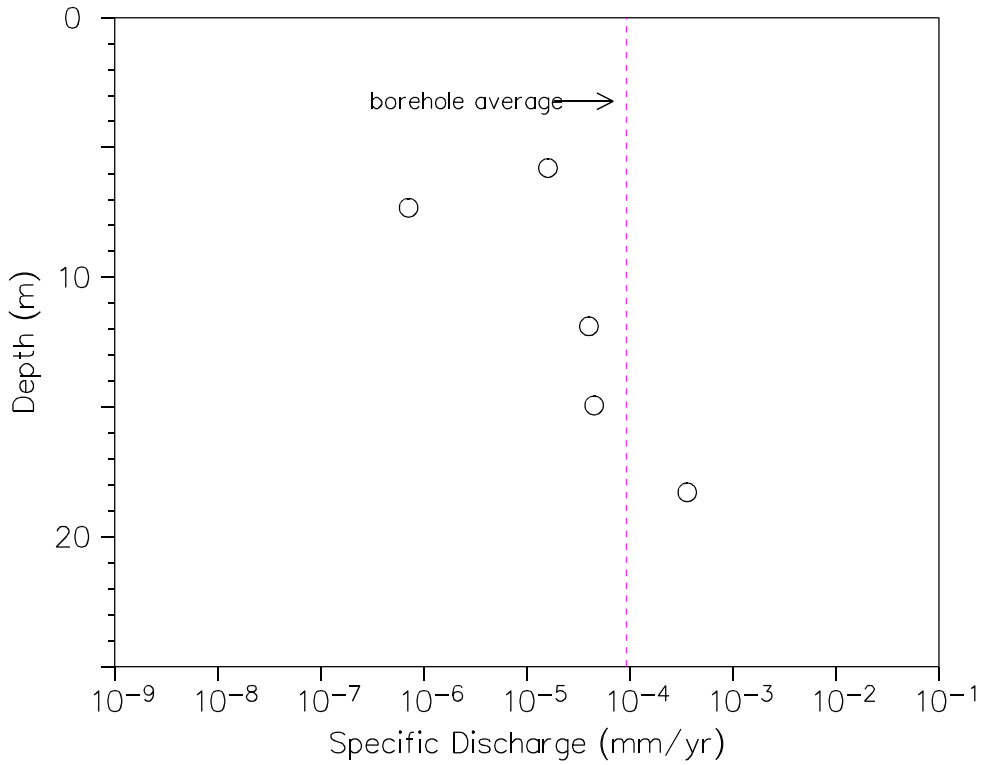

Figure D-6. Specific Discharge vs. Depth, AP-1.

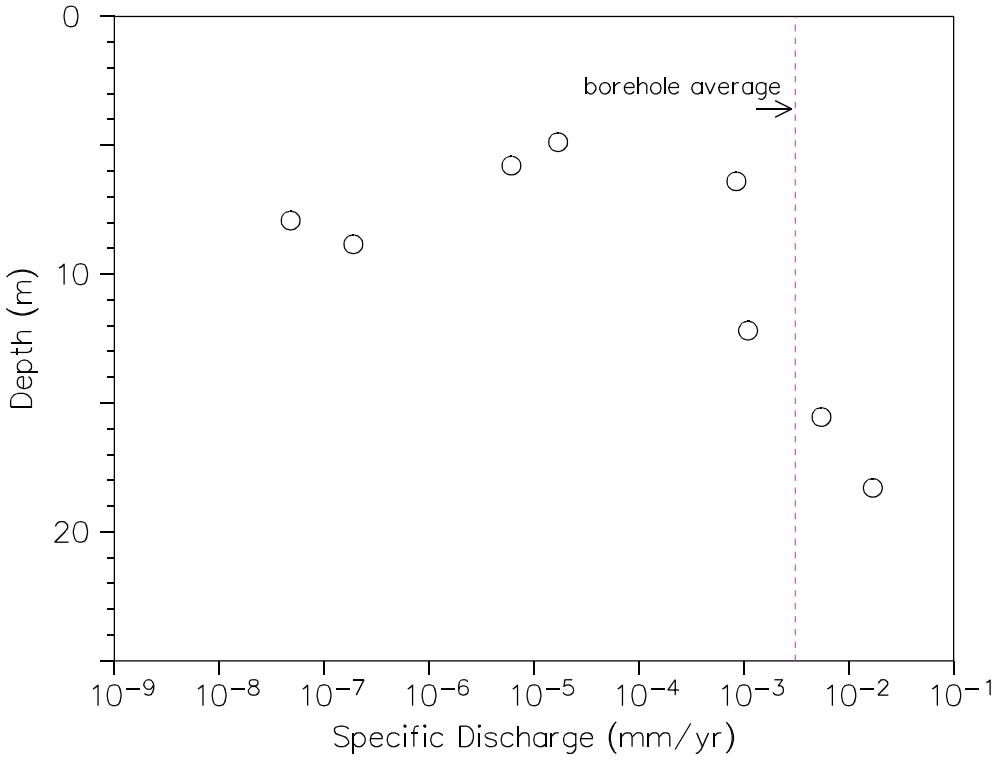

Figure D-7. Specific Discharge vs. Depth, AP-2.

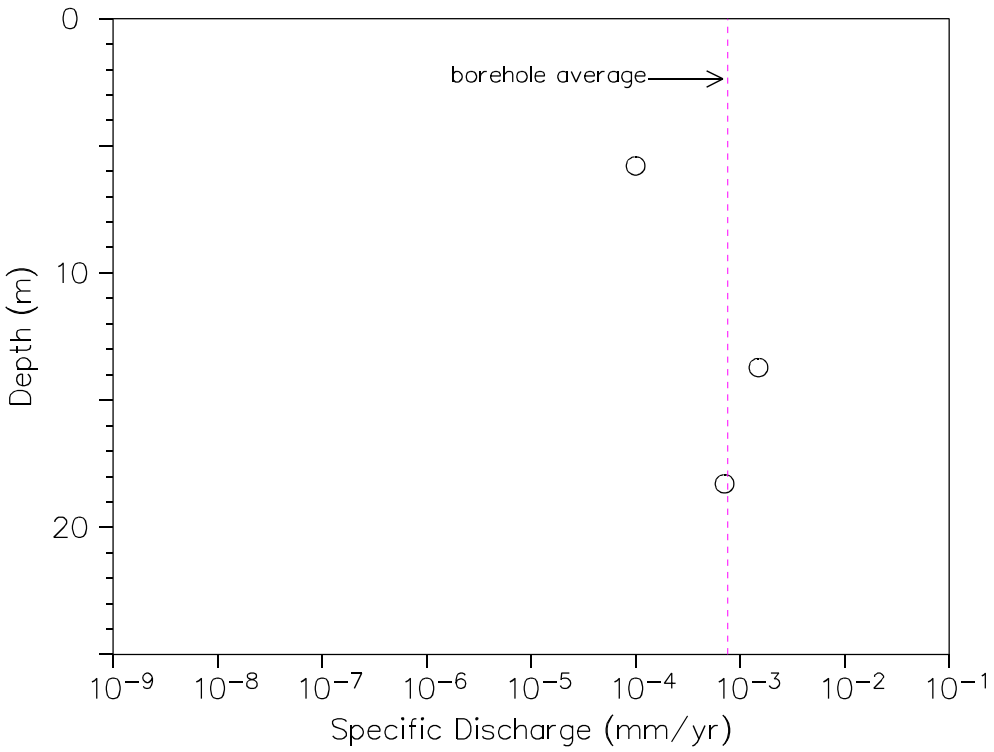

Figure D-8. Specific Discharge vs. Depth, RP-1.

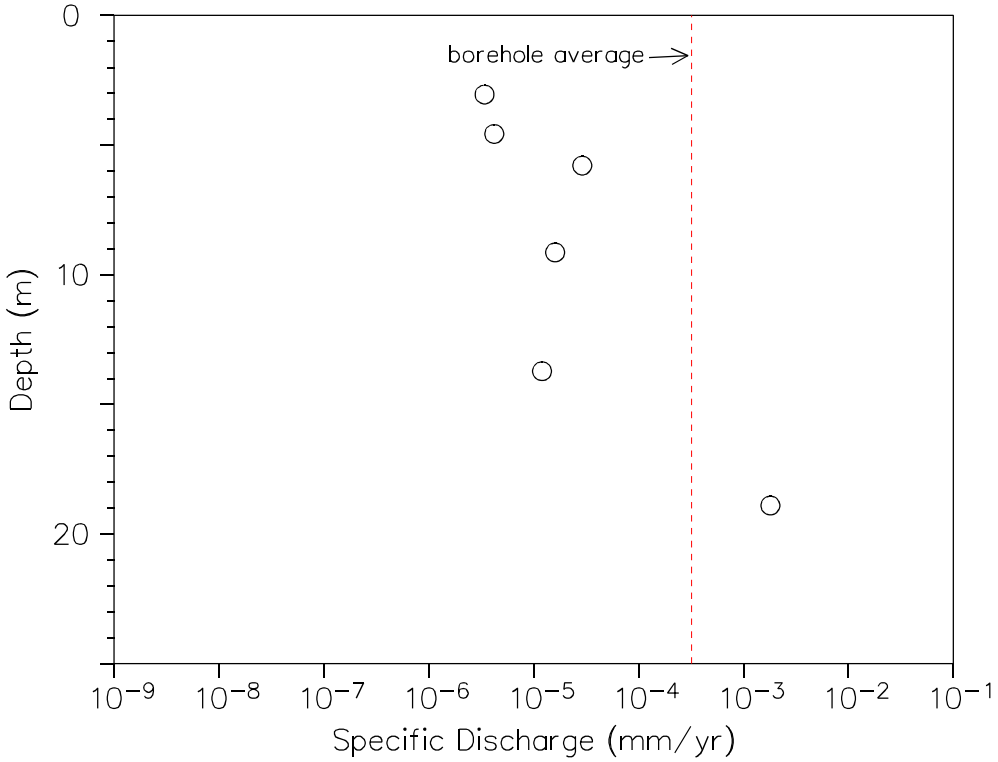

Figure D-9. Specific Discharge vs. Depth, RP-2.

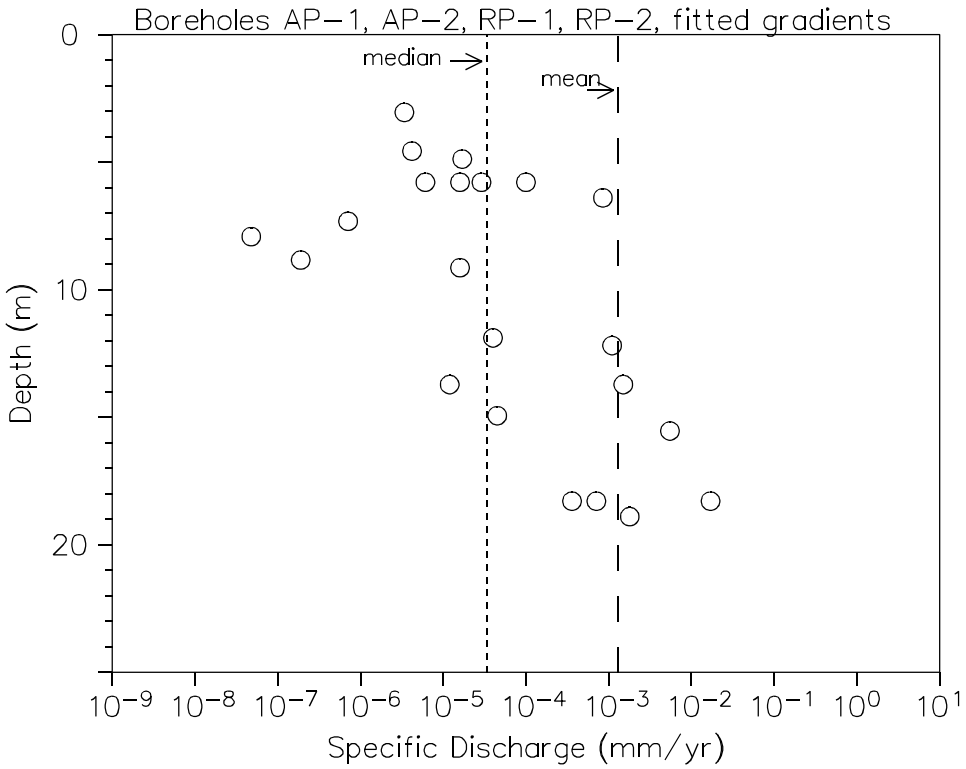

Figure D-10a. Specific Discharge Estimates vs. Depth.

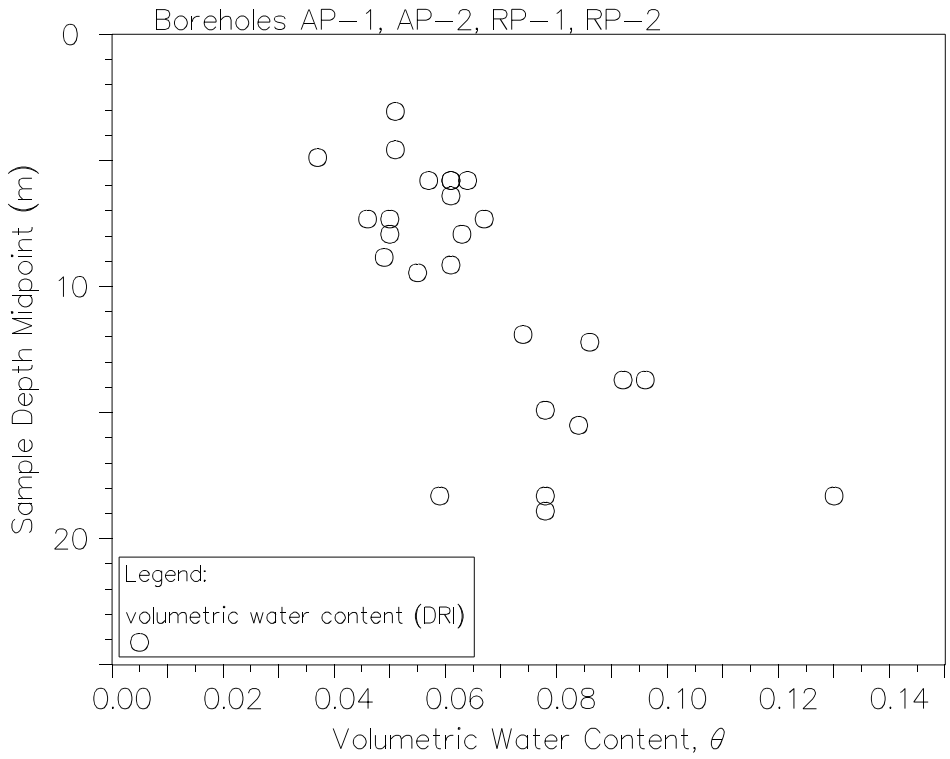

Figure D-10b. Volumetric Water Content vs. Depth.

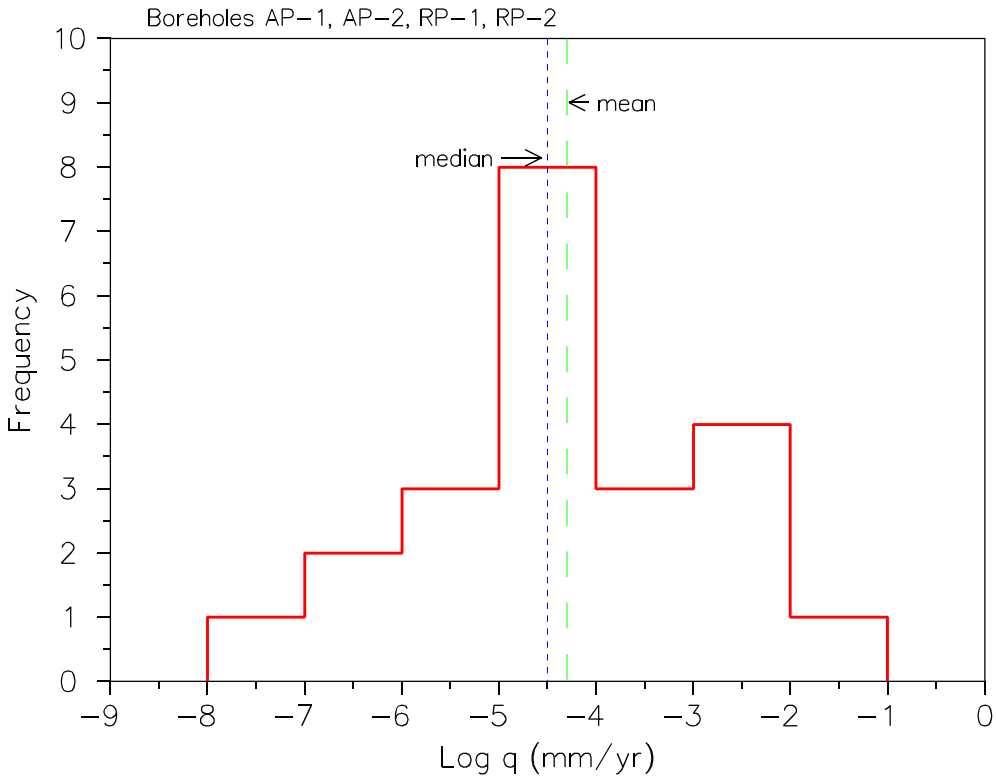

Figure D-11. Histogram of Log Specific Discharge.

RETC curve fit and solve this problem, an in-situ (θ,ψ) data point was added to the water retention curve in these cases. However, the $\theta_r > \theta$ result was encountered nonetheless. Therefore, specific discharge could not be calculated for these particular retention sets (see Attachment 2) because it was assumed that the model was invalidated by the data.

The curve-fitting procedure on several retention data sets did not converge to a value of θ_r. Under these circumstances RETC set the residual moisture content to zero, which was used in the calculation of S_e for those core samples. The zero value was used in these cases because the Mualem-van Genuchten model was not invalidated as a result of the lack of convergence in the mathematical solution, although a residual water content of zero will cause the flux to be over-estimated with respect to the use of the residual water content that is greater than zero.

Mualem, van Genuchten Models

The van Genuchten saturation model was used to estimate empirical constants and the Mualem model was used to calculate unsaturated hydraulic conductivity at the high observed suction pressures. According to van Genuchten et al. [1991], "the usefulness of these models...depends on the ability to reliably characterize the hydraulic properties of the unsaturated zone." It can be recognized that measurement of suction pressures and moisture contents under such dry conditions as those observed in the AP and RP boreholes most likely involves significant measurement error, making it difficult to accurately estimate hydraulic properties and empirical parameters.

The RETC-fitted 95% confidence limits of the empirical constant θ_r were very wide for all water retention curves, spanning ranges whose magnitudes are over twice their respective best-fit values with the exception of those which curves for which θ_r could not be estimated within the given closure criterion of the algorithm. Confidence limits for the fitted parameter *n* were also wide enough to suggest a significant effect on the specific discharge estimate. The large confidence interval is a result of fitting the sparse set of six or seven data points defining the water retention curves to the van Genuchten saturation model. Given more data points, particularly at high suction pressures, the fitted values of empirical constants may be different enough to produce significantly different flux estimates. Varying *n* and θ_r within their limits for some water retention curves, as an example, can produce significant changes in specific discharge estimates. A first indication of the effect of the value of *n* on the resulting retention curve is that the lower the value of n, the flatter the retention curve. The uncertainty in the empirical parameters *n*, α, and θ_r, according to the correlation and confidence limits established by the RETC program, will be incorporated into the estimate of the effective upward specific discharge value.

Use of Measured Data

The vadose zone alluvium was sampled at selected depth intervals [Blout et al., 1995]. Each depth interval was split between several separate core samples (see example, Figure D-12). In-situ water content (θ) was measured in all cores, while suction pressure ψ (as matric potential), saturated hydraulic conductivity and water retention characteristics were measured in selected ones. As a result of these analyses, for each sampled depth interval there are several measurements of θ (from separate cores) while there is only one ψ estimate. This situation requires a judgement as to which particular θ to include in the calculation because the magnitude of the resulting specific discharge flux is very sensitive to θ. In all but three of the calculations presented, the θ that was most closely associated with the measured ψ was used, that is, ψ and θ measured in the same core sample were considered to be in-situ.

There were three exceptions when ψ and θ measured from the same core sample were not used in the specific discharge calculation. These occurred in AP-2 at a reference depth of 15.5 m (51 ft), RP-1 at 18.3 m (60 ft) and in RP-2 at 18.9 m (62 ft). In RP-1, there was no measurement of ψ at or near 18.3 m; a value was therefore interpolated from the curve fit of suction pressure versus depth (see above section). The in-situ ψ and θ measurements in borehole AP-2 at a reference depth of 15.5, m (51 ft) and in RP-2 at 18.9 m (62 ft) appeared to be incongruous with the retention data set representing each depth interval. The assumed representative θ value was therefore taken from the same interval at which saturated hydraulic conductivity was measured. A more detailed discussion on this issue is taken up in Attachment 3.

Calculation Method Variations

As previously discussed, in-situ water content was measured in several cores within a sample depth interval, and the actual in-situ suction pressures in these depth intervals were fitted to develop a depth versus suction pressure function. To investigate the effect of altering the methodology, additional calculations of specific discharge were performed by directly calculating the local pressure head gradient at each sample depth. Calculating the pressure head gradient

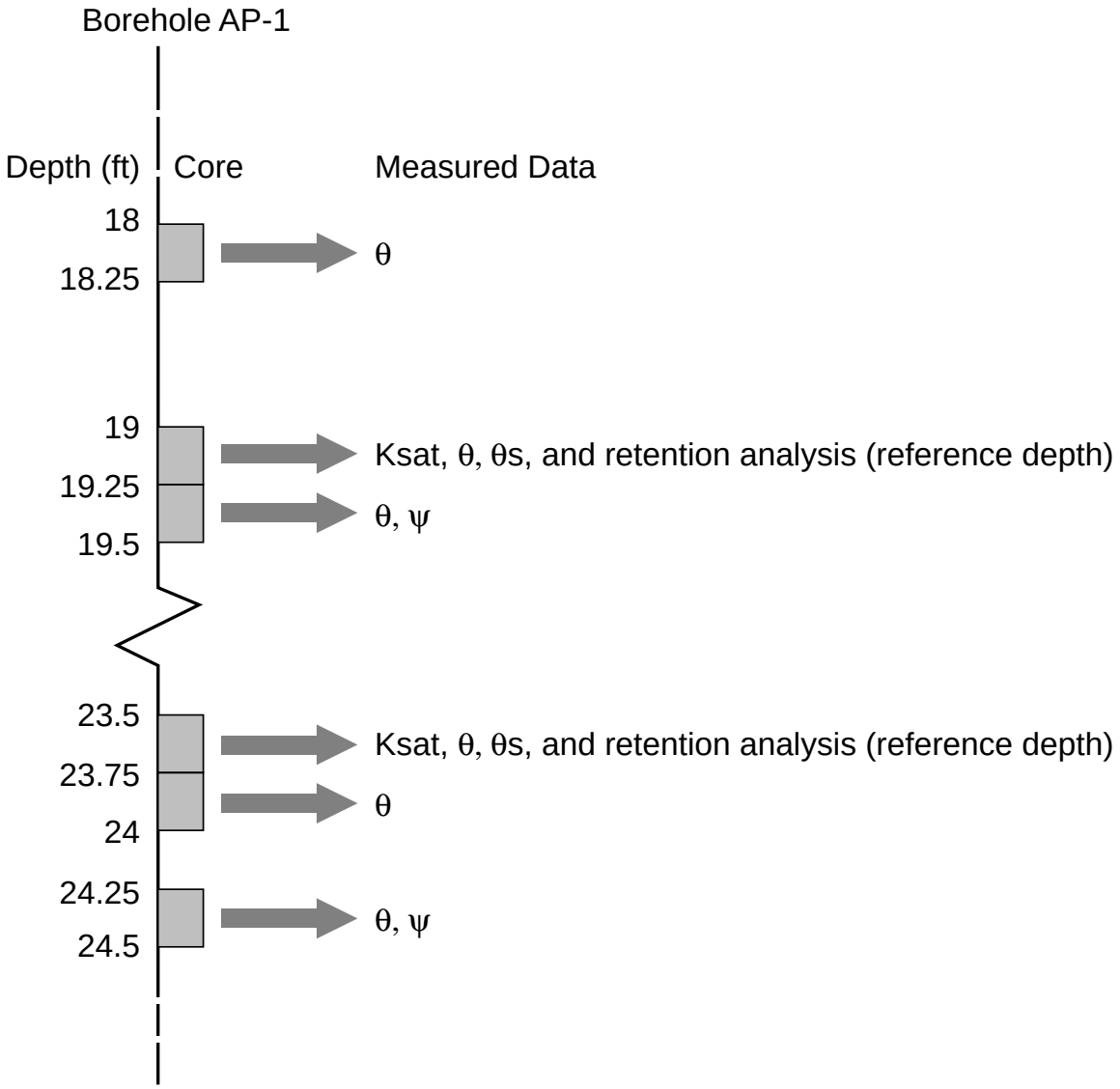

Figure D-12. Example of Origin of Available Measured Data within Boreholes (actual data are in Blout et al. [1995], Appendix D).

"directly" at a core was done by subtracting the nearest-neighbor suction pressure measurements and dividing by the distance between these measurements. The results, included in Attachment 4, show that when the pressure head gradient is calculated directly, downward flux occurs at several locations within the 3 m to 21 m depth interval in each borehole. However, no consistent downward trend is observed within or between boreholes and measurement error may play a part in these gradient reversals. The general shape and maximum value of the log transformed upward flux distribution are similar between the estimates produced with fitted or local pressure head gradients, but minimum upward values are higher when the pressure head gradients are directly calculated.

Representative Upward Specific Discharge Estimates

The estimates from this study can be used to develop a representative distribution of upward specific discharge that incorporates uncertainty in the effective value. The intent is to obtain a single effective specific discharge value from the specific discharge estimates consistent with the notion that the effective value is representative of the spatial average value in the soil overlying the waste at the scale of the GCD borehole.

The effective value of specific discharge was developed by creating a distribution that expresses uncertainty about the spatially averaged upward flux below the 10 m depth and over the area of the GCD model borehole under current conditions. This was done by a) using only those data below 10 m, b) Latin-Hypercube Sampling of parameters n, α, and θ_r while maintaining the correlation between them established by the RETC curve fit, c) calculating *q* at each reference depth from the sampled parameters and measured data, d) averaging all of the *q* values together to produce one single estimate of the spatial average of *q* for each sample realization, and e) creating a cumulative probability distribution over the sample realizations by assuming each average is an equally probable estimate of the effective value. To sample *n*, α, and θ_r, bounded normal distributions were used. The bounds for each of these parameters were based on the 95% confidence limits produced by the RETC program. The cumulative distribution of *q* produced by 1000 realizations is displayed in Figure D-13 and described in Table D-2.

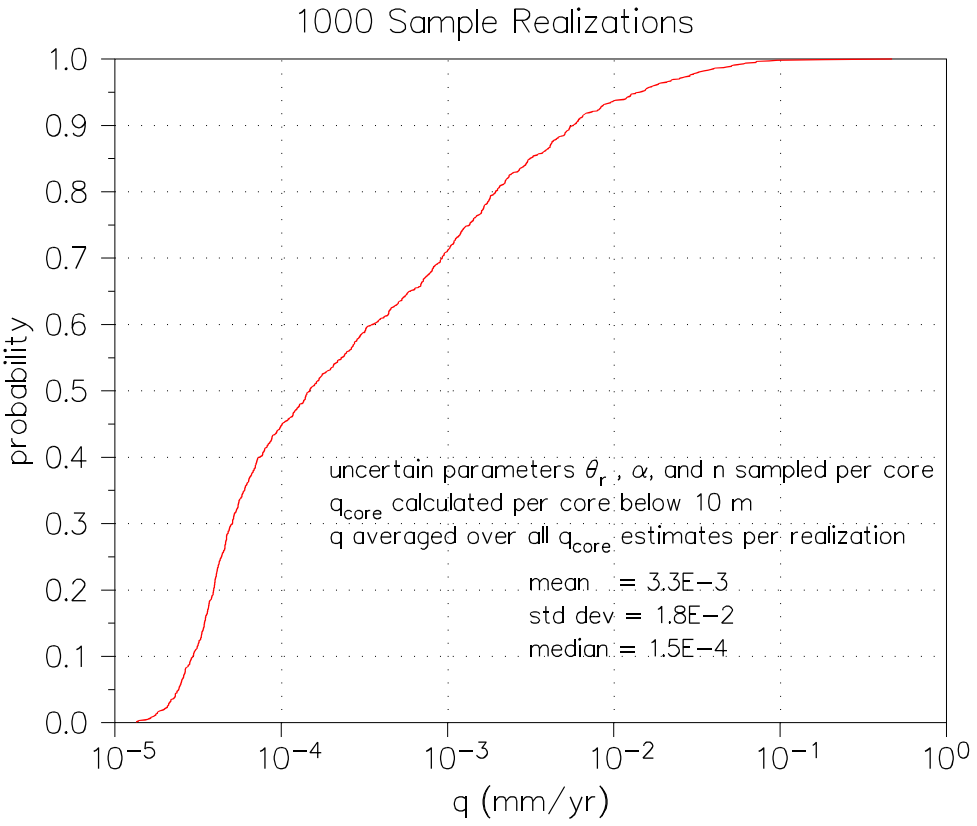

Figure D-13. Average Specific Discharge over GCD Borehole.

Table D-2. Average Upward Specific Discharge

Probability	Specific Discharge (mm/yr)
.05	2.4146E ! 005
.1	2.9386E ! 005
.15	3.4511E ! 005
.2	3.9167E ! 005
.25	4.3595E ! 005
.3	5.0734E ! 005
35	5.9809E ! 005
.4	7.4005E ! 005
.45	1.0116E ! 004
.5	1.4800E ! 004
.55	2.2917E ! 004
.6	3.5554E ! 004
.65	5.9689E ! 004
.7	9.2833E ! 004
.75	1.3450E ! 003
.8	1.9462E ! 003
.85	3.1349E ! 003
.9	5.7187E ! 003
.95	1.4217E ! 002

Conclusions

There is a large amount of uncertainty associated with estimating specific discharge in the vadose zone under such dry conditions. The calculations performed in this study suggest that the greatest uncertainty lies in the estimation of empirical parameters needed for the van Genuchten saturation model and Mualem hydraulic conductivity model. The curve-fitting method used to estimate these parameters results in wide confidence limits in most cases for the empirical parameter θ_r (and for some values of n) under the conditions of limited retention data points and high suction pressures, suggesting that the specific discharge estimates can be off by orders of magnitude. To develop any distribution for effective upward specific discharge, n and θ_r must be considered uncertain.

It was assumed that for the computational model, the use of suction pressure and water content values measured in the same core were more representative of the water retention characteristics of the soil at a particular depth interval than was the water content measured in a separate core with no associated suction pressure measurement. This assumption seemed to be confirmed (in all but two cases) by the placement of this water content-suction pressure point on the laboratory-derived water retention data curve from the neighboring core sample at each sample depth interval.

Upward specific discharge estimates with depth show two groupings, where higher values are below a depth of approximately 10 m (32.8 m) and lower flux estimates are above this depth. This zoning suggests that the drier, shallow region (below 2 m and above a depth of 10 m) is impacted by evaporation and plant root uptake to a much greater degree than the deeper region. Therefore the deeper region, below 10 m, is assumed to be more representative of the expected long-term steady upward specific discharge value.

Local pressure head gradients indicate either downward flow direction at some depth locations or significant measurement error. Fitting a function to the depth versus suction pressure data, as was done in this study, effectively ignores these local observations.

The specific discharge model shows that zero upward flux may be suggested directly in some calculations (see Attachment 2, AP-1 at 7.9 m (26 ft), for example), or is suggested indirectly by use of the upper confidence limit of the fitted parameter θ_r, which exceeds in-situ moisture content in most cores.

From this study, a suggested distribution for the effective upward specific discharge parameter can defined by the use of the data below a depth of 10 m, and latin-hypercube sampling of n, α, and θ_r within their respective confidence limits.

The recommended effective value of upward specific discharge based on this soil physics approach ranges from 1.3×10^{-15} to 4.7×10^{-11} mm/yr, with a mean of 3.3×10^{-13}, standard deviation of 1.8×10^{-12}, and a median value of 1.5×10^{-14} mm/yr.

References

Bechtel. 1998. "Estimation of Upward Advective Water Flux at the Greater Confinement Disposal Facility," work performed by Bechtel-Nevada under contract no. DE-AC08-96NV11718, submitted to Dept. Of Energy, Nevada Operations Office, September.

Blout, D.E., Birchfiel, W.S., Hammermeister, D.P., Zukosky, K.A., and K.D. Donnelson. 1995. "Site Characterization Data from the Area 5 Science Boreholes, Nevada Test Site, Nye County, Nevada," DOE/NV11432-170, February.

Mualem, Y. 1976. "A New Model for Predicting the Hydraulic Conductivity of Unsaturated Porous Media," Water Resources Research, 12:513-522.

van Genuchten, M.Th., Leij, F.J., and S.R. Yates. 1991. The RETC Code for Quantifying the Hydraulic Functions of Unsaturated Soils, Robert S. Kerr Environmental Research Laboratory, U.S. EPA, EPA/600/2-91/065, December.

Attachment 1. Curve-Fit Equations by Borehole for Depth $\mathbf{z}$ (m) vs Suction Pressure $\boldsymbol{\psi}$ (mH_20)

Fitted equation for Borehole AP-1: $\mathbf{z}(\boldsymbol{\psi}) = [4203407 - (3405.74\boldsymbol{\psi})] / [1 + (529.8\boldsymbol{\psi})]$

Slope of AP-1 equation = $d[\mathbf{z}(\boldsymbol{\psi})]/d\boldsymbol{\psi} = -2.23x10^{9} / (1 + 1.0596x10^{3}\boldsymbol{\psi} + 2.81x10^{5}\boldsymbol{\psi}^{2})$

Fitted equation for Borehole AP-2: $\mathbf{z}(\boldsymbol{\psi}) = [32473.14 - (29.55\boldsymbol{\psi})] / [1 + (4.6583\boldsymbol{\psi})]$

Slope of AP-2 equation = $d[\mathbf{z}(\boldsymbol{\psi})]/d\boldsymbol{\psi} = -1.513x10^{5} / (1 + 9.317\boldsymbol{\psi} + 21.7\boldsymbol{\psi}^{2})$

Fitted equation for Borehole RP-1: $\mathbf{z}(\boldsymbol{\psi}) = [5787235 - (2707.42\boldsymbol{\psi})] / (1 + 1069.876\boldsymbol{\psi})$

Slope of RP-1 equation = $d[\mathbf{z}(\boldsymbol{\psi})]/d\boldsymbol{\psi} = -6.1927x10^{9} / (1 + 2.14x10^{3}\boldsymbol{\psi} + 1.145x10^{6}\boldsymbol{\psi}^{2})$

Fitted equation for Borehole RP-2: $\mathbf{z}(\boldsymbol{\psi}) = [32.40 - (0.03\boldsymbol{\psi})]/ (1 + 1.5x10^{-3}\boldsymbol{\psi})$

Slope of RP-2 equation = $d[\mathbf{z}(\boldsymbol{\psi})]/d\boldsymbol{\psi} = -7.86x10^{-2} / (1 + 3x10^{-3}\boldsymbol{\psi} + 2.25x10^{-6}\boldsymbol{\psi}^{2})$

Attachment 2. Parameters for Calculations of Specific Discharge from Site-Specific Data

Borehole	Retention Analysis Sample Depth (ft)	Retention Analysis Sample Depth (m)	RETC-fitted residual water content	Measured saturated water content	Measured in-situ water content	Calculated effective saturation (Se)	Measured in-situ suction pressure (m)	Estimated pressure gradient (recip. of curve slope)	RETC-fitted Empirical constant (n)	Measured saturated hydraulic conductivity (cm/s)	Calculated unsaturated hydraulic conductivity (cm/s)	Specific Discharge (positive upward)
AP-1	19	5.79	0.042	0.37	0.057	4.6E-02	5.3E+02	-3.6E+01	1.37	7.6E-04	1.4E-15	1.6E-05
	24	7.32	0.044	0.34	0.050	2.0E-02	4.7E+02	-2.8E+01	1.43	1.1E-03	8.3E-17	7.1E-07
	26	7.92	0.061	0.40	0.050	-3.3E-02	6.0E+02	-4.5E+01	1.55	7.9E-04	ERR	ERR
	39	11.9	0.054	0.34	0.074	6.9E-02	3.9E+02	-1.9E+01	1.33	9.2E-04	6.9E-15	4.0E-05
	49	14.9	0.053	0.38	0.078	7.7E-02	3.8E+02	-1.8E+01	1.33	4.7E-04	8.4E-15	4.5E-05
	60	18.3	0.000	0.31	0.059	1.9E-01	3.6E+02	-1.6E+01	1.23	2.7E-04	7.5E-14	3.6E-04
AP-2	16	4.88	0.0093	0.33	0.037	8.5E-02	6.8E+02	-6.6E+01	1.27	6.9E-04	8.0E-16	1.7E-05
	19	5.79	0.037	0.36	0.064	8.3E-02	4.6E+02	-3.1E+01	1.25	3.5E-03	6.0E-16	6.1E-06
	21	6.40	0.046	0.25	0.061	7.2E-02	5.3E+02	-4.0E+01	1.41	2.0E-04	6.6E-14	8.5E-04
	24	7.32	0.048	0.33	0.046	-7.0E-03	5.5E+02	-4.3E+01	1.45	1.3E-03	ERR	ERR
	26	7.92	0.060	0.34	0.063	1.1E-02	4.3E+02	-2.7E+01	1.47	9.8E-04	5.3E-18	4.4E-08
	29	8.84	0.002	0.34	0.049	1.4E-01	4.5E+02	-2.9E+01	1.16	6.6E-03	2.0E-17	1.9E-07
	40	12.2	0.023	0.40	0.086	1.7E-01	3.8E+02	-2.1E+01	1.23	3.1E-04	2.3E-14	1.6E-04
	51	15.5	0.057	0.30	0.084	1.1E-01	2.8E+02	-1.1E+01	1.47	4.6E-04	1.6E-11	6.1E-02
	60	18.3	0.000	0.39	0.078	2.0E-01	3.4E+02	-1.6E+01	1.25	1.3E-04	2.2E-13	1.2E-03
RP-1	19	5.79	0.034	0.39	0.061	7.8E-02	6.4E+02	-7.5E+01	1.29	2.2E-03	4.2E-15	1.0E-04
	24	7.32	0.080	0.41	0.067	-3.9E-02	5.1E+02	-4.7E+01	1.71	1.5E-03	ERR	ERR
	31	9.45	0.058	0.39	0.055	-9.0E-03	4.3E+02	-3.5E+01	1.54	9.5E-04	ERR	ERR
	45	13.7	0.030	0.38	0.092	1.8E-01	3.2E+02	-1.9E+01	1.27	1.4E-04	2.3E-13	1.5E-03
*interpolated psi	60	18.3	0.061	0.36	0.13	2.4E-01	2.6E+02	-1.2E+01	1.2	4.0E-04	1.7E-13	7.1E-04
RP-2	10	3.05	0.032	0.39	0.051	5.2E-02	8.8E+02	-6.8E+01	1.33	2.3E-04	1.6E-16	3.4E-06
	15	4.57	0.035	0.34	0.051	5.3E-02	6.2E+02	-4.7E+01	1.33	3.8E-04	2.7E-16	4.2E-06
	19	5.79	0.043	0.33	0.061	6.2E-02	6.1E+02	-4.6E+01	1.37	9.3E-05	1.9E-15	2.9E-05
	30	9.14	0.000	0.37	0.061	1.6E-01	5.1E+02	-3.9E+01	1.18	2.5E-03	1.3E-15	1.6E-05
	45	13.7	0.000	0.33	0.096	2.9E-01	3.6E+02	-3.0E+01	1.13	4.1E-04	1.2E-15	1.2E-05
	62	18.9	0.065	0.35	0.078	4.6E-02	2.0E+02	-2.1E+01	1.53	5.6E-04	2.6E-13	1.8E-03

Attachment 3. Investigation into In-situ Water Content Data

In this study there was an issue as to which volumetric θ is most representative of the reference depth (depth of core sample at which water retention was analyzed). With the intent of maintaining the physical relationship between ψ and θ as much as possible, the general rule in this report was to use the θ measurement most closely associated with each ψ measurement (i.e., the ones observed in the same core). This assumption worked well with all but three depth intervals; the $\theta + \psi$ data points fit in with and were used to augment each water retention curve fit in these cases.

However, the general assumption for choosing a representative θ based on the location of ψ, as just described, did not hold at three locations: AP-2 at 18.3 m (60 ft), RP-1 at 18.3 m (60 ft), and RP-2 at 18.9 m (62 ft). In the case of RP-1, ψ was not available. For AP-2 and RP-2, the θ associated with ψ obviously did not fit in with the water retention analysis, and appeared to indicate local differences, or heterogeneity, between the core samples. For example, in borehole RP-2, θ was measured as 11.5 % at depth interval 19.13–19.2 m (62.75–63 ft), and 10.2 % at 18.4–18.52 m (60.5–60.75 ft). These values are consistent with values at approximately the same depth in the separate although closely located borehole RP-1, but are significantly higher than θ values measured less than one foot away, where θ = 8.7 % at depth interval 18.52–18.6 m (60.75–61 ft), and θ = 7.8 % at 18.82–18.9 m (61.75–62 ft) (Figure 3.1). The example of RP-2 at 18.9 m is of particular significance, because the use of the higher observed water contents results in a specific discharge estimate at this depth that is three orders of magnitude higher than observed within the vadose zone study region in the other boreholes or at any other location in borehole RP-2 down to the 90 ft core sample depth.

In the case of RP-2 at 18.9 m (62 ft), when high in-situ moisture content (and suction pressure) points are added to the water retention analysis results performed on the core at 18.82–18.9 m (61.75–62 ft), it is clear that they do not fit the overall theoretical trend of θ versus ψ (see Figure 3.2). The same observation is true for AP-2, but the difference is not as pronounced. Logs of RP-2 borehole cores and cuttings were inspected in this depth region to determine whether local grain size changes between these depths might explain the changes in water content (Blout et al., 1995, Appendix B). Cores with predominantly finer grain sizes would be expected to have the higher in-situ water contents and cores with coarser grain sizes would be associated with lower water contents in this region if lithology was causing these local differences. Review of the cuttings log, which contains information on predominant gravel and sand sizes, proved mainly inconclusive due to the wide depth range for which information is provided. The core logs indicate that the core taken from 19.13–19.2 m (62.75–63 ft), which had an in-situ θ value of 11.5 %, contained 5 to 10 % less gravel and slightly more sand than the cores with the 7.8 and 8.7 % in-situ θ.

It was concluded from these observations that the locally high θ measurements in RP-2 in the 18.9 m (62 ft) depth interval are valid, but they represent a θ versus ψ relationship that is possibly different from the other measured water contents in this depth interval and is likely different than the relationship indicated by water retention analysis performed at 18.82–18.9 m (61.75–62 ft). This difference is attributed to local heterogeneity between sample cores in this region. Therefore, when a poor fit was observed between the $\theta + \psi$ data point from one core and the water retention analysis results performed on a separate core, it was assumed that the moisture

content value measured in the core used for water retention analysis should be used as the in-situ water content. This was done for AP-2 at 18.3 m (60 ft), RP-1 at 18.3 m (60 ft), and RP-2 at 18.9 m (62 ft).

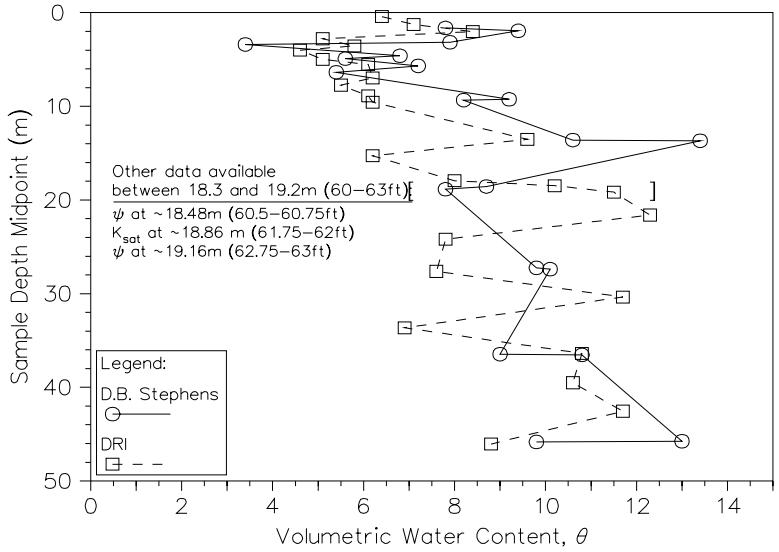

Figure 3.1. Water Contents in Borehole RP-2.

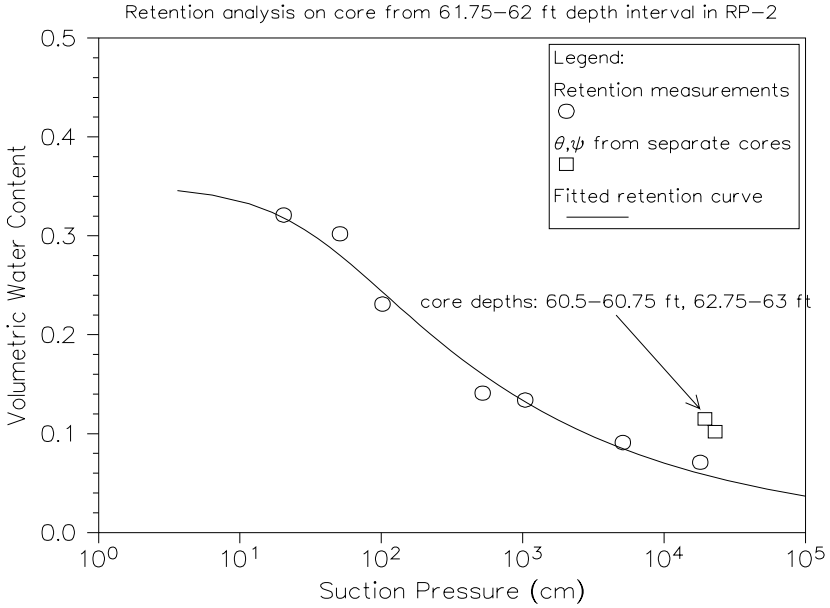

Figure 3.2. RP-2 Retention Data + Fitted Curve.

Attachment 4. Upward Specific Discharge Estimates - *using Local Pressure head gradient**

borehole	Upward Specific Discharge, **q** (mm/yr) mean	standard deviation	minimum	maximum	median	skewness	kurtosis
AP-1 (5 estimates)	5.9E-5	5.7E-5	1.1E-6	1.3E-4			
AP-2 (4 estimates)	3.9E-2	7.7E-2	3.1E-7	1.5E-1			
RP-1 (2 estimates)	1.3E-3	8.6E-4	6.5E-4	1.9E-3			
RP-2 (5 estimates)	5.3E-4	1.1E-3	6.6E-6	2.6E-3			
All boreholes	1.0E-2	3.8E-2	3.1E-7	1.5E-1	4.7E-5	4.0	16
All boreholes, log of **q**	-4.2	1.4	-6.5	-0.81	-4.3	-0.97	0.94

* The “local pressure head gradient” at each sample interval is the difference between nearest neighbor measured suction pressures divided by the distance between them.

This page intentionally left blank.

Appendix E

Root Length Data and Analyses

This page intentionally left blank.

E.1 Species Variability in Maximum Root Length

The plant root length data in Table E-1 have been grouped by lifeform for modeling the current and future plant communities and analyzing the root length data. The data analysis is based on the assumption that the set of measurements within each lifeform are representative of the measurements that would be made of plants in that lifeform at the GCD site. The measurements may be representative in at least two ways. First, they may approximate a random sample of plants at the site and, therefore, include the same plant species in the same proportions as would occur at the site. Second, the measurements for any particular species in a lifeform may have the same distribution as the measurements for any other species in the same lifeform. In this case, the particular species that are measured to characterize the lifeform need not represent the species that would occur at the site because variations among species are practically irrelevant.

Average maximum root lengths, as well as other data descriptors, are given in Table E-2. For each lifeform, the basic statistical parameters were found to be nearly identical for the data sets for current and future species. The data sets of maximum root length for current and future conditions were tested for differences with a Mann-Whitney U test. Strictly speaking, the assumption of independence required for the Mann-Whitney test is violated. The samples representing current and future conditions are not independent because the samples representing future conditions contain the same species as are currently found at the site. The relevant question for the test is whether the influence of the added species is sufficient to warrant defining a separate distribution for future conditions. This decision cannot be based on the added species alone, although such a comparison would satisfy the assumption of independence. The fact that future communities would include the same species, and simply the same "types" of species, as the current community is an important consideration in evaluating the need for separate current and future distributions. The Mann-Whitney test is therefore used as an indication of similarity in forming judgement about the value of defining separate distributions, but its results were not intended to provide proof at some specified level of significance. In no test were statistically significant differences detected (Table E-2). Thus, there appears to be no compelling reason to separate the root length data of current and future species of a lifeform.

Certain features of the data sets are consistent with assumptions being made about the various lifeform groups. First, the relative size and longevity of the lifeforms should be mirrored in the average maximum root length for each lifeform. Size and length of lifetime for the lifeforms can be ordered as follows: annuals < perennials < shrubs < trees. The average maximum root lengths follow this pattern, with annuals having the shortest average maximum root length (39 cm) and trees having the largest average maximum root length (436 cm). Second, the measured maximum root lengths follow this pattern, with annuals having the shortest (162 cm) and trees with the longest at 3,000 cm.

Table E-1. Root Length Data

Item[a]	Species	Length, cm	Root Type[b]	Lifeform[c]	Lifeform Grouping[c]
Annuals					
72	*Amsinckia rugosa*	120	t	a	a
14	*Amsinckia spectabilis*	13	t	a	a
15	*Astragalus nuttallianus*	13	t	a	a
615	*Avena sativa*	162	t	g	a
56	*Bromus tectorum*	30	t	g	a
77	*Calyptridium umbellatum*	120	t	a	a
21	*Erodium cicutarium*	2	l	a	a
9	*Kallstroemia grandiflora*	22	t	a	a
9	*Kallstroemia grandiflora*	21	l	a	a
26	*Linanthus bigelovii*	10	t	a	a
29	*Mentzelia albicaulis*	11	t	a	a
805	*Mentzelia albicaulis*	12	t	a	a
10	*Pectis prostrata*	13	t	a	a
33	*Phacelia tanacetifolia*	18	t	a	a
33	*Phacelia tanacetifolia*	6	l	a	a
34	*Plantago insularis*	13	t	a	a
35	*Rafinesquia neomexicana*	5	l	a	a
1	*Amaranthus palmeri*	10	t	a	a
1	*Amaranthus palmeri*	25	l	a	a
3	*Aster tanacetifolius*	15	t	a	a
3	*Aster tanacetifolius*	6	l	a	a
73	*Collomia linearis*	120	t	a	a
74	*Gayophytum diffusum*	120	t	a	a
Perennials					
837	*Ambrosia (Franseria) deltoidea*	38	t	p	p
838	*Ambrosia (Franseria) deltoidea*	18	t	p	p
839	*Ambrosia (Franseria) deltoidea*	180	t	p	p
839	*Ambrosia (Franseria) deltoidea*	140	l	p	p
238	*Ambrosia (Franseria) psilostachya*	183	t	p	p
356	*Anemone zephyra*	15	t	p	p
356	*Anemone zephyra*	18	l	p	p
603	*Aristida purpurea*	122	t	g	p
603	*Aristida purpurea*	18	l	g	p
266	*Astragalus arrectus*	183	t	p	p
266	*Astragalus arrectus*	61	l	p	p
409	*Astragalus arrectus*	178	t	p	p
788	*Astragalus cobrensis*	183	t	p	p
	Astragalus goniatus	60	t	p	p

Table E-1. Root Length Data (Continued)

Item[a]	Species	Length, cm	Root Type[b]	Lifeform[c]	Lifeform Grouping[c]
	Astragalus spp.	120	t	p	p
	Ceratoides (Eurotia) lanata	180	t	p	p
381	*Cryptantha flava*	91	t	p	p
619	*Curcurbita foetidissima*	122	t	p	p
373	*Eriogonum alatum*	64	t	p	p
373	*Eriogonum alatum*	81	l	p	p
349	*Eriogonum flavum*	91	t	p	p
64	*Eriogonum heracleoides*	235	t	p	p
803	*Eriogonum spp.*	122	t	p	p
374	*Eriogonum subalpinum*	104	t	p	p
374	*Eriogonum subalpinum*	122	l	p	p
804	*Euphorbia spp.*	6	t	p	p
840	*Krameria canescens*	18	t	p	p
787	*Lepidium montanum*	30	t	p	p
197	*Muhlenbergia montana*	81	t	p	p
197	*Muhlenbergia montana*	17	l	p	p
822	*Muhlenbergia montana*	85	t	p	p
822	*Muhlenbergia montana*	52	l	p	p
827	*Muhlenbergia montana*	104	t	p	p
827	*Muhlenbergia montana*	122	l	p	p
834	*Muhlenbergia montana*	82	t	p	p
834	*Muhlenbergia montana*	40	l	p	p
195	*Muhlenbergia montana*	23	t	p	p
195	*Muhlenbergia torreyi*	127	t	p	p
394	*Oenothera coronopifolia*	152	t	p	p
807	*Oenothera spp.*	137	t	p	p
807	*Oenothera spp.*	137	l	p	p
387	*Oenothera strigosa*	53	t	p	p
387	*Oenothera strigosa*	76	l	p	p
841	*Opuntia arbuscula*	2	t	p	p
841	*Opuntia arbuscula*	300	l	p	p
39	*Opuntia engelmanii*	25	t	p	p
40	*Opuntia engelmanii*	15	t	p	p
40	*Opuntia engelmanii*	50	l	p	p
41	*Opuntia leptocaulis*	15	t	p	p
41	*Opuntia leptocaulis*	10	l	p	p
42	*Opuntia leptocaulis*	8	t	p	p
42	*Opuntia leptocaulis*	61	l	p	p
43	*Opuntia versicolor*	30	t	p	p
44	*Opuntia versicolor*	25	t	p	p

Table E-1. Root Length Data (Continued)

Item[a]	Species	Length, cm	Root Type[b]	Lifeform[c]	Lifeform Grouping[c]
786	*Oryzopsis hymenoides*	122	t	g	p
60	*Penstemon glabra*	160	t	p	p
60	*Penstemon glabra*	60	l	p	p
359	*Penstemon glaucus*	36	t	p	p
359	*Penstemon glaucus*	91	l	p	p
388	*Penstemon unilateralis*	53	t	p	p
611	*Psoralea spp.*	213	t	p	p
609	*Psoralea tenuiflora*	274	t	p	p
11	*Solanum elaeagniflolium*	15	t	p	p
395	*Solidago decumbens*	107	t	p	p
	Sphaeralcea coccinea	180	t	p	p
810	*Sphaeralcea spp.*	229	t	p	p
755	*Sporobolus airoides*	457	t	g	p
756	*Sporobolus airoides*	823	t	g	p
736	*Stipa comata*	152	t	g	p
801	*Stipa comata*	168	t	g	p
	Stipa comata	107	t	g	p
	Stipa comata	63	t	g	p
	Stipa comata	99	t	g	p
	Stipa comata	110	t	g	p
	Stipa comata	85	t	g	p
55	*Stipa lettermani*	80	t	g	p
468	*Stipa richardsonii*	183	t	g	p
122	*Stipa spartea*	66	t	g	p
122	*Stipa spartea*	30	l	g	p
	Stipa spartea	80	t	g	p
	Stipa spartea	102	t	g	p
	Stipa spartea	68	t	g	p
	Stipa spartea	85	t	g	p
	Stipa spartea	105	t	g	p
	Stipa spartea	60	t	g	p
	Stipa spartea	127	t	g	p
57	*Achillea lanulosa*	14	t	p	p
57	*Achillea lanulosa*	60	l	p	p
390	*Achillea millefolium*	64	t	p	p
391	*Achillea millefolium*	23	t	p	p
460	*Achillea millefolium*	30	t	p	p
472	*Achillea millefolium*	183	t	p	p
51	*Agropyron inerme*	10	t	g	p
262	*Agropyron inerme*	152	t	g	p

Table E-1. Root Length Data (Continued)

Item[a]	Species	Length, cm	Root Type[b]	Lifeform[c]	Lifeform Grouping[c]
261	*Agropyron spicatum*	152	t	g	p
542	*Agropyron spicatum*	183	t	g	p
399	*Allium cernuum*	15	t	p	p
761	*Anemopsis californica*	122	t	p	p
207	*Antennaria parvifolia*	36	t	p	p
207	*Antennaria parvifolia*	13	l	p	p
208	*Antennaria parvifolia*	36	t	p	p
208	*Antennaria parvifolia*	27	l	p	p
209	*Antennaria parvifolia*	48	t	p	p
209	*Antennaria parvifolia*	15	l	p	p
462	*Antennaria spp.*	152	t	p	p
474	*Antennaria spp.*	91	t	p	p
341	*Antennaria umbrinella*	20	t	p	p
367	*Arenaria fendleri*	117	t	p	p
367	*Arenaria fendleri*	61	l	p	p
368	*Arenaria fendleri*	38	t	p	p
403	*Arenaria sajanensis*	76	t	p	p
458	*Arnica cordifolia*	61	t	p	p
369	*Arnica cordifolia*	142	t	p	p
204	*Artemesia frigida*	94	t	p	p
204	*Artemesia frigida*	16	l	p	p
205	*Artemesia frigida*	97	t	p	p
205	*Artemesia frigida*	22	l	p	p
206	*Artemesia frigida*	97	t	p	p
206	*Artemesia frigida*	22	l	p	p
384	*Artemesia frigida*	46	t	p	p
384	*Artemesia frigida*	91	l	p	p
385	*Artemesia frigida*	183	t	p	p
392	*Aster commutatus*	36	t	p	p
66	*Balsamorhiza sagittata*	270	t	p	p
267	*Balsamorhiza sagittata*	274	t	p	p
267	*Balsamorhiza sagittata*	91	l	p	p
107	*Bouteloua gracilis*	45	t	g	p
201	*Bouteloua gracilis*	102	t	g	p
201	*Bouteloua gracilis*	24	l	g	p
202	*Bouteloua gracilis*	109	t	g	p
202	*Bouteloua gracilis*	19	l	g	p
203	*Bouteloua gracilis*	84	t	g	p
203	*Bouteloua gracilis*	18	l	g	p
602	*Bouteloua gracilis*	98	t	g	p

Table E-1. Root Length Data (Continued)

Item[a]	Species	Length, cm	Root Type[b]	Lifeform[c]	Lifeform Grouping[c]
861	*Bouteloua gracilis*	122	t	g	p
861	*Bouteloua gracilis*	46	l	g	p
400	*Calochortus gunnisoni*	13	t	p	p
456	*Carex geyeri*	122	t	se	p
469	*Carex geyeri*	183	t	se	p
52	*Carex geyeri*	160	t	se	p
346	*Castilleja brachyantha*	30	t	p	p
386	*Castilleja linariaefolia*	25	t	p	p
386	*Castilleja linariaefolia*	61	l	p	p
68	*Clematis hirsutissima*	140	t	p	p
753	*Distichlis spicata*	234	t	se	p
851	*Elymus canadensis*	266	t	g	p
752	*Elymus condensatus*	366	t	g	p
370	*Epilobium angustifolium*	107	t	p	p
371	*Epilobium angustifolium*	122	t	p	p
461	*Galium boreale*	152	t	p	p
471	*Galium boreale*	183	t	p	p
270	*Haplopappus racemosus*	335	t	p	p
270	*Haplopappus racemosus*	61	l	p	p
350	*Heuchera bracteata*	41	t	p	p
271	*Heuchera glabella*	183	t	p	p
271	*Heuchera glabella*	30	l	p	p
789	*Hymenoxys acaulis*	24	t	p	p
123	*Koeleria cristata*	71	t	g	p
315	*Lithospermum caroliniense*	213	t	p	p
67	*Lithospermum ruderale*	300	t	p	p
272	*Lithospermum ruderale*	183	t	p	p
272	*Lithospermum ruderale*	70	l	p	p
273	*Lupinus leucophyllus*	168	t	p	p
273	*Lupinus leucophyllus*	91	l	p	p
408	*Lupinus leucophyllus*	168	t	p	p
274	*Lupinus obtusilobis*	335	t	p	p
274	*Lupinus obtusilobis*	122	l	p	p
407	*Lupinus obtusilobis*	335	t	p	p
65	*Lupinus spp.*	240	t	p	p
612	*Lygodesmia juncea*	213	t	p	p
345	*Phacelia sericia*	23	t	p	p
382	*Phacelia splendens*	122	t	p	p
347	*Phlox caespitosa*	23	t	p	p
347	*Phlox caespitosa*	81	l	p	p

Table E-1. Root Length Data (Continued)

Item[a]	Species	Length, cm	Root Type[b]	Lifeform[c]	Lifeform Grouping[c]
62	*Phlox longifolia*	75	t	p	p
54	*Poa secunda*	35	t	g	p
260	*Poa secunda*	61	t	g	p
406	*Potentilla diversifolia*	61	t	p	p
63	*Potentilla gracilis*	75	t	p	p
275	*Potentilla gracilis*	229	t	p	p
275	*Potentilla gracilis*	30	l	p	p
383	*Potentilla gracilis*	107	t	p	p
809	*Senecio spp.*	91	t	p	p
351	*Senecio taraxaciodes*	30	t	p	p
348	*Silene acaulis*	15	t	p	p
76	*Silene spp.*	120	t	p	p
340	*Stellaria crassifolia*	15	t	p	p
760	*Suaeda spp.*	213	t	p	p
344	*Trifolium dasyphyllum*	30	t	p	p
597	*Trifolium hybridum*	61	t	p	p
595	*Trifolium pratense*	173	t	p	p
596	*Trifolium pratense*	145	t	p	p
401	*Zygadenus elegans*	13	t	p	p
SHRUBS					
	Artemesia cana	240	t	s	s
790	*Artemesia spinescens*	152	t	s	s
180	*Artemesia tridentata*	213	t	s	s
181	*Artemesia tridentata*	160	t	s	s
181	*Artemesia tridentata*	152	l	s	s
182	*Artemesia tridentata*	183	t	s	s
182	*Artemesia tridentata*	152	l	s	s
183	*Artemesia tridentata*	183	t	s	s
183	*Artemesia tridentata*	122	l	s	s
184	*Artemesia tridentata*	168	t	s	s
184	*Artemesia tridentata*	122	l	s	s
818	*Artemesia tridentata*	914	t	s	s
	Artemesia tridentata	150	t	s	s
	Artemesia tridentata	110	t	s	s
765	*Atriplex canescens*	305	t	s	s
	Atriplex canescens	80	t	s	s
	Atriplex canescens	110	t	s	s
794	*Atriplex confertifolia*	152	t	s	s
	Atriplex nuttallii	180	t	s	s
767	*Atriplex torreyi*	274	t	s	s

Table E-1. Root Length Data (Continued)

Item[a]	Species	Length, cm	Root Type[b]	Lifeform[c]	Lifeform Grouping[c]
819	*Chrysothamnus nauseosus*	457	t	s	s
	Chrysothamnus nauseosus	180	t	s	s
	Chrysothamnus nauseosus	100	t	s	s
	Chrysothamnus nauseosus	300	t	s	s
38	*Encelia farinosa*	55	t	s	s
38	*Encelia farinosa*	60	l	s	s
792	*Ephedra viridis*	549	t	s	s
78	*Haplopappus lanuginosus*	200	t	s	s
328	*Haplopappus tenuisectus*	549	t	s	s
328	*Haplopappus tenuisectus*	122	l	s	s
764	*Hymenoclea monogyra*	305	t	s	s
47	*Larrea tridentata*	35	t	s	s
47	*Larrea tridentata*	300	l	s	s
48	*Larrea tridentata*	107	t	s	s
48	*Larrea tridentata*	210	l	s	s
763	*Pluchea sericea*	762	t	s	s
424	*Salvia apiana*	152	t	s	s
795	*Sarcobatus vermiculatus*	579	t	s	s
426	*Yucca whiplei*	76	t	s	s
412	*Arctostaphylos*	274	t	s	s
412	*Arctostaphylos*	76	l	s	s
854	*Arctostaphylos glandulosa*	518	t	s	s
816	*Arctostaphylos glauca*	259	t	s	s
833	*Arctostaphylos uva-ursi*	61	t	s	s
465	*Arctostaphylos uva-ursi*	91	t	s	s
477	*Arctostaphylos uva-ursi*	183	t	s	s
464	*Berberis repens*	183	t	s	s
476	*Berberis repens*	183	t	s	s
459	*Ceanothus crassifolius*	137	t	s	s
413	*Ceanothus leucodermis*	366	t	s	s
855	*Ceanothus leucodermis*	366	t	s	s
419	*Ceanothus oliganthus*	183	t	s	s
814	*Ceanothus spp.*	366	t	s	s
856	*Eriodictyon spp.*	137	t	s	s
856	*Eriodictyon spp.*	91	l	s	s
422	*Eriogonum fasciculatum*	122	t	s	s
799	*Gutierrezia divaricata*	244	t	s	s
176	*Gutierrezia sarothrae*	213	t	s	s
176	*Gutierrezia sarothrae*	61	l	s	s
605	*Gutierrezia sarothrae*	198	t	s	s

Table E-1. Root Length Data (Continued)

Item[a]	Species	Length, cm	Root Type[b]	Lifeform[c]	Lifeform Grouping[c]
279	*Rosa sufflata*	640	t	s	s
467	*Rosa woodsii*	91	t	s	s
479	*Rosa woodsii*	183	t	s	s
475	*Symphoricarpos albus*	183	t	s	s
463	*Symphoricarpos albus*	152	t	s	s
817	*Symphoricarpos spp.*	183	t	s	s
TREES					
696	*Acer rubrum*	2500	t	t	t
784	*Acer saccharinum*	91	t	t	t
784	*Acer saccharinum*	91	l	t	t
223	*Acer sp.*	2438	l	t	t
796	*Amelanchier utahensis*	640	t	t	t
420	*Cercocarpus betuloides*	152	t	t	t
	Cercocarpus montanus	50	t	t	t
	Cercocarpus montanus	40	t	t	t
823	*Cercocarpus montanus*	152	t	t	t
823	*Cercocarpus montanus*	244	l	t	t
828	*Cercocarpus montanus*	152	t	t	t
828	*Cercocarpus montanus*	305	l	t	t
835	*Cercocarpus montanus*	107	t	t	t
835	*Cercocarpus montanus*	152	l	t	t
797	*Cowania stansburiana*	152	t	t	t
798	*Fraxinus anomala*	305	t	t	t
791	*Juniperus monosperma*	579	t	t	t
	Juniperus monosperma	170	t	t	t
	Juniperus monosperma	600	t	t	t
820	*Pinus contorta*	122	t	t	t
820	*Pinus contorta*	488	l	t	t
	Pinus edulis	110	t	t	t
	Pinus edulis	130	t	t	t
	Pinus edulis	600	t	t	t
	Pinus edulis	300	t	t	t
	Pinus edulis	640	t	t	t
811	*Pinus ponderosa*	2438	t	t	t
826	*Pinus ponderosa*	171	t	t	t
826	*Pinus ponderosa*	610	l	t	t
832	*Pinus ponderosa*	85	t	t	t

Table E-1. Root Length Data (Continued)

Item[a]	Species	Length, cm	Root Type[b]	Lifeform[c]	Lifeform Grouping[c]
832	*Pinus ponderosa*	579	l	t	t
	Pinus ponderosa	160	t	t	t
	Pinus ponderosa	150	t	t	t
	Pinus ponderosa	200	t	t	t
776	*Populus fremontii*	610	t	t	t
831	*Populus tremuloides*	73	t	t	t
831	*Populus tremuloides*	610	l	t	t
771	*Prosopis spp.*	792	t	t	t
687	*Prunus persica*	272	t	t	t
687	*Prunus persica*	305	l	t	t
688	*Prunus persica*	152	t	t	t
688	*Prunus persica*	457	l	t	t
415	*Quercus chrysolepis*	732	t	t	t
416	*Quercus dumosa*	244	t	t	t
417	*Quercus dumosa*	853	t	t	t
793	*Quercus gambelii*	396	t	t	t
	Quercus gambelii	200	l	t	t
779	*Quercus lobata*	610	t	t	t
427	*Quercus macrocarpa*	335	t	t	t
785	*Quercus macrocarpa*	457	t	t	t
782	*Quercus maxima*	152	t	t	t
782	*Quercus maxima*	274	l	t	t
813	*Quercus spp.*	853	t	t	t
	Quercus spp.	320	t	t	t
	Quercus spp.	150	t	t	t
	Quercus spp.	175	t	t	t
	Quercus spp.	80	t	t	t
335	*Salix nivalis*	20	t	t	t
812	*Salix spp.*	366	t	t	t
694	*Tamarix spp.*	3000	t	t	t

[a] item number from original database, if available.
[b] l = lateral root; t = vertical root.
[c] a = annual; g = grass; p = perennial; s = shrub; se = sedge; t = tree.

Table E-2. Statistical Parameters for Maximum Root Length Data Sets (in cm)

Parameter	Annual	Perennial	Shrub	Tree
n	23	196	67	59
mean	39	106	227	436
median	13	85	183	272
stdev	49	95	172	566
min	2	2	35	20
max	162	823	914	3,000
Mann-Whitney U test p-value[a]	0.83	0.82	0.86	not performed

[a]Significance determined at a p-value # 0.05. All values greater than 0.05 are non-significant.

This page intentionally left blank.

Appendix F

Concentration Ratio Data and Analyses

This page intentionally left blank.

F.1 Discussion

The concentration ratio data show considerable variability in concentration ratio values from element to element (Table F-1). Particularly striking is that, within a data set, there can be values several orders of magnitude apart. For some elements, this variability is most likely a statistical consequence of the small size of the data set. While larger data sets might have enough data points to indicate that very high concentration ratio values are outliers that do not conform to assumptions of lognormality, this cannot be determined reliably for small data sets. Lacking a statistical basis to exclude high values from the analysis for these small data sets, all data were included. This is also a more conservative approach, as excluding high end "deviations" would skew the distributions to smaller values. Lognormal distribution test results are provided in Tables F-2 and F-3.

Nonuniform distributions of radionuclides in the soil also contribute to the tremendous variability in concentration ratio data. As Kinnear et al. [1981] discovered, concentration ratio values can range more than an order of magnitude with even the most careful attempt to obtain a uniform soil mixture. This nonuniformity is compounded by a number of other factors in the field, producing large ranges like those found here. To some degree, including all concentration ratio values that fit the qualifying criteria shows that, though the distribution of radionuclides in the soil is modeled as uniform, it really is not. As a result, the concentration ratio values used here incorporate actual variability in uptake by mirroring in-situ conditions.

While there should be reasonable explanations for concentration ratio variability, there is, unfortunately, often very little supporting documentation within a given study to provide such explanations or determine which factors might be influencing the variability in concentration ratio values. Lacking the necessary information to rigorously evaluate such variability, the approach being taken is that variability is an inherent feature of concentration ratio data, reflected in the data sets compiled to predict concentration ratio values.

Data specificity, due to detailed screening criteria, serves to lower the variability within a given data set [Sheppard and Evenden, 1997]. In a study of concentration ratio distributions by Sheppard and Evenden [1997], the broadest, fully generic data sets for elements have geometric standard deviations (GSDs) that range from 2.4 to 16. The narrowest data sets of site- and species-specific data have GSDs that range from 1.1 to 3.7. For the data sets compiled here, the variability within each data set, as measured by the GSD, never exceeds 1.34 (Table F-4). Thus, all data sets are well within the range of variability observed by Sheppard and Evenden [1997]. One conclusion is that, even though the absolute values of uptake for native species may seem high—often exceeding those found for agricultural species—the actual variability within the data sets is not excessive.

Concentration ratio values for native plants are not necessarily suspect simply because they may exceed those for agricultural species. In fact, efforts to remediate contaminated soil by plants within the southwest often capitalize on the ability of native plants to bioaccumulate (via high uptake rates) soil contaminants, especially metals. The next section provides a more detailed comparison of native and agricultural plant concentration ratio values.

Table F-1. Plant Concentration Ratio Data[a]

Radionuclide	Concentration Ratio	Community[b]	Citation[c]
Am	6.00E!05	c	1
Am	8.00E!05	c	1
Am	1.00E!04	c	1
Am	2.30E!04	c	1
Am	6.00E!04	c	1
Am	6.00E!04	c	1
Am	1.40E!03	c	1
Am	1.40E!03	c	1
Am	1.50E!03	c	1
Am	1.50E!03	c	1
Am	2.10E!03	c	1
Am	1.70E!02	c	1
Cs	5.36E!02	c	2
Pa	7.00E!03	c	1
Pa	1.10E!02	c	1
Pa	1.20E!02	c	1
Pa	1.30E!02	c	1
Pa	1.30E!02	c	1
Pa	1.50E!02	c	1
Pa	1.10E!01	c	1
Pa	1.12E!01	c	1
Pa	2.30E!01	c	1
Pa	2.40E!01	c	1
Pa	2.80E!01	c	1
Pa	2.80E!01	c	1
Pb	1.42E!03	c	3
Pb	5.67E!03	c	3
Pb	8.00E!03	c	4
Pb	9.20E!03	c	3
Pb	9.93E!03	c	3
Pb	1.00E!02	c	5
Pb	2.20E!02	c	5
Pb	1.10E!01	c	4
Pb	1.12E!01	c	3
Pb	1.20E!01	c	4
Pb	1.30E!01	c	4
Pb	1.42E!01	c	3
Pb	2.90E!01	c	4
Pb	5.00E!01	c	4
Pb	6.30E!01	c	4

Table F-1. Plant Concentration Ratio Data[a] (Continued)

Radionuclide	Concentration Ratio	Community[b]	Citation[c]
Pb	6.60E ! 01	c	4
Pb	8.79E ! 01	c	3
Pb	8.80E ! 01	c	4
Pb	9.50E ! 01	c	4
Pb	9.90E ! 01	c	4
Pu	1.40E ! 05	c	1
Pu	1.70E ! 05	c	1
Pu	1.70E ! 05	c	1
Pu	4.30E ! 05	c	1
Pu	4.60E ! 05	c	1
Pu	4.60E ! 05	c	1
Pu	4.80E ! 05	c	1
Pu	5.10E ! 05	c	1
Pu	5.30E ! 05	c	1
Pu	2.54E ! 04	c	1
Pu	2.73E ! 04	c	1
Pu	3.10E ! 04	c	1
Pu	8.60E ! 04	c	2
Ra	4.73E ! 03	c	3
Ra	1.53E ! 02	c	3
Ra	1.96E ! 02	c	3
Ra	2.52E ! 02	c	6
Ra	3.40E ! 02	c	5
Ra	3.74E ! 02	c	6
Ra	4.08E ! 02	c	3
Ra	4.09E ! 02	c	6
Ra	4.10E ! 02	c	5
Ra	4.89E ! 02	c	3
Ra	4.90E ! 02	c	5
Ra	5.61E ! 02	c	6
Ra	7.83E ! 02	c	3
Ra	1.03E ! 01	c	6
Ra	1.25E ! 01	c	6
Ra	1.29E ! 01	c	6
Ra	1.36E ! 01	c	6
Ra	1.40E ! 01	c	6
Ra	1.58E ! 01	c	6
Ra	2.08E ! 01	c	6
Ra	2.19E ! 01	c	6
Ra	2.19E ! 01	c	6

Table F-1. Plant Concentration Ratio Data[a] (Continued)

Radionuclide	Concentration Ratio	Community[b]	Citation[c]
Ra	2.70E!01	c	6
Ra	2.85E!01	c	6
Ra	3.10E!01	c	6
Ra	3.38E!01	c	6
Ra	3.90E!01	c	6
Ra	4.50E!01	c	5
Ra	4.80E!01	c	6
Ra	7.40E!01	c	5
Sr	4.18E+00	c	7
Sr	6.16E+01	c	7
Th	1.23E!02	c	8
Th	2.00E!02	c	9
Th	2.66E!02	c	8
Th	3.57E!02	c	8
Th	4.32E!02	c	8
Th	5.37E!02	c	8
Th	6.15E!02	c	8
Th	6.60E!02	c	8
Th	8.00E!02	c	9
Th	1.72E!01	c	8
Th	1.78E!01	c	8
Th	1.94E!01	c	8
Th	2.25E!01	c	8
Th	3.26E!01	c	8
Th	3.30E!01	c	9
Th	3.80E!01	c	8
Th	4.10E!01	c	9
Th	4.60E!01	c	9
Th	6.94E!01	c	8
Th	1.89E+00	c	8
Th	1.90E+00	c	9
Th	2.88E+00	c	8
Th	1.10E+01	c	9
Th	1.10E+01	c	9
U	4.27E!03	c	2
U	5.28E!03	c	3
U	7.95E!03	c	3
U	8.52E!03	c	3
U	9.66E!03	c	3
U	9.66E!03	c	3

Table F-1. Plant Concentration Ratio Data[a] (Continued)

Radionuclide	Concentration Ratio	Community[b]	Citation[c]
U	1.70E!02	c	3
U	3.94E!02	c	8
U	4.80E!02	c	8
U	6.00E!02	c	9
U	7.00E!02	c	9
U	7.44E!02	c	8
U	8.80E!02	c	8
U	2.30E!01	c	8
U	2.50E!01	c	7
U	2.70E!01	c	9
U	2.84E!01	c	7
U	2.90E!01	c	9
U	3.19E!01	c	8
U	3.30E!01	c	9
U	3.90E!01	c	9
U	8.09E!01	c	8
U	1.50E+00	c	9
U	1.90E+00	c	9
Am	5.00E!05	f	10
Am	4.80E!04	f	10
Cs	1.20E!02	f	11
Cs	1.31E!01	f	11
Cs	2.83E!01	f	11
Cs	2.95E!01	f	11
Cs	3.59E!01	f	11
Cs	4.00E!01	f	11
Cs	4.34E!01	f	11
Cs	4.41E!01	f	11
Cs	6.56E!01	f	11
Cs	7.62E!01	f	11
Cs	1.07E+00	f	11
Cs	1.29E+00	f	11
Pb	1.64E!01	f	12
Pb	2.51E!01	f	12
Pb	2.84E!01	f	12
Pb	3.66E!01	f	12
Pb	5.46E!01	f	12
Pb	3.04E+00	f	13
Pu	8.00E!06	f	10
Pu	5.20E!04	f	10

Table F-1. Plant Concentration Ratio Data[a] (Continued)

Radionuclide	Concentration Ratio	Community[b]	Citation[c]
Ra	2.20E ! 03	f	14
Ra	2.40E ! 03	f	12
Ra	2.42E ! 03	f	14
Ra	4.40E ! 03	f	14
Ra	4.73E ! 03	f	14
Ra	4.73E ! 03	f	14
Ra	4.76E ! 03	f	14
Ra	5.70E ! 03	f	12
Ra	1.58E ! 02	f	12
Ra	1.82E ! 02	f	12
Ra	4.88E ! 02	f	12
Th	3.15E ! 05	f	14
Th	7.26E ! 05	f	14
Th	7.55E ! 05	f	14
Th	9.13E ! 05	f	14
Th	1.84E ! 04	f	14
Th	5.40E ! 04	f	14
Th	8.15E ! 04	f	14
Th	1.10E ! 03	f	14
Th	2.76E ! 03	f	14
Th	8.00E ! 03	f	14
Th	1.70E ! 02	f	14
Th	2.13E ! 02	f	14
Th	2.79E ! 02	f	14
Th	3.79E ! 02	f	14
Th	4.08E ! 02	f	14
Th	4.74E ! 02	f	14
Th	6.43E ! 02	f	14
Th	8.01E ! 02	f	14
Th	8.97E ! 02	f	14
Th	1.19E ! 01	f	14
Th	1.19E ! 01	f	14
Th	1.37E ! 01	f	14
Th	1.54E ! 01	f	15
Th	2.24E ! 01	f	15
Th	2.37E ! 01	f	14
Th	2.70E ! 01	f	14
Th	2.88E ! 01	f	14
Th	3.54E ! 01	f	15
Th	3.90E ! 01	f	14

Table F-1. Plant Concentration Ratio Data[a] (Continued)

Radionuclide	Concentration Ratio	Community[b]	Citation[c]
Th	4.69E!01	f	14
Th	5.38E!01	f	14
Th	6.99E!01	f	14
Th	1.06E+00	f	14
Th	2.37E+00	f	14
U	7.00E!04	f	10
U	1.25E!03	f	10
U	1.70E!03	f	12
U	2.20E!03	f	12
U	2.30E!03	f	12
U	3.20E!03	f	12
U	7.69E!03	f	14
U	1.06E!02	f	10
U	1.31E!02	f	10
U	1.67E!02	f	14
U	2.21E!02	f	14
U	2.26E!02	f	14
U	2.50E!02	f	14
U	2.60E!02	f	16
U	2.61E!02	f	14
U	2.85E!02	f	14
U	3.00E!02	f	17
U	3.00E!02	f	17
U	4.53E!02	f	12
U	4.62E!02	f	14
U	7.50E!02	f	16
U	1.00E!01	f	14
U	1.38E!01	f	14
U	1.52E!01	f	15
U	3.60E!01	f	15
U	5.12E!01	f	16
U	5.63E!01	f	13
U	7.32E!01	f	16
U	8.05E!01	f	16
U	1.17E+00	f	16
U	2.10E+00	f	15
U	3.48E+00	f	16

[a] Plant concentration ratio = pCi activity per kg dry aboveground biomass/pCi activity per kg dry soil

[b] C = current and future communities; f = future community only

[c] Citations:

1 = Price [1972; 1973]
2 = Wenzel et al. [1987]
3 = Dreesen and Marple [1979]
4 = Ibrahim and Whicker [1987]
5 = Simon and Fraley [1986]
6 = Ibrahim and Whicker [1988b]
7 = Fresquez et al. [1995]
8 = Ibrahim and Whicker [1988a]
9 = Ibrahim et al. [1982]
10 = Garten [1980]
11 = Livens et al. [1991]
12 = Mahon and Mathewes [1983]
13 = Dunn [1981]
14 = Titaeva et al. [1979]
15 = Sheppard and Thibault [1981]
16 = Walker [1978]
17 = Sheppard and Sheppard [1985]

Table F-2. Results of Normality Tests on Log-Transformed Concentration Ratio Data for Current Shrubland Species

Radionuclide Element	Shapiro-Wilk	Lilliefors
Am (analogue for Ac)	p<0.35	p>0.20
Cs[1]	-----	-----
Np (analogue for Pa)	p<0.01	p<0.01
Pb	p<0.03	p<0.10
Pu	p<0.10	p<0.01
Ra	p<0.49	p>0.20
Sr[1]	-----	-----
Tc[1]	-----	-----
Th	p<0.36	p>0.20
U	p<0.17	p<0.10
all data (generic)	p<0.00	p<0.01

[1]There are insufficient data to run the normality tests.

Table F-3. Results of Normality Tests on Log-Transformed Concentration Ratio Data for Potential Future Species

Radionuclide Element	Shapiro-Wilk	Lilliefors
Am (analogue for Ac)	p<0.35	p>0.20
Cs	p<0.04	p<0.05
Np (analogue for Pa)	p<0.01	p<0.01
Pb	p<0.04	p<0.01
Pu	p<0.22	p<0.05
Ra	p<0.03	p<0.20
Sr[1]	-----	-----
Tc	p<0.39	p>0.15
Th	p<0.00	p<0.01
U	p<0.43	p>0.20
all data (generic)	p<0.00	p<0.01

[1]There are insufficient data to run the normality tests.

Table F-4. Geometric Standard Deviations of Concentration Ratio Distributions

Radionuclide Element	Current Shrubland Species[1]	Potential Future Species
Am (for Ac)	0.71	0.72
Cs	--	0.56
Np (for Pa)	0.66	0.66
Pb	0.90	0.86
Pu	0.55	0.62
Ra	0.52	0.73
Sr	--	--
Tc	--	0.66
Th	0.81	1.26
U	0.79	0.91
all data (generic)	1.34	1.29

[1]Dashed lines indicate insufficient data to perform analysis.

There are partial explanations for some of the highest concentration ratio values (e.g., Th). In the case of Th, the high values were for ^{230}Th uptake by plants growing at the edge of a contaminated tailings impoundment [Ibrahim et al., 1982; Ibrahim and Whicker, 1988a]. It is possible that acidity and wet conditions enhanced the solubility, availability, and thus, uptake, of ^{230}Th. The authors also suggest that foliar deposition of ^{230}Th in pond water spray and subsequent foliar

absorption may have been another uptake mechanism at the impoundment edge. However, evidence for foliar absorption of ^{230}Th is weak, as there is no evidence for this mechanism with other radionuclides in the study. Additionally, because the concentration ratio values reported for ^{230}Th fall far below what the authors expected due to external plant contamination, the high concentration ratio values for Th were assumed to be due to root uptake and were retained in the analysis.

The data do tend to follow the expected uptake pattern of actinides, which indicate CRs are often ordered as follows: Np>Am~U~Cm>Pu.

A consequence of using lognormal distributions is the potential for very high upper CR values. In these data sets, this is most obvious when the 0.999 quantile exceeds the measured maximum, sometimes by an order of magnitude. The likelihood of these high quantiles causing problems in the overestimation of uptake can be investigated on an individual basis.

By using the concentration ratio model of uptake, we are attempting to make generic what is actually plant-, element-, and site-specific. Whatever the physical, stochastic, and experimental reasons there are for the variability in concentration ratio values, it remains true that under some conditions, plants uptake very small amounts of radionuclides while under other conditions, plants can concentrate radionuclides to a great degree. This generic, albeit simplistic, approach to modeling plant uptake is validated by using distributions of reported concentration ratio values that can represent the uncertainty and the variability in the process and measurement of plant uptake for native species.

F.2 Native Versus Agricultural Plant Concentration Ratios

Concentration ratio values for native plants should be expected to differ from those for agricultural species. The main difference between the two plant types is that native plants tend to have higher concentration ratio values than agricultural plants for a given element. As shown by Sheppard and Evenden [1997], even the broadest distributions chosen to describe variability in agricultural plant concentration ratio values fail to capture 34% of the variability in concentration ratio values for native plants; relatively high concentration ratio values lie outside the distributions for agricultural species.

The concentration ratio values compiled here were compared to concentration ratio values compiled for agricultural species [Table C-5, Ng et al., 1982; Baes et al., 1984; Kennedy and Strenge, 1994]. The average concentration ratio values for native plants tend to exceed mean values for agricultural species by one or two orders of magnitude, though native plant concentration ratio averages exceed those for non-native species by three to five orders of magnitude in the case of Th. A two order of magnitude difference is well within the range of expected variability about an average concentration ratio value, even in studies with the most careful experimental controls [Kinnear et al., 1981]. More importantly, for all the elements (except Th for current species), the range of concentration ratio values for native plants encompassed ranges reported for agricultural species (Tables F-5). Similarly, the upper and

Table F-5. Average CR Values for Native and Agricultural Plants

Radionuclide Element	Mean Native Plant CR	Range of Means, Agricultural Plant CR
Am (analogue for Ac)	2.2E!03	5.9E!5 to 5.8E!4
Cs	na	2.6E!2 to 2.2E!1
Np (analogue for Pa)	1.1E!01	2.7E!3 to 1.3E!2
Pb	3.2E!01	3.2E!3 to 9.0E!3
Pu	1.6E!04	2.6E!5 to 3.9E!4
Ra	1.7E!01	1.2E!3 to 7.5E!2
Sr	3.3E+01	1.3E!1 to 1.6E+0
Tc	3.7E+00	7.3E!1 to 4.4E+1
Th	1.4E+00	3.4E!5 to 6.6E!3
U	2.9E!01	1.3E!3 to 1.7E!2

lower quantiles of the lognormal pdfs developed for each element (Tables 5-5 and 6-10) encompassed concentration ratio ranges reported for agricultural species (except Pb and Th for current species). For all three exceptions, the lower end of the concentration ratio values for native plants were equal to or exceeded the upper end of the concentration ratio values for agricultural plants, suggesting that concentration ratio values (for the three exceptions) are, at the very least, being modeled conservatively for native plants. Again, high concentration ratio values for native plants are not necessarily suspect simply because they exceed those for agricultural plants. As explained in the previous section, there are defensible reasons for retaining the Th data, even though some of the Th data are high relative to expected concentration ratio values for agricultural species.

In conclusion, this simple comparison suggests that the concentration ratio values compiled here for native plant species are not unreasonably high and should be used in the GCD PA in order to prevent an underestimation of the uptake of radionuclides by native plants.

References

Baes, C. F., III., R. D. Sharp, A. L. Sjoreen, and R. W. Shor. 1984. A review and analysis of parameters for assessing transport of environmentally released radionuclides through agriculture. ORNL-5786. Oak Ridge National Laboratory.

Dreesen, D.R., and M.L. Marple. 1979. Uptake of trace elements and radionuclides from uranium mill tailings by four-wing saltbush (*Atriplex canescensi*) and alkali sacaton (*Sporobolus airoides*). LA-UR-79-3045. CONF-791140-1.

Dunn, C.E. 1981. The biogeochemical expression of deeply buried uranium mineralization in Saskatchewan, Canada. *Journal of Geochemical Exploration* 15:437–452.

Fresquez, P. R., T. S. Foxx, and L. Naranjo, Jr. 1995. Strontium concentrations in chamisa (*Chrysothamnus nauseosus*) shrub plants growing in a former liquid waste disposal area in Bayo Canyon. Los Alamos National Laboratory Report LA-13050-MS, UC-721 and UC-702.

Garten, C.T., Jr. 1980. Comparative uptake of ^{234}U, ^{238}U, ^{239}Pu, ^{241}Am, and ^{244}Cm by boxelder trees (*Acer negundo*) inhabitating a contaminated Tennessee floodplain. *Health Physics* 39:334–338.

Ibrahim, S. A. and F. W. Whicker. 1987. Plant accumulation and plant/soil concentration ratios of ^{210}Pb and ^{210}Po at various sites within a uranium mining and milling operation. *Environmental and Experimental Botany* 27(2):203-213.

Ibrahim, S. A. and F. W. Whicker. 1988a. Comparative uptake of U and Th by native plants at a U production site. *Health Physics* 54(4):413-419.

Ibrahim, S. A. and F. W. Whicker. 1988b. Plant/soil concentration ratios of ^{226}Ra for contrasting sites around an active U mine-mill. *Health Physics* 55(6):903-910.

Ibrahim, S., S. Flot, and F. W. Whicker. 1982. Concentrations and biological availability of ^{238}U and ^{230}Th in the environs of a uranium milling operation. Symposium on Uranium Mill Tailing Management, Fort Collins, Colorado, December 9-10.

Kennedy, W. E., Jr., and D. L. Strenge. 1994. Residual radioactive contamination from decommissioning. NUREG/CR-5512. PNL-7994, Vol. 1.

Kinnear, J. E., A. Wallace, and E. M. Romney. 1981. Frequency distribution of ^{241}Am in a population of bush bean plants grown in soil in a glasshouse. *Soil Science* 132(1):122-126.

Livens, F. R., A. D. Horrill, and D. L. Singleton. 1991. Distribution of radiocesium in the soil-plant systems of upland areas of Europe. *Health Physics* 60(4):539–545.

Mahon, D. C. and R. W. Mathewes. 1983. Uptake of naturally occurring radioisotopes by vegetation in a region of high radioactivity. *Canadian Journal of Soil Science* 63:281–290.

Ng, Y. C., C. S. Colsher, and S. E. Thompson. 1982. Soil-to-plant concentration factors for radiological assessments. NUREG/CR-2975. UCID-19463.

Price, K. R. 1972. Uptake of ^{237}Np, ^{239}Pu, ^{241}Am, and ^{244}Cm from soil by tumbleweed and cheatgrass. BNWL-1688, 15 p.

Price, K. R. 1973. Tumbleweed and cheatgrass uptake of transuranium elements applied to soil as organic acid complexes. BNWL-1755, 9 p.

Sheppard, M. I. and S. C. Sheppard. 1985. The plant concentration ratio concept as applied to natural U. *Health Physics* 48:494-500.

Sheppard, M. I. and D. H. Thibault. 1981. Uptake of uranium, thorium and arsenic from refinery residue by *Pinus sylvestris* L. and the effect on growth. In *Proceedings of the 2nd Annual Conference of the Canadian Nuclear Society*, p. 54-61.

Sheppard, S. C. and W. G. Evenden. 1997. Variation in transfer factors for stochastic models: soil-to-plant transfer. *Health Physics* 72(5): 727-733.

Simon, S. L. and L. Fraley, Jr. 1986. Uptake by sagebrush of uranium progeny injected *in situ*. *Journal of Environmental Quality* 15(4):345-350.

Titaeva, N. A., A. I. Taskaev, V. Ya. Ovchenkov, R. M. Aleksakhin, and I. I Shuktomova. 1979. Content and characteristics of uranium, thorium, radium and radon uptake in plants growing under different radioecological conditions. *Ekologiya* 9:37-44, translated in *Soviet Journal of Ecology* (1979) 9:328-334.

Walker, N. C. 1978. Trace elements in vegetation and soils over the Key Lake uranium-nickel orebody in northern Saskatchewan, Canada. Geochemical Exploration, Proceedings of the 7th International Geochemical Exploration Symposium, Golden, Colorado, pp. 361–369.

Wenzel, W. J., T. S. Foxx, A. F. Gallegos, G. Tierney, and J. C. Rodgers. 1987. Cesium-137, plutonium-239/240, total uranium, and scandium in trees and shrubs growing in transuranic waste at Area B. LA-11126-MS. UC-70.

This page intentionally left blank.

Appendix G

Biomass Turnover Data and Analyses

This page intentionally left blank.

G.1 Cross-Correlation Analysis

Cross-correlation estimates the correlation between one time series at time *t* and a second time series at time *t-k* as a function of the lag or time differential *k*. At $t = 0$, the time series overlap completely and with each successive increment of *k*, the time series have one less pair of overlapping numbers. Some requirements of the analysis include: each data set must have the same number of observations; observations for paired data sets must have been taken at the same time periods; the lag lengths used in the analysis must not exceed one half of the length of the data series for meaningful results; and lastly, each data set must be stationary, lacking predictable or systematic changes in the mean through time.

With total litterfall as one time series, total productivity as the other series, and *k* in units of years, the data for each site were analyzed to determine whether total litterfall was correlated to total productivity measured within a particular year and for each of the preceding years for which there were data. Lag lengths varied from zero to four, depending on the site and number of years for which there were data. The stationarity requirement was met for all the data sets.

Table G-1. Productivity and Litterfall Data for Current Shrubland Community[a]

Location	Year	Lifeform			Data Type[b]	Citation[c]
		Shrub	Perennial	Annual		
Frenchman Flat	1987	217	49	--	anp	1
Frenchman Flat	1987	174	37	--	anp	1
Frenchman Flat	1987	357	20	--	anp	1
Frenchman Flat	1987	177	97	--	anp	1
Frenchman Flat	1987	261	56	--	anp	1
Jackass Flat	1987	432	154	--	anp	1
Jackass Flat	1987	120	206	--	anp	1
Jackass Flat	1987	246	132	--	anp	1
Jackass Flat	1987	224	181	--	anp	1
Jackass Flat	1987	170	155	--	anp	1
Yucca Flat	1987	344	36	--	anp	1
Yucca Flat	1987	546	50	--	anp	1
Yucca Flat	1987	455	53	--	anp	1
Yucca Flat	1987	299	36	--	anp	1
Yucca Flat	1987	286	71	--	anp	1
Yucca Flat	1987	505	12	--	anp	1
Mid Valley	1987	842	2	--	anp	1
Mid Valley	1987	697	3	--	anp	1
Frenchman Flat	1987	--	--	378	anp	1
Frenchman Flat	1987	--	--	43	anp	1
Jackass Flat	1987	--	--	80	anp	1
Yucca Flat	1987	--	--	520	anp	1
Rock Valley	1987	--	--	175	anp	1
Mid Valley	1986	--	--	26	anp	1
Mid Valley	1987	--	--	53	anp	1
Mojave Desert	1975	124	19	51	lf	2

Table G-1. Productivity and Litterfall Data for Current Shrubland Community[a] (Continued)

Location	Year	Lifeform			Data Type[b]	Citation[c]
		Shrub	Perennial	Annual		
Mojave Desert	1976	292	96	143	lf	2
Rock Valley	1964	--	--	6	anp	3
Rock Valley	1965	--	--	0.24	anp	3
Rock Valley	1966	312	176	178	anp	3
Rock Valley	1967	195	110	45	anp	3
Rock Valley	1968	276	155	248	anp	3
Rock Valley	1971	152	89	4	anp	3
Rock Valley	1972	131	98	3	anp	3
Rock Valley	1973	440	242	644	anp	3
Rock Valley	1974	141	80	17	anp	3
Rock Valley	1975	147	63	49	anp	3
Rock Valley	1976	312	167	137	anp	3

[a]Data are in units of kg dry plant biomass/ha.
[b]anp = annual net primary production; lf = litterfall.
[c]citations:
1 = Hunter and Medica [1989]
2 = Strojan et al. [1979]
3 = Turner and Randall [1989]
-- indicates no data for that lifeform.

Table G-2. Litterfall and Productivity Data for Potential Future Cummunities[a] (from Passey et al. [1982])

Year	Site	Litterfall					Productivity				
		Annual	Perennial	Shrub	Tree	Total	Annual	Perennial	Shrub	Tree	Total
1960	ID 8-60	1	160	182	--	343	1	190	217	--	408
1960	ID 9-60	28	512	349	--	889	19	345	235	--	599
1960	UT 3-58	19	889	38	--	946	26	1204	51	--	1281
1961	UT 2-58	4	801	159	115	1079	3	584	116	84	787
1961	UT 5-58	17	786	146	41	990	14	663	123	35	835
1961	ID 8-60	0	175	150	--	325	0.5	271	233	--	504
1961	ID 15-58	33	548	259	--	839	27	449	212	--	688
1961	ID 1-59	7	628	187	--	823	6	504	150	--	660
1961	ID 4-59	2	814	257	--	1072	1	520	164	--	685
1961	ID 9-60	0	446	270	--	716	0.5	321	194	--	515
1961	UT 3-58	36	888	60	--	984	28	690	47	--	765
1961	ID 6-58	12	697	99	--	809	10	563	80	--	653
1961	ID 12-58	6	455	150	--	610	5	389	128	--	522
1961	ID 13-58	14	829	283	--	1126	7	427	146	--	580
1961	ID 3-58	54	718	184	--	956	39	520	133	--	692
1962	UT 2-58	11	863	105	78	1056	16	1244	151	112	1523
1962	UT 5-58	30	611	73	28	741	47	950	113	43	1153
1962	ID 8-60	5	200	104	--	308	9	368	191	--	568

Table G-2. Litterfall and Productivity Data for Potential Future Cummunities[a] (from Passey et al. [1982]) (Continued)

Year	Site	Litterfall					Productivity				
		Annual	Perennial	Shrub	Tree	Total	Annual	Perennial	Shrub	Tree	Total
1962	ID 15-58	195	561	95	--	851	344	988	168	--	1500
1962	ID 1-59	7	871	155	--	1033	6	802	143	--	951
1962	ID 4-59	27	865	171	--	1064	24	757	150	--	931
1962	ID 9-60	13	569	245	--	827	11	481	207	--	699
1962	UT 3-58	35	390	23	--	448	81	896	53	--	1030
1962	ID 6-58	10	831	99	--	940	9	717	85	--	811
1962	ID 12-58	29	542	172	--	743	33	625	198	--	856
1962	ID 13-58	16	1134	277	--	1427	10	688	168	--	866
1962	ID 3-58	163	595	145	--	903	189	688	168	--	1045
1963	UT 2-58	6	663	107	76	853	6	617	100	71	794
1963	UT 5-58	47	789	212	63	1111	42	704	189	56	991
1963	ID 8-60	4	174	134	--	311	10	469	361	--	840
1963	ID 15-58	260	489	108	--	857	399	751	165	--	1315
1963	ID 1-59	45	691	115	--	851	57	870	145	--	1072
1963	ID 4-59	24	677	290	--	991	22	609	261	--	892
1963	ID 9-60	5	476	211	--	692	6	541	240	--	787
1963	UT 3-58	6	744	21	--	771	10	1253	36	--	1299
1963	ID 6-58	11	802	83	--	896	15	1092	113	--	1220
1963	ID 12-58	50	484	142	--	676	42	405	119	--	566
1963	ID 13-58	3	814	292	--	1109	2	554	199	--	755
1963	ID 3-58	233	551	151	--	935	317	748	205	--	1270
1964	UT 2-58	11	765	48	65	889	12	838	53	71	974
1964	UT 5-58	19	628	87	41	774	26	866	120	56	1068
1964	ID 8-60	0	213	149	--	362	0.5	325	228	--	553
1964	ID 15-58	169	465	194	--	828	173	476	199	--	848
1964	ID 1-59	9	635	258	--	902	8	597	243	--	848
1964	ID 4-59	7	520	117	--	644	11	798	179	--	988
1964	ID 9-60	13	319	294	--	626	19	455	420	--	894
1964	UT 3-58	7	526	20	--	553	15	1071	40	--	1126
1964	ID 6-58	4	755	66	--	825	5	967	84	--	1056
1964	ID 12-58	45	770	83	--	898	40	688	74	--	802
1964	ID 13-58	10	752	247	--	1009	7	527	173	--	707
1964	ID 3-58	147	585	84	--	816	200	796	114	--	1119
1965	UT 2-58	6	593	426	91	1117	5	460	331	71	867
1965	UT 5-58	2	534	218	68	823	2	437	178	56	673
1965	ID 8-60	1	207	167	--	375	1	216	175	--	392
1965	ID 15-58	97	944	108	--	1149	62	605	69	--	736
1965	ID 1-59	10	912	143	--	1065	7	636	100	--	743
1965	ID 4-59	7	633	200	--	840	5	481	152	--	638
1965	ID 9-60	5	258	239	--	502	5	268	248	--	521
1965	UT 3-58	2	520	79	--	601	2	675	103	--	780

Table G-2. Litterfall and Productivity Data for Potential Future Cummunities[a] (from Passey et al. [1982]) (Continued)

Year	Site	Litterfall					Productivity				
		Annual	Perennial	Shrub	Tree	Total	Annual	Perennial	Shrub	Tree	Total
1965	ID 6-58	3	695	58	--	756	3	745	62	--	810
1965	ID 12-58	34	551	44	--	629	36	586	47	--	669
1965	ID 13-58	2	571	27	--	600	2	515	24	--	541
1965	ID 3-58	254	972	175	--	1401	200	767	138	--	1105
1966	UT 2-58	3	611	233	95	941	2	457	174	71	704
1966	UT 5-58	1	943	124	98	1167	1	538	71	56	665
1966	ID 8-60	0	185	260	--	445	0.5	130	183	--	313
1966	ID 15-58	2	684	385	--	1071	1	370	208	--	579
1966	ID 1-59	3	392	302	--	697	3	285	220	--	505
1966	ID 4-59	4	612	197	--	813	2	304	98	--	404
1966	ID 9-60	0	166	311	--	477	0.5	188	351	--	539
1966	UT 3-58	1	650	179	--	830	1	437	120	--	557
1966	ID 6-58	1	1004	252	--	1257	2.5	628	158	--	786
1966	ID 12-58	2	472	32	--	506	1	253	17	--	271
1966	ID 13-58	1	529	93	--	623	1	371	65	--	436
1966	ID 3-58	4	823	170	--	997	2	382	79	--	463
1967	UT 2-58	8	704	228	83	1024	7	593	192	70	862
1967	UT 5-58	16	605	116	45	782	20	752	144	56	972
1967	ID 8-60	0	281	217	--	498	0.5	290	224	--	514
1967	ID 15-58	117	577	260	--	954	183	898	405	--	1486
1967	ID 1-59	14	975	263	--	1252	15	1068	288	--	1371
1967	ID 4-59	22	441	471	--	934	28	556	594	--	1178
1967	ID 9-60	14	537	293	--	844	13	497	271	--	781
1967	UT 3-58	10	644	94	--	748	13	814	119	--	946
1967	ID 6-58	5	1008	146	--	1159	6	1194	173	--	1373
1967	ID 12-58	6	322	30	--	357	11	631	58	--	700
1967	ID 13-58	8	535	112	--	655	12	781	163	--	956
1967	ID 3-58	86	502	79	--	666	118	690	108	--	916
1968	ID 8-60	2	155	329	--	486	3	201	427	--	632
1968	ID 1-59	20	523	201	--	744	20	513	197	--	730
1968	ID 4-59	8	498	212	--	718	7	420	179	--	606
1968	ID 9-60	1	295	230	--	525	1	430	335	--	766
1969	ID 8-60	1	221	134	--	355	1	352	213	--	567
1969	ID 9-60	12	249	176	--	437	28	562	396	--	986

[a] Data are in units of kg dry plant biomass/ha.
- indicates no data for that lifeform.

Table G-3. Dependent Sample t-test Results for Tests of Differences Between Productivity and Litterfall Data, Potential Future Communities

Lifeform (community)	n	p-value[1]
annual (shrubland)	79	0.44
perennial (shrubland)	79	0.72
shrub (shrubland)	79	0.79
total site-wide (shrubland)	79	0.62
annual (woodland)	14	0.33
perennial (woodland)	14	0.82
shrub (woodland)	14	0.18
tree (woodland)	14	0.32
total site-wide (woodland)	14	0.66
total site-wide (combined)	93	0.80

[1]Test is significant at $p < 0.05$; p $ 0.05 indicates no difference between sample populations.

References

Hunter, R. B. and P. A. Medica. 1989. Status of the flora and fauna on the Nevada Test Site: results of continuing basic environmental research January through December 1987. DOE/NV/10630-2.

Passey, H. B., V. K. Hugie, E. W. Williams, and D. E. Ball. 1982. Relationships between soil, plant community, and climate on rangelands of the intermountain west. USDA Soil Conservation Service, Technical Bulletin No. 1669.

Strojan, C. L., F. B. Turner, and R. Castetter. 1979. Litter fall from shrubs in the northern Mojave Desert. *Ecology* 60(5):891-900.

Turner, F. B. and Randall. 1989. Net production by shrubs and winter annuals in southern Nevada. *Journal of Arid Environments* 17:23-36.

This page intentionally left blank.

Appendix H

NTS Species that Excavate Burrows

This page intentionally left blank.

This list of burrowing species was taken from Thompson [1993] and Winkel et al. [1995], and includes all animals known to excavate their own burrow at the NTS.

Table H-1. NTS Species that Excavate Burrows

Species/Scientific Name	Common Name/Type
Mammals	
Ammospermophilus leucurus leucurus	white-tailed antelope squirrel
Anis latrans	Coyote
Dipodomys deserti deserti	desert kangaroo rat
Dipodomys merriami merriami	Merriam's kangaroo rat
Dipodomys microps occidentalis	chisel-toothed kangaroo rat
Dipodomys ordi monoensis	Ord's kangaroo rat
Eutamias dorsalis grinnelli	cliff chipmunk
Lagurus curtatus curtatus	sagebrush vole
Microdipodops megacephalus sabulonis	dark kangaroo mouse
Neotoma lepida lepida	desert wood rat
Notiosorex crawfordi crawfordi	desert shrew
Onychomys torridus longicaudus	southern grasshopper mouse
Perognathus formosus mohavensis	long-tailed pocket mouse
Perognathus longimembris	little pocket mouse
Perognathus parvus olivaceus	Great Basin pocket mouse
Peromyscus crinitus stephensi	canyon mouse
Peromyscus eremicus eremicus	cactus mouse
Peromyscus maniculatus sonoriensis	deer mouse
Peromyscus truei truei	pinon mouse
Reithrodontomys megalotis megalotis	western harvest mouse
Sorex merriami leucogenys	Merriam's shrew
Sorex tenellus	Inyo shrew
Spermophilus tereticaudus tereticaudus	Round-tailed ground squirrel
Spermophilus townsendii mollis	Townsend's ground squirrel
Spermophilus variegatus robustus	rock squirrel
Taxidea taxus	badger
Thomomys umbrinus nanus	southern pocket gopher
Vulpes macrotis	kit fox
Invertebrates	
Amitermes sp.	termite
Aphaenogaster megommatus	ant
Camponotus maccooki	ant
Crematogaster coarctata	ant
Crematogaster depilis	ant
Dorymyrmex bicolor	ant
Dorymyrmex pyramicus	ant
Iridomyrmex pruinosum	ant
Myrmecocystus comatus	ant
Myrmecocystus lugubris	ant
Myrmecocystus mexicanus	ant

Table H-1. NTS Species that Excavate Burrows (Continued)

Species/Scientific Name	Common Name/Type
Myrmecocystus mimicus	ant
Pheidole bicarinata	ant
Pheidole desertorum	ant
Pogonomyrmex californicus	ant
Pogonomyrmex imberbiculus	ant
Reticulitermes tibialas	termite
Solenopsis aurea	ant
Solenopsis molesta	ant
Solenopsis xyloni	ant
Veromessor lariversi	ant
Veromessor pergandei	ant

References

Thompson, M. 1993. Burrowing animals at the Nevada Test Site: a literature study. Unpublished supporting documentation for the Area 5 GCD Performance Assessment, prepared by Sandia National Laboratories for the U.S. Department of Energy under Contract DE-AC04-94AL85000.

Winkel, V. K., J. P. Angerer, D. B. Hall, M. W. Fariss, and K. R. Johnejack. 1995. Plant and Burrowing Animal Characteristics. Integrated Closure Program for the Area 3 and Area 5 Radioactive Waste Management Sites, Nevada Test Site. Prepared for U.S. Department of Energy, Nevada Operations Office under Contract No. DE-AC08-94-NV11432.

Appendix I

Memo from Lewis to Lojek

This page intentionally left blank.

-----Original Message-----
From: John A. Lewis [mailto:jalewis@sandia.gov]
Sent: Thursday, February 11, 1999 4:28 PM
To: Lojek, Carole A
Subject: Re: Request for Information

Hi Carole,

Per our conference telecon earlier today, I informed you that I gave you some misinformation in the past. Item #6 does NOT contain any TRU elements. This fact is unclassified (because the lack of TRU elements in specified or unspecified weapons is unclassified). This fact has been confirmed with Pat Bodin, DOE/NV Classification Officer.

Let me know if I can be of any more assistance.
John

John A. Lewis 16FEB99
JOHN A. LEWIS
CLASSIFICATION ANALYST, SNL/NM-7447

At 12:49 PM 2/1/99 -0700, you wrote:
>Hi John,
>
>Can you give me the following information for Package ID# M23 (or Item# 6):
>
>1) The number of curies of TRU elements in the above package
>2) The weight of the above package.
>
>I'd appreciate it if you can get this information for me as soon as you can.
>Thanks again for your assistance.
>
>Carole
>
>

Post-it® Fax Note 7671	Date 16FEB99	# of pages ▶ 01
To CAROLE LOJEK	From JOHN LEWIS	
Co./Dept. C6416	Co. DEPT 7447	
Phone # 284-2583	Phone # 845-9349	
Fax # 844-5404	Fax #	

This page intentionally left blank.

Appendix J

Radionuclide Chains

This page intentionally left blank.

The four complete radioactive decay chains resulting from radioactive decay of TRU waste disposed of in the GCD boreholes are shown in Figure J-1, and the half-lives of all radionuclides are given in Table J-1. The decay chains were taken from General Electric [1988], and half-lives were taken from the CRC [1992].

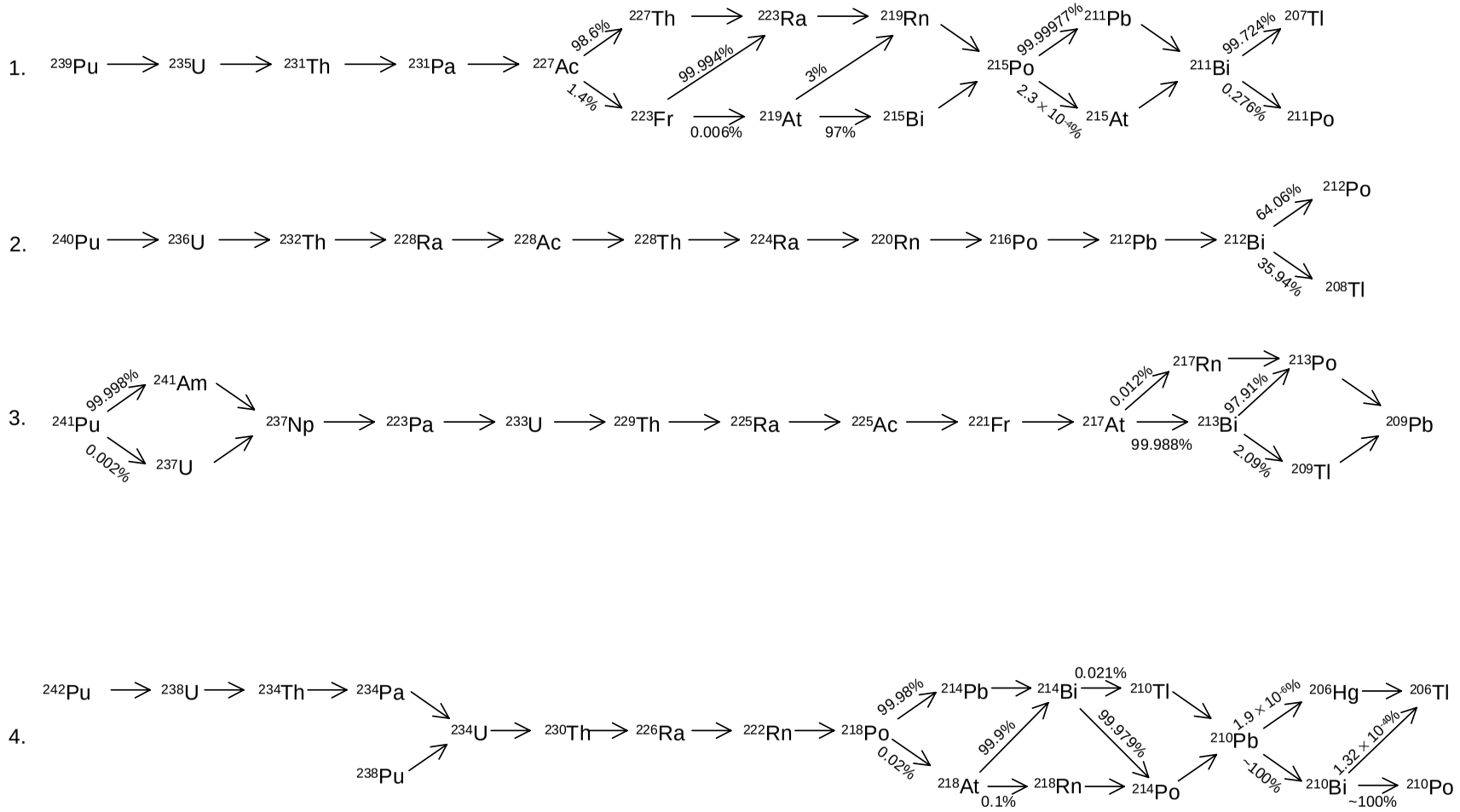

Figure J-1. Complete Radioactive Decay Chains.

Table J-1. Radionuclide Half-Lives

Chain 1		Chain 2		Chain 3		Chain 4	
Radio-nuclide	**Half-life (years)**	**Radio-nuclide**	**Half-life (years)**	**Radio-nuclide**	**Half-life (years)**	**Radio-nuclide**	**Half-life (years)**
^{239}Pu	2.41×10^{4}	^{240}Pu	6537	^{241}Am	432.2	^{242}Pu	3.76×10^{5}
^{235}U	7.04×10^{8}	^{236}U	2.34×10^{7}	^{237}Np	2.14×10^{6}	^{238}U	4.46×10^{9}
^{231}Th	$2.91 \times 10^{!3}$	^{232}Th	1.4×10^{10}	^{233}Pa	$7.39 \times 10^{!2}$	^{234}Th	$6.60 \times 10^{!2}$
^{231}Pa	3.25×10^{4}	^{228}Ra	5.76	^{233}U	1.59×10^{5}	^{234}Pa	$7.63 \times 10^{!4}$
^{227}Ac	21.77	^{228}Ac	$7.02 \times 10^{!4}$	^{229}Th	7.9×10^{3}	^{238}Pu	87.74
^{227}Th	$5.13 \times 10^{!2}$	^{228}Th	1.913	^{225}Ra	$4.08 \times 10^{!2}$	^{234}U	2.45×10^{5}
^{223}Ra	$3.13 \times 10^{!2}$	^{224}Ra	$1.00 \times 10^{!2}$	^{225}Ac	$2.73 \times 10^{!2}$	^{230}Th	7.54×10^{4}
^{219}Rn	$1.26 \times 10^{!7}$	^{220}Rn	$1.76 \times 10^{!6}$	^{221}Fr	$9.13 \times 10^{!6}$	^{226}Ra	1599
^{215}Po	$5.64 \times 10^{!11}$	^{216}Po	$4.60 \times 10^{!9}$	^{217}At	$1.01 \times 10^{!9}$	^{222}Rn	$1.05 \times 10^{!2}$
^{211}Pb	$6.86 \times 10^{!5}$	^{212}Pb	$1.21 \times 10^{!3}$	^{213}Bi	$8.67 \times 10^{!5}$	^{218}Po	$5.78 \times 10^{!6}$
^{211}Bi	$4.07 \times 10^{!6}$	^{212}Bi	$1.15 \times 10^{!4}$	^{213}Po	$1.27 \times 10^{!13}$	^{214}Pb	$5.12 \times 10^{!5}$
^{207}Tl	$9.07 \times 10^{!6}$	^{208}Tl	$5.81 \times 10^{!6}$	^{209}Pb	$3.71 \times 10^{!4}$	^{214}Bi	$3.75 \times 10^{!5}$
						^{214}Po	$5.19 \times 10^{!12}$
						^{210}Pb	22.6
						^{210}Bi	$1.37 \times 10^{!2}$
						^{210}Po	$3.79 \times 10^{!1}$

CRC Handbook of Chemistry and Physics, 73rd Edition (1992–1993), David R. Lide, Editor.

General Electric. 1988. *Chart of the Nuclides*, 14th Edition, Knolls Atomic Power Laboratory, operated by the General Electric Company, Nuclear Energy Operations, 175 Curtner Avenue, MIC684, San Jose, California, 95125.

This page intentionally left blank.

Appendix K

EQ3NR

This page intentionally left blank.

EQ3NR

The input for EQ3NR [Wolery, 1992b] consists of the composition of the solution of interest, and properties such as the pH and the temperature of the solution. The code calculates the distribution of each element among possible dissolved species (given as concentrations, thermodynamic activities, and the proportions of the total quantity of that element), and whether the solution is undersaturated, saturated, or supersaturated with respect to minerals or other solids that contain that element. EQ3NR also creates an input file for the reaction-path code EQ6.

EQ3NR uses two measures of the degree of saturation of solutions. The saturation index (SI) is defined as the log of the quotient Q/K, in which Q is the ion activity product and K the equilibrium constant for a reaction, typically the congruent dissolution of a mineral. The SI is negative for undersaturated minerals, zero for saturated minerals, and positive for supersaturated minerals. The other measure, the affinity (A), is defined as the product of the SI and the factor -2.303 × R × T, in which R is the gas constant (0.0821 × liter × atm × $mol^{!1}$ × $K^{!1}$) and T is the absolute temperature (EK). Because log (Q/K) changes sign when the reaction is reversed, the affinity to precipitate a mineral is defined as the product of the SI and the factor 2.303 × R × T. $A_{precipitation}$ therefore has the same sign as the SI. Although one generally uses the chemical analysis of a solution to compute the degree of saturation of minerals or other solids, it is possible to assume that a mineral is in equilibrium with the solution and compute what constraints this places on certain components, given that the values for other components are known and correct.

For solutions with ionic strengths less than about 1 M, EQ3NR uses an ion-association model for the speciation of solutes. This model explicitly recognizes the reaction of oppositely charged species to form complexes, and applies mass-action, mass-balance, and charge-balance equations to calculate the relative activities of the free (dissociated) ions and complexes. EQ3NR uses the extended Debye-Hückel equation of Helgeson [1969], commonly referred to as the B-Dot Equation, to determine activity coefficients for solute species.

The ion-association model, in conjunction with the B-Dot Equation, has proven very successful in modeling dilute aqueous solutions of geochemical interest, such as GCD vadose-zone groundwaters. Furthermore, sufficient thermodynamic data now exist for modeling the behavior of several important radionuclides in such systems.

For solutions with ionic strengths up to several molar, EQ3NR uses a mixed-electrolyte model for the speciation of solutes. Because the B-Dot Equation was used to determine activity coefficients for solute species, the mixed-electrolyte model is not discussed here.

EQ6

EQ6 [Wolery and Daveler, 1992] uses the model of an aqueous solution generated by EQ3NR as the starting point for simulations of reactions between the solution and minerals or other solids, gases, or other solutions. EQ6 calculates the extent to which these reactions occur, keeps track of the reaction products that precipitate or redissolve, and recalculates the species distribution and degree of saturation of the solution as its composition changes in response to the reactions.

Reaction-path codes generally assume that, as a reactant or reactants are incrementally added to the solution, chemical equilibrium is maintained within the solution, as well as between the solution and any solids that precipitate. Conceptually, this is equivalent to a system in which a reactant dissolves at a finite rate, but all other reactions occur instantaneously; the dissolution of the reactant is thus the rate-limiting step for the system as a whole.

EQ6 operates in three modes: a titration mode, a closed-system mode, and a pseudo-one-dimensional, "flow-through" mode which follows the evolution of a packet of solution moving through a reactant medium. (There is no provision in EQ6 for modeling actual flow through a column. Currently, the "flow-through" only models what happens to the "first" packet of solution.) The user can impose fixed fugacities for specified gases on all three of these reaction models to simulate systems open with respect to external reservoirs of these gases. This capability is useful in modeling systems open to the atmosphere, which contains highly reactive gases such as carbon dioxide and oxygen.

EQ6 allows the user to choose the function which describes the rates at which the reactants equilibrate with the solution. These functions may represent arbitrary, relative rates or actual, kinetic rate models. If the user employs arbitrary, relative rates, there is no time frame in the calculation, and the code measures the progress of the reaction with a progress variable ξ related to the quantities of reactants consumed. Each step of the calculation represents an equilibrium state of the system, the composition of which is changing as reactants enter the system. If the user specifies actual rate laws, the calculation includes a time frame. The rate at which a reactant dissolves can be negative, in which case the "reactant" is actually a product precipitating according to the rate law instead of instantaneously to satisfy solubility equilibrium. This is the principle behind the option to specify precipitation kinetics [Delany, Puigdomenech, and Wolery, 1986]. Unfortunately, few kinetic data exist yet for geochemical precipitation reactions.

References

Delany, J.M., I. Puigdomenech, and T.J. Wolery. 1986. Precipitation Kinetics Option for the EQ6 Geochemical Reaction Path Code, UCRL-53642, Lawrence Livermore National Laboratory, Livermore, CA.

Helgeson, H.C. 1969. "Thermodynamics of Hydrothermal Systems at Elevated Temperatures and Pressures," American Journal of Science, Vol. 267, 729–904.

Wolery, T.J. 1992b. *EQ3NR, A Computer Program for Geochemical Aqueous Speciation-Solubility Calculations: Theoretical Manual, User's Guide, and Related Documentation (Version 7.0).* UCRL-MA-110662 PT III. Livermore, CA: Lawrence Livermore National Laboratory.

Wolery, T.J., and S.A. Daveler. 1992. EQ6, A Computer Program for Reaction-Path Modeling of Aqueous Geochemical Systems: Theoretical Manual, User's Guide, and Related Documentation (Version 7.0). UCRL-MA-110662 PT IV. Livermore, CA: Lawrence Livermore National Laboratory.

Appendix L

Criticality Potential

This page intentionally left blank.

Gary A. Harms, Sandia National Laboratories, Albuquerque, New Mexico
Terry L. Steinborn, Applied Research Associates, Inc., Albuquerque, New Mexico

Final Performance Assessment

Introduction

The potential for nuclear criticality is of concern for the GCD boreholes, because they contain fissionable materials., i.e., plutonium and enriched uranium [Chu and Bernard, 1991]. With these constituents in the source-term inventory, the possibility of nuclear criticality either as a result of the waste emplacement in the GCD boreholes itself or as a result of postclosure radionuclide migration is a concern when assessing disposal-system performance.

Analyses were performed to evaluate the potential for nuclear criticality to determine whether this process can or cannot be eliminated as a concern when assessing disposal system performance. If nuclear criticality can occur, but the probability of occurrence is less than the value provided by the U.S. EPA as guidance (i.e., less than one chance in 10,000 in 10,000 years [EPA, 1985]), the process can be screened out of scenario development. If the occurrence of nuclear criticality either alone or in combination with other events and processes does not affect the performance of the disposal system (i.e., no or low consequence), the process need not be considered further. If the conditions necessary for nuclear criticality to occur are not physically reasonable or possible, the process need not be considered further. A detailed discussion of the calculations and assumptions of these analyses are available in Harms et al., 1998. This discussion is taken from that report, and presents no new analyses.

The approach used to screen nuclear criticality was to establish bounding conditions by modeling various highly idealized (i.e., noncredible) configurations of fissile radionuclides consistent with the radionuclide inventories present in the TRU boreholes and the physical properties of the materials within the disposal system. These bounding conditions optimized the conditions necessary for nuclear criticality to occur. This approach was selected as a more computationally-efficient alternative to attempting to simulate the relatively complex processes of radionuclide dissolution, migration, and reconcentration within and surrounding the TRU boreholes. If nuclear criticality cannot occur under these idealized conditions, then nuclear criticality certainly cannot occur under the actual conditions within the GCD disposal system, and the process need not be considered further. If nuclear criticality can occur under these idealized conditions, the next step is to examine less idealized configurations. If the analyses indicate that nuclear criticality can occur in modeled systems deemed to be sufficiently similar to the actual disposal system, the possible effects of nuclear criticality on system performance must be considered.

Basics of Nuclear Criticality

Nuclear criticality is commonly misunderstood to be the same as a nuclear explosion. Whereas the same radionuclides can participate in both phenomena, the specific conditions that will result in criticality are substantially different from the conditions resulting in an explosion. The following discussion defines nuclear criticality and identifies those factors that affect criticality.

Definitions

Nuclear criticality is a self-sustaining neutron chain reaction in which there is an exact balance between the production of neutrons (by the splitting of atomic nuclei) and the loss of neutrons in the absence of extraneous neutron sources. When the net production of neutrons exceeds the neutron leakage, the system will be super-critical, and a divergent chain reaction will occur. If, on the other hand, too many neutrons are lost through leakage, the effective reproduction factor for the system will be less than unity, and a self-sustaining chain reaction will not be possible [Wick, 1967, p. 877].

When the nuclei of certain (fissionable) radionuclides are struck by a neutron, the neutron will be absorbed, resulting in instability of the nucleus. The unstable nucleus will then split (fission) and produce one or more neutrons that, under specific conditions, can strike other nuclei, also causing instability and fissioning. Not all neutrons produced will strike other nuclei. In order for the chain reaction to be self-sustaining, at least one neutron from each fission must go on to cause another fission, on the average. If less than one neutron per fission goes on to produce another fission, the chain reaction will die out.

A nuclear explosion can only occur when the neutron chain reaction within a mass of radionuclides becomes supercritical with exponentially increasing energy levels occurring within a fraction of a second. Achieving the necessary geometry of this supercritical mass of radionuclides within the necessary time constraints is very difficult. The supercritical mass must be assembled quickly, so that the production of neutrons within the system can exceed the leakage of neutrons out of the system within the required time scale. As energy is released by fission, the mass of radionuclides expands, which increases the distance between nuclei thereby reducing the probability of neutrons within the system striking and destabilizing enough other nuclei to maintain a growing chain reaction. At some time after the initiation of the chain reaction, the probability of neutrons striking nuclei will be reduced (i.e., neutron leakage increases) to a level where the chain reaction cannot be increased or maintained (i.e., the system becomes subcritical). No realistic mechanism for assembling a supercritical mass of radionuclides on the short time scales required for an explosion has been proposed in a repository or geologic setting, as discussed in Harms et al., 1998, Appendix A. Nuclear explosions resulting from reconcentration of radionuclides within the GCD boreholes or along possible migration routes are excluded from further discussion because of the unrealistic conditions required for such events to occur. Because of these constraints, only nuclear criticality is considered further.

Neutron Economy

The state of a neutron multiplying system is most concisely described by its effective multiplication factor (k_{eff}). The k_{eff} is defined as the ratio of the production rate to the loss rate of neutrons in a system. When k_{eff} is less than one, the system is subcritical and has a decreasing or zero power level depending on the initial conditions. When k_{eff} is greater than one, the system is supercritical and has an increasing power level. When k_{eff} is exactly equal to one, the system is critical and has a constant power level.

The k_{eff} can be modified by changing the neutron production rate or the loss rate. Neutron production occurs predominately through fission, although minor contributions can be made by other reactions. Thus, the primary method of controlling the production rate is through controlling the amount of fissile material present in a system (i.e., controlling the number of nuclei that will decay as a function of half life and/or the number that can absorb neutrons, become unstable, fission, and produce more neutrons).

Neutrons are lost from a system through two processes: absorption and leakage. During absorption, a neutron is taken up in the nucleus of an atom creating a different, heavier isotope of the absorbing material. Both fissile and nonfissile atoms can absorb neutrons. The absorption probability (cross section) varies greatly from material to material and, in fact, from isotope to isotope of a given material. The neutron loss rate of a system can be increased (decreasing k_{eff}) by the inclusion of an absorbing material in the system. A predominantly absorbing material is referred to as a poison.

The leakage rate from a system is determined by the geometry of the system and by the presence or lack of materials external to the system that reflect neutrons back into the system. In general, leakage can be promoted (decreasing k_{eff}) by changing to a geometry with a higher surface area to volume ratio or by increasing the size of the system while holding the mass constant. Reflectors decrease the loss rate, increasing k_{eff}. The effectiveness of a given reflector material depends on the neutronic properties of the material. Substances that are absorbers when placed inside the critical mass can, in some instances, serve as good reflectors.

The fission and absorption cross sections of all materials depend on the energy of the impinging neutron. Neutrons are produced by fission at high energies where cross sections of the fissioning nuclei are generally small. Fission cross sections, as well as many absorption cross sections, are much larger for low neutron energies. Thus, the presence of materials called moderators, which can efficiently decrease the energy of the fission neutrons by collisions (and nonabsorption) between the neutrons and the moderator nuclei, can significantly change the balance between neutron production and loss in a system, generally increasing k_{eff}. Materials containing hydrogen (e.g., water) are good neutron moderators.

The effectiveness of a moderator is dependent on the characteristics of the system. For systems with a low absorption cross section relative to the fission cross section, an optimum ratio of moderator atoms to fissile atoms can exist. For a system with constant fissile mass, increasing the moderator to fissile ratio (i.e., increasing the number of moderator atoms) increases the size of the system. On a plot of k_{eff} versus system size, k_{eff} will initially increase with size up to an optimum value and then decrease beyond this value. The system is undermoderated below the optimum value and overmoderated above this value.

Assessment of Nuclear Criticality

This study began with a bounding analysis based on highly conservative assumptions. Required assumptions were made in the direction that increased the criticality of the system. For example, because the locations of the materials in the boreholes were not well known, all of the material in a given borehole was assumed to be localized in a small volume with the optimum geometry to promote criticality; in reality the fissionable materials were dispersed within the boreholes, much less likely to lead to criticality.

Methods and Data

The multigroup Monte Carlo code KENO-IV [Petrie and Cross, 1975] was used to calculate the k_{eff} for the various configurations investigated in this study. KENO-IV is a standard tool used in criticality safety analyses and was chosen over other Monte Carlo codes because this code is simple and thus computationally very fast without compromising accuracy. The neutron cross-section data used in this study came from the CSRL [Ford et al., 1976] library. This study included collapsing the original 218-group structure of the neutron cross sections in the CSRL library to 27 groups using the AMPX [Greene et al., 1976] code system.

The results of a number of benchmark criticality experiments have been published [Brookhaven National Laboratory, 1974] and can be used as an integral test of the accuracy of all computational schemes. The benchmarks are divided into two broad categories, thermal and fast, based on whether hydrogen is present or not to moderate the neutron energies. For the thermal benchmarks, the average energy of the neutrons causing the fissions is near the average thermal energy of a hydrogen atom at the ambient temperature. For the fast benchmarks, the average energy of a neutron causing a fission is close to the average energy of the neutrons produced by fission. The thermal benchmarks that are most directly applicable to the work presented here are those that include critical solutions of uranium or plutonium. Several of the benchmark experiments were modeled using KENO-IV and the 27-group cross section data.

The results of the calculations of the thermal category of benchmarks are shown in Table L-1. Listed in the table are the benchmark designation, the difference between the measured k_{eff} and the calculated k_{eff} ($\Delta k = k_{expt} - k_{calc}$), and a brief description of the benchmark. The Δk is a bias factor that must be added to the calculated k_{eff} to obtain the measured result. In general, the calculations underpredict the k_{eff} for the uranium solutions by a few tenths of a percent and overpredict the k_{eff} for the plutonium solutions by as much as 1.7 percent.

The results of the calculations of the fast category of benchmarks are shown in Table L-2. The same data are listed here as for the thermal category of benchmarks. The calculations overpredict the k_{eff} for the uranium-fueled systems by a few tenths of a percent and underpredict the k_{eff} for the plutonium-fueled systems by up to 2.4%.

The KENO-IV code and 27-group cross sections predict the k_{eff} for the uranium-fueled benchmarks within a few tenths of a percent and for the plutonium-fueled benchmarks within two to three percent. While none of the benchmarks are exactly the same as the configurations

Table L-1. Thermal Criticality Benchmarks*

Name	Δ*k*	Description
ORNL-1	+0.0033 ± 0.0016	Bare sphere of uranyl nitrate in water, H/^{235}U ratio: 1378, radius 35 cm
ORNL-2	+0.0066 ± 0.0016	Bare sphere of uranyl nitrate in water with boron, H/^{235}U ratio: 1177, radius 35 cm
ORNL-3	+0.0065 ± 0.0016	Bare sphere of uranyl nitrate in water with boron, H/^{235}U ratio: 1033, radius 35 cm
ORNL-4	+0.0017 ± 0.0015	Bare sphere of uranyl nitrate in water with boron, H/^{235}U ratio: 972, radius 35 cm
ORNL-10	+0.0052 ± 0.0012	Bare sphere of uranyl nitrate in water, H/^{235}U ratio: 1835, radius 61 cm
PNL-1	-0.0157 ± 0.0026	Bare sphere of plutonium nitrate in water, H/^{239}Pu ratio: 700, radius 20 cm
PNL-3	-0.0023 ± 0.0021	Bare sphere of plutonium nitrate in water, H/^{239}Pu ratio: 1204, radius 23 cm
PNL-4	-0.0061 ± 0.0021	Bare sphere of plutonium nitrate in water, H/^{239}Pu ratio: 911, radius 23 cm
PNL-5	-0.0166 ± 0.0020	Bare sphere of plutonium nitrate in water, H/^{239}Pu ratio: 578, radius 20 cm
PNL-6	-0.0119 ± 0.0025	Bare sphere of plutonium nitrate in water, H/^{239}Pu ratio: 125, radius 19 cm
PNL-7	-0.0131 ± 0.0021	Water-reflected sphere of plutonium nitrate in water, H/^{239}Pu ratio: 980, radius 18 cm
PNL-12	-0.0159 ± 0.0020	Water-reflected sphere of plutonium nitrate in water, H/^{239}Pu ratio: 1067, radius 19 cm

* Each benchmark was done with 145,000 histories.

Table L-2. Fast Criticality Benchmarks

Name	Δ*k*	Description	Neutron Histories
GODIVA	! 0.0071 ± 0.0006	Bare uranium metal sphere	1,450,000
FLATTOP-25	! 0.0030 ± 0.0013	Depleted-uranium-reflected uranium metal sphere	290,000
JEZEBEL	+0.0084 ± 0.0008	Bare plutonium metal sphere	1,450,000
FLATTOP-PU	+0.0188 ± 0.0014	Depleted-uranium-reflected plutonium metal sphere	290,000
VERA-11A	+0.0238 ± 0.0012	Depleted-uranium-reflected plutonium/graphite cylinder	290,000

modeled for the material in the GCD boreholes, the comparisons with benchmarks do give an indication of the expected accuracy of the calculations. Based on the results of the benchmark calculations, a calculated k_{eff} of 0.95 or less will be considered here to be evidence that the system modeled is safely subcritical.

Inventory In TRU Boreholes

The TRU borehole inventory is discussed in Section 5.8.3, which is based on information examined in an earlier study [Chu and Bernard, 1991]. Only Boreholes 1, 2, 3, and 4 were found to contain either enriched uranium or plutonium, and thus only these boreholes are considered for criticality evaluation. Because discrepancies existed between the several sources of information surveyed in Chu and Bernard [1991], the reported mass estimates were imprecise. The estimated material masses are shown in Table L-3. Many of the masses are listed as ranges, which indicate the spread of the reported data.

The material in Boreholes 1, 2, and 3 is the remains of weapons parts that were recovered from four nuclear weapon accident scenes. In all four accidents, the weapons were involved in either a fire or high-explosive detonation. In the accidents involving fire, the heat was intense enough to melt the weapon parts. The fissile material mixed with an undetermined amount of structural material before resolidifying. The fissionable material recovered from detonation accidents was embedded in surrounding structural material by the blast. The material buried in Boreholes 1, 2, and 3 was packaged in 15 containers of differing construction. Five containers were buried in Borehole 1, four in Borehole 2, and six in Borehole 3.

The plutonium buried in Borehole 4 is divided among 258 fifty-five gallon drums and consists of surficial plutonium contamination on metal, plastic, and graphite items used in the manufacture and disassembly of weapons. A minor amount of ^{235}U (up to 45 grams) is also contained in these drums. The large amount of depleted uranium buried in this hole is contained in eight boxes separate from the drums.

Table L-3. Estimated Material Masses in Boreholes 1, 2, 3, and 4
[from Chu and Bernard, 1991]

Borehole	Estimated Material Mass (kg)		
	Enriched Uranium	Depleted Uranium	Plutonium
1	18.105 - 31.5	423.4 - 722.4	0.895 - 2.03
2	1.11 - 23.44	2.63 - 68.6	0.044
3	1.40 - 11.2	6.1 - 10.1	1.27 - 1.43
4	0.297	1280	2.23

The assumed isotopic composition of the radionuclides buried in the GCD boreholes is shown in Table L-4. The enriched uranium was assumed to be 93% by weight ^{235}U. The depleted uranium was assumed to be 0.2% ^{235}U. The plutonium was assumed to be high in ^{239}Pu with low quantities of the higher mass number isotopes. *(Note - these isotopic compositions*

Table L-4. Assumed Isotopic Composition of the Depleted Uranium, Enriched Uranium, and Plutonium Buried in GCD Boreholes 1, 2, 3, and 4

Isotope	Depleted Uranium (wt %)	Enriched Uranium (wt %)	Plutonium (wt %)
^{234}U	0.0	0.93	0.0
^{235}U	0.2	92.99	0.0
^{236}U	0.0	0.41	0.0
^{238}U	99.8	5.67	0.0
^{239}Pu	0.0	0.0	93.75
^{240}Pu	0.0	0.0	5.85
^{241}Pu	0.0	0.0	0.40

differ slightly from information given elsewhere. The differences are small, and would have no substantive effect on the results of this study.)

Modeling Assumptions

The Harms, et al. study performed a bounding criticality analysis for the radionuclides buried at the GCD facility. To do this analysis, assumptions on the mass of radionuclides in each borehole were made that are as conservative as possible, while still remaining consistent with the documentation of the inventory. The analyses were done both for the solid form of the material as it was originally emplaced and for the form it would take if the radionuclides were to enter solution.

For cases where the radionuclides enter solution, both enriched and depleted uranium were included in the solution, because these radionuclides are chemically identical. Plutonium could conceivably behave differently from the uranium (e.g., enter solution where the uranium does not), and this possibility was addressed. For the boreholes that contained both enriched uranium and plutonium (Boreholes 1, 2, and 3), the upper limits on the masses of these radionuclides given in Table L-3 were used while the lower limit on the mass of the depleted uranium, which is a neutron absorber, was used. This approach yielded the highest ratio of fissile atoms to absorbing atoms consistent with the mass data, and overestimates the potential for criticality.

Because Borehole 4 contains a relatively small amount of enriched uranium compared to a large inventory of depleted uranium, the uranium was ignored and only the plutonium was considered in the analyses. The fission cross section of ^{238}U has a threshold at high neutron energies and thus ^{238}U contributes very little to the production of neutrons. The absorption cross section, however, is fairly large. As a result, ^{238}U is a net neutron absorber (poison) in a critical system and ignoring this isotope of uranium as a constituent of the material in Borehole 4 results in a large degree of conservatism to the analysis by eliminating a major poison from consideration. Borehole 4 has the largest plutonium inventory of the TRU boreholes, so results for this borehole will bound those of the other boreholes if plutonium alone is considered.

Solubilities of various radionuclides, including uranium and plutonium, in the ground water near the GCD site were collected and reported in Chu and Bernard [1991]. Solubilities were reported for two different groundwater compositions; J-13 water from near Yucca Mountain, and Well 5b water, which is from a well closer to the RWMS and thus possibly more representative of groundwater at the GCD location (Figure L-1). Using the solubility data and the mass of radionuclides in each borehole, the radius of a sphere of water that could contain all of the dissolved fissile radionuclides in a given borehole can be calculated. These radii are shown in Table L-5, assuming the higher of the two solubilities given in the table. In calculating these radii, only the mass of the most dominant fissile radionuclide (enriched uranium or plutonium) was used. In the analyses that follow, the fissile radionuclides in the TRU boreholes are assumed to be completely soluble. *(Note - more recent solubility data are reported elsewhere in this document, but their use for these calculations would not substantially affect the conclusions reached using the solubilities available at the time these calculations were performed.)*

Table L-5. Solubilities of the Materials in the TRU Boreholes and Radius of the Sphere That Could Contain a Volume of Water Sufficient to Dissolve the Given Radionuclides in Each Borehole (solubility data from Chu and Bernard, 1991)

Hole	Fissile Material	Solubility (g/g)		Sphere Radius (m)
		j-13 Water	Well 5b	
1	Enriched uranium	9.4×10^{-4}	1.0×10^{-5}	2.0
2	Enriched uranium	9.4×10^{-4}	1.0×10^{-5}	1.8
3	Enriched uranium	9.4×10^{-4}	1.0×10^{-5}	1.4
4	Plutonium	1.2×10^{-5}	6.0×10^{-5}	2.1

Criticality Calculations

Sets of calculations were performed for each of four sets of physical-chemical conditions. Results of these calculations are presented in detail by Harms et al. [1998, p. 22–32]; the cases and analytical results will be summarized here.

Isolated Radionuclides

The first set of calculations were done for a hypothetical worse case (maximum criticality potential. This case required that all of the fissile radionuclides in each borehole were concentrated into a metallic sphere (no admixed fill material or moderator). This physically impossible case was analyzed with three neutron reflector configurations: no reflector, a probertite reflector, and a water reflector. Because no moderator is included in this configuration, most of the fissions in a critical assembly will be produced by fast neutrons. As a result, the probertite, which was used as the backfill material to act as a good thermal-neutron poison, actually behaves as a good reflector, because the neutron energy is not degraded sufficiently for the poison to take effect. These results give a conservative bound on the actual case in the TRU boreholes, because the radionuclides in each borehole are contained in several (four to six) separate packages that are spread axially over the 15-meter height in which TRU waste was emplaced. The multiplication factors are well below 1 in all cases except for Borehole 2 with probertite and water reflectors.

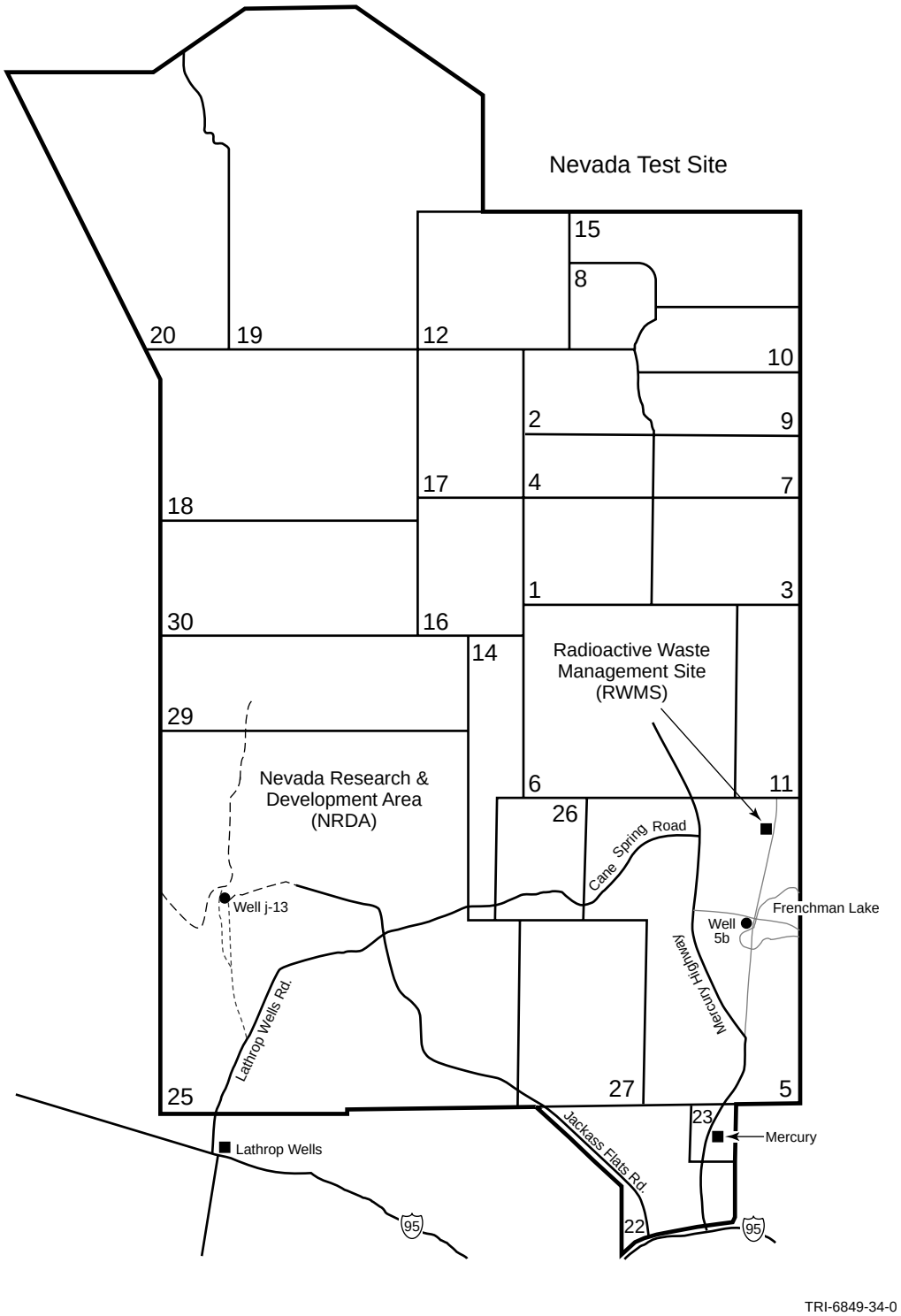

Figure L-1. Location of Wells J-13 and 5b at the NTS.

Two approaches were taken to examine the effects of a slightly more realistic dispersion of the fissile radionuclides. The first approach used spheres larger than the ideal minimum size used in the first calculation. For both reflectors, k_{eff} drops sharply as the radius of the sphere increases, because the neutron leakage increases as the surface to volume ratio of the sphere increases. The second approach was to divide the radionuclides in Borehole 2 into two equal hemispherical bodies and to calculate k_{eff} as a function of the distance separating the faces of the hemispheres. The reflector material filled the space between the hemispheres. At infinite separation (i.e., each hemisphere acts independently), k_{eff} was 0.737 for a probertite reflector and 0.820 for a water reflector. With the probertite reflector, a separation of 40 centimeters was sufficient to decrease k_{eff} to the infinite separation value. Because water is a better moderator than probertite, a separation of only 20 centimeters was adequate to decrease k_{eff} to the infinite separation value with the water reflector. Thus, because the radionuclides in the boreholes are actually more widely dispersed than the simple cases calculated, a criticality incident involving the radionuclides as buried is not credible, even in Borehole 2.

In Situ Solution of Radionuclides

The second set of calculations involved dissolving all the fissile radionuclides. In general, the effective multiplication factor of a given mass of fissile radionuclides can be increased by dispersing the material in a moderator; for example, by dissolution in water. In fact, under ideal conditions, less than 1 kilogram of ^{235}U can be made to go critical if properly dispersed in water. The reactivity of a solution is influenced by the amount of fissile radionuclides present, the amount of moderator available, the amount and neutron absorbing characteristics of other materials included in the solution, the characteristics of any reflector present, and the geometry of the system. For example, if all of the fissionable radionuclides in Borehole 2 were dissolved in water with no other materials and held in a spherical shape with a thick water reflector, the effective multiplication factor of the system would be a function of the radius of the sphere. The highest k_{eff} occurs at a radius of about 35 centimeters. For radii less than this value, the system is undermoderated. For radii greater than about 35 centimeters, the system is overmoderated. The calculations showed that the fissile nuclide solubilities are at least an order of magnitude too low to allow a criticality do develop under the most favorable conditions.

Most additional materials, such as naturally occuring dissolved salts, probertite and mineral grains, included in the solution with the radionuclides will decrease the effective multiplication factor of the system by absorbing neutrons. The mineral probertite was used as backfill in three of the TRU boreholes that contained fissile radionuclides, and local sedimentary material was used in the fourth (Borehole 4). Probertite is a mineral that contains a high boron content. Boron is a strong thermal-neutron absorber. The effect of the boron is to decrease substantially the effective multiplication factor of fissile solutions placed in the pores of the backfill material. Native soil materials decrease the effective multiplication factor, although not as substantially as probertite. Under these more realistic conditions, the solubilities are several orders of magnitude too low to permit criticality. In addition, the disposal volume is well above the water table, so saturated conditions in the vicinity of the waste cannot occur.

In Situ Deposition of Radionuclides

The third set of calculations required that the fissile radionuclides be dissolved in groundwater, transported and deposited into a small, continuous volume. The reported porosities of the existing alluvium at the GCD site are in the range of 33% to 36% [Holmes and Narver, Inc., 1983]. This range of porosity values is narrower than the results of more recent measurements of these sediments [REECo, 1993a,b], although the mean porosity value is approximately the same for these sets of data. The results of criticality calculations for cases where fissile radionuclides have been dissolved from the wastes and redeposited in pores in the alluvium are included in Harms, et al. [1998, p. 26–29]. While probertite was not used as backfill in Borehole 4, the results for the plutonium in the borehole are used to bound the results for the plutonium buried in the other three boreholes. In all cases, the maximum k_{eff} occurs at the radius where the fissile nuclides are packed tightly in the pores with no remaining pore space. The highest value of k_{eff} is about 0.6 for the radionuclides in Borehole 2. These results show that, even under the most conservative assumptions on the distribution of the radionuclides, a criticality incident is not possible in the boreholes containing probertite. No credible mechanism exists to precipitate large amounts of plutonium or uranium in the porosity surrounding the waste.

The results presented by Harms, et al. [1998] show that a criticality incident is not possible for the fissile material buried in Boreholes 1 through 4 without some sort of migration of the radionuclides away from the alluvium containing the wastes. Conditions that could lead to an increase in k_{eff} could be the relocation of the radionuclides into a high-porosity region of the probertite or migration of the radionuclides completely out of the probertite backfill. The minimum porosity in the probertite required to achieve criticality for any given mass of radionuclides was determined [Harms, et al., 1998, Table 8]. For all three boreholes, the minimum porosities are greater than 91%. In order to achieve criticality, the radionuclides would be required to migrate to a void in the backfill. A factor of 50 for uranium solubility and more than three orders of magnitude for plutonium would be required to hold an ample amount of the fissile material in solution to achieve criticality

Migration Of Radionuclides Out Of The Probertite

The case where the fissile radionuclides are transported away from the probertite was also analyzed [Harms et al., 1998, p. 29–32]. Complete segregation of radionuclides and probertite was assumed, although the segregation is not physically reasonable. For all boreholes, k_{eff} is less than 1, with a maximum of 0.92 for the material in Borehole 2. The minimum porosity of the alluvium at which the conservative criticality limit (k_{eff} = 0.95) can be achieved and critical radius were calculated for the radionuclides in each borehole. The minimum porosity required to achieve criticality varies by borehole with a minimum of about 39 percent for Borehole 2. Table 9 [Harms et al., 1998, p. 32] lists the ratios of the mass of fissile material to the mass of water in the pore space that holds the material in solution. Comparing these values with the solubilities of the fissile material in the local groundwater again shows that the solubilities of the fissile material would have to increase by more than a factor of 50 for uranium and more than three orders of magnitude for plutonium to keep the fissile material in solution.

This analysis assumed that the entire inventory of a hole migrated from a widely dispersed condition in the backfill of the borehole and concentrated in a compact volume in the native alluvium at the site. For Boreholes 1 through 3, the material would be required to move *en mass* from the probertite fill to the surrounding alluvium. For Borehole 4, the material would be required to migrate from the 258 drums to a 42-cm diameter sphere either inside or outside the borehole. No transport process has been identified that would allow movement and reconcentration of the radionuclides on this scale. For any given alluvium porosity, a minimum radionuclide fraction is required to be concentrated in a specific volume to reach criticality. At 50-percent porosity, over half of the inventory must be concentrated in a very small volume of the alluvium to approach criticality.

Time Dependence Of Effective Multiplication Factor

The half lives of the radionuclides originally buried in the GCD holes are shown in Table L-6. The original radionuclides will decay with time, producing other isotopes of differing nuclear properties. For example, ^{239}Pu decays by the emission of an alpha particle directly to ^{235}U, which decays through a series of radionuclides eventually to ^{207}Pb. Because the makeup of the fissile material changes, the k_{eff} of a given configuration is a function of time [Harms et al., 1998, Figure 4-14]. The material is assumed to be dissolved in water to the solubility limit in 35% porous alluvium with nearly the optimum spherical configuration. The k_{eff} for the material in Borehole 2 is constant over the first million years and then drops as a significant amount of the ^{235}U decays. The k_{eff} for the material in Borehole 4 is constant until about 10,000 years after disposal, beyond which significant decay of the ^{239}Pu occurs. The k_{eff} reaches a lower constant level after the ^{239}Pu has decayed to ^{235}U and then drops beyond a million years as a significant amount of the ^{235}U decays. In neither case does k_{eff} increase during the time period considered.

Table L-6. Half-lives of the Fissionable Radionuclides Buried in the TRU Boreholes

Nuclide	Half-Life (yr)
^{234}U	2.45×10^{5}
^{235}U	7.038×10^{8}
^{236}U	2.342×10^{7}
^{238}U	4.468×10^{9}
^{239}Pu	2.41×10^{4}
^{240}Pu	6.57×10^{5}
^{241}Pu	14.4×10^{0}

This decrease in k_{eff} with time contrasts with the behavior of systems that contain "spent" nuclear fuel, which has been irradiated in a reactor for a long period of time. The fissile radionuclides buried in the TRU boreholes are relatively "clean," in that they contain little of the nonfissile isotopes of plutonium (e.g., ^{240}Pu and ^{242}Pu) or of ^{241}Am (a decay product of short-lived ^{241}Pu), which are strong neutron absorbers. Spent fuel contains a higher proportion of these nonfissile isotopes. With spent fuel, the initial critical mass is larger because of the neutron losses to the absorbers. As the absorbers decay to less absorbing nuclides, the k_{eff} of the system can increase.

This behavior is not seen for the isotopic composition of the material disposed of in the TRU boreholes.

Summary and Conclusions

The study by Harms et al. [1998] has investigated the criticality safety of the TRU waste buried in Boreholes 1 through 4 at the GCD disposal facility in Area 5 of the NTS. Bounding analyses were done in which all of the radionuclides in a given borehole were assumed to concentrate in a small volume even though a mechanism for concentrating the radionuclides in this manner does not exist. All assumptions were made in the direction that increased the conservatism of the analyses. The four situations examined in the analyses are: (1) the radionuclides in each borehole are concentrated within the backfill as a metallic sphere having no porosity, (2) the radionuclides are dissolved in groundwater and maintained in a spherical shape within the backfill, (3) the radionuclides are deposited within the pore volume available within the backfill, and (4) the radionuclides are deposited in the pore space within the undisturbed alluvium outside the boreholes.

For radionuclides concentrated in metallic spheres, the analyses considered an absence of reflectors and the presence of probertite and water as reflectors. Of the 12 analyses for the four boreholes and three reflector arrangements, only the radionuclides in Borehole 2 when concentrated in a sphere of radius 6.1 cm with probertite and water reflectors resulted in values of k_{eff} in excess of 0.95, which is the value assumed for criticality to occur. Even relatively minor dispersal of the radionuclides from the spherical geometry (e.g., separating the hemispheres) resulted in values of k_{eff} substantially below 0.95.

For fissionable radionuclides in a spherically-shaped solution within the backfill and surrounded by a water reflector, the radionuclide inventories can result in values of k_{eff} equal to or greater than 0.95 for certain sphere radii and mass ratios of the solutions. The mass ratios necessary for criticality to occur require radionuclide solubilities at least one order of magnitude greater than the solubilities determined for the groundwater composition in the vicinity of the GCD facility. Criticality under these conditions is not possible, because no mechanism exists that can create the geometry of this analysis in the field, other materials in solution with the fissionable radionuclides will absorb neutrons, and the radionuclide solubilities necessary for criticality to occur are not physically achievable for GCD-specific groundwater properties.

Concentration of the fissile radionuclides of each borehole in the pore volume in the probertite backfill was also analyzed. The radionuclides were assumed to occupy a spherical volume within the backfill with the pores filled with various proportions of radionuclides and either air or water. For all analyses of all borehole inventories, k_{eff} did not exceed 0.6. In addition to the lack of a mechanism to concentrate the radionuclides within the backfill, the porosities of the backfill required for criticality to be a concern are physically unrealistic (> 0.91).

Complete segregation of the fissile radionuclides in the alluvium was also analyzed. The radionuclides were assumed to be concentrated in a spherical shape, occupying the pores within the alluvium. Calculation of the minimum porosity in the alluvium for criticality to occur indicates that only the porosity associated with the Borehole 2 inventory is within the range of

porosity values measured for samples associated with the GCD facility. No mechanism has been identified that can result in complete radionuclide concentration of a borehole's entire inventory. Fractional concentrations of radionuclides may be possible, but the porosities required for fractions of the radionuclide inventory to achieve criticality are higher than expected for alluvial deposits. A mechanism to achieve significant (i.e., with respect to criticality) fractional concentrations of radionuclides in the required geometry is also lacking.

Criticality analyses based on radionuclide inventories in the TRU boreholes do not consider the possible contributions to criticality by daughter products of the fissile radionuclides. Analyses of k_{eff} as a function of time (to 1 billion years) for radionuclides in Borehole 2 (nearly all uranium) and Borehole 4 (all plutonium) indicate that k_{eff} does not increase during this time frame for either inventory. These results are also applicable to the radionuclide inventories in Boreholes 1 and 3.

Based on the results of bounding analyses of criticality safety for the fissile-radionuclide inventories in the TRU boreholes at the GCD location, criticality cannot occur under conditions that either currently exist within the disposal system or will occur during the evolution of the disposal system. The conclusion derived from this study is that nuclear criticality is not only physically unreasonable, but physically impossible.

REFERENCES

Brookhaven National Laboratory. 1974. *ENDF-202 Cross Section Evaluation Working Group Benchmark Specifications*, BNL 19302 (with updates), Brookhaven National Laboratory, Upton, NY.

Chu, M.S.Y., and E.A. Bernard. 1991. *Waste Inventory and Preliminary Source Term Model for the Greater Confinement Disposal Site at the Nevada Test Site*, SAND91-0170, Sandia National Laboratories, Albuquerque, NM.

Ford, W.E., C.C. Webster, and R.M. Westfall. 1976. *A 218-Group Neutron Cross-Section Library in the AMPX Master Interface Format for Criticality Safety Studies*, ORNL/CSD/TM-4, Oak Ridge National Laboratory, Oak Ridge, TN.

Greene, N.M., W.E. Ford, III, J.L. Lucius, J.E. White, L.M. Petrie, and R.Q. Wright. 1976. *AMPX: A Modular Code System for Generating Coupled Multigroup Neutron-Gamma Libraries from ENDF/B*, ORNL/TM-3706, Oak Ridge National Laboratory, Oak Ridge, TN.

Harms, G.A., T.L. Steinborn, and R.V. Guzowski. 1998. *An Assessment of Nuclear Criticality for the Greater Confinement Disposal Facility, Area 5 of the Nevada Test Site*, SAND94-1854, Sandia National Laboratories, Albuquerque, NM.

Holmes and Narver, Inc. 1983. *Soil Characterization for the Greater Confinement Disposal Test Demonstration Project at the Nevada Test Site*, Holmes and Narver, Inc., Mercury, NV.

Petrie, L.M., and N.F. Cross. 1975. *KENO-IV—An Improved Monte Carlo Criticality Program*, ORNL-4938, Oak Ridge National Laboratory, Oak Ridge, TN.

REECo (Reynolds Electrical & Engineering Co., Inc.). 1993a. *Site Characterization and Monitoring Data from Area 5 Pilot Wells, Nevada Test Site, Nye County, Nevada*, Draft Report, Reynolds Electrical & Engineering Co., Inc., Las Vegas, NV.

REECo (Reynolds Electrical & Engineering Co., Inc.). 1993b. *Hydrogeologic Data for Science Trench Boreholes at the Area 5 Radioactive Waste Management Site, Nevada Test Site, Nye County, Nevada*, DE-AC08-94-NV11432 Reynolds Electrical & Engineering Co., Inc., Las Vegas, NV.

U.S. EPA (Environmental Protection Agency). 1985. *Environmental Standards for the Management and Disposal of Spent Nuclear Fuel, High-Level and Transuranic Radioactive Waste: Final Rule, 40 CFR Part 191*, Federal Register, v.50, no.182, p. 38066-38089.

Wick, O.J., ed. 1967. *Plutonium Handbook. A Guide to the Technology. Volume II*, Gordon and Breach, Science Publishers, Inc., New York, NY.

This page intentionally left blank.

Appendix M

Memos from Price to Brown, Brown to Cochran

This page intentionally left blank

date: January 10, 1996

to: Theresa Brown, 6851

from: Laura Price, 6331

subject: Selection of tortuosity values for PAIII (memo/95/S34)

Tortuosity is one of the most important variables in the liquid phase diffusion model used to estimate releases of radionuclides to the accessible environment, according to sensitivity analyses performed as a part of the second iteration of the performance assessment for the GCD boreholes at the Area 5 Radioactive Waste Management Site at the Nevada Test Site (NTS) [Baer et al., 1994]. The values of tortuosity used by Baer et al. [1994] were arrived at after only a cursory study, and so a more detailed study was required. That more detailed study is documented in this memo.

Introduction

Tortuosity, τ, is a dimensionless number that reflects the fact that radionuclides are diffusing through alluvium that contains a variety of pore sizes and that may not have a continuous water phase. Tortuosity can be defined in a number of ways. Sometimes it is represented by the ratio of the length of the actual diffusion path taken through the alluvium between two points to the straight line distance between the same points. Tortuosity is also sometimes represented by the square of that same ratio [Sadeghi et al., 1989]. Either of these two definitions yields a value of tortuosity that is always greater than or equal to one. Some workers define tortuosity as the reciprocal of the above definitions, yielding values that are always less than or equal to one [Jury et al., 1991; Shearer et al, 1973]. For the purpose of this study, the relationship between effective diffusion coefficient and tortuosity is defined as

$$D_{eff} = \frac{D_0}{\tau} \qquad \text{(M-1)}$$

where

D_0 = free-water diffusion coefficient, and
D_{eff} = effective diffusion coefficient in the alluvium.

Defined in such a manner, the tortuosity is always greater than or equal to one. Low values of tortuosity signify that the actual path taken through the alluvium *is not* very tortuous, and that the effective diffusion coefficient is not much lower than the free-water diffusion coefficient. Large values of tortuosity indicate that the actual path taken through the alluvium *is* tortuous and that the effective diffusion coefficient is much lower than the free-water diffusion coefficient. Therefore, in general, large values of tortuosity result in slower diffusion and lower cumulative releases of radionuclides to the accessible environment.

In the discussion that follows, I assume that tortuosity is a function of volumetric moisture content (VMC), θ, and/or porosity, ε. There is widespread, but not universal, support for this assumption. Conca and Wright [1992a] state that "diffusion coefficients for all materials fall into a narrow range of distribution and demonstrate that the diffusion coefficient is dependent primarily on the *volumetric* water content, and only secondarily on material type at any given water content." They support this statement with a plot of effective diffusion coefficient versus VMC for soils, silts, clay, gravel, and whole rock cores. Approximately 100 data points are plotted and all points follow the same general curve, regardless of rock type. This curve shows a steep increase in effective diffusion coefficient as VMC increases from 1% to about 5% with a more gradual increase in effective diffusion coefficient as VMC increases above 5%. Other researchers that have also found the effective diffusion coefficient to be dependent primarily on VMC include Conca and Wright [1992b], Jurinak et al. [1987], Shearer et al. [1973], and Wright [1990]. Sadeghi et al. [1989] found that relative water content (θ/ε) was a better predictor of effective diffusion coefficient than was VMC. On the other hand, Ryan and Cohen [1990] state that "there is no one single model that can be used to accurately predict individual phase tortuosities as a function of θ." The difference in opinion between these various researchers can be explained as follows. Ryan and Cohen [1990] were studying the diffusion of lindane and dieldrin, organic compounds that diffuse in all three phases: soil, air, and water. In contrast, those researchers that concluded that effective diffusion coefficient was primarily dependent on VMC (or relative water content) were studying diffusion in the water phase only. Therefore, perhaps the effective diffusion coefficient *is not* primarily a function of water content if the diffusing species diffuses in multiple phases, but *is* a function of water content if the species in question diffuses only in the aqueous phase. Because radionuclides diffuse primarily in the aqueous phase, available data support the assumption that the effective diffusion coefficient used in the performance assessments and, hence, the tortuosity, is a function of the VMC, θ, and/or the porosity, ε.

Background

In the first iteration of the performance assessment for the GCD boreholes at the NTS, known as the preliminary performance assessment (PPA) [Price et al., 1993], the relationship between tortuosity and effective diffusion coefficient was defined as

$$D_{eff} = \frac{\theta\, D_0}{\tau_{PPA}} \tag{M-2}$$

while in the second iteration of the performance assessment (PA2) [Baer et al, 1994] it was defined as

$$D_{eff} = \frac{D_0}{R\, \tau_{PA2}} \tag{M-3}$$

where

R = retardation coefficient (dimensionless).

The PPA relationship includes VMC, θ, while the others (Eq. M-1 and M-3) do not. The retardation coefficient was not included in the PPA definition because the liquid phase diffusion model

did not include retardation. In the PA2, retardation was included in the model of liquid phase diffusion, but each radionuclide in each radionuclide decay chain was assumed to have the same retardation coefficient; hence, the retardation coefficient could be included in the definition of the effective diffusion coefficient, which affects all radionuclides equally. This was done so that an analytical solution to the liquid phase diffusion problem could be implemented. The definition of effective diffusion coefficient used in the present study does not contain the retardation coefficient because the numerical solution that will be used to solve the liquid phase diffusion problem allows a unique retardation coefficient to be assigned to each radionuclide. Therefore, the retardation coefficient cannot be included in the definition of effective diffusion coefficient.

In the PPA [Price et al., 1993], the tortuosity was assumed to be uniformly distributed between 1 and 110, and was correlated with the VMC with a correlation coefficient of -0.9. This distribution was loosely based on the relationship of Campbell [1985], $\tau = 1/(2.8\ \theta^3)$. Because the PPA definition of D_{eff} included VMC in the numerator, the relationship from Campbell was modified to $\tau = 1/(2.8\ \theta^2)$. Using the modified Campbell relationship and the 0.999 quantile (0.17) and 0.001 quantile (0.06) values of the lognormal VMC pdf yielded minimum and maximum tortuosity values of 12.36 and 99.20, respectively. To account for uncertainty in the empirical relationship used above, the minimum and maximum values of tortuosity were assumed to be 1 and 110, respectively, yielding the pdf used in the PPA. To compare these values of tortuosity with those used in the PA2, these values need to be adjusted by dividing by the VMC. Doing so yields a lower value of (1/0.17) = 5.88 and an upper value of (110/0.06) = 1833.

In the second iteration of the performance assessment [Baer et al., 1994], the tortuosity was assumed to vary uniformly between 3 and 110, and was correlated with the VMC with a correlation coefficient of -0.9. In this iteration, the moisture content was assumed to vary lognormally (as before) but with a 0.001 quantile value of 0.0475 and a 0.999 quantile value of 0.181. Using these values in the original Campbell [1985] model to obtain maximum and minimum values of tortuosity yielded values of 3332 and 60 respectively. It was decided to keep the maximum value of tortuosity at 110, the value used in the PPA, because it was conservative to do so. However, it was not conservative to raise the minimum value from 5.88 to 60. Therefore, it was decided to use the value of tortuosity obtained under saturated conditions. Under saturated conditions, the VMC is equal to the porosity, 0.46. Using this value in the Campbell [1985] model yielded a minimum tortuosity value of 3.7. The minimum value was therefore set to 3.

A minimum of effort was expended in developing the pdf's of tortuosity for the PPA and the PA2 because tortuosity was not considered to be an important variable; therefore, investigating it did not merit a substantial amount of activity. However, the sensitivity analyses conducted as a part of the PA2 indicated that, under base case conditions, tortuosity and root depth were the most important variables in determining the value of the EPA Sum. The present study examines tortuosity more closely than it was examined for either the PPA or the PA2 and suggests defensible values of tortuosity to use in the next iteration of the performance assessment.

Tortuosity Models

After conducting a literature search and looking at the assorted models presented by a variety of researchers, I narrowed down the candidate models to three. These models were selected because they were presented along with data that supported them and because the data represented water contents that were roughly in the same range that we are interested in (0.05 # θ # 0.18). The three models are as follows.

Shearer et al. [1973] (as taken from Millington & Quirk [1961])

$$\tau = \frac{\in^2}{\theta^{10/3}} \tag{M-4}$$

Wright [1990]

$$\tau = \frac{e^{-b\theta}}{a}; \quad 0.001 \le a \le 0.005, \quad b = 10. \tag{M-5}$$

Sadeghi et al. [1989]

$$\tau = 5.56\left(\frac{\in}{\theta}\right)^{2.98} \tag{M-6}$$

Wright's [1990] model was actually taken from work by Kemper and Van Schaik [1966] and Olsen and Kemper [1968], but I will call it Wright's model for brevity. In Wright's model, *a* varies from 0.005 to 0.001, depending on soil type and texture. A value of 0.005 is used for sand and 0.001 is used for clay. In the calculations done below, a value of 0.005 was used. Note that the Wright model is not dependent on porosity (ε).

Plots of the tortuosity calculated by the three models as a function of VMC are given in Figures M-1 and M-2. These figures show the tortuosity for five different values of porosity, 0.248, 0.305, 0.362, 0.419, and 0.475. Figure M-1 gives τ(θ) for the Wright and Shearer et al. models while Figure M-2 gives τ(θ) for the Wright and Sadeghi et al. models. As is expected, the tortuosity increases with decreasing VMC. Also, for a given VMC, the tortuosity increases as the porosity increases. The Wright model gives the lowest (i.e., most conservative) value of tortuosity of the three models for VMCs less than about 0.12.

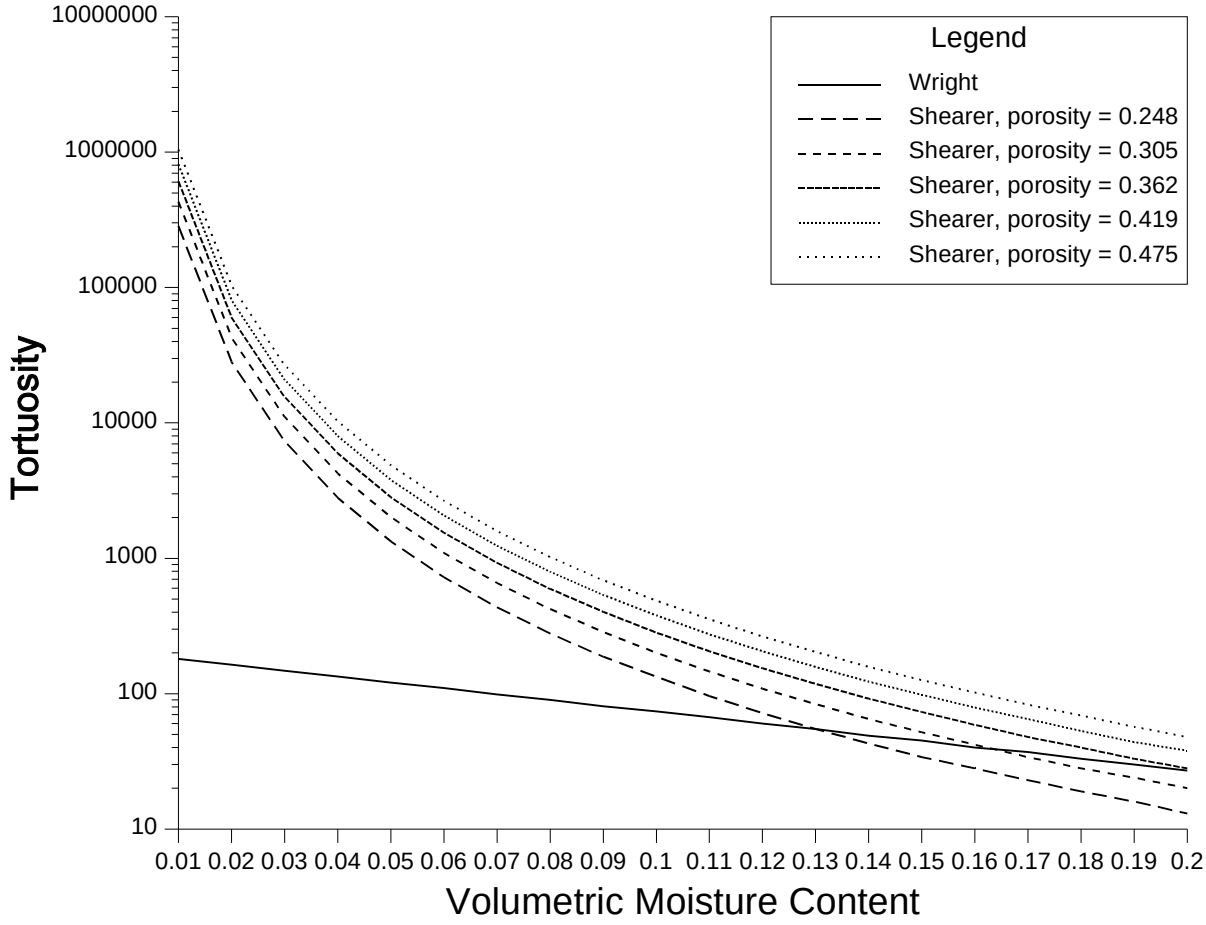

Figure M-1. Models of Shearer and Wright.

Comparison with Data

As stated above, each of the three models was presented along with data that supported that particular model. Of course, each model should be compared with data found in other publications. Such a comparison is shown in Figure M-3.[1] In this figure, data from six different publications are shown (discrete points) and are compared with the three models given above (lines). All the data represent measurements of diffusion of species in a single phase. Because diffusion in multiple phases is probably not a function of VMC, studies reporting measurements of diffusion coefficients for multiphase diffusion were not included in the study below. The data in this figure were collected from experiments that looked at a variety of rock types. The following paragraphs discuss each data set and how the data were collected.

[1] Shearer et al. (1973) presented models for both vapor and non-vapor phase diffusion within the context of the diffusion of lindane, a substance that diffuses in the vapor and non-vapor phases. Hence, the data presented by Shearer et al. represents multiphase diffusion and is not shown in Figure M-3.

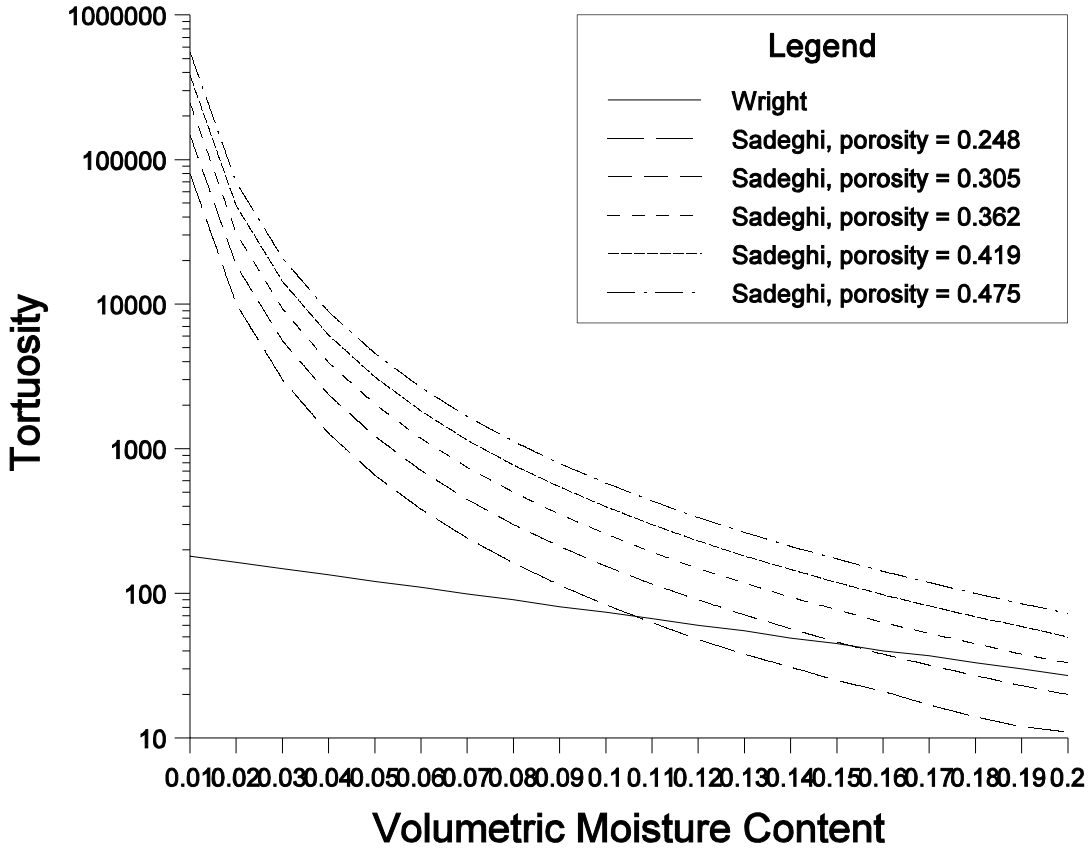

Figure M-2. Models of Sadeghi and Wright.

Sadeghi et al. [1989] studied the diffusion of urea in seven different soils (Cecil, Houston Black, Crete, Smolan, Richfield, Kahola, and Haynie) in which clay content ranged from 10% to 51%, sand content ranged from 9% to 41%, and silt content ranged from 16% to 67%. Urea is not adsorbed by these soils and does not have a significant vapor pressure at ambient temperatures; therefore, it was transported only in the liquid phase. The diffusion of urea was studied in the laboratory using packed soil columns of known water content. Urea diffused through the soil columns for 48 hours, after which the soil was sampled at various depths and analyzed for urea concentration. Urea concentrations were also calculated using numerical techniques to solve the diffusion equation. The effective diffusion coefficient, D_{eff}, was initially estimated and then modified incrementally until the root mean square error (RMSE) of the difference between calculated and measured urea concentrations with depth for a given soil column was minimized. These effective diffusion coefficients were reported in a table, along with the relative moisture content (θ/ε), and were plotted as a function of VMC. Tortuosity was calculated from these data by dividing the diffusion coefficient of urea in water (assumed to be $2.08 \times 10^{!9}$ m^2/s at 25EC [Sadeghi et al., 1988]) by the effective diffusion coefficient associated with the minimum RMSE. The corresponding VMCs were estimated from the plot.

The data from Sallam et al. [1984] were obtained from laboratory studies using an inert gas (Freon). Freon is sparingly soluble in water (0.028% by weight at 25EC and 1 atm) and so

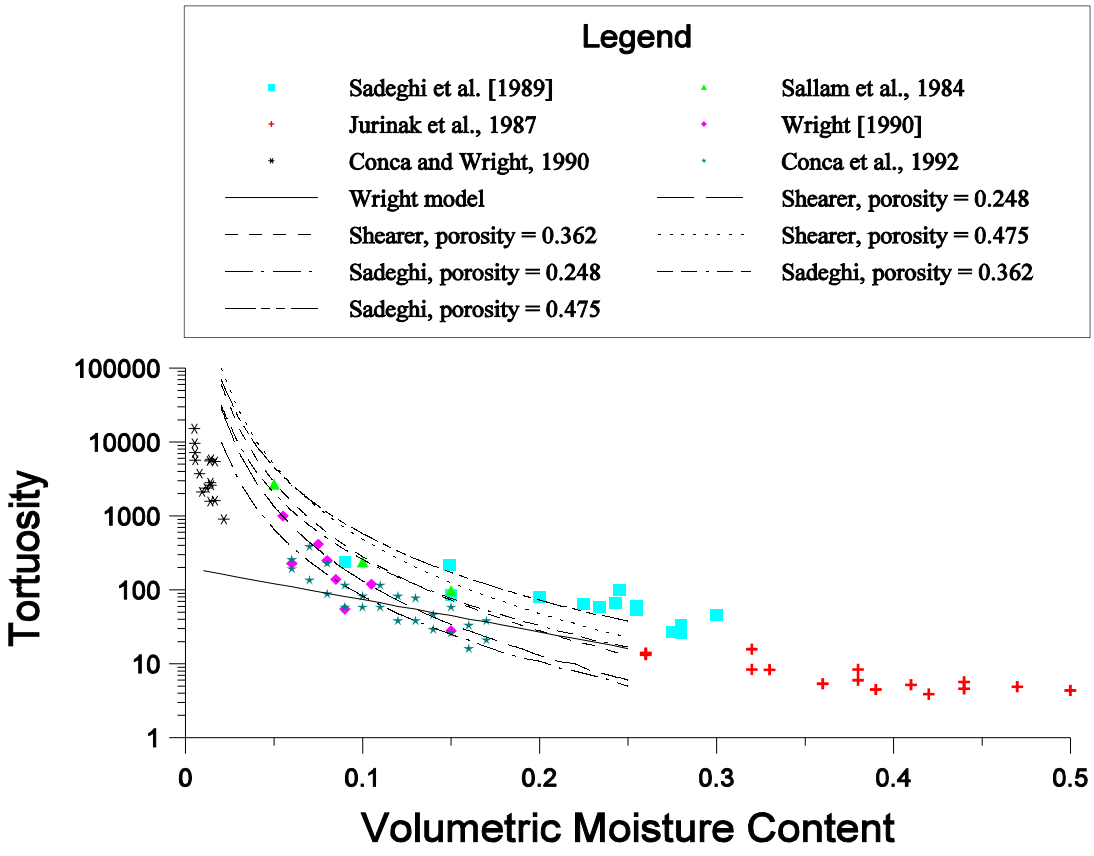

Figure M-3. Comparison of Tortuosity Data and Models

diffused only in the gas phase. The gas diffused through a Yolo silt loam that had been packed to 5, 10, and 15% air-filled porosity in a cylindrical soil chamber. The soil chamber was connected to two air-filled chambers, the inlet chamber on one side and the outlet chamber on the other. The effective diffusion coefficient was determined by measuring the freon concentration in the outlet chamber. Six experiments were performed for each value of air-filled porosity and the average effective diffusion coefficient determined from the six experiments was reported for each value of air-filled porosity. Sallam et al. [1984] gave the value of the Freon gas diffusion coefficient in air, so the tortuosity for a given value of air-filled porosity was calculated by dividing the free-air diffusion coefficient by the measured effective diffusion coefficient. Even though the data from this experiment are representative of diffusion in the gas phase, I believe they are relevant to liquid phase diffusion because the diffusion path is made tortuous by the same factors in each case (closed-end pores, discontinuous diffusion phase, variety of pore sizes) and diffusion is occurring in only one phase. Jury et al. [1991] confirm this, stating that "...liquid tortuosity modifies liquid diffusion in the same way that the gas tortuosity modifies gas diffusion..." Thus, I believe it is reasonable to use these gas-phase tortuosity data in this study.

The data from Jurinak et al. [1987] were obtained from laboratory studies that measured liquid phase ion diffusion coefficients for Na, Ca, and Cl in three different soils (Aiken clay loam, Yolo loam, and Kidman fine sandy loam) under saturated and unsaturated conditions. The measurements were made using bulk soil specific electrical conductivity data and the Nernst-Einstein equation. In this conductometric technique, "the diffusion coefficients of constituent ions can be estimated by determining their equivalent (molar) conductance and then applying the well-documented Nernst-Einstein equation (Bockris and Reddy, 1973)" [Jurinak et al., 1987]. According to Jurinak et al.[1987], various studies have found "reasonable" agreement between predicted and experimentally measured ionic diffusivities of Na, K, and Ca, supporting the use of the Nernst-Einstein equation in a charged porous medium. In this technique, the apparent specific conductance, K_a, is defined by the relationship

$$K_a = K_w \, \theta T + K_s \tag{M-7}$$

where

K_w = specific conductance of the solution,
θ = volumetric moisture content (VMC),
T = dimensionless transmission coefficient, and
K_s = apparent specific surface conductivity or excess conductance.

Jurinak et al. [1987] assume that θT is a "measure of the effect of the porous medium on the mobility of ions under an electric potential gradient similar to the situation when the ions are under a chemical potential gradient, i.e., diffusion." Thus, θT (or its inverse) can be considered as a tortuosity factor. The data shown in Figure M-3 were calculated from tabular values of K_s and K_a. The value of K_w was given in the text. The tortuosity was calculated from the equation

$$\tau = \frac{K_w}{K_a - K_s} \tag{M-8}$$

which was obtained by solving Equation (M-7) for $(\theta T)^{-1}$. The experiment was conducted by filling a moisture pressure cell with a soil to a given bulk density. The soil was initially saturated and allowed to desaturate. Measurements were taken at each of five different pressure settings (0.0 - 50 kP).

The data from Wright [1990] were obtained using conductometric techniques, similar to those of Jurinak et al. [1987], described above. In addition, an unsaturated flow apparatus (UFA) was used to hasten attainment of steady state conditions. The joint use of the UFA and electrical conductivity (EC) methods is called the UFA-EC technique. This technique involves the use of a rock core ultracentrifuge and a flow pump to provide fluid to the sample surface and is described further by Wright [1990] and by Conca and Wright [1992a and 1992b]. Wright [1990] used this technique with five different samples of Hanford G-1 soil and a solution of 0.1 M KCl to estimate liquid phase diffusion coefficients. The composition of the five Hanford G-1 soil samples ranged from 79–96% sand, 1–4% clay, and 2–18% silt. Data were reported in a graph of effective diffusion coefficient versus moisture content, so the data shown in Figure M-3 were estimated from this graph. Seven pairs of moisture content and diffusion coefficient values were

chosen from among the approximately 25 pairs of values given by Wright [1990]. The seven values were chosen because they spanned the range from 0.06 to 0.17 (the moisture content of NTS soil) and because they were readily estimated from the graph. The free diffusion coefficient of KCl in water was reported as 2.5×10^{-5} cm^2/sec, so tortuosity was easily calculated by dividing the free diffusion coefficient by the value taken from the graph. The porosity of the samples was not given.

The data given by Conca and Wright [1990] were obtained by using the UFA-EC technique to estimate the diffusion coefficient of KCl in 6.3 - 9.5 mm granitic gravel. The results of the experiments were reported in tables that gave the volume percent water and the estimated diffusion coefficient. Assuming that the diffusion coefficient of KCl in water was 2.5×10^{-5} cm^2/sec (see discussion of data from Wright [1990]), tortuosity was calculated simply by dividing the diffusion coefficient in water by the estimated effective diffusion coefficient. The porosity of the gravel was not given. As the data in Figure M-3 indicate, the VMCs in this experiment were very low, ranging from 0.005 to 0.0217. This range is below the range of VMCs at the NTS (approximately 0.06–0.17) but the data are still of interest because they demonstrate that tortuosity increases dramatically as moisture content drops to very low levels.

Conca et al. [1992] used the UFA-EC technique to estimate liquid phase diffusion coefficients of 0.1M KCl and 0.1M NaCl in soils, silts, whole rock cores, and gravel. They present approximately 100 data points in a graph of effective diffusion coefficient vs. VMC. The 24 data points shown in Figure M-3 were selected from this graph. These 24 data points were selected by choosing the highest value and lowest value of the effective diffusion coefficient shown that corresponded to VMCs of 0.06, 0.07, 0.08, ..., 0.016, 0.17. The diffusion coefficient in free water was shown on the graph and the value was estimated to be 2.3×10^{-5} cm^2/sec. Thus, the tortuosity was calculated by dividing the free water diffusion coefficient by the effective diffusion coefficients read off the graph. The porosity of the samples was not given.

The three models were regressed against the literature values of tortuosity to determine how well each model fit the data. The best R^2 value for the Shearer et al. model was 0.70 and the best R^2 value for the Sadeghi et al. model was 0.72. Both of these were obtained assuming a porosity of 0.248. The R^2 value for the Wright model (which is not dependent on porosity) was 0.42. These are not particularly good R^2 values.

Results of Data Regression

Because none of the three models obtained from the literature fit the data very well, the next step was to regress the data shown in Figure M-3 to try to find an appropriate tortuosity model. The tortuosity values obtained from the literature (shown in Figure M-3) were input into a spreadsheet program and were regressed against tortuosity values predicted by various models. Models were developed as follows. A model of the form

$$\tau = \frac{r}{\theta^s} \qquad \text{(M-9)}$$

was assumed. This form was assumed for several reasons. First, the data in Figure M-3 do not support a linear relationship between log of tortuosity and VMC, as assumed by the Wright [1990] model. Instead, the data seem to support relationships similar to those of Sadeghi et al. [1989] and Shearer et al. [1973], which both assume that tortuosity is a power function of VMC and porosity. Therefore, the power relationship was chosen. Second, porosity data were not available for most of the data shown in Figure M-3; only moisture content was known. Therefore, a model that did not incorporate porosity as an independent variable was needed.

The most appropriate value of *s* was not known. Therefore, multiple iterations were performed, each with a different value of *s*, until the best fit (as measured by the value of R^2) was obtained. The values of *s* used were 3.33, 3.1, 3.0, 2.5, 2.4, 2.0, 1.75, 1.7, 1.5, and 1.3. The value of *r* was obtained from each regression calculation as the coefficient of the model, and in each regression the *y*-intercept was set to zero. Using this method, four models with approximately equally good R^2 values were obtained. These four models, their R^2 values, and their tortuosity values at VMC's of 0.0475 and 0.181 were:

Model 1

$= \frac{1.0}{\theta^{1.7}}$, $R^2 = 0.79$; $\tau(0.0475) = 209.0$, $\tau(0.181) = 20.1$

Model 2

$= \frac{1.3}{\theta^{1.7}}$, $R^2 = 0.79$; $\tau(0.0475) = 232.8$, $\tau(0.181) = 23.9$

Model 3

$= \frac{3.68}{\theta^{1.50}}$, $R^2 = 0.81$; $\tau(0.0475) = 355.5$, $\tau(0.181) = 47.8$

Model 4

$= \frac{10.25}{\theta^{1.30}}$, $R^2 = 0.81$; $\tau(0.0475) = 538.3$, $\tau(0.181) = 94.6$

These R^2 values are somewhat better than those for the three models found in the literature. In addition, the spreadsheet's power trendline function was used to calculate the best fitting power-function curve through the data. The model given by that function was

Trendline Model

$= \frac{2.30}{\theta^{1.65}}$, $R^2 = 0.90$; $\tau(0.0475) = 350.9$, $\tau(0.181) = 38.6$.

Therefore, the best-fitting model is the Trendline Model. All five models are shown in Figure M-4. As shown in this figure, Model 1 is the most conservative model; that is, it consistently gives the lowest value of tortuosity for a given VMC, compared to the other models. The trendline model is less conservative than Model 2, while the other two models are less conservative than the Trendline Model.

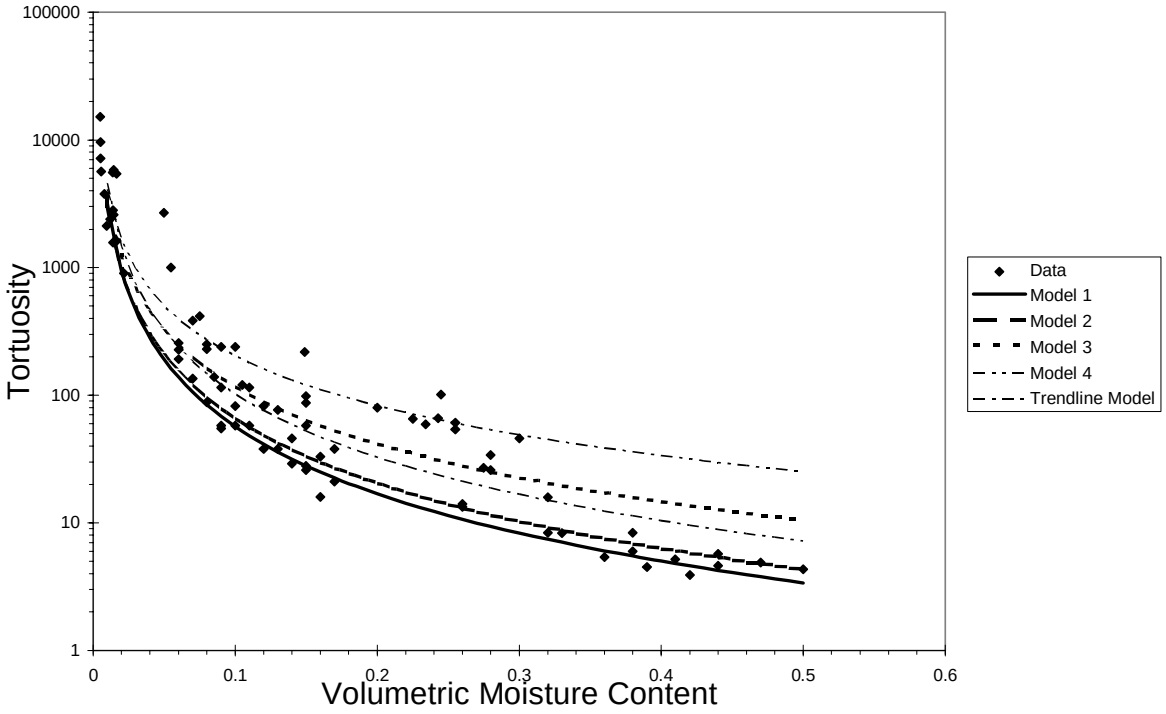

Figure M-4. Comparison of Tortuosity Data and Regressed Models

A comparison of tortuosity values used in the PPA and those predicted by the regressed models is given in Figure M-5. Figure M-6 compares tortuosity values used in the PA2 and those predicted by the regressed models. As demonstrated by Figure M-5, the values of tortuosity predicted by the regressed models are significantly lower (i.e., more conservative) than those used in the PPA, at least for values of VMC less than about 0.12. In contrast, Figure M-6 shows that the values of tortuosity used in the PA2 are lower than those predicted by the regressed models. Also, in both figures, the shape of the regressed curves is different from the shape of the distribution of sampled tortuosity values. The shape of the regressed curves mimics that of the data found in the literature, while the shape of the distribution of sampled tortuosity values results from assuming a uniform pdf for tortuosity and a lognormal pdf for VMC.

Conclusions

In this study we have looked at tortuosity models proposed by Sadeghi et al. [1989], Shearer et al. [1973], and Wright [1990]; examined approximately 75 experimentally obtained values of tortuosity; regressed the experimental values of tortuosity against proposed models to obtain new models; and compared the regressed models to values of tortuosity used in the PPA and the PA2. So, the question is, where do we go from here? What values of tortuosity should be used in the

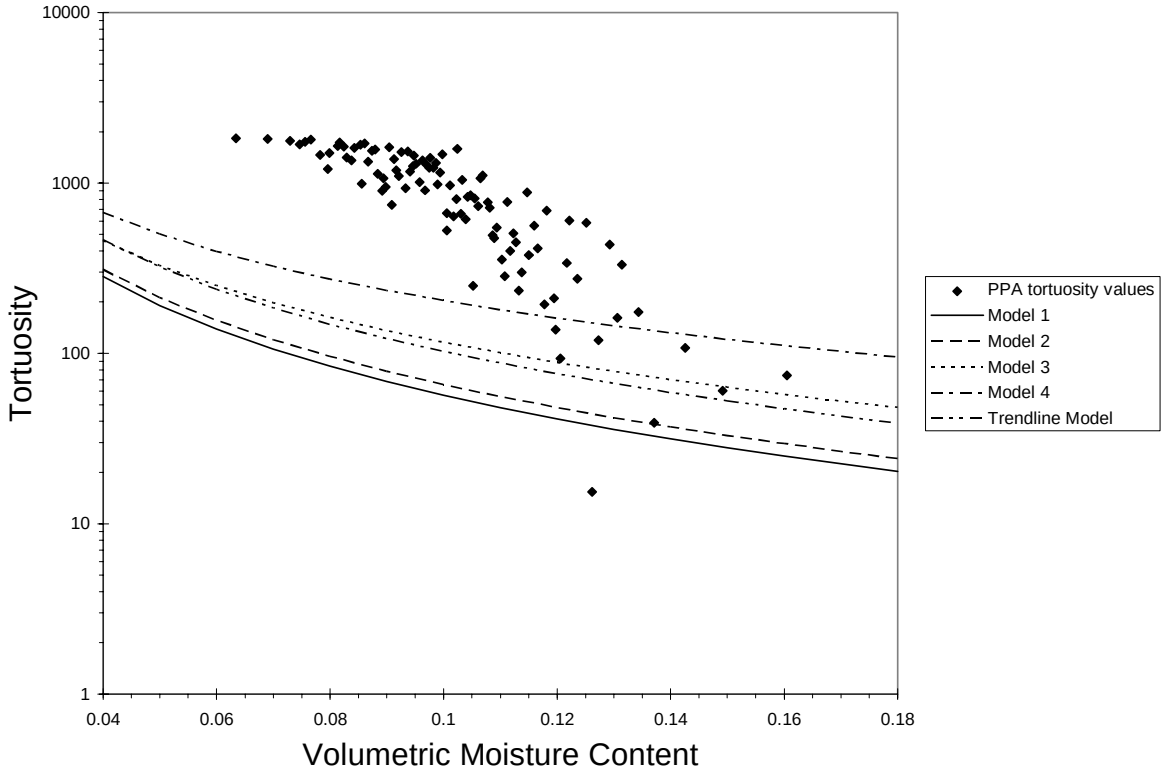

Figure M-5. Comparison of PPA Tortuosity Values and those Predicted by Regressed Models

third iteration of the NTS performance assessment? Before that question is answered, let us review some of the things we have learned so far.

First, for a given VMC, the tortuosity found by various researchers can vary by as much as an order of magnitude. For example, at a moisture content of about 0.15, Sadeghi et al. found a tortuosity of 217 while Wright found a tortuosity of 28. This is probably the biggest variation found; the variation at other values of VMC tends to be less. Such discrepancies make it impossible to find a single model that fits *all* the data, but it is still possible to find models that fit *most* of the data (e.g., the Trendline Model, with an R^2 of 0.90). Second, the models presented by Sadeghi et al. and Shearer et al. are very similar. Both are functions of both VMC and porosity and both increase dramatically as the moisture content drops to very low values (<0.05). Third, the data indicate that tortuosities tend to be very high at very low values of VMC. These data fall between values predicted by the Wright model and values predicted by the models presented by Sadeghi et al. and Shearer et al. Fourth, the Wright model is consistently more conservative than the other two models for porosities greater than about 0.36. For porosities less than 0.36, which model is more conservative is a function of the VMC. In general, though, between VMCs of 0.05 and 0.18, the Wright model is more conservative than the other two. Fifth, the data support the models presented by Sadeghi et al. and Shearer et al. more than the model presented by Wright . The data indicate that the relationship between log of tortuosity and VMC is not linear. The models given by Sadeghi et al. and Shearer et al. are not linear in this respect while the model given by Wright is. On the other hand, the Sadeghi et al. and Shearer et al. models tend to overpredict tortuosity somewhat at lower values of VMC and underpredict

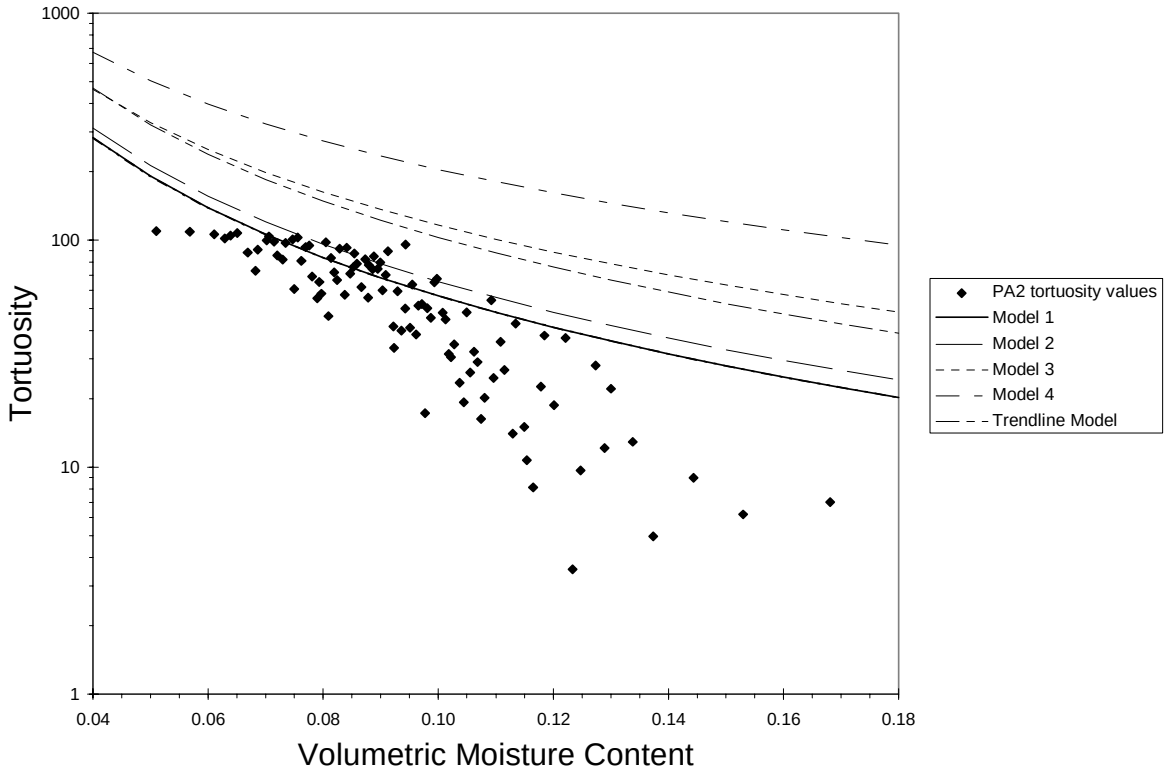

Figure M-6. Comparison of PA2 Tortuosity Values and those Predicted by Regressed Models

tortuosity at higher values of VMC. Finally, even the model that appears to fit the data the best, the Sadeghi et al. model, does not fit the data very well. Thus, none of the three models obtained from the literature fits the data very well.

Assuming that the data obtained from the literature represent the most defensible source of tortuosity values, one option is to use the Trendline Model for the third iteration of the performance assessment. The trendline model fits the data better than any of the other models (R^2 = 0.90), making it a better candidate than the other regressed models or the models found in the literature. Abandoning the values used in the PPA and the PA2 is warranted because these values do not match the values found in the literature, as indicated by the poor match between the PPA and PA2 values and the regressed models.

The other option would be to use the maximum and minimum values of tortuosity predicted by the Trendline Model (350.9 and 38.6, respectively) as endpoints for the tortuosity pdf and sample from VMC and tortuosity, as was done in the previous PA's. The type of pdf should be changed from uniform to lognormal to more closely imitate the relationship between tortuosity and VMC demonstrated by the data (Figure M-3). The result of assigning lognormal pdf's to both VMC and tortuosity is shown in Figure M-7.

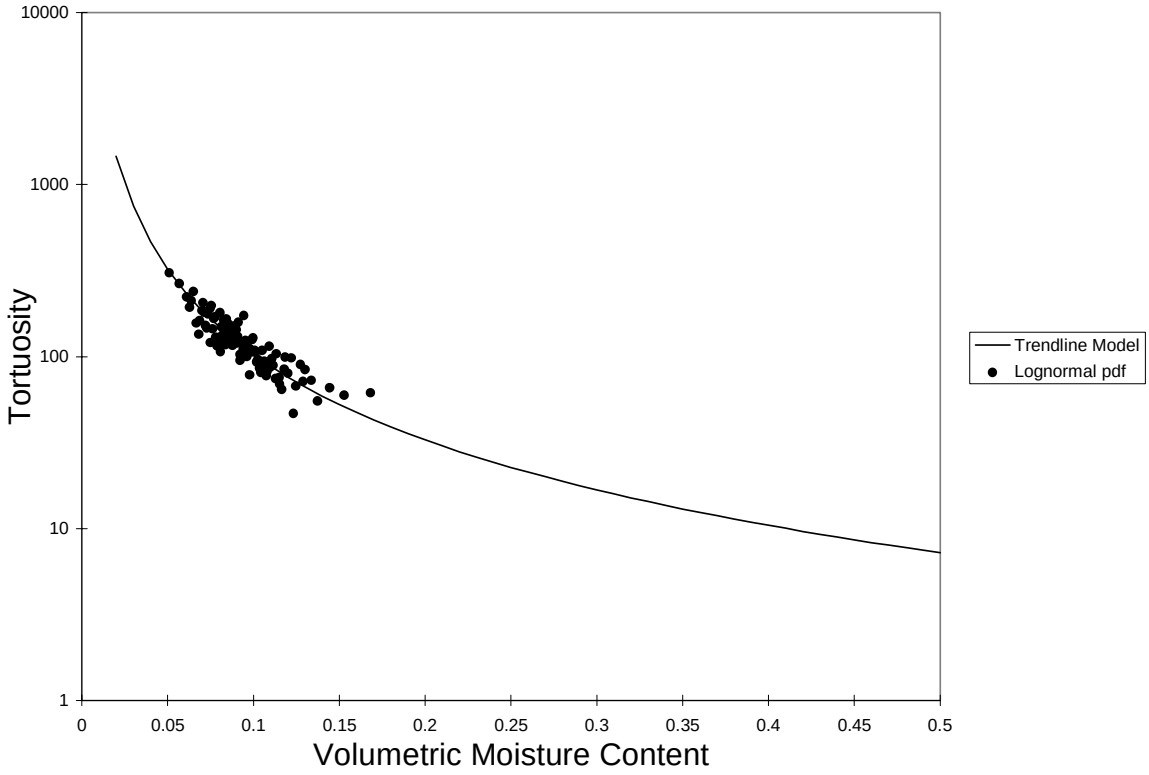

Figure M-7. Relationship Between Tortuosity and VMC with Lognormal PDFs.

References

Baer, T. A., L. L. Price, J. N. Emery, and N. E. Olague. 1994. *Second Performance Assessment Iteration of the Greater Confinement Disposal Facility at the Nevada Test Site*, SAND93-0089, Sandia National Laboratories, Albuquerque, NM.

Bockris, J. O'M., and A. K. N. Reddy. 1973. *Modern Electrochemistry, Vol. 1*, Plenum Press, New York.

Campbell, G. S. 1985. *Soil Physics with Basic: Transport Models for Soil-Plant Systems*, Developments in Soil Science 14, Elsevier Science Publishing Company, Inc., New York, NY.

Conca, J. L. and J. Wright. 1990. "Diffusion Coefficients in Gravel Under Unsaturated Conditions," *Water Resources Research*, Vol. 26, No. 5, pp. 1055–1066.

Conca, J. L. and J. Wright. 1992a. "A New Technology for Direct Measurements of Unsaturated Transport," *Proceedings of Spectrum '92 International Topical Meeting on Nuclear and Waste Management*, Boise, ID.

Conca, J. L., and J. Wright. 1992b. "Diffusion and Flow in Gravel, Soil, and Whole Rock," *Applied Hydrogeology International Journal*, Vol. 1, pp. 5–24.

Conca, J. L., M. Apted, and R. Arthur. 1992. "Aqueous Diffusion in Repository and Backfill Environments, " *Scientific Basis for Nuclear Waste Management,* 16th Symposium, ed. C. G. Interrante and R. T. Pabalan, pp. 395–402.

Jurinak, J. J., S. S. Sandhu, and L. M. Dudley. 1987. "Ionic Diffusion Coefficients as Predicted by Conductometric Techniques," *Soil Science Society of America Journal*, Vol. 51, pp. 625–630.

Jury, W. A., W. R. Gardner, and W. H. Gardner. 1991. *Soil Physics*, Fifth Edition, John Wiley and Sons, Inc., New York, NY.

Kemper, W. D. and J. C. Van Schaik, "Diffusion of Salts in Clay Water Systems." 1966. *Soil Science Society of America Proceedings*, Vol. 30, pp. 534–540.

Millington, R. J. and J. P. Quirk. 1961. "Permeability of Porous Solids," *Transactions of the Faraday Society*, Vol. 57, pp. 1200–1207.

Olsen, S. R. and W. D. Kemper. 1968. "Movement of Nutrients to Plant Roots," *Advanced Agronomy*, Vol. 30, pp. 91–151.

Price, L. L., S. H. Conrad, D. A. Zimmerman, N. E. Olague, K. C. Gaither, W. B. Cox, J. T. McCord, and C. P. Harlan. 1993. *Preliminary Performance Assessment of the Greater Confinement Disposal Facility at the Nevada Test Site: Volume 1 — Executive Summary; Volume 2 — Technical Discussion; Volume 3 — Supporting Details,* SAND91-0047, Sandia National Laboratories, Albuquerque, NM.

Ryan, P. A. and Y. Cohen. 1990. "Diffusion of Sorbed Solutes in Gas and Liquid Phases of Low-Moisture Soils," *Soil Science Society of America Journal*, Vol. 54, pp. 341–346.

Sadeghi, A.M., D. E. Kissel, and M. L. Cabrera. 1988. "Temperature Effects on Urea Diffusion Coefficients and Urea Movement in Soil," *Soil Science Society of America Journal*, Vol. 52, pp. 46–49.

Sadeghi, A. M., D. E. Kissel, and M. L. Cabrera. 1989. "Estimating Molecular Diffusion Coefficients of Urea in Unsaturated Soil," *Soil Science Society of America Journal*, Vol. 53, pp. 15–18.

Sallam, A., W. A. Jury, and J. Letey. 1984. "Measurement of Gas Diffusion Coefficient under Relatively Low Air-filled Porosity," *Soil Science Society of America Journal*, Vol. 48, pp 3–6.

Shearer, R. C., J. Letey, W. J. Farmer, and A. Klute. 1973. "Lindane Diffusion in Soil," *Soil Science Society of America Proceedings*, Vol. 37, pp. 189–193.

Wright, J. 1990. "Diffusion Coefficients and Hydraulic Conductivity in Unsaturated Hanford Soils and Sediments," *Proceedings of the First International High-Level Radioactive Waste Management Conference*, Vol. 1, pp. 835–842.

cc:
MS 1345 - 6352 GCD Records Center: S34;PA;tortuosity studies

date: April 14, 1997

to: John Cochran, MS 1345

from: Theresa Brown and Laura Price, MS 1345

subject: Addressing comments on tortuosity model (memo/97/S34)

A tortuosity model for use in the third iteration of the performance assessment (PAIII) of the Greater Confinement Disposal (GCD) boreholes at the Nevada Test Site (NTS) was developed and documented in a January 10, 1996 memo from Laura Price (then 6331) to Theresa Brown (then 6851). This memo presented the results of a literature search for tortuosity data and models, looked at five other models for tortuosity, and proposed a model for use in the PAIII. The model selected, the Trendline Model, was selected because it provided the best fit to the tortuosity data obtained from the literature. These data and the five tortuosity models that were examined are shown in Figure M-8.

In the Trendline Model, tortuosity is a power function of volumetric moisture content (VMC),

$$\tau = \frac{2.30}{\theta^{1.65}}. \qquad \text{(M-15)}$$

VMC is an uncertain parameter, having a lognormally distributed pdf with 0.001 and 0.999 quantiles of 0.04745 and 0.1810, respectively. Using these values for VMC in the Trendline Model yields values of tortuosity that range from 38.6 to 350.9.

In the memo discussed above, two options for obtaining tortuosity values for PAIII were presented. The first was to use the Trendline Model. In this option, VMC would remain an uncertain parameter but tortuosity would not. That is, tortuosity would not be a sampled variable; it would be determined directly by Equation (M-15). The second option was to continue to sample from both tortuosity and VMC, but make the pdf for tortuosity lognormal with 0.001 and 0.999 quantiles of 38.6 and 350.9. The two variables could also be correlated. Assigning lognormal pdf's to both VMC and tortuosity results in a relationship between tortuosity and VMC that closely imitates the relationship demonstrated by the data.

This model was presented at the October 1995 Area 5 Site Characterization/Performance Assessment meeting. One of the comments from Scott Tyler (DRI) was that the tortuosity model should predict a tortuosity of about 1.5 at a saturation of 1. This tortuosity value is based on theoretical models of tortuosity (capillary bundles with circular tubes; see Bear [1972]) and on experimental results for gas diffusion in air-dry porous media (e.g., Penman [1940a ,b]). As a

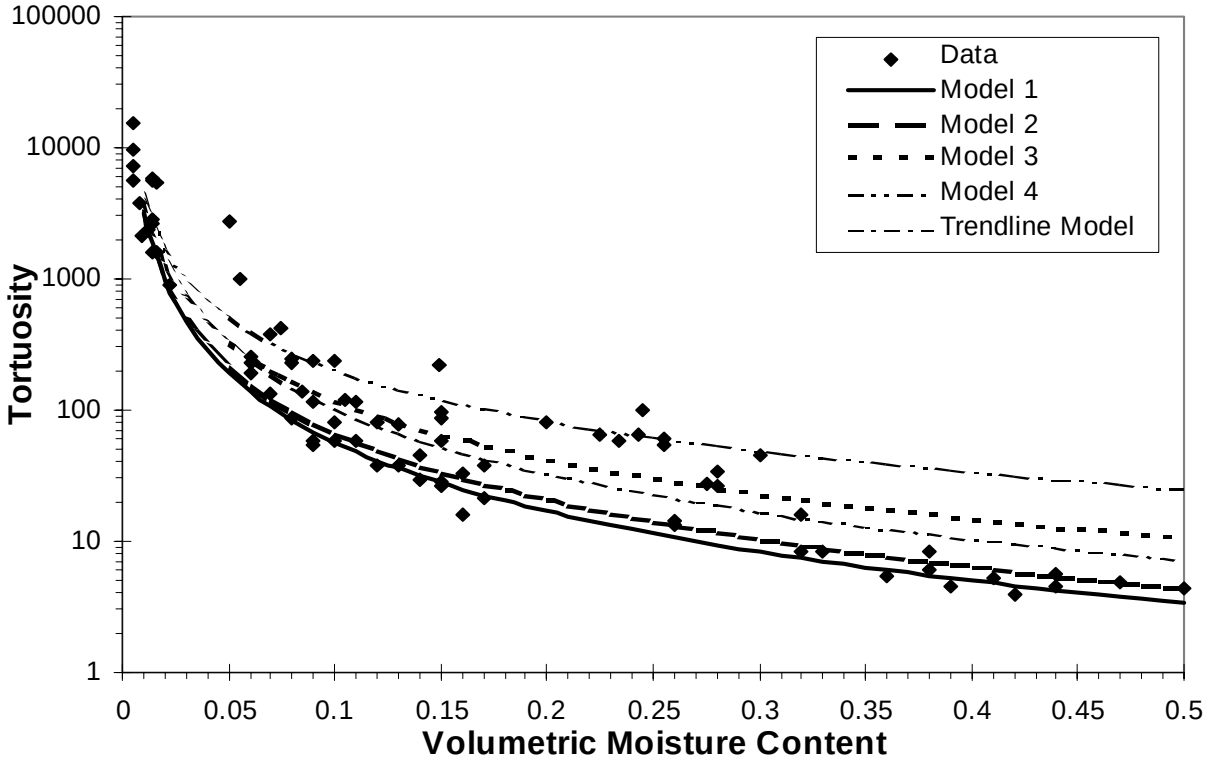

Figure M-8. Comparison of Tortuosity Data and Models as a Function of VMC.

result of this comment, we went back to the papers from which we had obtained tortuosity data and examined them to see if they contained enough information to plot the data as a function of saturation instead of VMC. Half the papers contained enough information and half did not. The tortuosity data that could be shown as a function of saturation are given in Figure M-9. Most of the data with VMC values between 0.05 and 0.2 are lost, and the data that remain tend to be those that report higher tortuosities for a given VMC. The data indicate that tortuosities approach a value of about 4 as the saturation approaches 1, not 1.5 as predicted by theoretical capillary-bundle models [Bear, 1972] and by gas diffusion in air-dry porous media [Penman, 1940a, b]. This variation between tortuosity values at S = 1 is reasonable because the higher tortuosity values represent results for liquid phase (not gas phase) transport in porous media (not smooth, round capillary tubes).

The tortuosity models found in the literature in the original tortuosity study were plotted as a function of saturation and compared with the tortuosity data. This comparison is shown in Figures M-10, M-11, and M-12. The three models, in terms of saturation (S) and porosity (n), are

Wright [1990]

$$\tau = \frac{e^{\&bnS}}{a}; \qquad a = 0.005, \quad b = 10. \tag{M-16}$$

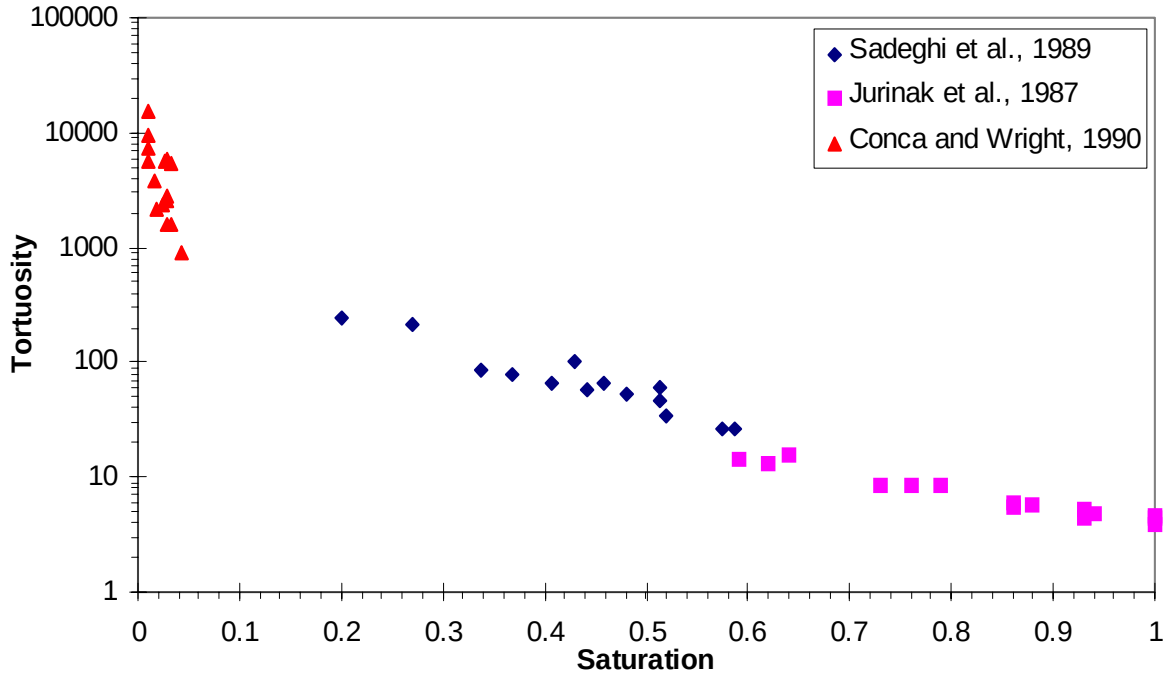

Figure M-9. Tortuosity as a Function of Saturation.

Shearer et al. [1973]

$$\tau = \frac{1}{S^{10/3} n^{4/3}} \qquad \text{(M-17)}$$

Sadeghi et al. [1989]

$$\tau = \frac{5.56}{S^{2.98}} \qquad \text{(M-18)}$$

Note that the Shearer et al. and Wright models are functions of both saturation and porosity, while the Sadeghi et al. model is a function only of saturation. All models are in fairly good agreement with the data when saturation is greater than about 0.1, but none of the models is in good agreement with the data at very low saturation values (< 0.1). At these low saturation values the models predict tortuosities that are too high, i.e., tortuosities that are not conservative for transport modeling. An analysis of variation between the data and these models is given in Table M-1. The residual sum of squares shown in this table is the sum of the squared difference between the measured tortuosity and the tortuosity predicted by the given model. Porosity values used to calculate tortuosities for the Shearer et al. and Wright models were taken from the same literature from which measured tortuosity values were taken.

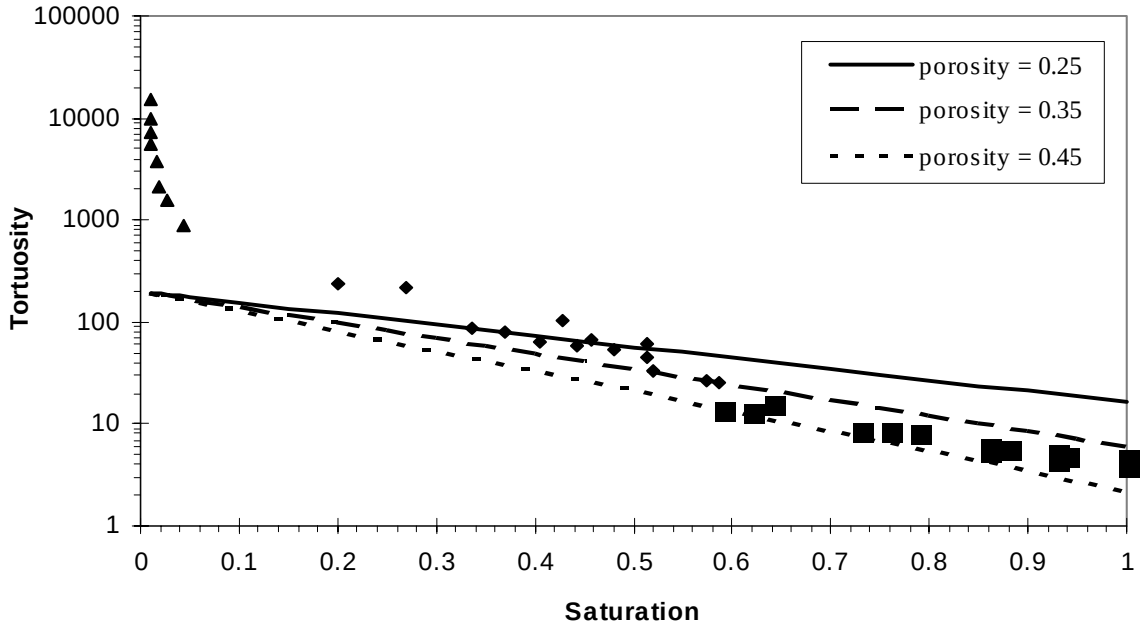

Figure M-10. Tortuosity as a Function of Saturation Compared with Wright [1990] Model.

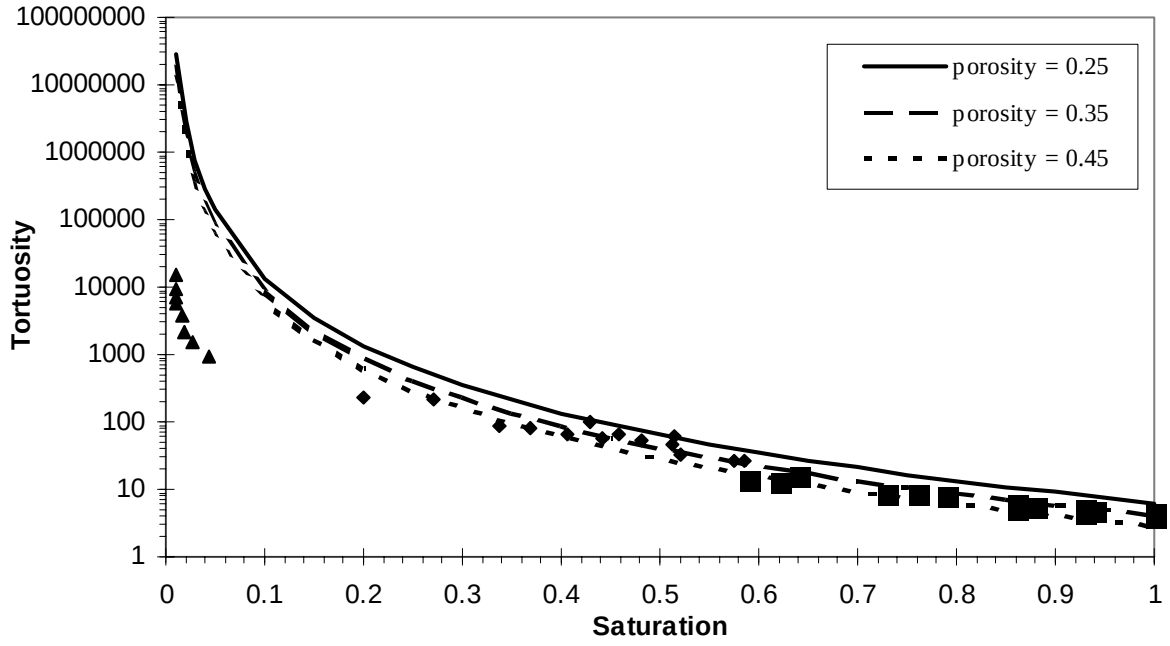

Figure M-11. Tortuosity as a Function of Saturation Compared with Shearer et al. [1973] Model.

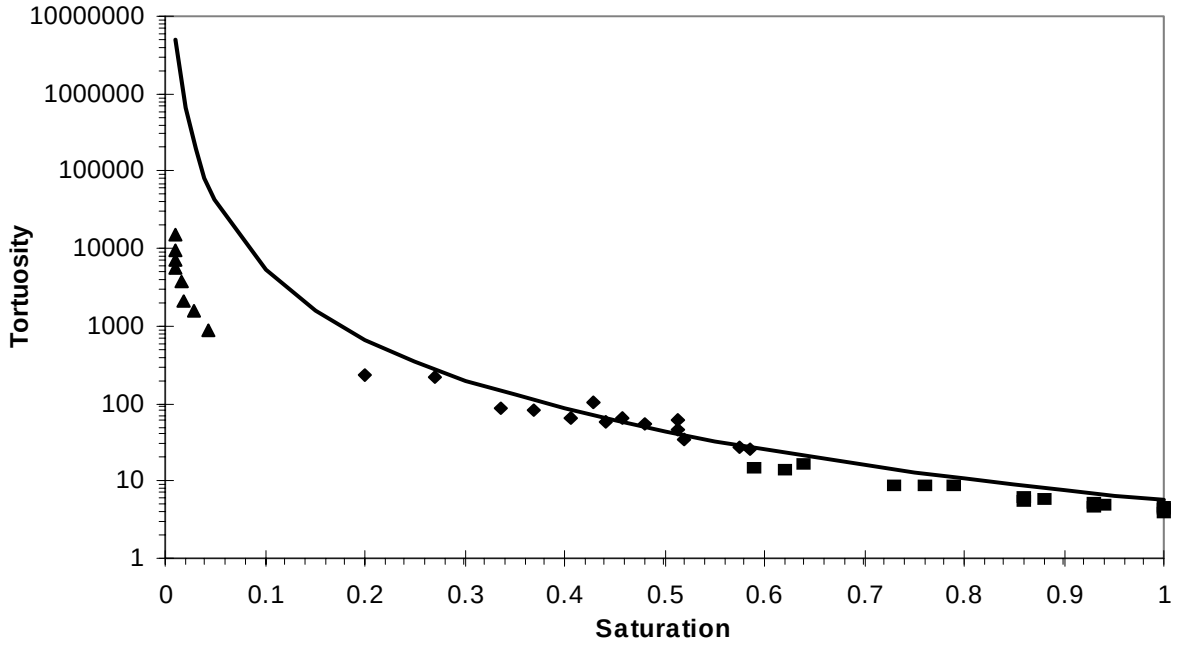

Figure M-12. Tortuosity as a Function of Saturation Compared with Sadeghi et al. [1989] Model

Table M-1. Results of Analysis of Variation Between Data and Models from the Literature

	Shearer et al.	Wright	Sadeghi et al.
Residual Sum of Squares	4.16×10^{14}	5.19×10^{8}	8.12×10^{13}
Residual Sum of Squares, Sat. > 0.1	1.58×10^{5}	7.83×10^{4}	1.98×10^{5}

In the PAIII, VMC ranges from 0.04745 to 0.1810 and porosity ranges from 0.2455 to 0.4576, yielding saturation values that range from 0.1037 to 0.7373. Therefore, we are interested primarily in the behavior of the models between these saturation values. According to Table M-1, the Wright model provides the best fit to the data for saturation values greater than 0.1, with a residual sum of squares that equals 7.83×10^{4}. The other two models have slightly higher residual sums of squares, indicating that they do not fit the data quite as well as the Wright model.

None of the three models presented above was developed using the composite data set and, as a result, we felt that we could find a model that fit the data better, particularly in the range of saturations and VMCs that we are modeling. In an attempt to find a model that fit the data better than the models obtained from the literature, we developed four models of our own based on the data. The models took one of two forms: power or exponential. As before, various forms of S^{-n} and e^{-nS} were regressed against the measured values of tortuosity until a balance between a good fit (as measured by R^2) and conservatism (i.e., model generally predicts values of tortuosity

similar to or lower than measured values) was obtained. Two models were developed for each model form, one with a tortuosity of 1.5 when saturation was 1.0 (see Bear [1972] and Penman [1940a, b]) and the other with a tortuosity of about 4 under fully saturated conditions (as supported by the data). These models and the data are shown in Figure M-13.

The results of an analysis of variation between tortuosity data and the four models we developed for saturation values greater than 0.1 is given in Table M-2. The models are also given in this table.

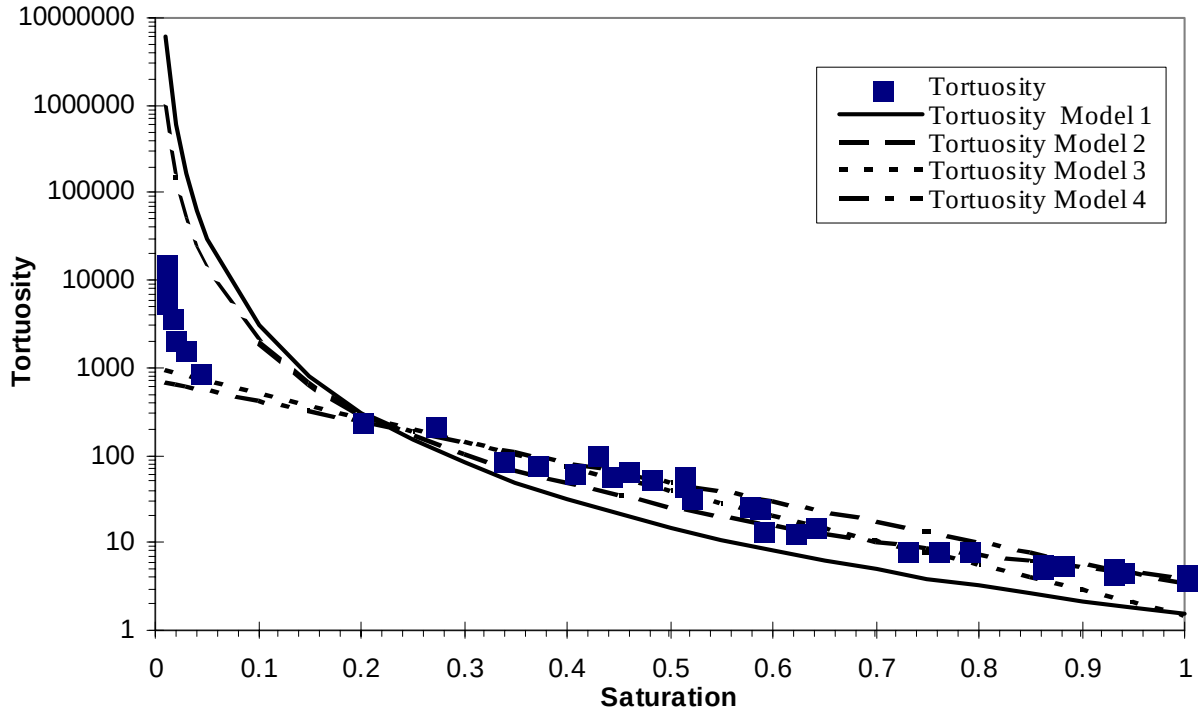

Figure M-13. Tortuosity Data and Four Saturation-based Models.

Table M-2. Results of Analysis of Variation Between Data and Developed Models

	Model 1 $\tau = 1.53\ S^{-3.3}$	**Model 2** $\tau = 3.98\ S^{-2.7}$	**Model 3** $\tau = 995e^{(-6.5)\ S}$	**Model 4** $\tau = 705e^{(-5.3)\ S}$
Residual Sum of Squares, Sat. > 0.1	3.42×10^4	2.03×10^4	6.68×10^3	5.96×10^3

As Table M-2 indicates, the exponential models (Models 3 and 4) have lower residual sums of squares than the power models (Models 1 and 2). Models 3 and 4 also have better R^2 values (0.93 and 0.94, respectively) than Models 1 and 2 (0.65 and 0.79, respectively). In addition, Models 1 and 2 predict non-conservative tortuosities for low values of saturation while Models 3 and 4 fit the data very well for saturation values as low as 0.04 before they produce overly

conservative results. All four of these models have lower residual sums of squares than the models found in the literature.

The last step of our analysis was to compare the tortuosities predicted by VMC-based models with those predicted by saturation-based models. We selected Model 1 and the Trendline Model from Figure M-8 and Model 3 from Figure M-13 for comparison. We then took 100 sampled values of VMC and porosity, calculated the tortuosity predicted by each model, and plotted the results, as shown in Figures M-14 and M-15. Figure M-14 presents the results as a function of VMC, while Figure M-15 presents them as a function of saturation. Both figures demonstrate that the VMC-based models give lower (i.e., more conservative) values of tortuosity than the saturation-based model. This is probably because the saturation-based model used only a subset of the data available for the VMC-based model, and this subset included data that tended to have higher tortuosities for a given VMC or saturation.

The conclusion we have drawn from all this analysis is that Model 1 from Figure M-8 should be used in the PAIII. This model is based on VMC, not saturation, and is the most conservative of all the models considered. The equation for this model is:

$$\tau \; ' \; \frac{1.01}{\theta^{1.75}} \qquad \text{(M-19)}$$

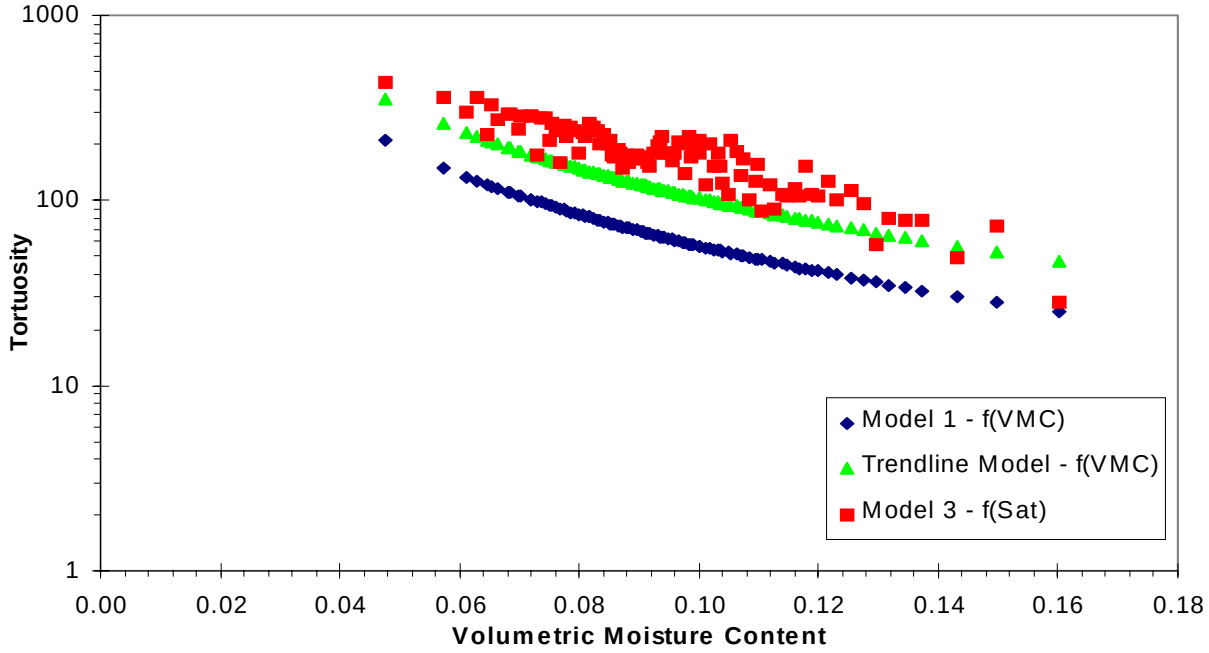

Figure M-14. Comparison of VMC-based and Saturation-based Tortuosity Models as a Function of VMC.

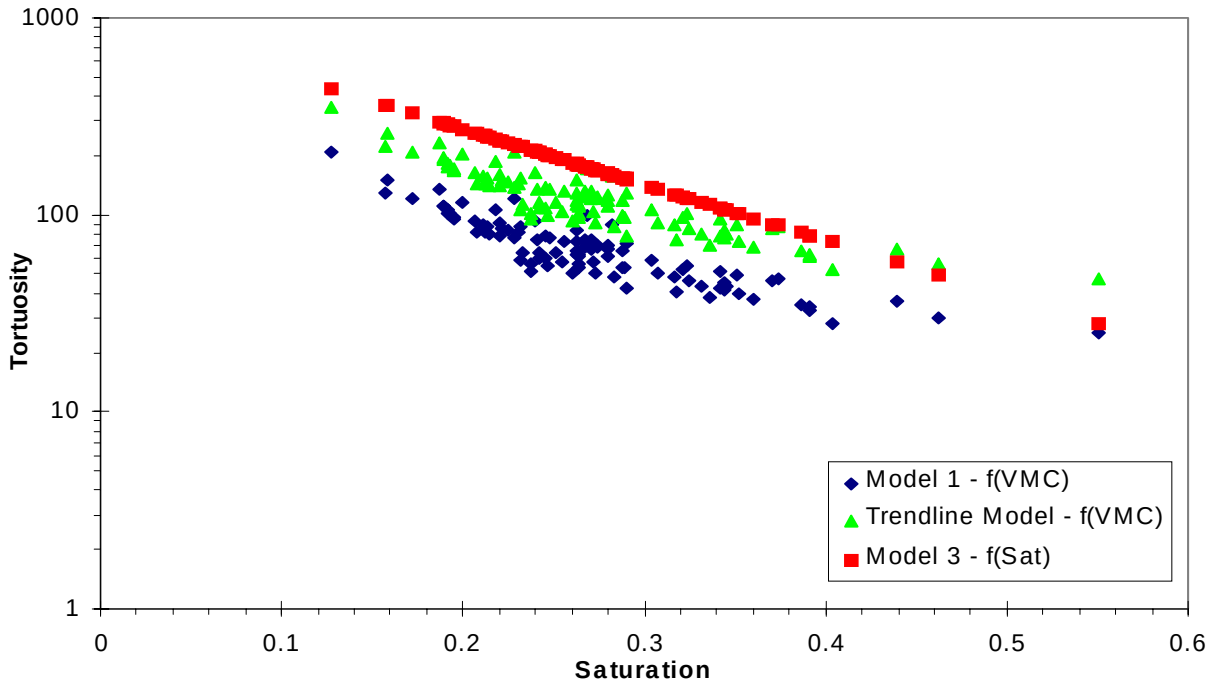

Figure M-15. Comparison of VMC-based and Saturation-based Tortuosity Models as a Function of Saturation.

References

Bear, J. 1972. *Dynamics of Fluids in Porous Media*, Dover Publications, Inc., New York, NY, pp. 110–113.

Conca, J. L. and J. Wright. 1990. "Diffusion Coefficients in Gravel Under Unsaturated Conditions," *Water Resources Research*, Vol. 26, No. 5, pp. 1055–1066.

Jurinak, J. J., S. S. Sandhu, and L. M. Dudley. 1987. "Ionic Diffusion Coefficients as Predicted by Conductometric Techniques," *Soil Science Society of America Journal*, Vol. 51, pp. 625–630.

Penman, H. L. 1940a. "Gas and Vapor Movements in Soil. I. The Diffusion of Vapors Through Porous Solids," *Journal of Agricultural Science*, Vol.30, pp. 437–462.

Penman, H. L. 1940b. "Gas and Vapor Movements in Soil. II. The Diffusion of Carbon Dioxide Through Porous Solids," *Journal of Agricultural Science*, Vol. 30, p. 570–581.

Sadeghi, A. M., D. E. Kissel, and M. L. Cabrera. 1989. "Estimating Molecular Diffusion Coefficients of Urea in Unsaturated Soil," *Soil Science Society of America Journal*, Vol. 53, pp. 15–18.

Shearer, R. C., J. Letey, W. J. Farmer, and A. Klute. 1973. "Lindane Diffusion in Soil," *Soil Science Society of America Proceedings*, Vol. 37, pp. 189–193.

Wright, J. 1990. "Diffusion Coefficients and Hydraulic Conductivity in Unsaturated Hanford Soils and Sediments," *Proceedings of the First International High-Level Radioactive Waste Management Conference*, Vol. 1, pp. 835–842.

cc:
MS 1345 - 6352 GCD Records Center: S34;PA;tortuosity studies

This page intentionally left blank.

Appendix N

Memo from Arnold to Brown

This page intentionally left blank.

Sandia National Laboratories
Albuquerque, New Mexico 87185-1326
INFORMATION ONLY

date: February 1, 1996

to: T. Brown, 6851, MS 1326

BWA

from: Bill W. Arnold, 6851, MS1326

subject: Estimating Dispersivity for GCD PA (revised)

The purpose of this memo is to report recommendations on the distribution of dispersivity in unsaturated solute transport for use in the GCD PA. Dispersivity is a relevant parameter for solute transport in the PA because current plans are to include an upward advective flux (on the order of 0.1 to 0.2 mm/year) in the transport modeling. This memo contains the results of a literature search for pertinent experiments (field and laboratory) in which dispersivity was derived. Some theoretical conclusions regarding unsaturated solute transport are also reviewed. Data on the chloride profiles in two boreholes, as presented in Tyler et al. (in press), are used to derive a possible range of dispersivity specific to the GCD site. Finally, the range of total dispersion coefficient and the relative importance of mechanical dispersion versus molecular diffusion, for the anticipated range of parameter values in the PA, are analyzed.

Experimental Estimates

Experimental studies of solute transport in unsaturated media span a wide range of conditions and experimental methods. The results of 12 experiments are summarized in Table 1. I have attempted to rank these studies in terms of their relevance to unsaturated transport at the GCD site. Criteria used in this ranking include the scale of the experiment, *in situ* versus disturbed medium, infiltration rates, tracer type, and general experimental methods. Some of the experiments tabulated below approach the scale of transport for GCD (about 20 m from the waste to the land surface), but most of the column experiments involve much shorter transport distances. All of these experiments were performed using infiltration rates and flow velocities many orders of magnitude higher than the inferred ambient rates at the GCD site. These higher flow velocities also resulted in higher moisture contents under experimental conditions. Tracers other than ^3H may have experienced significant interaction with the medium (e.g. retardation) in experiments; however, there is no consistent difference in dispersivity from experiments using various tracers. Note that for some studies values of velocity and moisture content were either not reported or were not measured.

Table 1: Unsaturated Dispersivity Studies

Reference	Range of Dispersivity (cm)	Range of Depths (m)	Range of Velocity (cm/day)	Range of Volumetric Moisture Content	Comments
Wierenga et al. (1988)	1.0 - 2.1	1.5 - 3.5	8.5 - 10.0	0.05 - 0.24	^{3}H tracer, *in situ* trench, arid site
Porro et al. (1993)	1.4 - 4.5	5.0	6.5 - 14.7	0.16 - 0.47	^{3}H tracer, column, loamy fine sand, layered and non-layered
Nyhan et al. (1986)	0.8 - 1.7	4.2	6 - 12	0.25 - 0.39	I^-, Br^- tracers, sandy silt, caisson
Fuentes and Polzer (1986)	4.2 - 13.8	4.2	1.2 - 4		Br^- tracer, caisson
Stephenson and de Jesus (1985)	10 - 40	~ 5	~ 150		^{46}Sc tracer, *in situ* injection
Butter and Jury (1989)	~ 40	13.0		0.07 - 0.20	Br^- tracer, *in situ*
Wierenga and van Genuchten (1989)	~ 5	6.0			^{3}H tracer, column, sandy soil
DeSmedt et al. (1986)	7.3	1.0	9.5 - 20.7	0.00 - 0.30	^{3}H tracer, column, sand
Schulin et al. (1987)	~ 4	0.50	0.16 - 41		^{3}H tracer, column, stony soil
Gvirtzman and Magaritz (1986)	0.05 - 0.15	8.5	~ 0.18		environmental ^{3}H tracer, *in situ* irrigated site, loess
James and Rubin (1986)	.012 - .023	0.10	4.8 - 48	0.17 - 0.22	Cl^- tracer, column, Delhi sand
Bresler and Laufer (1974)	0.04 - 0.12	0.45		0.03 - 0.42	Cl^- tracer, column, loam

Values of dispersivity reported in these studies range from near 0 to 40 cm. The majority of the more reliable studies estimate dispersivity to be less than 15 cm.

Theoretical and Numerical Conclusions

Theoretical and numerical analyses of solute transport in unsaturated media have reached differing conclusions regarding dispersivity. Numerical experiments by Russo (1991) of flow perpendicular to stratification in a geostatistically simulated layered medium indicate that solute movement undergoes a compression-expansion effect as the solute front encounters heterogeneities and that longitudinal dispersivity increases with travel distance to approach an asymptotic value. Further theoretical analysis of the results of this study by Russo and Dagan (1991) conclude that the asymptotic longitudinal dispersivity for unsaturated flow should be equal to the theoretical dispersivity for saturated flow (as derived by Gelhar and Axness, 1983). In contrast, analytical and numerical analyses by Harter and Yeh (in press) indicate that for an anisotropic, layered medium the longitudinal dispersivity for unsaturated flow would be less than the theoretical dispersivity for saturated conditions. The experimental study of James and Rubin (1986) indicates lower dispersivity for unsaturated flow than for saturated flow in the same column. The generally low range of unsaturated dispersivity apparent in Table 1 supports the concept that dispersivity of solute transport is smaller under unsaturated conditions than under saturated conditions. Comparison of the range of experimental dispersivity shown in Table 1 with the results of numerous solute transport experiments in the saturated zone (Gelhar et al., 1985) confirms that unsaturated-flow dispersivity is generally smaller than saturated-flow dispersivity.

An Estimate of Dispersivity at the GCD Site

Data on chloride profiles in boreholes PW-1 and PW-3, along with conclusions regarding the history of infiltration at the GCD site presented in Tyler et al. (in press), can be used to estimate the dispersivity for unsaturated flow. The deeper chloride bulges in both of these boreholes are assumed to have resulted from the flushing of shallow, accumulated chloride during an aborted recharge event corresponding to pluvial conditions in the late Wisconsinan. These deeper chloride bulges underwent spreading by mechanical dispersion during downward transport as well as molecular diffusion. The total dispersion coefficients have been estimated by fitting a Gaussian distribution to the concentration profiles, yielding values of 4×10^{-7} and 1×10^{-6} cm^2/s for PW-1 and PW-3, respectively.

Because of uncertainty in the tortuosity and moisture content of the medium during the aborted recharge event, dispersivity is analysed here for a range of these parameters. The ranges of tortuosity and moisture content used in the analysis include the anticipated ranges to be used in the GCD PA. Total dispersion is the sum of mechanical dispersion and molecular diffusion. Mechanical dispersion, D_α, for one-dimensional flow is defined as:

$$D_\alpha = \frac{q\alpha_l}{\theta} \qquad (1)$$

where q is the recharge rate, α_l is the longitudinal dispersivity and θ is the moisture content. The effective molecular diffusion coefficient, D_e, is defined as:

$$D_e = \frac{\theta D_m}{\tau} \qquad (2)$$

where D_m is the molecular diffusion coefficient (1.0×10^{-5} cm^2/s in these calculations) and τ is the tortuosity. An additional assumption is made that there is a general relationship between tortuosity and moisture content. Data on volumetric moisture content and tortuosity have been compiled by Laura Price and have been fitted by several models (T. Brown, pers. comm.). Analyses of dispersion coefficient are performed on the basis of two alternative models:

$$\tau = \frac{1.31}{\theta^{1.7}} \qquad \text{Model 1}$$

$$\tau = \frac{3.68}{\theta^{1.5}} \qquad \text{Model 2}$$

Using the relationships in Equations 1 and 2, the total dispersion coefficient can be calculated as a function of tortuosity/moisture content and longitudinal dispersivity for a given value of recharge rate. Plots of total dispersion coefficient for recharge rates of 2.0 and 10.0 mm/year, employing both Model 1 and Model 2 for the tortuosity/moisture content relationship are shown in Figure 1.

Using the estimates of total dispersion coefficient from the chloride concentration profiles, the corresponding range of dispersivity can be determined from the plots in Figure 1 for the range of volumetric water content considered. If we assume a lower recharge flux of 2.0 mm/year the values of dispersivity corresponding to the dispersion coefficients of 4×10^{-7} and 1×10^{-6} cm^2/s range from about 3 cm to greater than 40 cm. Alternatively, if we assume a recharge flux of 10.0 mm/year during the chloride flushing event, the corresponding values of dispersivity range from less than 1 cm to about 8 cm. The actual paleorecharge rates estimated in Tyler et al. (in press) are 4.4 and 7.6 mm/year. The analysis presented here was performed for the bounding values of 2.0 and 10.0 mm/year due to uncertainty in the estimates in paleorecharge rate in Tyler et al. (in press), as suggested by Steve Conrad (pers. comm.). The differences between the results for Model 1 and Model 2 of the tortuosity/moisture content relationship are not great, as shown in Figure 1.

The analysis presented above provides a conservative estimate (from the perspective of performance assessment) of dispersivity at the site. This analysis does not account for

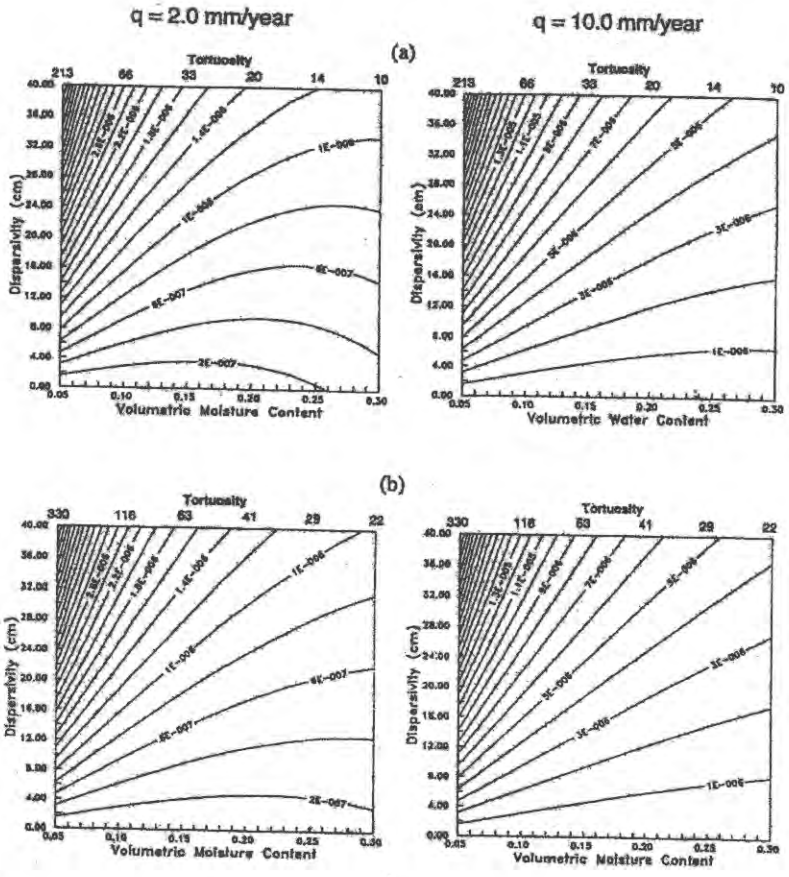

Figure 1. Contour plots of total dispersion coefficient (cm^2/s) as a function of tortuosity and dispersivity. The plots correspond to paleorecharge rates of 2.0 and 10.0 mm/year. Results for Model 1 of the tortuosity/volumetric water content relationship are shown in part (a) and model 2 of the tortuosity/volumetric water content relationship in part (b). Note that the tortuosity scale is not linear.

additional spreading of the chloride bulge by molecular diffusion following the cessation of pluvial recharge and thus tends to overestimate dispersivity.

The maximum value of dispersivity from this analysis can be further constrained by limiting the bounds of reasonable volumetric moisture content during the paleorecharge event. Present day measurements of volumetric moisture content in boreholes PW-1, PW-2, and PW-3 exceed 0.18 at only two points deep in the boreholes and near the water table (Kalinina, 1995). Volumetric moisture contents corresponding to the paleorecharge rates should be partially preserved at greater depths in these boreholes. Because unsaturated flow is highly non-linear, the higher paleorecharge rates would not have resulted in drastically higher volumetric moisture contents. From these observations it seems reasonable to limit the analysis of dispersivity to volumetric moisture content ranging from 0.05 to 0.20. Using these bounds, the highest value of dispersivity (about 30 cm) is calculated for a paleorecharge rate of 2.0 mm/year using Model 2 of the tortuosity/volumetric moisture content relationship at a volumetric moisture content value of 0.20.

If it becomes apparent from PA analyses that the higher values of dispersivity lead to failure of the site, the range of dispersivity may be further reduced by reconsidering the range of paleorecharge rates used in this analysis. The lower estimate of paleorecharge rate presented in Tyler et al. (in press) is 4.4 mm/year, which is over twice as great as the bounding rate of 2.0 mm/year used in this analysis. Examination of Figure 1 shows that the derived maximum dispersivity is sensitive to the assumed paleorecharge rate and would be reduced considerably if the minimum assumed paleorecharge rate was increased.

Relative Influence of Mechanical Dispersion and Molecular Diffusion

The total dispersion in unsaturated solute transport, as well as the relative effects of mechanical dispersion and molecular diffusion, vary as functions of groundwater flux, dispersivity, tortuosity, and moisture content. Figure 2 shows plots of total dispersion coefficient and molecular/mechanical dispersion ratio for the anticipated values of upward advective flux (0.1-0.2 mm/year) for the GCD PA. Note that the absolute values of total dispersion coefficient are much lower than those shown in Figure 1, because of the lower values of flux. The higher values of total dispersion occur at lower values of tortuosity where molecular diffusion becomes more prominent and at lower values of volumetric moisture content where increased flow velocity produces greater mechanical dispersion. Also note that dispersion is dominated by molecular diffusion (molecular/mechanical dispersion ratio greater than one) at values of low dispersivity and high moisture content. One conclusion from Figure 2 is that mechanical dispersion is an important process that dominates diffusive transport over most of the range of values to tortuosity/moisture content (and dispersivity) for the GCD PA analysis.

Fastest simulated transport of radionuclides to the surface (or rooting depth) in the PA analysis will occur by advective transport under conditions of high upward flux and by dispersive transport under conditions which result in high total dispersion coefficient.

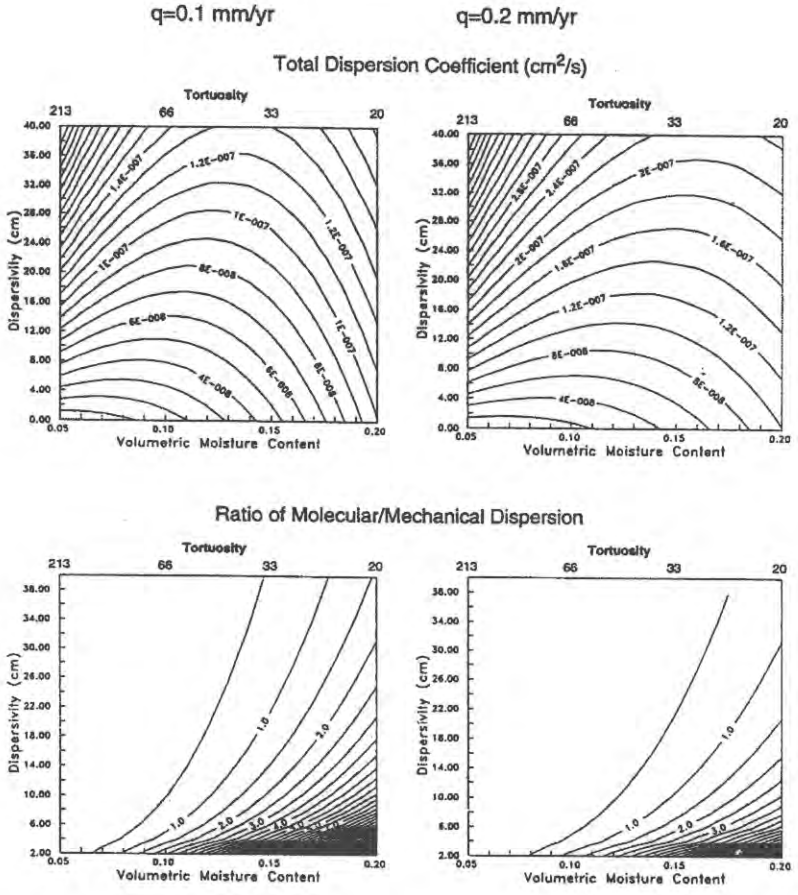

Figure 2. Contour plots of total dispersion coefficient and molecular/mechanical dispersion ratio for upward groundwater fluxes of 0.1 and 0.2 mm/year. Model 1 of the tortuosity/volumetric moisture content relationship is used.

Examination of Figure 2 shows that the highest values of total dispersion coefficient occur with high flux, high dispersivity, and low moisture content (high tortuosity). In reality we

would expect higher flux to result in higher volumetric moisture content. If a realistic, positive correlation between flux and moisture content is included in the PA analysis, the cases of highest dispersion would be avoided.

Summary

Overall, the results of tracer experiments in unsaturated media indicate a plausible range of dispersivity of a few to a few tens of centimeters for transport on the scale of GCD. Analysis of chloride concentration profiles from boreholes at the GCD site indicates a possible range of about 1 to 30 cm for dispersivity, using relatively conservative bounds on possible paleorecharge rates. For present upward fluxes of 0.1 to 0.2 mm/year at the GCD site, mechanical dispersion may be a significant or dominant component of dispersive transport.

My recommendation is to use a range of 1 to 30 cm for dispersivity in the unsaturated transport calculations for the GCD PA. Due to lack of any additional information on the distribution of possible values for dispersivity within these bounds, a uniform distribution seems to be the most appropriate. This relatively conservative range of dispersivity could be further constrained by limiting the bounds of assumed paleorecharge rate in the analysis of the chloride profile bulges from Tyler et al. (in press). Correlation between upward advective flux and moisture content is physically realistic and would tend to limit cases with the greatest diffusive transport.

References

Bresler, E. and A. Laufer, 1974, "Anion Exclusion and Coupling Effects in Nonsteady Transport Through Unsaturated Soils: II. Laboratory and Numerical Experiments," *Soil Science Society of America Proceedings*, **38**(2), 213-218.

Butter, G. L. and W. A. Jury, 1989, "Field Scale Transport of Bromide in an Unsaturated Soil, 2. Dispersion," *Water Resources Research*, **25**(7), 1583-1589.

DeSmedt, F., F. Wauters and J. Sevilla, 1986, "Study of Tracer Movement Through Unsaturated Sand," *Geoderma*, **38**, 223-236.

Fuentes, H. R. and W. L. Polzer, 1986, "Interpretive Analysis of Data for Solute Transport in the Unsaturated Zone," *NUREG/CR-4737*, U. S. Nuclear Regulatory Commission, Washington, DC.

Gelhar, L. W. and C. L. Axness, 1983, "Three-Dimensional Stochastic Analysis of Macrodispersion in Aquifers," *Water Resources Research*, **19**(1), 161-180.

Gelhar, Lynn W., A. Mantoglou, C. Welty, and K. R. Rehfeldt, 1985, A review of field-scale physical solute transport processes in saturated and unsaturated porous media: Electric Power Research Institute EPRI EA-4190 Project 2485-5, 116 p.

Gvirtzman, H. and M. Magaritz, 1986, "Investigation of Water Movement in the Unsaturated Zone Under an Irrigated Area Using Environmental Tritium," *Water Resources Research*, **22**(5), 635-642.

Harter, T. and T. -C. J. Yeh, in press, "Flow and Transport in Hetergeneous, Variably Saturated Porous Media: 2. Stochastic Analysis of Solute Transport From Small Sources," *Water Resources Research.*

James, R. V. and J. Rubin, 1986, "Transport of Chloride Ion in a Water-Unsaturated Soil Exhibiting Anion Exclusion," *Soil Science Society of America Journal*, **50**(5), 1142-1149.

Kalinina, Elena, 1995, *Volumetric Water Content Distribution Analysis for the Greater Confinement Disposal Facility Nevada Test Site*, unpublished report.

Nyhan, J., W. Polzer, E. Essington, E. Cokal, L. Lane, E. Lopez, E. Stallings and R. Walker, 1986, "Joint DOE-NRC Field Study of Tracer Migration in the Unsaturated Zone," *LA-10575-MS*, Los Alamos National Laboratories, Los Alamos, NM.

Porro, I., P. J. Wierenga and R. G. Hills, 1993, "Solute Transport Through Large Uniform and Layered Soil Columns," *Water Resources Research*, **29**(4), 1321-1330.

Russo, D., 1991, "Stochastic Analysis of Simulated Vadose Zone Solute Transport in a Vertical Cross Section of Heterogeneous Soil During Nonsteady Water Flow," *Water Resources Research*, **27**(3), 267-283.

Russo, D. and G. Dagan, 1991, "On Solute Transport in a Heterogeneous Porous Formation Under Saturated and Unsaturated Water Flows," *Water Resources Research*, **27**(3), 285-292.

Schulin, R., P., J. Weirenga, H. Fluher and J. Leuenberger, 1987, "Solute Transport Through a Stony Soil," *Soil Science Society of America Journal*, **51**(1), 36-42.

Stephenson, D. and A. S. M. de Jesus, 1985, "Estimate of Dispersion in an Unsaturated Aquifer," *Journal of Hydrology*, **81**, 45-55.

Tyler, S. W., J. B. Chapman, S. H. Conrad, D. P. Hannermeister, D. Blout, J. Miller, M. J. Sully and J. M. Ginanni, in press, "Soil Water Flux on the Nevada Test Site: Temporal and Spatial Variations Over the Last 120,000 Years," *Water Resources Research.*

Wierenga, P. J., D. Baschelet, J. R. Bilskie, H. Elabd, D. B. Hudson, M. Nash, I. Porro, W. R. Strong, A. Toorman and J. Vinson, 1988, *Validation of Stochastic Flow and Transport Models for Unsaturated Soils*, Annual Report for the Period October 1, 1986 - September 30, 1987, Research Report 88-SS-03, New Mexico State University, Las Cruces, NM.

Wierenga, P. J. and M. T. van Genuchten, 1989, "Solute Transport Through Small and Large Unsaturated Columns," *Groundwater*, 27(1), 35-42.

cc:

MS 1326	6851	J. Cochran
MS 1324	6331	S. H. Conrad
MS 1324	6331	D. P. Gallegos
MS 1326	6851	H. A. Dockery

File: dispers.memo.2

Appendix O

MPCs from ICRP2 and Resulting DCFs for Ingestion and Inhalation DCFs for External Exposure from FGR 12

This page intentionally left blank.

Table O-1. Radionuclide Activities and Maximum Permissible Concentrations in Air from ICRP 2 (µCi/cm^3)

Isotope	Activity Conversion (Ci/mole)	Whole Body	Bone	Liver	Kidney	Lower Large Intestine	Lung	Spleen	Upper Large Intestine	Stomach
Pu-242	9.53E!01	1E!11	2E!12	7E!12	1E!11	2E!07	4E!11			
U-238	8.00E!05	2E!09	6E!10		7E!11	2E!07	1E!10			
Th-234	5.42E+06	4E!07	6E!08	5E!07	9E!08	9E!08	3E!08			
Pa-234	4.68E+08									
U-234a	1.46E+00	2E!09	6E!10		1E!09	2E!07	1E!10			
Th-230a	4.64E+00	2E!11	2E!12	2E!11	4E!12	2E!07	1E!11			
Ra-226a	2.23E+02	5E!11	3E!11			2E!07				
Rn-222a	3.41E+07						3E!08			
Po-218a	6.16E+10									
Pb-214a	7.02E+09									
Bi-214a	9.46E+09									
Po-214a	6.87E+16									
Pb-210a	1.60E+04	1E!09	2E!10	4E!10	1E!10	9E!07	2E!10			
Bi-210a	2.61E+07	3E!07	1E!06	8E!08	6E!09	2E!07	6E!09	1E!07		
Po-210a	9.44E+05	5E!09	7E!09	2E!09	5E!10	2E!07	2E!10	5E!10		
Pu-238	4.08E+03	1E!11	2E!12	8E!12	1E!11	1E!07	3E!11			
U-234b	1.46E+00	2E!09	6E!10		1E!09	2E!07	1E!10			
Th-230b	4.64E+00	2E!11	2E!12	2E!11	4E!12	2E!07	1E!11			
Ra-226b	2.23E+02	5E!11	3E!11			2E!07				
Rn-222b	3.41E+07						3E!08			
Po-218b	6.16E+10									
Pb-214b	7.02E+09									
Bi-214b	9.46E+09									
Po-214b	6.87E+16									
Pb-210b	1.60E+04	1E!09	2E!10	4E!10	1E!10	9E!07	2E!10			
Bi-210b	2.61E+07	3E!07	1E!06	8E!08	6E!09	2E!07	6E!09	1E!07		
Po-210b	9.44E+05	5E!09	7E!09	2E!09	5E!10	2E!07	2E!10	5E!10		
Am-241	8.26E+02	2E!11	6E!12	9E!12	6E!12	1E!07	1E!10			
Np-237	1.67E!01	2E!11	4E!12	2E!11	7E!12	2E!07	1E!10			
Pa-233	4.84E+06	9E!07	9E!07	2E!06	6E!07	6E!07	2E!07			
U-233	2.25E+00	2E!09	5E!10		1E!09	2E!07	1E!10			
Th-229	4.90E+01	2.2E!12	6E!13	2.60E!11	5.50E!12	2.50E0-8	2.10E!12		5.00E!08	7.40E!07
Ra-225	8.76E+06	1.20E!09	1.30E!09	5.30E!07	1.90E!08		2.00E!10			
Ac-225	1.30E+07	2.80E!09	9.70E!10	3.90E!10	3.00E!09	3.0E!08	2.40E!10		5.90E!08	8.80E!7
Fr-221	2.73E+07									
At-217	3.53E+14									
Bi-213	4.12E+09									
Po-213	2.82E+18									
Pb-209	9.64E+08									

Table O-1. Radionuclide Activities and Maximum Permissible Concentrations in Air from ICRP 2 (µCi/cm^3) (continued)

Isotope	Activity Conversion (Ci/mole)	Whole Body	Bone	Liver	Kidney	Lower Large Intestine	Lung	Spleen	Upper Large Intestine	Stomach
Pu-240	5.45E+01	1E!11	2E!12	7E!12	9E!12	2E!07	4E!11			
U-236	1.53E!02	2E!09	6E!10		1E!09	2E!07	1E!10			
Th-232	2.54E!05	1E!11	2E!12	3E!11	5E!12	2E!07	1E!11			
Ra-228	6.22E+04	9E!11	7E!11			1E!07	4E!11			
Ac-228	5.11E+08	1E!07	9E!08	8E!08	6E!07		2E!08		4E!07	
Th-228	1.87E+05	5E!11	9E!12	3E!10	5E!11	7E!08	6E!12			
Ra-224	3.57E+07	8E!09	5E!09			3E!08	7E!10			
Rn-220	1.99E+11						3E!07			
Po-216	7.52E+13									
Pb-212	2.95E+08	2E!07	7E!08	2E!07	2E!08	9E!08	2E!08			
Bi-212	2.89E+10	2E!06	8E!06	1E!06	1E!07		2E!07	1E!06		2E!06
Tl-208	6.16E+10									
Pu-239	1.48E+01	1E!11	2E!12	7E!12	9E!12	2E!07	4E!11			
U-235	5.08E!04	2E!09	6E!10		5E!10	1E!07	1E!10			
Th-231	1.23E+08	4E!05	1E!05	1E!04	1E!05	1E!06	6E!06			
Pa-231	1.09E+01	5E!12	1E!12	2E!11	3E!12	1E!07	1E!10			
Ac-227	1.64E+04	7E!12	2E!12	1E!11	3E!11	2E!06	3E!11			
Th-227	6.97E+06	2E!09	3E!10	1E!08	2E!09	9E!08	2E!10			
Ra-223	1.14E+07	3E!09	2E!09			2E!08	2E!10			
Rn-219	2.86E+12						5.90E!08			
Po-215	6.34E+15									
Pb-211	5.21E+09									
Bi-211	8.78E+10									
Tl-207	3.94E+10									

Table O-2. Calculated Inhalation Dose Conversion Factors (mrem/mole)

Isotope	Whole Body (mrem/mole)	Bone	Liver	Kidneys	LLI	Lung	Spleen	ULI	Stomach
Pu-242	2E+11	6E+12	8E+11	6E+11	3E+07	1E+11			
U-238	8E+04	2E+06		7E+06	2E+03	5E+06			
Th-234	3E+13	1E+15	7E+13	4E+14	4E+14	1E+15			
Pa-234									
U-234a	1E+09	3E+10		9E+09	4E+07	9E+10			
Th-230a	5E+11	3E+13	1E+12	7E+12	1E+08	3E+12			
Ra-226a	9E+12	9E+13			7E+09				
Rn-222a						7E+15			
Po-218a									
Pb-214a									
Bi-214a									
Po-214a									

Table O-2. Calculated Inhalation Dose Conversion Factors (mrem/mole) (continued)

Isotope	Whole Body (mrem/mole)	Bone	Liver	Kidneys	LLI	Lung	Spleen	ULI	Stomach
Pb-210a	3E+13	1E+15	2E+14	1E+15	1E+11	5E+14			
Bi-210a	2E+14	3E+14	2E+15	3E+16	8E+14	3E+16	2E+15		
Po-210a	4E+14	2E+15	3E+15	1E+16	3E+13	3E+16	1E+16		
Pu-238	8E+14	2E+16	3E+15	2E+15	2E+11	8E+14			
U-234b	1E+09	3E+10		9E+09	4E+07	9E+10			
Th-230b	5E+11	3E+13	1E+12	7E+12	1E+08	3E+12			
Ra-226b	9E+12	9E+13			7E+09				
Rn-222b						7E+15			
Po-218b									
Pb-214b									
Bi-214b									
Po-214b									
Pb-210b	3E+13	1E+15	2E+14	1E+15	1E+11	5E+14			
Bi-210b	2E+14	3E+14	2E+15	3E+16	8E+14	3E+16	2E+15		
Po-210b	4E+14	2E+15	3E+15	1E+16	3E+13	3E+16	1E+16		
Am-241	8E+13	2E+15	6E+14	8E+14	5E+10	5E+13			
Np-237	2E+10	5E+11	5E+10	1E+11	5E+06	1E+10			
Pa-233	1E+13	6E+13	1E+13	5E+13	5E+13	1E+14			
U-233	2E+09	5E+10		1E+10	7E+07	1E+11			
Th-229	4.45E+13	9.80E+14	1.13E+13	5.34E+13	1.18E+10	1.40E+14		5.88E+09	3.97E+08
Ra-225	1.46E+16	8.09E+16	9.92E+13	2.77E+15		2.63E+17			
Ac-225	9.32E+15	1.61E+17	2.01E+17	2.61E+16	2.61E+15	3.26E+17		1.33E+15	8.90E+13
Fr-221									
At-217									
Bi-213									
Po-213									
Pb-209									
Pu-240	1E+13	3E+14	5E+13	4E+13	2E+09	8E+12			
U-236	2E+07	3E+08		9E+07	5E+05	9E+08			
Th-232	5E+06	2E+08	5E+06	3E+07	8E+02	2E+07			
Ra-228	1E+15	1E+16			4E+12	9E+15			
Ac-228	1E+16	7E+16	4E+16	5E+15		2E+17		8E+15	
Th-228	7E+15	2E+17	4E+15	2E+16	2E+13	2E+17			
Ra-224	9E+15	9E+16			7E+15	3E+17			
Rn-220						4E+18			
Po-216									
Pb-212	3E+15	5E+16	9E+15	9E+16	2E+16	9E+16			
Bi-212	3E+16	4E+16	2E+17	2E+18		9E+17	2E+17		9E+16
Tl-208									
Pu-239	3E+12	9E+13	1E+13	1E+13	4E+08	2E+12			
U-235	5E+05	1E+07		6E+06	3E+04	3E+07			
Th-231	6E+12	1E+14	7E+12	7E+13	7E+14	1E+14			
Pa-231	4E+12	1E+14	3E+12	2E+13	7E+08	7E+11			
Ac-227	5E+15	1E+17	1E+16	3E+15	5E+10	3E+15			

Table O-2. Calculated Inhalation Dose Conversion Factors (mrem/mole) (continued)

Isotope	Whole Body (mrem/mole)	Bone	Liver	Kidneys	LLI	Lung	Spleen	ULI	Stomach
Th-227	7E+15	3E+17	4E+15	2E+16	5E+14	2E+17			
Ra-223	8E+15	7E+16			3E+15	3E+17			
Rn-219						3E+20			
Po-215									
Pb-211									
Bi-211									
Tl-207									

Table O-3. Maximum Permissible Concentrations of Radionuclides in Water from ICRP 2 (µCi/cm^3)

Isotope	Whole Body	Bone	Liver	Kidney	Lower Large Intestine	Spleen	Upper Large Intestine	Stomach
Pu-242	1E!03	1E!04	6E!04	7E!04	9E!04			
U-238	4E!02	1E!02		2E!03	1E!03			
Th-234	8	1	10	2	5E!04			
Pa-234								
U-234a	4E!02	1E!02		3E!02	9E!04			
Th-230a	3E!04	5E!05	5E!04	1E!04	9E!04			
Ra-226a	6E!07	4E!07			9E!04			
Rn-222a								
Po-218a								
Pb-214a								
Bi-214a								
Po-214a								
Pb-210a	4E!06	6E!06	1E!05	4E!06	5E!03			
Bi-210a	7E!02	2E!01	2E!02	2E!03	1E!03	2E!02		
Po-210a	2E!04	3E!04	7E!05	2E!05	8E!04	2E!05		
Pu-238	1E!03	1E!04	6E!04	8E!04	8E!04			
U-234b	4E!02	1E!02		3E!02	9E!04			
Th-230b	3E!04	5E!05	5E!04	1E!04	9E!04			
Ra-226b	6E!07	4E!07			9E!04			
Rn-222b								
Po-218b								
Pb-214b								
Bi-214b								
Po-214b								
Pb-210b	4E!06	6E!06	1E!05	4E!06	5E!03			
Bi-210b	7E!02	2E!01	2E!02	2E!03	1E!03	2E!02		

Table O-3. Maximum Permissible Concentrations of Radionuclides in Water from ICRP 2 (µCi/cm^3) (continued)

Isotope	Whole Body	Bone	Liver	Kidney	Lower Large Intestine	Spleen	Upper Large Intestine	Stomach
Po-210b	2E!04	3E!04	7E!05	2E!05	8E!04	2E!05		
Am-241	4E!04	1E!04	2E!04	1E!04	8E!04			
Np-237	4E!04	9E!05	6E!04	2E!04	9E!04			
Pa-233	20	20	50	10	3E!03			
U-233	4E!02	1E!02		3E!02	9E!04			
Th-229	5.00E!05	1.40E!05	4.80E!04	9.90E!05	1.11E!04		2.26E!04	3.27E!03
Ra-225	1.50E!05	1.60E!05	6.40E!03	2.20E!04				
Ac-225	6.30E!02	2.30E!02	9.20E!03	8.10E!02	1.40E!04		2.70E!04	3.90E!03
Fr-221								
At-217								
Bi-213								
Po-213								
Pb-209								
Pu-240	1E!03	1E!04	5E!04	7E!04	8E!04			
U-236	4E!02	1E!02		3E!02	1E!03			
Th-232	3E!04	5E!05	6E!04	1E!04	1E!03			
Ra-228	1E!06	8E!07			7E!04			
Ac-228	3	2	2	20			3E!03	
Th-228	1E!03	2E!04	7E!03	1E!03	4E!04			
Ra-224	9E!05	7E!05			2E!04			
Rn-220								
Po-216								
Pb-212	6E!03	2E!03	6E!03	6E!04	5E!04			
Bi-212	5E!01	2	3E!01	2E!02		4E!01		1E!02
Ti-208								
Pu-239	1E!03	1E!04	5E!04	7E!04	8E!04			
U-235	4E!02	1E!02		1E!02	8E!04			
Th-231	900	200	2000	300	7E!03			
Pa-231	1E!04	3E!05	4E!04	7E!05	8E!04			
Ac-227	2E!04	6E!05	2E!04	7E!04	9E!03			
Th-227	5E!02	8E!03	2E!01	4E!02	5E!04			
Ra-223	4E!05	2E!05			1E!04			
Rn-219								
Po-215								
Pb-211								
Bi-211								
Tl-207								

Table O-4. Calculated Ingestion Dose Conversion Factors (mrem/mole)

Isotope	Whole Body (mrem/mole)	Bone	Liver	Kidneys	LLI	Spleen	ULI	Stomach
Pu-242	2E+07	1E+09	9E+07	7E+07	6E+07			
U-238	4E+01	9E+02		2E+03	4E+03			
Th-234	1E+10	6E+11	3E+10	1E+11	6E+14			
Pa-234								
U-234a	7E+05	2E+07		3E+06	9E+07			
Th-230a	3E+08	1E+10	5E+08	3E+09	3E+08			
Ra-226a	7E+12	6E+13			1E+10			
Rn-222a								
Po-218a								
Pb-214a								
Bi-214a								
Po-214a								
Pb-210a	7E+13	3E+14	9E+13	2E+14	2E+11			
Bi-210a	7E+12	1E+13	7E+13	7E+14	1E+15	7E+13		
Po-210a	9E+13	3E+14	7E+14	3E+15	6E+13	3E+15		
Pu-238	7E+10	4E+12	4E+11	3E+11	3E+11			
U-234b	7E+05	2E+07		3E+06	9E+07			
Th-230b	3E+08	1E+10	5E+08	3E+09	3E+08			
Ra-226b	7E+12	6E+13			1E+10			
Rn-222b								
Po-218b								
Pb-214b								
Bi-214b								
Po-214b								
Pb-210b	7E+13	3E+14	9E+13	2E+14	2E+11			
Bi-210b	7E+12	1E+13	7E+13	7E+14	1E+15	7E+13		
Po-210b	9E+13	3E+14	7E+14	3E+15	6E+13	3E+15		
Am-241	4E+10	9E+11	2E+11	5E+11	6E+10			
Np-237	8E+06	2E+08	2E+07	5E+07	1E+07			
Pa-233	4E+09	3E+10	5E+09	3E+10	7E+13			
U-233	1E+06	2E+07		4E+06	1E+08			
Th-229	1.78E+10	3.82E+11	5.57E+09	2.70E+10	2.41E+10		1.18E+10	8.17E+08
Ra-225	1.06E+16	5.97E+16	7.47E+13	2.17E+15				
Ac-225	3.77E+12	6.19E+13	7.74E+13	8.79E+12	5.08E+15		2.64E+15	1.82E+14
Fr-221								
At-217								
Bi-213								
Po-213								
Pb-209								

Table O-4. Calculated Ingestion Dose Conversion Factors (mrem/mole) (continued)

Isotope	Whole Body (mrem/mole)	Bone	Liver	Kidneys	LLI	Spleen	ULI	Stomach
Pu-240	1E+09	6E+10	6E+09	4E+09	4E+09			
U-236	7E+03	2E+05		3E+04	8E+05			
Th-232	2E+03	6E+04	2E+03	1E+04	1E+03			
Ra-228	1E+15	8E+15			5E+12			
Ac-228	3E+12	3E+13	1E+13	1E+12			9E+15	
Th-228	3E+12	1E+14	1E+12	1E+13	3E+13			
Ra-224	7E+15	6E+16			1E+16			
Rn-220								
Po-216								
Pb-212	9E+14	2E+16	3E+15	3E+16	3E+16			
Bi-212	1E+15	2E+15	5E+15	8E+16		4E+15		2E+17
Ti-208								
Pu-239	3E+08	2E+10	2E+09	1E+09	1E+09			
U-235	2E+02	6E+03		3E+03	3E+04			
Th-231	2E+09	7E+10	3E+09	2E+10	1E+15			
Pa-231	2E+09	4E+10	1E+09	8E+09	7E+08			
Ac-227	1E+12	3E+13	4E+12	1E+12	1E+11			
Th-227	3E+12	1E+14	2E+12	1E+13	8E+14			
Ra-223	5E+15	6E+16			6E+15			
Rn-219								
Po-215								
Pb-211								
Bi-211								
Tl-207								

Table O-5. Dose Conversion Factors for Immersion in a Contaminated Plume (rem/yr per mole/m^3)

Isotope	Effective	Adrenals	Bladder	Bone Surface	Brain	Breast	Esophagus	Stomach Wall	SI	ULI	LLI	Kidneys
Pu-242	4.46E+05	6.32E+04	9.10E+04	8.80E+05	8.04E+04	1.15E+06	4.75E+04	9.25E+04	5.27E+04	6.01E+04	5.30E+04	1.29E+05
U-238	3.18E+01	5.49E+00	7.40E+00	6.91E+01	7.43E+00	7.98E+01	3.93E+00	7.71E+00	4.56E+00	5.26E+00	4.64E+00	9.99E+00
Th-234	2.14E+14	1.38E+14	1.51E+14	7.08E+14	1.83E+14	2.55E+14	1.24E+14	1.61E+14	1.29E+14	1.39E+14	1.31E+14	1.68E+14
Pa-234	5.10E+18	4.13E+18	4.10E+18	8.20E+18	5.31E+18	5.68E+18	4.19E+18	4.42E+18	4.02E+18	4.15E+18	4.09E+18	4.46E+18
U-234a	1.30E+06	5.23E+05	5.96E+05	3.39E+06	6.94E+05	2.45E+06	4.57E+05	6.30E+05	4.79E+05	5.21E+05	4.86E+05	6.97E+05
Th-230a	9.43E+06	5.64E+06	6.18E+06	2.87E+07	7.48E+06	1.29E+07	5.07E+06	6.56E+06	5.25E+06	5.64E+06	5.31E+06	6.89E+06
Ra-226a	8.22E+09	6.08E+09	6.31E+09	2.07E+10	7.85E+09	9.24E+09	5.87E+09	6.68E+09	5.79E+09	6.11E+11	5.84E+09	6.81E+09
Rn-222a	7.62E+13	6.18E+13	6.18E+13	1.32E+14	7.90E+13	8.53E+13	6.06E+13	6.58E+13	5.86E+13	6.10E+13	5.94E+13	6.62E+13
Po-218a	3.22E+15	2.62E+15	2.58E+15	4.90E+15	3.38E+15	3.58E+15	2.67E+15	2.80E+15	2.55E+15	2.63E+15	2.61E+15	2.82E+15
Pb-214a	9.68E+18	7.57E+18	7.68E+18	2.00E+19	9.68E+18	1.09E+19	7.37E+18	8.15E+18	7.16E+18	7.51E+18	7.27E+18	8.20E+18
Bi-214a	8.45E+19	6.98E+19	7.07E+19	1.20E+20	8.90E+19	9.30E+19	7.15E+19	7.49E+19	6.88E+19	7.07E+19	6.98E+19	7.51E+19
Po-214a	3.27E+22	2.66E+22	2.61E+22	5.03E+22	3.43E+22	3.64E+22	2.70E+22	2.84E+22	2.58E+22	2.66E+22	2.64E+22	2.86E+22
Pb-210a	1.06E+11	4.98E+10	5.92E+10	3.65E+11	7.02E+10	1.53E+11	3.58E+10	6.38E+10	4.19E+10	4.85E+10	4.27E+10	7.30E+10
Bi-210a	1.00E+14	6.82E+13	7.24E+13	2.73E+14	8.92E+13	1.20E+14	6.33E+13	7.70E+13	6.39E+13	6.82E+13	6.45E+13	8.00E+13
Po-210a	4.58E+10	3.74E+10	3.67E+10	7.04E+10	4.82E+10	5.10E+10	3.79E+10	3.98E+10	3.63E+10	3.74E+10	3.70E+10	4.01E+10
Pu-238	2.32E+09	2.90E+08	4.33E+08	4.43E+09	3.64E+08	6.05E+09	2.14E+08	4.37E+08	2.38E+08	2.73E+08	2.39E+08	6.28E+08
U-234b	1.30E+06	5.23E+05	5.96E+05	3.39E+06	6.94E+05	2.45E+06	4.57E+05	6.30E+05	4.79E+05	5.21E+05	4.86E+05	6.97E+05
Th-230b	9.43E+06	5.64E+06	6.18E+06	2.87E+07	7.48E+06	1.29E+07	5.07E+06	6.56E+06	5.25E+06	5.64E+06	5.31E+06	6.89E+06
Ra-226b	8.22E+09	6.08E+09	6.31E+09	2.07E+10	7.85E+09	9.24E+09	5.87E+09	6.68E+09	5.79E+09	6.11E+11	5.84E+09	6.81E+09
Rn-222b	7.62E+13	6.18E+13	6.18E+13	1.32E+14	7.90E+13	8.53E+13	6.06E+13	6.58E+13	5.86E+13	6.10E+13	5.94E+13	6.62E+13
Po-218b	3.22E+15	2.62E+15	2.58E+15	4.90E+15	3.38E+15	3.58E+15	2.67E+15	2.80E+15	2.55E+15	2.63E+15	2.61E+15	2.82E+15
Pb-214b	9.68E+18	7.57E+18	7.68E+18	2.00E+19	9.68E+18	1.09E+19	7.37E+18	8.15E+18	7.16E+18	7.51E+18	7.27E+18	8.20E+18
Bi-214b	8.45E+19	6.98E+19	7.07E+19	1.20E+20	8.90E+19	9.30E+19	7.15E+19	7.49E+19	6.88E+19	7.07E+19	6.98E+19	7.51E+19
Po-214b	3.27E+22	2.66E+22	2.61E+22	5.03E+22	3.43E+22	3.64E+22	2.70E+22	2.84E+22	2.58E+22	2.66E+22	2.64E+22	2.86E+22
Pb-210b	1.06E+11	4.98E+10	5.92E+10	3.65E+11	7.02E+10	1.53E+11	3.58E+10	6.38E+10	4.19E+10	4.85E+10	4.27E+10	7.30E+10
Bi-210b	1.00E+14	6.82E+13	7.24E+13	2.73E+14	8.92E+13	1.20E+14	6.33E+13	7.70E+13	6.39E+13	6.82E+13	6.45E+13	8.00E+13
Po-210b	4.58E+10	3.74E+10	3.67E+10	7.04E+10	4.82E+10	5.10E+10	3.79E+10	3.98E+10	3.63E+10	3.74E+10	3.70E+10	4.01E+10
Am-241	7.89E+10	4.38E+10	4.99E+10	2.77E+11	6.01E+10	1.03E+11	3.61E+10	5.35E+10	3.95E+10	4.37E+10	4.00E+10	5.80E+10
Np-237	2.01E+07	1.29E+07	1.41E+07	6.24E+07	1.70E+07	2.46E+07	1.18E+07	1.49E+07	1.21E+07	1.31E+07	1.23E+07	1.56E+07
Pa-233	5.28E+15	4.06E+15	4.15E+15	1.18E+16	5.20E+15	5.93E+15	3.93E+15	4.40E+15	3.84E+15	4.03E+15	3.89E+15	4.45E+15
U-233	4.27E+06	2.73E+06	2.88E+06	1.08E+07	3.51E+06	5.82E+06	2.55E+06	3.04E+06	2.55E+06	2.70E+06	2.58E+06	3.17E+06

Table O-5. Dose Conversion Factors for Immersion in a Contaminated Plume (rem/yr per mole/m^3) (continued)

Isotope	Effective	Adrenals	Bladder	Bone Surface	Brain	Breast	Esophagus	Stomach Wall	SI	ULI	LLI	Kidneys
Th-229	2.19E+10	1.51E+10	1.61E+10	6.58E+10	1.97E+10	2.53E+10	1.41E+10	1.71E+10	1.43E+10	1.52E+10	1.44E+10	1.76E+10
Ra-225	2.85E+14	1.18E+14	1.47E+14	9.41E+14	1.68E+14	4.34E+14	7.36E+13	1.58E+14	9.29E+13	1.13E+14	9.37E+13	1.93E+14
Ac-225	1.10E+15	7.73E+14	8.20E+14	3.15E+15	1.01E+15	1.26E+15	7.27E+14	8.69E+14	7.31E+14	7.79E+14	7.41E+14	8.91E+14
Fr-221	4.65E+15	3.51E+15	3.63E+15	1.11E+16	4.53E+15	5.23E+15	3.41E+15	3.82E+15	3.35E+15	3.51E+15	3.38E+15	3.89E+15
At-217	6.09E+20	4.86E+20	4.86E+20	1.10E+21	6.22E+20	6.79E+20	4.82E+20	5.23E+20	4.61E+20	4.82E+20	4.73E+20	5.23E+20
Bi-213	3.08E+18	2.47E+18	2.48E+18	5.63E+18	3.15E+18	3.45E+18	2.42E+18	2.63E+18	2.33E+18	2.44E+18	2.37E+18	2.65E+18
Po-213	0.00E+00	0.00E+00	0.00E+00	0.00E+00	0.00E+00	0.00E+00	0.00E+00	0.00E+00	0.00E+00	0.00E+00	0.00E+00	0.00E+00
Pb-209	9.14E+14	5.73E+14	6.26E+14	2.74E+15	7.58E+14	1.15E+15	5.12E+14	6.64E+14	5.29E+14	5.73E+14	5.36E+14	7.06E+14
Pu-240	3.02E+07	3.96E+06	5.85E+06	5.89E+07	5.03E+06	7.83E+07	2.89E+06	5.93E+06	3.25E+06	3.74E+06	3.26E+06	8.40E+06
U-236	8.93E+03	2.60E+03	3.12E+03	2.12E+04	3.46E+03	1.96E+04	2.19E+03	3.28E+03	2.34E+03	2.58E+03	2.37E+03	3.81E+03
Th-232	2.58E+01	1.34E+01	1.49E+01	7.70E+01	1.79E+01	4.03E+01	1.17E+01	1.58E+01	1.23E+01	1.34E+01	1.25E+01	1.69E+01
Ra-228	0.00E+00	0.00E+00	0.00E+00	0.00E+00	0.00E+00	0.00E+00	0.00E+00	0.00E+00	0.00E+00	0.00E+00	0.00E+00	0.00E+00
Ac-228	2.85E+18	2.32E+18	2.31E+18	4.41E+18	2.99E+18	3.17E+18	2.37E+18	2.48E+18	2.26E+18	2.34E+18	2.31E+18	2.50E+18
Th-228	2.01E+12	1.38E+12	1.47E+12	5.76E+12	1.81E+12	2.38E+12	1.30E+12	1.56E+12	1.31E+12	1.39E+12	1.32E+12	1.60E+12
Ra-224	1.96E+15	1.50E+15	1.54E+15	4.46E+15	1.93E+15	2.20E+15	1.46E+15	1.63E+15	1.42E+15	1.50E+15	1.45E+15	1.65E+15
Rn-220	4.31E+17	3.51E+17	3.49E+17	7.28E+17	4.47E+17	4.82E+17	3.47E+17	3.72E+17	3.33E+17	3.47E+17	3.40E+17	3.75E+17
Po-216	7.28E+18	5.93E+18	5.82E+18	1.12E+19	7.64E+18	8.11E+18	6.03E+18	6.32E+18	5.75E+18	5.94E+18	5.89E+18	6.37E+18
Pb-212	2.36E+17	1.76E+17	1.83E+17	5.78E+17	2.28E+17	2.67E+17	1.70E+17	1.93E+17	1.67E+17	1.76E+17	1.69E+17	1.97E+17
Bi-212	3.11E+19	2.55E+19	2.54E+19	4.68E+19	3.27E+19	3.44E+19	2.59E+19	2.73E+19	2.49E+19	2.56E+19	2.53E+19	2.74E+19
Tl-208	1.27E+21	1.07E+21	1.11E+21	1.74E+21	1.34E+21	1.38E+21	1.10E+21	1.15E+21	1.06E+21	1.09E+21	1.08E+21	1.15E+21
Pu-239	7.35E+06	3.46E+06	3.78E+06	1.64E+07	4.47E+06	1.31E+07	3.20E+06	3.98E+06	3.22E+06	3.43E+06	3.26E+06	4.31E+06
U-235	4.27E+05	3.15E+05	3.29E+05	1.09E+06	4.07E+05	4.81E+05	3.05E+05	3.47E+05	3.01E+05	3.17E+05	3.04E+05	3.53E+05
Th-231	7.49E+15	4.50E+15	4.98E+15	2.34E+16	5.95E+15	9.74E+15	4.06E+15	5.28E+15	4.22E+15	4.55E+15	4.25E+15	5.60E+15
Pa-231	2.19E+09	1.67E+09	1.71E+09	4.63E+09	2.14E+09	2.53E+09	1.63E+09	1.81E+09	1.58E+09	1.65E+09	1.60E+09	1.83E+09
Ac-227	1.11E+10	7.58E+09	8.10E+09	3.22E+10	9.90E+09	1.34E+10	7.12E+09	8.56E+09	7.18E+09	7.64E+09	7.26E+09	8.83E+09
Th-227	3.97E+15	3.01E+15	3.09E+15	9.11E+15	3.87E+15	4.50E+15	2.91E+15	3.27E+15	2.85E+15	2.99E+15	2.88E+15	3.33E+15
Ra-223	8.12E+15	5.99E+15	6.23E+15	2.05E+16	7.75E+15	9.22E+15	5.72E+15	6.60E+15	5.67E+15	5.99E+15	5.74E+15	6.74E+15
Rn-219	8.95E+20	7.05E+20	7.11E+20	1.82E+21	8.98E+20	1.00E+21	6.85E+20	7.55E+20	6.65E+20	6.98E+20	6.75E+20	7.62E+20
Po-215	6.24E+21	5.03E+21	5.03E+21	1.13E+22	6.40E+21	6.98E+21	4.91E+21	5.35E+21	4.73E+21	4.95E+21	4.82E+21	5.38E+21
Pb-211	1.52E+18	1.22E+18	1.22E+18	2.55E+18	1.57E+18	1.70E+18	1.22E+18	1.31E+18	1.17E+18	1.22E+18	1.20E+18	1.32E+18
Bi-211	2.28E+19	1.80E+19	1.82E+19	4.55E+19	2.29E+19	2.55E+19	1.74E+19	1.93E+19	1.69E+19	1.77E+19	1.72E+19	1.94E+19
Tl-207	7.46E+17	5.80E+17	5.80E+17	1.39E+18	7.50E+17	8.47E+17	5.75E+17	6.26E+17	5.57E+17	5.80E+17	5.71E+17	6.35E+17

Table O-5. Dose Conversion Factors for Immersion in a Contaminated Plume (rem/yr per mole/m^3) (continued)

Isotope	Liver	Lungs	Muscle	Ovaries	Pancreas	Red Marrow	Skin	Spleen	Testes	Thymus	Thyroid	Uterus
Pu-242	8.88E+04	1.08E+05	4.84E+05	4.62E+04	4.73E+04	1.59E+05	3.64E+06	7.94E+04	5.95E+05	1.41E+05	3.70E+05	4.97E+04
U-238	7.57E+00	9.30E+00	3.45E+01	4.07E+00	4.08E+00	1.16E+01	2.72E+02	7.00E+00	4.10E+01	1.10E+01	2.54E+01	4.27E+00
Th-234	1.64E+14	1.90E+14	1.92E+14	1.21E+14	1.25E+14	1.58E+14	4.74E+14	1.64E+14	2.14E+14	1.82E+14	2.06E+14	1.25E+14
Pa-234	4.49E+18	4.97E+18	4.85E+18	4.08E+18	3.96E+18	4.84E+18	6.78E+18	4.51E+18	4.99E+18	4.64E+18	5.11E+18	3.90E+18
U-234a	6.37E+05	7.46E+05	1.30E+06	4.50E+05	4.60E+05	7.16E+05	7.24E+06	6.24E+05	1.50E+06	7.58E+05	1.14E+06	4.62E+05
Th-230a	6.67E+06	7.75E+06	8.73E+06	4.92E+06	5.09E+06	6.61E+06	2.45E+07	6.67E+06	9.76E+06	7.43E+06	8.84E+06	5.07E+06
Ra-226a	6.84E+09	7.70E+09	7.54E+09	5.64E+09	5.77E+09	7.05E+09	1.25E+10	6.84E+09	8.04E+09	7.31E+09	8.06E+09	5.69E+09
Rn-222a	6.66E+13	7.42E+13	7.22E+13	5.54E+13	5.78E+13	7.14E+13	9.09E+13	6.70E+13	7.46E+13	6.86E+13	7.58E+13	5.70E+13
Po-218a	2.84E+15	3.15E+15	3.07E+15	2.61E+15	2.50E+15	3.08E+15	5.44E+15	2.86E+15	3.16E+15	2.92E+15	3.24E+15	2.47E+15
Pb-214a	8.28E+18	9.27E+18	9.02E+18	6.86E+18	7.13E+18	8.69E+18	2.27E+19	8.28E+18	9.51E+18	8.69E+18	9.60E+18	7.00E+18
Bi-214a	7.59E+19	8.29E+19	8.10E+19	6.98E+19	6.83E+19	8.21E+19	1.41E+20	7.60E+19	8.22E+19	7.91E+19	8.47E+19	6.75E+19
Po-214a	2.88E+22	3.19E+22	3.11E+22	2.63E+22	2.53E+22	3.12E+22	3.78E+22	2.90E+22	3.21E+22	2.96E+22	3.28E+22	2.50E+22
Pb-210a	6.48E+10	7.96E+10	9.57E+10	3.73E+10	3.76E+10	5.88E+10	2.40E+11	6.33E+10	1.16E+11	7.94E+10	1.01E+11	3.88E+10
Bi-210a	7.85E+13	8.98E+13	9.16E+13	6.06E+13	6.24E+13	7.91E+13	7.00E+16	7.82E+13	1.01E+14	8.55E+13	9.80E+13	6.18E+13
Po-210a	4.04E+10	4.47E+10	4.36E+10	3.69E+10	3.56E+10	4.37E+10	5.30E+10	4.07E+10	4.50E+10	4.14E+10	4.61E+10	3.50E+10
Pu-238	4.17E+08	5.05E+08	2.54E+09	2.07E+08	2.11E+08	8.00E+08	1.95E+10	3.66E+08	3.12E+09	6.90E+08	1.91E+09	2.24E+08
U-234b	6.37E+05	7.46E+05	1.30E+06	4.50E+05	4.60E+05	7.16E+05	7.24E+06	6.24E+05	1.50E+06	7.58E+05	1.14E+06	4.62E+05
Th-230b	6.67E+06	7.75E+06	8.73E+06	4.92E+06	5.09E+06	6.61E+06	2.45E+07	6.67E+06	9.76E+06	7.43E+06	8.84E+06	5.07E+06
Ra-226b	6.84E+09	7.70E+09	7.54E+09	5.64E+09	5.77E+09	7.05E+09	1.25E+10	6.84E+09	8.04E+09	7.31E+09	8.06E+09	5.69E+09
Rn-222b	6.66E+13	7.42E+13	7.22E+13	5.54E+13	5.78E+13	7.14E+13	9.09E+13	6.70E+13	7.46E+13	6.86E+13	7.58E+13	5.70E+13
Po-218b	2.84E+15	3.15E+15	3.07E+15	2.61E+15	2.50E+15	3.08E+15	5.44E+15	2.86E+15	3.16E+15	2.92E+15	3.24E+15	2.47E+15
Pb-214b	8.28E+18	9.27E+18	9.02E+18	6.86E+18	7.13E+18	8.69E+18	2.27E+19	8.28E+18	9.51E+18	8.69E+18	9.60E+18	7.00E+18
Bi-214b	7.59E+19	8.29E+19	8.10E+19	6.98E+19	6.83E+19	8.21E+19	1.41E+20	7.60E+19	8.22E+19	7.91E+19	8.47E+19	6.75E+19
Po-214b	2.88E+22	3.19E+22	3.11E+22	2.63E+22	2.53E+22	3.12E+22	3.78E+22	2.90E+22	3.21E+22	2.96E+22	3.28E+22	2.50E+22
Pb-210b	6.48E+10	7.96E+10	9.57E+10	3.73E+10	3.76E+10	5.88E+10	2.40E+11	6.33E+10	1.16E+11	7.94E+10	1.01E+11	3.88E+10
Bi-210b	7.85E+13	8.98E+13	9.16E+13	6.06E+13	6.24E+13	7.91E+13	7.00E+16	7.82E+13	1.01E+14	8.55E+13	9.80E+13	6.18E+13
Po-210b	4.04E+10	4.47E+10	4.36E+10	3.69E+10	3.56E+10	4.37E+10	5.30E+10	4.07E+10	4.50E+10	4.14E+10	4.61E+10	3.50E+10
Am-241	5.44E+10	6.50E+10	7.05E+10	3.63E+10	3.71E+10	5.03E+10	1.24E+11	5.40E+10	8.28E+10	6.29E+10	7.55E+10	3.74E+10
Np-237	1.52E+07	1.76E+07	1.82E+07	1.14E+07	1.18E+07	1.50E+07	3.00E+07	1.52E+07	2.03E+07	1.68E+07	1.94E+07	1.18E+07
Pa-233	4.47E+15	5.02E+15	4.91E+15	3.66E+15	3.81E+15	4.67E+15	9.38E+15	4.49E+15	5.17E+15	4.71E+15	5.20E+15	3.75E+15
U-233	3.09E+06	3.54E+06	4.04E+06	2.43E+06	2.51E+06	3.25E+06	1.20E+07	3.09E+06	4.43E+06	3.38E+06	4.06E+06	2.48E+06

Table O-5. Dose Conversion Factors for Immersion in a Contaminated Plume (rem/yr per mole/m^3) (continued)

Isotope	Liver	Lungs	Muscle	Ovaries	Pancreas	Red Marrow	Skin	Spleen	Testes	Thymus	Thyroid	Uterus
Pu-242	8.88E+04	1.08E+05	4.84E+05	4.62E+04	4.73E+04	1.59E+05	3.64E+06	7.94E+04	5.95E+05	1.41E+05	3.70E+05	4.97E+04
Th-229	1.74E+10	2.00E+10	1.98E+10	1.36E+10	1.40E+10	1.73E+10	3.09E+10	1.74E+10	2.16E+10	1.90E+10	2.12E+10	1.39E+10
Ra-225	1.60E+14	2.01E+14	2.58E+14	7.49E+13	7.84E+13	1.45E+14	3.08E+15	1.55E+14	3.32E+14	2.07E+14	2.83E+14	8.28E+13
Ac-225	8.87E+14	1.01E+15	9.96E+14	6.98E+14	7.21E+14	8.88E+14	1.43E+15	8.87E+14	1.08E+15	9.57E+14	1.07E+15	7.13E+14
Fr-221	3.92E+15	4.40E+15	4.30E+15	3.25E+15	3.31E+15	4.05E+15	6.44E+15	3.92E+15	4.56E+15	4.14E+15	4.59E+15	3.28E+15
At-217	5.27E+20	5.89E+20	5.76E+20	4.45E+20	4.57E+20	5.64E+20	7.66E+20	5.31E+20	5.97E+20	5.48E+20	6.05E+20	4.53E+20
Bi-213	2.67E+18	2.97E+18	2.91E+18	2.21E+18	2.32E+18	2.85E+18	1.63E+19	2.68E+18	3.01E+18	2.76E+18	3.06E+18	2.27E+18
Po-213	0.00E+00	0.00E+00	0.00E+00	0.00E+00	0.00E+00	0.00E+00	0.00E+00	0.00E+00	0.00E+00	0.00E+00	0.00E+00	0.00E+00
Pb-209	6.77E+14	7.86E+14	8.30E+14	4.97E+14	5.12E+14	6.68E+14	1.05E+18	6.72E+14	9.43E+14	7.59E+14	8.91E+14	5.11E+14
Pu-240	5.67E+06	6.94E+06	3.29E+07	2.82E+06	2.88E+06	1.05E+07	2.49E+08	5.01E+06	4.05E+07	9.23E+06	2.49E+07	3.04E+06
U-236	3.28E+03	3.89E+03	9.31E+03	2.17E+03	2.21E+03	4.15E+03	6.36E+04	3.16E+03	1.09E+04	4.15E+03	7.47E+03	2.25E+03
Th-232	1.61E+01	1.89E+01	2.45E+01	1.15E+01	1.19E+01	1.63E+01	1.02E+02	1.60E+01	2.77E+01	1.84E+01	2.34E+01	1.19E+01
Ra-228	0.00E+00	0.00E+00	0.00E+00	0.00E+00	0.00E+00	0.00E+00	0.00E+00	0.00E+00	0.00E+00	0.00E+00	0.00E+00	0.00E+00
Ac-228	2.52E+18	2.78E+18	2.72E+18	2.32E+18	2.23E+18	2.72E+18	4.71E+18	2.53E+18	2.79E+18	2.61E+18	2.86E+18	2.20E+18
Th-228	1.59E+12	1.82E+12	1.83E+12	1.25E+12	1.29E+12	1.60E+12	3.27E+12	1.59E+12	1.99E+12	1.72E+12	1.94E+12	1.28E+12
Ra-224	1.66E+15	1.86E+15	1.82E+15	1.39E+15	1.42E+15	1.74E+15	2.65E+15	1.66E+15	1.92E+15	1.75E+15	1.93E+15	1.40E+15
Rn-220	3.77E+17	4.19E+17	4.10E+17	3.16E+17	3.28E+17	4.05E+17	5.12E+17	3.79E+17	4.21E+17	3.89E+17	4.31E+17	3.23E+17
Po-216	6.41E+18	7.11E+18	6.94E+18	5.86E+18	5.65E+18	6.95E+18	8.41E+18	6.45E+18	7.13E+18	6.58E+18	7.31E+18	5.57E+18
Pb-212	1.97E+17	2.22E+17	2.18E+17	1.61E+17	1.66E+17	2.04E+17	4.64E+17	1.97E+17	2.32E+17	2.10E+17	2.32E+17	1.64E+17
Bi-212	2.76E+19	3.04E+19	2.97E+19	2.52E+19	2.46E+19	2.99E+19	1.36E+20	2.77E+19	3.04E+19	2.86E+19	3.12E+19	2.42E+19
Tl-208	1.16E+21	1.26E+21	1.22E+21	1.06E+21	1.06E+21	1.25E+21	1.68E+21	1.16E+21	1.24E+21	1.21E+21	1.28E+21	1.06E+21
Pu-239	4.02E+06	4.59E+06	7.31E+06	3.03E+06	3.14E+06	4.63E+06	3.22E+07	3.95E+06	8.38E+06	4.63E+06	6.72E+06	3.12E+06
U-235	3.55E+05	4.00E+05	3.91E+05	2.92E+05	2.99E+05	3.65E+05	5.12E+05	3.55E+05	4.18E+05	3.79E+05	4.18E+05	2.95E+05
Th-231	5.37E+15	6.24E+15	6.81E+15	3.92E+15	4.06E+15	5.31E+15	3.62E+16	5.34E+15	7.73E+15	6.03E+15	7.17E+15	4.07E+15
Pa-231	1.83E+09	2.06E+09	2.05E+09	1.51E+09	1.58E+09	1.93E+09	3.11E+09	1.85E+09	2.18E+09	1.93E+09	2.16E+09	1.54E+09
Ac-227	8.75E+09	1.00E+10	1.02E+10	6.86E+09	7.07E+09	8.79E+09	2.11E+10	8.73E+09	1.11E+10	9.50E+09	1.07E+10	7.01E+09
Th-227	3.34E+15	3.75E+15	3.68E+15	2.74E+15	2.83E+15	3.48E+15	5.29E+15	3.34E+15	3.91E+15	3.53E+15	3.91E+15	2.78E+15
Ra-223	6.72E+15	7.60E+15	7.46E+15	5.40E+15	5.60E+15	6.88E+15	1.18E+16	6.74E+15	7.96E+15	7.16E+15	7.95E+15	5.54E+15
Rn-219	7.65E+20	8.55E+20	8.35E+20	6.35E+20	6.61E+20	8.12E+20	1.13E+21	7.68E+20	8.75E+20	8.02E+20	8.85E+20	6.48E+20
Po-215	5.41E+21	6.03E+21	5.89E+24	4.46E+21	4.71E+21	5.78E+21	7.48E+21	5.45E+21	6.10E+21	5.60E+21	6.20E+21	4.61E+21
Pb-211	1.33E+18	1.47E+18	1.44E+18	1.17E+18	1.16E+18	1.42E+18	1.86E+19	1.33E+18	1.48E+18	1.37E+18	1.52E+18	1.14E+18
Bi-211	1.95E+19	2.18E+19	2.13E+19	1.61E+19	1.68E+19	2.06E+19	3.15E+19	1.96E+19	2.23E+19	2.04E+19	2.25E+19	1.65E+19
Tl-207	6.35E+17	7.13E+17	7.04E+17	5.66E+17	5.48E+17	6.77E+17	1.41E+20	6.40E+17	7.36E+17	6.67E+17	7.46E+17	5.43E+17

Table O-6. Dose Conversion Factors for Exposure to Soil Contaminated to a Depth of 15 cm (mrem/yr per mole/m^3)

Isotope	Effective	Adrenals	Bladder	Bone Surface	Brain	Breast	Esophagus	Stomach Wall	SI	ULI	LLI	Kidneys
Pu-242	7.63E+01	2.17E+01	2.66E+01	1.57E+02	2.38E+01	1.47E+02	1.73E+01	2.69E+01	1.98E+01	2.14E+01	2.08E+01	3.18E+01
U-238	5.16E!03	1.41E!03	1.77E!03	1.23E!02	1.60E!03	9.90E!03	9.81E!04	1.83E!03	1.24E!03	1.40E!03	1.33E!03	2.17E!03
Th-234	8.16E+10	5.66E+10	6.28E+10	2.64E+11	6.58E+10	8.92E+10	5.05E+10	6.52E+10	5.52E+10	5.83E+10	5.71E+10	6.64E+10
Pa-234	2.94E+15	2.49E+15	2.55E+15	4.41E+15	2.80E+15	3.14E+15	2.36E+15	2.57E+15	2.40E+15	2.46E+15	2.47E+15	2.61E+15
U-234a	3.65E+02	2.11E+02	2.37E+02	1.01E+03	2.44E+02	4.91E+02	1.86E+02	2.44E+02	2.04E+02	2.15E+02	2.11E+02	2.56E+02
Th-230a	3.46E+03	2.36E+03	2.61E+03	1.02E+04	2.74E+03	3.96E+03	2.11E+03	2.70E+03	2.29E+03	2.42E+03	2.39E+03	2.77E+03
Ra-226a	4.31E+06	3.29E+06	3.57E+06	9.94E+06	3.81E+06	4.64E+06	3.11E+06	3.60E+06	3.24E+06	3.34E+06	3.34E+06	3.68E+06
Rn-222a	4.55E+10	3.67E+10	3.80E+10	7.18E+10	4.23E+10	4.90E+10	3.53E+10	3.86E+10	3.58E+10	3.68E+10	3.72E+10	4.03E+10
Po-218a	1.89E+12	1.61E+12	1.65E+12	2.71E+12	1.81E+12	2.02E+12	1.52E+12	1.66E+12	1.55E+12	1.59E+12	1.60E+12	1.68E+12
Pb-214a	5.50E+15	4.35E+15	4.58E+15	1.02E+16	5.02E+15	5.95E+15	4.14E+15	4.63E+15	4.24E+15	4.37E+15	4.40E+15	4.80E+15
Bi-214a	4.82E+16	4.20E+16	4.25E+16	6.58E+16	4.67E+16	5.09E+16	4.00E+16	4.25E+16	4.05E+16	4.13E+16	4.15E+16	4.36E+16
Po-214a	1.92E+19	1.63E+19	1.67E+19	2.77E+19	1.84E+19	2.05E+19	1.54E+19	1.68E+19	1.57E+19	1.61E+19	1.62E+19	1.71E+19
Pb-210a	2.45E+07	1.23E+07	1.51E+07	8.76E+07	1.43E+07	3.18E+07	8.41E+06	1.58E+07	1.10E+07	1.25E+07	1.16E+07	1.78E+07
Bi-210a	5.66E+10	4.20E+10	4.53E+10	1.39E+11	4.84E+10	6.24E+10	3.86E+10	4.63E+10	4.08E+10	4.23E+10	4.23E+10	4.78E+10
Po-210a	2.70E+07	2.28E+07	2.34E+07	3.89E+07	2.58E+07	2.89E+07	2.16E+07	2.36E+07	2.20E+07	2.26E+07	2.27E+07	2.39E+07
Pu-238	3.84E+05	1.00E+05	1.24E+05	7.47E+05	1.09E+05	7.62E+05	7.95E+04	1.25E+05	9.09E+04	9.81E+04	9.52E+04	1.50E+05
U-234b	3.65E+02	2.11E+02	2.37E+02	1.01E+03	2.44E+02	4.91E+02	1.86E+02	2.44E+02	2.04E+02	2.15E+02	2.11E+02	2.56E+02
Th-230b	3.46E+03	2.36E+03	2.61E+03	1.02E+04	2.74E+03	3.96E+03	2.11E+03	2.70E+03	2.29E+03	2.42E+03	2.39E+03	2.77E+03
Ra-226b	4.31E+06	3.29E+06	3.57E+06	9.94E+06	3.81E+06	4.64E+06	3.11E+06	3.60E+06	3.24E+06	3.34E+06	3.34E+06	3.68E+06
Rn-222b	4.55E+10	3.67E+10	3.80E+10	7.18E+10	4.23E+10	4.90E+10	3.53E+10	3.86E+10	3.58E+10	3.68E+10	3.72E+10	4.03E+10
Po-218b	1.89E+12	1.61E+12	1.65E+12	2.71E+12	1.81E+12	2.02E+12	1.52E+12	1.66E+12	1.55E+12	1.59E+12	1.60E+12	1.68E+12
Pb-214b	5.50E+15	4.35E+15	4.58E+15	1.02E+16	5.02E+15	5.95E+15	4.14E+15	4.63E+15	4.24E+15	4.37E+15	4.40E+15	4.80E+15
Bi-214b	4.82E+16	4.20E+16	4.25E+16	6.58E+16	4.67E+16	5.09E+16	4.00E+16	4.25E+16	4.05E+16	4.13E+16	4.15E+16	4.36E+16
Po-214b	1.92E+19	1.63E+19	1.67E+19	2.77E+19	1.84E+19	2.05E+19	1.54E+19	1.68E+19	1.57E+19	1.61E+19	1.62E+19	1.71E+19
Pb-210b	2.45E+07	1.23E+07	1.51E+07	8.76E+07	1.43E+07	3.18E+07	8.41E+06	1.58E+07	1.10E+07	1.25E+07	1.16E+07	1.78E+07
Bi-210b	5.66E+10	4.20E+10	4.53E+10	1.39E+11	4.84E+10	6.24E+10	3.86E+10	4.63E+10	4.08E+10	4.23E+10	4.23E+10	4.78E+10
Po-210b	2.70E+07	2.28E+07	2.34E+07	3.89E+07	2.58E+07	2.89E+07	2.16E+07	2.36E+07	2.20E+07	2.26E+07	2.27E+07	2.39E+07
Am-241	2.26E+07	1.35E+07	1.56E+07	8.13E+07	1.60E+07	2.64E+07	1.10E+07	1.65E+07	1.28E+07	1.41E+07	1.35E+07	1.74E+07
Np-237	8.12E+03	5.72E+03	6.30E+03	2.42E+04	6.59E+03	8.92E+03	5.19E+03	6.50E+03	5.58E+03	5.85E+03	5.77E+03	6.63E+03
Pa-233	2.92E+12	2.28E+12	2.41E+12	5.82E+12	2.63E+12	3.15E+12	2.16E+12	2.45E+12	2.23E+12	2.30E+12	2.31E+12	2.53E+12
U-233	1.90E+03	1.38E+03	1.49E+03	4.46E+03	1.60E+03	2.15E+03	1.29E+03	1.52E+03	1.35E+03	1.40E+03	1.40E+03	1.57E+03

Table O-6. Dose Conversion Factors for Exposure to Soil Contaminated to a Depth of 15 cm (mrem/yr per mole/m^3) (continued)

Isotope	Effective	Adrenals	Bladder	Bone Surface	Brain	Breast	Esophagus	Stomach Wall	SI	ULI	LLI	Kidneys
Th-229	9.72E+06	7.09E+06	7.78E+06	2.74E+07	8.18E+06	1.05E+07	6.52E+06	7.95E+06	6.98E+06	7.26E+06	7.21E+06	8.12E+06
Ra-225	6.04E+10	2.65E+10	3.35E+10	2.01E+11	2.87E+10	8.49E+10	1.48E+10	3.49E+10	2.15E+10	2.56E+10	2.27E+10	4.23E+10
Ac-225	5.09E+11	3.78E+11	4.10E+11	1.35E+12	4.36E+11	5.49E+11	3.50E+11	4.19E+11	3.70E+11	3.85E+11	3.82E+11	4.28E+11
Fr-221	2.52E+12	1.95E+12	2.09E+12	5.45E+12	2.25E+12	2.72E+12	1.84E+12	2.11E+12	1.91E+12	1.97E+12	1.98E+12	2.17E+12
At-217	3.54E+17	2.88E+17	2.99E+17	5.85E+17	3.31E+17	3.82E+17	2.75E+17	3.02E+17	2.80E+17	2.88E+17	2.90E+17	3.13E+17
Bi-213	1.81E+15	1.45E+15	1.51E+15	3.01E+15	1.68E+15	1.95E+15	1.39E+15	1.53E+15	1.42E+15	1.45E+15	1.47E+15	1.59E+15
Po-213	0.00E+00	0.00E+00	0.00E+00	0.00E+00	0.00E+00	0.00E+00	0.00E+00	0.00E+00	0.00E+00	0.00E+00	0.00E+00	0.00E+00
Pb-209	4.59E+11	3.22E+11	3.55E+11	1.27E+12	3.72E+11	5.16E+11	2.89E+11	3.64E+11	3.12E+11	3.28E+11	3.23E+11	3.77E+11
Pu-240	4.99E+03	1.30E+03	1.62E+03	1.01E+04	1.41E+03	9.86E+03	1.01E+03	1.63E+03	1.16E+03	1.27E+03	1.23E+03	1.97E+03
U-236	2.03E+00	9.84E!01	1.12E+00	5.33E+00	1.13E+00	3.14E+00	8.38E!01	1.16E+00	9.36E!01	9.96E!01	9.73E!01	1.24E+00
Th-232	8.23E!03	5.24E!03	5.86E!03	2.51E!02	6.10E!03	9.95E!03	4.59E!03	6.07E!03	5.06E!03	5.39E!03	5.27E!03	6.28E!03
Ra-228	0.00E+00	0.00E+00	0.00E+00	0.00E+00	0.00E+00	0.00E+00	0.00E+00	0.00E+00	0.00E+00	0.00E+00	0.00E+00	0.00E+00
Ac-228	1.65E+15	1.41E+15	1.44E+15	2.40E+15	1.58E+15	1.76E+15	1.33E+15	1.45E+15	1.36E+15	1.39E+15	1.40E+15	1.47E+15
Th-228	9.10E+08	6.70E+08	7.29E+08	2.42E+09	7.75E+08	9.89E+08	6.20E+08	7.46E+08	6.55E+08	6.83E+08	6.79E+08	7.62E+08
Ra-224	1.09E+12	8.50E+11	9.08E+11	2.25E+12	9.83E+11	1.18E+12	8.08E+11	9.17E+11	8.33E+11	8.58E+11	8.62E+11	9.42E+11
Rn-220	2.56E+14	2.09E+14	2.16E+14	3.98E+14	2.40E+14	2.77E+14	2.01E+14	2.19E+14	2.04E+14	2.09E+14	2.12E+14	2.27E+14
Po-216	4.28E+15	3.63E+15	3.72E+15	6.17E+15	4.09E+15	4.58E+15	3.43E+15	3.74E+15	3.50E+15	3.59E+15	3.61E+15	3.79E+15
Pb-212	1.24E+14	9.59E+13	1.03E+14	2.73E+14	1.11E+14	1.35E+14	9.01E+13	1.04E+14	9.35E+13	9.70E+13	9.70E+13	1.07E+14
Bi-212	1.81E+16	1.55E+16	1.58E+16	2.56E+16	1.74E+16	1.92E+16	1.47E+16	1.58E+16	1.50E+16	1.53E+16	1.53E+16	1.61E+16
Tl-208	6.96E+17	6.04E+17	6.20E+17	9.20E+17	6.80E+17	7.26E+17	5.91E+17	6.21E+17	5.98E+17	6.04E+17	6.12E+17	6.40E+17
Pu-239	2.63E+03	1.75E+03	1.89E+03	5.66E+03	2.01E+03	3.33E+03	1.63E+03	1.92E+03	1.70E+03	1.77E+03	1.77E+03	2.03E+03
U-235	2.22E+02	1.70E+02	1.84E+02	5.20E+02	1.96E+02	2.40E+02	1.60E+02	1.86E+02	1.67E+02	1.73E+02	1.73E+02	1.90E+02
Th-231	2.78E+12	1.89E+12	2.11E+12	8.64E+12	2.20E+12	3.13E+12	1.71E+12	2.18E+12	1.85E+12	1.95E+12	1.91E+12	2.24E+12
Pa-231	1.22E+06	9.57E+05	1.01E+06	2.33E+06	1.11E+06	1.34E+06	9.13E+05	1.02E+06	9.36E+05	9.65E+05	9.71E+05	1.06E+06
Ac-227	5.02E+06	3.68E+06	4.00E+06	1.36E+07	4.23E+06	5.46E+06	3.39E+06	4.10E+06	3.60E+06	3.75E+06	3.72E+06	4.17E+06
Th-227	2.16E+12	1.68E+12	1.79E+12	4.45E+12	1.94E+12	2.34E+12	1.59E+12	1.81E+12	1.64E+12	1.69E+12	1.70E+12	1.86E+12
Ra-223	4.13E+12	3.16E+12	3.37E+12	9.40E+12	3.65E+12	4.46E+12	2.96E+12	3.44E+12	3.08E+12	3.20E+12	3.20E+12	3.53E+12
Rn-219	5.14E+17	4.07E+17	4.28E+17	9.45E+17	4.71E+17	5.58E+17	3.87E+17	4.34E+17	3.97E+17	4.11E+17	4.14E+17	4.51E+17
Po-215	3.69E+18	2.96E+18	3.07E+18	6.10E+18	3.42E+18	3.99E+18	2.84E+18	3.12E+18	2.89E+18	2.97E+18	3.01E+18	3.26E+18
Pb-211	8.89E+14	7.36E+14	7.61E+14	1.38E+15	8.40E+14	9.55E+14	7.00E+14	7.67E+14	7.12E+14	7.30E+14	7.36E+14	7.85E+14
Bi-211	1.31E+16	1.04E+16	1.09E+16	2.37E+16	1.20E+16	1.43E+16	9.94E+15	1.11E+16	1.01E+16	1.05E+16	1.06E+16	1.15E+16
Tl-207	4.36E+14	3.54E+14	3.72E+14	7.50E+14	4.05E+14	4.70E+14	3.36E+14	3.75E+14	3.47E+14	3.56E+14	3.56E+14	3.82E+14

Table O-6. Dose Conversion Factors for Exposure to Soil Contaminated to a Depth of 15 cm (mrem/yr per mole/m^3) (continued)

Isotope	Liver	Lungs	Muscle	Ovaries	Pancreas	Red Marrow	Skin	Spleen	Testes	Thymus	Thyroid	Uterus
Pu-242	2.67E+01	3.06E+01	7.82E+01	1.98E+01	1.88E+01	3.25E+01	4.54E+02	2.57E+01	1.16E+02	3.21E+01	3.96E+01	1.90E+01
U-238	1.84E!03	2.19E!03	5.29E!03	1.21E!03	1.14E!03	2.04E!03	3.32E!02	1.79E!03	7.65E!03	2.21E!03	2.72E!03	1.18E!03
Th-234	6.64E+10	7.40E+10	7.40E+10	5.29E+10	5.40E+10	6.39E+10	9.49E+10	6.64E+10	8.48E+10	7.02E+10	6.96E+10	5.40E+10
Pa-234	2.60E+15	2.83E+15	2.86E+15	2.40E+15	2.33E+15	2.80E+15	3.40E+15	2.62E+15	3.07E+15	2.72E+15	2.64E+15	2.39E+15
U-234a	2.49E+02	2.78E+02	3.48E+02	1.98E+02	1.98E+02	2.49E+02	1.02E+03	2.47E+02	4.29E+02	2.68E+02	2.76E+02	1.98E+02
Th-230a	2.75E+03	3.06E+03	3.20E+03	2.24E+03	2.24E+03	2.69E+03	5.26E+03	2.77E+03	3.69E+03	2.94E+03	2.90E+03	2.24E+03
Ra-226a	3.68E+06	4.02E+06	4.04E+06	3.24E+06	3.18E+06	3.81E+06	4.91E+06	3.71E+06	4.46E+06	3.84E+06	3.73E+06	3.16E+06
Rn-222a	3.95E+10	4.31E+10	4.39E+10	3.51E+10	3.51E+10	4.23E+10	5.22E+10	3.97E+10	4.78E+10	4.11E+10	4.03E+10	3.54E+10
Po-218a	1.68E+12	1.82E+12	1.85E+12	1.55E+12	1.50E+12	1.81E+12	2.18E+12	1.68E+12	1.97E+12	1.76E+12	1.70E+12	1.55E+12
Pb-214a	4.74E+15	5.18E+15	5.25E+15	4.19E+15	4.17E+15	5.04E+15	6.41E+15	4.77E+15	5.76E+15	4.95E+15	4.84E+15	4.18E+15
Bi-214a	4.32E+16	4.66E+16	4.71E+16	4.06E+16	3.97E+16	4.67E+16	6.03E+16	4.36E+16	5.01E+16	4.46E+16	4.40E+16	4.00E+16
Po-214a	1.70E+19	1.85E+19	1.88E+19	1.56E+19	1.52E+19	1.84E+19	2.22E+19	1.72E+19	2.01E+19	1.79E+19	1.72E+19	1.56E+19
Pb-210a	1.61E+07	1.93E+07	2.23E+07	9.63E+06	9.96E+06	1.40E+07	4.23E+07	1.61E+07	2.83E+07	1.85E+07	1.98E+07	1.04E+07
Bi-210a	4.72E+10	5.20E+10	5.29E+10	3.99E+10	3.99E+10	4.81E+10	3.65E+12	4.75E+10	5.96E+10	4.96E+10	4.90E+10	3.99E+10
Po-210a	2.38E+07	2.59E+07	2.63E+07	2.20E+07	2.13E+07	2.58E+07	3.11E+07	2.40E+07	2.82E+07	2.51E+07	2.42E+07	2.20E+07
Pu-238	1.23E+05	1.41E+05	3.97E+05	9.24E+04	8.62E+04	1.57E+05	2.42E+06	1.18E+05	5.95E+05	1.51E+05	1.91E+05	8.76E+04
U-234b	2.49E+02	2.78E+02	3.48E+02	1.98E+02	1.98E+02	2.49E+02	1.02E+03	2.47E+02	4.29E+02	2.68E+02	2.76E+02	1.98E+02
Th-230b	2.75E+03	3.06E+03	3.20E+03	2.24E+03	2.24E+03	2.69E+03	5.26E+03	2.77E+03	3.69E+03	2.94E+03	2.90E+03	2.24E+03
Ra-226b	3.68E+06	4.02E+06	4.04E+06	3.24E+06	3.18E+06	3.81E+06	4.91E+06	3.71E+06	4.46E+06	3.84E+06	3.73E+06	3.16E+06
Rn-222b	3.95E+10	4.31E+10	4.39E+10	3.51E+10	3.51E+10	4.23E+10	5.22E+10	3.97E+10	4.78E+10	4.11E+10	4.03E+10	3.54E+10
Po-218b	1.68E+12	1.82E+12	1.85E+12	1.55E+12	1.50E+12	1.81E+12	2.18E+12	1.68E+12	1.97E+12	1.76E+12	1.70E+12	1.55E+12
Pb-214b	4.74E+15	5.18E+15	5.25E+15	4.19E+15	4.17E+15	5.04E+15	6.41E+15	4.77E+15	5.76E+15	4.95E+15	4.84E+15	4.18E+15
Bi-214b	4.32E+16	4.66E+16	4.71E+16	4.06E+16	3.97E+16	4.67E+16	6.03E+16	4.36E+16	5.01E+16	4.46E+16	4.40E+16	4.00E+16
Po-214b	1.70E+19	1.85E+19	1.88E+19	1.56E+19	1.52E+19	1.84E+19	2.22E+19	1.72E+19	2.01E+19	1.79E+19	1.72E+19	1.56E+19
Pb-210b	1.61E+07	1.93E+07	2.23E+07	9.63E+06	9.96E+06	1.40E+07	4.23E+07	1.61E+07	2.83E+07	1.85E+07	1.98E+07	1.04E+07
Bi-210b	4.72E+10	5.20E+10	5.29E+10	3.99E+10	3.99E+10	4.81E+10	3.65E+12	4.75E+10	5.96E+10	4.96E+10	4.90E+10	3.99E+10
Po-210b	2.38E+07	2.59E+07	2.63E+07	2.20E+07	2.13E+07	2.58E+07	3.11E+07	2.40E+07	2.82E+07	2.51E+07	2.42E+07	2.20E+07
Am-241	1.68E+07	1.94E+07	2.03E+07	1.22E+07	1.23E+07	1.51E+07	2.99E+07	1.69E+07	2.44E+07	1.86E+07	1.87E+07	1.24E+07
Np-237	6.59E+03	7.34E+03	7.43E+03	5.38E+03	5.46E+03	6.50E+03	9.75E+03	6.61E+03	8.49E+03	6.98E+03	6.89E+03	5.46E+03
Pa-233	2.50E+12	2.73E+12	2.77E+12	2.20E+12	2.19E+12	2.64E+12	3.35E+12	2.51E+12	3.05E+12	2.61E+12	2.56E+12	2.19E+12
U-233	1.55E+03	1.71E+03	1.79E+03	1.33E+03	1.32E+03	1.60E+03	2.75E+03	1.56E+03	2.03E+03	1.63E+03	1.61E+03	1.32E+03
Th-229	8.12E+06	8.98E+06	8.98E+06	6.81E+06	6.86E+06	8.06E+06	1.11E+07	8.12E+06	1.01E+07	8.52E+06	8.35E+06	6.81E+06

Table O-6. Dose Conversion Factors for Exposure to Soil Contaminated to a Depth of 15 cm (mrem/yr per mole/m^3) (continued)

Isotope	Liver	Lungs	Muscle	Ovaries	Pancreas	Red Marrow	Skin	Spleen	Testes	Thymus	Thyroid	Uterus
Ra-225	3.54E+10	4.30E+10	5.48E+10	1.60E+10	1.86E+10	3.05E+10	1.01E+11	3.50E+10	7.49E+10	4.29E+10	4.70E+10	2.00E+10
Ac-225	4.28E+11	4.71E+11	4.72E+11	3.61E+11	3.64E+11	4.31E+11	5.82E+11	4.28E+11	5.27E+11	4.48E+11	4.40E+11	3.63E+11
Fr-221	2.16E+12	2.36E+12	2.38E+12	1.91E+12	1.88E+12	2.26E+12	2.88E+12	2.17E+12	2.62E+12	2.25E+12	2.20E+12	1.87E+12
At-217	3.09E+17	3.36E+17	3.42E+17	2.76E+17	2.74E+17	3.31E+17	4.08E+17	3.10E+17	3.72E+17	3.23E+17	3.15E+17	2.77E+17
Bi-213	1.57E+15	1.71E+15	1.73E+15	1.39E+15	1.39E+15	1.68E+15	2.91E+15	1.57E+15	1.90E+15	1.64E+15	1.60E+15	1.40E+15
Po-213	0.00E+00	0.00E+00	0.00E+00	0.00E+00	0.00E+00	0.00E+00	0.00E+00	0.00E+00	0.00E+00	0.00E+00	0.00E+00	0.00E+00
Pb-209	3.70E+11	4.12E+11	4.25E+11	3.03E+11	3.04E+11	3.68E+11	4.39E+12	3.72E+11	4.89E+11	3.94E+11	3.91E+11	3.04E+11
Pu-240	1.62E+03	1.86E+03	5.14E+03	1.18E+03	1.10E+03	2.02E+03	3.10E+04	1.55E+03	7.70E+03	1.98E+03	2.51E+03	1.12E+03
U-236	1.17E+00	1.33E+00	2.00E+00	9.07E!01	9.04E!01	1.21E+00	8.22E+00	1.16E+00	2.60E+00	1.29E+00	1.38E+00	9.09E!01
Th-232	6.19E!03	6.96E!03	7.64E!03	4.89E!03	4.94E!03	6.01E!03	1.64E!02	6.19E!03	9.06E!03	6.63E!03	6.66E!03	4.94E!03
Ra-228	0.00E+00	0.00E+00	0.00E+00	0.00E+00	0.00E+00	0.00E+00	0.00E+00	0.00E+00	0.00E+00	0.00E+00	0.00E+00	0.00E+00
Ac-228	1.46E+15	1.59E+15	1.61E+15	1.36E+15	1.32E+15	1.58E+15	1.99E+15	1.48E+15	1.72E+15	1.53E+15	1.49E+15	1.35E+15
Th-228	7.59E+08	8.38E+08	8.45E+08	6.44E+08	6.44E+08	7.66E+08	1.09E+09	7.64E+08	9.45E+08	7.99E+08	7.81E+08	6.42E+08
Ra-224	9.37E+11	1.02E+12	1.03E+12	8.33E+11	8.21E+11	9.87E+11	1.25E+12	9.46E+11	1.14E+12	9.75E+11	9.54E+11	8.17E+11
Rn-220	2.24E+14	2.44E+14	2.49E+14	2.00E+14	1.99E+14	2.42E+14	2.96E+14	2.25E+14	2.70E+14	2.35E+14	2.29E+14	2.02E+14
Po-216	3.79E+15	4.12E+15	4.18E+15	3.50E+15	3.38E+15	4.09E+15	4.94E+15	3.81E+15	4.47E+15	3.99E+15	3.84E+15	3.49E+15
Pb-212	1.06E+14	1.16E+14	1.18E+14	9.32E+13	9.22E+13	1.11E+14	1.43E+14	1.07E+14	1.30E+14	1.11E+14	1.09E+14	9.18E+13
Bi-212	1.60E+16	1.74E+16	1.76E+16	1.49E+16	1.45E+16	1.74E+16	3.44E+16	1.62E+16	1.88E+16	1.67E+16	1.63E+16	1.48E+16
Tl-208	6.29E+17	6.74E+17	6.78E+17	5.94E+17	5.90E+17	6.81E+17	7.98E+17	6.37E+17	7.26E+17	6.45E+17	6.47E+17	5.86E+12
Pu-239	1.96E+03	2.17E+03	2.53E+03	1.67E+03	1.66E+03	2.08E+03	5.73E+03	1.96E+03	3.03E+03	2.08E+03	2.11E+03	1.67E+03
U-235	1.90E+02	2.08E+02	2.09E+02	1.66E+02	1.64E+02	1.97E+02	2.54E+02	1.91E+02	2.31E+02	1.97E+02	1.93E+02	1.64E+02
Th-231	2.21E+12	2.47E+12	2.55E+12	1.78E+12	1.81E+12	2.15E+12	3.67E+12	2.21E+12	2.96E+12	2.37E+12	2.34E+12	1.81E+12
Pa-231	1.05E+06	1.14E+06	1.17E+06	9.27E+05	9.20E+05	1.11E+06	1.44E+06	1.06E+06	1.29E+06	1.09E+06	1.07E+06	9.20E+05
Ac-227	4.17E+06	4.60E+06	4.63E+06	3.52E+06	3.54E+06	4.19E+06	6.09E+06	4.17E+06	5.21E+06	4.37E+06	4.29E+06	3.52E+06
Th-227	1.85E+12	2.02E+12	2.05E+12	1.63E+12	1.61E+12	1.95E+12	2.49E+12	1.86E+12	2.25E+12	1.93E+12	1.89E+12	1.61E+12
Ra-223	3.51E+12	3.85E+12	3.88E+12	3.04E+12	3.04E+12	3.63E+12	4.72E+12	3.53E+12	4.29E+12	3.68E+12	3.60E+12	3.03E+12
Rn-219	4.44E+17	4.84E+17	4.91E+17	3.94E+17	3.91E+17	4.71E+17	5.91E+17	4.48E+17	5.38E+17	4.61E+17	4.54E+17	3.91E+17
Po-215	3.21E+18	3.49E+18	3.55E+18	2.83E+18	2.84E+18	3.43E+18	4.25E+18	3.21E+18	3.89E+18	3.34E+18	3.27E+18	2.85E+18
Pb-211	7.79E+14	8.52E+14	8.64E+14	7.06E+14	6.94E+14	8.40E+14	2.25E+15	7.85E+14	9.31E+14	8.16E+14	7.91E+14	7.12E+14
Bi-211	1.13E+16	1.23E+16	1.25E+16	1.00E+16	9.98E+15	1.20E+16	1.51E+16	1.14E+16	1.37E+16	1.18E+16	1.16E+16	1.00E+16
Tl-207	3.80E+14	4.15E+14	4.21E+14	3.44E+14	3.35E+14	4.05E+14	1.16E+16	3.83E+14	4.56E+14	4.00E+14	3.88E+14	3.43E+14

This page intentionally left blank.

Appendix P

Supplementary Results and Analyses

This page intentionally left blank.

P.1 Introduction

The relevant results of the PA are described in the text. Supplementary analyses were performed to evaluate the effects of the approximations inherent in the numerical evaluation of the mathematical model, and to identify input parameters which have the strongest influence on the calculated performance measures. This appendix describes calculations that investigate the errors associated with three aspects of numerical approximation: sampling error arising from a finite number of parameter samples and numerical errors arising from discretizing space and time. The results of the sensitivity analysis are also presented. Finally, calculated concentrations in the garden soil are provided for the parameter sample set leading to the largest whole-body dose to the resident farmer.

P.2 Parameter Sampling Error

Five independent sets of 1000 parameter samples were generated using LHS in order to explore the effects of sampling error on the calculated CCDF. Figure P-1 shows the five CCDFs estimated using each of these five independent parameter sets. The variation among these five estimates is indicative of the sampling error associated with any one of the estimates. The sampling error is seen to increase as probability decreases. The more extreme quantile values of the CCDF are necessarily estimated using fewer observations than other quantities such as the median or mean, and are therefore more subject to sampling error. The estimates of the .001 quantile of integrated release (approximated by the largest value in each of the five sets) range from 4.2×10^{-13} to 1.9×10^{-11}. Although there is evidently uncertainty about the exact value of the .001 quantile value due to sampling error, it is clear that the exact value is very likely to be less than the regulatory limit of 10^{1}. The estimates of the 0.1 quantile value are not as sensitive to the particular set of parameter samples used, and range from 4.3×10^{-14} to 5.0×10^{-14}.

For the IPRs, the regulatory evaluation is based on the larger of the mean or median of the calculated dose distribution. Compared to the upper quantiles of the integrated release distribution, the estimates of both of these measures of central tendency converge very rapidly. One thousand parameter samples were assumed to produce an amply accurate estimate.

P.3 Discretization Error

Two sets of analyses were performed to identify the magnitude of the numerical error associated with the particular computational grid and timestep used to estimate integrated release. One analysis repeated the integrated release calculations using two alternative grids: one coarser and one finer than that used in the primary calculations. The second analysis used smaller and larger timesteps than those used in the primary calculations.

[1]Considering the logarithms of the five estimates, the distance between the average value and the regulatory limit is approximately nine times the standard error of the mean.

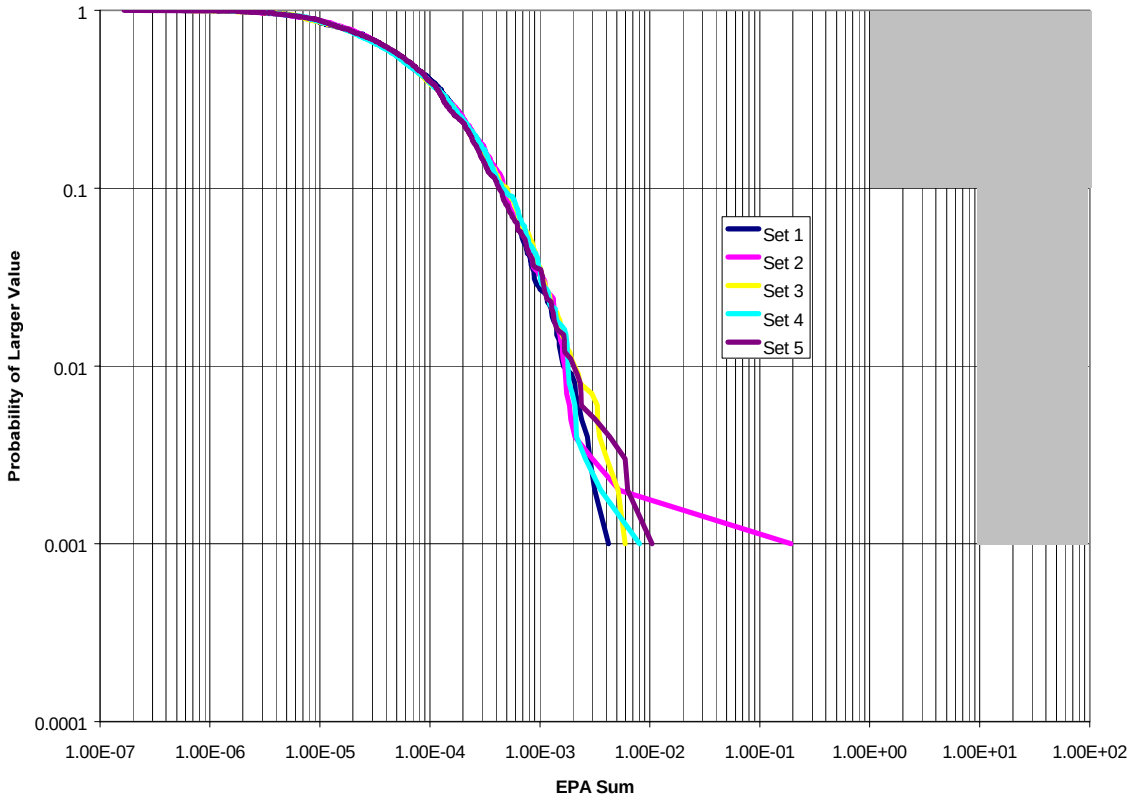

Figure P-1. CCDFs Calculated using Five Independent Sets of 1000 Parameter Samples.

The grid used in the primary calculations has a spacing of approximately 2 m (7 ft) in the first 16 m (13 ft) above the waste and a spacing of 1 m (3 ft) for the remaining distance below the flux boundary. The 1 m (3 ft) spacing in the upper portion of the profile was unchanged in the finer and coarser grids. The coarser grid used a spacing of approximately 5 m (16 ft) over the lower portion of the profile, while the finer grid used a spacing of 1 m (3 ft) over this region. Figure P-2 shows the CCDFs estimated using the primary grid and the two comparison grid for one of the five parameter sample sets. There are small differences between the coarse grid and the two finer grids; however, these differences are only evident at small values of integrated release. Increasing the grid resolution beyond that used in the primary calculations has no practical effect on the estimated CCDF. Continuous grid refined would decrease numerical dispersion in principle, causing the CCDF to shift leftward; however, the error arising from the existing gridding is evidently quite small.

The primary calculations used a uniform timestep size of 100 years for the integrated release calculations. Alternative uniform timestep sizes of 50 years and 200 years were used in a set of comparison calculations, producing the estimated CCDFs shown in Figure P-3. As in the case of grid refinement, more resolution leads to smaller calculated discharges; however, the amount of this reduction is practically irrelevant. A timestep size of 100 years apparently provides sufficient resolution.

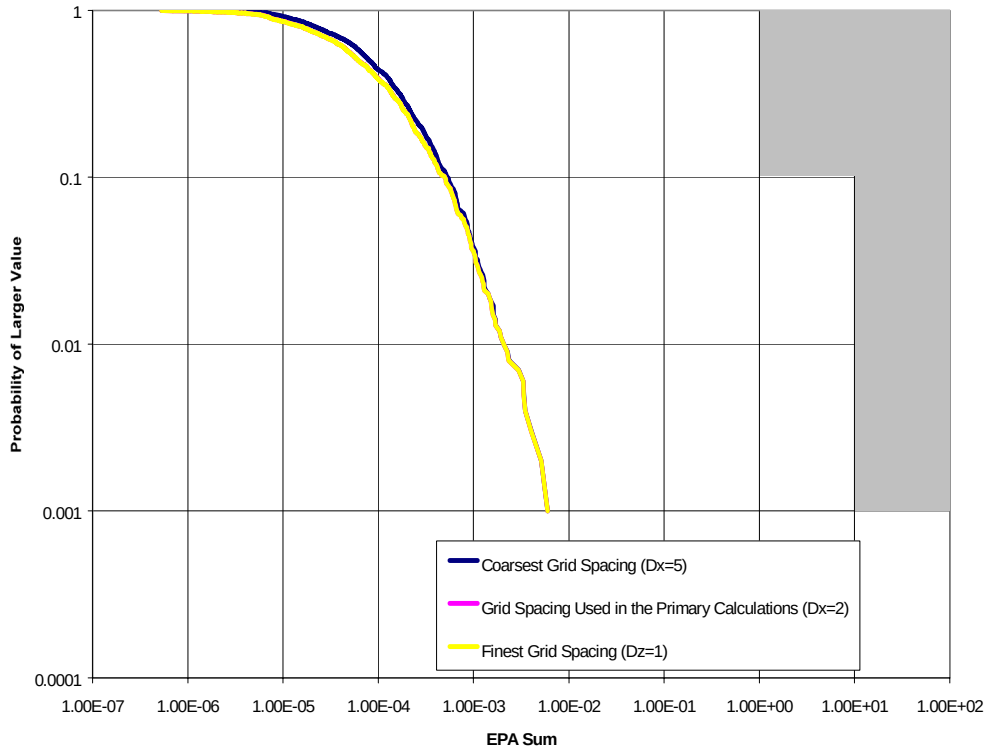

Figure P-2. CCDFs for Sample Set 3 Calculated Using Three Alternative Grid Spacings.

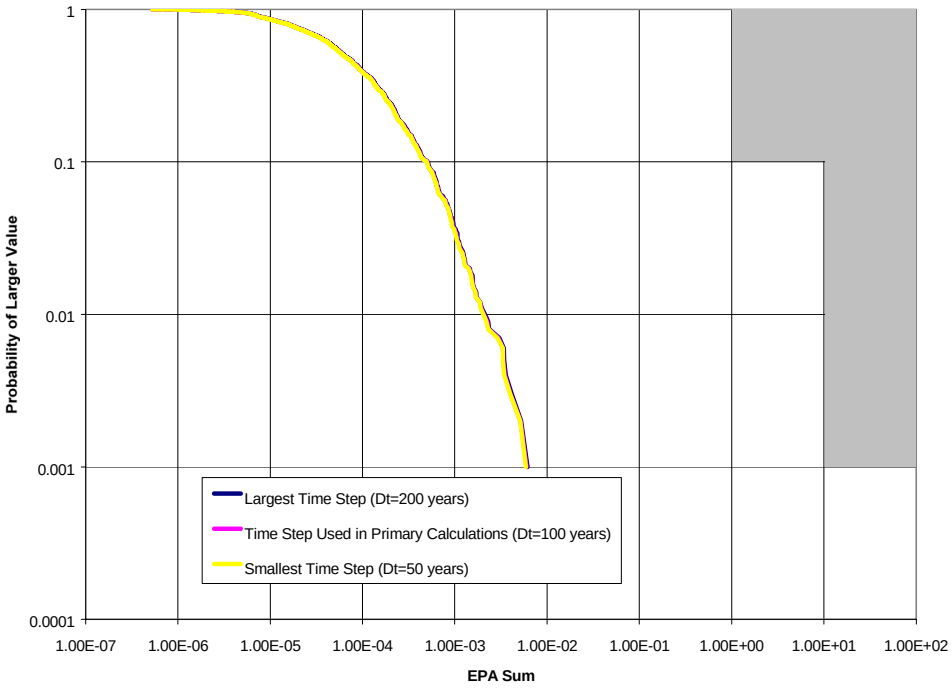

Figure P-3. CCDFs for Sample Set 3 Calculated Using Three Alternative Time Step Sizes.

P.4 Sensitivity Analysis

The calculated values of the regulatory performance measures (integrated normalized release and dose to a resident farmer) were examined to identify the controlling mechanisms and model parameters. The goal of the sensitivity analysis is to understand which parameter uncertainties make the largest contributions to uncertainty in the calculated performance measure value. Given the assumptions underlying the transport and exposure models, additional information about these parameters has the greatest potential to change the distribution of the performance measure.

Controlling parameters were identified by quantifying their influence on the regulatory performance measures, and by examining scatterplots of the transport and exposure parameters affecting those elements and isotopes that made large relative contributions to the performance measures. The observed relationships between the parameter values and the performance measure values, and the mathematical formulation of the transport and exposure models, helped to define parameter combinations that showed strong correlations with the performance measures. In addition to the regulatory performance measures, intermediate model results were also examined to help identify the role of individual process models in overall model behavior.

A quantitative test was used to identify parameters having a strong influence on the calculated performance measure value. First, a set of 1000 sample values was divided into two equal groups based on the performance measure value calculated for each sample. Second, the 500 parameter values leading to low performance measure values, and the 500 parameter values leading to high performance measure values were used to build two separate probability distributions for the parameter. Third, the Komolgovov-Smirnov test was used to determine whether the distribution of parameter values leading to high performance measures was significantly different from the distribution leading to low values. Parameters having a strong influence on the performance measure have significantly different distributions in the “high” and “low” performance measure groups. The difference between these distributions is therefore a measure of the strength of the influence of the parameter. This measure was used in preference to more common measures, such as linear regression coefficients, because it is sensitive to more complicated dependencies between the parameter and performance measure values.

Parameters and Processes Controlling Uncertainty in Integrated Release

Table P-1 lists the parameters whose values have the greatest influence on integrated release. The table includes parameters whose “high release” and “low release” distributions differed at a significance level of 5%. All parameters meeting this criterion had a significance level of 0.5% or less; all other parameters had a significance level of 10% or more.

Integrated release was found to be strongly correlated with the average root lengths of perennial shrubs and trees, the biomass turnover rates of all four plant lifeforms, and the invertebrate burrowing rate. The plant parameters directly control the rate of radionuclide uptake by plants, but they also control the way invertebrate burrowing varies with depth via the community average maximum root length. The scatterplot in Figure P-4 shows integrated release values

Table P-1. Sampled Parameters Having a Significant Influence on Calculated Integrated Release

Parameter	K-S Significance Level
Biomass Turnover Rate - Perennials, Current Climate	<0.005
Biomass Turnover Rate - Perennials, Subsidence Conditions	<0.005
Biomass Turnover Rate - Shrubs, Current Climate	<0.005
Biomass Turnover Rate - Shrubs, Subsidence Conditions	<0.005
Biomass Turnover Rate - Annuals, Current Climate	<0.005
Biomass Turnover Rate - Annuals, Subsidence Conditions	<0.005
Biomass Turnover Rate - Trees, Subsidence Conditions	<0.005
Soil Excavation Rate - Invertebrates	<0.005
Average Maximum Root Length - Shrubs	<0.005
Average Maximum Root Length - Trees	<0.005
Average Maximum Root Length - Trees	0.005

versus the community average maximum root length derived from the sampled values of productivity and maximum root length for each lifeform. The strong correlation indicates that the importance of the plant parameters in Table P-1 comes from their indirect effect on invertebrate burrowing rather than from their direct role in plant uptake.

Although invertebrate burrowing is *far* more active near the land surface than at depth, it is the only mechanism in the model that can transport radionuclides directly from the source region to the land surface. Other mechanisms that can transport waste to the land surface (mammal burrowing and plant uptake) operate primarily or exclusively at elevations above the top of the waste, and are especially vigorous near the land surface. In order for these processes to contribute to integrated release, advection or diffusion must first carry nuclides upward from the waste to the shallower regions where these processes are practically operative. Small advective fluxes and large Kd values usually prevent this from occurring.

To compare the relative importance of invertebrate burrowing within the waste region to burrowing above the waste region, an integrated release was also calculated which excluded releases directly from the waste region. Figure P-5 shows the CCDF of these releases, along with the CCDF including direct releases from the waste region (based on the 1000 parameter samples from Sample Set 2). In almost all cases, the integrated release that excludes direct transport from the source region is one or more orders of magnitude smaller than the overall release, indicating that direct transport from the source is the dominant mechanism for almost all parameter combinations. The largest value of integrated release, however, is practically the same in both calculations, indicating that a different mechanism can cause high release, albeit with low probability.

For the great majority of parameter samples, very slow upward advection and sorption confine radionuclides near the source, beyond reach of the relatively large extraction rates operating near the land surface. The highest value of integrated release, however, occurred due to the advection

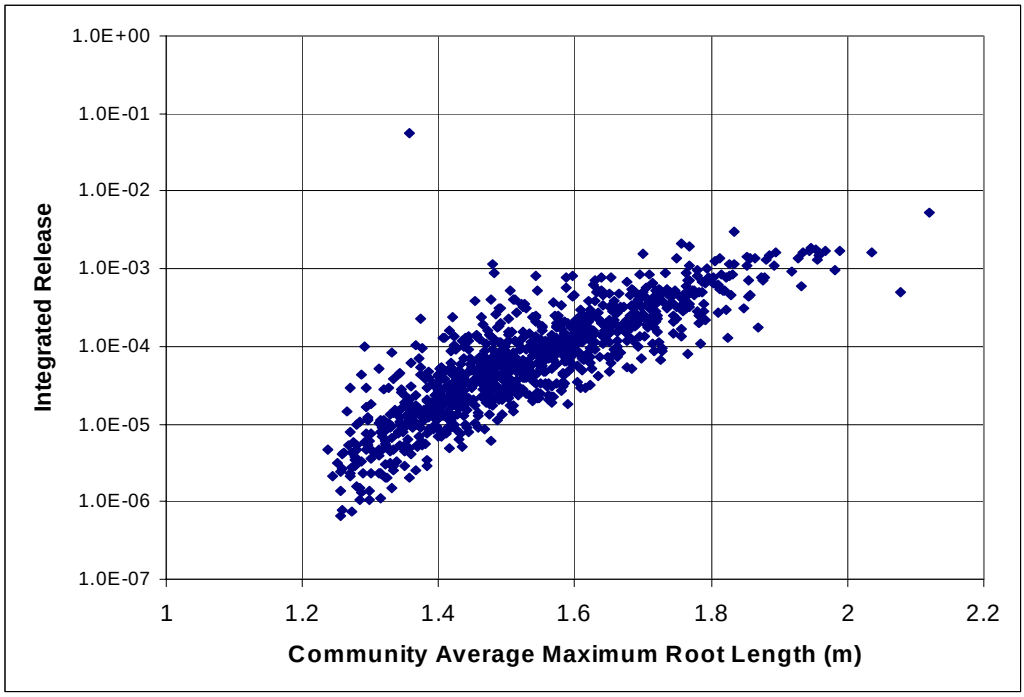

Figure P-4. Scatterplot Showing the Community Average Maximum Root Length and the Corresponding Value of Integrated Release from Sample Set 2

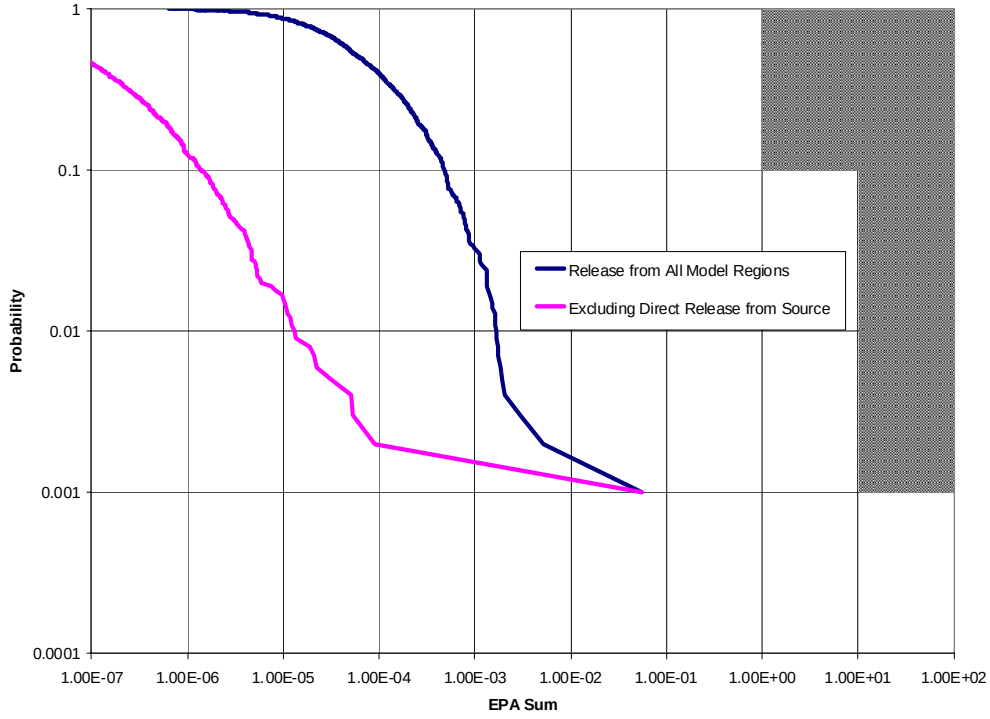

Figure P-5. Calculated CCDFs from Sample Set 2 With and Without Direct Release from the Source Region

of ^{231}Pa into the regions of greater plant and animal activity. Other relatively large releases occurred due to ^{237}Np advection. With low probability, the parameters affecting transport of Pa and Np led to relatively short travel times to the land surface, and therefore to significant contributions to integrated release by ^{231}Pa (and its daughter ^{227}Ac) and ^{237}Np. Figure P-6 is a scatterplot showing the relationship between the travel time of Pa from the top of the waste to the no-flux boundary and the integrated release of ^{231}Pa. Figure P-7 is an analogous plot for ^{237}Np. In most cases, travel times for Pa and Np are far larger than the performance period, and the integrated release due to these elements is negligible. In rare cases, the travel times approach the performance period, resulting in transport of appreciable amounts of these elements upward from the waste region to the elevations where plant uptake and bioturbation are more active.

Parameters and Processes Controlling Uncertainty in Dose

Table P-2 lists the parameters whose distributions for low and high whole-body dose to a resident farmer differed at a significance level of 5%. The IPR calculations and the CR calculations use a common underlying transport model. The dose performance measures for the IPR, like the integrated release values for the CR, are controlled by invertebrate burrowing and are therefore sensitive to the parameters that determine the rate and location of invertebrate burrowing. Figure P-8 shows the scatterplot of whole-body dose and community average maximum root length. Much of the uncertainty about dose is clearly related to uncertainty in this parameter, which is functionally derived from the biomass turnover rates and root lengths of the four lifeforms. Uncertainty in the other parameters identified as sensitive in Table P-2 contribute to the residual uncertainty about dose. Figure P-9 shows the scatterplot of whole-body dose and outdoor dust loading, for example. Higher dust loadings tend to produce higher doses; however, the dependency is clearly not as strong as that exhibited in Figure P-8.

A quantitative analysis was not done to identify the parameters controlling lung dose to an MOP residing over the virtual borehole. Scatterplots of the few parameters used in this calculation were inspected to evaluate parameter sensitivity. Figure P-10 shows the scatterplot of the lung dose and the fresh air infiltration rate. This parameter evidently accounts for much of the uncertainty about lung dose. This relationship suggests that under this scenario and exposure model, the primary dose would arise from chronic exposure to air in the basement rather than from short-term exposure during construction of the house.

P.5 Radionuclide Concentrations in Garden Soil

Doses to the resident farmer all arise from contamination in the garden soil, with the exception of radon flux through the land surface from the source region and overlying backfill. The contribution of radon flux was found to be negligible, however, so that the garden soil contamination is the sole practical source for the resident farmer's exposure. The concentrations in the garden soil of all radionuclides considered in the exposure calculations for the sample set leading to the largest calculated whole-body dose are given in Table P-3.

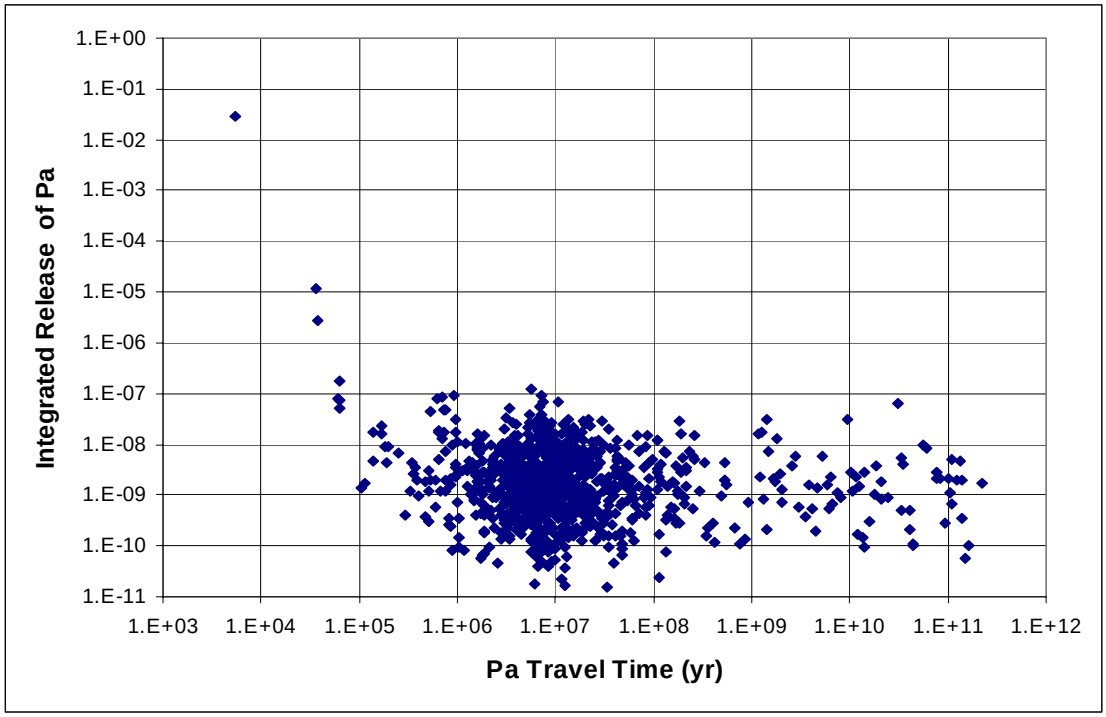

Figure P-6. Scatterplot Showing the Calculated Values of the Advective Travel Time of Pa and the Corresponding Value of Integrated Release of Pa from Sample Set 2

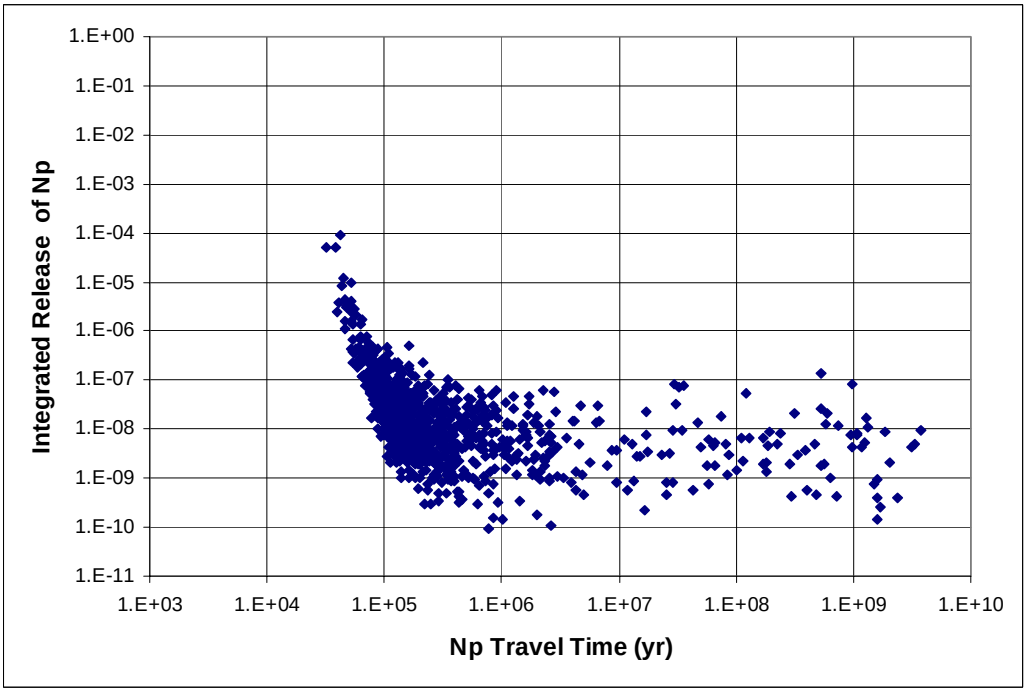

Figure P-7. Scatterplot Showing the Calculated Values of the Advective Travel Time of Np and the Corresponding Value of Integrated Release of Np from Sample Set 2

Table P-2. Sampled Parameters Having a Significant Influence on Calculated Whole-Body Dose to a Resident Farmer

Parameter	K-S Significance Level
Biomass Turnover Rate - Perennials, Current Climate	<0.005
Biomass Turnover Rate - Perennials, Subsidence Conditions	<0.005
Biomass Turnover Rate - Shrubs, Current Climate	<0.005
Biomass Turnover Rate - Shrubs, Subsidence Conditions	<0.005
Biomass Turnover Rate - Annuals, Current Climate	<0.005
Biomass Turnover Rate - Annuals, Subsidence Conditions	<0.005
Biomass Turnover Rate - Trees, Subsidence Conditions	<0.005
Outdoor Dust Loading	<0.005
Soil Excavation Rate - Invertebrates	<0.005
Average Maximum Root Length - Shrubs	<0.005
Average Maximum Root Length - Trees	<0.005
Average Maximum Root Length - Trees	0.005
Pa Concentration Ratio - Non-leafy Vegetables	0.05
Th Concentration Ratio - Native Plants	0.05
Pu Solubility	0.05

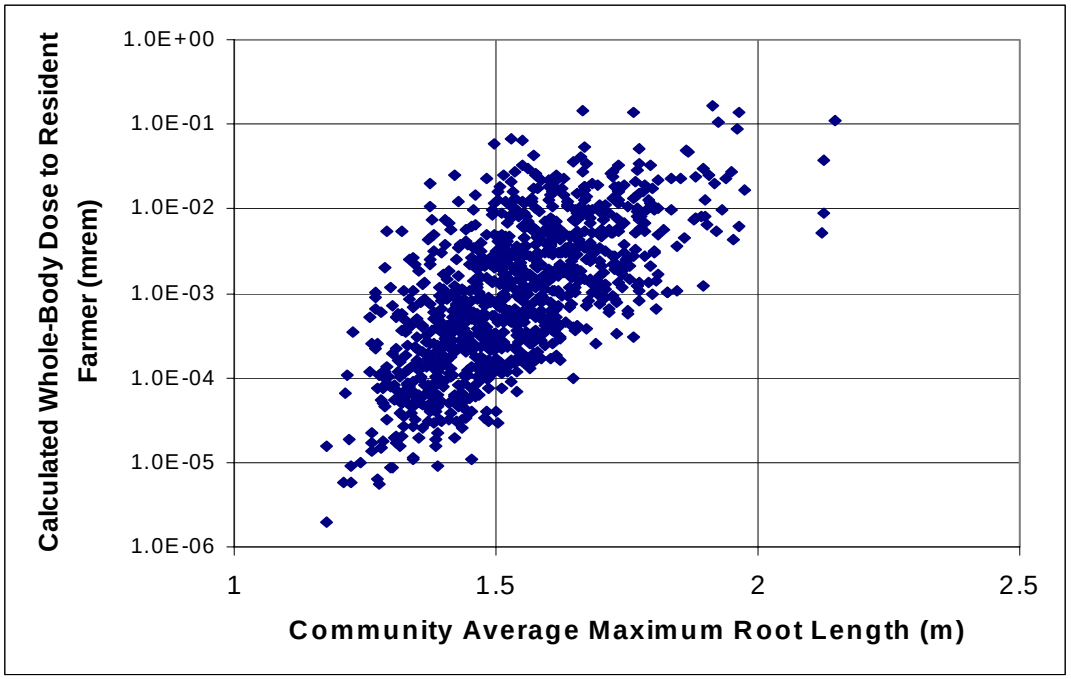

Figure P-8. Scatterplot Showing the Values of Community Average Maximum Root Length and the Corresponding Values of Whole-Body Dose to a Resident Farmer from the IPR Analysis

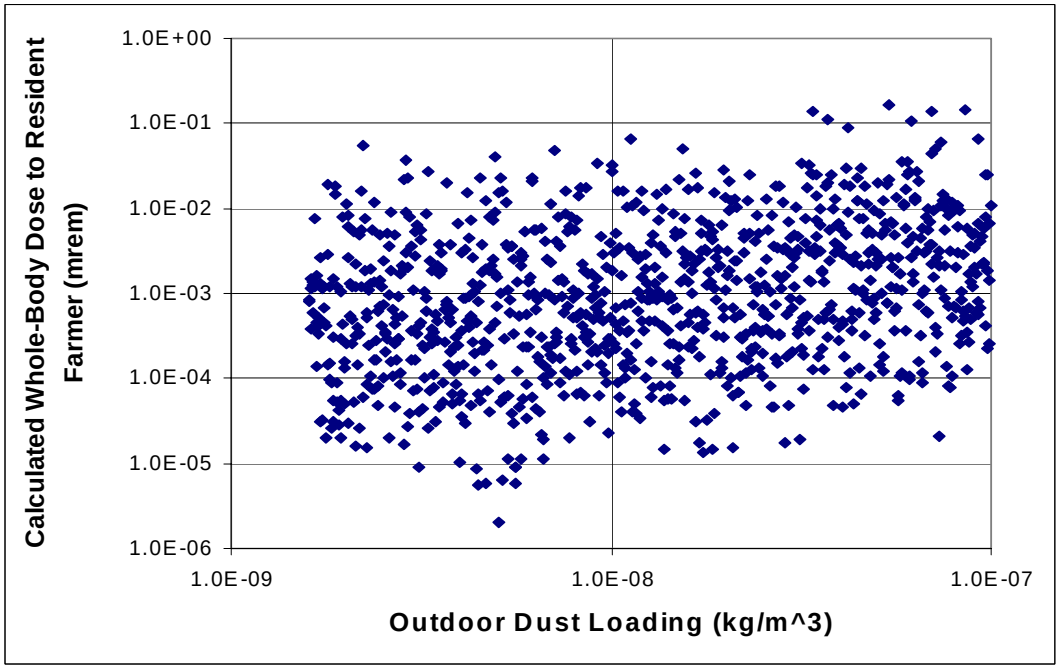

Figure P-9. Scatterplot Showing the Sampled Values of Outdoor Dust Loading and the Corresponding Values of Whole-Body Dose to a Resident Farmer from the IPR Analysis

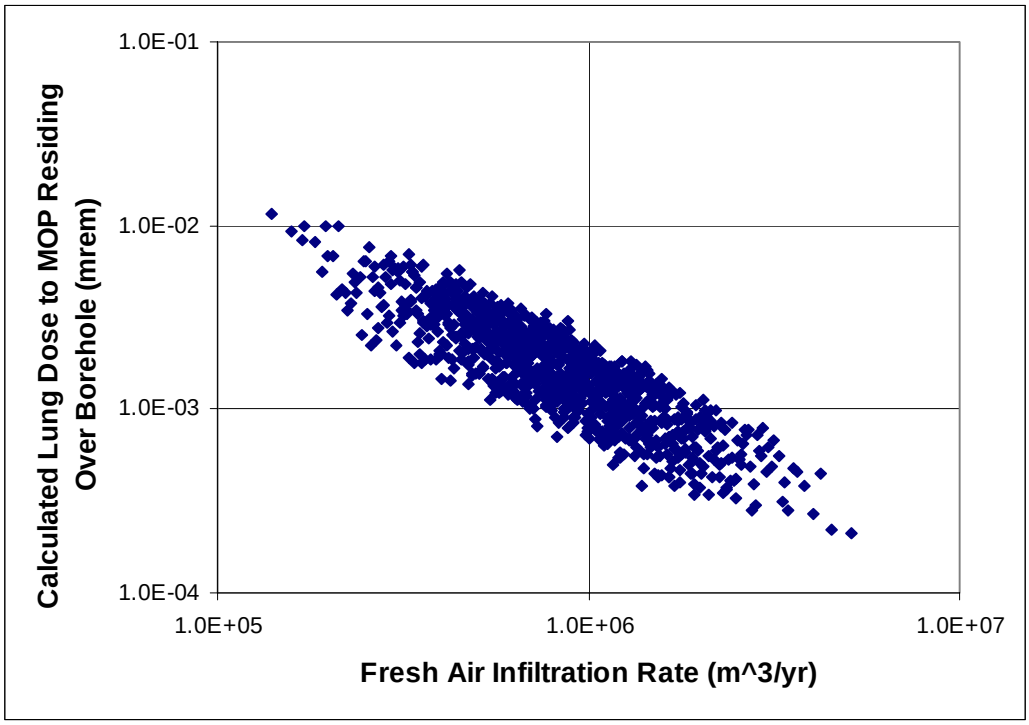

Figure P-10. Scatterplot Showing the Sampled Values of Fresh Air Infiltration Rate and the Corresponding Lung Doses to an MOP Residing Over the Virtual Borehole from the IPR Analysis

Table P-3. Calculated Radionuclide Concentrations in the Garden Soil Which Produce the Largest Value of Whole-Body Dose to the Resident Farmer

Radionuclide	Concentration (mole/m^3)	Radionuclide	Concentration (mole/m^3)	Radionuclide	Concentration (mole/m^3)
Ac-225	6.59E!25	Pb-212	1.08E!30	Rn-219	2.86E!27
Ac-227	4.96E!19	Pb-214	3.63E!25	Rn-220	1.56E!33
Ac-228	6.22E!31	Po-210	2.69E!21	Rn-222	7.42E!23
Am-241	1.52E!13	Po-213	3.05E!36	Th-227	1.17E!21
At-217	2.44E!32	Po-214	3.68E!32	Th-228	1.7E!27
Bi-210	9.73E!23	Po-215	1.28E!30	Th-229	1.9E!19
Bi-211	9.27E!26	Po-216	4.07E!36	Th-230	2.83E!15
Bi-212	1.02E!31	Po-218	4.1E!26	Th-231	3.25E!21
Bi-213	2.09E!27	Pu-238	5.48E!18	Th-232	1.24E!17
Bi-214	2.66E!25	Pu-239	1.31E!10	Th-234	3.35E!19
Fr-221	2.2E!28	Pu-240	7.36E!12	Tl-207	2.07E!25
Np-237	5.97E!13	Pu-241	2.22E!33	Tl-208	5.15E!33
Pa-231	7.65E!16	Pu-242	2.84E!14	U-233	1.2E!16
Pa-233	2.06E!20	Ra-223	7.13E!22	U-234	1.01E!12
Pa-234	3.88E!21	Ra-224	8.88E!30	U-235	7.87E!10
Pb-209	8.92E!27	Ra-225	9.81E!25	U-236	8.23E!13
Pb-210	1.6E!19	Ra-226	1.13E!17	U-238	2.27E!08
Pb-211	1.56E!24	Ra-228	5.1E!27		

This page intentionally left blank.

Appendix Q
Water Wells of the Frenchman Flat Basin

This page intentionally left blank

The following tables and discussion provide information regarding water wells in the Frenchman Flat Basin. This information is used to determine whether or not the GWPRs of 40 CFR 191 apply to the GCD boreholes.

Table Q-1. Water Wells of the Frenchman Flat Basin (from Gillespie et al., [1996]).

Water Well	Well Location	Well Construction	Hydrostratigraphic Unit
Water Well UE-5C	Central Frenchman Flat	1964 (out of service 1994)	Alluvial and Volcanic Aquifers
Water Well-5B	Central Frenchman Flat	1951	Alluvial Aquifer
Water Well-5C	Central Frenchman Flat	1954	Alluvial Aquifer
Water Well-5A	Central Frenchman Flat	Abandoned 1970	Alluvial Aquifer
Water Well 4	CP Basin, NW Frenchman Flat	1981	Volcanic Aquifer
Water Well 4A	CP Basin, NW Frenchman Flat	1990	Volcanic Aquifer

As of 1994, Water Well 4 and Water Well 4A were connected through a pipeline to the Yucca Flat water system and did not supply water to Mercury, and water well UE-5C was out of service [Chapman, 1994]. As of 1994, drinking water was supplied to the Mercury water system by Army #1 located southwest of Mercury, and water wells 5B and 5C in Frenchman Flat. Multiple water wells in Yucca Flat (Water Wells C-1, C, and 3), directly north of Frenchman Flat penetrate the lower carbonate aquifer but did not provide drinking water to Mercury during the period of testing, development, construction and waste emplacement for the GCD boreholes (1980's).

Table Q-2 provides water well discharge data for the Frenchman Flat water wells (5B, 5C, and UE-5C) and water well Army #1 that supply drinking water to Mercury.

Table Q-2. Well Discharge Data for the Water Supply Wells of Mercury During and Immediately Following the Primary Years of Disposal of TRU Waste in the GCD Boreholes (1984 - 1988).

Year	Water Well Army #1 (m^3)	Water Well UE-5C (m^3)	Water Well 5B (m^3)	Water Well 5C (m^3)	Total Frenchman Flat (m^3)
1983	215382	4779	121924	159551	286254
1984	311132	9107	219251	222397	450755
1985	157706	18855	257102	178566	454523
1986	132116	13409	221715	242408	477532
1987	131566	31680	191322	190557	413559
1988	201310	33295	217750	256897	507942
1989	433762	12059		134169	146228
1990	477684			145482	145482
Mean	257582	17598	204844	191253	360284
Std Dev	135697	11037	45713	45381	147791

This page intentionally left blank

Appendix R

Revisions to the CAD in Response to Review Team Comments

This page intentionally left blank.

This appendix summarizes revisions that were made to this document in response to issues identified by the DOE/HQ Federal Review Team in their draft report. All text within the CAD that was changed in response to a Review Team issue is marked with a sidebar. This table lists key Review Team issues and comments from the criteria matrices.

Table R-1. Federal Review Team Comments and Resulting Changes to the CAD.

Federal Review Team Key Issues	Revisions to the CAD
Drill cuttings were not included in analysis. (Containment Requirement (CR))	Additional analyses were performed to calculate the effect on the CCDF of including releases in drill cuttings. This analysis is documented in Section 8.3
Engineered Barrier Systems were not included in the analysis. (CR)	See Appendix B of Volume 4 of the CAD.
Mathematical models were not verified. (CR)	Two additional analyses that were conducted to address this concern. These analyses addressed the effects on the CCDF of extending the simulation time from 10,000 years to 20,000 years, and the effects on the CCDF of including extreme values of upward advection. These analyses are presented in Section 8.3.
Quality Assurance Requirements were not met. (CR)	Additional text was added in Section 4 explaining how QA requirements were met. The added explanations includes a discussion of two new QA-related activities: (1) the results of two software benchmarking exercises and (2) the results of an independent review of data qualification and software quality. Neither of these new studies found any reason to invalidate the data, software, or conclusion of the PA.
The PA does not describe the active institutional controls that will be used at the site.(Assurance Requirements (AR))	See Appendix B of Volume 4 of the CAD
No GCD borehole monitoring program is described. (AR)	See Appendix B of Volume 4 of the CAD and Bechtel Nevada [2000].

Markers, records, and other passive institutional controls are not adequately discussed. (AR)	See Appendix B of Volume 4 of the CAD
Lack of Engineered Barriers. (AR)	See Appendix B of Volume 4 of the CAD
Lack of information supporting the claim that the GCD boreholes avoid areas with resources. (AR)	See Appendix B of Volume 4 of the CAD
Insufficient evidence that removal of waste is not precluded. (AR)	See Appendix B of Volume 4 of the CAD
Non-transuranic waste packages excluded (Individual Protection Requirements (IPR))	Additional dose calculations were completed that included radionuclides in non-TRU waste packages in boreholes 2 and 4. These analyses are documented in Section 8.3.
Supplemental information regarding the robustness of mathematical models was not provided. (IPR)	This information is provided in Section 8.3.
Engineered barrier systems were not included in the analysis. (IPR)	See Appendix B of Volume 4 of the CAD.
Quality Assurance requirements were not met. (IPR)	Text was added to Section 4. See above issue for CRs.

Three additional issues identified in the criteria matrices were responded to by adding text to the CAD. These issues are: (1) a new Section 3.9 showing that Sandia's PA Methodology is equivalent to the Data Quality Objectives (DQO) process, (2) a new Section 5.6.3 providing further substantiation to the assumption that the aquifers are not a "special source of ground water," and, hence, that the ground water protection requirements of 40 CFR 191 do not apply to the GCD boreholes, and (3) Figure 7-1 was updated to remove the cow.

References

Bechtel Nevada, 2000. Integrated Closure and Monitoring Plan for the Area 3 and Area 5 Radioactive Waste Management Sites at the Nevada Test Site, DOE/NV/11718-449, submitted to U.S. DOE, Nevada Operations Office, Las Vegas, Nevada, October 2000.

Distribution:

4 U.S. Department of Energy
Nevada Operations Office
Waste Management Division
Attn: Frank Di Sanza
DOE/NV/WMD
232 Energy Way
North Las Vegas, NV 89030

	MS	ORG	Name
1	0771	6800	M. Chu
1	0735	6115	E. Webb
4	0735	6115	J. Cochran
2	0731	6850	NWMP Library
1	9018	8945-1	Central Technical Files
2	0899	9616	Technical Library
1	0612	9612	Review and Approval Desk for DOE/OSTI